De-Shuang Huang
Zhongming Zhao
Vitoantonio Bevilacqua
Juan Carlos Figueroa (Eds.)

LNCS 6215

Advanced Intelligent Computing Theories and Applications

6th International Conference
on Intelligent Computing, ICIC 2010
Changsha, China, August 2010, Proceedings

Springer

Lecture Notes in Computer Science 6215

Commenced Publication in 1973
Founding and Former Series Editors:
Gerhard Goos, Juris Hartmanis, and Jan van Leeuwen

De-Shuang Huang Zhongming Zhao
Vitoantonio Bevilacqua
Juan Carlos Figueroa (Eds.)

Advanced Intelligent Computing Theories and Applications

6th International Conference
on Intelligent Computing, ICIC 2010
Changsha, China, August 18-21, 2010
Proceedings

Springer

Volume Editors

De-Shuang Huang
Chinese Academy of Sciences, Intelligent Computing Laboratory
P.O. Box 1130, Hefei, Anhui 230031, China
E-mail: dshuang@iim.ac.cn

Zhongming Zhao
Vanderbilt University Medical Center, Department of Biomedical Informatics
2525 West End Avenue, Suite 600, Nashville, TN 37203, USA
E-mail: zhongming.zhao@vanderbilt.edu

Vitoantonio Bevilacqua
Polytechnic of Bari, Electrical and Electronics Department
Via Orabona 4, 70125 Bari, Italy
E-mail: bevilacqua@poliba.it

Juan Carlos Figueroa
District University Francisco José de Caldas, Faculty of Engineering
Cra. 7a, No. 40-53, Fifth Floor, Bogotá, Colombia
E-mail: jcfigueroag@udistrital.edu.co

Library of Congress Control Number: 2010931690

CR Subject Classification (1998): I.2, I.4, I.5, F.1, H.3, H.4

LNCS Sublibrary: SL 1 – Theoretical Computer Science and General Issues

ISSN 0302-9743
ISBN-10 3-642-14921-9 Springer Berlin Heidelberg New York
ISBN-13 978-3-642-14921-4 Springer Berlin Heidelberg New York

Printed in Germany

Typesetting: Camera-ready by author, data conversion by Scientific Publishing Services, Chennai, India
Printed on acid-free paper 06/3180

Preface

The International Conference on Intelligent Computing (ICIC) was formed to provide an annual forum dedicated to the emerging and challenging topics in artificial intelligence, machine learning, pattern recognition, image processing, bioinformatics, and computational biology. It aims to bring together researchers and practitioners from both academia and industry to share ideas, problems, and solutions related to the multifaceted aspects of intelligent computing.

ICIC 2010, held in Changsha, China, August 18-21, 2010, constituted the 6th International Conference on Intelligent Computing. It built upon the success of ICIC 2009, ICIC 2008, ICIC 2007, ICIC 2006, and ICIC 2005 that were held in Ulsan, Korea, Shanghai, Qingdao, Kunming and Hefei, China, respectively.

This year, the conference concentrated mainly on the theories and methodologies as well as the emerging applications of intelligent computing. Its aim was to unify the picture of contemporary intelligent computing techniques as an integral concept that highlights the trends in advanced computational intelligence and bridges theoretical research with applications. Therefore, the theme for this conference was "Advanced Intelligent Computing Technology and Applications". Papers focusing on this theme were solicited, addressing theories, methodologies, and applications in science and technology.

ICIC 2010 received 926 submissions from 29 countries and regions. All papers went through a rigorous peer review procedure and each paper received at least three review reports. Based on the review reports, the Program Committee finally selected 253 high-quality papers for presentation at ICIC 2010, of which 243 papers are included in three volumes of proceedings published by Springer: one volume of *Lecture Notes in Computer Science* (LNCS), one volume of *Lecture Notes in Artificial Intelligence* (LNAI), and one volume of *Communications in Computer and Information Science* (CCIS). The other 10 papers will be included in *Neural Computing & Applications*.

This volume of *Lecture Notes in Computer Science* (LNCS) includes 84 papers.

The organizers of ICIC 2010, including Hunan University, Institute of Intelligent Machines of Chinese Academy of Sciences, made an enormous effort to ensure the success of ICIC 2010. We hereby would like to thank the members of the Program Committee and the referees for their collective effort in reviewing and soliciting the papers. We would like to thank Alfred Hofmann from Springer for his frank and helpful advice and guidance throughout and for his continuous support in publishing the proceedings. In particular, we would like to thank all the authors for contributing their papers. Without the high-quality submissions from the authors, the success of the conference would not have been possible. Finally, we are especially grateful to the IEEE Computational Intelligence Society, the International Neural Network Society, and the National Science Foundation of China for their sponsorship.

June 2010

De-Shuang Huang
Zhongming Zhao
Vitoantonio Bevilacqua
Juan Carlos Figueroa

ICIC 2010 Organization

General Co-chairs	De-Shuang Huang, China
	Martin McGinnity, UK
Program Committee Co-chairs	Laurent Heutte, France
	Zhongming Zhao, USA
	Xiao-Ping Zhang, Canada
Organizing Committee Co-chairs	Renfa Li, China
	Jiawei Luo, China
	Kenli Li, China
	Wei Jia, China
Award Committee Chair	Kang-Hyun Jo, Korea
Publication Co-chairs	Vitoantonio Bevilacqua, Italy
	Carlos Alberto Reyes Garcia, Mexico
Special Session Co-chairs	Kang Li, UK
	Xiang Zhang, USA
	Vincent C. S. Lee, Australia
Tutorial Chair	Marco Loog, Denmark
International Liaison Chair	Prashan Premaratne, Australia
Publicity Co-chairs	Valeriya Gribova, Russia
	Kyungsook Han, Korea
	Lei Zhang, Hong Kong, China
	Juan Carlos Figueroa, Colombia
	Muhammad Khurram Khan, Saudi Arabia
Exhibition Chair	Chun-Hou Zheng, China
Organizing Committee Members	Bo Liao, China
	Shulin Wang, China
	Zhiyong Li, China
	Xinguo Lu, China

Program Committee Members

Khalid Mahmood Aamir, Pakistan
Andrea Francesco Abate, Italy
Shafayat Abrar, UK
Peter Andras, UK
Sabri Arik, Turkey
Vasily Aristarkhov, Russian Federation
Costin Badica, Romania
Martin Brown, UK
Uday K. Chakraborty, USA
Shih-Hsin Chen, Taiwan
Tan Kay Chen, Singapore
Wen-Sheng Chen, China
Xiyuan Chen, China
Yang Chen, China
Yuehui Chen, China
Ziping Chiang, Taiwan
Min-Sen Chiu, Singapore
Won-Ho Choi, Korea
Michal Choras, Poland
Tommy Chow, Hong Kong
Jose Alfredo F. Costa, Brazil
Mingcong Deng, Japan

Youping Deng, USA
Eng. Salvatore Distefano, Italy
Karim Faez, Iran
Jianbo Fan, China
Dimitar Filev, USA
Wai-Keung Fung, Canada
Liang Gao, China
Xiao-Zhi Gao, Finland
Dunwei Gong, China
Valeriya Gribova, Russia
Ping Guo, China
Sung Ho Ha, Korea
Kyungsook Han, Korea
Haibo He, USA
Nojeong Heo, Korea
Laurent Heutte, France
Wei-Chiang Hong, Taiwan
Yuexian Hou, China
Zeng-Guang Hou, China
Kun Huang, USA
Tingwen Huang, Qatar
Yufei Huang, USA
Peter Hung, Ireland
Li Jia, China
Zhenran Jiang, China
Robert I. John, UK
Dah-Jing Jwo, Taiwan
Sanggil Kang, Korea
Muhammad Khurram Khan, Saudi Arabia
Myung-Kyun Kim, Korea
Sungshin Kim, Korea
In-Soo Koo, Korea
Harshit Kumar, Korea
Yoshinori Kuno, Japan
Takashi Kuremoto, Japan
Vincent C.S. Lee, Australia
Guo-Zheng Li, China
Kang Li, UK
Peihua Li, China
Shutao Li, China
Hualou Liang, USA
Chunmei Liu, USA
Chun-Yu Liu, USA
Van-Tsai Liu, Taiwan, China
Marco Loog, Denmark
Jinwen Ma, China
Vishnu Vardhan Makkapati, India
Miguel Melgarejo, Colombia
Cheolhong Moon, Korea
Tarik Veli Mumcu, Turkey
Roman Neruda, Czech Republic
Ben Niu, China
Yusuke Nojima, Japan
Pedro Nuno Oliveira, Portugal
Sim-Heng Ong, Singapore
Ali Özen, Turkey
Shaoning Pang, New Zealand
Francesco Pappalardo, Italy
Witold Pedrycz, Canada
Caroline Petitjean, France
Prashan Premaratne, Australia
Daowen Qiu, China
Hong Qiao, China
Seeja K.R., India
Nini Rao, China
Marylyn Ritchie, USA
Angel Sappa, Spain
Ruhul Amin Sarker, Australia
Jiatao Song, China
Joao Miguel Sousa, Portugal
Stefano Squartini, Italy
Min Su, USA
Zhan-Li Sun, Singapore
Masahiro Takatsuka, Australia
Maolin Tang, Australia
Fariba Salehi, Iran
Ernesto Cuadros-Vargas, Peru
Anhua Wan, China
Jun Wan, USA
Jeen-Shing Wang, Taiwan
Ling Wang, China
Xue Wang, China
Xuesong Wang, China
Yong Wang, China
Zhi Wei, China
Ling-Yun Wu, China
Qingxiang Wu, UK
Shunren Xia, China
Yu Xue, China
Ching-Nung Yang, Taiwan
Jun-Heng Yeh, Taiwan
Myeong-Jae Yi, Korea
Zhi-Gang Zeng, China
Jun Zhang, China
Lei Zhang, Hong Kong, China
Xiang Zhang, USA
Xiaoguang Zhao, China
Xing-Ming Zhao, China
Zhongming Zhao, USA
Bo-Jin Zheng, China
Chun-Hou Zheng, China
Fengfeng Zhou, USA
Mianlai Zhou, China

Reviewers

Salim Kahveci, Mustafa Aktas, Birol Soysal, Mehmet Eker, Halil Brahim Sahin, Bekir Dizdaroglu, Huseyin Polat, Xinjiao Gao, Zexian Liu, Fengfeng Zhou, Anyuan Guo, Zhaolei Zhang, Sanggil Kang, Xiao-Zhi Gao, Quanming Zhao, Huisen Wang, Ying Qiu, Sajalendu Dey, Mandira Chakraborty, Chengyou Wang, H.S. Raymond Ng, Peter Baranyi, Carson K. Leung, Yu Xue, Michele Scarpiniti, Yibin Ye, Draguna Vrabie, Li-Wei (Leo) Ko, Kunikazu Kobayashi, Joaquín Torres-Sospedra, Takashi Kuremoto, Masanao Obayashi, Dongsheng Che, Junfeng Qu, Feng-Biao Guo, Gang Wang, Dimitar Filev, Jianxiu Guo, Joaquín Torres-Sospedra, Xiangzhen Kong, Xuesong Wang, K.C. Tan, Marco Alzate, Leonardo Leottau Forero, Oscar Méndez, Jairo Soriano, Sergio A. Rojas, Andres Eduardo Gaona Barrera, Juan Carlos Figueroa García, Vladimir Brusic, Filippo Castiglione, Santo Motta, Alessandro Cincotti, Ping Zhang, Selin Ozcira, Ibrahim Aliskan, Marzio Pennisi, Davide Alemani, Salvatore Musumeci, Zeeshan Rana, Jordi Solé-Casals, Ohmin Kwon, Fugang Zheng, Marcos Faundez-Zanuy, Sanqing Hu, Georgia Tourassi, Jun Qin, Lingling Wang, Weiwu Wang, Tsung-Han Chan, Xinyu Li, Xuezheng Chu, Ping Jiang, Iftikhar Ahmad, Usman Tariq, Lvzhou Li, Situ Haozhen, Qin Li, Gui Lu Long, Mohammad Rouhani, Chien-Cheng Tseng, Juan Cui, Weifeng Huo, Shan Wang, Song Zhu, Lei Liu, Feng Jiang, Ailong Wu, Haibin Duan, Quan-Ke Pan, Yong Wang, Lingpo Li, Ye Xu, Jia-qing Zhao, Bo Liu, Yuejiao Gong, Ying Lin, Jinghui Zhong, Ling Wang, Xianxia Zhang, Aravindan Chandrabose, Maqsood Mahmud, Fuchun Liu, Hongjun Jia, Liya Ding, Dawen Xu, Beijing Chen, Yehu Shen, Tiantai Guo, Chun Chen, Linhua Zhou, Liangxu Liu, Qingfeng Li, Shaojing Fan, Jianhua Che, Jianbo Fan, Aizhong Mi, Daoqing Sun, Jie Sun, Yu Wang, Rina Su, Hua Yu, Zhongkun He, Jie Sun, Davide Ciucci, Dominik Slezak, Xianlong Wang, Mingyu You, Tian-yu Liu, Yang Xiang, Zheng Su, Jianfei Hu, Jikui Shen, Xueping Yu, Changli Li, Shafayat Abrar, Chenglei Sun, Xiaoping Liu, Chong Shen, Xuefen Zhu, Yifeng Zhang, Cristiana Cuco, Zhiquan Feng, Min-Sen Chiu, Nikolay Mikhaylov, Olesya Kazakova, Dingfei Ge, Jiayin Zhou, Xiaoping Luo, Patrick Dempster, Ammar Belatreche, Huaizhong Zhang, Li Hong-chun, Gurumurthy Swaminathan, Gina Sierra, Héctor Daniel Bernal, Katherine Baquero, Edgar Forero, Xueping Yu, Xin Fang, Omar Orqueda, Carme Julià, Rafal Kozik, Prashan Premaratne, Sina Wafi, Haibo Deng, Qiao Wang, Hyunju Park, Myung-Kyun Kim, Chengjian Wei, Bo Peng, Shigang Liu, Zhang Kaihua, Weidi Dai, Jie Gui, Yingke Lei, Rong-xiang Hu, Lei Tang, Chunhou Zheng, Junfeng Xia, Zhuhong You, Min Wu, Ji-Guang Wang, Lin Zhu, Zhi-Ping Liu, Wei Jia, Xue-Ling Li, Lin wang, YuQing Qiu, Hong-Jie Yu, Sergio Pinheiro dos Santos, Renato Sassi, Anne Canuto, Adriao Duarte, Allan Martins, Claudio Medeiros, Min-Chih Chen, Sorin Ilie, Mihnea Scafes, Safeeullah Soomro, Dao Zhou, Li Zhu, Yenisel Plasencia, Yan Li, Mehrdad Gangeh, Bin Yang, I-Cheng Chang, Cheng-Chin Chiang, Wuchaun Yang, Kumar Rajamani, Chung-Ho Cho, Gyungjin Hong, Gwangju-Hyun Kim, Min Su, Changyan Xiao, Renato Sassi, Flora Jia, Wei Xiong, Jing Zhang, Litt Teen Hiew, Chuang Ma, Ismail Shah, Ni Chen, Hongshan Yu, Yanmin Liu, Bing Xue, Quande Qin, Yan Fan, Bei Ye, Z.H.L Zheng, J.l. Xu, Martin Pilat, Roman Neruda, Petra Vidnerová, Xiaomin Liu, Alfredo Pulvirenti, Akihiro Yorita, Xiao-Feng Wang, Yang Shi, Wen Feng, Kunlei Lian, Zhi-Hui Zhan, S. M. Kamrul Hasan, Nurhadi Siswanto, Tapabrata Ray, Abu S.S.M. Barkat Ullah, Xiao Sun, Zhuping Wang, Hui Liu, Long

Chen, Yan Yang, Yongsheng Dong, Yanqiao Zhu, Gang Chen, Irina Artemieva, Sabooh Ijaz, Keqin Liu, Sangyoon Oh, Kyung-Suk Lhee, Jianguo Wang, Min Zheng, Eung-Hee Kim, Yasuki Kansha, Bo Chen, Lu Jian, Chifeng Ma, Jianliang Tang, Jose Alfredo F. Costa, Diana Porro, Martha Ruth Ospina Torres, Ferro Roberto, Elvis Eduardo Gaona García, Junlin Chang, Alex Cheng, Huijun Li, Huijuan Lu, Quan-Ke Pan, Bin Qian, Jianyong Sun, Yong Zhang, Zhihua Cui, Nelson Perez, Licheng Jiao, Aimin Zhou, Jihui Zhang, Yan Zhang, Chuan Wu, Shangfei Wang, Lifeng Ai, Zeratul Yusoh, Haini Qu, Toshiaki Kondo, Yuanwei Zhang, Leandro Coelho, Vasily Aristarkhov, Sen-Chueh Peng, Kuo-Ting Huang, Shengjun Wen, Ajiboye Osunleke, Aihui Wang, Hui-Yu Huang, Barbara Zitova, Zheng-Jun Zha, Luis Felipe Albarracin Sanchez, Joao Sousa, Xiang Zhang, Jun Zhang, B.W., Xiangjuan Yao, Xiaoyan Sun, David Taniar, Gang Li, Kok-Leong Ong, Yi Sun, Wang Xiaojuan, Li Nie, Peilin Jia, Ping Liang, Ke Tang, Jifeng Ning, Kazunori Onoguchi, Yasuhiro Taniguchi, Nhan Nguyen-Thanh, Thuc Kieu Xuan, Youngdu Lee, Vu Van Hiep, Asaduzzaman., Kanghee Kim, Hyunho Yang, Sungsoo Choi, Seokjoo Shin, Jintae Park, Seok Woo, Dinesh Gautam, Min Hai, Michal Choras, Francesco Longo, Salvatore Distefano, Insoo Koo, A.D. Allan, Stanislav Slusny, Kesheng Wang, Arash Ghanbari, Tiejun Liu, Yongjie Li, Peng Xu, Zhongming Zhao, Rowena Chau, Dan Cuns, Ryuzo Okada, Rodrigo Herrera, Yuanlong Li, Wei-jie Yu, Jing Xiao, Qi Cheng, Teerasit Kasetkasem, Ying Lin, Yue Wang, Zujun Hou, Xin Hao, Nidhi Arora, Eugen Ganea, Amar Balla, Zhenhua Guo, Wei Li, Linlin Shen, Zhiyong Liu, Jin Liu, Zhiyi Lin, Shen Xianjun, Flavius Gorgonio, Roseli Romero, Michal Wozniak, Nilton Canto, Kang Li, Qun Niu, Jing Deng, Po-Chih Chou, Chao Wu, Yaou Zhao, Lizhi Peng, Qingfang Meng, Jian Chen, Bilal Khan, Aneel Rahim, Mohamed Eldefrawy, Dudy Lim, Lanshen Guo, Yunlong Liu, Gilbert Feng, Daniel Linares, Weidong Yang, Mill Sam, Rajalakshmi Krishnamurthi, Susana Vieira, Luis Mendon&ccedila, Wei-Chiang Hong, Li Shutao, Ming Zhao, Shiuh-Jeng Wang, S.J. Shyu, Wen-Chung Kuo, Jyun-Jie Lin, Chin Yuan Fan, Sheng Wang, Sun Xinyao, Chang Liu, Z. Zeng, Alberto Rey, Raquel Pati&ntildeo, Lin Zhang, Chien-Yuan Lai, Alberto Moraglio, Ruhul Sarker, Saber Elsayed, Yu-Liang Hsu, Tzu-Ping Kao, Fang-Chen Chuang, Wei-Chun Chiang, Yasuhiro Hitotsuyanagi, Tomasz Rutkowski, Ziping Chiang, James Kim, Senator Jeong, Eylem Yucel, Sibel Senan, Ermai Xie, Simon Bernard, Wlike Wang, Yunyo Chiang, Mingbo Zhao, Zhou Wu, Wei Huang, Shanping Qiao, Bin Yang, Yucheng Dong, Jong Min Lee, Ikhyeon Jang, Amelia Badica, Chunjiang He, Yong Wanng, Vincent C.S. Lee, Song Yang, Z.G. Hou, Yihai Zhu, LingFeng Liu, Yang Zhao, Xiaodong Dai, Shanwen Zhang, Meiling Hou, Jie Gui, Jixiang Du, Lei Yang, Xiao Yang Xue, Hangjun Wang, Muhammad Imran Razzak, John Ray.

Table of Contents

Neural Networks

Evolutionary Learning and Genetic Algorithms

Fuzzy Theory and Models

Fuzzy Systems and Soft Computing

Particle Swarm Optimization and Niche Technology

Supervised and Semi-supervised Learning

Unsupervised and Reinforcement Learning

Combinatorial and Numerical Optimization

Systems Biology and Computational Biology

Neural Computing and Optimization

Nature Inspired Computing and Optimization

Knowledge Discovery and Data Mining

Artificial Life and Artificial Immune Systems

Intelligent Computing in Image Processing

Special Session on New Hand-Based Biometric Methods

Special Session on Recent Advances in Image Segmentation

Special Session on Theories and Applications in Advanced Intelligent Computing

Special Session on Search Based Software Engineering

Special Session on Bio-inspired Computing and Applications

Special Session on Advance in Dimensionality Reduction Methods and Its Applications

Special Session on Protein and Gene Bioinformatics: Methods and Applications

Design of a Novel Six-Dimensional Force/Torque Sensor and Its Calibration Based on NN

Qiao-Kang Liang[1,2], Quan-Jun Song[1], Dan Zhang[3], Yun-Jian Ge[1], Guang-Bin Zhang[1,2], Hui-Bin Cao[1], and Yu Ge[1]

[1] Institute of Intelligent Machines, Chinese Academy of Sciences, Hefei, Anhui, P.R. China
[2] University of Science and Technology of China, Hefei, Anhui, P.R. China
[3] Faculty of Engineering and Applied Science, University of Ontario Institute of Technology, Oshawa, ON L1H 7K4, Canada
{Qiaokang.Liang,Dan.Zhang}@uoit.ca,
{qjsong,hbcao,Geyu}@iim.ac.cn, zgb@mail.ustc.edu.cn

Abstract. This paper describes the design of a six-axis force/torque sensor, the purpose of which is to provide decoupled and accurate F/T information for the closed-loop control of the manipulator system. Firstly, the manipulator system and the adopted measuring principle are introduced. Then, a novel static component based on dual annulus diaphragms is presented. At last, the calibration and decoupling test based on Neural Network (NN) is carried out. The results of calibration test show superiority of the structure of the elastic component of the developed sensor and the improvement of the calibration method.

Keywords: F/T sensor, calibration, Neural Network, dexterous manipulation, elastic component.

1 Introduction

Robot applications are widespread in industry such as material-handling, surveillance, surgical operations, rehabilitation and entertainment [1]. Of all robotic manipulators, besides their architectures and controls, F/T sensors mounted in the manipulators deserve special attention in order to perform dexterous and accurate tasks via feedback control. If it is to be autonomous, the manipulator system should have several kinds of sensors such as stereo vision, joint angle sensor, distance sensor, F/T sensor and tactile sensor. Force feedback and control have been discussed from the beginning of the robotics research [2] as its importance. A direct and simple method to measure the manipulator force is to place an F/T sensor closed to that, so-called wrist F/T sensor. Recently, some researchers set up F/T sensors on the finger tip of the manipulators, so-called fingertip F/T sensor, to detect more particular force/torque information. Among the F/T sensors, six-dimensional F/T sensor, with the ability of detecting three force components along the axes and three torque components about the axes, is one kind of the most important sensor in dexterous manipulators.

D.-S. Huang et al. (Eds.): ICIC 2010, LNCS 6215, pp. 1–8, 2010.

Force sensing has a long research history as the force control and theoretical and experimental investigation of the six-axis F/T sensors have been carried out by many scholars and researchers. Liu [3] developed a novel six-component force sensor with its force-sensing member in the form of four T-shaped beams, Chao [4] presented a six-axis force sensor based on cross beams using shape optimal design and finite-element method, and Kim [5, 6] designed some kinds of six-axis force/torque sensor with interference error of less than 2.85% based on cross beams, Kang [7] developed a transducer based on the Stewart platform by a closed-form solution of the forward kinematics. In the meantime, several six-axis F/T sensors with acceptable performances are commercially available by companies such as ATI, JR3, Kistler and Futek etc. A major problem in developing F/T sensor is the design of the elastic component, which is a main determinant but dependent on the experience of designers. Additionally, the theoretical evaluation of the designed F/T sensors and their comparative evaluation have not been done sufficiently [2]. Moreover, as all multi-axis F/T sensors have some degree of cross coupling, so the calibration and decoupling should be perform individually for each F/T sensor [8], which is investigated insufficiently either.

In response to the above needs, we focus our attention on designing a novel six-axis F/T sensor for manipulators to enable them to grasp and manipulate objects controllably and dexterously by providing systems F/T information about particular processes when manipulators interact with the environment. The sensor was newly modeled by the elastic body with two E-type membranes to measure the F_x, F_y, F_z, M_x, M_y and four lamellas to measure the M_z. At last, the calibration based on NN and the characteristic tests were carried out, which prove the developed sensor possesses of positive characteristics such as strong linearity, weak couplings and high sensitivity.

2 Description of the Manipulator and the Measuring Principle

Figure 1 represents a 5-DOF serial manipulator in which the first joint axis points up vertically, the second joint axis in perpendicular to the first with a small offset, the third and fourth joint axes are both parallel to the second, and the fifth joint axis intersects the fourth perpendicularly. A six-axis wrist F/T sensor is mounted at the end of the fifth link, and three four-axis fingertip F/T sensors are set up at the ends of fingers of the end-effector.

In the manipulator system, real-time feedback control loop has been developed to make sure that the system performs tasks dexterously and accurately. And the architecture of the manipulator control system is shown in Fig. 2. To accomplish the complex tasks of manipulation, the control system acts as a closed-loop system based on feedback data provided by different sensors. The wrist F/T sensor measures the three orthogonal force components along the x-, y- and z-axis, and the torques about these axes applied on the end-effector. At the same time, the fingertip F/T sensor detects more particular information such as tactile and frictional force/torque. Then this information is fed back to the controller in real time for analyzing and decision-making. Obviously, the performance of the system is heavily influenced by the need for real-time sensing. Therefore, high accurate F/T sensor is desired.

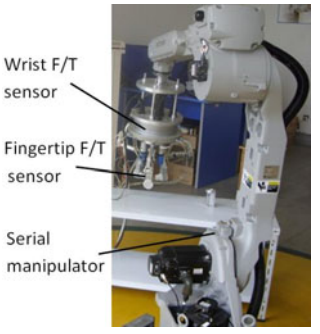

Fig. 1. The serial manipulator system featured by wrist and fingertip F/T sensor

There are a number of methods of detecting the forces and moments applied to an object, and the most common is electric measurement technique with strain gauges, whose electrical resistance is proportional to its length. When the strain gauges mounted onto the force-sensing element of sensor, they will undergo the changes of resistances as the force-sensing element deforms. Gage factor, a fundamental parameter about the sensitivity to strain, is defined as:

$$G_F = \frac{\Delta R / R}{\Delta L / L} = \frac{\Delta R / R}{\varepsilon} \tag{1}$$

where R is the original resistance of the strain gauge, L is the original length, and ε is the strain that the strain gauge experience.

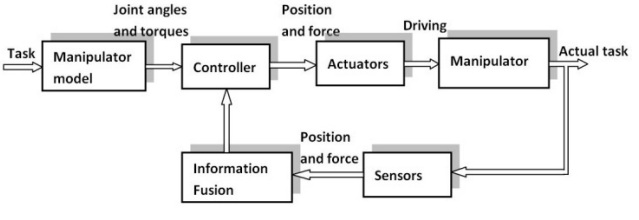

Fig. 2. Feedback control architecture of the manipulator system

A bridge circuit always used to measure such small changes in resistances. Full-bridge circuits, whose four arms are all active strain gages, increase the sensitivity of the circuit further. And its measurement sensitivity is:

$$V_0 / V_E = -G_F \cdot \Delta\varepsilon \tag{2}$$

where V_0 is the output of the circuit, V_ε is the voltage excitation source.

When forces in directions F_x, F_y, F_z and moments around the axis M_x, M_y, M_z are applied to the sensor, the outputs of strain gauges attached at various locations will be S(S_1, S_2, S_3, ⋯). Relationship could be expressed as below using detection matrix T:

$$S = TF \tag{3}$$

So, from the sensor outputs, applied forces and moments could be determined and calculated by using the inverse matrix of $\boldsymbol{T}$:

$$F = T^{-1}S \tag{4}$$

Finally, as wrist sensors measure forces and moments equivalent forces acting on the wrist which differ from the forces and moments applied on the manipulator's end. It is therefore necessary to transform forces from the sensor frame $f_s=[f_{xs}\ f_{ys}\ f_{zs}]^T$ and moments $ms=[m_{xs}\ m_{ys}\ m_{zs}]^T$ into the end-effector frame $f_c=[f_{xc}\ f_{yc}\ f_{zc}]^T$ and moments $m_c=[m_{xc}\ m_{yc}\ m_{zc}]^T$ [9]:

$$\begin{bmatrix} f_c \\ m_c \end{bmatrix} = \begin{bmatrix} R_s^c & 0 \\ S(r_{cs}^c)R_s^c & R_s^c \end{bmatrix} \begin{bmatrix} f_s \\ m_s \end{bmatrix} \tag{5}$$

which requires knowledge of the position ${r_{cs}}^c$ of the origin of Frame s with respect to Frame c as well as of the orientation ${R_s}^c$ of Frame s with respect to Frame c. And *S(*)* are the skew-symmetric operator.

3 Design of the Elastic Component

The elastic component connects the measured and strain gauges in the form of a sense organ, and its performances mainly determine the performance of the sensor. A drawback of most existing force/torque sensors is high coupled interference among axes, especially between Fx and My, Fy and Mx respectively, which need complicate and difficult calibration test to get decoupling matrix [8].

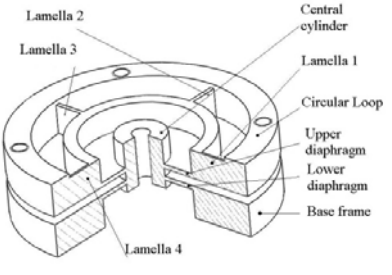

Fig. 3. A partially cutaway perspective view of the elastic component structure

In detail, as shown in Fig. 3, the elastic component consists of a base frame, a lower diaphragm, a circular loop, an upper diaphragm, a central cylinder that connects the lower diaphragm and the upper diaphragm, and four lamellas that connect the central hollow cylinder and the circular loop. The upper diaphragm that serve as an active sensing portion is sensitive to the moment about the X-axis and Y-axis (M_x, M_y), and the lower diaphragm that serve as an active sensing portion is sensitive to the

normal force (F_z) and both tangential force terms (F_x, F_y). On the other hand, the lamellas that serve as active sensing portions are responsive to the moment about the normal axis (M_z). Fig. 4 (a) shows the photograph of the prototype of the six-axis F/T sensor. The prototype is made of aluminum alloy and total diameter and height of the sensor is Φ60mm and 35mm, respectively. Twenty-four pieces of strain gauges are bonded onto the active sensing portions of the elastic component and form six full Wheatstone electrical bridges. The communication and signal-conditioning circuit board based on embedded system is integrated in the sensor, as shown in Fig.4 (b).

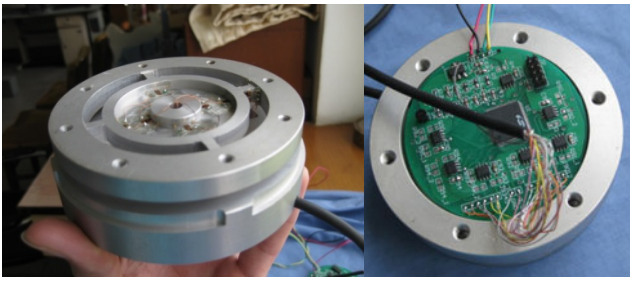

(a) (b)

Fig. 4. (a) Prototype of the six-axis F/T sensor; (b) The integrated circuit board of the sensor

4 Calibration and Decoupling

Cross-coupling causes the erroneous measurement of some particular axes as a result of an actual force or torque applied to another orthogonal axis [10]. Actually, all multi-axis force/torque sensors have some degree of cross coupling between components.

The calibration and decoupling procedure of the sensor was performed as follows.

1. Mount the F/T sensor in the center of the calibration platform horizontally with a loading hat bolted on its top, as shown in Fig. 5.
2. Adjust the zero point of the AMPs of the each component of the F/T sensor.
3. We applied single component of six components through hanging standard weights onto the sensor with a cycle series of values from minimum to maximum allowed loads within measurement range.
4. And perform the loading cycle three times for each component. In the meantime, recorded the output voltages of the sensitive bridge circuits as samples.
5. Train the Neural Network with the samples recorded at step 4, as show in Fig. 6. The input vector (S= $[S_{Fx}\ S_{Fy}\ S_{Fz}\ S_{Mx}\ S_{My}\ S_{Mz}]^T$) are the output voltages of the sensitive bridge circuits, and the output vector(F=$[F_x\ F_y\ F_z\ M_x\ M_y\ M_z]^T$) are the real forces/torques outputs of the sensor after decoupling.
6. After network training, the weight value (W= $[w_{ij}]$, i,j=1,2,…,6) is taken as a decoupling matrix. As,

$$F=WS\cdot b \tag{6}$$

Comparing formula (4) with Formula (12),

$$W=T^{-1} \tag{7}$$

So we can obtain decoupling matrix by neural network.

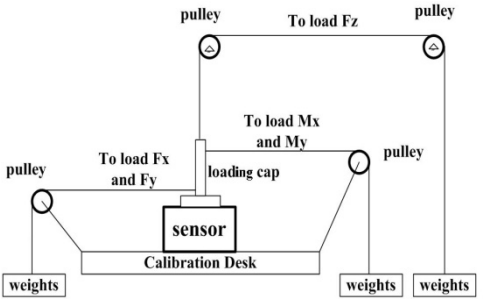

Fig. 5. Calibration schematic diagram

At last, we get the decoupling matrix as following

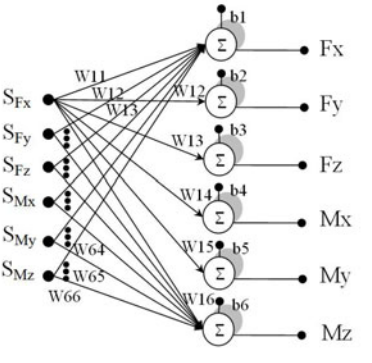

Fig. 6. Neural network model for wrist force sensor calibration

$$W = \begin{bmatrix} 6.2939 & 0.055 & 0.0352 & -0.0348 & 4.756 & -0.007 \\ 0.0466 & 6.3283 & 0.0459 & 4.5078 & 0.0557 & 0.0072 \\ 0.0375 & 0.032 & 0.9309 & -0.0136 & -0.0193 & -0.0093 \\ 0.0598 & 14.755 & 0.0521 & 19.3399 & 0.3772 & -0.03 \\ 14.7681 & 0.1232 & -0.0786 & -0.2420 & 20.421 & 0.0299 \\ -0.5449 & -3.1098 & 0.0069 & -2.4641 & -0.328 & 4.207 \end{bmatrix} \tag{8}$$

and the deviation value

$$b=[-0.3134\ -0.3022\ 0.8675\ -1.1652\ -0.0311\ -1.3375]^T \quad (9)$$

The experimental results, the output curves of the sensor, are shown in Fig.4. Here the X-coordinates and Y-coordinates are respectively the sample points of the data acquisition system and output of the A/D converter of the system. And when one component of six kinds of load calibrated, the others are set at zero.

After zero adjustment, the maximum interference errors of the F_x, F_y, F_z, M_x, M_y and M_z measurement are 1.4% F.S., 1.3% F.S., 1.5% F.S. and 1.6% F.S., 1.6% F.S., 1.0% F.S., respectively. So it could be confirmed that the developed wrist force sensor is excellent in the maximum error.

However, the fabricated sensors have the following disadvantages. First, the developed sensor the calibration procedure took too much time as the large sum of the sampling is needed.

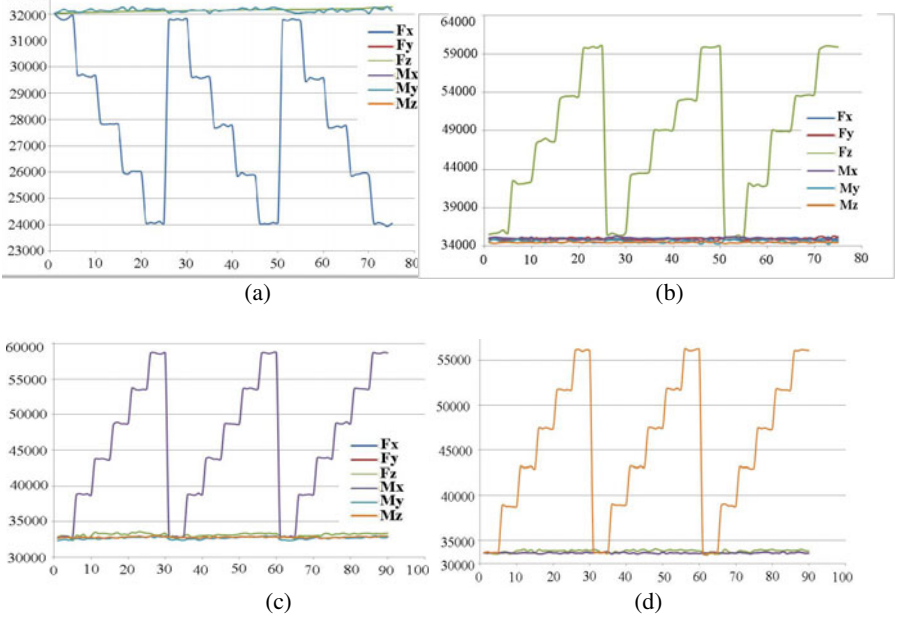

Fig. 7. Calibration results of the six-DOF F/T sensor: (a) component F_x (similar with F_y); (b) component F_z; (c) component M_x (similar with M_y); (d) component M_z

5 Conclusion

This study has endeavored in designing and fabricating a novel six-dimensional force sensor (60mm in diameter and 35mm in height) for manipulators with the elastic component based on double annulus diaphragm, as shown in Fig. 7. The novel structure of the force-sensing element and the calibration procedure based on NN make sure it has a relevant performance, and the experiment results demonstrate

maximum interference error and nonlinearity error are 1.6% F.S. and 0.17% F.S., respectively, and it has results in terms of the high measurement sensitivity, good linearity, and weak couplings between dimensions characteristics.

Acknowledgments. This work was supported in part by the National 863 Project under Grant No. 2006AA04Z244 and National Nature Science Foundation of China under Grant No. NSFC60874097 and No. NSFC60910005. The first author gratefully acknowledges the financial support from the China Scholarship Council, Ministry of Education of the P.R.C. and Innovation Program of USTC.

References

1. Angeles, J.: Fundamentals of robotic mechanical Systems. Springer, Heidelberg (2007)
2. Nakamura, Y.: Robotics: Redundancy and optimization. Addison-Wesley Publishing Company, Reading (1991)
3. Liu, S.A., Tzo, H.L.: A novel six-component force sensor of good measurement isotropy and sensitivities. Sensors & Actuators: A. Physical 100, 223–230
4. Chao, L.P., Chen, K.T.: Shape optimal design and force sensitivity evaluation of six-axis force sensors. Sensors & Actuators: A. Physical 63, 105–112 (1997)
5. Kim, G.S.: Design of a six-axis wrist force/moment sensor using FEM and its fabrication for an intelligent robot. Sensors & Actuators: A. Physical 133, 27–34 (2007)
6. Kim, G.S.: Development of 6-axis force/moment sensor for a humanoid robot's intelligent foot. Sensors & Actuators: A. Physical 141, 276–281 (2008)
7. Kang, C.C.: Closed-form force sensing of a 6-axis force transducer based on the stewart platform. Sensors & Actuators: A. Physical 90, 31–37 (2001)
8. Liang, Q., Zhang, D., Ge, Y.J., Song, Q.J.: A novel miniature four-dimensional force/torque sensor with overload protection mechanism. IEEE Sensors Journal 9, 1741–1747 (2009)
9. Liang, Q., Ge, Y., Song, Q., Ge, Y.: A Novel Thin Six-dimensional Wrist Force/Torque Sensor with Isotropy. In: International Conference on Information and Automation, ICIA 2009, pp. 1135–1139 (2009)
10. Liang, Q., Zhang, D., Song, Q., Ge, Y.: A potential four-dimensional fingertip force sensor for underwater robot manipulator. IEEE Journal of Oceanic Engineering 35 (2010)

Incremental-Based Extreme Learning Machine Algorithms for Time-Variant Neural Networks

Yibin Ye, Stefano Squartini, and Francesco Piazza

A3LAB, Department of Biomedics, Electronics and Telecommunications,
Università Politecnica delle Marche, Via Brecce Bianche 1, 60131 Ancona, Italy
{yibin.ye,s.squartini,f.piazza}@univpm.it
http://www.a3lab.dibet.univpm.it

Abstract. Extreme Learning Machine (ELM) is a novel learning algorithm for Neural Networks (NN) much faster than the traditional gradient-based learning techniques, and many variants, extensions and applications in the NN field have been appeared in the recent literature. Among them, an ELM approach has been applied to training Time-Variant Neural Networks (TV-NN), with the main objective to reduce the training time. Moreover, interesting approaches have been proposed to automatically determine the number of hidden nodes, which represents one of the limitations of original ELM algorithm for NN. In this paper, we extend the Error Minimized Extreme Learning Machine (EM-ELM) algorithm along with other two incremental based ELM methods to the time-variant case study, which is actually missing in the related literature. Comparative simulation results show the the proposed EM-ELM-TV is efficient to optimally determine the basic network architecture guaranteeing good generalization performances at the same time.

1 Introduction

A fast learning algorithm called Extreme Learning Machine (ELM) introduced by Huang et al[1,2], has recently caught much attention within the Neural Network (NN) research community. ELM is designed for single hidden layer feed-forward neural networks (SLFNs): it randomly chooses hidden nodes and then determines the output weight analytically. However, one of the open problem of ELM is how to assign the number of hidden neurons, which is the only factor that needs to be set by users, usually by trial-and-error. The first hidden nodes increment algorithm for ELM, referred to as Incremental Extreme Learning Machine (I-ELM)[3], randomly adds nodes to the hidden layer one by one and freezes the output weights of the existing hidden nodes when a new hidden node is added. However, due to the random generation of added hidden nodes, some of which may play a very minor role in the network output and thus may eventually increase the network complexity. In order to avoid this issue, an Enhanced method for I-ELM, called EI-ELM[4] have been proposed. At each learning step, several hidden nodes are randomly generated and the one leading to least error is then selected and added to the network.

D.-S. Huang et al. (Eds.): ICIC 2010, LNCS 6215, pp. 9–16, 2010.

Recently, another ELM-based hidden nodes incremental learning algorithm referred to as Error Minimized Extreme Learning Machine (EM-ELM)[5] was proposed. It can also add random hidden nodes to SLFNs one by one or even group by group, with all the previous output weights updated accordingly at each step. Compared with I-ELM and EI-ELM which keep the output weights of existing hidden nodes fixed when adding a new hidden node, EM-ELM attain a much better generalization performance.

Time-Variant Neural Networks(TV-NN) represent a relevant example in the field of neural architectures working properly in non-stationary environments. Such networks have time-variant weights, each being a linear combination of a certain set of basis functions. Titti et al[6], proposed an extended version of the Back-Propagation(BP) algorithm to suitably train such networks. An Extreme Learning Machine approach is also developed for TV-NN(ELM-TV-NN), introduced by Cingolani et al[7], accelerating the training procedure significantly. However, ELM-TV-NN also has the problem to determine the size of network, e.g. the number of hidden nodes, as ELM does.

In this paper, we attempt to extend I-ELM, EI-ELM and EM-ELM to time-variant networks, as well as testing and comparing them in 3 different task scenarios. We will show that similar behavior to the one achievable in the time-invariant case can be obtained, proving the effectiveness of the algorithm generalization to the TV-NN case study.

Due to the space constraint, we do not present more details for ELM algorithm and its three related incremental-based variants I-ELM, EI-ELM and EM-ELM. Please refer to [2,3,4,5] for more information.

2 The ELM Approach for Time-Variant Neural Networks

The application and extension of ELM to the time-variant case has been studied in [7]. In a time-variant neural network, the input weights, or output weights, or both are changing through the training and testing time. Each weight can be expressed as a linear combination of a certain set of basis functions: $w[n] = \sum_{b=1}^{B} f_b[n] \cdot w_b$, in which $f_b[n]$ is the known orthogonal function at n-th time instant of b-th order, w_b is the b-th order coefficient of the basic function to construct time-variant weight w_n, while B is the total number of the bases preset by user.

If time-variant input weights are introduced in a SLFN, hidden neuron output function can be rewritten as: $h_k[n] = g\left(\sum_{i=0}^{I} x_i[n] \cdot w_{ik}[n]\right)$, where $w_{ik}[n] = \sum_{b=1}^{B} f_b[n] \cdot w_{b,ik}$. Similarly, if time-variant output weights are introduced, the standard output equation can be rewritten as: $\sum_{k=1}^{K} h_k[n] \cdot \beta_{kl}[n] = t_l[n]$, where $\beta_{kl}[n] = \sum_{b=1}^{B} f_b[n] \cdot \beta_{b,kl}$.

To train a TV-NN, $\{w_{b,ik}\}$ can be randomly generated and then hidden-layer output matrix $\mathbf{H}$ can be computed. However, the values of a set of output weight parameters $\{\beta_{b,kl}\}$ can not be so straightforward calculated. Some transformations are needed. Let us expand the time-variant output weights $\beta_{kl}[n]$ and assume the following notation: $\mathbf{f}[n] = [f_1[n], f_2[n], \ldots, f_B[n]]^T \in \mathbb{R}^B$,

$\mathbf{h}[n] = [h_1[n], h_2[n], \ldots, h_K[n]]^T \in \mathbb{R}^K$, $\boldsymbol{\beta}_{kl} = [\beta_{1,kl}, \beta_{2,kl}, \ldots, \beta_{B,kl}]^T \in \mathbb{R}^B$, $\boldsymbol{\beta}_{(l)} = [\boldsymbol{\beta}_{1l}, \boldsymbol{\beta}_{2l}, \ldots, \boldsymbol{\beta}_{Kl}] \in \mathbb{R}^{B\times K}$, $\boldsymbol{\omega}_{(l)} = [\boldsymbol{\beta}_{1l}^T, \boldsymbol{\beta}_{2l}^T, \ldots, \boldsymbol{\beta}_{Kl}^T]^T \in \mathbb{R}^{B\cdot K\times 1}$. We can now state:

$$\begin{aligned} t_l[n] &= \sum_{k=1}^{K} h_k[n] \cdot \left(\sum_{b=1}^{B} f_b[n] \cdot \beta_{b,kl} \right) = \sum_{k=1}^{K} \mathbf{f}[n]^T \cdot \boldsymbol{\beta}_{kl} \cdot h_k[n] \\ &= \mathbf{f}[n]^T \cdot \boldsymbol{\beta}_{(l)} \cdot \mathbf{h}[n] = \left(\mathbf{h}[n]^T \otimes \mathbf{f}[n]^T \right) \cdot \boldsymbol{\omega}_{(l)} \end{aligned} \tag{1}$$

where $\otimes$ denotes the *Kronecker product* of $\mathbf{h}[n]^T$ and $\mathbf{f}[n]^T$. The last step consists in: $vec(\mathbf{ABC}) = (\mathbf{C}^T \otimes \mathbf{A})vec(\mathbf{B})$, (note that $vec(t_l[n]) = t_l[n]$.) and $\boldsymbol{\omega}_{(l)} = vec(\boldsymbol{\beta}_{(l)})$ is the vectorization of the matrix $\boldsymbol{\beta}_{(l)}$ formed by stacking the columns of $\boldsymbol{\beta}_{(l)}$ into a single column vector.

Moreover, we define: $\mathbf{G} = \mathbf{H} * \mathbf{F}$, where $\mathbf{H} = [\mathbf{h}[1], \mathbf{h}[2], \ldots, \mathbf{h}[N]]^T = \{h_k[n]\} \in \mathbb{R}^{N\times K}$, $\mathbf{F} = [\mathbf{f}[1], \mathbf{f}[2], \ldots, \mathbf{f}[N]]^T = \{f_b[n]\} \in \mathbb{R}^{N\times B}$, $*$ denotes the *Khatri-Rao product* of matrices $\mathbf{H}$ and $\mathbf{F}$, with $\mathbf{h}[n]^T$ and $\mathbf{f}[n]^T$ as their submatrices, respectively. Further assuming that: $\mathbf{T} = \{t_l[n]\} \in \mathbb{R}^{N\times L}$, $\boldsymbol{\Omega} = [\boldsymbol{\omega}_{(1)}, \boldsymbol{\omega}_{(2)}, \ldots, \boldsymbol{\omega}_{(L)}] \in \mathbb{R}^{B\cdot K\times L}$, we get: $\mathbf{G} \cdot \boldsymbol{\Omega} = \mathbf{T}$.

Since $\mathbf{F}$ is obtained by the type of the basis function predetermined by the user; $\mathbf{H}$ can be calculated once input weight parameters are randomly generated. Hence we can get $\mathbf{G}$. Similar to the ELM algorithm described in previous section, the time-variant output weight matrix $\boldsymbol{\Omega}$ can be computed by:

$$\hat{\boldsymbol{\Omega}} = \mathbf{G}^{\dagger} \cdot \mathbf{T} \tag{2}$$

where $\mathbf{G}^{\dagger}$ is the MP inverse of matrix $\mathbf{G}$, and consequently, $\hat{\boldsymbol{\Omega}}$ is a set of optimal output weight parameters minimizing the training error.

3 Proposed Incremental-Based ELM Algorithms for TV-NN

3.1 I-ELM-TV and EI-ELM-TV

It is proved in [3] and [4] that for one specific output neuron, when the k-th hidden neuron is added and $\beta_k = \frac{\tilde{\mathbf{h}}_k^T \cdot \tilde{\mathbf{e}}_{k-1}}{\tilde{\mathbf{h}}_k^T \cdot \tilde{\mathbf{h}}_k}$, $\|\tilde{\mathbf{e}}_k\| = \|\tilde{\mathbf{t}} - (\tilde{\mathbf{t}}_{k-1} + \beta_k \tilde{\mathbf{h}}_k)\|$ achieves its minimum and the sequence $\{\|\tilde{\mathbf{e}}_k\|\}$ decreases and converges. Note that $\beta_k = \frac{\tilde{\mathbf{h}}_k^T \cdot \tilde{\mathbf{e}}_{k-1}}{\tilde{\mathbf{h}}_k^T \cdot \tilde{\mathbf{h}}_k}$, is a special case of $\beta_k = \tilde{\mathbf{h}}_k^{\dagger} \tilde{\mathbf{e}}_{k-1}$ when $\tilde{\mathbf{e}}_{k-1}$ and $\tilde{\mathbf{h}}_k$ are vectors. Actually, the MP generalized inverse of $\tilde{\mathbf{h}}_k$ is just $\tilde{\mathbf{h}}_k^{\dagger} = (\tilde{\mathbf{h}}_k^T \cdot \tilde{\mathbf{h}}_k)^{-1} \tilde{\mathbf{h}}_k^T$ For our time-variant case, this can also be extended to matrix computations.

Let $\delta\boldsymbol{\Omega}_k = \begin{bmatrix} \beta_{1,k1}, \cdots, \beta_{1,kL} \\ \cdots, \cdots, \cdots \\ \beta_{B,k1}, \cdots, \beta_{B,kL} \end{bmatrix}_{B\times L}$ and $\delta\mathbf{G}_k = \begin{bmatrix} h_k[1] \cdot \mathbf{f}[1]^T \\ \cdots \\ h_k[N] \cdot \mathbf{f}[N]^T \end{bmatrix}_{N\times B}$,

(Note $\boldsymbol{\Omega} = \begin{bmatrix} \delta\boldsymbol{\Omega}_1 \\ \cdots \\ \delta\boldsymbol{\Omega}_K \end{bmatrix}$ and $\mathbf{G} = [\delta\mathbf{G}_1, \cdots, \delta\mathbf{G}_K]$.) Similarly, if $\delta\boldsymbol{\Omega}_k = \delta\mathbf{G}_k^{\dagger} \cdot \mathbf{E}_{k-1}$,

$\|\mathbf{E}_k\| = \|\mathbf{T} - (\mathbf{T}_{k-1} + \delta\mathbf{G}_k\delta\mathbf{\Omega}_k)\|$ achieve its minimum and the sequence $\{\|\mathbf{E}_k\|\}$ would decrease and converges.

It is noted in [4] that some newly added hidden nodes may make residual error reduce less than others. In the Enhanced I-ELM method, at any step, among P trial of hidden nodes, the hidden nodes with greatest residual error reduction is chosen and added. This method is also applied in this paper.

Hence, we have our time-variant version of I-ELM and EI-ELM. Assume we have a set of training data $\{(\mathbf{x}[n], \mathbf{t}[n])\}_{n=1}^{N}$, the target output matrix $\mathbf{T}$, the residual matrix $\mathbf{E}$, the maximum number of hidden nodes K_{max}, and the expected learning accuracy ϵ. We get Algorithm 1.

Algorithm 1. I-ELM-TV(in the case of $P = 1$) and EI-ELM-TV

1: Let $k = 0$ and residual error $\mathbf{E} = \mathbf{T}$,
2: **while** $k < K_{max}$ and $\|\mathbf{E}\| > \epsilon$, **do**
3: Increase by one the number of hidden nodes: $k = k + 1$;
4: **for** $p = 1 : P$ **do**
5: Assign random input weight and bias $\{w_{(p)b,ik}\}$ for new hidden node;
6: Calculate the hidden layer output submatrix for new hidden node

$$\delta\mathbf{G}_{(p)} = \begin{bmatrix} h_{(p)k}[1] \cdot \mathbf{f}[1]^T \\ \cdots \\ h_{(p)k}[N] \cdot \mathbf{f}[N]^T \end{bmatrix}_{N \times B}$$

7: Calculate the output weight $\delta\mathbf{\Omega}_{(p)}$ for the new hidden node

$$\delta\mathbf{\Omega}_{(p)} = \delta\mathbf{G}_{(p)}^{\dagger} \cdot \mathbf{E}$$

8: Calculate the residual error after adding the new hidden node k:

$$\mathbf{E}_{(p)} = \mathbf{E} - \delta\mathbf{G}_{(p)} \cdot \delta\mathbf{\Omega}_{(p)}$$

9: **end for**
10: Let $p^* = \{p | min_{1 \leqslant p \leqslant P} \|\mathbf{E}_{(p)}\|\}$.
11: Set $\mathbf{E} = \mathbf{E}_{(p^*)}$, $\{w_{b,ik} = w_{(p^*)b,ik}\}$, and $\delta\mathbf{\Omega}_k = \delta\mathbf{\Omega}_{(p^*)}$.
12: **end while**
13: The output weight matrix would be $\mathbf{\Omega} = \begin{bmatrix} \delta\mathbf{\Omega}_1 \\ \cdots \\ \delta\mathbf{\Omega}_K \end{bmatrix}_{B \cdot K \times L}$

3.2 EM-ELM-TV

Similarly, with certain transformation, Error Minimized ELM approach can also be extended in time-variant case. Replace $\mathbf{H}_0$, $\delta\mathbf{H}_k$, β with $\mathbf{G}_1$,$\delta\mathbf{G}_k$, $\mathbf{\Omega}$, respectively, we get our time-variant version of EM-ELM. For the sake of presentation clarity, we only add hidden nodes one by one in our proposed EM-ELM-TV algorithm, which can be easily generalized to the group-by-group node addition means.

Assume we have a set of training data $\{(\mathbf{x}[n], \mathbf{t}[n])\}_{n=1}^{N}$, the target matrix $\mathbf{T}$, the residual matrix $\mathbf{E}_k = \mathbf{G}_k\mathbf{G}_k^{\dagger}\mathbf{T} - \mathbf{T}$, the maximum number of hidden nodes K_{max}, and the expected learning accuracy ϵ. We get Algorithm 2.

Algorithm 2. EM-ELM-TV

1: Randomly generate one hidden node.
2: Calculate the time-variant hidden layer output matrix $\mathbf{G}_1$ by (**??**) and (**??**):

$$\mathbf{G}_1 = \begin{bmatrix} h_1[1] \cdot \mathbf{f}[1]^T \\ \cdots \\ h_1[N] \cdot \mathbf{f}[N]^T \end{bmatrix}_{N \times B}$$

3: Calculate the output error $\|\mathbf{E}_1\| = \|\mathbf{G}_1\mathbf{G}_1^{\dagger}\mathbf{T} - \mathbf{T}\|$.
4: Let $k = 1$
5: **while** $k < K_{max}$ and $\|\mathbf{E}_k\| > \epsilon$, **do**
6: Randomly add another hidden node. The corresponding hidden layer output matrix becomes $\mathbf{G}_{k+1} = [\mathbf{G}_k, \delta\mathbf{G}_k]$, where

$$\delta\mathbf{G}_k = \begin{bmatrix} h_k[1] \cdot \mathbf{f}[1]^T \\ \cdots \\ h_k[N] \cdot \mathbf{f}[N]^T \end{bmatrix}_{N \times B}$$

7: Update the output weight $\mathbf{\Omega}$

$$\begin{aligned} \mathbf{D}_k &= ((\mathbf{I} - \mathbf{G}_k\mathbf{G}_k^{\dagger})\delta\mathbf{G}_k)^{\dagger} \\ \mathbf{U}_k &= \mathbf{G}_k^{\dagger} - \mathbf{G}_k^{\dagger}\delta\mathbf{G}_k\mathbf{D}_k \\ \mathbf{\Omega}^{(k+1)} &= \mathbf{G}_{k+1}^{\dagger}\mathbf{T} = \begin{bmatrix} \mathbf{U}_k \\ \mathbf{D}_k \end{bmatrix} \mathbf{T} \end{aligned}$$

8: $k = k + 1$
9: **end while**

4 Simulation Results

In this section, we compare I-ELM-TV, EI-ELM-TV and EM-ELM-TV with ELM-TV in three identification problems. All the data depicted in figures are the average values of 10 trials. All the programs are run in MATLAB 7.8.0 environment with Windows Vista, Intel Core2 Duo CPU P8400 2.26GHz. The number P of trials of assigning random hidden nodes at each step for EI-ELM-TV, is set to 10. The chosen basis function type for all these time-variant algorithms is Prolate [6] and the number of bases have been set to 3. Varying the basis function type and number leads to different performances, but similar comparative conclusions as those drawn in following subsections can be done: therefore, for the sake of conciseness, such results have not been reported here.

4.1 Time-Variant Perceptron System Identification

In the first case, we construct a simple time-variant system: $y[n] = g(w[n] \cdot x[n])$, where $g(x)$ is a sigmoid activation function $g(x) = \frac{1}{1+e^{-x}}$, and $w[n]$ is a single time-variant coefficient, which is combination of 3 prolate function bases, $w[n] = \sum_{b=1}^{3} f_b[n] \cdot w_b$, with setting $w_b = 0.5, (b = 1, 2, 3)$. The inputs are normalized (within the range $[-1, 1]$).

In the simulation of single perceptron system, hidden neurons are gradually increase one by one from 1 to 20. Results show that EM-ELM-TV has similar performance as ELM-TV in terms of testing accuracy and outperforms over I-ELM-TV and EI-ELM-TV, but reach its minimum accuracy by only about 17 hidden nodes. Though the training time of EM-ELM-TV is more than ELM-TV when the number of hidden nodes is small, it only increase slightly when more hidden nodes are added. On the other hand, EI-ELM-TV achieves better testing accuracy than I-ELM-TV as expected, at the cost of more training time. Therefore, the incremental ELM algorithms seem not to be effective w.r.t. the common ELM. It can be justified saying that the simplicity of the addressed task do not ask for enough hidden nodes to appreciate the effectiveness of the EM based approach, as it will occur in next simulations.

4.2 Time-Variant MLP System Identification

The system to be identified here is the same with that in [6] and [7]: a time-variant IIR-buffered MLP with 11 input lines, one 5 neurons hidden layer, one neuron output layer. The input weights and output weights are combination of 3 Chebyshev basis functions; the lengths of the input and output TDLs are equal to 6 and 5 respectively. Note that the output neuron of this system is not linear, both the hidden neurons and output neuron use tangent sigmoid activation function.

A wider range of hidden nodes from 1 to 200 are tested in this scenario. The accuracy performance of EM-ELM-TV is quite the same with that of ELM-TV, and as the number of hidden nodes becomes larger, the training time of EM-ELM-TV is much less than that of ELM-TV.

4.3 Time-Variant Narendra System Identification

The next test identification system is a modified one addressed in [8], adding the coefficients $a[n]$ and $b[n]$ to form a time-variant system, as done in [6] and [7]:

$$y[n] = a[n] \cdot \frac{y[n-1] \cdot y[n-2] \cdot y[n-3] \cdot x[n-1] \cdot (y[n-3]-1) + x[n]}{1 + b[n] \cdot (y[n-3]^2 + y[n-2]^2)} \quad (3)$$

Simulation results for Narendra system are depicted in Fig 1 and Fig 2. For I-ELM-TV and EI-ELM-TV, better testing accuracies can be achieved gradually and smoothly as new hidden nodes are added. However, this is not true for ELM-TV and EM-ELM-TV. When adding new hidden nodes to EM-ELM-TV, the

training RMSE does decrease, but the testing RMSE may not. We can conclude from these that I-ELM-TV and EI-ELM-TV produce more stable results than ELM-TV and EM-ELM-TV in Narendra system, though they converge much slower. Again, same behavior as in the time-invariant case is recognized.

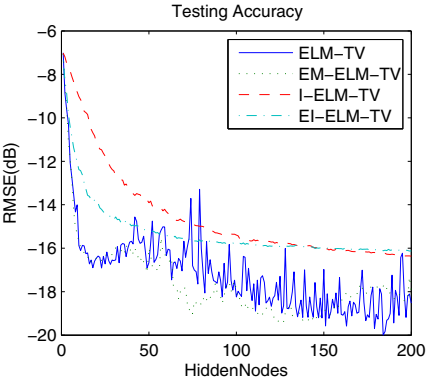

Fig. 1. Testing Accuracy of 4 algorithms for Narendra System

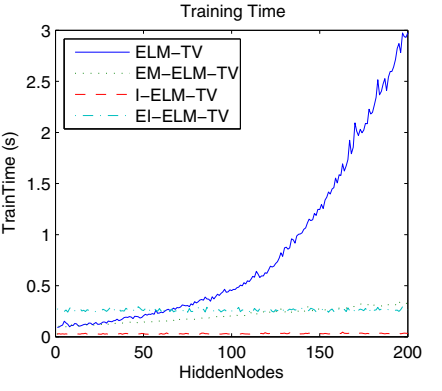

Fig. 2. Training Time of 4 algorithms for Narendra System

The performance comparison in terms of necessary hidden nodes between ELM-TV and EM-ELM-TV, has also been conducted in these time-variant systems. The target training RMSE(dB) ϵ are set as: -40 for perceptron system, -35 for MLP system and -18 for Narendra system. The optimal number of hidden nodes for ELM-TV is obtained by trial-and-error. Table 1 displays performance evaluation between ELM-TV and EM-ELM-TV, since I-ELM-TV and EM-ELM-TV are not able to reach the training goals of them within 500 nodes. Focusing on the MLP and Narendra Systems case studies for reasons explained above, results reported in Table 1 prove that EM-ELM-TV has similar generalization performance and optimal number of hidden nodes attainable with ELM-TV, but at reduced training time. Therefore, EM-ELM-TV is able to optimally select the

Table 1. Performance Comparisons for the Number(average of 10 trials) of Hidden Nodes When the Expected Accuracy is Reached

Systems [stop RMSE(dB)]	Algorithms	Training Time (s)	Testing RMSE(dB)	Hidden Nodes
Perceptron [-40]	ELM-TV	0.0775	-41.80	13.7
	EM-ELM-TV	0.1166	-41.75	13.2
MLP [-35]	ELM-TV	3.0707	-30.69	197.7
	EM-ELM-TV	0.3463	-30.07	203.8
Narendra [-18]	ELM-TV	0.2039	-16.13	48.1
	EM-ELM-TV	0.1604	-16.75	49.5

number of hidden nodes more efficiently than the trial-and-error approach typically used in common ELM-TV, as well as concluded in the time-invariant case.

5 Conclusions

In this paper, we have proposed three incremental-based Extreme Learning Machine algorithms for Time-Variant Neural Networks training. They are the extensions of the corresponding time-invariant counterparts and they have been addressed as I-ELM-TV, EI-ELM-TV and EM-ELM-TV. The main advantage of the incremental approach consists in automatically determining the number of hidden nodes, avoiding to use the trial-and-error method typically adopted in standard ELM. As it occurs in the time-invariant case, the EM method, in contrast to the others, is able to get generalization performances comparable to the original ELM, also significantly reducing the training time (when large number of hidden nodes are required). Future works are intended to apply the promising EM paradigm to the optimal selection of the number of bases functions, which is still assign by the users before TV-NN training.

References

1. Huang, G.B., Zhu, Q.Y., Siew, C.K.: Extreme learning machine: a new learning scheme of feedforward neural networks. In: Proc. IEEE International Joint Conference on Neural Networks, vol. 2, pp. 985–990 (2004)
2. Huang, G.B., Zhu, Q.Y., Siew, C.K.: Extreme learning machine: Theory and applications. Neurocomputing 70(1-3), 489–501 (2006)
3. Huang, G., Chen, L., Siew, C.: Universal approximation using incremental constructive feedforward networks with random hidden nodes. IEEE Transactions on Neural Networks 17(4), 879 (2006)
4. Huang, G., Chen, L.: Enhanced random search based incremental extreme learning machine. Neurocomputing 71(16-18), 3460–3468 (2008)
5. Feng, G., Huang, G.B., Lin, Q., Gay, R.: Error minimized extreme learning machine with growth of hidden nodes and incremental learning 20(8), 1352–1357 (2009)
6. Titti, A., Squartini, S., Piazza, F.: A new time-variant neural based approach for nonstationary and non-linear system identification. In: Proc. IEEE International Symposium on Circuits and Systems, ISCAS, pp. 23–26, 5134–5137 (2005)
7. Cingolani, C., Squartini, S., Piazza, F.: An extreme learning machine approach for training time variant neural networks. In: Proc. IEEE Asia Pacific Conference on Circuits and Systems, APCCAS, pp. 384–387 (2008)
8. Narendra, K., Parthasarathy, K.: Identification and control of dynamical systems using neural networks. IEEE Transactions on Neural Networks 1(1), 4–27 (1990)

Global Exponential Robust Stability of Hopfield Neural Networks with Reaction-Diffusion Terms

Xiaohui Xu and Jiye Zhang

Traction Power State Key Laboratory, Southwest Jiaotong University,
Chengdu 610031, China
xhxu@163.com

Abstract. Some sufficient conditions ensuring existence, uniqueness for a class of interval Hopfield neural networks with unbounded delays and reaction-diffusion terms are proposed in this paper. The obtained conditions including reaction-diffusion terms are less conservative than the existing results. The application of the conditions in practice is illustrated by an example.

Keywords: Neural networks, Stability, Reaction-diffusion, Unbounded delays, Robust.

1 Introduction

Many authors have recently dealt with the questions of the global exponential stability of Hopfield neural networks (HNN) [1], due to its potential applications in fields ranging from signal processing to optimal control and, meanwhile, the studied models have become more involved in order to take into account a wide variety of phenomena which occur in practice. Time delays, which may destroy the stability of a system giving rise to unstable or chaotic dynamics [2], have been introduced in Hopfield neural networks since they are unavoidable in implementations, see [3-7]. While they only considered that the neural states varied in time. However, strictly speaking, diffusion effect cannot be avoided in the neural networks when electrons are moving in asymmetric electromagnetic field, which could cause instability of the states [10]. The stability analysis for delayed neural networks with reaction-diffusion terms becomes increasingly significant. Wang [6] considered dynamical behavior of HNN with time delays and reaction-diffusion terms, and got the L_2-norm global exponential stability of HNN for the first time. Thereafter, numerous papers about neural networks with reaction-diffusion terms were studied see [7-12]. With regard to the study of the above system, the present research results can be classified into two categories: one category [7-10] got the existence, uniqueness and stability conditions for the system, but the obtained conditions without reaction-diffusion terms were relatively conservative; the other [11-12] proposed the stability conditions containing reaction-diffusion terms, but did not discuss the existence and uniqueness of solutions. To the best of our knowledge, although lots of papers have studied existence and uniqueness of HNN equilibrium point with unbounded delays and reaction-diffusion terms, the obtained conditions did

D.-S. Huang et al. (Eds.): ICIC 2010, LNCS 6215, pp. 17–24, 2010.

not include reaction-diffusion terms. In this paper, we will study the existence, uniqueness and global exponential stability of the equilibrium point of HNN with reaction-diffusion terms and unbounded delays.

2 Model Description

Assuming that $\Omega \in R^m$ (here R denotes real number) is a compact set with smooth boundary $\partial\Omega$, and $\operatorname{mes}\Omega = [\sum_{k=1}^{m} (x_k)^2]^{1/2} > 0$. Let $u_i(t,x)$ be the state of neural networks, $x \in \Omega$, $i = 1,2,...,n$. Denote $L^2(\Omega)$ the Lebesgue measurable function spaces, i.e. $\| u_i \|_{L^2} = (\int_\Omega | u_i |^2 dx)^{1/2} < \infty$, $i = 1,2,...,n$. For matrix $A = (a_{ij})_{n\times n}$, $|A|$ denotes the absolute-value matrix given by $|A| = (|a_{ij}|)_{n\times n}$; for vector $u = (u_1, u_2, ..., u_n) \in R^n$, $\| u \|$ denotes a vector norm defined by $\| u \| = (\sum_{i=1}^{n} \| u_i \|_{L^2}^2)^{1/2}$.

Hopfield neural networks with unbounded delays and reaction-diffusion terms can be described as follows:

$$\frac{\partial u_i}{\partial t} = \sum_{k=1}^{m} \frac{\partial}{\partial x_k}(D_{ik} \frac{\partial u_i(t,x)}{\partial x_k}) - d_i(u_i(t,x)) + \sum_{j=1}^{n} [a_{ij} g_j(u_j(t,x)) + c_{ij} \int_{-\infty}^{t} q_{ij}(t-s) g_j(u_j(s,x)) ds] + J_i, \quad t \geq 0,\ i = 1,2,...,n,\ x \in \Omega, \tag{1a}$$

$$u_i(t,x)\big|_{\partial\Omega} = 0,\ i = 1,2,...,n,\ x \in \Omega. \tag{1b}$$

Where $n \geq 2$ denotes the number of neurons, $u_i(t,x)$ represents the state variable of i-th neuron, $i = 1,2,...,n$. $D_{ik}(t,x) \geq 0$ denotes diffusion function and let $\theta_i = \min_{1\leq k\leq m} \{\sup_{t\geq 0, x\in\Omega} D_{ik}\}$, $i = 1,2,...,n$. $d_i(u_i(t,x))$ denotes behaved function, $A = (a_{ij})_{n\times n}$, $C = (c_{ij})_{n\times n}$, represent the weight matrices of the neurons, $g(u) = (g_1(u_1), g_2(u_2), ..., g_n(u_n))^T$ corresponds to the activation function of neurons. $q_{ij} : [0,\infty) \to [0,\infty)$ is piecewise continuous on $[0,\infty)$, and satisfy

$$\int_0^\infty e^{\beta s} q_{ij}(s) ds = \kappa_{ij}(\beta),\ i, j = 1,2,...,n, \tag{2}$$

where $\kappa_{ij}(\beta)$ is continuous function in $[0, \delta]$, $\delta > 0$, and $\kappa_{ij}(0) = 1$. J_i denotes the external input on the i-th neuron, let $J = (J_1, J_2, ..., J_n)^T$. The initial conditions of (1) are of the forms $u_i(s,x) = \phi_i(s,x)$, $s \leq 0$, where ϕ_i is bounded and continuous on $(-\infty, 0]$, $i = 1,2,...,n$.

Define interval matrix: $A_I = \{A = (a_{ij})_{n\times n} : \underline{A} \leq A \leq \overline{A}$, *i.e.* $\underline{a}_{ij} \leq a_{ij} \leq \overline{a}_{ij},\ i, j = 1,2,...,n\}$,

$C_I = \{C = (c_{ij})_{n\times n} : \underline{C} \leq C \leq \overline{C}$ *i.e.* $\underline{c}_{ij} \leq c_{ij} \leq \overline{c}_{ij},\ i, j = 1,2,...,n\}$,

let $A^0 = (a_{ij}^0)_{n\times n}$, $C^0 = (c_{ij}^0)_{n\times n}$, where $a_{ij}^0 = \max\{|\underline{a}_{ij}|, |\overline{a}_{ij}|\}$, $c_{ij}^0 = \max\{|\underline{c}_{ij}|, |\overline{c}_{ij}|\}$, $i, j = 1,2,...,n$. Let $u^* = (u_1^*, u_2^*, \hbar, u_n^*)^T$ be the equilibrium point of (1).

Definition 1. The equilibrium point of (1) is said to be exponentially robustly stable if there exist constant $M>0$ and $\lambda>0$ such that for all $J\in R^n$, $A\in A_I$ and $C\in C_I$, $\|u(t,x)-u^*\|\le M\|\phi(s,x)-u^*\|e^{-\lambda t}$ holds, where $t\ge 0$, $x\in\Omega$, $\|\phi(s,x)-u^*\|=\sup_{s\in(-\infty,0]}\sum_{i=1}^{n}\|\phi_i(s,x)-u_i^*\|_{L_2}$.

Definition 2. [3] A real matrix $A=(a_{ij})_{n\times n}$ is said to be a M-matrix if $a_{ij}\le 0$, $i,j=1,2,...,n$, $i\ne j$, and all successive principal minors of A are positive.

Lemma 1. Let $\Omega\in R^m$ is a compact set, which has smooth boundary $\partial\Omega$. Let $x\in\Omega$, $|x_k|\le\omega_k$ ($k=1,2,...,m$), and $u_i(x)$ be a real-valued function belonging to $C^1(\Omega)$ and $u_i(x)\big|_{\partial\Omega}=0$, then $m\int_\Omega u_i^2dx\le\pi^2\int_\Omega\nabla u_i^T\nabla u_i dx$, where $\pi=\max_{1\le k\le m}\omega_k$, $i=1,2,...,n$.

The detail proof of lemma 1 can be found in paper [11].

Assumption A1. For each function d_i, $i=1,2,...,n$, there exists constant $\gamma_i>0$ such that for all $u_i\ne v_i$, $0<\gamma_i(u_i-v_i)^2\le d_i(u_i)-d_i(v_i)(u_i-v_i)$.

Assumption A2. Each function $g_j: R\to R$, $j=1,2,...,n$, is monotone increasing, i.e. there exists constant $L_j>0$ such that for all $u_j\ne v_j$, $0\le[g_j(u_j)-g_j(v_j)](u_j-v_j)\le L_j(u_j-v_j)^2$.

Define $H(u)=[H_1(u),H_2(u),\hbar,H_n(u)]$ is a nonlinear map associated with (1), here

$$H_i(u)=\sum_{k=1}^{m}\frac{\partial}{\partial x_k}[D_{ik}\frac{\partial u_i}{\partial x_k}]-d_i(u_i)+\sum_{j=1}^{n}(a_{ij}+c_{ij})g_j(u_j)+J_i,\ i=1,2,...,n. \tag{3}$$

Lemma 2. [3]. If $H(u)\in C^0$ satisfies: (i) $H(u)$ is injective on R^n; (ii) $\|H(u)\|\to\infty$ as $\|u\|\to\infty$, then $H(u)$ is the homeomorphism of R^n.

In the following section, we will give a theorem ensuring (1) has a unique equilibrium point.

Theorem 1. Suppose that **Assumption A1-A2** are satisfied, then (1) has a unique equilibrium point u^* if for all $A\in A_I$, $C\in C_I$, $J\in R^n$, matrix P is a M-matrix, here

$$p_{ii}=\gamma_i+m\theta_i/\pi^2-0.5\sum_{j=1}^{n}(a_{ij}^0+c_{ij}^0)L_j;\ p_{ij}=-0.5\sum_{j=1}^{n}(a_{ij}^0+c_{ij}^0)L_j,\ i=1,2,...,n.$$

Proof. For all $A\in A_I$, $C\in C_I$, due to P is a M-matrix, from the property of M-matrix [3], we know that there exists $\xi_i>0$ ($i=1,2,...,n$) such that

$$\xi_i[m\theta_i/\pi^2+\gamma_i-0.5\sum_{j=1}^{n}(a_{ij}^0+c_{ij}^0)L_j]-0.5\sum_{j=1}^{n}\xi_j(a_{ji}^0+c_{ji}^0)L_j>0,$$

then for a sufficient small $\delta>0$, we have

$$\xi_i[m\theta_i/\pi^2+\gamma_i-0.5\sum_{j=1}^{n}(a_{ij}^0+c_{ij}^0)L_j]-0.5\sum_{j=1}^{n}\xi_j(a_{ji}^0+c_{ji}^0)L_j\ge\delta>0. \tag{4}$$

Consider the map (3) endowed with the norm $\|\cdot\|=(\sum\|\cdot\|_{L^2}^2)^{1/2}$. It is well known that if Eq. (3) is homeomorphism on R^n, then (1) has a unique equilibrium point.

First of all, we demonstrate the injective part.

When $H(u)=H(v)$, we get the following equation for $i=1,2,...,n$:

$$d_i(u_i)-d_i(v_i)=\sum_{k=1}^{m}\frac{\partial}{\partial x_k}[D_{ik}\frac{\partial(u_i-v_i)}{\partial x_k}]+\sum_{j=1}^{n}(a_{ij}+c_{ij})[g_j(u_j)-g_j(v_j)]. \quad (5)$$

Multiply both sides of (5) by u_i-v_i $(i=1,2,...,n)$ and considering **Assumption A1**, **Assumption A2**, we get

$$\gamma_i(u_i-v_i)^2\le(u_i-v_i)\sum_{k=1}^{m}\frac{\partial}{\partial x_k}[D_{ik}\frac{\partial(u_i-v_i)}{\partial x_k}]+|u_i-v_i|\sum_{j=1}^{n}(|a_{ij}|+|c_{ij}|)L_j|u_j-v_j|. \quad (6)$$

Integrate both sides of (6) on the domain Ω with respect to *x*, and from **Lemma 1**, we get

$$\begin{aligned}&\int_\Omega\gamma_i(u_i-v_i)^2dx\\ &\le\int_\Omega(u_i-v_i)\sum_{k=1}^{m}\frac{\partial}{\partial x_k}[D_{ik}\frac{\partial(u_i-v_i)}{\partial x_k}]dx+\int_\Omega|u_i-v_i|\sum_{j=1}^{n}(|a_{ij}|+|c_{ij}|)L_j|u_j-v_j|\\ &\le-(\theta m/\pi^2)\int_\Omega|u_i-v_i|^2dx+\int_\Omega\sum_{j=1}^{n}(|a_{ij}|+|c_{ij}|)L_j|u_j-v_j||u_j-v_j|dx,\ i=1,2,...,n. \quad (7)\end{aligned}$$

Estimation (7) through the use of the Holder inequality and Young inequality leads to

$$\begin{aligned}\int_\Omega\gamma_i|u_i-v_i|^2dx\le&-[\theta_i m/\pi^2-0.5\sum_{j=1}^{n}(|a_{ij}|+|c_{ij}|)L_j]\int_\Omega|u_i-v_i|^2dx+\\ &0.5\sum_{j=1}^{n}(|a_{ij}|+|c_{ij}|)L_j\int_\Omega|u_j-v_j|^2dx,\ \ i=1,2,...,n.\end{aligned}$$

Moreover

$$[\gamma_i+\theta_i m/\pi^2-0.5\sum_{j=1}^{n}(|a_{ij}|+|c_{ij}|)L_j]\|u_i-v_i\|_{L^2}^2-0.5\sum_{j=1}^{n}(|a_{ij}|+|c_{ij}|)L_j\|u_j-v_j\|_{L^2}^2\le0,$$

namely $\tilde{P}(\|u_1-v_1\|_{L^2}^2,\|u_2-v_2\|_{L^2}^2,...,\|u_n-v_n\|_{L^2}^2)^T\le0$.

Since P is a M-matrix, from the property of M-matrix [3], it follows that $\|u_i-v_i\|_{L^2}^2=0$, namely $u_i=v_i$, $i=1,2,...,n$. So the map $H(u)\in C^0$ is injective on R^n.

Next, we will demonstrate $\|H(u)\|\to\infty$ as $\|u\|\to\infty$. Let $\overline{H_i(u)}=H_i(u)-H_i(0)$, where $H_i(0)=-d_i(0)+\sum_{j=1}^{n}(a_{ij}+c_{ij})g_j(0)+J_i$, $i=1,2,...,n$, *i.e.*

$$\overline{H_i(u)}=\sum_{k=1}^{m}\frac{\partial}{\partial x_k}(D_{ik}\frac{\partial u_i}{\partial x_k})-[d_i(u_i)-d_i(0)]+\sum_{j=1}^{n}(a_{ij}+c_{ij})[g_j(u_j)-g_j(0)]. \quad (8)$$

It is suffice to show $\|\overline{H(u)}\|\to\infty$ as $\|u\|\to\infty$ in order to demonstrate the property $\|H(u)\|\to\infty$ as $\|u\|\to\infty$. Multiply both sides of (8) by u_i and integrate it on the domain Ω with respect to *x*, we get

$$\begin{aligned}\int_\Omega\overline{H_i(u)}\,u_i dx=\int_\Omega\{&u_i\sum_{k=1}^{m}\frac{\partial}{\partial x_k}(D_{ik}\frac{\partial u_i}{\partial x_k})-u_i[d_i(u_i)-d_i(0)]+\\ &u_i\sum_{j=1}^{n}(a_{ij}+c_{ij})[g_j(u_j)-g_j(0)]\}dx. \quad (9)\end{aligned}$$

Considering **Assumption 1** and in virtue of the Holder inequality and Young inequality, we have

$$\int_\Omega \overline{H_i(u)}\, u_i dx \le -[m\theta_i/\pi^2 + \gamma_i - 0.5\sum_{j=1}^n (|a_{ij}|+|c_{ij}|)L_j]\int_\Omega |u_i|^2\, dx$$
$$+0.5\sum_{j=1}^n (|a_{ij}|+|c_{ij}|)L_j \int_\Omega |u_j|^2 dx\ ,\ i=1,2,...,n\ . \qquad (10)$$

Multiply both sides of (10) by ξ_i and consider (4), we get

$$\sum_{i=1}^n \xi_i \int_\Omega \overline{H_i(u)}\, u_i dx \le \sum_{i=1}^n \xi_i \{-[m\theta_i/\pi^2 + \gamma_i - 0.5\sum_{j=1}^n (|a_{ij}|+|c_{ij}|)L_j]\int_\Omega |u_i|^2\, dx$$
$$+0.5\sum_{j=1}^n (|a_{ij}|+|c_{ij}|)L_j \int_\Omega |u_j|^2 dx\} \le -\delta\sum_{i=1}^n \|u_i\|_{L^2}^2\ ,\ i=1,2,...,n.$$

Furthermore

$$\delta\sum_{i=1}^n \|u_i\|_{L^2}^2 \le -\sum_{i=1}^n \xi_i \int_\Omega \overline{H}_i(u) u_i dx \le \max_{1\le i\le n}\{\xi_i\}\sum_{i=1}^n \|\overline{H_i(u)}\|_{L^2}\|u_i\|_{L^2}\ . \qquad (11)$$

Employing Holder inequality for (11), we obtain

$$\delta\|u\|^2 \le \max_{1\le i\le n}\{\xi_i\}\|\overline{H(u)}\|.\|u\|\ ,\ \text{i.e.}\ \delta\|u\| \le \max_{1\le i\le n}\{\xi_i\}\|\overline{H(u)}\|\ .$$

Apparently, $\|\overline{H(u)}\|\to\infty$ as $\|u\|\to\infty$, which directly implies that $\|H(u)\|\to\infty$ as $\|u\|\to\infty$. It can be concluded that $H(u)$ is a homeomorphism on R^n, namely, system (1) has unique equilibrium point. □

3 Main Results

In this section, we will establish a family of conditions ensuring global exponential robust stability of (1).

For convenience, we introduce coordinate translation for (1), let $z_i = u_i - u_i^*$, $i=1,2,...,n$, the system (1) can be rewritten as follows:

$$\frac{\partial z_i}{\partial t} = \sum_{k=1}^m \frac{\partial}{\partial x_k}[D_{ik}(t,x)\frac{\partial z_i}{\partial x_k}] - h_i(z_i(t,x)) + \sum_{j=1}^n [a_{ij}f_j(z_j(t,x)) +$$
$$c_{ij}\int_{-\infty}^t q_{ij}(t-s)f_j(z_j(s,x))ds]\ ,\ t\ge 0\ ,\ i=1,2,...,n\ ,\ x\in\Omega\ , \qquad (12a)$$
$$z_i(t,x)\big|_{\partial\Omega} = 0\ ,\ i=1,2,...,n\ , \qquad (12b)$$

where $h_i(z_i(t,x)) = d_i(z_i(t,x)+u_i^*) - d_i(u_i^*)$, $f_j(z_j(t,x)) = g_j(z_j(t,x)+u_j^*) - g_j(u_j^*)$.

The initial condition of (12) is $\varphi_i(s,x) = \phi_i(s,x) - u_i^*$, $\tau\le s\le 0$, $i=1,2,...,n$. Next, we will propose some sufficient conditions for (12).

Theorem 2. Suppose that **Assumption A1** and **Assumption A2** are satisfied, then the zero solution of (12) is globally exponentially robustly stable if for all $A\in A_I$, $C\in C_I$, matrix P is a M-matrix, where $p_{ii} = \gamma_i + \theta_i m/\pi^2 - 0.5\sum_{j=1}^n (a_{ij}^0 + c_{ij}^0)L_j$; $p_{ij} = -0.5\sum_{j=1}^n (a_{ij}^0 + c_{ij}^0)L_j$, $i=1,2,...,n$.

Proof. Firstly, from (4), it can be concluded that

$$-\xi_i[\gamma_i+\theta_i m/\pi^2-0.5\sum_{j=1}^{n}(|a_{ij}|+|c_{ij}|)L_j]+0.5\sum_{j=1}^{n}\xi_j[|a_{ij}|+|c_{ij}|]L_j<0,\ i=1,2,...,n.$$

Constructing the functions

$$F_i(\mu)=-\xi_i[-\mu+\gamma_i+\theta_i m/\pi^2-0.5\sum_{j=1}^{n}L_j(|a_{ij}|+|c_{ij}|]+0.5\sum_{j=1}^{n}[|a_{ij}|+|c_{ij}|\kappa_{ij}(\mu)]L_j\xi_j.$$

Obviously $F_i(0)<0$. Since $F_i(\mu)$, $i=1,2,...,n$, are continuous functions, so there exists a constant $\lambda>0$, such that $F_i(\lambda)<0$, i.e.

$$F_i(\lambda)=-\xi_i[-\lambda+\gamma_i+\theta_i m/\pi^2-0.5\sum_{j=1}^{n}L_j(|a_{ij}|+|c_{ij}|)]$$
$$+0.5\sum_{j=1}^{n}[|a_{ij}|+|c_{ij}|\kappa_{ij}(\lambda)]L_j\xi_j<0,\ i=1,2,...,n. \tag{13}$$

Let $V_i(t)=e^{\lambda t}\|z_i(t,x)\|_{L^2}^2$, $i=1,2,...,n$, calculating the upper right derivation D^+V_i of V_i along (12), we get

$$D^+V_i(t)=\lambda e^{\lambda t}\|z_i(t,x)\|_{L^2}^2+e^{\lambda t}\int_\Omega z_i(t,x)\{\sum_{k=1}^{m}\frac{\partial}{\partial x_k}[D_{ik}(x)\frac{\partial z_i(t,x)}{\partial x_k}]-h_i(z_i(t,x))$$
$$+\sum_{j=1}^{n}[a_{ij}f_j(z_j(t,x))+c_{ij}\int_{-\infty}^{t}q_{ij}(t-s)f_j(z_j(s,x))]\}dx,\ i=1,2,...,n. \tag{14}$$

By **Lemma 1**, we have

$$\int_\Omega z_i(t,x)\sum_{k=1}^{m}\frac{\partial}{\partial x_k}[D_{ik}\frac{\partial z_i(t,x)}{\partial x_k}]dx$$
$$\le-\theta_i\int_\Omega\nabla z_i^T(t,x)\nabla z_i(t,x)dx\le-(\theta_i m/\pi^2)\int_\Omega z_i^2(t,x)dx, \tag{15}$$

substituting (15) into (14), and from **AssumptionsA1-A2**, we have

$$D^+V_i(t)\le\lambda e^{\lambda t}\|z_i(t,x)\|_{L^2}^2-(\theta_i m/\pi^2)e^{\lambda t}\int_\Omega z_i^2(t,x)dx+e^{\lambda t}\int_\Omega\{-\gamma_i z_i^2(t,x)+$$
$$\sum_{j=1}^{n}L_j[|z_i(t,x)|.|a_{ij}|.|z_j(t,x)|+|z_i(t,x)|.|c_{ij}|.\int_{-\infty}^{t}q_{ij}(t-s)|z_j(t-\tau_{ij}(t),x)|]\}dx. \tag{16}$$

By using Holder inequality and Young inequality for (16), we get

$$D^+V_i(t)\le\lambda e^{\lambda t}\|z_i(t,x)\|_{L^2}^2-\theta_i\frac{m}{\pi^2}e^{\lambda t}\int_\Omega z_i^2(t,x)dx+e^{\lambda t}\int_\Omega\{-\gamma_i z_i^2(t,x)$$
$$+0.5\sum_{j=1}^{n}L_j|a_{ij}|[|z_i(t,x)|^2+|z_j(t,x)|^2]$$
$$+0.5\sum_{j=1}^{n}L_j|c_{ij}|.\int_{-\infty}^{t}q_{ij}(t-s)[|z_i(t,x)|^2+|z_j(s,x)|^2]ds\}dx,\ i=1,2,...,n.$$

From (2), we know that $\int_0^\infty q_{ij}(s)\,ds=\kappa_{ij}(0)=1$, so

$$D^+V_i(t)\le-[-\lambda+\theta_i m/\pi^2+\gamma_i-0.5\sum_{j=1}^{n}L_j(|a_{ij}|+|c_{ij}|)]v_i(t)$$
$$+0.5\sum_{j=1}^{n}L_j[|a_{ij}|v_j(t)+|c_{ij}|.\int_{-\infty}^{t}q_{ij}(t-s)e^{\lambda(t-s)}v_j(s)ds],\ i=1,2,...,n. \tag{17}$$

Defining the curve, $\zeta = \{y(\chi) : y_i = \xi_i \chi, \chi > 0\}$, and the sets $\Lambda(y) = \{z : 0 \le z \le y, y \in \zeta\}$. Let $\xi_{\min} = \min_{1 \le i \le n}\{\xi_i\}$, $\xi_{\max} = \max_{1 \le i \le n}\{\xi_i\}$. Taking $\chi_0 = \delta \| \varphi \|^2 / \xi_{\min}$, here $\delta > 1$ is a constant. Then $\{V : V = \mathrm{e}^{\lambda s} \| \varphi \|^2, -\tau \le s \le 0\} \subset \Lambda(y_0(\chi_0))$, i.e. $V_i(s) < \xi_i \chi_0$, $-\infty \le s \le 0$, $i = 1,2,...,n$.

We claim that $V_i(t) < \xi_i \chi_0$, $t \ge 0$, $i = 1,2,...,n$. If it is not true, then there exists some i and $t' > 0$, such that $V_i(t') = \xi_i \chi_0$, $D^+ V_i(t') \ge 0$ and $V_j(t) \le \xi_j \chi_0$, $-\infty < t \le t'$, $j = 1,2,...,n$. However, from (13) and (17), we get

$$D^+ V_i(t_1) \le -[-\lambda + \theta_i m / \pi^2 + \gamma_i - 0.5 \sum_{j=1}^{n} L_j (|a_{ij}| + |c_{ij}|)] \xi_i \chi_0 +$$

$$0.5 \sum_{j=1}^{n} L_j [|a_{ij}| + |c_{ij}| \kappa_{ij}(\lambda)] \xi_j \chi_0 < 0 .$$

This is a contradiction. So $V_i(t) < \xi_i \chi_0$, $t \ge 0$, $i = 1,2,...,n$, i.e. $\| z_i(t,x) \|_{L^2}^2 < e^{-\lambda t} \xi_i \chi_0$, namely, $\| z(t,x) \|_{L^2} < e^{-0.5\lambda t} (\xi_i \chi_0)^{0.5} \le M \| \varphi \| e^{-0.5\lambda t}$, here $M = (\xi_{\max} \delta / \xi_{\min})^{0.5}$.

From **Definition 1**, the zero solution of (12) is globally exponentially robustly stable, namely, the equilibrium point of (1) is globally exponentially robustly stable. The proof is completed. □

4 Example

Considering the system as follows:

$$\frac{\partial u_i}{\partial t} = \sum_{k=1}^{2} \frac{\partial}{\partial x_k} (D_{ik} \frac{\partial u_i(t,x)}{\partial x_k}) - d_i(u_i(t,x)) + \sum_{j=1}^{2} [a_{ij} g_j(u_j(t,x)) +$$

$$c_{ij} \int_{-\infty}^{t} q_{ij}(t-s) g_j(u_j(s,x)) ds] + J_i , \ t \ge 0 , \ i = 1,2,...,n , \ x \in \Omega , \qquad (18)$$

where $J_i = 0$, $q_{ij}(s) = e^{-s}$, $i, j = 1,2$. Suppose that $u_i(t,x)|_{\partial\Omega} = 0$, $i = 1,2,...,n$, $x \in \Omega$. Let $A_I = \begin{bmatrix} [-1,1] & [-2,-1] \\ [-2,1] & [-0.5,0.5] \end{bmatrix}$, $C_I = \begin{bmatrix} [1,2] & [-0.5,1] \\ [-1,0] & [-1.5,1] \end{bmatrix}$, so $A^0 = \begin{bmatrix} 1 & 2 \\ 2 & 0.5 \end{bmatrix}$, $C^0 = \begin{bmatrix} 2 & 1 \\ 1 & 1.5 \end{bmatrix}$. Let $d_1(u_1) = 6u_1$, $d_2(u_2) = 5u_2$, $g_1(u_1) = \tanh u_1$, $g_2(u_2) = \tanh u_2$. Apparently, $\gamma_1 = 6$, $\gamma_2 = 5$, $L_1 = L_2 = 1$. Taking $D(x) = \begin{bmatrix} \sin x_2 & 2 + \cos^2 x_1 \\ |3 - x_1| & 1 + 0.5 \cos x_2 \end{bmatrix}$, $|x_k| \le 3$ $(1 \le k \le 2)$. By simple calculation, we get $\theta_1 = 1$, $\theta_2 = 1.5$, $\pi = 3$, $m = 2$.

Based on that assumptions and the definition of matrix P in **Theorem 2**, it can be concluded that $P = \begin{bmatrix} 3.2 & -3 \\ -2.5 & 2.8 \end{bmatrix}$. Clearly, from **Definition 2**, we know that P is a M-matrix, so the equilibrium point of system (18) is globally exponentially robustly stable under the matrices interval.

5 Conclusion

In this paper, applying vector Lyapunov method and M-matrix theory, the analysis of existence, uniqueness and global exponential robust stability of the equilibrium point of Hopfield neural networks with unbounded delays and reaction-diffusion terms have been researched. The obtained sufficient conditions including reaction-diffusion terms are less conservative than the previous results. An example is given at last to illustrate the practicability of our results.

Acknowledgments. This work is supported by Natural Science Foundation of China (No. 10772152, 60974132), Doctoral Fund of Ministry of Education of China (No. 200806130003).

References

1. Hopfield, J.J.: Neural Networks and Physical Systems with Emergent Collective Abilities. Proceedings of the National Academy of Sciences, USA, 2554–2558 (1982)
2. Wei, J., Velarde, M.: Oscillatory Phenomena and Stability of Periodic Solutions in a Simple Neural Network with Delay. Nonlinear Phenomena in Complex Systems 5, 407–417 (2002)
3. Zhang, J.Y., Suda, Y., Iwasa, T.: Absolutely Exponential Stability of a Class of Neural Networks with Unbounded Delay. J. Neural Networks 17, 391–397 (2004)
4. Tan, X.H., Zhang, J.Y., Yang, Y.R.: Global Exponential Stability of Hopfield Neural Networks. J. Southwest Jiaotong University 40, 338–342 (2005)
5. Zhang, J.Y.: Absolutely Stability of a Class of Neural Networks with Unbounded Delay. J. International Journal of Circuit Theory and Applications 32, 11–21 (2004)
6. Wang, L.S., Xu, D.Y.: Global Exponential Stability of Hopfield Neural Networks with Variable Time Delays and Reaction-Diffusion Terms. J. Science China (Series E) 33, 488–495 (2003)
7. Allegretto, W., Papini, D.: Stability for Delayed Reaction–Diffusion Neural Networks. J. Physics Letters A 360, 669–680 (2003)
8. Li, K.L., Song, Q.K.: Exponential Stability of Impulsive Cohen-Grossberg Neural Networks with Time-Varying Delays and Reaction-Diffusion Terms. J. Neurocomputing 72, 231–240 (2008)
9. Wang, L., Gao, Y.: Global Exponential Robust Stability of Reaction-Diffusion Interval Neural Networks with Time-Varying Delays. J. Physics Letters A 350, 342–348 (2006)
10. Liang, J., Cao, J.: Global Exponential Stability of Reaction-Diffusion Recurrent Neural Networks with Time-Varying Delays. J. Physics Letters A 314, 434–442 (2003)
11. Lu, J.: Global Exponential Stability and Periodicity of Reaction-Diffusion Delayed Recurrent Neural Networks with Dirichlet Boundary Conditions. J. Chaos, Solitons and Fractals 35, 116–125 (2008)
12. Wang, J., Lu, J.: Global Exponential Stability of Fuzzy Cellular Neural Networks with Delays and Reaction-Diffusion Terms. J. Chaos, Solitons and Fractals 38, 878–885 (2008)

Direct Inverse Model Control Based on a New Improved CMAC Neural Network*

Yingqi Ge[1,2], Shanshan Ma[2], and Xiaoping Luo[3,**]

[1] China Jiliang University, Hangzhou, China, 310018
kangaroo1987@163.com
[2] Zhejiang University City College Key Laboratory of Intelligent Systems, Hangzhou, China, 310015
470146367@qq.com
[3] Zhejiang University City College Key Laboratory of Intelligent Systems, Hangzhou, China, 310015
luoxp@zucc.edu.cn

Abstract. In order to solve the difficulty in complicated system control, a new direct inverse model control strategy is proposed based on a new improved CMAC (Cerebellar Model Articulation Controller) neural network to control a kind of nonlinear system with strong hysteresis i.e. continuous-stirred tank reactor (CSTR). The idea of credit is introduced to help design a new Improved Credit Assigned CMAC (ICA-CMAC) with fast learning speed, which is helpful in real time control of CSTR. Simulation results show that the ICA-CMAC based method performs faster than conventional CMAC, and is strong in self-learning and helpful for improving the nonlinear control performance.

Keywords: direct inverse model control, neural network, ICA-CMAC, CSTR.

1 Introduction

The continuous-stirred tank reactor (CSTR) is a chemical reactor system with highly sensitive and nonlinear behavior. It is widely used in the polymerization industry. The hysteresis of CSTR has made it difficult to be mathematical modeled precisely, and the lack of well-developed nonlinear control techniques has caused difficulties in achieving good control performance of polymerization reactors[1]. However, the commonly used PID control can not meet the requirements of high precision and fast response[2]. In recent years, direct inverse model control, which uses a controller whose transfer characteristic is inverse to the plant to be controlled, has been a novel technology to the design of control systems with complex, unknown and uncertain dynamics. It has been demonstrated that the inverse model control has great potential in

* This work is supported by Zhejiang Nature Science Foundation under Grant Y1080776 and National Science Foundation, China under Grant 60702023.
** Corresponding author.

D.-S. Huang et al. (Eds.): ICIC 2010, LNCS 6215, pp. 25–32, 2010.

controlling nonlinear systems with flexible dynamics[3]. Consequently, the direct inverse model control is selected as the control system of CSTR in this paper.

Neural network is one of the most applied methods in identification and control of the nonlinear systems. Along with the development of artificial neural networks, they are applied for inverse control of nonlinear systems in many works[4-7]. Since Albus proposed the cerebellar model articulation controller (CMAC) in 1975, it has earned widespread interest because of its rapid learning convergence. In CMAC, complicated nonlinear functions can be represented by referring to a lookup table. However, it still needs several cycles to converge when the conventional CMAC is applied[8-9]. Therefore, the conventional CMAC needs to improve its learning accuracy to meet the requirements of real-time controls.

Based on this thought, an improved credit assigned CMAC (ICA-CMAC) is designed in this paper to accelerate the learning process of conventional CMAC. During the simulation of step signal in section 5, we find that ICA-CMAC performs five times faster than conventional CMAC and has a higher control precision in the initial stage of learning.

2 The CSTR System

The continuous-stirred tank reactor (CSTR) is a reactor widely used in industrial polymerization. In the experimental setup of CSTR control system of this paper, reactants flow through the reactor in a certain rate controlled by the feed pump, heat released from reaction is took away by the loop coolant in reactor, and the materials have reacted or partial reacted flow out from the reaction kettle continuously.

By using differential equations to describe the system, mathematical model is established as follows:

$$\frac{dx_1}{dt} = -x_1 u_F + D_a (1 - x_1) \exp\left(\frac{x_2}{1 + \frac{x_2}{\gamma}} \right) \tag{1}$$

$$\frac{dx_2}{dt} = -x_2 (u_F + \beta) + H D_a (1 - x_1) \exp\left(\frac{x_2}{1 + \frac{x_2}{\gamma}} \right) + u_c \beta \tag{2}$$

Where x_1 is the reaction conversion rate, x_2 is the reaction temperature, u_c denotes output of the controller. D_a is 3.0, β is 1.5, γ is 22.9, H is 2.55, u_F is 1.0, T is 0.005625.

3 Improved Credit Assigned CMAC

The basic ideas of CMAC are giving an input in the input space, finding the addresses of this input in memory locations, calculating the output by summing up the contents of the memory locations corresponding to this input, comparing this response value with desired value, and modifying the contents of the enabled memory locations according to learning algorithm. The training scheme of conventional CMAC is as follows:

$$W_j(t+1) = W_j(t) + \alpha \frac{(f_d - F(s))}{C} \tag{3}$$

Where f_d denotes the desired value, $F(s)$ is the actual output of CMAC, α is the learning rate, C is the generalization parameter. In conventional CMAC, errors are equally distributed into all addressed memory locations. In such an updating algorithm, previous learned information may be corrupted due to large error caused by unlearned information. As a result, when the conventional CMAC is applied, though it has rapid learning convergence, it still needs several cycles to converge. Therefore, the conventional CMAC is still unable to meet the needs of real-time applications.

To improve the learning speed of conventional CMAC, [10] proposed the concept of credibility (confidence) of the studied knowledge. In its CA-CMAC learning scheme, learned times of the addressed (enabled) memory locations are used as the credibility of the learned values and the correcting amounts of errors are distributed into the addressed memory locations according to the credibility of learned values. ZHU Da-qi[11] presented the concept of balanced learning which tries to find the best balance between learning of new knowledge and forgetting of old knowledge based on [10]. With the ideas of credibility and balanced learning, the learning speed gets improved, what makes the online learning possible.

Enlightened by these ideas, we ameliorate the conventional CMAC training algorithm to improve the learning speed. The improved CMAC training algorithm is as follows:

$$W_j(t+1) = W_j(t) + \alpha \left(\frac{\left(1 - \frac{f_t(j)}{\sum_{m=1}^{t} \sum_{l=1}^{C} f_m(l)} \right)^k}{\sum_{i=1}^{C} \left(1 - \frac{f_t(i)}{\sum_{m=1}^{t} \sum_{l=1}^{C} f_m(l)} \right)^k} \right) (f_d - F(s)) \tag{4}$$

Where k is the balanced learning constant defined by ZHU Da-qi, $f_t(j)$ is the learned time of the j th memory location in the t th updating of weight values. $f_t(j)$ is not cleared until the last cycle's training of the network is finished. Consequently, this algorithm can prevent the corruption produced by adjacent unlearned input not

only in the same cycle's training of the network but also in the next one. The basic idea of this algorithm is the same as that of [10]: in the process of updating weights, the more the memory location learned, the more knowledge it stored, then the higher credibility it has, then the less error correction it gets. In what follows, it can be observed that the performance of ICA-CMAC is significantly superior to that of conventional CMAC.

4 ICA-CMAC Network Inverse Control

Inverse model control can structure and memorize the model of target system, and then the corresponding input value can be gained on the basis of the desired value of the target system. According to the analysis in section 2, the CSTR system can be described as $\dot{X} = F(X,U)$, where the state $X = [x_1, x_2]^T$ and the controller output $U = [u_c]$. $F(\ )$ is a nonlinear function. The aim of inverse model learning control is to train the ICA-CMAC to learn the inverse mechanism of the system so as to find the relationship between U and (X, $\dot{X}$), i.e.

$$U = F^{-1}(X, \dot{X}) \tag{5}$$

Based on this idea, the ICA-CMAC learning control principle can be depicted as Figure 1.

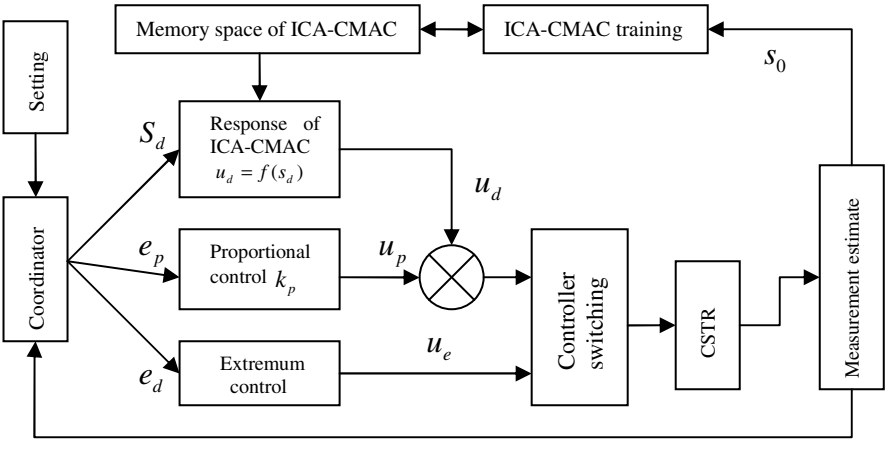

Fig. 1. Figure of ICA-CMAC inverse control

From figure 1, we can know that proportional control is inducted as the auxiliary controller of ICA-CMAC. In this way, the initial dynamic performance of the system can be improved to a certain extent. While the system is entering in or close to expectation, due to the absolute value of error e is less, therefore ICA-CMAC controller plays the main role rather than proportional control.

In addition, there is an additional extremum controller being used as an assistant controller to correct fast when the deviation is large, which is according to the principles of optimal control. The role of expert coordinator is to switch controller according to the current error signal. The operation is depicted as below:

$$u_c = \begin{cases} u_{bangbang} & e \geq e_+ \\ u_d + u_p & e \leq -e_+ \end{cases} \tag{6}$$

To get the solutions of the differential equations in section 2, the fourth order Runge-Kutta method is used in this paper. The formula is as follows:

$$y_{i+1} = y_i + \frac{h}{6}(K_1 + 2K_2 + 2K_3 + K_4) \tag{7}$$

Where $K_1 = f(x_i, y_i)$,

$$K_2 = f(x_i + \frac{h}{2}, y_i + \frac{h}{2}K_1),$$

$$K_3 = f(x_i + \frac{h}{2}, y_i + \frac{h}{2}K_2),$$

$$K_4 = f(x_i + h, y_i + hK_3).$$

In the simulation, with the state x_1 set of sine wave signal and step signal, ICA-CMAC network and conventional CMAC are used to control the actual state to track the set value. The desired output state vector s_d is defined as $s_d = \langle x_{1e}[k+1], x_2[k], e_d \rangle$, $e_d = x_{1e}(k+1) - x_1(k)$, where $x_{1e}[k+1]$ is the next desired output value. The current output state vector s_0 is defined as $s_0 = \langle x_1, x_2, dx_1 \rangle$, $dx_1[k] = x_1[k] - x_1[k-1]$.

5 Simulation Results

Parameters are selected as follows: the maximum of u_c is 4.87, the minimum of u_c is 0, e_+ is 0.01, T is 0.005625, K_p is 200, $[x_1(0), x_2(0)]$ is [0.94, 2.07]. When the state x_1 is set for sine wave signal, simulation result of ICA-CMAC is shown in Figure 2, and the simulation result of conventional CMAC is shown in Figure 3. According to the results of Figure 2 and Figure 3, the learning performance of ICA-CMAC is significantly superior to that of conventional CMAC.

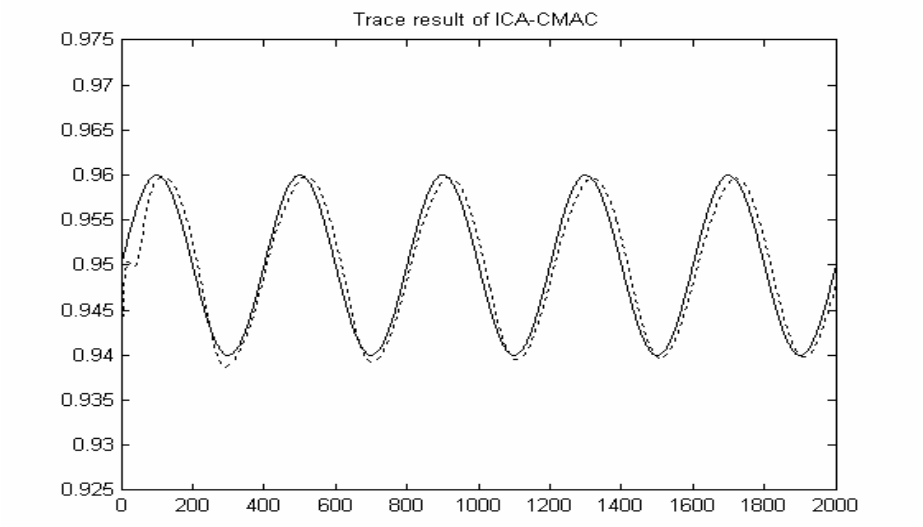

Fig. 2. Simulation result of ICA-CMAC

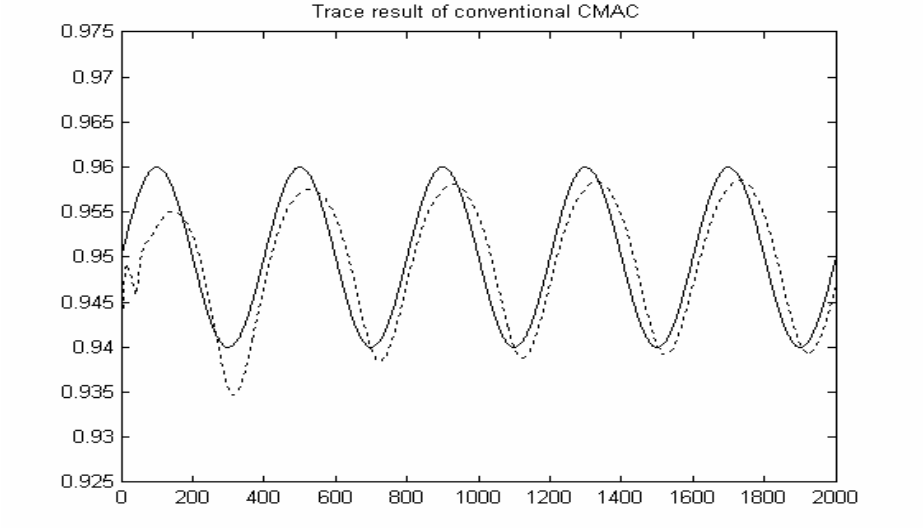

Fig. 3. Simulation result of conventional CMAC

When the state x_1 is set for the step signal, simulation result of ICA-CMAC is shown in Figure 4, and the simulation result of conventional CMAC is shown in Figure 5. By comparing Figure 4 with Figure 5, it can be concluded that the adjustment time of ICA-CMAC is much shorter than that of conventional CMAC. Consequently, it can be conclude that ICA-CMAC performs much faster than conventional CMAC.

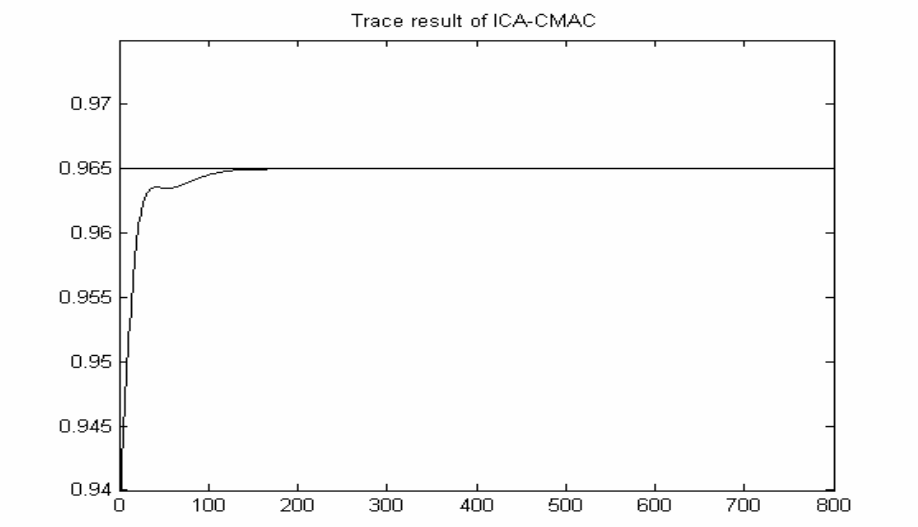

Fig. 4. Simulation result of ICA-CMAC

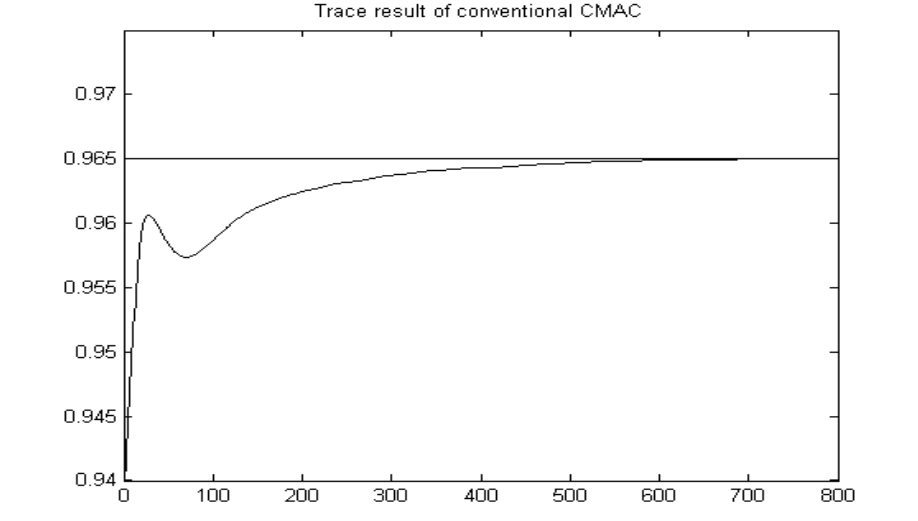

Fig. 5. Simulation result of conventional CMAC

From the simulations of sine wave signal and step signal, it can be seen that ICA-CMAC applied in direct inverse model control of CSTR can accelerate the convergence to achieve the needs of real-time control.

6 Conclusions

Inverse control combined with neural network can achieve the dynamic control of the nonlinear system. In this paper, a new Improved Credit Assigned CMAC is designed

based on the concept of credit assignment. As a result, the learning speed of conventional CMAC is improved. And the ICA-CMAC applied in direct inverse model control also improves the response speed, which is, therefore, better to meet the requirements of real-time controls. In this paper, ICA-CMAC is used for researching of CSTR control issues of a class of complicated nonlinear object. During the simulation, the new ICA-CMAC network performs much faster than conventional CMAC. The simulation results show that the improved CMAC has a faster learning speed and a higher precision in the initial stage of learning.

References

1. Xu, L., Jiang, J.-P., Zhu, J.: Supervised Learning Control of a Nonlinear Polymerization Reactor Using the CMAC Neural Network for Knowledge Storage. IEE Proc.-Control Theory Appl. 141(1), 33–38 (1994)
2. Ying, L., Wen-qi, G., Shao-Bin, W., Zheng-Ping, X.: Study of Adaptive Inverse Control to Stale Platform. In: Proc. 2008 International Conference on Computer Science and Software Engineering, pp. 807–810 (2008)
3. Li, J., Jinshou, Y.: Nonlinear Hybrid Adaptive Inverse Control Using Neural Fuzzy System And Its Application To CSTR Systems. In: Proceedings of the 4th World Congress on Intelligent Control and Automation, Shanghai, P.R.China, June 10-14, pp. 1896–1900 (2002)
4. Nazaruddin, Y.Y., Waluyo, J., Hadisupadmo, S.: Inverse Learning Control Using Neuro-Fuzzy Approach for a Process Mini-Plant. In: Proc. Physics and Control, St. Petersburg, Russia, vol. 1, pp. 247–252 (2003)
5. Tao, M., Jie, C., Wenjie, C., Fang, D.: Neural Network Based Inverse Control of Systems with Hysteresis. In: Proc. Mechtronic and Embedded Systems and Applications, pp. 353–356 (2008)
6. Anuradha, D.B., Reddy, G.P., Murthy, J.S.N.: Direct Inverse Neural Network Control of A Continuous Stirred Tank Reactor (CSTR). In: Proceedings of the International Multi Conference of Engineers and Computer Scientists 2009 IMECS 2009, Hong Kong, P.R.China, March 18-20, vol. II (2009)
7. Salman, R.: Neural Networks of Adaptive Inverse Control Systems. Applied Mathematics and Computation 163(2), 931–939 (2005)
8. Iiguni, Y.: Hierarchical Image Coding Via Cerebellar Model Arithmetic Computers. IEEE Transactions on image processing 5(10), 1393–1401 (1996)
9. Hong, C.M., Lin, C.H., Tao, T.: Grey-CMAC model. In: Proc. ISTED Int. Conf. High Technology Power Industry, San Francisco, pp. 39–44 (1997)
10. Shun, F.S., Ted, T., Hung, T.H.: Credit Assigned CMAC and Its Application to Online Learning Robust Controllers. IEEE Trans. on Systems, Man, and Cybernetics-part B: Cybernetics 33(2), 202–213 (2003)
11. Da-qi, Z., Wei, Z.: Nonlinear Identification Algorithm of the Improved CMAC Based on Balanced Learning. In: Proc. Control and Decision, vol. 19(12), pp. 1425–1428 (2004)
12. Ge, Y., Luo, X., Du., P.: A New Improved CMAC Neural Network. In: Proc. CCDC 2010 (accepted 2010)
13. Luo, X., Pang, W., Peng, Y.: A New Control Strategy of Artificial Climate Chest Temperature and Humidity on Bi-CMAC. In: Proc. 2009 Chinese Control and Decision Conference (CCDC 2009), vol. 17(7), pp. 3220–3223 (2009)

Further Research on Extended Alternating Projection Neural Network

Jingen Wang, Yanfei Wang, and Xunxue Cui

New Star Research Institute of Applied Technology,
451 Huangshan Road, Hefei, Anhui, China
wangjingen@126.com

Abstract. In order to apply the Extended Alternating Projection Neural Network (EAPNN) better in pattern recognition, signal processing and sensor network, the paper makes futher research on the EAPNN and deduces several important conclusions from the mathematical expression to the steady state value of EAPNN, and strict mathematical proofs to these corollaries are also given. In addition, the convergent speed of EAPNN has been discussed and analyzed.

Keywords: Alternating projection, neural network, signal processing, sensor network, pattern recognition.

1 Introduction

Alternating Projection Neural Network(APNN)[1] is firstly proposed by Marks II etc at Washington University in the United States. Marks II etc assume *N* library patterns to be linearly independent before they discuss APNN. Thus the interconnect matrix can be obtained by letting $T = F(F^T F)^{-1} F^T$; But in practice it is very difficult to ensure that *N* library patterns are linearly independent, so $F^T F$ can be singular or ill conditioned, the aforementioned method for obtaining *T* will be invalid. Therefore Marks II etc present a practical method which includes the case that *N* library patterns aren't linearly independent. However, APNN's convergent condition and its proofs are based on the precondition that *N* library patterns are linearly independent. Then is the interconnect matrix obtained by the practical method possible to ensure that APNN is stable? If possible, what is stable convergent condition of network used for CAM? In addition, all the researches on APNN have been done in the real domain. In order to APNN can be widely applied to signal processing, its application scope needs to be expanded from the real domain to the complex domain. Is it possible to directly expand? If impossible, how do we modify the network?

Aiming at the above problems, the literature [2] studies APNN thoroughly and proposes a new neural network—Extended Alternating Projection Neural Network (EAPNN) which functions in the complex domain. The topology architecture and association process of EAPNN are the same as those of APNN. In the literature [2] the stability of EAPNN has been studied and strict mathematical proofs to its stability

D.-S. Huang et al. (Eds.): ICIC 2010, LNCS 6215, pp. 33–40, 2010.

has also been given. The literature [3] obtains the mathematical expression to the steady state value of EAPNN and gives the sufficient and necessary condition of EAPNN used for CAM.

EAPNN is prone to parallel computation and VLSI design due to its simplicity, consequently has a bright future under the real time processing situations. It has been applied to the signal processing such as band-limited signal extrapolation[4], notch filters[5] and weak signal seperation[6]. In order to expand its application scope and apply it better in other field such as pattern recognition and sensor network, we need to make further research on the EAPNN.

In the paper we will deduce several important conclusions, which can be helpful to EAPNN application, from the mathematical expression to the steady state value of EAPNN.In addition, we will discuss and analyze the convergent speed of EAPNN.

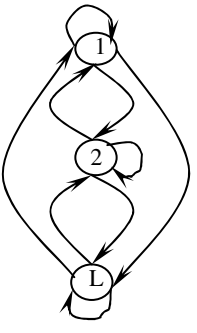

Fig. 1. Illustration of EAPNN

2 Extended Alternating Projection Neural Network (EAPNN)

EAPNN is full-interconnect neural network and its topology architecture is shown in Figure1. Assuming that EAPNN is made up of L neurons, the arbitrary neuron *i* and the neuron *j* are bidirectional connect. Weight t_{ij} equals t_{ji}. Neurons of EAPNN can be classified into clamped neurons or floating neurons according to their states. The state $s_i(m)$ of arbitrary floating neuron *i* at time *m* equals $\sum_{p=1}^{L} t_{pi} s_p(m-1)$, the state $s_j(m)$ of arbitrary clamped neuron *j* at time *m* is equal to $s_j(m-1) = \cdots = s_j(0)$. The weight-value of network can be obtained by the following training method.

2.1 Training Method

The library matrix *F* is equal to $[f_1 \quad f_2 \quad \cdots \quad f_N]$ which is formed by *N* complex patterns of length L: $f_1, f_2, \cdots, f_N$. Then the interconnect matrix, *T*, of EAPNN can be obtained by the following weight-learning method:

(a) Let the interconnect matrix T equal 0, $i \leftarrow 1$;

(b) $\varepsilon_i = (I - T) f_i$, where I is $L \times L$ identity matrix, f_i is complex pattern used for training the neural network;

(c) if $\|\varepsilon_i\| = 0$, then f_i is already in the subspace T and jump to (d)， else $T \leftarrow T + \varepsilon_i \varepsilon_i^H / \varepsilon_i^H \varepsilon_i$;

(d) $i \leftarrow i+1$, if $i > N$ then end, else jump to (b).

From the literature [2] we can learn that the interconnect matrix T obtained by the above method equals FF^+, where F^+ is pseudoinverse of the matrix F.

2.2 Stability and Steady State Value

After EAPNN has been trained, it is time to decide which neurons are clamped neurons and which neurons are floating neurons. We can assume without loss of generality that neurons 1 through P are clamped and the remaining Q=L-P neurons are floating. At time m=0 clamped neurons are initialized. If the state vector of EAPNN is $S(m) = [s_1(m) \quad s_2(m) \quad \cdots \quad s_L(m)]^T$ at time m, the state vector of clamped neurons is $S^P(m)$ and the state vector of floating neurons is $S^Q(m)$, then the state vector of EAPNN at time m+1 is

$$S(m+1) = \eta T S(m) = \begin{bmatrix} S^P(m+1) \\ S^Q(m+1) \end{bmatrix} = \eta \cdot \begin{bmatrix} T_2 & T_1 \\ T_3 & T_4 \end{bmatrix} \cdot \begin{bmatrix} S^P(m) \\ S^Q(m) \end{bmatrix} = \begin{bmatrix} S^P(m) \\ T_3 S^P(m) + T_4 S^Q(m) \end{bmatrix} \tag{1}$$

Where T is the interconnect matrix, operator η clamps the states of clamped neurons whose states will be altered by T. Thus the whole operating process of EAPNN is that operator T and operator η function by turns.

In the literature [2] the stability of EAPNN has been studied and detailed proof process has been provided. Its stability can be described by the following theorem 1.

Theorem 1. Assuming that N complex patterns f_i of length L form the matrix $F = [f_1 \quad f_2 \quad \cdots \quad f_N]$, rank of F equals K, the first P rows of F form the matrix F_P. We can assume without loss of generality that neurons 1 through P are clamped and the remaining Q=L-P neurons are floating. At time m=0, the states of all the neurons form vector $s(0)$ and the states of all the clamped neurons form vector $s^P(0)$. The interconnect matrix T which is created by F is equal to $FF^+ = \begin{bmatrix} T_2 & T_1 \\ T_3 & T_4 \end{bmatrix}$, where T_4 is $Q \times Q$ matrix, then EAPNN is stable.

What is its steady state value since EAPNN is stable? In the literature [3] a general expression and mathematical proof have been given. It can be denoted by the following theorem 2.

Theorem 2. The first P elements of inital state vector $s(0)$ of EAPNN form vector $s^P(0)$, The remaining Q elements form vector $s^Q(0)$, the first P rows of F form the matrix F_P, the remaining Q rows form the matrix F_Q, $A = R(F)$ is a subspace enclosed by all library patterns, B is a set of all vectors whose first P elements form $s^P(0)$, then $s(\infty)$ in the subspace B can be written as follows:

$$s_B(\infty) = \begin{bmatrix} s^P(0) \\ F_Q(I - F_P^+ F_P)(F_Q(I - F_P^+ F_P))^+ (s^Q(0) - F_Q F_P^+ s^P(0)) + F_Q F_P^+ s^P(0) \end{bmatrix} \tag{2}$$

$s(\infty)$ in the subspace A is equal to

$$s_A(\infty) = \begin{bmatrix} F_P F_P^+ s^P(0) \\ F_Q(I - F_P^+ F_P)(F_Q(I - F_P^+ F_P))^+ (s^Q(0) - F_Q F_P^+ s^P(0)) + F_Q F_P^+ s^P(0) \end{bmatrix} \tag{3}$$

3 Several Conclusions of EAPNN

Theorem 2 obtains a general expression which includes all kinds of situations. From the point of view of geometrical relation between two spaces, theorem 2 includes three situations, that is:(1) the two spaces don't intersect;(2) the intersection of the two spaces results in a linear variety of positive dimension;(3) the two spaces intersect at a unique point. From the point of view of rank of library matrix, theorem 2 includes $rank(F_P) = rank(F)$ and $rank(F_P) \neq rank(F)$.

By studying the general expression in theorem 2 we can deduce several important corollaries as follows:

Corollary 1. If $rank(F_P) = rank(F)$, then $s_A^Q(\infty) = s_B^Q(\infty) = F_Q F_P^+ s^P(0)$

Proof. Let $rank(F_P) = rank(F) = r$ decompose F as follows:

$F = \begin{bmatrix} C_1 \\ C_2 \end{bmatrix} \cdot D = C_0 \cdot D$, where $C_0 = \begin{bmatrix} C_1 \\ C_2 \end{bmatrix} \in C^{L \times r}$, $D \in C^{r \times N}$, $C_1 \in C^{P \times r}$, $C_2 \in C^{Q \times r}$

$F_P = C_1 D$, $F_Q = C_2 D$,

$$rank(F_P) = rank(F) = r = rank(C_1 D) \leq rank(C_1), \text{ namely } rank(C_1) \geq r \tag{4}$$

and

$$r = rank(C_1 D) \geq rank(C_1) + rank(D) - r = rank(C_1), \text{ namely } rank(C_1) \leq r \tag{5}$$

Combining (4) and (5), we obtain $rank(C_1) = r$. Thus $F_P^+ = (C_1 D)^+ = D^+ C_1^+$

$$F_Q(I - F_P^+ F_P) = F_Q - F_Q F_P^+ F_P = C_2 D - C_2 D D^+ (C_1^H C_1)^{-1} C_1^H C_1 D$$

$$= C_2 D - C_2 D D^+ D = C_2 D - C_2 D = 0$$

Since $F_Q(I-F_P^+F_P)=0 \Rightarrow (F_Q(I-F_P^+F_P))^+=0$, we can deduce $s_B^Q(\infty)=F_Q F_P^+ s^P(0)=s_A^Q(\infty)$, and our proof is complete.

From the above corollary we can learn that $s_A^Q(\infty)=s_B^Q(\infty)$ is unrelated to $s^Q(0)$ while $rank(F_P)=rank(F)$, that is to say, final steady states of the network are unrelated to the inital states of the floating neurons. This shows that the steady convergent condition of the network used for CAM is to require $rank(F_P)=rank(F)$. In practice, it is a sufficient and necessary condition according to the conclusions in the literature [3].Apparently, when all the rows of F are linearly independent, the steady convergent condition of EAPNN agrees with that of APNN.

Corollary 2. If $rank\ (F_P)=rank\ (F)$ and $s^P(0)=F_P\cdot\vec{k}$, where $\vec{k}=[k_1 \quad k_2 \quad \cdots \quad k_N]^T$ is constant vector, then $s_A^Q(\infty)=s_B^Q(\infty)=F_Q\cdot\vec{k}$.

Proof. $s^P(0)=F_P\cdot\vec{k}$, furthermore, from corollary 1,we obtain $s_A^Q(\infty)=s_B^Q(\infty)=F_Q F_P^+ s^P(0)$,Thus

$$s_A^Q(\infty)=s_B^Q(\infty)=F_Q F_P^+ F_P\cdot\vec{k}=C_2 D\cdot D^+ C_1^+\cdot C_1 D\cdot\vec{k}=C_2 DD^+(C_1^H C_1)^{-1}C_1^H C_1 D\cdot\vec{k}$$
$$=C_2 DD^+ D\cdot\vec{k}=F_Q\cdot\vec{k}$$ and our proof is complete.

Corollary 3. If $s(0)$ is linear combination of library patterns, then $s_A(\infty)=s_B(\infty)=s(0)$.

Proof. Since $s(0)$ is linear combination of library patterns, $s(0)$ can be expressed as follows:

$s(0)=F\cdot\vec{k}=F\cdot[k_1 \quad k_2 \quad \cdots \quad k_N]^T$ .Then $s^P(0)=F_P\cdot\vec{k}$ ， $s^Q(0)=F_Q\cdot\vec{k}$.

Substitute $s^P(0)=F_P\cdot\vec{k}$ and $s^Q(0)=F_Q\cdot\vec{k}$ for the general expression in theorem 2, then

$$s_A^Q(\infty)=s_B^Q(\infty)=F_Q(I-F_P^+F_P)(F_Q(I-F_P^+F_P))^+(F_Q\cdot\vec{k}-F_Q F_P^+F_P\cdot\vec{k})+F_Q F_P^+F_P\cdot\vec{k}$$
$$=F_Q(I-F_P^+F_P)(F_Q(I-F_P^+F_P))^+(F_Q(I-F_P^+F_P))\cdot\vec{k}+F_Q F_P^+F_P\cdot\vec{k}$$
$$=F_Q(I-F_P^+F_P)\cdot\vec{k}+F_Q F_P^+F_P\cdot\vec{k}=F_Q\cdot\vec{k}$$
$$s_A^P(\infty)=F_P F_P^+F_P\cdot\vec{k}=F_P\cdot\vec{k}=s^P(0)=s_B^P(\infty)$$

Thus $s_A(\infty)=s_B(\infty)=s(0)$, and our proof is complete.

Corollary 4. $T_4^\infty=\lim_{n\to\infty}T_4^n=F_Q(I-F_P^+F_P)(F_Q(I-F_P^+F_P))^+$. If $rank(F_P)=rank(F)$, then $T_4^\infty=0$.

Proof. From theorem 2, we obtain

$$s_B^Q(\infty)=F_Q(I-F_P^+F_P)(F_Q(I-F_P^+F_P))^+(s^Q(0)-F_Q F_P^+ s^P(0))+F_Q F_P^+ s^P(0) \tag{6}$$

According to the association process of EAPNN, the state vector of its floating neurons can be written as follows after *n* times association:

$$s_B^Q(n) = \sum_{i=0}^{n-1} T_4^i T_3 s^P(0) + T_4^n s^Q(0) \quad \text{(Here define } T_4^0 = I \text{)}$$

Due to randomicity of $s^P(0)$, we might as well let $s^P(0)$ =0, then $s_B^Q(n) = T_4^n s^Q(0)$

Thus

$$s_B^Q(\infty) = \lim_{n\to\infty} T_4^n s^Q(0) = T_4^\infty s^Q(0) \tag{7}$$

Considering (6), (7) and randomicity of $s^Q(0)$, we obtain

$$T_4^\infty = \lim_{n\to\infty} T_4^n = F_Q(I - F_P^+ F_P)(F_Q(I - F_P^+ F_P))^+ \tag{8}$$

Especially if $rank(F_P) = rank(F)$, we have $F_Q(I - F_P^+ F_P) = 0$ and $(F_Q(I - F_P^+ F_P))^+$ =0, according to the proof process of the corollary 1. Thereby $T_4^\infty = 0$, and our proof is complete.

Suppose that, eigenvalues of the matrix T_4 satisfy $\lambda_1 \geq \lambda_2 \geq \cdots \geq \lambda_Q$ and $l = rank(F) - rank(F_P) + 1$. According to our research, we conclude that the *l*-th eigenvalue of T_4 must be less than one and the speed of network reaching stable solution is related to magnitude of the *l*-th eigenvalue, more fast the network reach stable solution more larger magnitude of the eigenvalue is. When the network is applied to CAM, we have *l*=1 due to $rank(F_P) = rank(F)$, that is to say, speed of network reaching stable solution is related to spectral radius $\rho(T_4)$ of T_4. Suppose that the first *P* neurons of EAPNN are always clamped neurons, and the remaining *Q* neurons are floating , then $\rho(T_4)$ is related to *P* or related to *Q* . $\rho(T_4)$ decreases with the increase of *P* or with the decrease of *Q* . This conclusion can be theoretically proved.

Theorem 3. Suppose that EAPNN have *L* neurons (*L* is changeless), and have learned a group of library patterns. Assuming that the first P neurons are clamped and the remaining $Q = L - P$ neurons are floating. Let T_4 denote the interconnect matrix formed by weights of all floating neurons, then the spectral radius, $\rho(T_4)$, of T_4 will decrease with increase of P.

In order to prove the theorem, a definition and a theorem—*Courant* maximin theorem need to be introduced.

Definition 1. $R(X) = \dfrac{X^H A X}{X^H X}, \forall X (\neq 0) \in C^n$ is called *Rayleigh* quotient of the matrix *A*.

Courant maximin theorem[7]. Let $\lambda_1 \geq \lambda_2 \geq \cdots \geq \lambda_n$ be the eigenvalues of an $n \times n$ *Hermite* matrix A .Then for $k \leq n$, $\lambda_k = \min_{\dim S = n-k+1} \{\max_{X \in S} R(X)\}$ or $\lambda_k = \max_{\dim S = k} \{\min_{X \in S} R(X)\}$.

Proof of theorem 5

when $P = n$ ($1 \leq n \leq L-1$), let $T_4 = A = \begin{bmatrix} t & C \\ D & B \end{bmatrix}$, where t is a real number, $C \in C^{1\times(L-n-1)}$, $D \in C^{(L-n-1)\times 1}$, $B \in C^{(L-n-1)\times(L-n-1)}$, then while $P = n+1$, we have $T_4 = B$. Since $T_4^H = T_4$, then $D = C^H$ (or $C = D^H$). According to our research eigenvalues of *A,B* are real number lying in the interval [0,1]. Suppose that, eigenvalues of *A* satisfy $\lambda_1 \geq \lambda_2 \geq \cdots \geq \lambda_{L-n}$, eigenvalues of *B* satisfy $\mu_1 \geq \mu_2 \geq \cdots \geq \mu_{L-n-1}$, then $\rho(A) = \lambda_1$, $\rho(B) = \mu_1$. Due to randomicity of n we only need prove $\rho(A) = \lambda_1 \geq \rho(B) = \mu_1$.

Suppose that, $m = L - n$ and X_{m-1} is $m-1$ dimensional column vector, mark *Rayleigh* quotient of *A* and *B* as $R_1(X)$ and $R_2(X_{m-1})$ respectively,let *m* dimensional column vector $Y = \begin{bmatrix} 0 \\ X_{m-1} \end{bmatrix}$, Thus

$$R_1(Y) = \frac{Y^H A Y}{Y^H Y} = \frac{\begin{bmatrix} 0 & X_{m-1}^H \end{bmatrix} \cdot \begin{bmatrix} t & C \\ C^H & B \end{bmatrix} \cdot \begin{bmatrix} 0 \\ X_{m-1} \end{bmatrix}}{\begin{bmatrix} 0 & X_{m-1}^H \end{bmatrix} \cdot \begin{bmatrix} 0 \\ X_{m-1} \end{bmatrix}} = \frac{\begin{bmatrix} 0 & X_{m-1}^H \end{bmatrix} \cdot \begin{bmatrix} CX_{m-1} \\ BX_{m-1} \end{bmatrix}}{X_{m-1}^H \cdot X_{m-1}} = \frac{X_{m-1}^H B X_{m-1}}{X_{m-1}^H \cdot X_{m-1}} = R_2(X_{m-1}) \tag{9}$$

Let $W = \left\{ Y = \begin{bmatrix} 0 \\ X_{m-1} \end{bmatrix} \;\middle|\; \forall X_{m-1} \in C^{m-1} \right\}$, W_1 is one dimensional subspace of *W*, S_1 is one dimensional subspace of C^m, S_2 is one dimensional subspace of C^{m-1}. Since $\{W_1 | \dim W_1 = 1\} \subset \{S_1 | \dim S_1 = 1\}$, then

$$\max_{\dim S_1 = 1} \{\min_{X \in S_1} R_1(X)\} \geq \max_{\dim W_1 = 1} \{\min_{X \in W_1} R_1(X)\} \tag{10}$$

According to defines of W_1, S_2 and formula (10) we obtain

$\forall X \in W_1$, $\exists S_2$, $X_{m-1} \in S_2$, $R_1(X) = R_2(X_{m-1})$, and $\forall X_{m-1} \in S_2$, $\exists W_1$, $X \in W_1$, $R_2(X_{m-1}) = R_1(X)$, So right hand side of formula (10) equals

$$\max_{\dim S_2 = 1} \{\min_{X_{m-1} \in S_2} R_2(X_{m-1})\} \tag{11}$$

Left hand side of formula 6) equals λ_1 , formula (7) equals μ_1 , from *courant* maximin theorem, we have $\lambda_1 \geq \mu_1$, namely $\rho(A) \geq \rho(B)$, and our proof is complete.

4 Peroration

EAPNN is prone to parallel computation and VLSI design due to its simplicity, consequently has a bright future under the real time processing situations. It has been applied to the signal processing such as band-limited signal extrapolation, notch filters and weak signal seperation. In order to expand its application scope and apply it better in other field such as pattern recognition and sensor network, the paper makes further research on the EAPNN, deduces several important conclusions, which can be helpful to EAPNN application, from the mathematical expression to the steady state value of EAPNN,discusses and analyzes the convergent speed of EAPNN. All the conclusions are obtained by strict mathematical deduction.

Acknowledgments

This work was partially supported by the National Natural Science Foundation of China under grant No. 60773129; the Excellent Youth Science and Technology Foundation of Anhui Province of China under grant No.08040106808.

References

1. Marks, R.J., Oh, S., Atlas, L.E.: Alternating Projection Neural Networks. IEEE Trans. CAS 36, 846–857 (1989)
2. Wang, J.G.: Target signal detection and target localization. Naval University of Engineering, Wuhan (2001)
3. Wang, J.G., Gong, S.G., Chen, S.F.: Sufficient and necessary condition of the extended alternating projection neural network configured as a content addressable memory. Tien Tzu Hsueh Pao/Acta Electronica Sinica 32, 596–600 (2004)
4. Wang, J.G., Lin, C.S., Gong, S.G.: An extrapolation algorithm for band-limited signals based on Alternating Projection Neural Networks. Acta Electronica Sinica 28, 52–55 (2000)
5. Wang, J.G., Gong, S.G., Lin, C.S., Tang, J.F., Liu, S.D.: Notch filter based on Complex Alternating Projection Neural Networks. Journal of Data Acquisition & Processing 16, 440–445 (2001)
6. Wang, J.G., Chen, S.F., Gong, S.G., Chen, Z.Q.: An extended alternating projection neural networks based weak-signal separation algorithm. In: IEEE International Conference on Robotics, Intelligent Systems and Signal Processing, vol. 1, pp. 554–558 (2003)
7. Zhang, M.C.: Matrix Theory for Engineering. Southeast University Press, Nanjing (1995)

Global Synchronization in an Array of Hybrid Coupling Neural Networks with Multiple Time-Delay Components

Jian Feng and Dawei Gong

School of Information Science and Engineering, Northeastern University, Shenyang 110004, China
fjneu@163.com

Abstract. In this paper, synchronization problem is investigated for a new array of coupled neural networks with multiple time-delay components. The considered system is more general than those basic mathematical model with single delay. Based on a novel Lyapunov-Krasovskii functional and the Kronecker product technique, a delay-dependent criterion is derived to ensure the global synchronization. The criteria is expressed within the framework of linear matrix inequalities, which can be easily computed and checked. Finally, a typical example with chaotic nodes is given to illustrate the effectiveness of the proposed result.

Keywords: Global synchronization, Multiple time-delay components, Kronecker product, Hybrid coupling, Linear matrix inequalities.

1 Introduction

In recent years, there exists much increasing in the study of recurrent neural networks (NNs) due to its potential applications in various fields. Such as online optimization, static images processing, pattern recognition, signal processing, and associative memories. Most of the previous studies have been applied to the stability analysis, periodic oscillations and dissipativity of such kind of neural networks [1-4].

However, in such networks, there also exists more complicated dynamics. For example, the chaotic behavior has been found and investigated in [5-6]. Among all the issues of such networks, arrays of coupled network may play a crucial role in the emergence of synchronization phenomena in various fields. For example, they can be utilized in secure communication, chaos generators design and harmonic oscillation generation [7-8]. So it is necessary to give the further research on the arrays of coupled systems, and the synchronization of coupled systems have been attracted much attention to many researchers.

Meanwhile, time delays inevitably occur in the signal communication among the neurons, which may lead to the oscillation phenomenon or instability of the networks. Therefore, the study on the dynamical behavior of the delayed neural networks is attractive both in theory and in practice. On the other hand, in

D.-S. Huang et al. (Eds.): ICIC 2010, LNCS 6215, pp. 41–48, 2010.

practical situations, signals transmitted from one point to another may experience a few network segments, which can possibly induce successive delays due to variable network transmission conditions. In [9-10], some sufficient conditions have been proposed to ensure the asymptotic stability of such neural networks. However, to the best of the author's knowledge, there is no progress toward solving the synchronization problems arising from array of coupled networks with successive delay components.

Motivated by the above discussions, a new model for an array of coupled neural networks with successive time-varying delays is proposed. By constructing a special L-K functional, we obtain some novel sufficient conditions, which are expressed in terms of linear matrix inequality. Finally, our main results are illustrated through some numerical simulation examples.

Notations: R^n is the n-dimensional Euclidean space; $R^{m\times n}$ denotes the set of $m \times n$ real matrices. I_n represents the n-dimensional identity matrix. The superscript "T" denotes the transpose and the notation $X \geq 0$ (respectively, $X > 0$) means that X is positive semidefinite (respectively, positive definite). The notation $A \otimes B$ stands for the Kronecker product of matrices A and B.

2 Preliminaries

In this paper, the problem of delay-dependent technique for the synchronization of coupled neural networks with a new delay system is proposed. Consider the following successive time-delay neural networks:

$$\begin{aligned}\dot{x}_i(t) =& - Cx_i(t) + Af(x_i(t) + Bf(x_i(t - d_1(t) - d_2(t))) \\ &+ I(t) + \sum_{j=1}^{N} L_{ij}^{(1)} \Gamma_1 x_j(t) + \sum_{j=1}^{N} L_{ij}^{(2)} \Gamma_2 x_j(t - d_1(t) - d_2(t)) \end{aligned} \tag{1}$$

where $x_i(t) = (x_{i1}(t), x_{i2}(t), \cdots, x_{in}(t))^T \in R^n$ is the neuron state vector of the ith network at time t. $f(x_i(t)) = (f_1(x_{i1}(t)), f_2(x_{i2}(t)), \cdots, f_n(x_{in}(t)))^T$, $C = diag(c_1, c_2, \ldots, c_n) > 0$ is the state feedback coefficient, matrix A , B represent the connection weight matrix. $I(t) = (I_1^T(t), I_2^T(t), \cdots, I_n^T(t))^T \in R^n$ is an external input vector, $L^{(1)} = (L_{ij}^{(1)})_{N\times N}, L^{(2)} = (L_{ij}^{(2)})_{N\times N}$ represent the coupling connections, $\Gamma_1, \Gamma_2 \in R^{n\times n}$ represent the linking matrix and the discrete-delay linking matrix. The time delays $d_1(t)$ and $d_2(t)$ are time-varying differentiable functions which satisfy:

$$0 \leq d_1(t) \leq \bar{d}_1 < \infty, \dot{d}_1(t) \leq \mu_1 < \infty$$

$$0 \leq d_2(t) \leq \bar{d}_2 < \infty, \dot{d}_2(t) \leq \mu_2 < \infty$$

and we denote

$$d(t) = d_1(t) + d_2(t), \bar{d} = \bar{d}_1 + \bar{d}_2, \mu = \mu_1 + \mu_2$$

For simplicity, let $x(t) = (x_1^T(t), x_2^T(t), \cdots, x_N^T(t))^T$, $\mathbf{I}(t) = (I^T(t), I^T(t), \cdots, I^T(t))^T$, $F(x(t)) = (f^T(x_1(t)), f^T(x_2(t)), \cdots, f^T(x_N(t)))^T$, combining with the signal $\otimes$ of Kronecker product, model (1) can be rewritten as:

$$\begin{aligned}\dot{x}(t) =& -(I_N \otimes C)x(t) + (I_N \otimes A)F(x(t) + (I_N \otimes B)F(x(t - d_1(t) - d_2(t))) \\ &+ \mathbf{I}(t) + (L^{(1)} \otimes \Gamma_1)x(t) + (L^{(2)} \otimes \Gamma_2)x(t - d_1(t) - d_2(t)) \end{aligned} \tag{2}$$

In the following, some elementary situations are introduced, which play an important role in the proof of the main result.

Throughout this letter, the following assumptions are needed.

Assumption (H1): the outer-coupling configuration matrices of the neural networks satisfy:

$$\begin{cases} L_{ij}^{(q)} = L_{ji}^{(q)} \geq 0, i \neq j, q = 1, 2, 3 \\ L_{ii}^{(q)} = -\sum\limits_{j=1, j\neq i}^{N} L_{ij}^{(q)}, i, j = 1, 2, \cdots, N \end{cases}$$

Assumption(H2): for any constants σ_i^-, σ_i^+, the functions are bounded and satisfy:

$$\sigma_r^- \leq \frac{f_r(x_i) - f_r(x_j)}{x_i - y_j} \leq \sigma_r^+, r = 1, 2, \cdots, n$$

We denote

$$\Delta_1 = diag(\sigma_1^+\sigma_1^-, \cdots, \sigma_n^+\sigma_n^-), \Delta_2 = diag(\frac{\sigma_1^+ + \sigma_1^-}{2}, \cdots, \frac{\sigma_n^+ + \sigma_n^-}{2})$$

Next, we give some useful definitions and lemmas.

Definition 1. Model (2) is said to be globally synchronized if the following holds:

$$||x_i(t) - x_j(t)|| = 0, i, j = 1, 2, \cdots, N$$

Lemma 1. For any constant matrix $\Re \in R^{n\times n}, \Re^T = \Re > 0$, scalar $\rho > 0$ and vector function $\varpi : [0, \rho] \to R^n$, one has:

$$\rho \int_0^\rho \varpi^T(s)\Re\varpi(s)ds \geq (\int_0^\rho \varpi ds)^T \Re (\int_0^\rho \varpi ds)$$

Lemma 2. Let $\otimes$ denote the notation of Kronecker product. Then, the following relationships hold:

(1) $(\alpha A) \otimes B = A \otimes (\alpha B)$
(2) $(A + B) \otimes C = A \otimes C + B \otimes C$
(3) $(A \otimes B)(C \otimes D) = (AC) \otimes (BD)$

Lemma 3 [14]: let $\tilde{U} = (\alpha_{ij})_{N\times N}$, $P \in R^{n\times n}$, $x = (x_1^T, x_2^T, \cdots, x_N^T)^T$, and $y = (y_1^T, y_2^T, \cdots, y_N^T)^T$ with $x_k, y_k \in R^n, (k = 1, 2, \cdots, N)$. If $\tilde{U} = \tilde{U}^T$, and each row sum is zero, then

$$x^T(\tilde{U} \otimes P)y = -\sum_{1\leq i<j}^{N} a_{ij}(x_i - x_j)^T P(y_i - y_j)$$

3 Main Results

In this section, we are in the position to present our main results for synchronization criteria.

Theorem 1: Under assumptions H1,H2, system (2) is globally synchronized if there exist positive definite matrices $P_i > 0 (i = 1, 2, 3, 4, 5)$, $S_i (i = 1, 2, 3, 4)$, three positive definite diagonal matrix J, V, R, such that the following linear matrix inequalities hold for all $1 \leq i < j \leq N$:

$$\Omega_{ij} = \begin{bmatrix} \Xi_{11} & 0 & -NL_{ij}^{(2)} P_1 \Gamma_2 & P_1 A + J\Delta_2 & 0 & P_1 B \\ * & \Xi_{22} & 0 & 0 & V\Delta_2 & 0 \\ * & * & -(1-\mu)P_4 - R\Delta_1 & 0 & 0 & R\Delta_2 \\ * & * & * & \Xi_{44} & 0 & 0 \\ * & * & * & * & \Xi_{55} & 0 \\ * & * & * & * & * & -(1-\mu)P_5 - R \end{bmatrix} < 0 \tag{3}$$

where

$$\begin{aligned} \Xi_{11} &= -2P_1 C - 2NL_{ij}^{(1)} P_1 \Gamma_1 + P_2 + \bar{d}_1 S_1 + \bar{d}_2 S_2 - J\Delta_1 \\ \Xi_{22} &= -(1-\mu_1)P_2 + (1-\mu_1)P_4 - V\Delta_1 \\ \Xi_{44} &= P_3 + \bar{d}_1 S_3 + \bar{d}_2 S_4 - J \\ \Xi_{55} &= -(1-\mu_1)P_3 + (1-\mu_1)P_5 - V \end{aligned}$$

Proof. Let $e = (1, 1, \ldots, 1)^T$, $E_N = ee^T$, and $U = NI_N - E_N$. We introduce the following new Lyapunov functional for the coupled complex system:

$$V(t) = V_1(t) + V_2(t) + V_3(t) + V_4(t) \tag{4}$$

$$V_1(t) = x^T(t)(U \otimes P_1)x(t) \tag{5}$$

$$\begin{aligned} V_2(t) = &\int_{t-d_1(t)}^{t} x^T(s)(U \otimes P_2)x(s)ds + \int_{t-d_1(t)}^{t} F^T(x(s))(U \otimes P_3)F(x(s))ds \\ &+ \int_{t-d(t)}^{t-d_1(t)} x^T(s)(U \otimes P_4)x(s)ds + \int_{t-d(t)}^{t-d_1(t)} F^T(x(s))(U \otimes P_5)F(x(s))ds \end{aligned} \tag{6}$$

$$V_3(t) = \int_{t-\bar{d}_1}^{t} \int_{\theta}^{t} x^T(s)(U \otimes S_1)x(s)dsd\theta + \int_{t-\bar{d}}^{t-\bar{d}_1} \int_{\theta}^{t} x^T(s)(U \otimes S_2)x(s)dsd\theta \tag{7}$$

$$V_4(t) = \int_{t-\bar{d}_1}^{t} \int_{\theta}^{t} F^T(x(s))(U \otimes S_3)F(x(s))dsd\theta + \int_{t-\bar{d}}^{t-\bar{d}_1} \int_{\theta}^{t} F^T(x(s))(U \otimes S_4)F(x(s))dsd\theta \tag{8}$$

Calculating the time derivative of $V(t)$ along the trajectories of (2), and noting that $(U \otimes P_1)\mathbf{I}(t) = 0$, by using Lemma (3), one has:

$$\begin{aligned}\dot{V}_1(t) =& 2x^T(t)(U \otimes P_1)\dot{x}(t)\\ =& 2\sum_{i=1}^{N-1}\sum_{j=i+1}^{N}\{(x_i(t)-x_j(t))^T \times [((-P_1C - NL_{ij}^{(1)}P_1\Gamma_1)(x_i(t)-x_j(t)))\\ &+ P_1A(f(x_i(t)) - f(x_j(t))) + P_1B(f(x_i(t-d(t))) - f(x_j(t-d(t))))\\ &- NL_{ij}^{(2)}P_1\Gamma_2(x_i(t-d(t)) - x_j(t-d(t)))]\} \end{aligned} \tag{9}$$

Similarly, calculating the time derivative of $V_2(t)$ along the system (2), then one obtains:

$$\begin{aligned}\dot{V}_2(t) =& \sum_{i=1}^{N-1}\sum_{j=i+1}^{N}[(x_i(t)-x_j(t))^TP_2(x_i(t)-x_j(t)) - (1-\mu_1)\\ &\times (x_i(t-d_1(t)) - x_j(t-d_1(t)))^TP_2(x_i(t-d_1(t)) - x_j(t-d_1(t)))\\ &+ (f(x_i(t)) - f(x_j(t)))^TP_3(f(x_i(t)) - f(x_j(t))) - (1-\mu_1)(f(x_i(t-d_1(t)))\\ &- f(x_j(t-d_1(t))))^TP_3(f(x_i(t-d_1(t))) - f(x_j(t-d_1(t))))\\ &+ (1-\mu_1)(x_i(t-d_1(t)) - x_j(t-d_1(t)))^TP_4(x_i(t-d_1(t)) - x_j(t-d_1(t)))\\ &- (1-\mu)(x_i(t-d(t)) - x_j(t-d(t)))^TP_4(x_i(t-d(t)) - x_j(t-d(t)))\\ &+ (1-\mu_1)(f(x_i(t-d_1(t))) - f(x_j(t-d_1(t))))^TP_5(f(x_i(t-d_1(t)))\\ &- f(x_j(t-d_1(t)))) - (1-\mu)(f(x_i(t-d(t))) - f(x_j(t-d(t))))^T\\ &\times P_5(f(x_i(t-d(t))) - f(x_j(t-d(t))))] \end{aligned} \tag{10}$$

Calculating the time derivative of $V_3(t), V_4(t)$ along the trajectories of system (2), with Lemma 1, one has

$$\begin{aligned}\dot{V}_3(t) \le& \sum_{i=1}^{N-1}\sum_{j=i+1}^{N}[(x_i(t)-x_j(t))^T(\bar{d}_1S_1)(x_i(t)-x_j(t)) - (\int_{t-\bar{d}_1}^{t}(x_i(s)-x_j(s))ds)^T\\ &\times (\frac{1}{\bar{d}_1}S_1)(\int_{t-\bar{d}_1}^{t}(x_i(s)-x_j(s))ds) + \bar{d}_2(x_i(t)-x_j(t))^TS_2(x_i(t)-x_j(t))\\ &- (\int_{t-\bar{d}}^{t-\bar{d}_1}(x_i(s)-x_j(s))ds)^T(\frac{1}{\bar{d}_2}S_2)(\int_{t-\bar{d}}^{t-\bar{d}_1}(x_i(s)-x_j(s))ds)] \end{aligned} \tag{11}$$

$$\dot{V}_4(t) \le \sum_{i=1}^{N-1}\sum_{j=i+1}^{N}[(f(x_i(t)) - f(x_j(t)))^T \times (\bar{d}_1S_3)(f(x_i(t)) - f(x_j(t)))$$

$$
\begin{aligned}
&- \Big(\int_{t-\bar{d}_1}^{t} (f(x_i(s)) - f(x_j(s)))ds \Big)^T \times \Big(\frac{1}{\bar{d}_1} S_3\Big) \Big(\int_{t-\bar{d}_1}^{t} (f(x_i(s)) - f(x_j(s)))ds \Big) \\
&+ (f(x_i(t)) - f(x_j(t)))^T \times \bar{d}_2 S_4 (f(x_i(t)) - f(x_j(t))) \\
&- \Big(\int_{t-\bar{d}}^{t-\bar{d}_1} (f(x_i(s)) - f(x_j(s)))ds \Big)^T \times \Big(\frac{1}{\bar{d}_2} S_4\Big) \Big(\int_{t-\bar{d}}^{t-\bar{d}_1} (f(x_i(s)) - f(x_j(s)))ds \Big) \quad (12)
\end{aligned}
$$

From the assumption (H2) and reference [11], there exists positive definite diagonal matrix J, V, R, for any $1 \le i < j \le N$, the following equations are feasible:

$$
\begin{aligned}
&\begin{bmatrix} x_i(t) - x_j(t) \\ f(x_i(t)) - f(x_j(t)) \end{bmatrix}^T \begin{bmatrix} -J\Delta_1 & J\Delta_2 \\ J\Delta_2 & -J \end{bmatrix} \begin{bmatrix} x_i(t) - x_j(t) \\ f(x_i(t)) - f(x_j(t)) \end{bmatrix} \\
&+ \begin{bmatrix} x_i(t - d_1(t)) - x_j(d_1(t)) \\ f(x_i(d_1(t))) - f(x_j(d_1(t))) \end{bmatrix}^T \begin{bmatrix} -V\Delta_1 & V\Delta_2 \\ V\Delta_2 & -V \end{bmatrix} \begin{bmatrix} x_i(d_1(t)) - x_j(d_1(t)) \\ f(x_i(d_1(t))) - f(x_j(d_1(t))) \end{bmatrix} \\
&+ \begin{bmatrix} x_i(t - d(t)) - x_j(d(t)) \\ f(x_i(d(t))) - f(x_j(d(t))) \end{bmatrix}^T \begin{bmatrix} -R\Delta_1 & R\Delta_2 \\ R\Delta_2 & -R \end{bmatrix} \begin{bmatrix} x_i(d(t)) - x_j(d(t)) \\ f(x_i(d(t))) - f(x_j(d(t))) \end{bmatrix} \le 0
\end{aligned} \quad (13)
$$

From (9)-(13), Let $\xi_{ij}(t) = ((x_i(t) - x_j(t))^T, (x_i(t - d_1(t)) - x_j(t - d_1(t)))^T, (x_i(t - d(t)) - x_j(t - d(t)))^T, (f(x_i(t)) - f(x_j(t)))^T$,$(f(x_i(t - d_1(t))) - f(x_j(t - d_1(t))))^T$,$(f(x_i(t - d(t))) - f(x_j(t - d(t))))^T)^T$, then we have

$$
\begin{aligned}
\dot{V}(t) \le \sum_{i=1}^{N-1} \sum_{j=i+1}^{N} \{ &(\xi_{ij}(t))^T \Omega_{ij} (\xi_{ij}(t)) - \tfrac{S_1}{\bar{d}_1} \Big(\int_{t-\bar{d}_1}^{t} (x_i(s) - x_j(s))ds \Big)^T \Big(\int_{t-\bar{d}_1}^{t} (x_i(s) - \\
x_j(s))ds \Big) - \tfrac{S_2}{\bar{d}_2} \Big(\int_{t-\bar{d}}^{t-\bar{d}_1} (x_i(s) - x_j(s))ds \Big)^T \Big(\int_{t-\bar{d}}^{t-\bar{d}_1} (x_i(s) - x_j(s))ds \Big) - \tfrac{S_1}{\bar{d}_1} \Big(\int_{t-\bar{d}_1}^{t} (f(x_i(s)) - \\
f(x_j(s)))^T \Big(\int_{t-\bar{d}_1}^{t} (f(x_i(s)) - f(x_j(s))) - \tfrac{S_2}{\bar{d}_2} \Big(\int_{t-\bar{d}}^{t-\bar{d}_1} (f(x_i(s)) - f(x_j(s)))ds \Big)^T \Big(\int_{t-\bar{d}}^{t-\bar{d}_1} (f(x_i(s)) - \\
f(x_j(s)))ds \Big) \}
\end{aligned}
$$

where Ω_{ij} is defined as (3), According to Definition 1, it is easily seen that system (2) is global synchronized. Then the proof is completed.

4 Numerical Examples

In this section, the given results are illustrated by a typical chaotic CNN.

4.1 Chaotic Dynamical Behavior

Consider an 2-dimensional neural network with delay presented in (2):

$$
\dot{V}(t) = -Cy(t) + Af(y(t)) + Bf(y(t - d_1(t) - d_2(t))) + I(t) \quad (14)
$$

where $y(t) = (y_1(t), y_2(t))^T \in R^2$ is the state vector of the network, the activation function $f(y(t)) = (f_1(y_1(t)), f_2(y_2(t)))^T$ with $f_i(y_i) = 0.2(|y_i + 1| - |y_i - 1|)(i = 1, 2)$, obviously, the external input vector $I(t) = (0, 0)^T$; and the other matrices are as follows:

$$C = \begin{bmatrix} 1 & 0 \\ 0 & 1 \end{bmatrix}, A = \begin{bmatrix} 1.78 & 20 \\ 0.1 & 1.78 \end{bmatrix}, B = \begin{bmatrix} -1.8 & 0.1 \\ 0.1 & -1.43 \end{bmatrix},$$

$\mu_1 = 0.6, \mu_2 = 0.32, \bar{d}_1 = 1, \bar{d}_2 = 1$, the dynamical chaotic behavior with initial conditions $y_1(s) = 0.1, y_2(s) = 0.1$ is shown in Fig.1.

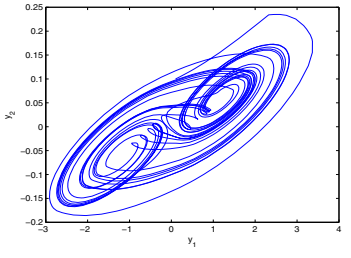

Fig. 1. The chaotic trajectory of model (14)

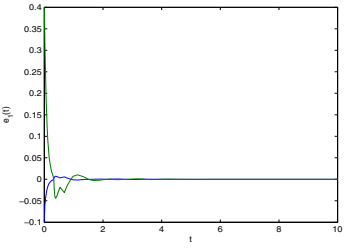

Fig. 2. Synchronization errors of $e_1(t)$

4.2 The Global Synchronization of Complex System

Now, consider the dynamical system consisting of hybrid coupling model (2), Choose the following matrix:

$$L^{(1)} = \begin{bmatrix} -4 & 2 & 2 \\ 2 & -4 & 2 \\ 2 & 2 & -4 \end{bmatrix}, L^{(2)} = \begin{bmatrix} -2 & 1 & 1 \\ 1 & -2 & 1 \\ 1 & 1 & -2 \end{bmatrix}, \Gamma_1 = \begin{bmatrix} 2 & 0 \\ 0 & 2 \end{bmatrix}, \Gamma_2 = \begin{bmatrix} 1 & 0 \\ 0 & 1 \end{bmatrix}$$

By applying the MATLAB LMI Control Toolbox, the feasible solutions can be solved as:

$$P_1 = \begin{bmatrix} 0.0503 & -0.0209 \\ -0.0209 & 1.0491 \end{bmatrix}, P_2 = \begin{bmatrix} 0.5680 & -0.2930 \\ -0.2930 & 11.7822 \end{bmatrix}, P_3 = \begin{bmatrix} 0.2086 & -0.5280 \\ -0.5280 & 2.0533 \end{bmatrix},$$

$$P_4 = \begin{bmatrix} 0.5390 & -0.2230 \\ -0.2230 & 11.0337 \end{bmatrix}, P_5 = \begin{bmatrix} 0.1524 & -0.2908 \\ -0.2908 & 1.9874 \end{bmatrix}, S_1 = \begin{bmatrix} 0.0179 & -0.0790 \\ -0.0790 & 0.5684 \end{bmatrix},$$

$$S_2 = \begin{bmatrix} 0.0170 & -0.0790 \\ -0.0790 & 0.5484 \end{bmatrix}, S_3 = \begin{bmatrix} 0.1089 & -0.2963 \\ -0.2963 & 1.3770 \end{bmatrix}, S_4 = \begin{bmatrix} 0.1080 & -0.2963 \\ -0.2963 & 1.3670 \end{bmatrix},$$

According to Theorem 1, the system (2) can achieve global synchronization. And the synchronization error is illustrated in Fig.2, where $e_j(t) = (x_{ij}(t) - x_{1j}(t)), i = 2, 3.$

5 Conclusion

In this paper, the coupled neural networks with successive time-delay components is proposed. Based on the Lyapunov functional method and Kronecker product properties, a new criterion has been developed to ensure the dynamical networks of global synchronization. The derived result, which in term of linear matrix inequalities, can be easily checked. Finally, a typical chaotic CNN is given to show the effectiveness of the proposed result.

Acknowledgment

This work was supported by the National Natural Science Foundation of China(60774093), the National High Technology Research and Development Program (2009AA04Z127), Program for New Century Excellent Talents in University (NCET-08-0101).

References

1. Ensari, T., Arik, S.: New results for robust stability of dynamical neural networks with discrete time delays. Expert Systems with Applications 02, 195–197 (2010)
2. Yoo, S.J., Park, J.B.: Neural-network-based decentralized adaptive control for a class of large-scale nonlinear systems with unknown Time-Varying Delays. IEEE Trans. Syst., Man, Cybern. B, Cybern. 39, 1316–1323 (2009)
3. Wang, Z., Liu, Y., Liu, X.: On global asymptotic stability of neural networks with discrete and distributed delays. Phys. Lett. A 345, 299–308 (2005)
4. Wang, Z., Liu, Y., Li, M., Liu, X.: Stability analysis for stochastic Cohen-Grossberg neural networks with mixed time delays. IEEE Trans. Neural Netw. 17, 814–820 (2006)
5. Huang, H., Feng, G.: Synchronization of nonidentical chaotic neural networks with time delays. Neural networks 22, 869–874 (2009)
6. Zhou, T.S., Lü, J.H., Chen, G., Tang, Y.: Synchronization stability of three chaotic systems with linear coupling. Phys. Lett. A 301, 231–240 (2002)
7. Wu, C.W.: Synchronization in arrays of coupled nonlinear systems with delay and nonreciprocal time-varying coupling. IEEE Trans. Circuits Syst. II, Exp. Briefs 52, 282–286 (2005)
8. Lu, Q., Ho, D.W.C.: Globally exponential synchronization in an array of asymmetric coupled neural networks. Phys. Lett. A 369, 444–451 (2007)
9. Gao, H., Chen, T., Lam, J.: A new delay system approach to network-based control. Automatica 44, 39–52 (2008)
10. Zhao, Y., Gao, H., Mou, S.: Asymptotic stability analysis of neural networks with successive time delay components. Neurocomputing 71, 2848–2856 (2008)
11. Liu, Y., Wang, Z., Liang, J., Liu, X.: Synchronization and State Estimation for Discrete-Time Complex Networks With Distributed Delays. IEEE Trans. Syst., Man, Cybern. B, Cybern. 38, 1026–1031 (2008)

Colour Image Segmentation Based on a Spiking Neural Network Model Inspired by the Visual System

QingXiang Wu, T.M. McGinnity, Liam Maguire, G.D. Valderrama-Gonzalez, and Patrick Dempster

Intelligent Systems Research Centre, University of Ulster at Magee Campus
Derry, BT48 7JL, Northern Ireland, UK
{q.wu,tm.mcginnity,lp.maguire,g.valderrama}@ulster.ac.uk
pa.dempster@ulster.ac.uk

Abstract. The human visual system demonstrates powerful image processing functionalities. Inspired by the visual system, a spiking neural network is proposed to segment visual images. The network is constructed in the two parts. The first part is a spiking neural network which is composed of photon receptors, cone and rod cells, and ON/OFF ganglion cells. Colour features can be extracted and passed through different ON/OFF pathways. The second part is a BP neural network which is trained to recognize the colour features and segment the visual image. The network has been successfully applied to segment leukocytes from blood smeared images.

Keywords: Spiking neural networks, image segmentation, visual system, visual image.

1 Introduction

The human visual system demonstrates powerful image processing functionalities. The retina contains complex circuits of neurons that extract salient information from visual inputs. Signals from photoreceptors are processed by retinal interneurons, integrated by retinal ganglion cells and sent to the brain by axons of retinal ganglion cells. Different cells respond to different visual features, such as light intensity, colour or moving objects [1–5]. Mammalian retinas contain approximately 55 distinct cell types, each with a different function [1]. Biological evidence shows that the retina contains two forms of photosensitive neurons, i.e. rods and cones [6]. Rod cells are highly sensitive to light and respond in dim light and dark conditions. Three types of cones have primary sensitivity of red, green, and blue lights. Inspired by the roles of rods and cones in retina, a spiking neural network model is proposed to separate colour images into different colour features which are provided through different ON/OFF pathways. An error back-propagation (BP) neural network is trained to segment the visual image.

The remainder of this paper is organized as follows. In Section 2, the architecture of the neural network is proposed to extract colour features and a BP neural network is

D.-S. Huang et al. (Eds.): ICIC 2010, LNCS 6215, pp. 49–57, 2010.

used to identify the colour features and segment the visual image. The spiking neural network model is based on simplified conductance-based integrate-and-fire neurons. The behaviours of the neural network are governed by a set of equations discussed in Section 3. Segmentation algorithms are introduced in Section 4. Experimental results are presented in Section 5. Section 6 gives a conclusion and a topic for further study.

2 Spiking Neural Network Model to Extract Colour Features

The human visual system performs feature extraction very efficiently. Neuroscientists have found that there are various receptive fields from simple cells in the striate cortex to those of the retina and lateral geniculate nucleus [6]. Inspired by the roles of rods and cones in retina, a spiking neural network is proposed to extract colour features and a colour image is separated by eight ON/OFF pathways. The eight features are then used to segment a colour image based on a BP neural network. The architecture of the spiking neural network is shown as in Fig.1.

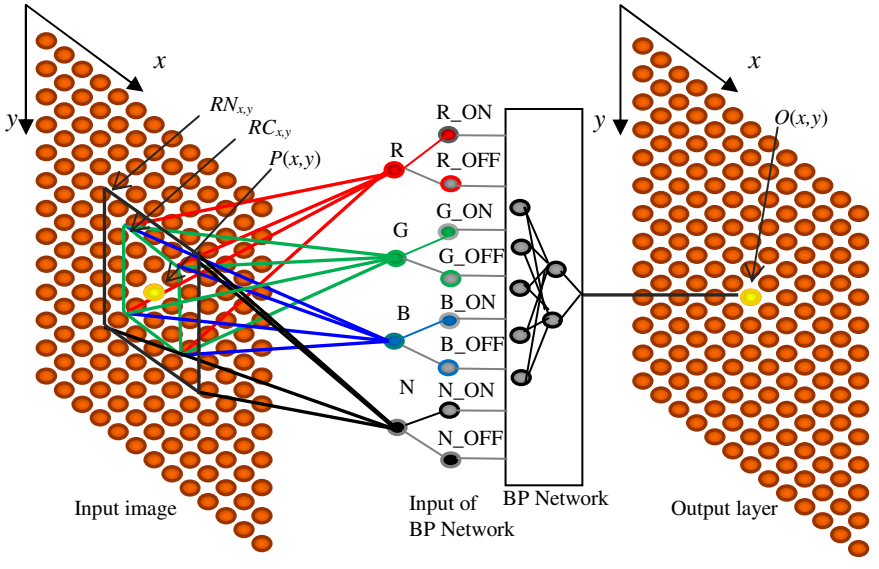

Fig. 1. Spiking neural network for eight ON/OFF pathways and BP neural network

Let the input image dimension be $P \times Q$. A colour pixel in the image is labeled as $P(x,y)$, where $x=1,2,\ldots,P$, $y=1,2,\ldots,Q$. The output layer is feature classification neurons with the same dimension as input image. The output value of neuron $O(x,y)$ is determined by the BP neural network according to outputs of eight ON/OFF ganglion cell pathways with receptive fields centred at $P(x,y)$ in the input image. Since biological cones have small receptive fields and have high spatial resolution, the small receptive field $RC_{x,y}$ is designed for three types of cones corresponding to three colours R, G, and B. Three types of receptive fields for cones are labeled with R, G, and B,

which form six ON/OFF pathways. The R receptive field responds to red light. The G receptive field responds to green light. The B receptive field responds to blue light. Biological rods with large receptive field are sensitive to brightness instead of colours. The N receptive field is designed to simulate rods which respond to gray scale in the large receptive field $RN_{x,y}$ and forms two ON/OFF pathways. The eight features from the eight ON/OFF pathways are used to train the BP neural network. After training, the segmentation of the colour image can be drawn in the output image $O(x,y)$. Therefore, the neural network can identify specific areas in the colour image. The algorithm is detailed in the next sections.

3 Spiking Neuron Model and Simulation Algorithms

Considering computational cost, a simplified conductance-based integrate-and-fire neuron model is used to simulate the network. Suppose that $P_{x,y}(t)$ represents the strength of red light from an image pixel at a point (x, y) at time t. Let $R_{x,y}(t)$ represent the normalized strength i.e. $R_{x,y}(t) = P_{x,y}(t)/P_{\max}$. Suppose that each red photon receptor transfers the red-light strength to a synapse current $I_{R\_ON(x,y)}(t)$. The synapse current can be represented as follows:

$$I_{R\_ON(x,y)} = \alpha R_{x,y}(t) \tag{1}$$

where α is a constant for transformation from the red-light strength to current. For the OFF pathway, the synapse current can be represented as follows:

$$I_{R\_OFF(x,y)} = \beta(1 - R_{x,y}(t)) \tag{2}$$

where β is a constant for transformation for the OFF pathway. According to the integrate-and-fire neuron model [7-13], the potential of an ON neuron $R\_ON(x, y)$ is governed by the following equation:

$$\begin{aligned} c\frac{dv_{R\_ON(x,y)}(t)}{dt} = g_l(E_l - v_{R\_ON(x,y)}(t)) + \sum_{(x',y')\in RC_{x,y}} w_{x',y'} I_{R\_ON(x',y')}(t) \\ \sum_{(x^*,y^*)\in RF^*_{x,y}} w_{\text{lateral}} S_{R\_ON(x^*,y^*)}(t) + I_0, \end{aligned} \tag{3}$$

where g_l is the membrane conductance, E_l is the reverse potential, $v_{R\_ON(x,y)}(t)$ is the membrane potential of the neuron $R\_ON(x, y)$, c represents the capacitance of the membrane, I_0 is simulated by an average current produced by background noise, $w_{lateral}$ is the synapse strength of lateral connections from the neghbourhood neurons, $RF^*_{x,y}$ is a set of neighborhood neurons, and $S_{R\_ON(x^*,y^*)}(t)$ is a spike train from neighborhood neurons. $W_{x',y'}$ is used to simulate the centre-ON and surround-OFF receptive field, which is represented by the following expression.

$$w_{x',y'} = w_0 e^{-\frac{(x-x')^2+(y-y')^2}{\delta^2}} - w_1 e^{-\frac{(\sqrt{(x-x')^2+(y-y')^2}-\Delta)^2}{\delta^2}} \tag{4}$$

where w_0 and w_1 are used to determine the maximal value of the weight distribution, δ is a decay constant for the distribution away from the centre point (x,y), Δ is corresponds to the radius of the OFF surround circle.

If the membrane potential passes a threshold v_{th}, then the neuron generates a spike. Let $S_{R\_ON(x,y)}(t)$ represent the spike train generated by the neuron such as that:

$$S_{R\_ON(x,\,y)}(t) = \begin{cases} 1 & \text{if neuron } R\_ON(x,y) \text{ fires at time } t. \\ 0 & \text{if neuron } R\_ON(x,y) \text{ does not fire at time } t. \end{cases} \tag{5}$$

Similar representation is used to $S_{R\_OFF(x,Y)}(t)$ for The firing rate for the neuron $F_{R\_ON(x,y)}$ is calculated by the following expression:

$$F_{R\_ON(x,y)}(t) = \frac{1}{T}\sum_{t}^{t+T} S_{R\_ON(x,y)}(t) \tag{6}$$

By analogy, using synapse current, a firing rate of R_OFF neuron can be obtained.

$$F_{R\_OFF(x,y)}(t) = \frac{1}{T}\sum_{t}^{t+T} S_{R\_OFF(x,y)}(t) \tag{7}$$

For colour green and blue, we can have

$$F_{G\_ON(x,y)}(t) = \frac{1}{T}\sum_{t}^{t+T} S_{G\_ON(x,y)}(t) \tag{8}$$

$$F_{G\_OFF(x,y)}(t) = \frac{1}{T}\sum_{t}^{t+T} S_{G\_OFF(x,y)}(t) \tag{9}$$

$$F_{B\_ON(x,y)}(t) = \frac{1}{T}\sum_{t}^{t+T} S_{B\_ON(x,y)}(t) \tag{10}$$

$$F_{B\_OFF(x,y)}(t) = \frac{1}{T}\sum_{t}^{t+T} S_{B\_OFF(x,y)}(t) \tag{11}$$

Let $N_{x,y}(t)$ represent the normalized value of the gray scale image at the point (x, y) at time t. For neuron $N\_ON(x,y)$, we have

$$I_{N\_ON(x,y)} = \alpha N_{x,y}(t). \tag{12}$$

$$\begin{aligned} c\frac{dv_{N\_ON(x,y)}(t)}{dt} &= g_l(E_l - v_{N\_ON(x,y)}(t)) + \sum_{(x',y')\in RN_{x,y}} w_{x',y'} I_{N\_ON(x',y')}(t) \\ &+ \sum_{(x^*,y^*)\in RF^*_{x,y}} w_{\text{lateral}} S_{N\_ON(x^*,y^*)}(t) + I_0. \end{aligned} \tag{13}$$

$$S_{N\_ON(x,\,y)}(t) = \begin{cases} 1 & \text{if neuron } N\_ON(x,y) \text{ fires at time } t. \\ 0 & \text{if neuron } N\_ON(x,y) \text{ does not fire at time } t. \end{cases} \tag{14}$$

The firing rate for the neuron $F_{N\_ON\,(x,y)}$ is calculated by the following expression:

$$F_{N\_ON(x,y)}(t) = \frac{1}{T}\sum_{t}^{t+T} S_{N\_ON(x,y)}(t) \tag{15}$$

Using the synapse current in the OFF pathway,

$$I_{N\_OFF(x,y)} = \beta(1 - N_{x,y}(t)). \tag{16}$$

By analog, firing rate of N_OFF neuron can be obtained as follows.

$$F_{N\_OFF(x,y)}(t) = \frac{1}{T}\sum_{t}^{t+T} S_{N\_OFF(x,y)}(t) \tag{17}$$

4. Segmentation Algorithms

Suppose $O(x,y)$ is an output of the BP neural network. Let ($F_{R\_ON(x,y)}$, $F_{R\_OFF(x,y)}$, $F_{G\_ON(x,y)}$, $F_{G\_OFF(x,y)}$, $F_{B\_ON(x,y)}$, $F_{B\_OFF(x,y)}$, $F_{N\_ON(x,y)}$, $F_{N\_OFF(x,y)}$) represent the input vectors of the network. The network is represented by the following expression.

$$\begin{aligned} O(x,y) = NET(&F_{R\_ON(x,y)}, F_{R\_OFF(x,y)}, F_{G\_ON(x,y)}, F_{G\_OFF(x,y)}, \\ &F_{B\_ON(x,y)}, F_{B\_OFF(x,y)}, F_{N\_ON(x,y)}, F_{N\_OFF(x,y)}) \end{aligned} \tag{18}$$

$O(x,y)$ can be defined as a classification label for a segmentation area. For example, this approach is applied to segment leukocytes from a blood smeared image. Four label numbers {0, 1, 2, 3} are defined. "0" represents background in a smear image. "1" represents erythrocyte. "2" represents cytoplasm of leukocytes. "3" represents nucleus of leukocytes. Biological rods have larger receptive fields than cones. In the experiments, the dimension of receptive field $RC_{x,y}$ is set to 5×5 and dimension of receptive field $RN_{x,y}$ is 7×7. These receptive fields can be adjusted according to different images. The larger the receptive fields, the more immune to noise, with trade off, loss of sharpness at the border of the leukocytes. In order to train the network, a training data set is sampled from four areas i.e. background, erythrocyte, cytoplasm, and nucleus areas, and at the same time a classification number for the corresponding area is assigned to each sample in the training set. If the network is trained with the training data set, the network can identify which area the image pixel belongs to. A set of masks is obtained in the output layer. The algorithm for segmentation of leukocytes is as follows.

Algorithm 1. Segmentation of leukocytes

1. Load a colour image
2. For x=3 to P-2
3. For y=3 to Q-2
4. Calculate eight firing rates.
5. Calculate $O(x, y) = NET(F_{R\_ON(x,y)}, F_{R\_OFF(x,y)}, F_{G\_ON(x,y)}, F_{G\_OFF(x,y)}, F_{B\_ON(x,y)}, F_{B\_OFF(x,y)}, F_{N\_ON(x,y)}, F_{N\_OFF(x,y)})$.
6. Case= (O(x,y)); switch to Case 1 Mask1(x,y)=1; Case 2 Mask2(x,y)=1; case 3 Mask3(x,y)=1; Otherwise Mask0(x,y)=1.
7. End for
8. End for

This algorithm gives four Masks corresponding to background, erythrocyte, cytoplasm, and nucleus areas. In order to remove noise, the objects with area less than a minimum size threshold (e.g. 200 pixels) are removed from *Mask0*, *Mask1*, *Mask2*, and *Mask3* respectively. Using the following algorithm, four areas can be separated in different images. Finally the algorithm 2 is used to obtain four separate areas.

Algorithm 2. Separate four images

1. Load original image P(x,y)
2. For x=1 to P
3. For y=1 to Q
4. P_background(x,y)= Mask0(x,y)* P(x,y).
5. P_erythrocyte (x,y)= Mask1(x,y)* P(x,y).
6. P_ cytoplasm (x,y)= Mask2(x,y)* P(x,y).
7. P_ nucleus (x,y)= Mask3(x,y)* P(x,y).
8. End for
9. End for

5 Experimental Results

The spiking neural network is simulated in Matlab using the Euler method with a time step of 0.1 ms. Corresponding to biological neurons [10], the following parameters for the network were used in the experiments. v_{th} = -60 mv. E_l= -70 mv. g_l=1.0 μs/mm^2. c=8 nF/mm^2. τ = 4ms. T=400ms. These parameters can be adjusted to get a good quality output image. α=4.8. β=11.2. I_0=7μA. $w_{Lateral}$=0.01. w_0=1. w_1=1/3. Δ=1.5. δ=1.5. These parameters can be determined by trial/error method according to single neuron behaviours. A blood smeared image, which is shown in the left of Fig. 2, presents to the spiking neural network. Eight images are obtained corresponding to the eight ON/OFF pathways as shown in the right of Fig. 2. It can be seen that different ON/OFF pathways separate different areas. For example, erythrocytes and cytoplasm

areas are difficult to identify in a gray scale image (see White_ON), but they are easly identified in both the Red_on and Green_on images.

Each colour pixel in the input image can be separated into eight values corresponding to eight ON/OFF pathways. The BP network is defined as eight inputs, 6 hidden neurons and one output neuron. Sampling points are obtained as shown in Fig. 3, and used to train the BP neural network. The stars indicate sample points for background and the target output value of the network is set to '0'. The squares indicate the sample points for erythrocytes, and the target output value of the network is set to '1'. By analogy, crosses indicate cytoplasm, and the target output value of the network is set to '2'. Circles indicate the sample points for nucleus of leukocytes and the target output value of the network is set to '3'. A training set is obtained by sampling about 20 points in each area. The Levenberg-Marquardt optimization is used as the training algorithm in this paper. Changes of error rate are shown in the right panel of Fig. 3.

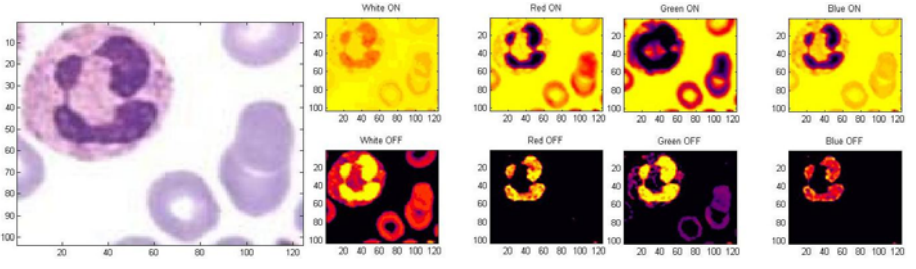

Fig. 2. Original smeared image and eight images in the eight ON/OFF pathways

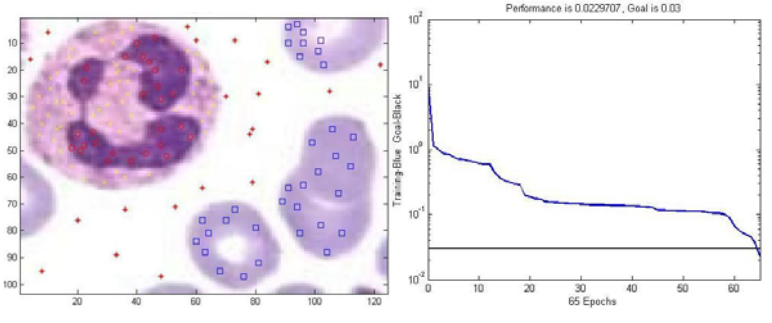

Fig. 3. Sampling points and errors in the training process

The trained network is applied in algorithm 1 to obtain to obtain *Mask0*, *Mask1*, *Mask2*, and *Mask3*. *Mask0* corresponds to background. Using the Matlab function e.g. *bwareaopen* (*Mask1, 200*), the objects with area less than 200 pixels are regarded as noise to be removed from *Mask0*, *Mask1*, *Mask2*, and *Mask3*. Clear masks are obtained in the left panel of Fig. 4. Applying algorithm 2, the separated images are obtained in the right panel of Fig. 4.

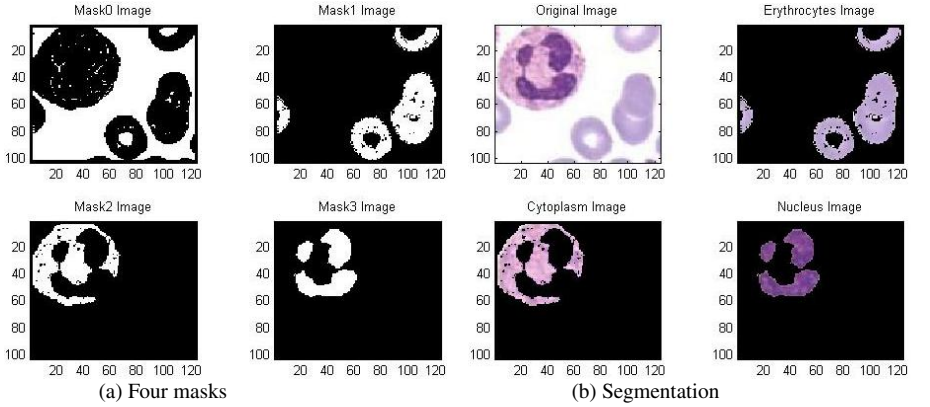

(a) Four masks (b) Segmentation

Fig. 4. Results of segmentation

6 Conclusion and Further Work

Using eight ON/OFF pathways inspired by the visual system, a spiking neural network is proposed to extract colour features from a visual image. An integrate-and-fire spiking neuron model is used to construct and simulate the spiking neural network. As multiple colour ON/OFF pathways have been used, it is possible to separate some areas with some gray scale values. Owing to the incorporation of lateral connections from neighborhood neurons, the network enables feature binding to form similar firing patterns. The eight ON/OFF colour values provide specific features to the BP neural network to allow it to identify areas. Results show that the approach can be successfully applied to segment leukocytes from a blood smeared image. Additionally other interesting features such as texture and shape can be easily identified by the visual system. Further research will be conducted into developing networks to efficiently extract these features, using the biological retina model as inspiration.

References

1. Masland, R.H.: The fundamental plan of the retina. Nature Neurosci. 4, 877–886 (2001)
2. Wassle, H.: Parallel processing in the mammalian retina. Nature Rev. Neurosci. 5, 747–757 (2004)
3. Nelson, R., Kolb, H.: On and off pathways in the vertebrate retina and visual system. In: Chalupa, L.M., Werner, J.S. (eds.) The Visual Neurosciences, pp. 260–278. MIT Press, Cambridge (2003)
4. Demb, J.B.: Cellular mechanisms for direction selectivity in the retina. Neuron 55, 179–186 (2007)
5. Taylor, W.R., Vaney, D.I.: New directions in retinal research. Trends Neurosci. 26, 379–385 (2003)
6. Kandel, E.R., Shwartz, J.H.: Principles of neural science. Edward Amold Ltd. (1981)
7. Koch, C.: Biophysics of Computation: Information Processing in Single Neurons. Oxford University Press, Oxford (1999)

8. Dayan, P., Abbott, L.F.: Theoretical Neuroscience: Computational and Mathematical Modeling of Neural Systems. The MIT Press, Cambridge (2001)
9. Gerstner, W., Kistler, W.: Spiking Neuron Models: Single Neurons, populations, Plasticity. Cambridge University Press, Cambridge (2002)
10. Wu, Q.X., McGinnity, T.M., Maguire, L.P., Belatreche, A., Glackin, B.: 2D Co-ordinate Transformation Based on a Spike Timing-Dependent Plasticity Learning Mechanism. Journal of Neural Networks 21, 1318–1327 (2008)
11. Wu, Q.X., McGinnity, T.M., Maguire, L.P., Belatreche, A., Glackin, B.: Processing Visual Stimuli Using Hierarchical Spiking Neural Networks. International Journal of Neurocomputing 71, 2055–2068 (2008)

The White Noise Impact on the Optimal Performance of the Hopfield Neural Network

Yaoqun Xu and Yulei Li

Institute of System Engineering, Harbin University of Commerce, 150028, Harbin, China
xuyq@hrbcu.edu.cn, sky_walker85@126.com

Abstract. Hopfield neural network (HNN) is an efficient optimization model, but it easily produces random noise. White noise is an ideal model and is more convenient in the mathematical analysis. This paper presents a new model of Hopfield neural network which is called White Noise Hopfield Neural Network. By introducing the white noise to the Hopfield neural network, we analyze the impact of noise on the neural network. The examples of the functional optimization and the traveling salesman problem (TSP) show as long as the appropriate adjustment Signal Noise Ratio (SNR), the performance of Hopfield network model for optimization has been greatly improved.

Keywords: White Noise; Hopfield Neural Network; Optimization Problems.

1 Introduction

Many optimization problems arising from science and technology are often difficult to solve entirely. Hopfield and Tank first applied the continuous-time, continuous-output Hopfield neural network (HNN) to solve TSP, thereby initiating a new approach to optimization problems. The Hopfield neural network [1], one of the well-known models of this type, converges to a stable equilibrium point due to its gradient decent dynamics; however, it causes sever local-minimum problems whenever it is applied to optimization problems [2-6]. In real applications, the Hopfield neural network so easily produces random noise because of its physical characteristics. Based on this common phenomenon in real applications, this paper introduces the white noise into the Hopfield neural network to simulate the actual application of the noise. White noise is the power spectral density in the entire frequency domain uniformly distributed noise. Strictly speaking, White noise is an ideal model, since the actual noise power spectral density can not have infinitely wide bandwidth, otherwise its average power will be infinite, which is physically unattainable. However, the white noise is more convenient in the mathematical analysis, so it is a powerful tool for system analysis. By means of adjusting the Signal Noise Ratio, this paper analyzes the noise impact on system and applies the model to optimization problems. Simulation results show that as long as the Signal Noise Ratio under certain range, the system still has a good optimization performance.

D.-S. Huang et al. (Eds.): ICIC 2010, LNCS 6215, pp. 58–65, 2010.

2 The Hopfield Neural Networks with White Noise

In this paper, the model of the Hopfield Neural Networks with White Noise is described as follows.

$$U_w = Gn(U) \tag{1}$$

$$V = 1/2(1+\tanh(U_w / U_0)) \tag{2}$$

$$V_w = Gn(V) \tag{3}$$

$$\mathrm{Gn}(\xi) = \mathrm{AWGN}(\xi, \mathrm{SNR}) \tag{4}$$

where U , V is the input and output of the Hopfield Neural Networks respectively, U_w , V_w is the input and output which has been interfered by the White Noise, Gn is the function which generates the Gauss White Noise, V is generated by the nonlinear function. In this model, the input and output of the neural networks has been interfered by the Gauss White Noise, the purpose is to study the white noise impact on the optimization performance of the Hopfield Neural Networks.

3 Application in Optimization Problems

Optimization problem is divided into functional optimization and combinatorial optimization, many practical problems can be converted into one of them to be solved. The objects of functional optimization are continuous variables within a certain range, while the objects of combinatorial optimization are discrete states in the solution space. In order to verify the Hopfield neural network with white noise is effective, it will be applied to functional optimization and combinatorial optimization problems respectively.

When using the Hopfield neural networks solve the optimization problems, the first should map the problems into a certain states of a kind of neural networks, these states may be the solution of the optimization problems; and then construct an Energy function E which is suited to the optimization problem. This E should be proportional to the cost function of the optimization problem. The general process of the Hopfield neural network for solving optimization is as follows:

1. For the unknown problem, select an appropriate representation make the neural network output correspond to the solution of the problem.
2. Construct energy function of the neural network, the minimum value is corresponding to the optimal solution.
3. From the energy function, we infer the neural network structure, that is, the weights of neurons and the bias input.
4. Establish the networks based on the network structure, the steady state is the optimal solution under certain conditions.

3.1 Continuous Function Optimization

We will use the Hopfield neural network with white noise in functional optimization to calculate the following function. The nonlinear optimization problem is as follows:

$$f(x_1, x_2) = (x_1 - 0.7)^2[(x_2 + 0.6)^2 + 0.1] + (x_2 - 0.5)^2[(x_1 + 0.4)^2 + 0.15] \quad (5)$$

The minimum of the function is 0, which is the global minimum of the objective function, and the corresponding coordinates are (0.7, 0.5). There are three local minimums: (0.6, 0.4), (0.6, 0.5) and (0.7, 0.4).

When the model proposed in this paper to solve the function, the parameters of the function to be optimized are set as follows: time step $\Delta t = 0.1$, $y_{1,2}(1) = 0.283$. Depending on the Signal Noise Ratio, the time evolution figures of the energy function and x_1, x_2 changes are shown as below:

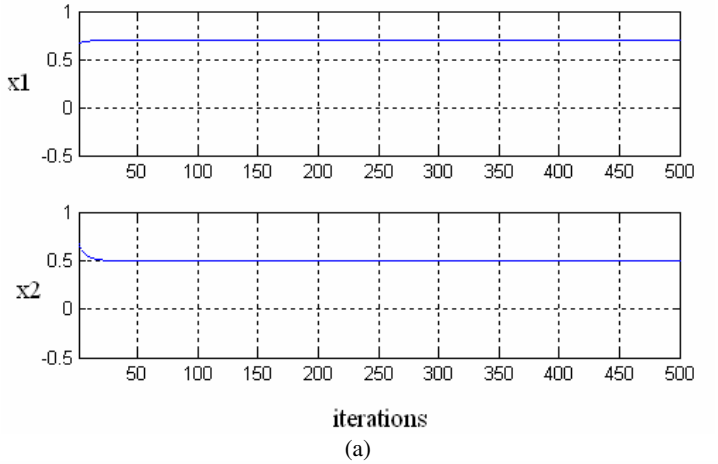

(a)

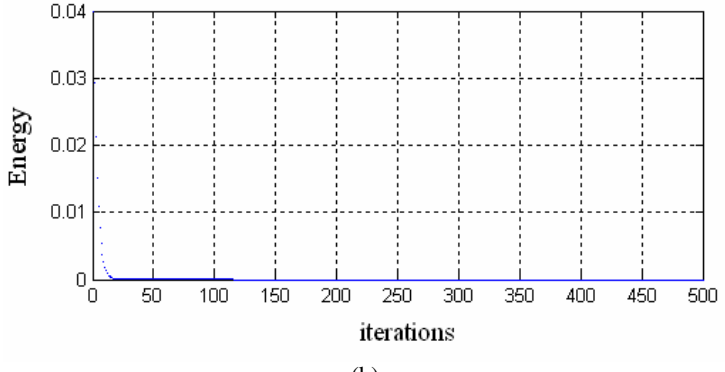

(b)

Fig. 1. (a) Evolutionary figure of state x1 and state x2 without noisy; (b) Evolutionary figure of energy function without noisy

From the time evolution of the function, we can see that the network first searches from a unstable state, and then begins to search with gradient descent. Finally, the network gradually reaches a steady state. The global minimum point is (0.7, 0.5) and the minimum value is 0.

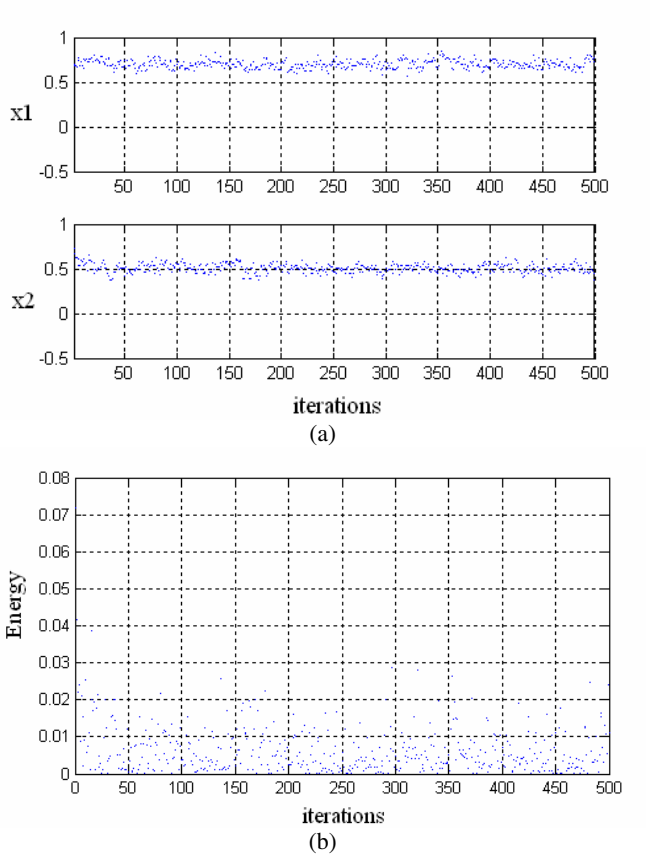

Fig. 2. (a) Evolutionary figure of state x1 and state x2 with noisy of SNR=30; (b) Evolutionary figure of energy function with noisy of SNR=30

The global minimum point is (0.7766, 0.4478) and the minimum value is 0.0112.

From the above experimental results, it can be concluded that the noise will cause the instability of the network model, and have an impact on the optimal performance. Especially when the SNR is less than 50, the noise has a great impact on solving ability. When the SNR is greater than 90, the noise has little impact on the network model, the optimal performance of the network model is close to the ideal environment without noise.

3.2 Application in Combinatorial Optimization

This paper applies the Hopfield neural network with white noise to 10-city traveling salesman problem (TSP). Traveling salesman problem is described as follows: Given n cities and the distance between each other, we seek the shortest route through them, visiting each once and only once and return the starting point.

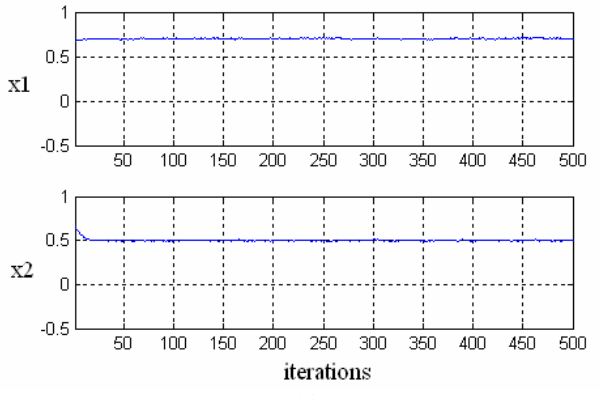

(a)

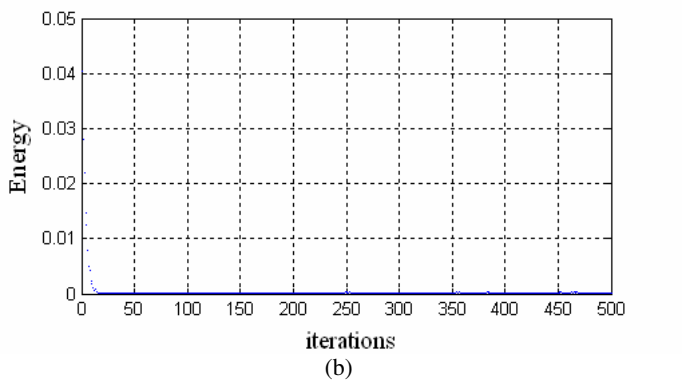

(b)

Fig. 3. (a) Evolutionary figure of state x1 and state x2 with noisy of SNR=50; (b) Evolutionary figure of energy function with noisy of SNR=50

The global minimum point is (0.6983, 0.4990) and the minimum value is 5.3560e-006.

An energy function reaching and satisfying all the constraints can be described as the following formula [7]. In the formula: V_{xi} represents the x th city will be visited after the other $(i-1)$ cities have been visited. d_{xy} is the distance between city x and y. Therefore, the global minimum value of E represents a shortest effective path.

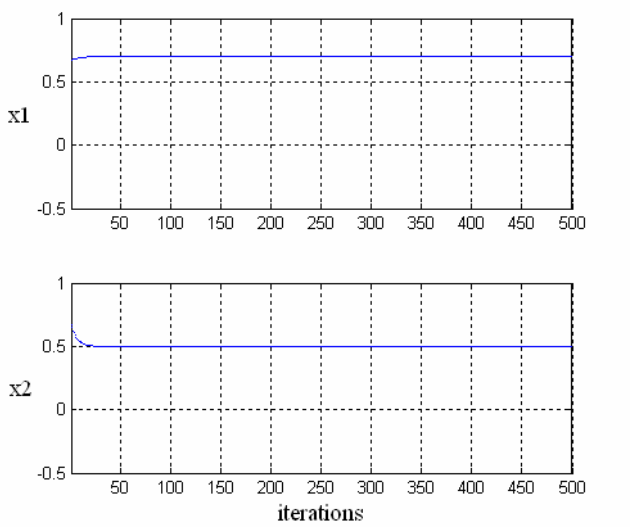

Fig. 4. Evolutionary figure of state x1 and state x2 with noisy of SNR=90

The global minimum point is (0.7000, 0.5000) and the minimum value is 6.2693e-010.

$$E = \frac{A}{2}\sum_{x=1}^{n}\left(\sum_{i=1}^{n}V_{xi}-1\right)^2 + \frac{B}{2}\sum_{x=1}^{n}\left(\sum_{i=1}^{n}V_{xi}-1\right)^2 + \frac{D}{2}\sum_{x=1}^{n}\sum_{y=1}^{n}\sum_{i=1}^{n}d_{xy}V_{xi}V_{y,i+1} \tag{6}$$

This paper adopts the following 10-city unitary coordinates:
(0.4, 0.4439),(0.2439, 0.1463),(0.1707, 0.2293),(0.2293, 0.716),(0.5171,0.9414), (0.8732,0.6536),(0.6878,0.5219),(0.8488,0.3609),(0.6683,0.2536),(0.6195,0.2634).
The shortest distance of the 10-city is 2.6776, as is seen in Fig.5.

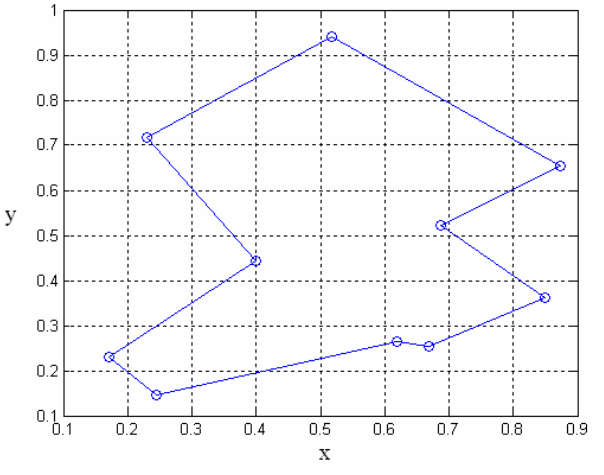

Fig. 5. The optimal solution of 10-city TSP

Solving the TSP problem with this model, the initialization parameters take the following values: $A = B = 1$, $D = 1$, $U_0 = 0.02$, the computer randomly initializes U. In the simulation experiment we use different SNR to solve the problem, and then summarize the experimental results. The results are shown in the following Table1. (VN= valid number; GN= global number; VP= valid percent; GP=global percent.)

As seen from Table 1, in the ideal case without noise, Hopfield neural network for solving TSP problems is easy to get a large number of invalid solution, and when introduce the appropriate noise, the capacity of Hopfield neural network to solve TSP problems has been improved, particularly control the SNR greater than 80, its optimal capabilities is obviously improved, and we also find when the SNR reaches a certain level, the optimal performance is not increasing as the SNR, but stable in a range. As the SNR is less than 50, the ability of the network model to solve the TSP declines. These data indicates that not all of the noise signal is useful, and can not to arbitrarily increase or decrease the noise, but should control the noise in a certain range. In practice, the noise signal should be controlled within a reasonable range, and by adjusting other parameters in order to make the network model has the strongest optimal performance.

Table 1. Results of 200 different initial conditions for different SNR on 10-city TSP

SNR	VN	GN	VP	GP
Non-noise	135	97	67.5%	48.5%
30	19	1	9.5%	0.5%
40	84	13	42%	6.5%
50	126	64	63%	32%
60	144	92	72%	46%
70	145	94	72.5%	47%
80	160	112	80%	56%
90	151	106	75.5%	53%
120	149	103	74.5%	51.5%
150	149	104	74.5%	52%
180	152	103	76%	51.5%

4 Conclusions

In real applications, Hopfield neural network so easily produces noise, and thus affect the capacity of the system in different degrees. This paper introduces the white noise in the simulation to analyze the white noise impact on the Hopfield neural network. By using the Hopfield neural network with white noise in functional optimization and combinatorial optimization, we can find the appropriate noise to improve the optimization ability of Hopfield network is a great help. At the same time, different SNR has different effects on the optimal performance of the model. Finding the optimal SNR in order to optimize the model's ability to achieve the maximum will be our future research directions.

References

1. Hopfield, J.J.: Neural networks and physical systems with emergent collective computational abilities. Proc. Natl. Acad. Sci. 79, 2554–2558 (1982)
2. Wang, L., Zheng, D.: Study on TSP and Optimization Based on Hopfield Neural Network. Control and Decision 14, 671–674 (1999)
3. Chen, L., Aihara, K.: Chaotic Simulated Annealing by a Neural Network Model with Transient Chaos. Neural Networks 8, 915–930 (1995)
4. Wang, L.: Intelligence optimization algorithm and its application, pp. 4–5. Press of TUP (2001)
5. Xu, Y., Sun, Y., Hao, Y.: A Chaos Hopfield Network and its Application in Optimization Computation. Computer Engineering and Applications 38, 41–42 (2002)
6. Shuai, J., Chen, Z., Liu, R.: Self-evolution Neural Model. Physics Letters A 221, 311–316 (1996)
7. Sun, S., Zheng, J.: A Modified Algorithm and Theoretical Analysis for Hopfield Network Solving TSP. Acta Electronica Sinica 1, 73–78 (1995)

The Study and Realization of Virtual Organization File System Based on DHT Technology

Jiqing Liu[1], Jinhua Huang[2], and Chen Xing[3]

[1,2] Wuhan Institute of Shipbuilding Technology, Wuhan, Hubei, 430050, China
[3] Zhejiang Water Conservancy and Hydropower College, Hangzhou, Zhejiang, 310018, China
LJQ6521@public.wh.hb.cn, Angela_icec@yahoo.cm.cn

Abstract. Virtual Organization File System (VOFS) allows users from different virtual organizations sharing and accessing files through the Internet. It is a dynamic file sharing system and quite different from conventional file sharing solutions. However, All peers in VOFS are global aware. For maintaining this global aware, peers of VOFS need abundant bandwidth and storage space. This paper tries to build a new version of VOFS based on DHT to overcome the old one's shortage. Since global aware costs a lot of resources, peers in the new DHT-based version of VOFS will not be global aware, each peer just knows part of entire namespace. This new version can help VOFS to reduce communication burden and balance requirement of storage space and can be tested in actual grid system effectively.

Keywords: Grid, Distributed Hash Table (DHT), Chord, Virtual Organization File System(VOFS), P2P network, Peer.

1 Introduction

Grid is a base architecture and a burgeoning conception which is developing rapidly in modern communication technology. It is defined as relative problems-solving and resource-sharing on dynamic virtual organization [1]. For it always faces problems in distributed and heterogeneous environment, grid system sets up a virtual lamellate layer on the available systems to shield the difference in understratum systems and provides the end user a sheer entire namespace [2]. So in distributed Virtual Organization File System(VOFS), all VO-members know and maintain entire namespace and other peers' status. This duplicated data can accelerates file accessing operation; but disk space requirement will be a problem when the file tree grows huge. And communication burden and synchronizing between peers are also problems. Once the VOFS file tree is changed, all peers of VOFS have to be notified. In a Distributed VOFS which has N peers, an expose operation needs more than 2N messages [3]. It is heavy burden for the peer who actives the expose operation, the peer might runs out of its bandwidth in short time for sending those notifications. Building a DHT-based VOFS can solves these problems mentioned above.

Distributed Hash Table [4] is a powerful tool, its ring structure with topologies fits for files sharing and flow-media transferring very well [5].It is popularly used in P2P

D.-S. Huang et al. (Eds.): ICIC 2010, LNCS 6215, pp. 66–71, 2010.

networks. By applying DHT, VOFS can splits file tree into parts, and allocates these fragments to different peers. Each peer of VOFS keeps part of whole file tree; it can balance the space cost and lower the disk space requirement of being a VO-member of VOFS. DHT-based VOFS doesn't like Distributed VOFS, each resource has some specific peers to maintain its status, not all peers. By using uniform algorithm, peers in VOFS can easily locate the peers who maintain the target resource's status. If VOFS tree map is changed, only peers who related with changed part should be notified and update the status. It saves abundant of communication inside VOFS.

2 Conceiving and Realization of DHT-Based VOFS

VO-members of DHT-based VOFS share resource with others. There is a hierarchical virtual file tree in this system[6], members can expose or unexpose resource into this tree, only VO-members has the right to access the tree and exposed resource in this tree. One major purpose of building DHT-based VOFS is balancing disk cost of VOFS system, two kinds of data in VOFS which consume disk space can be hashed: metadata and file resource. We choose only using metadata as DHT's value. No peer knows entire namespace, each peer keeps part of VOFS file tree map.

Strategy of resource storage is no different with Distributed VOFS. Peers only have right to expose and unexpose the resource they own. And the peer who exposes a resource has the responsibility of providing access service of this resource. It doesn't like conventional P2P file sharing system which split resource file into parts and distributes these parts around whole network[7]-[11].

2.1 Chord Ring Management

Chord is a distributed lookup protocol. The main purpose of Chord is providing a service that locates target node by a given key. For Chord, consistent hashing is heart. Each node in Chord is assigned a key by consistent hash function, consistent hash function uses base hash algorithm, e.g. SHA-1, to get the key. Normally, Chord chooses hashing node's IP address to generate the key for a node, each node in Chord has its own unique key. Chord makes all nodes into a ring by the numeric order of their keys. Node with bigger key is successor of the node with smaller key, and the smaller node is its predecessor.

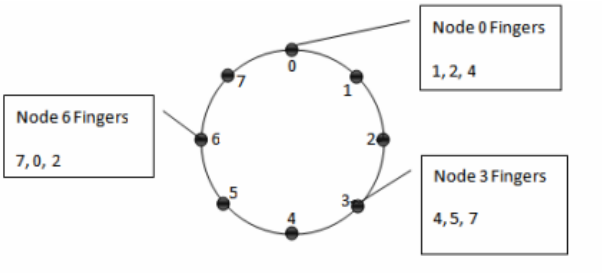

Fig. 1. Fingers for nodes

To speed up lookup operation, each node in Chord maintains a routing table called *finger table*. The entry with index *i* in node N's finger table, it keeps the location of node N.successor(2^{i-1}). Figure 1 shows an example of finger table of simple ring.

DHT-based VOFS utilizes Chord as lookup function. Each peer has its own unique ID to identify itself. This ID is generated by hashing peer's IP address including port number, which guarantees no two IDs are the same. Depending on different hash algorithms, the IDs might be geographic related or not. In DHT-based VOFS, we just utilize the simple algorithm to generate those IDs, so peers have similar IP addresses will be granted close IDs, that means these IDs are geographic related.

2.2 Storage of VOFS Path

VOFS path is used to indicate and locate the position of resource in VOFS file tree, and also is used to record and generate VO file tree map. There are two database files recording resource location information: *local.db* and *dht.db*.

(1) local.db

Each peer who used exposed resource has this file. It is the connection between practical resource and VOFS path. The content of this file is a hash map, each entry of this hash map has two tuples: local path and VOFS path. Local path represents the location of exposed resource in local file system.

(2) dht.db

This file is the connection between exposed resource and its host. The content of this file is also a hash map. The key of this map is VOFS path of a kind of resource, and the DHT_ENTRY is the value. Some information of resource is encapsulated in DHT_ENTRY, e.g. host address, resource type (directory or file).

Peers are completely free to modify the *local.db*, once a peer exposes or unexposes a resource in its local disk; it just adds or removes an entry from the *local.db* locally. But operating *dht.db* is much more complicated. Unlike *local.db*, the peer takes responsibility of maintaining the entry of *dht.db* that represents an exposed resource might not be the same peer that exposed the resource.

Table 1. Metadata table view

local.db	dht.db
<VOFS_PATH, LOCAL_PATH>	<VOFS_PATH, DHT_ENTRY>

Peer maintains DHT entry of a resource is selected by utilizing the same hash algorithm which used to generate peers' IDs. When a resource is exposed, system grants a Resource ID (RID) to it, this RID is generated by hashing resource's VOFS path. Then the DHT entry about this resource is sent to the peer whose ID is bigger and closest to this RID. And some replicas of this entry will be sent to the target peer's successors, these replicas are used to improve VOFS's reliability.

When peer joins or leaves, those related DHT entries should be allocated to new appropriate peers. New peers for Chord ring don't actively try to get those DHT entries that should be reallocated. When a new peer comes online and joins Chord ring, its closest successor browses its *dht.db* to see whether there are entries should be transmit to this new predecessor or not. If these entries exist, successor will transmit these DHT entries to the new peer. When peer leaves, it should send all DHT entries stored in it to its closest successor before it get offline. And DHT-based VOFS utilizes replicas of VOFS path entries to solve peer's crash, even if a peer crashes, other peers can still find DHT entries from its successors.

2.3 VOFS File Tree Browsing

We used a new solution to solve tree browsing problem. The main idea of this solution is maintaining separate sub-path metadata in VOFS, and using this metadata to provide fast and accurate browse service.

There is a file *sub_path.db* for storing sub-path metadata; the content of *sub_path.db* is hash map. The key of an entry of sub-path hash map is VOFS path of a resource, and the value is that key's parent path. Table 2 shows an example of *sub_path.db*.

There is a strict rule for allocating this sub-path metadata, not any peer can stores this kind of metadata. The peer who stores an entry of sub-path metadata is decided by the same hash algorithm that is used to generate peer ID and RID. Sub-path metadata is created and stored when peer exposes new resource. When a peer tries to expose a new resource, VOFS decomposes this new resource's VOFS path, finds all parent-children relationships in this VOFS path, and then allocate these sub-path metadata to corresponding peers.

For illustrating this solution, here is an example of creating and allocating sub-path metadata of a new resource with VOFS path "/user_1/home/a.txt", and the Chord ring is showed in Figure 2. Assumes that peer with ID 100 tries to expose this resource, there are three levels hypotaxis in this resource's VOFS path, and Table 3 shows them. VOFS hashes the first sub-path "/user_1/home/a.txt", and get the RID 9 for this sub-path. From Figure 2, we can see peer who has bigger and the closest ID with RID 9 is Peer 12, so system allocates the top entry of Table 3 in Peer 12. And similar storing for the left two pairs, the peers who store these three path pairs might be same one or not, it depends on the hash algorithm. Like other metadata, sub-path metadata also be replicated to enhance its reliability, its replicas are allocated to several successors of the host of sub-path metadata. Figure 2 gives an illustration of this simple sub-path disposal.

Table 2. Example of subpath.db

Key	Value
/user_1/home/a.txt	/user_1/home
/user_1/home/picture	/user_1/home

Table 3. Hypotaxis pairs of "/ user_1/home/a.txt"

Sub-path	Parent Path
/user_1/home/a.txt	/user_1/home
/user_1/home	/user_1
/user_1	/

When a peer tries to observe a directory, like "/user_1", it sends a query to the peer who has the closest and bigger peer ID to the path "/user_1"'s resource ID. Once a peer receives the query, it observes its sub_path.db to see whether it has queried metadata of path "/user_1" or not, and sends the result back to the requester.

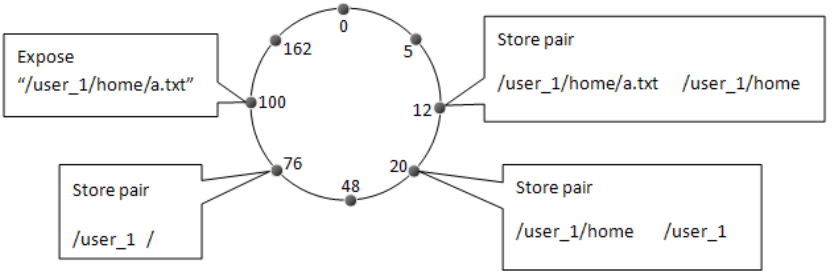

Fig. 2. Example of disposal subpath metadata

2.4 File Storage and Access

File Storage is completely borrowed from the Distributed VOFS. Only the peer who owns the resource has right to expose or unexpose the resource. The exposed resource is not copied to other peers in VOFS during the exposing process, it only be cached when a peer of VOFS tries to get it.

DHT-based VOFS file accessing is just like Distributed VOFS, the only thing that is modified is the way how to locate the peer who hosts target resource. In DHT-based VOFS, most of time peers have to query other peers to get metadata of target resource, and then use this metadata to locate the host of target resource and access the file. Since communication between requester and the metadata host peers costs time, file access of DHT-based VOFS is not as efficient as Distributed VOFS's.

3 Concluding Remarks

Both P2P network and grid are rapidly developing technologies in large-scale distributed systems. Though having different background and technological routes, these two aim similarly and tend to inter-gradate gradually. This paper provides the ideation and realization by applying DHT technology which is used popularly in P2P network to solve the problems in Virtual Organization File System for grid. By doing this can bring good features of P2P into grid system: taking the best use of self-organizing characteristic of P2P network, reducing management and allocation work efficiently, avoiding people's interference, etc. All these result in the flexibility of grid system which correspond with the spirit of the development of networks. On the other hand, P2P network and grid have different technological advantages and do little cooperation nowadays, so it is necessary to test the method which provided by the paper in practical grid environment. Further more, there are some alternatives in the realization of DHT technology, so it is also very important to select one which fits the actual grid environment best.

References

1. Foster, I., Kesselman, C., Tsudik, G.: The Anatomy of the Grid: Enabling Scalable Virtual Organizations. J. International Journal of Super Computer Applications 15, 200–222 (2001)
2. Huang, X., Ye, H.: A Dynamic Grid Naming Resolution Algorithm Based on DHT. J. Computer Engineering 32, 112–114 (2006)
3. Leif, L., Vladimir, V., Shahab, M.: Churn Tolerant Virtual Organization File System for Grids. Gabriele, Violino (2009)
4. Stoica, I., Morris, R., Karger, D., et al.: Chord: a scalable peer-to-peer lookup service for Internet applications. In: The International Conference of the Special Interest Group on Data Communication, pp. 149–160. ACM Press, New York (2001)
5. Hefeeda, M., Habib, A., Botev, B., et al.: Peer-to-peer media streaming using Collect Cast. In: 11th ACM International Conference on Multimedia, pp. 45–54. ACM Press, New York (2003)
6. Castrom, D.P., Kermarrec, A.M, et al.: Split Stream: High-bandwidth multicast in cooperative environments. In: 19th ACM Symposium on Operating Systems Principles, pp. 298–313. ACM Press, New York (2003)
7. Pouwelsej, A., Garbacki, P., Epema, D.H.J., et al.: The bit torrent P2P file-sharing system: measurements and analysis. In: Castro, M., van Renesse, R. (eds.) IPTPS 2005. LNCS, vol. 3640, pp. 205–216. Springer, Heidelberg (2005)
8. Zhang, X., Liu, J., Li, B., et al.: A data-driven overlay network for peer-to-peer live media streaming. In: 24th Annual Joint Conference of the IEEE Computer and Communications Societies, vol. 3, pp. 2102–2111. IEEE Press, USA (2005)
9. Liao, X., Jin, H., Liu, Y., et al.: peer-to-peer living streaming. In: 25th IEEE International Conference on Computer Communications, pp. 1–10. IEEE Press, USA (2006)
10. Liu, X., Zhang, Z., et al.: A measurement study of a peer-to-peer video-on-demand system. In: 6th International Workshop on Peer-to-Peer Systems, Bellevue, USA (2007)
11. Jin, H., Yao, H., Liao, X., et al.: A peer-to-peer middleware to support multiplayer online games. In: International Conference on Multimedia and Ubiquitous Engineering, Korea, pp. 54–59 (2007)

A Novel Quantum Genetic Algorithm for PID Controller

Jindong Wang[1] and Rigui Zhou[2,*]

[1] Shandong Computer Science Center, 250014, Jinan, Shandong, P.R. China
[2] College of Information Engineering, East China JiaoTong University, 330013, Nanchang, Jiangxi, P.R. China
zrg@ecjtu.jx.cn

Abstract. Based on subpopulation parallel computing， a novel quantum genetic algorithm (NQGA) is presented. In the algorithm, each axis of solution is divided into k parts, so m dimensional space is partitioned km subspaces, the individual (or chromosome) from different subspace code differently. Finally, NQGA and the classical quantum genetic algorithm (QGA) are applied to parameter optimization of PID controller, simulation results show that NQGA performs better than QGA on running speed and optimizing capability.

Keywords: Quantum Computing, space division, parallel computing.

1 Introduction

The description of quantum mechanical computers was formalized in the late 1980s [1]. And many efforts on quantum computers have progressed actively since the early 1990s because these computers were shown to be more powerful than classical computers on various specialized problems. And quantum genetic algorithm is a novel inter-discipline that includes quantum mechanics and genetic algorithm, researching on which has been started since late 1990s. In 1996, Ajit Narayanan, Mark Moore firstly introduced quantum multi-universe into genetic algorithm, and compared traditional evolutionary algorithm and quantum inspired genetic algorithm about a well-known mathematic problem of traveling salesperson problem (TSP), which found a precedent of combining quantum computing with evolutionary algorithm [2]. In the following years, many scholars research QGA and make lots of improvements, Jun-an YANG first proposed a novel Multi-universe Parallel Quantum Genetic Algorithm (MPQGA) and put forward a new blind source separation method based on the combination of MPQGA and independent component analysis In 2003 [3]. In the same year, Zexiang ZHANG advanced a novel parallel quantum genetic algorithm applying Q-bit phase comparison approach and hierarchical ring model, which is characterized by rapid convergence, good global search capability [4]. In 2004, Hui Chen et al raised a novel Q-gate updating algorithm called Chaos Updating Rotated Gates Quantum-inspired Genetic Algorithm, and this novel algorithm is more powerful in convergence speed [5]. In 2005 Ling Wang et al proposed a hybrid genetic algorithm to achieve better optimization performances by

* Corresponding author.

D.-S. Huang et al. (Eds.): ICIC 2010, LNCS 6215, pp. 72–77, 2010.

reasonably combining the Q-bit search of quantum algorithm in micro-space and classic genetic search of real-coded GA in macro-space [6].

2 Quantum Computing

Quantum theory is to reveal the motion law of atomic-scale, subatom-scale micro particles. The state of a quantum system is composed with a variety of particle's position, momentum, polarization, spin etc., and evolves over time. The process follows SchrÖdinger equation, while the state itself is full described by the vector in Hilbert space.

2.1 State-Space

Q-bit is the basic unit of quantum computation and quantum information, and a Q-bit can be viewed as a vector in two-dimensional Hilbert state space. Set $|0\rangle$ and $|1\rangle$ as a standard orthogonal basis of the state space, then any state $|\varphi\rangle$ of this space can be expressed as:

$$|\varphi\rangle = \alpha|0\rangle + \beta|1\rangle \tag{1}$$

where α, β is the complex, and $\alpha^2 + \beta^2 = 1$. In a sense, the quantum states exist simultaneously in the ground state of the space, $|\varphi\rangle$ corrects to $|0\rangle$ with the probability of α^2, and to $|1\rangle$ with the probability of β^2.

2.2 Quantum Evolutions

A closed quantum system's evolution can be characterized absolutely by a unitary transformation, that is, if the system's state is $|\varphi\rangle$ at time *t1*, and $|\varphi'\rangle$ at time *t2*, then these two states contact depending only on the unitary operator U: $|\varphi'\rangle = U|\varphi\rangle$. There is a major unitary operator in this paper:

$$U = \begin{bmatrix} \cos\theta & -\sin\theta \\ sin\theta & \cos\theta \end{bmatrix} \tag{2}$$

Quantum Evolutions could be characterized by SchrÖdinger education:

$$i\hbar \frac{d|\varphi\rangle}{dt} = H|\varphi\rangle \tag{3}$$

where $\hbar$ is Planck constant ascertained by experiments, H is Hermite operator.

3 A Novel Quantum Genetic Algorithm

3.1 Quantum Chromosome Redefining and Space Division

Q-bit is the smallest unit of information which could be expressed in the other form as follows:

$$|\varphi\rangle = \cos\theta|0\rangle + \sin\theta|1\rangle \tag{4}$$

$\cos^2\theta$ gives the probability that the Q-bit will be found in the "0" state and $\sin^2\theta$ gives the probability that the Q-bit will be found in the "1" state. So a Q-bit can be coded as $\begin{bmatrix}\cos\theta \\ \sin\theta\end{bmatrix}$, and a chromosome as a string of m Q-bits can be expressed as:

$$\begin{bmatrix}\cos\theta_1 & \cos\theta_2 & \ldots & \cos\theta_m \\ \sin\theta_1 & \sin\theta_2 & \ldots & \sin\theta_m\end{bmatrix} \tag{5}$$

Where $\cos\theta$ or $\sin\theta$ just represent a probability amplitude, but in this paper $\cos\theta$ and $\sin\theta$ are given a new meaning. For unit space $I^m = [-1,1]^m$, each Q-bit individual is regarded as two genes chains, that is, $\cos\theta$ and $\sin\theta$ are no longer probability amplitude but a certain value in a chromosome with two genes chains. The redefined quantum chromosome is vividly shown in Fig.1 as follows:

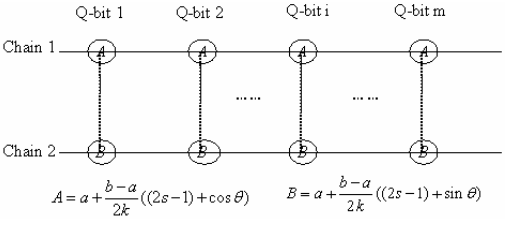

Fig. 1. Redefined chromosome

Because $\cos\theta$ or $\sin\theta$ all values among (-1, 1), redefined quantum chromosome is just for unit space. However, most realistic problems are not simple as unit space, so a method of dividing basis of solution space into *k* parts is proposed in NQGA.

Let us divide each basis of solution space into *k* subsets, that is, (a, b) is divided into *k* equal subsets and the subsets could be wrote as:

$$(a + s(\frac{b-a}{k}),\ a + (s+1)(\frac{b-a}{k})) \tag{6}$$

Where *s* represents *s*-th subset, therefore m-dimensional solution space is divided k^m subspaces. In the step of population initialization, we select individuals from all the subspaces, and individuals in different subspace are coded differently. Suppose every Q-bit of a chromosome belong to *s*-th subset, which could be coded as follows:

$$\begin{bmatrix} a+\frac{b-a}{2k}((2s-1)+\cos\theta_1),...,a+\frac{b-a}{2k}((2s-1)+\cos\theta_m) \\ a+\frac{b-a}{2k}((2s-1)+\sin\theta_1),...,a+\frac{b-a}{2k}((2s-1)+\sin\theta_m) \end{bmatrix}$$ And this chromosome can be expressed as Fig.2.

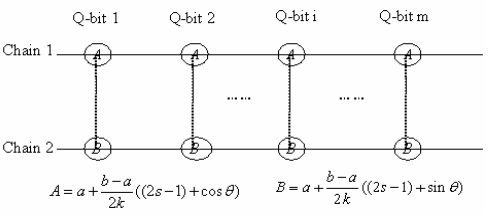

Fig. 2. Chromosome in subspace

3.2 The Procedure of NQGA

The following is the procedure of NQGA.

Step 1. In the step of "initialize P(t)", $\theta_{ji}^t\big|_{t=0} = 2\pi * rand(0,1)$

Step 2. Each chain of $p_j^t\big|_{t=0}$ is evaluated to give its fitness, and $p_j^t\big|_{t=0}$ has a pair of fitness. The initialized best individual is selected among this $P(0)$, and is stored in $B(0)$, $B(0)=\{b_1^0,b_2^0,...,b_{k^m}^0\}$ where b_j^0 $(j=1,2,...,k^m)$ is the same as p_j^0. Select the maximum among $B(0)$, which is stored in b. If the maximum b doesn't reach our required accuracy, population will be updated.

Step 3. In the while loop, $p(t)$ are got by updating $p(t-1)$ with the quantum gate U.

$$\begin{bmatrix} \cos\theta_{ji}^t \\ \sin\theta_{ji}^t \end{bmatrix} = \begin{bmatrix} \cos\Delta\theta_i & -\sin\Delta\theta_i \\ \sin\Delta\theta_i & \cos\Delta\theta_i \end{bmatrix} \begin{bmatrix} \cos\theta_{ji}^{t-1} \\ \sin\theta_{ji}^{t-1} \end{bmatrix}$$ And evaluate $p(t)$ as in step 2.

Step 4. The best solutions among $p(t)$ and $B(t-1)$ are selected and stored into $B(t)$, and if the best solution of $B(t)$ is fitter than the current b, the stored best solution will be instead by the new one.

Step 5. If the maximum b doesn't reach our required accuracy, the algorithm switches to step 3 to continue running.

4 Simulations

QGA and NQGA are applied to PID controller problem for verifying the feasibility and superiority of NQGA.

PID control is widely applied in industrial fabrication, and in order to obtain the good effect, the action of Proportional Integral Differential should interact closely in the process of forming controlled variable. Fig.3 shows a closed-loop system with a PID controller and we have:

$$u(t) = k_p e(t) + k_i de(t) + k_d \int e(t)dt \tag{7}$$

Where k_p, k_i and k_d are parameters which will be optimized by NQGA and QGA.

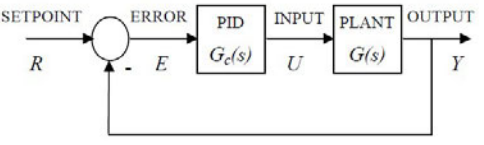

Fig. 3. A PID controller system

K_P, K_I, K_D could be regarded as the solution in three dimension space, and solution space is partitioned into 27 subspaces. The step response of PID control optimized by three algorithms is show as Fig.4. It is obvious that PID controller optimized by NQGA is better than the classical QGA on overshoot, rise time and stability.

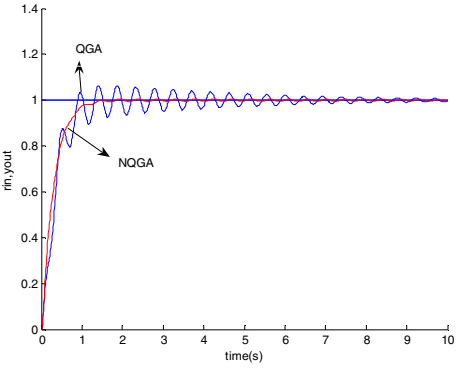

Fig. 4. Step response curve optimized by two algorithms

5 Conclusions

Based on quantum genetic algorithm, this paper proposes a novel quantum genetic algorithm by dividing each axis of solution space into k parts. We apply this novel

algorithm into PID controller. Through a comparison between simulation results of NQGA and QGA, it is obviously shown that the algorithm proposed in this paper performs better on running speed and optimizing capability.

Acknowledgment

The authors would like to thank the anonymous referees for their helpful comments and suggestions to improve the presentation of this paper. This work is supported by the Young Scholar Research Fund of Shandong Province under Grant No.2007BSC01001.

References

1. Benioff, P.: The Computer as a Physical System: A Microscopic Quantum Mechanical Hamiltonian Model of Computers as Represented by Turing Machines. J. Statist. Phys. 22, 563–591 (1980)
2. Ajit, N., Mark, M.: Quantum-inspired Genetic Algorithms. In: Proceeding of IEEE International conference on Evolutionary Computation, Nagoya, Japan, pp. 61–66 (1996)
3. Yang, J.A., Li, B., Zhuang, Z.Q.: Multi-universe Parallel Quantum Genetic Algorithm and its Application to Blind-source Separation. In: Proceedings of the International Conference on Neural Networks and Signal Processing, vol. 1, pp. 393–398 (2003)
4. Zhang, G.X., Jin, W.D., Hu, L.Z.: A Novel Parallel Quantum Genetic Algorithm. In: Proceedings of the fourth International Conference on Parallel and Distributed Computing, Applications and Technologies, pp. 693–697 (2003)
5. Chen, H., Zhang, J.H., Zhang, C.: Chaos Updating Rotated Gates Quantum-inspired Genetic Algorithm. In: Proceedings of the International Conference on Communications, Circuits and Systems, vol. 2, pp. 1108–1112 (2004)
6. Wang, L., Tang, F., Wu, H.: Hybrid Genetic Algorithm Based on Quantum Computing for Numerical Optimization and Parameter Estimation. Applied Mathematics and Computation 171(2), 1141–1156 (2005)
7. Li, P.C., Li, S.Y.: Quantum-inspired Evolutionary Algorithm for Continuous Spaces Optimization. Chinese Journal of Electronics 17(1), 80–84 (2008)
8. Li, P.C., Li, S.Y.: Quantum-inspired Evolutionary Algorithm for Continuous Spaces Optimization Based on Bloch Coordinates of Qubits. Neurocomputing 72, 581–591 (2008)
9. Yang, J.A., Li, B., Zhuang, Z.Q.: Research of Quantum Genetic Algorithms and its Application in Blind Source Separation. Journal of Electronics 20(1), 62–68 (2003)
10. Tao, Y.H.: A Novel PID Controller and its Application. Mechanical Industry Press (2003)
11. Li, C.Z.: Quantum Communication and Quantum computing. Chang Sha. National University of Defense Technology Press (2000)
12. Nielsen, M.A., Chuang, I.L.: Quantum Computation and Quantum information. Cambridge University Press, Cambridge (2000)
13. Guo, Z.L., Wang, S.A., Zhuang, J.: A Novel Immune Evolutionary Algorithm Incorporating Chaos Optimization. Pattern Recognition Letters 27(1), 2–8 (2006)
14. Liu, J., Xu, W.B., Sun, J.: Quantum-behaved Particle Swarm Optimization with Mutation Operator. In: Proceedings of the 17th IEEE International Conference on Tools with Artificial Intelligence (2005)

Research on Hybrid Evolutionary Algorithms with Differential Evolution and GUO Tao Algorithm Based on Orthogonal Design

Zhan-Fang Zhao[1], Kun-Qi Liu[1,2], Xia Li[1], You-Hua Zhang[1], and Shu-Lin Wang[3]

[1] Department of Computer Science, Shijiazhuang University of Economics, Shijiazhuang, 050031, China
[2] School of Computer, China University of Geosciences, Wuhan, 430074, China
[3]School of Computer and Communication, Hunan University, Changsha, Hunan, 410082, China
zhaozhanfang@sjzue.edu.cn

Abstract. This paper proposes an orthogonal mutation technology, which combines the orthogonal initialization technology and the orthogonal crossover technique. They are called the orthogonal processing technologies. The fusion of the differential evolution algorithm, the GuoTao operator and the orthogonal processing technology has formed several different hybrid evolutionary algorithms. The experimental results show that these new algorithms display the good performance in the solution precision, the stability and the convergence.

Keywords: Differential evolution algorithm; GuoTao operator; orthogonal design; orthogonal crossover; orthogonal mutation; hybrid evolutionary algorithm.

1 Introduction

How to design effective evolutionary algorithm is one of basic questions which need to be solved in the evolutionary computation research area [1][2]. The fusion of the existing evolutionary algorithm and other algorithms makes a new evolutionary algorithm (hybrid evolutionary algorithm), which is one of the basic ways to solve this problem [3][4]. As for this research, it can trace back to the combination of the genetic algorithm and the local search [4], at present it has already developed into the Memetic Algorithm[5][6]. For other fusion, such as the fusion of the evolutionary algorithm and the simulated annealing algorithm [7][15], the evolutionary algorithm and the genetic algorithm [7][11][13], and so on.

At present, the differential evolution algorithm (DE) [8] and the GuoTao algorithm[9][10] are two famous algorithms. In order to further enhance two algorithms' efficiency, the DE, particle swarm optimization [12], distributed evaluation algorithm[14] and ant colony algorithm[16] fuse to be a new algorithm[15]; moreover, the GuoTao algorithm, gene expression programming [17] and particle swarm optimization [18] fuse to be a new evolutionary algorithm. Inspired by the fusion of algorithms mentioned above, in this paper we will integrate DE, GuoTao operator and Orthogonal

D.-S. Huang et al. (Eds.): ICIC 2010, LNCS 6215, pp. 78–85, 2010.

design [19][20][21] to form a kind of hybrid evolutionary algorithms in different styles. The experimental results indicate that each algorithm of this kind has its own advantages, and is better than the evolutionary algorithm given in [22].

The remainder of this paper is organized as follows. In Section II we introduce DE and GuoTao operator. Section III is the discussion of orthogonal hybrid evolutionary algorithms. The simulation experiments and results analysis are presented in Section IV. Finally, Section V concludes this paper.

2 Differential Evolution Algorithm and GuoTao Operator

The differential evolution algorithm (DE) was introduced by Rainer Storn and Kenneth Price in 1995. For more details, please see [8].

The DE selects offspring with mechanism for the survival of the fittest, its search capability is powerful in early period, convergence speed becomes slow in later period, it can also easily be trapped in a local optimum. Therefore, we propose an improved DE in this paper. The basic idea is: First, DE generates many children in the crossover operation; then the GuoTao operator generates one child; lastly, offspring is generated by competition among all the children. The improved DE can greatly improve the global search capability and non-convex search capability.

The GuoTao algorithm is also called the Multi-Parent Crossover evolutionary algorithm. The details of the algorithm are given in [9]. In this paper, we regard Multi-Parent Crossover as an operator, which is GuoTao operator. In order to enhance the search efficiency, we apply subspace shrinking technology [10] to algorithm.

3 Hybrid Evolutionary Algorithms with DE and GuoTao Operator Based on Orthogonal Design

In this paper, we apply orthogonal initialization technology, the details are given in [19]. We apply orthogonal crossover technology, the details are given in [21].

3.1 Orthogonal Mutation Operator

In this paper, we integrate orthogonal design into the mutation, the basic idea of the orthogonal mutation is: one parent individual is selected at random, a perturbation is added to some genes by the difference vector. The parent individual can generate many new individuals according to the orthogonal array, which generates an orthogonal mutation sub-population. We select the best individual that inherits a great many best genes of the parent individual.

We have selected the orthogonal array with two levels per factor. The individual V is current parent individual, $V= (v_{11},v_{12},\ldots,v_{1N})$, X_1 and X_2 are selected randomly to generate difference vector, $X_1=(x_{11},x_{12},\ldots, x_{1N})$, $X_2=(x_{21},x_{22},\ldots,x_{2N})$. This individual V generates an mutation sub-population according to orthogonal array L[M][N].

Algorithm 1. Generate orthogonal mutation sub-population V(M, N).

```
for i= 1 to M do
 for j= 1 to N do
     k= L[i][j]
     if k = 1 then
        V[i][j]=V_ij + F(x_1j-x_2j)
     End if
     If k = 2 then
        V[i][j]= V_ij
     End if
  End
 End
```

3.2 Hybrid Algorithm with DE and GuoTao Operator Based on Orthogonal Design

The Idea of Hybrid Algorithm and the Framework of Orthogonal Hybrid Algorithm

The basic idea of the hybrid algorithm is: first, the DE generates five new individuals, we select the best individual, the DE model is DE/rand/1/bin; Afterwards, the GuoTao operator generates one new individual; lastly, the two new individuals compete with the parent individual, we select the best individual as an offspring. In addition, we use the subspace shrinking technology. The algorithm 2 is as follows:

Algorithm 2: Hybrid algorithm of the DE and GuoTao operator

For i=1 to PopulationSize do
  The DE generates five new individuals, we select the best individual as A;
  The GuoTao operator generates one new individual B;
  A and B compete with the parent, we select the best individual as offspring;
End

The basic idea of orthogonal Hybrid Algorithm is: Introducing the orthogonal design technology into the hybrid algorithm and putting the orthogonal initialization, the orthogonal mutation and the orthogonal crossover into the beginning, middle and end of the hybrid algorithm separately, we confirm the orthogonal technology's influence on the algorithm in the 3 different positions.

Hybrid Algorithm with Orthogonal Initialization (OIDE)

We place orthogonal initialization in front of hybrid algorithm， the detail is as follows:

Algorithm 3: Hybrid Algorithm with orthogonal initialization

Step 1: Construct the suitable orthogonal array;
Step 2: Generate the orthogonal initial population;
Step 3: Calculating the fitness, find out the current best and worst individual;
Step 4: While (stopping condition is not met)

Execute Algorithm 2 to generate new population;
Find out the best and worst individual in current population;
The subspace shrink;
End
Step 5: Output computation result.

Hybrid Algorithm with Orthogonal Crossover (OCDE)
We place orthogonal crossover the end of hybrid algorithm. The detail is as follows:

Algorithm 4: Hybrid Algorithm with orthogonal crossover

Step 1: Generate the initial population at random;
Step 2: Find out the best and worst individual in current population;
Step 3: Construct suitable orthogonal array;
Step 4: While (stopping condition is not met)
Execute Algorithm 2 to generate new population;
Find out the best and worst individual in current population;
Execute orthogonal crossover operator, then select the best individual to replace the worst individual in current population;
The subspace shrink;
End
Step 5: Output computation result.

Hybrid Algorithm with Orthogonal Mutation (OMDE)
We insert the orthogonal mutation algorithm between the DE and GuoTao operator.

Algorithm 5: Insert orthogonal mutation between the DE and GuoTao operator
For i=1 to PopulationSize do
The DE generates five new individuals, we select the best individual as A;
Execute Algorithm 1 , select the best individual B from mutation sub-population;
The GuoTao operator generates one new individual C;
A, B and C compete with the parent individual, we select the best individual;
End

Algorithm 6: Hybrid Algorithm with orthogonal mutation

Step 1: Generate the initial population at random;
Step 2: Find out the best and worst individual in current population;
Step 3: Construct suitable orthogonal array;
Step 4: While (stopping condition is not met)
Execute Algorithm 5 to generate new population;
Find out the best and worst individual in current population;
The subspace shrink;
End
Step 5: Output computation result.

Hybrid Algorithm with Several Orthogonal Technologies
We fix the position of the orthogonal initialization, the orthogonal mutation and the orthogonal crossover into the beginning, middle and end of the hybrid algorithm separately. The combinations of these three technologies examine many kinds of orthogonal technology's influence on the algorithm.

Algorithm 7: Hybrid Algorithm with the orthogonal initialization and orthogonal crossover (OICDE)

Step 1: Construct suitable orthogonal array;
Step 2: Generate the orthogonal initial population;
Step 3: While (stopping condition is not met)
Execute Algorithm 2 to generate new population;
Find out the best and worst individual in current population;
Execute orthogonal crossover operator, then select the best individual to replace the worst individual in current population;
The subspace shrink;
End
Step 4: Output computation result.

Algorithm 8: Hybrid Algorithm with the orthogonal mutation and orthogonal crossover (OMCDE)

Step 1: Generate the initial population at random;
Step 2: Find out the best and worst individual;
Step 3: Construct suitable orthogonal array;
Step 4: While (stopping condition is not met)
Execute Algorithm 5 to generate new population;
Find out the best and worst individual in current population;
Execute orthogonal crossover operator, then select the best individual to replace the worst individual in current population;
The subspace shrink;
End
Step 5: Output computation result.

Algorithm 9: Hybrid Algorithm with the orthogonal initialization, the orthogonal mutation and orthogonal crossover (OICMDE).

Step 1: Construct suitable orthogonal array;
Step 2: Generate the orthogonal initial population;
Step 3: While (stopping condition is not met)
Execute Algorithm 5 to generate new population;
Find out the best and worst individual in current population;
Execute orthogonal crossover operator, then select the best individual to replace the worst individual in current population;
The subspace shrink;
End
Step 4: Output computation result.

4 Simulation Experiments and Results Analysis

In this paper the operating environment is Windows XP operating system, Intel P4 Dual Core CPU with 2GB of RAM, 3GHz. The development environment is Visual C++ 6. The crossover constant is set CR=0.3, the scaling factor is set F=0.9, and the size of population is set PopulationSize=100.

In this paper, there are six hybrid evolutionary algorithms: OIDE, OCDE, OMDE, OMCDE, OICDE, OICMDE. We performed 50 independent runs for each algorithm on each test function and recorded.

The maximum evolutionary generation: Generation; The mean function value: Mean Best; The standard deviation of the function values: Std-dev. We have tested 18 functions which are given in [22], the optimal values of all function are given in [22], "F " denotes function in table. The detail of the comparison is as follows:

Table 1. Comparison with OIDE, OCDE, OMDE and boDE[22]

F	Generation				Mean Best				Std-Dev			
	boDE	OIDE	OCDE	OMDE	boDE	OIDE	OCDE	OMDE	boDE	OIDE	OCDE	OMDE
F01	1500	4000	4000	4000	1.7E-61	0	0	0	1.6E-61	0	0	0
F02	2000	6000	3500	6000	6.2E-48	0	0	0	4.5E-48	0	0	0
F03	5000	5000	5000	5000	4.6E-15	1.3E-45	8.6E-237	9.1E-196	8E-15	4.7E-45	6.8E-237	1.4E-197
F04	5000	5000	5000	5000	0	4.57	7.7E-267	4.4E-8	0	0.58	5.1E-267	2.4E-8
F05	20000	20000	20000	3000	0	1.1E-6	0	0	0	1.5E-6	0	0
F06	1500	500	500	500	0	0	0	0	0	0	0	0
F07	3000	3000	1000	3000	1.8E-3	1.8E-3	1.2E-3	1.7E-2	4.7E-4	6.8E-4	5.6E-4	1.5E-3
F08	9000	1000	1000	1000	-12569.48	-12569.49	-12569.49	-12569.49	7.3E-12	0	0	0
F09	5000	1500	500	1500	1.31	0	0	0	1.0	0	0	0
F10	1500	500	500	500	4.6E-15	4.4E-15	5.9E-16	4.14E-15	1.36E-15	1.0E-15	0	0
F11	2000	500	400	500	0	0	0	0	0	0	0	0
F12	1500	500	500	500	1.57E-32	1.78E-32	1.57E-32	1.57E-32	8.2E-48	2.6E-32	0	0
F13	1500	800	800	600	1.3E-32	1.3E-32	1.3E-32	1.3E-32	1.09E-47	0	0	0
F14	100	50	50	50	0.9980038	1.031138	0.9980038	0.9980038	7.69E-17	0.18	0	0
F15	4000	300	300	300	3.07E-4	3.0748E-4	3.0748E-4	3.1205E-4	2.76E-10	0	0	2.5E-5
F16	100	50	50	50	-1.031628	-1.031628	-1.031628	-1.031628	4.44E-16	0	0	0
F17	100	100	100	100	0.397887	0.397887	0.397887	0.397887	3.58E-16	0	0	0
F18	100	50	50	50	3	3	3	3	3.52E-15	0	0	0

Table 2. Comparison with OICDE, OMCDE, OICMDE and boDE[22]

F	Generation				Mean Best				Std-Dev			
	boDE	OICDE	OMCDE	OICMDE	boDE	OICDE	OMCDE	OICMDE	boDE	OICDE	OMCDE	OICMDE
F01	1500	3000	4000	3000	1.7E-61	0	0	0	1.6E-61	0	0	0
F02	2000	4000	6000	4000	6.2E-48	0	0	0	4.5E-48	0	0	0
F03	5000	5000	5000	4000	4.6E-15	2.24E-200	0	0	8.0E-15	7.3E-200	0	0
F04	5000	5000	5000	5000	0	5.7E-4	1.9E-300	7.7E-320	0	9.8E-5	4.5E-300	3.7E-320
F05	20000	20000	2000	2000	0	5.63E-101	0	0	0	3.5E-101	0	0
F06	1500	500	500	500	0	0	0	0	0	0	0	0
F07	3000	3000	3000	3000	1.8E-3	1.7E-3	1.0E-3	4.6E-2	4.7E-4	5.0E-4	8.1E-4	3.5E-3
F08	9000	1000	1000	1000	-12569.48	-12569.49	-12569.49	-12569.49	7.3E-12	0	0	0
F09	5000	500	500	500	1.31	0	0	0	1.0	0	0	0
F10	1500	1000	500	500	4.6E-15	5.9E-16	5.9E-16	5.9E-16	1.36E-15	0	0	0
F11	2000	500	500	500	0	0	0	0	0	0	0	0
F12	1500	800	500	500	1.57E-32	1.57E-32	1.57E-32	1.57E-32	8.2E-48	0	0	0
F13	1500	800	500	500	1.3E-32	1.3E-32	1.3E-32	1.3E-32	1.09E-47	0	0	0
F14	100	50	50	50	0.9980038	1.0641405	0.9980038	1.1302772	7.69E-17	0.36	0	0.5
F15	4000	300	300	300	3.07E-4	3.0748E-4	3.1097E-4	3.0748E-4	2.76E-10	0	1.7E-5	0
F16	100	50	50	50	-1.031628	-1.031628	-1.031628	-1.031628	4.44E-16	0	0	0
F17	100	100	100	100	0.397887	0.397887	0.397887	0.397887	3.58E-16	0	0	0
F18	100	50	50	50	3	3	3	3	3.52E-15	0	0	0

Firstly, the precision analysis: The six orthogonal hybrid algorithms are better than boDE for f1-f3, f9-f10. For f6-f8, f11-f18, applying the six orthogonal hybrid algorithms and boDE to solve them, the precision of solutions are the same. Three orthogonal hybrid algorithms and boDE algorithm obtain the same precision for f4. Four orthogonal hybrid algorithms and boDE can obtain the same precision for f5.

Secondly, the convergence speed analysis: For 16 test functions among 18 test functions, the six algorithms display the better performance than boDE.

Thirdly, the solution stability analysis: For most of the test functions, the six orthogonal hybrid algorithms are obviously better than boDE.

In conclusion, three orthogonal design technologies have their own respective characteristics and advantages. The orthogonal initialization may produce the initial population of high quality, which can enhance the quality and speed of the solution; The orthogonal crossover adopt a strategy: maintain stability and survival of the fittest, it can not only guarantee population's multiplicity, and also speed up population's convergence speed. When guaranteeing population multiple, the orthogonal mutation chooses the best individual which retains the outstanding genes of parent individual at maximum. For the most of test function, the orthogonal combinational algorithms enhance distinctly the convergence speed. The disadvantage of these algorithms is: for the function with extra dimensions, if the function dimensions are 100, orthogonal array can expand rapidly, which will greatly affect the solution quality and the speed.

5 Conclusion

In this paper, the DE, the GuoTao operator and the orthogonal technology are fused to form 6 different algorithms. Particularly, this paper brings forth an innovation, that is, the thought of orthogonal mutation and several different hybrid algorithms coming from the combination of orthogonal initialization, the orthogonal crossover and the orthogonal mutation. The simulation experiment indicated that these new algorithms display better performance than the existing algorithm in the solution precision, the stability and the convergence. It is a powerful explanation that the fusion of the orthogonal technology and evolutionary computation is one of the basic ways to enhance the evolutionary performance. It is the further research direction that the fusion of the orthogonal technology and evolutionary algorithm to solve the constrained function optimization and the multi-objective function optimization.

Acknowledgments

This work is supported by the National Natural Science Foundation of China (Grant Nos. 60772196 and 60973153), the Special Fund for Basic Scientific Research of Central Colleges (No. CUG090109), and the China Postdoctoral Science Foundation (No. 20090450825).

References

1. Qi, L.K., Shan, K.L., Zhuo, Z.Z.: Brief Report of Research on Cognizing the Subarea of Evolutionary Computation (I). J. Computer Science 36, 26–30 (2009)
2. Qi, L.K., Shan, K.L., Zhuo, Z.Z.: Brief Report of Research on Cognizing the Subarea of Evolutionary Computation(II). J. Computer Science 36, 35–39 (2009)
3. Moscato, P.: On evolution, search, optimization, genetic algorithms and martial arts: Towards memetic algorithms. California Institute of Technology, Pasadena, California, USA, Tech. Rep. Caltech Concurrent Computation Program, Report 826 (1989)
4. Grefenstette, J.J.: Lamarckian learning in multi-agent environments. In: Proc. Fourth Intl. Conf. of Genetic Algorithms, pp. 303–310. Morgan Kaufmann, San Mateo (1991)
5. Natalio, K., Jim, S.: A Tutorial for Competent Memetic Algorithms: Model, Taxonomy and Design Issues. IEEE Transactions on Evolutionary Computation 10, 472–488 (2006)
6. Dan, L.M.: The Development of Memetic Algorithm. J. Techniques of Automation and Applications. 26, 1–4 (2007)
7. Yong, L., Shan, K.L.: The Annealing evolution algorithm as function optimizer. J. Parallel Computing (21), 389–400 (1995)
8. Storn, R., Price, K.: Differential evolution: A simple and efficient heuristic for global optimization over continuous spaces. Journal of Global Optimization 11, 341–359 (1997)
9. Tao, G., Shan, K.L.: A new evolutionary algorithm for function optimization. J. Wuhan University Journal of Nature Sciences 4, 409–414 (1999)
10. Zhuo, K., Yan, L.: An all-purpose evolutionary algorithm for solving nonlinear programming problems. J. Journal of computer research and development 39, 1471–1474 (2002)
11. Lei, W., Cheng, J.L.: A novel genetic algorithim based on immunity. In: Proceedings of the 2000 IEEE International Symposium on Circuits and Systems (ISCAS), pp. 385–388 (2000)
12. Jun, Z.W., Feng, X.L.: DEPSO: hybrid particle swarm with differential evolution operator. In: IEEE International Conference on Systems, Man, and Cybernetics (SMCC), Washington, DC, USA, pp. 3816–3821 (2003)
13. Zhang, Q., Sun, J., Tsang, E.: Evolutionary Algorithm with Guided Mutation for the Maximum Clique Problem. IEEE Transaction on Evolutionary Computation 9, 192–200 (2005)
14. Sun, J., Zhang, Q., Tsang, E.: DE/DEA: New Evolutionary Algorithm for Global Optimisation. J. Information Sciences 169, 249–262 (2005)
15. Qi, L.K.: Differential Evolution Algorithm Based on Simulated Annealing. In: Kang, L., Liu, Y., Zeng, S. (eds.) ISICA 2007. LNCS, vol. 4683, pp. 120–126. Springer, Heidelberg (2007)
16. Yin, Z.X., Bin, D.H.: DEACO: Hybrid Ant Colony Optimization with Differential Evolution. In: Proceedings of the 2008 Congress on Evolutionary Computation, pp. 921–927 (2008)
17. Wei, L.X., Hua, C.Z.: Application of a novel GEP algorithm in evolutionary modeling and forecasting. J. Computer Applications 25, 2783–2786 (2005)
18. Chao, H.Y., Zhan, K.Y.: Hybrid particle swarm optimization algorithm based on global inferior-substitution strategy. J. Application Research of Computers 24, 75–78 (2005)
19. Leung, Y.W.: An Orthogonal Genetic Algorithm with Quantization for Global Numerical Optimization. IEEE Transactions on Evolutionary Computation 5, 91–96 (2001)
20. Yan, W.S., Fu, Z.Q.: A new evolutionary algorithm based on family eugenics. Journal of software 8, 137–144 (1997)
21. Yin, G.W., Bo, L.X.: Research on a Fast Differential Evolution Based on Orthogonal Design and its Application. Journal of Chinese Computer Systems 28, 1297–1300 (2007)
22. Feng, W.Z., Kuan, H.H.: A differential evolution algorithm with double trial vectors based-on Boltzmann mechanism. Journal of Nanjing university (natural sciences) 44, 199–200 (2008)

An Improved Evolution Strategy for Constrained Circle Packing Problem

Yan-jun Shi, Zhuang-Cheng Liu, and Shuai Ma

School of Mechanical Engineering,
Dalian University of Technology, Dalian, P.R. China 116024
syj@dlut.edu.cn

Abstract. This paper proposes an improved evolution strategy with crossover operator (ESCO for short) to tackle a combinatorial optimization problem, i.e., constrained circle packing problem. The proposed ESCO extend a canonical ES to deal with combinatorial optimization by employing the crossover operator from genetic algorithm, aiming to exchange the location of circles for obtaining a better packing scheme. The experimental results showed the effectiveness of ESCO compared with genetic algorithm and canonical evolution strategy.

Keywords: evolution strategy, combinatorial optimization, genetic algorithm, circle packing.

1 Introduction

Evolution strategy (ES) is an optimization technique based on ideas of adaptation and evolution[1]. This technique belongs to a class of evolutionary computation or artificial evolution, which was created in the early 1960s and developed further along the 1970s and later by Ingo Rechenberg, Hans-Paul Schwefel and et al. The canonical ES employs a simple procedure for selecting individuals, and often uses mutation as the search operator. The state-of-the-art of ES is CMA-ES[1] for difficult non-linear non-convex optimization problems in continuous domain. However, there is little report in the available literature on employing ES to tackle combinatorial optimization problem or discontinuous domain. For the discontinuous domain, e.g., circle packing problems in industrial application[2], 3D component layout[3],where the search space is discrete, non-linear and multi-modal, the canonical ES had to be improved or modified to search such problem space. This study attempts to extend ES to deal with such problems by employing crossover operator from genetic algorithm.

This paper aims to solve circle packing problem, which attempt to obtain a better arrangement of N arbitrary sized circles inside a container (e.g., a rectangle or a circle) such that no two circles overlap. We often measure the quality of the packing by (1) the size of the container, (2) the weighted average pair-wise distance between the centers of the circles, or (3) a linear combination of criteria (1) and (2). The constrained circle packing in this study can be formulated as simplification of layout design of a satellite module, which considers how to place the given apparatuses and equipment (component) in the limited space of the satellite module[4]. This placement must

D.-S. Huang et al. (Eds.): ICIC 2010, LNCS 6215, pp. 86–93, 2010.

satisfy various behavioral constraints of the interior and exterior environment. Additionally, circle packing problem can be applied to the other industry areas including circular cutting problems, communication networks, facility location, dashboard layout and etc.

As we know, heuristic solution strategies appear to be preferred when dealing with larger problem instances. These heuristic solution strategies included simulated annealing, genetic algorithm, and etc[2]. However, because of various requirements in the engineering, finding more alternative solutions was always welcome for solving this problem. Until now, there is little work on this problem using evolution strategy-based solvers. This study attempted to tackle the circle packing problems with constrains using the improving version of evolution strategy with crossover operator.

2 A Brief Introduction to Evolution Strategy

Together with genetic algorithm and evolutionary programming, evolution strategies form the class of evolutionary algorithms. The canonical ES use natural problem-dependent representations, and primarily mutation and selection as search operators. Like genetic algorithm, the operators are applied in an iterative process, which called a generation. The sequence of generations is continued until a termination criterion is met. The important features separate ES from genetic algorithm as follows. Firstly, ES uses a real coding of the decision vector, and model the organic evolution at the level of individual's phenotypes. Secondly, ES depends on deterministic selection of the individuals to the next generation, and the search is mainly driven by a high mutation rate. We take an individual in ES as a pair of real vectors, $v = (x, \sigma)$. The vector x represents a point in the search space (solution) and consists of a number of real-valued variables. The vector σ represents strategy parameters, called by the step size or mutation strength (i.e. the standard deviation of the normal distribution). Mutation is normally performed by adding a normally distributed random value $N(0, \sigma)$ to each vector component x. Individual step sizes for each coordinate or correlations between coordinates are either governed by self-adaptation or by covariance matrix adaptation (CMA-ES) [1]. Thirdly, the selection in evolution strategies is deterministic and only based on the fitness rankings, not on the actual fitness values. Note that ES does not use crossover operator as search operators.

The evolution strategies can be categorized according to the population size (μ) and the number of offspring (λ) created in each generation ($\lambda > \mu > 1$). The simplest ES operates on a population of size two: the current point (parent) and the result of its mutation. Only if the mutant's fitness is at least as good as the parent one, it becomes the parent of the next generation. Otherwise the mutant is disregarded. This is a $(1+1)ES$. More generally, λ mutants can be generated and compete with the parent, called $(1+\lambda)ES$. Thus, the common $(\mu+\lambda)ES$ denotes an ES that generates λ offspring from μ parents and selects the best μ individuals from the $(\mu+\lambda)$ individuals (parents and offspring) in total. This generation is believed to make them less prone to get stuck in local optima. In this study, we employ $(\mu+\lambda)ES$ with crossover operator for constrained circle packing.

3 The Proposed Evolution Strategy with Crossover Operator

The previous studies have shown that ES has the characteristic for solving a variety of complex continuous and non-convex function[1]. For circle packing problem, the search space is discrete, non-linear and multi-modal. The basic ES only employs mutation operator, which is good at continuous domain. To solve circle packing problem, ES still needs special optimization operator for the combinatorial problem. To find special optimization operator for ES, we firstly review the optimization operator from genetic algorithm in the literature. The optimization operators herein mean selection operator, crossover operator, and mutation operator. These operators from genetic algorithm for component layout design[4] included single-point crossover, two-point crossover, uniform crossover, etc. They were useful for obtaining a good packing topology by changing or swapping the location of component. These are the

```
μ ← number of parents selected
λ ← number of children generated by the parents
Initialize the population P
for λ times do
    P ← P ∪ { new random individual }
end for
Initialize best individual Best
repeat
    for each individual P_i ∈ P do
        Evaluate Fitness (P_i)
        if Fitness(P_i) > Fitness(Best) then
            Best ← P_i
        end if
    end for
    Q ← the μ individuals in P whose fitness are greater
    P ← Q
    for each individual Q_j ∈ Q do
        for λ times do
            perform n-point crossover operator to Q_j
            perform mutation operator to Q_j
            P ← P ∪ { Q_j }
        end for
    end for
until Best is the ideal solution or we have run out of generation
Output Best
```

Fig. 1. Computational flowchart of ESCO

reasons why these operators performed well in GA for solving layout optimization design problem. We borrowed the ideas from the aforementioned operators, and made an initial test to them in ES. Then we found that two-point crossover operator play an important role on location adjustment of circle packing.

Fig.1 shows the computational flowchart of the proposed ESCO. In ESCO, we initialize a population P of λ number of individuals, generated randomly. After the best individual *Best* is initialized, the process of ESCO is iterated as follows. Firstly, the fitness of all the individuals is evaluated. Thus, *Best* individual is assigned by fitness ranking. Secondly, we select μ fittest individuals as Q. Moreover, we perform crossover operator (n-point) for each individual Q_j from Q, then mutation operator. The join operation is simple: the children just replace the parents. The iteration continues anew. The crossover operator can be seen in Fig. 2. For two-point crossover, like genetic algorithm, two parents are chosen and two crossover points, k_1 and k_2, are selected, typically uniformly across the components. Two offspring are created by interchanging the segments defined by the points k_1 and k_2. That is, two offspring are generated by interchanging circles' locations of two parents in circle packing problem.

Parent

$$\boldsymbol{x}_1 = x_{1,1}x_{1,2}\ldots x_{1,k_1}x_{1,k_1+1}\ldots x_{1,k_2}x_{1,k_2+1}\ldots x_{1,d}$$
$$\boldsymbol{x}_2 = x_{2,1}x_{2,2}\ldots x_{2,k_1}x_{2,k_1+1}\ldots x_{2,k_2}x_{2,k_2+1}\ldots x_{2,d}$$

⇩

offspring

$$\boldsymbol{x}'_1 = x_{1,1}x_{1,2}\ldots x_{2,k_1}x_{2,k_1+1}\ldots x_{2,k_2}x_{1,k_2+1}\ldots x_{2,d}$$
$$\boldsymbol{x}'_2 = x_{2,1}x_{2,2}\ldots x_{1,k_1}x_{1,k_1+1}\ldots x_{1,k_2}x_{2,k_2+1}\ldots x_{2,d}$$

Fig. 2. Crossover operator (n-point) used in ESCO

The mutation of ESCO can be formulated as

$$\tilde{X}_i = X_i + N(0,\sigma_i)\,. \tag{1}$$

where σ_i is the variance of the normal distribution, i.e., mutation rate. The mutation can be considered as micro-adjustment of location of circles. Note that online adjustment of σ_i could provide better performance. This online adjustment is known as the one-fifth success rule, which states that around 1/5 of the mutations should be successful. If the actual number of successful mutations is greater than 1/5, increase the variance. If the number is less than 1/5, decrease the variance.

The proposed evolution strategy with crossover operator may be more exploitative than canonical ES because employing mutation only may causes the entire population to prematurely converge to some parent, at which point the whole population has been trapped in the local optimum surrounding the parent, especially for non-linear and multi-modal search space, e.g., circle packing problem.

4 Constrained Circle Packing Problems

The constrained circle packing problems in this study can be simplification of optimal layout problem of a simplified satellite module[4]. We describe it as follows. A total number of N components (circles) must be located within a cylindrical satellite module. The module rotates around axis z at an angular velocity. The bearing plate in the middle of the module, a vertical plane of axis z, is used to fix all the components. All the components are simplified as cuboids or cylinders in this study and regarded as rigid bodies with uniform mass distribution. The design target here is to optimize the inertia performance of whole module, subjected to following constraints: (1) All the components should be contained within the module, with no overlap among the objects and no clash between the module wall and each object; (2) Position error of the centroid of whole system should not exceed an allowable value, as small as possible; (3) Equilibrium error of the system should be permissible and, of course, the smaller the better.

Only cylinder components (circles) will be located within the module in this study. In this study, R denotes the radius of the bearing plate and ω denotes the angular velocity of module. The i th object can be denoted by $X_i(O_i, r_i, m_i), i = 1, 2, ..., N$, where $O_i = (x_i, y_i)$ is the center of the object X_i, and r_i, m_i is the radius and mass of X_i respectively. Then the mathematical model of above problem can be formulated as follows. To find a layout scheme $X = \{X_i \mid i = 1, 2, ..., N\}$, such that

$$\min f(X) = \min\left\{\max\left\{\sqrt{x_i^2 + y_i^2} + r_i\right\}\right\}, i = 1, 2, ..., N, \tag{2}$$

subject to

$$h(X) = \sum_{i=1}^{N-1} \sum_{j=i+1}^{N} \Delta S_{ij} + \sum_{i=1}^{N} \Delta S_i' = 0, \tag{3}$$

$$g(X) = \sqrt{\left(\sum_{i=1}^{N} m_i x_i\right)^2 + \left(\sum_{i=1}^{N} m_i y_i\right)^2} \le \delta_J, \tag{4}$$

where $f(X)$ denotes the maximum envelop radius of all the objects, $h(X)$ denotes the total overlap area among the objects and between the module wall and each object, ΔS_{ij} denotes the overlap area between X_i and X_j, $\Delta S_i'$ denotes the overlap area between the module wall and X_i, $g(X)$ is the distance between the centroid of the whole system and axis z, δ_J is the allowable error of the system should be permissible.

Here, the constrained circle packing problem was converted to an optimization problem using punishment coefficients method. The fitness function was used to evaluate the layout scheme and can be described as

$$F(X) = f(x) + w_1\lambda_1 \max(0, g(X)) + w_2\lambda_2 \left|h(X)\right|, \tag{5}$$

where $\lambda_i (i = 1,2)$ are the normalization factors of each sub objective functions; $w_i (i = 1,2)$ are the weight factors of each sub objective functions.

5 Experimental Study

To evaluate the proposed algorithms, we used the case study introduced by Qian[5], where there were 7 cylinder objects that will be located on the 1 bearing surfaces in the simplified satellite's module. Table 1 listed their dimensions and masses. The equilibrium error of the system should be smaller than a permissible value ($\delta_J = 3.4kg \cdot mm$). The radius of satellite module R was set to be $50mm$.

Table 1. The components' geometry and dimension and mass

No	radius(*mm*)	mass(*kg*)
1	10.0	100.0
2	11.0	121.0
3	12.0	144.0
4	11.5	132.25
5	9.5	90.25
6	8.5	72.25
7	10.5	110.25

5.1 Experiment Setup

A fair time measure must be used to compare the different optimizers. Considering that the number of function evaluations has a strong relationship with cost time, we used the number of function evaluations as a fair time measure in this study. All experiments were run for $3*10^5$ fitness function evaluations. And each of experiments was run 30 times with different random seeds. The reported results are the averages calculated from these 30 runs. Table 2 showed details of the experiment setup from ESCO, ES and GA, which were implement using Python.

Table 2. The experiment setup of ENCO, ES and GA

	ESCO	ES	GA
Selection Operator	all individuals are selected	all individuals are selected	fitness proportionate selection
Crossover Operator	1-point crossover		1-point crossover
Mutation Operator	Gaussian mutation	Gaussian mutation	Gaussian mutation
Mutation Rate	0.25	0.25	0.25

5.2 Experimental Results and Discussion

The experimental results are shown in Fig. 3, Table 3 and Table 4. Table 3 shows the statistic results, including the fitness values and the computing time cost of each algorithm. Table 4 lists the statistic results of performance, including the maximum enveloped radius, overlap area and static non-equilibrium. Fig. 3 shows the comparative

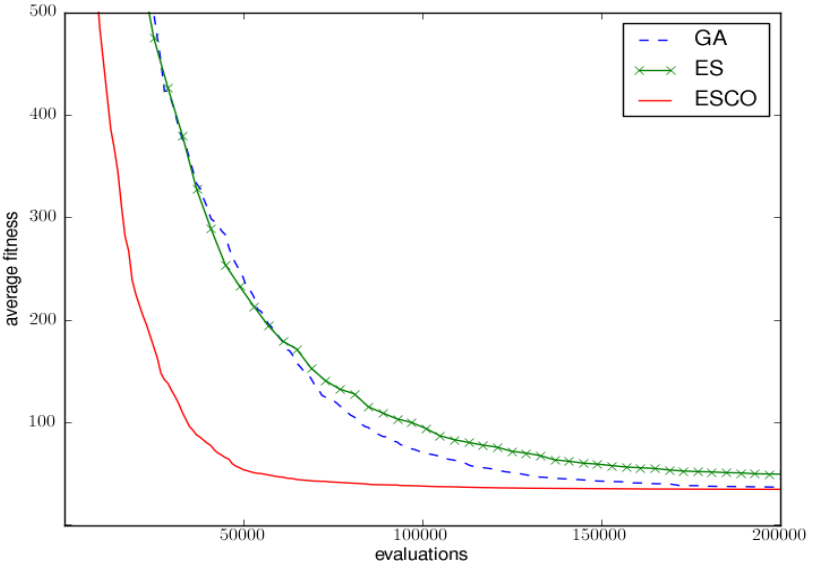

Fig. 3. The comparative result of ESCO, GA, and ES on circle packing problem

Table 3. The comparative results of ESCO, ES and GA

	Fitness values				Computing time			
	Mean	SD	Best	Worst	Mean	SD	Best	Worst
ESCO	34.18	0.95	33.07	37.09	24.87	0.45	23.77	26.33
ES	40.25	14.18	33.34	94.10	24.86	0.43	24.34	26.55
GA	34.58	1.59	33.20	40.65	27.06	1.04	25.73	29.31

Table 4. The comparative performance results of ESCO, ES and GA

	maximum envelop radius				Overlap area		static non-equilibrium			
	Mean	SD	Best	Worst	Mean	SD	Mean	SD	Best	Worst
ESCO	33.80	0.27	33.06	34.09	0.06	0.13	0.84	1.60	0.00	7.69
ES	33.86	0.31	33.16	34.69	1.20	2.75	4.52	4.06	0.00	13.37
GA	33.83	0.26	33.20	34.16	0.12	0.27	1.75	2.20	0.00	9.85

results on average fitness from ESCO, ES and GA. Note that static non-equilibrium in Table 4. shows dimensionless number, just for comparative study.

Table 3 and Table 4 showed that ESCO outperformed canonical ES on all of the packing performance, where the mean fitness value of ESCO decreased by 15.08% than that of ES. That is, ESCO can find better circle packing scheme then ES. The n-point crossover operator in ESCO exchanges the circles' location continually, thus the trend to good packing pattern can be kept. Using the same crossover, the mean fitness value of ESCO (34.18) is approximately equal to the one acquired from that of GA (34.58), but ESCO take less computing time then GA (decreased 2.19 seconds).

From Table 3, we can see that ESCO and GA were able to search feasible layout scheme, that is, overlap area come near to 0 through $3*10^5$ times or less evaluation of fitness function, but the proposed ESCO show the smallest mean overlap area.

Besides, the average static non-equilibrium of ESCO shows the best performance than ES and GA. Fig. 3 also showed ESCO outperformed ES and GA on convergence rate. That is, ESCO can obtain optimum faster than ES and GA. Note that the mentioned-above algorithm implement by Python language needs more time to run than that implement by C language.

6 Conclusion

We improve the basic ES with crossover for constrained circle packing with engineering background of satellite module, aiming at obtaining a better solution-scheme. The problem in this study is very difficult to solve in polynomial time [5] when the amount of circles increase. There was still no perfect solution-scheme in previous studies. We proposed the ESCO for a helpful exploration of this problem. The experimental results showed the effectiveness of ESCO compared with genetic algorithm and canonical evolution strategy. Moreover, the further study will employ the CMA-ES[1] for better performance.

Acknowledgements

This work was supported by National Natural Science Foundation of P R China (Grant No. 50975039).

References

1. Suttorp, T., Hansen, N., Igel, C.: Efficient Covariance Matrix Update for Variable Metric Evolution Strategies. Machine Learning 75, 167–197 (2009)
2. Castillo, I., Kampas, F.J., Pinter, J.D.: Solving Circle Packing Problems by Global Optimization: Numerical Results and Industrial Applications. European Journal of Operational Research 191, 786–802 (2008)
3. Aladahalli, C., Cagan, J., Shimada, K.: Objective Function Effect Based Pattern Search - Theoretical Framework Inspired by 3D Component Layout. Journal of Mechanical Design 129 (2007)
4. Sun, Z.G., Teng, H.F.: Optimal Layout Design of a Satellite Module. Engineering Optimization 35, 513–529 (2003)
5. Qian, Z.Q., Teng, H.F., Xiong, D.L.: Human-computer Cooperation Genetic Algorithm and Its Application to layout design. In: Proceeding of the 4th Asia-Pacific Conference on Simulated Evolution and Learning, Singapore, pp. 299–302 (2002)

Lecture Notes in Computer Science: Research on Multi-robot Avoidance Collision Planning Based on XCS

Jie Shao* and Jing-yu Yang

School of computer Science & Technology, Nanjing University of Science & Technology, Nanjing 210094, P.R. China
School of computer Science & Technology, Nanjing University of Science & Technology, Nanjing 210094, P.R. China
sj012328@163.com

Abstract. This paper presented a novel approach to solving the problem of robot path planning. A Learning Classifier System is an accuracy-based machine learning system that combines covering operator and genetic algorithm. The covering operator is responsible for adjusting precision and large search space according to some reward obtained from the environment. The genetic algorithm acts as an innovation discovery component which is responsible for discovering new better path planning rules. The advantages of this approach are its accuracy-based representation that can easily reduce learning space, improve online learning ability, robustness due to the use of genetic algorithm.

Keywords: Avoidance collision Planning, Multi-robot, Accuracy-based learning classifier system (XCS).

1 Introduction

Path planning is one of the most important topics in robotics research that aims to find a suitable collision-free path for a mobile robot to move from a start position to a target position. Path planning has been extensively explored for many years and many different methods varying degrees of success in a variety of conditions of motion and environments have been developed [1]. Path planning based on genetic algorithm in dynamic environments is still among the most difficult and important problems in mobile robotics. Despite successes of GA in robot path planning. GA has some common shortcomings. One is the computational time required when dealing with a large population, and the other is premature convergence. In addition, because GA is essentially applying discrete random sampling over the solution space, there is a balance

* Jie Shao, born in 1966 , Associate professor. He is currently pursuing the PhD degree in the department of computer science from Nanjing University of science and technology. His research interests include multi-robot path planning, reinforcement learning, neural networks. Jingyu Yang, born in 1941, professor and Ph.D. supervisor in Nanjing University of Science and Technology. His main research interests include pattern recognition, image processing, data fusion and so on.

D.-S. Huang et al. (Eds.): ICIC 2010, LNCS 6215, pp. 94–101, 2010.

between the accuracy of location of the global optimum and the computational resources require [2-4].

That is, in order to improve precision, large search space and premature convergence, this paper presented a novel approach to solving the problem of robot path planning. A Learning Classifier System is an accuracy-based machine learning system that combines covering operator and genetic algorithm. The covering operator is responsible for adjusting precision and large search space according to some reward obtained from the environment. The genetic algorithm acts as an innovation discovery component which is responsible for discovering new better path planning rules. The advantages of this approach are its accuracy-based representation, that can be easily reduce learning space, improve online learning ability, robustness due to the use of genetic algorithm.

The rest of this paper is organized as follows. Section 2 we provides a short review of XCS classifier system. Section 3 we describes our proposed framework. The experimental design and results are described in Section 4.Finally, conclusion and future works are given in Section 5.

2 Accuracy-Based Learning Classifier System

The XCS [5-8] classifier system is an LCS that evolves its classifier by an accuracy-based fitness approach. Each XCS classifier contains the usual condition, action, and reward prediction parts. Complementary, XCS contains a prediction error estimate and a fitness estimate, which represents the relative accuracy of a classifier.

2.1 Implementation Component

The initial classifier set is randomly generated, each classifier is represented as the state, action pair in $|P|$. According to the environmental input, the match set $|M|$ is formed from the population $|P|$, and then action sets $|A|$ composed of classifier's action is generated .The final, an action based on the classifier probability is choosed. The prediction array $P(a_i)$ of each action a_i is calculated by the following equation:

$$P(a_i) = \frac{\sum cl_k \in |M| a_i P_k \times F_k}{\sum cl_k \in |M| a_i F_k} \tag{1}$$

2.2 Reinforcement Component

Each classifier in the process of implementation component will obtain a reward from the environment and the reward prediction, classifier fitness strength will be updated as follows:

$$P \leftarrow R + \gamma \max_a P(a) \tag{2}$$

Where $0 \le \gamma \le 1$ learning rate, R serves as the reward from the environment.

$$P_j \leftarrow P_j + \beta(P - P_j) \tag{3}$$

$$\varepsilon_j \leftarrow \varepsilon_j + \beta(\left|P - \varepsilon_j\right| - \varepsilon_j) \tag{4}$$

$$k_j = \begin{cases} 1 & \text{if } \varepsilon_j \le \varepsilon_0 \\ \alpha(\varepsilon_j / \varepsilon_0)^{-v} & \text{otherwise} \end{cases} \tag{5}$$

$$k_j' = \frac{(kj \times num_j)}{\sum cl_k \in |A|_{-1} (k_k \times num_k)} \tag{6}$$

Where ε_0 （$\varepsilon_0 > 0$） Control prediction errors redundancy, $\alpha(0 < \alpha < 1)$ and $\nu(\nu > 0)$ denote constant, which control decline of accuracy k rate When ε_0 is exceeded. In action set the absolute accuracy value k is converted to a relative accuracy value k'. XCS fitness value is to be updated based on the relative precision of the value:

$$F_j \leftarrow F_j + \gamma^*(k_j' - F_j) \tag{7}$$

2.2.1 Rule Discovery System

The task of rule discovery system is to generate new classifiers by using covering operator and genetic algorithm. If the match set $|M|$ is empty, covering operator will generate new classifier whose condition part will be matched with the environmental message / input message and this new classifier will be added to the classifier store by replacing the worst classifier in order to keep the fixed size of the classifier store.

After reaching timed interval, XCS will select two classifiers from action set $|A|$ by using roulette wheel of fitness for running genetic operators. To sum up, XCS can evaluate the exiting rules and discover high performance rules by using covering operator and genetic algorithm. So its capabilities of implicit parallelism, robust and potential self-adaptive learning will benefit avoidance collision planning.

3 Avoidance Collision Planning Design

3.1 Encoding of Operating Message and Rules

Assume that robot sensors detect area is a fan-shaped region, the robot has 16 sonar that can sense the obstacles and obstructions distance in every area. Robot has three action effectors, with 6-bit binary code, which four of them are for steering angles, one is for speed control, one endnotes forward or backwards. Thus, the rule can be used 22 binary encoding, the format is as fellows:

$$<\text{Condition}>::=\{0,1,\#\}^{16} \tag{8}$$

$$<\text{Action}>::=\{0,1\}^{6} \tag{9}$$

Encoding format of environmental information as follows:

$$<\text{Condition}>::=\{0,1\}^{16}. \tag{10}$$

3.2 Fitness Function Design

We think it as the main elements of reinforcement learning that robot can avoid obstacles in dynamic or static. So we design the fitness function by whether robot is within safety limits and the robot strength.

3.2.1 Whether within the Security

We considered all obstacles as particles, each obstacle has a safe radius, if the distance between robot and obstacle is greater than the safety radius, then considered to be safe; if it is less than the safety radius, then that is not safe. Relationship between the radius R and distance d as follows:

$$fit1 = \begin{cases} 0 & \text{d} \geq \text{R} \\ -1 & \text{d} \leq R \end{cases} \tag{11}$$

where $d = \sqrt{(x_o - x_r)^2 + (y_o - y_r)^2}$, Obstacle coordinates(x_o , y_o) , robot current coordinates(x_r ,y_r). $fit1$ value indicates the robot particle and obstacles are in a safe distance , then its fitness is 0, if the robot particle and obstacles are not in a safe distance, then the fitness is -1.

3.2.2 The Fitness Function for Robot Strength

$$fit2 = S_i(t+1) \tag{12}$$

Taking these factors, the integration fitness function of robot reinforcement learning as follows:

$$f = (1 + fit1) * fit2 \tag{13}$$

3.3 Basic Behavioral Design

Robot behaviors that must execute in the simulated environment consist of three basic behaviors, these behaviors are: move to goal, avoiding collision, negotiation behavior.

3.3.1 Move to Goal

$$V_{goal} = \frac{v_{\max}}{\sqrt{(x_g - x_r)2 + (y_g - y_r)2}} * \begin{bmatrix} x_g - x_r \\ y_g - y_r \end{bmatrix} \tag{14}$$

where $v_{\max}$ denote robot's maximum speed, V_{goal} server as a velocity vector, goal coordinates (x_g,y_g), robot current coordinates(x_r, y_r).

3.3.2 Avoiding Collision

$$V_{col} = V_{goal}\begin{bmatrix}\cos\varphi & -\sin\varphi \\ \sin\varphi & \cos\varphi\end{bmatrix}[x_d \quad y_d]^T \tag{15}$$

where $[x_d \quad y_d]^T$ denote robot current direction, φ denote robot on its own axis of rotation center point of view, counter-clockwise is positive; V_{col} servers as a velocity vector.

3.3.3 Negotiation Behavior

It is closely related that robot collision avoidance behavior and real-time access to sensor information. Suppose information a robot get from environmental can be attributed to a series of a certain set of rules

$$M = \{M_1, M_2, \cdots, M_n\} \tag{16}$$

$$A = \{A_1, A_2, \cdots, A_8\} \tag{17}$$

where, M denote robot's sensor information total set M_i $(1 \le i \le n)$ denote the robot subset of sensor information, A server as total set of robot actions, A_i denote the robot subset of actions.

A robot with other robots consultation process is as follows:

① Establish an information list based on sensor information.

② LCS release own information through the broadcasting operation to other robots, while accepting other LCS information.

③ Establishing every robot LCS rules set, and sharing best path planning generated by the other LCS rules to avoid conflicts each other.

④ Producing their own path planning rules, and generating the entire multi-robot collision avoidance planning by using covering operator and genetic algorithm. otherwise returns to ②.

4 Experiments and Simulation

Suppose the activities region of the robot is a rectangular area, O1-O3 are three dynamic obstacles, the rest is static obstacles in the region. Fig.1 shows the robot reinforcement learning in a static environment. Fig.2 shows robot reinforcement learning in a dynamic environment, effectively improving the learning convergence speed.

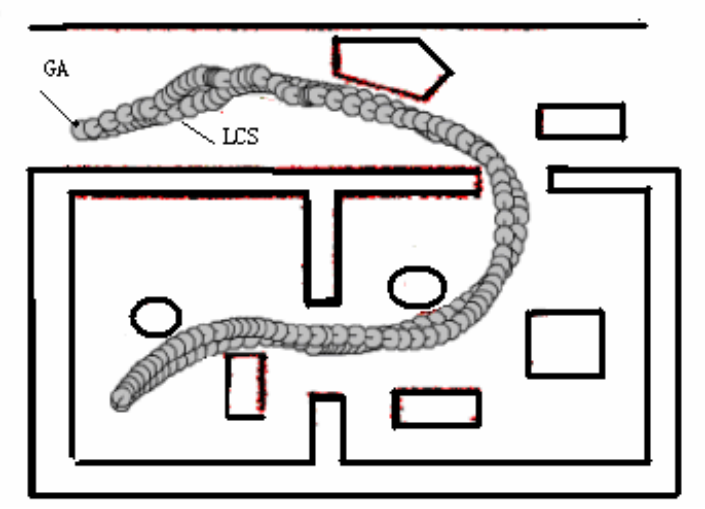

Fig. 1. The robot avoidance collision in a static environment based on GA or LCS

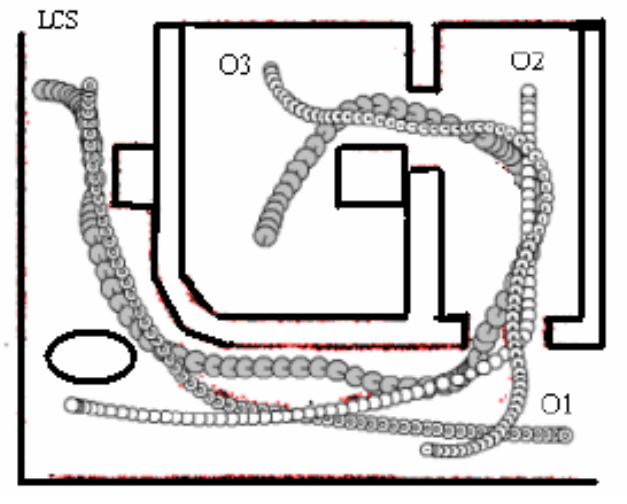

Fig. 2. The robot avoidance collision in a dynamic environment based on LCS

Fig.3 is the convergence curves in the static environment based on LCS or GA, robots have made a better learning convergence. Fig.4 is the convergence curves of the dynamic environment GA-based, robot have not made a better learning effect, due to the phenomenon of jumping behavior. Figure 5 shows convergence curve in a dynamic environment based on LCS, although the initial stage of learning turbulence, but with the increase in the number of iterations, the robot finally have achieved a good convergence, no convergence of the local minimum or local hopping phenomenon.

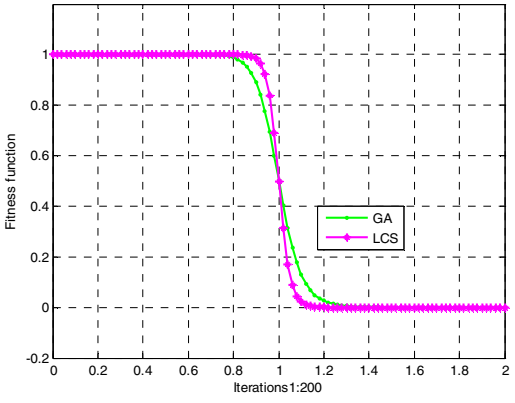

Fig. 3. Learn convergence curve in the dynamic environment based on LCS or GA

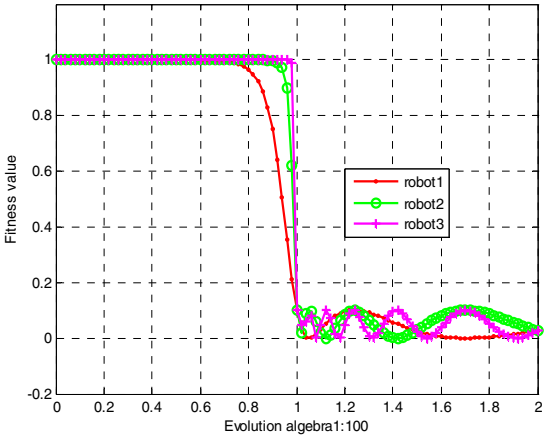

Fig. 4. Learn convergence curve under the dynamic environment based on GA

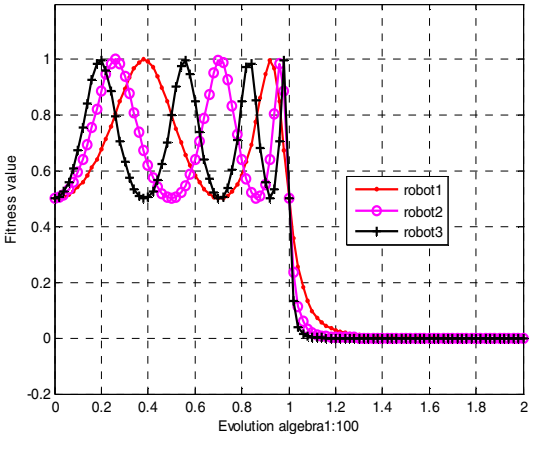

Fig. 5. Learn convergence curve under the dynamic environment based on LCS

5 Conclusions

This paper presented a novel approach to solving the problem of robot path planning. A Learning Classifier System is an accuracy-based machine learning system that combines covering operator and genetic algorithm. The covering operator is responsible for adjusting precision and large search space according to some reward obtained from the environment. The genetic algorithm acts as an innovation discovery component which is responsible for discovering new better path planning rules. The advantages of this approach are its accuracy-based representation, that can be easily reduce learning space, online learning ability, robustness due to the use of genetic algorithm. Simulation indicated that the accuracy-based learning classifier system used in the multi-robot's avoidance collision planning is effective.

Acknowledgements

This work was supported by National Natural Science Foundation of P. R. China (60705020).

References

1. Bernad'o-Mansilla, E., Garrell, J.: Accuracy-based Learning Classifier Systems: Models, Analysis and Applications to Classification Tasks. Evolutionary Computation 11(3), 209–238 (2003)
2. Hung, K.T., Liu, J.S., Chang, Y.Z.: Smooth Path Planning for a Mobile Robot by Evolutionary Multiobjective Optimization. In: IEEE Int. Symposium on Computational Intelligence in Robotics and Automation, Jacksonville, Florida (2007)
3. Berg, J., Lin, M., Manocha, D.: Reciprocal Velocity Obstacles for Real-time Multi-agent Navigation. In: Proc. IEEE Int. Conf. Robot. Autom., Pasadena, CA, pp. 1928–1935 (2008)
4. Gemeinder, M., Gerke, M.: GA-based Path Planning for Mobile Robot Systems Employing an Active Search Algorithm. Applied Soft Computing 3, 149–158 (2003)
5. Baneamoon, S.M., Abdul Salam, R., Talib, A.Z.Hj.: Learning Process Enhancement for Robot Behaviors. International Journal of Intelligent Technology 2(3), 172–177 (2007)
6. Bull, L., Studley, M., Bagnall, I., Whittley, I.: Learing Classifier System Ensembles with Rule-sharing. IEEE transactions on evolutionary computation (4) (August 2007)
7. Baneamoon, S.M., Salam, R.A.: Applying Steady State in Genetic Algorithm for Robot Behaviors. In: 2008 International conference on Electronic Design, Malasia, December 1-3 (2008)
8. Bull, L.: A Simple Accuracy-based Learning Classifier System. University of the West of England, Bristol (2003)

An Integrated Method for the Construction of Compact Fuzzy Neural Models

Wanqing Zhao[1], Kang Li[1], George W. Irwin[1], and Minrui Fei[2]

[1] Intelligent Systems and Control,
School of Electronics, Electrical Engineering and Computer Science,
Queen's University Belfast, Belfast, BT9 5AH, UK
[2] Shanghai Key Laboratory of Power Station Automation Technology,
School of Mechatronical Engineering and Automation,
Shanghai University, Shanghai 200072, China

Abstract. To construct a compact fuzzy neural model with an appropriate number of inputs and rules is still a challenging problem. To reduce the number of basis vectors most existing methods select significant terms from the rule consequents, regardless of the structure and parameters in the premise. In this paper, a new integrated method for structure selection and parameter learning algorithm is proposed. The selection takes into account both the premise and consequent structures, thereby achieving simultaneously a more effective reduction in local model inputs relating to each rule, the total number of fuzzy rules, and the whole network inputs. Simulation results are presented which confirm the efficacy and superiority of the proposed method over some existing approaches.

Keywords: Compact fuzzy neural models, Rule consequents and premises, Structure selection and parameter learning, Local model inputs.

1 Introduction

The fuzzy inference system, which is based on the concepts of fuzzy sets, if-then rules, and fuzzy reasoning, has been successfully used in many engineering applications due to its transparence, interpretability and ability to incorporate expert knowledge. Moreover, fuzzy neural networks (FNNs) are fuzzy inference systems that are implemented as neural nets. They aim to combine the learning capability of neural networks with the transparency and interpretability of rule-based fuzzy systems. This paper will focus on Takagi-Sugeno fuzzy neural modelling of nonlinear dynamic systems. The most well-known architecture for this kind of networks is the adaptive network-based fuzzy inference system (ANFIS) [1] [2]. Determining a fuzzy neural network representation of a dynamical system requires structural optimization plus estimation of the parameters.

The Takagi-Sugeno fuzzy model has proved to be a very good representation of a certain class of nonlinear dynamic systems. However, the resulting network complexity can be extremely high. The challenge then is to construct a useful model consisting of the smallest possible network based on the parsimonious

D.-S. Huang et al. (Eds.): ICIC 2010, LNCS 6215, pp. 102–109, 2010.

principle. To tackle this problem, a number of FNN construction methods have been proposed in the literature either to determine the number of inputs, the number of terms, or the number of rules. Given some fuzzy model construction criterion, this can be achieved by an exhaustive search of all possible combinations of regression terms using the least-squares method. To reduce computational demand, orthogonal least squares (OLS) and its variants are the most popular approaches for solve a model with redundancy in model terms [3] [4].

To further decrease the computational complexity, Li et al [5] proposed a fast recursive algorithm (FRA) which avoids any matrix decomposition. This has also been used for rule selection in the context of FNNs [6] [7]. The main limitation of most of these approaches is that they assume a linear-in-the-parameters model. More specifically, these methods mainly deal with the rule consequents, therefore failing to explore the full potential of the optimal structure and parameters in the premise thus the optimal local models relating to the corresponding linguistics. Further, input selection is often been performed prior to rule selection, leading to a less compact fuzzy neural model since input selection is closely related to rule selection. In this paper, a new integrated method for combined structure selection and parameter learning is used to simultaneously select the most significant local model inputs related to each rule, the total number of fuzzy rules, and all the network inputs to produce a model for entire system, thus leading to a more compact FNN.

2 Preliminaries

Consider a wide class of nonlinear dynamic systems with multiple inputs u_j, $j = 1, \ldots, n$ and an output y that can be represented using a discrete-time input/output NARX model (nonlinear autoregressive with exogenous input):

$$\begin{aligned} y(t) =& g(u_1(t-1), \ldots, u_1(t-n_u), \ldots, u_n(t-1), \ldots, \\ & u_n(t-n_u), y(t-1), \ldots, y(t-n_y)) + \varepsilon(t) \end{aligned} \tag{1}$$

where $y(t)$ is the system output at the time instant t ($t = 1, \ldots, N$), $g(\cdot)$ is some unknown nonlinear function comprised of a finite number of the past inputs and outputs (n_u and n_y are the input and output dynamic orders of the system), and $\varepsilon(t)$ represents the model residual which is an uncorrelated white noise sequence.

Typically, model (1) can be approximated using a set of local models based on the corresponding interpretable rules of the following form:

$$R_i: \ \textbf{IF}\ x_1(t) = A_{i1}\ \textbf{AND} \ldots \textbf{AND}\ x_n(t) = A_{in}\ \textbf{THEN}\ y(t) = f_i(\mathbf{x}(t)) \tag{2}$$

where $\mathbf{x}(t) = [x_1(t), \ldots, x_n(t)] \in \Re^n$ represents n inputs for the fuzzy system, $y(t)$ is the system output realized using a local model $f_i(\cdot)$, i is the rule index, A_{ij} denotes the fuzzy sets under rule i with regard to input x_j. Assuming Gaussian membership functions and first-order polynomials are used, the fuzzy inference mechanism can then be employed to calculate the model output as follows:

$$\hat{y}(t) = \sum_{i=1}^{N_r} f_i(\mathbf{x}(t), \mathbf{w}_i)\mu_i(\mathbf{x}(t), c_i, \sigma_i) \Big/ \sum_{i=1}^{N_r} \mu_i(\mathbf{x}(t), c_i, \sigma_i) = \sum_{i=1}^{N_r} v_i(t) f_i(\mathbf{x}(t), \mathbf{w}_i) \tag{3}$$

where $\mu_i(\mathbf{x}(t), c_i, \sigma_i)$ represents each individual rule defined as:

$$\mu_i(\mathbf{x}(t), c_i, \sigma_i) = \prod_{j=1}^{n} \mu_{ij}(x_j(t), c_{ij}, \sigma_{ij}) = \prod_{j=1}^{n} \exp\left\{-\frac{1}{2}\left(\frac{x_j(t) - c_{ij}}{\sigma_{ij}}\right)^2\right\} \quad (4)$$

where N_r is the total number of fuzzy rules, c_{ij} and σ_{ij} denote the centre and standard deviation of the ith membership function with regard to the jth input. Also $v_i(t)$ is the validity function which determines the valid region for each rule defined as:

$$v_i(t) = \mu_i(\mathbf{x}(t), c_i, \sigma_i) \Big/ \sum_{i=1}^{N_r} \mu_i(\mathbf{x}(t), c_i, \sigma_i) \quad (5)$$

$$f_i(\mathbf{x}(t), \mathbf{w}_i) = w_{i0} + \sum_{j=1}^{n} w_{ij} x_j(t) \quad (6)$$

Further $f_i(\mathbf{x}(t), \mathbf{w}_i)$ is the ith local linear model given by (6) where $\mathbf{w}_i = [w_{i0}\ w_{i1} \cdots w_{in}]^T \in \Re^{n+1}$ denotes the associated coefficient parameters. Assuming a set of observed data $\{\mathbf{x}(t) \in \Re^n, y(t) \in \Re\}, (t = 1, \ldots, N)$, substituting (3) into (1), gives:

$$\mathbf{y} = \mathbf{\Phi W} + \mathbf{\Xi} \quad (7)$$

where $\mathbf{y} = [y(1), \ldots, y(N)]^T \in \Re^N$ is the output vector, $\mathbf{W} = [w_{10}, \ldots, w_{1n}, \ldots, w_{N_r 0}, \ldots, w_{N_r n}]^T \in \Re^{(n+1)N_r}$ is the linear parameter vector associated with the rule consequent, $\mathbf{\Xi} = [\varepsilon(1), \ldots, \varepsilon(N)]^T \in \Re^N$ is the residual vector, and $\mathbf{\Phi}$ is the regression matrix defined in (8) with $\phi_i(t) = [v_i(t), \ldots, v_i(t)x_n(t)]^T \in \Re^{n+1}$, $i = 1, \ldots, N_r$, as the basis vectors.

$$\mathbf{\Phi} = [\phi_1, \phi_2, \ldots, \phi_{N_r}],\ \phi_i = [\phi_i(1), \phi_i(2), \ldots, \phi_i(N)]^T \quad (8)$$

3 Integrated Method for Structure Selection and Parameter Learning

The proposed integrated method for structure selection and parameter learning consists of the following steps. 1) Initial model construction; 2) Premise parameter optimization; 3) Consequent structure selection. In order to obtain the initial fuzzy rules to define approximate operating regions for the underlying system, Chiu's subtractive clustering method [8] can be applied. The following procedure is thus used on this initial model.

3.1 Premise Parameter Optimization

Consider the Takagi-Sugeno type fuzzy system described in Eqs. (2)-(8), assume a set of observed data $\{\mathbf{x}(t) \in \Re^n, y(t) \in \Re\}, (t = 1, \ldots, N)$, and define the following loss function:

$$\mathbf{E} = \frac{1}{2}\sum_{t=1}^{N} (y(t) - \hat{y}(t))^2 = \frac{1}{2}\mathbf{e}^T\mathbf{e} \quad (9)$$

where $\mathbf{e} = [e(1), e(2), \ldots, e(N)]^T \in \Re^N$, $e(t) = y(t) - \hat{y}(t)$, for $t = 1, \ldots, N$. The gradients of $e(t)$ with respect to the nonlinear parameters are computed using Eqs. (10)-(11).

$$\frac{\partial e(t)}{\partial c_{ij}} = -\frac{f_i(x(t), w_i) - \hat{y}(t)}{\sum_{i=1}^{N_r} \mu_i(x(t), c_i, \sigma_i)} \mu_i(x(t), c_i, \sigma_i) \frac{x_j(t) - c_{ij}}{\sigma_{ij}^2} \tag{10}$$

$$\frac{\partial e(t)}{\partial \sigma_{ij}} = -\frac{f_i(x(t), w_i) - \hat{y}(t)}{\sum_{i=1}^{N_r} \mu_i(x(t), c_i, \sigma_i)} \mu_i(x(t), c_i, \sigma_i) \frac{(x_j(t) - c_{ij})^2}{\sigma_{ij}^3} \tag{11}$$

Suppose $J_i(t) = \left[\frac{\partial e(t)}{\partial c_{i1}} \frac{\partial e(t)}{\partial \sigma_{i1}} \frac{\partial e(t)}{\partial c_{i2}} \frac{\partial e(t)}{\partial \sigma_{i2}} \cdots \frac{\partial e(t)}{\partial c_{in_i}} \frac{\partial e(t)}{\partial \sigma_{in_i}}\right]^T$, $i = 1, \ldots, N_r^l$, where n_i represents the number of inputs under the ith rule. The Jocobian matrix is then defined by (12) with N_r^l denotes the number of fuzzy rules at iteration l.

$$\mathbf{J}^{l)} = [J_1, J_2, \ldots, J_{N_r^l}],\ J_i = [J_i(1), J_i(2), \ldots, J_i(N)]^T \tag{12}$$

The Levenberg-Marquardt method is then applied to optimize the nonlinear parameters of centres and widths in the rule premise defined by (13), where $\mathbf{\Theta}^{l)} = \left[\theta_1, \theta_2, \ldots, \theta_{N_r^l}\right]^T$ and $\theta_i = [c_{i1}, \sigma_{i1}, \ldots, c_{in_i}, \sigma_{in_i}] \in \Re^{2n_i}$.

$$\mathbf{\Theta}^{l+1)} = \mathbf{\Theta}^{l)} - \left((\mathbf{J}^{l)})^T \mathbf{J}^{l)} + \gamma \mathbf{I}\right)^{-1} (\mathbf{J}^{l)})^T \mathbf{e}^{l)} \tag{13}$$

In (13), γ is the regularization factor, and $\mathbf{\Phi}^{l)}$ are given by (14) with $\varphi_i(t) = [v_i(t), v_i(t)x_1(t), \cdots, v_i(t)x_{n_i}(t)]^T \in \Re^{n_i+1}$.

$$\mathbf{\Phi}^{l)} = \left[\varphi_1, \varphi_2, \ldots, \varphi_{N_r^l}\right],\ \varphi_i = [\varphi_i(1), \varphi_i(2), \ldots, \varphi_i(N)]^T \tag{14}$$

3.2 Structure Selection Procedure

To improve the model compactness, the FRA [5] from our previous work within the context of fuzzy basis vectors defined by premise parameters can be applied. The structure selection procedure can be roughly described as follows. 1) In order to select the basis vectors, the net contribution of each candidate vector to the cost function is first computed. 2) The basis vector giving the maximal reduction in the cost function will then be added in the model. 3) The first two steps continue, until a stopping criteria is met, thus achieving a compact model.

The procedure starts by setting the number of selected basis vectors as $k = 0$, and initializing other intermediate matrices and vectors: $\mathbf{S}_k^{l)}$ is the selected pool including all selected vectors at step k initialized with an empty matrix at the beginning of the lth iteration, $\mathbf{C}_k^{l)}$ denotes the candidate pool at step k for the lth iteration including all the remaining basis vectors, and $\mathbf{C}_0^{l)} = \mathbf{\Phi}^{l)}$, $s_{k,m}^{l)}$ and $c_{k,j}^{l)}$ represent candidate basis vectors from $\mathbf{C}_{k-1}^{l)}$ and $\mathbf{C}_k^{l)}$, where $m = 1, \ldots, n-k+1$.

With these definitions it is obvious that: $\mathbf{S}_{k,m}^{l)} \triangleq [\mathbf{S}_{k-1}^{l)}] + [s_{k,m}^{l)}]$, $\mathbf{C}_{k,m}^{l)} \triangleq [\mathbf{\Phi}^{l)}] - [\mathbf{S}_{k,m}^{l)}]$, Now defining a recursive matrix $\mathbf{R}_{k-1}^{l)}$

$$\mathbf{R}_{k-1}^{l)} \triangleq \mathbf{I} - \mathbf{S}_{k-1}^{l)} \left(\left(\mathbf{S}_{k-1}^{l)} \right)^T \mathbf{S}_{k-1}^{l)} \right)^{-1} \left(\mathbf{S}_{k-1}^{l)} \right)^T \in \Re^{N \times N} \tag{15}$$

then $\mathbf{R}_{k,m}^{l)}$ is associated with a single new candidate vector selected from $\mathbf{C}_{k-1}^{l)}$. According to [5], the following properties hold:

$$\left(\mathbf{R}_{k-1}^{l)} \right)^T = \mathbf{R}_{k-1}^{l)}, \left(\mathbf{R}_{k-1}^{l)} \right)^2 = \mathbf{R}_{k-1}^{l)} \tag{16}$$

$$\mathbf{R}_{k,m}^{l)} = \mathbf{R}_{k-1}^{l)} - \mathbf{R}_{k-1}^{l)} s_{k,m}^{l)} \left(s_{k,m}^{l)} \right)^T \left(\mathbf{R}_{k-1}^{l)} \right)^T \Big/ \left(\left(s_{k,m}^{l)} \right)^T \mathbf{R}_{k-1}^{l)} s_{k,m}^{l)} \right) \tag{17}$$

Further defining $s_{k,i}^{l),k-1)} = \mathbf{R}_{k-1}^{l)} s_{k,i}^{l)}$, $i = 1, \ldots, n-k+1$, according to (16) and (17), the net contribution of $s_{k,m}^{l)}$ to the cost function is given as:

$$\delta \mathbf{E}_{k,m}^{l)} = \mathbf{y}^T \left(\mathbf{R}_{k-1}^{l)} - \mathbf{R}_{k,m}^{l)} \right) \mathbf{y} = \left(\mathbf{y}^T s_{k,m}^{l),k-1)} \right)^2 \Big/ \left(\left(s_{k,m}^{l),k-1)} \right)^T s_{k,m}^{l),k-1)} \right) \tag{18}$$

To simplify the computation of $\delta \mathbf{E}_{k,m}^{l)}$, $[a_{r,c}^{l)}]_k \in \Re^{k \times n}$ are defined with the first k columns computed as (19), and then define $[a_r^{l)}]_k \in \Re^k$ according to (20).

$$\left[a_{r,c}^{l)} \right]_{k,m} \triangleq \begin{cases} 0, & c < r \\ \left[a_{r,c}^{l)} \right]_{k-1}, & r \le c < k \\ \left[a_{r,k+m-1}^{l)} \right]_{k-1}, & c = k, r < k \\ \left(s_{k,m}^{l),k-1)} \right)^T s_{k,m}^{l),k-1)}, & c = k, r = k \end{cases} \tag{19}$$

$$\left[a_r^{l)} \right]_{k,m} \triangleq \begin{cases} \left[a_r^{l)} \right]_{k-1}, & 1 \le r < k \\ \left(s_{k,m}^{l),k-1)} \right)^T \mathbf{y}, & r = k \end{cases} \tag{20}$$

FRA accordingly used for updating these quantities recursively as:

$$\left(s_{k,m}^{l),k-1)} \right)^T s_{k,m}^{l),k-1)} = \left(s_{k,m}^{l)} \right)^T s_{k,m}^{l)} - \sum_{j=1}^{k-1} \left(\left[a_{j,k}^{l)} \right]_{k,m}^2 \Big/ \left[a_{j,j}^{l)} \right]_{k,m} \right) \tag{21}$$

$$\left(s_{k,m}^{l),k-1)} \right)^T \mathbf{y} = \left(s_{k,m}^{l)} \right)^T \mathbf{y} - \sum_{j=1}^{k-1} \left(\left[a_{j,k}^{l)} \right]_{k,m} \left[a_j^{l)} \right]_{k,m} \Big/ \left[a_{j,j}^{l)} \right]_{k,m} \right) \tag{22}$$

Finally the required value for $\delta\mathbf{E}_{k,m}^{l)}$ easily follows from:

$$\delta\mathbf{E}_{k,m}^{l)} = \left(\left[a_k^{l)}\right]_{k,m}^T\right)^2 \Big/ \left[a_{k,k}^{l)}\right]_{k,m} \tag{23}$$

The value of $\delta\mathbf{E}_{k,m}^{l)}$ is calculated for $m=1,\ldots,n-k+1$, then $s_k^{l)} = \arg\max \delta\mathbf{E}_{k,m}^{l)}$, the following quantities are updated ('$\leftarrow$' means the value has been determined):

$$\mathbf{R}_k^{l)} = \mathbf{R}_{k,m}^{l)}\{s_k^{l)} \leftarrow s_{k,m}^{l)}\}, \delta\mathbf{E}_k^{l)} = \delta\mathbf{E}_{k,m}^{l)}\{s_k^{l)} \leftarrow s_{k,m}^{l)}\}, s_k^{l),k-1)} = s_{k,m}^{l),k-1)}\{s_k^{l)} \leftarrow s_{k,m}^{l)}\}$$

and thus the full n columns of $[a_{r,c}^{l)}]_k$ and $[a_r^{l)}]_k$ can be computed as:

$$\left[a_{r,c}^{l)}\right]_k = \begin{cases} 0, & c < r \\ \left[a_{r,c}^{l)}\right]_{k-1}, & r \le c < k \\ \left[a_{r,k+m-1}^{l)}\right]_{k-1}, & c = k, r < k \\ \left[a_{r,k}^{l)}\right]_{k-1}, & c = k+m-1, c < k \\ \left(s_k^{l),k-1)}\right)^T s_k^{l),k-1)}, & c = k, r = k \\ \left(s_k^{l),k-1)}\right)^T \mathbf{R}_{k-1}^{l)} c_{k,c-k}^{l)}, & c > k, r = k \end{cases} \tag{24}$$

$$\left(s_k^{l),k-1)}\right)^T \mathbf{R}_{k-1}^{l)} c_{k,c-k}^{l)} = \left(s_k^{l)}\right)^T c_{k,c-k}^{l)} - \sum_{j=1}^{k-1} \left(\left[a_{j,k}^{l)}\right]_k \left[a_{j,c}^{l)}\right]_k \Big/ \left[a_{j,j}^{l)}\right]_k\right) \tag{25}$$

$$\left[a_r^{l)}\right]_k = \begin{cases} \left[a_r^{l)}\right]_{k-1}, & 1 \le r < k \\ \left(s_k^{l),k-1)}\right)^T \mathbf{y}, & r = k \end{cases} \tag{26}$$

The result is now that a new basis vector is added to the selected pool $\mathbf{S}_k^{l)} = [\mathbf{S}_{k-1}^{l)}] + [s_k^{l)}]$, and thus the candidate pool in turn changes to $\mathbf{C}_k^{l)} = [\mathbf{\Phi}^{l)}] - [\mathbf{S}_k^{l)}]$. Since the training error will fall rapidly at the start of the selection procedure, but the improvement will then decrease with time and excessive terms may be included to the model. In this paper, the error reduction ratio (ERR) [3] is modified to be the SSE (sum of squared error) ratio defined of two successive selected models. If ERR is greater than a predetermined threshold, then the procedure continues, otherwise it stops. Through the procedure, some fuzzy basis vectors and their associated input vectors will be eliminated from the corresponding local models. Thus the scope and characteristics of a local region are only determined by the most relevant local inputs. Moreover, at the end of each iteration, a local model that has insignificant terms will be removed together with its corresponding rule. Meantime, an input that is not included in any of the rules or is only expressed in a very small number of rules will be removed, which implement the required input selection.

4 Simulation Example

The proposed algorithm from section 3 is now applied to the modelling of the following nonlinear system [4].

$$y(t) = \frac{2.5y(t-1)y(t-2)}{1+y^2(t-1)+y^2(t-2)} + 0.3\cos(0.5(y(t-1)+y(t-2))) + 1.2u(t-1) + e(t)$$

where the system input and noise sequences are given by:

$$u(t) = (1/2)\left(\sin(\pi t/20) + \sin(\pi t/50)\right), e(t) \backsim N(0, 0.05^2)$$

A data sequence of 1000 samples was generated. The first 500 samples were used for modelling, while the remaining were used for validation. The full input set was initially set as

$$X = [u(t-1), u(t-2), y(t-1), y(t-2), y(t-3)],\ (n_u = 2, n_y = 3)$$

Chiu's subtractive clustering method [8] was first applied to generate an initial structure (the cluster radius is defined as 0.3), then the integrated method for structure selection and parameter learning algorithm was applied with five different ERR values tested separately. The results are summarized in Table 1.

Table 1. The results of proposed method with different ERR

ERR	Training SSE	Testing SSE	Selected Inputs	Number of Rules
1.000	1.0206	1.8208	1,2,3,4,5	9
1.001	1.0373	1.7621	1,2,3,4,5	9
1.002	1.0746	1.6103	1,2,3,4,5	8
1.003	1.2098	1.5249	1,3,4	6
1.004	1.7753	2.0394	1,3,4	4

The regularization factor γ in (13) was chosen as 0.5. According to Table 1, as the ERR value increases, the SSE in the modelling dataset increases, while the SSE on the validation dataset decreases for the first four cases while it increases

Table 2. The proposed method compared with different models/Algorithms

Model/Algorithm	Number of Rules	Training SSE	Testing SSE	Inputs
RBF [9]	20	1.67	1.86	1,2,3,4,5
ANFIS [1]	32	0.98	1.78	1,2,3,4,5
DENFIS [10]	14	1.29	1.59	1,2,3,4,5
FRSA [7][1]	19	1.24	1.77	1,3,4
The Proposed Method	6	1.21	1.52	1,3,4

[1] It is assumed that the inputs are known firstly as y(t-1), y(t-2), u(t-1).

for others. It can be seen that the best fuzzy neural model is the fourth one with six rules and three inputs. The proposed new technique is then compared with four other models/algorithms produced by terms of rules (nodes), testing error and system inputs. Table 2 shows that the proposed method outperforms the alternatives in terms of model compactness and performance.

5 Conclusion

A new integrated method for structure selection and parameter learning algorithm has been introduced for the construction of compact fuzzy neural network models. The most significant basis vectors are selected based on both the premise structure and consequent structure, thereby achieving effective reduction in local model inputs, fuzzy rules, and system inputs simultaneously. The effectiveness of the method has been confirmed in a simulation example.

Acknowledgments. This work is supported by UK-China Science Bridge grant EP/G042594/1, EP/F021070/1, the China Scholarship Council, and the Key Project of Science and Technology Commission of Shanghai Municipality under grant 08160512100 and 08160705900.

References

[1] Jang, J.S.R.: ANFIS: Adaptive-network-based fuzzy inference system. IEEE Trans. Systems, Man, Cybernetics 23, 665–685 (1993)
[2] Shoorehdeli, M.A., Teshnehlab, M., Sedigh, A.K.: Training ANFIS as an identier with intelligent hybrid stable learning algorithm based on particle swarm optimization and extended kalmanlter. Fuzzy Sets and Systems 160, 922–948 (2009)
[3] Chen, S., Hong, X., Luk, B.L., Harris, C.J.: Orthogonal-least-squares regression: A unied approach for data modelling. Neurocomputing 72, 2670–2681 (2009)
[4] Hong, X., Harris, C.J., Chen, S.: Robust neurofuzzy rule base knowledge extraction and estimation using subspace decomposition combined with regularization and d-optimality. IEEE Trans. Syst. Man Cybern-Pt B: Cybern. 34, 598–608 (2004)
[5] Li, K., Peng, J.X., Irwin, G.W.: A fast nonlinear model identication method. IEEE Transactions on Automatic Control 50, 1211–1216 (2005)
[6] Pizzileo, B., Li, K., Irwin, G.W.: A fast method for fuzzy neural modelling and renement. Int. Journal of Modelling, Identication and Control 8, 175–183 (2009)
[7] Pizzileo, B., Li, K.: A new fast algorithm for fuzzy rule selection. In: IEEE International Conference on Fuzzy Systems. Imperial College, London (2007)
[8] Chiu, S.L.: Fuzzy model identication based on cluster estimation. J. Intell. Fuzzy Systems 2, 267–278 (1994)
[9] Kasabov, N.K., Song, Q., et al.: Neucom - a neuro-computing decision support enviroment. AUT University, New Zealand (2008), http://www.theneucom.com/
[10] Kasabov, N.K., Song, Q.: Denfis: Dynamic evolving neural-fuzzy inference system and its application for time-series prediction. IEEE Transactions on Fuzzy Systems 10, 144–154 (2002)

Scalarization of Type-1 Fuzzy Markov Chains

Dusko Kalenatic[1,⋆], Juan C. Figueroa-García[2,⋆⋆], and Cesar Amilcar Lopez[3,⋆⋆⋆]

[1] Universidad de La Sabana, Chia - Colombia
dusko.kalenatic@unisabana.edu.co
[2] Universidad de La Sabana, Chia - Colombia
juan.figueroa@unisabana.edu.co
[3] Universidad de La Sabana, Chia - Colombia
cesar.lopez@unisabana.edu.co

Abstract. This paper presents a method to transform Fuzzy Markov chains into Crisp Markov chains by means of an equivalence matrix derived from the concept of *Scalar cardinality* of a fuzzy set. This proposal is a linear transformation of the fuzzy space into a probability space.

In this paper, a finite-state Fuzzy Markov Chain is transformed into a crisp Markov chain by a linear operator. It is a projection of the fuzzy space into a probability space which allows to compare them one another.

1 Introduction and Motivation

Markov chains is an important stochastic process studied by many staticians on a probabilistic context. Its application to many problems with successful results is wide. An appropriate treatment of this topic is given by Grimmet & Strizaker in [1], Ross in [2], Gordon in [3] and Stewart in [4].

The Fuzzy Markov chain *(FM)* stochastic process has been treated by Sanchez in [5] and [6], Avrachenkov and Sanchez in [7] and Araiza, et. al. in [8] defining algorithms, fuzzy relations and compositions to compute its stationary distribution.

The theoretical distinction between the FM and the CM lies in the functional form that represents the conditional statement given by the Markovian property. Even so, some similarity measures can be defined in that context, as the presented one.

This paper is divided into six sections. Section 1 is an Introductory section. In Section 2 some concepts of Type-1 Fuzzy Markov Chains (FM) are defined. Section 3 presents definitions about the Cumulative Membership Function. In Section 4 a linear transformation of the FM into a CM is defined. In Section 5 some application examples are provided, and finally the Section 6 presents the concluding remarks of the paper.

⋆ Dusko Kalenatic is member of the Logistic Systems group - Universidad de La Sabana.
⋆⋆ Corresponding author.
⋆⋆⋆ Cesar A. Lopez is member of the Logistic Systems research group - Universidad de La Sabana.

D.-S. Huang et al. (Eds.): ICIC 2010, LNCS 6215, pp. 110–117, 2010.

2 Basic Definitions of Fuzzy Markov Chains

Such as in the classical Markov processes analysis, the definition of a Fuzzy Markov Chain is based on a squared relational matrix that represents the possibility that a discrete state at instant t becomes into any state at next instant $t+1$ as follows:

$$P(X^{(t)} = s \mid X^{(t-1)} = x^{(t-1)}) \tag{1}$$

Here, $P(X^{(t)})$ is a fuzzy distribution of the process characterized by a membership function. In this paper, we use the definition of fuzzy randomness given by Yian-Kui Liu & Baoding Liu in [9].

Definition 1. *Let $S = \{1, 2, \cdots, n\}$. A finite fuzzy set for a fuzzy distribution on S is defined by a mapping x from S to $[0, 1]$ represented by a vector $x = \{x_1, x_2, \cdots, x_n\}$, with $0 \leqslant x_i \leqslant 1$, $i \in S$.*

In this definition, x_i is the membership degree[1] that a state i has regarding a fuzzy set S, $i \in S$ with cardinality m, $\mathcal{C}(S) = m$. All relations and compositions are defined by fuzzy sets theory since are useful tools to find a fuzzy stationary distribution.

Now, a fuzzy relational matrix P is defined in a metric space $S \times S$ by a matrix $\{p_{ij}\}_{i,j=1}^{m}$ with $0 \leqslant p_{ij} \leqslant 1$, $i, j \in S$. The complete set of all fuzzy sets is denoted by $\mathcal{F}(s)$ where $\mathcal{C}(S) = m$.

This fuzzy matrix P allows to define all relations among the m states of the fuzzy Markov Chain at each time instant t, as follows.

Definition 2. *At each instant t, $t = 1, 2, \cdots, n$, the state of system is described by the fuzzy set[2] $x^{(t)} \in \mathcal{F}(S)$. The transition law of a fuzzy Markov chain is given by the fuzzy relational matrix P at instant t, $T = 1, 2, \cdots, n$, as follows:*

$$x_j^{(t+1)} = \max_{i \in S} \{x_j^{(t)} \wedge p_{ij}\},\ j \in S. \tag{2}$$

$$x^{(t+1)} = x^{(t)} \circ P \tag{3}$$

Where i and j, $i, j = 1, 2, \cdots, m$ are the initial and final states of the transition and $x^{(0)}$ is the Initial Distribution *of the process.*

Thomason in [10] shows that the powers of a fuzzy matrix are stable if it is used the max-min operator. For further information about powers of a fuzzy matrix, see Sanchez in [5] and [6]. Now a *Stationary Distribution* of a fuzzy matrix is defined.

Definition 3 (Stationary Distribution). *Let the powers of the fuzzy transition matrix P converge in τ steps to a non-periodic solution, then the associated fuzzy Markov chain is called* Aperiodic Fuzzy Markov Chain *and $P^* = P^\tau$ is its* Stationary Fuzzy Transition Matrix.

Definition 4 (Ergodicity). *A fuzzy Markov chain is called $Ergodic$ if is aperiodic and its stationary distribution matrix has identical rows.*

Some Fuzzy matrices exhibit a periodical behavior. These cases are treated by Martin Gavalec in [11], [12] and [13] and these results can be applied to identify the

[1] Also known as $\alpha - cut$.

[2] This matrix is also known as the *Fuzzy Distribution* of x.

period of a fuzzy Markov chain. In a complementary way, it is possible to define two concepts of Markov processes in a fuzzy environment:

Definition 5 (Strong Ergodicity for Markov Chains). *A fuzzy Markov chain is called* ***Strong Ergodic*** *if it is aperiodic and its stationary transition matrix has identical rows.*

Definition 6 (Weak Ergodicity for Markov Chains). *A fuzzy Markov chain is called* ***Weakly Ergodic*** *if it is aperiodic and its stationary transition matrix is stable with no identical rows.*

Now, if the stationary distribution of P is given by $P^* = P^\tau$ where $\lim_{n\to\tau} P^n = P^*$, then P becomes an idempotent matrix. Sánchez in [6], [5] & [14] defined its stationary distribution by its *Eigen Fuzzy Set* which is defined next:

Definition 7. *Let P be a fuzzy relation in a given matrix form. Then x is called an Eigen Fuzzy set of P, iff:*

$$x \circ P = x \tag{4}$$

Definition 8. *The Fuzzy set $x \in \mathcal{F}(S)$ is contained in the fuzzy set $y \in \mathcal{F}(S)$, this is, $(x \subseteq y)$, iff $x_i \leqslant y_i$ for all $i \in S$.*

Definition 9. *Let $\mathcal{X}$ be the set of eigen fuzzy sets of the fuzzy relation P. Namely:*

$$\mathcal{X} \stackrel{\triangle}{=} \{x \in \mathcal{F}(S) \mid x \circ P = x\} \tag{5}$$

The elements of (X) are invariants of P according to the $\circ-(max-min)$ composition. Then, if there exists $\overset{\vee}{x} \in \mathcal{F}(S)$ such that $x \subseteq \overset{\vee}{x}$ for any $x \in (X)$, it is called the ***Greatest Eigen Fuzzy Set*** *of the relation P.*

We use the Method III proposed by Sánchez in [14], [6] and [5], which obtains $\overset{\vee}{x}$. If P is a *Strong Ergodic* fuzzy Markov chain, then its greatest eigen fuzzy set converges to an idempotent matrix P^τ with equal rows at any $n \geqslant \tau$.

Now, the scalar cardinality and the Cumulative Membership function of a fuzzy set is used to define a transformation of a FM into a CM.

3 Scalar Cardinality of a Type-1 Fuzzy Set

The well known *Scalar Cardinality* of a fuzzy set namely $|S|$ is a measure of amount and represents the total size of the membership function of S. $|S|$ is defined by crisp operations on S and gives the total area of μ_S. Its definition is presented next:

$$|S| = \int_{-\infty}^{\infty} \mu_S(x)\, dx, \quad x \in \mathbb{R} \tag{6}$$

3.1 Cumulative Membership Function $\psi_S(x)$

The probability cumulative function $F(x)$ used in many statistical approaches is:

$$F(x) = \int_{-\infty}^{x} f(t)\, dt \tag{7}$$

Where $x \in \mathbb{S}$, $t \in X$. The associated fuzzy definition is the following.

Definition 10 (CMF Function). *Consider a fuzzy number defined on a specific fuzzy set S with known bounds a and b and a central interval $c \in [c_1, c_2]$ that satisfies $\mu_S(c) = 1 \ \forall \ c$. By taking advantage from the $l(x), c(x), r(x)$ decomposition of a membership function, the cumulative membership function (CMF) is defined as:*

$$\psi_S(x) = \int_{-\infty}^{x} \mu_A(t)\ dt \tag{8}$$

This definition represents the possibility that all elements of S equal or less than a x value has into a set S, $Ps_S(X \leqslant x)$[3]. Note that in the probabilistic case $F(\infty) = 1$ while in the possibilistic case $1 < \psi(\infty) < \Lambda$, where Λ is a finite value defined itself as the *Total Area* of $\mu_S(x)$ namely $\Lambda = |S|$ and defined by(6).

Note that $\mu_S(\infty) > 1$ is an important issue to be solved. This is an interpretation problem since the definition of a *normalized* fuzzy set determines that $\sup_{x \in S} \mu_S(x) = 1$ and the above definition does not have this property. To solve it, an easy way to normalize $\psi_S(x)$ is dividing it by Λ, obtaining the following definition:

$$\psi_S(x) = \frac{1}{\Lambda} \int_{-\infty}^{x} \mu_S(t)\ dt \tag{9}$$

Remark 1 (Relation between $\psi_S(x)$ and $|S|$). *Recall that $\psi_S(\infty) = |S|$, that is $\Lambda = |S|$ so the notation Λ is used either to refer $\psi_S(\infty)$ or $|S|$.*

4 Transforming a Fuzzy Markov Chain into a Crisp Markov Chain

Now, the main idea is to obtain an easy way to project a fuzzy Markov chain into a crisp Markov chain, that is, find a method for projecting all the embedded conditional fuzzy sets of $\breve{P}$, into a probability space. To do so, the following proposition is useful.

Proposition 2. *Consider a fuzzy transition matrix $\breve{P}$ whose elements $\breve{p}_{ij}$ denotes the conditional statement of going from the i_{th} state to the j_{th} state. If $\breve{P}$ is a stochastic fuzzy Markov chain, then there exists a function that projects S_{ij} into a crisp Markov chain denoted by $f\{x_j|x_i\} = p_{ij}$.*

When a fuzzy Markov chain is defined, it is possible to obtain its cumulative membership function $\psi_{S_{ij}}$ and it is easy to show that $\psi_{S_{im}} = 1$, $i \in \mathbb{N}_m$ can be normalized $\psi_{S_{mj}}$, by dividing it into Λ.

This is an useful reasoning to project S_{ij} into a normalized fuzzy set $\psi_{S_{im}} = 1$ which agrees with all crisp laws, that is, the projection of S_{ij} into a new set obtained by dividing all their elements by Λ gets a crisp stochastic set. It results in the next theorem.

Theorem 3. *Let $\breve{P}$ a Type-1 fuzzy Markov chain with elements $\breve{p}_{ij} = \mu_{S_{ij}}$, then $\breve{P}$ can be transformed into a crisp Markov chain namely P by using the following linear transformation:*

$$P = \Lambda^{-1} \breve{P} \tag{10}$$

[3] This expression denotes a fuzzy measurement of an event occurs treated as a *Possibility (Ps)*.

Where Λ is a diagonal squared matrix whose components are the scalar cardinality of each set $|S_i|$ by row, denoted by Λ_i, $i \in m$.

Proof. First, the scalar cardinality of S_i, $|S_1|$ defined as Λ_i, $i \in m$ is obtained as:

$$\Lambda_i = \sum_{j=1}^{m} \mu_{S_{ij}},\ i \in m. \tag{11}$$

So, Λ, Λ^{-1} and $\breve{P}$ are defined as:

$$\Lambda = \begin{bmatrix} \Lambda_1 & & & \\ & \Lambda_2 & & \\ & & \ddots & \\ & & & \Lambda_m \end{bmatrix}; \Lambda^{-1} = \begin{bmatrix} \Lambda_1^{-1} & & & \\ & \Lambda_2^{-1} & & \\ & & \ddots & \\ & & & \Lambda_m^{-1} \end{bmatrix}; \breve{P} = \begin{bmatrix} \mu_{S_{11}} & \mu_{S_{12}} & \cdots & \mu_{S_{1m}} \\ \mu_{S_{21}} & \mu_{S_{22}} & \cdots & \mu_{S_{2m}} \\ \vdots & \vdots & \ddots & \vdots \\ \mu_{S_{m1}} & \mu_{S_{m2}} & \cdots & \mu_{S_{mm}} \end{bmatrix}$$

And finally we have:

$$P = \begin{bmatrix} \Lambda_1^{-1} & & & \\ & \Lambda_2^{-1} & & \\ & & \ddots & \\ & & & \Lambda_m^{-1} \end{bmatrix} * \begin{bmatrix} \mu_{S_{11}} & \mu_{S_{21}} & \cdots & \mu_{S_{m1}} \\ \mu_{S_{12}} & \mu_{S_{22}} & \cdots & \mu_{S_{m2}} \\ \vdots & \vdots & \ddots & \vdots \\ \mu_{S_{1m}} & \mu_{S_{2m}} & \cdots & \mu_{S_{mm}} \end{bmatrix}$$

Which is $P = \Lambda^{-1}\breve{P}$. Now, all their components result in the following matrix:

$$P = \begin{bmatrix} \frac{\mu_{S_{11}}}{\Lambda_1} & \frac{\mu_{S_{12}}}{\Lambda_1} & \cdots & \frac{\mu_{S_{1m}}}{\Lambda_1} \\ \frac{\mu_{S_{21}}}{\Lambda_2} & \frac{\mu_{S_{22}}}{\Lambda_2} & \cdots & \frac{\mu_{S_{2m}}}{\Lambda_2} \\ \vdots & \vdots & \ddots & \vdots \\ \frac{\mu_{S_{m1}}}{\Lambda_m} & \frac{\mu_{S_{m2}}}{\Lambda_m} & \cdots & \frac{\mu_{S_{mm}}}{\Lambda_m} \end{bmatrix}$$

This transformation obtains a matrix P whose elements satisfy all basic properties of a stochastic crisp distribution function, i.e.

i) $0 \leqslant p(x_{ij}) \leqslant 1$

ii) $\sum_{j \in S}^{\infty} p(x_{ij}) = 1,\ i \in S$

iii) $P(X \leqslant x_{ij}) = \sum_{i \leqslant S} p(x_{ij}) = F(x),\ i \in S$

In this way, it is possible to show that all elements of P obtained from $\breve{P}$ by using $P = \Lambda^{-1}\breve{P}$ conforms a crisp distribution function, agree to the Markovian property of a stochastic transition matrix. To that effect, their properties are shown next.

The property presented in i) refers to the domain of p_{ij}, and as $\mu_{S_{ij}} < \Lambda_i$, $i, j \in m$, then it asserts that $\frac{\mu_{S_{ij}}}{\Lambda_i} < 1$, $i, j \in m$.

The second statement ii) refers to the density of p_{ij} which should be 1 by row or column, now, the following calculation from $P = \Lambda^{-1}\breve{P}$ is true:

$$\frac{\mu_{S_{i1}}}{\Lambda_i} + \frac{\mu_{S_{i2}}}{\Lambda_i} + \cdots + \frac{\mu_{S_{im}}}{\Lambda_i} = \frac{\Lambda_i}{\Lambda_i} = 1, \forall\, i \tag{12}$$

It shows that P is a row Markovian stochastic matrix (See [1], [2], [3] and [4] for further information).

And finally the third statement refers to the cumulative probability function of p_{ij}, which is obtained from $\breve{P}$ by using the fuzzy approach defined in (9). Its adaptation to the conditional statement $i \rightarrow j$ is:

$$\psi_{S_i} = \frac{1}{\Lambda_i}\sum_{j=1}^{x} \mu_{S_{ij}},\ i \in m \tag{13}$$

This yields in $0 \leqslant \psi_{S_i} \leqslant 1$ and iii) is satisfied by all elements of $P = \Lambda^{-1}\breve{P}$.

Now, as all elements of $P = \Lambda^{-1}\breve{P}$ are agree with the probability function laws and the definitions of Crisp Markov chains presented in Section 4, then $P = \Lambda^{-1}\breve{P}$ is a crisp Markov chain and the proof is complete.

The Theorem 3 reveals an easy and efficient way to transform a fuzzy Markov chain into a crisp Markov chain defined on a probabilistic environment. To illustrate this result, in next section some application examples are given.

5 Application Examples

In this section, two introductory examples are presented. Both are FMs which have a size of 5×5 and are transformed into CM by using the results of the Theorem 3.

5.1 First Example: Strong Ergodic $\breve{P}$

Let $\breve{P}$ has the following transition matrix:

$$\breve{P} = \begin{bmatrix} 0.721 & 0.569 & 0.438 & 0.025 & 0.241 \\ 0.342 & 0.020 & 0.452 & 0.824 & 0.915 \\ 0.529 & 0.060 & 0.289 & 0.774 & 0.057 \\ 0.746 & 0.013 & 0.385 & 0.015 & 0.008 \\ 0.746 & 0.490 & 0.459 & 0.356 & 0.521 \end{bmatrix}$$

So Λ and $P = \Lambda^{-1}\breve{P}$ are:

$$\Lambda = \begin{bmatrix} 1.994 & & & & \\ & 2.553 & & & \\ & & 1.709 & & \\ & & & 1.167 & \\ & & & & 2.572 \end{bmatrix};\ P = \begin{bmatrix} 0.362 & 0.285 & 0.220 & 0.013 & 0.121 \\ 0.134 & 0.008 & 0.177 & 0.323 & 0.358 \\ 0.310 & 0.035 & 0.169 & 0.453 & 0.033 \\ 0.639 & 0.011 & 0.330 & 0.013 & 0.007 \\ 0.290 & 0.191 & 0.178 & 0.138 & 0.203 \end{bmatrix}$$

By using the Method III proposed by Sánchez, the stationary distribution of $\breve{P}$ converges to its greatest eigen fuzzy set $\overset{\vee}{x}_j$ which is:

$$\overset{\vee}{x} = [\ 0.721\ \ 0.569\ \ 0.459\ \ 0.569\ \ 0.569\ ]$$

This stationary fuzzy matrix is Weak Ergodic according to the Definition 6. It means that both $\breve{P}^{\tau}$ and $\overset{\vee}{x}$ have equal rows. The crisp stationary distribution of P is:

$$\pi = [\ 0.356\ \ 0.136\ \ 0.216\ \ 0.166\ \ 0.126\ ]$$

Note that the first state is the most probable and the most possible at once. It means that both approaches maintain the statement $\max_{x_j \in S}\{\overset{\vee}{x}_j\} = \max_{x_j \in S}\{\pi_j\}$.

5.2 Second Example: Weak Ergodic $\breve{P}$

Let $\breve{P}$ has the following transition matrix:

$$\overline{P} = \begin{bmatrix} 0.07 & 0.876 & 0.970 & 0.827 & 0.151 \\ 0.084 & 0.472 & 0.849 & 0.361 & 0.607 \\ 0.183 & 0.147 & 0.687 & 0.022 & 0.303 \\ 0.522 & 0.832 & 0.988 & 0.056 & 0.697 \\ 0.288 & 0.225 & 0.931 & 0.914 & 0.934 \end{bmatrix}$$

So Λ and $P = \Lambda^{-1}\breve{P}$ are:

$$\Lambda = \begin{bmatrix} 2.894 & & & & \\ & 2.373 & & & \\ & & 1.342 & & \\ & & & 3.094 & \\ & & & & 3.291 \end{bmatrix},\ P = \begin{bmatrix} 0.024 & 0.303 & 0.335 & 0.286 & 0.052 \\ 0.035 & 0.199 & 0.358 & 0.152 & 0.256 \\ 0.136 & 0.109 & 0.512 & 0.017 & 0.226 \\ 0.169 & 0.269 & 0.319 & 0.018 & 0.225 \\ 0.087 & 0.068 & 0.283 & 0.278 & 0.284 \end{bmatrix}$$

The fuzzy stationary matrix of $\breve{P}^{\tau}$ is:

$$\breve{P}^{\tau} = \begin{bmatrix} 0.586 & 0,586 & 0,481 & 0,481 & 0,481 \\ 0,706 & 0,832 & 0,481 & 0,481 & 0,481 \\ 0,686 & 0,686 & 0,861 & 0,784 & 0,686 \\ 0,686 & 0,686 & 0,760 & 0,840 & 0,686 \\ 0,706 & 0,812 & 0,481 & 0,481 & 0,521 \end{bmatrix}$$

This stationary fuzzy matrix is Weak Ergodic, it means that $\breve{P}^{\tau}$ does not agree with $\overset{\vee}{x}$ since $\breve{P}^{\tau}$ has no equal rows, according to the Definition 6. Now, Which of the stationary row vectors is the correct projection of the steady state of $\breve{P}$? Indeed, any of the 5 row vectors can be used for. A natural choice is to select a stationary distribution by using $\overset{\vee}{x}$. In this way, the greatest eigen fuzzy set of $\breve{P}$, $\overset{\vee}{x}_j$ is:

$$\overset{\vee}{x} = [\ 0.706\ \ 0.832\ \ 0.861\ \ 0.840\ \ 0.686\ ]$$

The crisp stationary distribution of P is:

$$\pi = [\ 0.102\ \ 0.153\ \ 0.395\ \ 0.124\ \ 0.226\ ]$$

In this case the third state is the most probable and the most possible at once. As in Example 1, both approaches maintain the statement $\max_{x_j \in S}\{\overset{\vee}{x}_j\} = \max_{x_j \in S}\{\pi_j\}$.

While the FM does not have a Strong Ergodic behavior, its projection matrix P achieves an ergodic behavior with a single steady state. It means that it has no periodic oscillations.

6 Concluding Remarks

Some conclusions and recommendations can be suggested:

1. A linear transformation of a FM into a CM is presented and some of their properties are described. This leads to define a new Theorem (See Theorem 3).
2. This transformation is an easy way to scalarize a FM into a CM to analyze their properties under both theoretical focuses: Fuzzy and Algebraic.
3. The concept of Cardinality and Cumulative membership function of a fuzzy set are applied to obtain a crisp projection of the fuzzy space of the FM into a probability space of a CM.
4. In the fuzzy Markov chains case, it is possible to transform the FM into a CM and analyze them by using both fuzzy and classical stochastic theory. In cases where $\breve{P}$ is Weak Ergodic, their projection P can be useful to analyze their stationary distribution.

Finally, this work lets view an important relation between $\psi_S(x)$ and $F(x)$. It means that any fuzzy set can be transformed into a probability distribution function by using the presented results.

References

1. Grimmet, G., Stirzaker, D.: Probability and Random Processes. Oxford University Press, Oxford (2001)
2. Ross, S.M.: Stochastic Processes. John Wiley and Sons, Chichester (1996)
3. Gordon, P.: Thorie des Chaines de Markov finies et ses applications, Dunod - Paris (1967)
4. Stewart, W.J.: Introduction to the Numerical Solution of Markov Chains. Princeton Press (1994)
5. Sanchez, E.: Resolution of eigen fuzzy sets equations. Fuzzy Sets and Systems 1, 69–74 (1978)
6. Sanchez, E.: Eigen fuzzy sets and fuzzy relations. Journal of mathematical analysis and applications 81, 399–421 (1981)
7. Avrachenkov, K.E., Sanchez, E.: Fuzzy markov chains and decision-making. Fuzzy optimization and Decision Making 1, 143–159 (2002)
8. Araiza, R., Xiang, G., Kosheleva, O., Skulj, D.: Under interval and fuzzy uncertainty, symmetric markov chains are more dificult to predict. In: 2007 Annual Meeting of the North American Fuzzy Information Processing Society (NAFIPS), June 2007, vol. 26, pp. 526–531. IEEE, Los Alamitos (2007)
9. Liu, Y.K., Liu, B.: Fuzzy random variables: A scalar expected value operator. Fuzzy optimization and Decision Making 2, 143–160 (2003)
10. Thomason, M.: Convergence of powers of a fuzzy matrix. Journal of mathematical analysis and applications 57, 476–480 (1977)
11. Gavalec, M.: Computing orbit period in max-min algebra. Discrete Applied Mathematics 100, 49–65 (2000)
12. Gavalec, M.: Periods of special fuzzy matrices. Tatra Mountains Mathematical Publications 16, 47–60 (1999)
13. Gavalec, M.: Reaching matrix period is np-complete. Tatra Mountains Mathematical Publications 12, 81–88 (1997)
14. Avrachenkov, K.E., Sanchez, E.: Fuzzy markov chains: Specifities and properties. In: IEEE (ed.) 8th IPMU 2000 Conference, Madrid, Spain, pp. 1851–1856. IEEE, Los Alamitos (2000)

Applying Fuzzy Differential Equations to the Performance Analysis of Service Composition*

Zuohua Ding and Hui Shen

Center of Math Computing and Software Engineering
Zhejiang Sci-Tech University
Hangzhou, Zhejiang, 310018, China
zouhuading@hotmail.com

Abstract. In this paper, a new method is proposed to measure the performance of service composition. Due to the nondeterministic response in the Internet, we model service composition by a group of fuzzy differential equations, where each equation describes the state change of the service composition. By using RKF method, approximate reasoning rules, and fuzzy simulation principle, we obtain the the numerical solutions. Our performance analysis is based on the solutions of the these equations. Three measure indexes have been considered: response time, throughput and resource utilization rate. A case study demonstrates the advantages.

Keywords: Service composition, performance analysis, fuzzy Petri net, fuzzy differential equation.

1 Introduction

Different approaches have been proposed in the literature for system performance analysis. Most of them exploit analytical models whose analysis is based on Petri net and Markov Theory. Stochastic Petri Nets (SPN) [2] are among the most popular modeling formalisms that have been used in the past decade. However, SPN has its limitations in modeling some real time systems, such as service compositions, because of the random waiting time, or non-deterministic response time in the Internet[7].

This paper presents a new method for performance analysis of service composition. The analytical model is based on relaxation idea proposed by David and Alla[4] for Continuous Petri nets. We introduce fuzzy execution rates to the transitions of Petri nets, and we get a new type of fuzzy Petri nets(FPN) by applying relaxation technique. The semantics of Fuzzy Petri net is defined by a set of fuzzy differential equations (FDEs). Hence, a service composition can be described by a group of fuzzy differential equations, where each equation describes a state change of the service. A state can be measured by a fuzzy number, called State Measure, indicating how much the state can be reached while the service is in execution. This information can help us to do performance analysis such as response time, throughput and resource utilization rate.

By using RKF method, approximate reasoning rules, and fuzzy simulation principle, we obtain the the numerical solutions. Thus we can make performance analysis in practice.

* This work is partially supported by NSF(No. 90818013) and Zhejiang NSF(No.Z1090357).

D.-S. Huang et al. (Eds.): ICIC 2010, LNCS 6215, pp. 118–125, 2010.

2 Modeling Service Composition with FDEs

A Web service behavior is basically a partially ordered set of operations. Therefore, it is straightforward to map it into a Petri net. Operations are modeled by transitions and the state of the service is modeled by places. The arrows between places and transitions are used to specify causal relations. The initial marking indicates the start state. Service composition can be described by many languages, such as BPEL, Petri net, etc. In this paper, we use Petri net to describe service composition.

In the system modeling, we need to describe its start time, end time and execution time if we describe an event. Since execution rate is the reciprocal of the execution time, an event p may has three cases for its execution rate: the smallest execution rate a, the biggest execution rate c, and the most probabilistic execution rate b. We use triangle fuzzy number to describe such nondeterministic rates.

Definition 1. *A* Fuzzy Petri Net *is a tuple* $FPN=< P, T, A, M_0, \tilde{d} >$*, where* (P, T, A, M_0) *is a underlying untimed Petri net:* $P = \{p_1, p_2, \ldots, p_n\}$ *is the set of places,* $T = \{t_1, t_2, \ldots, t_m\}$ *is the set of transitions,* $A \subset (P \times T) \cup (T \times P)$ *is the set of arcs, and* M_0 *is the initial marking.* $\tilde{d} = \{\tilde{d_1}, \tilde{d_2}, \ldots, \tilde{d_m}\}$ *is a set of triangle fuzzy numbers representing firing rates of transitions.*

Definition 2. *Let* $I = [0, \infty)$ *be the time interval and let* $m_i : I \to E, i = 1, 2, \ldots, n$ *be a set of mappings that associated with place* p_i*. A marking of a Fuzzy Petri Net* $FPN =< P, T, A, M_0, \tilde{d} >$ *is a mapping*
$m : I \to E^n$, $m(\tau) = (m_1(\tau), m_2(\tau), \ldots, m_n(\tau))$.

Definition 3. *(State Measure) Given any time moment* $t \in [0, \infty)$*, the marking value in a place is called the State Measure of this place, denoted as* $m(t)$*. State measures take fuzzy numbers as their values.*

A transition is enabled if all the input places have nonzero fuzzy number markings. Only enabled transitions can be fired. So, if some marking is moved into a place, we say that the state measure in this place is increasing; if some marking is moved out from a place, we say that the state measure in this place is decreasing. The change rate of state measure can be calculated as the following.

Let p_1 and p_2 be the input places of a transition t and their markings are $m_1(\tau)$ and $m_2(\tau)$, respectively. Let $\tilde{d_t}$ be the firing rate associated with t, then the marking moving out from p_1 and p_2 is defined by $\tilde{d_t} \times min\{m_1(\tau), m_2(\tau)\}$. If t has only one input p_1, then marking $\tilde{d_t} \times m_1(\tau)$ will be moved out from p_1. This definition is actually an extension of the semantics of Continuous Petri net defined by David and Alla [4].

Based on the above semantics, the state measure at each place can be calculated from an fuzzy differential equation. For example, the net with an input as shown in Fig. 1. Place p will get marking from place p_1 and p_2. Let the markings at place p_1, p_2 and p be m_1, m_2 and m, respectively. Assume that the firing rates at transition t_1 and t are $\tilde{d_1}$ and $\tilde{d}$, respectively. Then the state measure m can be represented as

$$m'(\tau) = \tilde{d_1} min\{m_1(\tau), m_2(\tau)\} - \tilde{d} m(\tau).$$

If t_1 is not enabled, then $m_1(\tau) = \tilde{0}$ or/and $m_2(\tau) = \tilde{0}$. If t is not enabled, then $m(\tau) = \tilde{0}$. Hence the above equation also covers these situations.

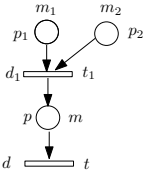

Fig. 1. Two places to one place model

3 Solutions of Fuzzy Differential Equations

From the last section, we will get a set of fuzzy differential equations:

$$\begin{cases} x_1' = f_1(t, x_1, x_2, \ldots, x_n, \tilde{d}_1, \tilde{d}_2, \ldots, \tilde{d}_m) \\ x_2' = f_2(t, x_1, x_2, \ldots, x_n, \tilde{d}_1, \tilde{d}_2, \ldots, \tilde{d}_m) \\ \vdots \\ x_n' = f_n(t, x_1, x_2, \ldots, x_n, \tilde{d}_1, \tilde{d}_2, \ldots, \tilde{d}_m) \\ x_1(0) = x_{10}, x_2(0) = x_{20}, \ldots, x_n(0) = x_{n0}. \end{cases}$$

where $\tilde{d}_i$ are triangle fuzzy numbers. This is equivalent to the fuzzy initial value problem:

$$(*) \quad X' = F(t, X, \tilde{d}),\ X(0) = X_0.$$

We can imitate[5] to prove the existence of the solutions of (*). The details are omitted here. We will focus on how to find the solutions of (*).

It is hard to get the analytical solutions for (*), thus we will find numerical solution instead. Our method is based on RKF method[1] to find the numerical solutions for the non-fuzzy initial value problem, then apply approximate reasoning rules[6], and fuzzy simulation principle, to get fuzzy numerical solution.

STEP 1. Find numerical solutions of non-fuzzy initial value problem. Let $d = (d_1, d_2, \ldots, d_m) \in R^m$ be a vector, and $f : [0, \infty) \times R^n \times R^m \to R^n$ is a mapping. Consider the normal initial value problem:

$$x' = f(t, x, d), t \geq 0,\ x(0) = x_0,$$

or

$$\begin{cases} x_1' = f_1(t, x_1, x_2, \ldots, x_n, d_1, d_2, \ldots, d_m) \\ x_2' = f_2(t, x_1, x_2, \ldots, x_n, d_1, d_2, \ldots, d_m) \\ \vdots \\ x_n' = f_n(t, x_1, x_2, \ldots, x_n, d_1, d_2, \ldots, d_m) \\ x_1(0) = x_{10}, x_2(0) = x_{20}, \ldots, x_n(0) = x_{n0}. \end{cases}$$

Its numerical solution by Runge-Kutta-Fehlberg (RKF) method is

$$(**)\quad \begin{cases} x_{1,k+1} = x_{1,k} + h(\frac{16}{135}K_{11} + \frac{6656}{12825}K_{13} + \frac{28561}{56430}K_{14} - \frac{9}{50}K_{15} + \frac{2}{55}K_{16}) \\ x_{2,k+1} = x_{2,k} + h(\frac{16}{135}K_{21} + \frac{6656}{12825}K_{23} + \frac{28561}{56430}K_{24} - \frac{9}{50}K_{25} + \frac{2}{55}K_{26}) \\ \vdots \\ x_{n,k+1} = x_{n,k} + h(\frac{16}{135}K_{n1} + \frac{6656}{12825}K_{n3} + \frac{28561}{56430}K_{n4} - \frac{9}{50}K_{n5} + \frac{2}{55}K_{n6}) \end{cases}$$

In the above expressions, h is the step size. RKF is a variable step size single step method, which has the global truncation error $o(h^5)$.

STEP 2. Find the numerical solutions of fuzzy initial problem. From the solution (**), we see that it characters the approximate relation between two sequential time moments of the system. So it is basically an approximate reasoning. Hence, for fuzzy number d_i, we may use fuzzy relations to replace function relations. Next we use fuzzy language to describe fuzzy relation R.

Let $\tilde{d_i}, i = 1, 2, \ldots, m$ be the triangular fuzzy numbers on universe of discourse. $U_{i0} = \{u_{i0} | d_i(u_{i0}) > 0, u_{i0} \in U\}$ is called effective universe of discourse of $\tilde{d_i}$. Denote $U_{i1} = \{u_{i1} | \tilde{d_i}(u_{i1}) = u_{i1}(1, u_{i0}), u_{i0} \in U_{i0}\}$. For any $(u_{i0}, u_{i1}) \in U_{i0} \times U_{i1}$, let

$$r_0^{(i)}(u_{i0}, u_{i1}) = \begin{cases} 1 \text{ if } u_{i1} = u_{i1}(1, u_{i0}), \\ 0 \text{ else.} \end{cases}$$

then $R_0^i = \{r_0^{(i)}(u_{i0}, u_{i1}) | (u_{i0}, u_{i1}) \in U_{i0} \times U_{i1}\}$ is a fuzzy relation on $U_{i0} \times U_{i1}$. Assume that $U_{ik} = \{u_{ik}\}$ is known, then based on the fuzzy approximate reasoning rules, we can rewrite (**) as

$$\begin{aligned} U_{i,k+1} = \{u_{i,k+1} | u_{i,k+1} = u_{i,k} + h(&\frac{16}{135}K_{i1} \\ &+ \frac{6656}{12825}K_{i3} + \frac{28561}{56430}K_{i4} - \frac{9}{50}K_{i5} + \frac{2}{55}K_{i6})\}, \end{aligned}$$

where $i = 1, 2, \ldots, n$, $k = 0, \ldots, n-1$, and $K_{i1}, K_{i2}, \ldots, K_{i6}$ are the same as in (**). If we define

$$r_k^{(i)}(u_{ik}, u_{ik+1}) = \begin{cases} 1, \text{ if } u_{,k+1} = u_{i,k} + h(\frac{16}{135}K_{i1} \\ \qquad\qquad + \frac{6656}{12825}K_{i3} + \frac{28561}{56430}K_{i4} \\ \qquad\qquad - \frac{9}{50}K_{i5} + \frac{2}{55}K_{i6}), \\ 0, \text{ else.} \end{cases}$$

then we call

$$\begin{cases} R^{(1)} = \{r_k^{(1)} | r_k^{(1)} = r_k^{(1)}(u_{1k}, u_{1,k+1})\} \\ R^{(2)} = \{r_k^{(2)} | r_k^{(2)} = r_k^{(2)}(u_{2k}, u_{2,k+1})\} \\ \vdots \\ R^{(n)} = \{r_k^{(n)} | r_k^{(n)} = r_k^{(n)}(u_{nk}, u_{n,k+1})\} \end{cases}$$

the RKF based fuzzy relations. If $x_{ik} = X_{ik}, i = 1, 2, \ldots, n$ is a fuzzy set, then the fuzzy state at the next time moment will be

$$
\begin{aligned}
& X_{i,k+1}(u_{i,k+1}) \\
= & \, sup_{u_{ik} \in U_{ik}} \{X_{ik}(u_{ik}) \wedge r_k^{(i)}(u_{ik}, u_{i,k+1})\}, \\
& i = 1, 2, \ldots, n, \;\; k = 0, 1, \ldots, n-1.
\end{aligned}
$$

The above numerical method is denoted as $\overline{RKF}$.

So far our solution calculating is for the case that the fuzzy equation group has one fuzzy number $\tilde{d}_i$ and all others $\tilde{d}_i$ are real numbers. If i goes through $1, 2, \ldots, n$, then we will have n values for variable X. The arithmetic average of these n values will be regarded as the numerical solution to this fuzzy variable X.

4 Performance Analysis with FDEs

We consider three performance indexes in this paper: response time, throughput, and resource utilization rate.

(1) Response Time: Response time is the time that cost in the process, which is from the beginning that the customers request to the end that the system responses to the customer. Thus the response time is actually a response between customers and a subsystem. We consider the problem to calculate response time as a queuing theory problem, and then we could calculate it using Little Rule and Flow Balance Principle. Thus the response time is the sum of all the average number of state measures in the subsystem (queue) divided by the average marking flow velocity of the subsystem. In Fig.2, the queue is $m_6 + m_7 + \cdots + m_{14}$, and the velocity is $d_4 min\{m_4, m_6\}$. Thus the response time $T = (m_6 + m_7 + \cdots + m_{14})/(d_4 min\{m_4, m_6\})$.

(2) Throughput: Throughput is the number of customer requests that the subsystem can accept or deal with in a given time period.

(3) Resource utilization rate: Resource utilization rate is the extension of resource utilization, which can be explained based on the state measure of FPN. In the Petri net model, based on the state descriptions, we need to select a place as the measuring place. Using the state measure of this place, we can analyze the efficiency of the system.

5 Case Study

For example, we consider Online Shop from IBM web site[1]. The system works as follows: First, a customer sends an order to the manufacturer. The manufacturer receivers the order, and then sends the customer's information to the bank to determine whether the account is in good standing. Bank will check the customer and then send the result to the manufacturer.The manufacturer receives the result, sends a message to the customer to notify him whether the order is accept.

The Petri net description of Online Shop is shown in Fig. 2. It has three services, Customer (Input to the system), manufacturer (ProcessOrder), and Bank (CustomerCheck).

[1] http://www.ibm.com/developerworks/websphere/techjournal/0603_gregory/0603_gregory.html.

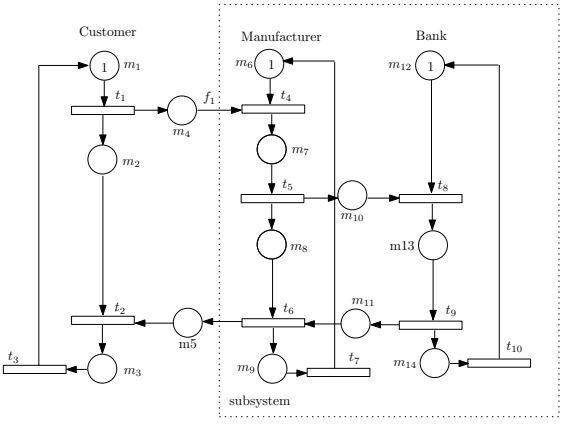

Fig. 2. Petri net representation of online shop

The fuzzy differential equation model is:

$$\begin{cases} m_1' = \tilde{d}_3 * m_3 - \tilde{d}_1 * m_1 \\ m_2' = \tilde{d}_1 * m_1 - \tilde{d}_2 * min(m_2, m_5) \\ m_3' = \tilde{d}_2 * min(m_2, m_5) - \tilde{d}_3 * m_3 \\ m_4' = \tilde{d}_1 * m_1 - \tilde{d}_4 * min(m_4, m_6) \\ m_5' = \tilde{d}_6 * min(m_8, m_{11}) - \tilde{d}_2 * min(m_2, m_5) \\ m_6' = \tilde{d}_7 * m_9 - \tilde{d}_4 * min(m_4, m_6) \\ m_7' = \tilde{d}_4 * min(m_4, m_6) - \tilde{d}_5 * m_7 \\ m_8' = \tilde{d}_5 * m_7 - \tilde{d}_6 * min(m_8, m_{11}) \\ m_9' = \tilde{d}_6 * min(m_8, m_{11}) - \tilde{d}_7 * m_9 \\ m_{10}' = \tilde{d}_5 * m_7 - \tilde{d}_8 * min(m_{10}, m_{12}) \\ m_{11}' = \tilde{d}_9 * m_{13} - \tilde{d}_6 * min(m_8, m_{11}) \\ m_{12}' = \tilde{d}_{10} * m_{14} - \tilde{d}_8 * min(m_{10}, m_{12}) \\ m_{13}' = \tilde{d}_8 * min(m_{10}, m_{12}) - \tilde{d}_9 * m_{13} \\ m_{14}' = \tilde{d}_9 * m_{13} - \tilde{d}_{10} * m_{14} \end{cases}$$

with the initial values: $m_1(0) = m_6(0) = m_{12}(0) = 1$, all other are 0.

At the beginning, we suppose d_6 is a fuzzy number. With some simulation data, in the most possible case, we get $d_1 = 6, d_2 = 3, d_3 = 6, d_4 = 12, d_5 = 10, d_7 = 18, d_8 = 8, d_9 = 12$, and $d_{10} = 18$. We also assume that the average number of orders from customers is 6/minute. From the experiment data, we find that $\tilde{d}_6$ is located in the interval $(0, 20]$. We partition $(0, 20]$ into four small intervals: $(0, 5], (5, 10], (10, 15], (15, 20]$. Let $\tilde{d}_6$ pick the values $1, 5, 10, 15$ and 20, and other $\tilde{d}_i$ take the most possible values. Then we will obtain five non-fuzzy differential equations. By calling the function *ODE45*(with algorithm RKF) in Matlab, we can solve all the state measures m_i.

Since we have ten fuzzy firing rates, after changing the position of fuzzy numbers, we will get ten values for each m_i. Table 1 shows the arithmetic average values of m_i of ten cases. Each row will give us a time dependent fuzzy number.

Table 1. Average values of m_i

	$d_i = 1, t = 20$	$d_i = 5, t = 40$	$d_i = 10, t = 60$	$d_i = 15, t = 80$	$d_i = 20, t = 100$
m_1	0.1271	0.1320	0.1324	0.1326	0.1327
m_2	0.7458	0.7361	0.7352	0.7348	0.7346
m_3	0.1271	0.1320	0.1324	0.1326	0.1327
m_4	0.1067	0.0732	0.0703	0.0693	0.0687
m_5	0.2092	0.2469	0.2533	0.2556	0.2568
m_6	0.4530	0.5027	0.5389	0.5421	0.5437
m_7	0.0941	0.0850	0.0828	0.0820	0.0816
m_8	0.3358	0.3311	0.3288	0.3280	0.3275
m_9	0.0884	0.0546	0.0496	0.0480	0.0472
m_{10}	0.1065	0.1026	0.1015	0.1011	0.1008
m_{11}	0.1436	0.1552	0.1570	0.1576	0.1580
m_{12}	0.8101	0.8722	0.8802	0.8828	0.8841
m_{13}	0.0858	0.0726	0.0703	0.0693	0.0687
m_{14}	0.1041	0.0546	0.0495	0.0480	0.0472

Based on the above data, we give the performance analysis of Online Shop system:

Response time: The response time is a time dependent fuzzy number. We regard the manufacturer and the bank as the subsystems. The queue length of the task is the sum of the average number of marking in each place in the subsystem. We have the following calculation result in Table 2. Based on the data in the table and the fitting method in [3], we get plot the response time as shown in Fig. 3(a).

Table 2. Values for Response Time and Throughput

	$t = 20$	$t = 40$	$t = 60$	$t = 80$	$t = 100$
Resp	17.702	3.4223	1.7054	1.1355	0.8511
Throughput	0.1271	0.6597	1.3243	1.9892	2.6543

Throughput: It is also a time dependent fuzzy number. We have the following calculation result in Table 2. Based on the table and the fitting method in [3], we get plot the throughput as shown in Fig. 3(b). From Fig. 3, we see that as the firing rates increase,

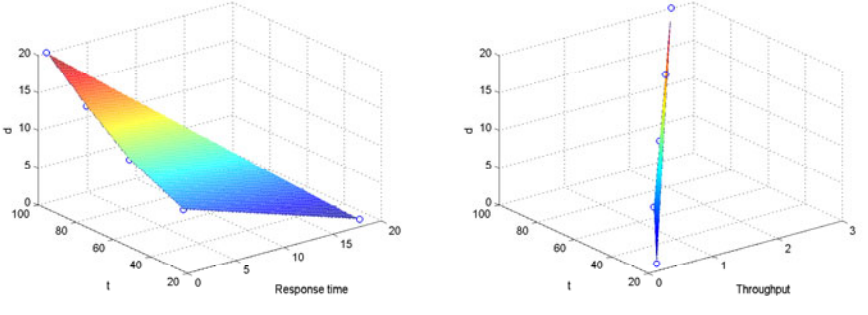

(a) (b)

Fig. 3. (a) Response time for online shop; (b) Throughput for online shop

the response time decreases and the throughput increases, which is consistent with the real situation.

Resource utilization rate: State m_2 stands for 'customer waiting for response'. We may choose m_2 as the measuring place. From Table 1 we see that the values of m_2 are mainly distributed between 0.73 and 0.75, so we can imply that most of the customers are waiting for the response. Thus, the resource utilization rate in the given time period is about $(1 - 0.74) = 26\%$, which is bad. From the further data analysis, we find the reason is that very small customer orders (m_4 is about 0.07) have been sent out to the manufacturer, and very little customer information(m_{10} is about 0.10) has been sent out for checking.

6 Conclusion and Discussion

We studied the performance analysis of service composition based on fuzzy differential equations. Three indexes have been used to measure the performance: response time, throughput and resource utilization rate. With our method we can avoid the state explosion problem. The reason is that we do not check the reachable state space, instead we solve a set of fuzzy differential equations.

References

1. Ascher, U.M., Petzold, L.R.: Computer methods for ordinary differential equations and differential-algebraic equations. Society for Industrial & Applied Mathematis, Philadelphia (1998)
2. Bause, F., Kritzinger, F.: Stochastic Petri Nets-An Introduction to the Theory. Vieweg Verlag (2002)
3. Chalco-Cano, Y., Román-Flores, H.: Comparation between some approaches to solvefuzzy differential equations. Fuzzy Sets and Systems 160, 1517–1527 (2009)
4. David, R., Alla, H.: Continuous Petri nets. In: Proceedings of the 8^{th} European Workshop on Application and Theory of Petri nets, pp. 275–294 (1987)
5. Kaleva, O.: Fuzzy differential equation. Fuzzy Sets and Systems 24, 301–317 (1987)
6. Zadeh, L.A.: The concept of a linguistic variable and its applications in approximate reasoning. Information Sciences 8, 119–251 (1975)
7. Zhou, Y., Murata, T., DeFanti, T.: Modeling and Performance Analysis Using Extended Fuzzy-Timing Petri Nets for Networked Virtual Environments. IEEE Transactions on Systems, Man, and Cybernetics-Part B: Cybernetics 30(5) (2000)

Lattice Structures of Fuzzy Soft Sets

Keyun Qin and Hua Zhao

College of Mathematics, Southwest Jiaotong University,
Chengdu, Sichuan 610031, China
keyunqin@263.net, zzh8008@gmail.com

Abstract. In this paper, we study the algebraic structures of fuzzy soft sets. Some operations on fuzzy soft sets are introduced and several related properties are investigated. Furthermore, two lattice structures of fuzzy soft sets are established. It is proved that certain De Morgan's laws hold in fuzzy soft set theory.

1 Introduction

To solve complicated problems in economics, engineering, environmental science and social science, methods in classical mathematics are not always successful because of various types of uncertainties present in these problems. While probability theory, fuzzy set theory [12], rough set theory [8], and other mathematical tools are well-known and often useful approaches to describing uncertainty, each of these theories has its inherent difficulties as pointed out in [7]. In 1992, Molodtsov [7] introduced the concept of soft sets, which can be seen as a new mathematical tool for dealing with uncertainties. This so-called soft set theory is free from the difficulties affecting existing methods.

Presently, works on soft set theory are progressing rapidly. Maji et al.[6] defined several operations on soft sets and made a theoretical study on the theory of soft sets. Aktas and Cagman [1] compared soft sets to the related concepts of fuzzy sets and rough sets. They also defined the notion of soft groups and derived some related properties. Jun [3] introduced the notion of soft BCK/BCI-algebras. Jun and Park [4] discussed the applications of soft sets in ideal theory of BCK/BCI-algebras. Furthermore, based on [6] , Ali et al.[2] introduced some new operations on soft sets and improved the notion of complement of soft set. They proved that certain De Morgan's laws hold in soft set theory.

In soft set theory, we observe that in most cases the parameters are vague words or sentences involving vague words. Considering this point, Maji et al.[5] introduced the notion of fuzzy soft sets by combining fuzzy sets and soft sets. Roy et al.[9] presented a fuzzy soft set theoretic approach towards a decision making problem. Xiao et al.[10] proposed a combined forecasting approach based on fuzzy soft set theory. Yang et al.[11] introduced the concept of interval-valued fuzzy soft set and a decision making problem is analyzed by the interval-valued fuzzy soft set.

D.-S. Huang et al. (Eds.): ICIC 2010, LNCS 6215, pp. 126–133, 2010.

Algebraic structures play a fundamental role in many fields of mathematics. In this paper, we deal with the algebraic structures of fuzzy soft sets. Some operations on fuzzy soft sets are introduced. Two lattice structures of fuzzy soft sets are established and several related properties are investigated. It is proved that the set of all fuzzy soft sets over a definite universe forms bounded distributive lattices. Furthermore, certain De Morgan's laws in fuzzy soft set theory are proved.

2 Preliminaries

This section presents a review of some fundamental notions of soft sets and fuzzy soft set. We refer to [5,7] for details.

Let U be an initial universe set and E the set of all possible parameters under consideration with respect to U. The power set of U (i.e., the set of all subsets of U) is denoted by $P(U)$. Usually, parameters are attributes, characteristics, or properties of objects in U. Molodtsov defined the notion of a soft set in the following way:

Definition 1. *[7] A pair (F, A) is called a soft set over U, where $A \subseteq E$ and F is a mapping given by $F : A \to P(U)$.*

In other words, a soft set over U is a parameterized family of subsets of U. For $e \in A$, $F(e)$ may be considered as the set of $e-$approximate elements of the soft set (F, A). For illustration, Molodtsov considered several examples in [7].

Example 1. [7] Suppose that there are six houses in the universe U given by $U = \{h_1, h_2, h_3, h_4, h_5, h_6\}$ and $E = \{e_1, e_2, e_3, e_4, e_5\}$ is the set of parameters. Where e_1 stands for the parameter 'expensive', e_2 stands for the parameter 'beautiful', e_3 stands for the parameter 'wooden', e_4 stands for the parameter 'cheap' and e_5 stands for the parameter 'in the green surroundings'.

In this case, to define a soft set means to point out expensive houses, beautiful houses, and so on. The soft set (F, E) may describe the 'attractiveness of the houses' which Mr.X is going to buy. Suppose that $F(e_1) = \{h_2, h_4\}$, $F(e_2) = \{h_1, h_3\}$, $F(e_3) = \{h_3, h_4, h_5\}$, $F(e_4) = \{h_1, h_3, h_5\}$, $F(e_5) = \{h_1\}$. Then the soft set (F, E) is a parameterized family $\{F(e_i); 1 \leq i \leq 5\}$ of subsets of U and give us a collection of approximate descriptions of an object. $F(e_1) = \{h_2, h_4\}$ means 'houses h_2 and h_4' are 'expensive'.

It is worth noticing that as set-valued mappings, different soft set may have different domains. So, nested fuzzy set is a special case of soft set. In[5], Maji et al. introduced the concept of fuzzy soft set by combining soft set and fuzzy set.

Definition 2. *[5] A pair (F, A) is called a fuzzy soft set over U, where $A \subseteq E$ and F is a mapping given by $F : A \to F(U)$, $F(U)$ is the set of all fuzzy subsets on U.*

Clearly, the notion of fuzzy soft set is a generalization of that of soft set.

3 The Properties of Operations in Fuzzy Soft Set Theory

Based on the operations on soft sets [2], in this section, we introduce some operations on fuzzy soft sets and investigate their related properties.

Definition 3. *The extended intersection of two fuzzy soft sets* (F, A) *and* (G, B) *over a common universe* U*, denoted by* $(F, A) \sqcap_{\varepsilon} (G, B)$*, is the fuzzy soft set* (H, C)*, where* $C = A \cup B$*, and* $\forall e \in C$*, if* $e \in A - B$*, then* $H(e) = F(e)$*; if* $e \in B - A$*, then* $H(e) = G(e)$*; if* $e \in A \cap B$*, then* $H(e) = F(e) \cap G(e)$*.*

Definition 4. *The restricted intersection of two fuzzy soft sets* (F, A) *and* (G, B) *over a common universe* U*, denoted by* $(F, A) \text{⋒} (G, B)$*, is the fuzzy soft set* (H, C)*, where* $C = A \cap B$*, and* $\forall e \in C$*,* $H(e) = F(e) \cap G(e)$*.*

Definition 5. *The union of two fuzzy soft sets* (F, A) *and* (G, B) *over a common universe* U*, denoted by* $(F, A)\widetilde{\cup}(G, B)$*, is the fuzzy soft set* (H, C)*, where* $C = A \cup B$*, and* $\forall e \in C$*, if* $e \in A - B$*, then* $H(e) = F(e)$*; if* $e \in B - A$*, then* $H(e) = G(e)$*; if* $e \in A \cap B$*, then* $H(e) = F(e) \cup G(e)$*.*

Definition 6. *The restricted union of two fuzzy soft sets* (F, A) *and* (G, B) *over a common universe* U*, denoted by* $(F, A) \cup_{\Re} (G, B)$*, is the fuzzy soft set* (H, C)*, where* $C = A \cap B$*, and* $\forall e \in C$*,* $H(e) = F(e) \cup G(e)$*.*

Definition 7. *(a)* (F, A) *is called a relative null soft set(with respect to the parameter set* A*), denoted by* $\emptyset_A$*, if* $F(e) = \emptyset$ *for all* $e \in A$*.*

(b) (G, A) *is called a relative whole soft set(with respect to the parameter set* A*), denoted by* U_A*, if* $F(e) = U$ *for all* $e \in A$*.*

Definition 8. *The relative complement of a soft sets* (F, A) *is denoted by* $(F, A)^r$ *and is defined by* $(F, A)^r = (F^r, A)$ *where* $F^r : A \to F(U)$ *is a mapping given by* $F^r(e) = \sim F(e)$ *for all* $e \in A$ *and* $\sim F(e)$ *is the complement of* $F(e)$*.*

Clearly, $((F, A)^r)^r = (F, A)$ and $((F, A)^c)^c = (F, A)$ hold.

Theorem 1. *Let* (F, A)*,* (G, B) *and* (H, C) *be fuzzy soft sets over the same universe* U*. Then*

(1)$(F, A)\widetilde{\cup}(F, A) = (F, A)$*,*

(2)$(F, A)\widetilde{\cup}(G, B) = (G, B)\widetilde{\cup}(F, A)$*,*

(3)$((F, A)\widetilde{\cup}(G, B))\widetilde{\cup}(H, C) = (F, A)\widetilde{\cup}((G, B)\widetilde{\cup}(H, C))$*.*

Proof. (1) and (2) are trivial. We only prove (3). Suppose that

$$((F, A)\widetilde{\cup}(G, B))\widetilde{\cup}(H, C) = (K, A \cup B \cup C),$$

$$(F, A)\widetilde{\cup}((G, B)\widetilde{\cup}(H, C)) = (L, A \cup B \cup C).$$

For all $e \in A \cup B \cup C$, it follows that $e \in A$, or $e \in B$, or $e \in C$. Without losing of generality, we suppose that $e \in C$.

(a) If $e \notin A$ and $e \notin B$, then $K(e) = H(e) = L(e)$;
(b) If $e \in A$ and $e \notin B$, then $K(e) = F(e) \cup H(e) = L(e)$;
(c) If $e \notin A$ and $e \in B$, then $K(e) = G(e) \cup H(e) = L(e)$;
(d) If $e \in A$ and $e \in B$, then $K(e) = (F(e) \cup G(e)) \cup H(e) = F(e) \cup (G(e) \cup H(e)) = L(e)$.

Since K and L are indeed the same set-valued mappings, we conclude that $((F, A)\widetilde{\cup}(G, B))\widetilde{\cup}(H, C) = (F, A)\widetilde{\cup}((G, B)\widetilde{\cup}(H, C))$ as required.

This theorem shows that the operation $\widetilde{\cup}$ is idempotent, associative and commutative. The following three theorems can be proved similarly:

Theorem 2. *Let (F, A), (G, B) and (H, C) be fuzzy soft sets over the same universe U. Then*
(1) $(F, A) \sqcap_\varepsilon (F, A) = (F, A)$,
(2) $(F, A) \sqcap_\varepsilon (G, B) = (G, B) \sqcap_\varepsilon (F, A)$,
(3) $((F, A) \sqcap_\varepsilon (G, B)) \sqcap_\varepsilon (H, C) = (F, A) \sqcap_\varepsilon ((G, B) \sqcap_\varepsilon (H, C))$.

Theorem 3. *Let (F, A), (G, B) and (H, C) be fuzzy soft sets over the same universe U. Then*
(1) $(F, A) \cup_\Re (F, A) = (F, A)$,
(2) $(F, A) \cup_\Re (G, B) = (G, B) \cup_\Re (F, A)$,
(3) $((F, A) \cup_\Re (G, B)) \cup_\Re (H, C) = (F, A) \cup_\Re ((G, B) \cup_\Re (H, C))$.

Theorem 4. *Let (F, A), (G, B) and (H, C) be fuzzy soft sets over the same universe U. Then*
(1) $(F, A) \Cap (F, A) = (F, A)$,
(2) $(F, A) \Cap (G, B) = (G, B) \Cap (F, A)$,
(3) $((F, A) \Cap (G, B)) \Cap (H, C) = (F, A) \Cap ((G, B) \Cap (H, C))$.

The following types of De Morgan's laws hold in soft set theory.

Theorem 5. *Let (F, A) and (G, B) be two fuzzy soft sets over the same universe U. Then*
(1) $((F, A)\widetilde{\cup}(G, B))^r = (F, A)^r \sqcap_\varepsilon (G, B)^r$,
(2) $((F, A) \sqcap_\varepsilon (G, B))^r = (F, A)^r \widetilde{\cup} (G, B)^r$.

4 The Lattice Structures of Fuzzy Soft Sets

In this section, we establish the lattice structures of fuzzy soft sets. The following theorem shows that the absorption law with respect to operations $\widetilde{\cup}$ and $\Cap$ holds.

Theorem 6. *Let (F, A) and (G, B) be fuzzy two soft sets over the same universe U. Then*
(1) $((F, A)\widetilde{\cup}(G, B)) \Cap (F, A) = (F, A)$,
(2) $((F, A) \Cap (G, B))\widetilde{\cup}(F, A) = (F, A)$.

Proof. (1) Suppose that $(F,A)\widetilde{\cup}(G,B) = (H, A\cup B)$ and $((F,A)\widetilde{\cup}(G,B)) \widetilde{\cap} (F,A) = (K,(A\cup B)\cap A) = (K,A)$. For all $e \in A$,

(a) if $e \in B$, then $K(e) = H(e)\cap F(e) = (F(e)\cup G(e))\cap F(e) = F(e)$;

(b) if $e \notin B$, then $K(e) = H(e)\cap F(e) = F(e)\cap F(e) = F(e)$.

Hence $((F,A)\widetilde{\cup}(G,B)) \widetilde{\cap} (F,A) = (F,A)$.

(2) Suppose that $(F,A)\widetilde{\cap}(G,B) = (H, A\cap B)$ and $((F,A)\widetilde{\cap}(G,B))\widetilde{\cup}(F,A) = (K,(A\cap B)\cup A) = (K,A)$. For all $e \in A$,

(a) if $e \in B$, then $K(e) = H(e)\cup F(e) = (F(e)\cap G(e))\cup F(e) = F(e)$;

(b) if $e \notin B$, then $e \notin A\cap B$. It follows that $K(e) = F(e)$.

Hence $((F,A)\widetilde{\cap}(G,B))\widetilde{\cup}(F,A) = (F,A)$.

We denote by $S(U,E)$ the set of all fuzzy soft sets over the universe U and the parameter set E, that is

$$S(U,E) = \{(F,A); A\subseteq E, F : A \to F(U)\}.$$

Theorem 7. *(1)* $(S(U,E),\widetilde{\cup},\widetilde{\cap})$ *is a lattice.*

(2) Let $\leq_1$ *be the ordering relation in lattice* $(S(U,E),\widetilde{\cup},\widetilde{\cap})$ *and* $(F,A),(G,B)\in S(U,E)$. $(F,A)\leq_1 (G,B)$ *if and only if:* $A\subseteq B$ *and* $F(e)\subseteq G(e)$ *for all* $e\in A$.

Clearly, $(S(U,E),\widetilde{\cup},\widetilde{\cap})$ is a bounded lattice, U_E and $\emptyset_\emptyset$ are the upper bound and lower bound respectively.

Theorem 8. $(S(U,E),\widetilde{\cup},\widetilde{\cap})$ *is a distributive lattice.*

We consider fuzzy soft sets over a definite parameter set. Let $A\subseteq E$ and

$$S_A = \{(F,A); F : A \to F(U)\}$$

be the set of soft sets over the universe U and the parameter set A. It is trivial to verify that $(F,A)\widetilde{\cup}(G,A), (F,A)\widetilde{\cap}(G,A)\in S_A$ for all $(F,A),(G,A)\in S_A$. That is to say

Corollary 1. S_A *is a sublattice of* $(S(U,E),\widetilde{\cup},\widetilde{\cap})$.

In $(S_A,\widetilde{\cup},\widetilde{\cap})$,$U_A$ and $\emptyset_A$ are the greatest element and the least element respectively.

In what follows, we consider another lattice structure of soft sets.

Theorem 9. *Let* (F,A) *and* (G,B) *be two fuzzy soft sets over the same universe* U. *Then*

(1)$((F,A)\cup_\Re (G,B))\sqcap_\varepsilon (F,A) = (F,A)$,

(2)$((F,A)\sqcap_\varepsilon (G,B))\cup_\Re (F,A) = (F,A)$.

Proof. (1) Suppose that $(F,A)\cup_\Re (G,B) = (H, A\cap B)$ and $((F,A)\cup_\Re (G,B))\sqcap_\varepsilon (F,A) = (K,(A\cap B)\cup A) = (K,A)$. For all $e\in A$,

(a) if $e\in B$, then $e\in A\cap B$ and $K(e) = H(e)\cap F(e) = (F(e)\cup G(e))\cap F(e) = F(e)$;

(b) if $e \notin B$, then $e \notin A \cap B$ and $K(e) = F(e)$.

Hence $((F, A) \cup_{\Re} (G, B)) \sqcap_{\varepsilon} (F, A) = (F, A)$.

(2) Suppose that $(F, A) \sqcap_{\varepsilon} (G, B) = (H, \cup B)$ and $((F, A) \sqcap_{\varepsilon} (G, B)) \cup_{\Re} (F, A) = (K, (A \cup B) \cap A) = (K, A)$. For all $e \in A$,

(a) if $e \in B$, then $e \in A \cap B$ and $K(e) = H(e) \cup F(e) = (F(e) \cap G(e)) \cup F(e) = F(e)$;

(b) if $e \notin B$, then $K(e) = H(e) \cup F(e) = F(e) \cup F(e) = F(e)$.

Hence $((F, A) \sqcap_{\varepsilon} (G, B)) \cup_{\Re} (F, A) = (F, A)$.

Theorem 10. *For all* $(F, A), (G, B), (H, C) \in S(U, E)$,

$$(F, A) \cup_{\Re} ((G, B) \sqcap_{\varepsilon} (H, C)) = ((F, A) \cup_{\Re} (G, B)) \sqcap_{\varepsilon} ((F, A) \cup_{\Re} (H, C)).$$

Proof. Suppose that

$$(F, A) \cup_{\Re} ((G, B) \sqcap_{\varepsilon} (H, C)) = (K, A \cap (B \cup C)),$$

$$((F, A) \cup_{\Re} (G, B)) \sqcap_{\varepsilon} ((F, A) \cup_{\Re} (H, C)) = (L, (A \cap B) \cup (A \cap C)) = (L, A \cap (B \cup C)).$$

For each $e \in A \cap (B \cup C)$, it follows that $e \in A$ and $e \in B \cup C$.

(a) if $e \in A$, $e \notin B$, $e \in C$, then $K(e) = F(e) \cup H(e) = L(e)$;

(b) if $e \in A$, $e \in B$, $e \notin C$, then $K(e) = F(e) \cup G(e) = L(e)$;

(c) if $e \in A$, $e \in B$, $e \in C$, then $K(e) = F(e) \cup (G(e) \cap H(e)) = (F(e) \cup G(e)) \cap (F(e) \cup H(e)) = L(e)$.

Hence $(F, A) \cup_{\Re} ((G, B) \sqcap_{\varepsilon} (H, C)) = ((F, A) \cup_{\Re} (G, B)) \sqcap_{\varepsilon} ((F, A) \cup_{\Re} (H, C))$.

Theorem 11. *(1)* $(S(U, E), \cup_{\Re}, \sqcap_{\varepsilon})$ *is a distributive lattice.*

(2) Let $\leq_2$ *be the ordering relation in lattice* $(S(U, E), \cup_{\Re}, \sqcap_{\varepsilon})$ *and* $(F, A), (G, B) \in S(U, E)$. $(F, A) \leq_2 (G, B)$ *if and only if:* $B \subseteq A$ *and for all* $e \in B$, $F(e) \subseteq G(e)$.

Proof. (1) This can be deduced from Theorem 2, Theorem 3, Theorem 9 and Theorem 10.

(2) Suppose that $(F, A) \leq_2 (G, B)$. Then $(F, A) \cup_{\Re} (G, B) = (G, B)$. By definition, $A \cap B = B$ and hence $B \subseteq A$. For all $e \in B$, by $F(e) \cup G(e) = G(e)$, it follows that $F(e) \subseteq G(e)$.

Conversely, suppose that $B \subseteq A$ and $F(e) \subseteq G(e)$ for all $e \in B$. It is trivial to verify that $(F, A) \cup_{\Re} (G, B) = (G, B)$ and hence $(F, A) \leq_2 (G, B)$.

We notice that the lattice structure $(S(U, E), \widetilde{\cup}, \widetilde{\cap})$ is different from that of $(S(U, E), \cup_{\Re}, \sqcap_{\varepsilon})$.

Corollary 2. S_A *is a sublattice of* $(S(U, E), \cup_{\Re}, \sqcap_{\varepsilon})$.

Theorem 12. *Let* (F, A) *and* (G, B) *be two fuzzy soft sets over the same universe* U. *Then*

(1) $((F, A) \widetilde{\cup} (G, B)) \sqcap_{\varepsilon} (F, A) = ((F, A) \sqcap_{\varepsilon} (G, B)) \widetilde{\cup} (F, A)$,

(2) $((F, A) \cup_{\Re} (G, B)) \widetilde{\cap} (F, A) = ((F, A) \widetilde{\cap} (G, B)) \cup_{\Re} (F, A)$.

Proof. (1) Suppose that $((F,A)\widetilde{\cup}(G,B)) \sqcap_\varepsilon (F,A) = (H, A\cup B)$ and $((F,A) \sqcap_\varepsilon (G,B))\widetilde{\cup}(F,A) = (K, A\cup B)$. For all $e \in A\cup B$,

(a) if $e \in A$ and $e \in B$, then $H(e) = (F(e)\cup G(e)) \cap F(e) = F(e) = ((F,e) \cap G(e)) \cup F(e) = K(e)$;

(b) if $e \in A$ and $e \notin B$, then $H(e) = F(e) \cap F(e) = F(e) = F(e) \cup F(e) = K(e)$;

(c) if $e \notin A$ and $e \in B$, then $H(e) = G(e) = K(e)$.

Hence $((F,A)\widetilde{\cup}(G,B)) \sqcap_\varepsilon (F,A) = ((F,A) \sqcap_\varepsilon (G,B))\widetilde{\cup}(F,A)$.

(2) Suppose that $((F,A) \cup_\Re (G,B)) \Cap (F,A) = (H, A\cap B)$ and $((F,A) \Cap (G,B)) \cup_\Re (F,A) = (K, A\cap B)$. For all $e \in A\cap B$, we have $e \in A$ and $e \in B$. It follows that

$$H(e) = (F(e)\cup G(e)) \cap F(e) = F(e) = (F(e)\cap G(e)) \cup F(e) = K(e).$$

Hence $((F,A) \Cap (G,B))\widetilde{\cup}(F,A) = (F,A)$.

The absorption laws with respect to operations $\widetilde{\cup}$ and $\sqcap_\varepsilon$, $\cup_\Re$ and $\Cap$ may not necessarily hold. That is to say:

(1) $((F,A)\widetilde{\cup}(G,B)) \sqcap_\varepsilon (F,A) = (F,A)$,

(2) $((F,A) \cup_\Re (G,B)) \Cap (F,A) = (F,A)$,

do not hold in general.

Example 2. Suppose that the universe $U = \{h_1, h_2, h_3, h_4, h_5, h_6\}$ and $E = \{e_1, e_2, e_3, e_4\}$ is the set of parameters. Let (F,A) and (G,B) be two soft sets over U, where $A = \{e_1, e_2\}$, $B = \{e_2, e_3\}$, $F(e_1) = \{h_1, h_2\}$, $F(e_2) = \{h_2, h_4\}$, $G(e_2) = \{h_1, h_3\}$, $G(e_3) = \{h_2, h_3, h_4\}$. By the definitions, we have $((F,A)\widetilde{\cup}(G,B)) \sqcap_\varepsilon (F,A) = (H, \{e_1, e_2, e_3\}$, $((F,A) \cup_\Re (G,B)) \Cap (F,A) = (K, \{e_2\})$. Where $H(e_1) = \{h_1, h_2\}$, $H(e_2) = \{h_2, h_4\}$, $H(e_3) = \{h_2, h_3, h_4\}$, $K(e_2) = \{h_2, h_4\}$.

Hence $((F,A)\widetilde{\cup}(G,B)) \sqcap_\varepsilon (F,A) \neq (F,A)$ and $((F,A) \cup_\Re (G,B)) \Cap (F,A) \neq (F,A)$.

5 Conclusions

In this paper, we study the algebraic structures of fuzzy soft sets. Two lattice structures of fuzzy soft sets are established and several related properties are investigated. It has been proved that certain De Morgan's laws hold in soft set theory. Based on these results, we can further prove the relationship among fuzzy soft sets, fuzzy sets and fuzzy rough set. The topological structure of fuzzy soft sets is another important and interesting issue to be addressed.

Acknowledgements

This work has been supported by the National Natural Science Foundation of China (Grant No. 60875034) and the Fundamental Research Funds for the Central University of China (Grant No. SWJTU09ZT37).

References

1. Aktas, H., Cagman, N.: Soft sets and soft groups. Information Sciences 177, 2726–2735 (2007)
2. Ali, M.I., Feng, F., Liu, X., Min, W.K., Shabir, M.: On some new operations in soft set theory. Computers and Mathematics with Applications 57, 1547–1553 (2009)
3. Jun, Y.B.: Soft BCK/BCI-algebras. Computers and Mathematics with Applications 56, 1408–1413 (2008)
4. Jun, Y.B., Park, C.H.: Applications of soft sets in ideal theory of BCK/BCI-algebras. Information Sciences 178, 2466–2475 (2008)
5. Maji, P.K., Biswas, R., Roy, A.R.: Fuzzy soft sets. The Journal of Fuzzy Mathematics 9, 589–602 (2001)
6. Maji, P.K., Biswas, R., Roy, A.R.: Soft set theory. Computers and Mathematics with Applications 45, 555–562 (2003)
7. Molodtsov, D.: Soft set theory-First results. Computers and Mathematics with Applications 37, 19–31 (1999)
8. Pawlak, Z.: Rough sets. International Journal of Computer and Information Science 11, 341–356 (1982)
9. Roy, A.R., Maji, P.K.: A fuzzy soft set theoretic approach to decision making problems. Journal of Computational and Applied Mathematics 203, 412–418 (2007)
10. Xiao, Z., Gong, K., Zou, Y.: A combined forecasting approach based on fuzzy soft sets. Journal of Computational and Applied Mathematics 228, 326–333 (2009)
11. Yang, X.B., Lin, T.Y., Yang, J.Y., Li, Y., Yu, D.J.: Combination of interval-valued fuzzy set and soft set. Computers and Mathematics with Applications 58, 521–527 (2009)
12. Zadeh, L.A.: Fuzzy sets. Information and Control 8, 338–353 (1965)

A Predicate Formal System of Universal Logic with Projection Operator

Yingcang Ma and Mei Zhang

School of Science, Xi'an Polytechnic University
Xi'an 710048, China
mayingcang@126.com

Abstract. The propositional calculus formal deductive system $\mathcal{UL}^{\triangle}_{h\in(0,1]}$ for 0-level universal AND operator with projection operator has been built up. In this paper, according to the propositional system, a predicate calculus formal deductive system $\forall\mathcal{UL}^{\triangle}_{h\in(0,1]}$ for 0-level universal AND operator with projection operator is built up. The soundness theorem and deduction theorem of system $\forall\mathcal{UL}^{\triangle}_{h\in(0,1]}$ are given.

Keywords: Universal logic; Fuzzy logic; Predicate calculus; Axiomatization.

1 Introduction

How to deal with various uncertainties and evolution problems have been critical issues for further development of AI. The well-developed mathematical logic is too rigid and it can only solve certainty problems. It is the new challenge for logics to make mathematical logic more flexible and to contain various uncertainties and evolution. Therefore, non-classical logic and modern logic develop rapidly, for example fuzzy logic and universal logic.

In recent years considerable progress has been made in logical foundations of fuzzy logic, especially for the logic based on t-norm and its residua (See [1-11]). Some well-known logic systems have been built up, such as the basic logic (BL)[1, 3] introduced by Hajek; the monoidal t-norm based logic (MTL)[2] introduced by Esteva and Godo; a formal deductive system $L*$ introduced by Wang (see [7-11]), and so on. Moreover the completeness of the above logical systems have been proven.

Universal logic[12] was proposed by Huacan He, which thinks that all things in the world are correlative, that is, they are either mutually exclusive or mutually consistent, and we call this kind of relation generalized correlation. Any two propositions have generalized correlation. The degree of general correlation can be described quantitatively by the coefficient of the generalized correlation $h \in [0, 1]$: If we define the h of operator $T(a, b)$ as the ratio between the volume of $T(a, b)$ and the volume of maximal operator , then $h = 1$ means the maximal attractive state; $h = 0.75$ means independency correlative state; $h = 0.5$ means neutral state; $h = 0$ means maximal exclusive state. The 0-level universal AND operators and 0-level universal IMPLICATION operators are defined as:

D.-S. Huang et al. (Eds.): ICIC 2010, LNCS 6215, pp. 134–141, 2010.

0-level universal AND operators are mapping $T : [0,1] \times [0,1] \to [0,1]$, $T(x,y,h) = \Gamma^1[(x^m + y^m - 1)^{1/m}]$, which is usually denoted by $\wedge_h$; the real number m has relation with the coefficient of generalized correlation h as:

$$m = (3 - 4h)/(4h(1-h)) \tag{1}$$

$h \in [0,1], m \in \mathbb{R}$. And $\Gamma^1[x]$ denotes x is restricted in $[0,1]$, if $x > 1$ then its value will be 1, if $x < 0$, its value will be 0. Four basic operators can be obtained through specifying the parameter h:

$T(x,y,1) = \min(x,y)$; $T(x,y,0.75) = xy$;
$T(x,y,0.5) = \max(0, x+y-1)$; $T(x,y,0) = ite\{\min(x,y) | \max(x,y) = 1; 0\}$.

In the above the $ite\{a|b;c\}$ denotes that the value is a if b is true, otherwise c.

0-level universal IMPLICATION operators are mapping $I : [0,1] \times [0,1] \to [0,1], I(x,y,h) = ite\{1|x \le y; 0|m \le 0 \text{ and } y = 0; \Gamma^1[(1 - x^m + y^m)^{1/m}]\}$, which is usually denoted by $\Rightarrow_h$. In the above the equation with m and h is the same as (1). Four basic operators can be obtained through specifying the parameter h:

$I(x,y,1) = ite\{1|x \le y, y\}$; $I(x,y,0.75) = \min(1, y/x)$;
$I(x,y,0.5) = \min(1, 1 - x + y)$; $I(x,y,0) = ite\{y|x = 1, 1\}$

The formal systems of propositional universal logic have been studied in [13-17], the predicate calculus formal deductive systems of universal logic have not been studied. In this paper, we focus on the formal system of universal logic according the propositional system $\mathcal{UL}^{\triangle}_{h\in(0,1]}$[15] for 0-level universal AND operator with projection operator. We build predicate formal system $\forall\mathcal{UL}^{\triangle}_{h\in(0,1]}$, and its soundness and deduction theorem are given.

The paper is organized as follows. After this introduction, Section 2 we will build the predicate calculus formal deductive system $\forall\mathcal{UL}^{\triangle}_{h\in(0,1]}$ for 0-level universal AND operator with projection operator. In Section 3 the soundness of system $\forall\mathcal{UL}^{\triangle}_{h\in(0,1]}$ will be proved, moreover, the deduction theorem will given. The final section offers the conclusion.

2 Predicate Formal System $\forall\mathcal{UL}^{\triangle}_{h\in(0,1]}$

In order to build first-order predicate formal deductive system based on 0-level universal AND operator with projection operator, we give the first-order predicate language as following:

First-order language J consists of symbols set and generation rules:

The symbols set of J consist of as following:

(1) Object variables: $x, y, z, x_1, y_1, z_1, x_2, y_2, z_2, \cdots$;
(2) Object constants: $a, b, c, a_1, b_1, c_1,$, Truth constants: $\overline{0}, \overline{1}$;
(3) Predicate symbols: $P, Q, R, P_1, Q_1, R_1, \cdots$;
(4) Connectives: $\&, \to, \triangle$;
(5) Quantifiers: $\forall$(universal quantifier), $\exists$(existential quantifier);
(6) Auxiliary symbols: (,), ,.

The symbols in (1)-(3) are called non-logical symbols of language J. The object variables and object constants of J are called terms. The set of all object constants is denoted by $\mathrm{Var}(J)$, The set of all object variables is denoted by $\mathrm{Const}(J)$, The set of all terms is denoted by $\mathrm{Term}(J)$. If P is n-ary predicate symbol, $t_1, t_2, \cdots, t_n$ are terms, then $P(t_1, t_2, \cdots, t_n)$ is called atomic formula.

The formula set of J is generated by the following three rules in finite times:

(i) If P is atomic formula, then $P \in J$;
(ii) If $P, Q \in J$, then $P\&Q, P \to Q, \triangle P \in J$;
(iii) If $P \in J$, and $x \in \mathrm{Var}(J)$, then $(\forall x)P, (\exists x)P \in J$.

The formulas of J can be denoted by $\varphi, \phi, \psi, \varphi_1, \phi_1, \psi_1, \cdots$. Further connectives are defined as following:

$\varphi \wedge \psi$ is $\varphi\&(\varphi \to \psi)$, $\quad \varphi \vee \psi$ is $((\varphi \to \psi) \to \psi) \wedge (\psi \to \varphi) \to \varphi)$,
$\neg\varphi$ is $\varphi \to \overline{0}$, $\quad \varphi \equiv \psi$ is $(\varphi \to \psi)\&(\psi \to \varphi)$.

Definition 1. *The axioms and deduction rules of predicate formal system* $\forall\mathcal{UL}^{\triangle}_{h\in(0,1]}$ *as following:*

(i)The following formulas are axioms of $\forall\mathcal{UL}^{\triangle}_{h\in(0,1]}$*:*

(U1) $(\varphi \to \psi) \to ((\psi \to \chi)(\varphi \to \chi))$
(U2) $(\varphi\&\psi) \to \varphi$
(U3) $(\varphi\&\psi) \to (\psi\&\varphi)$
(U4) $\varphi\&(\varphi \to \psi) \to (\psi\&(\psi \to \varphi))$
(U5) $(\varphi \to (\psi \to \chi)) \to ((\varphi\&\psi) \to \chi)$
(U6) $((\varphi\&\psi) \to \chi) \to (\varphi \to (\psi \to \chi))$
(U7) $((\varphi \to \psi) \to \chi) \to (((\psi \to \varphi) \to \chi) \to \chi)$
(U8) $\overline{0} \to \varphi$
(U9) $(\varphi \to \varphi\&\psi) \to ((\varphi \to \overline{0}) \vee \psi \vee ((\varphi \to \varphi\&\varphi) \wedge (\psi \to \psi\&\psi)))$
(U10) $\triangle\varphi \vee \neg\triangle\varphi$
(U11) $\triangle(\varphi \vee \psi) \to (\triangle\varphi \vee \triangle\psi)$
(U12) $\triangle\varphi \to \varphi$
(U13) $\triangle\varphi \to \triangle\triangle\varphi$
(U14) $\triangle(\varphi \to \psi) \to (\triangle\varphi \to \triangle\psi)$
(U15) $(\forall x)\varphi(x) \to \varphi(t)$ *(t substitutable for x in* $\varphi(x)$*)*
(U16) $\varphi(t) \to (\exists x)\varphi(x)$*(t substitutable for x in* $\varphi(x)$*)*
(U17) $(\forall x)(\chi \to \varphi) \to (\chi \to (\forall x)\varphi)$*(x is not free in* χ*)*
(U18) $(\forall x)(\varphi \to \chi) \to ((\exists x)\varphi \to \chi)$*(x is not free in* χ*)*
(U19) $(\forall x)(\varphi \vee \chi) \to ((\forall x)\varphi \vee \chi)$*(x is not free in* χ*)*

Deduction rules of $\forall\mathcal{UL}^{\triangle}_{h\in(0,1]}$ *are three rules. They are:*
Modus Ponens(MP):from $\varphi, \varphi \to \psi$ *infer* ψ*;*
Necessitation: from φ *infer* $\triangle\varphi$*;*
Generalization: from φ *infer* $(\forall x)\varphi$*.*

The meaning of "t substitutable for x in $\varphi(x)$" and "x is not free in χ" in the above definition have the same meaning in the classical first-order predicate logic,

moreover, we can define the concepts such as proof, theorem, theory, deduction from a theory T, T-consequence in the system $\forall\mathcal{UL}^{\triangle}_{h\in(0,1]}$. $T \vdash \varphi$ denotes that φ is provable in the theory T. $\vdash \varphi$ denotes that φ is a theorem of system $\forall\mathcal{UL}^{\triangle}_{h\in(0,1]}$. Let $\mathrm{Thm}(\forall\mathcal{UL}^{\triangle}_{h\in(0,1]}) = \{\varphi \in J| \vdash \varphi\}, \mathrm{Ded}(T) = \{\varphi \in J|T \vdash \varphi\}$. Being the axioms of propositional system $\mathcal{UL}^{\triangle}_{h\in(0,1]}$ are in predicate system $\forall\mathcal{UL}^{\triangle}_{h\in(0,1]}$, then the theorems in $\mathcal{UL}_{h\in(0,1]}$ are theorems in $\forall\mathcal{UL}_{h\in(0,1]}$. According the similar proof in [1,15,16] we can get the following lemmas.

Lemma 1. *The hypothetical syllogism holds in* $\forall\mathcal{UL}^{\triangle}_{h\in(0,1]}$, *i.e. let* $\Gamma = \{\varphi \to \psi, \psi \to \chi\}$, *then* $\Gamma \vdash \varphi \to \chi$.

Lemma 2. $\forall\mathcal{UL}^{\triangle}_{h\in(0,1]}$ *proves:*
(1) $\varphi \to \varphi$; *(2)* $\varphi \to (\psi \to \varphi)$; *(3)* $(\varphi \to \psi) \to ((\varphi \to \gamma) \to (\psi \to \gamma))$;
(4)$(\varphi\&(\varphi \to \psi)) \to \psi$; *(5)* $\Delta\varphi \equiv \Delta\varphi\&\Delta\varphi$.

Lemma 3. *If* $T = \{\varphi \to \psi, \chi \to \gamma\}$, *then* $T \vdash (\varphi\&\chi) \to (\psi\&\gamma)$.

In order to prove the soundness of predicate system $\forall\mathcal{UL}^{\triangle}_{h\in(0,1]}$, we should introduce the following definitions.

Definition 2. [1] *A BL-algebra is an algebra* $\mathrm{L} = (L, \cap, \cup, *, \Rightarrow, 0, 1)$ *with four binary operations and two constants such that*

1. $(L, \cap, \cup, 0, 1)$ *is a lattice with the greatest element* 1 *and the least element* 0 *(with respect to the lattice ordering* $\leq$*),*
2. $(L, *, 1)$ *is a commutative semigroup with the unit element* 1, *i.e.* $*$ *is commutative, associative and* $1 * x = x$ *for all* x,
3. *the following conditions hold for all* x, y, z:
   (i) $z \leq (x \Rightarrow y)$ *iff* $x * z \leq y$
   (ii) $x \cap y = x * (x \Rightarrow y)$
   (iii) $(x \Rightarrow y) \cup (y \Rightarrow x) = 1$.

Definition 3. [16] *A ŁΠG algebra is a BL-algebra in which the identity* $(x \Rightarrow x * y) \Rightarrow ((x \Rightarrow 0) \cup y \cup ((x \Rightarrow x * x) \cap (y \Rightarrow y * y))) = 1$ *is valid.*

Definition 4. [15] *A ŁΠG$_{\triangle}$-algebra is a structure* $\mathrm{L} =< L, *, \Rightarrow, \cap, \cup, 0, 1, \triangle >$ *which is a ŁΠG-algebra expanded by an unary operation* $\triangle$ *in which the following formulas are true:*

$\triangle x \cup (\triangle x \Rightarrow 0) = 1$
$\triangle(x \cup y) \leq \triangle x \cup \triangle y$
$\triangle x \leq x$
$\triangle x \leq \triangle\triangle x$
$(\triangle x) * (\triangle(x \Rightarrow y)) \leq \triangle y$
$\triangle 1 = 1$

Let J is first-order predicate language, L is linearly ordered ŁΠG$_{\triangle}$ algebra, $\mathrm{M} = (M, (r_P)_P, (m_c)_c)$ is called a L-evaluation for first-order predicate language J, which M is non-empty domain, according to each n-ary predicate P and object constant c, r_P is L-fuzzy n-ary relation: $r_P : M^n \to \mathrm{L}$, m_c is an element of M.

Definition 5. *Let J be predicate language,* M *is* L*-evaluation of J, x is object variable, $P \in J$.*

(i) A mapping V: $\mathrm{Term}(J) \to M$ *is called* M*-evaluation, if for each $c \in$*Const (J), $v(c) = m_c$;*

(ii)Two M*-evaluation v, v' are called equal denoted by $v \equiv_x v'$ if for each $y \in \mathrm{Var}(J)\backslash\{x\}$, there is $v(y) = v'(y)$.*

(iii) The value of a term given by M*, v is defined by:* $\|x\|_{\mathrm{M},v} = v(x)$; $\|c\|_{\mathrm{M},v} = m_c$. *We define the truth value* $\|\varphi\|^{\mathrm{L}}_{\mathrm{M},v}$ *of a formula φ as following. Clearly, $*, \Rightarrow, \triangle$ denote the operations of* L.

$\|P(t_1, t_2, \cdots, t_n)\|^{\mathrm{L}}_{\mathrm{M},v} = r_P(\|t_1\|_{\mathrm{M},v}, \cdots, \|t_n\|_{\mathrm{M},v})$

$\|\varphi \to \psi\|^{\mathrm{L}}_{\mathrm{M},v} = \|\varphi\|^{\mathrm{L}}_{\mathrm{M},v} \Rightarrow \|\psi\|^{\mathrm{L}}_{\mathrm{M},v}$

$\|\varphi \& \psi\|^{\mathrm{L}}_{\mathrm{M},v} = \|\varphi\|^{\mathrm{L}}_{\mathrm{M},v} * \|\psi\|^{\mathrm{L}}_{\mathrm{M},v}$

$\left\|\overline{0}\right\|^{\mathrm{L}}_{\mathrm{M},v} = 0$; $\left\|\overline{1}\right\|^{\mathrm{L}}_{\mathrm{M},v} = 1$

$\|\Delta\varphi\|^{\mathrm{L}}_{\mathrm{M},v} = \Delta\|\varphi\|^{\mathrm{L}}_{\mathrm{M},v}$

$\|(\forall x)\varphi\|^{\mathrm{L}}_{\mathrm{M},v} = \inf\{\|\varphi\|^{\mathrm{L}}_{\mathrm{M},v'} \mid v \equiv_x v'\}$

$\|(\exists x)\varphi\|^{\mathrm{L}}_{\mathrm{M},v} = \sup\{\|\varphi\|^{\mathrm{L}}_{\mathrm{M},v'} \mid v \equiv_x v'\}$

In order to the above definitions are reasonable, the infimum/supremum should exist in the sense of L. So the structure M is L-safe if all the needed infima and suprema exist, i.e. $\|\varphi\|^{\mathrm{L}}_{\mathrm{M},v}$ is defined for all φ, v.

Definition 6. *Let $\varphi \in J$,* M *be a safe* L*-structure for J.*

(i) The truth value of φ in M *is* $\|\varphi\|^{\mathrm{L}}_{\mathrm{M}} = \inf\{\|\varphi\|^{\mathrm{L}}_{\mathrm{M},v} \mid v \ \ \mathrm{M-evaluation}\}$.

(ii) A formula φ of a language J is an L*-tautology if* $\|\varphi\|^{\mathrm{L}}_{\mathrm{M}} = 1_{\mathrm{L}}$ *for each safe* L*-structure M. i.e.* $\|\varphi\|^{\mathrm{L}}_{\mathrm{M,v}} = 1$ *for each safe* L*-structure* M *and each* M*-valuation of object variables.*

Remark 1. For each $h \in (0, 1]$, $([0, 1], \wedge_h, \Rightarrow_h, \min, \max, 0, 1, \triangle)$ is a linearly ordered ŁΠG$_\triangle$-algebra. So the predicate system $\forall\mathcal{UL}^{\triangle}_{h\in(0,1]}$ can be considered the axiomatization for 0-level universal AND operator with projection operator.

3 Soundness of System $\forall\mathcal{UL}^{\triangle}_{h\in(0,1]}$

Definition 7. *A logic system is soundness if for its each theorem φ, we can get φ is a tautology.*

Theorem 1. *(Soundness of axioms) The axioms of $\forall\mathcal{UL}^{\triangle}_{h\in(0,1]}$ are* L*-tautologies for each linearly ordered ŁΠG$_\triangle$-algebra* L.

Proof. The axioms of (U1)-(U14) are L-tautologies can be get as in propositional calculus. We verify (U15)-(U19)

To verify (U15), (U16), let y is substitutable for x to φ, when $v'' \equiv_x v$ and $v''(x) = v(y)$, there is $\|\varphi(y)\|^{\mathrm{L}}_{\mathrm{M},v} = \|\varphi(x)\|^{\mathrm{L}}_{\mathrm{M},v''}$. So, $\|(\forall x)\varphi(x)\|^{\mathrm{L}}_{\mathrm{M},v} = \inf_{v'\equiv v}\|\varphi(x)\|^{\mathrm{L}}_{\mathrm{M},v'} \le \|\varphi(y)\|^{\mathrm{L}}_{\mathrm{M},v''} \le \sup_{v'}\|\varphi(x)\|^{\mathrm{L}}_{\mathrm{M},v'} = \|(\exists x)\varphi(x)\|^{\mathrm{L}}_{\mathrm{M},v}$, then $\|(\forall x)\varphi(x) \to \varphi(y)\|_{\mathrm{M},v} = \|(\forall x)\varphi(x)\|_{\mathrm{M},v} \to \|\varphi(y)\|_{\mathrm{M},v} = 1$.

For (U17), let x not free in χ, then for each M-valuation w, when $w \equiv_x v$, we have $\|v\|^{\mathrm{L}}_{\mathrm{M},w} = \|\varphi(x)\|^{\mathrm{L}}_{\mathrm{M},v}$. We have to show $\inf_w(\|v\|^{\mathrm{L}}_{\mathrm{M},w} \Rightarrow \|\varphi\|^{\mathrm{L}}_{\mathrm{M},w}) \leq (\|v\|^{\mathrm{L}}_{\mathrm{M},v} \Rightarrow \inf_w \|\varphi\|^{\mathrm{L}}_{\mathrm{M},w})$. Let $\|v\|^{\mathrm{L}}_{\mathrm{M},v} = \|v\|^{\mathrm{L}}_{\mathrm{M},w} = a$, $\|\varphi\|^{\mathrm{L}}_{\mathrm{M},w} = b_w$, thus we must prove $\inf_w(a \Rightarrow b_w) \leq (a \Rightarrow \inf_w b_w)$. On the one hand, $\inf_w b_w \leq b_w$, thus $a \Rightarrow b_w \geq (a \Rightarrow \inf_w b_w)$ for each w, thus $\inf_w(a \Rightarrow b_w) \geq (a \Rightarrow \inf_w b_w)$. On the other hand if $z \leq (a \Rightarrow b_w)$ for each w, then $z * a \leq b_w$ for each w, $z * a \leq \inf_w b_w$, $z \leq (a \Rightarrow \inf_w b_w)$. Thus $(a \Rightarrow \inf_w b_w)$ is the infimum of all $(a \Rightarrow b_w)$. So (U17) holds.

For (U18), we need to verify $\inf_w(a_w \Rightarrow b_w) = (\sup_w a_w \Rightarrow b)$. Indeed, $\sup_w \geq a_w$, thus $(\sup_w a_w \Rightarrow b) \leq (a_w \Rightarrow b)$, hence $(\sup_w a_w \Rightarrow b) \leq \inf_w(a_w \Rightarrow b)$, If $z \leq a_w \Rightarrow b$ for all w, then $a_w \leq (z \Rightarrow b)$ for all w, then $\sup_w a_w \leq (z \Rightarrow b)$, $z \leq (\sup_w a_w \Rightarrow b)$, so $\sup_w a_w \Rightarrow b$ is the infimum. So (U18) holds.

Finally we verify (U20), we need to verify $\inf_w(a \vee b_w) = a \vee \inf_w b_w$. Indeed, $a \leq a \vee b_w$, thus $a \leq \inf_w(a \vee b_w)$; similarly, $\inf_w b_w \leq \inf_w(a \vee b_w)$, thus $a \vee \inf_w b_w \leq \inf_w(a \vee b)$. Conversely, let $z \leq a \vee b_w$ for all w, we prove $z \leq a \vee \inf_w b_w$.

Case 1: Let $a \leq \inf_w b_w$. Then $z \leq b_w$ for each w, $z \leq \inf_w b_w$ and $z \leq a \vee \inf_w b_w$.

Case 2: Let $a \geq \inf_w b_w$. Then for some w_0, $a \geq b_{w_0}$, thus $z \leq a$ and $z \leq a \vee \inf_w b_w$.

So we prove the soundness of axioms.

Theorem 2. *(Soundness of deduction rules) (1) For arbitrary formulas φ, ψ, safe-structure* M *and evaluation v, $\|\psi\|^{\mathrm{L}}_{\mathrm{M},v} \geq \|\varphi\|^{\mathrm{L}}_{\mathrm{M},v} * \|\varphi \to \psi\|^{\mathrm{L}}_{\mathrm{M},v}$. In particular, if $\|\varphi\|^{\mathrm{L}}_{\mathrm{M},v} = \|\varphi \to \psi\|^{\mathrm{L}}_{\mathrm{M},v} = 1_{\mathrm{L}}$ then $\|\psi\|^{\mathrm{L}}_{\mathrm{M},v} = 1_{\mathrm{L}}$.*

(2) Consequently, $\|\psi\|^{\mathrm{L}}_{\mathrm{M}} \geq \|\varphi\|^{\mathrm{L}}_{\mathrm{M}} * \|\varphi \to \psi\|^{\mathrm{L}}_{\mathrm{M}}$, thus if $\varphi, \varphi \to \psi$ are then ψ is 1_{L}-true in M.

(3) If φ is 1_{L}-true in M *then $\triangle\varphi$ is 1_{L}-true in* M.

(4) If φ is 1_{L}-true in M *then $(\forall x)\varphi$ is 1_L-true in* M.

Proof. (1) is just as in propositional calculus(from the basic property of residuation).

To prove (2) put $\|\varphi\|_w = a_w, \|\psi\|_w = b_w, \inf_w a_w = a$. We have to prove $\inf_w(a_w \Rightarrow b_w) \leq \inf_w a_w \Rightarrow \inf_w b_w$. Observe the following: $\inf(a_w \Rightarrow b_w) \leq (a_w \Rightarrow b_w) \leq (a \Rightarrow b_w)$, thus $\inf_w(a_w \Rightarrow b_w) \leq \inf_w(a \Rightarrow b_w)$. It remains to prove $\inf_w(a \Rightarrow b_w) \leq a \Rightarrow \inf_w b_w$, this is holds from Theorem 1.

(3) If φ is 1_L-true in M then $\|\varphi\|^L_M = 1_{\mathrm{L}}$, so $\|\Delta\varphi\|^{\mathrm{L}}_{\mathrm{M},v} = \Delta\|\varphi\|^{\mathrm{L}}_{\mathrm{M},v} = 1_{\mathrm{L}}$. Then (3) holds.

(4) Being $\|\varphi\|^{\mathrm{L}}_{\mathrm{M}} = \inf\{\|\varphi\|^{\mathrm{L}}_{\mathrm{M},v} \mid v \ \ \mathrm{M}-\text{evaluation}\} \leq \inf\{\|\varphi\|_{\mathrm{M},v'} | v' \equiv v\} = \|(\forall x)\varphi\|^{\mathrm{L}}_{\mathrm{M}}$. So (4) holds.

So we can get the following soundness theorem.

Theorem 3. *(Soundness) Let* L *is linearly ordered ŁΠ$G_\triangle$-algebra and φ is a formula in J, if $\vdash \varphi$, then φ is* L*-tautology, i.e. $\|\varphi\|^{\mathrm{L}}_{\mathrm{M}} = 1_{\mathrm{L}}$.*

Similarly, we can get the following strong soundness theorem.

Definition 8. *Let T be a theory,* L *be a linearly ordered $L\Pi G_\triangle$-algebra and* M *a safe* L*-structure for the language of T.* M *is an* L*-model of T if all axioms of T are $1_{\mathrm{L}}-$true in* M*, i.e. $\|\varphi\| = 1_L$ in each $\varphi \in T$.*

Theorem 4. *(Strong Soundness) Let T be a theory,* L *is linearly ordered $L\Pi G_\triangle$-algebra and φ is a formula in J, if $T \vdash \varphi$ (φ is provable in T), then $\|\varphi\|^{\mathrm{L}}_{\mathrm{M}} = 1_{\mathrm{L}}$ for each linearly ordered $L\Pi G_\triangle$-algebra* L *and each* L*-model* M *of T.*

Proof. In fact, from the proof of theorem 1, for each L-model M of T, the axioms are true, and the formulas in T are true, from the proof of theorem 2, the deduction rules preserve true. So the theorem holds.

Theorem 5. *(Deduction Theorem) Let T be a theory, φ, ψ are closed formulas. Then $(T \cup \{\varphi\}) \vdash \psi$ iff $T \vdash \Delta\varphi \to \psi$.*

Proof. Sufficiency: Let $T \vdash \Delta\varphi \to \psi$, from $\varphi(\varphi \in (T \cup \{\varphi\})$), then $\Delta\varphi$ by necessitation, so we can get ψ by MP rules.

Necessity: Let m is the proof length from $T \cup \{\varphi\}$ to ψ, we prove by induction for the length m.

When $m = 1$, $\psi \in T \cup \{\varphi\} \cup \mathrm{Axm(C}\forall)$, if $\psi = \varphi$, The result holds. If $\psi \in T$ or ψ is axiom, from Lemma2(2), we have $\psi \to (\Delta\varphi \to \psi)$, then by $\psi, \psi \to (\Delta\varphi \to \psi)$, we get $\Delta\varphi \to \psi$, thus $T \vdash \Delta\varphi \to \psi$.

Assume that the result holds when $m \leq k$, i.e. we get γ at k step, then $T \vdash \Delta\varphi \to \gamma$. Now Let $m = k + 1$.

If ψ is obtained from MP rule by the above results $\gamma, \gamma \to \psi$ in the proof sequence, then by induction hypothesis, we get $T \vdash \Delta\varphi \to \gamma, T \vdash \Delta\varphi \to (\gamma \to \psi)$. From Lemma 3, we can get $T \vdash (\Delta\varphi \& \Delta\varphi) \to (\gamma \& (\gamma \to \psi))$. Being $T \vdash (\Delta\varphi) \& (\Delta\varphi) \equiv \Delta\varphi$, so $T \vdash \Delta\varphi \to (\gamma \& (\gamma \to \psi))$. From lemma 2(4) we have $(\gamma \& (\gamma \to \psi) \to \psi$, so we get $T \vdash \Delta\varphi \to \psi$ by the hypothetical syllogism.

If ψ is obtained from necessitation rule by the above step γ in the proof sequence, i.e. $\Delta\gamma = \psi$, then by induction hypothesis, we get $T \vdash \Delta\varphi \to \gamma$. $T \vdash \Delta(\Delta\varphi \to \gamma)$, from (U14) we can get $T \vdash \Delta\Delta\varphi \to \Delta\gamma$, from (U13) we can get $\Delta\varphi \to \Delta\Delta\varphi$, thus by the hypothetical syllogism we can get $T \vdash \Delta\varphi \to \Delta\gamma$, i.e. $T \vdash \Delta\varphi \to \psi$.

If ψ is obtained from generalization rule by the above step γ in the proof sequence, i.e. $(\forall x)\gamma = \psi$, then by induction hypothesis, we get $T \vdash \Delta\varphi \to \gamma$, From generalization rule we can get $T \vdash (\forall x)(\Delta\varphi \to \gamma)$, being $\Delta\varphi, \gamma$ are closed formula and from (U17), we can get $T \vdash \Delta\varphi \to (\forall x)\gamma$, i.e. $T \vdash \Delta\varphi \to \psi$.

So the theorem holds.

4 Conclusion

In this paper a predicate calculus formal deductive system $\forall\mathcal{UL}^{\triangle}_{h\in(0,1]}$ according to the propositional system $\mathcal{UL}^{\triangle}_{h\in(0,1]}$ for 0-level universal AND operator with projection operator is built up. We prove the system $\forall\mathcal{UL}^{\triangle}_{h\in(0,1]}$ is sound. The deduction theorem are also given. Based on the paper's work, the Completeness of $\forall\mathcal{UL}^{\triangle}_{h\in(0,1]}$ will be discussed in other papers.

Acknowledgement

This work is supported by the Special Scientific Research Plan Project of Shaanxi Provincial Education Department(No. 10JK597).

References

1. Hajek, P.: Metamathematics of Fuzzy Logic. Kluwer Academic Publishers, Dordrecht (1998)
2. Esteva, F., Godo, L.: Monoidal t-normbased Logic:Towards A Logic for Left-continous t- norms. Fuzzy Sets and Systems 124, 271–288 (2001)
3. Cignoli, R., Esteva, F., Godo, L., Torrens, A.: Basic Fuzzy Logic is the Logic of Continuous t-norms and Their Residua. Soft computing 4, 106–112 (2000)
4. Hohle, U.: Commutative, Residuated L-monoids. In: Hohle, U., Klement, E.P. (eds.) Non-Classical Logics and Their Applications to Fuzzy Subsets, pp. 53–106. Kluwer Academic Publishers, Dordrecht (1995)
5. Francesc, E., Godo, L., et al.: Residuated Fuzzy Logics with an Involutive Negation. Archive for Mathmatical Logic 39, 103–124 (2000)
6. Klement, E.P., Mesiar, R., Pap, E.: Triangular Norms. Kluwer Academic Publishers, Dordrecht (2000)
7. Pei, D.W., Wang, G.J.: The Completeness and Applications of the Formal System L*. Science in China (Series F) 45, 40–50 (2002)
8. Wang, S.M., Wang, B.S., Pei, D.W.: A Fuzzy Logic for an Ordinal Sum t-norm. Fuzzy Sets and Systems 149, 297–307 (2005)
9. Wang, G.J.: Non-classical Mathematical Logic and Approximate Reasoning. Science Press, Beijing (2000) (in Chinese)
10. Pei, D.W.: First-order Formal System K^* and its Completeness. Chinese Annals of Mathematics, Series A 23(6), 675–684 (2002)
11. Wu, H.B.: Competeness of $BL^*_{\triangle}$ System. Journal of Jishou University (Natural Science Edition) 30(6), 1–5 (2009)
12. He, H.C., et al.: Universal Logic Principle. Science Press, Beijing (2001) (in Chinese)
13. Ma, Y.C., He, H.C.: The Fuzzy Reasoning Rules Based on Universal Logic. In: 2005 IEEE International Conference on GrC, pp. 561–564. IEEE Press, Los Alamitos (2005)
14. Ma, Y.C., He, H.C.: A Propositional Calculus Formal Deductive System $\mathcal{UL}_{h\in(0,1]}$ of Universal Logic. In: Proceedings of 2005 ICMLC, pp. 2716–2721. IEEE Press, Los Alamitos (2005)
15. Ma, Y.C., Li, Q.Y.: A Propositional Deductive System of Universal Logic with Projection Operator. In: Proceedings of 2006 ISDA, pp. 993–998. IEEE Press, Los Alamitos (2006)
16. Ma, Y.C., He, H.C.: The Axiomatization for 0-level Universal Logic. In: Yeung, D.S., Liu, Z.-Q., Wang, X.-Z., Yan, H. (eds.) ICMLC 2005. LNCS (LNAI), vol. 3930, pp. 367–376. Springer, Heidelberg (2006)
17. Ma, Y.C., He, H.C.: Axiomatization for 1-level Universal AND Operator. The Journal of China Universities of Posts and Telecommunications 15(2), 125–129 (2008)

A Neuro-Evolutive Interval Type-2 TSK Fuzzy System for Volatile Weather Forecasting

Dusko Kalenatic*, Juan C. Figueroa-García**, and Cesar Amilcar Lopez***

Universidad de La Sabana, Chia - Colombia
{dusko.kalenatic,juan.figueroa,cesar.lopez}@unisabana.edu.co

Abstract. This paper presents an hybrid Neuro-Evolutive algorithm for a First-order Interval Type-2 TSK Fuzzy Logic System applied to a volatile weather forecasting case. All results are tested by statistical tests as Goldfeld-Quant, Ljung-Box, ARCH, Runs, Turning Points, Bayesian, Akaike and Hannan-Quin criteria. Some methodological aspects about a hybrid implementation among ANFIS, an Evolutive Optimizer and a First order Interval Type-2 TSK FLS are presented. The selected type-reduction algorithm is the *IASCO* algorithm proposed by Melgarejo in [1] since it presents better computing properties than other algorithms.

1 Introduction and Motivation

Volatile Time Series have become as a complex problem for identification and prediction, so the application of computational intelligence techniques is useful in those cases. A first approach to Interval Type-2 Takagi-Sugeno Fuzzy Logic System *(IT2FSK)* was given by Mendez & Castillo in [2] and Figueroa in [3].

This paper shows an strategy between an Artificial Neural-Based Fuzzy Inference System *(ANFIS)* and an Evolutionary optimizer to synchronize a First-order IT2TSK for volatile weather time series forecasting in Bogotá-Colombia, using the results of Figueroa in [4] and Figueroa in [3]. Some important aspects about the design of Type-2 fuzzy input sets, TSK outputs, rule base and inference process are described.study case.

The paper is organized as follows: Section I presents the introduction, Section 2 presents the case study. In Section 3 we briefly introduce an IT2TSK system, Section 4 presents the Neuro-Evolutive IT2TSK algorithm. Section 5 presents the obtained results and its analysis and Section 6 presents the concluding remarks.

2 Bogotá Weather Time Series

Colombia is a tropical country with a nonlinear weather, so its forecasting is highly encouraged to be accurate. Its capital city is Bogotá, it is 2600m above sea level and it has a changing weather, so the more complex problem for flower-growers in the region. is the minimum temperature because it is the most dangerous point for the flower-farms.

* Dusko Kalenatic is member of the Logistic Systems group - Universidad de La Sabana.
** Corresponding author.
*** Cesar A. Lopez is member of the Logistic Systems research group-Universidad de La Sabana.

D.-S. Huang et al. (Eds.): ICIC 2010, LNCS 6215, pp. 142–149, 2010.

Particularly, this time series presents deviations from linearity and a volatile behavior. It has no constant mean and variance, therefore we apply a differentiation operator $(1 - B)x_t = x_t - x_{t-1}$ to get a constant mean process as is shown in the Figure 1.

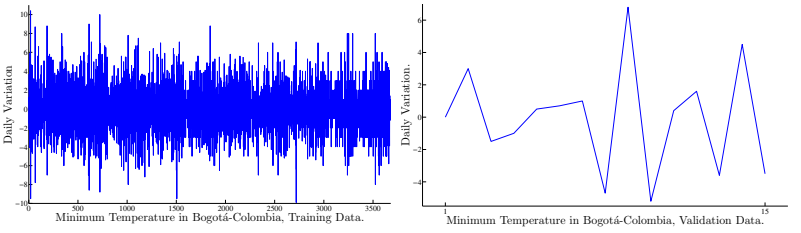

Fig. 1. Daily Variation of the Minimum Temperature in Bogotá-Colombia

Clearly, the structure of the variance of this time series is not constant and non-linear for which we perform three heteroscedasticity tests: The Golfeld-Quant [5], and the Ljung-Box tests [6] which are summarized in the Tables 1 and 2 respectively.

Table 1. Goldfeld-Quant Results

Training Data sets	F-test	p-value
1-1224; 2448-3572	1.244	0.0001

Table 2. Ljung-Box Test Results

Lag	L-B Stat	Test Stat	p-value
20	61.33	31.41	≈ 0
25	76.26	37.65	0.01596

These tests suggest that the series is not stationary neither it has a suitable structure for linear modelling, other tests on normality and randomness are shown in Table 3.

Table 3. Randomness and Normality Tests

Test	Stat	Test Stat	p-value
Randomness Tests			
Runs Test	16.47	1.9599	≈ 0
Turning Points	5.70	1.9599	≈ 0
Normality Tests			
Shapiro-Wilks Test	0.990	0.854	≈ 0
Kolmogorov-Smirnov Test	0.0646	0.0224	≈ 0
Anderson - Darling Test	12.3	2.49	≈ 0

In Tables 1 to 3, Stat is the statistic value, Test Stat is its critical value and the p-value is the probability of fulfillment of each test. All these tests suggest that the series is deviated from randomness and normality. It is a correct since weather is influenced by hundreds of environmental and unknown variables, being a clear sign of volatility.

2.1 Training and Testing Data

The training data set is defined as follows: Minimum temperature in Bogotá measured in 3676 days from 01/01/2000 to 31/01/2010. A test data set is defined on 15 days to test the generalization capability of the model. We use only 15 days due to weather time series has high sensibility regarding to ergodicity, that is, older than 30 days has no significant information about the present day.

Figueroa and Soriano in [4] show that ARIMA models have worst results than computational intelligence techniques as ANFIS, DBR or ANN. Given that antecedent, ARIMA or any linear model is not evaluated in this paper.

3 Interval Type-2 Fuzzy Logic System Design Methodology

The classical Time series model is General Linear Model:

$$x_t = \widehat{x}_t + e_t \tag{1}$$

Where x_t is an observation of the process $\{\widehat{X}_t\}$ in the time instant "t", $\widehat{x}_t$ is an *Estimation of* x_t and e_t is the model residual or residual estimation of $\widehat{x}_t$.

Box & Jenkins in [7] are focused on a statistical point of view. In this paper, $\widehat{x}_t$ is obtained by using a Neuro-Evolutive IT2TSK, so its goodness of fit is based on classical residual analysis theory. General facts about the proposed fuzzy inference engine are:

- Fuzzy input sets are interval Type-2 fuzzy sets and Outputs are TSK sets.
- Both upper and lower membership functions have the same rule base.
- Operators: *and:* $\min$, *or:* $\max$, *Aggregation:* $\max$.
- Type reduction: *IASCO* algorithm proposed by Melgarejo in [1] and Mendel en [8].

Now, we use 6 input vectors with 2 sigmoidal IT2 Fuzzy sets per input which result on 64 rules and 64 TSK output sets with 7 parameters (An intercept and one weight per input). By using the autocorrelation function, we selected the following 6 inputs: $x_{t-1}, x_{t-2}, x_{t-3}, z_{t-1}, z_{t-2}$ and z_{t-3} so the j_{th} TSK output Y^j is defined as:

$$Y^j = a_0^j + a_1^j x_{t-1} + a_2^j x_{t-2} + a_3^j x_{t-3} + a_4^j z_{t-1} + a_5^j z_{t-2} + a_6^j z_{t-3} \tag{2}$$

Here, x_{t-h} is the h_{th} lagged value of x_t and z_{t-p} is the p_{th} moving average of x_t. For each input, we use two linguistic variables: *Positive variation* (p), and *Negative Variation* (n) each one associated to an IT2FS. The lower and upper membership functions of each $\tilde{p}(x_t)$ and $\tilde{n}(x_t)$ fuzzy set are $\overline{\mu}_{\tilde{p}}(x_t), \underline{\mu}_{\tilde{p}}(x_t), \overline{\mu}_{\tilde{n}}(x_t)$ and $\underline{\mu}_{\tilde{n}}(x_t)$.

We use quadratic membership functions for each $\overline{\mu}_{\tilde{p}}(x_t), \underline{\mu}_{\tilde{p}}(x_t), \overline{\mu}_{\tilde{n}}(x_t)$ and $\underline{\mu}_{\tilde{n}}(x_t)$ set as is shown in the Figure 3. In this way, each rule R^j can be represented as:

$$R^j = \textit{IF } x_{t-1} \textit{ is } \tilde{n}_{t-1}^j \textit{ and } \cdots \textit{ and } z_{t-3} \textit{ is } \tilde{p}_{t-5}^j, \quad \textit{Then } \; Y^j = a_0^j + a_1^j x_{t-1} + a_2^j x_{t-2} + \cdots + a_6^j z_{t-3} \tag{3}$$

This configuration of IT2FS, rules and TSK outputs yield on 48 parameters for the input sets and 448 parameters for the TSK outputs which will define the size of each individual and its number of genes. The Figure 2 shows the used methodology.

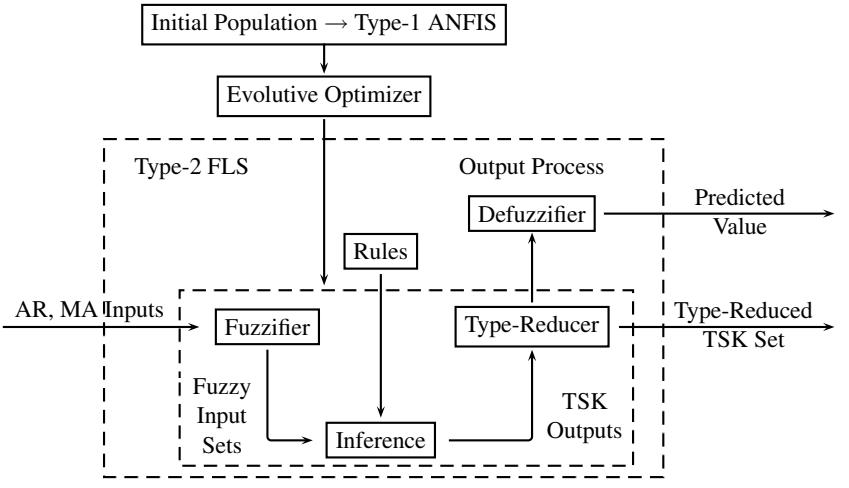

Fig. 2. Evolutive Type-2 TSK FLS design methodology

4 Neuro-Evolutive Optimizer

The selected strategy to synchronize the IT2TSK system is an Evolutionary Optimizer. Some of most important issues of the designed algorithm are described next.

4.1 Fitness Function Operator

The fitness function $\mathcal{F}$ tries to minimize the Mean Squared Error (MSE) between the original series and the output of the IT2TSK after Type-reduction and deffuzification, as follows:

$$\mathcal{F} = \sum_{i=1}^{n} \frac{(x_t - \hat{x}_t)^2}{n-1} \tag{4}$$

Where $\hat{x}_t$ is the estimate of x_t through the IT2TSK. Thus, the main goal is to find an evolutionary estimate of the parameters of the IT2 fuzzy input sets and the parameters of the TSK output sets which minimizes $\mathcal{F}$.

4.2 Random Number Generator, Individuals, Population Size and Number of Generations

The selected Random Generator R_j is the uniform generator defined as $R_j(a,b) = a + r_j(b-a)I_{[0,1]}(r_j)$, since it presents better practical properties than other generators. a, b are its lower and upper bounds.

An *Individual* is defined as a *chromosome* of size $m = 496$, where each gen or cell is a set of parameters of the IT2TSK system: The first 48 genes are the parameters of the IT2 fuzzy input sets and the other 448 are the parameters of the TSK output sets.

The size of the population is defined by two values: The m parameters and a pre-selected k number of individuals, creating a matrix called $P^g_{k,m}$ where g is the *Generation index*. It is defined that $m = 496$ and $k = 100$.

The generation index g is a genetic operator which is used as stop criterion. In this paper, the maximum number of generations is defined as $G = 1500$.

4.3 Initial Population: ANFIS Generator

ANFIS is a specialized neural net which synchronizes a Type-1 fuzzy logic system by using derivable membership functions and a complete specification of all rules for each fuzzy set. It is important to recall that ANFIS is only applied to Type-1 TSK systems, so we use it as starting point of the evolutive algorithm.

The designed ANFIS structure synchronizes twelve Type-1 FS combined on 64 rules, getting 64 outputs Y^j, similar to the defined in the Section 3 and (2). The main goal for ANFIS learning is to minimize an error measurement $E_t = \sum_{j=1}^{J}(x_t - Y^j)^2$. Where j is the j_{th} rule and J is the maximum number of rules.

Now, the initial population $P^1_{k,m}$ of the evolutive algorithm is summarized next:

1. The first individual is composed as: $p_{1,24}$ are the final parameters of ANFIS, $p_{1,48} = p_{1,24} + \triangle_{1,24}$ the next 224 genes are the final TSK outputs of ANFIS, and the last 224 genes are defined by a random generator.
2. The second individual is composed as: $p_{2,48}$ are the final parameters of ANFIS, $p_{2,24} = p_{2,48} - \triangle_{2,24}$ the next 224 genes are defined by a random generator, and the last 224 genes are the final TSK outputs of ANFIS.
3. The following 48 individuals are generated by using the same procedure of the first and second individuals.
4. The final 50 individuals are defined by R_j.

Given an initial population, the evolutionary algorithm has a good starting point to apply mutation and crossover operators, which are described as follows.

4.4 Mutation and Crossover Operators

– The selected Mutation strategy is described below:
  1. Select a random position for each orderly individual in $P^g_{k,m}$ by $\mathcal{F}$.
  2. Replace the selected position with a new individual by using R_j.
  3. Repeat Step 3 for the c_1 better individuals of each population $P^g_{k,m}$.

– The selected Crossover strategy is described below:
  1. Select the c_2 first individuals in the orderly Population $P^g_{k,m}$ by $\mathcal{F}$.
  2. Generate a new individual by replacing all even genes with its respective even gene located in the next individual.
  3. Generate a new individual by replacing all odd genes with its respective odd gene located in the next individual for each one.
  4. Repeat Step 3 for the c_2 better individuals of each population $P^g_{k,m}$.

To complete the population, an additional set of individuals is generated by replacing worst individuals with new ones, trying an exhaustive search. First, the best four individuals are preserved for the next generation and later a complementary population of size $\{k - 4 - c_1 - c_2 \times m\}$ is obtained by using R_j.

4.5 Finalization and Stopping Strategy

Two stopping criterions are used to stop the algorithm: A first one is by defining a maximum number of iterations called G, that is $g \rightarrow G$, and the second one stops when $\mathcal{F}$ has no significant improvement through a specific number of iterations. Finally, the best individual is selected by $\mathcal{F}$ and it is used to generate an IT2TSK, whose outputs Y^j are deffuzified to obtain an estimation $\hat{x}_t$.

5 Neuro-Evolutive Interval Type-2 Fuzzy Logic System Results

After the implementation of the Neuro-Evolutive IT2TSK, we obtain successful results of $\mathcal{F}$ and the properties of the residual of the model, improving the results of the Type-1 ANFIS model. The obtained residuals are shown in the Figure 4.

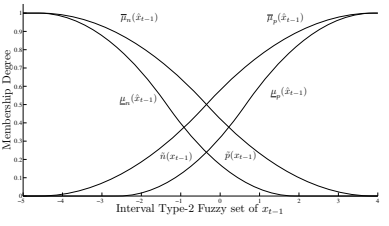

Fig. 3. IT2 Fuzzy Input sets for x_{t-1}

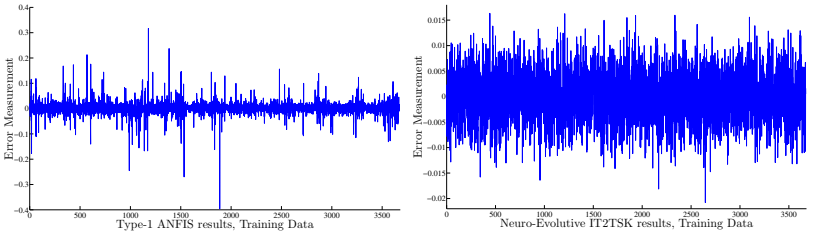

Fig. 4. Residuals of ANFIS and the Neuro-Evolutive IT2TSK models

5.1 Residual Analysis

The residual analysis is focused on e_t in (1), based on statistics as the Akaike Information criteria and Schwarz Information criteria (See [9]) and the Hannan-Quinn (HQC) information criterion (See [10]) which estimates the dimension of the model. The Ljung-Box and Goldfeld-Quant tests [11] are used to verify if the residuals are correlated. All these tests are shown in the Tables 4, 5 and 6.

Table 4. Residual Analysis

ANFIS Tests on Randomness.		
Test	Stat	p-value
Runs Test	4.258	≈ 0
Turning points	0.117	0.906
Model Adequation.		
AIC Criteria = -25388		
BIC Criteria = 2.050		
HQC Criteria = -24398		
MSE = 0.000778 ; SSE = 2.8593		

IT2TSK Tests on Randomness.		
Test	Stat	p-value
Runs Test	0.099	0.92
Turning points	0.261	0.793
Model Adequation.		
AIC Criteria = -37967		
BIC Criteria = -1.3737		
HQC Criteria = -36965		
MSE = 0.0000253 ; SSE = 0.093		

Table 5. Goldfeld-Quant Results

ANFIS Data sets	F-test	p-value
1-1224; 2448-3572	0.9355	0.2435

IT2TSK Data sets	F-test	p-value
1-1224; 2448-3572	1.0384	0.5048

Table 6. ARCH and Ljung-Box Tests Results

ANFIS ARCH Results.			
Lag	ARCH Stat	Test Stat	p-value
1	10.932	3.84	0.0009
2	14.367	5.99	0.0008
3	15.191	7.81	0.0017
ANFIS Ljung-Box Results.			
Lag	L-B Stat	Test Stat	p-value
20	21.01	31.41	0.3965
25	25.096	37.65	0.1505

IT2TSK ARCH Results.			
Lag	ARCH Stat	Test Stat	p-value
1	0.2326	3.84	0.6296
2	0.5606	5.99	0.7556
3	1.5876	7.81	0.6622
IT2TSK Ljung-Box Results.			
Lag	L-B Stat	Test Stat	p-value
20	28.18	31.41	0.3504
25	23.40	37.65	0.5518

Randomness tests suggest that residuals are independent from $\hat{X}$. The Ljung-Box and Goldfeld-Quant tests confirm the idea that ANFIS and IT2TSK are good methods. The ARCH test does not present correlation on errors or effect of heteroscedasticity, but ANFIS residuals shows that it has heteroscedasticity and correlation.

Goldfeld-Quant and Ljung-Box Tests confirm that the idea that there are no serial correlation among residuals. AIC, BIC, HQC and MSE criteria lead us to think that the Neuro-Evolutive IT2TSK model is better than ANFIS.

Based on that statistical evidence, the Neuro-Evolutive IT2TSK model is a better choice than ANFIS since it has independent, normal distributed, uncorrelated and smaller residuals than other methods, so it is a good forecaster.

6 Concluding Remarks

The proposed model obtains successful results for volatile weather forecasting in Bogotá-Colombia. Their residuals show good properties, improving its applicability. The validation data shows small differences regarding original data.

The proposed Neuro-Genetic structure is computationally expensive, even using the IASCO Type-reduction algorithm proposed by Melgarejo in [1], so the design of more efficient structures is a challenge for upcoming fuzzy models.

The analyst must consider the computing cost of finding solutions by using ANFIS and an evolutive structures. In addition to, Type-reduction process increases the computing time since it is an iterative process of an Interval Type-2 fuzzy set, so it is an interesting study field, furthermore if the main focus is optimize a fuzzy system.

Finally, the IT2TSK model outperforms classical techniques, obtaining good results for volatile weather time series forecasting. In fact, the presented algorithm got a successful IT2TSK for volatile weather forecasting.

References

1. Melgarejo, M., Bernal, H., Duran, K.: Improved iterative algorithm for computing the generalized centroid of an interval type-2 fuzzy set. In: 2008 Annual Meeting of the North American Fuzzy Information Processing Society (NAFIPS), vol. 27, pp. 1–6. IEEE, Los Alamitos (2008)
2. Mendez, G., Castillo, O.: Interval type-2 tsk fuzzy logic systems using hybrid learning algorithm. In: Proceedings of IEEE FUZZ Conference, vol. 27, pp. 230–235. IEEE, Los Alamitos (2005)
3. Figueroa, J.C.: An evolutive interval type-2 TSK fuzzy logic system for volatile time series identification. In: 2009 Conference on Systems, Man and Cybernetics, pp. 1–6. IEEE, Los Alamitos (2009)
4. Figueroa, J.C., Soriano, J.J.: A comparison of ANFIS, ANN and DBR systems on volatile time series identification. In: IEEE (ed.) 2007 Annual Meeting of the North American Fuzzy Information Processing Society, vol. 26, pp. 321–326. IEEE, Los Alamitos (2007)
5. Goldfeld, S., Quandt, R.: Nonlinear Methods in Econometrics. North Holland, Amsterdam (1972)
6. Brockwell, P., Davis, R.: Time Series: Theory and Methods. Springer, Heidelberg (1998)
7. Box, G., Jenkins, G.: Time Series Analysis: Forecasting and Control. Holden Day Publishing (1970)
8. Mendel, J.: Uncertain Rule-Based Fuzzy Logic Systems: Introduction and New Directions. Prentice Hall, Englewood Cliffs (1994)
9. Ljung, G.M., Box, G.E.P.: Information theory and the extension of the maximum likelihood principle. Biometrika 65, 553–564 (1978)
10. Hannan, E.J.: The estimation of the order of an arma process. Annals of Statistics 8, 1071–1081 (1981)
11. Ljung, G.M., Box, G.E.P.: On a measure of lack of fit in time series models. Biometrika 65, 297 (1978)

A Soft Computing Approach for Obtaining Transition Regions in Satellite Images

Jorge Morales[1,2], Jesus A. Gonzalez[1,2],
Carlos A. Reyes-Garcia[1], and Leopoldo Altamirano[1,2]

[1] INAOE (Coordination of Computer Science), A. P. 72840, Tonantzintla, Puebla, México
[2] Regional Centre of Science and Technology Education for Latin America and the aribbean, A. P. 72840, Tonantzintla, Puebla, México
{jorgemorales,jagonzalez,kargaxxi,robles}@ccc.inaoep.mx

Abstract. Most of the current satellite image classification methods consider rough boundaries among homogeneous regions. However; real images contain transition regions where pixels belong, at different degrees, to different classes. With this motivation, in this paper we propose a satellite image classification method that allows the identification of transition regions among homogeneous regions. Our solution is based on Soft Computing because of its ability to handle the uncertainties present in nature. We present our method as well as preliminary results that show how our method is able to solve real world problems.

Keywords: transition regions, soft computing, satellite image, uncertainties.

1 Introduction

The classification of satellite images is part of the process followed for the creation of thematic maps from remotely sensed images. The classification process usually involves three major steps: a) Segmentation, b) Feature Extraction, and c) Classification.

Traditional classifiers, known as hard classifiers, produce a hard decision about the identity of each pixel. The classification of each pixel of the image is done by assigning a single class, which is determined through a mechanism that measures the major relationship presented with the assigned class.

In nature, there are non homogeneous (or transition) areas in which land cover gradually changes from one class to another. For example, moving from an urban area to a vegetation one does not happen abruptly, but gradually. A disadvantage of hard classifiers is that they assign transition pixels to a single class when they actually belong to more than one class.

Soft classifiers appeared as an option to overcome the limitations of hard classifiers to get a more accurate classification and to solve ambiguity problems generated by the image acquisition [1].

Soft Classifiers are able express the degree to which a pixel belongs to each of the classes under consideration. For example, instead of deciding that a pixel represents a forest of coniferous or caduceus leaves, it may indicate that it belongs in a degree of 0.43 to the caduceus leaves class and in 0.57 to the conifers class (in this case, a hard classifier would conclude that the pixel belongs to the coniferous class).

D.-S. Huang et al. (Eds.): ICIC 2010, LNCS 6215, pp. 150–157, 2010.

Soft classifiers give us more information about the composition of a pixel within a satellite image. Using soft classifiers we are able to (1) determine the mixture of classes in the ground, (2) measure and report the strength of evidence in support to the best conclusion that can be obtained, and (3) use GIS data layers (Geographic Information Systems) and other models to complement the information considered to generate the final decision [2].

Our work attempts to determine the transition regions formed by land cover in nature. To accomplish this, we have implemented a segmentation algorithm based on information at both, the pixel and region levels. We use the segmentation algorithm to find the homogeneous coverages to then determine the location of the transition regions. After that, we use a fuzzy logic approach (our evaluation function) to evaluate the transition region.

The paper is organized as follows: Section 2 presents the related work to obtain transition regions. Section 3 presents the proposed method. In Section 4, experiments and results are shown, and finally in Section 5 the conclusions are presented.

2 Related Work

Gutierrez Gutierrez and Jegat presented in [3] a work where fuzzy logic was used for classification of satellite images. In this paper they considered transition regions or mixed areas (either man made or commonly found in nature). The developed work consists in the use of two types of supervised classification of an urban area in the city of Merida in Venezuela. The first classification approach is based on a traditional hard classification algorithm (where pixels are considered as well-defined, belonging to a unique class) and the second one uses a Fuzzy Logic or soft approach (where pixels may belong to more than one class with different membership degrees to each of them). They used the IDRISI Andes software.

Schiewe and colleagues in 2009 presented in [1] a work that focuses on the modeling of undetermined transition regions and the description of their uncertainties. The evaluation of these transition regions is modeled through fuzzy sets using the concepts of degrees of memberships to different basic categories in a satellite image. Based on the problem described above, their overall contribution is the definition of an extended quality or uncertainty measure able to consider the uncertainty, the transition area, and undetermined zones in both the reference image and the classification result. Other works proposed for acquisition and analysis of transition regions are: a pixel exchange algorithm [4], a mixed linear model [5], a mixed pixels algorithm [6], a method using neural networks [7], and others.

3 Proposed Method

The work presented in this paper attempts to determine the transition regions found among homogeneous coverages present in a satellite image. Once we identify these transition regions we evaluate them using fuzzy theory. Fig. 1 shows the blocks diagram of the proposed method.

The main blocks of this diagram describe, in general terms, the proposed classification process.

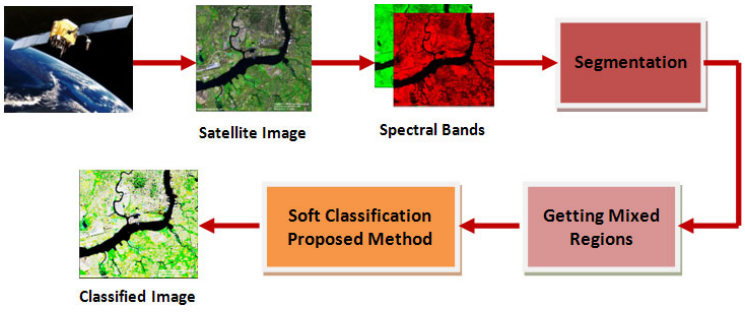

Fig. 1. Proposed method for the soft classification of satellite images

Segmentation. In this step we determine homogeneous land covers (e.g. forest, grassland, bare soil, urban, water, etc.) in order to identify them as homogeneous classes basically composed by a single land cover. These classes are the basic categories (hard classes) used to obtain the transition region. In order to determine these homogeneous classes we use the segmentation algorithm described in section 3.1.

Obtaining Mixed Regions. Once we determine the homogeneous covers, we use them to create the boundaries of the transition regions. For example, between a forest and a bare ground coverage, there exists a transition zone in which we gradually find a land cover change from forest to bare soil. In this work we only consider transition regions between two homogeneous regions but we can apply the same type of analysis to more than two coverages.

Transition Regions Evaluation. We evaluate the transition regions in order to determine the composition of each pixel with respect to homogeneous classes. At this point we use a fuzzy evaluation to establish the distance of each pixel to the homogeneous classes that are close to them. Our results are shown with the classification of an image. We also show each pixel composition with respect to the different homogeneous classes.

As mentioned at the beginning of this section, the aim of this paper is to report the identification of the transition regions from the segmentation of satellite images, as described in the following section.

3.1 Segmentation Algorithm

The image segmentation process separates an image into its meaningful units so that we can recognize objects located in the image. The main objective of our work is to find the transition regions through the identification of basic categories (homogeneous regions) through a segmentation algorithm. Our segmentation algorithm allows:

i. The identification of homogeneous coverages present in a satellite image.
ii. Controls the homogeneity level between pixels that belong to the same coverage.
iii. Once we have found the homogeneous regions, we identify the transition regions through a difference operation between the original and the image containing only the homogeneous regions.

Based on the above mentioned conditions we chose a region growing segmentation algorithm. This is a local technique in which we take a pixel or set of pixels as an initial region (called the seed) and create larger regions by making the seeds grow. For this, we add pixels to the region we are growing according to a similarity measure (and a similarity threshold). Currently, the seeds selection process is performed manually, in other words, the user indicates their location from the homogeneous regions of the image.

Segmenting a satellite image using only the pixels gray levels can be very inaccurate. This is the reason why we also take into account the relationship that each pixel keeps with its neighbors. We overcome this limitation using a texture based segmentation technique proposed by Ojala and colleagues in [8]. This method recognizes how certain local binary patterns, termed "uniform", are fundamental properties of local image texture and their frequency histogram is proven to be a very powerful texture feature. They proposed a generalized gray-scale representation and a rotation invariant operator that allows detecting "uniform" patterns from any quantization of the angular space and for any spatial resolution. They also present a method that combines multiple operators for multi-resolution analysis [8].

3.2 Transition Regions Evaluation

The strategy used in this study for the evaluation of transition regions, is an extension of the work shown in [9] by Amr and colleagues. This technique is based on the concept of fuzzy connectivity, which is used as a tool for segmenting objects with undefined or fuzzy boundaries. It uses the idea of "hanging together" between pixels of the image or SPatial ELements of the image (SPEL). Thus, it is possible to calculate a strength bond based on a fuzzy SPEL affinity. The fuzzy connectivity between any pair of pixels in the image is determined by the strongest connection chain among them. In their work, Amr and colleagues calculated the fuzzy connectivity between a seed pixel and each pixel in the image. The seed pixel is part of the objects of interest to segment.

We take advantage from the work by Amr and colleagues by modifying it to use the homogeneous coverages as seeds. From these homogeneous regions, we obtain their statistical values such as their mean (μ) and standard deviation (σ) of the gray levels of the pixels contained in each of those regions.

In this way, once we located the transition region, we evaluate each of its pixels with respect to each of the homogeneous regions. In order to evaluate the transition region pixels we calculate their fuzzy affinity through equation 1.

$$g(x) = e^{\frac{(x-\mu)^2}{-2\sigma^2}} \tag{1}$$

where x refers to the gray level of the transition region pixel being evaluated .

We calculate an affinity fuzzy value for each pixel from the region of transition in each of the four spectral bands of a Quick Bird image. We combine the results of the four bands through the MAX operation to take the maximum value as the value of fuzzy pixel affinity.

4 Experiments

For the experiments we used a Quick Bird satellite image of the zone of Puebla, Mexico. The analyzed coverages are vegetation and bare soil. Fig. 2a shows this area. Fig. 2b shows our image segmentation method using a region growing approach with information at both, pixel (thresholding) and region levels (local binary patterns). Fig. 3 shows the location of the transition region generated by these two coverages in several sub images.

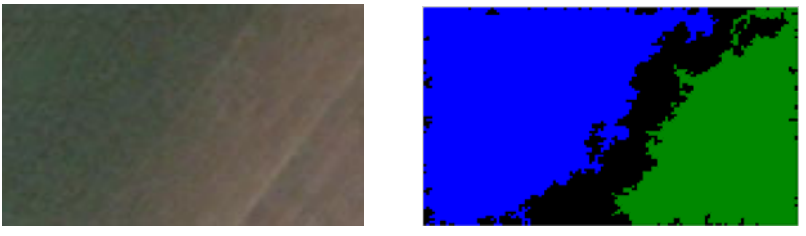

(a) (b)

Fig. 2. (a) Original satellite image, (b) Segmented image using region growing

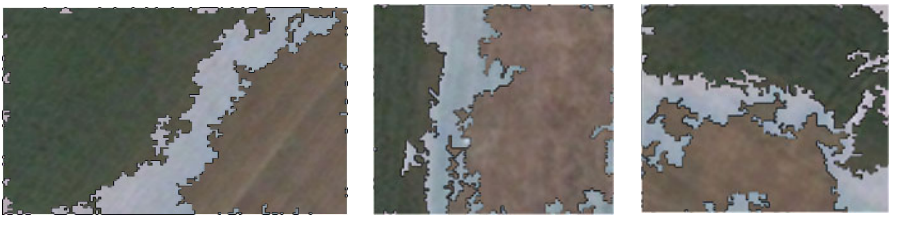

(a) (b) (c)

Fig. 3. Transition regions (in original image color) generated for the vegetation and bare soil coverage

The results of the classification of the transition region shown in fig. 3a are presented in Figs. 4a and 4b. Pixels colors represent the membership degree that each pixel keeps with respect to the seed region (homogeneous land coverages). The bright pixels represent a 100% ownership of the particular class. The dark pixels represent a 0% ownership of the particular class.

To compare the results of the proposed method, we used the soft classifiers implemented in IDRISI TAIGA. The classifiers used were: Bayesian (BAYCLASS), Fuzzy (FUZCLASS) and Nearest Neighbor (KNN). We selected three training sets for classes: vegetation, bare soil, and transition region. Table 1 shows the accuracy obtained for the classification of the sub image of fig. 2a using IDRISI TAIGA classifiers and the proposed method.

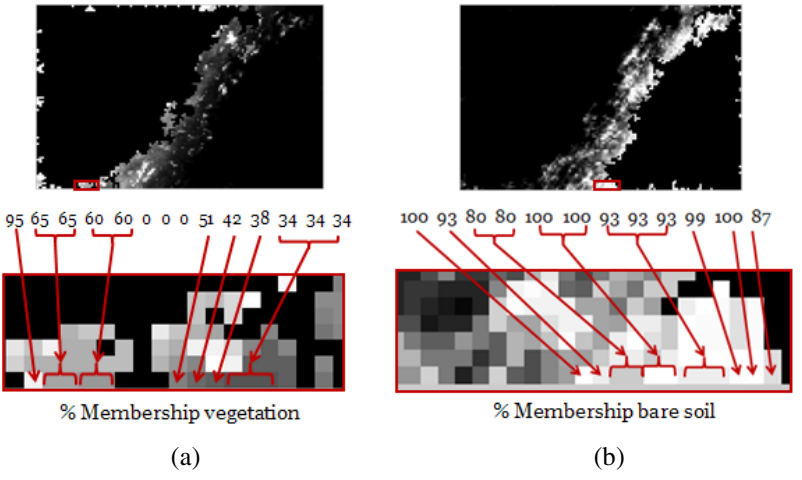

Fig. 4. Evaluation of the transition region: (a) with respect to the vegetation land cover and (b) with respect to the bare soil land cover

Table 1. Accuracy obtained in the classification of the sub image of Fig. 2a

Class	No. pixels	FUZCLASS	BAYCLASS	KNN	PROPOSED
Vegetation	50	86 %	84 %	68 %	100 %
Bare soil	32	62.5 %	81.2 %	62.5 %	90.6 %
Transition region	18	89 %	94.4 %	94.4 %	89 %
Average Accuracy		79.1 %	86.5 %	75 %	93.13 %

These results show that the proposed method has a higher average accuracy for the three given classes. BAYCLASS and KNN are slightly better than FUZCLASS and the proposed method for class Transition region.

In order to analyze the soft classification of the transition region shown if fig. 3a using the proposed method, 10 sampled pixels were selected by a domain expert, who determined the degree of membership in each class. This is shown in Table 2.

Table 2. Results of the membership degree of 10 sampled pixels selected from Fig. 3a

No. pixel	The domain expert		Proposed method	
	% Vegetation membership	% Bare soil membership	% Vegetation membership	% Bare soil membership
1	25	75	18	82
2	30	70	32	68
3	30	70	24	76
4	25	75	36	64

Table 2. (*continued*)

5	20	80	17	83
6	95	5	100	0
7	10	90	12	88
8	60	40	67	33
9	50	50	57	43
10	95	5	97	3

Schiewe and Kinkeldey in [10] proposed a class-specific fuzzy certainty measure (CFCM), which is obtained through equation 2:

$$CFCM(c) = 1 - \frac{1}{n}\sum_{i=1}^{n} |\mu_{i,REF}(c) - \mu_{i,CLASS}(c)| \quad \forall i \,|\, \mu_{i,REF} > 0 \vee \mu_{i,CLASS} > 0 \tag{2}$$

$\mu_{REF}(c)$: corresponds to the class membership value of a pixel / area for class c in the reference data (domain expert).
$\mu_{CLASS}(c)$: class membership value of a pixel / area for class c in classification data.
n: number of pixels / areas under examination.

The results obtained by applying CFCM are as shown in Table 3.

Table 3. CFCM value for the vegetation and bare soil classes of table 2

	Vegetation	**Bare soil**
CFCM	94.8 %	94.8%

5 Conclusions

Our method is able to locate land cover transition regions in satellite images from the identification of homogeneous land cover regions through a region growing segmentation approach. Finding accurate homogeneous regions is an important step of our method in order to avoid errors while locating the boundaries of transition regions. Our results to locate transition regions are really encouraging because we were able to find the transition regions between vegetation and bare soil regions. We were also able to determine the membership degree of each pixel to each of the homogeneous regions. With the use of fuzzy theory we are able to handle the uncertainties and ambiguities present in the transition regions of a satellite image. We are currently working with four spectral bands.

We thank Christina Connolly for providing us with a trial license of the IDRISI-TAIGA software used for the experiments.

References

1. Schiewe, J., Ehlers, M., Kinkeldey, C., Tomowski, D.: Implementation of Indeterminate Transition Zones for Uncertainty Modeling in Classified Remotely Sensed Scenes. In: International Conference on Geographic Information Science (2009)

2. Ronald Eastman, J.: Idrisi Taiga: Guide to GIS and Image Processing. Clark University (2006)
3. Gutiérrez, J., Jegat, H.: Uso de la Teoría de Lógica Difusa en la Clasificación de Imágenes Satelitales con Coberturas Mixtas: El Caso Urbano de Mérida, Venezuela, Interciencia, vol. 30, pp. 261–266. Asociación Interciencia, Caracas Venezuela (2005)
4. Makido, Y.K.: Land cover mapping at sub-pixel scales. Ph.D., Michigan State University, 149 p. (2006); AAT 3248589
5. Kumar, U., Kerle, N., Ramachandra, T.V.: Contrained linear spectral unmixing technique for regional land cover mapping using MODIS data. In: Innovations and advanced techniques in systems, computing sciences and software engineering, Springer, Heidelberg (2008)
6. Plaza, A., et al.: A new approach to mixed pixel classification of hyperspectral imagery based on extended morphological profiles. Pattern Recognition 37, 1097–1116 (2004)
7. Han, J., Chi, K., Yeon, Y.: Land Cover Classification of IKONOS Multispectral Satellite Data: Neuro-Fuzzy, Neural Network and Maximum Likelihood Methods. In: Ślęzak, D., Yao, J., Peters, J.F., Ziarko, W.P., Hu, X. (eds.) RSFDGrC 2005. LNCS (LNAI), vol. 3642, pp. 738–742. Springer, Heidelberg (2005)
8. Ojala, T., Pietikäinen, M.: Multiresolution Gray-Scale and Rotation Invariant Texture Classification with Local Binary Patterns. IEEE Transactions on Pattern Analysis and Machine Intelligence 24, 971–987 (2002)
9. Abdel-Dayen, A.R., El-Sakka, M.R.: Carotid Artery Ultrasound Image Segmentation Using Fuzzy Region Growing. In: Kamel, M.S., Campilho, A.C. (eds.) ICIAR 2005. LNCS, vol. 3656, pp. 869–878. Springer, Heidelberg (2005)
10. Schiewe, J., Kinkeldey, C.: Development of an Advanced Uncertainty Measure for Classified Remotely Sensed Scenes. In: Proceedings for ISPRS WG II/2+3+4 and Cost Workshop on Quality, Scale & Analysis Aspects of Urban City Models, Lund, Sweden (2009)

Particle Swarm Optimization for Two-Stage Fuzzy Generalized Assignment Problem

Xuejie Bai, Yajing Zhang, and Fengtao Liu

College of Science, Agricultural University of Hebei
Baoding 071001, Hebei, China
xjbai2009@163.com

Abstract. This paper constructs a new class of two-stage fuzzy generalized assignment problems, in which the resource amounts consumed are uncertain and assumed to be characterized by fuzzy variables with known possibility distributions. Motivated by the definitions of the positive part and negative part, we can transform the second-stage programming to its equivalent one. To calculate the expected value in the objective function, an approximation approach (AA) is employed to turn the fuzzy GAP model into an approximating one. Since the approximating GAP model is neither linear nor convex, traditional optimization methods cannot be used to solve it. To overcome this difficulty, we design a hybrid algorithm integrating the approximation approach and particle swarm optimization (PSO) to solve the approximating two-stage GAP model. Finally, one numerical example with six tasks and three agents is presented to illustrate the effectiveness of the designed hybrid algorithm.

Keywords: Generalized assignment problem; Two-stage fuzzy programming; Approximation approach; Particle swarm algorithm.

1 Introduction

The generalized assignment problem (GAP) appears as a subproblem in important real-life applications such as resource scheduling, vehicle routing and distribution, plant location and flexible manufacturing systems, and attracts more and more researchers' attention [3,4,5,15,16]. As we know, the majority of its applications [1,20] have a stochastic nature. Stochasticity occurs when the actual capacity of the agents or the amount of resource needed to process the tasks is not known in advance. For example, Toktas et al. [17] focused on GAP with stochastic capacities.

With the presentation of fuzzy set theory [18] and the concept of possibility measure [19] introduced by Zadeh, some scholars employed these theories to reflect the vagueness and ambiguity of the resource amount in GAP. For instance, Chang et al. [2] generalized fuzzy rules of a fuzzy modeling method and evolved the fuzzy modeling method for due-date assignment problem in manufacturing by a genetic algorithm. Majumdar and Bhunia [14] considered to solve a generalized assignment problem with imprecise cost(s)/time(s) instead of precise one by elitist genetic algorithm.

D.-S. Huang et al. (Eds.): ICIC 2010, LNCS 6215, pp. 158–165, 2010.

Recently, Liu and Liu [9] presented the credibility measure instead of possibility measure in the fuzzy decision system. Based on credibility theory [8,12,13], a two-stage fuzzy programming problem was studied in [10]. The purpose of this paper is to construct a class of two-stage fuzzy generalized assignment problems. In the proposed fuzzy GAP model, the resource consumed by agent i to perform task j is characterized by fuzzy variable with known possibility distribution, and the objective is to formulate an optimization problem via expectation criteria. It is assumed that some decisions must be taken before the outcome of fuzzy parameters is revealed and thus be based on the knowledge of the distribution of the parameters only. This is referred to as the first stage. In the second stage, outcomes of all fuzzy parameters have been observed and some recourse actions may be taken.

The rest of this paper is organized as follows. In Section 2 we propose two-stage fuzzy generalized assignment problem. In Section 3 we employ the AA [11] to approximate the objective function of the original generalized assignment problem model and the convergent result is also discussed. A hybrid algorithm incorporating AA and PSO is designed to solve the proposed model. One numerical example is given to illustrate the effectiveness of the designed algorithm in Section 4. Finally, Section 5 summarizes the main results.

2 Formulation of Fuzzy GAP Model

In this section, we employ fuzzy optimization methods to model generalized assignment problem from a new point of view. For the sake of simplicity of presentation, we adopt the notations listed in Table 1.

Table 1. List of notations

Notations	Definitions
i	index of agents, $i = 1, 2, \cdots, n$
j	index of tasks, $j = 1, 2, \cdots, m$
c_{ij}	qualification of processing task j by agent i
x_{ij}	binary variable indicating whether task j is assigned to agent i or not
r_i	capacity availability of agent i
ξ_{ij}	capacity consumption of task j processed by agent i
q_i^+	a penalty paid per unit of shortage resource
q_i^-	a penalty paid per unit of resource b_i in excess of $\sum_{j=1}^{m} \xi_{ij} x_{ij}$
y_i^+	the amount of unsatisfied require to agent i in state γ
y_i^-	the amount of remaining resource to agent i in state γ

GAP differs from the classical assignment problem in that each task j is assigned to a single agent, while each agent i can complete several tasks and the assignments have to be made taking into account the resource availability. However, the assignment of task j to agent i must be decided before the actual values of the demands for resource capacity are known. That is to say, the

decision variables x_{ij} must be taken before knowing the realization values of fuzzy variable ξ_{ij}. So we call x_{ij} the first-stage decisions. As a result of the uncertainty of resource capacity, the total consumed amount for agent i may not equal to the capacity availability. Thus, whether resource amount for agent i exceed the capacity availability or not, we all pay a penalty and introduce the second-stage decision variables y_i^+ and y_i^- indicating the insufficient amount and the under-utilization of capacity.

Using the notations above, in order to minimize the assigning cost and penalty cost over the two stages, we build a two-stage fuzzy GAP model as follows

$$\begin{cases} \min \sum\limits_{i=1}^{n}\sum\limits_{j=1}^{m} c_{ij}x_{ij} + E_\xi[Q(x,\xi)] \\ \text{s.t.} \sum\limits_{i=1}^{n} x_{ij} = 1, \quad j = 1,2,\cdots,m \\ \quad x_{ij} \in \{0,1\}, \quad i = 1,2,\cdots,n; j = 1,2,\cdots,m, \end{cases} \tag{1}$$

where

$$\begin{cases} Q(x,\xi(\gamma)) = \min \sum\limits_{i=1}^{n} q_i^+ y_i^+ + \sum\limits_{i=1}^{n} q_i^- y_i^- \\ \qquad\qquad \text{s.t. } r_i + y_i^+ - y_i^- = \sum\limits_{j=1}^{m} \xi_{ij}(\gamma)x_{ij}, \quad i = 1,2,\cdots,n \\ \qquad\qquad y_i^+ \geq 0, y_i^- \geq 0, \quad i = 1,2,\cdots,n. \end{cases}$$

Observing the second-stage problem of the proposed programming problem (1), y_i^+ and y_i^- actually have the following equivalent form

$$y_i^+ = \Big(\sum_{j=1}^{m} \xi_{ij}(\gamma)x_{ij} - r_i\Big)^+, \quad y_i^- = \Big(\sum_{j=1}^{m} \xi_{ij}(\gamma)x_{ij} - r_i\Big)^-.$$

So the recourse problem can be converted into the following equation

$$Q(x,\xi(\gamma)) = \sum_{i=1}^{n} q_i^+ \Big(\sum_{j=1}^{m} \xi_{ij}(\gamma)x_{ij} - r_i\Big)^+ + \sum_{i=1}^{n} q_i^- \Big(\sum_{j=1}^{m} \xi_{ij}(\gamma)x_{ij} - r_i\Big)^-.$$

Then, the two-stage fuzzy GAP model (1) can be expressed equivalently as follows

$$\begin{cases} \min \sum\limits_{i=1}^{n}\sum\limits_{j=1}^{m} c_{ij}x_{ij} + E_\xi[Q(x,\xi)] \\ \text{s.t.} \sum\limits_{i=1}^{n} x_{ij} = 1, \quad j = 1,2,\cdots,m \\ \quad x_{ij} \in \{0,1\}, \quad i = 1,2,\cdots,n; j = 1,2,\cdots,m, \end{cases} \tag{2}$$

where

$$Q(x,\xi(\gamma)) = \sum_{i=1}^{n} q_i^+ \Big(\sum_{j=1}^{m} \xi_{ij}(\gamma)x_{ij} - r_i\Big)^+ + \sum_{i=1}^{n} q_i^- \Big(\sum_{j=1}^{m} \xi_{ij}(\gamma)x_{ij} - r_i\Big)^-.$$

3 Hybrid PSO Algorithm

Since the fuzzy GAP model in Section 2 is not generally a convex programming, conventional optimization methods usually fail to find a global optimal solution. We suggest a hybrid PSO algorithm to solve the proposed fuzzy GAP model.

3.1 Approximation Approach

Suppose that $\xi = (\xi_{11}, \xi_{12}, \cdots, \xi_{nm})$ in the problem (2) is a continuous fuzzy vector with support $\Xi = \prod_{ij=11}^{nm}[a_{ij}, b_{ij}]$, where $[a_{ij}, b_{ij}]$ is the support of ξ_{ij}. In this case, we will try to use the AA to approximate the possibility distribution function of ξ by a sequence of possibility distribution functions of discrete fuzzy vectors $\{\zeta_s\}$. The detailed approach can be described as follows.

For each integer s, the discrete fuzzy vector $\zeta_s = (\zeta_{s,11}, \zeta_{s,12}, \ldots, \zeta_{s,nm})$ is constructed by the following method.

For each $ij \in \{11, 12, \cdots, nm\}$, define fuzzy variable $\zeta_{s,ij} = g_{s,ij}(\xi_{ij})$, where the functions $g_{s,ij}$'s are as follows

$$g_{s,ij}(u_{ij}) = \begin{cases} a_{ij}, & u_{ij} \in [a_{ij}, a_{ij} + \frac{1}{s}) \\ \sup\{\frac{k_{ij}}{s} | \, k_{ij} \in Z, \text{ s.t. } \frac{k_{ij}}{s} \le u_{ij}\}, & u_{ij} \in [a_{ij} + \frac{1}{s}, b_{ij}], \end{cases}$$

and Z is the set of all integers. By the definition of $\zeta_{s,ij}$, the possibility distribution of the fuzzy variable $\zeta_{s,ij}$, denoted $\nu_{s,ij}$ is

$$\nu_{s,ij}(a_{ij}) = \text{Pos}\{\zeta_{s,ij} = a_{ij}\} = \text{Pos}\left\{\gamma \,\middle|\, a_{ij} \le \xi_{ij}(\gamma) < a_{ij} + \frac{1}{s}\right\}$$

and

$$\nu_{s,ij}\left(\frac{k_{ij}}{s}\right) = \text{Pos}\{\zeta_{s,ij} = \frac{k_{ij}}{s}\} = \text{Pos}\left\{\gamma \,\middle|\, \frac{k_{ij}}{s} \le \xi_{ij}(\gamma) < \frac{k_{ij}+1}{s}\right\}$$

for $k_{ij} = [sa_{ij}], [sa_{ij}] + 1, \cdots, K_{ij}$. From the definition of $\zeta_{s,ij}$, for all $\gamma \in \Gamma$, we have

$$\left|\xi_{ij}(\gamma) - \zeta_{s,ij}(\gamma)\right| < \frac{1}{s}, \qquad ij \in \{11, 12, \ldots, nm\}$$

$$\left\| \zeta_s(\gamma) - \xi(\gamma) \right\| = \sqrt{\sum_{ij=11}^{nm} \left(\zeta_{s,ij}(\gamma) - \xi_{ij}(\gamma)\right)^2} \le \frac{\sqrt{nm}}{s}.$$

As a consequence, the sequence $\{\zeta_s\}$ of finitely support fuzzy vectors converges to ξ uniformly. The problem (2) is referred to as the original fuzzy GAP model. By generating a sequence $\{\zeta_s\}$ according to the distribution of ξ, one can obtain the approximating fuzzy GAP model as follows

$$\begin{cases} \min \sum_{i=1}^{n} \sum_{j=1}^{m} c_{ij} x_{ij} + E_{\zeta_s}[Q(x, \zeta_s)] \\ \text{s.t.} \sum_{i=1}^{n} x_{ij} = 1, \quad j = 1, 2, \cdots, m \\ \quad x_{ij} \in \{0, 1\}, \quad i = 1, 2, \cdots, n; j = 1, 2, \cdots, m, \end{cases} \tag{3}$$

where

$$Q(x,\zeta_s(\gamma)) = \sum_{i=1}^{n} q_i^+ \Big(\sum_{j=1}^{m} \zeta_{s,ij}(\gamma) x_{ij} - r_i \Big)^+ + \sum_{i=1}^{n} q_i^- \Big(\sum_{j=1}^{m} \zeta_{s,ij}(\gamma) x_{ij} - r_i \Big)^-. \quad (4)$$

The objective value of the approximating fuzzy GAP model (3) provides an estimator for that of the original fuzzy GAP model (2).

Theorem 1. *Consider the fuzzy generalized assignment problem (1). Suppose ξ is a continuous fuzzy vector such that $Q(x,\xi)$ is not $-\infty$ for any feasible decision x. If ξ is a bounded fuzzy vector and $\{\zeta_s\}$ is the discretization of ξ, then for any given feasible decision x, we have*

$$\lim_{s\to\infty} E[Q(x,\zeta_s)] = E[Q(x,\xi)].$$

Proof. Since for any feasible decision x and every realization γ of fuzzy vector ξ, $Q(x,\gamma)$ is not $-\infty$, which together with the suppositions of the theorem satisfy the conditions of [11, Theorem 3]. As a consequence, the assertion of the theorem is valid.

3.2 PSO Algorithm

Inspired by the social behavior of flocks of birds and/or schools of fish, Kennedy and Eberhart [6] proposed the PSO algorithm. Because of better intelligent background and theoretical framework, recently, the PSO algorithm has attracted much attention and been applied successfully in the fields of evolutionary computing, unconstrained continuous optimization problems and many others [7]. For the subsequent discussion, we will give more detailed explanations about the hybrid PSO algorithm for solving the approximating GAP model (3).

Representation Structure: Suppose there are *pop_size* particles to form a colony. In the two-stage GAP model, we use a vector $X = (x_{11}, x_{12}, \cdots, x_{nm})$ as a particle to represent a decision.
Initialization Process: Firstly, we generate *pop_size* initial feasible particles $X_1, X_2, \cdots, X_{pop\_size}$. For each particle X_k, $k = 1, 2, \cdots, pop\_size$, we can calculate the value of the recourse function $\mathcal{Q}_s(x) = E_{\zeta_s}[Q(x,\zeta_s)]$ at X_k via the AA. Thus, the objective value $z(x)$ of the fuzzy GAP model (3) can be computed by

$$z(X_k) = \sum_{i=1}^{n} \sum_{j=1}^{m} c_{ij} x_{ij} + \mathcal{Q}_s(X_k). \quad (5)$$

After that, we denote its current position of each particle by *pbest*, using P_k as abbreviation, $P_k = (p_{k,11}, p_{k,12}, \cdots, p_{k,n1}, \cdots, p_{k,nm})$ which represents the personal smallest objective value so far at time t. On the other hand, we set the global best particle of the colony as *gbest*, using P_g as abbreviation, $P_g = (p_{g,11}, p_{g,12}, \cdots, p_{g,n1}, \cdots, p_{g,nm})$ which represents the position of the best particle found so far at time t in the colony. Finally, we initialize the velocity V_k of the kth particle randomly, $V_k = (v_{k,11}, v_{k,12}, \cdots, v_{k,n1}, \cdots, v_{k,nm})$.

Updating Process: As mentioned above, the PSO algorithm is an evolutionary computation algorithm, and it searches for the optimal solution by renewing generations. Using the above notations, for the *pop_size* particles, the new velocity of the kth particle is updated by

$$V_k(t+1) = \omega_t V_k(t) + c_1 r_1 (P_k(t) - X_k(t)) + c_2 r_2 (P_g(t) - X_k(t)), \tag{6}$$

for $k = 1, 2, \cdots, pop\_size$, where ω_t is the inertia weight that decreases linearly from 0.9 to 0.4; c_1 and c_2 are nonnegative constants, called the cognitive and social parameter, respectively; and r_1 and r_2 are two independent random numbers generated from the unit interval $[0, 1]$. When the new velocity $V_k(t+1)$ is obtained, we can update the position of the kth particle by

$$X_k(t+1) = X_k(t) + V_k(t+1). \tag{7}$$

Summarizing the above process immediately yields the hybrid PSO algorithm as follows.

Step 1. Initialize *pop_size* particles and evaluate the objective values by the formula (5).
Step 2. Set *pbest* of each particle and its objective equal to its current position and objective value,and set *gbest* and its objective equal to the position and objective value of the best initial particle.
Step 3. Update the velocity and position of each particle.
Step 4. Calculate the objective values for for all particles.
Step 5. Renew *pbest* and its objective values with the current position and objective value.
Step 6. Renew *gbest* and its objective values with the position and objective value of the current best particle.
Step 7. Repeat the fifth to eighth steps for a given number of cycles.
Step 8. Return the *gbest* and its objective values.

4 One Numerical Example

To show the feasibility and effectiveness of the hybrid algorithm, consider the following generalized assignment problem with $n = 3, m = 6$. Capacity availability and penalty coefficient (r_i, q_i^+, q_i^-) are (50,40,80), (50,30,80) and (50,60,60), respectively. The cost c_{ij} and capacity consumption ξ_{ij} are displayed in Table 2. In addition, the fuzzy variables involved in this problem are supposed to be mutually independent.

Based on the related data, the two-stage fuzzy generalized assignment problem model is built as follows

$$\begin{cases} \min\ 130x_{11} + 30x_{12} + 510x_{13} + 30x_{14} + 340x_{15} + 20x_{16} \\ \quad +460x_{21} + 150x_{22} + 20x_{23} + 40x_{24} + 30x_{25} + 450x_{26} \\ \quad +40x_{31} + 370x_{32} + 120x_{33} + 390x_{34} + 40x_{35} + 30x_{36} + E_\xi[Q(x,\xi)] \\ \text{s.t.}\ \sum_{i=1}^{3} x_{ij} = 1 \quad j = 1, 2, \cdots, 6 \\ \quad x_{ij} \in \{0, 1\} \qquad i = 1, 2, 3; j = 1, 2, \cdots, 6, \end{cases} \tag{8}$$

Table 2. The parameters for the two-stage fuzzy GAP problem

Cost (c_{ij})						
	Task, j					
Agent, i	1.	2.	3.	4.	5.	6.
1.	130	30	510	30	340	20
2.	460	150	20	40	30	450
3.	40	370	120	390	40	30
Consumption (ξ_{ij})						
	Task, j					
Agent, i	1.	2.	3.	4.	5.	6.
1.	(28,30,32)	(48,50,51)	(8,10,13)	(10,11,13)	(10,13,14)	(7,9,15)
2.	(5,10,12)	(15,20,28)	(58,60,62)	(9,10,14)	(5,10,20)	(15,17,19)
3.	(68,70,72)	(8,10,12)	(6,10,12)	(12,15,18)	(6,8,10)	(8,12,16)

where $E_\xi[Q(x,\xi)]$ is the recourse function, and

$$\begin{aligned} Q(x,\xi(\gamma)) = 40\Big(\sum_{j=1}^{6}\xi_{1j}(\gamma)x_{1j} - 50\Big)^+ + 80\Big(\sum_{j=1}^{6}\xi_{1j}(\gamma)x_{1j} - 50\Big)^- \\ +30\Big(\sum_{j=1}^{6}\xi_{2j}(\gamma)x_{2j} - 50\Big)^+ + 80\Big(\sum_{j=1}^{6}\xi_{2j}(\gamma)x_{2j} - 50\Big)^- \\ +60\Big(\sum_{j=1}^{6}\xi_{3j}(\gamma)x_{3j} - 50\Big)^+ + 60\Big(\sum_{j=1}^{6}\xi_{3j}(\gamma)x_{3j} - 50\Big)^-. \end{aligned}$$

In order to solve the fuzzy generalized assignment problem (8), for each fixed first-stage decision variable x, we generate 3000 sample points via the approximation approach to calculate the recourse function $\mathcal{Q}_s(x)$. Then for each sample point $\widehat{\zeta}^k$, we can use the formula (4) to obtain the optimal value as $Q(x,\widehat{\zeta}^k)$ for $k = 1, 2, \cdots, 3000$. After that, the value $z(x)$ of the objective function at x can be computed by Equation (5). If we set the population size in the implementation of the hybrid PSO algorithm is 30, then a run of the proposed algorithm with 600 generations gives the optimal solution. An optimal assigns tasks 1 and 6 to agent 1, tasks 2, 4 and 5 to agent 2, and task 3 to agent 3 at a total cost of \$490095.1486.

5 Conclusions

In this paper, we took credibility theory as the theoretical foundation of fuzzy optimization and developed a two-stage fuzzy GAP model, where the resource amounts were uncertain and assumed to be fuzzy variables with known possibility distributions. Since it is inherently an infinite-dimensional optimization problem that can rarely be solved directly by conventional optimization algorithm, this paper employed the AA to the original two-stage fuzzy GAP model, and established a convergence ralation between the objective values of the original

problem and its approximating problem. Furthermore, we designed a AA-based PSO algorithm to solve the approximating two-stage GAP model. Finally, we gave one numerical example in order to demonstrate the fuzzy GAP modeling idea and the effectiveness of the designed hybrid PSO algorithm.

References

1. Balachandran, V.: An Integer Generalized Transportation Problem for Optimal Job Assignment in Computer Networks. Oper. Res. 24, 742–759 (1976)
2. Chang, P.C., Hieh, J.C., Liao, T.M.: Evolving Fuzzy Rules for due-date Assignment Problem in Semiconductor Manufacturing Factory. J. Intell. Manuf. 16, 549–557 (2005)
3. Chu, P.C., Beasley, J.E.: A Genetic Algorithm for the Generalized Assignment Problem. Comput. Oper. Res. 24, 17–23 (1997)
4. Diaz, J.A., Fernandez, E.: A Tabu Search Heuristic for the Generalized Assignment Problem. Eur. J. Oper. Res. 132, 22–38 (2001)
5. Haddadi, S.: Lagrangian Decomposition based Heuristic for the Generalised Assignment Problem. INFOR 37, 392–402 (1999)
6. Kennedy, J., Eberhat, R.C.: Particle swarm optimization. In: Proc. of the IEEE International Conference on Neural Networks, pp. 1942–1948. IEEE press, New York (1995)
7. Kennedy, J., Eberhart, R.C., Shi, Y.: Swarm Intelligence. Morgan Kaufmann Publishers, San Francisco (2001)
8. Liu, B.: Credibility Theory. Studies in Fuzziness and Soft Computing 154, 81–156 (2007)
9. Liu, B., Liu, Y.K.: Expected Value of Fuzzy Variable and Fuzzy Expected Value Models. IEEE Trans. Fuzzy Syst. 10, 445–450 (2002)
10. Liu, Y.K.: Fuzzy Programming with Recourse. Int. J. Uncertainty Fuzziness Knowl.-Based Syst. 13, 381–413 (2005)
11. Liu, Y.K.: Convergent Results about the Use of Fuzzy Simulation in Fuzzy Optimization Problems. IEEE Trans. Fuzzy Syst. 14, 295–304 (2006)
12. Liu, Y.K., Liu, B., Chen, Y.: The Infinite Dimensional Product Possibility Space and Its Applications. In: Huang, D.-S., Li, K., Irwin, G.W. (eds.) ICIC 2006. LNCS (LNAI), vol. 4114, pp. 984–989. Springer, Heidelberg (2006)
13. Liu, Y.K., Liu, Z.Q., Liu, Y.: Fuzzy Optimization Problems with Critical Value-at-Risk Criteria. In: Liu, D., Fei, S., Hou, Z., Zhang, H., Sun, C. (eds.) ISNN 2007. LNCS, vol. 4492, pp. 267–274. Springer, Heidelberg (2007)
14. Majumdar, J., Bhunia, A.K.: Elitist Genetic Algorithm for Assignment Problem with Imprecise Goal. Eur. J. Oper. Res. 177, 684–692 (2007)
15. Ross, G.T., Soland, R.M.: A Branch-and-Bound Algorithm for the Generalized Assignment Problem. Math. Program. 8, 91–103 (1975)
16. Savelsbergh, M.: A Branch-and-Price Algorithm for the Generalized Assignment Problem. Oper. Res. 45, 831–841 (1997)
17. Toktas, B., Yen, J.W., Zabinsky, Z.B.: Addressing Capacity Uncertainty in Resource-Constrained Assignment Problem. Comput. Oper. Res. 33, 724–745 (2006)
18. Zadeh, L.A.: Fuzzy Sets. Inf. Control 8, 338–353 (1965)
19. Zadeh, L.A.: Fuzzy Sets as a Basis for a Theory of Possibility. Fuzzy Sets Syst. 1, 3–28 (1978)
20. Zimokha, V.A., Rubinshtein, M.I.: R&D Planning and the Generalized Assignment Problem. Autom. Remote Control 49, 484–492 (1988)

A Novel Cyclic Discrete Optimization Framework for Particle Swarm Optimization

Qian Tao[1,*], Hui-you Chang[1], Yang Yi[1], Chun-qin Gu[2], and Wen-jie Li[1]

[1] Department of Computer Science, Sun Yat-sen University, Guangzhou, China
taoalex66@gmail.com
[2] Department of Computer Science, Zhongkai University of Agriculture and Engineering, Guangzhou, China
taoalex66@gmail.com

Abstract. To extend the existing PSO variants to their corresponding discrete versions, this paper presents a novel cyclic discrete optimization framework (CDOF) for particle swarm optimization. The proposed CDOF features the following characteristics. First, a general encoding method is proposed to describe the mapping relation between the PSO and the solution space. Second, a simple cyclic discrete rule is present to help the PSO to realize the extending from a continuous space to a discrete space. Two discrete PSO versions based on CDOF are tested on the traveling salesman problem comparing with each other. Experimental results show that the two discrete versions of the PSO algorithm based on CDOF are promising, and the framework is simple and effective for the PSO.

Keywords: particle swarm optimization, discrete space, cyclic discrete optimization framework, traveling salesman problem.

1 Introduction

Particle swarm optimization (PSO), originally developed by Kennedy and Eberhart [1] in 1995, is an important optimization approach based on stochastic population. The algorithm simulates preying behaviors of bird flocking and fish schooling, and searches for an optimal solution iteratively by adjusting the trajectories of individual particle vector in a multi-dimensional space.

As a simple and efficient optimization algorithm, PSO is widely used to solve all kinds of optimization problems in a continuous space [1-6], but can not be directly brought to solve discrete optimization problems. Hence, in 1997, Kennedy et al. [7] put forward a discrete PSO which adopts binary code to express position and Sigmoid function to restrain speed. Recently, different discrete PSO variants have been designed to successfully solve every type of discrete optimization problems, such as Traveling Salesman Problem [8], Flow Shop Scheduling [9, 10], Mixed Discrete Nonlinear Programming [11], Grid Service Optimal-Selection [12] etc. At the same time, many

* Corresponding author.

D.-S. Huang et al. (Eds.): ICIC 2010, LNCS 6215, pp. 166–174, 2010.

discrete optimize approaches have been developed to help PSO to resolve the discrete optimization problems and improve the performance, such as swap-operator [8], fuzzy matrix [13-15], ranked-order value (ROV) rule [9, 10], position vector-based transformation [8, 16], hybrid technology [11, 17] etc. Various discrete PSO algorithms have been proposed via the above approaches, but the performance is not competitive. On the other hand, various discrete PSO are generally designed for specific problems and their structures are more complicated. To extend the existing PSO variants to their corresponding discrete versions is a great challenge. To tackle this difficult problem effectively, this paper presents a novel cyclic discrete optimization framework (CDOF) for particle swarm optimization and achieves a high performance.

The remainder of this paper is organized as follows. Section 2 introduces the standard particle swarm optimization. Section 3 presents a cyclic discrete optimization framework for PSO. Comparison studies are shown in Section 4, and the conclusions are finally summarized in Section 5.

2 The Standard Particle Swarm Optimization

In the standard PSO, N particles cooperate to search for the global optimum in the M-dimensional search space. Each particle represents a potential solution. The $X_i = (x_{i1}, x_{i2}, ..., x_{ij}, ..., x_{iM})$ and $V_i = (v_{i1}, v_{i2}, ..., v_{ij}, ..., v_{iM})$ represent the position and velocity of the ith particle in an M-dimensional search space, respectively. The $PBest_i = (pBest_{i1}, pBest_{i2}, ..., pBest_{ij}, ..., pBest_{iM})$ is the best optimum of the ith particle. The $GBest = (gBest_1, gBest_2, ..., gBest_j, ..., gBest_M)$ is the best-so-far solution of the whole swarm. The velocity v_{ij} and positon x_{ij} of the jth dimension of the ith particle are update as follows:

$$v_{ij}(t+1) = \omega v_{ij}(t) + c_1 \cdot r_1 \cdot (pBest_{ij}(t) - x_{ij}(t)) + c_2 \cdot r_2 (gBest_j(t) - x_{ij}(t)) \tag{1}$$

$$x_{ij}(t+1) = x_{ij}(t) + v_{ij}(t+1) \tag{2}$$

where ω is an inertia weight of the velocity. c_1 and c_2 represent the cognition parameter and social parameter, which pull each particle toward own *pBest* poisition and *gBest* position of the whole swarm, respectively. r_1 and r_2 are random numbers uniformly distributed in [0, 1]. The ith particle's velocity on jth dimension is clamped to a maximum value v_{ij}^{max} and a minimum value v_{ij}^{min}.

3 Cyclic Discrete Optimization Framework

In this section, the cyclic discrete optimization framework is presented. To further verify the generality of the framework, we take the TSP for example, which is a classic discrete optimization problem. The definition of the TSP is described as follows:

A complete weighted graph $G=(V, E)$ is given, where V is the set of nodes, and E is the set of arcs. $|V|$ is the number of the nodes. Each arc $(i, j) \in E$ has the weight $w_{i,j}$,

which represents the length between i and j. In the symmetric TSP, $w_{i,j} = w_{j,i}$. The goal of the TSP is to find a minimum length Hamiltonian circuit.

3.1 Representation of the Problem

Let a graph $G=(V, E)$, the number of the cities $n=|V|$, $V = \{v_i\}, 1 \le i \le n$, $E = E_1 \cup E_2 \cup ... \cup E_n$, $E_i = (i, j_1) \cup (i, j_2) \cup ... \cup (i, j_n), i \ne j_1, j_2, ..., j_n$, the goal of the TSP is to find a path which is composed by arcs set (ArcSet) $ArcSet = arc_1 \cup arc_2 \cup ... \cup arc_n, arc_i = (i, j_i) \in E_i$, which makes the length $len(ArcSet) = len(arc_1) + len(arc_2) + ... + len(arc_n)$ is minimum. The TSP can be formulated as follows:

$$\text{minimize } len(arc_1, arc_2, ...arc_n) = \sum_{i=1}^{n} len(arc_i) \tag{3}$$

where n is the number of the cities in the TSP. Fig. 1 gives a example of the representation in the TSP. *ArcSet* is a candidate solution, which is composed of the lines with arrows. arc_i is selected from arcs set E_i.

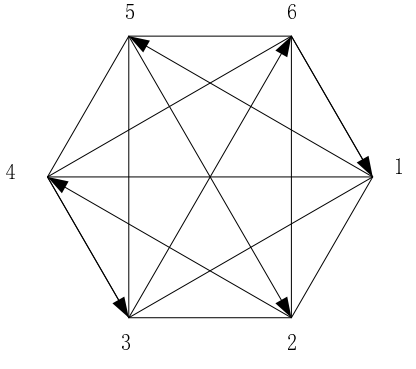

$E_1 = \{(1,2),(1,3),(1,4),(1,5),(1,6)\}$
$E_2 = \{(2,1),(2,3),(2,4),(2,5),(2,6)\}$
$E_3 = \{(3,1),(3,2),(3,4),(3,5),(3,6)\}$
$E_4 = \{(4,1),(4,2),(4,3),(4,5),(4,6)\}$
$E_5 = \{(5,1),(5,2),(5,3),(5,4),(5,6)\}$
$E_6 = \{(6,1),(6,2),(6,3),(6,4),(6,5)\}$
$E = E_1 \cup E_2 \cup E_3 \cup E_4 \cup E_5 \cup E_6$
$arc_1 = (1,5), arc_2 = (2,4), arc_3 = (3,6),$
$arc_4 = (4,3), arc_5 = (5,2), arc_6 = (6,1)$
$ArcSet = arc_1 \cup arc_2 \cup arc_3 \cup arc_4 \cup arc_5 \cup arc_6$
$path = 1 \to 5 \to 2 \to 4 \to 3 \to 6 \to 1$

Fig. 1. An example of the problem representation for the TSP

3.2 The Encoding Method of Particle

The encoding of particles is the premise of using particles to find the solution of the TSP. In this paper, the number of particles dimensions is equal to the number of the cities. The particle swarm can search an optimal solution in a 6-dimensional solution space. The ith dimension is corresponding to an index to the arcs that start from node i. Take the graph of Fig. 1 for example, the index to each E_i among E is shown as Table 1. A searching of 6-dimenisional particles is shown in Fig. 2. The number in the below of a square stands for the position in PSO. The process of searching optimum is to find the position in each dimension, and convert these positions into corresponding paths.

Table 1. The encoding of particles

Particles Dimension	Candidate arcs	Index to candidate arcs
1	$E_1 = \{(1,2),(1,3),(1,4),(1,5),(1,6)\}$	1,2,3,4,5
2	$E_2 = \{(2,1),(2,3),(2,4),(2,5),(2,6)\}$	1,2,3,4,5
…	…	1,2,3,4,5
6	$E_6 = \{(6,1),(6,2),(6,3),(6,4),(6,5)\}$	1,2,3,4,5

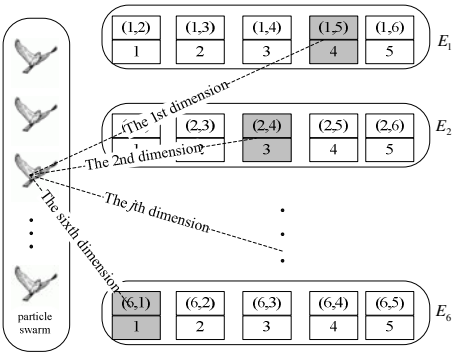

Fig. 2. The searching of particles in a 6-dimensional space

3.3 The Cyclic Discrete Rule (CD-Rule) of Multi-dimensional Space

In the discrete PSO, the position of a particle in each dimension is defined as an index to candidate solutions. The velocity of a particle, which acts a trigger of a position variation, is used to change the position of the particle, recorded as a group of float numbers. Hence, the searching of particles in each dimension is transformed into a rotation of a wheel by the action of the velocity. As shown in the Fig. 3, the position of a particle in the 1st dimension changes from 4 to 1 under the action of the velocity, and a turning wheel represents a dimension, and then a dimension of a particle corresponds to an arc that starts from node 1.

The CD-Rule of a particle is defined as follows:

Each wheel, which is composed of a candidate service set, rotates clockwise or anti-clockwise, and the velocity of a particle in a dimension is a positive number or a

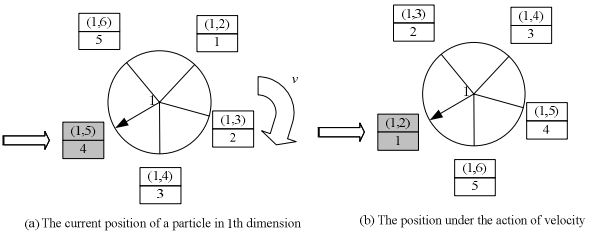

Fig. 3. The rotation discrete rule

negative number. If the velocity of a particle in the dimension is positive, the position of a particle change positively by the action of the velocity, so the number of the selected service increases simultaneously, and vice versa. In order to improve the searching effectiveness of particles, a mapping is defined between the maximum velocity of the *i*th dimension and the scale of candidate services set *i*, recorded as $v^i_{max} \to L(i)$, $L(i) >= 2$. At the same time, for the purpose of measuring the current velocity and realizing the accelerated searching of the particle, a unit velocity is recorded as $v_{unit} = v^i_{max} / L(i)$, when the value of current velocity is *k* times greater than v_{unit}, the step size of the position is *k*, then the wheel rotates *k* steps clockwise or counter-clockwise simultaneously. Whereas the variation of velocity is very small and less than v_ε, $v_\varepsilon = v_{max} / M, M \succ\succ L(i)$, the wheel stays still and the position does not change. Take $path_1, path_2$ for example, $path_1 = 1 \to 5 \to 2 \to 4 \to 3 \to 6 \to 1$, and $path_2 = 1 \to 2 \to 6 \to 5 \to 3 \to 4 \to 1$, the position of a particle and the process of changing the position are shown as Fig.4. Each wheel stands for a dimension, which is marked at the corner of the wheel. The number *j* outside the *i*th wheel stands for arc(*i*, *j*), and the *k* with circle presents that arc (*i*,*k*) is selected as the solution at *i*th dimension.

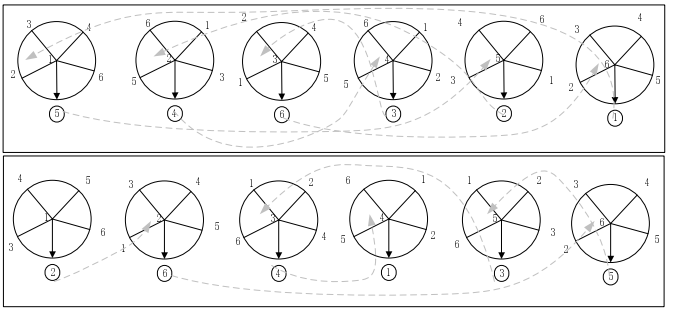

Fig. 4. The example of discrete PSO based on CDOF for the TSP

According to the CD-Rule, the formulas of the position and velocity can be expressed by Eq.(4)(6).

$$x_{ij}(t+1) = \begin{cases} x_{ij}(t), & -v_\varepsilon \le v_{ij}(t+1) \le v_\varepsilon \ or \ L(i) = 1 \\ x_{ij}(t)+1, & v_\varepsilon < v_{ij}(t+1) \le v_{unit} \\ x_{ij}(t)-1, & -v_{unit} \le v_{ij}(t+1) < -v_\varepsilon \\ x_{ij}(t)+k, & v_{unit} < v_{ij}(t+1) < v_{ij}^{max} \\ x_{ij}(t)-k, & -v_{ij}^{max} \le v_{ij}(t+1) < -v_{unit} \end{cases} \tag{4}$$

$$k = \begin{cases} \left\lceil v_{ij}(t+1)/v_{unit} \right\rceil, v_{ij}(t+1) > 0 \\ \qquad\qquad\qquad\qquad , v_{ij} \in \left[-v_{ij}^{max},\ v_{ij}^{max} \right] \\ \left\lfloor \left| v_{ij}(t+1)/-v_{unit} \right| \right\rfloor, v_{ij}(t+1) < 0 \end{cases} \tag{5}$$

where $x_{ij}(t)$, $v_{ij}(t)$ are the position and velocity of *i*th particles in *j*th dimension at iteration *t* respectively.

The particle's new velocity is updated by Eq. (6).

$$v_{ij}(t+1) = c_1 \cdot r_1 \cdot (pBest_{ij}(t) - x_{ij}(t)) + c_2 \cdot r_2 (gBest_j(t) - x_{ij}(t)) \tag{6}$$

where $pBest_{ij}(t)$ is the history best position of the *i*th particle in *j*th dimension at iteration *t*, and $gBest_j(t)$ is the *j*th dimensional best position in the whole particle swarm at iteration *t*.

4 Experimental Results and Comparison Studies

In this section, we present the numerical experimental results of two discrete PSO variants based on the proposed CDOF. The experiments are done on the TSP, comparing with each other. The TSP instances are extracted from the TSPLIB (http://www.iwr.uni-heidelberg.de/groups/comopt/software/TSPLIB95/tsp/), which is a library of sample instances for the TSP (and related problems) from various sources and of various types. The information of the burma14 instance is given in Table 2. The proposed algorithms were implemented on a machine with Pentium D 3.0 GHz CPU and 256 MB of RAM. The operating system is MS Windows XP and the compiler is VC++ 6.0.

Table 2. 14-Staedte in Burma (Zaw Win)

Node	1	2	3	4	5	6	7
X	16.47	16.47	20.09	22.39	25.23	22.00	20.47
Y	96.10	94.44	92.54	93.37	97.24	96.05	97.02
Node	8	9	10	11	12	13	14
X	17.20	16.30	14.05	16.53	21.52	19.41	20.09
Y	96.29	97.38	98.12	97.38	95.59	97.13	94.55

In our experiment, to avoid local optima and premature convergence in the discrete PSO variants, we take the chaotic logistic sequence perturbation to enrich the searching behavior of particles and enhance the performance of the PSO. The chaotic logistic sequence perturbation, which has the property of certainty, ergodicity and the stochastic, has great advantage to help particles to escape from local optimum and achieve a better searching quality than Gauss (normal) perturbation [18]. In order to realize chaotic dynamics search, the chaotic logistic sequence is selected as a perturbation technique to enhance the performance of PSO based on CDOF in this paper, defined as follows.

$$x(t+1) = r \cdot x(t) \cdot (1 - x(t)), r \in N, x(0) \in [0,1] \tag{7}$$

where *r* is the control parameter, *x* is a variable, $r = 4$ and $x \notin \{0, 0.25, 0.5, 0.75, 1\}$.

Meanwhile, modulus division remainder is adopted to modify the too big perturbation, to prevent the wheel from redundancy of rotation under the influence of a too big perturbation. The double perturbation of the pBest and gBest are given by Eq. (8) and Eq. (9).

$$pBest(t+1)=\begin{cases}\lceil pBest(t)+r_1\cdot x(t)\rceil\%l(i), & \varepsilon < p_m - r_3\\ l(i)-\lfloor \mid pBest(t)-r_2\cdot x(t)\mid\rfloor\%l(i), & r_3 > p_m\end{cases} \tag{8}$$

$$gBest(t+1)=\begin{cases}\lceil gBest(t)+r_4\cdot x(t)\rceil\%l(i), & \varepsilon < p_m - r_6\\ l(i)-\lfloor gBest(t)-r_5\cdot x(t)\rfloor\%l(i), & r_6 > p_m\end{cases} \tag{9}$$

where r_1, r_2, r_4, r_5 are large integer, r_3, r_6 are random number between 0 and 1, and p_m=0.45.

The following abbreviations represent the two PSO variants considered:

1) CD_V1_PSO: The discrete version of the standard PSO based on based on CDOF;
2) CD_V2_PSO: CD_V1_PSO without the history velocity $\omega v_{ij}(t)$ but with chaotic logistic sequence perturbation;

It can be seen from Fig. 5.that the two PSO variants based on CDOF can find a good solution for the TSP. the CD _V2_PSO outperforms the CD _V1_PSO in the test instances, and can search the optimal solution for the TSP (Best Known= 30.8785), the according route of the optimal solution is shown in the Fig.6. On the other hand, we can conclude that the chaotic logistic sequence perturbation can help the particles to escape from local optimum and achieve a better performance. The history velocity $\omega v_{ij}(t)$ of the particle will hinder the change of velocity and decrease the search capabilities of the particle in the search space.

As a discrete framework for the PSO, the CDOF is effective and can help the PSO algorithm to search an optimal solution in a multi-dimensional space. At the same time, to further improve the performance of the discrete PSO, we can take some hybrid technology to enhance the searching capability.

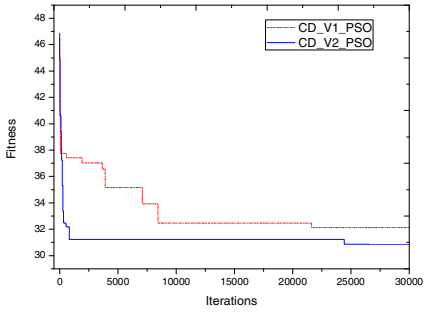

Fig. 5. Comparing CD _V1_PSO with CD _V2_PSO for the burma14

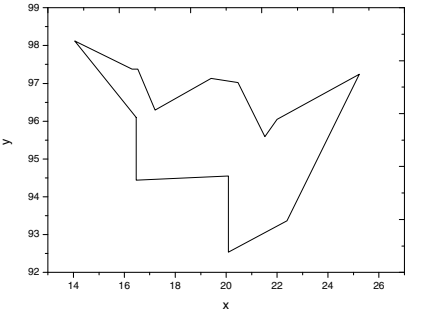

Fig. 6. The optimal solution of the burma14

5 Conclusion

To solve discrete optimize problems, a cyclic discrete Optimization framework has been proposed. Based on the proposed framework, the PSO was extended to two different discrete versions, CD _V1_PSO and CD_V2_PSO. The framework proposed a general encode method to describe the mapping relation between the PSO and the solution space, And presents a simple cyclic discrete rule to help the PSO to realize an extending from a continuous space to a discrete space. To further validate the performance of the two discrete PSO algorithms, we compare the two discrete PSO algorithms on the TSP. Experimental results show that the discrete versions of the PSO algorithm based on CDOF are promising, and the framework is simple and effective for the extending.

Acknowledgements

This work is supported by the Natural Science Foundation of China under Grant No. 60573159 and the Guangdong-Hong Kong Technology Cooperation Funding Scheme of China under Grant No. 2006Z1-D6021.

References

1. Kennedy, J., Eberhart, R.: Particle Swarm Optimization. IEEE, Piscataway (1995)
2. Liang, J., Qin, A.K., Suganthan, P.N., Baskar, S.: Comprehensive Learning Particle Swarm Optimizer for Global Optimization of Multimodal Functions. IEEE Transactions on Evolutionary Computation 10(3), 281–295 (2006)
3. Clerc, M., Kennedy, J.: The Particle Swarm - Explosion, Stability, and Convergence in a Multidimensional Complex Space. IEEE Transactions on Evolutionary Computation 6(1), 58–73 (2002)
4. Shi, Y., Eberhart, R.C.: Fuzzy Adaptive Particle Swarm Optimization. In: IEEE International Conference on Evolutionary Computation, pp. 101–106 (2001)
5. Yoshida, H., Kawata, K., Fukuyama, Y., Takayama, S., Nakanishi, Y.: A particle swarm optimization for reactive power and voltage control considering voltage security assessment. IEEE Transactions on Power Systems 15(4), 1232–1239 (2000)
6. Amin, A.M.A., EI Korfally, M.I., Sayed, A.A., Hegazy, O.T.M.: Efficiency Optimization of Two-Asymmetrical-Winding Induction Motor Based on Swarm Intelligence. IEEE Transactions on Energy Conversion 24(1), 12–20 (2009)
7. Kennedy, J., Eberhart, R.: A Discrete Binary Version of the Particle Swarm Algorithm. In: IEEE International Conference on Computational Cybernetics and Simulation, pp. 4104–4108 (1997)
8. Clerc, M.: 8 Discrete Particle Swarm Optimization, illustrated by the Traveling Salesman Problem. New optimization techniques in engineering (2004)
9. Liu, B., Wang, L., Jin, Y.H.: An Effective PSO-Based Memetic Algorithm for Flow Shop Scheduling. IEEE Transactions on Systems, Man, and Cybernetics, Part B: Cybernetics 37(1), 18–27 (2007)
10. Li, B.B., Wang, L., Liu, B.: An Effective PSO-Based Hybrid Algorithm for Multiobjective Permutation Flow Shop Scheduling. IEEE Transactions on Systems, Man and Cybernetics, Part A: Systems and Humans 38(4), 818–831 (2008)

11. Nema, S., Goulermas, J., Sparrow, G., Cook, P.: A Hybrid Particle Swarm Branch-and-Bound (HPB) Optimizer for Mixed Discrete Nonlinear Programming. IEEE Transactions on Systems, Man and Cybernetics, Part A: Systems and Humans 38(6), 1–1 (2008)
12. Tao, F., Zhao, D., Hu, Y., Zhou, Z.: Resource Service Composition and Its Optimal-Selection Based on Particle Swarm Optimization in Manufacturing Grid System. IEEE Transactions on Industrial Informatics 4(4), 315–327 (2008)
13. Liu, H., Abraham, A., Clerc, M.: An Hybrid Fuzzy Variable Neighborhood Particle Swarm Optimization Algorithm for Solving Quadratic Assignment Problems. Journal of Universal Computer Science 13(7), 1032–1054 (2007)
14. Abraham, A., Liu, H., Zhang, W., Chang, T.G.: Scheduling Jobs on Computational Grids Using Fuzzy Particle Swarm Algorithm. In: Gabrys, B., Howlett, R.J., Jain, L.C. (eds.) KES 2006. LNCS (LNAI), vol. 4252, p. 500. Springer, Heidelberg (2006)
15. Shen, B., Yao, M., Yi, W.: Heuristic Information Based Improved Fuzzy Discrete PSO Method for Solving TSP. In: Yang, Q., Webb, G. (eds.) PRICAI 2006. LNCS (LNAI), vol. 4099, p. 859. Springer, Heidelberg (2006)
16. Pang, W., Wang, K.P., Zhou, C.G.: Modified Particle Swarm Optimization Based on Space Transformation For Solving Traveling Salesman Problem. In: IEEE International Conference on Machine Learning and Cybernetics, pp. 2342–2346 (2004)
17. Ge, H.W., Sun, L., Liang, Y.C., Qian, F.: An Effective PSO and AIS-Based Hybrid Intelligent Algorithm for Job-Shop Scheduling. IEEE Transactions on Systems, Man and Cybernetics, Part A: Systems and Humans 38(2), 358–368 (2008)
18. Liu, B.: Improved Particle Swarm Optimization Combined With Chaos. Chaos, Solitons and Fractals 25(5), 1261–1271 (2005)

Economic Dispatch Considering Ancillary Service Based on Revised Particle Swarm Optimization Algorithm

Xin Ma[1] and Yong Liu [2]

[1] School of Management and Economic, North China University of Water Conservancy and Electric Power, Zhengzhou, Henan Province, 450011 China
[2] School of Electronic Information and Electrical Engineering, Shanghai Jiaotong University, Minhang, Shanghai City, 200240 China
maxin72@163.com, yliu2010@126.com

Abstract. A revised strategy particle swarm optimization algorithm is proposed to solve the economic dispatch problems in power systems. Many constraints such as ramp rate limits and prohibited zones are taken into account, and the loss is also calculated. On the basis of strategy particle swarm optimization algorithm, a new revised strategy is provided to handle the constraints and make sure the particles to satisfy the constraints. The strategy can guarantee the particles to search in or around the feasible solutions area combined with penalty functions. The accuracy and speed of the algorithm are improved for the particles will rarely search in the infeasible solutions area, and the results also show that the new algorithm has a fast speed, high accuracy and good convergence.

Keywords: Electricity market; economic dispatch; ancillary service; particle swarm optimization algorithm; revise strategy.

1 Introduction

Economic dispatch is the method of determining the most efficient, low-cost and reliable operation of a power system by dispatching the available electricity generation resources to supply the load on the system [1]. The primary objective of economic dispatch is to minimize the total cost of generation while honoring the operational constraints of the available generation resources [2].

Under the environment of electricity market, security-constrained economic dispatch benefits electricity consumers by systematically increasing the use of the most efficient generation units (and demand-side resources, where available). This can lead to better fuel utilization, lower fuel usage, and reduced air emissions than would result from using less efficient generation.

As the geographic and electrical scope integrated under unified economic dispatch increases, additional cost savings result from pooled operating reserves, which allow an area to meet loads reliably using less total generation capacity than would be needed otherwise. Economic dispatch requires operators to pay close attention to system conditions and to maintain secure grid operation, thus increasing operational reliability without increasing costs [3]. Economic dispatch methods are also flexible enough to incorporate policy goals such as promoting fuel diversity or respecting

D.-S. Huang et al. (Eds.): ICIC 2010, LNCS 6215, pp. 175–184, 2010.

demand as well as supply resources [4]. The model of problem slightly changes at the electricity market, the optimization objective changes from the minimizing the electricity generated cost to maximize the total generating profitable, and demand constraints are likely to become more loose inequality constraints [5].

How to deal with various constraints when using the particle swarm optimization algorithm to solve such constrained optimization problem, there are several approaches: one is to turn the optimization problem into unconstrained optimization problem and then use particle swarm optimization algorithm to solve it [6], but for more complex constrained optimization problem, it is very difficult to turn into an equivalent unconstrained optimization problem. Another is introduction of the concept of Pareto diagram of the multi-objective optimization problem and using multi-level information-sharing strategies [7], but this method is a more complex algorithm. There is also a relatively easy way, that is, when the initialization and update the particle only retain the particles that satisfy the constraint conditions [8] [9]. However, this method give up on or re-generate particles if they does not satisfy the constraints, the former due to fewer feasible solution in the particles will affect the accuracy of the algorithm, while the latter was due to randomness of regenerate, so re-generate particles is still a large probability of a non-feasible solution which would greatly extend the computing time of algorithm. Gaing discuss a variety of constraints so that economic dispatch problem model is closer to the actual power system operation, but the algorithm requested its initial value of the particles must all be a viable solution which is affecting the usefulness of the algorithm [10]. An adaptive algorithm with a shrinkage factor is introduced into the power system economic operation focus on the security constraints such as voltage and current of power grid through the penalty function, but it ignored technical constraints of the generating units. The equality constraints is treated through retain a viable solution, and inequality constraints is treated with an adaptive penalty function, and re-initialize the inactive particles in order to avoid the "premature" phenomenon of the algorithm, but its handling of the constraints are more negative, thereby the accuracy of the algorithm is affected [11].

In this paper, the economic dispatch model consider the ancillary services in electricity market is established, and then an revised particle swarm algorithm is putted up to solve them, a more positive patch strategy to achieve a good results has been taken for particles which does not meet the constraints. And the example analysis shows that the algorithm is effective and practical.

2 Economic Dispatch Model Consider the Ancillary Services

The economic dispatch model considers ancillary services built as follow, and the mode of power generation and spinning reserve in accordance with the tender mode. The objective function is the maximizing the total profit of power generation companies or minimizes the negative profit (it equals the cost minus benefits) when the reserved capacity is payoff according to contribution, the objective function as following:

$$Min\Psi = \sum_{i=1}^{N}[(1-\lambda)C_i(P_i) + \lambda C_i(P_i + R_i) - \theta_P P_i - \lambda\theta_R R_i] \tag{1}$$

Load demand and spinning reserve demand constraints:

$$\sum_{i=1}^{N} P_i \le P_D + P_{Loss} \tag{2}$$

$$\sum_{i=1}^{N} R_i \le R_D \tag{3}$$

Upper and lower limits of unit ramp constraints:

$$P_i^{\min} \le P_i \le P_i^{\max} \tag{4}$$

$$P_i \le P_i + R_i \le P_i^{\max} \tag{5}$$

Units climbing rate constraint:

$$-DR_i \le P_i - P_i^o \le UR_i \tag{6}$$

$$0 \le R_i \le UR_i / 6 \tag{7}$$

Units work dead-zone constraints:

$$P_i \in \begin{cases} P_i^{\min} \le P_i \le P_i^{1low} \\ P_i^{(j-1)up} \le P_i \le P_i^{jlow} \qquad j = 2,3,\cdots,z_i \\ P_i^{z_i up} \le P_i \le P_i^{\max} \end{cases} \tag{8}$$

$$P_i + R_i \in \begin{cases} P_i^{\min} \le P_i + R_i \le P_i^{1low} \\ P_i^{(j-1)up} \le P_i + R_i \le P_i^{jlow} \qquad j = 2,3,\cdots,z_i \\ P_i^{z_i up} \le P_i + R_i \le P_i^{\max} \end{cases} \tag{9}$$

Where, ψ is objective function; N is the total number of units; i is the unit number for the mark; j is the unit work dead-zone number for the mark; P_i^{min} is the minimum power output of unit i, unit is MW; P_i^{max} is the maximum power output of unit i, unit is MW, P_i^0 is the initial power output of unit i, unit is MW, DR_i is the decline climbing rate of unit i, unit is MW/h; UR_i is the increase climbing rate of unit i, unit is MW/h; P_i^{jlow} is the lower bound value of the number j work dead zone of unit i , unit is MW; P_i^{jup} is the upper bound value of the number j work dead zone of unit i , unit is MW; z_i is the number of unit work dead-zone; $C_i\ (P_i)$ is the cost function of unit i , generally taken as a quadratic function, that is,

$$C_i(P_i) = c_i P_i^2 + b_i P_i + a_i \tag{10}$$

Where, a_i, b_i and c_i are fuel cost coefficients of unit i; P_i is the power output of unit i, unit is MW; R_i is the spinning reserve capacity of unit i, unit is MW; θ_P is the spot price of electrical power, unit is \$/MWh; θ_R is the price of rotating reserve capacity, unit is \$/MWh; P_D is the load demand of system, unit is MW; R_D is the spinning

reserve demand of system, unit is MW; λ is the probability of spinning reserve is dispatched. Network loss is P_{Loss}, unit is MW, it generally calculate this value by B coefficient method, that is,

$$P_{Loss} = \sum_{i=1}^{N}\sum_{j=1}^{N} P_i B_{ij} P_j + \sum_{i=1}^{N} B_{0i} P_i + B_{00} \tag{11}$$

Load demand and spinning reserve demand may also be bound by equality constraints after bidding. The algorithm is relatively complex in dealing with constraints, but it does not fundamentally affect the algorithm steps.

3 Revised Particle Swarm Optimization for Solving Economic Dispatch

A positive approach is presented to revise the standard particle swarm optimization algorithm strategy to deal with a variety of constraints so that particles can execute its optimization search as much as possible in the feasible solution area or its vicinity.

3.1 Particles Encoding

Particles encoding is shown as follow.

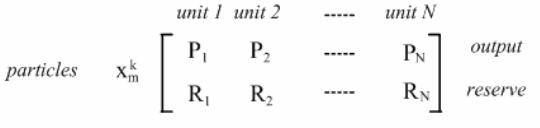

Fig. 1. Representation of the particle, the matrix structure are two rows and N columns, the first line represent the output value of active power of each unit, the second line represent the value of the rotating reserve of each units..

The particle's velocity and position update formula can be rewritten as:

$$\begin{bmatrix} v_{m,i}^{k+1,P} \\ v_{m,i}^{k+1,R} \end{bmatrix} = w \begin{bmatrix} v_{m,i}^{k,P} \\ v_{m,i}^{k,R} \end{bmatrix} + d_1\rho_1 \begin{bmatrix} \phi_{m,i}^{P} - x_{m,i}^{k+1,P} \\ \phi_{m,i}^{R} - x_{m,i}^{k+1,R} \end{bmatrix} + d_2\rho_2 \begin{bmatrix} \xi_{m,i}^{P} - x_{m,i}^{k+1,P} \\ \xi_{m,i}^{R} - x_{m,i}^{k+1,R} \end{bmatrix} \tag{12}$$

$$\begin{bmatrix} x_{m,i}^{k+1,P} \\ x_{m,i}^{k+1,R} \end{bmatrix} = \begin{bmatrix} x_{m,i}^{k,P} \\ x_{m,i}^{k,R} \end{bmatrix} + \begin{bmatrix} v_{m,i}^{k+1,P} \\ v_{m,i}^{k+1,R} \end{bmatrix} \tag{13}$$

$$v^{\min} \le v_m^k \le v^{\max} \tag{14}$$

$$w^{\min} \le w_m^k \le w^{\max} \tag{15}$$

Where, $x_{m,i}^{k,P}$ represents P_i; $x_{m,i}^{k,R}$ represents R_i; $v^{\min}$ is the lower limit of particle velocity; $v^{\max}$ is the up limit of particle velocity; v_m^k is the velocity at k iteration for particle m;

x_m^k is the location at k iteration for particle m; w is the particle inertia coefficient; $w^{\min}$ is the lower limit of particle inertia coefficient; $w^{\max}$ is the up limit of particle inertia coefficient; d_1 and d_2 are particle acceleration constants; ρ_1 and ρ_2 are uniformly distributed random number between [0, 1]; $\phi_{m,i}^P$ is the contribute output value of unit i in the extreme individuals for particle m; $\phi_{m,i}^R$ is the contribute reserve value of unit i in the extreme individuals for particle m; $\xi_{m,i}^P$ is the contribute output value of unit i in the global extreme of population; $\xi_{m,i}^R$ is the contribute reserve value of unit i in the global extreme of population.

3.2 Fitness Function

Particles fitness function is shown as follow,

$$f = \Psi + \sigma\left[\sum_{i=1}^{N} P_i - P_D - P\right] \tag{16}$$

The smaller total cost and the fewer deviation beyond the constraints of active power demand and reserve demand, the smaller the fitness value. When the constraints of load demand and reserve demand are all equality constraints, the fitness function formula changes as follow:

$$f = \Psi + \sigma\left[\left|\sum_{i=1}^{N} P_i - P_D - P\right|\right] + \sigma\left[\left|\sum_{i=1}^{N} R_i - R_D\right|\right] \tag{17}$$

$$\sigma(x) = \begin{cases} \tau x & x > 0 \\ 0 & otherwise \end{cases} \tag{18}$$

Where, τ is defined as penalty factor, it is generally a large positive number, and $\sigma(\bullet)$ is defined as penalty function.

3.3 Revised Strategy

If the output value of each unit beyond the up and lower limits, then it is limited to the corresponding boundary value and the formula expressed as:

$$P_i = \begin{cases} P_i^{\min} & P_i < P_i^{\min} \\ P_i^{\max} & P_i > P_i^{\max} \end{cases} \tag{19}$$

After comparing the output value of unit, and then compare the sum value of output and reserve, if contribute beyond the up limit, it has to be limited to the up limit value, if the reserve value is less than 0 and it need to be set to 0, the formula is expressed as:

$$R_i = \begin{cases} P_i^{\min} - P_i & P_i + R_i > P_i^{\max} \\ 0 & P_i + R_i < P_1 \end{cases} \tag{20}$$

If the output value of each unit violates the constraints of unit climbing rate, it will be limited at the boundary value, and the formula expressed as:

$$P_i = \begin{cases} P_i^0 - DR_i & P_i < P_i^0 - DR_i \\ P_i^0 + UR_i & P_i > P_i^0 + UR_i \end{cases} \tag{21}$$

If the rotating reserve value of each unit violates the constraints of unit climbing rate, it will also be limited at the boundary value and the formula expressed as:

$$R_i = \begin{cases} UR_i / 6 & R_i > UR_i / 6 \\ 0 & R_i < 0 \end{cases} \tag{22}$$

If the output value of each unit violates the constraints of work dead zone, then it is limited to the nearby boundary value and the formula expressed as:

$$P_i = \begin{cases} P_i^{jlow} & P_i > P_i^0, P_i \in (P_i^{jlow}, P_i^{jup}) \\ P_i^{jup} & P_i < P_i^0, P_i \in (P_i^{jlow}, P_i^{jup}) \end{cases} \tag{23}$$

After comparing the output value of unit, and then compare the sum value of output and reserve, if contribute beyond the work dead zone limit, it need to be adjusted in accordance with the following formula:

$$R_i = \begin{cases} P_i^{jlow} - P_i & P_i + R_i > P_i^0, P_i + R_i \in (P_i^{jlow}, P_i^{jup}) \\ P_i^{jup} - P_i & P_i + R_i < P_i^0, P_i + R_i \in (P_i^{jlow}, P_i^{jup}) \end{cases} \tag{24}$$

The deviation value is calculated as follow and it is similar with the handling on the constraint of load demand and also need calculate deviation:

$$\Delta P_{err} = \sum_{i=1}^{N} P_i - P_D - P \tag{25}$$

$$\Delta R_{err} = \sum_{i=1}^{N} R_i - R_D \tag{26}$$

3.4 Algorithm Steps

The algorithm steps are described as follow:

Step 1, input the parameters of system and the unit, set the number of particle swarm M and the total number of iterations K of particles population.

Step 2, set $k = 0$, $m = 1$, here k is temporary variables for the number of iterations. m is temporary variables for the number of particle.

Step 3, set $i = 1$, i is the serial number of the unit.

Step 4, if $k = 0$, the components of initial velocity of particles randomly generated between $[\, v^{\min}, v^{\max} \,]$ for unit i are $v_{m,j}^{0,P}$ and $v_{m,j}^{0,R}$, and the initial output value of unit i is,

$$x_{m,j}^{0,P} = P_i^0 + v_{m,j}^{0,P} \tag{27}$$

The initial reserve values of unit i is,

$$x_{m,j}^{0,R} = v_{m,j}^{0,R} \tag{28}$$

Otherwise update the velocity and location according to the equation (12), (13).

Step 5, if the output value and reserve value beyond the output constraint and the climb rate constraint and work done zone constraint, they will be revised to the boundary value nearby.

Step 6, if $i < N$, then $i = i+1$, and turn to step 4.

Step 7, if the output value and reserve value after the iteration can not meet the constraints of load demand and reserve demand, then revise these data through re-distributaries.

Step 8, the fitness value of particles are calculated, if $k = 0$, then set m ϕ_m and ξ_m are the particles of this iteration. Otherwise compare these parameters, if the fitness value of present particle less than ϕ_m , then save the present particle as ϕ_m , and if the fitness value of this particle also less than ξ_m, and it need to be saved as ξ_m.

Step 9, if $m < M$, then $m = m+1$, turn to the step 3 to generate next particle, otherwise it is means that all the particles have been generated and turn to the next step.

Step 10, if $k < K$, then $k = k+1$, $m = 1$, turn to the step 3 to next iteration, otherwise it is means that all the iteration have been over and turn to the next step.

Step 11, the result ξ_m is output and means the output value, reserve value and relation fitness of unit.

4 Simulation and Analysis

A system including three generating units is studied in this paper, total system load demand is 800MW, reserve demand is 80MW, spot price of electric power is 10.65$/MWh, the number of particle is 20, the number of iteration is 200, $w^{\max} = 0.9$, $\varepsilon = 0.01$, $\tau = 100$. Parameters of units are shown in Table 1, and the system load demand, spinning reserve and spot prices of 3-unit 12-hour system show in Table 2.

Table 1. The basic parameters of each unit in the 3-units system, $MUT_i(h)$ is the minimum continuous up time of unit i, MDT_i is the minimum continuous shutdown time of unit i, CSH_i is the start time of unit i, CT_i^0 is the cumulative duration state of unit i at time t, positive indicate continuous up time, negative values indicated that a continuous downtime.

Unit	1	2	3
P_0^{min}(MW)	100.00	100.00	50.00
P_0^{max}(MW)	600.00	400.00	200.00
a_i($/h)	500.00	300.00	100.00
b_i($/MWh)	10.00	8.00	6.00
c_i($/MW^{2}h)	0.002	0.0025	0.005
MUT_i(h)	3.00	3.00	3.00
MDT_i(h)	3.00	3.00	3.00
CSH_i(h)	3.00	3.00	3.00
CT_i^0(h)	-3.00	3.00	3.00

Table 2. System load demand, spinning reserve and spot prices of 3-units 12-hours system

Time	Load(MW)	Spinning reserve(MW)	Spot price($/MWh)
1	170.00	20.00	10.55
2	250.00	25.00	10.35
3	400.00	40.00	9.00
4	520.00	55.00	9.45
5	700.00	79.00	10.00
6	1050.00	95.00	11.25
7	1100.00	100.00	11.30
8	800.00	80.00	10.65
9	650.00	65.00	10.35
10	330.00	35.00	11.20
11	400.00	40.00	10.75
12	550.00	55.00	10.60

Table 3. The comparison of benefits under different λ, *NBP* means the negative benefits when using payment for power allocation, *NBR* means the negative benefits when using payment for reserve allocation

λ	*NBP*($)	*NBR*($)
0.005	-551.27	-576.66
0.010	-559.73	-576.42
0.015	-568.18	-576.19
0.020	-576.64	-575.96
0.025	-585.10	-575.73
0.030	-593.56	-575.50
0.035	-602.02	-575.27
0.040	-610.48	-575.04
0.045	-618.94	-574.81
0.050	-627.40	-574.58

When using payment for power delivered, the price of spinning reserve is taken to three times the spot price of power; the optimal solution is shown in Table 3 if the λ values change from 0.005 to 0.05 at this time. When using payment for reserve allocated, the price of spinning reserve is taken to 0.04 times the spot price of power, the optimal solution is shown in Table 3 if the λ values change from 0.005 to 0.05 at this time.

As can be seen from the table, when using the press to contribute to payment system for the distribution, The optimization results will be greater effected according to the changes of probability λ when using payment for power delivered, because the benefits of reserve capacity can be obtained only when it is dispatched, and the higher reserve price in this mode, so the optimization results are sensitive to the probability λ , the larger probability λ , the greater benefits received, and the greater chance to be dispatched while the cost of change is relatively small. The generator will have part of the proceeds regardless of dispatching or not dispatching when using the payment for reserve allocation.

The reserve prices are lower at this mode, so the optimization results are not sensitive to the probability λ. There may a small decline in the profit as shown in Table 3 at the current spot price and the output level with the λ increasing.

Table 4. Optimization result of the 3-units system using payment for reserve allocation

Unit	Output(MW)	Reserve(MW)	Negative benefits($)
1	162.10	80.00	-413.34
2	400.00	0.00	-360.00
3	200.00	0.00	-630.00
4	762.10	80.00	-576.66

Table 5. The solution quality for the 3-units system using payment for reserve allocation under two optimization methods, *BV* means best value, *WV* means worst value, *AV* means average value, *SD* means standard deviation and *ACT* means average calculation time.

Unit	PSO	Revised PSO
BV($)	-579.73	-576.66
WV($)	-571.42	-576.66
AV($)	-575.57	-576.66
SD($)	1.76	0.00
ACT($)	6.75	0.53

Take $\lambda = 0.005$, using payment for reserve allocation, spinning reserve price is 0.04 times the electricity spot price,repeat 50 times and calculate optimization results, Table 4 lists the optimal output distribution of 3-units system in order to compare with the revise particle swarm algorithm and particle swarm algorithm, the new algorithm get optimized solution is clearly better and the convergence and speed are greatly improved from the table.

5 Conclusion

Repair strategies presented in this paper is a positive amendment for particles which violate the various constraints,and penalty function technique is combined to make particles to search their optimization as much as possible in the area of feasible solution or its vicinity. The strategy effectively improves the accuracy of the algorithm and speed. Simulation results also clearly demonstrated the effectiveness of this method and good convergence. In this paper, power generation unit cost function takes the form of a smooth quadratic curve, this approach still apply for the form of nonsmooth quadratic curve. When the cost function using a more complex form, the calculation of slight increase rate will be correspondingly complicated and even may be unable to obtain exact value and the similar methods can be used to solve problem, there will have little impact on the accuracy of the algorithm.

Acknowledgement. The research is supported by China Postdoctoral Science Foundation 20060390669, and the authors also thank the help of professor Chuan-wen Jiang of Shanghai Jiaotong University.

References

1. Abdelaziz, A.Y., Kamh, M.Z., Mekhamer, S.F., Badr, M.A.L., et al.: A Hybrid HNN-QP Approach for Dynamic Economic Dispatch Problem. Electric Power Systems Research 78, 1784–1788 (2008)
2. Pothiya, S., Ngamroo, I., Kongprawechnon, W., et al.: Application of Multiple Tabu Search Algorithm to Solve Dynamic Economic Dispatch Considering Generator Constraints. Energy Conversion and Management 49, 506–516 (2008)
3. Yuan, X., Wang, L., Yuan, Y., et al.: A Modified Differential Evolution Approach for Dynamic Economic Dispatch with Valve-point Effects. Energy Conversion and Management 49, 3447–3453 (2008)
4. Basu, M.: Dynamic Economic Emission Dispatch Using Nondominated Sorting Genetic Algorithm-II. Electrical Power and Energy Systems 30, 140–149 (2008)
5. Ming, Z.: Methods for Analyzing Economic Dispatch of Power Grids. East China Electric Power 37, 0719–0723 (2009)
6. Liang, Z.X., Glover, D.: A Zoom Feature for a Dynamic Programming Solution to Economic Dispatch Including Transmission Losses. IEEE Trans. on Power Systems 7, 544–550 (2007)
7. El Gallad, A., El Hawary, M., Sallam, A., et al.: Particle Swarm Optimizer for Constrained Economic Dispatch with Prohibited Operating Zones. In: IEEE Conference on Electrical and Computer Engineering, pp. 78–81. IEEE Press, New York (2007)
8. Wong, K.P., Fung, C.C.: Simulated Annealing Based Economic Dispatch Algorithm. IEE Proceedings on Gener., Transm. and Distrib. 140, 509–515 (2008)
9. Shi, Y., Eberhart, R.C.: Empirical Study of Particle Swarm Optimization. In: Proceedings of the 1999 Congress on Evolutionary Computation, pp. 1945–1950. IEEE Press, New York (1999)
10. Gaing, Z.W.: Particle Swarm Optimization to Solving the Economic Dispatch Considering the Generator Constraints. IEEE Trans. on Power Systems 18, 1187–1195 (2005)
11. Yang, J., Zhou, J.Z., Wu, W., et al.: Application of Improved Particle Swarm Optimization in Economic Dispatching. Power System Technology 29, 1–4 (2009)

Particle Swarm Optimization-Based Extremum Seeking Control

Shi-Jie Yu[1], Hong Chen[2,3], and Li Kong[2]

[1] Electrical Engineering College,
Wuhan University, Wuhan 430074, China
[2] Department of Control Science and Engineering,
Huazhong University of Science and Technology,
Wuhan 430074, China
[3] Wuhan 2nd Ship Design and Research Institute, Wuhan 430064, China

Abstract. This paper devises a particle swarm optimization-based extremum seeking control (ESC) scheme. In the scheme, the system states are guided to the optimal point by the controller based on the output measurement, and the explicit form of the performance function is not needed. By measuring the performance function value online, a sequence, generated by the particle swarm optimization algorithm, steers the regulator that drives the system states approaching to the set point that optimizes the performance. We also propose an algorithm that first reshuffles the sequence, and then inserts intermediate states into the sequence, to reduce the regulator gain and oscillation induced by stochastic, population-based searching algorithms. Simulation examples demonstrate the effectiveness and robustness of the proposed scheme.

Keywords: particle swarm optimization; extremum seeking control; state regulation; adaptive control; swarm intelligence-based optimization.

1 Introduction

Regulation and tracking of system states to optimal setpoints or trajectories are typical tasks in control engineering. However, these optimal setpoints are sometimes difficult to be chosen a priori, or vary with the environmental condition changes. Extremum seeking control (ESC) is a kind of adaptive control schemes that can search for the optimal setpoints online, based on the measurement of the performance output or its gradient. ESC can be regarded as an optimization problem, and many of the schemes used in ESC are transferred from optimization algorithms.

Unlike the traditional variational calculus-involved optimal control method, the explicit form of the performance functions are not needed in ESC. Therefore, ESC is useful in the applications that performance functions are difficult to model. After Krstic and Wang's stability studies [11], research on ESC has received significant attention in recent years. The recent ESC application examples include active flow control [2], bioreactor or chemical process control [1] [7],

D.-S. Huang et al. (Eds.): ICIC 2010, LNCS 6215, pp. 185–196, 2010.

antilock braking system design [18], and fuel cell power plant [20]. There also have been considerable theoretical studies in ESC, such as stability studies on perturbation-based ESC [11][10], PID tuning by ESC [9], ESC for nonlinear dynamic systems with parametric uncertainties [6], and ESC for state-constrained nonlinear systems [4]. The recent studies of Zhang and Ordonez [18][19] presented a numerical optimization-based ESC (NOESC) framework that takes the advantage of numerical algorithms to find the optima online. However, these algorithms are unable to find the global optima if the assumptions that the performance functions are convex and continuous does not hold. Furthermore, the NOESC is sensitive to measurement noise, due to the poor robustness of the numerical algorithms.

Particle swarm optimization (PSO) algorithm is a stochastic, population-based optimization method which first devised by Kennedy and Eberhart [8]. PSO algorithm mimics the food-seeking behavior of birds or fishes. Due to its simplicity and effectiveness, PSO algorithm witnesses a considerable interest, and is applied in many areas. Studies have shown that PSO algorithm is able to handle a wide range of problems, such as integer optimization [12], multi-objective optimization [3], and global optimization of multimodal functions [13]. In control engineering, PSO algorithm is usually employed to identify the models [14], or to optimize the parameters of the controller offline [5]. PSO algorithm is usually regarded as an effective global optimization method, and often used in offline optimization, and depends on the explicit form and the solvability of the performance functions. However, for some complex models, e.g. active flow control problems, which are described by Navier-Stokes equations, it is difficult to obtain the optimal parameters of the controllers by time-consuming numerical simulations.

In this paper, we devise a novel ESC scheme that can optimize non-convex and discontinuous performance functions online by PSO. In the proposed scheme, the numerical optimization-based ESC [18] is extended by incorporating PSO algorithm into the extremum seeking framework. To improve the partibility of PSO-based ESC (PSOESC), we also propose a reshuffle-then-insertion algorithm, to reduce the control gain and oscillation introduced by the stochastic, population-based optimization algorithms.

2 Problem Statement

In control practice, the problem of seeking for an optimal set point is encountered usually. In general, this problem can be modeled as

$$\dot{x} = f(x, u), \tag{1}$$

$$y = J(x), \tag{2}$$

where $x \in \mathbb{R}^n$ is the state, $u \in (R)$ is the input, y is the performance output to be optimized, $f : D \times \mathbb{R} \to \mathbb{R}^n$ is a sufficiently smooth function, and $J : D \to \mathbb{R}$ is

an unknown function. For simplicity, we assume $D = \mathbb{R}^n$ in this paper. Without loss of generality, we consider the minimization of the performance function (2). Unlike optimal control, extremum seeking control finds the optimal set point by online measurement of the performance function, without the knowledge of its explicit form.

ESC can be considered as a class of constrained optimization problem whose constraint is the differential equation (1), instead of the algebraic constrains in traditional optimization problems. Then, ESC control problem can be stated as:

$$\begin{aligned} &\min_{x \in D} \quad J(x) \\ &s.t. \quad \dot{x} = f(x, u) \end{aligned} \tag{3}$$

When (1) is controllable, there always exists a control u such that state x transfers to any position in $\mathbb{R}^n$ in a finite time. We then can apply any optimization algorithm to produce a guidance sequence to determine a trajectory to the optimal set point in the state space [18].

Similar to numerical optimization-based ESC [18], we present a PSO-based ESC block diagram as Fig. 1, where the nonlinear plant $\mathbb{F}$ is modeled as (1) and the performance function J is (2). Unlike [18], we apply PSO algorithms to substitute the numerical optimization algorithms to produce the extremum seeking sequence $\{X_k\}$. This sequence is generated as the target state in every seeking iterative step, based on the online measurement of y. The regulator K regulates the state of $\mathbb{F}$ follows the sequence as $X_1, X_2, \cdots, X_k$, toward the optimal set point.

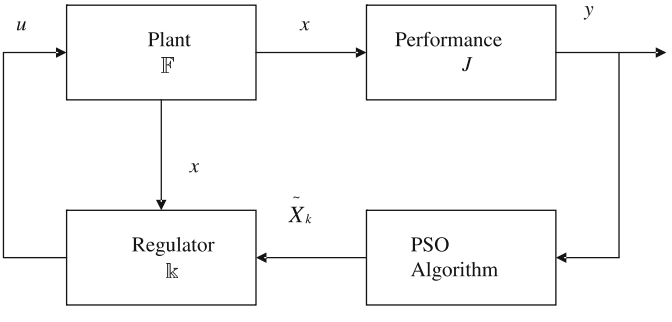

Fig. 1. PSO-based Extremum Seeking Block Diagram

3 Particle Swarm Optimization

PSO is a population-based random optimization algorithm that mimics the behavior of bird or fish swarm in searching food. In the swarm, each particle has a variable speed, moving toward the positions of its own best fitness achieved so far and the best fitness achieved so far by any of its neighbors.

Let $S \subset \mathbb{R}^n$ be an n-dimensional search space. The size of the particle swarm is denoted as N. The position of the ith particle is represented as an n-dimensional vector $\tilde{X}_i = (x_{i1}, x_{i2,} \cdots x_{in})^T \in S$, and its velocity is denoted as $V_i = (v_{i1}, v_{i2,} \cdots v_{in})^T \in S$, where $i = 1, 2, \ldots, N$, is the identity of each particle. The best position it has achieved so far is $P_i^{pbst} = (p_{i1}, p_{i2,} \cdots p_{in})^T \in S$. The best position achieved so far in its neighborhood is P_{gbst}. On the time step k , the update equation of the standard PSO algorithm is

$$V_i(k+1) = \omega V_i(k) + c_1 r_1(k) \left(P_i^{pbst}(k) - \dot{X}_i(k) \right) + c_2 r_2(k) \left(P_{gbst}(k) - \dot{X}_i(k) \right), \tag{4}$$

$$\tilde{X}_i(k+1) = \tilde{X}_i(k) + V_i(k+1). \tag{5}$$

where ω, c_1, c_2 are nonnegative constant real numbers, and r_1,r_2 are two independent random numbers with uniform distribution in the range of [0,1].

Because the positions of particles involve randomness, the convergence of PSO-involved algorithms is defined in a possibility sense in this paper. We say $X_i(k)$ converges in mean square to Q^*, when $\lim_{k \to \infty} \mathbf{E} |X_i(k) - Q^*|^2 = 0$, for $\forall i \in \{1, 2, \ldots, N\}$, where N is the population size of the swarm, and $\mathbf{E}$ represents the expectation operator.

It has been shown that the standard PSO algorithm guarantees every particle converges in mean square to the best position of the whole swarm [13]. However, that position may be neither the global optima nor the local optima. In order to ensure the convergence to the optimal value, modified PSO algorithms need to make tradeoffs between exploration and exploitation, and numerous papers have presented various modified PSOs for this issue [15] [17]. For simplicity, in the following section we will focus on standard PSO algorithm, assuming that the standard PSO algorithm can converge in mean square to the global optima in the ESC cases. For the same reason, we also drop the "mean square" in the convergence analysis.

4 PSO-Based Extremum Seeking Scheme

4.1 PSOESC for LTI Systems

Consider a single-input-single-output (SISO) linear time-invariant (LTI) system

$$\dot{x} = Ax + Bu, \tag{6}$$

with the performance function defined as (2). The matrices A and B are given, while J is unknown. We will find the minimum of J online by the measurement of the function value y. If the LTI system (6) is controllable, from the linear system theory, we have the following lemma that states the existence of a perfect regulator.

Lemma 1. For a controllable LTI system (6), given system state $x(t_k)$ on time t_k, regulation time δ_k, and X_{k+1}, let $t_{k+1} = t_k + \delta_k$, the control input

$$u(t) = -B^T e^{A^T(t_{k+1}-t)} G^{-1}(\delta_k)[e^{A\delta_k} x(t_k) - X_{k+1}], \tag{7}$$

where

$$G(\delta_k) = \int_0^{\delta_k} e^{A\tau} B B^T e^{A^T \tau} d\tau, \tag{8}$$

then we have $x(t_{k+1}) = X_{k+1}$.

From *Lemma 1*, there always exists a control u that regulates the state to any given state from any initial state, provided the LTI system is controllable. Thus, we can device a scheme that drives the state of the system to the global optima along a sequence produced by any optimization algorithms including that of swarm intelligence-based. By combining the PSO and ESC, the PSO-based ESC scheme can be formed as follows.

Algorithm 1. *PSO-based ESC scheme for LTI systems*

- step 1) Initialize the particle swarm, and let $i = 1$, $k = 1$.
- step 2) Let particle i's position as the ith target state, i.e. let $X_{k+1} = \tilde{X}_i(k)$ in (7) to get the control u.
- step 3) The u regulates the plant to the target state, and the performance output y is readily to be measured by sensors.
- step 4) Let the output y be the fitness $\tilde{y}_i$ of the particle.
- step 5) Let $i = i+1$, repeat 2) to 4), until $i = N$, where N is the predefined size of the particle swarm.
- step 6) Update the velocity and position according to (4) and (5).
- step 7) Let $k = k + 1$, repeat 2) to 5), until a stop criterion is met.

We say 2) - 4) is a PSO loop, and 2) - 7) an ESC loop. The convergence result of *Algorithm 1* can be shown by the combination of *Lemma 1* and the convergence proof of PSO [13], and is presented as the following theorem.

Theorem 1: Let X^* be the solution of the optimization problem (3), i.e. $X^* = \arg\min_{x \in D} J(x)$, if the solution of problem $\min_{x \in D} J(x)$, obtained online by PSO, converges to X^*, then *Algorithm 1* drives system (6) to its minimum performance function value J^* .

Since the standard PSO algorithm and its variants have shown their effectiveness in global optimization problems, it is safe to assume *Algorithm 1* converges to the global optima in ESC. Thanks to the global searching ability of PSO algorithm, we need not apply the assumptions in [18] [19] to ensure the global convergence condition for the numerical-based optimization algorithms. The performance function J can be nonconvex and discontinuous in ESC context now.

Since each state, represented by a particle in the swarm, can be tracked in a serial manner, the sensors needed in PSOESC are no more than other ESCs. It should be noted that, compared to NOESC, PSOESC have to spend more time

to obtain the best state in an ESC loop. However, this cost can be regarded as the expense paid for the global optima.

It is not difficult to extend the *Algorithm 1* to the multi-input-multi-output (MIMO) systems, like the NOESC schemes presented in [18]. Moreover, other designs of controller (10) can be applied for a more robust regulator as suggested in [18] and [19]. Moreover, The results on LTI systems can also be extend to state feedback linearizable systems and input-output feedback linearizable systems by substituting the regulator with appropriate designs, in a similar way as NOESC.

4.2 Regeneration of the Sequence Produced by the PSO Algorithm

Since *Algorithm 1* requires a regulator to drive the state of the system (6) from one to another along the sequence produced by the PSO loop, however, due to the randomness feature of the update equation (4), at some stages, the regulator gain may be very large, and the state of the system would oscillate rashly. This could cause serious problems in real-world applications, and may hinder PSO or any other swarm intelligence-based algorithms from being applied in the ESC context.

Consider system (6), and the state from time t_k to t_{k+1} . From (7), the output of the regulator $\mathbb{K}$ in a state transfer procedure is determined by the regulation time δ_k, the initial state $x(t_k)$, and the terminal state $x(t_{k+1})$. Given the regulation time δ_k, if we want to minimize the maximum control, then we need an algorithm to reshuffle the sequence $\{x_k\}$ to minimize the $\max\left(\underset{k=1,\ldots N}{u}(t_k)\right)$. However, the optimal regeneration is difficult to devise, because it is equivalent to the bottleneck traveling salesman problem(BTSP), and is shown NP-hard [16], i.e. there is no polynomial algorithm for this kind of problems so far. As a sub-optimal solution, we propose here an algorithm to regenerate the PSO-produced sequence for the practical use of PSOESC, based on the following consideration.

In practice, limiting maximum control gain within a certain bound is sufficient to have a practical controller. From *Lemma 1*, we have that for each predefined $\Sigma > 0$, there always exists a regulation time δ_k such that $\|u(t)\| < \Sigma$. Therefore, the control gain can be limited in a bound by choosing a sufficiently long regulation time δ_k. However, too long regulation time may be unacceptable in practice. Another feasible approach is to insert new intermediate states between two states that would lead to unacceptable large control gain. These new intermediate states would smooth the original state sequence produced by the PSO algorithm. However, this procedure may prolong the regulation time as well. Therefore, we propose a reshuffle procedure below, in order to reduce the requests of the insertion procedure as less as possible.

Consider the sequence $\{x_k\}$ produced by PSO in an ESC loop. First, we simply choose the nearest state to x_1 from $\{x_k\}$ as x_2 , then we choose the nearest state to x_2 from the remainder states in $\{x_k\}$ as x_3 , and so on. Repeating the procedure will lead to a new sequence in which each distance of two neighbor states of the first $k-1$ states is minimal. The distance between the last two state, i.e. x_{k-1} and x_k may be very large, and there may still be some

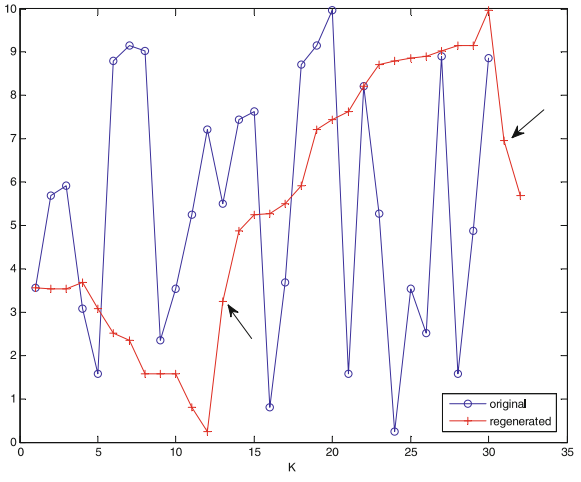

Fig. 2. The regeneration of the target state sequence.The two inserted intermediate states in the regenerated sequence are indicated by arrows.

unacceptable large distances in the reshuffled sequence $\{x_1, x_2, \ldots x_{k-1}\}$. However, the requests of the insertion procedure are much less than the original sequence.

By combination of the reshuffle procedure and the insertion procedure above, we have the reshuffle-then-insertion algorithm. The reshuffle-then-insertion algorithm is also applicable to ESC based other swarm-intelligence-based algorithms, such as Artificial Bee Colony, Ant Colony Swarm and Bacteria Foraging.

The result that the reshuffle-then-insertion algorithm is applied on a random sequence in the range of [0,10] is shown in Fig. 2. It can be seen that the algorithm smoothes the original sequence remarkably, and the control gain in each step is limited in a predefined bound.

5 Numerical Experiments

The numerical experiments were carried out on a personal computer running on the Matlab/Simulink environment. The parameters of the standard PSO were chosen as $w = 0.9$, $c_1 = 0.2$, and $c_2 = 0.012$. For the purpose of simulation, performance functions were provided explicitly, while they would be unknown in real-world applications. Since the convergence of the PSOESC scheme is described in mean square sense, we define the success rate of the PSOESC scheme as $R_c = \frac{N_c}{N_t}$, where N_c is the number of times that PSOESC converged to the known global optima, and N_t the number of repeated times of one test. We define the error limit as $\pm 0.05 J^*$, where J^* is the known global minimal value. We also present comparisons between PSOESC and NOESC, to show the ability and weakness of the proposed PSOESC algorithm.

5.1 First-Order Single-Input-Single-Output (SISO) LTI System

We first considered a LTI system

$$\dot{\theta} = -\theta + u \tag{9}$$

with the performance function defined as

$$J(\theta) = -0.4\sin(9\theta)\sin(\theta). \tag{10}$$

where u is the control obtained by (7). The two local minima of (10), 0.225 and 0.883, can be easily found by the *optimtool* toolbox in *Matlab* by choosing different start point. When setting the population size as 10 particles, we observed a 100 percent success rate in 120 repeated tests. We also tested a swarm with only 2 particles, and have a success rate of 82 percent with much less steps for convergence than that of 10 particles cases. By comparison, the performance of NOESC, which is based on the simplex search method in our experiment, depends on the initial point. It would convergence much faster than PSOESC, provided a *good* initial point was chosen. However, if we choose $\theta_0 = 0$ as the initial point, for example, the seeking procedure would converge to the local minimum 0.225. This comparison is shown in Fig.3.

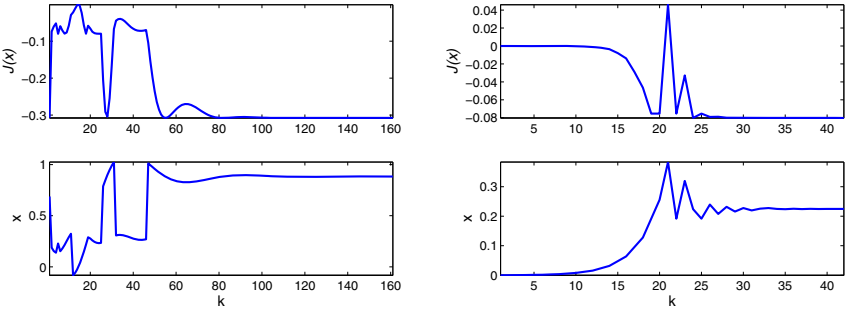

Fig. 3. Comparison between PSOESC (left) and NOESC (right) for the first-order LTI system (9), where k indicates the iterative steps

5.2 Second-Order LTI System

Consider a system discussed in [18]:

$$\dot{x} = \begin{bmatrix} 0 & 1 \\ -2 & -3 \end{bmatrix} x + \begin{bmatrix} 0 \\ 1 \end{bmatrix} u \tag{11}$$

$$y = J(x) = 100(x_2 - x_1^2)^2 + (1 - x_1)^2 \tag{12}$$

The performance function (12) is also known as Rosenbrock function whose minimum is $x^* = [1 \quad 1]^T$, and $J(x^*) = 0$. In this case, we use 10 particles.

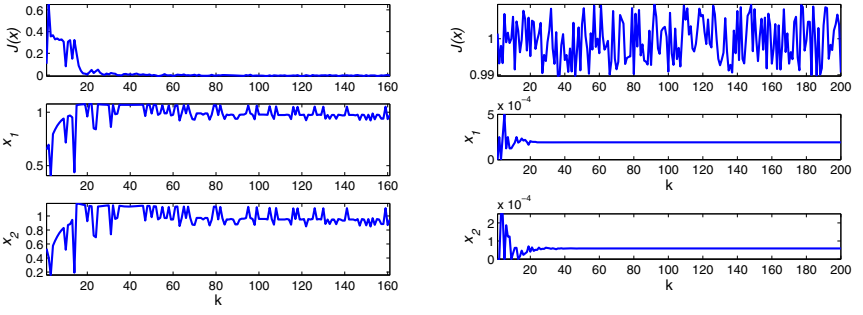

Fig. 4. Comparison between PSOESC (left) and NOESC (right) for the second-order LTI system (11) with measurement noise

To test the robustness of the PSOESC, we disturbed y with a random number uniformly distributed with amplitude 0.02. The PSOESC scheme drives the state of the system approaching to the optimal set point successfully, while NOESC converges to the wrong place near the initial point, the origin. This comparison is shown in Fig.4.

5.3 PSOESC for ABS Design

Consider a one wheel ABS design case which is usually used in ESC literatures. The problem is modeled as [18]

$$M\dot{v} = -N\mu(\lambda), \tag{13}$$

$$I\omega = -B\omega + NR\mu(\lambda) - u, \tag{14}$$

where v denotes the linear velocity, ω is the angular velocity, $N = Mg$ is the weight of the wheel, R is the radius of the wheel, I the moment of inertia of the wheel, $B\omega$ the braking friction torque, u the braking torque, $\mu(\lambda)$ the friction force coefficient, and $\lambda = \dfrac{v - \omega R}{v}$ is the slip, $0 \leq \lambda \leq 1$ for $\omega R \leq v$. There exists a maximum μ^* for the friction force coefficient $\mu(\lambda)$ at the optimal slip λ^*. Since λ^* and μ^* will change as the road condition changes, the design purpose is to device a control u to maximizes the $\mu(\lambda)$.

In the simulation, the parameters were chosen as: $M = 400kg$, $B = 0.01$, $R = 0.2m$, $\lambda(0) = 0$, $a = 1$, $\delta_k = 0.5$ [18]. For the simulation purpose, we also postulated that the relation of $\mu(\lambda)$ and λ satisfies

$$\mu(\lambda) = 2\mu^* \frac{\lambda^* \lambda}{{\lambda^*}^2 + \lambda^2}, \tag{15}$$

where, $\mu^* = 0.25$, $\lambda^* = 0.6$. Obviously, the optimal λ is $\lambda^* = 0.6$. To convert the problem into a minimizing one, we let $x = -\lambda$ and $J(x) = -\mu(\lambda)$. PSOESC scheme with 10 particles worked well, and we observed a 99 percent convergence

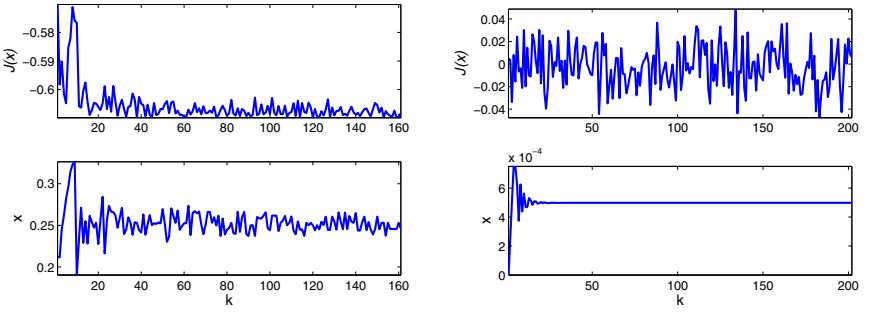

Fig. 5. Comparison between PSOESC (left) and NOESC (right) for the ABS with measurement noise

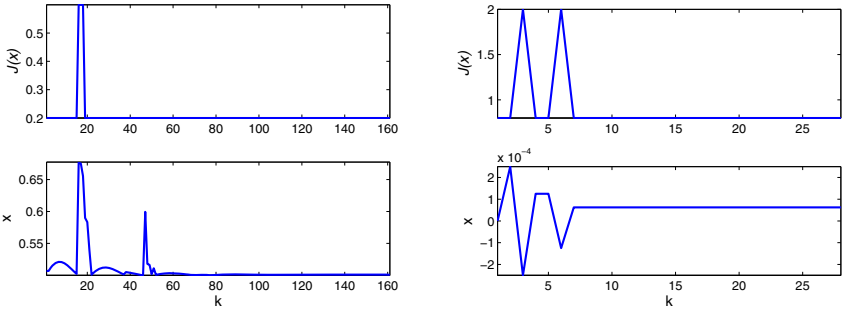

Fig. 6. Comparison between PSOESC (left) and NOESC (right) for the system with a discontinuous performance function

rate in 120 repeated simuulations. We also tested a swarm with only a single particle, and have a convergence rate of 61 percent. To test the robustness of the PSOESC, we added μ with a random disturbance with uniform distribution in the range of [-0.02, 0.02] to simulate the influence of noises. As Fig.5 shows, the PSOESC scheme drives the state of the system converging to the vicinity of the optimal slip. By comparison, the NOESC scheme converges fast to the optimal slip when no measurement noises are added, whereas it converges to the wrong point when measurement is disturbed by noise.

5.4 PSOESC for a System with Discontinuous Performance Function

Finally, we discuss a LTI system with a discontinuous performance function. Consider the system (20) with performance function defined as

$$y = J(\theta) = \begin{cases} 0.5 & ,\theta \in (-\infty, 0.5) \\ 0.2 & ,\theta \in [0.5, 0.6) \\ 0.8 & ,\theta \in [0.6, 0.9) \\ 2 & ,\theta \in [0.9, +\infty) \end{cases} . \tag{16}$$

As Fig.6 shows, the PSOESC scheme drives the performance output of the system converging to the optima. This test illustrates the intrinsic advantage of the PSOESC in solving discontinuous optimization problems. By comparison, it can be seen in Fig.6 that the existing NOESC is unable to deal with such kind of problem. Although it converges in no more than 8 steps, the optimum it found, 0, is not the true minimizer.

6 Conclusions

This paper presents a PSO-based ESC scheme that is able to find the optimal set point online. The PSO algorithm produces a sequence converging to the global optima. The sequence serves as a guidance to regulate the state of the plant approaching to the optimal set point. We also propose a reshuffle-then-insertion algorithm that is able to reduce the control gain and oscillation, thus improving the practicability of PSOESC scheme. The numerical experiments show the effectiveness of the scheme. The PSOESC scheme found the global optima successfully in various cases. The simulations also demonstrate the ability of PSOESC scheme for handling measurement noise. The disadvantage of PSOESC is that it costs more time in every ESC loop. However, the robustness to measurement noise makes PSOESC preferred to NOESC in some cases which NOESC cannot handle. The scheme proposed in this paper will be easily extend to other swarm intelligence-based algorithms, such as Artificial Bee Colony, Ant Colony Optimization and Bacteria Foraging Algorithm.

Acknowledgements. This work is partly supported by Hydrodynamics Research Foundation under the grant NO. 9140A14030308CB49.

References

1. Bastin, G., Nesic, D., Tan, Y., Mareels, I.: On extremum seeking in bioprocesses with multivalued cost functions. Biotechnol. Prog. 25(3), 683–689 (2009)
2. Beaudoin, J.F., Cadot, O., Aider, J.L., Wesfreid, J.E.: Drag reduction of a bluff body using adaptive control methods. Phys. Fluids 18(8) (August 2006)
3. Dasheng, L., Tan, K.C., Goh, C.K., Ho, W.K.: A multiobjective memetic algorithm based on particle swarm optimization. IEEE J. SMCB 37(1), 42–50 (2007)
4. DeHaan, D., Guay, M.: Extremum-seeking control of state-constrained nonlinear systems. Automatica 41(9), 1567–1574 (2005)
5. El-Zonkoly, A.M.: Optimal tuning of power systems stabilizers and avr gains using particle swarm optimization. Expert Systems with Applications 31(3), 551–557 (2006)
6. Guay, M., Zhang, T.: Adaptive extremum seeking control of nonlinear dynamic systems with parametric uncertainties. Automatica 39(7), 1283–1293 (2003)
7. Hudon, N., Guay, M., Perrier, M., Dochain, D.: Adaptive extremum-seeking control of convection-reaction distributed reactor with limited actuation. Comput. Chem. Eng. 32(12), 2994–3001 (2008)
8. Kennedy, J., Eberhart, R.: Particle swarm optimization. In: Neural Networks, pp. 1942–1948. IEEE Press, Proceedings (1995)

9. Killingsworth, N., Krstic, M.: Pid tuning using extremum seeking: online, modelfree performance optimization. IEEE Contr. Syst. Mag. 26(1), 70–79 (2006)
10. Krstic, M.: Performance improvement and limitations in extremum seeking control. Systems & Control Letters 39(5), 313–326 (2000)
11. Krstic, M., Wang, H.H.: Stability of extremum seeking feedback for general nonlinear dynamic systems. Automatica 36(4), 595–601 (2000)
12. Laskari, E.C., Parsopoulos, K.E., Vrahatis, M.N.: Particle swarm optimization for minimax problems. In: Proceedings of the 2002 Congress on Evolutionary Computation CEC 2002, vol. 2, pp. 1576–1581 (2002)
13. Liang, J.J., Qin, A.K., Suganthan, P.N., Baskar, S.: Comprehensive learning particle swarm optimizer for global optimization of multimodal functions. IEEE T. Evolut. Comput. 10(3), 281–295 (2006)
14. Panda, G., Mohanty, D., Majhi, B., Sahoo, G.: Identification of nonlinear systems using particle swarm optimization technique. In: IEEE Congress on Evolutionary Computation CEC 2007, pp. 3253–3257 (2007)
15. Rapaic, M.R., Kanovic, Z.: Time-varying pso - convergence analysis, convergencerelated parameterization and new parameter adjustment schemes. Information Processing Letters 109(11), 548–552 (2009)
16. Kabadi, A.P. (ed.): The Bottleneck TSP. The Traveling Salesman Problem and Its Variation. Kluwer Acadamic Publishers, Netherlands (2002)
17. Xin, C., Yangmin, L.: A modified pso structure resulting in high exploration ability with convergence guaranteed. IEEE J. SMCB 37(5), 1271–1289 (2007)
18. Zhang, C., Ordonez, R.: Numerical optimization-based extremum seeking control with application to abs design. IEEE T. Automat. Contr. 52(3), 454–467 (2007)
19. Zhang, C., Ordonez, R.: Robust and adaptive design of numerical optimization-based extremum seeking control. Automatica 45(3), 634–646 (2009)
20. Zhong, Z.d., Huo, H.b., Zhu, X.j., Cao, G.y., Ren, Y.: Adaptive maximum power point tracking control of fuel cell power plants. J. Power Sources 176(1), 259–269 (2008)

Image Contour Extraction Based on Ant Colony Algorithm and B-snake

Jinjiang Li

School of Computer Science and Technology,
Shandong Institute of Business and Technology, 264005, Yantai, China
lijinjiang@gmail.com

Abstract. In this paper, we present a novel image contour extraction by ant colony algorithm and B-snake model. Using ant colony algorithm, an initial curve of B-snake is get, which rapidly converging near image edge. When the B-snake begins to iterate, new control points are inserted, which can enhance the flexibility of B-snake to describe complex shape. A minimum energy method minimum mean square error (MMSE) is proposed for B-snake to push it to the target boundary. The experimental results demonstrate the efficiency and accuracy of our method.

Keywords: Contour extraction, Ant colony algorithm, B-snake.

1 Introduction

In most computer applications, image contour extraction constitutes a crucial initial step before performing the task of object recognition and representation. Snake [1], or active contour, are more accurate image methods, which are widely used in medical image processing, computer vision and other fields. It is defined within an image domain that can move under the influence of internal forces coming from within the curve itself and external forces computed from the image data. Snakes are widely used in many applications, including edge detection, shape modeling [2], segmentation [3], and motion tracking [4]. A great deal of research is made on curve evolution model and its numerical, a number of representative methods are proposed [5], [6], [7]. From the original philosophy of snake, an alternative approach is using a parametric B-spline representation of the curve, which is also called B-snake [8], [9]. Existing snakes have several limitations when a local regularization is wanted: with the original snake, a local regularization involves a matrix inversion step at each iteration, and B-snake avoids this by implicitizing the internal energy [10]. B-snake takes advantages of the B-spline representation, and a local control of the curve continuity and a limited number of processed points increase the convergence speed. B-snake model is described by parameterized B-spline, which is an energy minimizing spline parameterized by its control points. Due to some characteristic of B-spline curve, correspondingly, time of computing is reduced and constringency speed is improved [11]. The smoothness of the snake is implicitly given by the B-spline. The energy consists in two terms: the internal energy and the external energy [12]. Yue Wang

D.-S. Huang et al. (Eds.): ICIC 2010, LNCS 6215, pp. 197–204, 2010.

uses a minimum energy method which called Minimum Mean Square Error (MMSE) to push it to the target boundary [13].

In this paper, ant colony algorithm is used to quick search and optimizes the control points of B-spline, and it can quickly converge to the edge of the image. Ant algorithms were inspired by the observation of real ant colonies. Real ants are capable of finding the shortest path from a food source to their nest. It is a paradigm for designing metaheuristic algorithms for combinatorial optimization problems by using principles of communicative behaviour occurring in ant colonies. Its first application was the Traveling Salesman Problem. The algorithm has inherent parallelism, and we can validate its scalability. The characteristic of ant algorithms is their explicit use of elements of previous solutions. A colony of ants begins with no solutions. Each ant constructs a solution by making decisions stochastically, using existing problem constraints and heuristics combined with experience (which is analogous to a substance called pheromone) [14].

2 Ant Colony Algorithm

Ant algorithm is a heuristic algorithm, which is based on the behavior of real ants. It is a method to solve combinatorial optimization problems by using principles of communicative behavior occurring in ant colonies. Ants can communicate information about the paths they found to food sources by marking these paths with pheromone. The pheromone trails can lead other ants to the food sources. Ant algorithm is an evolutionary approach where several generations of artificial ants search for good solutions. Every ant of a generation builds up a solution step by step thereby going through several decisions until a solution is found. Ants that found a good solution mark their paths through the decision space by putting some amount of pheromone on the edges of the path. The following ants are attracted by the pheromone so that they will search in the solution space near good solutions.

Let τ_{ij} be the pheromone intensity on path form i to resource j; η_{ij} be the visibility of edge (i, j), and in general it taken as $\eta = 1/d_{ij}$; $\Delta\tau_{ij}^{k}$ be the change of pheromone on path (i, j) leaved by ant k; P_{ij}^{k} be transition probability of ant k; α be the importance of pheromone($\alpha \geq 0$); β be the importance of resource innate attributes ($\beta \geq 0$); ρ be the permanence of pheromone ($0 \leq \rho < 1$), and $1-\rho$ be evaporation of pheromone.

State transition rule the probability of selecting j as next point to visit, taking stochastic proportion, when ant k at point i. The probability can be calculated by the formula as follows.

$$P_{ij}^{k} = \begin{cases} \dfrac{\tau_{ij}^{\alpha}\eta_{ij}^{\beta}}{\sum_{r \in N_i} \tau_{ir}^{\alpha}\eta_{ir}^{\beta}}, & j \in N_i \\ 0, & \text{otherwise} \end{cases} \tag{1}$$

where N_k is the reachable point set of point i.

The local updating rule is used to reduce the pheromone value in the edge that an ant just visit in order to enhance the global search ability of the ant colony. The positive feedback mechanism of the ant colony algorithm only comes from the pheromone global updating rule excluding the pheromone local updating rule. In local updating, pheromone is updated on edge (i, j) when ant moves from point i to point j. The new quantity of pheromone deposited on an edge is inversely proportional to the edge length; thus, over time, shorter edges will receive more pheromone, which leads to a positive feedback loop of increased use and further reinforcement. During global updating, only one ant is allowed to update the trail values. This elitist strategy requires that only the ant with the iteration-best tour be allowed to deposit additional pheromone. Similar to local updating, the new quantity of pheromone deposited is inversely proportional to a certain value; this time, the value in question is tour length, not edge length. Thus, edges which constitute shorter tours are reinforced more which leads to another positive feedback loop of more use and greater reinforcement. Trail updating rule can be expressed as follows.

$$\tau_{ij}(t+1) = \rho\tau_{ij}(t) + \sum \Delta\tau_{ij} \tag{2}$$

3 B-snake Model

Let k be positive integer, arbitrarily gives a non-decreased knot vector: $T = \{t_0, t_1, \ldots, t_{n+k}\}$, control point: P_0, P_1, P_2, …, P_n ($n \geq k$). A B-spline curve of order k can be defined as:

$$C(t) = \sum_{i=0}^{n} P_i B_{i,k}(t), \quad t_{k-1} \leq t \leq t_{n+1} \tag{3}$$

where $B_{i,k}(t) = \begin{cases} 1, & t_i \leq t \leq t_{i+1} \\ 0, & otherwise \end{cases}$, $B_{i,k}(t) = \frac{t - t_i}{t_{i+k-1} - t_i} B_{i,k-1}(t) + \frac{t_{i+k} - t}{t_{i+k} - t_{i+1}} B_{i+1,k-1}(t)$.

If t in section $[t_j, t_{j+1}]$, $C(t)$ can be simplified as:

$$C(t) = \sum_{i=0}^{n} P_i B_{i,k}(t) = \sum_{i=j-k+1}^{j} P_i B_{i,k}(t) \tag{4}$$

Knot vectors of B-spline can be classified as clamped and unclamped[15]. For clamped knot vectors, knot vectors can be expressed as:

$$T_1 : \overbrace{0,0,\ldots 0}^{k}, t_k, \ldots, t_n, \overbrace{1,\ldots 1}^{k} \tag{5}$$

Unclamped knot vectors can be expressed as:

$$T_2 = \overbrace{0,0,\ldots 0}^{k}, t_k, \ldots, t_n, \overbrace{t_{n+1}, \ldots t_{n+k}}^{k}, \quad 1 \leq t_{n+1} \leq \ldots \leq t_{n+k-1} \leq t_{n+k} \tag{6}$$

Traditional active contour model is described as $v(s) = (x(s), y(s))$, where s is the arc length. Its energy can be written as:

$$E_{snake} = \int E(v(s))ds = \int E_{\text{int}}(v(s)) + E_{ext}(v(s))ds \tag{7}$$

Where E_{int} and E_{ext} are respectively the internal energy and the external energy. We can minimize the energy functional of Eq. (7) by the variational method.

The internal energy of traditional snake includes a first and second order derivative of the curve; respectively represent the flexibility and rigidity. But in the actual digital image processing, the curves is a discrete form. Thus the calculated first-order and second order derivative is often not continuous, curve smoothness are greatly affected. The B-spline has continuous first and second order derivatives in its left and right sides, and can use smaller control points to represent more data points. So B-spline needs not calculation the internal energy.

When using a parametric B-spline to represent the initial curve, and then the energy of the snake is minimized. In the B-spline representation, the snake is split into segments.

A B-snake is defined as follows:

$$C(s) = \sum_i b_i(s), \qquad where \qquad 0 \le s \le 1 \tag{8}$$

$b_i(s)$ is a B-spline. The external energy term on $C(s)$ is defined as $E(C(s))$. The total energy function of the B-snake can be defined as:

$$E_{B-snake} = \int_0^1 E(C(s))ds \tag{9}$$

Minimization of Eq. (9) will drive the B-snake to approach the object boundary in the image.

4 Boundary Extraction Model

4.1 Calculation of the Initial Curve

The mean-shift algorithm is a nonparametric statistical method for seeking the nearest mode of a point sample distribution. Mean shift is a simple iterative procedure that shifts each data point to the average of data points in its neighborhood. Given a set of data point x_i, the mean shift vector in a simple one-dimensional case can be expressed as[16]:

$$m(x) = \frac{\sum_{i=1}^{n} x_i g((x - x_i / h)^2)}{\sum_{i=1}^{n} g((x - x_i)^2)} - x \tag{10}$$

where x is an arbitrary point in the data space (it can even be one of the x_i points), h is a positive value called the analysis bandwidth and $g(u)$ is a special function

with bounded support; $g(u)$ is defined as the first derivative of another bounded-support function.

When $m(x)$ is applied to the original point, x, it results in anew position, x^1; this process can be repeated and an iterative procedure defined in this way:

$$x^{l+1} = m(x^l) + x^l \tag{11}$$

Here is the process of getting the control points of B-snake: (1) Given the initial control position; (2) Set every parameter of ant algorithms; (3) Calculate the probability P_{ij}^k that integrated x_j into x_i. If $P_{ij}^k \geq q_0$, x_j class will be integrated into x_i class; (4) Adjust the amount of permanence on the path; (5) Recalculate the initial position x_i'. $x_i' = \frac{1}{N}\sum_{k=1}^{N} x_k \ \ x_k \in class$ of x_i; (6) When iterative finished, the final control point is x_i'.

4.2 B-snake Iteration

Let take three B-spline curve as an example**.** Suppose a non-closure B-spline curve $C(S) = (m(s), n(s))$ with N data points and $K+1$ control points $\{Q_0, Q_1, ..., Q_n\}$, then it is composed by $K-1$ section curves. Ideally, when the B-snake's external energy is zero, the curve should be the true border, and this time the position and shape of the curve will not change. Therefore, the following formula makes the external forces zero can be defined as:

$$E_{ext} = \lambda[C(t) - C(t-1)] = \lambda\sum_{i=1}^{K-2} B_i(s)[Q_i(t) - Q_i(t-1)] = \lambda\sum_{i=1}^{K-2} B_i(s)\Delta Q_i(t) \tag{12}$$

where λ is a constant; t is the number of iterations. $\Delta Q(t)$ is the variation of control points in the t iterations. Using MMSE method to solution the Eq. (12), we can get the following matrix form:

$$\Delta Q(t) = v^{-1}[B^T B]^{-1} B^T E_{ext} \tag{13}$$

where E_{ext} is GVF(Gradient Vector Flow) force. Contrary to the traditional snake, B-snake has two advantages: few parameters and smoothness implicitly built into the model. Hence the resolution and convergence speed are greatly improved and no smoothness constraint is needed. GVF is selected here as the definition of external forces for B-snake. GVF is computed as a diffusion of the gradient vectors of binary edge map derived from the original planar curve. The resultant field has a large capture range and can force active contours into concave regions. In the GVF theory, the external force is replaced by the GVF vector spaces $V_{gvf} = (u(m,n), v(m,n))$.

$u(m,n)$ and $v(m,n)$ can be calculated by the following formula:

$$u_{t+1} = \mu\nabla^2 u_t - (u_t - f_m)(f_m^2 + f_n^2) \tag{14}$$

$$v_{t+1} = \mu\nabla^2 v_t - (v_t - f_m)(f_m^2 + f_n^2) \tag{15}$$

where f_m and f_n is the partial derivative of row and column direction respectively on the edge. t is the number of iterations.

The curve iterative process is described as follows:

(1) The initial curve is turn discrete N data points, and the initial control points are set to zero.
(2) Dividing the curve into $K-2$ section, and compute the knot parameters of each data point.
(3) Using the Eq. (13), we obtained a new $K+1$ control points.
(4) Calculate a new curve $C_{new}(s)$ by Eq. (3), and compute the GVF force E_{ext} of the curve.
(5) If the curve does not change, the iteration is stops. At this time $C_{new}(s)$ shall be the final result; otherwise go to Step (2).

5 Experiments

In order to examine the efficiency of our algorithm, we make a simulation on Pentium PC with 256MB RAM, 1.8GHz and running under Microsoft Windows 2000. The parameters of ant colony algorithm are: $\alpha = 3, \beta = 1, \rho = 0.3$. Figure 1(a) and 2(a) are the original image. Figure 1(b) and 2(b) are the B-snake method, which takes 50 iterations. The ant algorithm iteration process stops in 18 loops for figure 1, and 23 loops for figure 2. There are 21 points of initial zero level set curve for figure 1, and 34 ones for figure 2. The MMSE and control point insertion strategy has been involved after termination of search with the similar appearance and statistical information for landmark points. The final result of ours method are shown in figure 1(c) and 2(c). According to the results, it can be observed that our proposed method provides fine deformation for allowing the snake to accurately adapt to the desired object boundaries.

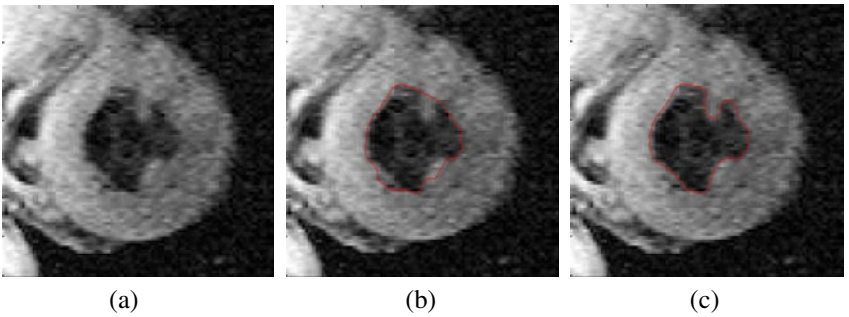

(a) (b) (c)

Fig. 1. (a) Original image (b) B-snake method (c) Ours

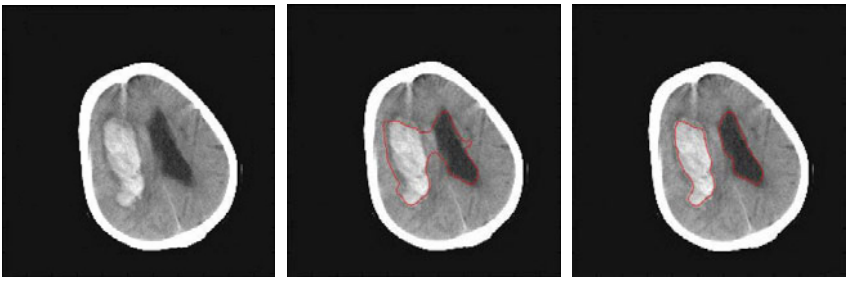

(a) (b) (c)

Fig. 2. (a) Original image (b) B-snake method (c) Ours

6 Conclusion

According to the results, it can be observed that our proposed method provides fine deformation for allowing the snake to accurately adapt to the desired object boundaries. According to the B-snake evolution theory and ant colony algorithm, a new image contour extraction algorithm is proposed. First, we use ant colony algorithm to get initial evolution curve. On this basis, the boundary is extraction by B-snake evolution. There is no manual intervention in the throughout extraction process. The calculated contour is close to the true edge. And the smoothness and accuracy of our algorithm is better than the traditional method. Experiments show that ours method can effectively lays out the fuzzy image and discontinuous marginal.

Acknowledgement

This work is supported by the National Natural Science Foundation of China (NSFC) under Grant No. 60773053 and 60970105; Natural Science Foundation of Shandong Provincial under Grant No. Y2007G22, ZR2009GQ005 and BS2009DX038; Science and technology projects of Shandong Province Education Department No. J08LJ06.

References

1. Kass, M., Witkin, A., Terzopoulos, D.: Snakes: Active contour models. International Journal of Computer Vision 1, 321–331 (1987)
2. McInerney, T., Terzopoulos, D.: A dynamic finite element surface model for segmentation and tracking in multidimensional medical images with application to cardiac 4D image analysis. Comput. Med. Imag. Graph. 19, 69–83 (1995)
3. Durikovic, R., Kaneda, K., Yamashita, H.: Dynamic contour: A texture approach and contour operations. Vis. Computer 11, 277–289 (1995)
4. Leymarie, F., Levine, M.D.: Tracking deformable objects in the plane using an active contour model. IEEE Transactions on Pattern Anal. Machine Intell. 15, 617–634 (1993)
5. Chan, T.F., Vese, L.A.: Active cContours without edges. IEEE Transactions on Image Processing 10, 266–277 (2001)

6. Li, J., Yang, X., Shi, P.F.: A fast level set approach to image segmentation based on mumford-shah model. Chinese Journal of Computers 25, 1175–1183 (2002)
7. Du, X.J., Tien, D.B.: A new model for image segmentation. IEEE Signal Processing Letters 15, 182–185 (2008)
8. Brigger, P., Hoeg, J., Unser, M.: B-spline snakes: A flexibletool for parametric contour detection. IEEE Transactions on Image Processin 9, 1484–1496 (2000)
9. Cheng, S.Y., Zhang, X.W., Jin, C.Y.: Finite element method based B-spline active contour. Journal of Information & Computational Science 1, 275–280 (2004)
10. Jerome, V., Hugues, B.C., Christophe, O.: Locally regularized smoothing B-Snake. EURASIP Journal on Advances in Signal Processing, 1–12 (2007)
11. Ye, B., Luo, D.S., Yu, Y.M., Wu, X.H.: Ultrasound image segmentation algorithm based on B-Snake. Science Technology and Engineering 8, 3007–3009 (2008)
12. Tauber, C., Batatia, H., Morin, G., Ayache, A.: Robust B-spline snakes for rltra-sound image segmentation. IEEE Computers in Cardiology 31, 325–328 (2004)
13. Wang, Y., Eam, K.T.: Object contour extraction using adaptive B-Snake model. Journal of Mathematical Imaging and Vision 24, 295–306 (2006)
14. Dorigo, M., Gambardella, L.M.: Ant colony system: A cooperative learning approach to the traveling saleman problem. IEEE Transactions on Evolutionary Computation 1, 53–56 (1997)
15. Hu, S.M., Tong, R.F., Ju, T., Sun, J.G.: Approximate merging of a pair of Bézier curves. Computer Aided Design 33, 125–136 (2001)
16. Cheng, Y.: Mean shift, mode seeking, and clustering. IEEE Transactions on Pattern Analysis and Machine Intelligence 17, 790–799 (1995)

An Improved Hidden Markov Model for Literature Metadata Extraction

Bin-Ge Cui and Xin Chen

College of Information Science and Engineering,
Shandong University of Science and Technology, 266510 Qingdao, China
cuibinge@yahoo.com.cn

Abstract. In this paper, we proposed an improved Hidden Markov Model (HMM) to extract metadata in the academic literatures. We have built a dataset including 458 literatures from the VLDB conferences, which contains the visual feature of text blocks. Our approach is based on the assumption that the text blocks in the same line have the same state (information type). The assumption is effective in more than 98% occasions. Thus, the state transition probability among the same states in the same line is much larger than that in different lines. According to this conclusion, we add one state transition matrix for HMM and modified the Viterbi algorithm. The experiments show that our extraction accuracy is superior to that of any existing works.

Keywords: HMM, Viterbi; Metadata Extraction, Text Block.

1 Introduction

With regard to the issue of metadata extraction, there have been three main approaches, i.e., heuristic approach [1], template-based approach [2], HMM-based approach [3]. Among these approaches, heuristic method has a low accuracy (only about 80%); template-based approach has a high accuracy (about 95%), but it requires manually writing template, thus it has poor adaptability; HMM-based approach has a medium accuracy (about 87%). It requires a large training sample to construct the transition matrix and emission matrix. However, to further improve the accuracy of HMM-based approach is very difficult.

In this paper, we proposed to add the text block visual features into the HMM. As we know, humans recognize the various parts of a PDF literature not just relying on the content of the text blocks, but also on their location, size, font and other information. In general, the text blocks in the same line is very likely to belong to the same information type, i.e., title, author, affiliation, etc. However, existing data sets do not provide the text block location information [4]. To solve this problem, we downloaded about 500 literatures from VLDB conferences and converted them into HTML format using an open-source utility [5]. The converted HTML document contains the text block location and other font information. Based on location information, we divide the state transition matrix of HMM into two transition matrixes. One matrix represents the state transition probability in the same line; the other represents the state transition probability in different lines. We modify Viterbi algorithm with the

D.-S. Huang et al. (Eds.): ICIC 2010, LNCS 6215, pp. 205–212, 2010.

two matrixes. Experimental results show that the exaction accuracy increases 4.5%, and the overall metadata exaction accuracy reaches 97.4%.

2 PDF File Conversion

2.1 HMM Profile

HMM is a double stochastic process, which can be defined as a five-tuple $\lambda=(X, O, \pi, A, B)$. X denotes a set of states, $X =\{S_1, S_2,..., S_N\}$, N denotes the state number, q_t denotes the state at time t; O denotes a set of observed symbols, $O= \{V_1, V_2, \ldots, V_M\}$, M denotes observed symbols number; π denotes the initial state distribution, $\pi = \{\pi_i\}$, $\pi_i = P\{q_1 = S_i\}$, $1 \le i \le N$; A denotes the state transition probability distribution, $A = \{a_{ij}\}$, $a_{ij} =\{q_{t+1} = s_j \mid q_t = s_i\}$, $1 \le i, j \le N$; B denotes the observation probability distribution of state j, $B = \{b_j(k)\}$, $b_j(k) = P\{O_t=V_k \mid q_t = S_j\}$, $1 \le j \le N$, $1 \le k \le M$. The detailed definitions can be found in reference [6].

2.2 Conversion of PDF Literature into HTML Files

In this section, we provide a sample PDF literature, which is shown in Figure 1. As we have seen, it contains title, authors, affiliations, addresses, emails, abstracts, etc. These items are called the literature metadata. They play an important role for the readers to understand a summary of the literature information. However, writing a program directly that can analyze the contents of PDF literature is very difficult. HTML documents are relatively easy to analyze and process. We utilize the open source Pdftohtml to convert PDF literatures into HTML format. The converted result is shown in Fig.2. From the 3rd line to the 25th line, each text block has its own location information.

3 HTML Document Pre-processing and Conversion

Many parts of the HTML document are not necessary for our follow-up metadata extraction, e.g., the font information, the background image, etc. Therefore, we need to pre-process the document collection, and then integrate all the HTML documents into an XML document. Pre-processing steps are as follows:

Step 1: Positioning the file pointer to the first position of a **DIV** appears;
Step 2: Loop read each line, and assign the content to the variable ***line***;
Step 3: Parse out the **top** and **left** property values in the **DIV** element's **style** attribute, and assign them to the variables ***vtop*** and ***vleft*** respectively;
Step 4: Parse out the text block content in the **span** element of ***line***, and reassign it to ***line***;
Step 5: Remove the ****, ****, ****, **, <a>, **, **
** tags and some other meaningless symbols from ***line***;

After the pre-processing steps, one DOM tree will be created, which contains the type (title, author, etc.) and location for all text blocks in all literatures.

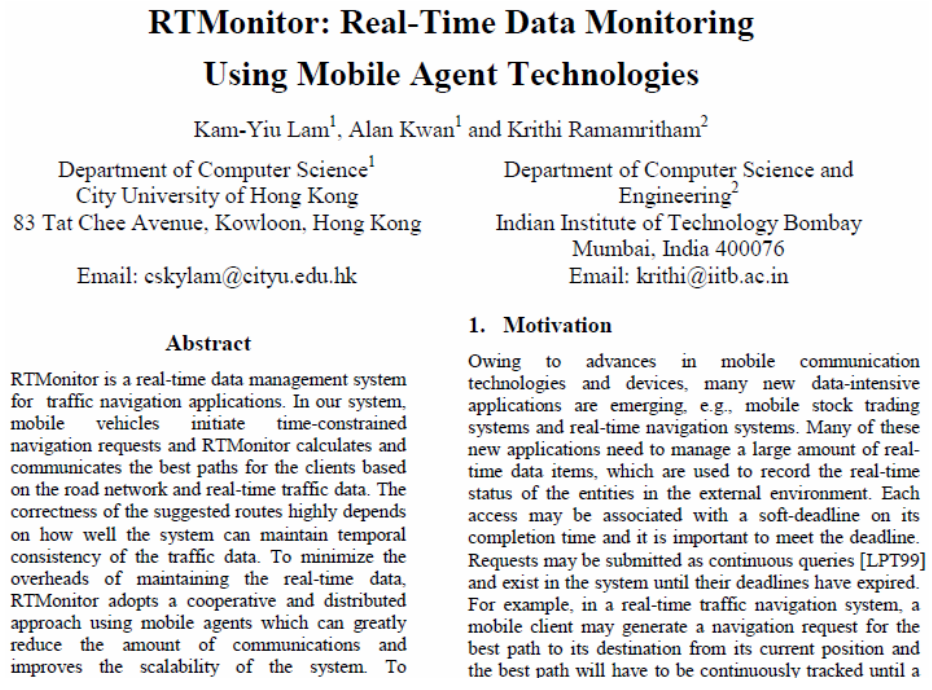

RTMonitor: Real-Time Data Monitoring Using Mobile Agent Technologies

Kam-Yiu Lam[1], Alan Kwan[1] and Krithi Ramamritham[2]

Department of Computer Science[1]
City University of Hong Kong
83 Tat Chee Avenue, Kowloon, Hong Kong

Email: cskylam@cityu.edu.hk

Department of Computer Science and Engineering[2]
Indian Institute of Technology Bombay
Mumbai, India 400076
Email: krithi@iitb.ac.in

Abstract

RTMonitor is a real-time data management system for traffic navigation applications. In our system, mobile vehicles initiate time-constrained navigation requests and RTMonitor calculates and communicates the best paths for the clients based on the road network and real-time traffic data. The correctness of the suggested routes highly depends on how well the system can maintain temporal consistency of the traffic data. To minimize the overheads of maintaining the real-time data, RTMonitor adopts a cooperative and distributed approach using mobile agents which can greatly reduce the amount of communications and improves the scalability of the system. To

1. Motivation

Owing to advances in mobile communication technologies and devices, many new data-intensive applications are emerging, e.g., mobile stock trading systems and real-time navigation systems. Many of these new applications need to manage a large amount of real-time data items, which are used to record the real-time status of the entities in the external environment. Each access may be associated with a soft-deadline on its completion time and it is important to meet the deadline. Requests may be submitted as continuous queries [LPT99] and exist in the system until their deadlines have expired. For example, in a real-time traffic navigation system, a mobile client may generate a navigation request for the best path to its destination from its current position and the best path will have to be continuously tracked until a

Fig. 1. One Typical PDF Literature

```
<BODY bgcolor="#A0A0A0" vlink="blue" link="blue">
<IMG width="892" height="1263" src="371001.png" alt="background image">
<DIV style="position:absolute;top:133;left:217"><nobr><span class="fc0"><b>RTMonitor: Real-Time Data Monitoring  </b></span></nobr></DIV>
<DIV style="position:absolute;top:172;left:259"><nobr><span class="fc0"><b>Using Mobile Agent Technologies </b></span></nobr></DIV>
<DIV style="position:absolute;top:219;left:252"><nobr><span class="fc1">Kam-Yiu Lam</span></nobr></DIV>
<DIV style="position:absolute;top:216;left:354"><nobr><span class="fc2">1</span></nobr></DIV>
<DIV style="position:absolute;top:219;left:360"><nobr><span class="fc1">, Alan Kwan</span></nobr></DIV>
<DIV style="position:absolute;top:216;left:450"><nobr><span class="fc2">1</span></nobr></DIV>
<DIV style="position:absolute;top:219;left:455"><nobr><span class="fc1"> and Krithi Ramamritham</span></nobr></DIV>
<DIV style="position:absolute;top:216;left:636"><nobr><span class="fc2">2</span></nobr></DIV>
<DIV style="position:absolute;top:219;left:642"><nobr><span class="fc1"> </span></nobr></DIV>
<DIV style="position:absolute;top:249;left:149"><nobr><span class="fc1">Department of Computer Science</span></nobr></DIV>
<DIV style="position:absolute;top:246;left:384"><nobr><span class="fc2">1</span></nobr></DIV>
<DIV style="position:absolute;top:249;left:390"><nobr><span class="fc1"> </span></nobr></DIV>
<DIV style="position:absolute;top:270;left:163"><nobr><span class="fc1">City University of Hong Kong </span></nobr></DIV>
<DIV style="position:absolute;top:290;left:115"><nobr><span class="fc1">83 Tat Chee Avenue, Kowloon, Hong Kong </span></nobr></DIV>
<DIV style="position:absolute;top:249;left:487"><nobr><span class="fc1">Department of Computer Science and </span></nobr></DIV>
<DIV style="position:absolute;top:270;left:574"><nobr><span class="fc1">Engineering</span></nobr></DIV>
<DIV style="position:absolute;top:267;left:659"><nobr><span class="fc2">2</span></nobr></DIV>
<DIV style="position:absolute;top:270;left:665"><nobr><span class="fc1"> </span></nobr></DIV>
<DIV style="position:absolute;top:290;left:481"><nobr><span class="fc1">Indian Institute of Technology Bombay </span></nobr></DIV>
<DIV style="position:absolute;top:310;left:539"><nobr><span class="fc1">Mumbai, India 400076  </span></nobr></DIV>
<DIV style="position:absolute;top:330;left:163"><nobr><span class="fc1">Email: cskylam@cityu.edu.hk </span></nobr></DIV>
<DIV style="position:absolute;top:330;left:536"><nobr><span class="fc1">Email: krithi@iitb.ac.in </span></nobr></DIV>
<DIV style="position:absolute;top:350;left:118"><nobr><span class="fc3"><b> </b></span></nobr></DIV>
<DIV style="position:absolute;top:381;left:230"><nobr><span class="fc3"><b>Abstract </b></span></nobr></DIV>
<DIV style="position:absolute;top:410;left:113"><nobr><span class="fc11">RTMonitor is a real-time data management system <br>for  traffic navigation applications. In
our system, <br>mobile vehicles initiate time-constrained <br>navigation requests and RTMonitor calculates and <br>communicates the best paths for the clients based
<br>on the road network and real-time traffic data. The <br>correctness of the suggested routes highly depends <br>on how well the system can maintain temporal
<br>consistency of the traffic data. To minimize the <br>overheads of maintaining the real-time data, <br>RTMonitor adopts a cooperative and distributed <br>approach
using mobile agents which can greatly <br>reduce the amount of communications and <br>improves the scalability of the system. To <br>minimize the space and message
overheads, we <br>have designed a two-level traffic graph scheme to <br>organize the real-time traffic data to support <br>navigation requests. In the framework, the
agents <br>use an Adaptive PUSH OR PULL (APoP) scheme <br>to maintain the temporal consistency of the traffic <br>data. Our experiments using synthetic traffic data
<br>show that RTMonitor can provide efficient support <br>to serve navigation requests in a timely fashion. <br>Although several agents may be needed to serve a
<br>request, the size of each agent is very small (only a <br>few kilobytes) and the resulting communication <br>and processing overheads for data monitoring can
<br>be maintained within a reasonable level. </span></nobr></DIV>
```

Fig. 2. Partial Content of newfile-1.html

4 HMM Definition and Parameters Estimation

HMM comprises of two sequences, i.e., state sequence and observation sequence. In the PDF metadata extraction, states correspond to the types of text blocks, observation symbols correspond to the content of text blocks. Metadata Extraction is performed by determining state sequence that was most likely to generate the observation sequence.

The header information of each literature includes title, author, affiliation, address, email, abstract, etc. Thus, the state set of HMM is defined as: X = {title, author,

affiliation, address, email, abstract, **final**}. If a text block is the last one in the literature, then we define that the next state of current state is the **final** state. The observation symbols contain all the words and numbers in all text blocks, which can be obtained through statistics of all training literatures. The initial state distribution contains the probabilities of each state that is in the first text block. The observation probability distribution contains the probabilities of each word appeared in each state.

In this paper, we have a text block as the smallest unit of information processing. Each text block corresponds to a unique state. Traditionally, HMM contains only one state transition matrix, which treats the whole literature as a data stream of text blocks. Although this approach retains the text blocks sequential relationship, it loses the text blocks location relationship. However, the location relationship is very important to determine the type of text block. For example, if we know a text block indicates the author, then the text blocks on the same line is very likely to indicate author too. In Fig. 2, the text blocks from the 5^{th} to the 11^{th} row are all authors, and they are on the same line. Of course, the punctuation, number and other symbols are not author names, but they are ancillary information that associated with the authors. For example, the superscript 1 denotes that the author in front of it belongs to the first affiliation.

Through the above analysis, we can draw the following conclusions: 1) in the same line, the transition probability between the same states is **much larger** than the normal one; 2) in the same line, the transition probability between different states is **smaller** than the normal one; 3) in different lines, the transition probability between the same states is **smaller** than the normal one; 4) in different lines, the transition probability between different states is **larger** than the normal one. These conclusions have been verified through the experiment results in Table 1, Table 2 and Table 3. The original state transition matrix A has been divided into two matrixes, A' A''.

Table 1. The Original State Transition Probability Matrix A

Current \ Next	title	author	affiliation	address	email	abstract	final
title	**0.3181**	0.6750	0.0000	0.0000	0.0000	0.0068	0.0000
author	0.0000	**0.4095**	0.5521	0.0000	0.0356	0.0026	0.0000
affiliation	0.0000	0.0146	**0.3532**	0.2775	0.3067	0.0464	0.0013
address	0.0000	0.0000	0.0092	**0.3588**	0.5797	0.0521	0.0000
email	0.0000	0.2528	0.1245	0.0000	**0.1566**	0.4452	0.0207
abstract	0.0026	0.0066	0.0000	0.0000	0.0000	**0.6071**	0.3834

Table 2. The State Transition Probability Matrix in the Same Line A'

Current \ Next	title	author	affiliation	address	email	abstract	final
title	**1.0000**	0.0000	0.0000	0.0000	0.0000	0.0000	0.0000
author	0.0000	**0.9903**	0.0048	0.0000	0.0000	0.0048	0.0000
affiliation	0.0000	0.0000	**0.8783**	0.0684	0.0532	0.0000	0.0000
address	0.0000	0.0000	0.0731	**0.8536**	0.0731	0.0000	0.0000
email	0.0000	0.0000	0.0000	0.0138	**0.9861**	0.0000	0.0000
abstract	0.0000	0.0000	0.0000	0.0000	0.0000	**1.0000**	0.0000

Table 3. The State Transition Probability Matrix in Different Lines A''

Current \ Next	title	author	affiliation	address	email	abstract	final
title	**0. 3055**	0.6944	0.0000	0.0000	0.0000	0.0000	0.0000
author	0.0000	**0.0186**	0.9285	0.0000	0.0527	0.0000	0.0000
affiliation	0.0000	0.0048	**0.2396**	0.3374	0.3300	0.0855	0.0024
address	0.0000	0.0000	0.0139	**0.3162**	0.5860	0.0837	0.0000
email	0.0000	0.0526	0.1085	0.0000	**0.0296**	0.7894	0.0197
abstract	0. 0000	0.0027	0.0000	0.0000	0.0000	**0.5931**	0.4041

Now that whether is in the same line has great impact for the transition probability between states, how can we know whether the two text blocks are in the same line? We proposed a simple way to solve it. Firstly, all text blocks are aggregated into multiple groups. In each group, the difference between the max **top** value and the min **top** value should be less than a threshold. This approach is basically correct. The recommended threshold value can be 6-10.

5 Viterbi Algorithm Improvement and Enhancement

Viterbi algorithm uses dynamic programming technology. Firstly, we briefly introduce how Viterbi algorithm finds the "best" state sequence.

We define $\delta_t(i) = \max_{q_1 q_2 \cdots q_{t-1}} P[q_1 q_2 ... q_{t-1}, q_t = i, O_1, O_2, ... O_t \mid \lambda]$

What we try to find is the state sequence that corresponds to the maximum $\delta_t(i)$ at time t. The steps are as follows:

1) Initialization

$\delta_t(i) = \pi_i b_i(O_1),\ 1 \le i \le N; \quad \phi_1(i) = 0,\ 1 \le i \le N;$ (1)

2) Recursive

$$\delta_t(j) = \max_{1 \le i \le n}[\delta_{t-1}(i) a_{ij}] b_j(O_t),\ 2 \le t \le T;\ 1 \le j \le N; \quad (2)$$

$$\phi_t(j) = \arg\max_{1 \le i \le n}[\delta_{t-1}(i) a_{ij}],\ 2 \le t \le T;\ 1 \le j \le N; \quad (3)$$

3) Terminate

$$P^* = \max_{1 \le i \le N}[\delta_t(i)]; \qquad q_t^* = \arg\max_{1 \le i \le N}[\delta_t(i)] \quad (4)$$

4) Find the S sequence

$$q_t^* = \phi_{t+1}(q^*_{t+1}), \qquad t = T-1, T-2 \ldots, 1 \quad (5)$$

We can improve the Viterbi algorithm by adjusting two factors, i.e., B and A. In this paper, the emission probability of each text block is the sum of that for all words in the text block. Assume that the block sequence is: $O = O_1 O_2 \ldots O_T$, and the length of the t^{th} block is K (i.e., it contains K words), $O_t = O_{t1}\ O_{t2}\ \ldots O_{tK}$. The probability that state j emits the t^{th} block is:

$$b_j(O_t) = \sum_{k=1}^{K} b_j(O_{tk}) \tag{6}$$

We found that some $b_j(O_t) = 0$, which lead to the extraction accuracy decrease remarkably. In order to avoid this problem, we assign a very small value for them (about one ten-thousandth), and the accuracy return normal level. Similarly, for the transition probability $a_{ij} = 0$, we also assign a very small value to them (about one thousandth).

In the formula (2) and (3), a_{ij} denotes the transition probability from state i to state j, which did not concern the location information of text blocks. Based on the discussion in section 4, we can modify the formula (2) as follows:

$$\delta_t(j) = \begin{cases} \max\limits_{1\le i\le n}[\delta_{t-1}(i)a'_{ij}]b_j(O_t) & line(O_t) = line(O_{t-1}) \ \ 2\le t\le T \\ \max\limits_{1\le i\le n}[\delta_{t-1}(i)a''_{ij}]b_j(O_t) & line(O_t) \ne line(O_{t-1}) \ \ 1\le j\le N \end{cases} \tag{7}$$

The function **line** returns the line number of the text block. From the formula (7) we can see that, if the two adjacent text blocks belong to the same line/group, then the matrix A' should be used; otherwise, the matrix A'' should be used.

6 Experiments and Analysis

Because there are no text blocks location information in the existing dataset, we downloaded and compiled more than 500 PDF literatures from VLDB conferences manually. However, some literatures became garbled after treatment by the tool pdftohtml-0.39. At last, we collected 458 valid PDF literatures. These literatures are divided into two groups: the former 300 as the training dataset, and the latter 158 as the test dataset. We evaluate the algorithm performance using the precision and recall, which are defined as follows:

Precision for each state is defined as the number of text blocks with the correct tag for the state divided by the total number of text blocks with the machine tag for the state.

Recall is defined as the number of text blocks with the correct tag for the state divided by the total number of text blocks with the manual tag for the state.

We did a total of three experiments. In the first experiment, we use the text block based way to extract metadata. The precision and recall are shown in the 2nd and 3rd columns of Table 4. The text block based way is superior to the word based way, which has been verified in reference [7], so we did not do that experiment again. In the second experiment, we considered the text block location information, and computed the new state transition matrixes as shown in Table 2 and Table 3. By using the two matrixes and the formula (7), the accuracy of Viterbi algorithm on average is increased about 4.5%. We can see that title precision and recall, author precision and recall, affiliation precision and recall, address precision, email recall and abstract precision are all increased remarkably.

Table 4. The Precision and Recall for Text Block Location Based Way

Accuracy State	Text Block Based Way		Location Based Way	
	Precision	Recall	Precision	Recall
title	0.975207	0.925490	**1.000000**	**1.000000**
author	0.894488	0.948247	**0.993266**	**0.984975**
affiliation	0.869469	0.825630	**0.930526**	**0.928571**
address	0.738739	0.858639	**0.943182**	0.869110
email	0.933993	0.792717	0.941333	**0.988796**
abstract	0.961538	0.992063	**0.990777**	0.994709

7 Related Works

Existing literature metadata extraction can be divided into two categories: extract metadata from the paper list on a Web page; extract metadata from a lot of PDF literatures. They are usually concerned with different metadata items. The former mainly extract the title, author, journal, year, conference, column, issue, page, etc; the latter mainly extract the title, author, affiliation, address, email, abstract, keyword, etc. Both of them can be extracted using HMM. Most HMMs are constructed automatically [8, 9]. For example, Seymore [9] proposed to extract the title, author, keyword and other metadata for each literature using HMM in Cora [4], which has an average accuracy of up to 92.9%.

In order to improve the accuracy of HMM-based metadata extraction algorithm, many people attempted to take full advantage of the feature of the text. Ling Zhang [10] proposed a HMM structure learning method based on symbol feature extraction, in which each feature corresponds to a state. She also modified Viterbi algorithm through add a type parameter to each state. The extraction accuracy of her algorithm is superior to that of [9]. Ming Zhang et al. [11] proposed a hybrid statistic model for metadata extraction: SVM + BiHMM. The BiHMM model modifies the HMM model with both Bigram sequential relation and position information of words, by means of distinguishing the beginning emitting probability from the inner emitting probability. The average extraction accuracy of their model can reach 96.5%.As a result of the different datasets, the accuracy of our algorithm cannot be compared directly to other algorithms. However, the practical application of our algorithm has achieved good results, which has an average accuracy of up to 97.4%.

8 Conclusions

In this paper, we proposed a new PDF academic literatures metadata extraction approach. It used the location information of text blocks and modified the definition of HMM by adding one state transition matrix. The two matrixes reflect such fact that the transition probability between the same states in the same line is far greater than that in different lines. From the above experiments we can see that the accuracy for the improved Viterbi algorithm is increased greatly. We also found that the number or symbol superscript is useful for the metadata analysis. It can tell us which affiliation that each author belongs to. Next, we will be in this area for further research.

Acknowledgments

This Work is Supported by Project of "Taishan Scholar" Funded by Government of Shandong Province and Foundation for Outstanding Young Scientist in Shandong Province.

References

1. Giles, C.L., Kurt, D.B., Steve, L.C.: An automatic citation indexing system. In: Digital Libraries 1998 (1998)
2. Ying, D., Gobinda, C., Schubert, F.: Template mining for the extraction of citation from digital documents. In: Proc. Second Asian Digital Library Conference, Taiwan, pp. 47–62 (1999)
3. Dayne, F., Andrew, K.M.: Information extraction with HMMs and shrinkage. In: AAAI 1999 (1999)
4. Cora Dataset (2003), http://www.cs.umass.edu/~mccallum/data/cora-hmm.tar.gz
5. pdftohtml (2006), http://sourceforge.net/projects/pdftohtml/files/
6. Du, L.: Hidden markov model (HMM), http://math.sjtu.edu.cn/teacher/wuyk/HMM-DL.pdf
7. Cui, B.: Scientific literature metadata extraction based on HMM. In: Luo, Y. (ed.) Cooperative Design, Visualization, and Engineering. LNCS, vol. 5738, pp. 64–68. Springer, Heidelberg (2009)
8. Zhang, N.R.: Hidden markov models for information extraction (June 2001)
9. Seymore, K., McCallum, A., Ronal, R.: Learning hidden markov model structure for information extraction. In: AAAI 1999 Workshop on Machine Learning for Information Extraction (1999)
10. Zhang, L.: Research and application of web information extraction technology. Master's thesis. Chinese Academy of Sciences (2003)
11. Zhang, M., Yin, P., Deng, Z.H., Yang, D.Q.: SVM+BiHMM: A hybrid statistic model for metadata extraction. Journal of Software 19, 358–368 (2008)

Discriminative Training of Subspace Gaussian Mixture Model for Pattern Classification

Xiao-Hua Liu and Cheng-Lin Liu

National Laboratory of Pattern Recognition (NLPR),
Institute of Automation, Chinese Academy of Sciences
95 Zhongguancun East Road, Beijing 100190, P.R. China
{xhliu,liucl}@nlpr.ia.ac.cn

Abstract. The Gaussian mixture model (GMM) has been widely used in pattern recognition problems for clustering and probability density estimation. For pattern classification, however, the GMM has to consider two issues: model structure in high-dimensional space and discriminative training for optimizing the decision boundary. In this paper, we propose a classification method using subspace GMM density model and discriminative training. During discriminative training under the minimum classification error (MCE) criterion, both the GMM parameters and the subspace parameters are optimized discriminatively. Our experimental results on the MNIST handwritten digit data and UCI datasets demonstrate the superior classification performance of the proposed method.

Keywords: Subspace GMM, EM algorithm, Discriminative training, MCE.

1 Introduction

The Gaussian mixture model (GMM) is widely used in pattern recognition problems for clustering, probability density estimation and classification. Many methods have been proposed for GMM parameter estimation and model selection (e.g. [1][2]). Despite the capability of GMM to approximate arbitrary distributions, the precise density estimation requires a large number of training samples, especially in high-dimensional space (say, dimensionality over 20). Researchers have proposed structure-constrained GMMs for high-dimensional data, such as diagonal covariance, tied covariance, semi-tied covariance [3], and GMM in subspace [4-5]. On the other hand, the GMM is a generative model, with parameters estimated for each class independently by maximum likelihood (ML) using the expectation-maximization (EM) algorithm [1]. Without considering decision boundaries in training, the obtained models do not necessarily give high classification accuracy. Discriminative training methods, typically using the maximum mutual information (MMI) [6] or minimum classification error (MCE) criterion [7], have been proposed to optimize the GMM parameters aiming for classification.

For sequence recognition problems like speech recognition, the GMM is commonly used to model the states of hidden Markov models (HMMs). Discriminative training has been applied to GMMs with diagonal covariance [8] and semi-tied covariance [9].

D.-S. Huang et al. (Eds.): ICIC 2010, LNCS 6215, pp. 213–221, 2010.

GMM with semi-tied covariance is also called orthogonal GMM [10], where an orthogonal transformation matrix is shared by multiple diagonal Gaussian components. With diagonal covariance, discriminative training criteria MMI and MCE can be easily optimized by gradient descent. Batch-mode updating algorithms are also available for MMI (called extended Baum-Welch algorithm [11]) and MCE training [12], and they can learn full covariance matrices.

Dimensionality reduction can help improve the classification performance of GMM in high-dimensional space. The subspace GMM of Moghaddam and Pentland [4] formulates the density function as the combination of a GMM in principal feature subspace and a spherical Gaussian in complement subspace. It utilizes the flexibility of density approximation of GMM and exploits the information in complement subspace, and has shown efficiency in classification [13].

In this paper, we propose a classification method using subspace GMM density model and discriminative training based on MCE. The discriminative training of subspace GMM has not been reported before, and in discriminative training of semi-tied GMMs (orthogonal GMMs), the transformation matrix was not trained discriminatively [9][10][14]. A previous method, called discriminative learning quadratic dsicriminant function (DLQDF) [15], optimizes the Gaussian parameters and subspace parameters discriminatively for single Gaussian. Our method optimizes both the GMM parameters and the subspace parameters discriminatively, and is suitable for classification in cases of non-Gaussian distributions. As to the training criteria, we choose the MCE criterion because it is flexible for various discriminant functions and is easier to implement by gradient descent. We can alternatively use the MMI criterion and can expect similar performance.

We have evaluated the proposed method on multitude of high-dimensional datasets, including the MNIST handwritten digit data [16] and some datasets from the UCI Machine Learning Repository [17]. Our experimental results show that the discriminative training of subspace GMMs yields significantly higher classification accuracies than ML estimation, and the joint training of subspace parameters outperforms that of training GMM parameters only. Our results are also superior to a recent discriminative training method for orthogonal GMM [14].

The rest of this paper is organized as follows. Section 2 briefly describes the subspace Gaussian mixture density model. Section 3 describes the discriminative training method. Section 4 presents our experimental results and Section 5 offers concluding remarks.

2 Subspace Gaussian Mixture Model

Denote a pattern as a point (vector) $\mathbf{x}$ in d-dimensional feature space. The subspace GMM density function of [4] combines a GMM in the principal subspace and a spherical Gaussian in complement subspace:

$$p(\mathbf{x} \mid \omega) = p_F(\mathbf{x} \mid \omega)\, p_{\bar{F}}(\mathbf{x} \mid \omega), \tag{1}$$

where $p_F(\mathbf{x} \mid \omega)$ is the GMM in principal subspace spanned by k principal eigenvectors $\mathbf{A} = [\phi_1, \ldots, \phi_k]$ of $\mathbf{x}$ space centered at $\mathbf{m}_x$:

$$p_F(\mathbf{x} \mid \omega) = \sum_{j=1}^{M} \pi_j p_j(\mathbf{y} \mid \boldsymbol{\theta}_j), \tag{2}$$

where $\mathbf{y} = \mathbf{A}^T(\mathbf{x} - \mathbf{m}_x)$ and $p_j(\mathbf{y} \mid \boldsymbol{\theta}_j)$ is a component Gaussian with parameters $\boldsymbol{\theta}_j = \{\mu_j, \Sigma_j\}$ in *k*-dimensional subspace. $p_{\bar{F}}(\mathbf{x} \mid \omega)$ is a spherical Gaussian in *d-k* dimensional complement subspace:

$$p_{\bar{F}}(\mathbf{x} \mid \omega) = \frac{1}{(2\pi\rho)^{(d-k)/2}} \exp\left(-\frac{\varepsilon^2(\mathbf{x})}{2\rho}\right), \tag{3}$$

where $\varepsilon^2(\mathbf{x}) = \| \mathbf{x} - \mathbf{m}_x \|^2 - \| \mathbf{y} \|^2$, and $\rho = \frac{1}{d-k} \sum_{l=k+1}^{d} \lambda_l$ is the average of the eigenvalues in complementary subspace [4].

We use the ML estimate of subspace GMMs (one for each class) as the initialization of discriminative training [5]. The principal subspace of each class is spanned by the *k* largest eigenvectors of the class covariance matrix, and the GMM parameters in the principal subspace are estimated by the EM algorithm. The classification performance is rather sensitive to the value of ρ. We select a common value of ρ by cross-validation for high classification accuracy [5].

3 Discriminative Training of Subspace GMM

The subspace GMM density model has been shown effective for pattern classification, but the parameters are estimated in generative learning: the training data of each class is used to estimate the class parameters independently. By discriminative training to optimize the decision boundary, the classification performance can be further improved.

3.1 MCE Training

In the MCE criterion, the misclassification loss of each training sample is approximated from the difference of discriminant functions between the genuine class and competing classes. The empirical loss is minimized by stochastic gradient descent to optimize the classifier parameters.

For classifiers based on probability density models and reasonably assumed equal prior probabilities, the discriminant function is $g_i(\mathbf{x}) = \log p(\mathbf{x} \mid \omega_i)$. In MCE training [7], the misclassification measure of a sample $\mathbf{x}$ from labeled class ω_c is

$$h_c(\mathbf{x}) = -g_c(\mathbf{x}) + g_r(\mathbf{x}), \tag{4}$$

where $g_r(\mathbf{x}) = \max_{i \neq c} g_i(\mathbf{x})$ is the discriminant function of the most competing class (rival class). It is obvious that $h_c(\mathbf{x})>0$ indicates misclassification while $h_c(\mathbf{x})<0$ indicates correct classification. The misclassification measure is transformed to loss by the sigmoidal function:

$$L_c(\mathbf{x}) = \sigma(\xi h_c) = \frac{1}{1 + \exp(-\xi h_c)}, \tag{5}$$

where ξ is a constant to control the hardness of sigmoidal nonlinearity.

On a training dataset $\{(\mathbf{x}^n, c^n) | n=1,\ldots,N\}$, the empirical loss is

$$\Gamma = \frac{1}{N}\sum_{n+1}^{N}\sum_{i=1}^{C} L_i(\mathbf{x}^n) I(\mathbf{x}^n \in \omega_i), \tag{6}$$

where $I(\cdot)$ is the indicator function. The aim of parameter adjustment is to minimize the objective Γ: $\Theta^* = \arg\min \Gamma(\Theta)$. By stochastic gradient descent, the parameters are updated iteratively on each input training sample:

$$\theta_i(t+1) = \theta_i(t) - \gamma(t)\frac{\partial L_i(\mathbf{x})}{\partial \theta_i}, \tag{7}$$

where θ_i denotes a parameter of class ω_i. In the case of density based discriminant functions, the parameters are class-modular. Since $L_c(\mathbf{x})$ only involves the parameters of two classes: genuine class ω_c and rival class ω_r, only the parameters of two classes are updated on an input training sample:

$$\begin{cases} \dfrac{\partial L_c(\mathbf{x})}{\partial \theta_c} = -\xi L_c(1-L_c)\dfrac{\partial g_c(\mathbf{x})}{\partial \theta_c}, \\ \dfrac{\partial L_c(\mathbf{x})}{\partial \theta_r} = \xi L_c(1-L_c)\dfrac{\partial g_r(\mathbf{x})}{\partial \theta_r}. \end{cases} \tag{8}$$

3.2 MCE Training for Subspace GMMs

For classification using subspace GMM density models, we use diagonal covariance matrices for the Gaussian components for the sake of simple computation in training. The diagonal GMM in principal subspace is actually a semi-tied GMM.

For multi-class classification, each class ω_i has a principal subspace specified by class-specific mean $\mathbf{m}_{xi}$ and principal eigenvectors $\mathbf{A}_i = [\phi_{i1},\ldots,\phi_{ik}]$, and the class-specific subspace projection (k-dimensional vector) is $\mathbf{y}_i = \mathbf{A}_i^T(\mathbf{x}-\mathbf{m}_{xi})$. Inserting the density function of Eq. (1), the class discriminant function is

$$g_i(\mathbf{x}) = \log\left(\sum_{j=1}^{M}\pi_{ij}p_{ij}(\mathbf{x}\,|\,\boldsymbol{\theta}_{ij})\right) - \frac{\varepsilon_i^2(\mathbf{x})}{2\rho_i} - \frac{d-k}{2}\log\rho_i, \tag{9}$$

where a constant term has been omitted. $\varepsilon_i^2(\mathbf{x})$ is the projection residual in the principal subspace of ω_i: $\varepsilon_i^2(\mathbf{x}) = \|\mathbf{x}-\mathbf{m}_{xi}\|^2 - \|\mathbf{y}_i\|^2$. The Gaussian component p_{ij} in class-specific principal subspace, with diagonal covariance $\Sigma_{yij} = \Lambda_{ij} = diag[\lambda_{ij1},\ldots,\lambda_{ijk}]$ and mean $\mu_{yij} = [\mu_{ij1},\ldots,\mu_{ijk}]^T$, is

$$p_{ij}(\mathbf{x}\,|\,\boldsymbol{\theta}_{ij}) = p_{ij}(\mathbf{y}_i\,|\,\boldsymbol{\theta}_{ij}) = \frac{1}{(2\pi)^{k/2}(\prod_{l=1}^{k}\lambda_{ijl})^{1/2}}\exp\left[-\frac{1}{2}\sum_{l=1}^{k}\frac{(y_{il}-\mu_{ijl})^2}{\lambda_{ijl}}\right]. \tag{10}$$

To preserve the positivity of parameters (ρ_i, π_{ij}, λ_{ijl}) in gradient descent learning, they are transformed: $(\rho_i, \pi_{ij}, \lambda_{ijl}) = (\exp(\delta_i), \exp(\alpha_{ij}), \exp(\nu_{ijl}))$, and the parameters

(δ_i, π_{ij}, v_{ijl}) are updated instead of (ρ_i, π_{ij}, λ_{ijl}). After each updating, the values of (ρ_i, π_{ij}, λ_{ijl}) are resumed, and further, the mixing weights π_{ij} are normalized to unity sum for each class.

For gradient descent learning by Eqs. (7) and (8), we can get the derivative of $g_i(\mathbf{x})$ with respect to parameters (δ_i, π_{ij}, v_{ijl}, μ_{ijl},m_{ip}, φ_{ilp}) as below:

$$
\begin{cases}
\dfrac{\partial g_i(\mathbf{x})}{\partial \delta_i} = \dfrac{\varepsilon_i^2(\mathbf{x})}{2} e^{-\delta_i} - \dfrac{d-k}{2}, \qquad i = 1,\ldots,C, \\
\dfrac{\partial g_i(\mathbf{x})}{\partial \alpha_{ij}} = \dfrac{p_{ij}(\mathbf{x}\,|\,\boldsymbol{\theta}_i)}{p_F(\mathbf{x}\,|\,\omega_i)} e^{\alpha_{ij}}, \quad i = 1,\ldots,C,\ j = 1,\ldots,M, \\
\dfrac{\partial g_i(\mathbf{x})}{\partial \mu_{ijl}} = \dfrac{p_{ij}(\mathbf{x}\,|\,\boldsymbol{\theta}_i)}{p_F(\mathbf{x}\,|\,\omega_i)} e^{\alpha_{ij}} e^{-v_{ijl}} (y_{il} - \mu_{ijl}), \quad i = 1,\ldots,C,\ j = 1,\ldots,M,\ l = 1,\ldots,k, \\
\dfrac{\partial g_i(\mathbf{x})}{\partial v_{ijl}} = \dfrac{p_{ij}(\mathbf{x}\,|\,\boldsymbol{\theta}_i)}{p_F(\mathbf{x}\,|\,\omega_i)} e^{\alpha_{ij}} [\frac{1}{2} e^{-v_{ijl}} (y_{il} - \mu_{ijl})^2 - \frac{1}{2}], \\
\qquad\qquad i = 1,\ldots,C,\ j = 1,\ldots,M,\ l = 1,\ldots,k, \\
\dfrac{\partial g_i(\mathbf{x})}{\partial m_{ip}} = \dfrac{\sum_{j=1}^{M} p_{ij}(\mathbf{x}\,|\,\boldsymbol{\theta}_i) e^{\alpha_{ij}} [\sum_{l=1}^{k} e^{-v_{ijl}} (y_{il} - \mu_{ijl}) \phi_{ilp}]}{p_F(\mathbf{x}\,|\,\omega_i)} + [e^{-\delta_i}(x_p - m_{ip}) - \sum_{l=1}^{k} e^{-\delta_i} y_{il} \phi_{ilp}], \\
\qquad\qquad i = 1,\ldots,C,\ p = 1,\ldots,d, \\
\dfrac{\partial g_i(\mathbf{x})}{\partial \phi_{ilp}} = \dfrac{\sum_{j=1}^{M} p_{ij}(\mathbf{x}\,|\,\boldsymbol{\theta}_i) e^{\alpha_{ij}} [-e^{-v_{ijl}} (y_{il} - \mu_{ijl})(x_p - m_{ip})]}{p_F(\mathbf{x}\,|\,\omega_i)} + e^{-\delta_i} y_{il} (x_p - m_{ip}), \\
\qquad\qquad i = 1,\ldots,C, l = 1,\ldots,k,\ p = 1,\ldots,d.
\end{cases}
\tag{11}
$$

Inserting these derivatives into Eqs. (7) and (8), we can update the parameters iteratively in stochastic gradient descent.

In implementation, the learning rate $\gamma(t)$ is initially set as a small value, and it progressively decreases during training. On the contrary, the hardness control parameter ξ increases in training such that the loss function (9) gradually approaches the 0-1 loss (classification error rate). Similar to [15], the initial value of ξ is set as the average of $1/h_c$.

According to the Newton's method, the optimal learning rate is inversely proportional to the eigenvalues of the Hessian matrix, or simply the second-order derivatives when assuming diagonal Hessian. Inspired by this relationship, we use three learning rates for three groups of parameters: γ_1 for $\{\delta_i, \pi_{ij}, v_{ijl}\}$, γ_2 for $\{\mu_{ijl}, m_{ip}\}$ and γ_3 for $\{\varphi_{ilp}\}$. Similar to [15], we set $\gamma_1=\gamma_3$ and $\gamma_2=var\cdot\gamma_1$ (*var* is the average within-class variance estimated on training samples).

3.3 Regularization and Ortho-normalization

Discriminative learning may lead to overfitting when the classifier model is complicated and the training dataset is relatively small. Regularization to confine the parameter change in learning is helpful to improve the generalization performance. One

way of regularization is done by adding to the empirical loss a term proportional to the log-likelihood of density:

$$\Gamma_1 = \frac{1}{N}\sum_{n=1}^{N}[L_c(\mathbf{x}^n) - \beta \cdot g_c(\mathbf{x}^n)], \tag{12}$$

Where β is the regularization coefficient. Because the maximization of sum of $g_c(\mathbf{x}^n)$ leads to ML estimate, this regularization effects to attract the parameters in the vicinity of ML estimate during discriminative training. This has been shown effective in discriminative learning quadratic discriminate function (DLQDF) [15]. Similarly, the value of β is set to be inversely proportional to the average G of discriminant function $g_i(\mathbf{x})$: $\beta = \hat{\beta}/G$, where $\hat{\beta}$ is a moderate number between 0 and 1.

In discriminative training, the ortho-normalization of eigenvectors is also influential [15][18]. Especially, if eigenvector normalization is not imposed, the empirical loss can be decreased by simply shrinking the eigenvectors. We perform ortho-normalization on the eigenvectors of one class whenever they are updated during MCE training. Ortho-normalization is performed by first normalizing the first eigenvector and then for each following eigenvector, subtracting its projection on the preceding eigenvectors and normalizing the difference vector.

4 Experiment Results

To evaluate the performance of the proposed method, we carried out experiments of density-based classification on the MNIST handwritten digit dataset and some datasets from the UCI Machine Learning Repository.

4.1 Experiments on MNIST Dataset

The MNIST dataset contains 60,000 training samples and 10,000 test samples. In order to compare our results with those of discriminative OGMM [14], we use the same feature data, 8-direction gradient feature (200D). In our experiments, the dimensionality k of the principal subspace ranges from 10 to 40 incremented by 10, and the number of Gaussian components ranges from 5 to 30 incremented by 5. Note that the number of Gaussians is much fewer than that used in a previous work of MMI training of diagonal GMMs [8].

Figure 1 shows the classification accuracies on test data using the subspace GMM classifier. M1 denotes the classifier with parameters estimated by ML, M2 denotes the version trained by MCE without regularization and M3 denotes the version of MCE training with regularization. We can see that MCE training improves the classification accuracy significantly compared to the classifier of ML estimate. Comparing the results of MCE training with and without regularization, the favor of regularization is justified.

It is seen in Figure 1 that when the dimensionality of principal subspace increases from k=10, the accuracies of three versions of subspace GMM classifier increases as well, but the accuracy increase from k=30 to k=40 is very small. The highest accuracy of M2 (MCE without regularization) is 99.45% (k=40 and M=25), and the highest

accuracy of M3 (MCE with regularization) is 99.49% (k=40 and M=15). The classification accuracy turns out to be rather stable against the model order (number of Gaussian components).

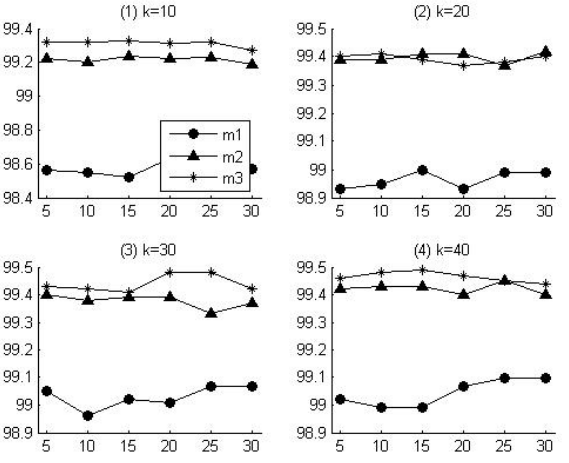

Fig. 1. Test accuracies on the MNIST dataset. X-axis denotes the number of Gaussian components, y-axis denotes the classification accuracies (%), and k denotes the dimensionality of principal subspace.

In [14] the OGMM also adopts diagonal covariance and eigenvalue decomposition. But it totally abandons the information of complementary subspace. In its discriminative learning, the transformation matrix was not optimized. [14] reported a best error rate 0.69%, while the best error rate of our method is 0.55%. It is obvious that our discriminative subspace GMM classifier is superior to discriminative OGMM. This result is also better than the result of DLQDF reported in [19], 0.71% error rate.

4.2 Experiments on UCI Datasets

To further illuminate the effectiveness of our method, we compared the proposed method with DLQDF in experiments of classification on 10 datasets from the UCI Repository. DLQDF is a discriminative learning method based on MCE to optimize the Gaussian parameters and subspace parameters, but it only uses a single Gaussian to estimate the class density. More details of DLQDF can be found in [15].

In the UCI Repository, some of the datasets have been divided into standard training and test sets before. For the other datasets, we randomly picked half data of each class for training and the remaining for testing. The specifications of the selected UCI datasets and the classification results on them are shown in Table 1. We simply fixed the number of Gaussian components as 4 without attempt to optimize the model order, but we can see that this still yield superior classification performance compared to the DLQDF. Both the subspace GMM classifier and the DLQDF are given three versions (M1: ML estimate; M2: MCE without regularization; M3: MCE with regularization).

Table 1. Specifications of UCI datasets and classification accuracies (%). #d: number of features; #c: number of classes; #n: number of samples; #k: dimensionality of principal subspace.

					Subspace GMM			DLQDF		
	#d	#c	*#n*	*#k*	M1	M2	M3	M1	M2	M3
Pendigits	16	10	10,992	10	97.5	98.0	**98.7**	96.1	97.8	**98.7**
Vehicle	18	4	846	10	69.7	72.3	**72.8**	67.1	69.5	**73.0**
Segment	19	7	2,210	10	90.1	**94.8**	93.8	89.3	91.1	**93.9**
Waveform21	21	3	5,000	10	85.0	85.6	**85.9**	85.4	**86.0**	85.6
Satimage	36	6	6,435	20	87.8	**90.3**	90.1	85.9	88.2	**89.7**
Waveform40	40	3	5,000	20	85.1	**85.3**	84.3	**85.0**	84.7	84.0
Mfeat-zer	47	10	2,000	20	84.7	**84.9**	84.6	**83.5**	80.1	80.5
Optdigits	64	10	5,620	20	98.4	**98.9**	**98.9**	98.2	**98.7**	**98.7**
Mfeat-kar	64	10	2,000	10	98.0	**98.5**	98.4	98.0	**98.3**	98.2
Mfeat-fou	76	10	2,000	20	83.3	**84.2**	83.9	**83.3**	82.5	82.5

From the results in Table 1, we can see that the two versions of discriminative subspace GMM classifier mostly give comparably high accuracies, and the accuracies are mostly higher than those of the ML version. Comparing the accuracies of subspace GMM classifier and DLQDF, the discriminative subspace GMM classifier gives higher accuracies than DLQDF on 7 of 10 datasets, and performs comparably on the remaining datasets. On some datasets, the DLQDF with ML estimate (M1) outperforms the DLQDF training by MCE. This can be explained that the sample data of each class is close to Gaussian distribution, and hence a Gaussian classifier with ML estimate performs sufficiently. On most datasets, however, using GMM density instead of single Gaussian by the subspace GMM classifier has led to significant improvement of classification accuracy.

5 Conclusion

In this paper, we proposed a classification method using subspace GMM density model with parameters optimized by discriminative training. The subspace GMM combines a GMM density function in the principal subspace and a spherical Gaussian in the complement subspace for each class. It inherits the merit of GMM of complicated distribution modeling while overcome the curse of dimensionality. During discriminative training under the MCE criterion, both the GMM parameters and the subspace parameters are optimized discriminatively. Experiments of pattern classification on the MNIST handwritten digit data and UCI datasets demonstrate the superior classification performance of the proposed method compared to previous discriminative GMM and Gaussian methods. Our future work will consider model order selection for subspace GMM to optimize the model structure.

Acknowledgements

This work was supported by the National Natural Science Foundation of China (NSFC) under grant no.60825301.

References

1. Dempster, A.P., Laird, N.M., Rubin, D.B.: Maximum Likelihood from Incomplete Data Via the EM Algorithm. J. Royal Statistical Soc. Ser. B 39(1), 1–38 (1977)
2. Figueiredo, M.A.T., Jain, A.K.: Unsupervised Learning of Finite Mixture Models. IEEE Trans. Pattern Analysis and Machine Intelligence 24(3), 381–396 (2002)
3. Gales, M.J.F.: Semi-tied Covariance Matrices for Hidden Markov Models. IEEE Trans. Speech and Audio Processing 7(3), 272–281 (1999)
4. Moghaddam, B., Pentland, A.: Probabilistic Visual Learning for Object Representation. IEEE Trans. Pattern Analysis and Machine Intelligence 19(7), 696–710 (1997)
5. Liu, X.-H., Liu, C.-L., Hou, X.-W.: A Pooled Subspace Mixture Density Model for Pattern Classification in High-dimensional Spaces. In: Proc. IJCNN 2008, Hong Kong, pp. 2467–2472 (2008)
6. Bahl, L., Brown, P., de Souza, P., Mercer, R.: Maximum Mutual Information Estimation of Hidden Markov Model Parameters for Speech Recognition. In: Proc. Int'l. Conf. on Acoustics, Speech and Signal Processing, Tokyo, vol. 1, pp. 49–52 (1986)
7. Juang, B.-H., Chou, W., Lee, C.-H.: Minimum Classification Error Rate Methods for Speech Recognition. IEEE Trans. Speech Audio Process. 5(3), 257–265 (1997)
8. Dahmen, J., Schluter, R., Ney, H.: Discriminative Training of Gaussian Mixtures for Image Object Recognition. In: Proc. 21st Symposium of German Association for Pattern Recognition, Bonn, Germany, pp. 205–212 (1999)
9. Zhou, X., Wang, X.: Optimisation of Gaussian Mixture Model for Satellite Image Classification. IEE Proc.-Vision, Image and Signal Processing 153(3), 349–356 (2006)
10. Zhang, R., Ding, X.: Offline Handwritten Numeral Recognition Using Orthogonal Gaussian Mixture Model. In: Proc. 6th Int. Conf. Document Analysis and Recognition, pp. 1126–1129 (2001)
11. Schluter, R., Macherey, W., Muller, B., Ney, H.: Comparison of Discriminative Training Criteria and Optimization Methods for Speech Recognition. Speech Communication 34(1), 287–310 (2001)
12. Li, Q., Juang, B.-H.: A New Algorithm for Fast Discriminative Training. In: Proc. ICASSP 2002, Orlando, vol. 1, pp. 97–100 (2002)
13. Moghaddam, B., Jebara, T., Pentland, A.: Bayesian Face Recognition. Pattern Recognition 33(11), 1771–1782 (2000)
14. Chen, X., Liu, X., Jia, Y.: Unsupervised Selection and Discriminative Estimation of Orthogonal Gaussian Mixture Models for Handwritten Digit Recognition. In: Proc. 10th ICDAR, Barcelona, Spain, pp. 1151–1155 (2009)
15. Liu, C.-L., Sako, H., Fujisawa, H.: Discriminative Learning Quadratic Discriminant Function for Handwriting Recognition. IEEE Trans. Neural Networks 15(2), 430–444 (2004)
16. LeCun, Y., Bottou, L., Bengio, Y., Haffner, P.: Gradient-based Learning Applied to Document Recognition. Proc. IEEE 86(11), 2278–2324 (1998)
17. UCI Machine Learning Repository, `http://archive.ics.uci.edu/ml/`
18. Watanabe, H., Katagiri, S.: Subspace Method for Minimum Error Pattern Recognition. IEICE Trans. Information Syst. E80-D(12), 1095–1104 (1997)
19. Liu, C.-L., Nakashima, K., Sako, H., Fujisawa, H.: Handwritten Digit Recognition: benchmarking of state-of-art techniques. Pattern Recognition 36, 2271–2285 (2003)

A Stage by Stage Pruning Algorithm for Detecting the Number of Clusters in a Dataset

Yanqiao Zhu and Jinwen Ma*

Department of Information Science, School of Mathematical Sciences & LMAM
Peking University, Beijing, 100871, P.R. China
jwma@math.pku.edu.cn

Abstract. Determining the number of clusters in a dataset has been one of the most challenging problems in clustering analysis. In this paper, we propose a stage by stage pruning algorithm to detect the cluster number for a dataset. The main idea is that from the dataset we can search for the representative points of clusters with the highest accumulation density and delete the other points from their neighborhoods stage by stage. As the radius of the neighborhood increases, the number of searched representative points decreases. However, the structure of actual clusters of the dataset makes the representative point number be stable at the true cluster number in a relative large interval of the radius, which helps us to detect the cluster number. It is demonstrated by the simulation and practical experiments that the proposed algorithm can lead to an effective estimate of the cluster number for a general dataset.

Keywords: Clustering analysis, Cluster number detection, Accumulation density, Representative point, Stage by stage pruning.

1 Introduction

As a powerful data analysis tool, clustering analysis has been widely used in information processing and pattern recognition. Actually, there have been a variety of clustering approaches such as the k-means algorithm [1] as well as the fuzzy c-means algorithm [2], the frequency sensitive competitive learning (FSCL) algorithm [3], the mixture models with the EM algorithm [4] and the spectral clustering. However, most of these approaches take the number k of clusters as a pre-known information, i.e., the cluster number should be given in advance. Due to the great diversity of data structure, the determination of the cluster number for a general dataset has been still a rather challenging problem in clustering analysis. In fact, many attempts have been made to detect or estimate the number of clusters in a dataset.

The traditional approach is to choose an optimal number k^* of clusters in the dataset via one of information, coding and statistical selection criteria such as Akaike's Information Criterion (AIC) [5], Bayesian Inference Criterion (BIC) [6], Minimum Message Length (MML) [7] and GAP statistic [8]. But the validating

* Corresponding author.

D.-S. Huang et al. (Eds.): ICIC 2010, LNCS 6215, pp. 222–229, 2010.

process is computationally consumptive because we need to repeat the entire parameter learning process (such as the implementation of the EM algorithm on all the dataset) at a large number of possible values of k. Moreover, all the existing selection criteria have their limitations and often lead to a wrong result.

Alternatively, there are split-and-merge or split clustering algorithms which can also lead to the true number of clusters in the dataset from any initial setting of k. In fact, the ISODATA algorithm [9], the general competitive clustering [10], and the BYY split-and-merge EM algorithm [11] all have no requirement on the initial setting of k, but it is certain that such a clustering algorithm will converge more quickly and correctly if the initial setting of k is close to the correct value, i.e., the true number of clusters in the dataset. In certain cases, the proper setting of k is even necessary. So, it is very valuable to detect or even estimate the number of clusters in the dataset before the implementation of clustering.

Practically, we can design a search algorithm or procedure on the data to detect or estimate the number of clusters in the dataset. In fact, there have been already such search approaches. The visual method and the subtractive clustering method are two typical examples. The visual method firstly constructs a reordered dissimilarity image where the dark blocks along the diagonal represent the clusters and can be detected by certain image processing techniques [12,13]. In the subtractive clustering method, the accumulation density of each data point is computed such that each peak of the density distribution corresponds to a cluster center. Thus, the number of peaks of the density distribution can give an estimate of the cluster number [14]. Moreover, Yu and Cheng tried to discover the searching scope of the optimal cluster number for the FCM algorithm from the perspective of information theory [15].

In the current paper, we try to propose a stage by stage pruning method to detect the cluster number in a dataset. We begin to define the accumulation density for each data point. We then search for the representative points of clusters with the highest accumulation density and delete the other points from their neighborhoods stage by stage. As the radius of the neighborhood increases, the number of searched representative points decreases. But the dividable cluster structure of the dataset enables the representative point number to be stable at the true cluster number in a relative large interval of the radius. This flat level gives a good estimate of the cluster number. Actually, the simulation experiments demonstrate that the proposed algorithm can lead to an effective estimate of the cluster number for a general dataset.

The rest of this paper is organized as follows. Section 2 presents the stage by stage pruning algorithm. The simulation and practical experiments are conducted in Section 3. Section 4 contains a brief conclusion.

2 The Stage By Stage Pruning Algorithm

2.1 The Basic Idea

We begin with a description of the basic idea for our stage by stage pruning algorithm. Actually, it comes from the intuition that if we can prune the data

such that there is only one representative point left in each cluster, we can easily get the number of clusters just as the number of representative points left.

In order to implement this idea, we can utilize the accumulation density distribution of the data point which can be defined and computed on the dataset. A representative point for a cluster is supposed to own the highest density around its neighborhood, serving as the cluster center. So we first search for the data point with the highest accumulation density and let it be the representative point and prune the other points in its neighborhood with a given and fixed radius. In the remaining data points except the representative one, we can again search another representative point and prune the other points in the neighborhood of this representative point. In such a way, we can obtain a set of representative points stage by stage.

Clearly, the number of representative points can equal to the number of clusters when the radius of the neighborhood is properly set. But it is rather difficult to set the radius of the neighborhood properly. However, we can increase the radius step by step and get the representative point number for each value of the radius. As the radius of the neighborhood increases, the number of searched representative points decreases. But the dividable cluster structure of the dataset enables the representative point number to be stable at the true cluster number in a relative large interval of the radius. This flat level actually gives a good estimate of the cluster number.

So far, we need only to define the accumulation density of a data point. The most convenient way is to count up the number of its neighbors (whose distances to this data point are less than the given threshold r which will be consistent with the radius of the neighborhood used each search step). In fact, with such a density of the data point, the above stage by stage pruning procedure can be conducted on the three-cluster dataset given in the left part of Fig. 1, in which the radius of the neighborhood increases from one to 50 times of the initial radius[1] (in 50 steps). It can be clearly observed from the right part of Fig. 1 that the attenuating curve of the number of representative points has a clear flat level 3 corresponding to the true number of clusters in the dataset. This simulation result demonstrates that the idea of the stage by stage pruning procedure with the change of the radius of the neighborhood is effective and can be applied to detect the number of clusters in a dataset.

2.2 The Presentation of the Algorithm

We further present the stage by stage pruning algorithm according to the above basic idea. For clarity, we refer to the number of representative points left at the end of a pruning step as the state of the algorithm. Suppose that the dataset consists of N data points being denoted by $x_i \in R^n, i = 1, 2, \ldots, N$. $maxDist = max\{\|x_i - x_j\| \mid 1 \leq i < j \leq N\}$ denotes the maximum distance between any two data points, which is also referred to as the diameter of the dataset. We adopt

[1] The initial radius is set to be 1/50 of the maximum distance between any two data points in the dataset.

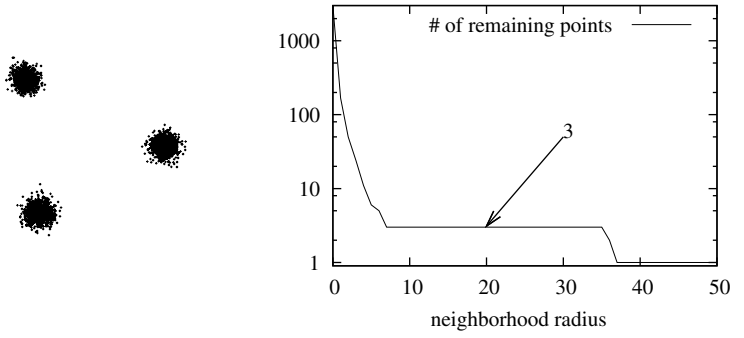

Fig. 1. The demonstration of the stage by stage pruning procedure

the following neighborhood increasing scheme and algorithm stop criterion. We equally divide the interval $[0, maxDist]$ into M parts and use $\{i \times maxDist/M : i = 1, 2, \ldots, M/2\}$ as the increasing radius sequence[2], i.e., $r = i \times maxDist/M$ is used to define the size of the neighborhood for the i-th step. As for the stop criterion, we introduce another parameter K. If one state sustains more than K steps (in other words, it appears more than $K + 1$ times consecutively), we then stop the algorithm and use the number of remaining representative data points in the state as an estimate of the cluster number. Details of our proposed stage by stage pruning algorithm are summarized in Algorithm 1.

3 Experimental Results

In this section, various simulation experiments are carried out to demonstrate the performance of the stage by stage pruning algorithm for detecting the number of clusters in a dataset. Moreover, the stage by stage pruning algorithm is implemented to detect the number of clusters in certain real-world datasets such as the Iris and wine datasets.

3.1 On Five Synthetic Datasets

We begin with a brief description of five synthetic datasets (shown in Fig. 2) used in our simulation experiments:

1. The clusters in $\mathcal{D}_1$ and $\mathcal{D}_2$ have equal number of samples, but those in the other three datasets have different numbers of samples.
2. The clusters in $\mathcal{D}_1, \mathcal{D}_3$ are well separated, but those in each of the other three datasets are overlapped at certain degree.
3. The clusters in $\mathcal{D}_1$ and $\mathcal{D}_2$ are spherical in shape, but those in the other three datasets are elliptic in shape.

[2] Usually we can take an even number for M, when $i = M/2$, $r = 1/2 \times maxDist$ is just the radius of the whole data.

Input: attribute vectors of data
Output: estimate of the cluster number
begin
  choose values for parameters M and K;
  compute the distance between data points (Euclidean distance between corresponding attribute vectors);
  compute neighbors of each data point for each radius in $\{i/M \times maxDist\colon i = 1, 2, \ldots, M/2\}$;
end
set $count = 0$, $preSet = \emptyset$, $curSet = \{1, 2, \ldots, \mathrm{N}\}$, $r = 1/M \times maxDist$;
while $count \leq K$ *and* $r \leq 1/2 \times maxDist$ **do**
  $preSet = curSet$;
  $curSet = \emptyset$;
  repeat
    begin
      find the data point in the remaining data which owns the most neighbors for current r (randomly choose one if there are a few);
      add the corresponding index to $curSet$;
      delete all of its neighboring data points and set its neighbors to 0.;
    end
  until *all of the data has been processed, either deleted or reserved* ;
  if $curSet == preSet$ **then**
    $count = count + 1$
  else
    $count = 0$
  end
  $r = r + 1/M \times maxDist$;
end
output the number of remaining data points in current state;

Algorithm 1. The stage by stage pruning algorithm

We now implement the stage by stage pruning algorithm on the five synthetic datasets with $M = 50$ and $K = 2$. Since there is some randomness when more than one data points own the largest number of the neighbors, different simulations may lead to different results, especially for datasets with complicated structure. So, we run 10 simulations for each dataset, and take the mode of the corresponding results as the final output. The results are summarized in Tab. 1.

For $\mathcal{D}_1$ and $\mathcal{D}_3$, nine out of the ten simulations give the correct cluster number, and so does the final output. For $\mathcal{D}_2$, $\mathcal{D}_4$, the advantage of the correct cluster number is not so obvious. As for $\mathcal{D}_5$, the correct cluster number 3 and the wrong cluster number 5 both win 3 times. So we take the average value 4 as the final output, which is 1 larger than the true cluster number.

By studying the simulation results on the five synthetic datasets, we can find that as the level of overlap among clusters increases, the ratio of correct cluster number in the simulation results tends to decrease. And the overall performance of the algorithm on $\mathcal{D}_1$ and $\mathcal{D}_2$ is better than that on each of the other three

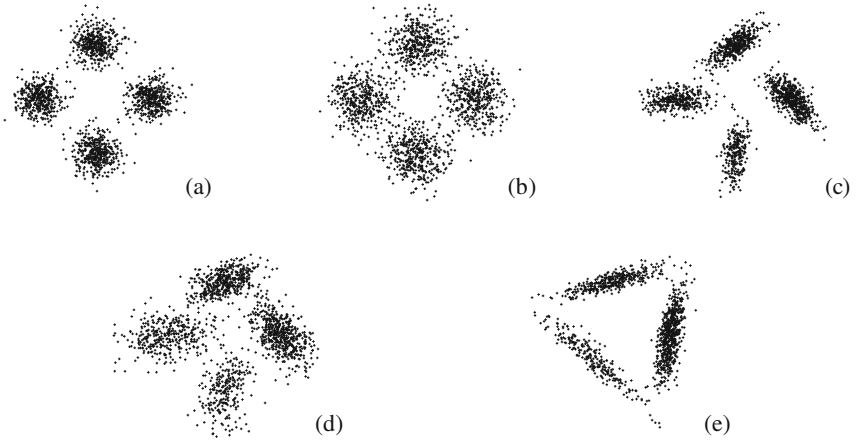

Fig. 2. Five synthetic datasets used in the simulation experiments. (a) dataset $\mathcal{D}_1$; (b) dataset $\mathcal{D}_2$; (c) dataset $\mathcal{D}_3$; (d) dataset $\mathcal{D}_4$; (e) dataset $\mathcal{D}_5$.

Table 1. Experimental results on five synthetic datasets (frequency of each output in 10 simulations)

Dataset \ Output	2	3	4	5	6	others	final output
$\mathcal{D}_1$	0	0.1	0.9(True)	0	0	0	4
$\mathcal{D}_2$	0.1	0.1	0.6(True)	0.1	0.1	0	4
$\mathcal{D}_3$	0	0.1	0.9(True)	0	0	0	4
$\mathcal{D}_4$	0.1	0.1	0.5(True)	0.3	0	0	4
$\mathcal{D}_5$	0	0.3(True)	0	0.3	0.2	0.2	4

datasets. Two reasons may account for this. First, in the algorithm, we will randomly choose one if a few data points all own the highest accumulation density at the same time. As the level of overlap among clusters increases, the randomness plays a more active role. Second, the algorithm is designed based on spherical neighborhood, which is not so appropriate for clusters in elliptic shape. As for $\mathcal{D}_5$, since clusters in the dataset are far from spherical-shaped, our algorithm cannot find an accurate result, but we can still get an effective estimate.

The algorithm is not sensitive to the differences among sample sizes of clusters, which can be supported by simulation results on $\mathcal{D}_3$. However, due to the neighborhood increasing scheme, the increment of neighborhood radius for all the clusters is the same, so we can expect the algorithm may not work well on datasets with clusters of dramatically different geographical sizes, say, one with diameter of 1000, while the others with diameter of 1.

3.2 On Real-World Datasets

On the Iris Data. The Iris dataset consists of 150 samples of three classes: Iris Versicolor, Iris Virginical and Iris Setosa, with each class containing 50 samples. Each datum consists of four attributes which represents measures of the plants morphology. Parameters are the same as previous settings. Six out of the ten simulations give the correct cluster number, so does the final output.

On the Wine Data. The wine data are typical high-dimensional real-world data. It contains 178 samples of three types of wine with 13-dimensional attributes. Ten experiments are conducted under $M = 50$ and $K = 2$. The results are better than that of Iris data with 80% of the simulations providing the correct cluster number.

3.3 Further Discussions

There are two free parameters in our proposed algorithm, M and K. Actually, M controls the increment of neighborhood radius, while K represents the stabling scale to output the result. Larger M means more computational cost since the radius increases slower, but the corresponding results are supposed to be more accurate. Meanwhile, with M being fixed, larger K means that we expect the clusters are farther away from each other, so clusters neighboring each other may be mistaken as one. Moreover, larger M usually is supposed be accompanied with larger K. The ideal case is that we can choose appropriate parameters based on the data to be processed, which is what we will look into in the future.

We can also consider the introduction of certain pre-process techniques before performing the algorithm, which aims at removing possible noisy data and making the boundaries more clear. For example, removing those data with few neighbors may improve the search result. Here we use Euclidean distance to define the neighborhood in this paper. But there are other choices such as the Mahalanobis distance or weighted Euclidean distance which treats each attribute differently based on their properties, which may be more proper for the datasets with more complicated structure.

4 Conclusions

We have established a stage by stage pruning algorithm for detecting the number of clusters in a dataset. The proposed algorithm searches for the representative points of clusters owning the highest accumulation densities with their neighborhoods with the neighborhood radius increasing stage by stage and takes the first stable representative point number as the estimate of the cluster number. It is demonstrated well by the experiments on both the synthetic and real-world datasets that the stage by stage pruning algorithm can provide an effective estimate of the cluster number.

Acknowledgements

This work was supported by the Natural Science Foundation of China for grant 60771061.

References

1. MacQueen, J.B.: Some Methods for classification and Analysis of Multivariate Observations. In: Proceedings of 5-*th* Berkeley Symposium on Mathematical Statistics and Probability, vol. 1, pp. 281–297. University of California Press, Berkeley (1967)
2. Bezdek, J.C.: Pattern Recognition with Fuzzy Objective Function Algorithms. Plenum Press, New York (1981)
3. Ahalt, S.C., Krishnamurty, A.K., Chen, P., Melton, D.E.: Competitive learning algorithms for vector quantization. Neural Networks 3, 277–291 (1990)
4. Dempster, A.P., Laird, N.M., Rubin, D.B.: Maximum likelihood from incomplete data via the EM algorithm. Journal of the Royal Statistical Society, B 39, 1–38 (1977)
5. Akaike, H.: A new look at the statistical model identification. IEEE Transactions on Automatic Control AC-19, 716–723 (1974)
6. Schwarz, G.: Estimating the dimension of a model. The Annals of Statistics 6, 461–464 (1978)
7. Wallace, C., Dowe, D.: Minimum Message Length and Kolmogorov Complexity. Computer Journal 42, 270–283 (1999)
8. Tibshirani, R., Walther, G., Hastie, T.: Estimating the number of clusters in a data set via the gap statistic. Journal of Royal Statistical Society, Series B (Statistical Methodology) 63, 411–423 (2001)
9. Ball, G.H., Hall, D.J.: ISODATA: a novel method of data analysis and pattern classification. Technique Report No. 699616, Stanford Research International (1965)
10. Boujemaa, N.: Generalized competitive clustering for image segmentation. In: Proc. of 19th International Conference of the North American Fuzzy Information Processing Society, pp. 133–137 (2000)
11. Li, L., Ma, J.: A BYY Split-and-Merge EM Algorithm for Gaussian Mixture Learning. In: Sun, F., Zhang, J., Tan, Y., Cao, J., Yu, W. (eds.) ISNN 2008, Part I. LNCS, vol. 5263, pp. 600–609. Springer, Heidelberg (2008)
12. Wang, L., Leckie, C., Ramamohanarao, K., Bezdek, J.: Automatically determining the number of clusters in unlabeled data sets. IEEE Transactions on Knowledge and Data Engineering 21, 335–350 (2009)
13. Sledge, I., Huband, J., Bezdek, J.: (Automatic) Cluster cluster count extraction from unlabeled datasets. In: Joint Proc. Fourth Int'l.Conf. Natural Computation and Fifth Int'l. Conf. Fuzzy Systems and Knowledge Discovery (2008)
14. Yager, R.R., Filev, D.P.: Approximate Clustering via the Mountain Method. IEEE Transactions Systems, Man, and Cybernetics 24, 1279–1284 (1994)
15. Yu, J., Cheng, Q.: The optimal range of number of clusters for the Fuzzy clustering methods. Science in China 32, 274–280 (2002)

Adaptive Independent Component Analysis by Modified Kernel Density Estimation*

Yunfeng Xue[1], Yujia Wang[2], and Yujie Han[3]

[1] School of Electronic and Electrical Engineering,
Shanghai Second Polytechnic University, Shanghai, P.R. China, 201209
[2] Department of Automation, Shanghai University of Engineering Science, Shanghai, P.R. China, 201620
[3] Collage of Mechanical and Electrical Engineering, Northeast Forestry University Harbin, P.R. China, 150040
yfxue@ee.sspu.cn

Abstract. In this paper, an adaptive algorithm for linear instantaneous independent component analysis is proposed, which is is based on minimizing the mutual information contrast function. Adaptive density estimation by modified kernel density estimation is applied to estimate the unknown probability density functions as well as their first and second derivatives. Empirical comparisons with several popular algorithms confirm the efficiency of the proposed algorithm.

1 Introduction

One of the most difficult problems in signal processing is blind source separation (BSS) [1]. Independent component analysis (ICA) [2] is an efficient method for solving this problem. The instantaneous linear noiseless ICA model is formulated by

$$\mathbf{x} = \mathbf{A}\mathbf{s} \tag{1}$$

where $\mathbf{s} \in \mathbf{R}^n$ is a zero mean vector with stationary and statistically independent signals termed as the source signals, $\mathbf{x} \in \mathbf{R}^n$ is the observed signals, and the mixing matrix $\mathbf{A} \in \mathbf{R}^{n\times n}$ is a full rank constant matrix. The aim of ICA is to find a demixing matrix $\mathbf{B}$ so that the components of the transformed data $\mathbf{y} = \mathbf{B}\mathbf{x}$ are as independent as possible without any knowledge on $\mathbf{A}$ and $\mathbf{s}$, because the only obtainable data is $\mathbf{x}$. The basic assumption for ICA model (1) to be solvable is that the components of the sources are mutually independent, which can often be satisfied in practical problems. Another two assumptions make (1) identifiable up to scale and permutation ambiguities are [2]: (a) the mixing matrix is a full rank matrix; and (b) at most one component of the sources is allowed to have Gaussian distribution. If the sources are successfully separated, the demixing matrix $\mathbf{B}$ is

* This work is supported by natural science foundation of Shanghai, China, No.10ZR1413000, and scientific research foundation for excellent young teachers of Shanghai, China, No.gjd09005.

D.-S. Huang et al. (Eds.): ICIC 2010, LNCS 6215, pp. 230–237, 2010.

equal to $\mathbf{PDA}^{-1}$ where $\mathbf{P}$ is a permutation matrix and $\mathbf{D}$ is a diagonal scaling matrix. Model (1) under the above assumptions has been studied thoroughly and many efficient algorithms have been developed [3,4,5,6,7].

The critical problem in ICA is how to estimate the source densities efficiently and accurately. A modified kernel density method is introduced in this paper to estimate the densities accurately and fast, where the histogram of the data is utilized. At the same time, Newton's method [8] is used to solve the ICA problem by means of solving the gradient equation which is derived from the mutual information contrast function. The advantage of Newton's method is that it does not need a learning rate and its convergence rate is faster than the (stochastic) gradient descent/ascent learning method.

The rest of this paper is organized as follows. In Section 2, the gradient equation is introduced through the mutual information contrast function. In Section 3, Newton's method is used to solve the gradient equation. In Section 4, the unknown density functions in the gradient equation along with their first and second derivatives are estimated by the modified kernel density method. Simulations are given in Section 5 with comparisons to several popular ICA algorithms, and finally, conclusions are drawn in Section 6.

2 Contrast Function and Gradient Equation for ICA

The key strategy of an ICA algorithm is to find a contrast function (also called objective function) which is the representation of the independence between the components of the transformed data. The ICA problem can be solved by maximizing or minimizing the contrast function, which is typically an optimization problem [2]. A lot of contrast functions have been proposed through different methods. One good choice is the mutual information contrast function formulated by

$$L(\mathbf{B}) = \sum_{i=1}^{n} H(y_i) - H(\mathbf{y}) \tag{2}$$

where $H(y_i)$ and $H(\mathbf{y})$ are the entropy of y_i and $\mathbf{y}$ respectively. After some algebraic manipulations and using basic information theory equalities [9], (2) can be reduced to the following form

$$L(\mathbf{B}) = -\sum_{i=1}^{n} \mathrm{E}\{\log p_{y_i}(y_i)\} - \log|\det \mathbf{B}| \tag{3}$$

where $H(\mathbf{x})$ has been dropped because it is a constant with respect to $\mathbf{B}$. Here, $p_{y_i}(y_i)$ is the pdf of $y_i = \mathbf{b}_i^T\mathbf{x}$ where $\mathbf{b}_i^T$ is the i-th row vector of $\mathbf{B}$, log denotes the natural logarithm, and the symbol E stands for the expectation operator.

The ICA problem can be solved by minimizing (3), which can be changed into the following gradient equation

$$\mathbf{F}(\mathbf{B}) = -\frac{\partial L}{\partial \mathbf{B}} = \mathrm{E}\{\mathbf{g}(\mathbf{B})\mathbf{x}^T\} + (\mathbf{B}^{-1})^T = \mathbf{0} \tag{4}$$

where $\mathbf{g}(\mathbf{B}) = (g_{y_1}(y_1), \ldots, g_{y_n}(y_n))^T$ and $g_{y_i}(y_i) = \frac{p'_{y_i}(y_i)}{p_{y_i}(y_i)}$.

3 Solving the Gradient Equation by Newton's Method

Newton's method is applied to obtain the approximate solution. The basic idea can be described as follows. If $\mathbf{B}$ is not an exact solution to (4), one can assume that $\mathbf{B}+\delta\mathbf{B}$ is a solution where $\delta\mathbf{B}$ is a perturbation matrix. Thus, $\mathbf{F}(\mathbf{B}+\delta\mathbf{B}) = \mathbf{0}$, and Taylor method can be used to expand $\mathbf{F}(\mathbf{B}+\delta\mathbf{B})$, then $\delta\mathbf{B}$ can be solved from the expansion. Therefore, the solution can be obtained iteratively. The most important step in Newton's method is to obtain the perturbation matrix $\delta\mathbf{B}$ from the expansion of $\mathbf{F}(\mathbf{B}+\delta\mathbf{B})$.

First, we will find the expansion of $\mathrm{E}\{\mathbf{g}(\mathbf{B}+\delta\mathbf{B})\mathbf{x}^T\}$. Denote $\mathbf{b}_i^T$ as the i-th row vector of $\mathbf{B}$, and similarly, $\delta\mathbf{b}_i^T$ for $\delta\mathbf{B}$. Thus, the i-th element of $\mathbf{g}(\mathbf{B}+\delta\mathbf{B})$ is $g_{y_i}(\mathbf{b}_i^T\mathbf{x}+\delta\mathbf{b}_i^T\mathbf{x})$, which can be expanded by Taylor method as follows

$$g_{y_i}(\mathbf{b}_i^T\mathbf{x}+\delta\mathbf{b}_i^T\mathbf{x}) \approx g_{y_i}(y_i) + g'_{y_i}(y_i)\delta\mathbf{b}_i^T\mathbf{x}.$$

So $\mathbf{g}(\mathbf{B}+\delta\mathbf{B})\mathbf{x}^T$ can be expanded as

$$\begin{aligned}\mathbf{g}(\mathbf{B}+\delta\mathbf{B})\mathbf{x}^T &\approx \begin{pmatrix} g_{y_1}(y_1)\mathbf{x}^T + g'_{y_1}(y_1)\delta\mathbf{b}_1^T\mathbf{x}\mathbf{x}^T \\ \vdots \\ g_{y_n}(y_n)\mathbf{x}^T + g'_{y_n}(y_n)\delta\mathbf{b}_n^T\mathbf{x}\mathbf{x}^T \end{pmatrix} \\ &= \mathbf{g}(\mathbf{B})\mathbf{x}^T + \mathbf{K}\delta\mathbf{B}\mathbf{x}\mathbf{x}^T\end{aligned}$$

where $\mathbf{K} = \mathrm{diag}(g'_{y_1}(y_1), \ldots, g'_{y_n}(y_n))$, and

$$\mathrm{E}\{g'_{y_i}(y_i)\} = \mathrm{E}\left\{\frac{p''_{y_i}(y_i)p_{y_i}(y_i) - (p'_{y_i}(y_i))^2}{(p_{y_i}(y_i))^2}\right\} \quad i = 1, \ldots, n$$

Thus, we finally obtain

$$\begin{aligned}\mathrm{E}\{\mathbf{g}(\mathbf{B}+\delta\mathbf{B})\mathbf{x}^T\} &\approx \mathrm{E}\{\mathbf{g}(\mathbf{B})\mathbf{x}^T\} + \mathrm{E}\{\mathbf{K}\delta\mathbf{B}\mathbf{x}\mathbf{x}^T\} \\ &\approx \mathrm{E}\{\mathbf{g}(\mathbf{B})\mathbf{x}^T\} + \mathrm{E}\{\mathbf{K}\}\delta\mathbf{B}\mathrm{E}\{\mathbf{x}\mathbf{x}^T\} \\ &= \mathrm{E}\{\mathbf{g}(\mathbf{B})\mathbf{x}^T\} + \mathbf{D}_{g'}\delta\mathbf{B}\mathbf{C}_{\mathbf{x}}. \end{aligned} \tag{5}$$

where $\mathbf{C}_{\mathbf{x}}$ is the covariance matrix of $\mathbf{x}$.

Next, $(\mathbf{B}+\delta\mathbf{B})^{-1}$ can be expanded as

$$(\mathbf{B}+\delta\mathbf{B})^{-1} \approx \mathbf{B}^{-1} - \mathbf{B}^{-1}\delta\mathbf{B}\mathbf{B}^{-1}. \tag{6}$$

Thus, expanding $\mathbf{F}(\mathbf{B}+\delta\mathbf{B})$ through (5) and (6) and letting $\mathbf{F}(\mathbf{B}+\delta\mathbf{B}) = \mathbf{0}$ yields

$$\begin{aligned}\mathbf{D}_{g'}\delta\mathbf{B}\mathbf{C}_{\mathbf{x}} - (\mathbf{B}^{-1})^T\delta\mathbf{B}^T(\mathbf{B}^{-1})^T &= -\mathrm{E}\{\mathbf{g}(\mathbf{B})\mathbf{x}^T\} - (\mathbf{B}^{-1})^T \\ &= -\mathbf{F}(\mathbf{B}). \end{aligned} \tag{7}$$

Equation (7) is a specific form of the following matrix equation

$$\mathbf{R}\mathbf{X}\mathbf{S} + \mathbf{U}\mathbf{X}^T\mathbf{V} = \mathbf{G} \tag{8}$$

where $\mathbf{R}$, $\mathbf{S}$, $\mathbf{U}$, $\mathbf{V}$, $\mathbf{G}$ and $\mathbf{X}$ are $n \times n$-size matrices and only $\mathbf{X}$ is unknown. The solution to (8) can be obtained by the following lemma.

Lemma 1. *Equation (8) can be changed into the following linear equation*

$$(\mathcal{A}+\mathcal{B})\mathcal{X}=\mathcal{G} \tag{9}$$

where $\mathcal{A}=\mathbf{R}\otimes\mathbf{S}^T$, *and* $\otimes$ *denotes the Kronecker product operator.* $\mathcal{B}$ *is defined by*

$$\mathcal{B}=\begin{pmatrix}\mathbf{v}_1\mathbf{u}_1^T & \dots & \mathbf{v}_n\mathbf{u}_1^T\\ \vdots & \ddots & \vdots\\ \mathbf{v}_1\mathbf{u}_n^T & \dots & \mathbf{v}_n\mathbf{u}_n^T\end{pmatrix} \tag{10}$$

where $\mathbf{u}_i^T$ *and* $\mathbf{v}_i^T$ *are the* i*-th row vector of* $\mathbf{U}$ *and* $\mathbf{V}$ *respectively.* $\mathcal{G}$ *and* $\mathcal{X}$ *are two* n^2*-dimensional column vectors defined by*

$$\mathcal{G}=(\mathbf{g}_1^T,\dots,\mathbf{g}_n^T)^T,\quad \mathcal{X}=(\mathbf{x}_1^T,\dots,\mathbf{x}_n^T)^T \tag{11}$$

where $\mathbf{g}_i^T$ *and* $\mathbf{x}_i^T$ *are the* i*-th row vector of* $\mathbf{G}$ *and* $\mathbf{X}$ *respectively.*

Proof. First calculate the term $\mathbf{L}=\mathbf{RXS}$. Let $\mathbf{L}=(\mathbf{l}_1,\dots,\mathbf{l}_n)^T$, $\mathbf{R}=(r_{ij})$, $\mathbf{S}=(\mathbf{s}_1,\dots,\mathbf{s}_n)$ and $\mathbf{X}=(\mathbf{x}_1,\dots,\mathbf{x}_n)^T$, where $\mathbf{l}_i^T$ stands for the i-th row vector of $\mathbf{L}$, r_{ij} stands for the ij-th element of $\mathbf{R}$, $\mathbf{s}_i$ stands for the i-th column vector of $\mathbf{S}$, and $\mathbf{x}_i^T$ stands for the i-th row vector of $\mathbf{X}$. Directly calculating $\mathbf{l}_i^T$ and changing this row vector into a column vector yields

$$\mathbf{l}_i=\left(\sum_{k=1}^{n}r_{ik}\mathbf{s}_1^T\mathbf{x}_k,\dots,\sum_{k=1}^{n}r_{ik}\mathbf{s}_n^T\mathbf{x}_k\right)^T=\left(r_{i1}\mathbf{S}^T,\dots,r_{in}\mathbf{S}^T\right)\begin{pmatrix}\mathbf{x}_1\\ \vdots\\ \mathbf{x}_n\end{pmatrix}.$$

Thus $\mathbf{L}$ can be changed into the following n^2-dimensional column vector

$$\begin{pmatrix}\mathbf{l}_1\\ \vdots\\ \mathbf{l}_n\end{pmatrix}=\begin{pmatrix}r_{11}\mathbf{S}^T & \dots & r_{1n}\mathbf{S}^T\\ \vdots & \ddots & \vdots\\ r_{n1}\mathbf{S}^T & \dots & r_{nn}\mathbf{S}^T\end{pmatrix}\begin{pmatrix}\mathbf{x}_1\\ \vdots\\ \mathbf{x}_n\end{pmatrix}=\mathbf{R}\otimes\mathbf{S}^T\begin{pmatrix}\mathbf{x}_1\\ \vdots\\ \mathbf{x}_n\end{pmatrix} \tag{12}$$

where $\otimes$ denotes the Kronecker product operator.

Then, through the same method, matrix $\mathbf{M}=\mathbf{UX}^T\mathbf{V}$ can be changed into the following n^2-dimensional column vector

$$\begin{pmatrix}\mathbf{m}_1\\ \vdots\\ \mathbf{m}_n\end{pmatrix}=\begin{pmatrix}\mathbf{v}_1\mathbf{u}_1^T & \dots & \mathbf{v}_n\mathbf{u}_1^T\\ \vdots & \ddots & \vdots\\ \mathbf{v}_1\mathbf{u}_n^T & \dots & \mathbf{v}_n\mathbf{u}_n^T\end{pmatrix}\begin{pmatrix}\mathbf{x}_1\\ \vdots\\ \mathbf{x}_n\end{pmatrix} \tag{13}$$

where $\mathbf{m}_i^T$, $\mathbf{u}_i^T$ and $\mathbf{v}_i^T$ stand for the i-th row vector of $\mathbf{M}$, $\mathbf{U}$ and $\mathbf{V}$ respectively.

Finally, change matrix $\mathbf{G}$ into an n^2-dimensional column vector, i.e., $\mathcal{G}=(\mathbf{g}_1^T,\dots,\mathbf{g}_n^T)^T$ where $\mathbf{g}_i^T$ is the i-th row vector of $\mathbf{G}$. Therefore, by (12) and (13),

it can be concluded that matrix equation (8) can be changed into the following linear equation

$$(\mathcal{A}+\mathcal{B})\mathcal{X}=\mathcal{G}$$

where $\mathcal{A}=\mathbf{R}\otimes\mathbf{S}^T$, $\mathcal{B}$ is defined by (10) and $\mathcal{X}$ and $\mathcal{G}$ is defined by (11). This completes the proof.

Thus $\delta\mathbf{B}$ in equation (7) can be solved out by this lemma, and $\mathbf{B}$ can be obtained iteratively.

4 Density Estimation by Modified Kernel Density Method

It is clear that the density function $p_{y_i}(y_i)$ as well as its first and second derivatives should be estimated to solve (4). One popular density estimation method is the kernel density method formulated by (assume that we have sample size T for y_i, i.e., $Y_i(1),\ldots,\ldots,Y_i(T)$)

$$p_{y_i}(y_i)=\frac{1}{Th}\sum_{t=1}^{T}K\left(\frac{y_i-Y_i(t)}{h}\right) \tag{14}$$

where h is the kernel bandwidth (also called smooth parameter) and $K(u)$ is the standard Gaussian kernel defined by

$$K(u)=\frac{1}{\sqrt{2\pi}}\exp\left(\frac{u^2}{2}\right). \tag{15}$$

It has been shown in [10] that estimation (14) can be calculated by fast Fourier transform (FFT). However, it is noted that in the proposed method, the first and second derivatives of $p_{y_i}(y_i)$ are also needed to be estimated, which may lead to high computational cost. To overcome this difficulty, a modified kernel density estimation is used in this paper, where the histogram of y_i is utilized. The idea of the modified kernel density estimation can be described as follows.

Note that if $Y_i(t_1),Y_i(t_2),\ldots,Y_i(t_k)$ are very close, then their contributions to (14) will be approximately the same, which can be calculated by

$$\begin{aligned}\frac{1}{T}\sum_{j=1}^{k}\frac{1}{\sqrt{2\pi}h}\exp\left(-\frac{(y_i-Y_i(t_j))^2}{2h^2}\right)&\approx\frac{1}{T}\sum_{j=1}^{k}\frac{1}{\sqrt{2\pi}h}\exp\left(-\frac{(y_i-\mu)^2}{2h^2}\right)\\&=\frac{k}{T}\phi(y_i;\mu,h)\end{aligned} \tag{16}$$

where μ is the center of $Y_i(t_1),Y_i(t_2),\ldots,Y_i(t_m)$, and $\phi(y_i;\mu,h)$ is the Gaussian kernel defined as

$$\phi(y_i;\mu,h)=\frac{1}{\sqrt{2\pi}h}\exp\left(-\frac{(y_i-\mu)^2}{2h^2}\right). \tag{17}$$

This inspires us to use the histogram of y_i to approximate its pdf. Thus, by calculating each bin of the histogram using (16), $p_{y_i}(y_i)$ can be approximated by the modified kernel density method as follows

$$p_{y_i}(y_i) = \sum_{j=1}^{L} k_j \phi(y_i; \mu_j, h). \tag{18}$$

Here L is the number of the bins of the histogram which should be a large number, for example, 100, to approximate the density in a relatively good performance, and μ_j is the center of each bin, and k_j is the frequency calculated from the histogram of y_i. The first and second derivatives of $p_{y_i}(y_i)$ can be approximated by the same way as follows

$$p'_{y_i}(y_i) = -\sum_{j=1}^{L} k_j \frac{y_i - \mu_j}{h^2} \phi(y_i; \mu_j, h) \tag{19}$$

$$p''_{y_i}(y_i) = \sum_{j=1}^{L} k_j \frac{(y_i - \mu_j)^2}{h^4} \phi(y_i; \mu_j, h) - \sum_{j=1}^{L} k_j \frac{1}{h^2} \phi(y_i; \mu_j, h). \tag{20}$$

The bandwidth parameter h is very critical in the modified kernel density method. An improper choice of h will lead to a wrong estimation of the density. It is shown in [11] that for one-dimensional estimation the heuristic choice of h is $1.06\sigma T^{-1/5}$ where σ is the standard deviation of y_i. Pham [12] points out that the optimal rate of h is $\sigma T^{-1/5}$, and h should go to zero when $T \to \infty$. However, in real applications, it can not be chosen that $h \to 0$ because the sample size T is a finite number. Thus, in this paper, h is chosen to be $0.75\sigma T^{-1/5}$.

5 Simulations

In this section, experiments are provided to verify the performance of the proposed algorithm and the results are compared with standard symmetric FastICA algorithm [13], EFICA algorithm [14] and JADE algorithm [15] with their default settings. The number of Gaussian mixtures in our algorithm is $L = 100$. All algorithms are repeated for 200 trials. In each trial, the sources are mixed by a randomly generated full rank matrix (condition number less than 1000), whose elements are drawn from a uniform distribution in $[-1, 1]$. All experiments are performed in Matlab 7.0 on a Pentium IV 2.66GHz PC with 1GB RAM.

In order to evaluate the efficiency of an algorithm, the performance index (PI) [16] is used in this paper, which is defined by

$$\mathrm{PI} = \frac{1}{2n} \left(\sum_{i=1}^{n} \left(\frac{\sum_{j=1}^{n} |g_{ij}|}{\max_j |g_{ij}|} - 1 \right) + \sum_{j=1}^{n} \left(\frac{\sum_{i=1}^{n} |g_{ij}|}{\max_i |g_{ij}|} - 1 \right) \right)$$

where g_{ij} is the element of $\mathbf{G} = \mathbf{BA}$. The PI measurement is invariant to permutation and scaling, thus it measures how close $\mathbf{B}$ is to the true demixing matrix $\mathbf{A}^{-1}$. The performance index is always nonnegative, and the smaller the PI value, the better performance of the algorithm is.

5.1 Experiment with Artificial Signals

Five Rayleigh signals (parameter $\beta = 5$) with skewness and kurtosis equal to 0.631 and 0.245 respectively, are used as the sources. Four different sample sizes, i.e., $T = 500, 1000, 1500, 2000$, are used to test the performance of an algorithm for different lengths of data. The separation results are presented in Table 1. It can be seen that our algorithm achieves the best performance. The results of FastICA is not satisfactory because the nonlinear function used in this algorithm is an approximation of a symmetric density, while the sources are skewed in this experiment. The performance of EFICA is not satisfactory because it uses the generalized Gaussian (GG) distribution model, a symmetric model, to approximate the source density. For JADE, it can be seen that its performance becomes better when the sample size becomes larger. However, the performance of our algorithm is better in all sample sizes. It can also be seen that the mean CPU time of our algorithm is higher because of the density estimation process.

Table 1. Separation results of five Rayleigh sources with four different sample size T = 500, 1000, 1500, 2000: mean performance index and mean CPU time (seconds)

T	Mean Performance Index				Mean CPU Time (seconds)			
	FastICA	EFICA	JADE	Our Algorithm	FastICA	EFICA	JADE	Our Algorithm
500	1.43	1.54	1.24	0.411	1.45	0.08	0.009	13.95
1000	1.56	1.53	1.16	0.127	1.83	0.10	0.009	15.16
1500	1.46	1.53	1.04	0.086	2.15	0.13	0.011	16.13
2000	1.50	1.56	0.97	0.075	2.60	0.15	0.014	17.31

6 Conclusion

A source adaptive ICA algorithm is proposed in this paper. The proposed algorithm is based on solving the gradient equation by Newton's method. At the same time, a modified kernel density method is used to estimate the unknown densities as well as their first and second derivatives, which makes the proposed algorithm adaptive to source distribution. A series of simulations is performed on artificially generated signals, real sound signals and image data. The experimental results show that our proposed algorithm is a good choice when several other ICA algorithms fail to separate all sources.

References

1. Comon, P., Jutten, C., Herault, J.: Blind separation of sources, part II: problems statement. Signal Processing 24, 11–20 (1991)
2. Comon, P.: Independent component analysis, a new concept? Signal Processing 36, 287–314 (1994)

3. Cardoso, J.F., Souloumiac, A., Paris, T.: Blind beamforming for non-Gaussian signals. IEE Proceedings F, Radar and Signal Processing 140, 362–370 (1993)
4. Bell, A.: An information-maximization approach to blind separation and blind deconvolution. Neural Computation 7, 1129–1159 (1995)
5. Lee, T.: Independent component analysis using an extended infomax algorithm for mixed subgaussian and supergaussian sources. Neural Computation 11, 417–441 (1999)
6. Koldovský, Z., Tichavský, P., Oja, E.: Efficient variant of algorithm FastICA for independent component analysis attaining the Cramer-Rao lower bound. IEEE Transactions on Neural Networks 17, 1265–1277 (2006)
7. Hyvärinen, A.: Fast and robust fixed-point algorithms for independent component analysis. IEEE Transactions on Neural Networks 10, 626–634 (1999)
8. Nocedal, J., Wright, S.J.: Numerical Optimization. Springer, Heidelberg (1999)
9. Cover, T.M., Thomas, J.A.: Elements of information theory. John Wiley & Sons, Chichester (1991)
10. Silverman, B.: Kernel density estimation using the fast Fourier transform. Applied Statistics 31, 93–99 (1982)
11. Silverman, B.: Density Estimation. Chapman and Hall, London (1986)
12. Pham, D.: Blind separation of instantaneous mixture of sources via an independent component analysis. IEEE Transactions on Signal Processing 44, 2768–2779 (1996)
13. The FastICA package, `http://www.cis.hut.fi/projects/ica/fastica/`
14. The EFICA package, `http://itakura.kes.tul.cz/zbynek/efica.htm`
15. The JADE package, `http://www.tsi.enst.fr/icacentral/Algos/cardoso/JnS.tar`
16. Amari, S., Cichocki, A., Yang, H.H.: A new learning algorithm for blind signal separation. In: Touretzky, D.S., Mozer, M.C., Hasselmo, M.E. (eds.) Advances in Neural Information Processing Systems, vol. 8, pp. 757–763. MIT Press, Cambridge (1996)

Cross System Bank Branch Evaluation Using Clustering and Data Envelopment Analysis

Zijiang Yang

School of Information Technology, York University, 4700 Keele Street
Toronto, ON, Canada M3J 1P3
zyang@mathstat.yorku.ca

Abstract. This paper introduces clustering method to traditional Data Envelopment Analysis (DEA) in order to examine the performance of 982 branches of one big Canadian bank nation wide. This improved method can address the effects exerted by different operating environment. K-means, one of the most popular clustering techniques is used to cluster the branches into 8 clusters in order to make a fair comparison. The system differentiated DEA model used in the paper considers the systematic difference among different clusters. The potential management uses of the DEA results were also presented. All the findings are discussed in the context of the Canadian banking market.

Keywords: Optimization, Clustering, Data Envelopment Analysis, Banking.

1 Introduction

Productivity and competitiveness analysis in the banking industry has attracted more attention than ever and has become a crucial management practice as bank managers continue to pursue all the opportunities available to enhance the productivity and competitiveness of their organizations. Top bank management wants to identify and eliminate the underlying causes of inefficiencies, thus helping their firms to gain competitive advantage, or, at least, meet the competitive challenges from others. Since Sherman and Gold [1] wrote the first significant DEA bank analysis paper, DEA has become a leading approach for the performance analysis in banking industry. Berger and Humphrey [2] reviewed 130 studies on financial institutions efficiency in 21 countries. Cook et al. [3] investigated the use of quantitative variable in bank branch evaluation using DEA. Asmild et al. [4] evaluate the performance of Canadian banking industry over time. Bala and Cook [5] incorporate expert knowledge within the DEA framework. Camanho and Dyson [6] investigated the bank branch performance under price uncertainty. Halkos and Salamouris [7] measured the Greek bank performance using DEA. Isik and Hassan [8] utilized a DEA-type Malmquist Total Factor Productivity Change Index to examine productivity growth, efficiency change, and technical progress in Turkish commercial banks during the deregulation of financial markets in Turkey.

However, there is an especially important situation when the branches belong to different systems. Some units may have an advantageous environment that the others

D.-S. Huang et al. (Eds.): ICIC 2010, LNCS 6215, pp. 238–245, 2010.

cannot adopt yet comparisons are useful. This reality challenges the traditional methods of applying DEA theory to real-world cases since the DEA analysis requires a consistent operating environment to make a fair comparison. Cooper et al. [9] introduced a method to do the cross-system comparison. They make use of mixed integer LP (linear programming) problem with binary variables to evaluate DMUs in different systems. This approach has a pre-requisite: they must know in advance which system the units belong to. Therefore, how to decide which system the units belong to becomes crucial. The traditional method assumes all the bank branches in the same region have the same operating environment. But it is not necessarily true in reality. Even the same region can have difference such as population mix, customers' income level, economy, culture and etc. This paper presents an evaluation of 982 branches of one big Canadian bank nation wide. Those branches are located in different geographical regions such as Atlantic, Central Canada, Greater Toronto area, Ontario, Pacific, Prairie, and Quebec. It is obvious that all the branches in Ontario (or other region) may have different operating environment. In order to solve this problem, this paper introduces a clustering method to cluster the bank braches into similar systems instead of using each region as one system and then apply Cooper et al. [9]'s cross-system analysis to make the fair comparison.

The rest of the paper is organized as follows. Section 2 gives a brief review of clustering method and DEA. Section 3 provides the models and methodology utilized in this paper. Section 4 presents the DEA results and the potential use of the DEA results is provided in Section 5. Finally, our conclusions are given.

2 Technical Basics

2.1 Clustering Method

Clustering algorithms are a collection of methods to divide a set of n observations into g clusters so that members of the same cluster have more common characteristics than members from different groups. The objective of this clustering process is to provide a comparable peer group and conduct the comparison on a common ground. K-means, the most popular clustering technique is used in this paper.

2.2 Data Envelopment Analysis

DEA provides a comprehensive analysis of relative efficiencies for multiple input-multiple output situations by evaluating each DMU and measuring its performance relative to an envelopment surface composed of other DMUs. Those DMUs forming the efficiency reference set are known as the peer group for the inefficient units. As the inefficient units are projected onto the envelopment surface, the efficient units closest to the projection and whose linear combination comprises this virtual unit form the peer group for that particular DMU. The targets defined by the efficient projections give an indication of how this DMU can improve to be efficient. Consider n DMUs to be evaluated, DMU_j (j=1,2…n) consumes amounts $X_j = \{x_{ij}\}$ of inputs (i=1, 2, …, m) and produces amounts $Y_j = \{y_{rj}\}$ of outputs (r=1 ,…, s). The efficiency of a particular DMU_0 can be obtained from the following linear programs (input-oriented VRS model [10]).

$$\begin{aligned} \min_{\theta,\lambda,s^+,s^-} \quad & z_0 = \theta - \varepsilon \cdot \vec{1} s^+ - \varepsilon \cdot \vec{1} s^- \\ \theta X_0 - X\lambda - s^- &= 0 \\ \vec{1}\lambda &= 1 \\ \lambda,\ s^+, s^- &\geq 0 \end{aligned} \tag{1}$$

Performing a DEA analysis actually requires the solution of *n* linear programming problems of the above form, one for each DMU. The optimal variable θ is the proportional reduction to be applied to all inputs of DMU_0 to move it onto the frontier. The vector λ indicates the contribution of the efficient DMUs to the peer group that forms the reference set for the DMU under evaluation. Their magnitude indicates the degree to which the characteristics of the efficient DMUs are used to construct the virtual DMU on the frontier to which the inefficient one is projected. The slack variables (s^+ and s^-) are variables added to the linear programming model in order to convert inequality constraints to equality constraints. Theoretically, the presence of the non-Archimedean ε in the objective function effectively allows the minimization over θ to preempt the optimization involving the slacks [10]. A DMU is termed efficient if and only if the optimal value θ* is equal to 1 and all the slack variables are zero. This model allows variable returns to scale. The dual program of the above formulation is illustrated by:

$$\begin{aligned} \max_{\mu,,\nu} \quad & w_0 = \mu^T Y_0 + u_0 \\ s.t. \quad & v^T X_0 = 1 \\ & \mu^T Y - v^T X + u_0 \vec{1} \leq 0 \\ & -\mu^T \leq -\varepsilon \bullet \vec{1} \\ & -v^T \leq -\varepsilon \bullet \vec{1} \\ & u_0 \ \text{ free} \end{aligned} \tag{2}$$

The dual problem yields an alternative geometric interpretation. In the dual form, ν and μ are the vectors of input and output weights. Efficiency is measured as a function of these weights. Each DMU is then allowed to choose weights that maximize its efficiency, provided that the set of weights yield efficiency scores that do not exceed unity, for all DMUs. The variable *u* is the measure of scale efficiency.

If the convexity constraint ($\vec{1}\lambda = 1$) in (1) and the variable u_0 in (2) are removed, the feasible region is enlarged, which results in the reduction in the number of efficient DMUs, and all DMUs are operating at constant returns to scale. The resulting model is referred to as the CRS model. The reader is advised to consult the textbook by Cooper, Seiford and Tone [9] for a comprehensive treatment of DEA theory and application methodology.

3 Models and Methodologies

K-means is chosen to cluster the bank branches because of its popularity. Based on the bank management's inputs, 17 variables are selected to cluster the branches. These 17 variables include average customer age, average household income, total population of 25 years and over * labour force activity, total population of 15-24 years * labour force activity, median employment income of all families, percent of all families with employment income, percent of all families with an estimated gross financial asset value of $500,000 or greater, percent of total estimated gross financial asset value of $750,000 or greater report by families, percent of taxfilers reporting more than $64, 000 total income, percent of all families receiving UI benefits, percent of taxfilers 0-24 years of age, percent of taxfilers 25-34 years of age, percent of taxfilers 35-44 years of age, percent of taxfilers 45-54 years of age, percent of taxfilers 55-64years of age, percent of taxfilers aged 65+, and branch age.

An operational efficiency model which adopts a production approach is introduced to model the banking process. This model examines how well different branches combine their resources to support the largest amount of possible services. There is a general agreement among the literature relating to bank branches' efficiency on the inputs used to assess performance. Most of the studies which adopt the production approach use personnel cost as the primary input. In terms of output measures, number of money in accounts and number of money out accounts are chosen as outputs. Figure 1 shows the model details.

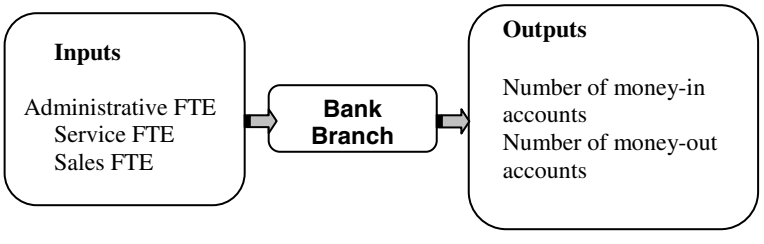

Fig. 1. DEA model

Input orientation (the LP is oriented to minimize inputs) is selected for the DEA models in this research. I point out that management was more interested in minimizing the consumption of inputs subject to attaining the desired output levels. In addition, VRS model is chosen in order to address the scale effect.

In order to remove the disadvantage caused by the economic and other reasons, system differentiated DEA models are adopted. Normal DEA models assume that a production possibility set *P* is convex and any convex combination of points in P also belongs to set *P*. This is valid if the production possibility set belongs to a homogeneous population. However, comparisons of bank branches nation wide become more complicated because the population is no longer homogeneous, i.e., the branches belong to different systems. Hence, the convexity assumption may be violated. Under system differentiated DEA model a DMU is evaluated in terms of each individual system and then the least of the values will be the efficiency score given to the unit.

4 Results and Discussions

The sample includes 982 branches of one big Canadian bank nation wide. The k-means method separates the branches into 8 clusters. Summary statistics for the inputs and outputs are reported in Table 1, which shows the large data variations for each variable. This further validates our choice of VRS model.

Table 1. Summary statistics of outputs and inputs

	Max	Min	Average	Standard Deviation
Inputs				
Administrative FTE	7.56	0.00	1.48	1.38
Service FTE	49.82	0.00	6.39	4.07
Sales FTE	53.32	0.00	6.85	4.39
Outputs				
No. of Money-in accounts	114911	606	22737	13672
No. of Money-out accounts	48551	54	5268	3629

Table 2. Distribution of the bank branches

Cluster No.	No of Branches
1	45
2	92
3	44
4	385
5	45
6	261
7	40
8	70
Total	982

Since input orientation is adopted in this study, technical efficiency scores in this paper can be interpreted as the proportion of inputs that could produce the DMU's output vector if the DMU was operating on the frontier. Moreover, the amount and type of resource saving that can be achieved by making each inefficient unit become efficient are identified. The DEA results are summarized as follows in Table 3:

Table 3. DEA results

	System differentiated DEA model
Average Score	0.60
Standard Deviation	0.17
Maximum Efficiency Score	1
Minimum Efficiency Score	0.16
Number (and %) of Efficient DMUs	44 (4%)

From this table, we can conclude that the DEA model identified 60% technical efficiency on average. This indicates if all the branches can perform efficiently, by using the target input and output values, the bank could save as much as 40% of its resources from a theoretical point of view. In practice, the saving will almost certainly be substantially less. Nevertheless, this indicates that significant potential savings can be achieved for the examined bank.

The Bank's top management also wants to know the performance at cluster level. Therefore, the efficiency distribution by cluster is also examined. Since this paper adopts system differentiated DEA model, the disadvantage caused by the economic and other reasons have been removed by the model. The comparison here is fair and on the same basis. Table 4 shows the results.

Table 4. DEA results by cluster

Cluster No	# of branches	Average score	Standard Deviation
1	45	0.65	0.17
2	92	0.60	0.18
3	44	0.61	0.19
4	385	0.59	0.17
5	45	0.55	0.18
6	261	0.62	0.16
7	40	0.61	0.21
8	70	0.60	0.18

The normal DEA model that does not address the system difference among the bank branches nation wide is also run based on the data set. Table 5 compares the results from normal input-oriented DEA model and system differentiated input-oriented DEA model.

Table 5. Comparison between normal DEA model and system differentiated DEA model

	Normal DEA model	System differentiated Model
No. of Efficient DMUs	35	44
% Efficient	3.6%	4%
Average Efficiency Score	0.58	0.60
Maximum Efficiency Score	1	1
Minimum Efficiency Score	0.15	0.16

Table 5 clearly shows that the average efficiency score from system differentiated DEA model is slightly higher than the normal DEA model. In addition, it identifies more efficient branches than the normal DEA model. In general, system differentiated input-oriented DEA models will cause efficiency scores to appear more favourable than normal DEA.

5 Management Use of the Results

DEA results also highlight the reasons for both favourable and poor use/production of resources/outcomes involved in the unit's performance – factors that contributed to or detracted from the DMUs' efficiency rating. Nevertheless, one of the most powerful pieces of information that is obtained by a DEA analysis is the set of target values for those assessed as inefficient. The reference set provides strong indications of what type and amounts of inputs and outputs are needed to make the inefficient units efficient. Since input oriented DEA models are used in the analysis, there will be target input values that the inefficient units could use to achieve an efficiency score of 1.0. Please note that it is possible that the reference set includes the DMUs from other systems using system differentiated DEA model. Table 6 provides DEA efficiency scores and reference sets for some of the DMUs in this analysis. For example, in order for DMU_{174} in Cluster 1 to become efficient, it should reduce each of its input resources including administrative FTE, service FTE and sales FTE by 19%. More specifically, based on the reference sets DMU_{174} should consume X_{1029}*0.90+X_{1590}*0.10 (X_i is the input vector for DMU i) amount of input to generate its observed output level. Please notice that X_{1029} and X_{1590} belong to Cluster 4.

Table 6. DEA efficiency scores and reference sets

DMU No. (Cluster)	Score	Reference set (lambda)			
174(C1)	0.81	1029 (C4)	0.90	1590 (C4)	0.10
1328(C1)	1	1328 (C1)	1		
10 (C2)	0.63	1304 (C1)	0.46	1328 (C1)	0.54
3203(C3)	0.71	1856 (C6)	0.86	3512 (C6)	0.14
114(C4)	0.59	1029 (C4)	0.39	1282 (C4)	0.61
3213 (C5)	0.68	2827 (C4)	1		

6 Conclusions

This paper adopts clustering method and system differentiated DEA model to evaluate the branch performance for a large Canadian bank. The branches operate fairly efficiently on the whole although there is still a lot of room for improvement. Special emphasis was placed on investigating the environmental variables which exert significant influence to the branch performance. Finally, recommendations to management's use of DEA results were given.

References

1. Sherman, H.D., Gold, F.: Bank branch operating efficiency: Evaluation with data envelopment analysis. Journal of Banking and Finance 9, 297–315 (1985)
2. Berger, A.N., Humphrey, D.B.: Efficiency of Financial Institutions: International Survey and Directions for Future Research. European Journal of Operational Research 98, 175–212 (1997)

3. Cook, W.D., Hababou, M., Tuenter, H.J.: Multicomponent efficiency measurement and shared inputs in data envelopment analysis: An application to sales and service performance in Bank Branches. Journal of Productivity Analysis 14, 209–224 (2000)
4. Asmild, M., Paradi, J.C., Aggarwall, V., Schaffnit, C.: Combining DEA window analysis with the malmquist index approach in a study of the Canadian Banking Industry. Journal of Productivity Analysis 21, 67–89 (2004)
5. Bala, K., Cook, W.D.: Performance measurement with classification information: An enhanced additive DEA model. Omega 31, 439–450 (2003)
6. Camanho, A.S., Dyson, R.G.: Cost efficiency measurement with price uncertainty: A DEA application to bank branch assessments. European Journal of Operational Research 161, 432–446 (2005)
7. Halkos, G.E., Salamouris, D.S.: Efficiency measurement of the Greek Commercial Banks with the use of financial ratios: A data envelopment analysis approach. Management accounting Research 15, 201–224 (2004)
8. Isik, I., Kabir, H.M.: Financial deregulation and total factor productivity change: An empirical study of turkish commercial bank. Journal of Banking and Finance 27, 1455–1485 (2003)
9. Cooper, W.W., Seiford, L.M., Tone, K.: Data envelopment analysis: A comprehensive text with models, applications, references and DEA-solver software, 2nd edn. Springer, New York (2006)
10. Banker, R.D., Charnes, A., Cooper, W.W.: Models for estimating technical and scale efficiencies in DEA. Management Science 30, 1078–1092 (1984)

He's Variational Iteration Method for Solving Convection Diffusion Equations*

Yiliang Liu[1] and Xinzhu Zhao[2]

[1] School of Mathematics and Computer Science,
Guangxi University for Nationalities, Nanning, Guangxi 530006, P.R. China
yiliangliu100@126.com
[2] School of Mathematics and Computing Science,
Changsha University of Science and Technology, Changsha 410114, Hunan, P.R.China
583192531@qq.com

Abstract. The variational iteration method is applied to solve convection diffusion equations. These equations play an important role in mathematical,physical and engineering sciences. The exact and approximating solutions will be obtained by variational iteration method. Some examples are given to illustrate the effectiveness and convenience of the method.

Keywords: Variational iteration method, restricted variation, convection diffusion equation.

2000 Mathematics Subject Classification: 65L05; 65L06; 26A33.

1 Introduction

The governing equation of unsteady water contamination problems, which are convection dispersion problems, is the convection diffusion equation and has a more or less mixed hyperbolic or parabolic character. In this paper, we consider the following initial-boundary one-dimensional unsteady convection diffusion problem

$$\begin{cases} \frac{\partial u(x,t)}{\partial t} = D\frac{\partial^2 u(x,t)}{\partial x^2} + \mu\frac{\partial u(x,t)}{\partial x} + \kappa u(x,t) - \sigma(x,t), & (x,t) \in \Omega \times (0,T) \\ u(x,0) = u_0(x), & x \in \Omega \\ u(x,t) = g(x,t), & (x,t) \in \partial\Omega \times (0,T), \end{cases} \tag{1}$$

where t is the time dimension. x is the space dimension of an open domain Ω with boundary $\partial\Omega$. $u(x,t)$ is the instantaneous concentration of material. μ is the instantaneous fluid velocity component in the x direction. D is the diffusion coefficient. κ is the rate of decay of material from control volume and $\sigma(x,t)$ is any local sources of the mass of substance.

* Project supported by Guangxi Natural Science Foundation Grant No.2010GXNSFA013114.

D.-S. Huang et al. (Eds.): ICIC 2010, LNCS 6215, pp. 246–251, 2010.

Efficient numerical solutions of convection diffusion equations are an important area for research. Recently many authors have paid attention to study solutions of convection diffusion equations by using various methods, such as Petrov-Galerkin method, Multigrid method and Galerkin finite element method [1,2,3,4,5,6]. It is,however,well know that applying these methods to (1) will in certain circumstances result in a discrete solution ,which exhibits non-physical oscillations.

In this paper, the variational iteration method is applied to solve the one-dimensional convection diffusion equations. The variational iteration method was first proposed by He and was success fully applied to autonomous ordinary differential equations, to nonlinear polycrystal line solids, and other fields (see, e.g. [7,8,9,10,11]). This method has been proved by many authors to be a powerful mathematical tool for kinds of nonlinear problem. Besides its mathematical importance tool and its links to other branches of mathematics, it is widely used in all ramifications modern sciences. The solution procedure of this method is very simple by means of variation theory and only few iterations lead to high accurate solutions which are valid for the whole solution domain. The motivation of this paper is to extend the variational iteration method to convection diffusion equations. Several examples are given to illustrate the reliability and performance of the proposed method.

2 Variation Iteration Method

To illustrate the basic idea of the variational iteration method, we consider the following general nonlinear equation

$$Lu(t) + Nu(t) = g(t) \tag{2}$$

where L is a linear operator, N is a nonlinear operator, and $g(t)$ is an inhomogeneous term.

According to the variational iteration method [7,8,10,11],we consider the correction functional in the following form

$$u_{n+1}(t) = u_n(t) + \int_0^t \lambda \left\{ Lu_n(s) + \widetilde{N}u_n(s) - g(s) \right\} ds \tag{3}$$

where λ is the general Lagrange multiplier, which can be identified optimally via the variational theory, the subscript n denotes the nth approximation and $\widetilde{u_n}(t)$ is considered as a restricted variation, i.e. $\delta\widetilde{u}_n = 0$.

To solve (3) by the variational iteration method, we first determine the Lagrange multiplier λ that will be identified optionally via integration by parts. Then the successive approximation $u_n(t)(n \geq 0)$ of the solution $u(t)$ will be readily gotten by using the obtained Lagrange multiplier and any selective function $u_0(t)$. The zeroth approximation u_0 may be selected by any function that just satisfies at least the initial and boundary conditions. Consequently, the exact solution may be obtained by using

$$u(t) = \lim_{n \to \infty} u_n(t). \tag{4}$$

Consider the one-dimension convection diffusion problem (1). Let $f(x,t) = Du_{n_{xx}} + \mu u_{n_x} + \kappa u_n - \sigma$, μ and κ are given variable coefficients. According to the variational iteration method, we can construct the following correction functional

$$u_{n+1} = u_n + \int_0^t \lambda \left\{ u_{n_\tau} - \widetilde{f(x,\tau)} \right\} d\tau \tag{5}$$

where the Lagrange multiplier can be easy identified by the variation theory.

Next section, we consider several examples of convection diffusion equations, which can be solved iteratively by using the variational iteration method.

3 Applications

In order to illustrate its general process, we solve three examples by means of variation iteration method.

Example 1. Let us first consider the following one-dimensional unsteady convection diffusion Cauchy problem

$$\begin{cases} u_t = u_{xx} - \frac{x}{2} u_x + \frac{x}{2} u - \frac{x^2}{2} + \frac{x}{2} \\ u(x,0) = e^x + x. \end{cases} \tag{6}$$

To solve Eq.(6) by means of the variational iteration method, we can construct a correct functional which reads

$$u_{n+1} = u_n + \int_0^t \lambda \left\{ u_{n_s} - \widetilde{f(x,s)} \right\} ds \tag{7}$$

where $f(x,s) = u_{n_{xx}} - \frac{x}{2} u_{n_x} + \frac{x}{2} u_n - \frac{x^2}{2} + \frac{x}{2}$, $\widetilde{f(x,s)}$ is considered as a restricted variation. Its stationary conditions can be obtained as following

$$\lambda(s)|_{s=t} + 1 = 0, \lambda'(s) = 0.$$

The Lagrange multiplier, therefore, can be easily identified as

$$\lambda = -1 \tag{8}$$

and the following iteration formula can be obtain

$$u_{n+1} = u_n - \int_0^t \left\{ u_{n_s} - u_{n_{xx}} + \frac{x}{2} u_{n_x} - \frac{x}{2} u_n + \frac{x^2}{2} - \frac{x}{2} \right\} ds \tag{9}$$

We choose its initial approximate solution in the form

$$u_0(x,t) = u(x,0) = e^x + x \tag{10}$$

Substituting Eq.(10) into Eq.(9), we have

$$\begin{aligned}
u_1 &= u_0 - \int_0^t \left\{ u_{0_s} - u_{0_{xx}} + \tfrac{x}{2} u_{0_x} - \tfrac{x}{2} u_0 + \tfrac{x^2}{2} - \tfrac{x}{2} \right\} ds = e^x + e^x t + x \\
u_2 &= e^x + e^x t + e^x \tfrac{t^2}{2} + x \\
u_3 &= e^x + e^x t + e^x \tfrac{t^2}{2} + e^x \tfrac{t^3}{3!} + x \\
&\cdots\cdots \\
u_n &= e^x + e^x t + e^x \tfrac{t^2}{2} + e^x \tfrac{t^3}{3!} + \ldots + e^x \tfrac{t^n}{n!} + x
\end{aligned}$$

Thus we have

$$\lim_{n\to\infty} u_n(t) = e^{x+t} + x$$

which is the exact solution.

Example 2. Consider the following convection diffusion Cauchy problem with variable coefficient

$$\begin{cases} u_t = \frac{1}{2} u_{xx} - \frac{3}{2} x^2 u_x + (2 - 3x) u \\ u(x, 0) = e^{x^3}. \end{cases} \tag{11}$$

To solve problem (11) by means of the variational iteration method, we can construct a correct functional which reads

$$u_{n+1} = u_n + \int_0^t \lambda \left\{ u_{n_s} - \widetilde{f(x,s)} \right\} ds$$

where $f(x,s) = \frac{1}{2} u_{n_{xx}} - \frac{3}{2} x^2 u_{n_x} + (2-3x) u_n$, $\widetilde{f(x,s)}$ is considered as a restricted variation. Like (8),the Lagrange multiplier $\lambda = -1$ and the iteration formula can be obtain

$$u_{n+1} = u_n - \int_0^t \left\{ u_{n_s} - \frac{1}{2} u_{n_{xx}} + \frac{3}{2} x^2 u_{n_x} - (2 - 3x) u_n(x, s) \right\} ds \tag{12}$$

We choose its initial approximate solution in the form

$$u_0(x,t) = u(x,0) = e^{x^3} \tag{13}$$

Substituting Eq.(13) into Eq.(12), we have

$$\begin{aligned}
u_1 &= u_0 - \int_0^t \left\{ u_{0_s} - \tfrac{1}{2} u_{0_{xx}} + \tfrac{3}{2} x^2 u_{0_x} - (2 - 3x) u_0 \right\} ds = e^{x^3} + 2te^{x^3} \\
u_2 &= e^{x^3} + 2te^{x^3} + \tfrac{(2t)^2}{2!} e^{x^3} \\
u_3 &= e^{x^3} + 2te^{x^3} + \tfrac{(2t)^2}{2!} e^{x^3} + \tfrac{(2t)^3}{3!} e^{x^3} \\
&\cdots\cdots \\
u_n &= e^{x^3} + 2te^{x^3} + \tfrac{(2t)^2}{2!} e^{x^3} + \tfrac{(2t)^3}{3!} e^{x^3} \ldots + \tfrac{(2t)^n}{n!} e^{x^3}.
\end{aligned}$$

Thus we have

$$\lim_{n\to\infty} u_n(t) = e^{2t+x^3}.$$

which is the exact solution.

Example 3. Consider the following convection diffusion Cauchy problem with variable coefficients

$$\begin{cases} u_t = u_{xx} - (\cos x + \sin x)u_x + [\frac{1}{2}(\sin x + \cos x)^2 + \sin x]u \\ u(x,0) = e^{\sin x}. \end{cases} \tag{14}$$

Its correct functional can be written in the following form

$$u_{n+1} = u_n + \int_0^t \lambda \left\{ u_{n_s} - \widetilde{f(x,s)} \right\} ds$$

where $f(x,s) = u_{xx} - (\cos x + \sin x)u_x + [\frac{1}{2}(\sin x + \cos x)^2 + \sin x]u$, $\widetilde{f(x,s)}$ is considered as a restricted variation. Also we may get that the Lagrange multiplier $\lambda = -1$ and the iteration formula can be obtain

$$u_{n+1} = u_n - \int_0^t \left\{ u_{n_s} - u_{n_{xx}} + (\cos x + \sin x)u_{n_x} - [\frac{1}{2}(\cos x + \sin x)^2 + \sin x]u_n \right\} ds \tag{15}$$

We choose its initial approximate solution in the form

$$u_0(x,t) = u(x,0) = e^{\sin x} \tag{16}$$

Substituting Eq.(16) into Eq.(15), we have

$$\begin{aligned} u_1 &= u_0 - \int_0^t \left\{ u_{0_s} - u_{0_{xx}} + (\cos x + \sin x)u_{0_x} - [\tfrac{1}{2}(\cos x + \sin x)^2 + \sin x]u_0 \right\} ds \\ &= e^{\sin x} + e^{\sin x}\tfrac{t}{2} \\ u_2 &= e^{\sin x} + e^{\sin x}\tfrac{t}{2} + e^{\sin x}\tfrac{(\frac{t}{2})^2}{2!} \\ &\cdots\cdots \\ u_n &= e^{\sin x} + e^{\sin x}\tfrac{t}{2} + e^{\sin x}\tfrac{(\frac{t}{2})^2}{2!} + \ldots + e^{\sin x}\tfrac{(\frac{t}{2})^n}{n!}. \end{aligned}$$

Thus we have

$$\lim_{n\to\infty} u_n(t) = e^{\frac{t}{2}+\sin x}$$

which is the exact solution.

4 Conclusions

In this paper, we applied the variational iteration method to solve convection diffusion equations. All examples show that the variational iteration method is very powerful and effective for solving convection diffusion equations. Moreover, the variational iteration method can reduce the calculation and obtain good approximate solution.

References

1. Elman, H.C., Silvester, D.J., Wathen, A.J.: Finite Elements and Fast Iterative Solvers. Oxford University Press, Oxford (2005)
2. Liu, Z.H.: A Class of Evolution Hemivariational Inequalities, Nonlinear Analysis. TMA 36(1), 91–100 (1999)

3. Liu, Z.H.: Browder-Tikhonov Regularization of Non-coercive Evolution Hemivariational Inequalities. Inverse Problems 21, 13–20 (2005)
4. Liu, Z.H.: Existence Results for Quasilinear Parabolic Hemivariational Inequalities. J. Differential Equations 244, 1395–1409 (2008)
5. Liu, Z.H.: Anti-periodic Solutions to Nonlinear Evolution Equations. J. Functional Analysis 258, 2026–2033 (2010)
6. Liu, Z.H.: On Boundary Variational-hemivariational Inequalities of Elliptic Type. Proceedings of the Royal Society of Edinburgh: Section A Mathematics 140(2), 419–434 (2010)
7. He, J.H.: Variational Principles for Some Nonlinear Partial Differential Equations with Variable Coefficients. Chaos Solitons Fractals 19, 847–851 (2004)
8. He, J.H.: Variational Iteration Method-some Recent Results and New Interpretations. J. Comput. Appl. Math. 207, 3–17 (2007)
9. He, J.H., Lee, E.W.M.: Variational Principle for the Differential.Difference system arising in stratified hydrostatic flows. Phys. Lett. A 373, 1644–1645 (2009)
10. Liu, J.B., Tang, J.: Variational Iteration Method for Solving an Inverse Parabolic Equation. Phys. Lett. A 372, 3569–3572 (2008)
11. Shou, D.H., He, J.H.: Beyond Adomian Method: The Variational Iteration Method for Solving Heat-like and Wave-like Equations with Variable Coefficients. Phys. Lett. A 372, 233–237 (2008)

GRASP for Low Autocorrelated Binary Sequences

Huchen Wang and Shaowei Wang

Nanjing University, School of Electronic Science and Engineering, China
wangsw@nju.edu.cn

Abstract. The search for *low autocorrelated binary sequences*(LABS) is a combinatorial optimization problem, which is NP-hard. In this paper, we apply *Greedy Randomized Adaptive Search Procedures* (GRASP) to tackle the LABS problem. The algorithm is capable of systematically recovering best-known solutions reported by now. Furthermore, it can find out good autocorrelated binary sequences sequences in considerably less time as comparison with other heuristic methods.

Keywords: combinatorial optimization, greedy randomized adaptive search procedure, low autocorrelation binary sequences.

1 Introduction

Let S be a binary sequence of length L with elements s_0, s_1, ..., s_{L-1} where each s_i takes on the value +1 or -1, the aperiodic autocorrelation of the binary sequence S at shift k is given by

$$R_k(S) = \sum_{i=0}^{L-k-1} s_i s_{i+k}, \text{ for } k = 1, \ldots, L-1. \tag{1}$$

The quadratic sum of all autocorrelation functions

$$E(S) = \sum_{k=1}^{L-1} R_k^2(S) \tag{2}$$

is called energy because of the relation to an Ising-spin system with long-range four-spin interaction [1]. The aim of finding sequences with low autocorrelation can be formulated to maximize the so-called *merit factor*

$$F(S) = L^2/2E(S) \tag{3}$$

introduced by Golay in 1977 [2].

As a combinatorial problem, the search space for the LABS problem has size 2^L. Obviously using exhaustive enumeration to find optimal sequences is impractical for large L. *Systematic search* such as branch-and-bound [3] was proposed to reduce the size of the search tree. For larger L, some *heuristic methods* such

D.-S. Huang et al. (Eds.): ICIC 2010, LNCS 6215, pp. 252–257, 2010.

as neural networks and evolutionary algorithms (EAs) [4,5,6] were proposed. In 2006, a pure Tabu Search(TS) [9] with frequent restarts was proposed and could find optimal LABS solutions for $L \leq 48$ much quicker than the exact branch-and-bound [3]. It was roughly on par with the Kernighan-Lin(KL) [10] solver which could find optimal LABS solutions for $L \leq 64$. In 2009, a new LABS solver called MA_{TS} [7], combining a memetic algorithm with TS, was proposed and was shown to be much faster than TS and KL algorithm.

Since it is difficult to find the optimum solution when L is very large, *skew-symmetry* sequences are applied to restrict the search to a promising subspace. The skew-symmetry sequence is only of odd length and can be defined as

$$s_{n+i} = (-1)^i s_{n-i}, \text{ for } i = 1, 2 \ldots n-1, \ L = 2n+1; \tag{4}$$

Such sequences often have good merit factors because $R_k = 0$ for all odd distance k.

In this paper, we apply a GRASP based algorithm to search for the desired binary sequences. This algorithm generates a set of binary sequences randomly and update them until the sequence with largest merit factor is found. The algorithm converges very quickly and the computational complexity is much lower than that of most other stochastic methods.

2 GRASP Based Algorithm

GRASP is an iterative multi-start metaheuristic for solving difficult combinatorial problems. Each GRASP iteration consists of two phases: a greedy adaptive randomized construction phase and a local search phase. The construction phase of GRASP is essentially a randomized greedy algorithm. Repeated applications of the construction procedure yields diverse starting solutions for the local search which explores its neighborhood until a local optimum is found. The best solution found overall the different iterations is kept as the result.

Consider a combinatorial optimization problem, where one is given a discrete set X of solutions and an objective function $f(x)$: $x \in X \rightarrow \mathbb{R}$, and one seeks a solution $x^* \in X$ with $f(x^*) \geq f(x)$ for all $x \in X$. The termination criterion is either a threshold of fitness value or the limited searching times. A basic GRASP [8] for a maximization problem is described in Table 1.

Unfortunately, using greedy solutions as starting points for local search will usually lead to suboptimal solutions. Because a greedy starting solution is less likely to be in the basin of attraction of a global optimum. To avoid producing the same solution in each iteration, a list of best candidates called the *restricted candidate list*(RCL) [8] is constructed according to their greedy function values. One of the best solutions but not necessarily the top candidate is then selected randomly from RCL. In this paper, we apply the value based scheme and the RCL for a maximization problem can be constructed as

$$RCL = \{x \in X | f(x) \geq f(x)_{\min} + \alpha(f(x)_{\max} - f(x)_{\min})\} \tag{5}$$

where $\alpha \in [0, 1]$, $f(x)_{\max} = \max\{f(x)|x \in X\}$, $f(x)_{\min} = \min\{f(x)|x \in X\}$. If $\alpha = 0$, it is a greedy algorithm, and if $\alpha = 1$, it is a random search. The pseudo code in Table 2 describes our GRASP based algorithm, where $f(s)$ is the merit factor of binary sequence s. In our practice, We apply $\alpha = 0.8$ to avoid getting stuck in local optima. After finding local optima s^*, we then flip $L/10$ bits of it randomly for several times to generate a new set of initial sequences for the next iteration.

Table 1. A Basic GRASP Algorithm

```
Initialization:
    let f(x*) := 0;
Loop:
  while (termination criterion is not satisfied)
    1) generate a set of greedy randomized solutions;
    2) find local optimum solution x_opt with local search;
    3) if f(x_opt) > f(x*), then
         f(x*) := f(x_opt), x* := x_opt;
       end if
  end while
```

Table 2. GRASP Based Semi-Greedy Algorithm

```
Initialization:
    randomly generate initial binary sequences;
    let f(s*) := 0;
Loop:
  while (termination criterion is not satisfied)
    1) update initial sequences with local search;
    2) sort all merit factors, find f(s)_max and f(s)_min;
    3) construct RCL := {s ∈ S|f(s) ≥ f(s)_min + α(f(s)_max − f(s)_min)},
       randomly select one sequence from RCL as s_opt;
    4) if f(s_opt) > f(s*), then
         f(s*) := f(s_opt), s* := s_opt;
       end if
    5) flip a few bits of s* to generate new initial sequences;
  end while
```

We apply a *steepest descent local search* (SDLS) [7] procedure, that moves to the best sequence in the neighborhood until reaching a local optimum. The pseudo code for this algorithm is depicted in Table 3, where $flip(s_1 \cdots s_i \cdots s_L, i) = s_1 \cdots - s_i \cdots s_L$.

Table 3. Steepest Descent Local Search

```
Initialization:
    let s* := s, f(s*) := f(s), f(s)max := 0, flag := true;
Loop:
  while (flag := true)
   1) for i := 1 : L
        s' := flip(s*, i)
        if f(s') > f(s)max then
          f(s)max := f(s'), smax := s*;
        end if
      end for
   2) if f(s)max > f(s*), then
        f(s*) := f(s)max, s* := smax, flag := true;
      else
        flag := false;
      end if
  end while
```

3 Experimental Results

The optimal binary sequences obtained by our GRASP based algorithm are listed in Table 4 and Table 5. For larger sequences, we apply skew-symmetry sequence

Table 4. Merit Factors and Example Sequences On Different Instance Sizes

L	MF	Time(S)	Example Sequence
40	7.40	18	5A5C3BC444
41	7.78	25	16900CCAB87
42	8.73	20	3BBB8478B4B
43	8.48	34	09A4FEAC79D
44	7.93	107	AB5B6671F00
45	8.58	121	0AB1E3725B00
46	8.07	144	003693B1E355
47	8.18	221	255B4C4C3807
48	8.22	230	9699384E0157
49	8.82	443	1144432F342F4
50	8.16	600	30BD0CBCD1104
51	8.50	1334	1C395EEE81B49
52	8.14	1665	05FB6D5D9D8E3
53	8.26	2255	01F451CFBB35A9
54	8.33	2492	300661C5D66A52
55	8.84	3731	0036C6D0E4E355
56	8.16	3654	FE04C58C2A349A
57	8.64	4530	039CFC54FED4D92
58	8.53	4818	1E4B21CBAA46C40
59	8.49	4420	544E47FBC973C69
60	8.25	6260	FE05215161A334C
61	8.23	6374	16C0F928AB718108
62	8.18	5411	18CF5C2D7D5FC9B2
63	9.59	7567	4631ABFAF85BE993
64	9.85	6763	D93602A0A5E28673
65	8.80	9247	0E73950141E9059B2
66	8.47	20393	30F866AACC006694B
67	9.31	15558	2B15C65247064813F
68	9.25	21297	DB348418D8C07A155
69	8.69	35809	0E33C5D64E4D5A17FF
70	8.31	31975	1B2D1EACC5D4358DFF

Table 5. Merit Factors and Example Sequences for Large Skew-Symmetry Sequences

L	MF	Time(S)	Example Sequence
73	7.66	12	1AD2A68A377208603C1
75	8.25	18	49B925AA2BF7F871B9C
77	8.28	38	15C54BC619D9A6D0FEDF
79	7.67	107	78FD73BA47247BB20ADA
81	8.20	316	00E05188B71B7089BEA4A
83	9.14	594	7381C62FE7EA6AF6495B2
85	8.17	711	1C013E76DC7D6DC7653AAD
87	8.39	813	78BCF37D46EEE40A32CBDA
89	8.18	1040	0DD2457F160E4A7B57EE3DC
91	8.68	1128	38BA861FC273274A965FBDB
93	8.61	1343	07C18F8051308B3BEA949AD6
95	9.42	1291	7319C1FE828FADF5EA949932
97	8.78	1433	19C7543A14C4F4ECFA12FF6D9
99	8.49	1573	0307C9B003A6167B5539CA535
101	8.82	1910	1F9F06C9FF8B3D309558C6B595
103	9.56	2840	34A6A55CCEF9AF9AECC807E7C3
105	8.89	7677	0004A5BD22DCC98CDC23D1E0EAA
107	8.46	12574	180E807530B8F32DBD30255ED59
109	8.97	15740	038558742A39982999202F69FE92
111	8.97	14930	6A31C46AE0BCB8DBCBD6FE44937E
113	8.49	18533	01F07D90DB600133AAA71CB9D6B5A
115	8.88	25668	56BED74A41847333245947C20EBE0
117	8.71	34870	03FA03B5951CCF3D34CDBF9F12A152
119	8.48	50722	76FDED93852BBD720BBF05B18E8AE2
121	8.67	73490	1DEB84604A3342CB0C2F320EA6E905D

to reduce the searching space. To simplify the denotation of a binary sequence, all -1's in a sequence are represented by 0's. The hexadecimal numbers are then used to denote the example sequences. Since it is usually difficult to analyze the computational complexity of one algorithm, we list the mean CPU time (on a 2.33 GHz PC) for searching the optimal sequences to compare the computation cost of different stochastic methods. We also implement other stochastic methods such as Tabu Search(TS) [9], Kernighan-Lin (KL) [10] and MA_{TS} [7] on our computer. Take a few short sequences for instance, for $L = 48$, the CPU time of TS and KL algorithm are respectively 630s and 890s. Table shows that, our algorithm also found the optimum but this is done in a mean time of 230s. The KL algorithm found the optimum for $L = 60$ in 12h of execution time, whereas our algorithm needs less than 2h which is comparable with MA_{TS}'s 1.3h. In general, our algorithm shows significantly improved the execution times of most approaches reported in the literature.

4 Conclusions

We proposed a GRASP based algorithm method to search for the low autocorrelation binary sequence of a given length. In order to test the algorithm on even larger instances, we also adapt it to explore only skew-symmetric solutions. Experimental results show that the algorithm proposed outperforms other algorithms to date for the LABS problem. In the following stage, we will analyze the characteristics of the problem and modify the parameters of the algorithm to improve the performance.

Acknowledgement

This work was supported by a grant from Natural Science Foundation of Jiangsu Province, China (No.BK2008261) and National Natural Science Foundation of China (No.60932002).

References

1. Bernasconi, J.: Low Autocorrelation Binary Sequences: Statistical Mechanics and Configuration Space Analysis. Journal de Physique 48, 559–567 (1987)
2. Golay, M.: Sieves for Low Autocorrelation Binary Sequences. IEEE Transactions on Information Theory 23(1), 43–51 (1977)
3. Mertens, S.: Exhaustive Search for Low-autocorrelation Binary Sequences. Journal of Physics A: Mathematical and General 29, L473–L481 (1996)
4. Golay, M.: The Merit Factor of Long Low Autocorrelation Binary Sequences. IEEE Transactions on Information Theory 28(3), 543–549 (1982)
5. Militzer, B., Zamparelli, M., Beule, D.: Evolutionary Search for Low Autocorrelated Binary Sequences. IEEE Transactions on Evolutionary Computation 2(1), 34–39 (1998)
6. Wang, S.: Efficient Heuristic Method of Search for Binary Sequences with Good Aperiodic Autocorrelations. Electronics Letters 44(12), 731–732 (2003)
7. Dotu, I., Hentenryck, P.V.: A Note on Low Autocorrelation Binary Sequence. In: Nikoletseas, S.E., Rolim, J.D.P. (eds.) ALGOSENSORS 2006. LNCS, vol. 4240, pp. 685–689. Springer, Heidelberg (2006)
8. Brglez, F., Li, X.Y., Stallman, M.F., Militzer, B.: Reliable Cost Prediction for Finding Optimal Solutions to Labs Problem: Evolutionary and Alternative Algorithms. In: Cantu-Paz, E. (ed.) 5th International Workshop on Frontiers in Evolutionary Algorithms, September 2003, pp. 26–30 (2003)
9. Gallardo, J.E., Cotta, C., Fernandez, A.J.: Finding Low Autocorrelation Binary Sequences with Memetic Algorithms. Applied Soft Computing 9, 1252–1256 (2009)
10. Feo, T.A., Resende, M.G.C.: Greedy Randomized Adaptive Search Procedures. Journal of Global Optimization 6, 109–133 (1995)

miRNA Target Prediction Method Based on the Combination of Multiple Algorithms

Lin Zhang[1], Hui Liu[1], Dong Yue[2], Hui He[1], and Yufei Huang[2,3,⋆]

[1] SIEE, China University of Mining and Technology, Xuzhou, China
[2] ECE, University of Texas at San Antonio
[3] GCCRI, University of Texas Health Science Center at San Antonio

Abstract. MicroRNAs(miRNAs) are around 22 nucleotides known to have important post-transcriptional regulatory functions. The computational target prediction algorithms are important to instruct effective experimental tests. However, different existing algorithms rely on different features and different classifiers, there is a poor agreement between the results of different algorithms. To take full advantage of all the algorithms, we proposed an algorithm to combine the prediction of different algorithms based on decision fusion. This approach was evaluated and tested on the ground truth retrieved from proteomics data. The results show that this method improves the sensitivity, specificity and consistency of each individual algorithm.

Keywords: miRNA target prediction, decision fusion, logistic regression.

1 Introduction

MicroRNAs (miRNAs) are single-stranded non-coding RNAs with about 22 nucleotides in length[1] known to mainly inhibit target translation or cleave target mRNA by binding to the complementary sites in the 3' UTR of targets. miRNAs have been shown and are speculated to play many important post-transcriptional regulatory roles in a wide range of biological processes and diseases including development, stress responses, viral infection, and cancer[2] [3]. Despite rapid advance in miRNA research, the detailed functions and regulatory mechanisms of most of miRNAs are still poorly understood. To gain better understanding, an important task herein is to identify miRNAs' regulatory targets. However, the current knowledge about the known targets is disproportional to that of the known miRNAs.

Therefore it is urgent to come up with effective target identification method for genome wide target discovery. Past work produced many target prediction algorithms based on miRNA-target sequence paring including TargetScan[2] [3] [4], MirTarget[5], PicTar[6], SVMicrO[7] [8] and others[9] [10] [11] [12] [13] [14] [15]. Usually, for a given training data set, each one of the algorithms will come up with

⋆ Corresponding author.

D.-S. Huang et al. (Eds.): ICIC 2010, LNCS 6215, pp. 258–265, 2010.

a set of different target prediction scores, but none of them is totally perfect. The prediction results of existing algorithms are still of low precision and poor sensitivity. A mass spectrometry (MS) approach was used to validate the prediction results of TargetScan, PicTar, etc[16]. And a precision of about 30% was achieved. Therefore, the existing algorithms still cannot be used as target screening for bench testing.

In this paper, we propose to improve the performance of existing target prediction algorithms. The motivation is that there seems to be a poor agreement between the results of different algorithms and yet they achieve similar performance; this fact indicates that different algorithms rely on different mechanisms in making decision, each of which has its own advantages. Although a few important features including "seed region complementary", "binding free energy" and "sequence conservation" are among the most common adopted ones, different algorithms utilize different sets of features. Moreover, different algorithms use different classifiers. The differences in features and classifiers contribute to the differences in their prediction results. Then it is desirable to integrate prediction scores of different algorithms together so that a more reliable result could be achieved. Then a decision fusion approach was adopted in this paper by building up a general model to combine the confidence scores of all the algorithms. The performance of our proposed method on combining the predictions of TargetScan, MirTarget and PicTar was tested and validated on the proteomics data. This method shows some improvement, and it can be easily extended to combine more algorithms. The final implementation is computationally efficient.

2 Methods

2.1 Overview of TargetScan, MirTarget and PicTar

TargetScan uses a scoring system in (1) to assign score to the 3'UTR for miRNA target prediction.

$$S_{TargetScan} = S_1 + S_2 + S_3 + S_4 \tag{1}$$

It is the summation of four types of contributions. S_1 presents the score of seed-type contribution, S_2 is of 3' pairing contribution, S_3 is of local AU contribution, while S_4 is of position contribution.

MirTarget uses a scoring system in (2) to assign score to the 3'UTR for target prediction.

$$S_{MirTarget} = 100 \times (1 - \sum_{i=1}^{n} p_i) \tag{2}$$

Where n represents the total number of candidate target sites in one UTR and p_i represents the statistical significance p-value for each of these candidate sites estimated by SVM.

PicTar uses a HMM to assign a score to the 3'UTR for target prediction. It assums the 3'UTRwas generated by the HMM, whose states were target sites of co-expressed miRNAs plus the background nucleotide sequence. PicTar computes the log ratio of the probability of the probing sequence being generated

by this HMM versus the probability that it was generated by the background process alone as a score. The final score S_{PicTar} is the average of the PicTar scores for all 3'UTRs that were used to define anchor sites.

For the above algorithms, scores obtained can be regarded as confidence for target prediction. In TargetScan, the lower the score is, the more confident the mRNA is a target, while in MirTarget and PicTar, the higher the score is, the more confident the mRNA is a target.

2.2 Decision Fusion

Decision fusion is regarded as a high level fusion to combine decisions from several experts. By extension, we speak of decision fusion even if the experts return a confidence (score) and not a decision[17].

Model Formulation. Genome-wide predictions of TargetScan, MirTarget and PicTar are all reported in terms of confidence scores. Considering the fact that each algorithm only regards some aspects of miRNA:mRNA features, it is more reliable to make decision by fusing the confidence of different algorithms. Since fusing information from several sources always requires some pre-analysis of the raw data to obtain homogeneous information referring to the same entity, so the involved confidence scores for fusion should first be mapped into a general range. To this end, we proposed the combined score, which is a function of confidence scores of individual algorithms.

$$Score = \mathcal{F}(\mathcal{T}_T(S_{TargetScan}), \mathcal{T}_M(S_{MirTarget}), \mathcal{T}_P(S_{PicTar})) \tag{3}$$

Here T_* is the pre-processing function for each algorithm, and $\mathcal{F}$ denotes the function for combination. Considering the fact that each algorithm only regards some aspects of prediction features, the simplest function to combine the three groups of score is shown in (4).

$$Score = a_T\mathcal{T}_\mathcal{T}(S_{TargetScan}) + a_M\mathcal{T}_\mathcal{M}(S_{MirTarget}) + a_P\mathcal{T}_\mathcal{P}(S_{PicTar}) \tag{4}$$

Where a_* is the weight for scores of each algorithm.

Pre-processing step. We first map the scores of each algorithm to probabilities by logistic function. Standard logistic function is shown in (5).

$$P(t) = \frac{1}{1 + e^{-t}} \tag{5}$$

By logistic function, variable t ranging over the real numbers from $-\infty$ to $+\infty$ can be mapped to a probability space which is $[0, 1]$.

In our case, a more general logistic model is used to carry out the pre-processing, shown in (6).

$$p = P(\alpha_0 + \alpha_1 S) \tag{6}$$

Where S represents the scores of each algorithm,α_0,α_1 are model parameters to be trained and $P()$ is the logistic function in (5).

$$\alpha_0 = \tau_L - t_{min}\frac{\tau_M - \tau_L}{t_{max} - t_{min}} \tag{7}$$

$$\alpha_1 = \frac{\tau_M - \tau_L}{t_{max} - t_{min}} \tag{8}$$

Where t_{max} represents the maximum of t while t_{min} represents the minimum.

Because each algorithm only retains the scores of about 100 to 1000 potential targets out of the entire 27,000 UTRs in genome wide for a specific miRNA, the scores need to be mapped into a more significant range $[\tau_L, \tau_M]$ instead of entire $[0, 1]$. Here τ_L represents the least significant probability while τ_M represents the most significant probability. Intuitively, we are more willing to believe the case a UTR is a target predicted by more algorithms even if confidence of each algorithm is low comparing to the case a UTR is a target but predicted by fewer algorithms with higher confidence of each algorithm. Based on this concept, there is the restrict for τ_L and τ_M in (9).

$$\alpha_0 = \tau_L - t_{min}\frac{\tau_M - \tau_L}{t_{max} - t_{min}} \tag{9}$$

Where n is the number of algorithms to be combined. TargetScan, MirTarget and PicTar are considered in this paper, so $n = 3$. There is the prior knowledge that each miRNA can regulate about 1% human genes, so we make $\tau_M = 0.99$. As in (9), τ_L should be larger than 0.66. If we think more of the decision of majority algorithms rather than extreme opinion of minority algorithms, a larger τ_L should be chosen. So we make $\tau_L = 0.8$ in this paper. In the three algorithms, only scores of potential targets are retained, those mRNAs predicted to be negative don't have any scores. A prior equals to 0.01 is assigned to those potential negative mRNAs as the output of function $\mathcal{T}_*$ directly.

Combination step. We propose to get more refined information by combining the above pre-processed confidence in this step. Each discrimination mechanism is considered to contribute equally to miRNA target prediction. Therefore the same weight is adopted for combination of all three algorithms in this paper.

3 Results

To investigate the performance of our proposed method, predictions for human miR-1, let-7b, miR-16, miR-30a, miR-124 and miR-155 are carried out and tested on the ground truth retrieved from proteomics data [16] [18].

3.1 Test on the proteomics Data

As is known, mRNA degradation and translation inhibition will lead to down regulation in protein level. In [16] [18], protein fold change due to the over-expression

of specific miRNAs were measured by stable-isotope-labeling-of-amino-acids-in culture (SILAC) and quantified by LC/MS. Obviously, a protein with a larger down-fold in the experiment means the corresponding mRNA is more likely to be a true target. However, due to the limitation of LC/MS coverage, only a subset of proteome was identified. Therefore, target prediction was only done among these proteins. Fig.1 and Fig.2 depicts the CFC (Cumulative Fold Change) for the predictions of let-7b and miR-1. Intuitively, CFC rewards higher confidence prediction with a drop and penalizes false prediction with a raise in the fold change. A better algorithm with higher precision and smaller false positive is expected to show faster drop in CFC. For let-7b, MirTarget and our proposed method clearly set them apart from the others, with proposed method performing slightly better up to top 20, shown in Fig. 3. At top 40 and top 80, the proposed method has clear advantage over the others. For miR-1, shown in Fig.4 proposed method is still among the better performing algorithms. After top 20, our method achieves apparently much sharper drops than the others. Moreover, same validation was also carried out for miR-124, miR-30a, miR-155

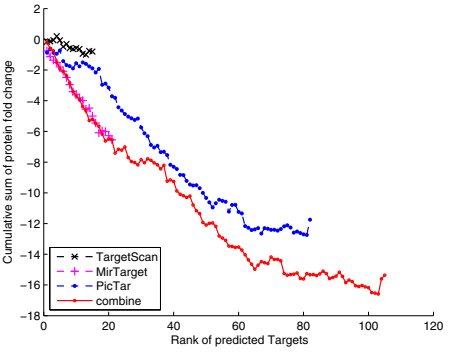

Fig. 1. Entire Cumulative sum of protein fold change for predictions of let-7b

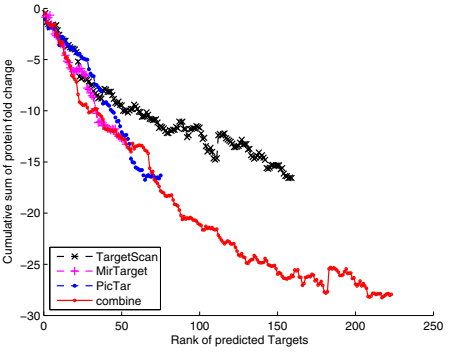

Fig. 2. Entire Cumulative sum of protein fold change for predictions of miR-1

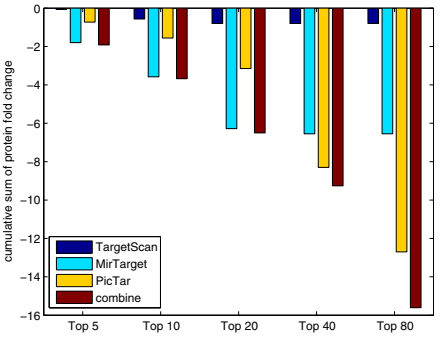

Fig. 3. Cumulative sum of protein fold change for different number of top ranked predictions of let-7b

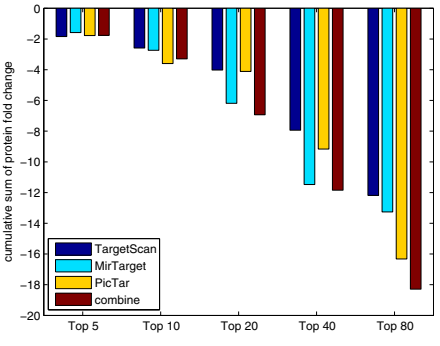

Fig. 4. Cumulative sum of protein fold change for different number of top ranked predictions of miR-1

and miR-16(not shown in this paper). Based on above results of proteomics experimental data, we also investigated the consistency of each algorithm over all the 6 miRNAs. Obviously, a good algorithm should have a cumulative sum curve with two characteristics, 1) drop fast at the beginning and 2) drop deep over all. Therefore, we calculate the averaged area under cumulative sum curve (shown in (10)) as an overall measurement of the performance of each algorithm.

$$\mathcal{M}(n) = \frac{1}{n} \int_0^n c(x)dx \tag{10}$$

Where $c(x)$ denotes the function of cumulative sum curve and $\mathcal{M}(n)$ indicates the averaged area under cumulative sum curve of top n predicted targets. Intuitively, the smaller $\mathcal{M}(n)$ is, the better performance the algorithm achieves. Subsequently, a consistency measurement of $n \in \{5, 10, 20, 40, 80, 100\}$ was defined as the average value of all the six $\mathcal{M}(n)$s.

$$\mathcal{C}(n) = \frac{1}{6}\sum_{i=1}^{6}\mathcal{M}_i(n) \tag{11}$$

The result in Table 1 clearly shows that proposed method overcomes other algorithms nearly in all cases. Consequently, a conclusion can be drawn that performance of proposed method is not only good but also consistent.

Table 1. Average cumulative sum rank of each algorithm

	TargetScan	MirTarget	PicTar	Combined
# of target	125	61	78	205
Top 10	4	2	3	1
Top 20	4	2	3	1
Top 40	3	2	4	1
Top 80	2	3	4	1
Top 200	2	3	4	1

4 Conclusion

In this paper, we presented a new method for miRNA target prediction by combining the prediction results of TargetScan, MirTarget and PicTar. A logistic transformation was designed to obtain homogeneous information from the three groups of results and a combination algorithm was designed to fuse the pre-processed prediction confidence. The validation results on proteomics data demonstrated the better performance of our proposed method.

Acknowledgments. Miss Lin Zhang is supported by "Qi-hang" Project of China University of Mining and Technology. Dr. Yufei Huang is supported by an NSF Grant CCF-0546345.

References

1. Bartel, D.P.: MicroRNAs:: Genomics, Biogenesis, Mechanism, and Function. Cell 116(2), 281–297 (2004)
2. Grey, F., Hook, L., Nelson, J.: The Functions of Herpesvirus-encoded MicroRNAs. Medical microbiology and immunology 197(2), 261–267 (2008)
3. Medina, P.P., Slack, F.J.: microRNAs and Cancer: an Overview. Cell cycle (Georgetown, Tex.) 7(16), 2485 (2008)
4. Grimson, A., Farh, K.K.H., Johnston, W.K., Garrett-Engele, P., Lim, L.P., Bartel, D.P.: MicroRNA Targeting Specificity in Mammals: Determinants Beyond Seed Pairing. Molecular cell 27(1), 91–105 (2007)
5. Lewis, B.P., Burge, C.B., Bartel, D.P.: Conserved Seed Pairing, Often Flanked by Adenosines, Indicates That Thousands of Human Genes Are MicroRNA Targets. Cell 120(1), 15–20 (2005)

6. Lewis, B.P., Shih, I., et al.: Prediction of Mammalian MicroRNA Targets. Cell 115(7), 787–798 (2003)
7. Yue, D., Liu, H., Huang, Y.: Survey of Computational Algorithms for MicroRNA Target Prediction. Current Genomics 10(7), 478–492 (2009)
8. Liu, H., Zhang, L., Gao, S.J., Huang, Y.: A Bayesian Approach for Identifying miRNA Targets by Combining Sequence Prediction and Expression Profiling
9. Wang, X., El Naqa, I.M.: Prediction of Both Conserved and Nonconserved MicroRNA Targets in Animals. Bioinformatics 24(3), 325 (2008)
10. Krek, A., Grün, D., Poy, M.N., Wolf, R., Rosenberg, L., Epstein, E.J., MacMenamin, P., da Piedade, I., Gunsalus, K.C., Stoffel, M., et al.: Combinatorial microRNA Target Predictions. Nature genetics 37(5), 495–500 (2005)
11. Miranda, K.C., Huynh, T., Tay, Y., Ang, Y.S., Tam, W.L., Thomson, A.M., Lim, B., Rigoutsos, I.: A Pattern-based Method For the Identification of MicroRNA Binding Sites and Their Corresponding Heteroduplexes. Cell 126(6), 1203–1217 (2006)
12. Rajewsky, N., Socci, N.D.: Computational Identification of MicroRNA Targets. Genome Biology 5(2), 5 (2004)
13. Rehmsmeier, M., Steffen, P., HÖChsmann, M., Giegerich, R.: Fast and Effective Prediction of MicroRNA/Target Duplexes. RNA 10(10), 1507 (2004)
14. Rusinov, V., Baev, V., Minkov, I.N., Tabler, M.: MicroInspector: a Web Tool for Detection of MiRNA Binding Sites in an RNA Sequence. Nucleic acids research 33(Web Server Issue), W696 (2005)
15. Saetrom, O., Snøve, O., Sætrom, P.: Weighted Sequence Motifs as an Improved Seeding Step in MicroRNA Target Prediction Algorithms. RNA 11(7), 995 (2005)
16. Selbach, M., Schwanhäusser, B., Thierfelder, N., Fang, Z., Khanin, R., Rajewsky, N.: Widespread Changes in Protein Synthesis Induced by MicroRNAs. Nature 455(7209), 58–63 (2008)
17. Yousef, M., Jung, S., Kossenkov, A.V., Showe, L.C., Showe, M.K.: Naive Bayes for MicroRNA Target Predictions Machine Learning for MicroRNA Targets. Bioinformatics 23(22), 2987 (2007)
18. Baek, D., Villén, J., Shin, C., Camargo, F.D., Gygi, S.P., Bartel, D.P.: The Impact of MicroRNAs on Protein Output. Nature 455(7209), 64–71 (2008)

Imperialistic Competitive Algorithm for Solving a Dynamic Cell Formation Problem with Production Planning

Fatemeh Sarayloo[1] and Reza Tavakkoli-Moghaddam[2]

[1] Department of Industrial Engineering, Graduate School Islamic Azad University-South Tehran Branch, Tehran, Iran
[2] Department of Industrial Engineering and Department of Engineering Science, College of Engineering, University of Tehran
f.saraylou@yahoo.com, tavakoli@ut.ac.ir

Abstract. Cellular manufacturing system, an application of group technology, has been considered as an effective way to obtain productivity in a factory. For design of manufacturing cells, several mathematical models and various algorithms have been proposed in literature. However, most of algorithms and models have more or fewer drawbacks. A dynamic cell formation problem with production planning is considered in this paper, where the sum of costs consisting constant machine costs, variable machine costs, intra-inter movement costs, production planning costs and reconfiguration costs is to be minimized. Because this type of problem is Np-hard, evolutionary algorithms are applied. In this paper the Imperialistic Competitive Algorithm (ICA), which optimizes inspired by imperialistic competition, is used. ICA is compared with other well-known evolutionary algorithms, *i.e.* genetic algorithm (GA) and particle swarm optimization (PSO), to show its efficiency. The computational results show the considerable superiority of ICA compared with PSO and GA.

Keywords: Cellular manufacturing, Production Planning, Evolutionary Algorithm, Imperialistic Competitive Algorithm.

1 Introduction

Group technology (GT) is a manufacturing philosophy that has established the potential to contribute positively in batch-type production, and it endeavors to combine the flexibility of the job production system with the high productivity of the flow production system [1]. Burbidge [2] defined GT as an approach to the optimization of work in which the organizational production units are relatively independent groups, each responsible for the production of a given family of products. By recognizing similarities among parts to be processed in the same facility, GT principles have provided the basis for converting the conventional job shop into a cellular layout with several manufacturing cells, each with a dedicated part mix [3].

D.-S. Huang et al. (Eds.): ICIC 2010, LNCS 6215, pp. 266–276, 2010.

The major benefits of CM have been reported in the literature as simplification and reduction in material handling, decreasing the work-in-process inventories, reduction in set-up time, increment in flexibility, better production control and shorter lead time [4][5]. However cell formation is the first step in designing, other aspects such as production planning is important to be considered.

The CF problem is known as NP-hard. This type of problem has complex computation; therefore, achieving optimal solution is not possible in large size problems with reasonable amount of time. There are several approaches to solve NP-hard problems approximately but in polynomial time.

2 Literature Review

The CF problem consists of two important aspects: part family formation and machine group formation. Accordingly, part oriented and machine oriented are two major categories which are called also the process oriented and production oriented method, respectively. In industrial applications, the part oriented methods are not as popular as process oriented methods, because there are a lot of parts which are similar but have to be made in different manufacturing cells. The part oriented methods include two methods: the visual inspection method and part coding analysis. The process-oriented methods can be further classified as cluster analysis, graph partitioning, mathematical programming, artificial intelligence, or heuristics [3].

Heuristic method: The meta heuristic and heuristic methods are applied broadly in various NP-hard problems. The heuristic methods help us to achieve near optimal solutions in large size problems with a reasonable time. The most common heuristic methods are genetic algorithm, particle swarm optimization, ant colony algorithm, tabu search algorithm and simulated annealing algorithm. The brief review of PSO is as follow[6]:

PSO is initialized with a group of random particles (solutions) and then searches for optima by updating generations. In every iteration, each particle is updated by following two "best" values. The first one is the best solution (fitness) it has achieved so far. (The fitness value is also stored.) This value is called pbest. Another "best" value that is tracked by the particle swarm optimizer is the best value, obtained so far by any particle in the population. This best value is a global best and called gbest. After finding the two best values, the particle updates its velocity and positions with following equation (1) and (2).

$$v[i] = w * v[i] + R_1(pbest[i] - present[i]) + R_2(gbest[i] - present[i]) \quad (1)$$

$$present[i] = parent[i] + v[i] \quad (2)$$

$v[i]$ is the velocity of particle i, $present[i]$ is the current particle i (solution). $pbest[i]$ and $gbest[i]$ are defined as stated before.R_1,R_2 are learning factors.w is inertia weight. The pseudo code of the procedure is as follows[6]:

```
For each particle
Initialize particle
END
Do
  For each particle
      Calculate fitness valu
           If the fitness value is better than the best
        fitness value (pBest) in history
        set current value as the new pBest
  End
Choose the particle with the best fitness value of all the
particles as the gBest
    For each particle
       Calculate particle velocity according equation(1)
        Update particle position according equation (2)
         EndWhile maximum iterations or minimum error criteria
     is not attained
```

3 Problem Formulation

In this section, the integrated optimization problem is formulated as a nonlinear mixed-integer programming model. The problem is formulated as follows [7]:

Indices:

c	index for manufacturing cells, c=(1,…,C)
m	index for machine types, m=(1,…,M)
p	index for part types, p=(1,…,P)
h	index for time periods, h=(1,…,H)
j	index for operations which belongs to part j=(1,…, O_p)

Input parameters:

P	number of part types
O_p	number of operations for part p
M	number of machine types
C	maximum number of cells that can be formed
D_{ph}	demand for part p in period h
$\gamma^{\text{int}\,er}$	Inter-cell movement cost
$\gamma^{\text{int}\,ra}$	Intra-cell movement cost
α_m	constant cost of machine type m in each period
β_m	variable cost of machine type m for each unit time
δ_m	relocation cost of machine type m
T_m	time-capacity of machine type m in each period
UB	maximal cell size

t_{jpm} processing timer required to perform operation j of part type p on machine type m

a_{jpm} equals to1,if operation j of part p can be done on machine type m; 0 otherwise

η_p inventory carrying cost per unit part p during each period

ρ_p backorder cost per unit part p during each period

l lead time where $l \le H-1$

Decision variables:

N_{mch} number of machines type m allocated to cell c in period h

x_{jpmch} the portion of operation j of part type p is done on machine type m in cell c in period h

Q_{ph} number of production of part p produced in period h

I_{ph} inventory/backorder level of part p at the end of period h. A negative value of I_{ph} means the backordered level or shortage.

Mathematical model:

By using mentioned notations, the proposed model is written as follows[42]:

$$\min Z = \sum_{h=1}^{H}\sum_{m=1}^{M}\sum_{c=1}^{C} N_{mch}\alpha_m \tag{3}$$

$$+\sum_{h=1}^{H}\sum_{c=1}^{C}\sum_{p=1}^{P}\sum_{j=1}^{O_p}\sum_{m=1}^{M} B_m Q_{ph} t_{jpm} x_{jpmch} + \frac{1}{2}\sum_{h=1}^{H}\sum_{p=1}^{P}\sum_{j=1}^{O_p-1}\sum_{c=1}^{C} Q_{ph}\gamma^{\text{int}\,er} \times \left|\sum_{m=1}^{M} x_{(j+1)pmch} - \sum_{m=1}^{M} x_{jpmch}\right|$$

$$+\frac{1}{2}\sum_{h=1}^{H}\sum_{p=1}^{P}\sum_{j=1}^{O_p-1}\sum_{c=1}^{C} Q_{ph}\gamma^{\text{int}\,ra} \times \left(\sum_{m=1}^{M}\left|x_{(j+1)pmch} - x_{jpmch}\right| - \left|\sum_{m=1}^{M} x_{(j+1)pch} - \sum_{m=1}^{M} x_{jpch}\right|\right)$$

$$+\frac{1}{2}\sum_{h=1}^{H}\sum_{c=1}^{C}\sum_{m=1}^{M}\delta_m\left|N_{mch} - N_{mch-1}\right| + \sum_{h=1}^{H}\sum_{p=1}^{P}(\eta_p I_{hp}^{+} + \rho_p I_{hp}^{-})$$

s.t.

$$\sum_{c=1}^{C}\sum_{m=1}^{M}\sum_{p=1}^{P}\sum_{j=1}^{Op} a_{jpm} x_{jpmch} = 1 \qquad \forall h \tag{4}$$

$$\sum_{p=1}^{P}\sum_{j=1}^{Op} Q_{ph} t_{jpm} x_{jpmch} \le T_m N_{mch} \qquad \forall m,c,h \tag{5}$$

$$\sum_{m=1}^{M} N_{mch} \le UB \qquad \forall c,h \tag{6}$$

$$\sum_{c=1}^{C}\sum_{m=1}^{M} N_{mch} \ge 1 \qquad \forall h \tag{7}$$

$$N_{mc(h-1)} + K^{+}_{mch} + K^{-}_{mch} = N_{mch} \qquad \forall m,c,h \tag{8}$$

$$I_{ph} = I_{p(h-1)} + Q_{ph} - D_{ph} \qquad \forall p,h \tag{9}$$

$$I^{+}_{ph} \le I_{ph}, I^{-}_{ph} \ge -I_{ph} \qquad \forall p,h \tag{10}$$

$x_{jpmch} \in [0,1], N_{mch}, Q_{ph}, I^{+}_{ph}, I^{-}_{ph}, \ge 0$ And integer

$-\infty \langle I_{ph} \langle \infty$ and integer

The objective function of model (Eq.3) consists of six terms. The first term is the total sum of constant costs. The second one is the variable costs of machines. The third and fourth term signify intra-cellular and inter-cellular movement costs. Coefficient 1/2 in this term is embedded because each movement is taken into account twice in calculation.

The fifth term presents cell reconfiguration costs which are sum of adding, removing and relocating costs of machines between cells in consecutive periods. Coefficient 1/2 in this term is embedded because each reconfiguration cost is taken into account twice in calculation. The last term is production planning cost consisting of inventory and backorder costs.

Equation (4) guarantees that all part-operation is assigned to machines. Equation (5) ensures that machine capacities are not exceeded and must satisfy the demand. Equation (6) guarantees the maximum cell size is not violated. Equation (7) guarantees that the number of all machines in one period is not 0. Equation (8) is called a balance constraint ensuring that the number of machines in the current period is equal to the number of machines in the previous period, plus the number of machines being moved in, and minus the number of machines being moved out. Equation (9, 10) indicate the balance inventory constraint between periods for each part type at each period. It means that the inventory level of each part at the end of each period is equal to the inventory level of the part at the end of the previous period plus the quantity of production minus the part demand rate in the current period.

4 Imperialistic Competitive Algorithm

Cell formation problem with considering production planning is defined as an NP-hard problem. Meta heuristic and evolutionary algorithms are useful methods to solve NP-hard problems. Imperialistic Competitive Algorithm is classified into population based method, like Genetic Algorithm. ICA can be a useful method in optimization because of its reasonable run time and effectiveness.

4.1 Main Steps of ICA

[8] Presented ICA as a novel evolutionary algorithm. In this section, we apply ICA for our model and its steps are as follows [8].

a) Generating Initial Empires

The goal of optimization is to find an optimal solution in terms of the variables of the problem. [8] formed an array of variable values to be optimized. In GA terminology, this array is called "*chromosome*", but here the term "*country*" is used for this array. In an N_{var} – dimensional optimization problem, a country is a $1 \times N_{var}$ array. This array is defined by(Eq.11)

$$contury = [p_1, p_2, p_3, \dots, p_{N_{var}}] \tag{11}$$

The variable values in the country are represented as floating point numbers. The cost of a country is found by evaluating the cost function *f* at the variables $(p_1, p_2, p_3, \dots, p_{N_{var}})$. Then (Eq.12):

$$cost = f(country) = f(p_1, p_2, p_3, \dots, p_{N_{var}}) \tag{12}$$

To start the optimization algorithm we generate the initial population of size N_{pop}. We select N_{imp} of the most powerful countries to form the empires. The remaining N_{col} of the population will be the colonies each of which belongs to an empire. Then we have two types of countries; *imperialist* and *colony*.

To form the initial empires, we divide the colonies among imperialists based on their power. That is the initial number of colonies of an empire should be directly proportionate to its power. To divide the colonies among imperialists proportionally, we define the normalized cost of an imperialist by Eq.13:

$$C_n = c_n - max_i\{c_i\} \tag{13}$$

Where c_n is the cost of *n*th imperialist and C_n is it normalized cost. Having the normalized cost of all imperialists, the normalized power of each imperialist identified by Eq.14:

$$p_n = \left| \frac{C_n}{\sum_{i=1}^{N_{imp}} C_i} \right| \tag{14}$$

From another point of view, the normalized power of an imperialist is the portion of colonies that should be possessed by that imperialist. Then the initial number of colonies of an empire will be (Eq.15)

$$N.C._n = round\{p_n.N_{col}\} \tag{15}$$

Where $N.C._n$the initial is number of colonies of *n*th empire and N_{col} is the number of all colonies. To divide the colonies, for each imperialist, [8] randomly chose $N.C._n$of the colonies and give them to it. These colonies along with the imperialist will form *n*th empire. Figure 1 shows the initial population of each empire. As

shown in this figure bigger empires have greater number of colonies while weaker ones have less. In this figure imperialist 1 has formed the most powerful empire and has the greatest number of colonies.

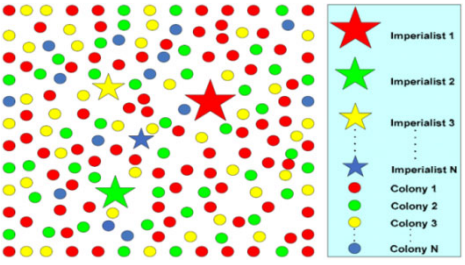

Fig. 1. Generating the initial empires: the more colonies an imperialist possess, the bigger is its relevant ★mark

b) Moving the Colonies of an Empire toward the Imperialist

Imperialists countries started to improve their colonies. They have modeled this fact by moving all the colonies toward the imperialist. This movement is shown in figure 2 in which the colony moves toward the imperialist by x units. The new position of colony is shown in a darker color. The direction of the movement is the vector from colony to imperialist. In this figure x is a random variable with uniform (or any proper)

$$x \backsim U(0, \beta \times d)$$

Where β is a number greater than 1 and d is the distance between colony and imperialist. A $\beta > 1$ causes the colonies to get closer to the imperialist state from both sides.

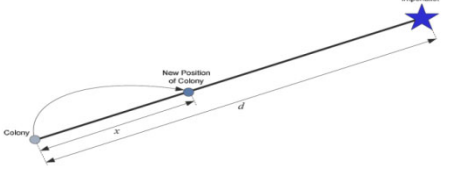

Fig. 2. Moving colonies toward their relevant imperialist

c) *Exchanging Positions of the Imperialist and a Colony*

While moving toward the imperialist, a colony may reach to a position with lower cost than that of imperialist. In such a case, the imperialist moves to the position of that colony and vise versa. Then algorithm will continue by the imperialist in a new position and then colonies start moving toward this position. Figure 3a depicts the position exchange between a colony and the imperialist. In this figure the best colony of the empire is shown in a darker color. This colony has a lower cost than that of imperialist. Figure 3b shows the whole empire after exchanging the position of the imperialist and that colony.

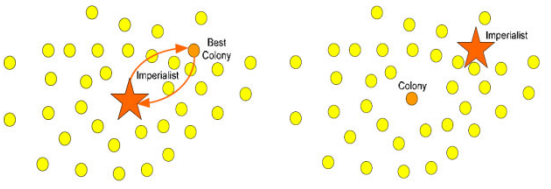

Fig. 3. (a) Exchanging the positions of a colony and the imperialist (b) The entire empire after position exchange

d) *Total Power of an Empire*

Total power of an empire is mainly affected by the power of imperialist country. But the power of the colonies of an empire has an effect, albeit negligible, on the total power of that empire. We have modeled this fact by defining the total cost by Eq. 16:

$$T.C._n = Cost(imperialist_n) + \xi mean\{Cost(colonies\ of\ empire_n)\} \quad (16)$$

Where $T.C._n$*the total is* cost of the nth empire and ξ is a positive number which is considered to be less than 1. A little value for ξ causes the total power of the empire to be determined by just the imperialist and increasing it will increase the role of the colonies in determining the total power of an empire.

e) *Imperialistic Competition*

All empires try to take possession of colonies of other empires and control them. This imperialistic competition gradually brings about a decrease in the power of weaker empires and an increase in the power of more powerful ones. [8] modeled this competition by just picking some (usually one) of the weakest colonies of the weakest empires and making a competition among all empires to possess these (this) colonies. Figure 4 shows a big picture of the modeled imperialistic competition. Based on their total power, in this competition, each of empires will have a likelihood of taking possession of the mentioned colonies. In other words these colonies will not be possessed by the most powerful empires, but these empires will be more likely to possess them.

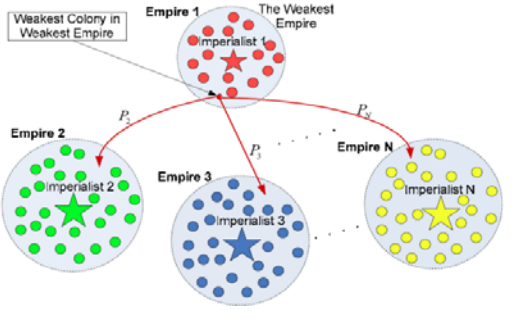

Fig. 4. Imperialistic competition. The more powerful empire is, the more likely it will possess the weakest colony of the weakest empire.

To start the competition, first, we find the possession probability of each empire based on its total power. The normalized total cost is simply obtained by Eq.17:

$$N.T.C._n = T.C._n - max_i\{T.C._i\} \tag{17}$$

Where $T.C._n$ and $N.T.C._n$ are respectively total cost and normalized total cost of nth empire. Having the normalized total cost, the possession probability of each empire is given by Eq. 18:

$$p_{p_n} = \left| \frac{N.T.C._n}{\sum_{i=1}^{N_{imp}} N.T.C._i} \right| \tag{18}$$

To divide the mentioned colonies among empires based on the possession probability of them, we form the vector P as Eq.19:

$$P = [p_{p_1}, p_{p_2}, p_{p_3}, \ldots, p_{p_{N_{imp}}}] \tag{19}$$

Then we create a vector with the same size as P whose elements are uniformly distributed random numbers.(Eq.20)

$$R = \left[r_1, r_2, r_3, \ldots, r_{N_{imp}}\right] \tag{20}$$

$$r_1, r_2, r_3, \ldots, r_{N_{imp}} \backsim U(0,1)$$

Then vector D is formed by simply subtracting R from .

$$D = P - R = \left[D_1, D_2, D_3, \ldots, D_{N_{imp}}\right] = \tag{21}$$

$$[p_{p_1} - r_1,\ p_{p_2} - r_2, p_{p_3} - r_3, \ldots, p_{p_{N_{imp}}} - r_{N_{imp}}]$$

Referring to vector D, [8] handed the mentioned colonies to an empire whose relevant index in D is maximum.

f) *Eliminating the Powerless Empires*

Powerless empires will collapse in the imperialistic competition and their colonies will be divided among other empires. In modeling collapse mechanism different criteria can be defined for considering an empire powerless. In most of our implementation, we assume an empire collapsed and eliminate it when it loses all of its colonies.

g) *Convergence*

After a while all the empires except the most powerful one will collapse and all the colonies will be under the control of this unique empire. In this ideal new world all the colonies will have the same positions and same costs and they will be controlled by an imperialist with the same position and cost as themselves. In this ideal world, there is no difference not only among colonies but also between colonies and imperialist. In such a condition we put an end to the imperialistic competition and stop the algorithm.

5 Experimental Result

In this section, ICA is tested with five test problems. All of these problems are generated randomly. The details of these problems are shown in Tab.1.

To make comparison, we applied GA and PSO for these test problems.

Algorithm assumptions:

General assumption: number of population=100, max iteration =100
ICA: $\beta = 2, \xi = 0.1$, number of empires:5
PSO: W=0.7, R_1=1.5, R_2=1.5
GA: the crowded comparison is used for selection operator.simulated binary cross over (SBX) and polynomial mutations are used as genetic operators.

Fig.5. (a) and (b). depict the best cost of two test problem 1 and 2 respectively, versus generation in ICA, PSO and GA.

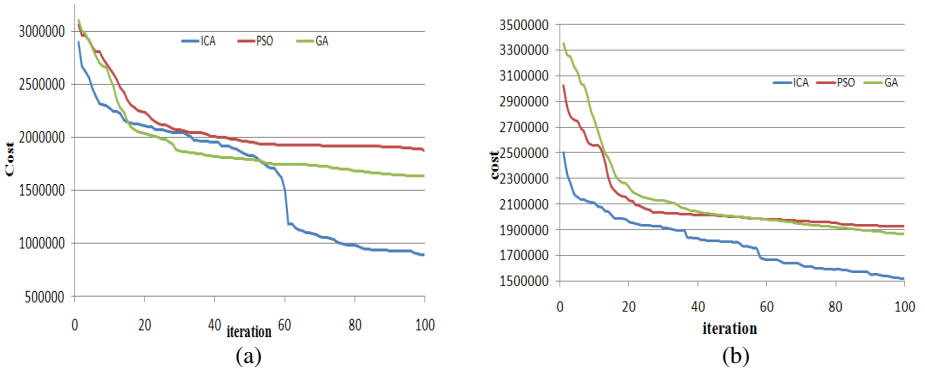

Fig. 5. (a):Comparison between algorithms on Test Problem 1,(b):Comparison between algorithms on Test Problem 2.

The computational results shown in Table.2 depict that ICA considerably obtain better result compared with GA and PSO.

Table 1. Test problems

No. test problem	$p(\sum Op)\times M\times H$
1	5(11)×5×3
2	7(12)×6×2
3	8(18)×7×2
4	9(27)×8×2
5	10(23)×9×2
6	14(30)×15×3
7	20(30)×20×4

Table 2. Computation results

Test Pro.	ICA Cost ($*10^6$)	ICA Time (Sec)	PSO Cost ($*10^6$)	PSO Time (Sec)	GA Cost ($*10^6$)	GA Time (Sec)
1	**0.98**	**15**	**1.7**	**20**	**1.9**	**24**
2	**1.5**	**55**	**1.9**	**70**	**2**	**87**
3	**2.3**	**130**	**3.6**	**190**	**3.8**	**210**
4	**2.7**	**400**	**3.9**	**480**	**3.6**	**520**
5	**3.2**	**630**	**3.7**	**786**	**3.8**	**834**
6	**4.1**	**860**	**5**	**950**	**5.6**	**980**
7	**4.8**	**1100**	**5.6**	**1300**	**5.7**	**1400**

6 Conclusion

In this paper, a dynamic cell formation problem with production planning was considered. Because this type of problem is Np-hard, we applied ICA which is an evolutionary algorithm. The computational results show that ICA has a better performance and runtime compared with PSO and GA. Parameter setting and considering other real production factors are interesting and important aspects to be investigated in future works.

References

1. Ham, I., Hitomi, K.: Group technology applications to production management. Kluwer-Nijhoff, Boston (1985)
2. Burbidge, J.L.: Group technology in engineering industry (1979)
3. Liu, C.G., Yin, Y., Yasuda, K., Lian, J.: A heuristic algorithm for cell formation problems with consideration of multiple production factors. Int. J. Adv. Manuf. Technol., 1201–1213 (2009)
4. Asking, R.G., Estrada, S.: Investigation of cellular manufacturing practices. In: Hand book of cellular manufacturing systems, ch. 1, pp. 25–34. John Wiley, New York (1999)
5. Aramoon-Bajestani, M., Rabbani, M., Rahimi–Vahed, A.R., Baharian khoshkhou, G.: A multi objective scatter search for a dynamic cell formation problem. Computers and Operation Research 36, 777–794 (2009)
6. http://www.swarmintelligence.org
7. Safaei, N., Tavakkoli-Moghaddam, R.: Integrated multi-period cell formation and subcontracting production planning in dynamic cellular manufacturing systems. Int. J. Production Economics, 301–314 (2009)
8. Atashpaz, G.E., Lucas, C.: Imperialist Competitive Algorithm: An Algorithm for Optimization Inspired by Imperialistic Competition. In: IEEE congress on Evolutionary computation CEC 2007, pp. 4661–4667 (2007)

Genome-Wide DNA Methylation Profiling in 40 Breast Cancer Cell Lines

Leng Han[1,2], Siyuan Zheng[1,2], Shuying Sun[3], Tim H.-M. Huang[4], and Zhongming Zhao[1,2,5,*]

[1] Department of Biomedical Informatics, Vanderbilt University School of Medicine, Nashville, TN, 37232, USA
[2] Bioinformatics Resources Center, Vanderbilt University, Nashville, TN, 37203, USA
[3] Case Comprehensive Cancer Center, Case Western Reserve University, Cleveland, OH, 44106, USA
[4] Human Cancer Genetics Program, The Ohio State University, Columbus, OH 43210, USA
[5] Department of Cancer Biology, Vanderbilt University School of Medicine, Nashville, TN, 37232, USA
zhongming.zhao@vanderbilt.edu

Abstract. DNA methylation plays important roles in gene regulation and functions. Aberrant methylation, either hypomethylation or hypermethylation, has been reported to cause various diseases, especially cancers. Breast cancer ranked the fifth according to the number of cancer deaths in the world. To systematically characterize the epigenetic modification in breast cancer, we examined the genome-wide methylation profiling in 40 breast cancer cell lines. We identified a gene signature consisting of 345 differentially methylated genes, which could be used to discriminate estrogen receptor (ER)-negative and ER-positive breast cancer cell lines. This gene signature is promising for diagnosis and therapies of breast cancer. In the follow up functional analysis of this gene signature, three enriched networks could be highlighted. Interestingly, one of these networks contained estrogen receptor, implying its functional importance of ER-centric module. Finally, we examined the correlation between methylation and expression of these breast cancer cell lines. Very few genes showed significant correlation, suggesting that gene expression regulated by methylation is a complex biological process.

Keywords: breast cancer, estrogen receptor, methylation, network, expression.

1 Introduction

1.1 Breast Cancer and Estrogen Receptor (ER)

Breast cancer causes the fifth largest amount of cancer deaths in the world (World Health Organization, WHO, http://www.who.int/). Among breast cancer genes, ER is a

* Corresponding author.

D.-S. Huang et al. (Eds.): ICIC 2010, LNCS 6215, pp. 277–284, 2010.

successful therapeutic target for the treatment of ER-positive breast cancers, which account for approximately 60–65% of primary breast cancers. Unfortunately, this treatment does not work well for ER-negative breast cancers, indicating different mechanisms underlying the breast cancer carcinogenesis. At the molecular level, ER-negative breast cancers are characterized by low expression of estrogen receptor. However, ER-negative breast cancers have aggressive clinical behavior, distinct patterns of metastasis, fewer cancer prevention, and lack of targeted therapies [1]. These distinctions suggest that the two subtypes of breast cancer cell lines might have a very different genomic and epigenomic context. Extensive investigation of such distinctions is important for us to understand their biology and to develop effective therapies.

1.2 Breast Cancer and DNA Methylation

DNA methylation is ubiquitous in the human genome, e.g., ~ 80% of the CpG dinucleotides are methylated [2]. It has been commonly accepted that methylation plays important roles in gene regulation and functions [3]. The global hypomethylation in cancer cells may either aberrantly activate expression of normally silent genes [4] or increase genomic stability [5, 6]. Conversely, human tumors may be caused by aberrant hypermethylation in the promoters of some genes [7], especially tumor-suppressor genes [8]. Both hypomethylation and hypermethylation have been found to cause different kinds of cancers, including breast cancer [9, 10].

Although methylation is an important regulatory mechanism for gene expression and chromatin stability in the cellular system, so far, it has still been a great challenge to explore its global pattern because of its dynamic and ubiquitous properties by traditional biochemical experiments. Recent advances in high throughput microarray technology make it possible to generate genome-wide methylation status data. In a typical bench experiment, methylation dependent DNA pretreatments were developed to reveal the methylation status of cytosine residues. These pretreatments include enzyme digestion, affinity enrichment and sodium bisulphate, followed by either hybridization array or resequencing [11].

2 Materials and Methods

2.1 DMH Microarray and Data Processing

Methylation profiling of 40 breast cancer cell lines were generated from Agilent 244K human CGI array, which contains 237,220 probes [12]. The raw array signal was normalized based on the description in Sun *et al.* [12]. Then, all probes within the promoter region of a gene were collapsed with quantile method implement in R package. Here, a promoter region was defined as -500 bp (upstream) to +500 bp (downstream) of the transcriptional start site (TSS) of a gene, i.e., 1 kb. When a gene had multiple TSSs, its most upstream TSS was used. Genes with less than 3 probes mapped to their promoter regions were discarded [12]. Gene annotation was downloaded from the UCSC Genome Browser (http://genome.ucsc.edu/, hg18).

2.2 Identification of Differentially Methylated Genes and Hierarchical Cluster Analysis

Among these 40 breast cancer cell lines, 25 belonged to estrogen receptor negative (ER-) cell lines, and the rest of them belonged to ER positive (ER+) cell lines. We used two-sample unequal variance (heteroscedastic) *t*-test to identify the genes differentially methylated in the two subtypes of breast cancer cell lines (ER- vs. ER+). Those genes whose *P*-values were less than 0.05 were considered as differentially methylated genes.

The methylation signal for each gene across all samples was mean centered, and hierarchical cluster analysis was used to cluster breast cancer cell lines.

2.3 Gene Enrichment in Network

To explore functional features of the differentially methylated genes, we used Ingenuity Pathway Analysis (IPA) tool (http://www.ingenuity.com/) to identify the enriched networks. For each pathway in analysis, a *P*-value was calculated by Fisher's exact test [13]. According to the IPA tool, a *P*-value based score, calculated by $-\log_{10}P$, was used to evaluate the significance of the network.

2.4 Correlation between Methylation and Gene Expression

We obtained gene expression data for breast cancer cell lines from Neve *et al*. [14]. A total of 4690 genes had both methylation and expression data. For each gene, we calculated spearman correlation between DNA methylation and gene expression intensities across the breast cancer cell lines. To evaluate statistical significance of each gene, we permuted the gene expression matrix and methylation matrix by swapping sample labels randomly for 1000 times. This permutation process generated a background distribution for each gene while keeping the correlation structure among genes. One-side *P*-value was obtained by calculating the percentage of the number of background correlation coefficients (cc) that were larger than the real correlation coefficient if the real cc >=0, as well as, the percentage of the background cc smaller than the real cc if the real cc <0. Then, we calculated False Discovery Rate (FDR) using Benjamini and Hochberg multiple testing corrections to adjust the *P*-values.

3 Results

3.1 Number of Probes in the Promoter Regions

Among the 237,202 probes on Agilent 244K array, we mapped 86,947 (36.7%) to the promoter regions of 12,005 genes. Figure 1 displays the distribution of the number of probes in the promoter regions. The maximum number of probes mapped to a promoter region of a gene was 14. Genes with less than 3 probes in their promoter regions were discarded. This process resulted in 11,260 genes whose methylation profiling could be further analyzed.

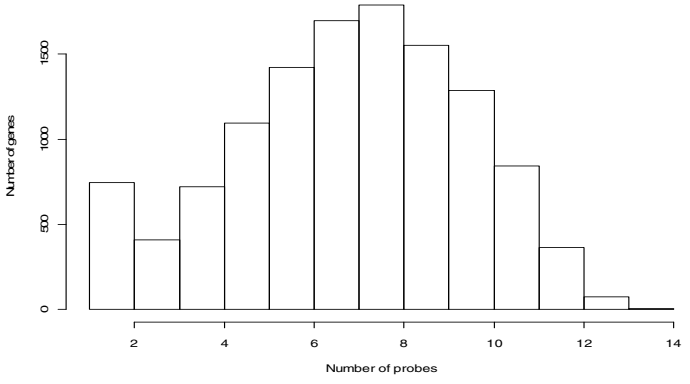

Fig. 1. Distribution of number of probes in the promoter regions

3.2 Distinguish Subtypes of Breast Cancer Cell Lines

Statistical analysis was performed using R package (version R2.9.2). Supervised hierarchical clustering of methylation data was performed using the subset of genes (n=345) with P-value < 0.05.

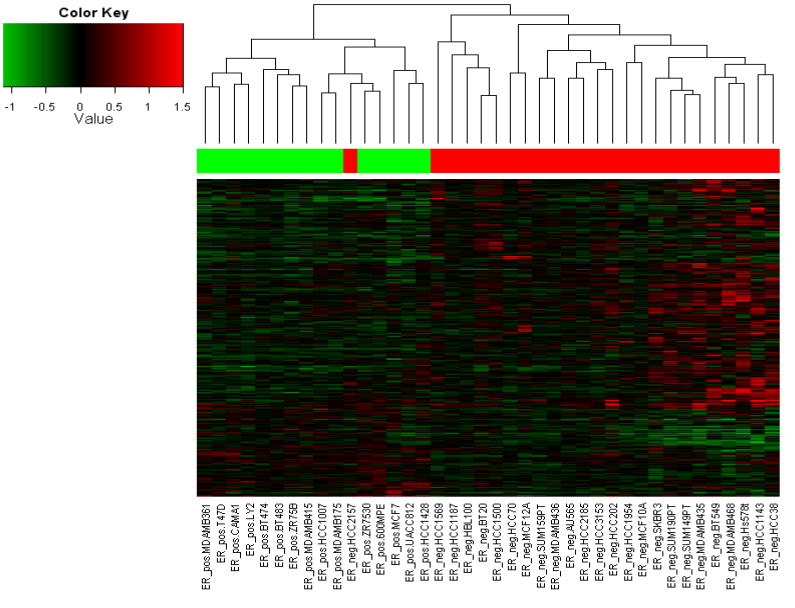

Fig. 2. Hierarchical cluster analysis of two subtypes of breast cancer cell lines. Dendrogram in red denotes ER- breast cancer cell lines and green denotes ER+ breast cancer cell lines. Methylation profiling in red indicates relatively higher methylation level, while profiling in green indicates relatively lower methylation level.

These 345 genes were considered as differentially methylated genes between two subtypes of breast cancer cell lines (Figure 2). The majority of 40 breast cancer cell lines could be clustered according to their subtype, except for HCC2157 (error rate: 1/40=2.5%). This breast cancer cell line, which belongs to ER-group, was clustered with other ER+ breast cancer cell lines. This false classification might be due to its positive expression of progesterone receptor (PR+) [15]. Interestingly, among these 345 differentially methylated genes, the majority (249, 72.2%) displayed higher average methylation levels in ER- breast cancer cell lines while only 96 (27.8%) genes had higher average methylation level in ER+ breast cancer cell lines.

3.3 Gene Enrichment at the Network Level

For 345 differentially methylated genes, three groups were significantly enriched in the human Global Molecular Network (GMN) with *P*-score greater than 20. Group 1 (*P*-score=47) contained 29 differentially methylated genes and had the top functions in gene expression, dermatological diseases and conditions, and infectious disease. Group 2 (*P*-score=39) contained 25 differentially methylated genes and had top functions in reproductive system disease, genetic disorder, and metabolic disease. Group 3 (*P*-score=32) contained 22 differentially methylated genes and had top functions in nervous system development and function, cellular development, and molecular transport.

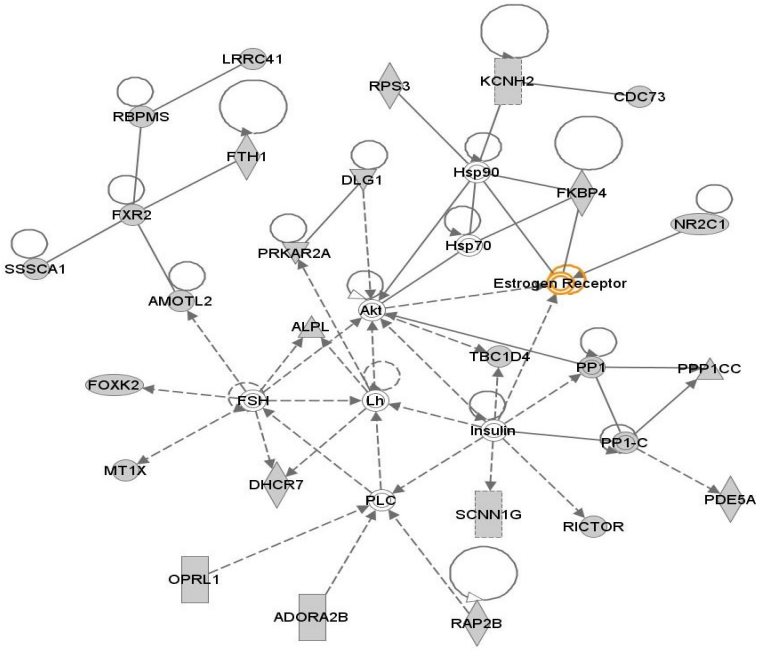

Fig. 3. Enriched network contains estrogen receptor (highlighted in orange). Grey nodes denote the differentially methylated genes in the network. A solid line indicates a physical interaction, a dashed line with an arrow indicates a regulation relationship, and a solid line with an arrow indicates both a physical interaction and a regulation relationship.

Specifically, among the three significantly enriched networks, group 2 contained estrogen receptor (Figure 3). Thus, we dicussed this network with more details here. Two differentially methylated genes (*FKBP4* and *NR2C1*) directly interacted with ER. *FKBP4* encodes a protein belonging to a member of the immunophilin protein family. It also has a functional association with two heat shock proteins (hsp90 and hsp70) and thus may play a role in the intracellular trafficking of hetero-oligomeric forms of the steroid hormone receptors. *NR2C1* encodes a nuclear hormone receptor characterized by a highly conserved DNA binding domain. This protein also belongs to a large family of ligand-inducible transcription factors that regulate gene expression by binding to specific DNA sequences within promoters of target genes. Although not identified as differentially methylated gene, *Akt*, an oncogene, plays an important role in the group 2 that it is in the center of the network and connects with many differentially methylated genes.

3.4 Correlation between Methylation and Expression

DNA methylation has been well documented to play an important role in gene expression regulation [16]. Current genome-wide microarray technologies allow us to examine the relationship between methylation and expression for specific samples, thus giving a detailed view of their regulation. One important question is whether DNA methylation plays a universal regulatory role in gene expression for all genes. Figure 4 shows the distribution of correlation coefficients (cc) between methylation and expression. However, distribution of FDR (data not shown) suggests that methylation and expression have almost no correlation. One possible reason is that transcription factor and other regulatory mechanisms may play more important roles in the regulation of gene expression [17].

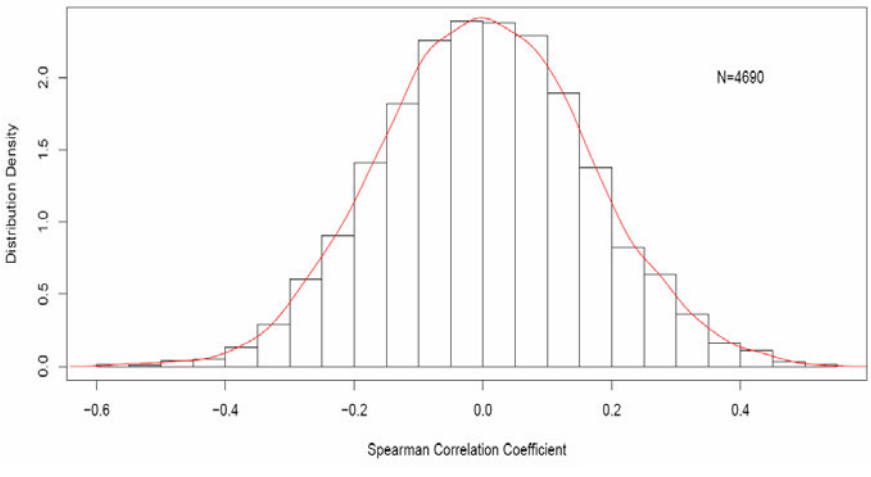

Fig. 4. Distribution of Spearman correlation coefficient (cc) between methylation and gene expression

4 Discussion and Future Perspectives

DNA methylation, as well as transcription factors and microRNAs, are among the key regulatory mechanisms for gene expression. While there have been numerous discussions on the roles of transcription factors and microRNAs in gene expression, similar discussion of DNA methylation on gene expression lag behind largely because of the current experiment limitations. In this study, we systematically examined genome-wide DNA methylation profiling of 40 breast cancer cell lines based on the methylation array technology. Further, we used the methylation profiles to distinguish the ER- and ER+ breast cancer subtypes. Our results showed that different breast cancer subtypes have distinct methylation patterns, extending previous findings of different gene expression profiling among cancer subtypes [14]. Interestingly, functional analysis of the methylation signature identified an Akt and ER centric module. Considering the methylation signature consists of differentially methylated genes between ER+ and ER- subtypes, this module may reflect a highly methylation-regulated pathway in breast cancers.

We further investigated the correlation between gene expression and methylation. The majority of genes did not show significant correlation, suggesting that methylation alone might have limited influences on gene expression of many genes. However, this conclusion may need further validation from other data because methylation and gene expression are all in highly dynamic processes. For instance, in different cell states (e.g., cell cycle phases), the cells may show very different profiles. In this case, correlation between gene expression and methylation may not be captured by a simplistic linear correlation.

Different DNA methylation profiling methods are often limited by their resolution, accuracy, reproducibility and types of bias [11]. With the development of DNA methylation profiling methods, particularly the next-generation sequencing [18] and single-molecule DNA sequencing technologies [19], large-scale and high-resolution methylation profiling will help us to understand the roles of methylation in cancer and other diseases.

Acknowledgments

This work was partially supported by NIH grant (LM009598) from the National Library of Medicine and Virginia Commonwealth University Institutional Research Grant IRG-73-001-31 from the American Cancer Society. Z. Zhao received additional support from Vanderbilt's Specialized Program of Research Excellence in GI Cancer grant (50CA95103) and the VICC Cancer Center Core grant (P30-CA68485).

References

1. Putti, T.C., El-Rehim, D.M., Rakha, E.A., Paish, C.E., Lee, A.H., Pinder, S.E., Ellis, I.O.: Estrogen Receptor-negative Breast Carcinomas: a Review of Morphology and Immunophenotypical Analysis. Mod. Pathol. 18(1), 26–35 (2005)
2. Antequera, F.: Structure, Function and Evolution of CpG Island Promoters. Cell Mol. Life Sci. 60(8), 1647–1658 (2003)

3. Jones, P.A., Baylin, S.B.: The Fundamental Role of Epigenetic Events in Cancer. Nat. Rev. Genet. 3(6), 415–428 (2002)
4. Cho, B., Lee, H., Jeong, S., Bang, Y.J., Lee, H.J., Hwang, K.S., Kim, H.Y., Lee, Y.S., Kang, G.H., Jeoung, D.I.: Promoter Hypomethylation of a Novel Cancer/testis Antigen Gene CAGE is Correlated with its Aberrant Expression and is Seen in Premalignant Stage of Gastric Carcinoma. Biochem. Biophys. Res. Commun. 307(1), 52–63 (2003)
5. Chen, R.Z., Pettersson, U., Beard, C., Jackson-Grusby, L., Jaenisch, R.: DNA Hypomethylation Leads to Elevated Mutation Rates. Nature 395(6697), 89–93 (1998)
6. Eden, A., Gaudet, F., Waghmare, A., Jaenisch, R.: Chromosomal Instability and Tumors Promoted by DNA Hypomethylation. Science 300(5618), 455 (2003)
7. Baylin, S.B., Herman, J.G.: DNA Hypermethylation in Tumorigenesis: Epigenetics Joins Genetics. Trends Genet. 16(4), 168–174 (2000)
8. Sakai, T., Toguchida, J., Ohtani, N., Yandell, D.W., Rapaport, J.M., Dryja, T.P.: Allele-specific Hypermethylation of the Retinoblastoma Tumor-suppressor Gene. Am. J. Hum. Genet. 48(5), 880–888 (1991)
9. Ito, Y., Koessler, T., Ibrahim, A.E., Rai, S., Vowler, S.L., Abu-Amero, S., Silva, A.L., Maia, A.T., Huddleston, J.E., Uribe-Lewis, S., et al.: Somatically Acquired Hypomethylation of IGF2 in Breast and Colorectal Cancer. Hum. Mol. Genet. 17(17), 2633–2643 (2008)
10. Fernandez, S.V., Snider, K.E., Wu, Y.Z., Russo, I.H., Plass, C., Russo, J.: DNA- Methylation Changes in a Human Cell Model of Breast Cancer Progression. Mutat. Res. (2010) (Advanced online)
11. Laird, P.W.: Principles and Challenges of Genome-wide DNA Methylation Analysis. Nat. Rev. Genet. 11(3), 191–203 (2010)
12. Sun, S., Yan, P.S., Huang, T.H., Lin, S.: Identifying Differentially Methylated Genes Using Mixed Effect and Generalized Least Square Models. BMC Bioinformatics 10, 404 (2009)
13. Guo, A.Y., Sun, J., Riley, B.P., Thiselton, D.L., Kendler, K.S., Zhao, Z.: The Dystrobrevin-binding Protein 1 Gene: features and networks. Mol. Psychiatry 14(1), 18–29 (2009)
14. Neve, R.M., Chin, K., Fridlyand, J., Yeh, J., Baehner, F.L., Fevr, T., Clark, L., Bayani, N., Coppe, J.P., Tong, F., et al.: A Collection of Breast Cancer Cell Lines for the Study of Functionally Distinct Cancer Subtypes. Cancer Cell 10(6), 515–527 (2006)
15. Gazdar, A.F., Kurvari, V., Virmani, A., Gollahon, L., Sakaguchi, M., Westerfield, M., Kodagoda, D., Stasny, V., Cunningham, H.T.: Wistuba, II et al: Characterization of Paired Tumor and Non-tumor Cell Lines Established from Patients with Breast Cancer. Int. J. Cancer 78(6), 766–774 (1998)
16. Klein, C.B., Costa, M.: DNA Methylation and Gene Expression: Introduction and Overview. Mutat. Res. 386(2), 103–105 (1997)
17. Flanagan, J.M., Cocciardi, S., Waddell, N., Johnstone, C.N., Marsh, A., Henderson, S., Simpson, P., Silva, L., Khanna, K., Lakhani, S., et al.: DNA Methylome of Familial Breast Cancer Identifies Distinct Profiles Defined by Mutation Status. Am. J. Hum. Genet. 86(3), 420–433 (2010)
18. Metzker, M.L.: Sequencing Technologies - the Next Generation. Nat. Rev. Genet. 11(1), 31–46 (2010)
19. Clarke, J., Wu, H.C., Jayasinghe, L., Patel, A., Reid, S., Bayley, H.: Continuous Base Identification for Single-molecule Nanopore DNA Sequencing. Nat. Nanotechnol. 4(4), 265–270 (2009)

GRIDUISS – A Grid Based Universal Immune System Simulator Framework

Francesco Pappalardo[1,*], Marzio Pennisi[1], Ferdinando Chiacchio[1], Alessandro Cincotti[2], and Santo Motta[1]

[1] University of Catania, Dept. of Mathematics and Computer Science
V.le A. Doria, 6, I-95125 Catania, Italy
{francesco.pappalardo,mpennisi,fchiacchio,motta}@dmi.unict.it
[2] School of Information Science, Japan Advanced Institute of Science and Technology, Japan
cincotti@jaist.ac.jp

Abstract. GRIDUISS is a simulation framework to model the immune system using grid technologies. It integrates simulation engines, optimization techniques and other prediction models. GRIDUISS is then capable to reproduce general immune system behavior connected to several immune system response (to viruses, bacteria, tumors and auto-immune disease) and drug-induced immune system responses. This framework has been inspired from the EC funded ImmunoGrid project.

Keywords: Immune system, systems biology, grid simulations.

1 Introduction

The last decade has been characterized by a vigorous fast innovation along the whole sectors. Computer technologies and the Internet grew up rapidly favoring the born of new computational frameworks. Nowadays clusters of computers connected by heterogeneous networks can deliver powerful computational capabilities to face up to previously unresolved problems of the most disparate scientific fields.

Breakthroughs in the fields of genetics, biochemistry, and molecular biology, in conjunction with this technological growth, pushed out the born of a new hybrid discipline called computational immunology, whose aim is to improve and extend our biological and immunological knowledge. Connected research areas involve vaccine design and drug discovery in which this new science can produce a multitude of new applications, resulting in a great contribute for the research community.

Mathematical and computational models can help to speed-up research in these fields. Three potential areas for computational modeling can in fact be developed: cell signal behavior models which aid to understand how compounds affect intracellular signaling, cell signal-cell behavior response models used to correlate intracellular signals to the cell behaviors and physiological models, able to simulate the organ level behavior and predict the system response.

* Corresponding author.

D.-S. Huang et al. (Eds.): ICIC 2010, LNCS 6215, pp. 285–290, 2010.

Simulation results coming from computing environments can be compared, through the use of validation tools, with a large amounts of clinical data, organized into ontologies and stored in databases (i.e. gene sequencing maps, radiographic exams, medical analysis, etc.). The results of these experiments either further validate the model or identify novel biology that is then incorporated into the model. So, it is fair that the development of such kind of simulation environments is an ongoing process which takes into account new knowledge from science and new available technology, achieving the cyclical refinements by means of interdisciplinary efforts and opening the scene to what can be considered the in silico prediction methods.

GRIDUISS is a simulation framework to model the immune system using grid technologies. It integrates simulation engines, optimization techniques and other prediction models. GRIDUISS is then capable to reproduce general immune system behavior connected to several immune system response (to viruses, bacteria, tumors and auto-immune disease) and drug-induced immune system responses.

The need for Grid resources has arisen from the increasing numbers of simulations to be run and the growing size of the simulation space modeled. A web server is being implemented in order to provide a centralized location for the development of the GRIDUISS framework and to provide a public resource to access these resources. The web server is a mixture of web pages containing information on the simulator and mechanisms to launch monitor and view simulations results. The ability to centralize the access to the GRIDUISS avoids the need for local versions of software.

The plan of the paper is the following. Section 2 presents the main GRIDUISS core infrastructure. Section 3 describes successful stories in which GRIDUISS framework has been applied. Section 4 draws final remarks and conclusions.

2 GRIDUISS Core Infrastructure

The immune system is the most complex (along with the central nervous system) biological scenario we know. To model such a scenario, one needs to include all the crucial entities (cells, molecules, cytokines, interactions) that biologists and medical doctors recognize as relevant in the game.

GRIDUISS is a multi-scale, multi-organ three dimensional framework simulator of the immune system. We summarize entities and interactions that are relevant in modeling the immune system in the conceptual model showed in Figure 1. We considered both cellular and molecular entities. Cellular entities can take up a state from a certain set of suitable states and their dynamics is realized by means of state changes. A state change takes place when a cell interacts with another cell or with a molecule or both of them. We considered the relevant lymphocytes, i.e. B lymphocytes, helper, cytotoxic and regulatory T lymphocytes and natural killer cells. Monocytes are represented as well and we take care of macrophages and dendritic cells. For what concerns molecules, the model distinguishes between simple small molecules like interleukins or signaling molecules in general and more complex molecules like immunoglobulins and antigens, for which we need to represent the specificity.

Looking at the Figure 1, at the same level of entities we find immune system activities. They include both interactions and functions. Functions refer to the main immune system tasks. In particular GRIDUISS takes care of the diversity of specific

elements, major histocompatibility classes restriction, clonal selection by antigen affinity, thymus education of T cells, antigen processing and presentation (both the cytosolic and endocytic pathways are implemented), cell–cell cooperation, homeostasis of cells created by the bone marrow, hypermutation of antibodies, cellular and humoral response and immune memory.

Our model represents receptors and ligands as bit strings and use a string matching rule to model affinity. This clever idea was introduced by Farmer et al. [1] as a way to perform calculations for determining molecular complementarity and predicting the optimal size of an epitope. From immunology, we know that binding is a threshold effect consisting of two components: the affinity of a single receptor and ligand, and the total binding, or avidity of multiple binding pairs. Binding is modeled by a string matching rule by counting the number of positions in the string at which the symbols are complementary (known as Hamming distance). Repertoires are represented in the model as sets of strings. This fundamental modeling abstraction ignores nearly all of the physical and chemical details that determine receptor/ligand interactions. By adopting bit strings, many binding events can be simulated quickly, making it feasible to study large-scale properties of the immune system. Although character strings are a poor representation of the reality, they produced accurate models when benchmarked to experiment, suggesting that the abstraction captures important features of receptor/ligand binding.

In particular, specificity is implemented in GRIDUISS by a bit-string polyclonal lattice method. Bit-string refers to the way the molecules and the specificity among molecules is represented, polyclonal indicates that more clones of different specificity of lymphocytes are represented and lattice means that we use a discrete lattice to represent the space, that is, the space is discrete. The set of lymphocytes receptors is represented by bit-strings of length h which then forms the so called shape space. A clonal set of cells is characterized by the same clonotypic receptor, i.e. by the same bit-string of length l. The potential repertoire of receptors scales as 2^l. The receptor–coreceptor binding among the entities are described in terms of matching between binary strings with fixed directional reading frame. Bit-strings represent the generic binding site between cells (through their receptors) and target molecules (through peptides and epitopes).

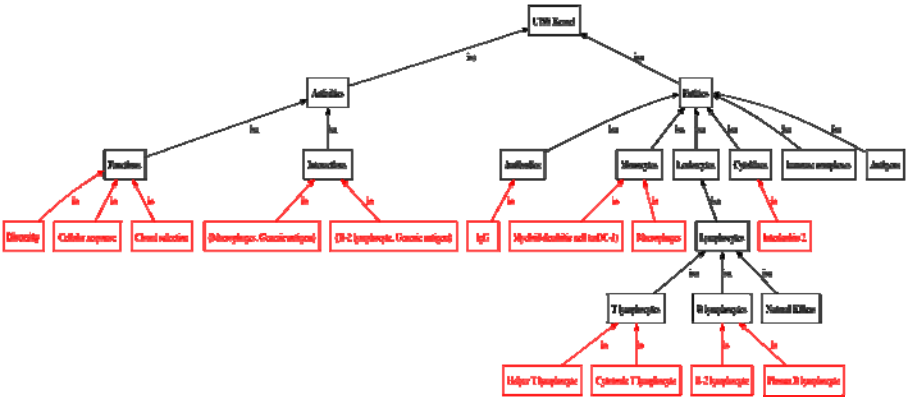

Fig. 1. GRIDUISS framework

2.1 GRID Implementation

The need for Grid resources has arisen from the increasing numbers of simulations to be run and the growing size of the simulation space modelled. The philosophy of the UISS grid implementation was inspired by ImmunoGrid project [2]. It provides access to multiple diverse grid middlewares through a single interface. This approach effectively hides the complexity of the implementation from the user. This is achieved by centralizing a job launcher on the GRIDUISS web services (GUWS) and providing uniformed mechanisms to upload, and define a job. Without this approach, the average user would need to deal with complexities such as VMware, applications servers and authentication. Our centralised approach encapsulates this complexity in the job launcher. With this approach, the final user view of the grid implementation is as simple as using an average web form. The actual implementation of the individual middlewares is completely dealt with by the technician in charge of the GUWS. Figure 2 provides an overview of the GRIDUISS grid design and shows how each individual grid middleware is accessible via a job launcher. Here we mainly present the creation of methods to allow the integration of the gLite middleware with the GUWS. Other middleware's that have been integrated are the Application Hosting Environment (AHE), DESHL client [3] (UNICORE) and simple GUWS access. The AHE provides the ability to launch jobs on resources which are globus enabled as well as local (non-national grid) resources which are GRIDSam enabled. GRIDSam is a web service which is capable of forking jobs to local systems as well as building Resource Specific Language (RSL) requests to launch jobs on globus enabled machines.

An AHE client is implemented on the GRIDUISS web services to allow interaction with the AHE server. DESHL is a command line client which is able to launch jobs on UNICORE enabled machines. This is an ideal solution to allow access to group resources at the DEISA site – CINECA.

A group portal certificate has been acquired to allow authentication of jobs launched via the GUWS rather than authentication of individual users. In order to allow resources which do not have any grid middleware to be made available through the GUWS, a simulator web service has been created. This service is able to run on an application server on the host resource and fork jobs to the local system. The simulator web service has been implemented in Java, Perl and PHP. Access to these services is available through simple SOAP protocols and PHP libraries.

The web interface provides transparent access to the various different resources available through IG. The interface is presented as standard web pages and forms which are familiar to most users. The GUWS is implemented in PHP, AJAX and DHTML to provide a modern look and feel to the site. The interface is used to create and prepare jobs to be launched onto the grid. The actual communication with any grid middleware is completely dealt with by the web services job launcher. This launcher is written as a PHP script (also available as Perl scripts) which is able to interact with the various middleware clients.

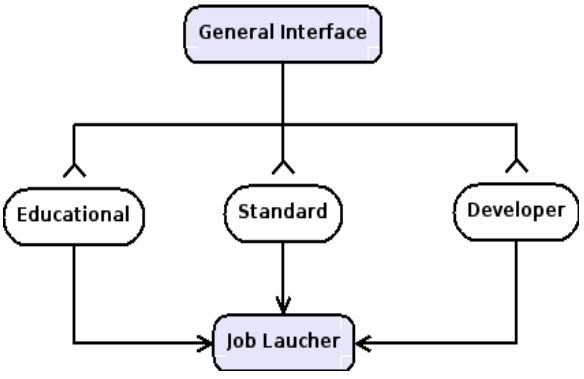

Fig. 2. Different 'levels' of access available in the web services

3 GRIDUISS Current Applications

The GRIDUISS framework has been used for successfully modeling and simulating multiple immune system related pathologies. It has initially used to model and simulate the immune system responses to mammary carcinoma tumor cells in naive mice and in mice vaccinated with an immunopreventive vaccine [4] (named Triplex), showing the ability to accurately reproduce the experimental results. In silico experiments carried out on two large statistical samples of virtual mice underlined that the humoral response is fundamental in controlling the tumor growth and therefore suggest the selection and timing of experiments for measuring the activity of T cells. The resulting model has been then used in conjunction with two famous optimization techniques in order to suggest vaccination protocols capable to guarantee the same survival rates entitled with the use of a Chronic protocol with the lowest possible number of vaccine administrations.

Genetic Algorithms have at the start been used in an high performance computing (HPC) environment showing as a result a reduction of approx. 50% in the number of vaccinations [5]. Furthermore the use of Simulated Annealing (SA) improved the quality of the suggested solution and the required computational time of an order of approx. 102. The SA found protocol has been obtained using the COMETA sicilian grid [http://www.consorzio-cometa.it/] infrastructure for both protocol search and validation.

The GRIDUISS framework has then specialized to model the effects of the Triplex vaccine as a therapeutic agent against lung metastases derived by mammary carcinoma [6]. The model has been validated against the in vivo experiment and it is at the present time being used with SA on the COMETA grid to predict optimal vaccine protocols for longer in vivo experiments.

Moreover GRIDUSS has been used to model the first state of atherosclerosis (atherogenesis) [7]. The resulting model simulates both the immune response to atherogenesis and the atheromatous plaque progression in a generic artery wall. The level of oxidized low density lipoproteins (LDLs), the immune humoral response with production of autoantibodies, the macrophages activity and the formation of foam cells are in good agreement with available clinical data, including the formation of atheromatous plaques in patients affected by hypercholesterolemia.

4 Conclusions

The central nervous system and the immune system are the two most complex systems of the human body. At variance with the central nervous system the immune system is a distributed system, with dynamic learning and adaptation, self-monitoring and error control. The primary goal of the immune system is the defense from harmful foreign pathogens and cancer. For this purpose the immune system includes a variety of cells, molecules, signals and organs with specific functions, which cooperate and exchange informations across the lymphatic system. All these components must be included in a modeling approach of the immune system leading to computational models which cannot be afforded on single computing machine in a reasonable time.

In this paper we presented a simulation framework to model the immune system using grid technologies. Thanks to these technologies we have been able to approach some pathologies where the role of the immune defense play a fundamental role. The grid computational framework can be used either as a tool for knowledge discovery or as a tool for drug discovery. In the former case the process is driven by the experiment-model-experiment cycle refinement; in the latter case one can simulate the result of specific stimulation of the immune system, artificial immunity. In this way the model framework can be used as a tool to fasten drug discovery.

Human health is the result of a good surveillance of the immune system. Thus most pathologies are related to malfunctioning of the immune system of escaping its surveillance. Here we have presented some examples of pathologies; we are currently working on other pathologies, like multiple sclerosis, and results will be published in due course.

References

1. Farmer, J.D., et al.: The Immune System, Adaption, and Machine Learning. Phisica D 22, 187–204 (1986)
2. Pappalardo, F., et al.: ImmunoGrid, an Integrative Environment for Large-scale Simulation of the Immune System for Vaccine Discovery, Design, and Optimization. Briefings in Bioinformatics 10(3), 330–340 (2009)
3. Sloan, T.M., Menday, R., Seed, T.P., Illingworth, M., Trew, A.S.: DESHL–Standards Based Access to a Heterogeneous European Supercomputing Infrastructure. In: Proceedings of the Second IEEE International Conference on e-Science and Grid Computing, p. 91 (2006)
4. Pappalardo, F., Lollini, P.-L., Castiglione, F., Motta, S.: Modeling and Simulation of Cancer Immunoprevention Vaccine. Bioinformatics 21(12), 2891–2897 (2005)
5. Pappalardo, F., Pennisi, M., Castiglione, F., Motta, S.: Vaccine Protocols Optimization: in Silico Experiences. Biotechnology Advances 28, 82–93 (2010)
6. Pennisi, M., Pappalardo, F., Motta, S.: Agent Based Modeling of Lung Metastasis-immune System Competition. In: Andrews, P.S. (ed.) ICARIS 2009. LNCS, vol. 5666, pp. 1–3. Springer, Heidelberg (2009)
7. Pappalardo, F., Musumeci, S., Motta, S.: Modeling Immune System Control of Atherogenesis. Bioinformatics 24(15), 1715–1721 (2008)

Performance Comparison of Tumor Classification Based on Linear and Non-linear Dimensionality Reduction Methods

Shu-Lin Wang[1,2], Hong-Zhu You[1], Ying-Ke Lei[1,3], and Xue-Ling Li[1]

[1] Intelligent Computing Laboratory, Hefei Institute of Intelligent Machines, Chinese Academy of Science, Hefei, 230031, China
[2] School of Computer and Communication, Hunan University, Changsha, Hunan, China
[3] Electronic Engineering Institute, Hefei, 230037, China
jt_slwang@hotmail.com

Abstract. Gene expression profiles play more and more important roles in accurate tumor diagnosis and treatment. However, the curse of dimensionality that the number of genes far exceeds the number of samples issues the challenges to the traditional dimensionality reduction methods. Here based on two-stage dimensionality reduction model we design 18 tumor classification methods by combining two classical gene filters with three common dimensionality reduction methods: principal component analysis (PCA), linear discriminative analysis (LDA) and multidimensional scaling (MDS) method to extract discriminative features and use three common machine learning methods to evaluate the prediction accuracy of the extracted features on six tumor datasets, respectively. Although gene expression presents the non-linear characteristics, non-linear dimensionality reduction method MDS is not always the best in prediction accuracy among the three dimensionality reductions on all six tumor datasets. Moreover, the performance comparison indicates that no single dimensionality reduction is always superior to the others on all of the six tumor datasets. Our results also suggest that the prediction accuracy obtained depends strongly on the dataset, and less on the gene selection and classification methods.

Keywords: Gene expression profiles, tumor classification, dimensionality reduction, principal component analysis, linear discriminative analysis, multidimensional scaling.

1 Introduction

Various tumors affect our quality of life, health and lives greatly. The death rate caused by tumor has been greatly increasing with the development of society. Although it is difficult to perform early tumor diagnosis by using traditional appearance-based diagnosis methods, the advent of DNA microarray technique brings hope into the tumor diagnosis [1]. In fact, tumor classification is one of major applications of DNA microarray technique. Over the last decade, a great number of tumor classification methods based on gene expression profiles (GEP) have been proposed and extensively studied [2], but

D.-S. Huang et al. (Eds.): ICIC 2010, LNCS 6215, pp. 291–300, 2010.

the challenges from GEP still exist due to the curse of dimensionality that the number of genes far exceeds the number of samples. Particularly, there are a great number of tumor-unrelated genes and much noise in GEP that can greatly affect the classification performance. Even so, DNA microarrays remain a useful technology to address a wide array of biological problems [3] and to extract meaningful results from the GEP-based analysis still pose many bioinformatics challenges [3].

When facing these problems, it is usually difficult for single dimensionality reduction to extract efficient and powerful features to realize tumor classification. Previous studies show that two-stage dimensionality reduction model is more efficient for the feature extraction of GEP than single method. First stage is to select those differentially expressed genes from GEP dataset so as to enhance the discriminative information. Second stage is to extract few features from those genes that include importantly discriminative information. For example, Wang *et al*. [4] combined Kruskal-Wallis rank sum test with factor analysis to extract few factors that were successfully applied to tumor classification of three cross-platform datasets. This paper mainly focuses on the performance comparison of tumor classification on six tumor datasets based on two-stage dimensionality reduction model that combines two gene filter methods with three classical dimensionality reduction methods: principal component analysis (PCA), linear discriminative analysis (LDA) [5] and non-linear multidimensional scaling (MDS) [6]. Although PCA, LDA and MDS have also been applied to the analysis of GEP [7-11], here we mainly compare the classification performance of the three feature extraction methods with three classifiers on six tumor datasets under the same circumstance to validate whether or not there is an optimal method among these methods on all selected datasets.

2 Methods

2.1 Analysis Framework

To avoid the effects of different division of dataset, we randomly split whole dataset into two parts: training set and test set. The whole construction process of classification model including gene filters, feature extraction and training prediction model are performed only on training set, as shown in Fig. 1. The constructed model is used to evaluate the test set.

Dimensionality reduction is an important task in tumor classification based on GEP so as to overcome or alleviate the curse of dimensionality. Our dimensionality reduction method involves two key steps: gene filters and feature extraction. Gene filters is to rank genes and select differentially expressed gene according to a criterion. Among many existing gene filter methods we will adopt Kruskal-Wallis rank sum test (KWRST) [12] and Relief-F [13] to filter genes, respectively. Both methods are suitable for multi-class dataset. KWRST is equivalent to an ordinary one-way ANOVA that uses the ranks instead of the original data. Especially, KWRST does not require the data following Gaussian distribution. The main idea of Relief-F is to select samples at random, compute their nearest neighbors, and adjust a feature weighting vector to assign more weight to features that discriminate the sample from the neighbors belonging to different subclasses.

Feature extraction is to extract few features so as to construct prediction model to evaluate the classification performance of test set. We will adopt three classical dimensionality reduction methods: PCA, LDA and MDS to extract features from the pre-selected genes. Furthermore, we will adopt three machine learning methods: *k*-nearest neighbor (*k*-NN), probabilistic neural network (PNN) and support vector machines (SVM) to construct classification model with the extracted features. Therefore the number of the combined methods is $2 \times 3 \times 3 = 18$. Our task is to evaluate the classification performance of the 18 methods on six tumor datasets, respectively.

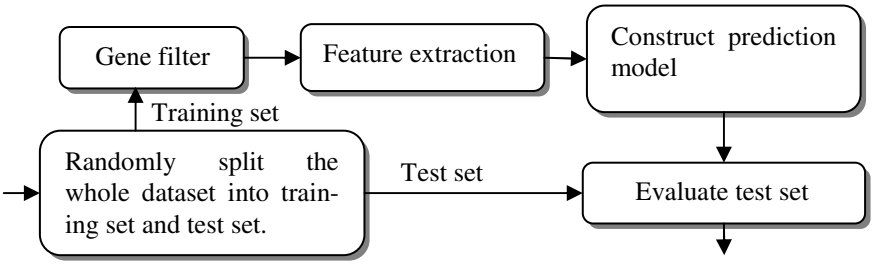

Fig. 1. The framework of our analysis method

2.2 Representation of GEP

DNA microarray is composed of thousands of individual DNA sequences printed in a high density array on a glass microscope slide. Samples are generated under multiple conditions which may be a time series during a biological process or a collection of different tissue samples. Let $G = \{g_1, \cdots, g_n\}$ be a set of genes and $S = \{s_1, \cdots s_m\}$ be a set of samples with k subclasses $C = \{c_1, \cdots, c_k\}$. The corresponding gene expression matrix can be represented as $X = \{x_{i,j} | 1 \le i \le m, 1 \le j \le n\}$. The matrix X is composed of m row vectors. $x_i \in R^n, i = 1,2, \cdots, m$, m denotes the number of samples, and n denotes the number of genes measured.

Suppose the dataset has the intrinsic dimensionality d (where $d \ll n$). A dimensionality reduction technique attempts to find a matrix A so as to transform dataset $X = \{x_1, \cdots, x_m\}$ $(x_i \in R^n)$ into a new dataset $Y = \{y_1, \cdots, y_m\}$ $(y_i \in R^d)$ with dimensionality d, while retaining the geometry of dataset X as much as possible. That is $Y = A^T X$.

2.3 Three Feature Extractions

We briefly review two linear dimensionality reduction methods (unsupervised PCA and supervised LDA) and one nonlinear dimensionality reduction method MDS below, respectively. Principal component analysis (PCA) attempts to find a linear basis of reduced dimensionality for dataset, in which the amount of variance in the dataset is maximal, to construct a low-dimensionality representation of the dataset. To achieve dimensionality reduction, PCA find a linear transformation T that maximize $T^{\mathrm{T}} \mathrm{cov}_{X-\bar{X}}\, T$, where $\mathrm{cov}_{X-\bar{X}}$ is the covariance matrix of the dataset X. Hence PCA solves the eigenproblem.

$$\mathrm{cov}_{X-\bar{X}}\ v = \lambda v \tag{1}$$

The eigenproblem is solved for the d principal eigenvalues λ. The corresponding eigenvector form the columns of the linear transform matrix T. The low-dimensionality representation Y of the original dataset X are computed by linear transform matrix T, i.e., $Y = (X - \bar{X})T$.

Linear discriminative analysis (LDA) attempts to maximize the linear separability between data points belonging to different classes. Unlike PCA, LDA is a supervised dimensionality reduction method. LDA optimize the ratio between the within-class scatter S_w and the between-class scatter S_b in the low-dimensionality representation of the data. LDA considers maximizing the following criterion:

$$J(W) = \frac{W^T S_b W}{W^T S_w W} \tag{2}$$

where S_w is the within-class scatter matrix and S_b is the between-class scatter matrix.

$$S_w = \sum_c p_c\ cov(X^c - \bar{X}^c) \tag{3}$$

$$S_w = cov(X - \bar{X}) - S_w \tag{4}$$

where p_c is the prior information of class label c, and $cov(X^c - \bar{X}^c)$ is the covariance matrix of the zero mean data points x assigned to class label $c \in C$. The optimization problem in Eq. 1 equals to solve the following generalized eigenvector problem.

$$S_b a = \lambda S_w a \tag{5}$$

For the d largest eigenvectors a_i to form the transformation matrix W associated with their eigen-values, where $d < |C|$. The low-dimensionality representation Y of the original dataset X can be computed by mapping them onto the linear basis W, i.e., $Y = (X - \bar{X})W$.

Multidimensionality scaling (MDS) represents a collection of non-linear dimensionality reduction techniques that maps the high-dimensional data onto a low-dimensional representation while retaining the pairwise distances between the data points as much as possible. The quality of the mapping is evaluated by a stress function. Two important examples of stress functions are the raw stress function and the Sammon cost function. The raw stress function is defined by

$$f(Y) = \sum_{ij}(\|x_i - x_j\| - \|y_i - y_j\|)^2 \tag{6}$$

in which $\|x_i - x_j\|$ denotes the Euclidean distance between the high-dimensional datapoints x_i and x_j; $\|y_i - y_j\|$ denotes the Euclidean distance between the low-dimensional data points y_i and y_j. The Sammon cost function is defined by

$$f(Y) = \frac{1}{\sum_{ij}\|x_i - x_j\|}\sum_{ij}\frac{(\|x_i - x_j\| - \|y_i - y_j\|)^2}{\|x_i - x_j\|} \tag{7}$$

3 Experiments

3.1 Descriptions of Six Tumor Datasets

Six tumor datasets are applied to our experiments. They are Leukemia1 [14], high-grade gliomas (Gliomas) [15], Leukemia2 [1], Diffuse Large B-cell Lymphomas

(DLBCL) [16], Acute Lymphoblastic Leukemia (ALL) [17], and Small Round Blue Cell Tumor (SRBCT) [18], which are briefly described in Table 1. The Leukemia2 dataset contains 7129 genes in each sample and 72 samples that belong to three subtypes: AML, ALL-T and ALL-B. The ALL dataset totally contains 248 samples that belong to six tumor subtypes: BCR-ABL, E2A-PBX1, Hyperdip>50, MLL, T-ALL and TEL-AML1. The SRBCT dataset contains 88 samples with 2,308 genes in each sample. According to the original literature, there are 63 training samples and 25 test samples containing five non tumor-related samples. The 63 training samples contain 23 Ewing family of tumors (EWS), 20 rhabdomyosarcoma (RMS), 12 neuroblastoma (NB), and eight Burkitt lymphomas (BL) samples. The test samples contain six EWSs, five RMSs, six NBs, three BLs, and five non tumor-related samples that were removed in our experiments.

Table 1. The descriptions of six tumor datasets

No.	Datasets	Platform	#Samples	#Genes	#Subclasses
1	Leukemia1	Affy HGU95a	72	12,582	3
2	Gliomas	Affy U95Av2	50	12,625	2
3	Leukemia2	Affy HU6800	72	7,129	3
4	DLBCL	Affy HU6800	77	7,129	2
5	ALL	Affy HGU95Av2	248	12,626	6
6	SRBCT	cDNA	83	2,308	4

3.2 Parameter Setting

To achieve honest and reliable results there are many parameters to be appropriately set for each method before evaluating test set. In another words, all parameters must be determined within training set. Inappropriate parameter selection can easily lead to over-fitting and selection bias. For example, if gene selection is performed on whole dataset including training set and test set, the obtained prediction accuracy on the test set will be upwardly biased [19]. If we set the parameters according to the prediction accuracies, the bias of results can also be caused. If we repeatedly optimize the parameters on training set, over-fitting might be occurred. Hence to simplify experiments and avoid over-fitting and bias we set the parameters in methods in the following, which might not be the optimal parameter combinations.

For both KWRST and Relief-F, top 300 genes are selected to be further analyzed. For PCA, we fixedly extract 5 principal components for each dataset. For LDA, we extract $|C|-1$ components to be used for classification features. For MDS, the intrinsic dimensionality d of each dataset is first estimated for each dataset and then we extract d components to be used for classification features. For KNN classifier, 5 nearest neighbors are used for label decision. For PNN, the smoothing parameter σ is fixedly set to 0.5. For SVM, we adopt Gaussian kernel to be used for the kernel function of SVM. In our experiments, we use the software LIBSVM (http://www.csie.ntu.edu.tw/ ~cjlin/libsvm) to classify the tumor samples, in which the kernel parameter γ and the regularization parameter C can be determined by performing two-dimensional grid search. At last, we perform the construction process of classification model shown in Fig. 1 500 times to obtain average accuracies for each

method and dataset. In each time, 50% samples in whole dataset are used for training set and the remains are used for the test set.

3.3 Experimental Results

The prediction accuracies obtained by PCA, LDA and MDS with three different classifiers and two gene filters on the six tumor datasets are shown in Table 1, 2, and 3, respectively. Our observations indicate that among the three feature extraction methods (PCA, LDA and MDS) no single method is obviously superior to other two methods in prediction accuracy on all six tumor datasets and that among the three classifiers (5NN, PNN and SVM) no single classifier is always obviously superior to other two classifiers on all six tumor datasets. It can be seen that the prediction accuracy is greatly affected by datasets and less affected by classification methods and gene selection. For example, LDA is very suitable for the classification of the SRBCT dataset, and all methods with LDA can achieve greater than 99% average accuracy on this dataset. However, for the Gliomas dataset, no method can achieve greater than 73% average accuracy on this dataset.

Fig. 2 and 3 show the boxplots of prediction accuracies obtained by nine methods (PCA+5NN, PCA+PNN, PCA+SVM, LDA+5NN, LDA+PNN, LDA+SVM, MDS+5NN, MDS+PNN and MDS+SVM) with KWRST and the nine methods with Relief-F gene selection on all six tumor datasets, respectively. It is obvious that the different divisions of training set and test set can greatly affect the prediction accuracy. For example, for Gliomas dataset KWRST+LDA+PNN can achieve from 28% to 92% prediction accuracies due to different divisions of dataset, shown in Fig. 2. The experimental results suggest that the prediction accuracies obtained by each method on each dataset presents a random phenomena.

Table 2. The accuracies obtained by PCA with three different classifiers

Datasets	KWRST			Relief-F		
	PCA+5NN	PCA+PNN	PCA+SVM	PCA+5NN	PCA+PNN	PCA+SVM
Leukemia1	90.67±4.67	90.53±4.39	92.61±3.62	90.51±4.40	90.60±4.10	92.39±3.85
Gliomas	72.09±9.85	71.82±8.85	72.33±9.90	71.46±9.07	70.63±8.50	72.56±8.43
Leukemia2	93.53±3.86	93.97±3.53	94.94±3.36	93.52±3.66	94.37±3.34	95.46±3.12
DLBCL	87.92±5.09	87.81±5.04	88.28 ±5.10	92.21±4.19	91.63 ±4.63	93.14±4.26
ALL	89.12±1.72	88.47±2.00	89.79±2.07	88.50±1.88	87.80±2.02	88.95±2.25
SRBCT	97.12±3.01	97.98±2.64	97.89±2.88	97.74±2.90	98.67 ±2.05	98.42 ±2.43

Table 3. The accuracies obtained by LDA with three different classifiers

Datasets	KWRST			Relief-F		
	LDA+5NN	LDA+PNN	LDA+SVM	LDA+5NN	LDA+PNN	LDA+SVM
Leukemia1	93.80±3.54	93.82±3.47	93.56±3.55	94.11±3.43	94.10±3.49	93.67±3.46
Gliomas	62.17±11.59	62.20±11.56	62.17±11.59	66.58±10.36	66.70±10.33	66.58±10.36
Leukemia2	95.74±3.11	95.72 ±2.99	95.74±3.11	96.25±3.10	96.25±3.00	96.25±3.10
DLBCL	87.07±7.40	88.06±7.39	89.24 ±7.40	89.54±5.09	90.26±5.14	90.49±5.38
ALL	95.74±1.73	95.66±1.75	95.74±1.73	95.48±1.74	95.46±1.76	95.48±1.74
SRBCT	99.43±1.58	99.44±1.56	99.41±1.60	99.31±1.91	99.36±1.80	99.36±1.67

Table 4. The accuracies obtained by MDS with three different classifiers

Datasets	KWRST			Relief-F		
	MDS+5NN	MDS+PNN	MDS+SVM	MDS+5NN	MDS+PNN	MDS+SVM
Leukemia1	92.18±3.88	86.36±5.69	92.16±3.96	92.67±3.58	87.03±4.92	92.46±4.10
Gliomas	72.29±10.73	67.27±9.50	72.52±9.05	69.88±9.18	68.47±9.00	70.75±8.97
Leukemia2	93.74±3.91	87.51±4.83	92.05±4.35	93.88±3.79	88.56±4.42	92.39±3.84
DLBCL	89.32±5.25	82.91±5.73	89.26±5.07	92.40±4.21	85.15±5.35	91.65±4.69
ALL	92.14±1.59	91.82±2.19	95.32±1.73	91.88±1.72	92.52±2.08	94.79±1.80
SRBCT	97.28±2.97	95.05±3.34	96.94±3.25	97.99±2.71	96.11±3.60	97.85±2.85

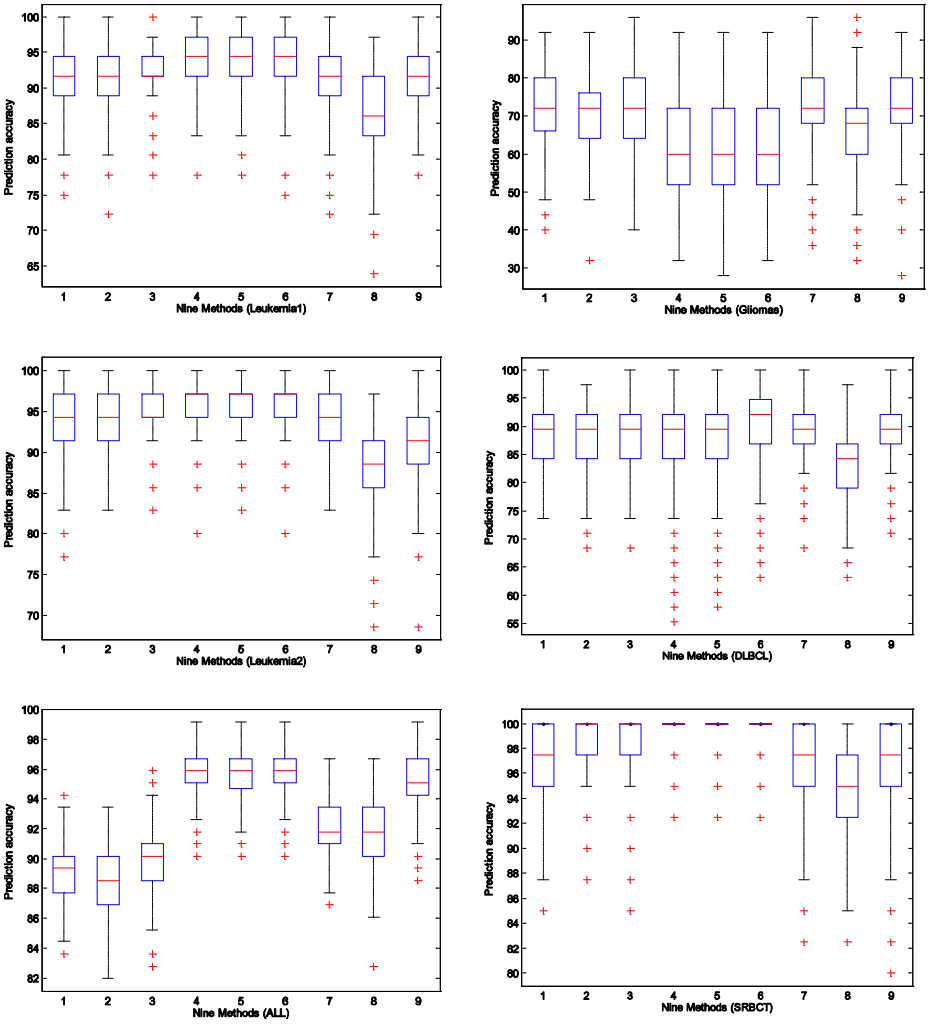

Fig. 2. The boxplots of various methods with KWRST on all six tumor datasets. The nine numbers on x-axis denote PCA+5NN (1), PCA+PNN (2), PCA+SVM (3), LDA+5NN (4), LDA+PNN (5), LDA+SVM (6), MDS+5NN (7), MDS+PNN (8) and MDS+SVM (9), respectively.

Although gene expression levels present the non-linear characters, non-linear dimensionality reduction method MDS does not always outperform the other two linear methods in prediction accuracies. In fact, it is very difficult to design the best dimensionality reduction approach to tumor classification due to what we do not know about the statistical distribution of measured gene expression levels. Especially, the distribution across transcripts of true expression values is dependent on the biological state of the cell, and for a given state this is unknown [3].

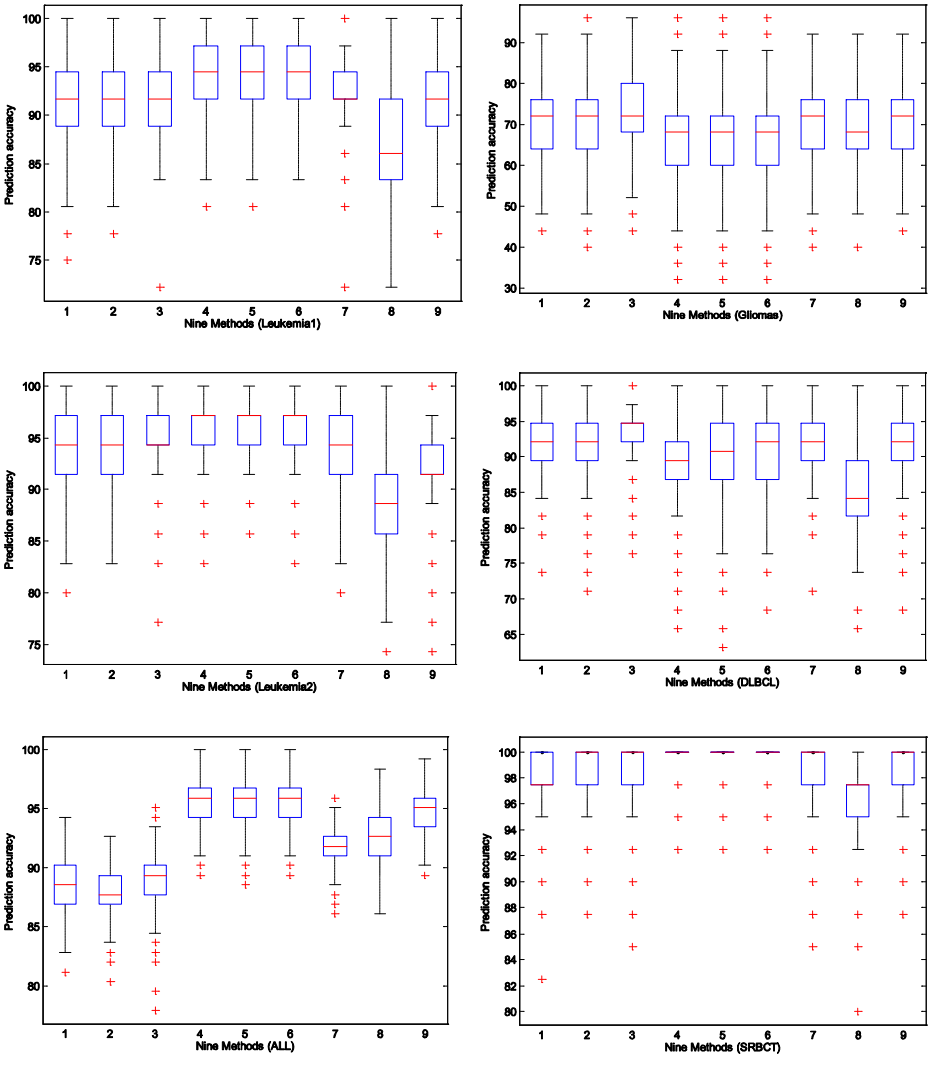

Fig. 3. The boxplots of various methods with Relief-F on all six tumor datasets. The nine numbers on x-axis denote PCA+5NN (1), PCA+PNN (2), PCA+SVM (3), LDA+5NN (4), LDA+PNN (5), LDA+SVM (6), MDS+5NN (7), MDS+PNN (8) and MDS+SVM (9), respectively.

4 Conclusions

Based on two-stage dimensionality reduction model we design 18 combined classification methods that combine two gene filters, three classical dimensionality reduction methods with three common machine learning methods to evaluate six tumor datasets to attempt to find the best methods for tumor classification. However, our experimental results suggest that no single method is always superior to other methods in prediction accuracy on all six tumor datasets and SVM is not always superior to KNN and PNN in prediction accuracy. Our results also suggest that the classification performance obtained depends strongly on the dataset, and less on the gene selection and classification methods. More importantly, our experiments indicate that those classical and simple methods can achieve satisfactory classification performance.

Acknowledgments

This work was supported by the National Science Foundation of China (grant nos., 30700161, 30900321, and 60973153), the China Postdoctoral Science Foundation (grant no. 20090450825), and the Knowledge Innovation Program of the Chinese Academy of Sciences (0823A16121).

References

1. Golub, T.R., Slonim, D.K., Tamayo, P., Huard, C., Gaasenbeek, M., Mesirov, J.P., Coller, H., Loh, M.L., Downing, J.R., Caligiuri, M.A., Bloomfield, C.D., Lander, E.S.: Molecular classification of cancer: Class discovery and class prediction by gene expression monitoring. Science 286, 531–537 (1999)
2. Asyali, M.H., Colak, D., Demirkaya, O., Inan, M.S.: Gene expression profile classification: A review. Current Bioinformatics 1, 55–73 (2006)
3. Rocke, D.M., Ideker, T., Troyanskaya, O., Quackenbush, J., Dopazo, J.: Papers on normalization, variable selection, classification or clustering of microarray data. Bioinformatics 25, 701–702 (2009)
4. Wang, S.L., Gui, J., Li, X.L.: Factor analysis for cross-platform tumor classification based on gene expression profiles. Journal of Circuits Systems and Computers 19, 243–258 (2010)
5. Belhumeur, P.N., Hespanha, J.P., Kriegman, D.J.: Eigenfaces vs. Fisherfaces: Recognition using class specific linear projection. IEEE Transactions on Pattern Analysis and Machine Intelligence 19, 711–720 (1997)
6. Cox, T., Cox, M.: Multidimensional scaling. Chapman & Hall, London (1994)
7. Wang, S.L., Wang, J., Chen, H.W., Zhang, B.Y.: SVM-based tumor classification with gene expression data. In: Li, X., Zaïane, O.R., Li, Z.-h. (eds.) ADMA 2006. LNCS (LNAI), vol. 4093, pp. 864–870. Springer, Heidelberg (2006)
8. Lu, Y.J., Tian, Q., Sanchez, M., Wang, Y.F.: Hybrid PCA and LDA analysis of microarray gene expression data. In: Proceedings of the 2005 IEEE Symposium on Computational Intelligence in Bioinformatics and Computational Biology, pp. 372–377 (2005)
9. Taguchi, Y., Oono, Y.: Relational patterns of gene expression via non-metric multidimensional scaling analysis. Bioinformatics 21, 730–740 (2005)

10. Chen, Y., Meltzer, P.S.: Gene expression analysis via multidimensional scaling. Curr. Protoc. Bioinformatics, ch. 7, Unit 7.11 (2005)
11. Ye, J.P., Li, T., Xiong, T., Janardan, R.: Using uncorrelated discriminant analysis for tissue classification with gene expression data. IEEE-ACM Transactions on Computational Biology and Bioinformatics 1, 181–190 (2004)
12. Kruskal, W.H., Wallis, W.A.: Use of ranks in one-criterion variance analysis. Journal of the American Statistical Association 47, 583–621 (1952)
13. Kononenko, I.: Estimating attributes: Analysis and extensions of Relieff. In: European Conference on Machine Learning, pp. 171–182. Springer, Catana (1994)
14. Armstrong, S.A., Staunton, J.E., Silverman, L.B., Pieters, R., de Boer, M.L., Minden, M.D., Sallan, S.E., Lander, E.S., Golub, T.R., Korsmeyer, S.J.: MLL translocations specify a distinct gene expression profile that distinguishes a unique leukemia. Nature Genetics 30, 41–47 (2002)
15. Nutt, C.L., Mani, D.R., Betensky, R.A., Tamayo, P., Cairncross, J.G., Ladd, C., Pohl, U., Hartmann, C., McLaughlin, M.E., Batchelor, T.T., Black, P.M., von Deimling, A., Pomeroy, S.L., Golub, T.R., Louis, D.N.: Gene expression-based classification of malignant gliomas correlates better with survival than histological classification. Cancer Research 63, 1602–1607 (2003)
16. Shipp, M.A., Ross, K.N., Tamayo, P., Weng, A.P., Kutok, J.L., Aguiar, R.C.T., Gaasenbeek, M., Angelo, M., Reich, M., Pinkus, G.S., Ray, T.S., Koval, M.A., Last, K.W., Norton, A., Lister, T.A., Mesirov, J., Neuberg, D.S., Lander, E.S., Aster, J.C., Golub, T.R.: Diffuse large B-cell lymphoma outcome prediction by gene-expression profiling and supervised machine learning. Nature Medicine 8, 68–74 (2002)
17. Yeoh, E.J., Ross, M.E., Shurtleff, S.A., Williams, W.K., Patel, D., Mahfouz, R., Behm, F.G., Raimondi, S.C., Relling, M.V., Patel, A., Cheng, C., Campana, D., Wilkins, D., Zhou, X.D., Li, J.Y., Liu, H.Q., Pui, C.H., Evans, W.E., Naeve, C., Wong, L.S., Downing, J.R.: Classification, subtype discovery, and prediction of outcome in pediatric acute lymphoblastic leukemia by gene expression profiling. Cancer Cell 1, 133–143 (2002)
18. Khan, J., Wei, J.S., Ringner, M., Saal, L.H., Ladanyi, M., Westermann, F., Berthold, F., Schwab, M., Antonescu, C.R., Peterson, C., Meltzer, P.S.: Classification and diagnostic prediction of cancers using gene expression profiling and artificial neural networks. Nature Medicine 7, 673–679 (2001)
19. Ambroise, C., McLachlan, G.J.: Selection bias in gene extraction on the basis of microarray gene-expression data. Proceedings of the National Academy of Sciences of the United States of America 99, 6562–6566 (2002)

PH Optimal Control in the Clarifying Process of Sugar Cane Juice Based on DHP

Xiaofeng Lin[1], Qianli Teng[1], Chunning Song[1], Shaojian Song[1], and Huixia Liu[2]

[1] School of Electrical Engineering, Guangxi University,
Nanning Guangxi 530004, China
[2] School of Light Industry and Food Engineering, Guangxi University
Nanning Guangxi 530004, China
gxulinxf@163.com

Abstract. This paper proposes the use of error back proragation (BP) neural network to efficiently control the pH in the clarifying process of sugar cane juice. In particular approximate dynamic programming (ADP) is implemented to solve this nonlinear control problem. The neural network model of the clarifying process of sugar cane juice and a neural network controller based on the idea of ADP to achieve optimal control are developed. The strategy and training procedures of dual heuristic programming (DHP) are discussed. The result is the "plant" has been effectively controlled using DHP.

Keywords: approximate dynamic programming, dual heuristic programming, optimal control, clarifying process.

1 Introduction

Dynamic programming is a very useful tool in solving the nonlinear multiple-input and multiple-output (MIMO) control cases most of which can be formulated as cost minimization or maximization problem.

Suppose that one is given a discrete-time nonlinear (time-varying) system

$$x(k+1) = F[x(k), u(k), k]. \tag{1}$$

where $x \in R^n$ represents the state vector of the system, $u \in R^m$ denotes the control action, F is the system function and k is the initial time. Suppose that one associates with this system the performance index (or cost)

$$J\left[x(k), k\right] = \sum_{i=k}^{\infty} \gamma^{i-k} U\left[x(i), u(i), i\right]. \tag{2}$$

where U is called the utility function, and γ is the discount factor, with $0 < \gamma \leq 1$. Note that J is dependent on the initial time k and the initial state $x(k)$, and it is referred to as the cost-to-go of state $x(k)$. The objective is to choose a control sequence $u(i)$, $i = k, k+1, \ldots$, so that the function J (i.e., the cost) in (2) is minimized.

D.-S. Huang et al. (Eds.): ICIC 2010, LNCS 6215, pp. 301–308, 2010.

Suppose that one has computed optimal cost $J^*[x(k+1).k+1]$ from time k+1 onward for all possible states $x(k+1)$ and that one has also found the optimal control sequences from time k+1 onward. The optimal cost from time k onward is equal to

$$J^*\left[x(k),k\right]=\min_{u(k)}\left\{U\left[x(k),u(k),k\right]+\gamma J^*\left[x(k+1),k+1\right]\right\}. \tag{3}$$

Equation (3) is the principle of optimality for discrete-time systems. Its importance lies in the fact that it allows one to optimize over only one control vector at a time by working backward in time. However, this procedure requires a backward numerical process, and it is too computationally expensive to determine the solutions due to the so-called "curse of dimensionality" [1].

2 Approximate Dynamic Programming (ADP)

In recent years, ADP has been gained much attention from many researchers in order to obtain approximate solutions of the Hamilton–Jacobi–Bellman (HJB) equation, cf. [2]-[5]. A typical design of ADP consists of three modules: 1) critic (for evaluation); 2) dynamic system (for prediction); and 3) action (for decision). When in ADP, the critic network (i.e., the evaluation module) takes the action/control signal as part of its inputs. The main idea of ADP is shown in fig. 1 [6].

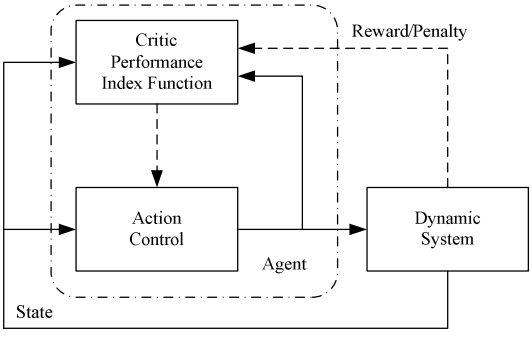

Fig. 1. Learn from the environment

The critic network outputs an estimate of J function in equation (2). This is done by minimizing the following error measure over time,

$$\left\|E_h\right\|=\sum_k E_h(k)=\sum_k\left[\hat{J}(k)-U(k)-\gamma\hat{J}(k+1)\right]^2. \tag{4}$$

where $\hat{J}(k)=\hat{J}[(x(k),u(k),k,Wc)]$ and Wc represents the parameters of the critic network. The function U is the same utility function as the one in (2) which indicates the performance of the overall system. When $E_h=0$ for all k, (4) implies that

$$\begin{aligned}\hat{J}(k) &= U(k) + \gamma \hat{J}(k+1) \\ &= U(k) + \gamma[U(k+1) + \gamma \hat{J}(k+2)] \\ &= \cdots = \sum_{i=k}^{\infty} \gamma^{i-k} U(i).\end{aligned} \tag{5}$$

which is exactly the same as the cost in (2). It is therefore clear that by minimizing the error function in (4).

2.1 Dual Heuristic Programming (DHP)

DHP is the fundamentally structure of ADP. A schematic diagram of components the DHP is shown in Figure 2. DHP is a method for estimating the gradient of the cost function, rather than J itself. To do this, a function is needed to describe the gradient of the instantaneous cost function with respect to the state of the system. In the DHP structure, the action network, with the control as its output and the state variables as its inputs, but for the second network, which is called the critic network, with the costate as its output and the state variables as its inputs [6], [7].

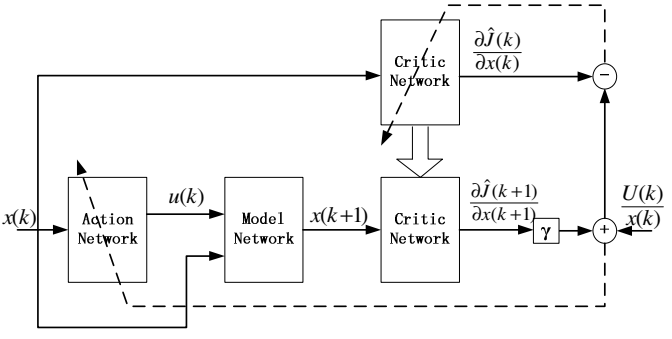

Fig. 2. The DHP structure

The critic network's training is complex since we need to take into account all relevant pathways of back propagation. This is done by minimizing the following error measure over time

$$\|E_D\| = \sum_k E_D(k) = \frac{1}{2} \sum_k \left[\frac{\partial \hat{J}(k)}{\partial x(k)} - \frac{\partial U(k)}{\partial x(k)} - \gamma \frac{\partial \hat{J}(k+1)}{\partial x(k+1)} \right]^2. \tag{6}$$

where $\partial \hat{J}(k) / \partial x(k) = \partial \hat{J}[(x(k), u(k), k, Wc)] / \partial x(k)$ and Wc represents the parameters of the critic network. When $E_D = 0$ for all k, (6) implies that [8]

$$\frac{\partial \hat{J}(k)}{\partial x(k)} = \frac{\partial U(k)}{\partial x(k)} + \gamma \frac{\partial \hat{J}(k+1)}{\partial x(k)}. \tag{7}$$

3 The BP Neural Network Modeling and DHP to Control the pH

The clarifying process of sugar cane juice is a complicated physical-chemistry process. The flowchart of sugarcane juice clarification is shown in fig.3 [8].

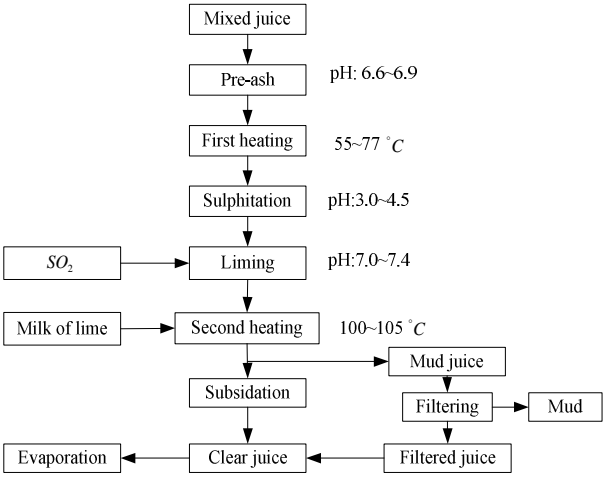

Fig. 3. Flow diagram of the clarifying process of sugar cane juice

At present, sulfurous acid method is popularly used in most sugar factories in China. To control the pH within a required range is the vital significance for acquiring high quality purified juice. The purpose of the clarifying process is to clear the most juice from a large number of impurities and control the neutralized pH and purified juice pH within a required range [8]: the neutralized pH is between 7.0 to 7.4, and purified juice pH is between 7.0 to 7.2.

3.1 The BP Neural Network (BPNN) Modeling

The 1200 data points are sampled for the model network training. The period is 10 minutes, which means one time step. The pre-ash's pH value (u_1), flow of juice (u_2), intensity of sulfur (u_3), flow of lime milk (u_4), neutralized pH value (y_1), and purified juice pH value (y_2), are needed for modeling. As we know, the pre-ash's pH is about 5 time-steps lagging the neutralized pH, the flow of juice, intensity of sulfur and flow of lime milk are about 1 time-steps lagging the neutralized pH value respectively, and the neutralized pH value is 6 time-steps lagging the purified juice pH. Suppose the nonlinear plant is formulated as [9]

$$\begin{aligned} y_1(k) &= f[y_1(k-1), u_1(k-6), u_2(k-2), u_3(k-2), u_4(k-2)]. \\ y_2(k) &= f[y_1(k-1), u_1(k-12), u_2(k-8), u_3(k-8), u_4(k-8)]. \end{aligned} \tag{8}$$

In this section, the structures of model network are three layers and the hidden layer are composed of 32 neurons. The BPNN model is shown in fig. 4.

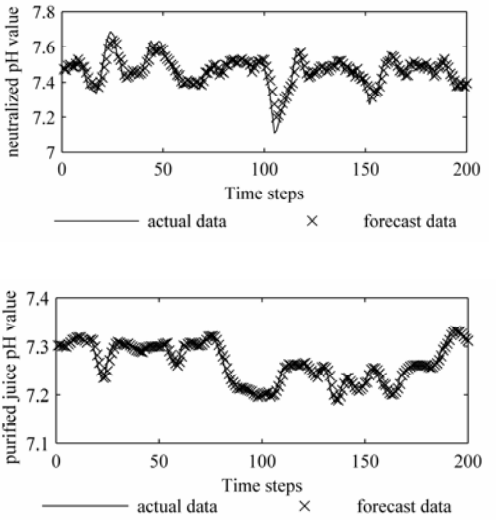

Fig. 4. The BPNN model for the pH

3.2 The Algorithm of DHP to Control the pH Value

We consider the use of the BPNN to efficiently control the pH in the clarifying process of sugar cane juice. Assume that the control objective is to have $x(k)$ in (1) track another signal given by 7.2. The local cost function is defined $U(k)$ as

$$U(k) = \frac{1}{2}(x(k) - 7.2)^2 . \tag{9}$$

For the critic network (critic NN), whose output is $\lambda(k)$, the weight update needs an error between the real output and the "desired output" of the critic NN. So a value must be calculated as the "desired output", defined as $\lambda^*(k)$. And the control vector $u(k)$ is also partial inputs for the critic NN. Then training critic network, the error team is calculated in the form

$$e_c(k) = \lambda(k) - \lambda^*(k). \tag{10}$$

$$E(k) = \frac{1}{2} e_c^{\,2}(k). \tag{11}$$

The critic network weights updating rule can be described as [10], [11]

$$Wc(k+1) = Wc(k) + \Delta Wc(k). \tag{12}$$

$$\Delta Wc = -\beta_1 \frac{\partial E(k)}{\partial Wc(k)}. \tag{13}$$

where Wc denotes the weight of the critic NN, $0 < \beta_1 \leq 1$ is a given learning rate for the critic network.

The main objective of action network (action NN) is to generate a sequence control signal $u(i)$, $u(i + 1)$, $u(i + 2)$ ···. The action network weights updating rule can be described as

$$Wa(k+1) = Wa(k) + \Delta Wa(k). \tag{14}$$

$$\Delta Wa = -\beta_2 \frac{\partial E(k)}{\partial Wa(k)}. \tag{15}$$

where Wa denotes the weight of the action NN, $0 < \beta_2 \leq 1$ is also a given learning rate and can be computed like critic neural network.

4 Simulation Results

In neural network implementation, two training plans can be adopted. One is training one network while the other's weight is unchanged. The other strategy is that both the action and critic NN are trained simultaneously. In this paper, we adopt the latter. The structures of both action and critic NN are three layers and the hidden layer are composed of 10 neurons. The weights of both action and critic NN are set with random state during [0, 1].

Then the training strategy can be formulated as following [10], [12]:

1. Scale $u_1(k\text{-}6)$, $u_2(k\text{-}2)$, $u_3(k\text{-}2)$, $u_4(k\text{-}2)$, $y_1(k\text{-}1)$ to model NN and obtain $y_1(k)$;
2. Apply $u_1(k\text{-}12)$, $u_2(k\text{-}8)$, $u_3(k\text{-}8)$, $u_4(k\text{-}8)$, $y_2(k\text{-}1)$ to model NN and obtain $y_2(k)$;
3. Calculate desired $\lambda^*(k)$ for critic NN and obtain the error.
4. Calculate/execute weight changes for action NN.
5. Calculate/execute weight changes for critic NN.
6. Increment k and go to 1.

In the training propagating path, for the hidden layers of both action and critic network, standard log-sigmoid transformation function are adopted. The simulation results are shown in fig. 5 and fig. 6.

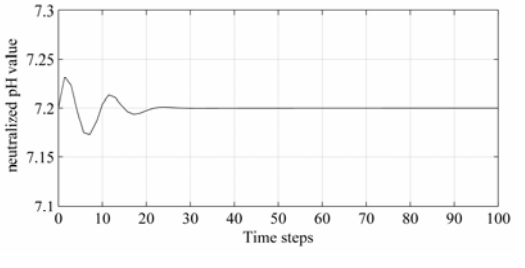

Fig. 5. Typical trajectories of control

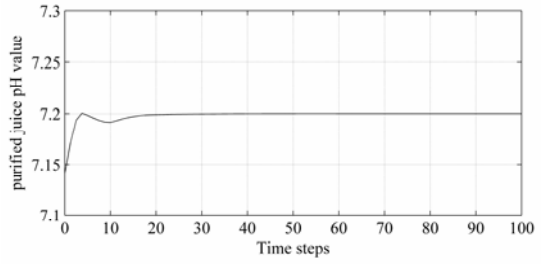

Fig. 5. (*continued*)

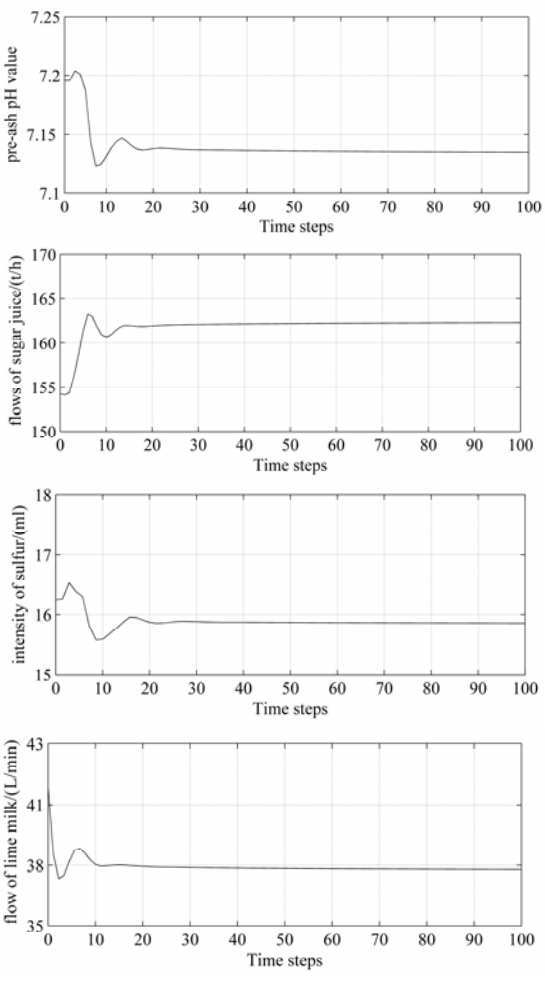

Fig. 6. Typical trajectories of pre-ash pH value, flows of sugar juice, intensity of sulfur and flow of lime milk respectively

5 Conclusions

The paper proposes the use of the BPNN to efficiently control the pH in the clarifying process of sugar cane juice. In particular ADP is implemented to solve this nonlinear control problem. First, in DHP, a "desired output" (target) is needed for training the critic NN, and this is typically calculated by running the critic NN one more computational cycle to provide its next-in-time output, and then use this value to compute the target for the present-time cycle. Secondly, DHP method is suitable for nonlinear systems, and can meet the system requirement or accommodate new environments. Besides, calculating the derivative of the performance function can improve the accuracy. Simulation results indicate that the proposed DHP is effective in achieving control of pH control through neural network learning.

References

1. Danil, V.P., Donald, C.W.: Adaptive critic designs. IEEE Trans. on Neural Networks 8, 997–1007 (1997)
2. Asma, A.T., Frank, L.L., Murad, A.K.: Discrete-Time Nonlinear HJB Solution using Approximate Dynamic Programming. Convergence Proof. IEEE Trans. Syst., Man., Cyberm. B 38, 943–949 (2008)
3. Paul, J.W.: Using ADP to understand and replicate brain intelligence: The next level design. In: Proc. of the 2007 IEEE Symposium on Approximate Dynamic Programming and Reinforcement Learning, pp. 209–216 (2007)
4. Brett, B., Jonathan, P.H.: Approximate dynamic programming using bellman residual elimination and gaussian process regression. In: 2009 American Control Conference Hyatt Regency Riverfront, St. Louis, MO, USA (2009)
5. Warren, B.P.: Approximate dynamic programming: Solving the courses of dimensionality. Wiley-Interscience, San Francisco (2007)
6. Feiyue, W., Huaguang, Z., Derong, L.: Adaptive dynamic programming: An introduction. Proc. of the IEEE Computational Intelligence Magazine (2009)
7. Jennie, S., Yutsung, W.: On-line learning by association and reinforcement. IEEE Trans. on Neural Networks 12, 349–360 (2001)
8. Weijun, C., Sixin, X.: Sugar cane production principle and technology, vol. 2. Chinese Light industry publishing house, Beijing (2000)
9. John, J.M., Chadwick, J.C., George, G.L.: Adaptive dynamic programming. IEEE Trans. on Systems, Man, and Cybernetic–Part C, Applications & Reviews 32, 140–153 (2002)
10. Derong, L., Hossein, J., Olesia, K.: Adaptive critic learning techniques for engine torque and air-fuel ratio control. IEEE Trans. on Syst., Man., and Cybern. B 38, 988–993 (2008)
11. Balakrishnan, S.N., Ding, J., Lewis, F.L.: Issues on stability of ADP feedback controllers for dynamical systems. IEEE Trans. Syst., Man., Cyberm. B 38, 913–917 (2008)
12. George, G.L., Thaddeus, T.S., Andres, R.: A comparison of training algorithms for DHP adaptive critic neuro-control. In: 1999 International Joint Conference on Neural Network, pp. 2265–2270. IEEE Press, Washington D.C (1999)

Parameter-Free Deterministic Global Search with Simplified Central Force Optimization

Richard A. Formato

Registered Patent Attorney & Consulting Engineer
P.O. Box 1714, Harwich, MA 02645, USA
rf2@ieee.org

Abstract. This note describes a simplified parameter-free implementation of Central Force Optimization for use in deterministic multidimensional search and optimization. The user supplies only the objective function to be maximized, nothing more. The algorithm's performance is tested against a widely used suite of twenty three benchmark functions and compared to other state-of-the-art algorithms. CFO performs very well.

Keywords: Central Force Optimization, CFO, Deterministic Algorithm, Multidimensional Search and Optimization, Parameter-Free Optimization, Gravitational Kinematics Metaphor, Metaheuristic.

1 Introduction

Central Force Optimization (CFO) is a *deterministic* Nature-inspired metaheuristic for an evolutionary algorithm (EA) that performs multidimensional global search and optimization [1-13]. This note presents a simplified parameter-free CFO implementation that requires only one user-specified input: the objective function to be maximized. The algorithm performs quite well across a wide range of functions.

A major frustration with many EAs is the plethora of setup parameters. For example, the three Ant Colony Optimization algorithms described in [14] (AS, *MAX-MIN*, ACS) require the user to specify nine parameters The generalized Particle Swarm Optimization algorithm in [15] requires the user to specify a population size and six "suitable bounded coefficients". This frustration is compounded by the facts that (a) there usually is no methodology for picking "good" values; (b) the "right" parameters are often problem-specific; (c) the solutions often are sensitive to small changes; and (d) run upon run, exactly the same parameters never yield the same results because the algorithm is *inherently stochastic*.

CFO is quite different. It is based on Newton's laws of motion and gravity for real masses moving through the real Universe; and just as these laws are mathematically precise, so too is CFO. It is completely deterministic at every step, with successive runs employing the same setup parameters yielding precisely the same results. Its inherent determinism distinguishes CFO from all the stochastic EAs that fail completely if randomness is removed. Moreover, CFO's metaphor of gravitational kinematics appears to be more than a simple analogy. While many metaheuristics are

D.-S. Huang et al. (Eds.): ICIC 2010, LNCS 6215, pp. 309–318, 2010.

inspired by natural processes, ant foraging or fish swarming, for example, the resulting algorithm is not (necessarily) an accurate mathematical model of the actual process. Rather, it truly is a metaphor. By contrast, CFO and real gravity appear to be much more closely related. Indeed, CFO's "metaphor" actually may be reality, because its "probes" often exhibit behavior that is strikingly similar to that of gravitationally trapped near earth objects (NEOs). If so, the panoply of mathematical tools and techniques available in celestial mechanics may be applicable to CFO directly or with modification or extension (see [1,7-9]). CFO may be interpreted in different ways depending upon the underlying model (vector force field, gravitational potential, kinetic or total energy) [3,13]. These observations, although peripheral to the theme of this note, provide additional context for the CFO metaheuristic.

There are, of course, other gravity-inspired metaheuristics, notably Space Gravitational Optimization [16]; Integrated Radiation Optimization [17]; and Gravitational Search Algorithm [18, 19]. But each one is *inherently* stochastic. Their basic equations contain true random variables whose values must be computed from a probability distribution and consequently are unknowable in advance. CFO, by contrast, is completely deterministic. Even arbitrarily assigned variables (for example, the "repositioning factor" discussed below), are known with absolute precision. At no point in a CFO run is any value computed probabilistically, which is a major departure from how almost all other Nature-inspired metaheuristics function.

2 CFO Algorithm

Pseudocode for the parameter-free CFO implementation appears in Fig. 1. Simplification of the algorithm is accomplished by hardwiring all of CFO's basic parameters, which results in simplified equations of motion as described below. CFO searches for the global *maxima* of an *objective function* $f(x_1, x_2, ..., x_{N_d})$ defined on the N_d-dimensional decision space Ω: $x_i^{\min} \le x_i \le x_i^{\max}$, $1 \le i \le N_d$. The x_i are *decision variables*, and i the coordinate number. The value of $f(\vec{x})$ at point $\vec{x}$ in Ω is its *fitness*. $f(\vec{x})$'s topology or "landscape" in the N_d-dimensional hyperspace is unknown, that is, there is no *a priori* information about the objective function's maxima. CFO searches Ω by flying "probes" through the space at discrete "time" steps (iterations). Each probe's location is specified by its position vector computed from two *equations of motion* that analogize their real-world counterparts for material objects moving through physical space under the influence of gravity without energy dissipation.

Probe p's position vector at step j is $\vec{R}_j^{\,p} = \sum_{k=1}^{N_d} x_k^{p,j} \hat{e}_k$, where the $x_k^{p,j}$ are its coordinates and $\hat{e}_k$ the unit vector along the x_k-axis. The indices j, $0 \le j \le N_t$, and p, $1 \le p \le N_p$, respectively, are the iteration number and probe number, with N_t and N_p being the corresponding *total* numbers of time steps and probes.

In metaphorical "CFO space" each of the N_p probes experiences an acceleration created by the "gravitational pull" of "masses" in Ω (see [1,12] for details). Probe p's acceleration at step $j-1$ is given by

$$\vec{a}_{j-1}^{\,p} = \sum_{\substack{k=1 \\ k\neq p}}^{N_p} U(M_{j-1}^{k} - M_{j-1}^{p}) \cdot (M_{j-1}^{k} - M_{j-1}^{p}) \times \frac{(\vec{R}_{j-1}^{k} - \vec{R}_{j-1}^{p})}{\left\| \vec{R}_{j-1}^{k} - \vec{R}_{j-1}^{p} \right\|}, \qquad (1)$$

which is the first of CFO's two equations of motion. In (1), $M_{j-1}^{p} = f(x_1^{p,j-1}, x_2^{p,j-1}, ..., x_{N_d}^{p,j-1})$ is the objective function's fitness at probe p's location at time step $j-1$. Each of the other probes at that step (iteration) has associated with it fitness $M_{j-1}^{k}, k = 1,..., p-1, p+1,..., N_p$. $U(\cdot)$ is the Unit Step function, $U(z) = \begin{cases} 1, & z \geq 0 \\ 0, & otherwise \end{cases}$. If $\vec{R}_{j-1}^{k} = \vec{R}_{j-1}^{p}, k \neq p$, then $\vec{a}_{j-1}^{\,p} \equiv 0$ because $M_{j-1}^{k} = M_{j-1}^{p}$ and $\vec{a}_{j-1}^{\,p}$ is indeterminate (probes k and p have coalesced so that k cannot exert a gravitational force on p). The acceleration $\vec{a}_{j-1}^{\,p}$ causes probe p to move from position $\vec{R}_{j-1}^{p}$ at step $j-1$ to position $\vec{R}_{j}^{p}$ at step j according to the trajectory equation

$$\vec{R}_{j}^{p} = \vec{R}_{j-1}^{p} + \vec{a}_{j-1}^{\,p}, \quad j \geq 1 \ , \qquad (2)$$

which is CFO's second equation of motion. These simplified CFO equations result from hardwiring CFO's basic parameters to $G = 2$, $\Delta t = 1$, $\alpha = 1$, and $\beta = 1$ (see [1,11,12] for definitions and discussion). The "internal parameters" in Fig. 1 are *not* fundamental CFO parameters, but rather specific to this *particular* implementation.

Every CFO run begins with an Initial Probe Distribution (IPD) defined by two variables: (a) the total number of probes used, N_p; and (b) where the probes are placed inside Ω. The IPD used here is an orthogonal array of N_p / N_d probes per dimension deployed uniformly on "probe lines" parallel to the coordinate axes and intersecting at a point that slides along Ω's principal diagonal. Fig. 2 provides a two-dimensional (2D) example of this type of IPD (9 probes shown on each probe line, 2 overlapping, but any number may be used). The probe lines are parallel to the x_1 and x_2 axes intersecting at a point on Ω's principal diagonal marked by position vector $\vec{D} = \vec{X}_{\min} + \gamma(\vec{X}_{\max} - \vec{X}_{\min})$. The diagonal's endpoints are at

Procedure $CFO[f(\vec{x}), N_d, \Omega]$

Internals: N_t, F_{rep}^{init}, ΔF_{rep}, $F_{rep}^{\min}$, $\left(\frac{N_p}{N_d}\right)_{MAX}$, γ_{start}, γ_{stop}, $\Delta\gamma$.

Initialize $f_{\max}^{global}(\vec{x})$ = very large negative number, say, -10^{+4200}.

For $N_p/N_d = 2$ to $\left(\frac{N_p}{N_d}\right)_{MAX}$ by 2:

(a.0) Total number of probes: $N_p = N_d \cdot \left(\frac{N_p}{N_d}\right)$

For $\gamma = \gamma_{start}$ to γ_{stop} by $\Delta\gamma$:

(a.1) Re-initialize data structures for position/ acceleration vectors & fitness matrix.

(a.2) Compute IPD [see text].

(a.3) Compute initial fitness matrix, $M_0^p, 1 \le p \le N_p$.

(a.4) Initialize $F_{rep} = F_{rep}^{init}$.

For $j = 0$ to N_t [or earlier termination – see text]:

(b) Compute position vectors, $\vec{R}_j^p, 1 \le p \le N_p$ [eq.(2)].

(c) Retrieve errant probes ($1 \le p \le N_p$):

If $\vec{R}_j^p \cdot \hat{e}_i < x_i^{\min} \therefore \quad \vec{R}_j^p \cdot \hat{e}_i = \max\{x_i^{\min} + F_{rep}(\vec{R}_{j-1}^p \cdot \hat{e}_i - x_i^{\min}), x_i^{\min}\}$.

If $\vec{R}_j^p \cdot \hat{e}_i > x_i^{\max} \therefore \quad \vec{R}_j^p \cdot \hat{e}_i = \min\{x_i^{\max} - F_{rep}(x_i^{\max} - \vec{R}_{j-1}^p \cdot \hat{e}_i), x_i^{\max}\}$.

(d) Compute fitness matrix for current probe distribution, $M_j^p, 1 \le p \le N_p$.

(e) Compute accelerations using current probe distribution and fitnesses [eq. (1)].

(f) Increment F_{rep}: $F_{rep} = F_{rep} + \Delta F_{rep}$; If $F_{rep} > 1 \therefore F_{rep} = F_{rep}^{\min}$..

(g) If $j \ge 20$ and $j \; MOD \; 10 = 0 \; \therefore$

(i) Shrink Ω around $\vec{R}_{best}$ [see text].

(ii) Retrieve errant probes [procedure Step (c)].

Next j

(h) Reset Ω boundaries [values before shrinking].

(i) If $f_{\max}(\vec{x}) \ge f_{\max}^{global}(\vec{x}) \quad \therefore \quad f_{\max}^{global}(\vec{x}) = f_{\max}(\vec{x})$.

Next γ

Next N_p/N_d

Fig. 1. Parameter-free CFO Pseudocode

$\vec{X}_{\min} = \sum_{i=1}^{N_d} x_i^{\min} \hat{e}_i$ and $\vec{X}_{\max} = \sum_{i=1}^{N_d} x_i^{\max} \hat{e}_i$, and parameter $0 \le \gamma \le 1$ determines where along the diagonal the probe lines intersect.

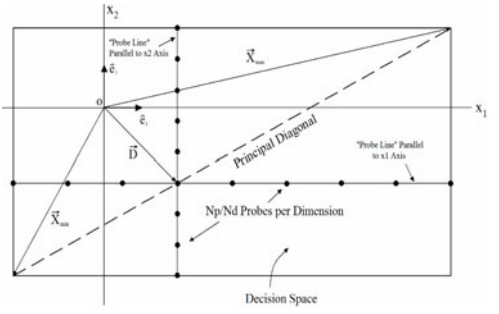

Fig. 2. Variable 2D Initial Probe Distribution

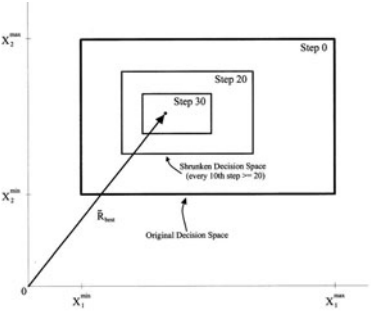

Fig. 5. 2D Decision Space Adaptation

Fig. 3 shows a typical 2D IPD for different values of γ, while Fig. 4 provides a 3D example. In Fig. 4 each probe line contains 6 equally spaced probes. For certain values of γ three probes overlap at the probe lines' intersection point on the principal diagonal. Of course, this IPD procedure is generalized to the N_d -dimensional decision space Ω to create N_d probe lines parallel to the N_d coordinate axes. While Fig. 2 shows equal numbers of probes on each probe line, a different number of probes per dimension can be used instead. For example, if equal probe spacing were desired in a decision space with unequal boundaries, or if overlapping probes were to be excluded in a symmetrical space, then unequal numbers could be used. Unequal numbers might be appropriate if *a priori* knowledge of Ω's landscape, however obtained, suggests denser sampling in one region.

Errant probes are a concern in CFO because a probe's acceleration computed from equation (1) may be too great to keep it inside Ω. If any coordinate $x_i < x_i^{\min}$ or $x_i > x_i^{\max}$, the probe enters a region of *unfeasible* solutions that are not valid for the problem at hand. The question (which arises in many algorithms) is what to do with an errant probe. While many schemes are possible, a simple, empirically determined one is used here. On a coordinate-by-coordinate basis, probes flying outside Ω are placed a fraction $F_{rep}^{\min} \le F_{rep} \le 1$ of the distance between the probe's starting coordinate and the corresponding boundary coordinate. F_{rep} is the "repositioning factor" introduced in [2]. See step (c) in the pseudocode of Fig. 1 for details. F_{rep} starts at an arbitrary initial value F_{rep}^{init} which is then incremented by an arbitrary amount ΔF_{rep}

at each iteration (subject to $F_{rep}^{\min} \le F_{rep} \le 1$). This procedure provides better sampling of Ω by distributing probes throughout the space.

This particular CFO implementation includes adaptive reconfiguration of Ω to improve convergence speed. Fig. 5 illustrates in 2D how Ω's size is adaptively reduced around $\vec{R}_{best}$, the location of the probe with best fitness throughout the run up to the current iteration. Ω shrinks every 10th step beginning at step 20. Its boundary coordinates are reduced by one-half the distance from the best probe's position to each boundary on a coordinate-by-coordinate basis, that is, $x_i'^{\min} = x_i^{\min} + \frac{\vec{R}_{best} \cdot \hat{e}_i - x_i^{\min}}{2}$ and $x_i'^{\max} = x_i^{\max} - \frac{x_i^{\max} - \vec{R}_{best} \cdot \hat{e}_i}{2}$, where the primed coordinate is Ω's new boundary, and the dot denotes vector inner product. For clarity, Fig. 5 shows $\vec{R}_{best}$ as being fixed, but generally it varies throughout a run. Changing Ω's boundary every 10 steps instead of some other interval is arbitrary.

The internal parameter values were: $N_t = 1000$, $F_{rep}^{init} = 0.5$, $\Delta F_{rep} = 0.1$, $F_{rep}^{\min} = 0.05$, $\left(\frac{N_p}{N_d}\right)_{MAX} = 14$ for $N_d \le 6$, $\left(\frac{N_p}{N_d}\right)_{MAX} = 6$ for $21 \le N_d \le 30$, $\gamma_{start} = 0$, $\gamma_{stop} = 1$, $\Delta\gamma = 0.1$, with N_t reduced to 100 for function f_7 because

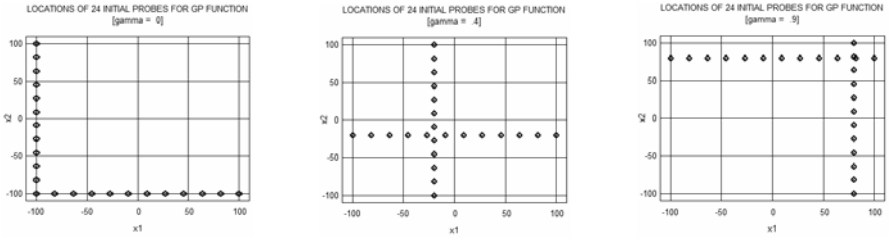

Fig. 3. Typical 2D IPD's for Different Values of γ

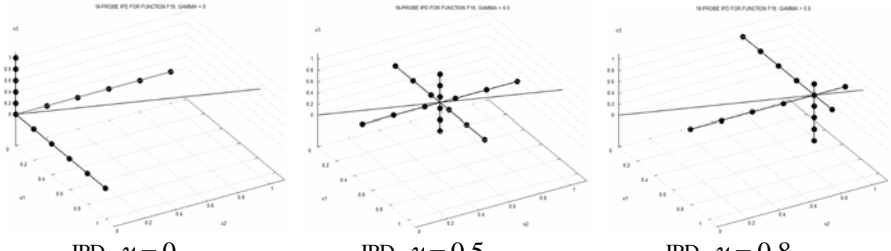

IPD, $\gamma = 0$ IPD, $\gamma = 0.5$ IPD, $\gamma = 0.8$

Fig. 4. Typical Variable 3D IPD for the GSO f_{19} Function (probes as filled circles)

this benchmark contains a random component that may result in excessive runtimes. The test for early termination is a difference between the average best fitness over 25 steps, including the current step, and the current best fitness of less than 10^{-6} (absolute value). This test is applied starting at iteration 35 (at least 10 steps must be computed before testing for saturation). The internal parameters, indeed all CFO-related parameters, were chosen empirically. These particular values provide good results across a wide range of test functions. Beyond this empirical observation there currently is no methodology for choosing either CFO's basic parameters or the internal parameters for an implementation such as this one. There likely are better parameter sets, which is an aspect of CFO development that merits further study.

3 Results

Group Search Optimizer (GSO) [20,21] is a new stochastic metaheuristic that mimics animal foraging using the strategies of "producing" (searching for food) and "scrounging" (joining resources). GSO was tested against 23 benchmark functions from 2 to 30D. GSO thus provides a superior standard for evaluating CFO. CFO therefore was tested against the same 23 function suite. The results are reported here.

In [20], GSO (inherently *stochastic*) was compared to two other stochastic algorithms, "PSO" and "GA". PSO is a Particle Swarm implemented using "PSOt" (MATLAB toolbox of standard and variant algorithms). The standard PSO algorithm was used with recommended default parameters: population, 50; acceleration factors, 2.0; inertia weight decaying from 0.9 to 0.4. GA is a real-coded Genetic Algorithm implemented with GAOT (genetic algorithm optimization toolbox). GA had a fixed population size (50), uniform mutation, heuristic crossover, and normalized geometric ranking for selection with run parameters set to recommended defaults. A detailed discussion of the experimental method and the toolboxes is at [20, p. 977].

Thus, while this note compares CFO and GSO directly, it indirectly compares CFO to PSO and GA as well. Table 1 summarizes CFO's results. F is the test function using the same function numbering as [20]. $f_{\max}$ is the known global *maximum* (note that the negative of each benchmark in [20] is used here because, unlike the other algorithms, CFO locates maxima, not minima). N_{eval} is the total number of function evaluations made by CFO. $<\cdot>$ denotes average value. Because GSO, PSO and GA are inherently stochastic, their performance must be described statistically. The statistical data in Table 1 for those algorithms are reproduced from [20].

Of course, no statistical description is needed for CFO because CFO is inherently *deterministic* (but see [11] for a discussion of *pseudorandomness* in CFO). For a given setup, only one CFO run is required to assess its performance. In the first group of high dimensionality unimodal functions ($f_1 - f_7$), CFO returned the best fitness on all seven functions, in one case by a wide margin (f_5). In the second set of six high dimensionality multimodal functions with many local maxima ($f_8 - f_{13}$), CFO performed best on three (f_9 - f_{11}) and essentially the same as GSO on f_8. In the last group of ten multimodal functions with few local maxima (f_{14} - f_{23}), CFO returned the best fitness on four (f_{20} - f_{23}, and by wide margins on f_{21} - f_{23}); equal fitnesses on four (f_{14}, f_{17}, f_{18}, f_{19}); and only very slightly lower fitness on two (f_{15} , f_{16}).

CFO did not perform quite as well as the other algorithms on only 2 of the 23 benchmarks (f_{12}, f_{13}). But its performance may be improved if a second run is made using a smaller Ω based on the first run. For example, for f_{12} the 30 coordinates returned on the run #1 are in the range $[-1.03941458 \le x_i \le -0.99688049]$ (known maximum at $[-1]^{30}$). If based on this result Ω is shrunk from $[-50 \le x_i \le 50]$ to $[-5 \le x_i \le 5]$ and CFO is run again, then on run #2 the best fitness improves to $-7.39354\text{x}10^{-35}$ ($N_{eval} = 273{,}780$), which is a good bit better than GSO's result.

Table 1. CFO Comparative Results for 23 Benchmark Suite in [20]

(* negative of the functions in [20] are computed by CFO because CFO searches for maxima instead of minima).

F^*	N_d	$f_{\max}{}^*$	*<Best Fitness>/ Other Algorithm*	*- - - CFO - - -*	
				Best Fitness	N_{eval}
Unimodal Functions (other algorithms: average of 1000 runs)					
f_1	30	0	-3.6927x10^{-37} / PSO	0	222,960
f_2	30	0	-2.9168x10^{-24} / PSO	0	237,540
f_3	30	0	-1.1979x10^{-3} / PSO	-6.1861x10^{-5}	397,320
f_4	30	0	-0.1078 / GSO	0	484,260
f_5	30	0	-37.3582 / PSO	-4.8623x10^{-5}	436,680
f_6	30	0	-1.6000x10^{-2} / GSO	0	176,580
f_7	30	0	-9.9024x10^{-3} / PSO	-1.2919x10^{-4}	399,960
Multimodal Functions, Many Local Maxima (other algorithms: avg 1000 runs)					
f_8	30	12,569.5	12,569.4882 / GSO	12,569.4865	415,500
f_9	30	0	-0.6509 / GA	0	397,080
f_{10}	30	0	-2.6548x10^{-5} / GSO	4.7705x10^{-18}	518,820
f_{11}	30	0	-3.0792x10^{-2} / GSO	-1.7075x10^{-2}	235,800
f_{12}	30	0	-2.7648x10^{-11} / GSO	-2.1541x10^{-5}	292,080
f_{13}	30	0	-4.6948x10^{-5} / GSO	-1.8293x10^{-3}	360,000
Multimodal Functions, Few Local Maxima (other algorithms: avg 50 runs)					
f_{14}	2	-1	-0.9980 / GSO	-0.9980	78,176
f_{15}	4	-3.075x10^{-4}	-3.7713x10^{-4} / GSO	-5.6967x10^{-4}	143,152
f_{16}	2	1.0316285	1.031628 / GSO	1.03158	87,240
f_{17}	2	-0.398	-0.3979 / GSO	-0.3979	82,096
f_{18}	2	-3	-3 / GSO	-3	100,996
f_{19}	3	3.86	3.8628 / GSO	3.8628	160,338
f_{20}	6	3.32	3.2697 / GSO	3.3219	457,836
f_{21}	4	10	7.5439 / PSO	10.1532	251,648
f_{22}	4	10	8.3553 / PSO	10.4029	316,096
f_{23}	4	10	8.9439 / PSO	10.5364	304,312

4 Conclusion

CFO is not nearly as highly developed as GSO, GA and PSO, but it performs very well with nothing more than the objective function as a user input. CFO performed better than or essentially as well as GSO, GA and PSO on 21 of 23 test functions. By contrast, GSO compared to PSO and GA returned the best performance on only 15 benchmarks. CFO's performance thus is better than GSO's, which in turn performed better than PSO and GA on this benchmark suite.

CFO's further development lies in two areas: architecture and theory. While this note describes one CFO implementation that works well, there no doubt is room for considerable improvement. CFO's performance is a sensitive function of the IPD, and there are limitless IPD possibilities. One approach applies precise geometric and combinatorial rules of construction to create function evaluation "centers" in a hypercube using extreme points, faces, and line segments [22-24]. Successively shrinking Ω as described for f_{12} is another possible improvement. Theoretically, gravitationally trapped NEOs may lead to a deeper understanding of the metaheuristic, as might alternative formulations involving the concepts of kinetic or total energy for masses moving under gravity. At this time there is no proof of convergence or complexity analysis for CFO, which is not unusual for new metaheuristics. As discussed in [1,14], for example, the first Ant System proof of convergence appeared four years after its introduction for a "rather peculiar ACO algorithm." Just as ACO was proffered on an empirical basis, so too is CFO. Perhaps the CFO-NEO nexus [7] provides a basis for that much desired proof of convergence?

These observations and the results reported here show that CFO merits further study with many areas of potentially fruitful research. Hopefully this note encourages talented researchers to become involved in CFO's further development. For interested readers, a complete source code listing of the program used for this note is available in electronic format upon request to the author (`rf2@ieee.org`).

References

1. Formato, R.A.: Central Force Optimization: A New Metaheuristic with Applications in Applied Electromagnetics. Prog. Electromagnetics Research 77, 425–449 (2007), `http://ceta.mit.edu/PIER/pier.php?volume=77`
2. Formato, R.A.: Central Force Optimization: A New Computational Framework For Multidimensional Search and Optimization. In: Krasnogor, N., Nicosia, G., Pavone, M., Pelta, D. (eds.) Nature Inspired Cooperative Strategies for Optimization (NICSO 2007). Studies in Computational Intelligence, vol. 129, pp. 221–238. Springer, Heidelberg (2008)
3. Formato, R.A.: Central Force Optimisation: A New Gradient-Like Metaheuristic for Multidimensional Search and Optimisation. Int. J. Bio-Inspired Computation 1, 217–238 (2009)
4. Formato, R.A.: Central Force Optimization: A New Deterministic Gradient-Like Optimization Metaheuristic. OPSEARCH 46, 25–51 (2009)
5. Qubati, G.M., Formato, R.A., Dib, N.I.: Antenna Benchmark Performance and Array Synthesis using Central Force Optimisation. IET (U.K.) Microwaves, Antennas & Propagation 5, 583–592 (2010)

6. Formato, R.A.: Improved CFO Algorithm for Antenna Optimization. Prog. Electromagnetics Research B, 405–425 (2010)
7. Formato, R.A.: Are Near Earth Objects the Key to Optimization Theory? arXiv:0912.1394 (2009), http://arXiv.org
8. Formato, R.A.: Central Force Optimization and NEOs – First Cousins?. Journal of Multiple-Valued Logic and Soft Computing (2010) (in press)
9. Formato, R.A.: NEOs – A Physicomimetic Framework for Central Force Optimization?. Applied Mathematics and Computation (review)
10. Formato, R.A.: Central Force Optimization with Variable Initial Probes and Adaptive Decision Space. Applied Mathematics and Computation (review)
11. Formato, R.A.: Pseudorandomness in Central Force Optimization, arXiv:1001.0317 (2010), http://arXiv.org
12. Formato, R.A.: Comparative Results: Group Search Optimizer and Central Force Optimization, arXiv:1002.2798 (2010), http://arXiv.org
13. Formato, R.A.: Central Force Optimization Applied to the PBM Suite of Antenna Benchmarks, arXiv:1003-0221 (2010), http://arXiv.org
14. Dorigo, M., Birattari, M., Stűtzle, T.: Ant Colony Optimization. IEEE Computational Intelligence Magazine, 28–39 (November 2006)
15. Campana, E.F., Fasano, G., Pinto, A.: Particle Swarm Optimization: dynamic system analysis for Parameter Selection in global Optimization frameworks, http://www.dis.uniroma1.it/~fasano/Cam_Fas_Pin_23_2005.pdf
16. Hsiao, Y., Chuang, C., Jiang, J., Chien, C.: A Novel Optimization Algorithm: Space Gravitational Optimization. In: Proc. of 2005 IEEE International Conference on Systems, Man, and Cybernetics, vol. 3, pp. 2323–2328 (2005)
17. Chuang, C., Jiang, J.: Integrated Radiation Optimization: Inspired by the Gravitational Radiation in the Curvature Of Space-Time. In: 2007 IEEE Congress on Evolutionary Computation (CEC 2007), pp. 3157–3164 (2007)
18. Rashedi, E., Nezamabadi-pour, H., Saryazdi, S., Farsangi, M.: Allocation of Static Var Compensator Using Gravitational Search Algorithm. In: Proc. First Joint Congress on Fuzzy and Intelligent Systems, Ferdowsi University of Mashad, Iran, pp. 29–31 (2007)
19. Rashedi, E., Nezamabadi-pour, H., Saryazdi, S.: GSA: A Gravitational Search Algorithm. Information Sciences 179, 2232–2248 (2009)
20. He, S., Wu, Q.H., Saunders, J.R.: Group Search Optimizer: An Optimization Algorithm Inspired by Animal Searching behavior. IEEE Tran. Evol. Comp. 13, 973–990 (2009)
21. CIS Publication Spotlight. IEEE Computational Intelligence Magazine 5, 5 (February 2010)
22. Glover, F.: Generating Diverse Solutions For Global Function Optimization (2010), http://spot.colorado.edu/~glover/
23. Glover, F.: A Template for Scatter Search and Path Relinking, http://spot.colorado.edu/~glover/
24. Omran, M.G.H.: private communication, Dept. of Computer Science, Gulf University for Science & Technology, Hawally 32093, Kuwait

Comparison of Optimality and Robustness between SA, TS and GRASP Metaheuristics in FJSP Problem

Tadeusz Witkowski, Arkadiusz Antczak, and Paweł Antczak

Warsaw University of Technology, Narbutta 85 street, Warsaw, Poland
tawit@poczta.onet.pl, {arkadij,pantczak}@op.pl

Abstract. The paper presents the comparison of optimality and robustness between Greedy Randomized Adaptive Search Procedure (GRASP), Simulated Annealing (SA) and Tabu Search (TS) metaheuristics in solving of flexible job shop problem (FJSP). Each of the scheduling problems have been tested with metaheuristics and have been run a number of times to get the best solution. All the results have been analyzed on certain parameter of performance for the metaheuristics - makespan. Overall, testing showed that the TS+GRASP algorithm was slightly more competitive than the SA+GRASP algorithm in the optimality and robustness test. The robustness of the algorithm increased as the best solutions produced by the algorithm were closer to the know optimal.

Keywords: robustness, greedy randomized adaptive search procedure, tabu search, simulated annealing, metaheuristics, flexible job shop.

1 Introduction

An objective of computational experiment in the theoretical context is to study the computational complexity (giving lower bounds) of optimization problems, and to devise efficient algorithms (giving upper bounds) whose complexity preferably matches the lower bounds. That is, not only are we interested in the intrinsic difficulty of computational problems under a certain computational model, but we are also concerned with the algorithmic solutions that are efficient or provably optimal in the worst or average case. Due to its applications to various science and engineering related disciplines, researches in this field have begun to address the efficacy of the algorithms, the issues concerning robustness and numerical stability [1].

Robust algorithm, i.e. an algorithm that is insensitive to its changes. Analyzing the stability of a heuristic algorithm is conceivably easier than analyzing the stability of an exact or approximate solution, science heuristic need not have any sort of performance guarantee. For example, Hall and Posner [2] study the behavior of greedy heuristics for two NP-hard problems: scheduling two machines to minimize the weighted completion time and scheduling two machines to minimize the makespan. They provide approaches to obtain bounds on the upper tolerances of each heuristic to changes in the processing time.

Intuitively, since a simple heuristic uses less of the input information than an exact algorithm, it may produce a poor result, but the solution should be less susceptible to

D.-S. Huang et al. (Eds.): ICIC 2010, LNCS 6215, pp. 319–328, 2010.

parameter changes than the optimal solution. This intuition is supported by the work of Kolen et al. [3] comparing two heuristics for scheduling jobs on identical parallel machines to minimize the makespan: Shortest Processing Time (SPT) and Longest Processing Time (LPT). The ratios between the solution returned and the optimum are 2-1/m for SPT, where m is the number of machines and 4/3 -1/(3m) for LPT [4]. The test comparison of evaluating 10 job shop problems with the artificial immune system model against a genetic algorithm model using the dimensions of optimality and robustness have been described in [5]. This paper presents the comparison of robustness between GRASP, SA+GRASP and TS+GRASP metaheuristics in solving of FJSP problem.

The paper is organized as follows. Section 2 gives the formulation of the FJSP problem. Section 3 introduces to optimality and robustness of the results. Section 4 presents the computer's experiments and section 5 gives some concluding remarks.

2 Formulation of the Problem

In job shop scheduling problem (JSP), there are n jobs and m machines, each job is to be processed on a group of machines satisfying precedence constraints. Each operation of job is to be processed only on one predetermined machine. Though the JSP has been well studied, its application to real-word scenarios is often undermined by the constraint of the one-to-one mapping of operations to machines. Hence, FJSP problem [6] extends the JSP problem by allowing each operation to be processed on more than one machine. With this extension, we are now confronted with two subtasks: assignment of each operation to an appropriate machine and sequencing operations on each machine.

The FJSP problem is formulated as fellows. There is a set of jobs $Z = \{Z_i\}$, $i \in I$, where $I = \{1, 2, ..., n\}$ is an admissible set of parts, $U = \{u_k\}$, $k \in 1, m$, is a set of machines. Each job Z_i is a group of parts Π_i of equal partial task p_i of a certain range of production. Operations of technological processing of the i-th part are denoted by $\{O_{ij}\}_{j=\xi}^{H_i}$. Then for Z_i, we can write $Z_i = (\Pi_i \{O_{ij}\}_{j=\xi}^{H_i})$, where $O_{ij} = (G_{ij}, t_{ij\,(N)})$ is the j-th operation of processing the i-th group of parts; ξ_i is the number of operation of the production process at which one should start the processing the i- th group of parts; H_i is the number of the last operation for a given group; G_{ij} is a group of interchangeable machines that is assigned to the operation O_{ij}; $t_{ij\,(N)}$ is an elementary duration of the operation O_{ij} with one part d_i that depends on the number of machine N in the group (on the specified operations); t'_{ij} is the duration of set up before the operation O_{ij}.

The most widely used objective is to find feasible schedules that minimise the completion time of the total production program, normally referred to as makespan (*Cmax*). We need comparison of robustness and optimality between the GRASP, SA+GRASP and TS+GRASP metaheuristics in solving FJSP.

3 Optimality and Robustness of the Results

There is no commonly acceptable definition of robustness. Different alternative definitions exist for robustness. In general, robustness is insensitivity against small

deviations in the input instances (data) or the parameters of the metaheuristics. The lower the variability of the obtained solutions the better the robustness [7]. In the metaheuristics community, robustness also measures the performance of the algorithms according types of input instances and/or problems. The metaheuristic should be able to perform well on a large variety of instances and/or problems using the same parameters. The parameters of the metaheuristic may be overfitted using the training set of instances and less efficient for other instances. The paper [8] discusses the comparison between Ant Colony (AC), Genetic-TS, Hybrid Genetic Algorithm (HGA) and Robust-Hybrid Genetic Algorithm (R-HGA). R-HGA produces statistically the same result as AC, Genetic-TS, and HGA. Testing hypothesis was applied for evaluating the performance of HGA. The result shows that the capability of HGA was not enough compare to the other algorithms in term of makespan.

In stochastic algorithms (i.e. GRASP, SA), the robustness may also be related to the average/deviation behavior of the algorithm over different runs of the algorithm on the same instance [9,10]. Each of the scheduling problems being tested with the GRASP, SA+GRASP and TS+GRASP metaheuristics will be run a number of times to get the best solution. All the iterations will then be analyzed on certain parameters of performance for the metaheuristics. The following will be used as the basis for evaluating the metaheuristics [5]:

- Optimality: attaining the know optimal for the problem is the primary test of the metaheuristic. All the problems being tested have known optimal solutions. If the known optimal is not reached, the solution which is closest to the known optimal will be chosen as the optimal solution reached by this metaheuristic.
- The robustness of the solution or the most optimal solution obtained by this metaheuristic will be measured by the number of times the optimal solution is reached as a percent of the total number of iterations that were run.

In this work when defining the robustness we use the depenance given below. The metaheuristic is robust, if the *Cmax* values for acceptable solutions x_i obtained as a result of a number of trials, for given criterion function $f(x_i)$:

- are equal to the values optimal solution problem $f(x^*)$ or fall within the range of $< f(x^*),\ f(x^*) + \varepsilon f(x^*) >$,
- are equal to the value of the optimal solution found by a metaheuristic $f(x_{BEST})$ or fall withing the range of $< f(x_{BEST}),\ f(x_{BEST}) + \varepsilon\ f(x_{BEST}) >$, where ε – deviation. Robustness therefore must fulfil this condition:

$$robustness \Leftrightarrow \forall x_i \exists \varepsilon \begin{cases} [f(x_i) - f(x^*)] = 0 \mid \dfrac{f(x_i) - f(x^*)}{f(x^*)} \le \varepsilon \\ \\ [f(x_i) - f(x_{BEST})] = 0 \mid \dfrac{f(x_i) - f(x_{BEST})}{f(x_{BEST})} \le \varepsilon \end{cases} \tag{1}$$

where $\varepsilon > 0$.

Solutions whose makespan values fall within specific ranges, with the deviation ε specified in advance, are suboptimal solutions, acceptable by the user for whom finding the global optimality is unattainable because for example it is too time-consuming or there are too many possible solutions in the searching space etc. That is why it is important to adequately select the deviation ε, on which the stability of the algorithm depends.

With the ε too high, the results generated by the metaheuristics can differ significantly from the global extreme and will still fall within the specified range, which testifies to the acceptability of solutions which are much worse than the suboptimal solution and recognising the method as stable.

With the ε too low, the situation is reverse - few solutions can be taken into account and few of them will belong to the specified stability range, which will be interpreted as rejection of quite good solutions which near the optimality.

4 The Computer Experiments

The resluts of the GRASP algorithm experiment were compared with the results of other algorithms, such as the hybrids SA+GRASP and TS+GRASP (table 1- 5 and figure 1- 8). Two FJSP problems were concidered: serial route FJS1 and parallel route FJS2 (problems with 10 jobs, 160 operations and 27 machines) and a great number of test JSP problems. Such sizes correspond to real dimensions of industrial problems. The real FJSP taken from manufacruring was used as the cases study (FJS1 and FJS2) for finding minimum makespan. Each of the metaheuristics was run 20 times, and the number of iterations was for the serial route iter.=1000, and for the parallel one iter. = 100.

For the solution of this problem, realizing software and Pentium 1,81 GHz with 1GB of RAM were used in the experiments.

Table 1. Difference in makespan between GRASP, SA+GRASP and TS+GRASP

1%			GRASP		SA+GRASP		TS+GRASP	
Problem #	Name of	Optimal Solution	Best Solution	Difference in Makespan	Best Solution	Difference in Makespan	Best Solution	Difference in Makespan
1	*FJS-1*	50242,2	50242,2	0	50242,2	0	50242,2	0
2	*FJS-2*	24830	25225,1	395,1	25038,8	208,8	24830	0
3	*FT06*	55	57	2	55	0	55	0
4	*FT10*	930	992	62	1021	91	938	8
5	*FT20*	1165	1249	84	1233	68	1177	12
6	*LA01*	666	668	2	666	0	666	0
7	*LA06*	926	926	0	926	0	926	0
8	*LA11*	1222	1231	9	1222	0	1222	0
9	*LA16*	945	1012	67	995	50	956	11
10	*LA21*	1046	1207	161	1167	121	1092	46
11	*TA01*	1231	1384	153	1392	161	1292	61
12	*TA31*	1764	2193	429	1979	215	2018	254
13	*TA51*	2760	3213	453	2890	130	3030	270
14	*TA61*	2868	3530	662	3125	257	3325	457
15	*TA71*	5464	6171	707	5712	248	5892	428

Table 2. Summary of comparison: GRASP, SA+GRASP, TS+GRASP (ε=1%)

1%			GRASP		SA+GRASP		TS+GRASP	
Problem #	Name of Problem	Optimal Solution	Best Solution	No. Best Solutions (%)	Best Solution	No. Best Solutions (%)	Best Solution	No. Best Solutions (%)
1	*FJS-1*	50242,2	50242,2	90	50242,2	100	50242,2	100
2	*FJS-2*	?	25225,1	40	25038,8	20	24830	20
3	*FT06*	55	57	30	55	60	55	25
4	*FT10*	930	992	5	1021	30	938	10
5	*FT20*	1165	1249	15	1233	40	1177	80
6	*LA01*	666	668	5	666	30	666	100
7	*LA06*	926	926	30	926	100	926	100
8	*LA11*	1222	1231	35	1222	100	1222	100
9	*LA16*	945	1012	5	995	5	956	35
10	*LA21*	1046	1207	30	1167	5	1092	5
11	*TA01*	1231	1384	15	1392	15	1292	25
12	*TA31*	1764	2193	25	1979	35	2018	45
13	*TA51*	2760	3213	15	2890	15	3030	35
14	*TA61*	2868	3530	5	3125	15	3325	60
15	*TA71*	5464	6171	20	5712	10	5892	10

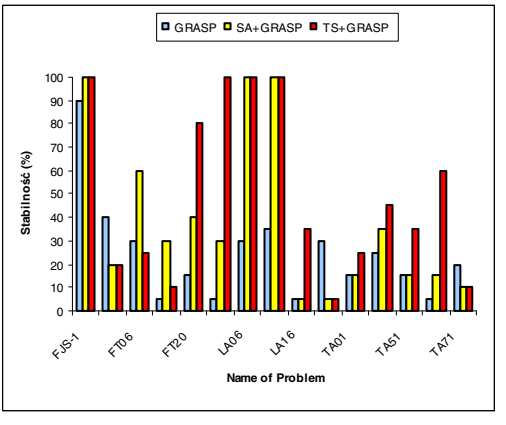

Fig. 1. Comparison of the robustness: GRASP, SA+GRASP, and TS+GRASP (ε=1%)

Table 3. Summary of comparison: GRASP, SA+GRASP, TS+GRASP (ε=2 %)

2%			GRASP		SA+GRASP		TS+GRASP	
Problem #	Name of Problem	Optimal Solution	Best Solution	No. Best Solutions (%)	Best Solution	No. Best Solutions (%)	Best Solution	No. Best Solutions (%)
1	*FJS-1*	50242,2	50242,2	100	50242,2	100	50242,2	100
2	*FJS-2*	?	25225,1	55	25038,8	70	24830	35
3	*FT06*	55	57	70	55	85	55	100
4	*FT10*	930	992	10	1021	50	938	25
5	*FT20*	1165	1249	40	1233	85	1177	100
6	*LA01*	666	668	15	666	55	666	100
7	*LA06*	926	926	35	926	100	926	100
8	*LA11*	1222	1231	60	1222	100	1222	100
9	*LA16*	945	1012	45	995	20	956	50
10	*LA21*	1046	1207	60	1167	5	1092	45
11	*TA01*	1231	1384	15	1392	50	1292	70
12	*TA31*	1764	2193	65	1979	90	2018	95
13	*TA51*	2760	3213	35	2890	70	3030	90
14	*TA61*	2868	3530	55	3125	70	3325	90
15	*TA71*	5464	6171	95	5712	80	5892	70

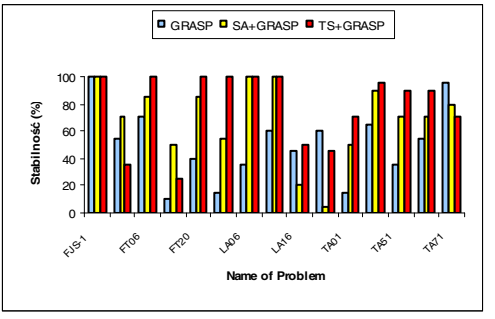

Fig. 2. Comparison of the robustness: GRASP, SA+GRASP, TS+GRASP(ε=2%)

Table 4. Summary of comparison: GRASP, SA+GRASP, TS+GRASP (ε=3%)

3%			GRASP		SA+GRASP		TS+GRASP	
Problem #	Name of Problem	Optimal Solution	Best Solution	No. Best Solutions (%)	Best Solution	No. Best Solutions (%)	Best Solution	No. Best Solutions (%)
1	*FJS-1*	50242,2	50242,2	100	50242,2	100	50242,2	100
2	*FJS-2*	?	25225,1	75	25038,8	100	24830	80
3	*FT06*	55	57	70	55	85	55	100
4	*FT10*	930	992	15	1021	85	938	90
5	*FT20*	1165	1249	75	1233	100	1177	100
6	*LA01*	666	668	20	666	60	666	100
7	*LA06*	926	926	75	926	100	926	100
8	*LA11*	1222	1231	100	1222	100	1222	100
9	*LA16*	945	1012	85	995	60	956	100
10	*LA21*	1046	1207	85	1167	10	1092	85
11	*TA01*	1231	1384	45	1392	80	1292	100
12	*TA31*	1764	2193	85	1979	100	2018	100
13	*TA51*	2760	3213	85	2890	100	3030	100
14	*TA61*	2868	3530	100	3125	100	3325	100
15	*TA71*	5464	6171	100	5712	100	5892	100

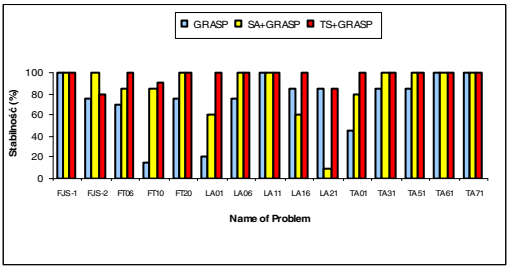

Fig. 3. Comparison of the robustness: GRASP, SA+GRASP, TS+GRASP (ε=3%)

Table 5. Summary of comparison: GRASP, SA+GRASP, TS+GRASP (ε=5%)

5%			GRASP		SA+GRASP		TS+GRASP	
Problem #	Name of Problem	Optimal Solution	Best Solution	No. Best Solutions (%)	Best Solution	No. Best Solutions (%)	Best Solution	No. Best Solutions (%)
1	*FJS-1*	50242,2	50242,2	100	50242,2	100	50242,2	100
2	*FJS-2*	?	25225,1	100	25038,8	100	24830	100
3	*FT06*	55	57	90	55	100	55	100
4	*FT10*	930	992	50	1021	100	938	100
5	*FT20*	1165	1249	100	1233	100	1177	100
6	*LA01*	666	668	35	666	100	666	100
7	*LA06*	926	926	90	926	100	926	100
8	*LA11*	1222	1231	100	1222	100	1222	100
9	*LA16*	945	1012	100	995	100	956	100
10	*LA21*	1046	1207	100	1167	40	1092	100
11	*TA01*	1231	1384	95	1392	100	1292	100
12	*TA31*	1764	2193	100	1979	100	2018	100
13	*TA51*	2760	3213	100	2890	100	3030	100
14	*TA61*	2868	3530	100	3125	100	3325	100
15	*TA71*	5464	6171	100	5712	100	5892	100

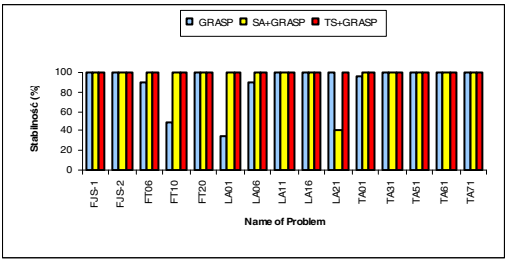

Fig. 4. Comparison of the robustness: GRASP, SA+GRASP, TS+GRASP (ε=5 %)

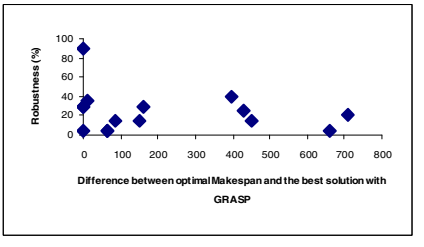

Fig. 5. Relationship between optimality and robustness for GRASP (ε=1%)

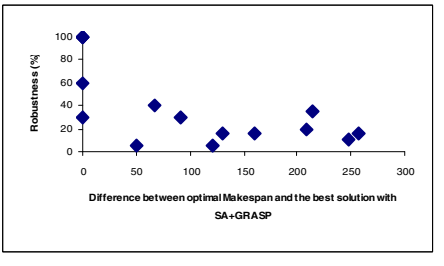

Fig. 6. Relationship between optimality and robustness for SA+GRASP (ε=1%)

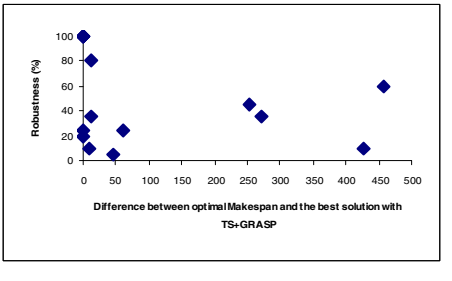

Fig. 7. Relationship between optimality and robustness for TS+GRASP (ε=1%)

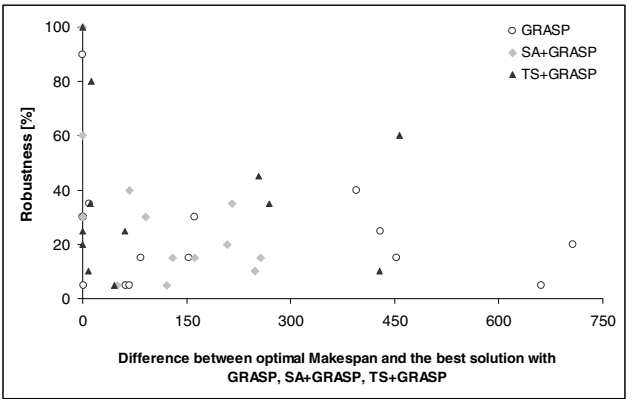

Fig. 8. Summary of relationship between optimality of solution and robustness for GRASP, SA+ GRASP and TS+GRASP (for ε=1%)

The results obtained with the GRASP, SA+GRASP and TS+GRASP [11,12] have been compared. The two flexible problems (FSJ1 and FSJ2) and 13 job shop problems have been tested with metaheuristics. 20 simulations of each problem were run with the 1000 iteration for serial and 100 iteration for parallel route. Table 1 summarizes the results for the 15 problems that were run with the GRASP, SA+GRASP and TS+GRASP. The two attributes compared are the best solution and the number of best solutions. The best solution for each problem refers to the solution obtained with GRASP, SA+GRASP and TS+GRASP, individually, with the lowest makespan (this may or may not be equal to the optimal solution). The optimal solution of each problem is also listed. The number of best solutions refers to the number of times the best solution was reached as a percent of the total 20 simulations that were run for each problem and is a test of the robustness of the solutions.

TS+GRASP and SA+GRASP obtained the optimal solution in 33,3% of the cases (5/15 problems: FJS1, FT06, LA01, LA06, LA11) while the GRASP reached the optimal makespan in 13,3 % of the cases (2/15 problems: FJS1, FT06). For most of the remainder of the problems that were tested (6 cases), the results generated by TS+GRASP reached nearer to the optimal solutions than the SA+GRASP (4 cases).

Overall, TS+GRASP produced insignificantly better optimality solutions compared to SA+GRASP algorithm (and significantly better than GRASP). The robustness of the results produced by the three algorithms was estimated by the number of times the best solution was reached out of the total 20 times that each problem was run by each algorithm (for given level value ε).

For ε=1% TS+GRASP and SA+GRASP algorithm had a higher or equal degree of robustness as compared to the GRASP in all problems as is observed with fig. 1 TS+GRASP had a higher degree of robustness as compared to the SA+GRASP in problems FT20, LA01, LA16, TA01, TA31, TA51, TA61, and an equal degree in problems FJS1, LA06 and LA11. SA+GRASP had a higher degree of robustness as compared to the three algorithms in problems FT06 and FT10. For ε=2% (fig. 2) TS+GRASP had a higher degree of robustness as compared to the SA+GRASP in problems FT06, FT20, LA01, LA16, TA01, TA31, TA51, TA61, and an equal degree

in problems LA06 and LA11. GRASP had a higher degree of robustness as compared to the three algorithms in problems LA16, LA21 and TA71, and an equal degree in problem FJS1.

For ε=3% (fig. 3) TS+GRASP had a higher degree of robustness as compared to the SA+GRASP in problems FT06, FT10, LA01, LA01, LA16, TA01, and an equal degree in problems FT20, LA06, TA31 and TA51. All three algorithms have an equal degree of robustness in problems FJS1, LA11, TA61 and TA71. GRASP had a higher degree of robustness as compared to the SA+GRASP in problems LA16 and LA21. For ε=5% (fig. 4) TS+GRASP had an equal degree of robustness as compared to the SA+GRASP in almost all problems (without problem LA21). Another measure of comparison was looking at the interaction between the degree of optimality of the solution and the robustness. Fig. 5, fig. 6, fig. 7 and fig. 8 depict this relationship for three metaheuristics respectively (for ε=1%).

5 Conclusion

The 15 problems tested covered a wide variety of job scheduling problems in terms of the size and difficulty of the problems. Metaheuristics constructed for generate of schedules in FJSP (problems FJS1 and FJS2) too. Relation between robustness and optimality of the GRASP, SA+GRASP and TS+GRASP solutions have been evaluated. In almost all non-optimal solutions, TS+GRASP got closer to optimal solution than the SA+GRASP did.

TS+GRASP had a higher degree of robustness as compared to the SA+GRASP in most JSP problems. SA+GRASP had a higher degree of robustness as compared to the TS+GRASP in FJSP problem (parallel route). The robustness of the algorithm increased as the best solutions produced by the algorithm were closer to the know optimal. As a future, it will be interesting to compare the proposed approach to others methods (e.g. SA/TS) and to study it on large set of benchmark and real problems.

References

1. Atallah, M.J.: Algorithms and theory of computation handbook. CRC Press, Corporate Blvd, Boca Raton (2000)
2. Hall, N.G., Posner, M.E.: Sensitivity analysis for scheduling problems. Journal Scheduling 7 (2004)
3. Kolen, A.W.J., Rinnooy Kan, A.H.G., Van Hoesel, C.P.M., Wagelmans, A.P.M.: Sensitivity analysis of list scheduling heuristics. Discrete Appl. Math. 55 (1994)
4. Gonzalez, T.F.: Handbook of algorithms and metaheuristics. Chapman & Hall/CRC, Boca Raton (2007)
5. Bondal, A.A.: Artificial immune systems applied to job shop scheduling. The Russ College of Engineering and Technology of Ohio University (2008)
6. Kacem, I., Hammadi, S., Borne, P.: Approach by localization and multiobjective evolutionary optimization for flexible job-shop scheduling problems. IEEE Transactions on Systems, Man and Cybernetics 32, 1–13 (2002)

7. Montgomery, D.C.: Design and analysis of experiments. Wiley, Chichester (2009)
8. Octavia, T., Sahputra, I.H.: Robust-Hybrid Denetic Algorithm for a Flow-Shop Scheduling Problem (A Case Study at PT FSCM Manufacturing Indonesia). Jurnal Teknik Industri 9, 144–151 (2007)
9. Talabi, E.C.: Metaheuristics. From Design to Implementation. Wiley, Chichester (2009)
10. Burke, E.K., Kendall, G.: Search methodologies. In: Introductory Tutorials in Optimization and Decision Support Techniques. Springer, Heidelberg (2005)
11. Witkowski, T., Antczak, P., Antczak, A.: Tabu search and GRASP used in hybrid procedure for optimize flexible job shop problem. In: Liu, Y., Chen, G., Ying, M. (eds.) 11th Internat. Fuzzy Systems Association - World Congress, Soft Computing and Computational Intelligence, Beijing, vol. 3, pp. 1620–1625. Tsinghua University Press/Springer (2005)
12. Witkowski, T., Antczak, P., Antczak, A.: The application of simulated annealing procedure for the flexible job shop scheduling problem. In: Proceedings 11th International Conference-Information Processing and Management of Uncertainty in Knowlegde Based Systems - Industrial Track, pp. 21–26 (2006)

Hardware Emulation of Bacterial Quorum Sensing

Fredy H. Martínez[1] and Jesús Alberto Delgado[2]

[1] Distrital University "Francisco José de Caldas", Bogotá D.C, Colombia
fhmartinezs@udistrital.edu.co
[2] National University of Colombia, Bogotá D.C., Colombia
jadelgador@unal.edu.co

Abstract. A digital architecture for the emulation of dynamic bacterial quorum sensing is presented. The architecture is completely scalable, with all parameters stored in artificial bacteria. It shows that self-organizing principles can be emulated in an electronic circuit, to build a parallel system capable of processing information, similar to cell-based structure of biological creatures. A mathematical model of artificial bacteria and their behavior reflecting the self-organization of the system are presented. The bacteria implemented on an 8-bit microcontroller; and a framework with CPLDs to build the hardware platform where the bacterial population increases are shown. Finally, simulation results show the ability of the system to keep working after physical damage, just as its biological counterpart.

1 Introduction

The theory of self-organization is based on the assumption that the system functionality is not a result of the individual performance of its elements; but rather a result of the interaction between the elements, i.e., a result of self-organization.

Studying the characteristics of self-organizing dynamic systems [1], it is possible to identify three key aspects of a self-organized system [2]: (1) The existence in the system of a lot of units (agents) [3] that interact among themselves, so that the system passes from a less organized state to a more organized state dynamically, along time, and maintains some kind of exchange. (2) The organization is evident in the global system behavior as a result of the interaction of agents [4], its functioning is not imposed on the system by any kind of external influence, and (3) the agents, all of them with identical characteristics, have only local information [5,2], which implies that the process of self-organization involves some transfer of local information.

Self-organization has been a subject of great theoretical research, but its practical applications have been somewhat neglected [1]. Mange et al. [6,7] have worked long applications of FPGAs in bio-inspired hardware, the most important process that they involve is the cellular construction, therefore, their artificial hardware implements cellular processes of replication and regeneration.

D.-S. Huang et al. (Eds.): ICIC 2010, LNCS 6215, pp. 329–336, 2010.

This research aims at providing a new approach into the application of self-organization principles to one aspect of electronic systems, digital processing. Our approach has been to devise reconfigurable logic hardware and an architecture that permits self-organizing processes; and then to begin methodically to develop self-organization concepts and their translation into practice within this framework.

Specifically, in this paper the hardware emulation of bacterial quorum sensing is presented. A system composed of a set of simple processing units, all identical in structure and programming, which collectively self-organize and perform a complex task, with the broader aim of addressing engineering applications.

This paper is organized as follows: in Section II, a brief general introduction on the theory of system structure is presented, followed by the description of the design used in these experiments. Section III, show how to model mathematically the behavior of a unit, which ultimately leads to self-organize the system. Section IV presents a series of circuit simulation results, that allow to analyze the behavior of the system. Finally, in Section V conclusions are presented.

2 System Structure

Approaches to self-organization can be grouped into at least two main categories: a statistical approach and an engineered approach [1]. Statistical approaches seek to manage complexity by discovering algorithms or techniques. Such approaches are not necessarily concerned with how the given task is accomplished, but with how well it is actually accomplished. Examples of statistical approaches include phylogenetic (genetic algorithms and systems based on theories of evolution [8,9]), epigenetic (neural networks and models of immune and endocrine systems [10,11]) and ontogenetic models (cell development, ontogenesis [12]).

In contrast to statistical approaches, engineered approaches seek to achieve, more deliberately, some set of goals by following a predefined algorithm. Surprisingly, several engineered approaches also draw inspiration from biology, including the electronic embryology (embryonics) [13,14]. The discussion in this paper falls into the domain of the engineered approach, taking as a design idea ontogenetic principles of living beings.

At the cellular level, the higher animals have an extraordinary redundancy and complex patterns of organization and operation that have been filtered as optimum throughout the evolution of a good number of generations. Other simpler cellular structures such as bacteria, with similar schemes have made the survival of thousands of communities, proving its robustness. The purpose of this research is to propose a new system of electronic hardware design that exhibits these same properties of cell development.

Particularly there is a control mechanism of gene expression dependent on cell density, observed in biology in the area of antibiotics [15]. This phenomenon is responsible for a set of independent cells, under the generation of extra-cellular signals, producing coordinated social behaviors. The pathogenic bacteria that

carry higher living organisms are not virulent until they reach a sufficient majority to enforce a massive attack against the immune system. When bacteria determine that their rates are sufficient to trigger an attack, they transform and become virulent. This phenomenon is called quorum sensing.

The search for a robust system that emulates the behavior of a community of bacteria for information processing, led to the development of a specific reconfigurable platform called Bacterial Platform (BP). The BP, inspired by the Cell Matrix architecture [16], is a regularly tiled collection of simple processing units called Bacterium. This platform is mainly an internally configured device, the configuration of each bacterium is written and read by the bacterium connected to it, i.e., its immediate adjacent neighbors, without the need for an external system (e.g., a PC). Only bacteria located on the perimeter of the platform can be accessible from other systems (communication with the platform). As cellular automata, the BP is a dynamic system that evolves in discrete steps according to local interaction, but unlike them, every BP cell is part of a more complex system.

In this first prototype, bacteria are arranged in a fixed, identical topology throughout the matrix, in a two-dimensional plane (Fig. 1). Each bacterium receives a dedicated input (called chemical signal input, CSI) from each of its neighbors, and generates a dedicated output (chemical signal output, CSO) to each of those neighbors. In this topology, each bacterium has four immediate neighbors, and there is no physical displacement.

Each bacterium contains a small 8-bit microcontroller (Fig. 2) that stores the genetic code of the bacterium, and reacts according to environmental conditions (communication with its neighbors). This interaction allows the execution of two basic functions:

– Reproduction: Scheme by which an artificial bacterium reproduces in the system. It is basically a process of cell division, where the growth limit is defined by the amount of resources needed to implement the operation of the system.

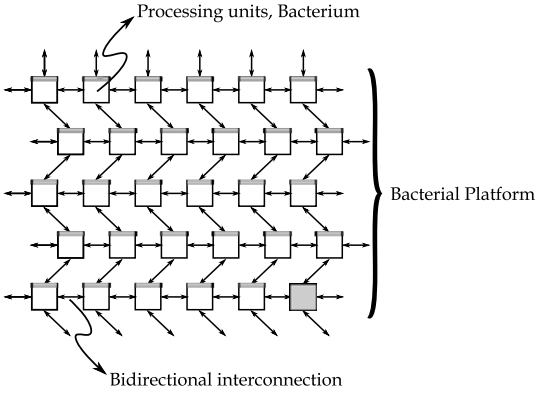

Fig. 1. Details of the two-dimensional structure of the BP

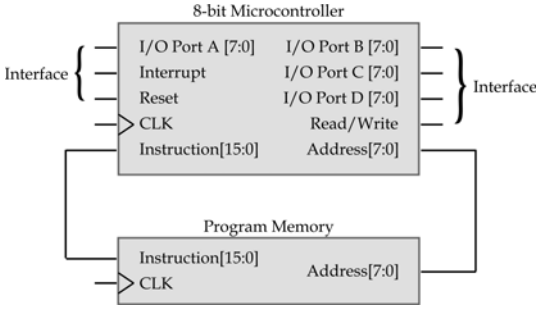

Fig. 2. Microcontroller block diagram

– Cell differentiation: Each artificial bacterium in the system has an identical copy of the genome. However, depending on population density and its physical position, each bacterium interprets it in a particular way.

The act of loading the genome (program the microcontroller with the information about its functionality) from one bacterium to another neighbor, is called reproduction. Similarly, the act of loading the genome in a number of bacteria is called population growth. The system architecture is infinitely scalable; there is no architectural impediment to scale a system to any desired size.

3 Algorithm Operation

This section presents the basic definitions from which it is mathematically possible to determine the structure of the system. Subsequently, the rules for self-organization of the bacteria are defined.

Definition 1. *A bacterium is a pair*

$$V = (f, P) \tag{1}$$

where f is a nonnegative integer ($f \in \mathbb{Z}$) that indicates the amount of neighboring bacteria in direct contact, and P is a point in q*-dimensional space ($P \in \mathbb{R}^q$). For the particular case of the hardware prototype developed in this research (Fig. 1), f takes values 0, 1, 2, 3 and 4 for each bacteria over time (the value changes when reproducing the bacterial population), and P is a point in two-dimensional plane $\big(q = 2, \Rightarrow P \in \mathbb{R}^2 \Rightarrow P = (p_1, p_2)\big)$.*

The bacterial recognition occurs in a bacterium V_i when the bacterium defines its values f and P. This definition corresponds to an extension of the cell definition in the antibody-antigen recognition mathematical model built by Tarakanov [17].

Definition 2. *The population density is evaluated using the distance between bacteria. Let:*

$$d_{ij} = d\left(V_i, V_j\right) \tag{2}$$

as the distance between bacteria V_i and V_j. which is calculated by any appropriate norm.

Definition 3. *A bacterial population is defined as a nonempty set of bacteria.*

$$W_0 = \{V_1, V_2, V_3, \cdots, V_m\} \tag{3}$$

with non-zero distance between bacteria:

$$d_{ij} \neq 0, \qquad \forall i, j \quad , \quad i \neq j \tag{4}$$

The bacteria that implement the final application (signal processing) are called Application Bacteria, AB, and are a subset of the bacterial population (Fig. 3).

$$W \subseteq W_0 \tag{5}$$

Definition 4. *The neighborhood threshold ρ, indicates the maximum amount of direct neighboring bacteria that a cell can have. For the prototype hardware (Fig. 1), $\rho = 4$ for all bacteria.*

The density threshold h, indicates the minimum distance between bacteria needed to define the bacterial population in order to implement the final application.

The behavior of bacteria (self-organization) is coordinated by the following rules (the model does not include cell death; if there is cell death, it is caused by an external action):

Reproduction Rule: If the bacterium $V_i \in W_0 \setminus W$ can reproduce, ie:

$$f_i < \rho \quad \text{and} \quad d_{ij} < h, \qquad \forall V_j \in W \tag{6}$$

then V_i must reproduce by duplicating their DNA (code) in the available medium.

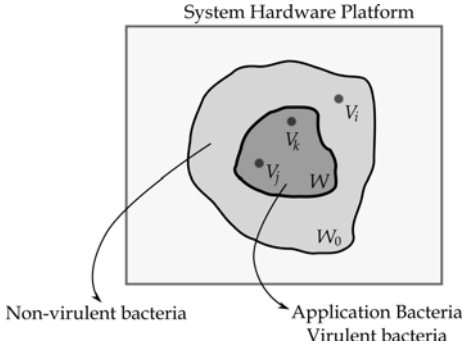

Fig. 3. Bacterial population and application bacteria in the proposed system

Virulence, Activation or Cell Differentiation Rule: If the bacterium $V_k \in W$ is the nearest to the bacterium $V_i \in W_0 \setminus W$ among all AB, ie (Fig. 3):

$$d_{ik} < d_{ij}, \qquad \forall V_j \in W,\ k \neq j \quad \text{and} \quad d_{kj} < h, \qquad \forall V_j \in W,\ k \neq j \tag{7}$$

then V_i must be added to AB (the bacterium becomes virulent).

4 Simulation and Results

The system's hardware platform was constructed by assembling 12 identical blocks (Fig. 4) each with total three Xilinx CoolRunner™-II CPLD (XC2C256). Each CPLD has the ability to communicate with its four neighbors (Fig. 1).

Each CPLD is programmed with a PicoBlaze soft processor of 8-bit RISC architecture. Initially, these processors do not have program code (empty CPLD), and therefore they are not considered part of the system. When the artificial bacterium program is loaded within the CPLD processor, it is said that the environment is contaminated and has a new bacterium, which can be virulent or not depending on bacterial density.

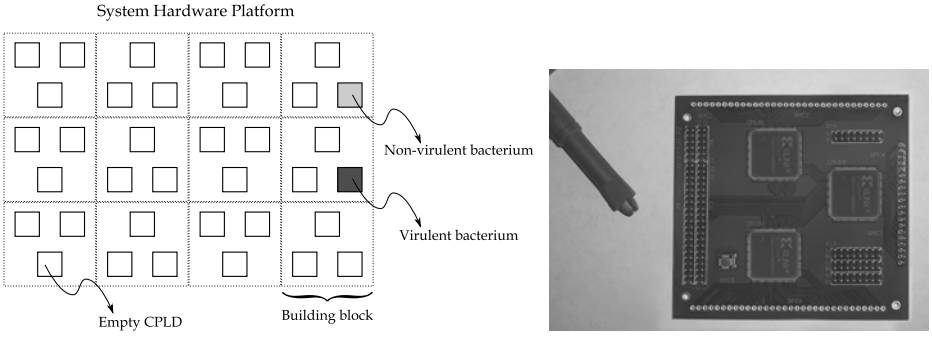

Fig. 4. (a) System hardware platform, (b) Building block system with three processors

In order to analyze the behavior of bacterial algorithm on the platform, a simulation of bacterial growth based on the rules of reproduction and cell differentiation was done. An array that can change the status of each unit in each bacterial operation cycle (one complete cycle of the bacterium program) was designed.

Fig. 5 shows the growth of the bacterial population after an initial infection (Fig. 5(b)). Fig. 5(e) shows the appearance of the first virulent bacterium. In this simulation, a density threshold of five ($h = 5$) was used; it is for this reason that in Fig. 5(i) population growth ended.

In order to evaluate the robustness and reliability of the system, one of the blocks was eliminated (lower right block) simulating the sudden death of three bacteria, and the response of the system was observed. Fig. 6 shows a

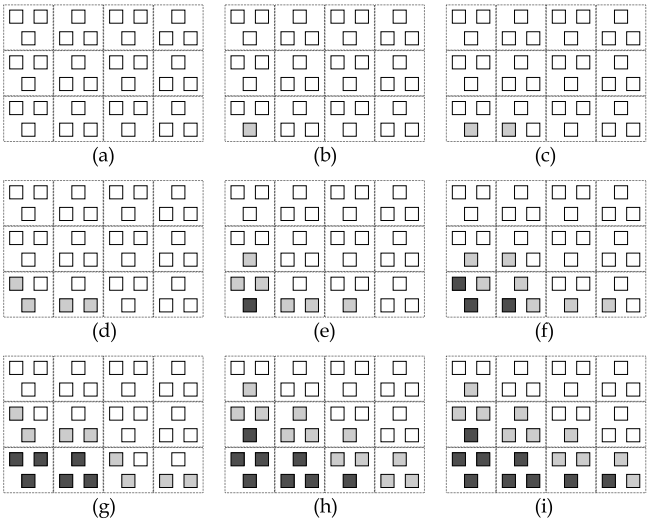

Fig. 5. Bacterial growth on the platform

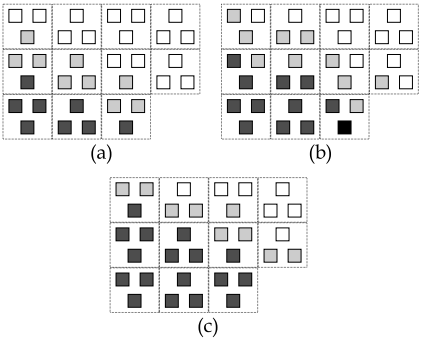

Fig. 6. Bacterial growth on the platform after some bacteria die

new behavior where bacterial growth begins again, and again it meets the threshold density after two bacterium cycles.

5 Conclusions

The circuit design and architecture for an emulator as an example of biology-oriented quorum sensing in bacterial population has been presented. The results of the system simulation help to understand the behavior of bacterial communities, and in particular they show that in the self-organization configuration investigated, the system's overall behavior is robust and scalable like the biological model.

References

1. Prokopenko, M.: Advances in Applied Self-organizing Systems. Advanced Information and Knowledge Processing. Springer, Heidelberg (2008)
2. Polani, D.: Measuring self-organization via observers. In: Banzhaf, W., Ziegler, J., Christaller, T., Dittrich, P., Kim, J.T. (eds.) ECAL 2003. LNCS (LNAI), vol. 2801, pp. 667–675. Springer, Heidelberg (2003)
3. Russell, S., Norvig, P.: Artificial Intelligence: A Modern Approach, 2nd edn. Pearson - Prentice Hall (2002)
4. Camazine, S., Deneubourg, J., Franks, N., Sneyd, J., Theraulaz, G., Bonabeau, E.: Self-Organization in Biological Systems. Princeton University Press, Princeton (2001)
5. Santini, C., Tyrrell, A.: Investigating the Properties of Self-Organization and Synchronization in Electronic Systems. IEEE Trans. on Pub. 8, 237–251 (2009)
6. Mange, D., Goeke, M., Madon, D., Stauer, A., Tempesti, G., Durand, S.: Embryonics: A New Family of Coarse-Grained Field Programmable Gate Array with Self-Repair and Self-Reproducing Properties. In: Sanchez, E., Tomassini, M. (eds.) Towards Evolvable Hardware 1995. LNCS, vol. 1062, pp. 197–220. Springer, Heidelberg (1996)
7. Freitas, R., Gilbreath, W.: Replicating Systems Concepts: Self-Replicating Lunar Factory and Demostration. In: Advanced Automation for Space Missions, 1980 NASA/ASEE Summer Study, Washington D.C (1980)
8. Greenwood, G., Tyrrell, A.: Introduction to Evolvable Hardware: A Practical Guide for Designing Self-Adaptive Systems. IEEE Press Series on C. I. Wiley, Chichester (2007)
9. Koza, J., Keane, M., Streeter, M.: The Importance of Reuse and Development in Evolvable Hardware. In: Conference NASA of Evolution Hardware, pp. 33–42 (2003)
10. Arbib, M.A.: The Handbook of Brain Theory and Neural Networks, 2nd edn. MIT Press, Cambridge (2003)
11. Wai-Yin, L.: Computer Immunology, Tesis Department of information Technology and Electrical Engineering, University of Queensland, NewYork (2002)
12. Sipper, M., Mange, D., Stauer, A.: Ontogenetic Hardware. BioSystems 44(3), 193–207 (1997)
13. Ortega-Sanchez, C., Mange, D., Smith, S., Tyrrell, A.: Embryonics: A bio-inspired cellular architecture with fault-tolerant properties. In: Genetic Programming and Evolvable Machines, pp. 187–215 (2000)
14. Prodan, L., Tempesti, G., Mange, D., Stauffer, A.: Embryonics: Electronic stem cells. In: 8th International Conference on Artificial Life, pp. 101–105. MIT Press, Cambridge (2003)
15. Otero, A.M., Muñoz, A., Bernández, M.I., Fábregas, J.: Quorum Sensing el lenguaje de las bacterias, 1st edn., Acribia, Spain (2005)
16. Macias, N.J., Durbeck, L.J.K.: A Hardware Implementation of the Cell Matrix Self-configurable Architecture: the Cell Matrix MOD 88™. In: Evolvable Hardware NASA/DoD 2005, pp. 103–106 (2005)
17. Tarakanov, A.O., Dasgupata, D.: A formal model of artificial immune system. Biosystems 55(3), 151–158 (2000)

Finding Research Community in Collaboration Network with Expertise Profiling

Hao Wu[1], Jun He[2], Yijian Pei[1], and Xin Long[1]

[1] School of Information Science and Engineering, Yunnan University,
No.2, North Green Lake Road, Kunming, P.R. China, 650091
{haowu,pei3p}@ynu.edu.cn, xinlong@126.com
[2] School of Electronic and Information Engineering,
Nanjing University of Information Science and Technology, Nanjing, P.R. China, 210044
hejun.zz@gmail.com

Abstract. As a new task of expertise retrieval, finding research communities for scientific guidance and research cooperation has become more and more important. However, the existing community discovery algorithms only consider graph structure, without considering the context, such as knowledge characteristics. Therefore, detecting research community cannot be simply addressed by direct application of existing methods. In this paper, we propose a hierarchical discovery strategy which rapidly locates the core of the research community, and then incrementally extends the community. Especially, as expanding local community, it selects a node considering both its connection strength and expertise divergence to the candidate community, to prevent intellectually irrelevant nodes to spill-in to the current community. The experiments on ACL Anthology Network show our method is effective.

1 Introduction

As a new task of expertise retrieval [1], finding research communities for scientific guidance and research cooperation has become more and more important. Unlike other complex networks, such as genetic networks and biological networks, the collaboration network character with more obvious hierarchy feature [2]. Collaboration networks usually consist of the communities with clearly different sizes or scales. Within the research community, the core usually contains a few individuals, and most of individuals make up the subsidiary. For example, the central professors or scholars of the research community are smaller, while the majority is students or ordinary researchers. More importantly, the research community is with a strong characteristic of expertise cohesion, that is of interests or expertise in the research community usually concentrate in a few directions. However, the existing community discovery algorithms only consider graph structure [3], without taking into account the context, such as knowledge characteristics. Therefore, the detection of research community cannot be simply addressed by direct application of existing methods. Instead, we propose a hierarchical discovery strategy which rapidly locates the core of the research community, and then incrementally extends the community. Especially, as expanding local community, it selects a node considering both its connection strength

D.-S. Huang et al. (Eds.): ICIC 2010, LNCS 6215, pp. 337–344, 2010.

and expertise divergence to the candidate community, to prevent intellectually irrelevant nodes to spill-in to the current community.

The rest of paper is structured as follows. Section 2 presents how to make expertise profiling based on latent topic model. Next, how to detect seed set and locally extend community with considering expertise divergence are explained. We also introduce what the incremental policy is. Then, experiments on ACL Anthology Network are carried out to watch the effect of our method. Finally, we review the state-of-art of research community detection and give some conclusion.

2 Topic Model Based Expertise Profiling

Topic models extract a set of latent topics from a corpus and as a result represent documents in a new latent semantic space. One of the well-known topic models is the Latent Dirichlet Allocation (LDA) model [4]. The basic idea of LDA is that documents are represented as random mixtures over latent topics, where each topic is characterized by a distribution over words. Suppose the expertise of a member r in a research community can be inferred by the topics of the paper collection $\mathcal{D}_r = \{d_0, \ldots d_i, \ldots d_n\}$ authored by him or her. Then, by using LDA, we get the likelihood $P(z_j|d_i)$ of topic z_j to d_i for each paper in $\mathcal{D}_r$, we can estimate the likelihood $P(z_j|r)$ of topic z_j to r as Eq.**1**, where |Dr| is the total number of papers. Let $Z = \{z_i | i = 1, \ldots, n\}$ be the expertise areas for whole collection, $EX(e,z_i)$ be the knowledge level of r on expertise area z_i, we define the expertise profile of a researcher as $profile(r) = < EX(e, z_1), \ldots, EX(e, z_i), \ldots, EX(e, z_n) >$.

$$P(z_j \mid r) = \frac{1}{|D_r|} \sum_{d_i \in D_r} P(z_j \mid d_i) \tag{1}$$

3 Finding Research Communities in Collaboration Network

3.1 Community Seed Set Detection

The community seed set detection is based on *(μ,ε)-cores* introduced in [5]. For a graph G = (V, E), the definition of *(μ,ε)-cores* is based on *structural similarity* and *ε-neighborhood*. The structural similarity between two nodes v and w is defined as $\sigma(v,w) = |\Gamma(v) \cap \Gamma(w)| / \sqrt{\Gamma(v) \cdot \Gamma(w)}$, where $\Gamma(v) = \{w \in V \mid (v,w) \in E\} \cup \{v\}$. *ε-neighborhood* ($\varepsilon \in [0,1]$) is the subset of a node's structure containing only those nodes that are at least ε-similar with the node; in math symbol: $N_\varepsilon(v) = \{w \in \Gamma(v) \mid \sigma(v,w) \geq \varepsilon\}$. Then a vertex v is called a (μ,ε)-core if its ε-neighborhood contains at least μ vertices; formally: $CORE_{\mu,\varepsilon}(v) \leftrightarrow N_\varepsilon(v) \geq \mu$. A node is directly structure reachable from a (μ,ε) core if it is at least ε-similar to it: $DirReach_{\mu,\varepsilon}(v,w) \leftrightarrow CORE_{\mu,\varepsilon}(v) \wedge w \in N_\varepsilon(v)$. Once the (μ,ε) -cores of a network have been identified, it is possible to start attaching adjacent nodes to them if they are reachable through a chain of nodes which are direct reachable from each other. We call the resulting set of nodes as a community seed set.

One issue that is not addressed concerns to selecting boundaries μ and ε. Higher values for (μ,ε) will result in fewer detected cores. Here, we propose an incremental strategy. First, given a ε-*boundary* value ε_B, splitting the range of ε into two sections, namely $[0, \varepsilon_B]$ and $[\varepsilon_B, 1]$. Second, deciding μ-*boundary* value as $\mu_B = avg\{N_{\varepsilon_B}\}$, namely, the average size of the ε_B-*neighborhood* collection. Finally, in each iteration of incremental community detection, using two sections $[1, \mu_B]$ and $[\mu_B, max(N_{\varepsilon_B})]$ to detect seed sets in unallocated node collection. In this way, it can avoid depending parameter initialization and achieve the ability to cover the global network so all potential communities can be detected.

Each time, after detecting the seed sets, there are usually some overlapping subsets. We can simply merge them by estimating their overlaps. The overlap metric between two subset s_1 and s_2 is Jaccard index: $|s_1 \cap s_2| / |s_1 \cup s_2|$. Specially, we fix the overlap 1.0 as $|s_1 \cap s_2| = min(|s_1|, |s_2|)$, because that s_1 is subset of s_2, or s_2 is subset of s_1 under this condition. The amalgamation also uses a recursive strategy, and the process stops as soon as it does not make a new subset.

3.2 Community Expansion

After the merging the seed set collection, we also use a recursive strategy for the gradual expansion of community, until the community structures stabilize. The detail shows as *Algorithm 1*. Here, the vertex set are splitted into two subsets, allocated node set: $in \leftrightarrow \{v \in CORE_{\mu,\varepsilon} \wedge v \in V\}$ and unassigned node set: $out \leftrightarrow \{v \notin in \wedge v \in V\}$.

For each recursion, the first step is to test whether the *coverage* (It means the rate of assigned nodes to the whole vertex set, *namely* $|in|/|V|$) is satisfied or not. If it is satisfied, the recursion ends. Otherwise, for each unassigned node $v \in out$, an optimal community which can maximize connections strength and minimize expertise divergence to the node is selected to join in. Link Strength (*LS*) is calculated using

Algorithm 1: RecursiveExpandCommunity

Require: Network $G = \{V, E\}$, Collection of seed set $\Omega = \{s \leftrightarrow DirReach_{\mu,\varepsilon}\}$;

1: **if** $Coverage \geq threshold$ **then return**;
2: **else** $\forall s \in \Omega$ update expertise profiling by Eq.4;
3: **for each** $v \in out$ **do**
4: **for each** $s \in \Omega$ **do**
5: Calculate $LS(v, s)$ by Eq.2; Calculate $KL(v, s)$ by Eq.3;
6: **end for**
7: Select s which results in maximum $LS(v, s) / KL(v, s)$;
8: Add v to s and in; Remove v from out;
9: **end for**
10: **if** $newCoverage - Coverage \leq DIFF$ **then return**;
11: **end if**
12: Invoke *RecursiveExpandCommunity*;

Eq.2, where $L_{v,w} = 1$ if $(v, w) \in E$, otherwise $L_{v,w} = 0$. $| s |$ is the size of the seed set s, and used to normalize connection strength value.

$$LS(v, s) = \sum_{w \in s} L_{v,w} / | s | \tag{2}$$

To detect the divergence of the expertise distribution between the node *v* and the seed set *s*, we use the Kullback-Leibler divergence (*KL*) as Eq.3 which is a non-symmetric measure for the difference between two likelihood distributions.

$$KL(profile(v) \| profile(s)) = \sum_{j} EX(v, z_j) \cdot \log(EX(v, z_j) / EX(s, z_j)) \tag{3}$$

Moreover, the extended seed sets need to update their expertise profiles at each recursion, this can be done by using following formula:

$$EX(s, z_j) = \frac{\sum_{w \in s} EX(w, z_j)}{\sum_{z_j \in Z} \sum_{w \in s} EX(w, z_j)} \tag{4}$$

Generally, we need to set the expanding level to control community scale. However, according to the well-known small-world principle, any two nodes inside a collaboration network can typically find out contact by no more than six hops. Therefore, it will not exceed six steps to expand the seed set. The behind experimental results can support this observation.

3.3 Incremental Community Detection

It is not able to detect all potential communities using only one combination of μ and ε. However, selecting high (μ,ε) are usually able to produce large-scale communities, because a strong connected seed set implies the corresponding community contains long chains. For detecting potential small-scale communities, we need adjust the value pair of (μ,ε). Based on the above-mentioned method to select boundaries μ and ε, we design an incremental algorithm 2 for community detection. When the incremental processing finally finishes, the unallocated node set will be a default community.

Algorithm 2: IncrementalDetection (STEP)

Require: Network $G = \{V, E\}$, $out = V$, $in = \{\}$;

1: **for each** $\forall v, w \in out$ **do** Calculate $\sigma(v, w)$;
2: **end for**
3: Get ε_B and μ_B for current unallocated node set;
4: Get and Merge the collection of seed set Ω by $[\varepsilon_B, 1]$ and $[\mu_B, max(N_{\varepsilon_B})]$;
5: Do *RecursiveExpandCommunity;*
6: Get and Merge the collection of seed set Ω by $[\varepsilon_B, 1]$ and $[1, \mu_B]$;
7: Do *RecursiveExpandCommunity;*
8: **if** $Coverage \geq threshold$ **then return**;
9: Invoke *IncrementalDetection(STEP--);*

In fact, coverage threshold is not easy to settle, it depends on the graph connectivity. However, because of the high efficiency of our algorithm, we can adjust the incremental step to make the coverage reach a satisfactory goal. In addition, it can also manually set μ and ε to get more flexible results.

4 Experiments on ACL Anthology Network

4.1 Data Preparation

For experiments, we select a reference corpus-the ACL Anthology Reference Corpus (ACL ARC) which is a digital archive of conference and journal papers in natural language processing and computational linguistics. The ACL ARC is refined as a standard test bed for experiments in both Bibliographic and Bibliometric research. It also has a parallel initiative, named ACL Anthology Network (AAN) [6], to build the matching citation networks. The AAN (2008 version) contains about 14245 papers with extracted metadata, and 54538 internal citations.

In general, clustering is time-consuming work; the topic model is no exception. To improve the efficiency of the LDA estimate, we first use feature selection technique based on TF-IDF to reduce the literature content. Here, the Lucene toolkit and the Porter-Stemming algorithm are exploited to tokenize the literatures. In each article, if the TF-IDF value of a word is greater than the threshold value of 0.03, and its etyma length is less than 12, the word keeps to form a new word-vector for the article expression. Then, we get a new corpus consists of 13966 word-vectors, the average vector length becomes 340, instead of the original length near 3000. Here, to obtain a stable theme set for our experiment, rather than setting random topical number, we use the Perplexity [4] to find a desirable number of topics where the perplexity curve starts stabilized. By this, we get the desirable K=65.

4.2 Finding Research Communities

We complete our algorithm in Java and run experiments on a computer equipped with Intel T7200 CPU and 2GB memory. The collaboration network of AAN contains 11124 authors. It takes about 4.5 seconds to load graph data and the likelihood distribution data produced by LDA, and about 13.6 seconds to find research community. The ε-*boundary* and μ-*boundary* are decided by default setting. The threshold to merge communities is 0.4. The properties of community with different boundaries are shown as Table 1. *No.* means the number of detected community in each step. *Avg. Size* means the average size of the community. For the algorithm *RecursiveExpandCommunity* and *IncrementalDetection,* we set the convergence threshold *DIFF* as 0.0001 to control recursive steps. As mentioned above, the step to expand the seed core is no more than six. The experiment result confirms this conclusion. As shown in Fig.1, when setting different ranges for ε and μ, expanding community always converges within 3-5 steps. Finally, *IncrementalDetection* takes four steps to reach convergence; the final coverage is 93.39%.

Table 1. The properties of detected community with different parameters

Parameters		Community		
ε	μ	*No.*	*Avg. Size*	*Coverage (%)*
[0.615,1.0]	[3, 24]	960	10.46	81.74
[0.615,1.0]	[1, 3]	545	2.37	11.36
[0.187,0.615]	[2, 20]	15	4.67	0.18
[0.187,0.615]	[1, 2]	28	3.43	0.11

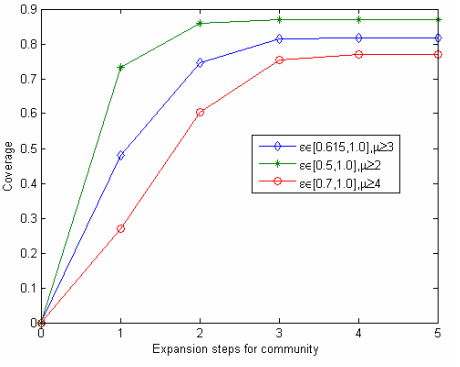

Fig. 1. The convergence of incremental community detection

For now, there is no uniform standard to assess the performance of the community mining. But within a series of studies in the local community, the commonly used method is *local modularity* [7]. We use *outwardness*, a variant measure of the local modularity, to compare two policies when extending the local community: LS (using only connection strength) and LS+KL (with expertise profiling). Let us define the "*outwardness$_v$(s)*" of node $v \in s$ from community s : $1/k_v \sum_{i \in n(v)} ([i \notin s] - [i \in s])$, where *n(v)* are the neighbors of *v*. The *outwardness$_v$(s)* has a minimum value of *-1* if all neighbors of *v* are inside *s*, and a maximum value of *1-2/|k$_i$|*, since any *v* must have at least one neighbor in *s*. Further, let us define the "*expertise cohesion(EC)*" of a community *s* as Eq.5, where *SKL(v,w)* is the Symmetric Kullback-Leibler divergence of expertise distribution between node *v* and node *w*, formally: *SKL(v,w)=KL(v||w)+ KL(w||v)*. The value of *SKL(v,w)* is non-negative.

$$EC(s) = (2/|s||s-1|)\sum_{v,w \in s} SKL(v,w) \tag{5}$$

We choose different boundaries to compare likenesses and differences between *outwardness* and *EC*. The results show in Table 2. Using expertise profiling does not reduce local modularity, and will increase the expertise cohesion of the community. We also note the expertise cohesion does not significantly increase; it is because the candidate community choosed by the LS and the LS + KL are the same in the vast majority of cases. Occasionally, a node connecting to multiple communities becomes a bridge between communities. (This is consistent with the nature of research

Table 2. The effect comparison of expanding community with LS and LS+KL strategy

Parameters		LS		LS+KL	
ε	μ	*outwardness*	*EC*	*outwardness*	*EC*
[0.615,1.0]	[3, 24]	-0.62	2.71	-0.62	2.62
[0.6,1.0]	[6, 24]	-0.70	3.74	-0.69	3.68
[0.7,1.0]	[7, 24]	-0.74	4.29	-0.74	4.24
[0.4,1.0]	[2, 24]	-0.51	2.55	-0.51	2.55

community). At this point, LS+KL strategy chooses a community candidate whose interests are closest to current node to join. Table 2 lists four grouped conditions. In each case, the different choices with LS and LS+KL are more than 200 times.

5 Related Discussion and Conclusion

Considering community detection, the most influential work perhaps is the method by Girvan and Newman [9]. By using betweenness centrality, network edges are removed resulting in the progressive fragmentation of the network. Later, they introduced the notion of modularity as a measure of the profoundness of community structure in a network. This triggered a series of models that attempted to detect community structure in a network with maximizing modularity, such as hierarchical clustering [10], simulated annealing [11], extremal optimization [12] and spectral optimization [13]. However, modularity maximization methods result in that community of small scales is likely to remain undetected. Then, methods integrating different notions of community-ness have been devised, such as SCAN algorithm [5]. However, all these algorithms consider graph structure of community, without considering its knowledge characteristics. In this paper, some policies are put forward to satisfy the special demands on research community discovery. By expertise modeling in mining community, considering the constraints on both connection strength and community expertise will find better knowledge coherent communities.

A set of methods of particular interest to our study are based on the notion of seed-based community expansion where the community detection is seen as an expansion process, which, starting from a seed node, progressively attracts adjacent nodes with the goal of maximizing some local community-ness measure, e.g. local modularity [14] or node outwardness [8]. However, when expanding community, we relax the constraint to maximize local community-ness measure, thus allow making communities on larger scales. Further, compared with the works specialized in mining research community, we propose seriously different algorithms. Zaïane et al. [15] used the random walk strategy, while we design the incremental expansion strategy. Different from topic identification presented in [16], we adopt the topic model to capture the semantics of theme more accurately.

In addition, our methods largely avoid depending on parameter initialization. The incremental detection strategy will improve the algorithmic scalability and the applicability of research community mining on large-scale networks. As the latent topic model is computation-intensive, we will consider the use of other text summary technologies (e.g., TF-IDF) to provide more efficient ways for modeling expertise.

Acknowledgments. This work is supported by the Scientific Research Funding of Department of Education of Yunnan Province under Grant No. 09Y0035.

References

1. Wu, H., Pei, Y.J., Yu, J.: Detecting academic experts by topic sensitive link analysis. Frontiers of Computer Science in China 3, 445–456 (2009)
2. Porter, M.A., Onnela, J.P., Mucha, P.J.: Communities in networks. Notices of the American Mathematical Society 56, 1082–1097, 1164–1166 (2009)
3. Fortunato, S.: Community Detection in Graphs. Physics Reports 486, 75–174 (2010)
4. Blei, D.M., Ng, A.Y., Jordan, M.I.: Latent dirichlet allocation. Journal of Machine Learning Research 3, 993–1022 (2004)
5. Xu, X., Feng, N.Y.Z., Schweiger, T.A.J.: Scan: A Structural Clustering Algorithm for Networks. In: Proceedings of KDD 2007, pp. 824–833. ACM Press, New York (2007)
6. Radev, D.R., Muthukrishnan, P., Qazvinian, V.: The ACL anthology network corpus. In: Proceedings of the 2009 Workshop on Text and Citation Analysis for Scholarly Digital Libraries, pp. 54–61. ACL, Suntec (2009)
7. Bagrow, J.P.: Evaluating local community methods in networks. Journal of Statistical Mechanics 7 (2008)
8. Fortunato, S., Barthelemy, M.: Resolution limit in community detection. Proceedings of the National Academy of Sciences 104, 36–41 (2007)
9. Girvan, M., Newman, M.E.J.: Community Structure in Social and Biological Networks. Proceedings of the National Academy of Sciences 99, 7821–7826 (2002)
10. Clauset, A., Newman, M.E.J., Moore, C.: Finding Community Structure in Very Large Networks. Physical Review E 70 066111 (2004)
11. Massen, P., Doye, J.P.K.: Identifying 'Communities' within energy landscapes. Physical Review E 71 046101 (2005)
12. Duch, J., Arenas, A.: Community detection in complex networks using extremal optimization. Physical Review E 72 027104 (2005)
13. Newman, M.E.J.: Finding community structure in networks using the eigenvectors of matrices. Physical Review E 74 036104 (2006)
14. Clauset, A.: Finding Local Community Structure in Networks. Physical Review E 72 027104 (2005)
15. Zaïane, O.R., Chen, J.Y., Goebel, R.: Mining research Communities in bibliographical data. In: Zhang, H., Spiliopoulou, M., Mobasher, B., Giles, C.L., McCallum, A., Nasraoui, O., Srivastava, J., Yen, J. (eds.) WebKDD 2007. LNCS, vol. 5439, pp. 59–76. Springer, Heidelberg (2009)
16. Ichise, R., Takeda, H., Muraki, T.: Research community mining with topic identification. In: Proceedings of the 10th International Conference on Information Visualisation, pp. 276–281. IEEE Computer Society Press, Los Alamitos (2006)

The Ideal Data Representation for Feature Extraction of Traditional Malay Musical Instrument Sounds Classification

Norhalina Senan[1], Rosziati Ibrahim[1], Nazri Mohd Nawi[1], Musa Mohd Mokji[2], and Tutut Herawan[3]

[1] FTMM, Universiti Tun Hussein Onn Malaysia, Malaysia
[2] FKE, Universiti Teknologi Malaysia, Malaysia
[3] PEND. MAT, Universitas Ahmad Dahlan, Yogyakarta, Indonesia
{halina,nazri,rosziati}@uthm.edu.my, musa@fke.utm.my, tutut81@uad.ac.id

Abstract. In presenting the appropriate data sets, various data representation and feature extraction methods have been discovered previously. However, almost all the existing methods are utilized based on the Western musical instruments. In this study, the data representation and feature extraction methods are applied towards Traditional Malay musical instruments sounds classification. The impact of five factors that might affecting the classification accuracy which are the audio length, segmented frame size, starting point, data distribution and data fraction (for training and testing) are investigated. The perception-based and MFCC features schemes with total of 37 features was used. While, Multi-Layered Perceptrons classifier is employed to evaluate the modified data sets in terms of the classification performance. The results show that the highest accuracy of 97.37% was obtained from the best data sets with the combination of full features.

Keywords: data representation; feature extraction; Traditional Malay musical instruments; Multi-Layered Perceptrons.

1 Introduction

An automatic feature extraction of musical instruments sounds has elevated many research interests [1–3]. These growing of interests are actuated from the increasing numbers of the collection of musical instruments sounds data and features schemes. The purpose of extraction is to obtain the relevant information from the input data to execute certain task. Consequently, the reliability of the input data has a significant role in extracting good features for the classifier to perform well. Without presenting a good input data and features schemes, the overall classification performance might be affected and cause to the failure of producing the desired output. Hence, these varying original input data need to be trimmed and analyzed systematically before the features can be extracted and evaluated.

Several approaches for data representation and feature extraction have been discovered [1,2]. Most of these studies are conducted based on the Western musical

D.-S. Huang et al. (Eds.): ICIC 2010, LNCS 6215, pp. 345–353, 2010.

instrument sounds. To date, a study on non-Western musical instruments is inadequate and still needs an intensive research. However, adapting the existing approaches for different musical instruments sounds domain might not be as that simple. The reason is different musical instruments sounds may have different characteristic or behavior [4].

Thus, the aim of this paper is to employ the data representation and feature extraction methods to different domain which is Traditional Malay musical instruments sounds. In order to accomplish this study, the original data sets are acquired from multiple sources with assortment of audio representation (i.e. file format, sample rate, audio type). Therefore, in order to create the best data sets for feature extraction, five factors are considered which are: (a) the maximum length of interval time for the audio file, (b) the size of the segmented frame, (c) the starting point for the sound tracks, (e) the distribution of the data set, and (d) the ratio of training and testing data sets. The combination of the two categories of features schemes which are perception-based and MFCC is used. While, Multi-Layered Perceptrons (MLP) classifier is employed in order to evaluate the performance of the data sets.

The rest of this paper is organized as follows: Section 2 discuss a related work on data representation and feature extraction. The proposed method will be explained in Section 3. Then, Section 4 presents the comparison result and discussion followed by the conclusion in Section 5.

2 Related Work

In literature, the data sets used have an assortment of audio representation and sources. It shows that different researchers have their own different ways to represent and obtain their data. In general, the difference is based on the length of audio file, length of segmented frame, audio format, audio type, size of sample rate (in Hertz) and filter technique used. Benetos *et al.* [6] used about 300 audio that were extracted from 6 different instrument classes. The audio files are discretized at 44.1kHz of sample rate and have a duration about 20 seconds. Eronen [2] perform the experiment by using 5286 samples of 29 Western Orchestral instruments. Two different frame lengths for two different states (onset with 20ms and steady with 40ms) were examined. The sample rate is 44.1 kHz. It can be seen that both of them use a uniformed length of audio file. Norowi *et al.* [7] also recommend that a standard length for each data file was required to avoid poor classification result. However, there were some researchers had use a certain length of audio files range. For instance, Liu and Wan [3] employ an interval time between 0.1 second to around 10 seconds for each audio file. Every audio file is divided into hamming-windowed frames of 256 samples, with 50% overlaps. In this study, this method will be adopted due to the limited sources problem (where some of the original data had a complete signal sound per cycle less than 1 second). These variety of parameters used in the literature show that there were no standard benchmarking in determining the best parameter for data representation. It shows that initial experiment in the early stage (data representation) of musical instrument classification system is vital to determine the reliability of data used.

In term of features schemes available, there were various features schemes that have been extracted and adopted by past research either by individual sets or combination of them. Normally, the features used consists both spectral and temporal domain.

Loughran *et al.* [10] highlighted that the combination of both spectral and temporal features is essential in order to provide an accurate description of sounds timbre. In our preliminary work [5], two categories of features schemes which are perception-based and MFCC were examined. Result from the study found that the combination of these features able to produce highest accuracy compared to single features subsets. With that encouraging performance, these two groups of features schemes are used in this study. For the purpose of musical instrument classification, various classification algorithms have been employed. In this study, the accuracy rate produced by the MLP is used to measure the performance of the data sets. From the observation, MLP can be considered as one of the famous techniques applied in musical instrument sounds classification. Studies performed using MLPs to classify musical instrument sounds have found able to produce a good result [1,8,10]. With the overall satisfactory performance achieved in previous research, MLP technique is applied in this study as well.

3 The Proposed Method

The method of this study was designed and conducted in order to accomplish the main objective stated in Section 1. This method comprises five main phases which are data acquisition, sound editing, data processing (representation), feature extraction, data elimination and data classification. Fig. 1 illustrates the phases of this method. Matlab functions were fully utilized in this study except for data acquisition and sound editing. The details for each phase as follows:

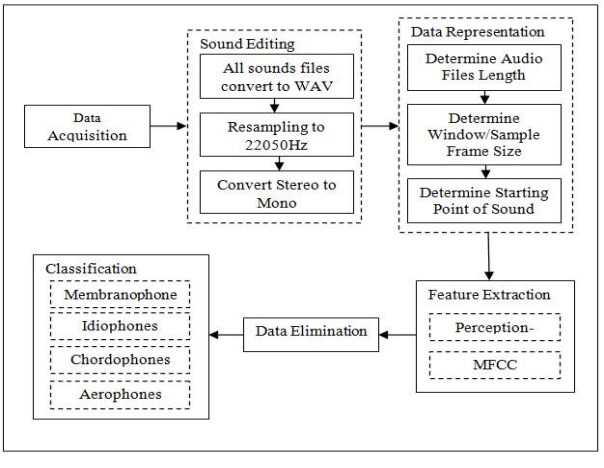

Fig. 1. The proposed method for identifying the ideal data representation for feature extraction of the Traditional Malay musical instruments sounds.

3.1 Data Acquisition and Sound Editing

The 150 sounds samples of Traditional Malay musical instruments were downloaded from personal [11] and *Warisan Budaya Malaysia* web page [12]. These 150 sounds consist of different number of instruments from four different families which are 41

membranophones, 75 idiophones, 23 aerophones and 11 chordophones. The original data collection came in MP3 and WAV files format with assortment of sample rate which are 22.1 kHz and 44.1 kHz. In order to utilize Matlab function in this study, all the sound files are converted into WAV format. Then the sounds are down-sampled to 22.1 kHz, and the sounds channel is converted to mono. The reason is to reduce the computational time compared using stereo file with high sample rate. Schmidt and Stone [13] also discovered that mono files provide better overall models. All these processes are done using sound editing software.

3.2 Data Representation

In this study, this phase can be considered as the most important stages in identifying the best data sets based on the factors stated in Section 1. There are three main steps were setup in this phase. In the first step, the original data collections were trimmed into three different data sets with different interval time. The first data set (F1A) comprises sound files range from 0.1 to 10 seconds, the second data set (F1B) with range from 0.1 to 20 seconds, and the range for the third data set (F1C) is assigned from 0.1 to 30 seconds. This is done in order to examine whether the length of audio files plays important role in determining the classification result. In addition, with the very limited number of instruments sounds obtained, this approach can be used to construct a diversity of data samples as well. This to ensure that the optimal number of data sets (for both training and testing) used for the classification process is sufficient.

Then, the second step focused on identifying whether the size of segmented frame has significant consequence to the output. For that, every audio file is then segmented into frames of two different sample sizes which are 256 and 1024 with 50% overlap. The overlap procedure is done to ensure there are no missing signals during the segmentation process. In addition, each frame is hamming-windowed in order to improve the frequency selectivity of an analysis. The hamming-windowed is preferred in this study because it has been widely used in the literature. Afterwards, in the third step, the starting points of each data set were altered to 0 second, 0.05 seconds, 0.1 seconds and 0.3 seconds. The purpose of this step is to determine the appropriate starting point of the sound tracks. Moreover, it is also essential to identify whether the unnecessary signal (such as noise) present at the beginning of the sounds has major effect to the performance of the data sets. In the next phase, all these modified data sets were used to extract all the features stated in Table 1.

Table 1. Features Descriptions

Number	Description
1	Zero Crossing
2-3	Mean and Standard Deviation of Zero Crossings Rate
4-5	Mean and Standard Deviation of Root-Mean-Square
6-7	Mean and Standard Deviation of Spectral Centroid
8-9	Mean and Standard Deviation of Bandwidth
10-11	Mean and Standard Deviation of Flux
12-37	Mean and Standard Deviation of the First 13 MFCCs

3.3 Feature Extraction

In this phase, 37 features from two categories of features schemes which are perception-based and MFCC features were extracted. As shown in Table 1, the first 1-11 features represent the perception-based features and 12-37 are MFCC's features. The mean and standard deviation were then calculated for each of these features. These features are extracted using the formula in [1].

3.4 Data Elimination

The number of the original sounds per family are not consistent which also had differ in the lengthwise. This will cause to the inconsistent number of the sample size per family after the original data was trimmed into certain interval time (as explained in data representation phase) correspondingly. This imbalance sample size might give a biased classification and have an effect on the overall classification result. In order to investigate the fourth factors, the data are eliminated to uniform size.

3.5 Data Classification Using MLP

Classification process was carried out using the modified data sets based on factors stated in Section 1. The database is split into two parts: training and testing. In this study, the split ratio for the training and testing is also considered in examining the effectiveness of the classification performance. Thus, two split ratios which are 70:30 and 60:40 (training and testing) are investigated. Neural network with MLP algorithm is used to classify the musical instruments into four different families which are membranophones, idiophones, chordophones and aerophones. The network structure was defined with one input layer, one hidden layer with five nodes and one output layer. Each MLP was trained with a minimum error of 0.001, a learning rate of 0.5 and a momentum rate of 0.2. Each data set was trained over ten times and the average of accuracy rate was then calculated. Finally, the results were analyzed and compared to determine the performance of the data sets with the several factors declared.

4 Result and Discussion

The aim of this study is to observe the characteristic of the data sets and features schemes used, as the initial step for further exploration in Traditional Malay musical instrument sounds classification system. For that, several factors that might give a significant role in classification performance were determined and tested. Therefore, in this section, the results from the comparison test are presented. Results were evaluated in terms of accuracy rate produced by the classifier based on the stated factors. Thus, the results are as follows:

4.1 Length of Audio Files Is Not Necessary Long

For many cases, it was originally well-known that the longer duration of the audio files, the better classification accuracy can be produced. However, with the consideration of storage size and computational load, optimum duration of audio files need to be determined. Norowi *et al.* [5] claimed that many of previous researchers use 30

seconds in their work. However, they found that 10 seconds able to produce better result compared to 30 seconds and 60 seconds duration tested in their experiment. In our work, three different values for the maximum interval time for each sample sounds which are 10 seconds, 20 seconds and 30 seconds were investigated. For this experiment, the segmented frame size was set on 256 samples and the sound was taken from the start (starting point = 0 second). Then the performance of the classification rate produced by these three data sets is compared. Table 2 summarized the accuracy rate achieved based on the length of audio files used.

Table 2. The comparison of the classification performance for the length of audio file

No	% of Training and Testing	Classification Performance (%)		
		F1A (0.1 to 10 sec)	F1B (0.1 to 20 sec)	F1C (0.1 to 30 sec)
1	60:40	91.50	95.02	95.04
2	70:30	89.57	**95.56**	93.33

From the table, it can be seen that, the result from the data size of 70:30 (training and testing) achieved highest accuracy rates up to 95.56% for the Data Set F1B (with the interval time from 0.1 to 20 seconds). It is better about 2% from Data Set F1C (interval time from 0.1 to 30 seconds) and almost 6% from the Data Set F1A (interval time from 0.1 to 10 seconds). Although there are only a slight difference in terms of the classification performance between Data Set F1B and Data Set F1C, however, this finding explains that the common maximum length of audio apply in previous work (30 seconds) may not suitable to the Traditional Malay musical instrument. Moreover, it also shows that the length of the audio is not necessary long. On the other hand, 10 seconds is might not that sufficient to represent the all data sets. Additionally, this approach also can be used to increase the number of sample size. In this study, the size of data sets was increase from 150 samples (original sounds files) to 3086 samples (Data Set F1A), 2482 samples (Data Set F1B), and 1886 (Data Set F1C). The larger data sets are important in order to ensure an adequate data was fed into the classifier. Yale [14] also claimed that the sample size must be large enough to provide an acceptable high confidence level especially in neural network. As result, highest accuracy more than 95% confidence level can be achieved in this experiment.

4.2 Smaller Segmented Frame Is Favourable

The second experiment is to analyze the impact of segmented frame size in classification accuracy. For the same reasons stated above (computational load and storage size), the small size of two difference segmented frame which are 256 and 1024 was compared. At this time, the best data set (with audio files range from 0.1 to 20 seconds) determined above was used. At the same time, the starting point is still remaining at kept the zero point of the sound tracks. The result shows that the segmented frame with 256 samples produce highest accuracy rate with 95.56% as demonstrate in

Table 3. The comparison of the classification performance for the frame size

No	% of Training and Testing	Classification Performance (%)	
		256	1024
1	60:40	95.02	91.86
2	70:30	**95.56**	94.68

Table 3. This means that the audio files with small frame size use in this experiment have significant local features.

4.3 Starting from the Beginning Might Be More Exciting

It was assumed that in order to get a very high quality data, it is important to eliminate a few seconds from the start of the sounds tracks. The purpose is to remove unnecessary signal such as noise to ensure the represented data is the actual sounds of the instruments. Thus, there were important needs to determine the best starting point for the data used. By utilized the parameters established before, the next experiment is to verify whether this factor can provide any impact to the classification performance. For that reason, four different starting points was examined which are 0 second, 0.05 seconds, 0.1 seconds and 0.3 seconds. This small size of the starting points was determined by considering some of the original data used in this study have very short length of audio (less than 1 second).

As can be seen in Table 4, it is surprising to discover that the classification performance is increase significantly when the sounds are processed from the start of the sound tracks compared to the modified starting point. This finding is associated with Norowi *et al.* [7]. However, this finding is not essential pertinent to all sounds data sets. In our case, the original data might not contain so much noise at the beginning which not gives so much affect to the overall performance. In addition, the fluctuated classification performance achieved in data sets with 70:30 portions for training and testing indicate that the best starting point need to be determined appropriately if it needs to be considered in the process. The improper selection of the starting point might cause some important data can be eliminated accidentally and will affect to the classification performance.

Based on the highest accuracy obtained from these three experiments, it can be concluded that the best data set revealed from this study is the data set with the following characteristics which are: (a) audio files length between 0.1 second to 20 seconds, (b) hamming-windowed frames of 256 samples, (c) starting point for the sound tracks at 0 second, (d) 22.1kHz sampling rate, and (e) single audio channel or mono.

Table 4. The comparison of the classification performance for the starting point

No	% of Training and Testing	Classification Performance (%)			
		0 sec	0.05 sec	0.1 sec	0.3 sec
1	60:40	95.02	92.18	90.65	90.67
2	70:30	**95.56**	93.25	92.91	94.06

Instead of the above factors, there are other two factors that also examined in this study which are the ratio of training and testing and the distribution of the data set. The result as discuss below:

4.4 Larger Training Portion for the Best Performance

In common practise, the fraction of the data set for the training is larger than testing. The purpose is to train the classifier to well learn about the data behaviour and able to produce better classification result respectively. In this study, two different ratios which are 70:30 and 60:40 are studied. Table 2 shows that the larger portion of training data used in classifier (with the ratio of 70:30 for training and testing) able to produce highest classification rate about 95.56%. However, this does not mean that the ratio of 70:30 for training and testing is the best for all classification problems. Nevertheless, this finding supports the theory that the training data set has to be larger than testing in order to produce higher classification accuracy.

4.5 Uniform Distribution of the Data Set for Unbiased Classification

After consider these four factors, the best accuracy rate achieved is 95.56% which is over than 95 percent confidence level. However, this encouraging result is still not considering the consistent number of the samples size for each class (family). Even though in the real situation, the distribution of the sample size is not uniform. However, the idea is to create the best learning data set that can represent the real data for the classifier to converge better. Thus, investigation on the effect of uniform distribution of sample data per family is done to ascertain whether it can give better classification accuracy as commonly used by many. For that, some of the samples in the best data set (with the best parameter obtained from previous experiments) are eliminated to uniform distribution. From the result, it is found that the overall classification performance is increased up to 97.37%. This shows consistent number of sample sounds per family able to produce a better result and avoid biased classification accuracy.

5 Conclusions

In this paper, study on data representation and feature extraction of Traditional Malay musical instruments sounds has been done. The impact of five factors which are the length of audio files, the size of frame sample, the starting point for the sound tracks, the distribution of the data set, and the percentage of data sets for both training and testing towards the classification performance were studied. Overall, results obtained show that the highest classification accuracy can be improved by taking into consideration of all factors identified. From this result, it is suggested to use tracks with maximum 20 seconds in length, shorter frame size to represent more local attribute, and starting from the beginning of the sounds track in order to perform feature extraction for Traditional Malay musical instruments sounds. While, in terms of data distribution and data fraction (for training and testing), it is prove that the common practise can be adapted just as good. In our future work, we plan to investigate the important of feature selection towards the Traditional Malay musical instruments sounds.

Acknowledgement. This work was supported by the Universiti Tun Hussein Onn Malaysia.

References

1. Deng, J.D., Simmermacher, C.: Cranefield. S.: A Study on Feature Analysis for Musical Instrument Classification. IEEE Transactions on System, Man, and Cybernetics-Part B: Cybernetics 38(2), 429–438 (2008)
2. Eronen, A.: Comparison of Features for Musical Instrument Recognition. In: IEEE Workshop on the Applications of Signal Processing to Audio and Acoustics, New York, pp. 19–22 (2001)
3. Liu, M., Wan, C.: Feature Selection for Automatic Classification of Musical Instrument Sounds. In: JCDL 2001: Proceedings of the 1st ACM/IEEE-CS Joint Conference on Digital Libraries, pp. 247–248 (2001)
4. Golzari, S., Doraisamy, S., Sulaiman, M.N., Udzir, N.I., Norowi, N.M.: Artificial Immune Recognition System with Nonlinear Resource Allocation Method and Application to Traditional Malay Music Genre Classification. In: Bentley, P.J., Lee, D., Jung, S. (eds.) ICARIS 2008. LNCS, vol. 5132, pp. 132–141. Springer, Heidelberg (2008)
5. Senan, N., Ibrahim, R., Nawi, N.M., Mokji, M.M.: Feature Extraction for Traditional Malay Musical Instruments Classification. In: International Conference of Soft Computing and Pattern Recognition, SOCPAR 2009, Malacca, pp. 454–459 (2009)
6. Benetos, E., Kotti, M., Kotropoulus, C.: Musical Instrument Classification using Non-Negative Matrix Factorization Algorithms and Subset Feature Selection. In: IEEE International Conference on Acoustics, Speech and Signal Processing, ICASSP 2006 Proceedings, Toulouse, vol. 5 (2006)
7. Norowi, N.M., Doraisamy, S., Wirza, R.: Factors Affecting Automatic Genre Classification: An Investigation Incorporating Non-Western Musical Forms. In: 6th International Conference on Music Information Retrieval Proceeding, ISMIR 2005, London, pp. 13–20 (2005)
8. Ding, Q., Zhang, N.: Classification of Recorded Musical Instruments Sounds Based on Neural Networks. In: IEEE Symposium on Computational Intelligence in Image and Signal Processing, Honolulu, pp. 157–162 (2007)
9. Piccoli, D., Abernethy, M., Rai, S., Khan, S.: Applications of Soft Computing for Musical Instrument Classification. In: Gedeon, T(T.) D., Fung, L.C.C. (eds.) AI 2003. LNCS (LNAI), vol. 2903, pp. 878–889. Springer, Heidelberg (2003)
10. Loughran, R., Walker, J., O'neill, M., O' Farrell, M.: Musical Instrument Identification Using Principal Component Analysis and Multi-Layered Perceptrons. In: IEEE International Conference on Audio Language and Image Processing, Shanghai, pp. 643–648 (2008)
11. Shriver, R.: Webpage, `http://www.rickshriver.net/hires.htm`
12. Warisan Budaya Malaysia: Alat Muzik Tradisional, `http://malaysiana.pnm.my/kesenian/Index.htm`
13. Schmidt, A.P., Stone, T.K.M.: Music Classification and Identification System (2009)
14. Yale, K.: Preparing the Right Data Diet for Training Neural Network. In: IEEE Spectrum, pp. 64–66 (1997)

Mining Reputation of Person/Product from Comment and Reply on UCC/Internet Article

Joonsuk Ryu, Wonyoung Kim, Jaeho Jeong, and Ungmo Kim

Dept of Electrical and Computer Engineering, Sungkyunkwan University
{jsryu,wykim,umkim}@ece.skku.ac.kr, skynettx@skku.edu

Abstract. Increasing Internet users and generalization of internet brought many changes to our Society. One of the most important changes is internet media start to provide their contents to people who have internet connection and these people express their opinions about UCC/Internet Articles as reply/comment after they read it. Replies/Comments written by users are from many different age groups which various opinions exist and these opinions are very useful for marketing in business or politician. However, collecting and analyzing opinions of users manually costs very high amount of money and a lot of labor. Therefore, this paper proposes a new method to extract opinions from reply or comment and to summarize extracted opinions to provide reputation of person/product in which we are interested.

Keywords: Data Mining, Opinion Mining, Reply, Comment, Reputation mining.

1 Introduction

As the number of internet media users increased, more users freely express their opinions about UCC/Internet Article using comment or reply. Through these opinions, we extract negative/positive side of person/product that we are interested in and numerate reputation of person/product. Knowing the reputation is very important for some people such as politician and marketing analyzer because they enhance the public's view of person/product by analyzing extracted reputation. UCC/Internet Articles are written/created, just after event occurred and spread all over the world in very short period of time. Consequently, we can extract very diverse and huge opinions of person/product. In the past, market analyzer or politician conducted manual survey to find reputation of person/product, in the past. However, manual survey not only costs high but also requires lots of labor. Therefore, we use opinion mining.

Opinion mining is a technology that extracts meaningful opinions from huge information which include texts written by users. In this paper, we propose a opinion mining method to automatically extract opinions from comments and to summarize extracted opinions. This paper is organized as follow. Section 2 shows background concept. Section3 describe how we apply some techniques to our method. Finally, we conclude with summary and direction for future work in Section 4.

D.-S. Huang et al. (Eds.): ICIC 2010, LNCS 6215, pp. 354–361, 2010.

2 Background Concept

Our work is mainly related to four research areas. In addition, some other minor works are related. In [1], many of techniques that are related to opinion mining are proposed. [2] has shown different ways of identifying opinion through WordNET word. [3] presented different approach from ours to mine from ParseTree.

2.1 Association Rule Mining

We use association rule mining which is one of the most popular algorithms proposed by Agrawal et al [4]. It discovers interesting patterns in transactions in very large database. Association rule mining[5] progresses through the following steps:

Let $I = \{I_1, I_2, \ldots, I_n\}$ is non-empty set of items, $D = \{ t_1, t_2, \ldots, t_n\}$ is the database of transactions and a rule is defined as an implication of the form X Y, where $X, Y \subset I$ and $X \cap Y = \phi$. To select interesting rules, usually two measures are used, support and confidence threshold. Support of an item X is defined as proportion of transactions in the data set in the itemset, sup(X Y)/N. Confidence of a rule is defined as following conf(X Y)= $\sup(X \cap Y)/\sup(X)$.

Table 1. Transaction Examples

Transaction ID	Milk	Bread	Butter	Beer
1	1	1	0	0
2	0	1	1	0
3	0	0	0	1
4	1	1	1	0
5	0	1	0	0

For example, from Table 1, let support and confidence are both 0.4. Rules that satisfy support threshold are {milk, bread},{bread, butter}and that satisfy confidence threshold are {milk, bread} $\Rightarrow$ {butter}. Now we can get example rule {milk, bread} $\Rightarrow$ {butter} which means if customers who buy milk and bread, also buy butter.

2.2 Part-Of-Speech Tagging

POS Tagging is Natural Language Process (NLP) of tagging the words as corresponding to a particular Part Of Speech such as Noun, Adjective and Adverb. Stanford-POS tagger[6] is one of POS Tagging programs. For example, if a sentence "When I watched this film, I hoped it ended as soon as possible" is inputted to Stanford-POS tagger, it outputs sentence with tags as below.

"When/WRB I/PRP watched/VBD this/DT film,/NN I/PRP hoped/VBD it/PRP ended/VBD as/IN soon/NN as/IN possible/JJ."

2.3 Latent Semantic Analysis

Latent Semantic Analysis (LSA) conceptually uses co-occurrence information. Co-occurrence information indicates that LSA uses semantic of word, not morphology as

other analyzer. Using LSA, hidden information between documents or terms can be extracted, including similarity between two terms.

To compute LSA, there are three steps. In first step, we count and score the number of words counted for each document as below matrix A,.

Matrix A

WORD\DOCUMENT	D1	D2	D3	D4	D5	D6
Cosmonaut	1	0	1	0	0	0
Astronaut	0	1	0	0	0	0
Moon	1	1	0	0	0	0
Car	1	0	0	1	1	0
truck	0	0	0	1	0	1

In second step, Singular Value Decomposition (SVD) is applied to Matrix A. SVD decomposes matrix A into three new matrixes, T, S, D. More information about SVD is in [7].

$$A_{t\,x\,d} = T_{t\,x\,n}\, S_{n\,x\,n}\, (D_{d\,x\,n})$$

t, d, n indicate the number of words and documents and min(t, d) respectively. Three matrixes below are matrixes decomposed from above matrix A.

Matrix T

	Dim1	Dim2	Dim3	Dim4	Dim5
Cosmonaut	-0.44	-0.3	0.57	0.85	0.25
Astronaut	-0.13	-0.33	-0.59	0	0.73
Moon	-0.48	-0.51	-0.37	0	-0.61
Car	-0.7	0.35	0.15	-0.58	0.16
truck	-0.26	0.65	-0.41	0.58	-0.09

Matrix D

	D1	D2	D3	D4	D5	D6
Dimension1	-0.75	-0.28	-0.2	-0.45	-0.33	-0.12
Dimension2	-0.29	-0.53	-0.19	0.63	0.22	0.41
Dimension3	-0.28	-0.75	0.45	-0.2	0.12	-0.33
Dimension4	0	0	0.58	0	-0.58	0.58
Dimension5	-0.53	0.29	0.63	0.19	0.41	-0.22

Matrix S

2.16	0	0	0	0
0	1.59	0	0	0
0	0	1.28	0	0
0	0	0	1.00	0
0	0	0	0	0.39

Then, we use matrix multiplication 2*2 from matrix S with matrix D to generate new Matrix B as below.

Matrix B

	D1	D2	D3	D4	D5	D6
Dimension1	-1.62	-0.60	-0.40	-0.97	-0.71	-0.26
Dimension2	-0.46	-0.84	-0.30	1.00	0.35	0.65

Finally, using equation below, we extract similarity of two documents.

$$Sim(A,B) = \cos\theta = \frac{A \cdot B}{|A||B|} = \frac{x_1 \times x_2 + y_1 \times y_2}{(x_1^2 + y_1^2)^{1/2}(x_2^2 + y_2^2)^{1/2}}$$

In [8], these three steps are explained in detail.

2.4 WordNET

WordNET is a large lexical database for the English language. In WordNet, words are grouped into sets of synonym called synsets. Synset provides simple definition of word and recodes semantic relations between synonym sets in a synset. More information of WordNET can be found in [9].

3 Proposed Method

In this section, we will describe our proposed approach to extract reputation of person/product from comments/replies.

3.1 Collect Comments and Replies on UCC/Internet Articles

A lot of UCC/Internet Articles are usually created just after event occurs. Therefore, for the convenient of users, UCC/Internet Articles are categorized as soon as they are created or reported. We collect UCC/Internet Articles categories related to our object and filter some unrelated documents then decompose comments/replies on these documents into one sentence with tags presenting where this sentence was decomposed from.

3.2 Generate ParseTree

Although not all opinions are expressed by adjectives, it is still worthwhile extracting adjectives as opinions of user because most of opinions are expressed by adjective. Thus, in this paper, we only extract a sentence containing at least one adjective.

ParseTree[10] is NLP tool used for analyzing and identifying Part-Of-Speech and constructing trees having POS as nodes. While tree is being constructed, we search adjectives in the tree and store sentences if more than one adjective exists in a sentence. For example, if sentence “Graphic is fantastic” is entered as input, tree with POS node is create as below.

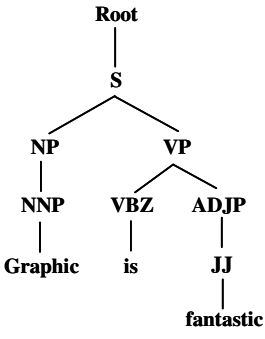

Fig. 1. Example of ParseTree

As above tree has ADJP, which stands for adjective phrase, sentence "Graphic is fantastic" is saved as a candidate comment.

3.3 Generate Candidate Comments and Replies from ParseTree

In this section, we describe the most important part of our approach that is how we apply our algorithm to extract opinions and features from ParseTree from section 3.2. We are required to find JJ in ParseTree then saved as opinion. Based on this opinion, we extract features in sentence.

```
Input: ParseTree
Output:  Nouns, Adjective, Adverb
Steps: 1. Search ParseTree until JJ is detected
2. Let Opinion, Recent  = jj
3. Find first NP ascendant of detected JJ before get to first ascendant
S
4. If NP exist as ascendant of JJ
  4.1. Let Recent = NP 4.2. Let Feature = Recent without jj
  4.3. If RB exist as sibling of Recent or Opinion
    4.3.1. Let RB = RB sibling of Recent or Opinion
5. Else If sibling of JJ is S
  5.1. Let Recent = S
  5.2. Let Feature = VB descendent of Recent
  5.3. If RB exist as sibling of ADJP parent of Recent
    5.3.1 Let RB = RB sibling of ADJP parent of Recent
6. Else
  6.1. Let Recent = VP ascendant of JJ
  6.2. Feature = NP sibling of Recent
7. Store Features(NNs), Opinion(JJ) and Adverb(RB) as
[(NN,NN,NN),(JJ,RB)]
```

Above algorithm extract candidate features and related opinions from ParseTree. For instance:

"Movie has very good graphic quality"

"It is easy to use"

In the first sentence, we extract "good" as the opinion word which describe "graphic quality" then extract graphic quality as a feature based on opinion word and word "very" which adverbial modifier of opinion word "good" is extracted as RB. In the second sentence, the word "easy" is extracted as opinion word and word "use" is extracted as feature because easy is complemented by "to use."

3.4 Prune Candidate Features and Opinions Applying LSA

We use LSA to solve metaphorical word problem and to find unrelated words. Before applying LSA to features, we use collected UCC/Article with replies/comments as base corpus and create feature table that is constituted by explicit feature words. After feature table is created, the features extracted from Section 3.3 is compared to feature table then if same feature word exist in feature table, skip LSA process, but if it is not in the list, we apply LSA to get similarity between two words. We set similarity threshold to 0.70, and we pick a word which has highest similarity among words satisfying threshold. After LSA process is done, we put new word into feature table. Example from 2.3, Let we assume a word "Cosmonaut" is explicit feature word in feature table. And we use matrix production between Matrix S and Matrix T and apply cosine similarity equation. After applying LSA, we get below Matrix W[1] showing similarity between words.

Matrix W

	Cosmonaut	Astronaut	Moon	Car	Truck
Cosmonaut	1				
Astronaut	0.811764	1			
Moon	0.978079	0.915575	1		
Car	0.687557	0.134084	0.52128		
Truck	0.431365	-0.548426	-0.165849	0.75513	1

As a result from matrix W, although word "Car" and "cosmonaut" appear together in document 1 from section 2.3, it is shown that similarity between cosmonaut and car does not satisfy LSA threshold, 0.70. Therefore word "Car" is discarded from feature word list. Through this work, we can prune feature words not related to our product/person.

3.5 Extract Features from Pruned Candidates

After we apply LSA in Section 3.4 some of related features can be pruned. We employ apriori rule[4] to opinion mining to reselect features from discarded features. In [11], the author stated the words used in sentences are converged, when people talking about one thing. How aprior algorithm is applied to opinion mining is presented in [11]. We only extract noun words that satisfy minimum support and minimum confidence. For example, if word "staker" appears 10 times out of 100 sentences which is 10%, then it is treated as feature word.

[1] Matrix W shows percentage of similarity between row words and column words. It is computed using example Matrix S and Matrix T from Section 2.3.

3.6 Summarize Opinions

Our method is based on WordNET. First, we select seed adjective words from opinion words and find their adjective synset to store them in a standard word list. Now, we compare each opinion word with words in a standard word list. If opinion word exists in standard word list, get value of standard word matched. But if it is not in standard word list, we use WordNET to find synset starting from synset including one standard word to synset including opinion word. But this process can reach infinite loop, so we limit depth of searching for each synsets of one standard word. After finding the synset, we store opinion word in standard word list with value of standard word included together.

With this process, we can explore opinion words. For example, standard word list starts as following Table 3. Opinion word "well" is compared with words in the list, and as word "well" is in the list, we put value of standard word into extracted word. Next word "fine" is compared, but this word not exist in the list, therefore we search WordNET based on seed words and extract the synsets that are searched and contain word "fine" and put value of a seed word. Table 4 shows after comparison of word "fine" is done.

Table 2. Standard Word List

Word	Value
Bad	-0.8
Good, Well	0.8
Excellent	1

Table 3. New Standard Word List

Word	Value
Bad	-0.8
Good, Well, OK, Satisfactory, Fine	0.8
Excellent	1

To get more precise opinion value, we apply adverb such as very, pretty, so etc. For instance, Let "this movie is so good" is candidate sentence. Opinion word "good" has value 0.8 but actual opinion is "so good" which has higher than 0.8. Multiplying value of opinion word by two is our approach. Therefore "so good" imply value 1.6. Now, we add up all values and divide that by the number of opinions to get average reputation of a person/product.

4 Conclusion and Feature Work

In this paper, an approach to extract reputation of person/products is introduced. Our aim is to gather reputation automatically without time consuming work such as survey and to provide politician or marketing analyzer helpful information to improve their reputation. Our approach starts with collecting comments/replies from UCC/Internet Articles and decomposing them into a sentence with tag presenting where this sentence is decomposed from. Then, using ParseTree, Tree with POS node is constructed. While tree is constructing, we prune sentences without adjective and save not pruned sentences. LSA is now applied to prune feature not related to our object and we extract features from pruned by LSA. Lastly, we summarize opinions using WordNET. This approach enables extracting reputations from comments/replies on

internet contents. In the future work, Firstly, we will show how our work is done in real world and effectiveness of our work. Secondly, we will increase accuracy of matching feature word by other approach including LSA and preciseness of summarization of opinions. Finally, more semantic information will be considered to improve accuracy of extracted opinions such as verb.

Acknowledgement

This work was supported by the Korea Science and Engineering Foundation (KOSEF) grant funded by the Korea government (MEST) (NO. 2009-0075771).

References

1. Pang, B., Lee, L.: Opinion Mining and Sentiment Analysis. Foundations and Trends in Information Retrieval AI 2(1-2), 1–135 (2008)
2. Smrž, P.: Using WordNet for Opinion Mining. In: GWC 2006 Proceedings, pp. 333–335 (2006)
3. Dey, L., Mirajul Haque, S.K.: Opinion Mining from Noisy Text Data. In: Proc. of the 2th workshop on Analytics for noisy unstructured text data, Singapore, pp. 83–90 (2008)
4. Agrawal, R., Srikant, R.: Fast Algorithm for Mining Association Rules. In: VLDB 1994 (1994)
5. Tan, P., Steinbach, M., Kumar, V.: Introduction to Data Mining. Association Analysis: Basic Concept and Algorithms (2006)
6. Stanford Tagger Version 1.6 (2008), http://nlp.stanford.edu/software/tagger.shtml
7. Singular Value Decomposition (SVD) tutorial, http://web.mit.edu/be.400/www/SVD/Singular_Value_Decomposition.htm
8. Latent Semantic Indexing (LSI) A Fast Track Tutorial, http://www.miislita.com/information-retrieval-tutorial/latent-semantic-indexing-fast-track-tutorial.pdf
9. WordNet – About WordNet, http://wordnet.princeton.edu
10. Stanford Parser Version 1.6 (2008), http://nlp.stanford.edu/software/lex-parser.shtml
11. Hu, M., Liu, B.: Mining and Summarizing Customer Reviews. In: Proc. of the 10th ACM SIGKDD international conference on Knowledge discovery and data mining, Seatle, pp. 168–177 (2004)

Interaction Analysis for Adaptive User Interfaces

Kawa Nazemi, Christian Stab, and Dieter W. Fellner

Fraunhofer Institute for Computer Graphics Research,
Fraunhoferstrasse 5, 64283 Darmstadt, Germany
{kawa.nazemi,christian.stab,d.fellner}@igd.fraunhofer.de
http://www.igd.fraunhofer.de

Abstract. Adaptive User Interfaces are able to facilitate the handling of computer systems through the automatic adaptation to users' needs and preferences. For the realization of these systems, information about the individual user is needed. This user information can be extracted from user events by applying analytical methods without the active information input by the user. In this paper we introduce a reusable interaction analysis system based on probabilistic methods that predicts user interactions, recognizes user activities and detects user preferences on different levels of abstraction. The evaluation reveals that the prediction quality of the developed algorithm outperforms the quality of other established prediction methods.

Keywords: Probabilistic Models, Interaction Analysis, User Modeling, Adaptive User Interfaces, Adaptive Visualization.

1 Introduction

The present operators of computer systems vary not only in different ages, gender and interests but also in working aptitudes, precognition and experience. As a consequence of the increasing heterogeneity of computer users, the user interfaces offer more and more features to cover the needs of every individual user. The effect of the increasing functional range is that the handling of computer systems becomes more and more complex [14]. To facilitate the handling of computer systems, Adaptive User Interfaces can be used to adapt the graphical presentation and representation of information to meet users' demands and to support them during their work process [18,13,2,5].

For all kinds of Adaptive User Interfaces and the realization of user supporting adaptations, information about the users and their handling with the computer system is needed. This user information is either prompted directly from the user or captured automatically and implicit by the system [21]. The explicit acquisition by questioning the user is not approved [18]. Through the observation of the users, the needed information can be captured implicit during the usage of the software system without the active information input by the users [4]. A possible data source for capturing user information in an implicit way is the sequence of interaction events that occurs as natural consequence of the usage

D.-S. Huang et al. (Eds.): ICIC 2010, LNCS 6215, pp. 362–371, 2010.

of the user interface. The interaction events contain information about the user and their handling of the computer system and can be captured without high effort [11,17]. However automatic analytical methods are required to extract the information about the user.

In this paper we introduce a reusable interaction analysis system based on probabilistic methods. In particular we describe an extension of the KO-Algorithm [14] that allows, alongside the prediction of user interactions, the detection of behavioral patterns. The detected patterns are used to discover user activities and to identify changes in user behavior. Furthermore the presented interaction analysis system captures user preferences by quantitative analysis of the interaction events and allows querying the extracted preferences on different grades of abstractions. The evaluation shows that the prediction quality of the extended algorithm outperforms the quality of other established methods.

In the next section we give an overview of existing probabilistic models and their usage in Adaptive User Interfaces followed by the detailed description of our interaction analysis system. Afterwards we present an evaluation of our new developed algorithm and its result compared to other established prediction algorithms.

This work has been carried out within the THESEUS Program, partially funded by the German Federal Ministry of Economics and Technology.

2 Related Work

One type of methods that are suitable for the implicit extraction of user information from interaction events, are probabilistic methods. Probabilistic methods are unsupervised learning algorithms which have the ability to infer conclusions from observations. For this reason they are well suited for the implicit extraction of user information from interaction events [1,16].

For example Horvitz et al. [12] use *Bayesian Networks* (BN) to extract the goals and needs of users from interaction events to realize an intelligent help system. Hancock [10] uses BNs to determine the handedness and the position of users to adapt the visualization of a tabletop display. The challenge for the usage of BNs is the construction of the causal dependency structure. This task requires knowledge from interdisciplinary domains (e.g. psychology or pedagogy). Indeed there are methods which determine a dependency structure automatically for given input data [7] but the interpretation of the automatic created structure constitutes another challenge.

Another type of probabilistic methods for the extraction of user information from interaction events are *Probabilistic Relational Models* (PRM). Getoor et al. [8] determine user interests with PRMs to filter products of a commercial internet platform. Noguez et al. [15] use PRMs for an Intelligent Tutor System (ITS) that assists students during the work with a virtual laboratory. Beside the dependency structure analog to BNs, for the usage of PRMs a relational schema is needed what implies even a higher configuration effort.

Markov Models are used to describe a sequence of events. They can be used to calculate predictions and allow quantitative analysis. For example Guzdial [9] uses *Markov Chains* (MC) to estimate usage patterns from users of *Emile* With the calculation of the *Steady State Vector* (SSV) from the transition matrix , Guzdial is able to identify parts of the application that are often used. Another Markov Model was developed by Anderson et al. [3]. They developed a *Relational Markov Model* (RMM) and use it for the automatic adaption of web sites to minimize user effort in reaching their goals. The RMM uses a relational structure of the web site to predict user behavior even for web sites that the user never visited before [3]. Davison and Hirsh [6] use an extended version of MCs to model users of a UNIX console and to predict user commands. The extension is called *Incremental Probabilistic Action Modeling* (IPAM). The model weights newer observations higher than older observations. So the model is able to adjust itself to changes of user behavior. The advantage of Markov Models adverse BNs or PRMs is that they are usable without high configuration effort. For the usage of Markov Chains the interaction events are needed in advance to define the states and the transition matrix of the model. For RMMs the relational structure of the observable data is needed additionally. In case of incremental methods the model is build incrementally when new observations are observed. They can be used with minor configuration effort for different application scenarios.

Other probabilistic methods are the *LEV-* and *KO-Algorithm* from Künzer et al. [14]. These algorithms calculate predictions of interactions by searching recurring similar (LEV) or identical (KO) sequences in the interaction events. Künzer et al. use these algorithms for an intelligent help system and evaluate the prediction quality of the two algorithms by comparing them with other prediction algorithms and the results show that especially the KO-Algorithm offers the best prediction quality [14].

3 Analysis of User Interactions

In this section we provide a detailed description of our interaction analysis system and introduce the KO*/19-Algorithm as an essential part of the system. In the first part we describe the representation of the interaction events and the associated context information. Afterwards we present three different analysis methods for capturing user preferences, predictions and user activities. Figure 1 illustrates the process of the interaction analysis system and the co-operation with an Adaptive User Interface. Every interaction event observed in the User Interface (UI) is sent to the analysis system where the user information is captured. The extracted user information is sent back to the UI to realize user-centered adaptations.

3.1 Representation of Interaction Events

The context information of interaction events constitutes an useful knowledge source for understanding and analysing the behavior of the user [11]. In order

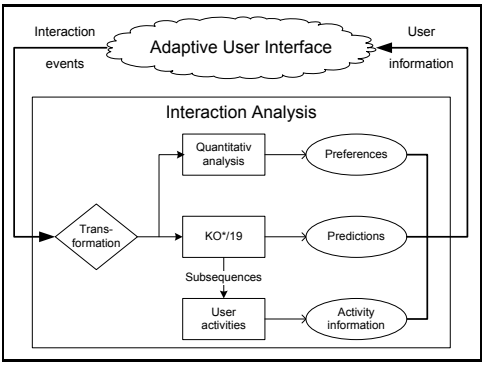

Fig. 1. Process of the interaction analysis system and co-operation with an Adaptive User Interface

to allow the usage of the introduced interaction analysis system for different application scenarios, the context information is defined with individually definable domains. A domain is a tree, representing an abstraction hierarchy [3] and indicates a certain field of knowledge about interaction events. An interaction event I is described as a relation instantiated with leaf values of the domains as

$$I = r(k_1, ..., k_n), \quad k_i \in leaves(D_i) \quad \text{with} \quad 1 \leq i \leq n, \tag{1}$$

in which $leaves(D_i)$ are the leaf nodes of the domain D_i and r is a relation over domains $D_1, ..., D_n$.

3.2 Quantitative Analysis of Interaction Events

Having described the representation of interaction events, we describe the quantitative analysis for the acquisition of user preferences in this section. After the transformation of the interaction events in an internal, numerical representation the Steady State Vector (SSV) is determined as a relative measurement for the occurrence of interaction events. The SSV is defined as $\boldsymbol{s} = (p_1, p_2, ..., p_n)$, in which n is the count of all possible interaction events and p_i is the probability that an interaction i occurs. Furthermore $\sum_{i=1}^{n} p_i = 1$ holds. Thus the Steady State Vector is a probability distribution over all possible interaction events. The context information of the interaction events is used to query the results of the quantitative analysis on different grades of abstraction. Analogue to RMMs, abstractions of interaction events are defined as sets of interaction events by instantiating the relation r with inner nodes of the domains. A quantitative query is defined as $query(depth_{D_1}, ..., depth_{D_n})$, where $depth_{D_i}$ is the grade of abstraction for every domain D_i. Thus with every query the set of abstractions

$$L = \{r(\delta_1, ..., \delta_k) | \delta_i \in nodes_i(depth_{D_i}), \forall i, 1 \leq i \leq k\} \tag{2}$$

is defined where $nodes_i(depth_{D_i})$ are the nodes of the domain D_i on the depth $depth_{D_i}$. With the defined set of abstractions all interaction events are partitioned into subsets of interaction events which account some similarity in respect of their context information. The probability p_α for every abstraction $\alpha \in L$ is calculated with the probabilities from the SSV as $p_\alpha = \sum_{q_i \in \alpha} ssv(q_i)$ where $ssv(q_i)$ is the probability of the interaction q_i from the SSV. Hence the result of a quantitative query is a probability distribution over sets of interaction events. The calculated probabilities permit statements concerning the preferences of the users. For example, elements of the user interface can be identified which are used frequently or not at all. Depending on the given context information of the interaction events, the user preferences can be queried on different grades of abstraction which increases the information content.

3.3 Prediction of Interaction Events

Beside the quantitative analysis, predictions of user interactions are calculated with the KO-Algorithm. The original version of the KO-Algorithm from Künzer et al. [14] calculates predictions of interaction events by the search of recurring identical subsequences with maximal length of three interaction events. By the recognition of recurring subsequences it is possible to identify usage patterns, which can be used to identify changes in user behavior and to recognize user activities [19]. For this purpose the behavioral patterns should not be limited to a fixed length, because this reduces the information content of the identified activities. Hence we extended the KO-Algorithm so that with every prediction calculation the longest subsequence of interaction events is identified. This extension of the algorithm is called KO*/19-Algorithm and is described below. For every occurrence of an interaction a at the position v in the interaction sequence $O = i_1, i_2, ..., i_n$, the last interaction events in the interaction sequence O are compared with the interaction events before v as long as no match is identified. In the first step i_n is compared with i_{v-1}. If they are identical, i_{n-1} is compared with i_{v-2} and so on (Fig. 2). Thereby the longest identical recurring interaction sequence is discovered. The lengths of each subsequence are weighted with $w(i) = i^{19}$ and summed. This process is accomplished for every observable interaction event. With the resulting values the probability distribution for the prediction of the next interaction event is calculated by normalization.

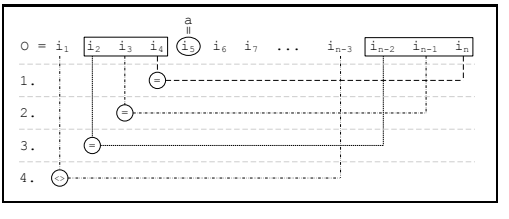

Fig. 2. Procedure of the KO*/19-Algorithm

3.4 Detection of User Activities

The behavior of a computer user change in the course of time [20]. So it is necessary that systems which collect user information are able to adapt themselves to these changes. Beside the adaptation of the user information to the changes of user behavior, our method is able to identify these changes by recognizing transitions between behavioral patterns. For this task we define an user activity as recurring similar sequence of interaction events.

With every new interaction event that is sent to the interaction analysis system the KO*/19-Algorithm identifies a behavioral pattern as the longest recurring subsequence in the interaction sequence of the user. These behavioral patterns are compared and grouped to similar sequences and constitute a user activity. To identify an activity, the first recognized subsequence is added to a new activity. For every new subsequence a similarity function is used to measure if the new sequence matches to the activity created in the first step. If the similarity value exceeds a threshold, the sequence is added to the activity. If the similarity value doesn't exceed the threshold a new activity is created and the sequence is added to it. In this process the actual activity of the user is detected as the activity that matches to the subsequence or a new created activity, if no matching activity could be identified.

The choice of the threshold has direct influence on the number of detected activities. If the threshold is too high, it is possible that for every detected sequence a new activity is created and so no similarities between the sequences are recognized. If the threshold is too low, all sequences are added to the same activity and the differentiation of user activities is not possible. Thus the threshold has to be determined for every application scenario.

For the cognition of the semantic meaning of the recognized activities, we implement the same querying method as for user preferences. Therefor the SSV of every activity is calculated from the interaction events of every sequence belonging to the activity. The context information of the activity interaction events is used to calculate probabilities of abstraction sets which are defined by the parameters of the query as described above. So for the derivation of the semantic meaning every activity can be also queried on different grades of abstraction.

4 Evaluation

To estimate the quality of the captured user information we evaluate the developed interaction analysis system. The focus of this evaluation is the estimation of the prediction quality of the KO*/19-Algorithm. For that purpose we use two assessment criteria that we describe below and compare the results of the KO*/19-Algorithm with those of other prediction methods. Additionally we evaluate the recognition of user activities.

For the estimation of the prediction quality we use the Mean Prediction Probability and the Mean Prediction Rank. The *Mean Prediction Probability* (MPP) is defined as the average probability that is calculated with the prediction algorithm for really occurring interaction events. Formally the MPP is defined as

$$MPP = \frac{1}{|o|} \sum_{i=1}^{|o|} P(o_i | o_{1:i-1}) \tag{3}$$

where o is the interaction sequence and $P(o_i|o_{1:i-1})$ is the calculated probability that the interaction o_i occurs after the sequence $o_{1:i-1}$. The second criterion we use for evaluating the prediction quality is the *Mean Prediction Rank* (MPR). Formally the MPR is defined as

$$MPR = \frac{1}{|o|} \sum_{i=1}^{|o|} rank(o_i) \tag{4}$$

where $rank(o_i)$ denotes the rank of the occurred interaction o_i. The rank of a prediction is defined as the position in the sorted probability distribution. So the most possible interaction has a rank of 1 and the second possible has a rank of 2 and so on. Hence, the lower the MPR of a prediction algorithm is, the better is the quality of the prediction calculation.

4.1 Evaluation Scenario

For the first evaluation scenario we chose the application *PKITool*, which allows the creation of certificates for building a public key infrastructure. The application allows the creation of three different certificate types, the visualization of certificate attributes and the revocation of certificates. The interaction events that occur during the usage of the user interface were stored and serve as base for our evaluation. Altogether 27 interaction events which are defined with two domains as context information can be observed. For the estimation of the prediction quality the interaction events of 26 different users were recorded and stored in a file. Afterward we determine the MPP and MPR of every prediction method. Therefor every method was learned with one file and the interaction events of the other files were used for the continuous learn process and the calculation of the two criteria.

Results. As expected the original KO-Algorithm outperforms the prediction quality of the other established methods (Table 1). So we can approve the results of Künzer et al. [14]. In respect of the MPP, the KO3/19-Algorithm is significantly better than other methods. The algorithm achieved a MPP of 45.23% in our test scenario and thus the algorithm is about 12.12% better than Markov Chains. Remarkable is that the KO*/19-Algorithm achieved in spite of the extension for the recognition of behavioural patterns even a better MPP as the KO3/19-Algorithm. The algorithm attains a MPP of 46.57% and is in this context the best algorithm in our evaluation scenario (Fig. 3). The results concerning the MPR show that the KO3/19-Algorithm is in the midfield in comparison with the other methods (Fig. 3). The algorithm achieves a MPR of 5.42. In respect of the MPR our extended algorithm improves the MPR of the KO3/19-Algorithm by 2.16 (Table 1).

[1] The difference denotes the distance between the assessment criteria of the KO*/19-Algorithm and the best other method.

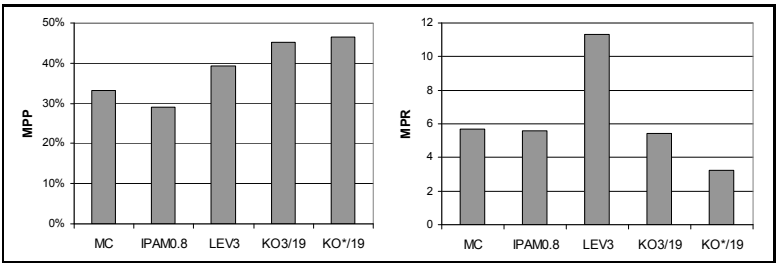

Fig. 3. Mean Prediction Probability (MPP) and Mean Prediction Rank (MPR)

Table 1. Comparison of the MPP and MPR for different prediction methods (PKITool)

Method	**MPP**	**MPR**
MC	33,11%	5,68
IPAM0.8	29,00%	5,57
LEV3	39,26%	11,34
KO3/19	45,23%	5,42
KO*/19	**46,57%**	**3,26**
Difference[1]	+1,34%	-2.16

4.2 Evaluation of Activity Detection

Additionally to the evaluation of the prediction quality we evaluate the detection of user activities and the recognition of behavioral changes respectively. For this purpose we implement a test bench which visualizes the extracted user information and especially the recognized user activities. So we are able to directly observe the acquired user information and to estimate the detection of user activities while the test person uses the application.

During the first tests we recognize that the detected user activities were sparse meaningful. For example the system detects an activity which was active while the creation of a certificate and during the browsing of certificate attributes. The adaption of the threshold indeed changes the number of the detected activities but the expressiveness of the recognized activities was not affected thereby. For the improvement of the activity detection we use a special trainings file for a second test. The trainings file contains the sequences of expected user activities. Altogether the file contains the sequences of five different activities: Three activities for the creation process of the different certificate types, one for the navigation and an activity for the revocation of a certificate. The activity sequences were separated with a special interaction event, which could not be executed in the user interface. So the subsequences which were detected with the KO*/19-Algotihm are separated concerning the expected activities. The further tests indicate that all expected activities were detected as expected and also the changes between the activities were recognized adequately. Thus it is possible to identify changes of user behavior with the usage of a special trainings file and to recognize user activities.

5 Conclusion

In this paper we introduced an interaction analysis system that extracts user information from interaction events for adapting user interfaces to the needs and requirements of the users. The developed system is applicable for different user interfaces and application scenarios without high configuration effort and detects user preferences by quantitative analysis of the interaction events. For increasing the information content we used the context information of the interaction events to query the preferences on different grades of abstraction.

Furthermore we described the KO*/19-Algorithm, which allows, alongside the prediction of interaction events, the detection of behavioral patterns. Therefor we extended the original KO-Algorithm so that the longest recurring subsequences in the interaction sequence of the user are detected as coproduct of the prediction calculation. The result of the evaluation revealed that the new developed algorithm outperforms the original version of the algorithm and other established prediction methods concerning the MPP. In addition our algorithm achieved a significant improvement of the MPR in comparison to other methods.

We used the recurring subsequences which are detected by the KO*/19-Algorithm for the definition of user activities. For this task we grouped similar subsequences and defined user activities as recurring similar sequences of interaction events. So the system is able to identify the present activity of the user by comparing the actual sequence with the detected activities.

References

1. Albrecht, D., Zukerman, I., Nicholson, A.: Bayesian Models for Keyhole Plan Recognition in an Adventure Game. In: UMUAI 1998, vol. 8, pp. 5–47 (1998)
2. Álvarez-Corés, V., Zayaz-Pérez, B., Zárate-Silvia, V., Uresti, J.: Current Trends in Adaptive User Interfaces: Challenges and Applications. CERMA, 312–317 (2007)
3. Anderson, C.R., Domingos, P., Weld, D.S.: Relational Markov Models and their Application to Adaptive Web Navigation. In: ACM SIGKDD, KDD 2002, pp. 143–152 (2002)
4. Armentano, M.G., Amandi, A.A.: Recognition of User Intentions for Interface Agents with Variable Order Markov Models. In: Houben, G.-J., McCalla, G., Pianesi, F., Zancanaro, M. (eds.) UMAP 2009. LNCS, vol. 5535, pp. 173–184. Springer, Heidelberg (2009)
5. Danine, A., Lefebvre, B., Mayers, A.: TIDES - Using Bayesian Networks for Student Modeling. In: ICALT 2006, pp. 1002–1007. IEEE Computer Society, Los Alamitos (2006)
6. Davison, B., Hirsh, H.: Predicting Sequences of User Actions. In: Predicting the Future: AI Approaches to Time Series Problems, pp. 5–12. AAAI Press, Menlo Park (1998)
7. Friedman, N.: The Bayesian Structural EM Algorithm. In: UAI 1998, pp. 129–138 (1998)
8. Getoor, L., Sahami, M.: Using Probabilistic Relational Models for Collaborative Filtering. In: Working Notes of the KDD Workshop on Web Usage Analysis and User Profiling (1999)
9. Guzdial, M.: Deriving Software Usage Patterns from Log Files. Georgia Institute of Technology (1993)

10. Hancock, M.S.: A Bayesian Network Model of a Collaborative Interactive Tabletop Display. University of British Columbia (2003)
11. Hilbert, D., Redmiles, D.: Extracting Usability Information from User Interface Events. ACM Comput. Surv. 32, 384–421 (2000)
12. Horvitz, E., Breese, J., Heckerman, D., Hovel, D., Rommelse, K.: The Lumiere project: Bayesian User Modeling for inferring the Goals and Needs of Software Users. In: UAI 1998, pp. 256–265. Morgan Kaufmann, San Francisco (1998)
13. Jameson, A.: Adaptive Interfaces and Agents. In: Human-computer Interaction Handbook, pp. 305–330 (2003)
14. Künzer, A., Ohmann, F., Schmidt, L.: Antizipative Modellierung des Benutzerverhaltens mit Hilfe von Aktionsvorhersage-Algorithmen. MMI-Interaktiv (7), 61–83 (2004)
15. Noguez, J., Sucar, L.E.: A Probabilistic Relational Student Model for Virtual Laboratories. In: ENC 2005, pp. 2–9. IEEE Computer Society, Los Alamitos (2005)
16. Papatheodorou, C.: Machine Learning in User Modeling. In: Paliouras, G., Karkaletsis, V., Spyropoulos, C.D. (eds.) ACAI 1999. LNCS (LNAI), vol. 2049, p. 286. Springer, Heidelberg (2001)
17. Guo, Q., Murphy, A., Deemer, S., Agichtein, E.: Modeling User Interactions for Automatic Library Search Evaluation: Preliminary Results. In: Joint Conference on Digital Libraries (2008)
18. Ross, E.: Intelligent User Interfaces Survey and Research Directions. University of Bristol (2000)
19. Stab, C.: Interaktionsanalyse für Adaptive Benutzerschnittstellen, Diploma Thesis, Technical University Darmstadt (2009)
20. Webb, G.I., Pazzani, M.J., Billsus, D.: Machine Learning for User Modeling. In: UMUAI 2001, pp. 19–29. Kluwer Academic Publishers, Dordrecht (2001)
21. Zukerman, I., Albrecht, D.W.: Predictive Statistical Models for User Modeling. In: UMUAI 2001, pp. 5–18. Kluwer Academic Publisher, Dordrecht (2001)

Unsupervised Subjectivity-Lexicon Generation Based on Vector Space Model for Multi-Dimensional Opinion Analysis in Blogosphere

Hsieh-Wei Chen[1], Kuan-Rong Lee[2], Hsun-Hui Huang[1], and Yaw-Huang Kuo[1]

[1] Intelligent System/Media Processing (ISMP) Lab, Dept. of Computer Science and Information Engineering, National Cheng Kung University, Tainan, Taiwan, ROC
[2] Dept. of Information Engineering, Kun Shan University, Yung-Kang, Tainan, Taiwan, ROC
hsiehwei@ismp.csie.ncku.edu.tw, leekr@mail.ksu.edu.tw, {hhhuang,kuoyh}@ismp.csie.ncku.edu.tw

Abstract. This paper presents an unsupervised framework to generate a vector-space-modeled subjectivity-lexicon for multi-dimensional opinion mining and sentiment analysis, such as criticism analysis, for which the traditional polarity analysis alone is not adequate. The framework consists of four major steps: first, creating a dataset by crawling blog posts of fiction reviews; secondly, creating a "subjectivity-term to object" matrix, with each subjectivity-term being modeled as a dimension of a vector space; thirdly, feature-transforming each subjectivity-term into the new feature-space to create the final multi-dimensional subjectivity-lexicon (MDSL); and fourthly, using the generated MDSL for opinion analysis. In the experiments, it shows that the improvement by the feature transform can be up to 31% in terms of the entropy of features. In addition, the subjectivity-terms and objects are also successfully and reasonably clustered in the demonstration of fiction review (literary criticism) analysis.

Keywords: weblogs, information retrieval, opinion mining, sentiment analysis, subjectivity classification, text mining.

1 Introduction

In recent years, more and more internet users own one or more blogs, with which many of the users enjoy sharing opinions and comments. To learn the spectrum of subjective opinions toward certain objects on the ever exploding blogosphere without an efficient opinion retrieval tool will be a difficult task in the study of an emerging area of information retrieval - opinion mining and sentiment analysis [1]-[3]. The process of sentiment analysis and opinion mining can be divided into the following four tasks: (i) topic-relevant document retrieval, (ii) opinionated document retrieval [4]-[8], (iii) opinion orientation classification (mostly polarity, i.e. positive or negative opinion, thumbs up or thumbs down) [9]-[12], and (iv) summarization and visualization [13][14]. Generally speaking, while task 1 can be categorized into the traditional document classification/clustering and retrieval task, tasks 2, 3, and 4 compose the major study area and pose challenges in opinion mining distinct from traditional information retrieval. Specifically, the three distinct major tasks usually involve either

D.-S. Huang et al. (Eds.): ICIC 2010, LNCS 6215, pp. 372–379, 2010.

an internal or external resource to determine the subjectivity and polarity semantic orientation (positive or negative) of a *phrase* and the overall opinion orientation in a document or a set of documents. The resource is commonly a *dictionary*, or a *lexicon* database (e.g. General Inquirer), which consist of entities (word, phrase, or syntactic patterns) tagged with their polarity orientations.

However, for more refined opinion analysis such as criticism analysis (e.g. criticism towards a film, a person, economy, politics, or literature), merely determining the polarity semantic orientation is not adequate Indeed, in literary criticism, a phrase with negative semantic orientation (e.g. poor, pity, and unfortunate) may imply sympathy, disproval, disappointment, tragedy, or sorrow etc. We cannot say that a reviewer has a negative attitude towards a character or a fiction merely because the overall polarity semantic orientation is negative. In political and social criticism, a phrase with positive semantic orientation (e.g. efficient, free, and respectful) may imply social justice, equality, freedom, instrumental rationality, value rationality, idealism etc. A person who is against assembly line system may imply he or she regards human value more important than instrumental rationality. It is difficult to find the author's value behinds an article by merely evaluating its polarity semantic orientation. A policy or a law has a statistically positive semantic orientation may merely due to the effect of advertisement and promotion. It is hard to know whether most people really approve of a government proposal or not. Therefore, the limitations of polarity opinion analysis are obvious and a more sophisticated *subjectivity-lexicon* is needed to achieve a deeper, more thorough, *multi-dimensional* opinion analysis (MDOA) system.

In this paper, a framework is proposed to learn the reviewers' opinions to the characters (objects) of fictions, rather than their recommendations of the fictions as a whole. The task of MDOA is to learn the dimensions of opinions towards objects, and to analyze opinions and objects from the learned dimensions. A *multi-dimensional* subjectivity-lexicon (MDSL) is learned and generated from corpus. A "subjectivity-term to object" matrix is firstly created from modeling fiction reviews in the blogosphere, and then transforming the subjectivity-terms into a feature-space. The transformation is based on measuring the similarity (or redundancy) between subjectivity-terms. The entities in the MDSL are represented by real-value vectors rather than polarity signs (+/-), which are commonly used in previous studies [9]-[12].

The rest of the paper is organized as following: in the next section, the proposed framework is formally described. In section 3, experiment results are shown. Section 4 is conclusions and future work.

2 Multi-dimensional Opinion Analysis

The proposed framework aims to generate a *vector-space-modeled subjectivity-lexicon* for fiction review analysis. The system structure is shown in Figure 1; the framework consists of four major parts, namely: (i) data collecting, (ii) preprocessing, (iii) transformation, and (iv) opinion analysis.

2.1 Data Collecting

The goal of the data collecting phase is to construct a raw dataset of fiction reviews for building the subjectivity-lexicon. In this phase, reviews (blog posts) of fictions are

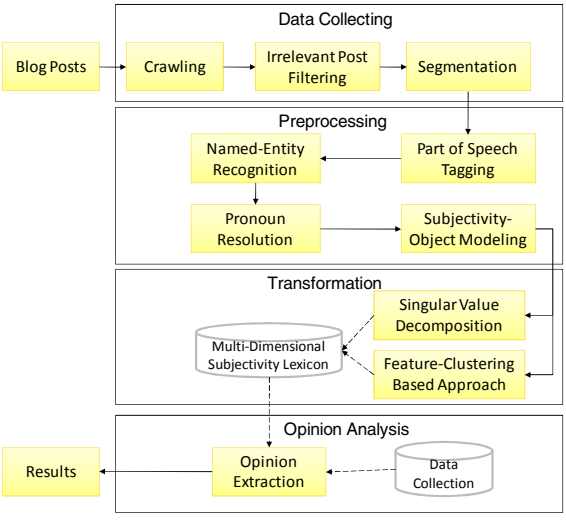

Fig. 1. The overview of multi-dimensional opinion analysis framework

crawled by querying the Google blog search service. Irrelevant posts (not a criticism or irrelevant to the given fictions) are filtered out by a rule-based scheme and human intervention; those remaining posts are considered as relevant reviews, denoted by $R = \{r_i | \ 1 \leq i \leq \text{number of reviews}\}$, and each r_i is segmented into individual sentences, denoted by $\{s_{i,j} | \ 1 \leq j \leq |r_i|\}$, where $|r_i|$=number of sentences in review r_i.

2.2 Preprocessing

The preprocessing phase is to create the "subjectivity-term to object" matrix, the source of the transformation phase, for forming the final vector-space-modeled subjectivity-lexicon. In the current implementation, only adjectives are considered as subjectivity-terms. In this phase, firstly, adjectives (JJs) are identified; secondly, since the objects are referred as person names or person pronouns mentioned in reviews, the named-entity recognition and pronoun resolution are needed; and thirdly, to create the JJ-object matrix, the dependencies between JJs (hereby, denoted as set *JJ*) and objects (hereby, denoted as set *O*) are modeled.

To build the JJ-object matrix, every token in review sentences is tagged by the Stanford POS Tagger and person names are identified by the Stanford Named Entity Recognizer. Also, person pronoun resolution (anaphora resolution) is performed; every third person pronoun is resolved to a person named-entity, which will be resolved to a corresponding fiction character next. Finally, a subjectivity-term to object matrix is constructed by modeling the dependencies of the objects (fiction characters) and their modifiers in reviews. The final "subjectivity-term to object" matrix is denoted as $C_{|JJ|x|O|}=[c_{ij}]$.

2.3 Transformation

The vector model is employed to represent an object $\hat{o}_j$ and a subjectivity-term $\hat{t}_i$. In the transformation phase, the subjectivity-term to object matrix is transformed into a

smaller feature space for three sakes: execution-efficiency in later use, finding semantic relationships between features, and finding subjective relationships between objects. The transformed subjectivity-term vectors are then saved as the multi-dimensional subjectivity-lexicon. Note that, entities in the subjectivity-lexicon are represented as real vectors, and the elements of the vectors are seen as the corresponding degrees between the subjectivity-terms and the un-semantically-tagged attributes, that is, how similar they are from the views of the learned *dimensions*.

The proposed framework employs four different transformation models: Weighting (TF-IDF), Singular Value Decomposition (SVD), Subjectivity-Clustering (SC) (or feature-clustering) based approach [19], and their combination. For the final constructed feature-space, represented by centroids $f_1,f_2,\ldots f_n$, subjectivity-term $\hat{t}_i=(\text{sim}(f_1,t_i), \text{sim}(f_2,t_i),\ldots,\text{sim}(f_n,t_i))$, and object $\hat{o}_j=(\text{P}(f_1|o_j), \text{P}(f_2|o_j),\ldots, \text{P}(f_n|o_j))$ where

$$\text{P}(f_k|o_j) = \log\left(1+\sum_{t_i\in JJ}\text{sim}\left(f_k,t_i\right)c_{ij}\right)$$

2.4 Opinion Analysis

Once the multi-dimensional subjectivity-lexicon (MDSL) is generated, the MDSL can be used for sentiment analysis and mining. A simple clustering is performed on the fiction review collection for evaluation and demonstration, which is given in the experiment section.

3 Experiments

The dataset was created from the blogosphere literature reviews about Gustave Flaubert's *Madame Bovary*, Jane Austen's *Pride and Prejudice*, Fyodor Dostoevsky's *Crime and Punishment*, and Leo Tolstoy's *War and Peace*. The total reviews collected are 191 blog posts, segmented into 8250 sentences, and 73 fiction characters. Taking negation factors into account, the dataset contained 1785 unduplicated subjectivity-terms, as shown in Table 1.

Table 1. Data set

Fiction	Reviews	Sentences	JJs	Characters
Madame Bovary	76	3137	843	13
Pride and Prejudice	61	2561	763	18
Crime and Punishment	23	748	281	19
War and Peace	31	1759	437	23
All Collection	191	8250	1785	73

In the SC transformation and clustering evaluation, the EM algorithm was employed. The generated MDSL was evaluated in terms of the feature entropy of subjectivity-terms and objects. The computation of entropy was specified in [19], in which a lower value indicates a better performance.

The example output of subjectivity-term clustering and object clustering of the proposed MDOA model are shown in Table 2 and 3. The examples show that the

Table 2. Example of subjectivity-term clustering results (MDOA)

Cluster	Words		
Cluster 1	true		
Cluster 2	attractive	decisive	lovely
	clever	smart	quick
	genuine	strong-willed	tolerable
	pretty	female	
Cluster 3	annoyed	generous	ironic
	handsome	ideal	sensible
	inferior	shy	snobbish
	proud	sympathetic	wealthy
Cluster 4	abusive	beloved	dull
	amiable	boring	emotional
	angry	confident	frivolous
	arrogant	crazy	self-centered
Cluster 5	-good	beautiful	desperate
	-happy	young	selfish
	afraid	broken-hearted	naïve
	unhappy	devoted	self-absorbed

Table 3. Example of object-clustering results (MDOA)

Cluster	Characters		
Cluster 1	Lheureux	Homais	Heloise Bovary
	Leon	Justin	Mrs. Bennet
	Berthe Bovary	Lydia Bennet	Miss Bingley
	Mr. Bennet	Charlotte Lucas	Georgiana Darcy
Cluster 2	Emma Bovary	Elizabeth Bennet	Fitzwilliam Darcy
	Charles Bovary		
Cluster 3	Rouault	Katerina Ivanovna	Zossimov
	Hippolyte		
Cluster 4	Rodolphe	Jane Bennet	George Wickham
	Mr. Bingley	Sonya Semyonovna	Rodion
	Mr. Collins	Andrew Bolkonski	Romanovich
	Pierre Bezukhov		

subjectivity-terms and objects clustered together are semantically or subjectively similar to each other. Indeed, in Table 2, the subjectivity-terms in cluster 2 indicate some attractive personalities; cluster 3 consists of some unattractive personalities; cluster 5 implies some unpleasant emotional states. However, cluster 1 consists of only one subjectivity-term, this phenomenon is due to the over-frequently used terms were not filtered out. In Table 3, we can see that characters with common personalities were clustered together; for instance, most characters in cluster 2 are supporting roles with lovely and innocent characteristics (except Lheureux, Homais, and Leon), while in cluster 4, most characters have honest personalities and draw sympathies (except Rodolphe and George Wickham). In cluster 2, those are major characters that encircle love, and are most widely and thoroughly discussed by readers. The result is meaningful and useful for opinion and sentiment analysis. The performance and accuracy may be improved if a larger and more complete dataset is built.

Table 4. Feature evaluation of subjectivity lexicon and objects (with negation and filtering)

Model	Entropy (# of attributes)	
	Subjectivity-Lexicon	Objects
MDOA-weighting	0.966 (73)	0.774 (195)
MDOA-weighting-SVD	0.964 (39)	0.800 (39)
MDOA-weighting-SC	0.921 (4)	**0.644 (4)**
MDOA-weighting-SVD-SC	0.908 (4)	0.805 (4)
MDOA-weighting-SVD-SC (without filtering)	**0.808 (4)**	0.751 (4)
SO	**0.799 (1)**	**0.650 (1)**

To compare with existing polarity opinion analysis approaches, the semantic orientation (hereby, denoted as SO) computed by PMI was implemented [9]. A comparison of the SO model with the proposed MDOA model is shown in Table 4. Here, the MODA model incorporates a cumulative frequency filter and negation factor. The subjectivity-terms (lexicon) and the subjectivity-term to object relationship matrix used in the SO model and the proposed MDOA model are the same; both are constructed by the MDOA model. However, in the SO model, the subjectivity-terms and objects were modeled by calculating their overall SO value, that is object $\hat{o}_j = (\Sigma_i [c_{ij} \mathrm{SO}(t_i)])$. We can see that, both the proposed MDOA model and the SO model had comparable result in terms of the entropy metric. But in the SO model, which was a polarity model, subjectivity-terms and objects were modeled as a value along one dimension.

The example output of object clustering with the SO model used is given in Table 5. We can see that, with the traditional polarity semantic orientation analysis, the clustering could only be done by separating the SO value range. Note that, most characters have negative SO value. Besides, the magnitude of the value could provide little, if any semantic meanings. The magnitude of the value merely implies how often the objects were mentioned in reviews. As mentioned before, a lot of attitudes (such as sympathy, disapproval, disappointment, tragedy, sorrow etc) have negative SO, the SO value alone cannot provide adequate information to distinguish and determine the differences of the subjectivity-terms as well as the objects. Polarity opinion analysis is not adequate for more refined analysis. On the other hand, the proposed MDOA provided a promising result for criticism analysis.

Table 5. Example of object-clustering results (SO)

Cluster	Characters (SO)		
Cluster 1	Leon (4.89)		
Cluster 2	Lheureux (-0.54) Elizabeth Bennet (-5.42) Mr. Bingley (-5.34) Mr. Collins (-9.27)	Berthe Bovary (-10.21) Homais (-1.89) Sofya Semyonovna (0.85) Natasha Rostova (-5.62) George Wickham (-4.50)	Heloise Bovaryais (0.61) Lydia Bennet (-7.545) Miss Bingley (-1.64) Lizaveta Ivanovna (1.05)
Cluster 3	Emma Bovary (-42.1) Charles Bovary (-32.56)	Rodion Romanovich (-28.00)	Pierre Bezukhov (-22.23)
Cluster 4	Rodolphe (-12.37) Jane Bennet (-2.16)	Fitzwilliam Darcy (-12.98) Semyon Zakharovitch (-12.39)	Catherine Bennet (-12.16)

4 Conclusions and Future Work

In this paper, the process flow of opinion mining and sentiment analysis is introduced, and the need of a more sophisticated subjectivity-lexicon for multi-dimensional opinion analysis (MDOA) is described. Moreover, the proposed multi-dimensional subjectivity-lexicon (MDSL) generation framework engineered for analyzing literary criticism, blog posts of fiction reviews, is also formally described. Finally, the merits of this proposed approach are illustrated in the experimental results: first, a MDSL can be generated by learning the usage of subjectivity-terms; secondly, a performance evaluation in terms of feature entropy achieves an up to 31% improvement by applying the proposed transformations; thirdly, reasonable subjectivity-term and object clustering results were obtained in the demonstration of fiction review analysis, and fourthly, the comparison and limitation of traditional polarity opinion analysis is also demonstrated. The proposed framework can also be adapted to other domains which require MDOA techniques.

In the future, we intend to test the proposed MDOA framework with a larger scale database that includes other literature reviews. The framework is planned to incorporate sentence–level opinion extraction and classification mechanisms. To improve the accuracy, more subjectivity-term selection algorithms and criteria, such as graph-based clustering or one which integrates the existing lexicon (General Inquirer), will also be studied. In addition, more completed experiments, such as precision and recall of retrieval and classification results evaluated by expert judgment, will also be performed.

Acknowledgment

This study was supported by the National Science Council, Taiwan, Grant Nos. NSC 98-2221-E-168-032 and NSC97-2221-E-006-144-MY3.

References

1. Liu, B.: Sentiment Analysis and Subjectivity. In: Handbook of Natural Language Processing, 2nd edn. (2010)
2. Pang, B., Lee, L.: Opinion Mining and Sentiment Analysis. Found. Trends Inf. Retr. 2, 1–135 (2008)
3. Tang, H., Tan, S., Cheng, X.: A Survey on Sentiment Detection of Reviews. Expert Systems with Applications 36, 10760–10773 (2009)
4. Riloff, E., Wiebe, J., Wilson, T.: Learning Subjective Nouns Using Extraction Pattern Bootstrapping. In: Proceedings of the seventh conference on Natural language learning at HLT-NAACL, vol. 4, pp. 25–32 (2003)
5. Riloff, E., Patwardhan, S., Wiebe, J.: Feature Subsumption for Opinion Analysis. In: Proceedings of the 2006 Conference on Empirical Methods in Natural Language Processing, Sydney, Australia, pp. 440–448 (2006)
6. Riloff, E., Wiebe, J.: Learning Extraction Patterns for Subjective Expressions. In: Proceedings of the 2003 Conference on Empirical Methods in Natural Language Processing, vol. 10, pp. 105–112 (2003)

7. He, B., Macdonald, C., He, J., Ounis, I.: An Effective Statistical Approach to Blog Post Opinion Retrieval. In: Proceeding of the 17th ACM conference on Information and knowledge management. ACM, Napa Valley (2008)
8. Zhang, W., Yu, C., Meng, W.: Opinion Retrieval from Blogs. In: Proceedings of the Sixteenth ACM Conference on Information and Knowledge Management. ACM, Lisbon (2007)
9. Turney, P.D.: Thumbs Up or Thumbs Down? Semantic Orientation Applied to Unsupervised Classification of Reviews. In: Proceedings of the 40th Annual Meeting on Association for Computational Linguistics, Philadelphia, Pennsylvania, pp. 417–424 (2002)
10. Pang, B.: Thumbs Up? Sentiment Classification Using Machine Learning Techniques. In: Proceedings of the ACL-2002 Conference on Empirical Methods in Natural Language Processing, vol. 10, pp. 79–86 (2002)
11. Shandilya, S.K., Jain, S.: Opinion Extraction and Classification of Reviews from Web Documents. In: IEEE International Advance Computing Conference, pp. 924–927 (2009)
12. Mei, Q., Ling, X., Wondra, M., Zhai, C.M.: Topic Sentiment Mixture: Modeling Facets and Opinions in Weblogs. In: Proceedings of the 16th International Conference on World Wide Web. ACM, Banff (2007)
13. Lu, Y., Zhai, C.X., Sundaresan, N.: Rated Aspect Summarization of Short Comments. In: Proceedings of the 18th International Conference on World Wide Web, pp. 131–140. ACM, Madrid (2009)
14. Chang, C.H., Tsai, K.C.: Aspect Summarization from Blogsphere for Social Study. In: The Seventh IEEE International Conference on Data Mining Workshops, pp. 9–14 (2007)
15. Marneffe, M.C., Manning, C.D.: The Stanford Typed Dependencies Representation. In: Workshop on Cross-framework and Cross-domain Parser Evaluation (2008)
16. Ge, N., Hale, J., Charniak, E.: A Statistical Approach to Anaphora Resolution. In: Proceedings of the Sixth Workshop on Very Large Corpora, pp. 161–171 (1998)
17. Brennan, S.E., Friedman, M.W., Pollard, C.J.: A Centering Approach to Pronouns. In: The Proceedings of the 25th Annual Meeting on Association for Computational Linguistics, Stanford, California, pp. 155–162 (1987)
18. Lappin, S., Leass, H.J.: An Algorithm for Pronominal Anaphora Resolution. Comput. Linguist. 20, 535–561 (1994)
19. Mitra, P., Murthy, C.A., Pal, S.K.: Unsupervised Feature Selection Using Feature Similarity. IEEE Transactions on Pattern Analysis and Machine Intelligence 24, 301–312 (2002)

Enhancing Negation-Aware Sentiment Classification on Product Reviews via Multi-Unigram Feature Generation

Wei Wei[1], Jon Atle Gulla[1], and Zhang Fu[2]

[1] Department of Computer and Information Science,
Norwegian University of Science and Technology, Trondheim, Norway
{wwei,jag}@idi.ntnu.no
[2] Department of Computer Science and Engineering,
Chalmers University of Technology, Gothenburg, Sweden
zhafu@chalmers.se

Abstract. Sentiment classification on product reviews has become a popular topic in the research community. In this paper, we propose an approach to generating multi-unigram features to enhance a negation-aware Naive Bayes classifier for sentiment classification on sentences of product reviews. We coin the term "multi-unigram feature" to represent a new kind of features that are generated in our proposed algorithm with capturing high-frequently co-appeared unigram features in the training data. We further make the classifier aware of negation expressions in the training and classification process to eliminate the confusions of the classifier that is caused by negation expressions within sentences. Extensive experiments on a human-labeled data set not only qualitatively demonstrate good quality of the generated multi-unigram features but also quantitatively show that our proposed approach beats three baseline methods. Experiments on impact analysis of parameters illustrate that our proposed approach stably outperforms the baseline methods.

Keywords: Sentiment Classification, Multi-Unigram Feature Generation, Negation-Aware Classifier.

1 Introduction

As the internet reaches almost every corner in this world, more and more people are used to accessing information on the World Wide Web (WWW). At the meantime, with rapid expansion of Web 2.0 technologies that facilitate people to write reviews and share opinions on products, a large amount of review texts are generated online. These user-generated product reviews not only provide useful information to potential customers but also form credible resources that companies and organizations might make use of to investigate on products and brands. However, as the amount of online product reviews grows rapidly, it becomes impossible for an individual to study product review texts one by one manually. Faced with this problem, research on sentiment analysis was proposed and has become a popular research topic at the crossroads of information retrieval and computational linguistics.

Sentiment analysis concerns analyzing sentiment information expressed within texts. Existing works on sentiment analysis can be divided into two categories. One category

D.-S. Huang et al. (Eds.): ICIC 2010, LNCS 6215, pp. 380–391, 2010.

of works (e.g., [8,1,5,6,7,10,3,27,25,26,22]) are devoted to determining sentiment attitude expressed in texts, which is referred to as "sentiment classification" task. The other category of works (e.g., [9,11,18,12,13,20,28,14,23]) are dedicated to analyzing which aspect of the topic the sentiment is expressed on, which is usually referred to as "attribute-based sentiment analysis" task. In this paper, we mainly focus on the purely "sentiment classification" task, i.e., classifying target texts as positive or negative. The target texts we analyze in this paper are subjective sentences from product reviews.

Unlike other user-generated online texts, product review texts hold a unique intrinsic property, i.e., vocabularies used in product reviews tend to be highly overlapping. For one product, there only exist a finite number of aspects (product's attributes) that can be commented on. For example, for a digital camera, attributes that are usually mentioned in reviews are "price", "LCD", "picture quality" and "battery life", etc. For each reviewed attribute, there are a finite number of vocabularies that are usually involved in sentiment expressing. Therefore, words referred to attributes of a product as well as words for describing sentiment on the attributes will co-appear in the product's review texts with high frequency. For example, in reviews for a digital camera, it is common to locate sentences commenting on a camera's LCD, e.g., "The big and bright LCD makes me enjoy reviewing pictures". In this sentence, words such as "LCD", "big", "bright" not only guide people to catch the sentiment information expressed therein but also are potentially candidate terms to be frequently utilized to express the same opinion on a camera by others. Hence, it is reasonable to argue that if highly-repeated paired terms, e.g., [LCD, big] and [LCD bright], can be appropriately identified as selected features, the accuracy of sentiment classification on product reviews will be improved.

In this paper, we propose an approach to generating multi-unigram features to enhance a negation-aware Naive Bayes classifier for sentiment classification on sentences of product reviews. We coin the term "multi-unigram feature" to represent the process that a new kind of features are produced by our generation algorithm that takes an initial set of unigram feature candidates as input. A negation-aware Naive Bayes classifier implies that in the training and classification process, negation expressions within each review sentences are captured to eliminate the confusion of the classifier. The proposed approach is evaluated against a human-labeled data set. Experimental results demonstrate significant effectiveness of ideas of both the generated multi-unigram features and the negation-aware classifier on improving the classification accuracy. Moreover, extensive experiments on parameters testing show that our proposed approach stably outperforms the other three baseline methods.

The rest of the paper is organized as follows. In Section 2, we present an overview of related works. In Section 3, we present a review on Naive Bayes classifier. After that, we formulate our method in Section 4. The empirical analysis and the results are presented in Section 5, followed by a conclusion and future work presented in Section 6.

2 Related Work

The problem of sentiment classification has drawn great attention within research community. There have already been a lot of research works that are dedicated to solving this problem. With different grouping criterion existing research works can be grouped into different categories.

According to different granularity levels on which sentiment classification is to be analyzed, existing works will mainly fall into two categories: *word-level sentiment classification* and *phrase-level sentiment classification*. The *word-level sentiment classification* is to utilize the polarity orientation of words in each sentence and summarize the overall sentiment of each sentiment-bearing word to infer the overall sentiment within the text [8,1,5,6,7,10,3,27]. The *phrase-level sentiment classification* focused sentiment orientation on phrases not words with concerns that atomic units of expression is not individual words but rather appraisal groups [25]. In [26], the concepts of *prior polarity* and *contextual polarity* were proposed. That paper presented a system that is able to automatically identify the *contextual polarity* for a large subset of sentiment expressions. In [22], an unsupervised learning algorithm was proposed to classify reviews as recommended or not recommended by the average semantic orientation of phrases in the review that contain adjectives or adverbs. Compared with these existing works, our work not only analyzes word-level features but also extends the analysis on multi-word level features. In contrast with phrase-level sentiment analysis, our work is more flexible for dealing with co-appeared words that is not only limited to phrase words.

According to techniques that sentiment classification mainly utilize, existing works can be roughly grouped into rule-based sentiment classification and machine learning sentiment classification. Rule-based methods for sentiment classification is to develop a certain of rules based on which sentiment information can be extracted from texts. In [1], a rule-based algorithm was presented for extracting sentiment-bearing adjectives from WordNet[1]. In [4], the authors proposed to use some linguistic rules to deal with the sentiment classification problem together with a new opinion aggregation function. Machine learning sentiment classification is to utilize traditional machine learning techniques to classify texts by therein sentiment. In [17], it is found that the three employed machine learning methods did not perform as well on sentiment classification as on traditional topic-based categorization. In [16], the relationship between opinion detection and sentiment classification was examined. In that paper, text categorization technique was applied to extract subjective portions of text from documents. In [24], Whitelaw et. al. proposed a Naive Bayes version of Turney's model and provided a framework that enabled human-provided information to be with unlabeled and labeled documents. Although existing machine learning works have already made a certain success on sentiment classification, they did not pay enough attention to co-appeared words and selected them whole as features. In this sense, our work differs with above previous works and is expected to enhance the performance of a Naive Bayes sentiment classifier by the generated multi-unigram features.

Among all the existing publications, ideas in works of [2] and [15] are the most similar to ours. In [2], the authors investigated on the relationships between features and opinion words using a corpus-based approach. However, this work didn't propose to utilize the extracted relationships to generate features for enhancing machine learning sentiment classification. In [15], a range of feature selectors and feature weights with both Naive Bayes and Support Vector Machine classifiers were systematically evaluated. However, it failed to break a new path on generating new features. Unlike this work, our approach is a pioneer on proposing the concept of multi-unigram features

[1] http://wordnet.princeton.edu/

and design an algorithm to identify these features for the accuracy improvement of sentiment classification.

3 Naive Bayes Classifier Review

In this section we will review the basic concept of a Naive Bayes (NB) classifier. An NB classifier is a simple but effective probabilistic classifier on text classification based on applying Bayes' theorem. With the Bayes' rule, the probability of a document d being in class c is computed as:

$$P(c|d) = \frac{P(c)P(d|c)}{P(d)}.$$

Since for each class c, the probability of a document d, i.e., $P(d)$, can be treated equally, with conditional independent assumption on term features of the document d, the probability of d being in c can be derived as:

$$P(c|d) \propto P(c) \prod_{\forall f \in d} P(f|c),$$

where $P(f|c)$ is the conditional probability of a feature f occurring in a document that belongs to class c.

4 Our Method

In this section, we will formulate our method on enhancing the NB classifier of sentiment classification on sentences of product reviews. First, we propose a multi-unigram feature generation algorithm to generate features for NB classification. The generated features not only contains unigram features but also contains multi-unigram features that is a combination of highly-repeated co-appeared terms. Then we make the NB classifier aware of negation expressions in the training and classification process to eliminate the confusions of the classifier that is caused by negation expressions within sentences.

4.1 Multi-Unigram Feature Generation for NB Classifier

In this section we present our proposed method on multi-unigram feature generation for enhancing the NB classifier. In a unigram language model, each unigram presence is usually treated as a feature of the NB classifier. In our method, we coin the term "multi-unigram feature" to represent a new kind of features that are generated with capturing high-frequently co-appeared unigrams in the training data. Before presenting the algorithm on multi-unigram features generation, we need to first perform some necessary preprocessing on the training data to get a set of initial unigram feature candidates.

Preprocessing for Unigram Feature Generation. For the purpose of generating a set of unigram feature candidates, we first employ an existing POS-tagger [21] to conduct a POS-tagging process on all the training data. According to the POS tags associated with each word, we select words only with interesting POS tags, e.g. verbs, nouns, adjectives,

etc. to be unigram feature candidates. Then we perform a stop-word-removing process on the list of unigram feature candidates so that meaningless words, e.g. this, that, will be removed. Furthermore, we transform each word to its stem with the porter stemming algorithm [19] and get a set of stems. We use the set of stems as initial unigram feature candidate set and denote it by F_0.

Multi-Unigram Feature Generation Algorithm. Based on the initial unigram feature candidate set F_0, we propose a Multi-Unigram Feature Generation algorithm to generate a set of multi-unigram features in Algorithm 1. Let $D_{training}$ denote the training data

Algorithm 1. Multi-Unigram Feature Generation Algorithm

1: $F \leftarrow \emptyset$; ▷ initialized to be empty set
2: $F_1 \leftarrow \{f_0 | f_0 \in F_0, f_0.count \geqslant \theta_1\}$; ▷ select unigram features based on appearance frequency
3: **for** ($k = 2$; $F_{k-1} \neq \emptyset$; k++) **do**
4: $F_{cand} \leftarrow \emptyset$; ▷ initialized to be empty set
5: $F_k \leftarrow \emptyset$; ▷ initialized to be empty set
6: **for** all $f_0 \in F_0$ **do** ▷ feature f_0 contains one stem t_0
7: **for** all $f_{k-1} \in F_{k-1}$ **do** ▷ feature f_{k-1} contains $k-1$ stems $\{t_1, t_2, ..., t_{k-1}\}$
8: with $f_0 = \{t_0\}$ and $f_{k-1} = \{t_1, t_2, ..., t_{k-1}\}$
9: **if** $t_0 \notin f_{k-1}$ **then** ▷ if feature f_{k-1} does not contain stem t_0
10: $f_{cand} \leftarrow \{t_0, t_1, t_2, ..., t_{k-1}\}$; ▷ combine f_0 and f_{k-1} to generate a candidate
11: $F_{cand} \leftarrow F_{cand} \cup \{f_{cand}\}$; ▷ put candidate f_{cand} into set F_{cand}
12: **end if**
13: **end for**
14: **end for**
15: **for** all $f_{cand} \in F_{cand}$ **do**
16: **for** all sentences $d \in D_{training}$ **do**
17: **if** f_{cand} occurs in d **then**
18: f_{cand}.count++; ▷ record f_{cand} occurs in d
19: **end if**
20: **end for**
21: **if** $f_{cand}.count \geqslant \theta_2$ **then** ▷ if the number of occurrence satisfy the threshold
22: $F_k \leftarrow F_k \cup \{f_{cand}\}$; ▷ f_{cand} is promoted to be a feature in F_k
23: **end if**
24: **end for**
25: **end for**
26: **return** $F \leftarrow \cup_k F_k$; ▷ return the generated feature set F as a union of all the generated F_k

set. F represents the set of features generated by the proposed algorithm. F is initialized to be an empty set. F_k ($k \geqslant 1$) represents the set of features generated in the k^{th} round. It is worth noting that each feature $f_k \in F_k$ generated in the k^{th} round must contain k stems. When k is equal to 1, any unigram feature candidate $f_0 \in F_0$ is selected to be a member of F_1, if $f_0.count$, i.e., the number of times f_0 occurring in $D_{training}$ is equal to or greater than the threshold θ_1. In the k^{th} ($k \geqslant 2$) round, if the generated feature set in the last round is not an empty set, i.e., $F_{k-1} \neq \emptyset$, the algorithm will continue to generate F_k until the terminal condition is satisfied. In the module of F_k's generation (line 3 - 25

in the Algorithm 1), the candidate feature set F_{cand} and the generated feature set F_k is initialized to be an empty set. The algorithm firstly generates a set of feature candidates in F_{cand} (line 6 - 14 in the Algorithm 1) and then filters out those candidates that occurs in $D_{training}$ less than a threshold of θ_2 times to generate the feature set F_k (line 15 - 24 in the Algorithm 1). In the module between line 6 and line 14 in the Algorithm 1, each feature f_{k-1} generated in the previous round will be combined with each unigram feature candidate f_0. If the stem t_0 of the unigram feature candidate f_0 is not in the stem set $\{t_1, t_2, ..., t_{k-1}\}$ of the feature f_{k-1}, f_0 and f_{k-1} can be combined into be a new feature candidate and be put into F_{cand}. In the module between line 15 and line 24 in the Algorithm 1, the number of occurrence f_{cand}.count of each candidate feature is recorded. The feature candidate f_{cand} in F_{cand} will become a member of F_k, if f_{cand}.count is equal to or greater than the threshold θ_2. Finally, the returned feature set F is a union of all the generated feature set F_k in each round.

4.2 Negation-Aware Classifier

When the NB classifier is applied to sentiment classification on each sentence, negation words like "not", "never", etc. will always be treated as stop words and not be selected as classification features. This is reasonable for text classification according to topics. However, when it comes to sentiment classification, these negation words might become pivotal terms. For instance, a sentence like "I never had a problem with image quality of this camera" is obviously a positive comment on the camera. However, without the negation word "never", this sentence becomes a negative statement. In order to eliminate the confusion caused by negation words, we utilize some specific regular expressions and a list of negation words, e.g., "won't", "never", "without", etc. to catch negation expressions within sentences. Therefore the classifier is able to make necessary adaptation in the training and classification process when negation expressions are identified.

Negation-Aware Training. Let $\mathfrak{n}$ be number of negation expressions identified in a sentence. For example, in sentences like "I cannot take beautiful pictures without this camera" and "This camera is not expensive", $\mathfrak{n}$ will be set to 2 and 1 respectively. In the training process, if $\mathfrak{n}$ of a labeled sentence is not an even number, the training sentence will be treated as from the opposite class of its label. In the above example, although both sentences are positive sentences, feature terms in the first sentence, e.g., "beautiful picture", will be counted in positive class, whereas feature terms in the second sentence, e.g., "expensive" will be counted in negative class.

Negation-Aware Classification. Let $C = \{1, -1\}$ represent a set of classes in the classification, where positive class is represented by 1 ,and negative class is represented by -1. The output of an NB classifier on a sentence d is denoted by $\mathcal{NB}(d)$, i.e., $\mathcal{NB}(d) \in \{1, -1\}$. Then the negation-aware NB classifier should classify a sentence d to be in a class $c \in C$ as:

$$c = (-1)^{\mathfrak{n}_d} \mathcal{NB}(d),$$

where n_d is the number of negation expressions identified in the sentence d. In this way, when observing a testing case like the second sentence in the above example, the

negation-aware NB classifier will be able to classify it to be a positive sentence. However, if without being aware of the negation words, the NB classifier might probably classify the sentence to be a negative one due to the occurrence of the term feature "expensive".

5 Empirical Analysis

In this section, we conduct experiments to perform empirical analysis on our proposed approach. With three implemented baseline methods, our experiments are intended to verify the following issues: (1) whether the generated multi-unigram features enhance the performance of the NB classifier; (2) whether negation-aware NB classifier performs better than the NB classifier without being aware of negation expressions; (3) how the performances of methods in comparison are impacted by the threshold θ_1; (4) how the performances of methods in comparison are impacted by the threshold θ_2.

5.1 Experimental Settings

The proposed approach is empirically analyzed against a human-labeled data set that contains 700 sentences of customer reviews on digital cameras selected from a customer review website[2]. In order to catch the statistical significance of the experimental results, we carry out five separate executions for each experiment. In each separate running of experiment, we randomly select out 100 positive sentences and 100 negative sentences to make a uniformly-distributed testing data so that the accuracy of random-choice method becomes 50%. All the experimental results are averages on results of the five separate executions of the experiments.

5.2 Experimental Results

In order to show the effectiveness of generated multi-unigram features and negation-aware concept respectively, we implement baseline approaches of NB classifier on Unigram features (denoted by NB-U), NB classifier on Multi-Unigram features (denoted by NB-MU), and Negation-Aware NB classifier on Unigram features (denoted by NANB-U). We compare our proposed Negation-Aware NB classifier on Multi-Unigram features (denoted by NANB-MU) with the three implemented baseline methods. In the experiments, the threshold θ_1 is set to 1 for all the approaches, which means that all the unigram feature candidates in the initial set F_0 are selected as features and are utilized to generate new multi-unigram features. The threshold θ_2 is set to 5 for approaches NB-MU and NANB-MU, which means that for a new generated multi-unigram feature candidate, it will be selected as a feature only if it appears at least 5 times in the training data.

Qualitative Evaluation on Generated Features. Tab. 1 presents top ranked generated features according to their frequencies in the training data of "positive" and "negative" classes with our proposed NANB-MU approach in one execution running. From Tab. 1, we can see that most top ranked features for respectively "positive" and "negative"

[2] http://www.consumerreview.com/

Table 1. Top Ranked Features according to Frequencies in Each Class

Class	Top Frequency Features
Positive	<good qualiti build>,<batteri long life>,<excel qualiti imag>, <great len>,<great pictur>,<valu monei>,<good life>,<good grip>,<good pictur>,<high qualiti>, <best camera>,<camera solid>,<feel hold>,<big lcd>,<long life>,<imag fantast>,<imag sharp>, <batteri long>,<great imag>,<built bodi>,<good camera>,<good feel>,<good build>,<feel solid>, <low nois>,<qualiti build>,<work>,<great>,<solid>,<good qualiti>,<good>,<great camera>, <good imag>,<camera like>,<excel>,<nice>,<ergonom>,<best>,<focu fast>
Negative	<heavi weight>,<limit>,<poor>,<problem>,<wait>,<heavi>, <disappoint>,<less>,<paid>,<problem camera>,<bit heavi>,<small>,<disapoint>,<regret>, <plastic>,<hate>,<unaccept>,<creep>,<gear>, <weak>,<flaw>,<shake>,<distort>,<clip>, <late>,<stretch>,<dislik>,<slow speed>,<cost>,<bad>,<dark>,<feel grip>,<nois iso>,<expens>

Table 2. Performance Comparisons

Approaches	Features	Negation-Aware	Parameters		Accuracies in Percent
NB-U	unigrams	no	$\theta_1 = 1$	N/A	0.6630
NB-MU	multi-unigrams	no	$\theta_1 = 1$	$\theta_2 = 5$	0.6850
NANB-U	unigrams	yes	$\theta_1 = 1$	N/A	0.7200
NANB-MU	multi-unigrams	yes	$\theta_1 = 1$	$\theta_2 = 5$	**0.7480**

classes are reasonable and consistent with human beings intuition. Especially, there are features containing multiple unigram stems, such as <good qualiti build> for "positive" class and <heavi weight> for "negative" class, that won't exist in unigram feature set. These multi-unigram features generated by our proposed algorithm are believed to be pivotal features that benefit the NB classifier.

Quantitative Evaluation. Tab. 2 summarizes the results of the three implemented baseline methods as well as our proposed method. From Tab. 2, we can observe that our proposed NANB-MU approach beats the other three baseline approaches. The NB-MU approach performs better than the NB-U approach, which implies that the performance of the NB classifier is improved by the generated multi-unigram features. The NANB-U approach outperforming the NB-U approach verifies that the negation-aware NB classifier produces better results than the NB classifier without being aware of negation expressions.

Impact of Parameter θ_1. The parameter θ_1 controls the frequency threshold that feature candidates in the initial set F_0 are selected as features. If θ_1 is set too small, some non-relevant stems might be selected as unigram features. If θ_1 is set too large, some important stems might be missed. Therefore, the parameter θ_1 is a factor that might impact quality of the generated features and hence affects the classification accuracy. Fig. 1 demonstrates the impact of θ_1 on the classification accuracies of the four approaches, where θ_1 varies from 1 to 30 and θ_2 is set to 5 (if applicable). From Fig. 1, it is interesting to observe that all the four approaches achieve their best performances when the value of θ_1 is set to 1, i.e., all the feature candidates in F_0 are selected as unigram features. It is reasonable since that all the feature candidates in the initial set F_0 are not on the stop-word list and further selected according to their POS tags. This probably ensures that most considered stems in the initial set F_0 are relevant stems. It can be also observed from the Fig. 1 that the accuracies of the four approaches generally decrease as the threshold θ_1 increases. This means when θ_1 becomes larger more useful stems

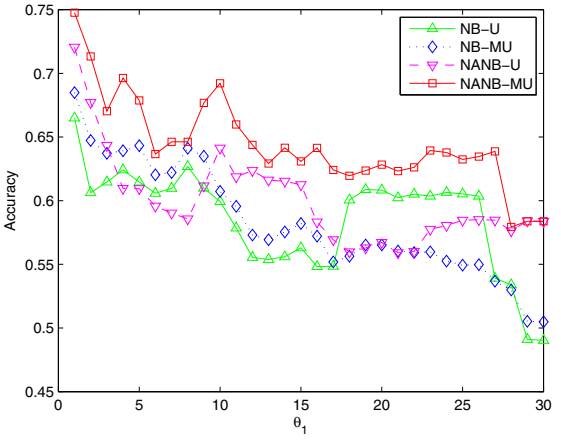

Fig. 1. Impact of θ_1 ($\theta_2 = 5$, if applicable)

will be filtered out of the feature list, so that the performance of classification will be depressed. In Fig. 1, it is important to notice that no matter how the parameter θ_1 varies, our proposed approach always generally outperforms the other three baseline methods.

Impact of Parameter θ_2. The parameter θ_2 controls the frequency threshold that multi-unigram feature candidates are promoted to be features. If θ_2 is set too small, some meaningless multi-unigram features is expected to be generated. If θ_2 is set too large, some useful multi-unigram features is expected to be missed. Therefore, the parameter θ_2 is a factor that might impact quality of the generated features and hence affect the classification accuracy. Fig. 2 shows the impact of θ_2 on the classification accuracy of

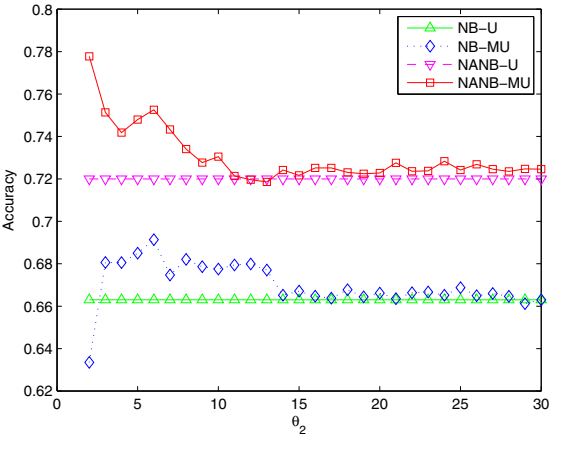

Fig. 2. Impact of θ_2 ($\theta_1 = 1$)

the approaches NB-MU and NANB-MU, where θ_2 varies from 2 to 30 and θ_1 is set to be 1. From Fig. 2, we can observe that as the value of θ_2 increases, the performances of both the approaches of NB-MU and NANB-MU eventually decrease until they reaches respectively the result levels of the approaches of NB-U and NANB-U. This implies that as θ_2 becomes larger, the effectiveness of multi-unigram features will disappear since less multi-unigram features that contains multiple stems can be generated to benefit the classifier. In Fig. 2, it is important to notice that no matter how the parameter θ_2 varies, classifiers with negation-aware (NANB-U and NANB-MU) always beats the classifiers without negation aware (NB-U and NB-MU). From the Fig. 2, It is also observable that as far as some multi-unigram features can be generated (i.e., when θ_2 is not too large), classifiers on the generated multi-unigram features (NANB-MU and NB-MU) outperform classifiers on unigram features (NANB-U and NB-U).

6 Conclusions and Future Work

In this paper, we propose an approach to generating multi-unigram features to enhance a negation-aware Naive Bayes classifier. The term "multi-unigram feature" is coined to represent the process that the generated features are produced by our generation algorithm that takes an initial set of unigram feature candidates as input. We further make the Naive Bayes classifier aware of negation expressions in the training and classification process to eliminate the confusions of the classifier that is caused by negation expressions within sentences. Extensive experiments not only qualitatively show the good quality of the generated features but also quantitatively demonstrate that our proposed approach beats other three baseline methods. That implies a significant effectiveness of ideas of both the multi-unigram features generation and the negation-aware classifier on improving the performance of the original Naive Bayes classifier. Experiments on parameter testings of θ_1 and θ_2 further illustrate that with variance of the parameters our proposed approach is stably superior to the three baseline methods.

Sentiment classification is a very challenging task. Since natural language expression is complicated and varies from time to time, no method can deal with every situation exhaustively. Although our proposed method succeeds in some aspects, when we look at some cases where our proposed method fails, we can still find some situations that are not dealt with very well. When encountering sentences, e.g., "I expected the image would be more sharp", our method will probably fail due to the feature of "image sharp" that is deemed as a strong evidence for "positive" class. Currently our proposed method cannot detect this kind of "hidden" meanings behind words in sentences, e.g., subjunctive sentences. We would like to tackle this problem in the future work.

Acknowledgments

The authors would like to thank the anonymous reviewers for many helpful comments on the manuscript. This work is funded by the Research Council of Norway under the VERDIKT research programme (Project No.: 183337).

References

1. Andreevskaia, A., Bergler, S.: Mining wordnet for a fuzzy sentiment: Sentiment tag extraction from wordnet glosses. In: Proceedings of 11th Conference of the European Chapter of the Association for Computational Linguistics (EACL 2006), Trento, Italy (2006)
2. Chan, K.T., King, I.: Let's tango — finding the right couple for feature-opinion association in sentiment analysis. In: Theeramunkong, T., Kijsirikul, B., Cercone, N., Ho, T.-B. (eds.) PAKDD 2009. LNCS, vol. 5476. Springer, Heidelberg (2009)
3. Devitt, A., Ahmad, K.: Sentiment polarity identification in financial news: A cohesion-based approach. In: Proceedings of 45th Annual Meeting of the Association for Computational Linguistics (ACL 2007), Prague, Czech Republic (2007)
4. Ding, X., Liu, B.: The utility of linguistic rules in opinion mining. In: Proceedings of 30th Annual International ACM Special Interest Group on Information Retrieval Conference (SIGIR 2007), Amsterdam, The Netherlands (2007)
5. Esuli, A., Sebastiani, F.: Determining the semantic orientation of terms through gloss classification. In: Proceedings of 14th ACM Conference on Information and Knowledge Management (CIKM 2005), Bremen, Germany (2005)
6. Esuli, A., Sebastiani, F.: Sentiwordnet: A publicly available lexical resource for opinion mining. In: Proceedings of 5th International Conference on Language Resources and Evaluation (LREC 2006), Genoa, Italy (2006)
7. Hatzivassiloglou, V., McKeown, K.R.: Predicting the semantic orientation of adjectives. In: Proceedings of 35th Annual Meeting of the Association for Computational Linguistics (ACL 1997), Madrid, Spain (1997)
8. Hatzivassiloglou, V., Wiebe, J.M.: Effects of adjective orientation and gradability on sentence subjectivity. In: Proceedings of 18th International Conference on Computational Linguistics (COLING 2000), Saarbrüken, Germany (2000)
9. Hu, M., Liu, B.: Mining and summarizing customer reviews. In: Proceedings of 10th ACM SIGKDD Conference on Knowledge Discovery and Data Mining (KDD 2004), Seattle, USA (2004)
10. Kamps, J., Marx, M., Mokken, R., de Rijke, M.: Using WordNet to measure semantic orientation of adjectives. In: Proceedings of 4th International Conference on Language Resources and Evaluation (LREC 2004), Lisbon, Portugal (2004)
11. Liu, B., Hu, M., Cheng, J.: Opinion observer: analyzing and comparing opinions on the web. In: Proceedings of 14th International World Wide Web Conference (WWW 2005), Chiba, Japan (2005)
12. Liu, Y., Huang, X., An, A., Yu, X.: ARSA: a sentiment-aware model for predicting sales performance using blogs. In: Proceedings of the 30th Annual International ACM Special Interest Group on Information Retrieval Conference (SIGIR 2007), Amsterdam, The Netherlands (2007)
13. Lu, Y., Zhai, C.: Opinion integration through semi-supervised topic modeling. In: Proceedings of 17th International World Wide Web Conference (WWW 2008), Beijing, China (2008)
14. Lu, Y., Zhai, C., Sundaresan, N.: Rated aspect summarization of short comments. In: Proceedings of 18th International World Wide Web Conference (WWW 2009), Madrid, Spain (2009)
15. OḰeefe, T., Koprinska, I.: Feature selection and weighting methods in sentiment analysis. In: Proceedings of the 14th Austraasian Document Computing Symposium (2009)
16. Pang, B., Lee, L.: A sentimental education: Sentiment analysis using subjectivity summarization based on minimum cuts. In: Proceedings of 42nd Annual Meeting of the Association for Computational Linguistics (ACL 2004), Barcelona, Spain (2004)

17. Pang, B., Lee, L., Vaithyanathan, S.: Thumbs up? sentiment classification using machine learning techniques. In: Proceedings of 7th Conference on Empirical Methods in Natural Language Processing (EMNLP 2002), Philadelphia, US (2002)
18. Popescu, A.-M., Etzioni, O.: Extracting product features and opinions from reviews. In: Proceedings of Human Language Technology Conference and Empirical Methods in Natural Language Processing Conference (HLT/EMNLP 2005), Vancouver, Canada (2005)
19. Porter, M.F.: An algorithm for suffix stripping. Readings in Information Retrieval, 313–316 (1997)
20. Titov, I., McDonald, R.T.: Modeling online reviews with multi-grain topic models. In: Proceedings of 17th International World Wide Web Conference (WWW 2008), Beijing, China (2008)
21. Toutanova, K., Manning, C.D.: Enriching the knowledge sources used in a maximum entropy part-of-speech tagger. In: Proceedings of the Empirical Methods in Natural Language Processing Conference (EMNLP 2000), Hong Kong, China (2000)
22. Peter, D.: Turney. Thumbs up or thumbs down? semantic orientation applied to unsupervised classification of reviews. In: Proceedings of 40th Annual Meeting of the Association for Computational Linguistics (ACL 2002), Philadelphia, USA (2002)
23. Wei, W., Gulla, J.A.: Sentiment learning on product reviews via sentiment ontology tree. In: Proceedings of 48th Annual Meeting of the Association for Computational Linguistics (ACL 2010), Uppsala, Sweden (2010)
24. Whitelaw, C., Garg, N., Argamon, S.: Using appraisal groups for sentiment analysis. In: Proceedings of 14th ACM Conference on Information and Knowledge Management (CIKM 2005), Bremen, Germany (2005)
25. Whitelaw, C., Garg, N., Argamon, S.: Using appraisal taxonomies for sentiment analysis. In: Proceedings of 14th ACM Conference on Information and Knowledge Management (CIKM 2005), Bremen, Germany (2005)
26. Wilson, T., Wiebe, J., Hoffmann, P.: Recognizing contextual polarity in phrase-level sentiment analysis. In: roceedings of Human Language Technology Conference and Empirical Methods in Natural Language Processing Conference (HLT/EMNLP 2005), Vancouver, Canada (2005)
27. Yu, H., Hatzivassiloglou, V.: Towards answering opinion questions: Separating facts from opinions and identifying the polarity of opinion sentences. In: Proceedings of 8th Conference on Empirical Methods in Natural Language Processing (EMNLP 2003), Sapporo, Japan (2003)
28. Zhou, L., Chaovalit, P.: Ontology-supported polarity mining. Journal of the American Society for Information Science and Technology (JASIST) 59(1), 98–110 (2008)

Building Associated Semantic Overlay for Discovering Associated Services

Shunxiang Zhang[1,2], Xiangfeng Luo[1,2], Wensheng Zhang[3], Jie Yu[1,2], and Weimin Xu[1,2]

[1] School of Computer Engineering and Science, Shanghai University,
[2] High Performance Computing Center, Shanghai University,
200072, Shanghai, China
[3] Lab. of Complex Systems and Intelligence Science, Institute of Automation, CAS, 100190, Beijing, China
{sxzhang,luoxf,jieyu,wmxu}@shu.edu.cn, wensheng.zhang@ia.ac.cn

Abstract. Due to the lack of associated links among web resources, it is hard for knowledge-based system to provide flexible associated services for users. To solve this problem, Associated Semantic Overlay (*ASO*) is proposed to semantically organize the loose web domain resources and provide support for associated services. First, using the Element Fuzzy Cognitive Maps (*E-FCM*) as the semantic representation of web resources, mapping from keywords to web resources is built to make *ASO* appropriate for the discovery of associated services. Secondly, based on domain keywords and domain association rules, an efficient computing approach of associated links among web resources is presented to automatically build the *ASO*, which can assist the discovery of associated services. Experimental results demonstrate that *ASO* can efficiently provide associated services for users.

Keywords: knowledge discovery, associated semantic overlay, associated service.

1 Introduction

With the growth of web domain resources such as the news of health, sports and environment, how to discover the knowledge (e.g. associated knowledge) from these resources and provide knowledge services for users is a very meaningful work.

The key problem is how to organize web resources to facilitate knowledge discovery. Currently, two types of links are used to organize web resources, hyperlink and Semantic Web (SW). However, hyperlink does not involve any semantic information, which makes it unable to discover associated knowledge. The semantic relations in SW are very detailed and accurate, but the non-automatic construction of SW schemas expressed in either RDF/S[1] or OWL[2] still hinder automatically organizing web resources by machine. To solve the problem mentioned above, Associated Link Networks (ALN) has been proposed in [3] to automatically organize web resources. In the approach of ALN, Element Fuzzy Cognitive Maps (E-FCM [3],[4]) is used as the original semantic representation of data to overcome the non-automatic construction of OWL.

D.-S. Huang et al. (Eds.): ICIC 2010, LNCS 6215, pp. 392–398, 2010.

Associated links among *E-FCM*s can solve the problem that the hyperlink is non-semantics, which are based on domain keywords [5] and association rules [6],[7] among web resources. Associated links in *ALN* are very precise and valuable. However, massive associated links will take up a lot of memory space.

In this paper, we propose Associated Semantic Overlay (*ASO*), which is used as an optional approach of semantic organization of resources. In *ASO*, only a few required associated links are built by real-time computing to discover associated services. Therefore, although the precision of associated links of *ASO* is slightly lower that of *ALN*, *ASO* can avoid storing massive links. Fig.1 shows the layer structure of *ASO*-based associated services system. The bottom level is the domain-oriented data which represents texts of classified web resources on a given website or a domain literature in databases such as Springer. There are no any associated semantic links among these data, so it can not provide associated services directly. Upon this level, *ASO* is built to semantically organize these domain-oriented data and can provide associated links among domain data. Based on *ASO*, the system can automatically discover associated knowledge and provide flexible associated services for users.

The major contributions of our work include two aspects: 1) we propose a building method of *ASO* to solve the lack of associated semantic links among *E-FCM*s (each *E-FCM* semantically represents a description text of web resource); 2) We present an *ASO*-based approach of associated services to meet user's requirements of associated knowledge.

The rest of this paper is organized as follows: Section 2 introduces the building method of *ASO*. Section 3 presents the *ASO*-based approach for discovering associated services. Section 4 presents experimental evaluation of associated services. Conclusions are given in Section 5.

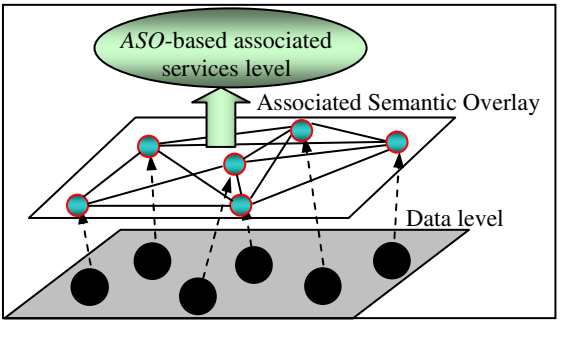

Fig. 1. The layer structure of *ASO*-based associated services system. *ASO* can semantically organize web resources of a domain and provide support for associated services.

2 Building Method of ASO

The procedure of building *ASO* mainly involves two steps computing. The first step is mapping from keywords to *E-FCM*s to help rapidly find those nodes associated with a given node. The second step is computing associated semantic links among the discovered associated nodes.

2.1 Mapping from Keywords to E-FCMs for Building ASO

Based on the extracted domain keywords and all generated *E-FCM*s of a domain, we can complete the mapping from keywords to *E-FCM*s. The computing procedures are as following.

(a) **Matrix construction:** Let m denote the number of *E-FCM*s of a domain and n denote the number of domain keywords, the mapping from *E-FCM*s to keywords can be denoted as matrix EK (i.e.Formula (1)) which can be automatically built according to domain *E-FCM*s. If the i^{th} *E-FCM* contains the j^{th} keyword of a domain, then element $e_i k_j = 1$; else $e_i k_j = 0$.

$$EK = \begin{bmatrix} e_1k_1 & e_1k_2 & \cdots & e_1k_{n-1} & e_1k_n \\ e_2k_1 & e_2k_2 & \cdots & e_2k_{n-1} & e_2k_n \\ \vdots & \vdots & \ddots & \vdots & \vdots \\ e_{m-1}k_1 & e_{m-1}k_2 & \cdots & e_{m-1}k_{n-1} & e_{m-1}k_n \\ e_mk_1 & e_mk_2 & \cdots & e_mk_{n-1} & e_mk_n \end{bmatrix} \tag{1}$$

(b) **Matrix transposition:** Carrying out transposition of matrix EK, we can get transposition matrix $KE = EK^{'}$. The element nonzero $k_i e_j$ in KE represents that the i^{th} domain keyword is an element semantic of the j^{th} *E-FCM*.

(c) **Matrix reduction:** Deleting all zero elements of matrix KE and record column index of nonzero elements of KE, we can complete the mapping from keywords to *E-FCM*s. It is the preliminary organization of *E-FCM*s to help rapidly find associated *E-FCM*s with a given *E-FCM*.

In the procedure of building mapping, the application of matrix operation can facilitate concurrent computation and enhance computing efficiency of this mapping. The time complexity of building mapping from keywords to *E-FCM*s is $O(m*n)$.

2.2 Computing Associated Links among E-FCMs for Building ASO

In this section, an efficient computing approach for building associated links among *E-FCM*s is provided to complete the building of *ASO*. The computing procedure of this approach can be described as follows.

(a) **Matrix construction:** All association rules of a domain can be reflected by matrix KK (i.e.Formula (2)). The element locating in the i^{th} row and the j^{th} column of this matrix is denoted as $k_i k_j$. If there is an association rule from the i^{th} keyword to the j^{th} keyword in a domain, then the element $k_i k_j = 1$; else $k_i k_j = 0$, where, $i, j = 1 \cdots n$.

$$KK = \begin{bmatrix} 0 & k_1k_2 & \cdots & k_1k_{n-1} & k_1k_n \\ k_2k_1 & 0 & \cdots & k_2k_{n-1} & k_2k_n \\ \vdots & \vdots & \ddots & \vdots & \vdots \\ k_{n-1}k_1 & k_{n-1}k_2 & \cdots & 0 & k_{n-1}k_n \\ k_nk_1 & k_nk_2 & \cdots & k_nk_{n-1} & 0 \end{bmatrix} \tag{2}$$

(b) **Picking sub-matrix:** All association rules between two *E-FCM*s are denoted by sub-matrix S_KK (i.e.Formula (3)). The sub-matrix S_KK is generated by directly selecting crossing point of corresponding row and column of matrix KK. That is, we can take the keyword's ID of one *E-FCM* as row index and take the keyword's ID of another *E-FCM* as column index, select corresponding element in matrix KK to constitute sub-matrix S_KK. Suppose the former *E-FCM* contains s keywords and the latter *E-FCM* contains t keywords, obviously, S_KK is a $s \times t$ matrix. Note that there is inequality $s,t \ll n$.

$$S\_KK = \begin{bmatrix} 0 & k_1k_2 & \cdots & k_1k_{t-1} & k_1k_t \\ k_2k_1 & 0 & \cdots & k_2k_{t-1} & k_2k_t \\ \vdots & \vdots & \ddots & \vdots & \vdots \\ k_{s-1}k_1 & k_{s-1}k_2 & \cdots & 0 & k_{s-1}k_t \\ k_sk_1 & k_sk_2 & \cdots & k_sk_{t-1} & k_sk_t \end{bmatrix} \tag{3}$$

(c) **Computation of associated links' strength:** Associated semantic link between two *E-FCM*s is computed by summing up the confidence of all existing association rules as well as all non-zero elements in sub-matrix S_KK.

The second step of building *ASO* provides a fast computing approach of associated semantic link between any two nodes (or two *E-FCM*s), because the small sub-matrix is directly selected from larger matrix KK, not global scanning of larger matrix KK. Therefore, computing of strength of associated semantic link between two nodes is very efficient, and the time complexity is $O(s*t)$.

3 Discovering Associated Services Based on ASO

Associated knowledge is a type of knowledge which has dependency with given knowledge or object. Associated knowledge and the given knowledge are linked by a general relation, association relation, which has many types such as instance, causality, inclusion, affiliation and other relations. Therefore, associated knowledge can provide comprehensive understanding of the given knowledge for users. In this paper, we do not distinguish which type an associated link belongs to, and only focus on how to provide services of associated knowledge. In section 2, we have explained that each node of *ASO* semantically represents a corresponding resource. Therefore, discovering of associated knowledge is find those resources containing associated knowledge with given resource.

From views of graph theory, services of associated knowledge are the computing procedure of finding all 1-order adjacent nodes of the given node from complex associated *ASO*. To efficiently discover all associated knowledge with a given resource, we present the *ASO*-based method of discovering associated services. Consider a given node contains s keywords, and the unique identifier of the i^{th} keyword of the given node is denoted as ID_i. Then the set of keywords' identifiers of this node can be denoted as $Sr = \{ID_i \mid 1 \le i \le s\}$. Fig.3 presents detailed algorithm of *ASO*-based approach for discovering associated knowledge.

Input: a node of given resource; Output: associated services;
(1) According to the *E-FCM* of this node, building the set $Sr = \{ID_i \mid 1 \le i \le s\}$;
(2) for(*i*=1;*i*++;*i*<=*s*)
Picking the column index of nonzero element of ID_i row in sparse binary matrix KK, adding them into $Sc = \{ID_j \mid 1 \le j \le \cdots \le n\}$;
(3) for(*j*=1;*j*++;*j*<=*the number of element in Sc*)
Scanning the ID_j row in the *KE* matrix, adding *E-FCM* ID to the set $Se = \{ID_k \mid 1 \le k \le \cdots \le l\}$;
(4) for(*k*=1;*k*++;*k*<=*the number of element in Se*)
calculate the associated link between the given node and the ID_k node
(5) Output the discovering nodes as associated service
(6) end;

Fig. 2. The algorithm of *ASO*-based associated services

This algorithm mainly includes three sequential computing (i.e. step (2)(3)(4)). The first computing takes each keyword of current node as antecedent to find possible descendant by scanning some rows of association rules matrix KK, and add the possible descendant into the set Sc. The second computing starts from each possible descendant in the set Sc, rapidly finding possible associated nodes by scanning some rows of *KE* matrix. The third computing is calculating associated links among current node and possible associated nodes to prepare the provision of associated services. This algorithm adapts to concurrent computation and efficiently enhances computational efficiency of associated services.

4 Experiments

In this section, we present our experimental evaluation method and the experimental results of associated services.

(a) Evaluation method

In research papers, authors usually propose an approach (or a theory) for solving a problem (or explaining an idea), and arrange all the sections of a paper by a certain sequence, aiming to improve the readability of the paper. Based on this common sense, we propose an evaluation method to verify the precision of associated services.

We pick the sections of every paper except the front-most parts (e.g. abstract) and the rear-most parts (e.g. conclusion, reference). Assigning a unique identifier (i.e. ID) for each selected section to facilitate recognition of all sections, and building corresponding *ASO* by our proposed approach. Starting from each node of *ASO*, we find a maximal associated link by fast computing approach given in section 3. We divide maximal associated links into two types (see Fig.3). If two nodes linked by the discovered associated link belong to the same paper, we name this associated link as inner associated link. On the contrary, we name it as outer associated link. The ratio of inner associated link can be as a measurement of precision of associated services.

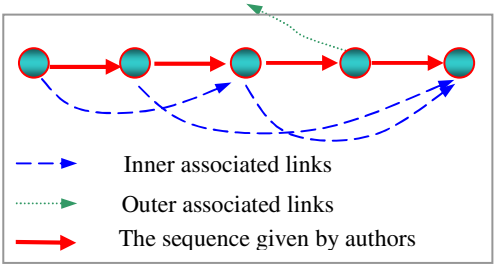

Fig. 3. Two types of maximal associated links

(b) Experimental results

We download all papers on "Transactions on knowledge and data engineering" during 2009.01 to 2009.12, and build seven *ASO*s according to literature in different time spans. The experimental data and results of the seven *ASO*s are listed in table 1.

Table 1. Evaluation of associated services

size	*n-papers*	*n-sections*	*support*	*ratio*	*Time span*
s1	30	168	3.57%	0.81	2009.01 ~ 2009.03
s2	32	184	3.26%	0.82	2009.04 ~ 2009.06
s3	30	178	3.37%	0.83	2009.07 ~ 2009.09
s4	30	175	3.43%	0.80	2009.10 ~ 2009.12
s5	62	352	3.13%	0.82	2009.01 ~ 2009.06
s6	60	353	3.12%	0.83	2009.07 ~ 2009.12
s7	122	705	2.84%	0.85	2009.01 ~ 2009.12

In table 1, *n-papers* and *n-sections* represent the numbers of papers and the picked sections during a given time span; the given *support* (about 3%) ensures that enough associated links are built to help provide associated services; and the *ratio* is the number of inner associated links versus the total of maximal associated links.

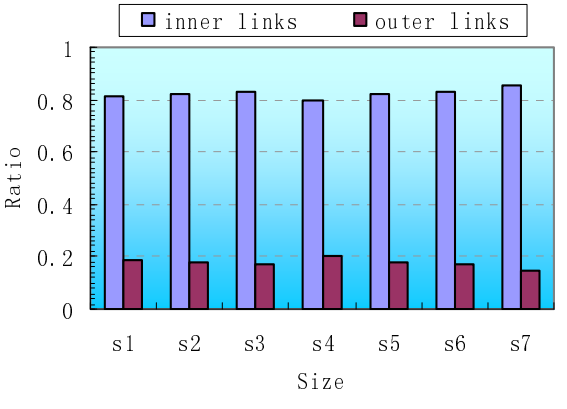

Fig. 4. The measurement of precision of associated services

In Fig.4, we plot the ratio of forward associated links for the seven *ASO*s, comparing it with the ratio of backward associated links. From Fig.4, we find that the ratios of forward associated links all greater than 0.8. It shows that the directions of maximal associated links are consistent with the sequence given by authors, which demonstrates that our approach of associated services is very precise.

5 Conclusion

With the growth of domain-oriented web resources, how to discover associated knowledge from these resources and provide flexible knowledge services for users is a very meaningful task. In this paper, we have proposed a systematic approach for automatically building Associated Semantic Overlay (ASO). ASO is a new virtual technique of semantically organizing and managing the resources of a domain, which can provide associated links among web resources. Based on ASO, an efficient computing approach of services has been proposed, which can automatically discover associated services to satisfy the requirement of users' associated knowledge. The basic operations of matrix including transpose of matrix, picking sub-matrix can facilitate for parallel computing and enhance the efficiency of processing massive data. Experimental results have demonstrated the validity of this method.

Acknowledgement. This Research work is supported by the Shanghai Municipal Science and Technology Commission (project no.09JC1406200), the National Science Foundation of China (project no. 90612010, 60703018) and the Shanghai Leading Academic Discipline Project (J50103). We thank Professor Jin Liu (Wuhan University) for his precious proposal.

References

1. Brickley, D., Guha, R.V.: Resource Description Framework Schema (RDF/S) Specification 1.0, W3C candidate recommendation (2000)
2. Dean, M., Schreiber, G.: OWL Web Ontology Language Reference, W3C recommendation (2004)
3. Luo, X.F., Xu, Z., et al.: Discovery of Associated Topics For the Intelligent Browsing. In: First IEEE International Conference on Ubi-Media Computing, pp. 119–125 (2008)
4. Luo, X.F., Fang, N., et al.: Semantic Representation of Scientific Documents for the E-science Knowledge Grid. Concurrency and Computation: Practice and Experience 20, 839–862 (2008)
5. Luo, X.F., Fang, N., et al.: Experimental Study on the Extraction and Distribution of Textual Domain Keywords. Concurrency and Computation: Practice and Experience 20, 1917–1932 (2008)
6. Orlando, S., Palmerini, P., Perego, R.: Enhancing the Apriori Algorithm for Frequent Set Counting. In: Kambayashi, Y., Winiwarter, W., Arikawa, M. (eds.) DaWaK 2001. LNCS, vol. 2114, pp. 71–82. Springer, Heidelberg (2001)
7. Jiang, T., Tan, A., et al.: Mining Generalized Associations of Semantic Relations from Textual Web Content. IEEE Transactions on knowledge and data engineering 19, 164–179 (2007)

Immunity-Based Model for Malicious Code Detection*

Yu Zhang, Lihua Wu, Feng Xia, and Xiaowen Liu

College of Information Science and Technology, Hainan Normal University,
571158 Haikou, China
bullzhangyu@yahoo.com.cn

Abstract. More and more unknown malware that hide itself in the operating system kernel make the traditional antivirus difficult to detect. Inspired by the biological immune system, we proposed a novel immunity-inspired model for malware detection---IMD. The IMD model extracts the I/O Request Packets (IRPs) sequence produced by the process running in kernel mode as antigen, defines the normal benign programs as self programs, and defines the malwares as nonself programs. By the process behavior monitoring and the family gene analysis, the model can monitor the evolution of malware. The model generates the immature antibodies by vaccination, produces mature antibodies by clonal selection and gene evolution, and then learns and evolutionary identifies the unknown malware by the mature antibodies. Experiments show that the proposed model for unknown malware detection has high detection rate, low false-positive rate, and low omission rate.

Keywords: Malicious code detection, artificial immune system, IRPs sequence, antivirus.

1 Introduction

The rapid development of Internet technology promotes the malware technology with two remarkable characteristics as follows: (1) the increasing number of unknown malwares; (2) the gradual rootkits techniques used by malwares. The former leads to update frequently the malware database, while the latter results in malware hidden in the system kernel, which will steal user sensitive data, monitor user network behavior and attack the networks. The traditional signature antivirus technology is difficult to effectively respond to the challenges of malware of new generation [1]. Therefore, how to effectively deal with such challenges of malware has become an important and urgent problem to resolve [2,3].

Biological immune system with the characteristic of robustness, adaptability, scalability, and efficiency, has the similar functions with the information security system, which brings inspirations for the design of the information security system [4]. Inspired by the biological immune system, researchers have proposed a variety of algorithms and models of artificial immune system that focus on malware detection. Forrest et al. [5] for the first time applied the immune principle to information

* This work was supported by the Science and Technology Project of Hainan Normal University (00203020214).

D.-S. Huang et al. (Eds.): ICIC 2010, LNCS 6215, pp. 399–406, 2010.

security systems, and proposed a general-purpose artificial immune system model named ARTIS. Kephart et al. [6] in IBM corporation proposed a digital immune system---DIS. Harmer et al. [7] proposed a computer immune system model called CDIS. Tao Li [8] presented a dynamic immune-based model for computer virus detection. These artificial immune systems draw inspirations from the biological immune system and have some similar features in functions that regard the normal programs as *Self*, suspicious programs as *Nonself*, malware detectors as antibodies or immune cells, all procedures in the network system as antigen. Moreover, these artificial immune systems generate qualified malware detectors by negative selection mechanism, clonal selection mechanism and genetic evolution mechanism, and detect malware by detectors/antigens matching.

However, the immune systems above still have some shortcomings: (1) the definitions of *Self* and *Nonself* lack flexibility, which do not reflect the dynamic evolution of network environment; (2) low generation efficiency of antibody (detector), which do not make use of the reservation of the best antibody genes; (3) insufficiency of antibody diversity; (4) antigen extraction method is simple and does not reflect the process behavior. These deficiencies led to the big cost of antibody (detector) generation, long detection time, and high false-positive rate.

Given these considerations, the paper proposed a novel immunity-inspired model for malware detection named IMD. The model extracts the I/O Request Packets (IRPs) sequence produced by the process running in kernel mode as antigen, defines the normal benign programs as *Self*, and defines malware as *Nonself*. Moreover, the IMD model can monitor the evolution of malware by the process behavior monitoring and genetic analysis of family genes of malware, learn and evolutionary identify the unknown malware through vaccination, clonal selection, genetic evolution, and afterwards extract the malware genes to update the antibody genes pool. Both theoretical analysis and experiments show that the proposed model has high detection rate and low false-positive rate for unknown malware.

2 Theory of Proposed Model

2.1 The Proposed Model Architecture

The architecture of the proposed model is shown in Figure 1. First, the model forms immature antibody set (immature detectors) by both some new antibodies vaccinated with vaccines extracting from the antibody genes pool and some randomly generated antibodies. Second, the immature antibody set will be divided into two groups by undergoing self-tolerance (negative selection). Those who endure the self-tolerance will evolve into mature antibody set (mature detectors), while those who fail to pass through the self-tolerance (or match one of self) will be removed. Third, some of the mature antibodies will be activated and evolve into memory antibody set (permanent detectors) if they match enough antigens (learning process) in their life cycle, otherwise some mature antibodies will be apoptosis. During this learning process, mature antibodies could cause initial response if they detect and identify malware antigen. These memory antibodies that evolved from the mature antibody set have infinite length of life cycle, during which they will be immediately activated once matching

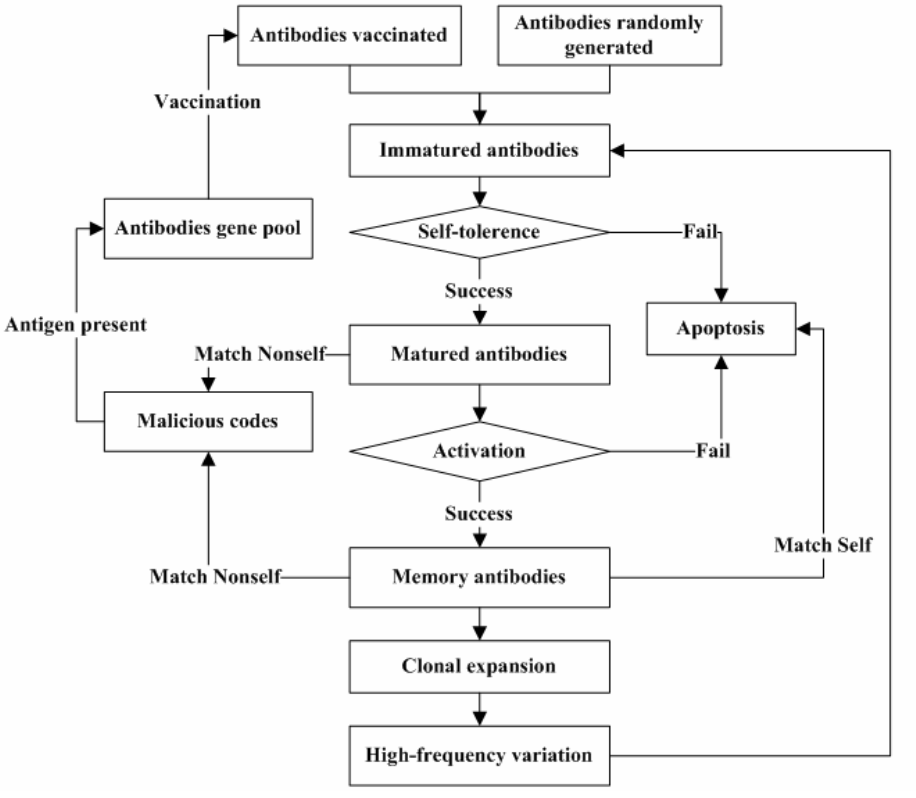

Fig. 1. The Proposed Model Architecture

any antigen, resulting in secondary response. In addition, part of memory antibodies will go through high-frequency variation and clonal expansion to produce new next generation immature antibodies. Finally, the model will extract malware gene by antigen-presenting from these detected malware to form the antibody gene pool. Moreover, the memory antibody set used to detect known malware and the mature antibody set used to unknown malware have different activation threshold values, respectively.

2.2 Antigen

We use I/O Request Packets (IRPs) sequence created by the process running in the kernel mode as antigen based on the following reasons. First, all user mode or running time API functions eventually execute the kernel mode system calls through the system call gate (INT 2E or SYSENTER). Second, those malwares that use rootkits techniques running in kernel mode will directly or indirectly call or hook the kernel mode system calls. Third, the I/O (input and output) operations conducted by the kernel mode system calls eventually complete by passing corresponding IRPs [9] created by I/O Manager to the device driver. Finally, the process dynamic behavior can be acquired by intercepting its IRPs sequence whether generated by user mode

API or kernel mode API. Therefore, the antigen extraction method used in this model reflects the essential characteristics of running process, and thereby overcomes traditional artificial immune system defects in antigen-extracting.

According to experimental observation, the commonly used IRPs types are fifteen or more. For the sake of simplicity, we have encoded these IRPs with hexadecimal characters from 0 to F, respectively, and the others are encoded with character "*". The commonly used IRPs types and their corresponding codes are shown in Table 1.

Table 1. IRPs types and the corresponding codes

IRPs types	Corresponding codes
IRP_MJ_CREATE	0
IRP_MJ_READ	1
IRP_MJ_WRITE	2
IRP_MJ_CLEANUP	3
IRP_MJ_CLOSE	4
IRP_MJ_SHUTDOWN	5
IRP_MJ_PNP	6
IRP_MJ_POWER	7
IRP_MJ_FLUSH_BUFFERS	8
IRP_MJ_QUERY_INFORMATION	9
IRP_MJ_SET_INFORMATION	A
IRP_MJ_DEVICE_CONTROL	B
IRP_MJ_INTERNAL_DEVICE_CONTROL	C
IRP_MJ_SYSTEM_CONTROL	D
IRP_MJ_QUERY_VOLUME_INFORMATION	E
IRP_MJ_SET_VOLUME_INFORMATION	F
Others	*

Definition 1: *Antigen space* is an IRPs sequence set generated by the running processes, which can be expressed as $A = \bigcup_{i=1}^{\infty} H^i$,where H={0,1,2,3,4,5,6,7,8,9,A,B,C,D,E,F,*}, and i is a positive integer.

Definition 2: The *antigen* is an IRPs sequence created by the running process expressed as $Ag = \{x \mid x = \text{IRPs sequence created by the running process}, x \in A\}$.

Definition 3: *Self* are benign Windows system files and application programs in computer, indicted as $N = \{x \mid x = \text{ IRPs sequence created by the malicious codes}, x \in A\}$.

Definition 4: *Nonself* are the files and processes with unusual suspicious behavior in a computer system, expressed as $N = \{x \mid x = \text{IRPs sequence created by the malicious codes}, x \in A\}$.

The above *Self* and *Nonself* meet these conditions as follows: $S \subset Ag$, $N \subset Ag$, $S \cup N = Ag, S \cap N = \phi$.

2.3 Antibody

Definition 5: Antibody is the malware detector extracted from IRPs sequence of *Nonself*, expressed as $Ab = \bigcup_{j=1}^{\infty} H^j$, in which $j < i$ is a positive integer and $Ab \subset N$.

As presented in the literature [1], a negative selection algorithm based on self-tolerance was designed to establish the model ARTIS. Although this elegantly simple algorithm seemed to make a lot of sense, it had problems in training costly the eligible antibodies. To address this problem, we propose a novel negative selection algorithm that creates eligible antibodies based on both *Self* and *Nonself*. The reason we propose such idea is that *Self* and *Nonself* in the process antigen space exist intersection. To specifically speaking, some *Self* programs(benign codes) may be refer a certain technology of *Nonself* programs(malware), and vice versa.

To better simulate real biological functions of antibody in the immune system, the model has establish corresponding antibody evolutionary mechanism as follows.

$$Ab(t) = \begin{cases} Ab_{initial} & , t = 0 \\ Ab(t-1) + Ab_{new}(t), t \geq 1 \end{cases} \quad (1)$$

$$Ab(t-1) = Ab_{immature}(t-1) + Ab_{mature}(t-1) + Ab_{memory}(t-1) \quad (2)$$

$$Ab_{immature}(t-1) = Ab_{new}(t-1) + Ab_{vaccination}(t-1) \quad (3)$$

$$Ab_{mature}(t-1) = \{v \mid v \in Ab_{immature}(t-1) \wedge \forall y \in N \wedge affinity(v, y) \geq \beta\} \quad (4)$$

$$Ab_{memory}(t-1) = \{v \mid v \in Ab_{mature}(t-1) \wedge \forall y \in N \wedge affinity(v, y) \geq \delta\} \quad (5)$$

As shown in above equations, $Ab(t), Ab(t-1) \subset A$ represent the antibody set at time t and t-1, respectively. $Ab_{immature}(t-1), Ab_{mature}(t-1), Ab_{memory}(t-1) \subset A$ mean the immature antibody set, the mature antibody set, and the memory antibody set at time t-1, respectively. $Ab_{new}(t-1)$ stands for the newly random generated antibodies at time t-1. $Ab_{vaccination}(t-1)$ represents the antibodies vaccinated by the vaccines from the antibody genes pool at time t-1. *affinity* ( ) is the affinity function (see section 2.4 below).

2.4 Affinity

The proposed r-step-matching algorithm is based on both immunological theory and software behavior theory. The immunological theory is as follows. First, the antibody in the biological immune system consists of a constant region and a variable region. Second, the gene diversity in antibody variable region makes the antibody combine different antigens. Third, the affinity between the antibody and the antigen is a kind of approximate matching, of which the antibody that has relatively large affinity will be

proliferated. The software behavior theory is as shown below. First, the static property of a program is represented by a data-and-instruction code source file. Second, the dynamic property of a program is expressed by running processes, which is the execution of the program. Third, programs whether malware or benign codes have some commonalities in static source files and dynamic processes. Finally, in terms of malware commonalities, they are composed of a series of malware gene fragments. Therefore, if these malware gene fragments appear in a program, the program could be identify as a malware.

The proposed *r*-step-matching rule is described below in detail.

$$affinity(x, y) = \sum Match(x, y) / l, |x| = l \tag{6}$$

$$Match(x, y) = \begin{cases} 1, & \sum_{i=1}^{n} match(x \rightarrow x_i, y)/n \geq \varepsilon \\ 0, & otherwise \end{cases} \tag{7}$$

$$match(x \rightarrow x_i, y) = \begin{cases} 1, & \exists i, j, j-i \geq |x|, 0 < i \leq j \leq l, x_i = y_j, x_{i+1} = y_{j+1}, ..., x_{|x|} = y_{j+|x|-1} \\ 0, & otherwise \end{cases} \tag{8}$$

where $affinity(x, y)$ indicates the affinity between antibody x and antigen y; $Match(x, y)$ expresses the total match value between antibody x and antigen y; $match(x \rightarrow x_i, y)$ describes the match value between antibody gene fragment x_i and antigen y, l the length of the antibody x, ε the matching threshold value, and n the dimension of the antibody x.

3 Experiments and Results

Due to the specificity of malware detection, the experiments were carried on in an isolated environment or a virtual environment. This study was tested in such virtual environment as VMWare 5.5. The antigen in the model is defined as IRPs sequences created by the processes running in the system kernel-mode, so we use the tool IRP-Trace to capture IRPs sequence. As for the malware type in the experiments, we choose computer viruses, worms, and Trojan horse. These malware were selected from the international authority malware library named WildList [10], which is the source library of the International Computer Security Association ICSA, and the National Software Testing Laboratory NSTL. However, the WildList is only available for malware name and does not provide malware samples. Therefore, the malware samples used in the experiments were derived from VX Heavens [11], which provides a large number of timely updating malware samples.

The Experimental data shown in Table 2 were divided into two groups of which one is for learning and the other is for testing.

Table 2. Experimental sample classification

Self		Malware	
Self-tolerance (for learning)	Immune Recognition (for testing)	Antibody gene pool	Immune Recognition (for testing)
500	500	400	600

As shown in Table 2, there are 500 *Self* for antibody learning and 500 malware for establishing the antibody gene pool. The test samples consist of 500 *Self* and 600 malware which are composed of 500 learned samples(simulating known malware) and 100 unlearned samples(simulating unknown malware).

The steps of the experiments are as follows.

(1) The establishment of *Self* set. The *Self* in the model is the IRPs sequence extracted from 1000 normal Windows system files and application programs with the tool IRPTrace. The *Self* set is composed of 1000 *Self*, of which 500 *Self* are for antibody learning and the rest 500 *Self* for malware test.

(2) The establishment of the antibody gene pool. The whole antibody gene pool consists of 200 malware gene fragments, which are extracted from 200 malware samples. The malware gene fragments are the IRPs sequence captured by the IRPTrace when malware running in a virtual environment VMWare + Windows XP.

(3) The creation of antibodies. The 100 mature antibodies are generated by successfully undergoing the self-tolerance, of which the tolerance objects are composed of both 500 *Self* and 400 *Nonself* samples.

(4) The evolutionary identification and detection of malware. The detection of malware is executed by 100 mature antibodies. The test objects consist of 500 *Self* and 600 malware samples. During the test, if any mature antibody matches a Self, it will be removed; otherwise, if the number of malware it detects is equal to or larger than the threshold value, this mature antibody will evolve into a memory antibody.

The experimental parameters are deployed as follows. The antibody length l is variable, ranging from 4 to 8; the self-tolerance threshold value α=0.1; the mature antibody matching threshold value β=0.4; the memory antibody matching threshold value δ=0.5; the malware detection threshold value ε=0.5. We use detection rate, false-positive rate, and omission rate to assess the proposed detection model performance.

The experimental results are shown in Table 3.

Table 3. The experimental results

Antibody Length l	Detection Rate	Omission Rate	False-positive Rate
4	94.35%	5.65%	1.58%
5	97.56%	2.46%	1.25%
6	95.82%	4.18%	1.42%
7	92.68%	7.32%	3.18%
8	85.12%	14.82%	2.46%

4 Conclusions

The trends that networks are everywhere, system complexity is rising, and systems are easily extensible have a large influence on the recent wide spread propagation of malware. Malwares have been becoming invisible in our computer systems when using rootkits and thus making traditional antivirus difficult to detect. Fortunately, artificial immune system has brought a ray of hope for network security community.

However, traditional artificial immune system has problems of *Self* integrity and detector completeness, which lead to high training costs and difficult to expand. We present a novel immunity-inspired model for malware detection---IMD . We propose the IRPs sequence as the antigen for the first time, and present *Self/Nonself* evolutionary equations, antibody gene pool evolutionary equation, and antibody evolutionary equation which can improve the efficiency of mature antibody generation. By vaccination, self-tolerance, and clonal selection, IMD could dynamically monitor malware evolution, which also improved the detection rate and lower the false-positive rate. The main innovations of the paper are as follows. First, a novel antigen extraction method was proposed which extracts the IRPs sequence of the process running the system kernel-mode as antigen. Second, a novel immature antibody generation method that vaccinates the randomly created antibody was presented. Third, a new self-tolerance method that is based on both *Self* and *Nonself* to produce mature antibody was proposed. Finally, a new antibody/antigen matching algorithm called *r*-step-matching algorithm was presented.

References

1. William, A.W., Anita, K.J.: Reflections on Cybersecurity. Science 13(26), 943–944 (2009)
2. Richard, F., Eugene, H.S.: Happy birthday, dear viruses. Science 13(317), 210–211 (2007)
3. Chang, F.R.: Is Your Computer Secure? Science 31(325), 550–551 (2009)
4. Li, T.: Computer Immunology. Publishing House of Electronics Industry, Beijing (2004)
5. Forrest, S., Perelson, A.S., Allen, L., et al.: Self-Nonself Discrimination in a Computer. In: Proceedings of the IEEE Symposium on Research in Security and Privacy, Oakland, USA (1994)
6. Kephart, J.O.: A Biologically Inspired Immune System for Computers. In: Proceedings on the 4th International Workshop on the Systhesis and Simulation of Living Systems and Artificial Life, pp. 130–139. MIT Press, Cambridge (1994)
7. Harmer, P.K., Paul, D.W., Gregg, H.G., et al.: An artificial immune system architecture for computer security applications. IEEE Transactions on Evolutionary Computation 6, 252–280 (2002)
8. Li, T.: Dynamic Detection for Computer Virus based on Immune System. Science In China Series F: Information Science 51, 1475–1486 (2008)
9. IRP (2010), `http://en.wikipedia.org/wiki/I/O_request_packet`
10. The WildList Organization International (2010), `http://www.wildlist.org`
11. VX Heavens (2010), `http://vx.netlux.org`

Sparse Representation-Based Face Recognition for One Training Image per Person

Xueping Chang, Zhonglong Zheng*, Xiaohui Duan, and Chenmao Xie

Department of Computer Science, Zhejiang Normal University, Zhejiang, China
zhonglong@zjnu.cn cxp0407@163.com

Abstract. In this paper, motivated by the recent development of sparse representation (SR) and compressive sensing (CS), in order to address one sample problem, we propose two approaches: shifted images +SRC (SSRC) and reconstructed images +SRC (RSRC). Specifically, we generate the multiple images by shifting the original image or reconstructing the original image via PCA(Principle Component Analysis), and regard new images as training samples, and then apply SRC (Sparse Representation-based Classification) on new training samples set. The experimental results on the two popular face databases (ORL and Yale) demonstrate the feasibility and effectiveness of our proposed methods.

Keywords: Face recognition, One sample problem, PCA, SRC.

1 Introduction

Face recognition (FR) is one of the most active research areas in computer vision and pattern recognition. However, in many application scenarios, such as law enforcement, driver license or passport card identification, surveillance photo identification, we actually collect one training sample per person, which makes the task of FR more difficult.

Recently, sparse representation (SR) has proven to be an extremely powerful tool for acquiring, representing, and compressing high-dimensional signals[1-5]. In the past few years, compressive sensing (CS) proposed by D. Donoho, E. Candes, T. Tao et al make SR reach a new level. SR has been successfully applied to solve many practical problems in signal processing, statistics, and pattern recognition [6-10].

In this paper, motivated by the recent development of SR and CS, in order to address one sample problem, we generate the multiple images by shifting the original image, and regard shifted images as new training samples, or consider the reconstructed images of the original image by PCA and the original ones as new training samples, and then apply SRC on the new training images available. Experiments on the well-known ORL database show that the proposed two methods are about 5.56%

* Corresponding author.
The authors confirm that the research was supported by National Natural Science Foundation (No.60805001), National High-Tech Research and Development Plan (No.2007AA01Z164), and Zhejiang Provincial Natural Science Foundation (Y1090579), China.

D.-S. Huang et al. (Eds.): ICIC 2010, LNCS 6215, pp. 407–414, 2010.

and 2.78% more accurate than the original SRC method when considered in the context of one training sample face recognition problem. Moreover, the feasibility and effectiveness of the proposed two methods are also verified on the famous Yale database with promising results.

2 Generating Redundant Samples

The lack of adequate training samples in the available image collections is one key technical barrier that one sample problem for face recognition solutions have to overcome. Increasing redundant information of the sample is an effective way to solve one sample problem.

2.1 Generating Shifted Images

Given a face image matrix D of size $M \times N$, we generate the following $m \times n$ number of synthesized (shifted) images with size of $l \times r$:

$$D_{ij} = D(i:(l+i-1), j:(r+j-1)), \qquad 1 \le i \le m, 1 \le j \le n, \tag{1}$$

where m and n are parameters, $l = M - m + 1$ and $r = N - n + 1$. When $m = n = 1$, there is only one shifted image, i.e., the original face image; when m and n are relatively small, say $m = n = 3$, there are 9 shifted images (illustrated in Fig.1) that resemble the original face image visually; and when m and n are very large, say $m = M$ and $n = N$, there are $M \times N$ number of shifted images that contain little visual information, since they reduce to points. Therefore, the values of m and n trade off the number of the shifted images and the information delivered [11].

We regard the multiple images by shifting the original image as new training samples for training. For example, we select one sample image per person for training in the experiments based on ORL database (There are 10 sample images of each of 40 distinct persons in the ORL database). when $m = n = 3$, we can get 360 shifted images (9 shifted images of each of 40 distinct persons) for training.

Fig. 1. Illustration of a face image D and its 9 shifted images D_{ij}'s with $m = n = 3$

2.2 Generating Reconstructed Images by PCA

PCA is one of the most successful techniques used in face recognition. And it is an unsupervised linear technique which provides an optimal, in the mean square error sense, representation of the input in a lower dimensional space. It tries to find eigenvectors of sample covariance matrix that corresponds to the direction of principal components of original data.

One can compute the eigenvalues and eigenvectors of the sample covariance matrix. The first k eigenvectors, corresponding to the k largest eigenvalues are forming the transform matrix. The cardinality of the transform matrix, namely k, is chosen such that $\frac{\sum_{i=1}^{k}\lambda_i}{\sum_{i=1}^{c}\lambda_i}$ is greater than a threshold θ [12].where λ_i is the i th eigenvalue of the sample covariance matrix.

According to these characters of PCA, we reconstruct face images by setting different value of θ so as to obtain redundant samples. And we regard reconstructed face images as independent samples, combined with the original face images, for training. An example is depicted in Fig.2.

Fig. 2. The original image and reconstructed images by PCA according to different value of θ ($\theta = 0.99, \cdots, 0.85$).

3 SRC

The key idea of SRC is that one can exploit the discriminative nature of sparse representation to perform classification. Instead of using the generic dictionaries discussed above, one can represent the test sample in an overcomplete dictionary whose base elements are the training samples themselves. If sufficient training samples are available from each class, it will be possible to represent the test samples as a linear combination of just those training samples from the same class. This representation is naturally sparse, involving only a small fraction of the overall training database. We argue that in many problems of interest, it is actually the sparsest linear representation of the test sample in terms of this dictionary and can be recovered efficiently via l_1-minimization. Seeking the sparsest representation therefore automatically discriminates between the various classes present in the training set (see [2-3] for details).

4 Experimentation

In order to demonstrate the validity of the proposed solution, the well-known ORL database[2] and Yale database[3] are used in our experimentation. Before the experiment, all face images are rotated and scaled so that the centers of the eyes are placed on specific pixels and the image size is normalized to 32×32. For each person, we select one sample image per person for training and the rest images for testing.

[2] http://cvc.yale.edu/projects/yalefaces/yalefaces.html
[3] http://www.cl.cam.ac.uk/Research/DTG/attarchive/facesataglance.html

4.1 ORL Database

Fig.3 dipicts 10 sample images of one person in the ORL database. In the experiment SSRC, the value of m and n trade off the number of the shifted images and the information delivered. Therefore, one can obtain different number of shifted images according to different values of m and n. We have observed in the experiments that $m = n = 4$ is better for the proposed SSRC approach. As shown in the table 1, experiments show that the proposed two methods are about 5.56% and 2.78% more accurate than the original SRC method, respectively. Fig.4 shows the recognition rates of SSRC when m and n take different values. Similarly, we can get different recognition results of RSRC with varying the number of θ we take when reconstructing images by PCA, as shown in Fig.5. Fig.6 and Fig.7 illustrate the recognition rate of SPCA (shifted images + PCA+NNC) and SLDA (shifted images + LDA(Linear Discriminative Analysis)+NNC) with varying values of m and n.

Fig. 3. Some sample images of ORL database

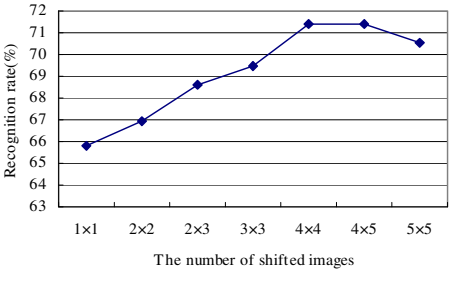

Fig. 4. Recognition rate of SSRC with varying values of m and n

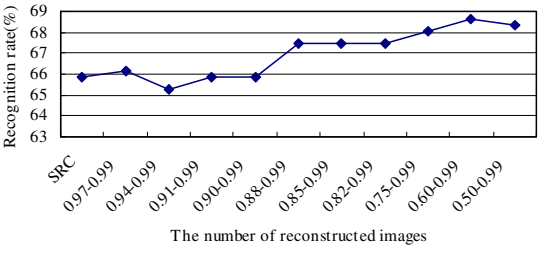

Fig. 5. Recognition rate of RSRC with varying the number of θ

Table 1. Comparison of recognition rate of SSRC, RSRC and SRC

Methods	Recognition rate
SSRC	71.39% ($m = n = 4$)
RSRC	68.61% （ $\theta = 0.99,\cdots,0.60$ ）
SRC	65.83%

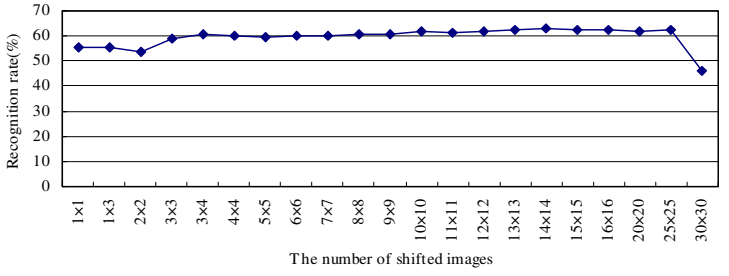

Fig. 6. Recognition rate of SPCA with varying values of m and n

Fig. 7. Recognition rate of SLDA with varying values of m and n

The following table 2 depicts that SPCA outperforms significantly the traditional PCA+NNC method and SLDA and RLDA (reconstructed images +LDA +NNC) extraordinary outperform the traditional LDA+NNC method. The recognition rate of SPCA is 62.78% ($m = n = 14, \theta = 0.95$), while that of PCA+NNC is 55.56% ($\theta = 0.95$). SPCA is about 7.22% more accurate than the traditional PCA+NNC method. Comparing with the traditional LDA+NNC method (12.22%), SLDA (66.94%) and RLDA (58.06%) give 54.72% and 45.84% improvement respectively. Experimental results of RLDA with varying the number of θ are given by the following Fig.8.

Table 2. Comparison of recognition rate of SPCA, SLDA, RLDA, PCA+NNC and LDA+NNC

Methods	Recognition rate
SPCA	62.78% ($m = n = 14, \theta = 0.95$)
SLDA	66.94% ($m = n = 2$,39 dimension)
RLDA	58.06%($\theta = 0.99, \cdots, 0.94$,39dimension)
PCA+NNC	55.56% ($\theta = 0.95$)
LDA+NNC	12.22%(39 dimension)

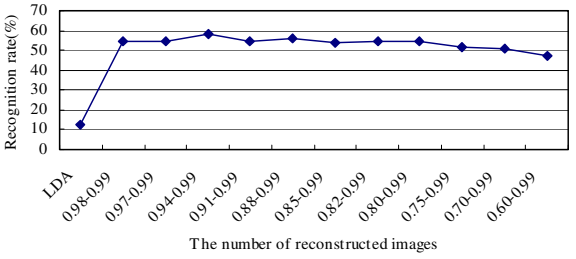

Fig. 8. Recognition rate of RLDA with varying the number of θ

4.2 Yale Database

Fig.9 shows some sample images of one individual in the Yale database. Recognition rates of SSRC with varying values of m and n are given by the following Fig 10. As shown in Fig.10, we can see that in the best situation, the recognition rate of SSRC achieves 70%. Similarly, we can get different recognition results of RSRC with varying the number of θ we take when reconstructing images by PCA. However, as shown in Fig.11, RSRC performs poorly in the Yale database. Experiments in the following table 3 show that SSRC outperform the original SRC method. For instance, SSRC achieves 70% recognition rate, whereas SRC (57.33%) performs poorly. SSRC are about 12.67% more accurate than the original SRC method.

Fig. 9. Some sample images of Yale database

Fig. 10. Recognition rate of SSRC with varying values of *m* and *n*

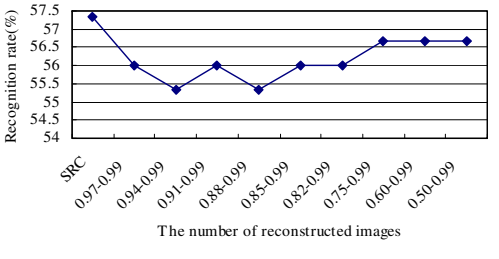

Fig. 11. Recognition rate of RSRC with varying the number of θ

Table 3. Comparison of recognition rate of SSRC, RSRC and SRC

Methods	Recognition rate
SSRC	70% ($m = n = 6$)
SRC	57. 33%

Experimental results given by the following table 4 show that SPCA, SLDA, and RLDA outperform significantly the traditional PCA+NNC and LDA +NNC method. The recognition rate of SPCA is 71.33% ($m=n=25, \theta=0.95$), while that of PCA+NNC is 44.67% ($\theta=0.95$).Comparing with the traditional LDA+NNC method (16%), SLDA (66%) and RLDA (52.67%) give 50% and 36.67% improvement respectively. Fig. 12 and Fig.13 illustrate the recognition rate of SPCA and SLDA with varying values of m and n. Experimental results of RLDA with varying the number of θ we take are given by the following Fig. 14.

Table 4. Comparison of recognition rate of SPCA, SLDA, RLDA, PCA+NNC and LDA+NNC

Methods	Recognition rate
SPCA	71.33% ($m=n=25, \theta=0.95$)
SLDA	66% ($m=3, n=4$,14 dimension)
RLDA	52.67%($\theta=0.99,0.98$,14 dimension)
PCA+NNC	44.67%($\theta=0.95$)
LDA+NNC	16%(14 dimension)

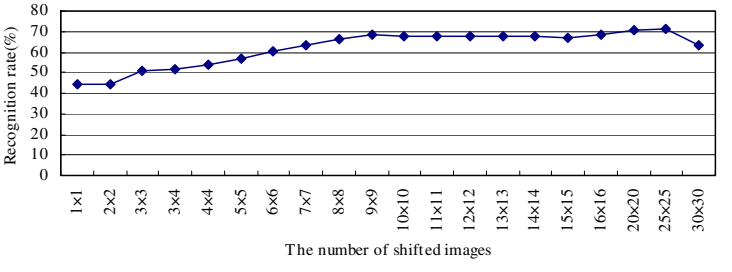

Fig. 12. Recognition rate of SPCA with varying values of m and n

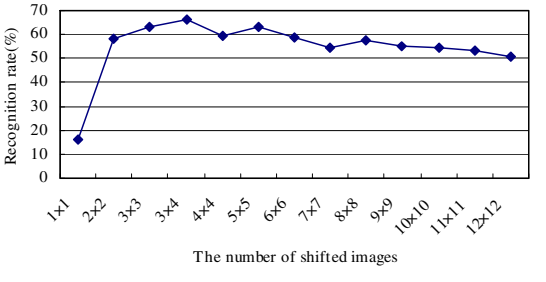

Fig. 13. Recognition rate of SLDA with varying values of m and n

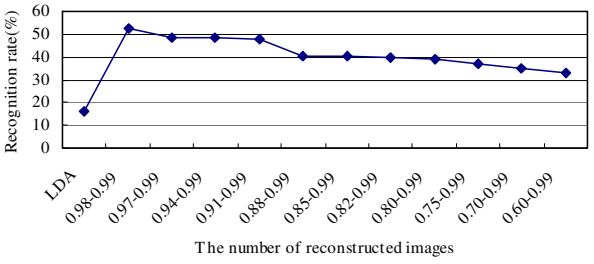

Fig. 14. Recognition rate of RLDA with varying the number of θ

5 Conclusion

In this paper we have proposed SSRC and RSRC, the extension of SRC to perform face recognition when just one sample per training class is available. The feasibility and effectiveness of the proposed methods are verified on the two famous face databases (ORL and Yale) with promising results.

References

1. Boufounos, P., Baraniuk, R.: Quantization of sparse representations. In: Proceedings of the 2007 Data Compression Conference (2007)
2. Wright, J., Yang, A.Y., Ganesh, A., Sastry, S.S., Ma, Y.: Robust face recognition via sparse representation. IEEE Transactions Pattern Analysis and Machine Intelligence 31, 210–227 (2009)
3. Wright, J., et al.: Sparse representation for computer vision and pattern recognition. Proceedings of IEEE (2009)
4. Huang, K., Aviyente, S.: Sparse representation for signal classification. In: Neural Information Processing Systems (2006)
5. Qiao, L., Chen, S., Tan, X.: Sparsity preserving projections with applications to face recognition. Pattern Recognition 43, 331–341 (2010)
6. Donoho, D.: Compressed sensing. IEEE Transactions on Information Theory 52, 1289–1306 (2006)
7. Candès, E.: Compressive sampling. International Congress of Mathematicians 3, 1433–1452 (2006)
8. Baraniuk, R.: Compressive sensing. IEEE Signal Processing Magazine 24, 118–121 (2007)
9. Candes, E.J., Tao, T.: Decoding by Linear Programming. IEEE Transactions on Information Theory 51, 4203–4215 (2005)
10. Candès, E.J., Tao, T.: Reflections on compressed sensing. IEEE Information Theory Society Newsletter 58, 20–23 (2008)
11. Liu, J., Chen, S., Zhou, Z., Tan, X.: Single image subspace for face pecognition. In: Zhou, S.K., Zhao, W., Tang, X., Gong, S. (eds.) AMFG 2007. LNCS, vol. 4778, pp. 205–219. Springer, Heidelberg (2007)
12. Wang, J., Plataniotis, K.N., Venetsanopoulos, A.N.: Selecting discriminant eigenfaces for face recognition. Pattern Recognition Letters 26, 1470–1482 (2005)

Semi-supervised Local Discriminant Embedding

Chuan-Bo Huang and Zhong Jin

School of Computer Science and Technology,
Nanjing University of Science and Technology, Nanjing 210094, China
huangjunfengcq@126.com

Abstract. In the paper, we present an improved approach based on Semi-supervised Discriminant Analysis (SDA), called semi-supervised local discriminant embedding (SLDE), for reducing the dimensionality of the feature space. We take the manifold structure into account and try to learn a subspace in which the Euclidean distances can better reflect class structure of the images. The weight matrix and the scatter matrices in SDA are improved to make efficient use of both labeled and unlabeled images. After being embedded into a low-dimensional subspace, the similar images maintain their intrinsic neighbor relations, whereas the dissimilarity neighboring images no longer stick to one another. Experiments have been carried out to validate our approach.

Keywords: semi-supervised learning, local discriminant embedding, nearest neighbor, label propagation.

1 Introduction

Dimensionality reduction is broad in solving many computer vision and pattern recognition problems. Principle component analysis (PCA) is widely used for linear dimensionality reduction. Techniques originated from manifold learning such as Isomap, LLE , and Laplacian Eigenmap consider nonlinear dimensionality reduction by investigating the local geometry of data set. Such embeddings are good for representation, but only concern with the training data. To facilitate nearest-neighbor searches for new test data, BoostMap and locality preserving projection (LPP) attempt to reconstruct data localities or similarities in the low-dimensional Euclidean space. LPP is linear and more crucially is defined everywhere in ambient space rather than just on the training data points. LPP has been applied to face recognition and image retrieval. More recently, Local discriminant embedding (LDE) is proposed to overcome the drawbacks of LPP.

The above-mentioned linear or nonlinear dimensionality reduction approaches are generally not devised for classification. However, Linear Discriminant Analysis (LDA) seeks the best projection subspace for separating data, and is shown to be an useful tool for feature extraction of classification. However, when there is no sufficient labeled samples relative to the number of dimensions, the covariance matrix of each class may not be accurately estimated. In this case, the generalization capability on labeled samples can not be guaranteed. A possible solution to deal with insufficient labeled samples could be learning by making use of both labeled and unlabeled

D.-S. Huang et al. (Eds.): ICIC 2010, LNCS 6215, pp. 415–422, 2010.

data. It is natural and reasonable since in reality we usually have only part of input labeled data, along with a large number of unlabeled data. Thus, semi-supervised dimensionality reduction, using some labeled data and lots of unlabeled data to find a low-dimensional representation, is of great practical importance.

In the last decades, semi-supervised learning has attracted an increasing amount of attention. Recently, there are considerable interest and success on graph based semi-supervised learning algorithms, which consider the graph over all the samples as a prior to guide the decision making. All these algorithms considered the problem of classification, either transductive or inductive. In this paper, we introduce a improved Semi-supervised dimensionality reduction algorithm based on semi-supervised Discriminant Analysis (SDA)[1], semi-supervised local discriminant embedding (SLDE), which can more accurately characterize the geometrical and discriminant structure of the data manifold.

2 Related Work

2.1 Linear Neighborhood Propagation (LNP)

LNP[2] is carried out under the framework of an intrinsic Gaussian Markov random field, which can iteratively propagate the labels of the labeled data to the remaining unlabeled data on the constructed graph.

2.1.1 Construct the Graph

Let $X = \{x_1, x_2, \cdots, x_i, \cdots x_n\}$, $X \subset R^m$ be an m-dimensional data feature space, $\{x_i\}_{i=1}^{l}$ is a labeled data set, the remaining $\{x_i\}_{i=l+1}^{n}$ is an unlabeled data set. LNP constructs the graph not only by considering pairwise relationships in traditional graph-based methods, but also by using the neighborhood information of each point. For computational convenience, assume that all these neighborhoods are linear, i.e. each data point can be optimally reconstructed using a linear combination of its neighbors. Hence objective is to minimize:

$$E_i = \left\| x_i - \sum_{j:x_j \in N(x_i)} w_{ij} x_j \right\|^2 \tag{1}$$

Where $N(x_i)$ is the set of the k-nearest neighbors of the point x_i .To avoid having a negative energy, we further constrain $\sum_{j:x_j \in N(x_i)} w_{ij} = 1$ and $w_{ij} \geq 0$. Usually, the more similar x_j is to x_i, the larger w_{ij} will be. Thus, w_{ij} can be used to measure the similarity degree from x_j to x_i.

After all the reconstruction weights are computed, a sparse matrix W is constructed by:

$$W = (w_{ij})_{n \times n} \tag{2}$$

2.1.2 Label Propagation

Suppose there are b class data in the data database. Let $F = [F_1^T, F_2^T, \cdots, F_n^T]^T$, $F \in R^{n \times b}$ be the predicted label matrix, where $F_i \in R^b$ $(1 \le i \le n)$ are row vectors and $0 \le F_{ij} \le 1$. Initially, we set the label matrix $B = [B_1^T, B_2^T, \cdots, B_n^T]^T$, $B \in R^{n \times b}$, where $B_i \in R^b$, $(1 \le i \le n)$ are row vectors. $B_{ij} = 1$ if x_i is labeled as l_j and $B_{ij} = 0$ otherwise. In order to facilitate the calculating, we normalize the weight matrix W, i.e., $P = D^{-1}W$, where D is the diagonal matrix, $D_{ii} = \sum_j W_{ij}$. The labels of each data object will be updated until convergence, as follows [3]:

$$F = (I - I_\alpha)(I - I_\alpha P)^{-1} B \tag{3}$$

where I_α is an $n \times n$ diagonal matrix with the i-th entry being α_i $(0 \le \alpha < 1)$, α_i is the fraction of label information that data x_i receives from its neighbors during the iteration.

2.2 Semi-supervised Discriminant Analysis

For X, we can use a k-nearest neighbor graph G to model the relationship between nearby data points. Specifically, we put an edge between nodes i and j if x_i and x_j are "close", i.e., x_i and x_j are among k nearest neighbors of each other. Let the corresponding weight matrix be S, defined by

$$S_{d,ij} = \begin{cases} 1, & if\ x_i \in N_k(x_j)\ or\ x_j \in N_k(x_i) \\ 0, & otherwise. \end{cases} \tag{4}$$

Let a is a projection vector, then $y_i = a^T x_i$. If two data points are linked by an edge, they are likely to be in the same class. Moreover, the data points lying on a densely linked subgraph are likely to have the same label. Thus, a reasonable criterion for choosing a good map transformation vector a is to optimize the following objective functions:

$$\min \sum_{i,j} \left\| a^T x_i - a^T x_j \right\|^2 S_{d,ij} \tag{5}$$

where $S_{d,ij}$ evaluate the local structure of the data space. The objective function with the choice of symmetric weights $S_{d,ij}$ ($S_{d,ij} = S_{d,ji}$) incurs a heavy penalty if neighboring data points x_i and x_j are mapped far apart. Therefore, minimizing it is for the purpose of ensuring that if x_i and x_j are close then y_i and y_j are close as well. $S_{d,ij}$ can be thought of as a similarity measure between objects.

For the objective function of LDA, when there is no sufficient training sample, overfitting may happen. A typical way to prevent overfitting is to impose a regularizer, the optimization problem of the regularized version of LDA can be written as follows:

$$\max_{a} \frac{a^T S_b a}{a^T S_t a + \beta(a^T X L_d X^T a)} \tag{6}$$

The projective vector a that maximizes the objective function is given by the maximum eigenvalue solution to the generalized eigenvalue problem:

$$S_b a = \lambda(S_t + \alpha X L X^T)a \tag{7}$$

3 SLDE Method

In this section, we combining two ideas together and introduce an improved construction algorithm i.e., SLDE method.

3.1 Idea

Denote by X the data matrix whose column vectors are data points. In order to discover both geometrical and discriminant structures of the data manifold, construct graphs G_d. Let $N_k(x_i)$ denotes the set of k-nearest neighbors of x_i. For each data point x_i, the set $N_k(x_i)$ may contain unlabeled data. However, there is reason to assume that these data are likely to be related to x_i if they are sufficiently close to x_i [4]. Try to learn a subspace in which the Euclidean distances can better reflect class structure of the images. Let $S_d \in R^{n \times n}$ be the weight matrices of G_d. It is defined as follows:

$$S_{d,ij} = \begin{cases} \gamma, \ \textit{if both nodes } x_i \textit{ and } x_j \textit{ have the same label}, \\ 1, \ \textit{if node } x_i \textit{ or } x_j \textit{ is unlabeled} \\ \quad \textit{but } x_i \in N_k(x_j) \textit{ or } x_j \in N_k(x_i), \\ 0, \ \textit{otherwise.} \end{cases} \tag{8}$$

where r is a suitable constant. When both data points are relevant, it is with high confidence that they share the same label. Therefore, the value of $S_{d,ij}$ should relatively be large.

In order to keep the labeled data with the initial label information, for the each step iteration, Eq.(3) can be changed as follows:

$$F_i = \begin{cases} B_i, \ if \ x_i \ is \ labeled, \\ (I - I_\alpha)(I - I_\alpha P)^{-1} B_i, \ otherwise. \end{cases} \tag{9}$$

After finishing the label propagation, we obtain the probability F_{ij} of each data x_i belonging to class j. In LDA, the scatter matrices S_b and S_t are defined as $\tilde{S}_b$ and $\tilde{S}_t$ based on the probability F_{ij} of x_i belonging to class j, the l_j is either 0 or 1. Thus, the objective function Eq.(6) can be rewritten to the follows:

$$\max_a \frac{a^T \tilde{S}_b a}{a^T \left(\tilde{S}_t + \beta (X L_d X^T) \right) a} \tag{10}$$

The projective vector a that maximizes (10) is given by the maximum eigenvalue solution to the generalized eigenvalue problem:

$$\tilde{S}_b a = \lambda (\tilde{S}_t + \beta X L_d X^T) a \tag{11}$$

Let the column vector $a_1, a_2, \cdots, a_d$ be the solutions of (11) ordered according to their eigenvalues $\lambda_1, \lambda_2, \cdots \lambda_d$. Thus, the embedding is given as $y_i = A^T x_i$, where y_i is a d-dimensional vector, and A is an $m \times d$ matrix.

3.2 Algorithm Description

Based on the above analysis, a dimensionality reduction algorithm by label transduction, called semi-supervised local discriminant embedding (SLDE), is proposed. It propagates label information from labeled data to unlabeled data according to the distribution of labeled and unlabeled data.

The algorithmic procedure of semi-supervised local discriminant embedding (SLDE) is stated below:

Input: Data matrix $X \in R^{m \times n}$ (each column is a data point), Projected dimension d and other related parameters.

Output: The d dimensional subspace Y.

Algorithm:

Step 1. For each data point x_i of the database, find its k nearest neighbors.

Step 2. Calculate the weight matrix W by Eqs. (1) and (2); Construct the weight matrix S_d as in Eq. (8) and calculate the graph Laplacian $L_d = D_d - S_d$.

Step 3. Calculate the label matrix F: Perform label propagation by Eq. (9) and obtain the label matrix F.

Step 4. Construct the labeled scatter matrice $\tilde{S}_b$ and total scatter matrix $\tilde{S}_t$ respectively.

Step 5. Solve the eigen-value problem: Compute the eigenvectors with respect to the non-zero eigenvalues for the generalized eigenvector problem Eq. (11) and obtain the projection matrix A.

Step 6. Linear embedding: A is a $n \times d$ transformation matrix. The samples can be embedded into d dimensional subspace by $X \to Y = A^T X$.

4 Experimental Results

In order to evaluated the performance of the method SLDE and compare it to LDA [5] and SDA [1]. In the experiments of this section, α_i is set to 0.99.

4.1 Test on USPS Handwritten Dataset

The effectiveness of the SLDE method is illustrated by the problem of classifying hand-written digits. The adopted dataet is the USPS handwritten digits dataet, which consists of 8-bit grayscale images of "0" through "9". The 110 images of digits that is randomly selected in each class are used in this experiments , and there are a total of 1100 examples in experiment database.

The learning performance of some methods usually vary with different choices of the parameters, then we evaluate the performance of the algorithm with different values of the parameters. In SLDE algorithm, there are four parameters, i.e., a parameters of nearest neighbors: k , a parameters r controls the weight, β is the regularization parameters, α_i is the fraction of label information that x_i receives from its neighbors. We make α_i as 0.99. Since the algorithm tries to obtain the local discriminant structures and class information of the data space, k is often set to a small number. In the parameters analysis experiment, empirically set $k = 13$, $r = 1.4$, $\beta = 1.7$, the 11 samples per class are used as the labeled data and the remaining data are as unlabeled data. Euclidean distance and nearest neighborhood classifier are used in the experiments. Fig.1 shows the diversification of the parameters values.

According to the experiment on the analysis of the parameters, set $k = 10$, $r = 1.3$, $\beta = 1.2$ for the SLDE method in the USPS handwritten digits dataset. The experiment settings for LDA and SDA are as same as described in [5] and [1]. Table.1 and Fig.2(a) shows the overall classification precision on the USPS handwritten digits dataset.

4.2 Test on COREL Database

In the experiment, choose COREL database to test the method on image classification application. The used dataset contains 1000 color images from COREL database (http://wang1.ist.psu.edu). The dataset consists of 10 classes. The images are represented by a 256-dimensional Color Histogram[6], a 5-dimensional Edge Histogram[6], a 5-dimensional Color Moment[6], a 18-dimensional Wavelet texture[7] and a 18-dimensional Edge Direction Histogram [8].

In the paramenter analysis experiment, also set $k=8$, $r=1.3$, $\beta=1.6$, the 10 samples per class are used as the labeled data and the remaining data are as unlabeled data. For consistency and simplicity, nearest neighborhood classifier are used in the projected space. Fig.1 shows the diversification of the parameters values.

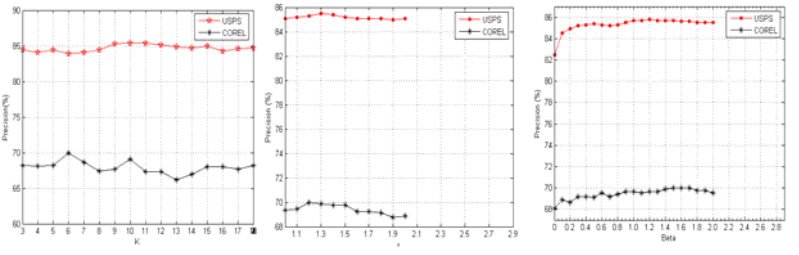

(a) (b) (c)

Fig. 1. Parameter selection for SLDE: classification precision versus different values of the parameters k, Beta, and r.

According to the parameters analysis, we set $k=6$, $r=1.2$, $\beta=1.5$ for our method in the COREL dataset. Table.1 and Fig.2(b) shows the overall classification precision on the COREL dataset.

Table 1. Classification precision on USPS and COREL

Train number	USPS			COREL		
	LDA	SDA	SLDE	LDA	SDA	SLDE
5 Train	56.3810	74.6190	79.1221	55.0526	70.1813	71.2849
10 Train	73.2000	84.5000	86.1500	63.1111	70.8889	71.7053
15Train	80.4211	86.4737	87.0831	66.7059	73.4445	74.5036
20 Train	82.7778	89.2222	90.6133	69.5000	75.4445	75.6163
25 Train	86.0000	91.1176	91.1456	72.4000	76.9112	77.8477
30 Train	84.5000	90.2500	90.8839	72.7143	77.3016	78.2024

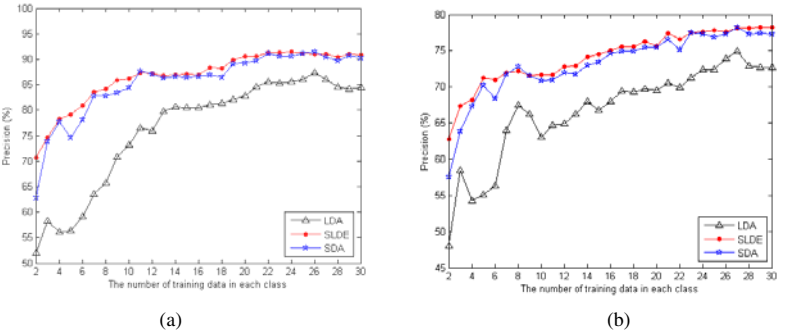

(a) (b)

Fig. 2. Comparison with other methods LDA and SDA

The result in Fig.1 shows the effect of the size of the three paramenters on the classification performance. It is clear that the classification precision is better improved in the two database when the β is from 0 to 0.1. The paramenter r is also important to get best classification performance for SLDE, bcause the different value of r can reflect the relativity between the data points. It is crucial for SLDE that the paramenter are in most setting.

From Table.1 and Fig.2, we have the following observations:

- SDA and SLDE methods perform better than LDA because they take care of both discriminant and geometrical structures in the data.
- SLDE assigns higher weights to the data with the same label data pairs and make more use of both labeled and unlabeled data by label propagation procedure, which is helpful to separate the different class images, that is why it outperforms the LDA and SLDE.

5 Conclusion

We have an improved manifold embedding method for dimensionality reduction based on SDA. The approach can make efficient use of both labeled and unlabeled data points and achieve good accuracy by rectifying the neighbor relations with weight matrix. Experiments are designed and conducted on USPS dataset and COREL dataset for performance evaluation. The results have shown the encouraging performance of the method.

Acknowledgment

This work is partially supported by the National Science Foundation of China under grant no. 60973098, 60873151, 90820306.

References

1. Cai, D., He, X., Han, J.: Semi-supervised Discriminant Analysis. In: Proceedings of the International Conference on Computer Vision (2007)
2. Wang, F., Zhang, C.S.: Label Propagation through Linear Neighborhoods. Knowledge and Data Engineering 20, 55–67 (2008)
3. Wang, J.D., Wang, F., Zhang, C.: Linear Neighborhood Propagation and Its Applications. Pattern Analysis and Machine Intelligence 31, 1600–1615 (2009)
4. He, X.F., Cai, D.: Learning a Maximum Margin Subspace for Image Retrieval. IEEE Trans. Knowledge and data engineering 20, 189–201 (2008)
5. Duda, R., Hart, P., Stork, D.: Pattern Classification. Wiley, Chichester (2001)
6. Manjunath, B.S., Ohm, J.R., Vasudevan, V.V., Yamada, A.: Color and texture descriptors. IEEE Trans. CSVT 11, 703–715 (2001)
7. Pinheiro, A.M.G.: Image Description Using Scale-Space Edge Pixel Directions Histogram. In: Semantic Media Adaptation and Personalization. In: Second International Workshop, pp. 211–218 (2007)
8. Huijsmans, D.P., Sebe, N.: How to Complete Performance Graphs in Content-Based Image Retrieval: Add Generality and Normalize Scope. IEEE Trans. Pattern Analysis and Machine Intelligence 27, 245–251 (2005)

Orthogonal Discriminant Local Tangent Space Alignment

Ying-Ke Lei[1,2,3], Hong-Jun Wang[1], Shan-Wen Zhang[2], Shu-Lin Wang[2,4], and Zhi-Guo Ding[1]

[1] State Key Laboratory of Pulsed Power Laser Technology, Electronic Engineering Institute, Hefei, Anhui 230027, China
[2] Intelligent Computing Lab, Institute of Intelligent Machines, Chinese Academy of Sciences, P.O. Box 1130, Hefei, Anhui 230031, China
[3] Department of Automation, University of Science and Technology of China, Hefei, Anhui 230027, China
[4] School of Computer and Communication, Hunan University, Changsha, Hunan, China
leiyingke@163.com

Abstract. In this paper, a novel linear subspace leaning algorithm called orthogonal discriminant local tangent space alignment (O-DLTSA) is proposed. Derived from local tangent space alignment (LTSA), O-DLTSA not only inherits the advantages of LTSA which uses local tangent space as a representation of the local geometry so as to preserve the local structure, but also makes full use of class information and orthogonal subspace to improve discriminant power. The experimental results of applying O-DLTSA to standard face databases demonstrate the effectiveness of the proposed method.

Keywords: Dimensionality reduction, subspace learning, manifold learning, face recognition.

Introduction

Recently, a large number of nonlinear manifold learning methods have been proposed, including isometric feature mapping (ISOMAP) [1], locally linear embedding (LLE) [2], Laplacian eigenmaps (LE) [3], Hessian-based locally linear embedding (HLLE) [4], and local tangent space alignment (LTSA) [5]. Each manifold learning method attempts to preserve local structures in small neighborhoods and successfully derives the intrinsic features of nonlinear manifold. However, current manifold learning methods suffer from some drawbacks when they are applied to pattern recognition tasks. One problem is that they yield an embedding restrictedly limited on the training data set, but, because of the implicitness of the nonlinear map, when applied to a new sample, they cannot find the sample's image in the embedded space. The other problem is that classical manifold learning methods neglect the class information, which will inevitably lead to a heavy weakening of their performance on pattern recognition.

To overcome these drawbacks, many subspace learning methods which characterize locally geometrical structure and discriminant power of the data have been

D.-S. Huang et al. (Eds.): ICIC 2010, LNCS 6215, pp. 423–429, 2010.

presented, such as marginal Fisher analysis (MFA) [6] and locality sensitive discriminant analysis (LSDA) [7]. Following this notion, a supervised version of LTSA, namely orthogonal discriminant local tangent space alignment (O-DLTSA), is proposed for feature extraction. In the proposed method, we attempt to enhance the recognition ability of the original LTSA from two aspects. On the one hand, we convert the optimization problem of LTSA into multi-object optimization problem, i.e., a linear transformation matrix, which maps the input data to a low-dimensional feature space, is obtained by solving multi-object optimization that captures the discrepancy of the local geometries and introduces the maximum margin criterion (MMC) [8] in the reduced space simultaneously. Therefore, our method effectively combines the ideas of LTSA and MMC. It not only holds the strong dsicriminant power of MMC, but also preserves the intrinsic geometry of the data samples. On the other hand, in order to improve the discriminant power, we take an orthogonal step to obtain a set of orthogonal basis eigenvectors.

2 A Brief Review of LTSA

Let $X = [x_1, x_2, ..., x_n] \in \mathbb{R}^{m \times n}$ denote n data points in a high m dimensional space. The goal of dimensionality reduction is to project the high-dimensional data into a low-dimensional feature space. Let us denote the corresponding set of n points in the reduced space as $Y = [y_1, y_2, ..., y_n] \in \mathbb{R}^{d \times n}$, with $d \ll m$, in which y_i is a low-dimensional representation of x_i $(i = 1, 2, ..., n)$.

Local tangent space alignment (LTSA) [5] is developed from the framework of part optimization and whole alignment. Each data point is represented in different local coordinate systems by part optimization. But its global coordinate should be maintained unique. Whole affine transformation is constructed to achieve this goal. For each point x_i, let $X_i = [x_{i_1}, x_{i_2}, ..., x_{i_k}] \in \mathbb{R}^{m \times k}$ denote the collection of its k nearest neighbors. To preserve the local geometry of each X_i, performing a singular decomposition of the centralized matrix of X_i, we have

$$X_i H_k = U_i \sum_i V_i^T, \quad i = 1, ..., n,$$

where $H_k = I - ee^T / k$ is the centering operator, $\sum_i = diag(\sigma_1, ..., \sigma_k)$ contains the singular values in descending order, U_i is an $m \times m$ matrix whose column vectors are the left singular vectors , and V_i is a $k \times k$ matrix whose column vectors are the right singular vectors. The local tangent space coordinates can be obtained from the following formula:

$$\Theta_i = U_i^T X_i H_k = \sum_i V_i^T = [\theta_1^{(i)}, \theta_2^{(i)}, ..., \theta_k^{(i)}], \tag{1}$$

where $\theta_j^{(i)}$ is the local tangent coordinate of the jth nearest neighbor of data point x_i. In essence, it is equal to performing a local principal component analysis (PCA); Θ_i is the projection of the points in a local neighborhood on the local PCA.

We now consider constructing the global coordinates $y_i, i = 1,...,n$, in the d-dimensional feature space based on the local coordinates $\theta_j^{(i)}$ which represents the local geometry. Let $Y_i = [y_{i_1}, y_{i_2},..., y_{i_k}] \in \mathbb{R}^{d \times k}$ contain the corresponding global coordinates of the k data points in Θ_i and $E_i = [\varepsilon_1^i,...,\varepsilon_k^i]$ be the local reconstruction error matrix. To preserve as much of the local geometry in the low-dimensional feature space, we seek to find y_i and the local affine transformations L_i to minimize the reconstruction errors E_i, i.e.,

$$\arg\min_{Y_i, L_i} \sum_i \|E_i\|_2^2 = \arg\min_{Y_i, L_i} \sum_i \|Y_i H_k - L_i \Theta_i\|_2^2. \tag{2}$$

Obviously, the optimal alignment matrix L_i is given by $L_i = Y_i H_k \Theta_i^+$, and thus $E_i = Y_i H_k (I - \Theta_i^+ \Theta)$, where Θ_i^+ is the Moore-Penrose generalized inverse of Θ_i.

Let $Y = [y_1, y_2,..., y_n]$ and S_i be the 0-1 selection matrix such that $YS_i = Y_i$. We need to find Y to minimize the overall reconstruction error

$$\arg\min_Y \sum_i \|E_i\|_F^2 = \arg\min_Y \|YSW\|_F^2 = \arg\min_Y tr(YSWW^T S^T Y^T) = \arg\min_Y tr(YBY^T), \tag{3}$$

where $S = [S_1,..., S_n]$, $B = SWW^T S^T$, and $W = diag(W_1,..., W_n)$ with $W_i = H_k(I - \Theta_i^+ \Theta_i)$. Let $\Theta_i^T = Q_i R_i$ be the QR decomposition of Θ_i^T, then $\Theta_i^+ \Theta_i = Q_i Q_i^T$. We can rewrite W_i as

$$W_i = I - [e/\sqrt{k}, Q_i][e/\sqrt{k}, Q_i]^T \equiv I - G_i G_i^T. \tag{4}$$

To uniquely determine Y, we impose the constraint $YY^T = I$. Then, the optimal d-dimensional global embedding Y is given by the d eigenvectors of the matrix B, corresponding to the 2nd to $(d+1)$st smallest eigenvalues of B.

3 Orthogonal Discriminant Local Tangent Space Alignment

In this section, we propose a supervised LTSA algorithm named as O-DLTSA. O-DLTSA aims to take full advantage of class information and orthogonal subspace to improve discriminant power of the original LTSA.

3.1 The Linearization of LTSA

In order to circumvent the out-of-sample problem, an explicit linear map from X to Y, i.e. $Y = V^T X$, is constructed. Thus the objective function for the original LTSA can be converted to the following form:

$$J_1(Y) = \min tr(YBY^T) = \min tr(V^T XBX^T V). \tag{5}$$

Mapping new data points to the low-dimensional space becomes trivial once linear transformation matrix V is determined. Some studies have found that the linearization of LTSA (LLTSA) [9-10] shows better recognition ability than the original LTSA [5]. However, since LLTSA does not take class information into account which is important for recognition problem, the linear transformation is not always the optimal one that the proposed O-DLTSA pursues. That is to say, O-DLTSA needs a criterion that can be used to automatically find an optimal linear transformation for classification.

3.2 Optimal Linear Discriminant Embedding

LLTSA only puts stress on preserving as much as possible local structure defined by the nearest neighbors, however, class information is ignored. In order to obtain optimal linear discriminant embedding, we introduce the MMC presented above to the LLTSA, which characterizes as much as possible local neighborhood structure on the original data manifold, and at the same time, maximizes the average margin between classes in the embedded space. That is to say, the linear transformation obtained by LLTSA can satisfy maximum margin criterion (MMC) [8] simultaneously, i.e., maximizing the average margin between classes in the projected space.. Thus the problem can be written as the following multi-object optimized problem:

$$\begin{cases} \min tr\{V^T XBX^T V\} \\ \max tr\{V^T (S_b - S_w)V\} \\ \text{s.t. } V^T XX^T V = I. \end{cases} \tag{6}$$

The constrained multi-object optimization is conducted to minimize the reconstruction error and maximize the margin between difference classes simultaneously. We formulate this discriminator by using the linear manipulation as follows:

$$\begin{aligned} &\min tr\{V^T (XBX^T - (S_b - S_w))V\} \\ &\text{s.t. } V^T XX^T V = I. \end{aligned} \tag{7}$$

The solution of Eq. (7) is obtained by solving the generalized eigenvalue decomposition problem:

$$(XBX^T - (S_b - S_w))v = \lambda XX^T v. \tag{8}$$

Therefore, the transformation matrix V which minimizes the objective function is composed of the d smallest generalized eigenvectors of $XBX^T - (S_b - S_w)$ and XX^T corresponding to the d smallest eigenvalues. The transformation matrix V which minimizes the objective function is as follows:

$$V = [v_1, v_2, ..., v_d].$$

3.3 Obtaining Orthogonal Eigenvectors

The generalized eigenvectors obtained by solving Eq. (8) are nonorthogonal. This makes it difficult to faithfully represent the manifold. We use Gram-Schmidt orthogonalization to produce orthogonal basis vectors, which is called O-DLTSA. Set

$g_1 = v_1$, and assume that $k-1$ orthogonal basis vectors $g_1, g_2, ..., g_{k-1}$ have been worked out, thus g_k can be computed as follows:

$$g_k = v_k - \sum_{i=1}^{k-1} \frac{g_i^T v_k}{g_i^T g_i} g_i. \tag{9}$$

Then $G = [g_1, g_2, ..., g_d]$ is the transformation matrix of O-DLTSA.

3.4 The Outline of O-DLTSA

The algorithmic procedure of O-DLTSA can be summarized as follows:

Step 1: Project the data set X into the PCA subspace by discarding the minor components.

Step 2: For each data point x_i, determine its k nearest neighbors by KNN or ε-ball algorithm.

Step 3: Compute the d left singular vector matrix U_i of $X_i H$. Set Θ_i as in Eq. (1).

Step 4: Compute the orthogonal basic matrix Q_i of Θ_i^T by QR decomposition, and form $G_i = [e/\sqrt{k}, Q_i]$.

Step 5: Construct affine alignment matrix B by locally summing as follows:

$$B(I_i, I_i) \leftarrow B(I_i, I_i) + I - G_i G_i^T \quad i = 1, 2, ..., n$$

with the initial $B = 0$, where $I_i = \{i_1, ..., i_k\}$ denotes the set of indices for the k nearest neighbors of x_i.

Step 6: Compute matrix XBX^T.

Step 7: Compute the between-class scatter S_b, within-class scatter S_w, and their difference $S_b - S_w$, respectively.

Step 8: Compute the d eigenvectors corresponding to the d smallest eigenvalues based on Eq. (8).

Step 9: Orthogonalize the d basis vectors based on Eq. (9) and obtain $G = [g_1, g_2, ..., g_d]$.

4 Experiments

In this section, the performance of O-DLTSA is evaluated on Olivetti Research Laboratory (ORL) face image databases and compared with the performances of PCA [11], MMC [8], LDA [12], marginal Fisher analysis (MFA) [6], and supervised LLTSA (SLLTSA) [9-10]. In our experiments, each image was manually cropped and resized to 32×32 pixels. Thus, each image can be represented by a 1024-dimensional vector in image space. The k-nearest neighborhood parameter in SLLTSA and O-DLTSA can be chosen as $k = l - 1$, where l denotes the number of training samples per class.

For each individual, seven images were randomly selected for training and the rest were used for testing. The experimental design is the same as before. We averaged the results over 20 random splits. The best mean recognition rates are shown in Table 1. As can be seen, O-DLTSA algorithm significantly outperforms the other techniques. We investigate the maximal average recognition accuracy at 278, 36, 39, 51, 111, and 39 dimensions for PCA, MMC, LDA, MFA, SLLTSA, and O-DLTSA, respectively. The best mean recognition rates of PCA, MMC, LDA, MFA, SLLTSA, and O-DLTSA are 91.42(±2.26)%, 94.92(±1.77)%, 95.71(±1.86)%, 96.46(±1.97)%, 94.21(±1.92)%, and 97.03(±1.70)%, respectively. The corresponding face subspaces obtained by carrying out the methods mentioned above are called optimal face subspace for each method.

Moreover, the effect of the training sample number is also tested in the following experiment. We randomly selected 3, 4, 5, 6, and 7 training samples and then the rest samples for test ones. We repeated these trails 20 times and computed the average results. The best results obtained in the optimal subspace are shown in Fig. 1. It can be seen that our O-DLTSA algorithm significantly performs the best among all the cases.

Table 1. Performance comparison and the corresponding standard deviations (percent) with the reduced dimensions for BASELINE, PCA, MMC, LDA, MFA, SLLTSA, and O-DLTSA

Method	Dimension	Recognition rate
BASELINE	1024	90.92±2.26
PCA	278	91.42±2.26
MMC	36	94.92±1.77
LDA	39	95.71±1.86
MFA	51	96.46±1.97
SLLTSA	111	94.21±1.92
O-DLTSA	39	97.03±1.70

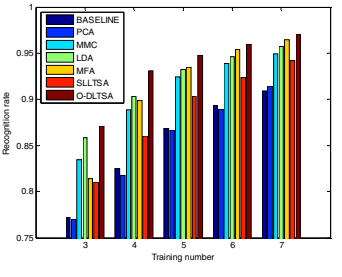

Fig. 1. Performance comparison of recognition rates with different training sample number using BASELINE, PCA, MMC, LDA, MFA, SLLTSA, and O-DLTSA

5 Conclusions

In this paper, we develop an orthogonal discriminant local tangent space alignment (O-DLTSA) technique for supervised feature extraction of high-dimensional data. The

projection of O-DLTSA can be viewed as a linear approximation of the nonlinear map that faithfully preserves both discriminant power and local geometrical structure hidden in the data. The experimental results on ORL databases show that the new method is indeed effective and efficient.

Acknowledgments. This work was supported by the grants of the National Science Foundation of China (grant nos. 60905023, 60975005, 60873012, 60805021, 60973153, and 60705007), and the China Postdoctoral Science Foundation (grant no. 20090450825).

References

1. Tenenbaum, J., de Silva, V., Langford, J.: A Global Geometric Framework for Nonlinear Dimensionality Reduction. Science 290, 2319–2323 (2000)
2. Roweis, S., Saul, L.: Nonlinear Dimensionality Reduction by Locally Linear Embedding. Science 290, 2323–2326 (2000)
3. Belkin, M., Niyogi, P.: Laplacian Eigenmaps for Dimensionality Reduction and Data Representation. Neural Computation 15(6), 1373–1396 (2003)
4. Donoho, D., Grimes, C.: Hessian Eigenmaps: New Locally Linear Embedding Techniques for High-dimensional Data. Proc. Nat'l academy of sciences 100(10), 5591–5596 (2003)
5. Zhang, Z., Zha, H.: Principal Manifolds and Nonlinear Dimension Reduction via Local Tangent Space Alignment. IAM J. Scientific Computing 26(1), 313–338 (2005)
6. Yan, S., Xu, D., Zhang, B., Zhang, H.J., Yang, Q., Lin, S.: Graph Embedding and Extension: A General Framework for Dimensionality Reduction. IEEE Trans. Pattern Anal. Mach. Intell. 29(1), 40–51 (2007)
7. Cai, D., He, X., Zhou, K., Han, J., Bao, H.: Locality Sensitive Discriminant Analysis. In: 20th International Joint Conference on Artificial Intelligence, pp. 708–713 (2007)
8. Li, H., Jiang, T., Zhang, K.: Efficient and Robust Feature Extraction by Maximum Margin Criterion. IEEE Trans. Neural Networks 17(1), 157–165 (2006)
9. Zhang, T.H., Yang, J., Zhao, D.L., Ge, X.L.: Linear Local Tangent Space Alignment and Application to Face Recognition. Neurocomputing 70, 1547–1553 (2007)
10. Li, H.Y., Teng, L., Chen, W.B., Shen, I.F.: Supervised Learning on Local Tangent Space. In: Wang, J., Liao, X.-F., Yi, Z. (eds.) ISNN 2005. LNCS, vol. 3496, pp. 546–551. Springer, Heidelberg (2005)
11. Turk, M., Pentland, A.: Eigenfaces for Recognition. J. Cognitive Neuroscience 3(1), 71–86 (1991)
12. Belhumeour, P.N., Hespanha, J.P., Kriegman, D.J.: Eigenfaces vs. Fisherfaces: Recognition Using Class Specific Linear Projection. IEEE Trans. Pattern Anal. Mach. Intell. 19(7), 711–720 (1997)

Separating Pigment Components of Leaf Color Image Using FastICA

Yuan Tian[1,2], Chunjiang Zhao[1], Shenglian Lu[1], and Xinyu Guo[1]

[1] Department of Automation, University of Science and Techonology of China, Hefei, Anhui 230026, P.R. China
[2] National Engineering Research Center for Information Technology in Agriculture, Beijing 100097, P.R. China
zhaocj@nercita.org.cn

Abstract. In this paper, the spatial distributions of pigments in foliage which lead to color variation are separated by independent component analysis (ICA) from a single leaf color image. The results can be applied to the reproduction of leaf color, the diagnosis of leaf disease, and leaf texture synthesis. Our results shows that the components of pigments which are different color influential factor are separated from leaf color image. We use images to demonstrate results and show how each component of pigment affects the leaf color.

Keywords: image processing, leaf color, leaf texture, texture synthesis, independent component analysis.

1 Introduction

In the field of botany and agriculture, for a long time the digital images of the plants leaves have been used to get intrinsic characteristics of color and texture by image process for higher-level application such as pattern recognition, texture synthesis and so on. Recently, digital photography has been used to assess viral infection of leaves by extracting the color features [1] and insect feeding [2]. Schaberg et al. [3] and Murakami et al. [4] developed a method for leaf color analysis using the Scion Image software package (Scion Corporation, Frederick, MD). El-Helly [5] developed a preprocessing system interface for preprocessing diseased plant images for diagnosis. Another application of analysis of the leaf image is to render a virtual plant realistically in Computer Graphics. Desbenoit [6] built leaf model map stencil groups, and synthesized all kinds of texture of leaf combing with circumstance parameters. Shigenori Mochizuki [7] used color-stealing algorithm (CSA) to extract natural-like color from some photographic images to realize the autumn colorings. Also by analyzing the leaf image sequence, many other advanced leaf models such as BRDF and BTDF model [8] had been developed for the real-time rendering of plant leaves.

The color and texture of a leaf are mainly caused by the pigments it contains, and more precisely the light absorption behavior of these pigments [9]. In this research, the spatial distributions of pigments which influence the main color of leaf are separated by independent component analysis (ICA). Recently, some researchers applied ICA to learn efficient codes of natural images that utilize a set of linear basis

D.-S. Huang et al. (Eds.): ICIC 2010, LNCS 6215, pp. 430–437, 2010.

functions or features [10-12]. In the field of color processing, Inoue et al.[13] firstly proposed a technique to separate each pigment from compound color images, and the technique is improved by N.Tsumura [14, 15] to synthesize various skin color and texture by changing the extracted amount of hemoglobin and melanin spatially in the human skin color image. Similar to N.Tsumura [14], we focus on the separation of the pigments which influence the color appearance. In our approach, we use FastICA to learn the basis independent components of a leaf color image. Compared with conventional methods, the proposed method is based on the fact that variation of color or texture is caused by two factors: First the kind of pigments that the leaf containing in different time and situation, the second is the situation that pigments increasing, decreasing spatially and temporally. So we firstly described the type of influenced pigments according to priori knowledge. And then we used a leaf model to separate leaf image into the intrinsic component images, which is also the spatial distribution of the pigment relative quantities. The intrinsic image representation of pigment distribution may be useful as a stepping-stone to high lever application like disease diagnosis, texture synthesis and so on.

2 FastICA of Color Image

Independent Component Analysis (ICA) is a signal processing method originally developed for the blind signal separation (BSS) problem [15]. Recently, there have been a considerable amount of papers presenting the applications of ICA algorithms on image data [16, 17]. Aapo Hyvärinen [18] proposed an efficient and popular FastICA algorithm to find independent components by separately maximizing the negentropy of each mixture. The deflation approach of FastICA is able to use some non-quadratic contrast function to provide estimates of negentropy [18].

The update rule for the deflation method is given by:

$$w^*(k) = C^{-1}E[xg(w(k-1)^T x)] - E[g'(w(k-1)^T x)]w(k-1). \tag{1}$$

$$w(k) = \frac{w^*(k)}{\sqrt{w^*(k)^T C w^*(k)}} \tag{2}$$

where E is the expectation operation, $w^*(k)$ is the complex conjugate of $w(k)$, g can be any suitable non-linear contrast function, with derivative g', and C is the covariance matrix of the mixtures, X.

In this paper, for color image separation, it is assumed that the different pigment quantity as independent component, the observation x_i $(i=1, 2, 3)$ is optical density domain of each color channel. To simplify the description, first assuming that the media in color image includes three pigments and it is captured by an image acquisitive system with three color channels. We denote $s_i(j, k)$ $(i=1, 2, 3)$ as the quantity of three pigments and $S(j, k)=[s_1(j, k), s_2(j, k), s_3(j, k)]^T$, a_i denotes the pure color vectors of every pigments. The dimension of the a_i is equivalent to the number of color channel, and each element is the pure color value of one unit pigment. N.Tsumura assumed

that compound color vector $X(j, k)$ from three channels can be calculated by linear combination of pure color vectors with the quantity matrix X:

$$X(j,k) = AS(j,k). \tag{3}$$

where $X(j, k)= [x_1(j, k),x_2(j, k), x_3(j, k)]^T$, each element indicates the pixel value of each channel.

By applying the ICA to the compound color vectors in the image, the relative quantity and pure color vector a_i of each pigment are extracted without a priori information on the quantity and color vector under the assumption that quantities of pigments are mutually independent for the image coordinate. Let define the separating equation:

$$Y(j,k) = MX(j,k). \tag{4}$$

where the separating matrix $M=[m_1,m_2]$, the intrinsic signals $Y(j,k)= [Y_1(j, k),Y_2(j, k), Y_3(j, k)]^T$.

The extracted signal matrix $Y(j, k)$ is not the absolute quantity of $S(j, k)$ without an assumption, Therefore the extracted independent vector:

$$Y(j,k) = RTS(j,k). \tag{5}$$

where R is the permutation matrix that may substitute the elements of the vector each other, T is the diagonal matrix to relate the absolute quantities to relative qualities, using (3)(4)(5), the mixing matrix A is calculated as follows:

$$A = M^{-1}RT. \tag{6}$$

Note that relative quantities and directions of compound color vectors are pragmatically enough in most cases.

3 Leaf Color Model

Figure 1 shows a color image from a cucumber leaf with 500×500 pixels. We choose samples that have disease or lack nutrition like aging to analyze for further applications. The image is taken by digital camera (SONY DSC-F717) with 3648×2736 pixels under a fixed light source. Every color image has three color channels: red, green, blue. And denote $r(j, k)$, $g(j, k)$, $b(j, k)$ to be three pixel color value on the image coordinate (j, k), respectively.

Two assumptions on leaf color were made in this section. First, Lambert-Beer law or modified Lambert-Beer law holds in the reflected light among the quantities and observed color signals. Second, these quantities are mutually independent spatially. The first assumption assures the linearity among the observed color signals and pure color signals of pigments in the spectral density domain.

We use optical density domain of three channels: $log(r(j, k))$, $log(g(j, k)$, $log (b(j, k))$ as compound signals. Denote color density vector $C(j, k)$ on image coordinate (j, k) as

$$C(j,k) = [-\log(r(j,k)), -\log(g(j,k)), -\log(b(j,k))]. \tag{7}$$

Fig. 1. The analyzed cucumber aging image with 500×500 pixels

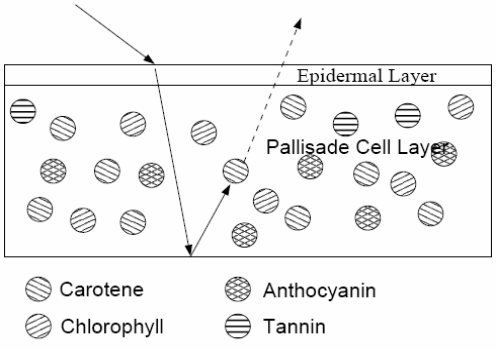

Fig. 2. Biological model of leaf with epidermal layer and palisade cell layer

Various pigments such as chlorophyll, carotene, anthocyanin, tannin are contained in the epidermal layer and palisade cell layer of leaf (Fig.2). Chlorophyll is responsible for the greenish color, during the aging process in autumn, carotene, anthocyanin and tannin grow more, and they create yellow-orange color, or even red color. To simplify the description we define chlorophyll as the Greenish Pigment (GP), other pigments as Aging Pigment (AP). Therefore in Fig.1, the aging cucumber leaf color is determined by AP and GP. Note that this definition is simplified and also can be adjusted to some other cases. For example maple leaf, which turns yellow and red in autumn, it can also denote the chlorophyll, carotene, anthocyanin as three independent signals in compound color.

Since we assumes there are two types of pigments in aged leaf and disease leaf, the color density vector of skin can be denoted as

$$C(j,k) = BQ(j,k) + c_3(j,k)\,. \tag{8}$$

where $B=[b_1, b_2]^T$, $C(j, k)=[c_1(j, k), c_2(j, k)]$, $c_1(j, k)$ and $c_2(j, k)$ are normalized as $\|c_1(j,k)\| = \|c_2(j,k)\| = 1$ .And b_1 and b_2 are pure color vectors of two types of

pigments (GP, AP or DP), q_1, q_2 are relative quantities of the pigments respectively, $c_3(j, k)$ is spatially stationary vector caused by other pigments and leaf structure.

Note that the number of pigments is smaller than the number of channels, we project the three optical density domain on the two dimensional plane that c_1 and c_2 spanned using Principal component analysis (PCA). Let denote the principal component matrix as $P=[p_1,p_2,p_3]$, p_1 and p_2 are the first and second principal component vectors which can span the plane spanned by c_1 and c_2. The projection Matrix is

$$PP^T = [p_1, p_2][p_1, p_2]^T . \tag{9}$$

The color density can be divided into two components as:

$$C(j,k) = PP^T(BQ(j,k) + c_3(j,k)) + (I - PP^T)c_3(j,k) . \tag{10}$$

where matrix I is an identity matrix. The first term indicates the component in the two dimensional subspace while the second term indicates the component in one dimensional subspace.

4 Pigment Components Separation and Results

In two dimensional plane proposed in the previous section, the FastICA can be used to estimate the quantity matrix Q and color density matrix A as follows.

In preprocessing of FastICA, firstly to center $C(j, k)$, the elements in $C(j, k)$ were made zero-mean variable by subtracting the mean vector of $C(j, k)$. Secondly, to whitening the signal, which means to transform $C(j, k)$ linearly, the observed vector was multiplied with the whitening matrix. The whiten vector can be indicated as:

$$X(j,k) = D^{-\frac{1}{2}}P^T(C(j,k) - \overline{C(j,k)}) . \tag{11}$$

where $\overline{C(j,k)}$ is the mean vector of $C(j, k)$, D is the diagonal matrix of its first two eigenvalues , $D = diag(d_1, d_2)$ and $D^{-1/2} = diag(d_1^{-1/2}, d_2^{-1/2})$. Substitute (10) into (11) gives:

$$X(j,k) = D^{-1/2}P^T B[Q(j,k) + B^{-1}c_3(j,k) - (D^{-1/2}P^T B)^{-1}\overline{C(j,k)}] . \tag{12}$$

Here, the independent component vector is defined as:

$$S(j,k) = Q(j,k) + B^{-1}c_3(j,k) - (D^{-1/2}P^T B)^{-1}\overline{C(j,k)} . \tag{13}$$

Also, we define:

$$A = D^{-1/2}P^T B . \tag{14}$$

The mixed matrix A is obtained by FastICA described in previous section, substituting into (9), the estimated pure color density matrix B is calculated as:

$$B = (D^{-1/2}P^T)H^{-1}RT . \tag{15}$$

Using FastICA Matlab toolbox proposed by Aapo Hyvärinen, we get the separation matrix M and mixed matrix A, and using deflation approach to provide estimates of negentropy. After Estimation of the color density vector B, similar as [19], we denote the color separation and synthesis equation as:

$$C'(j,k) = BKY(j,k) + i(I - PP^T)C(j,k). \tag{16}$$

where $C'(j, k)$ is the synthesized color, $Y(j, k)$ is independent component matrix after analysis, K is a diagonal matrix to change quantities of pigments $Q(j, k)$, i is the value to change quantities of stationary color vector $c_3(j, k)$. Through changing the K and i, the two images that are only influenced by different independent component respectively can be separated. We set the $K=diag[1,0]$ and $i=0$ to get the image that the first independent component determined, also $K=diag[0,1]$ and $i=0$ get the second one(Fig.3).

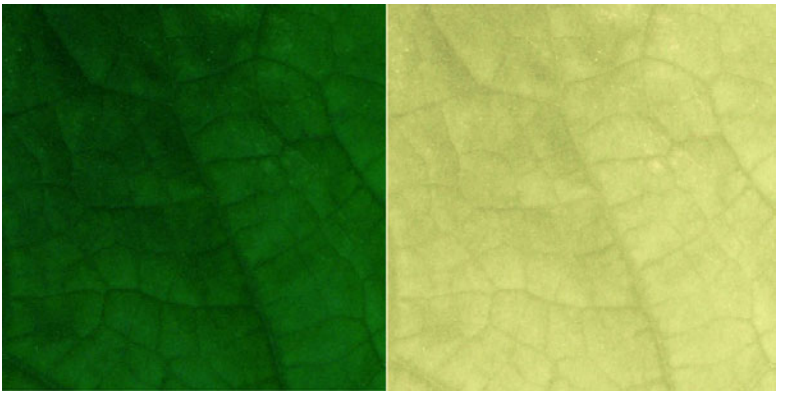

Fig. 3. Two separated independent component image of the leaf color image. The synthesis parameters are set as $K=diag[1, 0]$ and $i=0$ in the left, $K=diag[0, 1]$ and $i=0$ in the right.

Since the yellow and brown point and speckle which are caused by Aging Pigments are not appeared in first component image (Fig.3), but appeared in the second, it is considered that the first image component is caused by Greenish Pigments and the second is caused by Aging Pigments. In this case, it is possible to segment any other region which color is caused by different pigments from a single leaf image. The statistical characteristics can be extracted from the independent component image. Also, for image-based material weathering[19], using color synthesis equation(16), it is possible to change the pigments relative quantity to change the appearance of a single leaf image according to weathering process including aging and disease development.

5 Conclusion and Discussion

We have presented fixed-point independent component analysis (FastICA) of a single leaf color image, and separated it into two independent component images. And it is

believed that the separated images correspond to the spatial distribution of different independent pigments. For a higher application, this approach may acquire remarkable characteristics from independent distribution of leaf appearance, which can be applied to analyze plant disease and aging degree. Also, based on physiological knowledge or a database containing the spatio-temporal variation of leaf texture, the amount of the pigments can be changed nonlinearly to synthesize the weathering process from a single leaf image.

In this paper, the Lamber-Beer Law is assumed for the leaf surface. However, in practical applications, there is shading on the surface caused by directional light. Therefore, in the future work, our technique needs to be fixed for a more correct estimation of the pigment density in the shading area, which can be dealt with using reflectance/shading separation from a single image [20]. Another of our goals in future work is to handle the weathering effects on a single leaf image using texture analysis, also extending to a natural weathering scene including a lot of leaves.

Acknowledgement

This work is supported by Beijing Natural Science Foundation of China under grant No.4081001, National High Tech. R&D Program of China under grant No.2007AA10Z226, and National Fund Project for Transformation of Agricultural Scientific and Technological Achievements under grant No.2009GB2A000001.

References

1. Martin, D.P., Rybicki, E.P.: Microcomputer-based quantification of maize streak virus symptoms in Zea mays. Phytopathology 88, 422–427 (1998)
2. Chen, N., Hsiang, T.H., Goodwin, P.H.: Use of green fluorescent protein to quantify the growth of Colletotrichum during infection of tobacco. J. Microbiol. Methods 53, 113–122 (2003)
3. Schaberg, P.G., Van Den Berg, A.K., Murakami, P.F., Shane, J.B., Donnelly, J.R.: Factors influencing red expression in autumn foliage of sugar maple trees. Tree Physiol. 23, 325–333 (2003)
4. Murakami, P.F., Turner, M.R., Van den Berg, A.K., Schaberg, P.G.: An instructionalguide for leaf color analysis using digital imaging software. United States Department of Agriculture Publication. Tech. Rep. NE-327 (2005)
5. El-Helly, M., El-Beltagy, S., Rafea, A.: Image analysis based interface for diagnosticexpert systems. In: Proceedings of the Winter international synposium on information and Communication Technologies, pp. 1–6. Trinity College, Dublin (2004)
6. Desbeoint, B., Galin, E., Akkouche, S., Grosjean, J.: Modeling autumn sceneries Eurographics 2006 Conference, Short Papers Proceedings, Vienna, Austria. pp. 107–110 (2006)
7. Mochizuki, S., Cai, D., Komori, T., Kimura, H., Hori, R.: Virtual autumn coloring system based on biological and fractal model. In: Pacific Graphics 2001 Computer Graphics and Applications, pp.348–354 (2001)
8. Wang, L.F., Wang, W.L., Dorsey, J., Yang, X., Guo, B.N., Shum, H.Y.: Real-Time Rendering of Plant Leaves. ACM Tran. On Graphics 24, 712–719 (2005)
9. Mochizuki, S., Horie, D., Cai, D.S.: Stealing Autumn Colors. In: ACM SIGGRAPH 2005 (2005)

10. Bell, A., Sejnowski, T.: The independent components of nature scenes are edge filters. Vision Research 37, 3327–3338 (1997)
11. Lewicki, M., Olshausen, B.: Inferring sparse, overcomplete image codes using an efficient coding framework. In: Advances in Neural Information Processing Systems, vol. 10, pp. 556–562 (1998)
12. Li, Y., Chi, Z.R., Feng, D.: Leaf vein extraction using independent component analysis. In: 2006 IEEE International Conference on Systems, Man and Cybernetics, pp. 8–11 (2006)
13. Inoue, T., Fujii, Y., Itoh, K., et al.: Independent component analysis for a small number of elements in high-dimensional space. In: Proceedings of Japan Optics 1995, pp. 105–106 (1995)
14. Tsumura, N., Haneishi, H., Miyake, Y.: Independent component analysis of skin color image. Journal of Optical Society of America A 16(9), 2169–2176 (1999)
15. Tsumura, N., Ojima, N., Sato, K., Shiraishi, M., Shimizu, H., Nabeshima, H., Akazaki, S., Hori, K., Miyake, Y.: Image-based skin color and texture analysis/ synthesis by extracting hemoglobin and melanin information in the skin. ACM Transactions on Graphics 22, 770–779 (2003)
16. Comon, P.: Independent component analysis - a new concept? Signal Processing 36, 287–314 (1994)
17. Park, W.B., Ryu, E., Song, Y.J.: Visual feature extraction under wavelet domain for image retrieval. Key Engineering Materials 277, 206–211 (2005)
18. Lee, T.W., Lewicki, M.: Unsupervised Image Classification, Segmentation and Enhancement Using ICA Mixture Models. IEEE Transactions on Image Processing 11, 270–279 (2002)
19. Hyvarinen, A., Hoyer, P., Hurri, J.: Extensions of ICA as Models of Natural Images and Visual Processing. In: 4th International Symposium on Independent Component Analysis and Blind Signal Separation, Nara, Japan, pp. 963–974 (2003)
20. Xue, S., Wang, J.P., Tong, X., Dai, Q.H., Guo, B.N.: Image-based Material Weathering. In: Eurographics 2008, Computer Graphics Forum, vol. 27 (2008)
21. Tappen, M.F., Freeman, W.T., Adelson, E.H.: Recovering Intrinsic Images from a Single Image. IEEE Transactions on Pattern Analysis and Machine Intelligence 27(9), 1459–1472 (2005)

Fast Algorithm for Multisource Image Registration Based on Geometric Feature of Corners

Shaohua Jiang[1,2,*], Cheng Wang[1], Xuejun Xu[1] Wensheng Tang[2], Hongbo Zhu[1], and Xuesong Chen[1]

[1] Digital Engineering and Simulation Center, Huazhong University of Science and Technology, Wuhan, China
[2] Institute of Image Recognition & Computer Vision, Hunan Normal University, Changsha, China
jiangshaohua@smail.hust.edu.cn

Abstract. Due to the different imaging characteristics of sensor, there are big differences of multisource images in gray and trend of gray gradient. And the existing algorithms of image registration were time-consuming or low matching. In view of the status quo, a brief review of the SIFT algorithm is firstly given, and the shortcoming of SIFT, in which the matching rate is vulnerable to influence by gray feature, is pointed out. Then a fast algorithm for multisource image registration based on geometric feature of corners was presented. It adopts geometric feature of corners rather than gray feature. So the shortcoming of SIFT can be overcome. The novel algorithm can be used to register multisource images with large differences in gray or with different wavebands, and can increase the speed and raise the matching rate of registration. This section focused on how to select the corners, how to calculate feature vectors, and the feature matching algorithm. Finally, experiments have been done to prove that this algorithm can register images quickly and efficiently.

Keywords: Registration, multisource image, geometric feature, corner, SIFT.

1 Introduction

With the development of sensor technology, different imaging characteristics were showed by various sensors, so it has become an important means of obtaining information by synthesize multi-sensor images for extracting features and analyzing the images. But multi-sensor images must have been registered strictly on geometry and grayscale before extracting features and analyzing its. This makes image registration to be one of rapidly developing image processing technologies in recent years, and it has been widely used in medicine, pattern recognition, computer vision, remote sensing and military application [1-4].

Image registration technology can be classified as grey-based and feature-based. The grey-based registration technology needs manual intervention generally, which largely restricts its applications, and feature-based uses common feature of two

* Correspondence author.

D.-S. Huang et al. (Eds.): ICIC 2010, LNCS 6215, pp. 438–446, 2010.

(or more) images to register, so the more features, the higher registration accuracy. As the feature-based registration technology does not require manual intervention, it has become the mainstream of image registration technology [5-7].

Feature-based image registration technologies is made up of feature extraction, feature vector calculation and feature matching. According to image features, Feature-based image registration technologies can fall into three categories: image registration based on corner feature, line feature and surface feature. The interest point detector plays an important role in image registration based on corner feature, which is widely used currently, and includes the Harris [9-10], Forstner [9-11], SUSAN [9], Moravec [12-14] interest point detector, etc. The SIFT algorithm [14-16] proposed by Lowe is relatively good, and it is a scale invariant, rotation invariant, illumination invariant and affine invariant. But it is time-consuming because of high dimensions of feature vector. So Y. Ke1 [17] proposed PCA-SIFT algorithm to improve it, which draw lessons from principal component analysis (PCA), and convert to high- dimensional feature vector to several independent Components to reduce the dimension of feature vector. So it can greatly improve the matching speed, and maintain the original feature invariance.

The remainder of this paper is as follows. Firstly, a brief review of the SIFT algorithm is given. Then, a fast algorithm for multisource image registration based on geometric feature of corners is presented, and the shortcoming of SIFT, in which matching rate is vulnerable to influence by gray feature, is overcome. Lastly, the new algorithm can be used to register multisource images with large differences in gray or with different wavebands, and can increase the speed and raise the matching rate.

2 A Brief Review of the SIFT Algorithm

David G. Lowe proposed the SIFT (Scale Invariant Feature Transform) feature matching algorithm in 2004 [15], which detected the local maximum as feature points simultaneously in image two-dimensional plane space and the DoG (Difference-of-Gaussian) scale space, in order to have good uniqueness and stability. DoG operator is defined as the difference of two Gaussian kernels with different scales, the characteristics of its simple computation, and that is approximation of normalized LoG (Laplacian-of-Gaussian) operator. DoG operator is defined as follow:

$$D(x,y,\sigma) = (G(x,y,k\sigma) - G(x,y,\sigma)) * I(x,y) = L(x,y,k\sigma) - L(x,y,\sigma). \quad (1)$$

SIFT features matching algorithm includes two stages. The first stage is to calculate the SIFT features vector, and the second stage is to match the SIFT feature vector. While calculate SIFT feature vector of images, gray gradient distribution character of neighboring pixels is used to calculate the direction parameters for each corner, so that SIFT operator will have rotation invariance. In practical applications, we sample in the neighborhood of the key point and count the neighboring pixels gradient direction by the histogram. Gradient histogram ranges from 0° to 360°, and it is one column per 10°and total to 36 columns. The peak of histogram represents the main gradient direction of the neighborhood, i.e., the direction of the key point. In the gradient histogram, where there is another peak that has 80% energy of the principal peak, the direction will be defined as the secondary direction of the key point. One key point may be specified with multiple directions (one main direction, more than one supplementary direction) to enhance the robustness of matching.

3 Geometric Features of Corners

The SIFT features vector not only is invariant to shift, rotation, and scale, but also take advantage of distinctiveness and calculation speed. However, because the algorithm depends on gray level of key point, but the gray level of the heterogeneous sensor images of the same goal may be inconsistent, so the rate of matching may be low due to difference of the gray level of two images.

The gradient amplitude and gradient direction of corners and neighborhood may affect the applicability of SIFT. Assuming there are many images of the same scene, the image A may have a distinct Contour, and image B may be similar to the black-white negative film, or the gray distribution of some regions in A is contrast to that in B, thus the gradient of edge in two images may be opposite; all would affect the matching results. On account of above reasons, gradients of corners and neighborhood are no longer used, but the geometric feature of corners is only. The algorithm we presented (named as Fast Algorithm Based on Geometric Feature of Corners, FABGFC) is divided into steps as follows: ①Extract the potential feature points using SIFT algorithm; ②extract the contour [18]; ③locate points on the contour as the primary key points to generate the geometric feature vector; ④register images using the geometric feature vector. For image taken by fisheye lens or distorted image, in step 3, points with local maximum but not in the contour are considered as the secondary key points. Link every other secondary key points, and if there are intersections of two lines, remove the longer line and keep the rest one. Register triangle regions which are made up of these lines again. The above steps will be described further as follows.

3.1 Determination of the Corners

There are many methods to extract feature point, such as the SUSAN operator [9], the Harris operator [10] and SIFT operator [15], etc. In SIFT algorithm, the procedure of extraction extremum in scale-space are: ①.calculate the convolution of input image $f(x, y)$ and Gaussian integrable function $G(x, y, \sigma)$, product the corresponding scale space $L(x, y, \sigma)$, and express with a Gaussian Pyramid; ②. subtract adjacent two-layer Gaussian Pyramid to generate differential Gaussian pyramid; ③. in differential Gaussian pyramid, detect the maxima points of the same layer 3×3 neighborhood and adjacent layer 3×3 neighborhood. In order to reduce computational complexity and ensure consistency and speed of our algorithm, the method of extract feature point which is used in SIFT is used.

According to the previous analysis, feature points obtained by above three steps have scale invariance. In order to extract more stable geometric feature, the contour which through the point can apply to calculate the feature vector, and points which have no intersection with the contour are ignored. But even so, feature points of different images which are photographed by different sensor have different feature vectors. The contour needs to be extracted in different scale spaces so as to obtain more stable and fewer feature points to accelerate the matching speed.

Edges of image are extracted as contour, but because of the presence of noise, contour through points will appear intermittent or not clear enough, so it needs to remove miscellaneous redundant edge and patch the edge according to contour characteristics

of objects. In this paper, a Canny operator is used to extract the image edge [19-20]. The Canny operator firstly proposed in 1986 by Canny. It is widely used in edge detection. The specific algorithm is as follows: ①filter images with Gauss-filter to remove noise; ②calculate the gradient amplitude $A(x, y)$ and direction $\theta(x, y)$ for each pixel in the filtered image to obtain gradient image; ③use non-maxima suppression technology on each point of gradient image, determine whether the candidate points are the corner, then generate the thinning edge; ④remove false edge by the Double Threshold Algorithm, link interruption to get the edge image. Obviously, the advantages of Canny Edge Detection Algorithm are as follows: ①suppress the noise interference with the Gaussian filter. ② obtain refined edge by non-maxima suppression technique. ③Use the Double Threshold Algorithm to eliminate impact of the false edge and increase the accuracy of edge locating. Research shows that in most cases, Canny Edge Detection Algorithm can generate a single pixel successive edge, but occasionally lead to phenomena such as breaking edge. Many algorithms were put forward to get continuous edge or profile. But these methods are complex, and the purpose of extracting profile is only to extract the geometric feature from corners, so the absolute accuracy of contour is not required. To make calculations simple and fast, an adjacent area (usually is a belt zone which containing the contour) that has a clear gradient change (judged by a threshold) is calculated firstly, and then, the skeleton of neighborhood is calculated to obtain more stable contour, which is denote by $profile(f(x, y))$.

Geometric feature of a point include point size, the number of lines through the point and the angle between the lines through the point and so on. Obviously, point size is not a good feature, because it is not an invariant to scale. Therefore, in FABGFC algorithm the geometric feature vectors of key points are composed of the number of lines through key points which is defined as $Degree$ (Denote briefly by N), and angles sequence. As a number of lines can form multiple angles, from maximum angle, clockwise, point by point take angles sequence as $(\theta_1, \theta_2 \cdots \theta_n)$, so total $(N + 1)$ feature values are obtained, and these feature parameters are more stable than gradient in the above cases. Furthermore, the calculation is simple and fast. Then, we can get the feature vector of a corner as $X = (N, \theta_1, \theta_2, \cdots, \theta_n)^T$.

3.2 Calculating Feature Vector of Corners

For calculating feature vectors, we define the distance of two corners $p(x_1, y_1)$ and $p(x_2, y_2)$ (denoted briefly by p_1 and p_2) which are in the same image as follow:

$$d(p_1, p_2) = distance(p_1, p_2) = \sqrt{(x_1 - x_2)^2 + (y_1 - y_2)^2}. \tag{2}$$

And define the minimum distance of image d_{min} as follow:

$$d_{min} = \left\{ d(p_i, p_j) | d(p_i, p_j) \leq d(p_k, p_l), i \neq j, k \neq l, and, if i = k then j \neq l, if j = l then i \neq k \right\}. \tag{3}$$

Let $R = \frac{d_{min}}{2}$ is the radius, and points $P(x_c, y_c)$are the centre, we get a circle, denote the circumference by $Circle(p_c, R)$, then the number of intersections of the circle and contour is defined as Degree:

$$Degree(p_c) = \#\{p | p \in Circle(p_c, R) \cup profile(f(x, y))\}. \tag{4}$$

And "#" express the Cardinality of set, this namely fore-mentioned 3.1 N of $X = (N, \theta_1, \theta_2, \cdots, \theta_n)^T$. Furthermore, the angles sequence of θ_i are need to calculate. So, the intersection points of circumference $Circle(p_c, R)$ and contour $profile(f(x, y))$ are numbered according to following algorithm for calculating the angle θ.

1. To the points in the Fourth Quadrant of Cartesian coordinate system, we number them according to the order of x decreasing gradually, y decreasing gradually also.

i. Determine the initial point; and take the point with the maximum x coordinate value as the initial point.

$$p_1 = \{p(x_{init}, y_{init}) | x_{init} > x_i, i \in [1 \cdots N], x_i, x_{init} \in Circle(p_c, R) \cup profile(f(x, y))\};\ i = 1;\ k = 1$$

ii. Initialize the point set with the points in the Fourth Quadrant, but p_1 is excluded.

$$set = \{p(x, y) | p(x, y) \in Circle(p_c, R) \cup profile(f(x, y)) - p_1, x \in [0..x_{init}], y \leq 0\}$$

iii. In the rest points, the point with maximum x and maximum y is the succeed one, and loop this step until $set = \emptyset$

$$p_{i+1} = \{p(x, y) | p(x, y) \in set, x \geq x_j, y \geq y_j, j \in [1..(N - i)]\}$$
$$set = set - p_{i+1};\ i = i + 1;\ k = k + 1$$

2. Number the points in the Third Quadrant of Cartesian coordinate system according to x decreasing gradually, and y increasing gradually.

i. Initialize the point set with points in the Third Quadrant

$$set = \{p(x, y) | p(x, y) \in Circle(p_c, R) \cup profile(f(x, y)), x < 0, y \leq 0\};\ i = 0$$

ii. In the rest points, the point with maximum x and minimum y is the succeed one, and loop this step until $set = \emptyset$

$$p_{i+1} = \{p(x, y) | p(x, y) \in set, x > x_j, y < y_j, j \in [1..(N - i)]\}$$
$$set = set - p_{i+1};\ i = i + 1;\ k = k + 1$$

3. Number the points in the Second Quadrant of Cartesian coordinate system according to x increasing gradually and y increasing gradually.

i. Initialize the point set with the points in the Second Quadrant

$$set = \{p(x, y) | p(x, y) \in Circle(p_c, R) \cup profile(f(x, y)), x \leq 0, y > 0\};\ i = 0$$

ii. In the rest point, the point with minimum x and minimum y is the succeed one, and loop this step until $set = \emptyset$

$$p_{i+1} = \{p(x, y) | p(x, y) \in set, x < x_j, y < y_j, j \in [1..(N - i)]\}$$
$$set = set - p_{i+1};\ i = i + 1;\ k = k + 1$$

4. Number the points in the First Quadrant of Cartesian coordinate system according to x decreasing gradually and y increasing gradually.

i. Initialize the point set with the points in the First Quadrant

$$set = \{p(x, y) | p(x, y) \in Circle(p_c, R) \cup profile(f(x, y)), x \geq 0, y > 0\};\ i = 0$$

ii. In the rest points, the point with minimum x and maximum y is the succeed one, and loop this step until $set = \emptyset$

$$p_{i+1} = \{p(x, y) | p(x, y) \in set, x < x_j, y > y_j, j \in [1..(N - i)]\}$$
$$set = set - p_{i+1};\ i = i + 1;\ k = k + 1$$

The intersections points of $Circle(p_c, R)$ and $profile(f(x,y))$ are numbered $P_1, P_2, \cdots, P_n$ according to clockwise direction. Especially, if $N=0$, define $\theta_1(P_c)=4\pi$ (or $\theta_1(P_c)=720$), respectively, if $N=1$, define $\theta_1(P_c)=2\pi$ (or $\theta_1(P_c)=360$). When $N \geq 2$, take any three consecutive points $P(x_c, y_c)$,$P(x_{i-1}, y_{i-1})$,$P(x_i, y_i)$, we judge whether they are in the same line, if so, let $\theta_1(P_c)=\pi$ and $\theta_2(P_c)=\pi$; Else if they are not in a line, then a triangle can form by these three points. Thus we can define:

$$\theta_i(p_c) = arccos\left(\frac{(d(p_c,p_{i-1})^2 + d(p_c,p_i)^2 - d(p_{i-1},p_i)^2)}{2d(p_c,p_{i-1})d(p_c,p_i)}\right). \tag{5}$$

where the subscript $i \in [1 \cdots N]$, N is the number of intersections points (i.e. Degree). Thus the geometry feature vector is defined as

$$X = (Degree, \theta_1, \theta_2, \cdots, \theta_N)^T. \tag{6}$$

Since the $Degree(P_i)$ will change while the i is change, the dimension of the feature vector will change, the calculation become difficult. So,
(a) traverse $\theta_1, \theta_2, \cdots, \theta_N$, let:

i. $\theta'_1 = \{\theta_i | \theta_i \geq \theta_j, i, j \in N, i \neq j\}$

ii. $\theta'_{1+k} = successor(\theta'_k) = \{\theta_{(i+k) mod N} | \theta_i \geq \theta_j, i, j, k \in [1 \cdots N], i \neq j\}$

iii. $successor(\theta_N) = \theta_1$

In the above formula,$successor(\theta_k)$ express the successor of θ_k, and θ_{i+k} express the k-th successor of θ_i, and mod denote calculating remainder. So the different between sequence $\{\theta'_i\}$ and $\{\theta_i\}$ is: θ'_1 is the maximum of $\{\theta_i\}$, and the order of other elements are keep invariable.
(b) We can stipulate that the first N_0 angles are adopted, if the number of angles is less than N_0, for instance, the number is m, then, the latter $N_0 - m$ angles are assigned 0. And if the number of angles is exceed N_0, the latter $(N - N_0)$ angles are ignored. According to (a) and (b), we can get N_0 angles, so the feature vector of corner can express as:

$$X(p_c) = (Degree(p_c), \theta_1(p_c), \theta_2(p_c), \cdots, \theta_N(p_c))^T. \tag{7}$$

In this example, we let $N_0 = 5$, and N_0 may be assigned other value in other cases. If necessary, the grey feature which is used in the SIFT algorithm and the length ratio of the angle both sides line [21] may be utilized also to enhance the description abilities of feature vector. But it needs to consider weight of each feature suitably, and make a compromise between the calculation complexity and feature stability.

3.3 Feature Matching

Feature matching is a process to find matching point in another image for each point in an image. An effective method of finding matching point is the Nearest Neighbor Algorithm, and the Nearest Neighbor point is a neighbor point of corner which has the shortest European distance to it.

In the European distance, weights for each component of feature vectors are the same. But in practical application, components of feature vector have a different

contribution to identify the corner in image. For images have no occlusion, the stability of $Degree(P_c)$ is higher than the angle θ. But if images have occlusion or camouflage, the stability of $Degree(P_c)$ may lower than the angle θ. If there is a disturbance, the relative error of $Degree(P_c)$ is different to angle θ. If it is in absence of occlusion and camouflage, the $Degree(P_c)$ almost have no error, but angle θ may have error. Generally, the $Degree(P_c)$ and θ are given different weights. So the definition of weighted distance l_{P_1,P_2} between two feature vectors is as follow:

$$l_{P_1,P_2} = \sqrt{(Degree(P_1) - Degree(P_2))^2 * w_1 + (\theta_1(P_1) - \theta 2(P_2))^2 * w_2 + \cdots + (\theta_N(P_1) - \theta_N(P_2))^2 * w_N}. \quad (8)$$

The Exhaustive Algorithm is an effective algorithm to find the Nearest Neighbor point. But if there are a large number of corners, the computational complexity will grow exponentially. To solve this problem, Friedman proposed the K-D Tree Algorithm in 1977 [13, 22]. The K-D Tree algorithm bases on the Exhaustive Algorithm and accelerates the computation. However, when the dimension of feature vector is greater than 10, the computational efficiency is still not much higher than the Exhaustive Algorithm. Subsequently, Beis and Lowe [23] proposed a approximation algorithm of the k-d tree (named Best-Bin-Fist, BBF). This algorithm can find the nearest neighbor with more rapidly and higher probability.

D. Lowe [15, 23] pointed out that if a global threshold was set to eliminate the false matching points. Although the false matching points may be eliminated, the right points may be removed also because each descriptor has high uniqueness. So the ratio of the nearest neighbor distance to the second nearest neighbor distance is used, and a threshold ratio is specified to determine whether a point is a matching point. In this paper, the threshold value is assigned 0.6, i.e., p_c^f is a point of image f, the nearest neighbor point p_r^g and the second nearest neighbor point p_s^g in reference image g are found, then the distance $l(p_c^f, p_r^g)$ and the second nearest neighbor distance $l(p_c^f, p_s^g)$ are calculated according to the formula (8), let $ratio = \frac{l(p_c^f, p_r^g)}{l(p_c^f, p_s^g)} > threshold = 0.6$. In the BBF algorithm, when the number of leaf nodes is 150, the BBF algorithm can find out the nearest neighbor by more than 90% probability [23]. Therefore, the number of leaf nodes is assigned 160. For each feature point, the nearest neighbor point and the second nearest neighbor point are found in the reference image according to the BBF algorithm. Then, the distance ratios are judged by the threshold value 0.6, if the ratio is less than 0.6, a matching point is found, otherwise, it is not a match point. Other matching points are found in the same way. The transformation matrix can be calculated by using these points in theory. However, in order to improve the accuracy of registration, RANSAC [24] consistency testing is done with these points, and removes these point-pairs which may cause the registration errors.

4 Experimental Results

The experiments were done by using the SIFT algorithm and the FABGFC algorithm, and the match results and time-consumed of two algorithm were given as follows.

Fig.1 shows the registration results of the SIFT algorithm and the FABGFC algorithm. Among them, the left part is the results of SIFT algorithm and the right part is the result of FABGFC algorithm. As can be seen from Figure 1, FABGFC algorithm

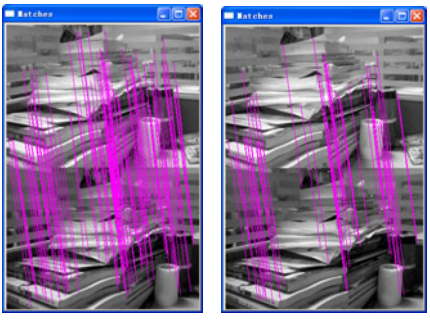

(a) (b)

Fig. 1. The registration result of experiments, (a) used SIFT algorithm and (b) used FABGFC algorithm

has a better result than SIFT algorithm. Because the FABGFC algorithm do not excessively extract many point-pairs with similar features, simultaneously, it extracts the feature points used the geometric feature and rejects some less accurate feature point, the FABGFC algorithm can calculate more rapidly and more accurately.

The FABGFC algorithm uses geometric feature which is invariant to rotation, gray scale, texture, shift, and scale, but is not gray, texture and edge. So it can match images of different sensors, and can automatically register images. Moreover, the algorithm has very intuitive registration criteria and high computation speed. In addition, if the FABGFC algorithm is used to register the multi-source images which are photographed by heterogeneous sensor, the actual effect of registration should be better. The related experiment is in progress. In practical application, the grey feature which is used in the SIFT algorithm and the ratio of the line lengths which formed the angle [21] may be utilized to significantly improve registration effect, if it is necessary.

Table 1. The matching result comparison of SIFT and FABGFC algorithm

	Elapsed time(s)	Matching / Extracted points	Matching ratio
SIFT	3.4177	200/624	0.3205
FABGFC	3.0639	77/173	0.4451

It is worth noting that the data of Table1 have not been optimized, if optimize the algorithm, it will significantly improve the speed and match effect. And the optimization of the FABGFC Algorithm, i.e., how to further improve the speed and accuracy of registration, is the work of next step.

References

1. Ruwwe, C., Keck, B., Rusch, O., Zolzer, U., Loison, X.: Image registration by means of 3D octree correlation. In: IEEE 10thWorkshop on Multimedia Signal Processing (MMSP), pp. 515–519 (2008)
2. Wei, B.Z., Zhao, Z.M., Peng, X.: A novel method of medical image registration based on feature point mutual information. Journal of Information and Computational Science 7, 559–566 (2010)

3. Wen, J.T., Wang, B.X., Qin, Y.: Rapid image registration based on local grey scale gradient characteristics. Journal of Tsinghua University 49, 673–675 (2009)
4. Xu, M., Chen, A., Varshney, P.K.: Ziv-Zakai bounds on image registration. IEEE Transactions on Signal Processing 57, 1745–1755 (2009)
5. Klein, S., Staring, M., Pluim, J.: Evaluation of optimization methods for nonrigid medical image registration using mutual information and b-splines. IEEE Transactions on Image Processing 16, 2879–2890 (2007)
6. Brown, L.G.: A survey of image registration techniques. ACM Computing Surveys 24, 326–376 (1992)
7. Fonseca, L.M.G., Costa, M.H.M.: Automatic registration of satellite images. In: Proceedings of the Brazilian Symposium on Computer Graphic and Image Processing, pp. 219–226 (1997)
8. Belongie, S., Malik, J., Puzicha, J.: Shape matching and object recognition using shape contexts. IEEE Transactions on Pattern Analysis and Machine Intelligence 24, 509–522 (2002)
9. Smith, S.M., Brady, J.M.: SUSAN: A new app roach to low level image processing. Journal of Vision 1, 45–78 (1997)
10. Harris, C.G., Stephens, M.J.: A Combined Corner and Edge Detector. In: Proceedings of Fourth Alvey Vision Conference, Manchester, pp. 147–152 (1988)
11. Forstner, W., Gulch, E.: A fast operator for detection and precise location of distinct points, corners and centres of circular features. In: Proceeding of Intercom-mission Workshop on Fast Processing of Photogrammetric Data, Interlaken, Switzerland, pp. 167–170 (1987)
12. Moravec, H.P.: Towards automatic visual obstacle avoidance. In: Proc.5th Intern. Joint Conf. Artif Intett., Cambridge, VIA, USA, pp. 584–589 (1977)
13. Philippe, C., Devroye, L., Carlos, Z.C.: Analysis of range search for random k-d trees. Acta Informatica 37, 4–5 (2001)
14. Viola, P., Jones, M.J.: Robust Real Time Face Detection. International Journal of Computer Vision 57, 137–154 (2004)
15. Lowe, D.G.: Distinctive image features from scale-invariant key points. International Journal of Computer Vision 60, 91–110 (2004)
16. David, G.L.: Object recognition from local scale-invariant features. In: Proceedings of the International Conference on Computer Vision, pp. 1150–1157 (1999)
17. Ke1, Y., Sukthankar, R.: PCA-SIFT: a more distinctive representation for local image descriptors. In: Proceedings of the 2004 IEEE Computer Society Conference on Computer Vision and Pattern Recognition, Washington D.C., USA, pp. 506–513. IEEE Computer Society, Los Alamitos (2004)
18. Zou, B.X., Lin, J.R.: Contour extraction research of image. Computer Engineering and Applications 44, 161–165 (2008)
19. Bao, P., Zhang, L., Wu, X.L.: Canny Edge Detection Enhancement by Scale Multiplication. IEEE Transactions on Pattern Analysis and Machine Intelligence 27, 1485–1490 (2005)
20. Canny, J.: A Computational Approach to Edge Detection. IEEE Transactions on Pattern Analysis and Machine Intelligence 8, 679–698 (1986)
21. Jiang, S.H., Wang, C., Chen, X.S., Zhu, H.B.: A Method of Recognizing Military Object from Occluded Images. Journal of Chinese Computer Systems, 1196–1203 (2010)
22. Friedman, J.H., Bentley, J.L., Finkel, R.A.: An algorithm for finding best matches in logarithmic expected time. ACM Transactions on Mathematical Software 3, 209–226 (1977)
23. Beis, J., David, G.L.: Shape indexing using approximate nearest-neighbor search in high-dimensional spaces. In: Conference on Computer Vision and Pattern Recognition, Puerto Rico, pp. 1000–1006 (1997)
24. Fischler, M.A., Bolles, R.C.: Random sample consensus: a paradigm for model fitting with applications to image analysis and automated cartography. ACM Commun. 24, 381–395 (1981)

Newborn Footprint Recognition Using Subspace Learning Methods

Wei Jia[1], Jie Gui[1,2], Rong-Xiang Hu[1,2], Ying-Ke Lei[1,2,3], and Xue-Yang Xiao[1,2]

[1] Hefei Institute of Intelligent Machines, CAS, Hefei, China
[2] Department of Automation, University of Science and Technology of China
[3] Department of Information, Electronic Engineering Institute, Hefei, China
icg.jiawei@gmail.com

Abstract. In this paper, we propose a novel online newborn personal authentication system based on footprint recognition. Compared with traditional offline footprinting scheme, the proposed system can capture digital footprint images with high quality. We also develop a preprocessing method for orientation and scale normalization. In this way, a coordinate system is defined to align the images and a region of interest (ROI) is cropped. In recognition stage, several representative subspace learning methods such as PCA, LDA are exploited for recognition. A newborn footprint database is established to examine the performance of the proposed system, and the promising experimental results demonstrate the effectiveness of proposed system.

Keywords: Biometric, Newborn, Infant, Footprint recognition, Subspace learning methods.

1 Introduction

In information and network society, there are many occasions in which the personal authentication is required. There is no doubt that biometric is one of the most important and effective solutions for this task. Generally, biometric is a field of technology that uses automated methods for identifying or verifying a person based on a physiological or behavioral trait [1]. In real applications, the traits that are commonly measured in different systems are the face, fingerprints, hand geometry, palmprint, handwriting, iris, and voice, etc [1]. However, most biometric systems mentioned above are developed for adults. How to design a biometric system for newborns and infants has not been well studied in the past. Therefore, few literatures and products about this issue can be found from scientific document databases and markets.

Actually, in many countries, footprint recognition has been used for newborn personal authentication for a long time. Usually the footprints are collected with ink spread on the foot with a cylinder or a paper, and then printed on the newborn's medical record, along with the mother's fingerprint [2].

Fig. 1 depicts two inked newborn footprint images. It can be seen that some thin lines can't be clearly observed, and some thick lines become white areas. Due to bad image quality of offline footprinting, it is nearly impossible to obtain desirable recognition rates.

D.-S. Huang et al. (Eds.): ICIC 2010, LNCS 6215, pp. 447–453, 2010.

Fig. 1. Inked footprint images

Several researchers have conducted experiments to evaluate the recognition performance of offline footprinting. Unfortunately, they drawn a conclusion that newborn' offline footprinting can't be used for identification purposes, and then the acquisition of footprints in hospital should be abandoned because it only generates unnecessary work and costs [2].

As stated previously, offline footprinting can't satisfy the demanding for fast and reliable newborn personal authentication. The online system based on digital image acquisition and processing is becoming a promising choice for this task. Generally, an online system captures footprint images using a digital capture sensor that can be connected to a computer for fast processing. In this paper, we propose an online newborn footprint recognition system based on low-resolution imaging. The resolution of image used for recognition is less than 100 dpi.

2 Image Acquisition and Preprocessing

In our system, the first step is image acquisition. We captured the newborns' footprint images using a digital camera, whose type is Cannon Powershot SX110 IS. The image capturing work was done in Anhui Province Hospital, which is one the biggest hospital in Anhui province, China. When capturing images, two persons are needed. One person is one of the authors of this paper, whose task is to take pictures using camera. The other person is a nurse of hospital, whose tasks are to pacify the newborn and hold the foot.

In order to facilitate image segmentation, we used a black cloth to wrap the ankle. Fig. 2 depicts a captured color footprint image, whose cloth background has been removed by image segmentation method. It can be seen that the quality of online footprint image is much better than that of inked footprint image. So it is possible to achieve promising recognition rates using online system.

All the images were collected in one session during the first two days following birth. After we explained some knowledge about the importance and significance about Newborn's Biometrics to newborn's parents, they consented that we can capture footprint images once and use these images for scientific research purpose. However, we failed to collect the images again from a same newborn since most parents declined our request of second image capturing. The main reason is that, in China, a newborn is so important for a family that the parents are unwilling to let other persons, especially strangers, to touch their baby once again. So they were very impatient for our second request. At last, we regretted to abandon the second image collection.

Fig. 2. A captured digital footprint image

In image acquisition stage, a crucial problem is to select an opportune time to capture images. If a newborn is hungry or crying, he/she will ceaselessly move his/her hands, feet, and whole body. In this time, it is difficult to capture footprint images with desirable quality. On the contrary, if a newborn is calm or sleeping, the task of image capturing will become easy. In this paper, all images were captured when newborns were calm or sleeping.

After image acquisition, the next task is image preprocessing. In our image acquisition system, orientation and scale changes between different images captured from a same foot are inevitable caused by unconstrained image acquisition. Thus, several tasks should be done in preprocessing stage, i.e., orientation normalization, scale normalization and ROI extraction.

In [3], Nakajima et al. proposed a footprint recognition scheme utilizing pressure-sensing, and described an orientation normalization method for footprint pressure images, which can also be used in our system. The main steps of orientation normalization are given in Fig. 3.

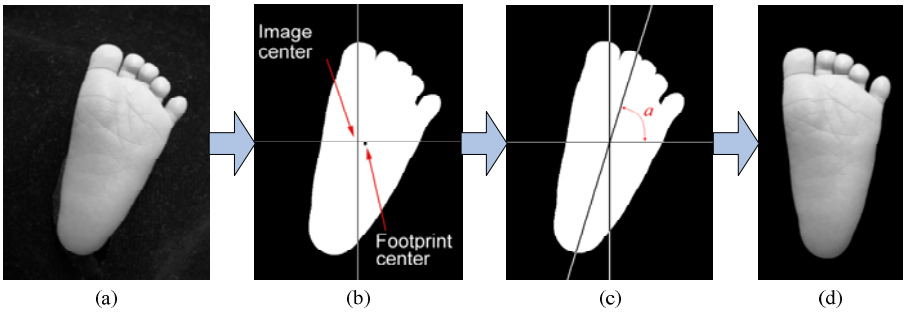

Fig. 3. Orientation normalization. (a) Original gray image $G(x,y)$, (b) Binary image $B(x,y)$, and the center of footprint, (c) estimating the angle of major axes of footprint, from image $C(x,y)$, (d) orientation normalized

We can perform the scale normalization at the vertical or horizontal direction. Vertical based scale normalization means that all footprints should have the same height in the position of crossing foot center. However, toes of the foot may have different poses. Thus, vertical based scale normalization may be not very reliable. In this paper, we conducted the scale normalization at the horizontal direction. Here, WH denotes the horizontal width of foot crossing foot center. For horizontal based scale normalization, all footprints were normalized to have the same WH, i.e., 246 pixels, which is the mean of all footprints' WH. Fig. 4(a) and (e) are two images captured from a same newborn's foot. Obviously, there exist scale changes between them. Their normalization images are Fig. 4(b) and (f), respectively. It can be observed that the scale varieties have been well corrected. After scale normalization, the center part (ROI) of normalized image was cropped for feature extraction (see Fig. 4(c), (d), (g), and (h)). The size of ROI image is 220×180.

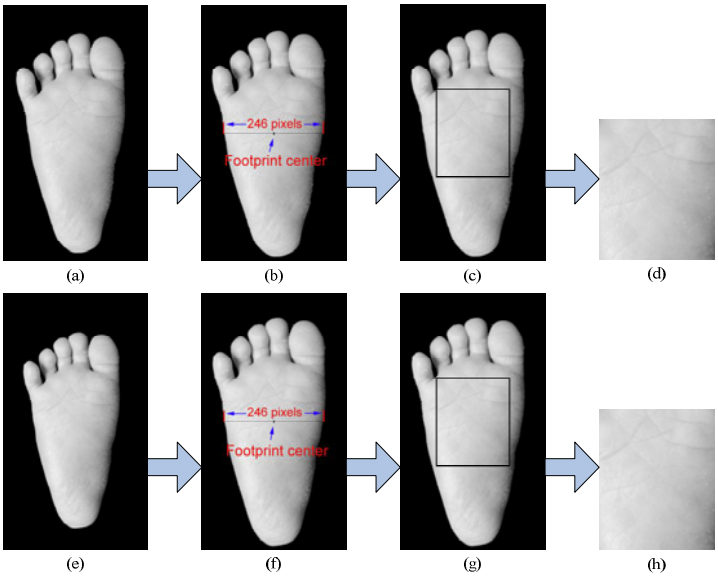

Fig. 4. Scale normalization and ROI extraction

3 Several Representative Subspace Learning Methods

Generally, classical subspace learning methods seek to find a low-dimensional subspace in a high-dimensional input space by linear transformation, which are also called appearance methods or subspace analysis methods. This low-dimensional subspace can provide a compact representation or extract the most discriminant information of the high-dimensional input data. It is well known that principal component analysis (PCA) [4] and linear discriminant analysis (LDA) [4] are two typical subspace learning methods. PCA is the optimal representation of the input data in the sense of the minimum reconstruction error. In contrast to PCA, LDA takes the class labels into consideration and can produce optimal discriminant projections. As we know, kernel PCA (KPCA) and kernel LDA (KLDA) are kernel based versions of

PCA and LDA, 2DPCA [5] and 2DLDA [6] are matrix based versions of PCA and LDA, and concurrent subspaces analysis (CSA) [7] and multilinear discriminant analysis (MDA) [8] are tensor based versions of PCA and LDA.

It should be noted that many subspace learning methods have been proposed in recent years. In this paper, due to space limitation, only PCA, LDA and their improved versions will be used for newborn's footprint recognition.

4 Experiments

A newborn's footprint database was established. In total, the database contains 1968 images from 101 newborns' feet. That is, about 19~20 images were collected from each foot. In each class, we use the first three footprint images for training and leave the remaining footprint images for test. Therefore, the numbers of images for training and test are 303 and 1635, respectively. In experiments, the nearest neighbor rule (1NN) is used for classification. The the accuracy recognition rate is exploited to evaluate the identification performance. For convenience, the top part of ROI image whose size is 180×180 is used for feature extraction. And then we resize this part from 180×180 to 128×128. Fig 5~8 depict the recognition rates of different methods under different dimensions. Table 1 lists the highest recognition rate of different

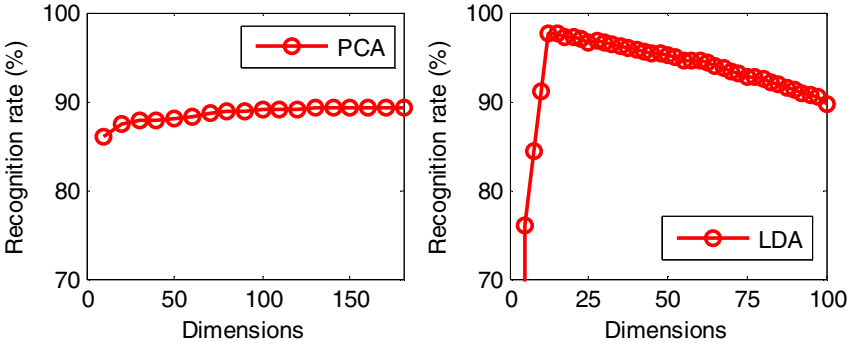

Fig. 5. Recognition rates of PCA and LDA under different dimensions

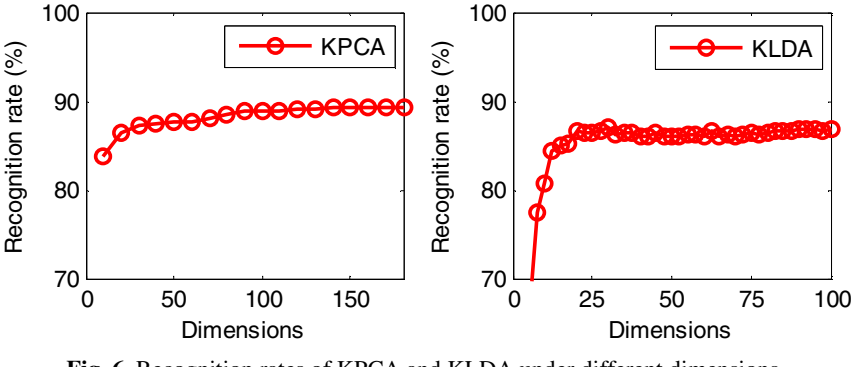

Fig. 6. Recognition rates of KPCA and KLDA under different dimensions

methods and corresponding dimension. Among all methods, 2DLDA achieves the best recognition rate of 98.04%. From Fig 4~7 and Table 1, it can be concluded that subspace learning methods are very effective for newborn's footprint recognition.

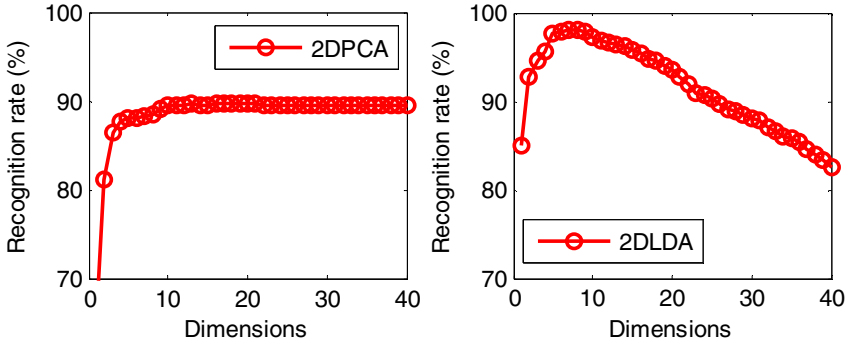

Fig. 7. Recognition rates of KPCA and KLDA under different dimensions

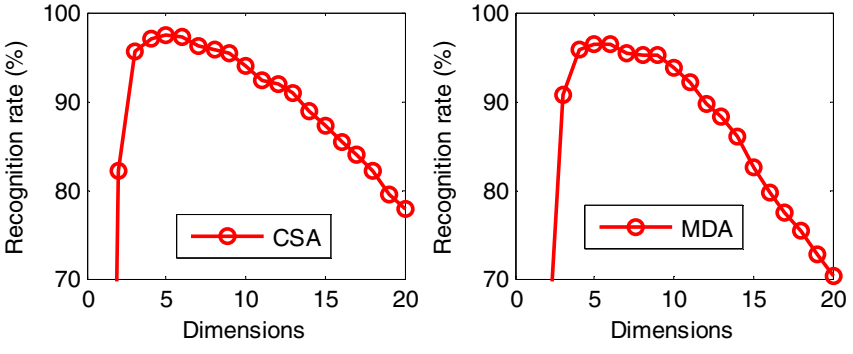

Fig. 8. Recognition rates of KPCA and KLDA under different dimensions

Table 1. Highest recognition rate (%) of different methods and corresponding dimension

	PCA	LDA	KPCA	KLDA	2DPCA	2DLDA	CSA	MDA
Highest recognition rate (%)	89.36	97.74	89.30	95.33	89.60	98.04	97.37	96.51
Dimension	140	10	150	100	13×128	7×128	5×5	5×5

5 Conclusion

In this paper, we proposed a novel online newborn recognition system for newborn personal authentication. We developed preprocessing methods for orientation and scale normalization of footprints, and utilized several representative subspace learning methods for recognition. Compared with traditional offline footprinting scheme, the proposed system can capture footprint images with high quality, has fast processing

speed, and more importantly, achieves very promising recognition performance. So, our work has important significance in the research of newborn personal authentication. In the future, we will develop other new algorithms to further improve the recognition performance.

Acknowledgment. This work was supported by the grants of the National Science Foundation of China, Nos. 60705007, 60905023, 60975005, 60873012, and 60805021, the grant of Postdoc Foundation of China, No. 200801231, and the grant of the Knowledge Innovation Program of the Chinese Academy of Sciences.

References

1. Jain, A.K., Ross, A., Prabhakar, S.: An Introduction to Biometric Recognition. IEEE Transactions on Circuits and Systems for Video Technology. Special Issue on Image and Video based Biometrics 14(1), 4–20 (2004)
2. Weingaertner, D., Bello, O., Silva, L.: Newborn's Biometric Identification: Can It Be Done? In: Proceedings of the VISAPP, vol. (1), pp. 200–205 (2008)
3. Nakajima, K., Mizukami, Y., Tanaka, K., Tamura, T.: Footprint-based Personal Recognition. IEEE Transactions on Biomedical Engineering 47(11), 1534–1537 (2000)
4. Belhumeur, P., Hespanha, K.: Eigenfaces vs. Fisherfaces: Recognition Using Class Specific Linear Projection. IEEE Trans. Pattern Anal. Mach. Intell. 19(7), 711–720 (1997)
5. Yang, J., Zhang, D., Frangi, A., Yang, J.: Two-Dimensional PCA: A New Approach to Appearance-Based Face Representation and Recognition. IEEE Trans. Pattern Analysis and Machine Intelligence 26(1), 131–137 (2004)
6. Li, M., Yuan, B.: 2D-LDA: A Novel Statistical Linear Discriminant Analysis for Image Matrix. Pattern Recognition Letter 26(5), 527–532 (2005)
7. Xu, D., Yan, S., Zhang, L., Lin, S., Zhang, H., Huang, T.: Reconstruction and Recognition of Tensor-based Objects with Concurrent Subspaces Analysis. IEEE Trans. on Circuits Systems for Video Technology 18(1), 36–47 (2008)
8. Yan, S., Xu, D., Yang, Q., Zhang, L., Tang, X., Zhang, H.: Multilinear Discriminant Analysis for Face Recognition. IEEE Trans. on Image Processing 16(1), 212–220 (2007)

Plant Classification Using Leaf Image Based on 2D Linear Discriminant Analysis

Minggang Du[1] and Shanwen Zhang [2]

[1] School of Urban and Environment Science, Shanxi Normal University,
Linfen, Shanxi 041004, P.R. China
[2] Institute of Intelligent Machines, Chinese Academy of Sciences,
Hefei 230031, P.R. China
wjdw716@163.com, dumg966@163.com

Abstract. The 2D-LDA algorithm operates on data represented as 2D matrices, instead of 1D vectors, so that the dimensionality of the data representation can be kept small as a way to alleviate the SSS problem. Given a set of samples of each class, the 2D-LDA extracts most informative features which could establish a high degree of similarity between samples of the same class and a high degree of dissimilarity between samples of two classes. In this paper, we apply 2D-LDA to plant leaf classification. The experiments on the real plant leaf database demonstrate that 2D-LDA is effective and feasible for plant leaf classification.

Keywords: Linear discriminant analysis (LDA), 2D-LDA, small-sample-size problem, plant leaf classification.

1 Introduction

Dimensional reduction is an important issue when facing high dimensional data. Linear discriminant analysis (LDA) [1] encodes discriminatory information by finding directions that maximize the ratio of between-class scatter to within-class scatter. However, there are some main drawbacks of LAD. To solve these problems, a principle component analysis (PCA) plus LDA method was proposed [2]. In this approach, PCA is used as a preprocessing step for dimensionality reduction so as to discard the null space of the within-class scatter matrix of the training data set. Then LDA is performed in the lower dimensional PCA subspace. However, the PCA step may discard dimensions that contain important discriminant information. There is another approach to address the SSS problem, with 2D LDA (2D-LDA) [3-14] being the representative of this approach. The major difference between the 2D-LDA algorithms and the LDA algorithms lies in their data representation. Specifically, 2D-LDA operates on data represented as (2D) matrices, instead of (1D) vectors, so that the dimensionality of the data representation can be kept small as a way to alleviate the SSS problem. They pointed out that from the bias estimation point of view, 2D-LDA might be more stable than 1D LDA. In this paper, the 2D-LDA algorithm is introduced to classify the plant leaf images. 2D-LDA helps to overcome the SSS problem and improve the classification results.

D.-S. Huang et al. (Eds.): ICIC 2010, LNCS 6215, pp. 454–459, 2010.

The rest of this paper is organized as follows: Section 2 gives a brief review of the LDA and 2D-LDA algorithms. Experimental results on plant leaf classification are given in Section 3. Finally, some concluding remarks are provided in Section 4.

2 Linear Discriminant Analysis (LDA)

LDA is one of the most popular dimensional reduction methods, which tries to find an optimal projection that best discriminates the different data classes by optimizing the ratio between the within-class scatter S_w and the between-class scatter S_b in the low-dimensional representation of the data. S_w and S_b are defined respectively as follows

$$S_b = \sum_{i=1}^{c} \|C_i\| \cdot (\overline{M_i} - \overline{M})(\overline{M_i} - \overline{M})^T \tag{1}$$

$$S_w = \sum_{i=1}^{c} \sum_{x_k \in C_i} (x_k - \overline{M_i})(x_k - \overline{M_i})^T \tag{2}$$

where $\overline{M_i}$ is the class mean of the class C_i, $\overline{M}$ is the global mean of all samples, and $\|C_i\|$ is the cardinality of C_i.

LDA finds a projection matrix A by maximizing the following objective function:

$$A_{LDA} = \arg\max_{A} \frac{\left|A^T S_b A\right|}{\left|A^T S_w A\right|} \tag{3}$$

where the solution $\{a_i | i = 1,2,...,d\}$ is a set of generalized eigenvectors of S_b and S_w corresponding to the d largest generalized eigenvalues $\{\lambda_i | i = 1,2,...,d\}$, i.e., $S_b a_i = \lambda_i S_w a_i$, $i = 1,2,...,d$. The projection matrix is formed by $A = [a_1, a_2, ..., a_d]$.

3 Two-Dimensional LDA (2D-LDA)

2D-LDA is based on 2D matrices rather than 1D-vector, which is introduced as follows. Suppose 2D-LDA $X = [X_1, X_2, ..., X_N]$ be N image matrices of size $m \times n$, which belong to C known pattern classes, $C_1, C_2, ..., C_c$, N is the total number of training samples and $|C_i|$ is the number of training samples in class C_i. The jth training image in class C_i is denoted by an $m \times n$ matrix X_j^i. The mean image of training samples in class C_i is denoted by $\overline{X_j^i}$ and the mean image of all training sample is $\overline{X}$. Then the between-class scatter matrix G_b and the within-class scatter matrix G_w of the training images are written as follows:

$$G_b = \sum_{i=1}^{c} \|C_i\| \cdot (\overline{X^i} - \overline{X})(\overline{X^i} - \overline{X})^T \tag{4}$$

$$G_w = \frac{1}{N}\sum_{i=1}^{c}\sum_{X_k \in C_i}(X_k - \overline{X^i})(X_k - \overline{X^i})^T \tag{5}$$

2D-LDA attempts to seek a set of optimal discriminating vectors to form a transform A by maximizing the following Fisher criterion:

$$J(A) = \frac{\left|A^T G_b A\right|}{\left|A^T G_w A\right|} \tag{6}$$

It can be proven that the eigenvector corresponding to the maximum eigenvalue of $G_w^{-1}G_b$ is the optimal projection vectors which maximizes $J(W)$. Generally, as it is not enough to have only one optimal projection vector, we usually look for d projection axes, say $a_1, a_2, ..., a_d$, which are the eigenvectors corresponding to the first d largest eigenvalues of $G_w^{-1}G_b$. In 2D-LDA, once these projection vectors are computed, each training image X_j^i is then projected to Y_j^i of size $m \times d$ of the training image X_j^i. The solution to the optimization problem (6) is obtained by an eigenvalue decomposition of $G_w^{-1}G_b$ and taking the d eigenvectors corresponding to the d largest eigenvalues. So, during training, for each training image X_j^i, a corresponding feature matrix of size $m \times d$ is constructed and stored for matching at the time of recognition and classification. So the given n-dimensional images reduce to $d (d < n)$ dimensions.

Let $A = [a_1, a_2, ..., a_d]$ be the Fisher optimal projection matrix, and the new data X is projected onto A by the following linear transformation:

$$Y = A^T X \tag{7}$$

The main aim of data classification is to seek a projection characterized by within-class compactness and between-class separability. The 2D-LDA algorithm can be applied to data classification. The classification procedure is formally summarized as follows:

Step 1: Use training data to compute the between-class scatter matrix G_b and the within-class scatter matrix G_w by Eqs.(4) and (5).

Step 2: Construct the objective function, i.e., Eq.(6) and compute the eigenvectors of $G_w^{-1}G_b$, then form the transformation matrix A.

Step 3: Project the test data points into low-dimensional subspace by Eq.(7).

Step 4: Predict the corresponding class labels by using the nearest neighbor classifier. The principle of the nearest neighbor classifier is simply explained as follows:

For the projection Y_{test} corresponding to the test image X_{test}, compute the distance $d(Y_{test}, Y_m) = \|Y_{test} - Y_m\|$. If the distance between Y_{test} and Y_m is minimal, and Y_m belong to the mth class, then X_{test} is classified as belonging to the mth class.

4 Experiment Results

Whether for agriculture informization or ecological protection, the study of the plant leaf classification is very necessary. In this subsection, using the plant leaf images, we try to classify the plant by the 2D-LDAmethod.

All the plant leaf images are collected at Hefei Botanical Garden in Hefei, the capital city of Anhui province of China by people from Intelligent Computing Laboratory (ICL) in Institute of Intelligent Machines, Chinese Academy of Sciences. For the whole dataset, there are 17032 plant leaf images of 220 species and image number of each class is unequal. To verify the 2D-LDA method for plant classification, we select 1500 leaf images from 50 kinds of plants; each kind of plant leaf contains 30 images, in this subset all classes are carefully selected and most of the shapes could be distinguished easily by human. All kinds of plants are also carefully selected and most of the shapes are similar but still distinguishable. Fig.1 shows some examples.

Fig. 1. Typical images from the ICL leaf data set

Since the original leaf images are not squares, we enlarge them with background color to form square images before resizing. All images are cropped and normalize (in scale and orientation) and resized to 32×32 pixels by histogram equilibrium with 255 gray levels per pixel and with the white background. The preprocessed images are shown in Fig.2, where (B) are gray images with the white background.

Then we reduce the dimension of images by 2D-LDA, this dimension reduction process significantly improves the classification performance. After dimension reduction, the k nearest neighbor classifier is used for the final classification.

The leaf dataset randomly is split into two parts which are used for training set and the second part is kept for test set. For each kind of plant, we randomly select l leaf images from each class as training set, and the rest (30-n) are considered as test set. For each given l, we perform 50 times experiments to choose randomly the training set. The final result is the average classification rate over 50 splits. Table 1 shows the maximal average classification results of the Baseline, LDA and 2D-LDA. For Baseline, we simply perform nearest-neighbor classification in the original 1024-dimensional space. For LDA, we transform the 2D leaf images into 1024-dimensional vectors. PCA is adopted as preprocess in before performing LDA.

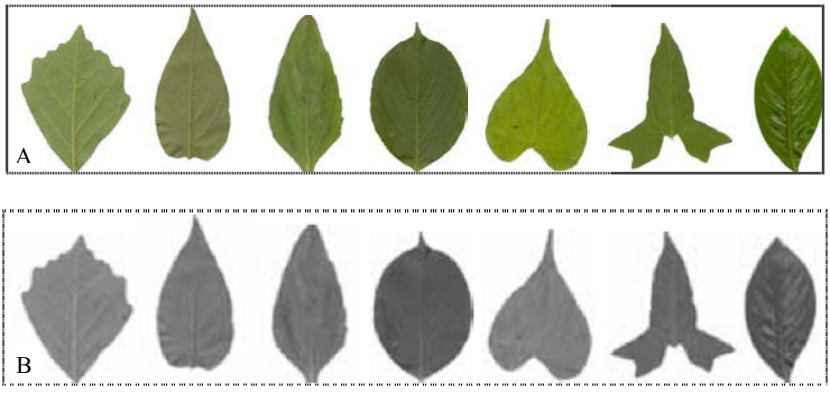

Fig. 2. Preprocessed leaf images

Table 1. The maximal average classification rates with standard deviations of Baseline, LDA and 2D-LDA

Method	l =6	l =10	l =14	l =18	l =22	l =24
Baseline	0.5934 ±0.031	0.7879 ±0.033	0.8203 ±0.024	0.8639 ±0.025	0.9125 ±0.028	0.9215 ±0.024
LDA	0.6474 ±0.053	0.8484 ±0.035	0.9074 ±0.038	0.9272 ±0.034	0.9443 ±0.034	0.9574 ±0.038
2D-LDA	0.7332 ±0.034	0.8812 ±0.036	0.9459 ±0.037	0.9543 ±0.034	0.9647 ±0.033	0.9742 ±0.031

LDA and 2D-LDA take full advantage of class information and try to find a projection to map the nearby points with the same label as close as possible while map the nearby points with different labels as far apart as possible. The key difference between LDA and 2D-LDA lies in the model for data representing form. LDA works with vectorized representations of data, while 2D-LDA works with matrix representation of data. By encoding each image as a matrix, 2D-LDA can capture higher-order structures in the data without requiring a large sample size. That is to say that 2D-LDA can overcome the curse of dimensionality dilemma and the singularity problem implicitly. Not only does 2D-LDA have a lower computational complexity than LDA, but it is superior to LDA in terms of its recognition accuracy.

5 Conclusions

This paper introduced the 2D linear discriminant analysis algorithm for plant leaf classification. By encoding each image as a naturally matrix, 2D-LDA can capture higher-order structures in the data without requiring a large sample size and has a lower computational complexity than other image-as-vector methods. In plant leaf classification experiments, 2D-LDA is adopted to extract the classification feature. Experimental

results showed that 2D-LDA is effective and feasible. 2D-LDA is linear projection algorithm, which may fail to discover the intrinsic geometrical structure when the data are highly nonlinear. Our future work is to generalize the 2D-LDA algorithm to nonlinear case. This is another future work.

Acknowledgment

This work was supported by the grants of the National Science Foundation of China, Nos. 60975005, 60905023, 60873012 & 60805021, the grant of the Guide Project of Innovative Base of Chinese Academy of Sciences (CAS), No.KSCX1-YW-R-30.

References

1. Yang, J., Yang, J.Y.: Why can LDA be performed in PCA transformed space? Pattern Recognition 36(2), 563–566 (2003)
2. Li, M., Yuan, B.: 2D-LDA: a statistical linear discriminant analysis for image matrix. Pattern Recognition Letters 26, 527–532 (2005)
3. Yang, J., Zhang, D., Xu, Y., Yang, J.J.: Two-dimensional discriminant transform for face recognition. Pattern Recognition 38, 1125–1129 (2005)
4. Xiong, H.L., Swanmy, M.N.S., Ahmad, M.O.: Two-dimensional FLD for face recognition. Pattern Recognition 38, 1121–1124 (2005)
5. Jing, X.Y., Wong, H.S., Zhang, D.: Face recognition based on 2D fisher-face approach. Pattern Recognition 39, 707–710 (2006)
6. Zheng, W.S., Lai, J.H., Li, S.Z.: 1D-LDA vs. 2D-LDA: when is vector-based linear discriminant analysis better than matrix-based. Pattern Recognition 41(7), 2156–2172 (2008)
7. He, X.F., Cai, D., Niyogi, P.: Tensor Subspace Analysis. In: Advances in Neural Information Proceeding Systems, Vancouver, Canada, vol. 18 (2005)
8. Tao, D.C., Li, X.L., Wu, X.D., et al.: General tensor discriminant analysis and gabor features for gait recognition. IEEE Transactions on Pattern Analysis and Machine Intelligence 29(10), 1700–1715 (2007)
9. Tao, D.C., Li, X.L., Hu, W.M., et al.: Supervised tensor learning. Knowledge and Information Systems (Springer: KAIS) 13(1), 1–42 (2007)
10. Yang, J., Zhang, D., Frangi, A.F., Yang, J.Y.: Two-dimensional PCA: a new approach to appearance-based face representation and recognition. IEEE Transactions on Pattern Analysis and Machine Intelligence 26(1), 131–137 (2004)
11. Yan, S., Xu, D., Yang, Q., Zhang, L., Tang, X., Zhang, H.: Multilinear discriminant analysis for face recognition. IEEE Trans. on Image Processing, 212–220 (January 2007)
12. Chen, S., Zhao, H., Kong, M., Luo, B.: 2D-LPP: A two-dimensional extension of locality preserving projections. Neurocomputing 70, 912–921 (2007)
13. Yu, W.: Two-dimensional discriminant locality preserving projections for face recognition. Pattern Recognition Letters 30, 1378–1383 (2009)
14. Chen, H.T., Chang, H.W., Liu, T.L.: Local discriminant embedding and its variants. In: Proceedings of the IEEE Computer Society Conference on Computer Vision and Pattern Recognition, vol. 2, pp. 846–853 (2005)

Palmprint Recognition Combining LBP and Cellular Automata

Xiao Dong Dai, Bing Wang, and Pei ZhenWang

Institute of Electrical and Information
Anhui University of Technology, Maanshan, China
dxdong.everyday@gmail.com

Abstract. In this paper, we present a palmprint recognition method which combines local binary pattern (LBP) and cellular automata. The LBP descriptor is proposed as a unifying texture model that describes the formation of a texture with micro-textons and their statistical placement rules. Because texture is one of the most important features in palmprint image, so we think the features based on LBP will be good discriminative for palmprint identification. Cellular automata can be generally described as discrete dynamic systems completely defined by a set of rules in a local neighborhood. In this paper, we use cellular automata to extract features as the part of feature vector. The experiments conducted on Polytechnic University Palmprint Database I demonstrates the effectiveness of proposed method.

Keywords: biometric, newborn, infant, footprint recognition, subspace learning methods.

1 Introduction

Nowadays, palmprint recognition, as a new biometric technology, has been receiving wide attentions from researchers [1]. So far, there have been many approaches proposed for palmprint recognition. Kong et al. made a survey for this technique and divided the approaches into several different categories [2]. For texture based approaches, Wavelet transform, DCT, and some statistical method are often used for texture feature extraction [3]. There are also some line based approaches since lines including principal lines and wrinkles are essential and basic features of palmprint [4]. Coding approaches are deemed to have the best performance on both accurate recognition rate and matching speed. The representative coding methods are Competitive Code [5], Ordinal Code [6], and Robust Line Orientation Code [7]. In addition, some representative appearance based approaches were also applied to palmprint recognition [8].

As we have mentioned above, there are many texture based approaches proposed for palmprint recognition. Among them, Local Binary Pattern (LBP) is an excellent and powerful descriptor for texture feature analysis, and robust to illumination and rotation invariances. In this paper, we propose a new LBP descriptor for palmprint recognition, which combines the original multi-scale LBP and cellular automata. The new LBP descriptor has better recognition performance than original one. The

D.-S. Huang et al. (Eds.): ICIC 2010, LNCS 6215, pp. 460–466, 2010.

experiments conducted on Polytechnic University Palmprint Database I demonstrates the effectiveness of proposed method.

2 LBP Descriptor and Cellular Automata

2.1 Introduction of LBP

LBP is very effective for texture description. Due to its rotation invariance, the gray-scale invariance and other obvious advantages, it has been widely used in texture classification, texture segmentation, facial image analysis and other fields. LBP was proposed by Ojala T and developed by many researchers based on gray level co-occurrence matrix method [9].

The premier LBP assigns a label to every pixel of an image by thresholding the 3×3-neighborhood of each pixel with the center pixel value and considering the result as a binary code. Fig. 1 gives an example of generating LBP representation. By considering the label result as a decimal number, pattern=11110001_2=241, a 256-bin histogram of the LBP labels computed over a region will be created.

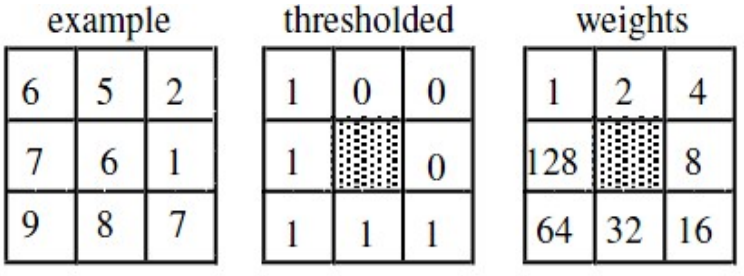

Fig. 1. A Sample graph of LBP

After the original LBP descriptor was proposed, it was extended to use different neighborhood with different sizes, and use circular region instead of square neighborhood area. In addition, the improved LBP descriptor allows any number of neighborhood pixels in a circular radius R region. Generally, common LBP descriptor s are $LBP_{8,1}$, $LBP_{16,2}$ and $LBP_{24,3}$, as shown in Fig 2.

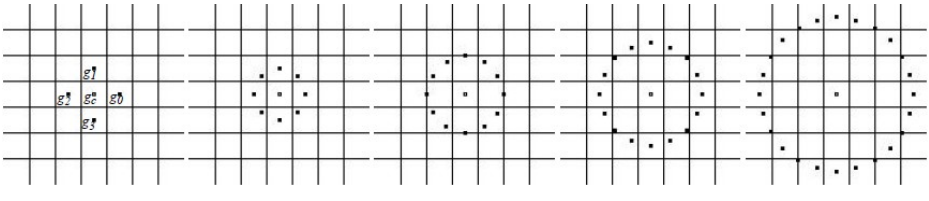

Fig. 2. Circularly symmetric neighbor sets for different (P, R), where P is the number of pixels around the center, and R denotes the radius of LBP descriptor

The later extension to the original operator is the method named "uniform patterns". In a local binary pattern, when the continuous bitwise transitions from 0 to 1 or 1 to 0 changed at most 2, this pattern called a "uniform patterns", and it was denoted as $LBP_{P,R}^{riu2}$. When accumulating the patterns which have more than 2 transitions, it belongs to the other one single bin. Experiments show that the use of $LBP_{8,1}^{riu2}$ operator for feature extraction, the "uniform patterns" accounts for about 90% of the total model.

2.2 The Cellular Automata

Generally speaking, cellular automata is a dynamic system which consists of cells and defined in a discrete, finite state cells space and developed in discrete time dimension with some certain local rules. The rule of cellular automata is simple but it can result in very complex behavior, like the branch of the system, attractor and self-similarity etc. Cellular automata model is raised by Von Neumann to simulate the self-replicating of biology [11]. In Von's model, the state of a system was presented within a two dimensional grid of ones and zeros - just like a digital binary image. The value of a slot in the state grid at time instant $t + 1$ was determined by the values of its nearest neighbors at time instant t [10]. Fig 3(a) shows one cellular automaton rule, in which one is represented by white and zeros is denoted by black squares. The automaton number of this particular automaton is $10001001_2 = 137$[12].

It looks the relation between multi-scale LBP and cellular automata may not be quite obvious. However, if we think of the thresholded circular neighborhoods as one dimensional circular binary signals, the notation of "time" in the evolution of the cellular automaton pattern is replaced by the radius of the circular neighborhood, we can regard cellular automata as texture features. As Fig 3(b) shows, two $LBP_{8,R}$ codes are dressed to form the two rows of a two-dimensional pattern[13].

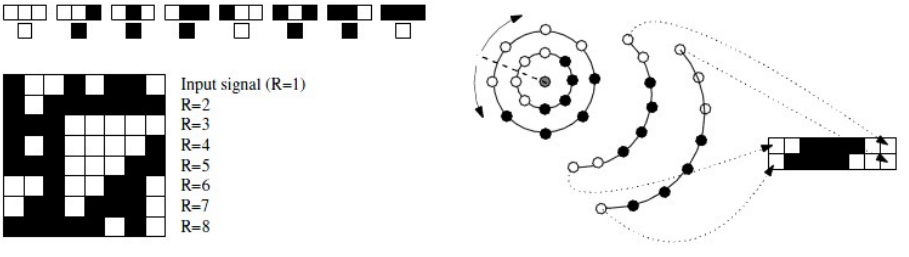

Fig. 3. A cellular automaton rule and turning a LBP into a two-dimensional pattern

3 Results and Discussion

PolyU I [15]database contains 600 grayscale palmprint images from 100 palms corresponding to 50 individuals. In PolyU database I, 6 samples from each of these palms were collected in two sessions, where 3 samples were captured in the first session and the second session, respectively. The total numbers of images captured in the first

session and the second session are all 300. In PolyU database II, we use first three palmprints from the first session for training and leave the palmprints from the second session for test.

In our paper, b**y** using the similar preprocessing approach described in literature [1], palmprint is orientated and the ROI, whose size is 128×128, is cropped in both databases.

In this paper, the whole feature consists of two parts. The first part is using 3 scales "uniform patterns": LBP, $LBP_{8,1}^{riu2}$, $LBP_{16,2}^{riu2}$ and $LBP_{24,3}^{riu2}$. The extracted feature vector for $LBP_{P,R}^{riu2}$ descriptor is a histogram, include P+2 dimensional component, and the P+1 were derived from "uniform patterns", the other one isn`t the "uniform patterns", so the joint three-scale LBP characteristic dimensions is 10+18+26=54. It can be calculated by formulation (1), in which $f(x, y)$ is $LBP_{P,R}^{riu2}$ binary code.

$$H_i = \sum_{x,y} I\{f(x,y) = i\}, i = 0,...P+1 \qquad I(X) = \begin{cases} 1, & \text{X is ture} \\ 0, & \text{X is false} \end{cases} \tag{1}$$

Since LBP is a local operator, a large number of experiments and literature suggested that the recognition rate would be low if we only used the histogram of the whole pictures as a feature. Therefore, we need divide the whole image into appropriate sub-image blocks, and then to calculate characteristics in each of the small pieces. Experimental results have shown that after blocking, the recognition rate has been significantly improved. Here, we divide the image into R_1, R_2 ..... R_n regions (see Fig. 4), and can calculate the LBP histogram characters by the following formula:

$$H_{i,j} = \sum_{x,y} I\{f(x,y) = i\} I\{(x,y) \in R_j\} \tag{2}$$

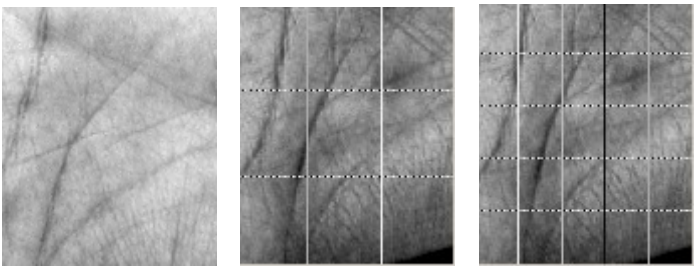

(a)original image (b) 3×3 blocks (c) 5×5 blocks

Fig. 4. The original palmprint image and two blocking image

The second part of feature in our method was derived from the statistics of cellular automata rule which produced by $LBP_{8,1}^{riu2}$, and $LBP_{8,2}^{riu2}$. Here we do not use cellular automata number as a characteristic, but directly use the values generated from statistical rules, which can be found in [14]. So that we can get 16-dimensional characteristics of components of use cellular automata. And therefore, we get 70-dimensional vector

Table 1. The recognition rate obtained under the different sub-blocks and operator

	$LBP_{8,1}^{riu2}$	$LBP_{16,2}^{riu2}$	$LBP_{24,3}^{riu2}$	$LBP_{8,1}^{riu2}$ + $LBP_{16,2}^{riu2}$ + $LBP_{24,3}^{riu2}$	Three LBP+CA
3×3	0.923	0.933	0.93	0.97	0.988
5×5	0.903	0.92	0.918	0.963	0.98
7×7	0.878	0.893	0.903	0.94	0.973

in each sub-block concatenation with 3 scales "uniform patterns" features as in the first part mentioned. In this paper, the different sub-blocks are used, and the detailed results are shown in Table 1.

We use the χ^2 distance as the matching distance, and use the nearest neighbor as criterion. The χ^2 distance can calculate as:

$$\chi^2(S,M) = \sum_{i,j} \frac{(S_{i,j} - M_{i,j})^2}{S_{i,j} + M_{i,j}} \tag{3}$$

where S and M represent the features of training samples and test samples separately. All of experiments are executed on a computer system of Intel(R) Dual-Core CPU E4500 @2.20GHz and 2GB RAM with Visual studio C++2008.

In our experiment ,we have test different sub-blocks from 2 to 7, but we only list three different sub-blocks, the effects of others are between the three listed. From this table ,we can see the recognition rate of our method are 5~6 percentage points higher than merely use "uniform patterns"LBP, and 1~3 percentage points higher than use of three joint "uniform patterns" LBP. In next figure (Fig 5), we show the experiment indicators FRR and FAR.

We also make a performance comparison between proposed method and other methods such as PCA and LDA, which is listed on Table 2. It can be seen that the recognition rate is better than that of PCA and LDA.

Table 2. Performance comparison between proposed method and other methods

methods	**Recognition rates (%)**
PCA	84.33
LDA	96.3
Propsed method	98.8

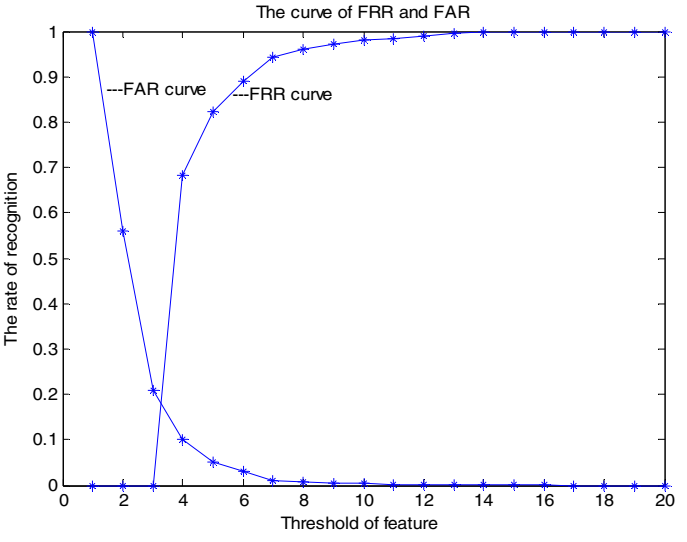

Fig. 5. Relation curve of FRR and FAR

From Fig 5 and Table 1 we can see that ,the equal error rate is about 18.3% when the threshold is about 3.5,and the topmost recognition of our method is 98.8%, so our method have some comparability compared with other palmprint recognition methods.

4 Conclusion

In this paper, we proposed a novel palmprint recognition method which combines LBP and cellular automate. Through experiments, we can see that the recognition rate of proposed method is about 99%, which is better than that of original LBP method. So our method is effective, and comparable with some other palmprint recognition methods. But our method also has one shortcoming which is the length of our feature vector is too long. As a result, the matching is very time-consuming. Our future work is trying to reduce the cost of computing and to further improve the recognition performance.

Acknowledgements

This work was supported by the National Science Foundation of China (No.60803107).

References

1. Zhang, D., Kong, A., You, J., Wong, M.: Online Palmprint Identification. IEEE Transactions on Pattern Analysis and Machine Intelligence 25(9), 1041–1050 (2003)
2. Kong, A., Zhang, D., Kamel, M.: A Survey of Palmprint Recognition. Pattern Recognition 42(7), 1408–1418 (2009)

3. Chen, G.Y., Xie, W.F.: Pattern Recognition with SVM and Dual-tree Complex Wavelets. Image and Vision Computing 25(6), 960–966 (2007)
4. Huang, D.S., Jia, W., Zhang, D.: Palmprint Verification Based on Principal Lines. Pattern Recognition 41(4), 1316–1328 (2008)
5. Kong, A., Zhang, D.: Competitive Coding Scheme for Palmprint Verification. In: Proc. of the 17th ICPR, vol. 1, pp. 520–523 (2004)
6. Sun, Z.N., Tan, T.N., Wang, Y.H., Li, S.Z.: Ordinal Palmprint Representation for Personal Identification. In: Proceedings of CVPR, pp. 279–284 (2005)
7. Jia, W., Huang, D.S., Zhang, D.: Palmprint Verification Based on Robust Line Orientation Code. Pattern Recognition 41(5), 1504–1513 (2008)
8. Jia, W., Huang, D.S., Tao, D.C., Zhang, D.: Palmprint Identification Based on Directional Representation. In: IEEE International Conference on Systems, Man, and Cybernetics (IEEE SMC 2008), Singapore, October 12-15, pp. 1562–1567 (2008)
9. Ojala, T., Pietikainen, M.: Multiresolution Gray Scale and Rotation Invariant Texture Classification with Local Binary Patterns. J. IEEE Transactions on Pattern Analysis and Machine Intelligence 24(7), 971–987 (2002)
10. Wolfram, S.: Statistical Mechanics of Cellular Automata. Reviews of Modern Physics 55, 601–644 (1983)
11. Wolfram, S.: Theory and Applications of Cellular Automata, pp. 7–50. World Scientific Publishing Company, M. Singaprot (1986)
12. Wolfram, S.: A New Kind of Science. Wolfram Media, Inc., Champaign (2002)
13. Maenpaa, T., Pietikainen, M.: Multi-Scale Binary Patterns for Texture Analysis. In: Bigun, J., Gustavsson, T. (eds.) SCIA 2003. LNCS, vol. 2749, pp. 885–892. Springer, Heidelberg (2003)
14. Maenpaa, T.: The Local Binary Pattern Approach to Texture Analysis – Extensions and Applications. M. Oulu University Press (2003)
15. PolyU Palmprint Database, `http://www.comp.polyu.edu.hk/~biometrics/`

Dual Unsupervised Discriminant Projection for Face Recognition

Lei Tang[1,2] and Jie Gui[1,2,*]

[1] Intelligent Computing Lab, Hefei Institute of Intelligent Machines, Chinese Academy of Sciences, P.O. Box 1130, Hefei Anhui 230031, China
[2] Department of Automation, University of Science and Technology of China, Hefei Anhui 230031, China
{knightanglei,guijiejie}@gmail.com

Abstract. In this paper we proposed a dual unsupervised discriminant projection (DUDP) method for dimensionality reduction tasks. The proposed method is derived from the efficient unsupervised method called unsupervised discriminant projection (UDP). UDP takes into account both the local and nonlocal characteristics to seek a projection that simultaneously maximizes the nonlocal scatter and minimizes the local scatter. While UDP adopt PCA procedure to avoid a singular scatter matrix by ruling out some small principal components in which it lost a lot of potential and valuable discriminant information of original data. To overcome this problem, we proposed our algorithm to carry out discriminant analysis both in null space and range space to avoid loss of discriminant information. The advantage of our algorithm is borne out by comparison with some other widely used methods in the experiments on Yale face database.

Keywords: Dimensionality reduction, unsupervised discriminant projection, subspace learning, face recognition.

1 Introduction

In many areas of computer sciences, people often confronted with intrinsically low dimensional data lying in a very high dimensional space. In order to benefit decision making and data analyzing, people try to find appropriate representations by projecting high dimensional data into a low-dimensional feature subspace that can reflect the important intrinsic structure of the original complex data. In recent years, dimensionality reduction have aroused large amount of attention and many useful algorithms have been proposed.

Among the numerous methods, some well-known classical methods such as Principal Component Analysis (PCA) [1], Linear Discriminant Analysis (LDA) [2, 3] have been extensively applied in many areas. As representatives of linear dimensionality reduction methods, PCA and LDA both provide linear projection matrices that could directly transform the original high-dimensional data into a low-dimensional subspace. However, recently, it is discovered that many high-dimensional data are intrinsically

* Corresponding author.

D.-S. Huang et al. (Eds.): ICIC 2010, LNCS 6215, pp. 467–473, 2010.

low-dimensional and lying on a low-dimensional manifold where the nonlinear data structural could not be effective discovered by traditional linear dimensionality reduction methods. Hence, people developed several powerful nonlinear dimensionality reduction algorithms, such as Isometric Mapping (ISOMAP) [4], locally linear embedding (LLE) [5] and Laplacian eigenmap (LE) [6] and are proved to show exciting good performance in nonlinear dimensionality reduction tasks. Since these manifold learning based methods attempt to preserve original data structure when performing dimensionality reduction.

However the nonlinear method shares a common drawback which is they can not deal with "out-of-sample" problem [7]. Therefore, many researchers have paid a lot of attention on linearized approximation methods of the manifold learning algorithms. Among them, UDP [8] is an effective unsupervised linearized method which focuses on not only local scatter but also nonlocal scatter which could be seen as a linear approximation of multi-manifolds learning method. It also provides a linear projection matrix to transform the original data into a low dimensional space where the nonlocal scatter is maximized and meanwhile the local scatter is minimized. But UDP suffers a disadvantage that, it should take PCA ahead of other procedures so that PCA cause discriminant information loss when transforming high-dimensional data into low-dimensional subspace since it throw away some small principal components. This weaken the performance of UDP in practical applications, we therefore proposed a modified algorithm named dual unsupervised discriminant projection (DUDP) which is motivated by [9] in order to overcome the dilemma. DUDP makes full use of two kinds of discriminant information, regular and irregular, which is a powerful strategy proved in our experiments.

The remainder of this paper is organized as follows: Section 2 introduced the algorithm in detail; In section 3, the proposed method is examined on a well-known face database to show its effectiveness. Section 4 finishes this paper with some conclusions.

2 Algorithm Discription

The generic dimensionality reduction problem can be described as follows. Original data can be represented as a $D \times n$ matrix $X = \{x_1, x_2, ..., x_n\} \subset \mathbb{R}^{D \times n}$. The goal of dimensionality reduction is to project the high-dimensional data into a low-dimensional feature space $\mathbb{R}^d$ as $Y = \{y_1, y_2, ..., y_n\} \subset \mathbb{R}^{d \times n}$, where y_i is a low-dimensional representation of x_i in $\mathbb{R}^d$ space, often $d \ll D$.

In the following parts, we will give the characterizations of the nonlocal scatter and the local scatter as introduced in [8].

2.1 Characterize the Local Scatter

Here the local scatter is defined as below:

$$J_L(w) = \frac{1}{2}\frac{1}{N}\frac{1}{N}\sum_{i=1}^{N}\sum_{j=1}^{N} H_{ij}\left(y_i - y_j\right)^2 \tag{1}$$

where N is the number of training samples and H_{ij} is a denoter of whether the two data are neighboring point, which means:

$$H_{ij}=\begin{cases}1, & \textit{if } x_i \textit{ is among } \kappa-\textit{nearest neighbors of } x_j \textit{ or vice versa.}\\ 0, & \textit{otherwise}\end{cases} \tag{2}$$

All the H_{ij}'s constitute a adjacent matrix H . Then we can transform local scatter matrix as follows:

$$J_L(w)=\frac{1}{2}\frac{1}{N}\frac{1}{N}\sum_{i=1}^{N}\sum_{j=1}^{N}H_{ij}\left(w^T x_i-w^T x_j\right)^2=w^T S_L w \tag{3}$$

where S_L is the local scatter matrix:

$$S_L=\frac{1}{2}\frac{1}{N}\frac{1}{N}\sum_{i=1}^{N}\sum_{j=1}^{N}H_{ij}\left(x_i-x_j\right)\left(x_i-x_j\right)^T \tag{4}$$

Due to the symmetry of H , we have

$$\begin{aligned}S_L&=\frac{1}{2}\frac{1}{N}\frac{1}{N}\left(\sum_{i=1}^{N}\sum_{j=1}^{N}H_{ij}x_i x_i^T+\sum_{i=1}^{N}\sum_{j=1}^{N}H_{ij}x_j x_j^T-2\sum_{i=1}^{N}\sum_{j=1}^{N}H_{ij}x_i x_j^T\right)\\&=\frac{1}{N}\frac{1}{N}\left(XDX^T-XHX^T\right)=\frac{1}{N}\frac{1}{N}XLX^T\end{aligned} \tag{5}$$

where $X=(x_1,x_2,x_3,...,x_N)$ and D is a diagonal matrix whose elements on diagonal are column sum of H ,i.e., $D_{ii}=\sum_{j=1}^{N}H_{ij}$. $L=D-H$ is called the Laplacian matrix.

2.2 Characterize the Nonlocal Scatter

Similar to local scatter, we can naturally describe the nonlocal scatter as follows:

$$J_{\mathrm{N}}(w)=\frac{1}{2}\frac{1}{N}\frac{1}{N}\sum_{i=1}^{N}\sum_{j=1}^{N}\left(1-H_{ij}\right)\left(\mathrm{y}_i-\mathrm{y}_j\right)^2 \tag{6}$$

By some simple algebra transformation, we can reduce $J_{\mathrm{N}}(w)$ as:

$$J_{\mathrm{N}}(w)=\frac{1}{2}\frac{1}{N}\frac{1}{N}\sum_{i=1}^{N}\sum_{j=1}^{N}\left(1-H_{ij}\right)\left(w^T x_i-w^T y_j\right)^2=w^T S_N w \tag{7}$$

Where $$S_N=\frac{1}{2}\frac{1}{N}\frac{1}{N}\sum_{i=1}^{N}\sum_{j=1}^{N}\left(1-H_{ij}\right)\left(x_i-x_j\right)\left(x_i-x_j\right)^T \tag{8}$$

S_N is called the nonlocal scatter matrix which has a close relation to S_T and S_L. That is $S_T = S_L + S_N$, which means $J_T(w) = J_L(w) + J_N(w)$.

2.3 Discriminant Criterion

UDP proposed an integrated discriminant criterion:

$$J(w) = \frac{J_N(w)}{J_L(w)} = \frac{w^T S_N w}{w^T S_L w} \tag{9}$$

Since $J_T(w) = J_L(w) + J_N(w)$, (9) is actually equivalent to:

$$w_{opt} = \arg\max \frac{J_T(w)}{J_L(w)} = \arg\max \frac{w^T S_T w}{w^T S_L w} \tag{10}$$

The Rayleigh quotient can be solved as a generalized eigen-equation:

$$S_N w = \lambda S_L w \tag{11}$$

The criterion is similar to the Fisher criterion in LDA. Also, (10) shares the same problem as it is in LDA that is, the local scatter matrix S_L usually is singular, especially in the small-sample-problem [10]. Therefore, UDP adopted the same strategy as LDA did which is to perform a PCA procedure first to eliminate or reduce "superfluous" information contained in the original data set. By this means, we can mathematically assure that S_L is nonsingular. But, the problem is, we may lost much useful information in this procedure. How to solve this dilemma is the central concern in this paper.

2.4 Dual Unsupervised Discriminant Projection

As we discussed above in UDP, a PCA procedure is adopt to eliminate matrix singularity of S_L. However, there is a dilemma that S_L might still be singular if we keep too much energy in PCA processing and on the contrary, if we abandon too much energy to ensure the nonsingularity of S_L, many useful discriminant information will be lost. Therefore, we propose dual unsupervised discriminant projection to deal with the problem. We adopt a profound analysis developed by Yang in [9] to try our best to preserve original useful discriminant information in dual space including null space and range space.

According to Theorem 1 [9], we can conclude that al optimal discriminant vectors can be derived from ϕ_t without any loss of optimal discriminantory information with respect to the discriminant criterion. The algorithm steps are as follows:

Step 1. Construct the adjacency diagram. For the given training data set $X = \{x_1, x_2, ...x_N\}$, find K nearest neighbors of each data point and build up the adjacency matrix H.

Step 2. Construct the local scatter matrix and nonlocal scatter matrix according to Eq.(4) and Eq.(8).

Step 3. Perform PCA transform of data, in PCA transformed space $\mathbb{R}^d$, work out the local scatter matrix $\tilde{S}_L$, nonlocal scatter matrix $\tilde{S}_N$ and $\tilde{S}_T$. Calculate $\tilde{S}_L$*'s* eigenvalues $\{\lambda_1, \lambda_2, ...\lambda_m\}$, and the associated orthonormal eigenvectors $\{\gamma_1, \gamma_2, ...\gamma_m\}$. We suppose the first q eigenvalues are zero.

Step 4. Let $P_1 = \{\gamma_{q+1}, \gamma_{q+2}, ...\gamma_m\}$ and $\overline{S}_N = P_1^T \tilde{S}_N P_1$, work out $\overline{S}_N$'s orthormal eigenvectors $Z_1, Z_2, ..., Z_l$,then, the optimal discriminant vector contained in $\tilde{\phi}_w^{\perp}$ are $Y_j = P_1 Z_j$, $j = 1, 2, ..., l$.

Step 5. Let $P_2 = \{\gamma_1, \gamma_2, ...\gamma_q\}$ and $\overline{S}_N = P_2^T \tilde{S}_N P_2$, $\overline{S}_T = P_2^T \tilde{S}_T P_2$ work out the $d - l$ orthormal eigenvectors $Z_{l+1}, Z_{l+2}, ..., Z_d$, then the optimal discriminant vector contained in $\tilde{\phi}_w$ are $Y_j = P_2 Z_j$, $j = l+1, l+2, ..., d$.

Step 6. Integrate P_1 and P_2 to form the final projection matrix $\phi = (Y_1, Y_2, ...Y_l, Y_{l+1}, ..Y_d)$.

By this way, we can reduce the dimensionality of original with loss of discriminant information and meanwhile overcome the singularity of S_L. In the next part we will conduct experiments to validate the advantage of our proposed method.

3 Experimental Results

To evaluate the effectiveness of the proposed method, the experimental results on real world face database are presented in this section. In the experiment, some other well-known algorithms are also applied to do comparison with DUDP, i.e., PCA [1], LDA [2, 3] and also UDP [8]. First of all, we do some data preparation.

3.1 Data Preparation

Yale database [11] includes 165 face images belonging to 15 individuals. The images demonstrate variations in lighting condition (left-light, center-light and right-light), facial expression (normal, happy, sad, sleepy, surprised and wink), and with or without glasses. The original face images were then cropped and resized to 32×32 pixels with 256 gray levels per pixel as shown in Fig.1. Thus each image can be represented as a 1024-dimensional vector in $\mathbb{R}^{1024}$ space. Before performing the algorithms, the data vectors need to be normalized.

3.2 Experiments on Yale Face Database

We randomly selected 2, 3, 4, 5, 6, 7, 8 images each individual to construct 2Train, 3Train, 4Train, 5Train, 6Train, 7Train, 8Train dataset respectively with their labels, and each time we use the remaining images as test sets. We randomly selected p images (p varies from 2 to 8) for 20 times to constructed 20 different data splits for experimental training and test. The recognition rates of algorithms are acquired as the mean of 20 recognition rates on 20 different splits.

Fig. 1. Two persons in Yale face database are drawn here and each person has eleven cropped and resized samples. Each line represents a person.

Shown in Table 1 are the recognition rates of PCA, LDA, UDP and the proposed DUDP. From this table, it can be found that our method outperforms the other algorithms in all training sets.

Table 1. The Experimental Results on Yale face database

Methods	2 Train	3Train	4Train	5Train	6Train	7Train	8Train
Baseline	42.63	48.08	52.86	55.44	58.80	59.67	63.44
PCA	42.63	48.08	52.86	55.44	59.13	59.83	64.33
LDA	45.19	59.42	68.95	74.89	79.27	79.83	83.22
UDP	55.93	65.08	73.43	78.65	82.56	85.83	87.89
DUDP	**57.19**	**66.92**	**75.14**	**79.22**	**83.63**	**86.15**	**88.22**

The experimental results illustrate that our proposed algorithm presents better performance than those competing methods and supported our idea and analysis.

4 Conclusion

In this paper, we proposed an effective unsupervised dimensionality reduction method which can be used as a powerful discriminator for classification task. We constructed local and nonlocal scatter matrix to represent local and nonlocal characters of original dataset and try to preserve the local characters and meanwhile enlarge nonlocal scatter. Also, we make good use of the discriminant information by conducting our method both in range space and null space to avoid information loss. The effectiveness of the proposed method has been testified in the experiments on Yale face database.

Acknowledgement

The authors would like to thank all the anonymous reviewers for their constructive advices. This work was supported by the grants of the National Science Foundation of China, Nos. 60905023, 60975005, 60873012, 60805021, and 60705007.

References

1. Jolliffe, I.T.: Principal Component Analysis. Springer, Heidelberg (1989)
2. Duda, R., Hart, P.E., Stork, D.G.: Pattern Classification, 2nd edn. John Wiley & Sons, Chichester (2001)
3. Belhumeur, P.N., Hepanha, J.P., Kriegman, D.J.: Eigenfaces vs. Fisherfaces: Recognition Using Class Specific Linear Projection. IEEE Transactions on Pattern Analysis and Machine Intelligence 19, 711–720 (1997)
4. Tenenbaum, J., de Silva, V., Langford, J.: A Global Geometric Framework for Nonlinear Dimensionality Reduction. Science 290, 2319–2323 (2000)
5. Roweis, S., Saul, L.: Nonlinear Dimensionality Reduction by Locally Linear Embedding. Science 290, 2323–2326 (2000)
6. Belkin, M., Niyogi, P.: Laplacian Eigenmaps and Spectral Techniques for Embedding and Clustering. Advances in Neural Information Processing Systems 14, 585–591 (2001)
7. Bengio, Y., Paiement, J.F., Vincent, P.: Out-of-sample Extensions for LLE, Isomap, MDS, Eigenmaps, and Spectral Clustering. Technical Report 1238 Université de Montreal (2003)
8. Yang, J., Zhang, D., Yang, J.Y., Niu, B.: Globally Maximizing, Locally Minimizing: Unsupervised Discriminant Projection with Application to Face and Palm Biometrics. IEEE Transactions on Pattern Analysis and Machine Intelligence 29, 650–664 (2007)
9. Yang, J., Yang, J.-y.: Why can LDA be performed in PCA transformed space? Pattern Recognition 36, 563–566 (2003)
10. Raudys, S.J., Jain, A.K.: Small Sample Size Effects in Statistical Pattern Recognition: Recommendations for Practitioners. IEEE Transactions on Pattern Analysis and Machine Intelligence 13, 252–264 (1991)
11. Yale Univ. Face Database, `http://cvc.yale.edu/projects/yalefaces/yalefaces.html`

Applying Wikipedia-Based Explicit Semantic Analysis for Query-Biased Document Summarization

Yunqing Zhou, Zhongqi Guo, Peng Ren, and Yong Yu

Dept. of Computer Science and Engineering, Shanghai Jiao Tong University
800, Dongchuan Road, Shanghai, China
{yunqing.zhou,gzq,renpeng,yyu}@apex.sjtu.edu.cn

Abstract. Query-biased summary is a query-centered document brief representation. In many scenarios, query-biased summarization can be accomplished by implementing query-customized ranking of sentences within the web page. However, it is a tough work to generate this summary since it is hard to consider the similarity between the query and the sentences of a particular document for lacking of information and background knowledge behind these short texts. We focused on this problem and improved the summary generation effectiveness by involving semantic information in the machine learning process. And we found these improvements are more significant when query term occurrences are relatively low in the document.

Keywords: query-biased summary, explicit semantic analysis, Wikipedia, machine learning.

1 Introduction

Living with tens of billions of web pages on the Internet, users are found growingly relying heavily on Search Engines to locate their specific resources. Typically a short piece of text (a generated query-biased summary) is given after every result entry. As Tombros et al. mentioned in [10], a query customized summary plays an important role in improving both the accuracy and the speed of judging document relevance.

Query-biased summaries can be generated in several different algorithms, and in many cases, query-biased summarization is performed in the sentence selection framework[11] [12] [8]. It is based on the assumption that the best piece of summary should lie in the article itself. The advantage of this method is that the original texts are best kept for users. Some recent work proposed a framework to use machine learning to guide the sentence selection process, but the features used in their paper are still constrained to the terms and cannot measure the hidden semantic relationship.

In the purpose of assigning semantic meaning to short texts such as queries, a lot of works have been focused on utilizing semantic knowledge collected from

D.-S. Huang et al. (Eds.): ICIC 2010, LNCS 6215, pp. 474–481, 2010.

collaborative knowledge bases, such as Wikipedia, to optimize search in information retrieval systems. Explicit Semantic Analysis (ESA) [6]systems are used to determine the semantic aspects behind an arbitrary text. It maps the text snippets directly to a series of concrete human cognizable concepts extracted from large collaborative edited knowledge sources. ESA bridges short texts to semantic concepts, leading to a great improvement in classification and relationship measuring.

In this paper, we add new features derived from ESA into the existing machine-learning-based query-bias summary generation method to further improve the summary generation effectiveness. We summarize our contributions as follows: First, we applied Wikipedia based ESA to the sentences and query texts, from which we derived two features *Concept TFIDF* and *Concept Vector Similarity* as the metrics of the two texts. Second, we combined these Wikipedia-based features and traditional sentence selection features, applying them to machine learning algorithm and achieved improvements in query-biased summary generation effectiveness. Third, we found these improvements are more significant when query term occurrences are rare in the document. So we can only apply this method to part of the document set to improve performance.

The rest of the paper is organized as follows. In Section 2, we show some related work on query-biased summary generation and explicit semantic analysis. And we describe our method in detail in Section 3. Extensive experiment results will be given in Section 4. Finally, we conclude in Section 5.

2 Related Work

A query-biased summary is a summary extracted from the document to present the information relevant to both the search query and the document rather than the document only. In modern search engines, it is very useful for user to determine whether a result entry meets his needs conveniently.

In many cases, query-biased summarization can be considered as a sentence selection task, and this sentence selection problem can be solved by either classification[2] [3] or ranking [8] [12] [11] techniques. Traditionally, in ranking methods, conventional metrics such as TF-IDF or BM25 are used. However, recent research has proposed methods to perform this job through machine learning. In these methods, a ranking model is trained by the features extracted from every sentence of the documents. And the top ranking ones of the document will be selected as the summary [8] [12]. Both query-dependent and query-independent features are involved to predict the score of sentences according to a specified query. However, the conventional methods failed to go beyond the constraints of the text literals. In other words, lacking of semantic information for short texts, traditional method is only well performed with exact match by terms, but not conceptual related sentences.

Extensive research has been done on the data mining on the Wikipedia data set. Gabrilovich and Markovich [6] found a method to enhance text classification performance using semantic analysis, which called the Explicit Semantic Analysis (ESA) method. This method is an efficient tool to measure the semantic

relationship (SR) between text snippets. By using Wikipedia, they measure the semantic relationship between the text snippets by calculating the similarity between concept vectors which are extracted from the snippets by Wikipedia. For example, given query "Search Engine", a concept vector *("Web Search Engine", weight 0.28), ("World Wide Web", weight 0.21) ...* can be generated by ESA. This method has been proved to be effective in problems dealing with either short texts or long ones. This information can be very useful in many IR tasks.

3 Apply Wikipedia Knowledge to Query-Biased Summary

Our method shares the same framework with [8]. First, we need some manually identified sentence selections. Second, numerous features are extracted from the sentences and a learning model is trained from these features. And finally, in summary generation, we can use this model to rank all the sentences to select the top ones, which is the origin of the summary. The learning model we used is Gradient boosted decision trees (GBDTs)[5] , which is a technique can be used for estimating a regression model, and is proved to be effective in web search related problems[14]. To begin with, we now introduce the features we used, both traditional ones and the ones we developed.

3.1 Traditional Features

We employ several traditional features extracted from every query-sentence pair. These features belong to two categories: query-independent and query-dependent. we use the same traditional feature set as [8].

Query-dependent Features. Query-dependent features are used to measure the relationship of the query and the sentence. Given a particular query Q and a sentence S, the extracted query-dependent features are shown below: (Note: Before extracting these features, all terms in the sentences are normalized and stemmed.)

Feature Name	Description
Exact Match	$f_{EXACT}(Q,S) = I(Q\ substringof\ S)$
Overlap	$f_{OVERLAP}(Q,S) = \frac{\sum_{w \in Q} I(w \in S)}{\lvert Q \rvert}$
Overlap-syn	$f_{OVERLAP-SYN}(Q,S) = \frac{\sum_{SYN(w) \in Q} I(w \in S)}{\lvert Q \rvert}$
Language Model Feature	$f_{LM}(Q,S) = \sum_{w \in Q} tf_{w,Q} \log \frac{tf_{w,S} + \mu P(w\lvert C)}{\lvert S \rvert + \mu}$

where I is the indicator function that has a value of 1 if satisfied and $|Q|$ is the number of non-stopword terms that occur in Q. SYN(w) denotes the set of

synonyms of w. The language model feature mentioned is developed by F.Song. et. al[9]to describe the relationship between query and texts. It is computed as the log likelihood of query being generated from the sentence. As what it is used in [13], we also apply a Dirichlet smoothing here. In the equation, $tf_{w,Q}$ is the number of occurrences of w in the query, while $tf_{w,S}$ is the number of occurrences of w in the sentence. $|S|$ is the number of terms in the sentence, $P(w|C)$ is the behind language model and μ is a tunable smoothing parameter.

Query-independent Features. Besides query-dependent features, there are also some features for describing the probability of a sentence to be part of the summary. Two features in this category are :

Feature Name	Description
Sentence Length	$f_{LENGTH}(S) = \|S\|$
Sentence Location	$f_{LOCATION}(S, D) = \frac{sentnum_D(S)}{\max_S, sentnum_D(S')}$

where $|S|$ is the number of terms in sentence S, $sentnum_D(S)$ is the sentence number for S in D and $\max_S, sentnum_D(S')$ is the total number of sentences in D.

3.2 Features Derived from Wikipedia

One of the highlights of this paper is to employ Wikipedia knowledge in the machine learning process. The features we introduced are:

Concept TF-IDF. Using ESA, we can get a weighted vector of related concepts of a particular query. For example, for a query "Explicit Semantic Analysis", we can acquire a concept vector like: Semantic, Semantic Web, ..., Latent Semantic Indexing, ... As we all know, ESA shares a similar idea with LSA(Latent Semantic Analysis)[4] and can be used in many semantic web applications. So if a sentence has a snippet "Semantic Web has the idea...", it is more likely to be selected as the summary corresponding to the query "ESA", initiatively. We introduce this feature to indicate the case, which is the weighted sum of the TF-IDF measure of every concept relative to the sentence. It is denoted as *CTFIDF* in the following experiments, which can be computed as:

$$f_{CTFIDF}(S, Q) = \sum_{C \in V_Q} w_C \sum_{t \in C} tf_{t,S} \log \frac{|D|}{df_t} \quad (1)$$

where V_Q is the query's concept vector retrieved by ESA with w_C as its corresponding weight. $tf_{t,S}$ is the concept term t's number of occurrence in the sentence, while df_t is term t's global document frequency and $|D|$ is the number of the documents in the data set from which df is computed. The original TF-IDF formula replaced tf with the ratio between tf and $|S|$, but since we've included the sentence length information independently in the above traditional features, we removed this factor from this formula.

Concept Vector Similarity. As we described above, by using ESA, for which text snippet, a vector of related concepts can be obtained. So the similarity between the query text and the sentence can be measured by comparing the corresponding concept vectors. We use simple cosine similarity here. It is denoted CSIM in the following experiments, which can be computed as:

$$f_{CSIM}(S,Q) = \frac{\sum_{C_Q \in V_Q} \sum_{C_S \in V_S} g(C_Q, C_S) w_{C_Q} w_{C_S}}{\sqrt{\sum_{C_Q \in V_Q} w_{C_Q}^2} \sqrt{\sum_{C_S \in V_S} w_{C_S}^2}} \tag{2}$$

where V_Q and V_S are the concept vectors of the query and the sentence respectively. w_{C_Q} and w_{C_S} are the corresponding weights of the concepts. And $g(C_Q, C_S)$ is a boolean function that has a value of 1 when $C_Q = C_S$. Although not showed and used here, more information can be added to create more features, such as paragraph information, etc.

4 Experiment

We have done extensive experiments to evaluate our method's effectiveness. We performed our experiment on different data sets and compared the results with the baseline method [8], and we also evaluated the features' and its parameters' effectiveness as well.

4.1 Experiment Setup

We implemented Metzler's method[8] by ourselves with GBDTs as the learning model, which is denoted "baseline" in the following experiments. Our own method use the same set of traditional features as the baseline method, and additional Wikipedia-based features CTFIDF and CSIM are employed. In both methods, Wordnet database[1] is used as the synonym source in the overlap-syn feature.

Real-world web pages are used to evaluate our methods' effectiveness. The data set is constructed by submitting 400 random chosen non-navigational queries from the AOL query set to the Google search engine and retrieve the top 5 result pages. For each page, 10 sentences were labeled a relatedness score ranging from 1 to 5 manually to every query. Half of these sentences were selected using cosine similarity measure, and the other half were selected randomly throughout the whole article.

4.2 Evaluation Metrics

Here normalized Discounted Cumulative Gain (nDCG)[7] is used as the metric of the effectiveness of the summarization. DCG(Discounted Cumulative Gain) is computed by accumulating the gains from the top of the rank list to the bottom with each gain entry discounted at lower ranks. nDCG is the normalized version of DCG, which is the ratio between the rank's DCG value and the idealized DCG value. In order to generalize our experiments to independent data sets, we applied a 5-fold cross validation to each of the experiments.

4.3 Results

Different Data Sets. We first apply our algorithm to different data sets divided by the frequency of query term occurrence in the document. The data sets we organized include: **All**, The entire data set, which contains all the documents; **L(n)** the data set representing the documents in which the query term occurs not too often, We put the query-document pair into this data set if any of the query terms occur in less than **n** sentences of the document. **GE(n)**, the data set consist of the query-document pairs that query term occurs in no less than **n** sentences, i.e., the complement of L(n).

4.4 Effectiveness

We now perform the experiment of four feature sets (baseline, baseline + CTFIDF, baseline + CSIM, baseline + CTFIDF + CSIM) on four different data sets (All, GE(10), L(10), L(5)). Here *baseline* denotes the traditional feature set we mentioned above, both query-dependent and query-independent. GE(10) contains 54.9% of the query-document pair in the training, while L(10), L(5) contains 45.1% and 36.0% respectively. The results are shown in Figure 1.

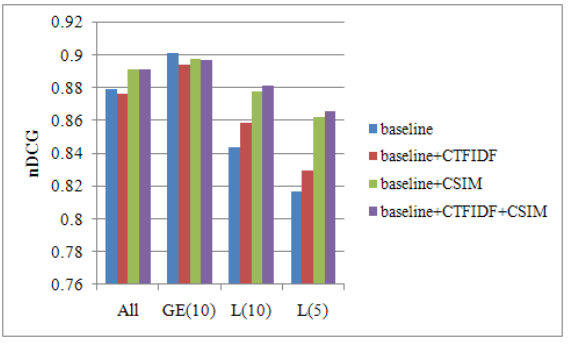

Fig. 1. Effectiveness, measured in terms of nDCG, on different data sets

From the Figure 1 we can get the following points. First, the feature set *baseline + CTFIDF + CSIM* achieved an obvious boost in all data sets except GE(10), and the drop on GE(10) dataset is relatively small. In GE(10) data set, the group of lexical features plays a decision role in the summary generation process, so semantic features may be hard to lead a gain. Second, our method caused a significant improvement when dealing with the documents with low occurrence of query terms (e.g., L(10) and L(5)). For the L(5) data set, our method achieved a 5% improvement in nDCG compared with the baseline method, which is significant enough for users to feel the improvement of the summarization quality. After carefully examining the sentence selection result,

we found that this improvement is caused by the involvement of semantic information. For example, when applying query *pink eye* to a document describing *Conjunctivitis*, traditional methods will get confused because they cannot found any *pink eye* occurrences. Third, we found that CSIM is the most effective feature among the newly-added ones, even without CTFIDF, CSIM can still lead to good enough results. Though CTFIDF behaves not so good in the experiments, we still notice a considerable gain it when it is combined with CSIM, compared with CSIM only.

4.5 Concept Vector Lengths

One of the parameters in our method is the length of the concept vector for each piece of text. Short vector cannot bring enough information of the semantics of the text, while very long vectors will bring a lot noise and spoil the summary generation. So we conducted an experiment on concept vector lengths to investigate how concept vector length affects the generation effectiveness. We applied baseline + CTFIDF + CSIM method with all the above features to the data set L(5), L(10), All. By varying the concept vector length from 10 to 450, the result is as follows.

	0	10	50	100	150	200	250	300	350	400	450
All	0.879	0.879	0.884	0.891	0.891	0.891	0.891	0.892	0.892	0.891	0.893
L(10)	0.844	0.869	0.864	0.881	0.885	0.884	0.888	0.885	0.885	0.887	0.884
L(5)	0.817	0.834	0.844	0.865	0.864	0.870	0.859	0.866	0.868	0.859	0.859

From the result, we can infer that on each data set the effectiveness increases with the growth of the concept length when the length is lower than 100. But further growth of concept vector length doesn't bring significant boost in the effectiveness. We even noticed a drop in effectiveness on L(5) data set when concept vector length exceeds 100. From the figure we found a concept length around 150 is the best for most of the cases.

5 Conclusions and Future Work

In this paper, we applied Wikipedia-based explicit semantic analysis to query-biased summary generation process. Our Experiment results showed our method achieved a significant gain in summary generation effectiveness, especially for the documents with rare occurrences of query terms. We also investigated how the concept vectors' length affects our method and found too long concept vectors may cause a drop in summary generation quality. As part of future work, we plan to try different machine learning techniques and involve more features derived from Wikipedia.

Acknowledgement

Authors thank the support by the grants from NSFC project (NO. 60873211) and RGC/NSFC project (NO. 60910123).

References

1. http://wordnet.princeton.edu
2. Amini, M.-R., Gallinari, P.: The use of unlabeled data to improve supervised learning for text summarization. In: SIGIR, pp. 105–112 (2002)
3. Chuang, W.T., Yang, J.: Extracting sentence segments for text summarization: a machine learning approach. In: SIGIR, pp. 152–159 (2000)
4. Deerwester, S.C., Dumais, S.T., Landauer, T.K., Furnas, G.W., Harshman, R.A.: Indexing by latent semantic analysis. JASIS 41(6), 391–407 (1990)
5. Jerome, H.: Friedman. Greedy function approximation: A gradient boosting machine. Annals of Statistics 29, 1189–1232 (2000)
6. Gabrilovich, E., Markovitch, S.: Computing semantic relatedness using wikipedia-based explicit semantic analysis. In: IJCAI 2007: Proceedings of the 20th international joint inproceedings on Artifical intelligence, pp. 1606–1611. Morgan Kaufmann Publishers Inc., San Francisco (2007)
7. Järvelin, K., Kekäläinen, J.: Cumulated gain-based evaluation of ir techniques. ACM Trans. Inf. Syst. 20(4), 422–446 (2002)
8. Metzler, D., Kanungo, T.: Machine Learned Sentence Selection Strategies for Query-Biased Summarization. Learning to Rank for Information Retrieval, 40
9. Song, F., Bruce Croft, W.: A general language model for information retrieval. In: Proceedings of the 1999 ACM SIGIR Conference on Research and Development in Information Retrieval, pp. 279–280 (1999)
10. Tombros, A., Sanderson, M.: Advantages of query biased summaries in information retrieval. In: SIGIR 1998: Proceedings of the 21st annual international ACM SIGIR inproceedings on Research and development in information retrieval, pp. 2–10. ACM, New York (1998)
11. Turpin, A., Tsegay, Y., Hawking, D., Williams, H.E.: Fast generation of result snippets in web search. In: SIGIR, pp. 127–134 (2007)
12. Wang, C., Jing, F., Zhang, L., Zhang, H.-J.: Learning query-biased web page summarization. In: CIKM 2007: Proceedings of the sixteenth ACM inproceedings on Conference on information and knowledge management, pp. 555–562. ACM, New York (2007)
13. Zhai, C.X., Lafferty, J.D.: A study of smoothing methods for language models applied to ad hoc information retrieval. In: SIGIR, pp. 334–342 (2001)
14. Zheng, Z., Zha, H., Zhang, T., Chapelle, O., Chen, K., Sun, G.: A general boosting method and its application to learning ranking functions for web search. In: NIPS (2007)

A New Approach for Vein Pattern-Based Recognition

Mohit Soni[1], Sandesh Gupta[2], and Phalguni Gupta[2]

[1] The Directorate of Forensic Science, CGO Complex, New Delhi-110003 India
myk.soni@gmail.com
[2] Indian Institute of Technology Kanpur, Kanpur, UP-208014 India
sandesh@iitk.ac.in, pg@iitk.ac.in

Abstract. This paper presents an efficient human verification system based on vein patterns of the hand. A new absorption based technique has been proposed to collect good quality images with the help of a low cost camera and light source. The system automatically detects the region of interest from the image and does the necessary processing to extract various features. Matching technique based on Euclidean Distance has been used for making the decision. It has been tested on a data set of 1750 image samples collected from 341 individuals. The accuracy of the recognition system is found to be 99.26% with FRR of 0.03%.

Keywords: Recognition system, Palma Dorsa, Region of Interest, Vein Structure, Minutiae, Ridge Forkings.

1 Introduction

Vein pattern of the palma dorsa is the geometry of the network of veins running under the skin, in the back of the hand. Since this geometry of the network is random, it can be considered as a possible biometric trait [12]. The existing biometric traits, with varying capabilities, have proven successful over the years. Traits like Face, Ear, Iris, Fingerprints, and Signatures etc. have dominated the world of biometrics over the years. But each of these biometric traits has its shortcomings. Ear and iris pose a problem during sample collection. Not only is an expensive and highly attended system required for iris but it also has a high failure to enroll rate. In case of ear data, it is hard to capture a non-occluded image in real time environment. In case of the most well known face recognition systems, there exist some limitations like aging, background, etc [2]. Fingerprints, though most reliable, still have the problem of automation and viability as they are also susceptible to wear and aging. Signatures are liable to forgery. Venal patterns, on the other hand, have the potential to surpass most of these problems. Apart from the size of the pattern, the basic geometry always stays the same. Unlike fingerprints, veins are located underneath the skin surface and are not prone to external manipulations. Vein patterns are also almost impossible to replicate because they lie under the skin surface.

D.-S. Huang et al. (Eds.): ICIC 2010, LNCS 6215, pp. 482–489, 2010.

It seems the first known work in the field of venal pattern has been found in [8]. Badawi [1] has also established the uniqueness of vein patterns using the patterns from the palma dorsa. The data acquisition technique mentioned in [1] is based on a clenched fist holding a handle to fixate the hand during image capture. This method is found to have limitations with respect to orientation. Substantial works in this field have been done by Leedham and Wang [9] [10] [11]. Thermal imaging of the complete non-fisted hand has been done using infra-red light sources. These lamps are found to be costly. Also infra-red light has been used to either reflect or transmit light to the desired surface [7] [9] [10] [12]. These techniques have both their advantages and disadvantages. It has been observed that the images captured through a reflection based system may not produce consistent results owing to excessive noise generated due to unnecessary surface information [9]. The surroundings need to be controlled always and the skin color or skin abnormalities are bound to have an effect. The best results can only be expected after exposure from the near infra-red lamps which are costly.

Matching technique in a biometric system is a crucial step because the accuracy of the system alone can determine its effectiveness. Badawi [1] has used a correlation based matching algorithm and achieved excellent results. However, correlation-based techniques, though the most popular, become costly on larger databases. Wang and Leedham [11] have used a matching technique based on Hausdorff distancing which is limited, in principle, by the slightest change in orientation.

This paper proposes an efficient absorption based technique for human identification through venal patterns. It makes use of a low cost sensor to acquire images. It uses a fully automated foreground segmentation technique based on active contouring. Reduced manual interference and an automatic segmentation technique guarantee the uniform segmentation of all samples. The paper also employs a rotation and translation invariant matching technique. The proposed system uses critical features of veins to make the decision. The results, thus far, have been found to be encouraging and fulfilling.

Next section presents the experimental setup used to acquire images. Its various sub-sections deal with the proposed venal pattern based biometric system. Critical issues such as use of a low cost sensor for acquiring images, automatic detection of region of interest, rotation and translation invariant matching etc. are discussed in this section. This system has been tested on the IITK database consisting of 1750 image samples collected from 341 individuals under a controlled environment, over the period of a month. Experimental results have been analyzed in Section 3. Concluding remarks are given in the last section.

2 Proposed System

Like any other biometric system, the venal pattern based system consists of four major tasks and they are (i) image acquisition (ii) preprocessing of acquired image data (iii) feature extraction (iv) matching. Flow diagram of the proposed system is given in Fig. 1.

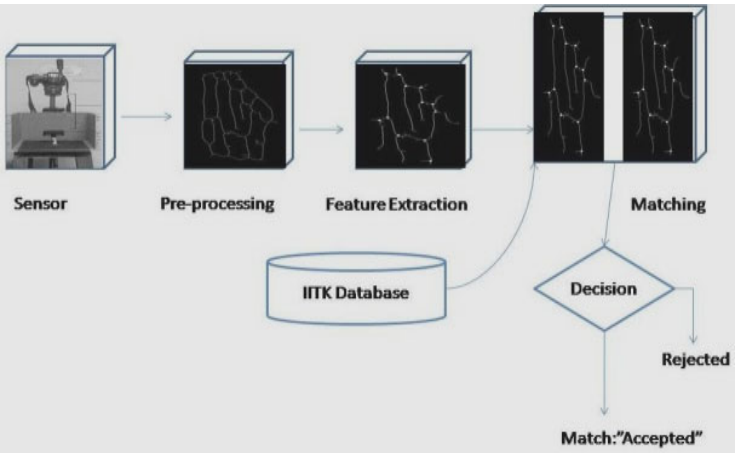

Fig. 1. Flow Diagram of the Proposed System

2.1 Image Acquisition

Performance of any biometric system depends on the quality of the acquired images. This system aims to capture the best possible images with cost effective equipment.

In our experiment, a simple digital SLR camera combined with an infra-red filter has been used for data acquisition. It employs a low cost night vision lamp of wavelength 940 nm as its light source. The proposed set-up is a modest wooden box with a hollow rod lodged in the middle accommodating the infra-red lamp. The camera is fixed at a perpendicular to the light source and is held on a tripod attached to the box. The robustness and the flat face of the night vision lamp provide a sturdy plinth for the subject's hand. The sensor is kept on the opposite side of the light source as shown in Fig. 2. The subject has to place his palm on the plinth surface to provide the image.

The experimental setup for the proposed system is not only the cost effective but also provides good quality images. The light source is placed behind the surface to be captured. It helps to make an ideal data scheme and standard, as all parameters can be fixed. Unlike [7] [9] [10] and [12] where infra-red light has been reflected or transmitted to the desired surface, this paper proposes an absorption-based technique to acquire images. The technique provides a good quality image regardless of the skin color or any aberrations or discolorations, on the surface of the hand. In this technique the veins pop out when the hand is fisted and it becomes much easier to capture high contrast images. The time and cost of image processing therefore can be kept to a minimum. The image capturing however would be limited by anomalies on the palma dorsa itself, like tattoos etc. On the other hand, skin color or the gradual change of it (due to diseases or sunlight exposure, etc.) or, the gain and loss of weight would not hamper the pattern collection process. Since the light illuminates the entire hand, it is a common notion that the veins in the front of the hand might interfere with the pattern at the back. However, it is crucial to note, that infra-red light does not make the hand transparent. It simply illuminates the hemoglobin in the veins which appear

black. The partition of the bone between the two planes in the front and the back of the hand does not allow interference. And since the sensor is always facing the dorsal surface, it becomes the only captured surface.

2.2 Data Pre-processing

The color image acquired through a camera generally contains some additional information which is not required to obtain the venal pattern. So there is a need to extract the region of interest from the acquired image and finally to convert into a noise free thinned image for generating the raw venal pattern. Badawi [1] has considered the skin component of the image as the region of interest (ROI). Wang and Leedham [9] have used anthropometric points of a hand to get ROI from the images. In [7] there is a similar work which is based on ROI selection employ arbitrary and inconsistent techniques and so end up enhancing manual intervention during processing. The extracted region is used for processing to obtain the venal pattern.

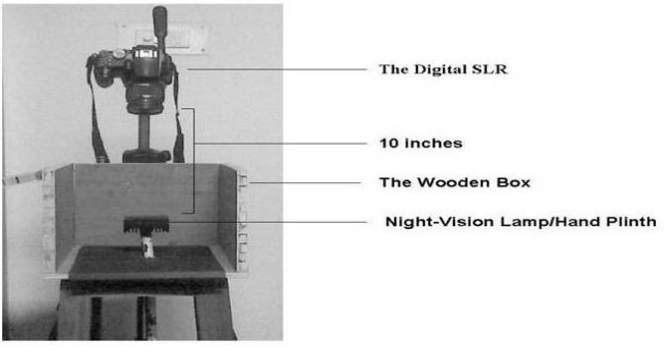

Fig. 2. Experimental Setu

In this paper the segmentation technique used to segregate the skin area from the acquired image selects the ROI in a systematic manner and it successfully gets rid of all manual intervention. It fuses a traditional technique based on active contouring [5] with a common cropping technique. It works on the principle of intensity gradient where the user initializes a contour to detect the boundary of the object easily. A traditional active contour is defined as a parametric curve $v(s) = [x(s), y(s)], s \in [0, 1]$ which minimizes the energy function:

$$E_{contour} = \int_0^1 \frac{1}{2}(\eta_1 |v'(s)|^2 + \eta_2 |v''(s)|^2) + E_{ext}(v(s))ds \quad (1)$$

where η_1 and η_2 are weights to control the relative importance of the elastic and bending ability of the active contour respectively; $v'(s)$ and $v''(s)$ are the first and second order derivatives of $v(s)$, and E_{ext} is derived from the image which takes smaller values at the feature of interest like object boundaries etc.

The active contour deforms itself with time to exactly fit around the object. It can thus be represented as a time varying curve:

$$v(s, t) = [x(s, t), y(s, t)] \tag{2}$$

where $s \in [0, 1]$ is arc length and $t \in R^+$ is time.

Active contouring helps the contours to settle at the object boundary. It is followed by the iterative use of a cropping tool to extract the object automatically [3]. In this paper this active contouring snake has been modified from its regular run. Instead of initiating the snake from the outside in, it is run in reverse, after initiating it from the centre of the image. This initiation is done automatically since the images are of fixed size.

The extracted ROI of the colored image is converted into a grey scale image [3]. The segmented image has been enhanced using Gaussian filtering technique and is then normalized by converting it to an image having a pre-defined mean and variance. The resultant image is then binarized by mean filtering. It may still contain noise like dots, blobs and stains, etc. Median filtering is used to remove these noise particles. The image may consist of a few edges of the vein pattern that may have been falsely eroded during filtering. These edges are reconnected by dilation and then skeletonized. To obtain only desired components amongst veins, all connected components are labeled and others are discarded.

From the skeleton of the hand, the skeletonized veins are extracted. The Connected Component Labeling (CCL) algorithm [6] is modified to determine all the connected components in an image and remove the isolated and disconnected components of size less than a specified threshold from the final skeleton.

2.3 Feature Extraction

This section extracts forkings from the skeleton image by examining the local neighborhood of each ridge pixel using a 3X3 window. The ridges representing vein patterns can be used to extract features. Features like ridge forkings are determined by computing the number of *arms originating from a pixel (AN)*. The *AN* for a pixel *P* can be given as:

$$AN = 0.5 \sum_{i=1}^{8} | P_i - P_{i+1} |, P_9 = P_1 \tag{3}$$

For a pixel *P*, its eight neighbors are scanned in an anti-clockwise direction as follows:

P_4	P_3	P_2
P_5	P	P_1
P_6	P_7	P_8

A given pixel *P* is termed as a ridge forking for a vein pattern if the value of *AN* for the pixel is 3 or more. This ridge forking pixel is considered as a feature point which can be defined by (x, y, θ) where x and y are coordinates and θ is the orientation with respect to a reference point. Figure 3 shows the final image of the extracted vein pattern with all forking points.

2.4 Matching Strategy

Suppose, N and M are two patterns having n and m features respectively. Then the sets N and M are given by:

$$N = \{(x_1, y_1, \theta_1), (x_2, y_2, \theta_2), \ldots, (x_n, y_n, \theta_n)\}$$
$$M = \{(a_1, b_1, \varphi_1), (a_2, b_2, \varphi_2), \ldots, (a_m, b_m, \varphi_m)\} \quad (4)$$

where (x_i, y_i, θ_i) and (a_j, b_j, φ_j) are the corresponding features in pattern N and M respectively. For a given minutiae (x_i, y_i, θ_i) in N, it first determines a minutiae (a_j, b_j, φ_j) such that the distance $sd_i = \left|\sqrt{(x_i - a_j)^2 + (y_i - b_j)^2}\right|$ is minimum for all j, $j=1,2,3 \ldots,m$. Let the corresponding difference between two directions be dd_i, where $dd_i = \left|\theta_i - \varphi_j\right|$.

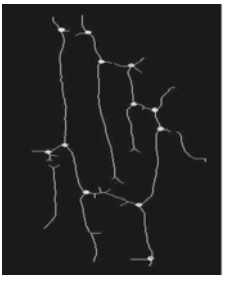

Fig. 3. Final Vein Pattern with all Forking Points

This is done for all features in N. To avoid the selection of same feature in M for a given minutiae in N, one can follow the following procedure. Suppose, for the i^{th} feature in N, one gets sd_i for the j^{th} feature in M. Then, in order to determine sd_{i+1}, one considers all features in M which are not selected in sd_1, $sd_2 \ldots sd_i$. Let A be a binary array of n elements satisfying:

$$A[i] = \begin{cases} 1 & if\ (sdi \le ti)\ and\ (ddi \le t2) \\ 0 & otherwise \end{cases} \quad (5)$$

where t_1 and t_2 are predefined thresholds.

Then the percentage of match for the pattern N having n features against the pattern can be computed by

$$V = \frac{\sum_{i=1}^{n} A[i]}{n} X100\% \quad (6)$$

If V is more than a given threshold then one can draw the conclusion that both the patterns are matched [4].

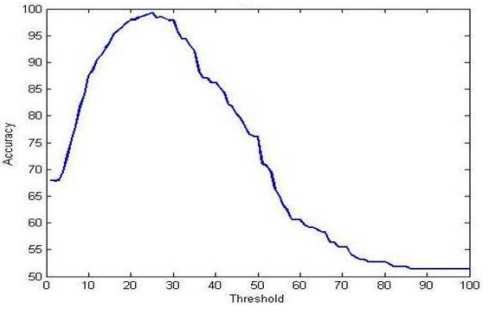

Fig. 4. Graph Accuracy

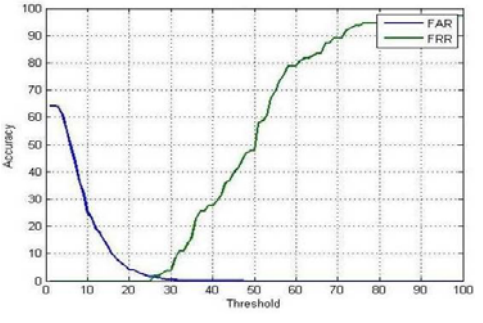

Fig. 5. Graph indicating FAR and FRR

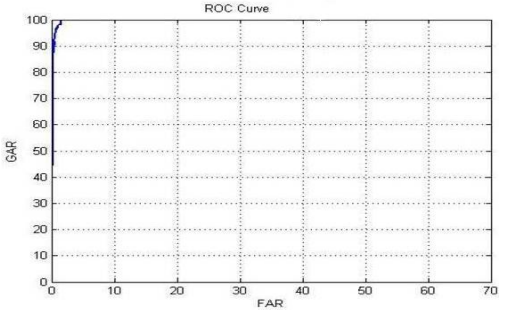

Fig. 6. The ROC Curve- GAR v/s FAR

3 Experimental Results

The system has been tested on the IITK database consisting of 1750 images obtained from 341 individuals under controlled environment. Out of these images, 341 are used as query samples. A graph is plotted for the achieved accuracy against the various threshold values as shown in Fig.4. It is observed that the maximum accuracy of 99.26% can be achieved at the threshold value, *T*, of 25. Graphs showing FAR and

FRR against various thresholds are plotted in Fig. 5 while the ROC curve between the values of GAR and the FAR is given in Fig. 6. These figures reveal that the value of FRR for which the system achieves maximum accuracy is achieved when FRR is 0.03%.

4 Conclusion

This paper has proposed a new absorption based vein pattern recognition system. It has a very low cost data acquisition set up. It has made an attempt to handle issues such as effects of rotation and translation on acquired images, minimizing the manual intervention to decide on the verification of an individual. The experimental results provide an accuracy of 99.26% with FRR 0.03%.

References

1. Badawi, A.: Hand vein biometric verification prototype: A testing performance and patterns similarity. In: Proceedings of the International Conference on Image Processing, Computer Vision, and Pattern Recognition, pp. 3–9 (2006)
2. De Luis Garcia, R., Alberola-Lopez, C., Aghzoutb, O.: Ruiz,A. Biometric identification systems. Signal Processing 83, 2539–2557 (2003)
3. Gonzalez, R.C., Woods, R.E.: Digital image processing using MATLAB, 1st edn. Prentice Hall, Englewood Cliffs (2003)
4. Halici, U., Jain, L.C., Erol, A.: Introduction to fingerprint recognition. Intelligent Biometric Techniques in Fingerprint and Face Recognition, 3–34 (1999)
5. Kass, M., Witkin, A., Terzopoulos, D.: Snake: Active contour models. International Journal of Computer Vision 1, 321–333 (1988)
6. Khanna, V., Gupta, P., Hwang, C.J.: Finding connected components in digital images by aggressive reuse of labels. International Vision Computing 20, 557–568 (2002)
7. Lakshmi, D.C., Kandaswamy, A.: An algorithm for improved accuracy in unimodal biometric systems through fusion of multiple feature sets. ICGST-GVIP Journal 9, 33–40 (2009)
8. Im, S.K., Park, H.M., Kim, Y.W., Han, S.C., Kim, S.W., Kang, C.H.: Improved vein pattern extracting algorithm and its Implementation. Journal of the Korean Physical Society 38, 268–272 (2001)
9. Wang, L., Leedham, C.G.: A thermal hand vein pattern verification system. In: Singh, S., Singh, M., Apte, C., Perner, P. (eds.) ICAPR 2005. LNCS, vol. 3687, pp. 58–65. Springer, Heidelberg (2005)
10. Wang, L., Leedham, C.G.: Near and far-infrared imaging for vein pattern biometrics. In: Proceedings of IEEE International Conference on Advanced Video and Signal Based Surveillance (2006)
11. Wang, L., Leedham, G., Cho, S.Y.D.: Minutiae feature analysis for infrared hand vein pattern biometrics. Pattern Recognition 41, 920–929 (2008)
12. Watanabe, M., Endoh, T., Shiohara, M., Sasaki, S.: Palm vein authentication technology and its applications. In: Proceedings of the Biometric Consortium Conference (2005)

Study of Hand-Dorsa Vein Recognition

Yiding Wang[1], Kefeng Li[1], Jiali Cui[1], Lik-Kwan Shark[2], and Martin Varley[2]

[1] College of Information Engineering,
North China University of Technology, Beijing,100144, China
[2] School of Computing, Engineering and Physical Sciences,
University of Central Lancashire, Preston. PR1 2HE. United Kingdom
wangyd@ncut.edu.cn,seafrog1984@hotmail.com,jialicui@gmail.com,
LShark@uclan.ac.uk, MRVarley@uclan.ac.uk

Abstract. A new hand-dorsa vein recognition method based on Partition Local Binary Pattern (PLBP) is presented in this paper. The proposed method employs hand-dorsa vein images acquired from a low-cost, near infrared device. After preprocessing, the image is divided into sub-images. LBP uniform pattern features are extracted from all the sub-images, which are combined to form the feature vector for token vein texture features. The method is assessed using a similarity measure obtained by calculating the Chi square statistic between the feature vectors of the tested sample and the target sample. Integral histogram method, original LBP and Partition LBP with 16, 32, 64 sub-images are tested on a database of 2040 images from 102 individuals built up by a custom-made acquisition device. The experimental results show that Partition LBP performs better than original LBP, Circular Partition LBP performs better than Rectangular Partition LBP, and when the image was divided into 32 performs better than others.

Keywords: Biometrics, hand-dorsa vein, Partition Local Binary Pattern (PLBP).

1 Introduction

Personal verification is becoming an increasingly important and widely used technique for security access systems. Biometric feature authentication technology is a process using inherent physiological or behavior characteristics to enable identification of individuals. It has high security and reliability compared to the traditional authentication modes such as password or code, because biometric features are hard to forge and relatively easy to use.

Vein patterns have attracted significant attention in the research community recently, as a new means of biometric recognition. Compared to more established biometric patterns, such as finger, face and iris, vein patterns have higher convenience and higher security [1] [2]. A typical vein pattern recognition system is shown in Fig.1.

D.-S. Huang et al. (Eds.): ICIC 2010, LNCS 6215, pp. 490–498, 2010.

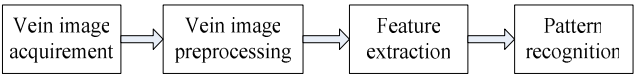

Fig. 1. A typical vein pattern recognition system

Former researchers usually obtain the vein structure first and use shape descriptors to extract features. Wang et al. [3] use endpoints and cross points. Cross and Smith [4] consider every vascular as a short straight vector, which has position and angle. Li et al. [5] use modified moment invariants to extract features.

However, all of these methods extracted features on the images after segmentation. In fact, segmentation errors cannot be avoided. Some thin vessels could be missed, and some dark regions could be considered as vein patterns by mistake. To solve this problem, we employ LBP uniform pattern as the feature of vein pattern. In this case, the images do not need thinning and pruning.

And the acquired vein images may exhibit different rotations, they usually should be normalized for angle before feature extraction. In this work, we use Circle Partition LBP as the feature. It has rotation invariance, so the normalization for angle is not necessary.

2 Vein Image Acquisition

The acquisition of hand vein images using near IR (NIR) imaging has been studied in [6], [7], and [8]. In this work, a low-cost NIR camera, traditionally used for medicine, was employed for image acquisition.

A database of hand-dorsa vein images was created using our custom-made device. Our database contains 2040 images from 102 individuals in which 52 are female and 50 are male. Ten images of the right hand and ten images of the left hand were captured for every individual. The database obtained by custom-made acquisition device is shown in Fig.2. Some image samples acquired from our device are reproduced in Fig.3.

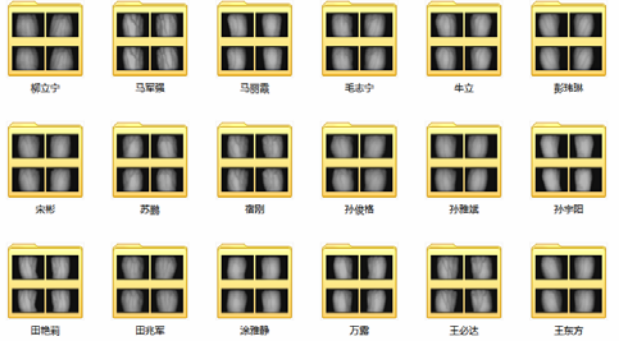

Fig. 2. The database obtained by our vein images acquisition device

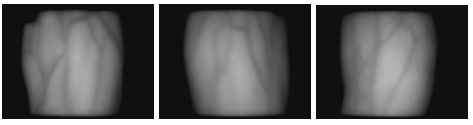

Fig. 3. Samples obtained by our device

3 Vein Image Preprocessing

3.1 Filtering

Our camera is not a professional one. It introduces noise to the images we obtained, therefore noise removal is required. Possible noise removal methods are discussed in [3], [6]. As our images exhibit different noise characteristics, these methods are not necessarily suitable. In this work, we employ a filtering process comprising a matched filter, a wiener filter and a smoothing filter, as shown in Fig.4. The results of filtering are shown in Fig.5.

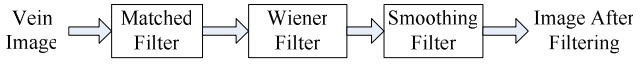

Fig. 4. Multi-stage filtering process

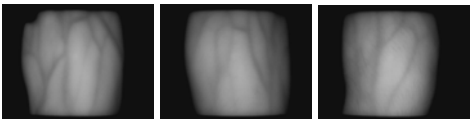

(a) Original vein images

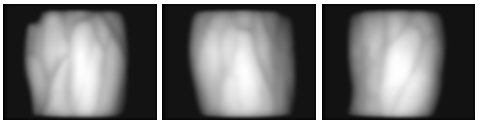

(b) Vein images after filtering

Fig. 5. Original and filtered vein images

Because our images are natural images, it is not easy to calculate signal-to-noise ratio (SNR) exactly. So we use total variation (TV) as the evaluation for noise [6]. For a digital image I (x, y), TV is calculated as shown in equation (1).

$$TV(I) = \sum_i \sum_j \begin{pmatrix} (I(i,j) - I(i-1,j))^2 \\ + (I(i,j) - I(i+1,j))^2 \\ + (I(i,j) - I(i,j-1))^2 \\ + (I(i,j) - I(i,j+1))^2 \end{pmatrix}^{\frac{1}{2}} \quad (1)$$

A bigger *TV* value means more noise. Table 1 shows the *TV* values of the original and filtered images shown in Fig. 5.

Table 1. *TV* values of original and filtered images

	Original	After filtering
***TV* value**	4273.4	1822.6
	4207.2	1744.6
	4175.6	1716.4

3.2 Region of Interest

In the vein images, the region that we are interested in is only the region which contains the information of the vein pattern. So we extract the region of interest (ROI) from the filtered images.

Extraction of ROI has been discussed in [9] [10]. In this work, we employ the centroid as the centre to extract the ROI. The centroid (x_0, y_0) of vein image $f(x, y)$ can be calculated as shown in equation (2).

$$x_0 = \frac{\sum_{i,j} i \times f(i,j)}{\sum_{i,j} f(i,j)}; y_0 = \frac{\sum_{i,j} j \times f(i,j)}{\sum_{i,j} f(i,j)} \tag{2}$$

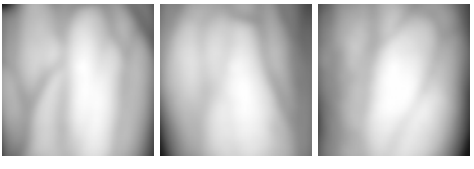

Fig. 6. ROI of the vein images

We get the region of size 360×360 with the centroid as the centre according to our vein images. The results are shown in Fig.6.

Because the centroid of the hand-dorsa vein region is invariable, extracting ROI using this method can correct the location difference.

3.3 Segmentation

Since the light intensity may vary at different times, the grey scale distribution of vein images is different. To reduce these differences and thereby simplify the segmentation process, a method of grey scale normalization is adopted, defined by equation (3).

$$y = ((x - \min) \times 255) / (\max - \min) \tag{3}$$

Where x is the grey scale value of the original image; y is the grey scale value after normalization; and min and max are the minimum and maximum grey scale values of the original image respectively.

Vein pattern images have low contrast. We choose Shi Zhao's improved threshold image segment method [6]. The main idea of this method is calculating a threshold for each pixel as (4).

$$T(x, y) = m(x, y) + k \times s(x, y) \tag{4}$$

Where $m(x, y)$ is the mean, $s(x, y)$ is the variance of the $r \times r$ region. k is the coefficient of correction. $m(x, y)$ and $s(x, y)$ are calculated as follows.

$$m(x, y) = \frac{1}{r^2} \sum_{i=x-r/2}^{x+r/2} \sum_{j=y-r/2}^{y+r/2} f(i, j) \tag{5}$$

$$s(x, y) = \sqrt{\frac{1}{r^2} \sum_{i=x-r/2}^{x+r/2} \sum_{j=y-r/2}^{y+r/2} (f(i, j) - m(x, y))} \tag{6}$$

Then the segmentation follows the equation (7). And the results of segmentation are shown as Fig. 7.

$$\begin{cases} f(x, y) = 0 & f(x, y) \geq T(x, y) \\ f(x, y) = 255 & f(x, y) < T(x, y) \end{cases} \tag{7}$$

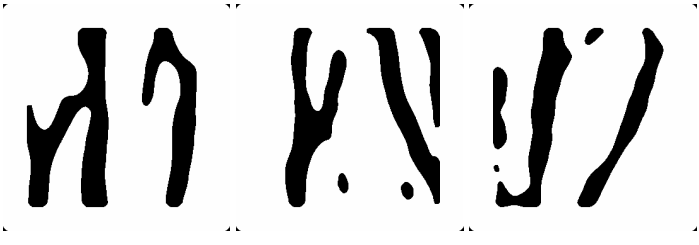

Fig. 7. Segmentation results

4 Feature Extraction

Former researchers usually obtain the vein structure first and use shape descriptors to extract features. Wang *et al.* [3] use endpoints and cross points. Cross and Smith [4] consider every vascular as a short straight vector, which has position and angle. Xueyan *et al.* [5] use modified moment invariants to extract features.

However, all of these methods extracted features on the images after segmentation. In fact, segmentation errors cannot be avoided. Some thin vessels could be missed, and some dark regions could be considered as vein patterns by mistake. To solve this

problem, we employ LBP uniform pattern as the feature of vein pattern. In this case, the images do not need thinning and pruning.

LBP is a powerful means of texture description [11]. It is an efficient rotation-invariant texture classification technique. The original LBP labels the pixels of an image by comparing the 3×3-neighbourhood of each pixel with the centre value, and considering the result as a binary number. Then the histogram of the labels can be used as a texture descriptor. An illustration of the basic LBP operator is shown in Fig.8.

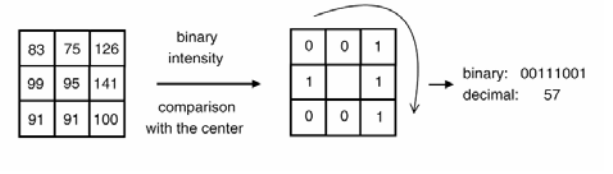

Fig. 8. Example of basic LBP operator

Ojala *et al.* [11] extended the operator to use neighborhoods of different sizes. Using circular neighborhoods and bilinearly interpolating the pixel values allows any radius and number of pixels in the neighborhood. $LBP_{P,R}$ means P sampling points on a circle of radius of R. Examples of the circular neighborhood are shown in Fig.9.

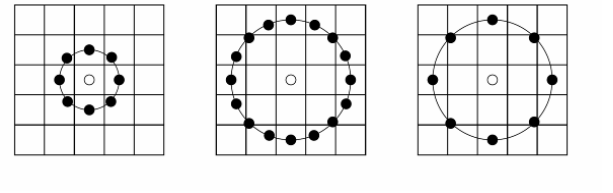

(a) $LBP_{8,1}$ (b) $LBP_{16,2}$ (c) $LBP_{8,2}$

Fig. 9. Circular neighborhoods for LBP

To remove the effect of rotation, the operator $LBP_{P,R}^{ri}$ is defined as shown in equation (8)

$$LBP_{P,R}^{ri} = \min\left\{ROR(LBP_{P,R}, i \middle| i = 0,1,2 \ldots P-1\right\} \tag{8}$$

Where $ROR(x,i)$ performs a circular bitwise right shift on the P-bit number x i times.

Another extension to the original method is called uniform patterns [11]. A Local Binary Pattern is called uniform if it contains at most two bitwise transitions from 0 to 1, or vice versa, when the binary string is considered circular. For example, 00000000, 00011110 and 10000011 are uniform patterns. The operator $LBP_{P,R}^{riu2}$ is defined to indicate LBP uniform patterns.

In this work, we use $LBP_{8,2}^{riu2}$ as the features for the vein images.

To describe the vein pattern in more detail, the vein image is divided into N regions as shown in Fig.10. $LBP_{8,2}^{riu2}$ features are extracted from all the sub images. Then 32 features are connected to form a 59×N dimensions vector, which describes the vein pattern more accurately than the original $LBP_{8,2}^{riu2}$ with a 59 dimensions vector.

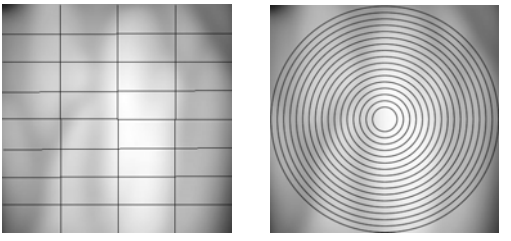

(a) Rectangular partitions (b) Circular partitions

Fig. 10. Sketches of image partitions

The similarity score of two vein images needs to be calculated for judging if they are from the same person or not. Chi square statistic similarity measures has been proposed by Ahonen et al. for histograms of LBP [12]. It is defined as shown in equation (9)

$$\chi(F,T) = \sum_i \frac{(F_i - T_i)^2}{F_i + T_i} \tag{9}$$

Where F and T are two images' LBP histograms to be compared. For Partition LBP, F and T are two images' feature vectors.

5 Experiments and Results

To test the proposed algorithm, we created a database of hand-dorsa vein images using our custom-made device. Our database contained 2040 images from 102 individuals in which 52 are female and 50 are male. Ten images of the right hand and ten images of the left hand were captured for every individual. To simulate the actual application environment, each image was captured at different times and some of them have shift and rotation.

The database was divided into two sets A and B. Set A had five images of every hand, and set B had the other five. We used set A for registering, and tested on set B. Integral histogram method and three LBP methods were applied to the database: $LBP_{P,R}^{riu2}$, Rectangular Partition LBP and Circular Partition LBP. The results are shown in Table 2.

Table 2. Results of Integral histogram, $LBP_{P,R}^{riu2}$, Rectangular Partition LBP and Circular Partition LBP

			images	correct	error	correct rate	error rate
Original LBP $LBP_{P,R}^{riu2}$			1020	756	264	74.12%	25.88%
PLBP	Rectangular Partition LBP	16 sub-images	1020	811	209	79.50%	20.50%
		32 sub-images	1020	836	184	81.96%	18.04%
		64 sub-images	1020	854	166	83.73%	16.27%
	Circular Partition LBP	16 sub-images	1020	813	207	79.71%	20.29%
		32 sub-images	1020	927	93	**90.88%**	**9.12%**
		64 sub-images	1020	853	167	83.63%	16.37%
Integral histogram			1020	886	134	86.86%	13.14%

It is evident from these results that Partition LBP gives an improved performance compared to original LBP. Furthermore, the performance of Circular Partition LBP is seen to be better than Rectangular Partition LBP. And Circular Partition LBP with 32 sub-images performs better than others.

Acknowledgements

This work is supported by the NCUT Scientific Research Foundation.

References

1. Kresimir, D., Mislav, G.: A survey of biometric recognition methods. In: 46th International Symposium Electronics in Marine, pp. 184–193 (2004)
2. Ding, Y.H., Zhuang, D.Y., Wang, K.J.: A study of hand vein recognition method. In: Proceedings of the IEEE International Conference on Mechatronics & Automation Niagara Falls, Canada, pp. 2106–2110 (2005)
3. Wang, K.J., Zhang, Y., Yuan, Z., Zhuang, D.Y.: Hand vein recognition based on multi supplemental features of multi-classifier fusion decision. In: Proceeding of the IEEE, International Conference on Mechatronics and Automation (2006)
4. Cross, J.M., Smith, C.L.: Thermographic imaging of the subcutaneous vascular network of the back of the hand for biometric identification In: Proceedings, Institute of Electrical and Electronics Engineers 29th Annual International Carnahan Conference Security Technology, Sanderstead, UK (1995)
5. Li, X.Y., Guo, S.X., Gao, F.L.: Vein pattern recognitions by moment invariants. In: IEEE Conference on Bioinformatics and Biomedical Engineering, pp. 612–615 (2007)
6. Zhao, S., Wang, Y., Wang, Y.: Biometric verification by extracting hand vein patterns from low-quality images. In: Proc. 4th ICIG, August 2007, pp. 667–671 (2007)
7. Cross, J.M., Smith, C.L.: Thermo Graphic Imaging of the Subcutaneous Vascular Network of the Back of the Hand for Biometric Identification. In: Proc. IEEE 29th Annu. Int. Carnahan Conf. Security Technology, Sander-Stead, Surrey, U.K., pp. 20–35 (1995)

8. Wang, L., Leedham, G.: Near and far-infrared imaging for vein pattern biometrics. In: Proc. IEEE Int. Conf. Video Signal Based Surveillance, Sydney, pp. 52–57 (2006)
9. Kumar, A., Prathyusha, K.V.: Personal authentication using hand vein triangulation and knuckle shape. IEEE Transactions on Image Processing 18, 2127–2136 (2009)
10. Lin, C.L., Fan, K.C., Chou, F.D.: A novel approach to palmprint verification utilizing finger-webs as datum points. Image and Vision Computing
11. Ojala, T., Pietikäinen, M., Mäenpää, T.: Multiresolution gray-scale and rotation invariant texture classification with local binary patterns. IEEE Transactions on Pattern Analysis and Machine Intelligence 24 (2002)
12. Ahonen, T., Pietikainen, M., Hadid, A., Maenpaa, T.: Face recognition based on the appearance of local regions. In: ICPR (2004)

DHV Image Registration Using Boundary Optimization

Jiali Cui, Yiding Wang, and Kefeng Li

North China University of Technology,
5 Jinyuanzhuang Rd, Beijing 100144, P.R. China
{jialicui,wangyd}@ncut.edu.cn, seafrog1984@hotmail.com

Abstract. An image registration method using boundary optimization is proposed to register dorsal-hand vein (DHV) images of different rotation angles. Since image rotation is inevitable during image capture, the proposed method is important in human identification based on DHV images. The proposed method consists of two main procedures, i.e., boundary detection and boundary optimization. Boundary detection is used to create a boundary map, and boundary optimization is used to find the best rotation angle with the boundary map. Simulations and extensive experiments show that the proposed method can reduce equal error rate (EER) efficiently. The experiments also show that the method is fast and can be completed in 50 milliseconds.

Keywords: Biometrics, DHV images, Image registration, Boundary optimization, EER.

1 Introduction

As a newly emerged topic, biometrics has attracted more and more attention in the past decades. Biometrics aims to recognize human identification using the physiological or behavioral characteristics, such as fingerprint, face, iris, dorsal hand vein, voice, gait, signature, and so on. Because of its high reliability and convenience, biometrics has many potential applications in surveillance, access control, network security, etc [1, 2].

As a new branch of biometric techniques, human identification based on DHV images attracts increasing interests of researchers due to its potential advantages. It can be non-invasive because the images can be captured without touching the device. Moreover, the DHV images are difficult to be forged.

However, most researchers focus on recognition algorithms and put less focus on pre-processing of DHV images. Thus, there is usually a handle in the capture device to fix the hand pose and position [3-5, 7]. This makes the capture device invasive. The motivation of this paper is to remove the handle to make the device non-invasive.

Without the handle, the users can show their hands under the camera with different poses; however removing the handle results in translation and rotation in the captured images. In this paper, we try to correct the rotation.

Some researchers obtained some progress in rotation correction of images. Koichi et al. developed a phase-only method to estimate the rotation angle between two palmprint images [6]. The method is based on the FFT transform of each image, thus,

D.-S. Huang et al. (Eds.): ICIC 2010, LNCS 6215, pp. 499–506, 2010.

the method has to deal with a lot of operations of floating point numbers and the computational complexity is high. Although the computation time is acceptable if the code is optimized carefully on some PCs, it does not work in some clips which do not support floating point computations. Kumar and Zhang proposed a hand geometry recognition using entropy-based discretization [8]. By analyzing these methods, we proposed a method to correct the rotation using a boundary optimization method. Our idea is to create a boundary map of the DHV images to describe the hand pose and finds the rotation angle with a boundary optimization procedure.

The remainder of the paper is organized as follows. Section 2 details the proposed registration method. Experimental results are reported in section 3. Section 4 concludes the whole paper. Acknowledgements and references are given at the end of the paper.

2 Algorithm Description

It is challenging to estimate the rotation angle between two DHV images. First, our low-cost ordinary camera brings much noise to the images. Moreover, the distribution of the dorsal hand veins is almost random and different subjects have different key points. It is like iris recognition, in which rotation correction is done in feature matching procedure.

In the subsequent parts, we try to use the DHV image boundary to estimate the rotation angle. The proposed method contains two main procedures, i.e., boundary detection and boundary optimization. Boundary detection creates a boundary map with a triangle model. Boundary optimization determines the rotation angle using the boundary map by maximizing a criterion which measures the distribution of the boundary points.

2.1 Boundary Detection

To detect the hand boundary while remaining the boundary shape, a geometric method is adopted. The method uses a triangle model which can be illustrated with Fig.1.

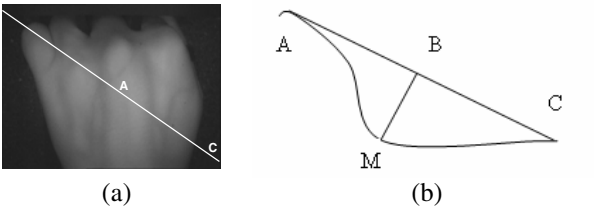

Fig. 1. Illustration of triangle model

In Fig.1(b), curve AMC, denoted with C_{AMC}, represents the sampling along the white line in Fig.1(a). Point A represents the point of maximum gray value in

C_{AMC} and point C stands for an edge point of the image. A straight line is obtained by connecting point A and C and the line can be denoted with L_{ABC}. Curve C_{AMC} and line L_{ABC} combine an approximate triangle and point M is the point which is farthest to line L_{ABC}. Therefore, the boundary point M can be found as follows.

$$M = \arg\max_{p \in C_{AMC}} D(p, L_{ABC}) \tag{1}$$

where $D(p, L_{ABC})$ is the distance between point p and line L_{ABC} and p is a point lying on curve C_{AMC}.

For each possible sampling line which is similar to the white line in Fig.1(a), we first obtain the position of the maximal gray value, then repeat Eq.(1) to detect all the boundary points. These boundary points give a boundary map which describes the hand contour.

The reason to adopt the above model is the noise in the captured images. The SNR is low in our images captured with low-cost cameras. Thus, simple threshold method may induce much noise in the binary images. Moreover, threshold method may destroy the hand boundary when lighting is not distributed equally.

2.2 Boundary Optimization

Boundary optimization is used to estimate the rotation angle. We rotate an image by each candidate angle and compute the corresponding variance of the boundary projection. If the variance reaches its maximum, we obtain the angle by which the image should be rotated.

Suppose I represents the boundary map and I_θ represents the boundary map rotated by an angle θ, then the best angle can be estimated using the following equations.

$$S = P(I_\theta) \tag{2}$$

$$\theta_{opt} = \arg\max_{\theta \in (-45^\circ, 45^\circ)} Var(S) \tag{3}$$

where $P(I_\theta)$ is the vertical projection of the rotated boundary map. $Var(S)$ is the variance of the projection.

Since the rotation angle is estimated with the same criterion, all the images are registered after rotated by the angle θ_{opt}. It is equivalent to normalize all the images to a fixed pose.

By analyzing Eqs.(1) to (3), we can see that all the computations are integer operations if we make several small look-up tables. Thus, the whole method can be completed in short time.

3 Experimental Results

In our previous work, a capture device is designed as a fundamental work. The device consists of a general-purpose camera, an infrared filter and a well designed light source. Two databases are collected and used in the following experiments.

The first database is called Dataset_Rotation. It contains the images of both left and right hands of 5 subjects. There are 10 images for each hand. Although there is still a handle in our device, we do not hold the handle with the same pose, so that we can simulate the distortions as if the handle is removed. However, to make the problem simple, only rotation is simulated. The rotation angle of the images is distributed from -30 to 30 degrees. Dataset_Rotation is used to evaluate the accuracy of the proposed method. Two examples in Dataset_Rotation are shown in Fig.2. The handle is marked with a white circle in Fig.2(b).

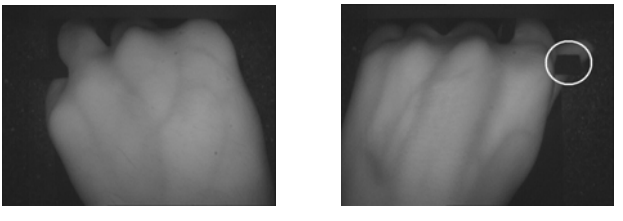

(a) (b)

Fig. 2. Samples of DHV images

The second database is called Database_Regular. We collected a large database which contains the images of both left and right hands of 102 men and women subjects. There are 10 images for each hand. We collected only one picture every time the users hold the handle. No obvious rotation can be seen in the images in the database.

Extensive experiments are done to evaluate the performance of the proposed method. The first experiment is a simulation to test the accuracy of the proposed method. The second experiment is done on Dataset_Rotation to show that the EER can be reduced with the proposed method. The last experiment is done on Database_Regular to test if the method works for the regular images without obvious rotation.

3.1 Results of Boundary Detection

An image is selected to show the performance of the boundary detection method introduced in Section 2.1. The detection results are shown in Fig.3, where white pixels represent the boundary points. These white pixels form the boundary map which can be used by the subsequent boundary optimization procedure.

Fig. 3. Results of boundary detection

3.2 Simulations

The simulations are used to test the accuracy of the proposed method. We randomly select one image in Dataset_Rotation and normalize the image so that the image has zero rotation angle according to Eq.(3). Then the normalized image is rotated by a random angle α distributing in (-45, 45) degrees and a nearest-neighbor interpolation is adopted during image rotation. Finally, the estimated angle $\hat{\alpha}$ is obtained with our method. The estimation angle error is defined with $\hat{\alpha}-\alpha$ and the histogram of the errors between α and $\hat{\alpha}$ is drawn in Fig.4. The simulation shows that the error is small.

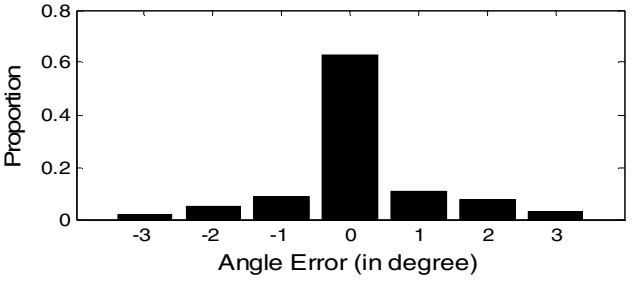

Fig. 4. Histogram of estimation errors

3.3 Experiments on Dataset_Rotation

To show the efficiency of the proposed method, we did a comparison experiment on Dataset_Rotation. The experiment computes the EER with and without the proposed method, respectively, to test if the EER is reduced when the proposed method is adopted.

Because our focus is not the recognition algorithm, we use arc-cosine of the correlation coefficient as the distance measure. We select this measure because the method is simple and it is not rotation invariant, as can be illustrated in Fig.5. It can be seen

that the distance increases when the rotation angle becomes bigger. When the rotation angle is bigger than a fixed threshold, the image may be regarded as a picture from a different subject.

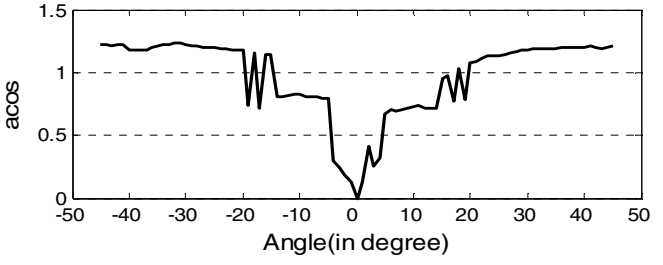

Fig. 5. Draw of arc-cosine distance vs rotation angle

Since recognition rate depends on the rotation angle, the following experiments are done to show the performance of the proposed method. First, all the images are registered, then the EER is obtained on the collected database. We show some examples in Dataset_Rotation in Fig.6 and the corrected images in Fig.7.

On this dataset, the EER is reduced from 20.2% to 4.96%. The EER decreases sharply because rotation exceeds the threshold of correlation method and rotation correction can compensate the rotation efficiently.

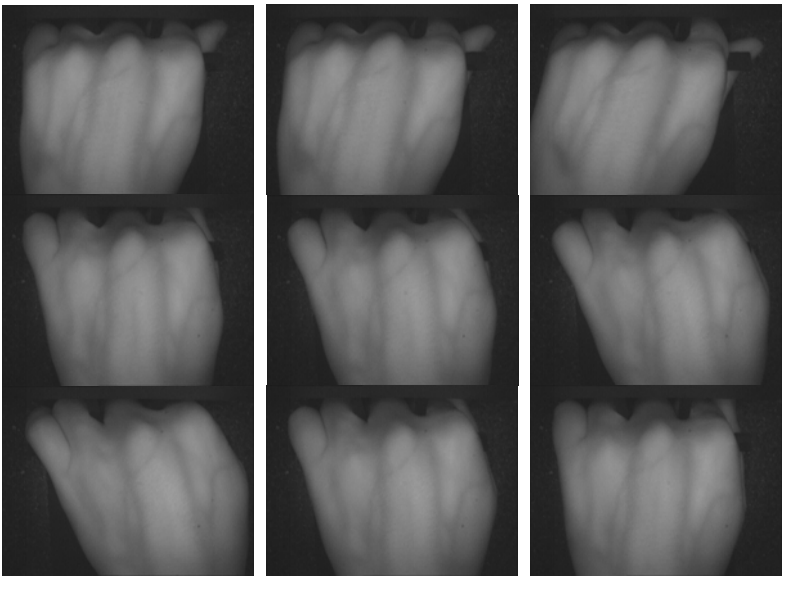

Fig. 6. Examples of the same subject in Dataset_Rotation

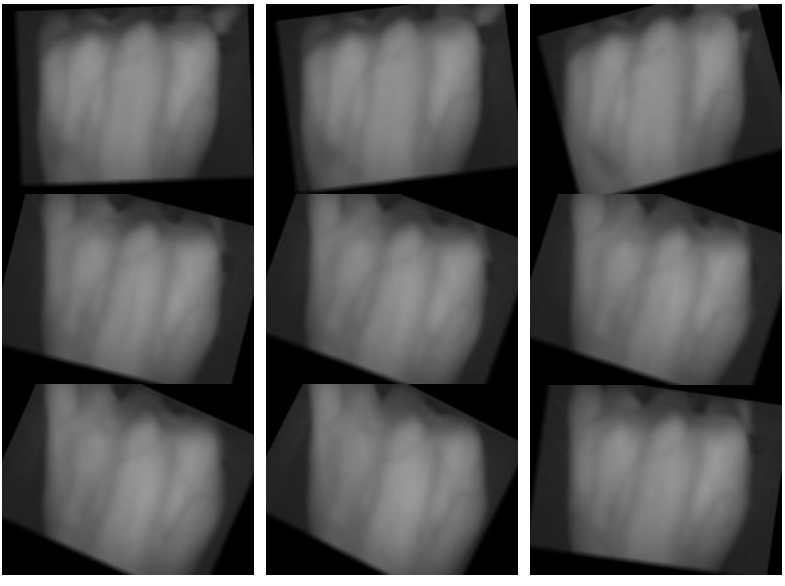

Fig. 7. Images after rotation correction

3.4 Experiments on Database_Regular

When the proposed method is applied to Database_Regular, the EER is reduced from 3.57% to 3.51%. This indicates that small rotation still exists though there is a handle in our device. And the EER can be reduced slightly for the regular images by adopting our method.

3.5 Speed of the Proposed Method

The experimental results also show that the proposed method can be completed in about 50ms on a desktop of 2G DRAM and 1.6G CPU. The reason is analyzed at the end of section 2. The method in reference [6] which is realized by us takes more than 400 ms to register a pair of DHV images of the same resolution.

4 Conclusions

The paper proposed a DHV image registration method using boundary optimization. The method can correct the rotation induced by different capture poses. All the samples are normalized according to a statistical criterion. The distribution of the hand boundary points is used to estimate the rotation angle by maximizing the variance of the projection of the boundary maps. Extensive experiments are reported to evaluate the performance of the proposed method.

The originality can be described in the following three aspects.

(1) The rules are simple. Only two maximization procedures are used to find the best rotation angle.

(2) All the samples are normalized according to the same statistical criterion. By doing this, we do not need to compare a sample with every template in the registration database. This increases the matching efficiency especially when the registration database is quite big. This means that the identification can be done in short time, therefore, the system based on DHV images can work not only in verification mode, but also in identification mode. Moreover, by doing this, we do not need to store the original images of every template to compute the rotation angle between a sample and the template, so the proposed method saves a lot of disk spaces.

(3) The method is quite robust. By adopting a statistical model, the method works well even when the SNR is small. This is helpful for the images captured with low-cost ordinary cameras.

In the future, we will make a comparison with the previous rotation correction [6] and rotation-invariant features, such as LBP based features. We will also focus on correcting the defocusing and affine distortion.

Acknowledgements

The authors want to present their thanks to Hai Wang for his fundamental work in the design and making of capture device. The authors also want to thank the volunteers from whom we collected our databases. This work is supported by the NCUT Scientific Research Foundation.

References

1. Jain, A.K., et al.: Biometrics: Personal Identification in a Networked Society. Kluwer, Norwell (1999)
2. Zhang, D.: Automated Biometrics: Technology and Systems. Kluwer, Norwell (2000)
3. Ahmed, M.B., et al.: Hand Vein Biometric Verification Prototype: A Testing Performance and Patterns Similarity. In: Proceedings of the 2006 International Conference on Image Processing, Computer Vision, and Pattern Recognition, Las Vegas, USA, June 26-29 (2006)
4. Maleika, H.K., et al.: A New Method to Extract Dorsal Hand Vein Pattern using Quadratic Inference Function. (IJCSIS) International Journal of Computer Science and Information Security 6(3) (2009)
5. Lin, X.R., et al.: Measurement and Matching of Human Vein Pattern Characteristics. Journal of Tsinghua University, Sci. and Tech. (2003)
6. Koichi, I., et al.: A Palmprint Recognition Algorithm using Phase-Only Correlation. IEICE Trans. Fundamentals E91-A(4) (April 2008)
7. Khan, M.M.: Low Dimensional Representation of Dorsal Hand Vein Features Using Principle Component Analysis (PCA). World Academy of Science, Engineering and Technology 49 (2009)
8. Ajay, K., Zhang, D.: Hand: Geometry Recognition Using Entropy-based Discretization. IEEE Trans. Information Forensics & Security 2, 181–187 (2007)

A Novel Level Set Model Based on Local Information

Hai Min[1,2], Xiao-Feng Wang[1,3,*], and Ying-Ke Lei[1,2]

[1] Hefei Institute of Intelligent Machines, CAS, P.O. Box 1130, Hefei, 230031, China
[2] Department of Automation, University of Science and Technology of China, Hefei 230027, China
[3] Key Lab of Network and Intelligent Information Processing, Department of Computer Science and Technology, Hefei University, Hefei, 230022, China
minhai361@yahoo.com.cn, xfwang@iim.ac.cn

Abstract. Local image information is crucial for accurate segmentation of image with intensity inhomogeneity. However, the local information is not embedded in Chan-Vese model. In this paper, we propose a novel level set model which takes the local boundary information into account. The proposed model can overcome the difficulty that CV model suffered, i.e., the unsuccessful segmentation of object with intensity inhomogeneity. Finally, we validate the efficiency of our model on some synthetic and real images.

Keywords: Level set, Image segmentation, Local information.

1 Introduction

Active contour model have become very important in the image segmentation filed [1], in which active contour based on level set is quiet popular. One of the most famous models is the Chan-Vese (CV) model (the detailed description can be found in [2]). CV model can detect objectives whose boundaries are not necessarily defined by gradient. However, the model that attempt to model regions using global statistic are usually not ideal for segmenting image with intensity inhomogeneity.

In order to accurately segment these heterogeneous objectives, several methods in the literatures which combined global information with local information were proposed. The idea of incorporating localized statistics into a framework begins with the work of Brox and Cremers [3] who show that segmenting with local means is a first order approximation of the piecewise smooth simplification [4] of the Mumford-Shan functional [5]. Li [6] proposed a method which can coordinate the local and global minimization. Sum [7] presented a new method that integrates CV model with local model. Besides, some methods utilized window function to obtain local information. Darolti [8] proposed novel local region descriptors, which can segment objects that have largely overlapping global probability densities. In [9] and [10], intensity information extracted from image region can be incorporated into an edge-based energy function to make active contour more robust. Further results for energies based on a linear combination of edge and region terms can be found in [11] and [12]. Paragios

* Corresponding author.

D.-S. Huang et al. (Eds.): ICIC 2010, LNCS 6215, pp. 507–514, 2010.

and Deriche [13] presented a method in which edge-based energies and region-based energies were explicitly summed to create a joint energy.

In this paper, we propose a level set model which incorporates the local information to segment the images with intensity inhomogeneity. The efficacy of our method is validated by experiments on some synthetic and real images.

In the remainder of the paper, we shall describe our model in section 2, and then show the experimental results in section 3. In section 4, we make concluding remarks and give directions for future research.

2 Model Description

The proposed level set model is composed of three parts: the global term, the local term and the regularize term. We define Ω as an entire image domain, and ω as an inside area of active contour C. u_0 denotes the original image.

2.1 Global Term

We adopt the fitting term from the CV model as the global term:

$$E_G(C) = \lambda_1 \int_{\omega} |u_0(x,y) - c_1|^2 dxdy + \lambda_2 \int_{\Omega \setminus \omega} |u_0(x,y) - c_2|^2 dxdy , \quad (1)$$

where λ_1 and λ_2 are respectively positive constant weighting parameters, and c_1 and c_2 denote the average intensity value of image area inside and outside contour C.

As discussed in the former paragraph, the global term is only an auxiliary term in our method. The local term plays a decisive role in detecting objective boundary accurately.

2.2 Local Term

Since the global model can't extract some image boundaries with intensity inhomogeneity, we proposed our local term. Let us first explain the model in a simple case. We assume that the change of image intensity is a maximum in the neighbor of objective boundary. First, the idea of neighboring difference is used to enhance the contrast between boundary and inner region. Then, the region-based method is used to construct the local term.

We define the local term as follows:

$$E_L(C) = \lambda_3 \int_{\omega} |u_N(x,y) - c_3|^2 dxdy + \lambda_4 \int_{\Omega \setminus \omega} |u_N(x,y) - c_4|^2 dxdy , \quad (2)$$

where λ_3 and λ_4 are still the weighting factors. The treated image is defined as u_N, c_3 and c_4 are the average intensity value of the area inside and outside of C in u_N. $u_N(x,y)$ is transformed from $u_0(x,y)$, (i,j) stands for the position of matrix.

$$u_N(i,j) = z_1(i,j) - z_2(i,j)\,. \tag{3}$$

z_1 and z_2 are respectively written as:

$$z_1(i,j) = \max(u_n(i,j))\,, \tag{4}$$

$$z_2(i,j) = \min(u_n(i,j))\,, \tag{5}$$

where u_n denotes a series of matrix of $a \cdot b$, and a and b respectively represent the row and column of u_0. We define a neighboring window of $(2m+1)\times(2m+1)$ in image $u_0(x,y)$. Thus, $u_n(i,j)$ can be written as:

$$u_n(i,j) = \begin{bmatrix} u_0(i-m,j-m) & \cdots & u_0(i-m,j) & \cdots & u_0(i-m,j+m) \\ \vdots & & \vdots & & \vdots \\ u_0(i-1,j-1) & & u_0(i-1,j) & & u_0(i-1,j+1) \\ u_0(i,j-m) \cdots u_0(i,j-1) & & u_0(i,j) & & u_0(i,j+1) \cdots u_0(i,j+m) \\ u_0(i+1,j-1) & & u_0(i+1,j) & & u_0(i+1,j+1) \\ \vdots & & \vdots & & \vdots \\ u_0(i+m,j-m) & \cdots & u_0(i+m,j) & \cdots & u_0(i+m,j+m) \end{bmatrix}. \tag{6}$$

Generally speaking, we assume that the image intensity is very similar in a small image region. The gray image has maximum intensity differences only in boundary. So we utilize this idea to design a local term for enhancing the local contrast. In (6), we define a $(2m+1)\times(2m+1)$ window in which the corresponding value is replaced by the difference between maximum and minimum value of window as defined in (3). $u_N(x,y)$ has the maximum value in object boundary, and has more minor value in other position. Obviously, our purpose is to enhance the contrast between boundary and inner region. Finally, the part of larger intensity is the boundary of image. After the process as before described, we derive the term as defined in formula (2).

2.3 Regularization Term

In this section, as described in [2], we choose the length of active contour as a regularization term, and then add to our energy function. It is used to keep smoothing of the active contour when the contour evolution directs for objective boundary. Let C as the active contour $C(p)$: $[0,1] \to \Omega$ parameterized by parameter $p \in [0,1]$. The regularization term can be written as:

$$E_R(C) = \mu \oint_C dp\,, \tag{7}$$

where μ is a positive constant weighting parameter. Besides, it is demand to meet with the Newman boundary condition [2].

2.4 Level Set Formulation

In the level set formulation, the curve C is replaced by the zero level set of a Lipschitz function ϕ. Our energy function is written as:

$$\begin{aligned} E(\phi) &= E_G(\phi) + E_L(\phi) + E_R(\phi) \\ &= \lambda_1 \int_\Omega |u_0(x,y) - c_1|^2 \cdot H(\phi) dxdy + \lambda_2 \int_\Omega |u_0(x,y) - c_2|^2 \cdot (1 - H(\phi)) dxdy \\ &+ \lambda_3 \int \Omega |u_n(x,y) - c_3|^2 \cdot H(\phi) dxdy + \lambda_4 \int_\Omega |u_n(x,y) - c_4|^2 \cdot (1 - H(\phi)) dxdy \\ &+ \mu \int_\Omega \delta_0(\phi(x,y)) \cdot |\nabla \phi(x,y)| dxdy \end{aligned} \tag{8}$$

where $H(\phi)$ and $\delta(\phi)$ denote the Heaviside function and Dirac Delta function [2], which divide the image into three parts: inside C, outside C and on C. c_1, c_2, c_3 and c_4 can be written as:

$$c_1(\phi) = \frac{\int_\Omega u_0(x,y) \cdot H(\phi(x,y)) dxdy}{\int_\Omega H(\phi(x,y)) dxdy}, \tag{9}$$

$$c_2(\phi) = \frac{\int_\Omega u_0(x,y) \cdot (1 - H(\phi(x,y))) dxdy}{\int_\Omega (1 - H(\phi(x,y))) dxdy}, \tag{10}$$

$$c_3(\phi) = \frac{\int_\Omega u_n(x,y) \cdot H(\phi(x,y)) dxdy}{\int_\Omega H(\phi(x,y)) dxdy}, \tag{11}$$

$$c_4(\phi) = \frac{\int_\Omega u_n(x,y) \cdot (1 - H(\phi(x,y))) dxdy}{\int_\Omega (1 - H(\phi(x,y))) dxdy}. \tag{12}$$

Keeping c_1, c_2 c_3 and c_4 fixed, and then minimizing formula (8) with respect to ϕ. We deduce the associated Eular—lagrange equation for ϕ by steepest descent method, parameterize the descent direction by an artificial time t, and then we derive the evolution equation (13) of ϕ.

$$\begin{aligned} \frac{\partial \phi}{\partial t} &= \delta_0(\phi)[-\lambda_1 (u_0(x,y) - c_1)^2 \\ &+ \lambda_2 (u_0(x,y) - c_2)^2 - \lambda_3 (u_N(x,y) - c_3)^2 + \lambda_4 (u_N(x,y) - c_4)^2 + \mu \cdot div(\frac{\nabla \phi}{|\nabla \phi|})] \end{aligned} \tag{13}$$

In traditional level set method, re-initialization step is demanded in the process of evolve. However, our numerical method ignored the re-initialization process.

3 Experiment Results

In this section, three experiments are used to demonstrate the capability of the proposed model. In all three experiments, the proposed model is compared with the CV model. Some parameters used in this paper are $m=1$, $\lambda_3 = \lambda_4 =1$, $\mu = 0.001\times 255\times 255$.

In the first experiment, a synthetic image with non-uniform illumination is segmented. What we emphasized is that our model can extract the very accurate objective boundary (as shown in Fig.1(c)). In general, our model with smaller scale parameter m can extract more accurate location of the object boundary. However, CV model can't produce an accurate result. As the Fig.1 showed, the original image and initial contour are shown in (a) and (b) respectively, (c) and (d) are the result produced by our model and CV model.

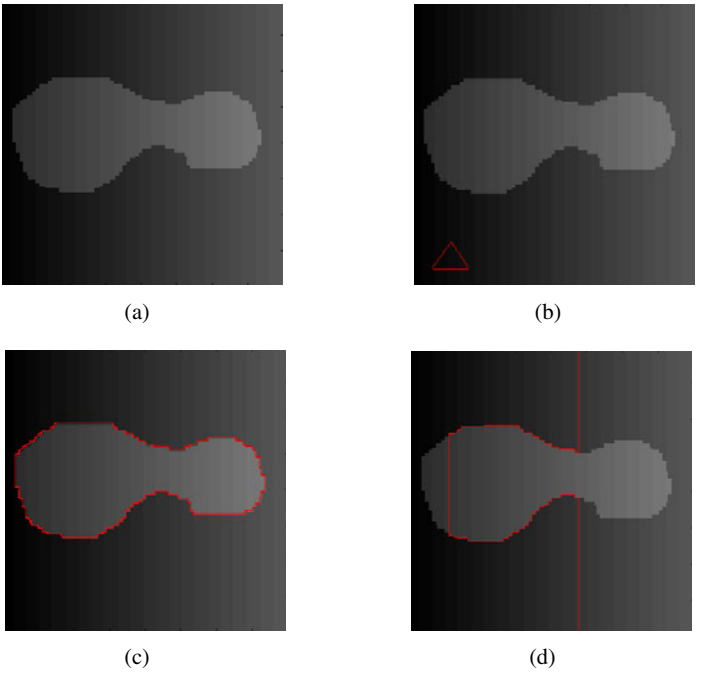

Fig. 1. Comparison of our model with CV model: (a) the original image. (b) Initial contour. (c) Result of our model after 15 iterations with parameters $\lambda_1 = \lambda_2 =0.03$. (d) Result of CV model after 150 iterations.

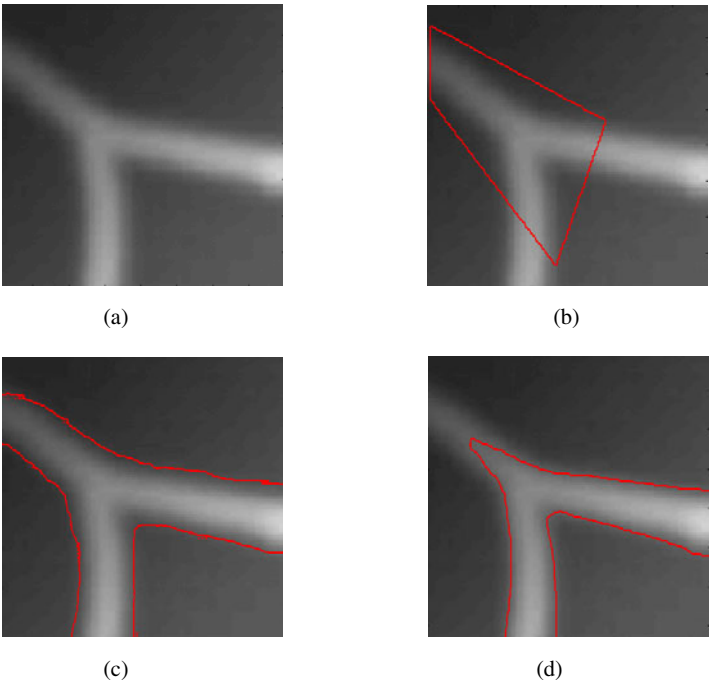

Fig. 2. The result of vessel extraction under non-uniform illumination: (a) the original image. (b) Initial contour. (c) Segmentation result with our model with parameters $\lambda_1 = \lambda_2 = 0.001$. (d) Segmentation result of CV model.

A synthetic image of blood vessel with inhomogeneity is shown in Fig.2 (a). The initial contour is placed in Fig.2 (b), the result of our model and CV model are respectively shown in Fig.2(c) and Fig.2 (d). It can be seen that the proposed model efficiently improves the segmentation performance of CV model while segmenting the blood vessel image with intensity inhomogeneity.

In fig.2, we show that our model works on an intensity non-uniform image, and we are very satisfied with the result. The original image and initial contour are shown in (a) and (b) respectively, and (c) show that our result is very accurate, however, (d) show that CV model can't extract this objective accurately.

In Fig.3, we show that our model works on a real image with intensity inhomogeneity, and we got a satisfying result. The original image and initial contour are shown in (a) and (b) respectively. Fig.3(c) shows that our result is accurate to some extent. However, it can be seen from Fig.3 (d) that CV model can't extract this objective accurately. In this experiment, the advantage of our model is fully reflected. The CV model only measures the global statistics information in the whole evolution process. On the contrary, our model combines the global information with local information, and provides a better solution than CV model.

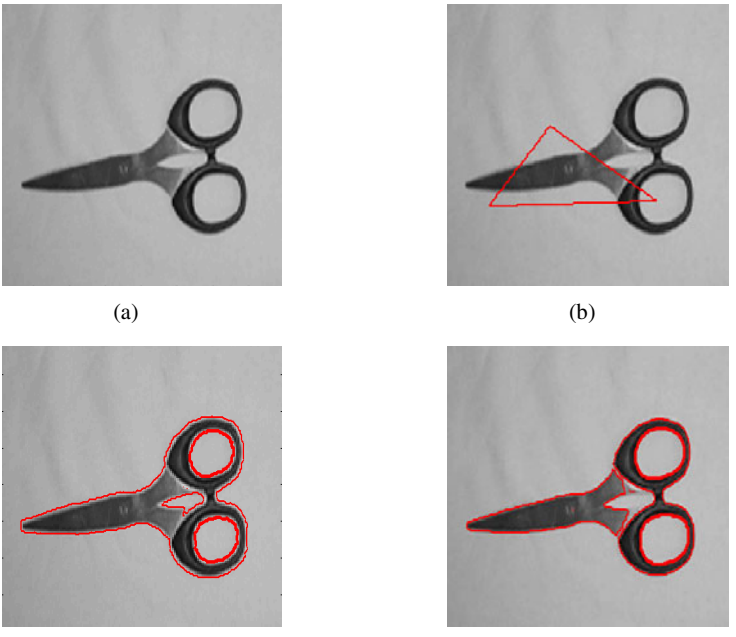

(a) (b)

(c) (d)

Fig. 3. Comparison between the segmentation results of our model and CV model. (a) Image with intensity inhomogeneity. (b) Initial contour. (c) Segmentation result of our model with parameters after 5 iterations with parameters $\lambda_1 = \lambda_2 = 0.3$. (d) Segmentation result of CV model with the same parameters.

It should be noted that the velocity of the curve evolution of our model is quiet fast. In Fig.1, the active contours arrive at the accurate objective boundary after only 15 iterations. Actually, the local term play an important role in our model, and the global term only strengthen the stability of the curve evolution.

4 Conclusion and Further Discussion

In this paper, we proposed a novel and efficient level set model which integrates the global and local information of image. We made full use of local information in image with intensity inhomogeneity. The experiments show that our method is effective. Besides, we can change the value of the parameters to regulate the final segmentation results.

Our future works will focus on utilizing the prior information to improve the image segmentation effect of our model.

Acknowledgement. This work was supported by the grants of the National Science Foundation of China, Nos. 60805021, 60905023, 60705007, 60873012 & 60975005. the grant of the Key Scientific Research Foundation of Education Department of Anhui Province, No. KJ2010A289.

References

1. Kass, M., Witkin, A., Terzopoulos, D.: Snakes: Active contour models. Int.J. Compu. Vis. 1, 321–331 (1988)
2. Chan, T., Vese, L.: Active Contours without Edges. IEEE Trans. Image Process. 10, 266–277 (2001)
3. Brox, T., Cremers, D.: On the Statistical Interpretation of the Piecewise Smooth Mumford-Shah Functional. In: Sgallari, F., Murli, A., Paragios, N. (eds.) SSVM 2007. LNCS, vol. 4485, pp. 203–213. Springer, Heidelberg (2007)
4. Mumford, D., Shah, J.: Optimal Approximations by Piecewise Smooth Functions and Associated Variational Problems. Comm. Pure Appl. Math. 42, 577–685 (1989)
5. Mumford, D.: A Bayesian Rationale for Energy Functionals. In: Romeny, B. (ed.) Geometry Driven Diffusion in Computer Vision, pp. 141–153. Kluwer, Dordrecht (1994)
6. Li, C., Kao, C.Y., Gore, J.C., Ding, Z.: Implicit Active Contours Driven by Local Binary Fitting Energy. In: IEEE Conference on CVPR, pp. 1–7 (2007)
7. Sum, K., Cheung, P.: Vessel Extraction under Non-Uniform Illumination: A Level Set Approach. IEEE Trans. Biomed. Eng. 55, 358–360 (2008)
8. Darolti, C., Mertins, A., Bodensteriner, C., Hofmann, U.: Local Region Descriptors for Active Contours Evolution. IEEE Trans. Image processing 17, 2275–2288 (2008)
9. Paragios, N., Deriche, R.: Unifying Boundary and Region-Based Information for Geodesic Active Tracking. In: IEEE Conf. Computer vision and Pattern Recognition, vol. 2, pp. 300–305 (1999)
10. Cohen, L., Bardinet, E., Ayache, N.: Surface Reconstruction using Active Contour Models. In: SPIE Conf. Geometric Methods in Computer Vision, pp. 1–13 (1993)
11. Ecabert, T.O.: Variational Image Segmentation by Unifying Region and Boundary Information. In: 16th Int. Conf. Pattern Recognition, vol. 2, pp. 885–888 (2000)
12. Bession, S.J., Barlaud, M., Aubert, G.: Detection and Tracking of Moving Objects Using a New Level Set Based Method. In: Int. Conf. Pattern Recognition, vol. 3, pp. 1100–1105 (2000)
13. Paragios, N., Deriche, R.: Geodesic Active Regions: A New Framework to Deal with Frame Partition Problems in Computer Vision. Int. J. comput. Vis. 46, 223–247 (2002)

A Multi-Descriptor, Multi-Nearest Neighbor Approach for Image Classification*

Dongjian He[1], Shangsong Liang[2,**], and Yong Fang[2]

[1] College of Mechanical and Electronic Engineering,
Northwest A&F University. Yangling, ShaanXi 712100, China
[2] College of Information Engineering,
Northwest A&F University. Yangling, ShaanXi 712100, China
{hdj168,lss,fangyong}@nwsuaf.edu.cn

Abstract. Three practices commonly used in image classification methods have led to the inferior performance of Nearest-Neighbor (NN) based image classifiers: (i)Way of constructing "bag-of-visual-words". (ii)Using only one kind of descriptor. (iii)Without considering which category the NN comes from. We propose a novel NN-based classifier –MDMNN (Multi-Descriptor Multi-Nearest Neighbor), which classifies an unlabeled image by employing its nearest neighbors coming from all of the categories and different kinds of feature descriptors to images. Empirically, we conduct experiments on two real-world image databases, and show that although MDMNN requires no learning phase, its performance ranks some outstanding learning-based image classifiers.

Keywords: Image Classification, Nearest Neighbor, Bag-of-Visual-Words.

1 Introduction

Despite of some merits, it has been proved that non-parametric NN-based image classifiers provide inferior performance compared to learning-based methods [2].We argue that three practices lead to significant degradation in the performance of non-parametric image classifiers: (i)"Bag-of-visual-words" has been used in image classification [2] [15] [13]. However, the choice of dimension, selection and the weight of visual words has not been deal with successfully [13]. (ii)Some approaches represent image by only one kind of feature. However, some classes in the database will be more distinctive to other classes using other kind of feature descriptor [7] [11]. (iii)It is difficult to set optimal number of nearest neighbors [3] and the ignorance of other images which are not the K nearest neighbors will be likely to degrade the performance of image classification.

In this paper we propose a novel and generalized non-parametric NN-based classifier, which can tackle the problems mentioned above to some extent. Nearest Neighbors mentioned in this paper are a set of Nearest Neighbors generating

* This work was funded in part by the National Natural Science Foundation of China 60975007.

** Corresponding author.

D.-S. Huang et al. (Eds.): ICIC 2010, LNCS 6215, pp. 515–523, 2010.

from all of the classes the labeled images in rather than the K nearest neighbors. We call them "Multi-Nearest-Neighbor"s. For brevity, we refer to this classifier as "MDMNN", which stands for "Multi-Descriptor, Multi-Nearest-Neighbor".

Figure 1 shows the framework of MDMNN. Firstly, we detect salient points for each image. Secondly, we construct each image's "bag-of-visual-words". After finding its Nearest Neighbors under the same type of descriptor in all of the classes, we compute the Earth Mover's Distance (EMD) between the unlabeled image and all of the Nearest Neighbors. Finally, unlabeled image is classified by using the rule in Sec.5.

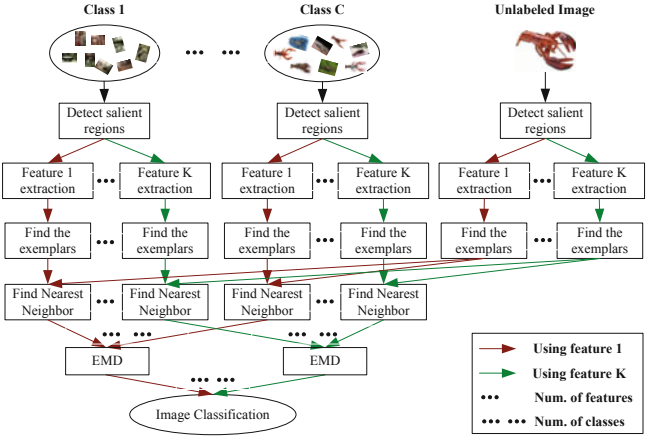

Fig. 1. A Framework of Multi-Descriptor Multi-Nearest-Neighbor Image Classification. Input is subclasses of labeled images coming from all categories in a database and unlabeled images. Output is the class labels for the unlabeled images.

This paper is organized as follows. Sec.2 discusses saliency image patches in images. Sec.3 discusses our method of constructing "bags-of-visual-words" for images. Sec.4 shows image-to-image distance. Sec.5 provides our formulation for classifying unlabeled images. Sec.6 provides empirical evaluation and comparison to other methods. Finally, Sec.7 concludes this paper and gives our further work.

2 Saliency Image Patches

We use the Harris-Laplace detector [11] to automatically detect saliency image patches (keypoints) from an image. Denoted by small crosses in Figure 2(b), keypoints are usually around the corners and edges of image objects, such as the outline of the Mountain, beach and the sea. According to [7] the size of the normalized region is arbitrarily set to 41 pixels in this paper. Subsequently, salient patches are depicted using Color Moments, Color Moment Invariants,

RGB histogram, rg histogram, Hue-SIFT and SIFT respectively in this paper, all of which are evaluated in [11].

Let us denote the *j-th* patch depicted with the *k-th* type of feature descriptor d_k in the *i-th* image I_i^c belong to the *c-th* class in database as $p_j(I_i^c, d_k)$, where $j = 1, 2, \ldots, J_i^c$, $k = 1, 2, \ldots, K$, $i = 1, 2, , |c|$. J_i^c, K and $|c|$ are the total number of patches in I_i^c, total number of feature descriptors and total number of images in the *c-th* class, respectively. We also denote the corresponding feature $f(x_j|p_j(I_i^c, d_k))$, which is a n-dimensional real-valued feature vector and n decided by the *k-th* type of feature descriptors d_k.

3 Constructing Bag-of-Visual-Words

Although some methods such as those used in [5] have been proposed for constructing "bag-of-visual-words", they still suffer from the choice of dimension, selection and the weight of visual words in the representation [13]. Since the exemplars of the patches can usually present the whole image well [15], we use the exemplars to construct "bag-of-visual-words". There are several algorithms to obtain the exemplars, such as K-means++ [3]. However, these cluster algorithms require to choose some original points and are time-consuming, which are unrealistic [4]. We use affinity propagation algorithm [4] to generate the exemplars of the patches, which can tackle these problems mentioned above to some extend.

In brief, the affinity propagation algorithm propagates two kinds of information between each two data points: the "responsibility" r(m, n) sent from data point m to data point n, which reflects how well n serves as the exemplar of m considering other potential exemplars for m, which also reflects how appropriate m chooses n as its exemplar considering other potential points that may choose n as their exemplar. The information are updated in an iterative way as:

$$\begin{aligned} r(m,n) &:= s(x_m, x_n) - \max_{n' \neq n} \{a(m,n') + s(x_m, x_{n'})\}, \\ a(m,n) &:= \min\{0, r(n,n) + \sum_{m' \notin (m,n)} \max\{0, r(m',n)\}\} \end{aligned} \tag{1}$$

Where, the function $s(x_a, x_b)$ is the similarity measure between two points x_a and x_b . We let $s(x_a, x_b) = \|x_a - x_b\|_2$ in our paper. The self-availability is updated in a slightly different way as:

$$a(n,n) := \sum_{m' \neq n} \max\{0, r(m',n)\} \tag{2}$$

Upon convergence, the exemplar for each data point x_m is chosen as $e(x_m) = x_n$ where n maximizes the following criterion:

$$\arg\max_k \; a(m,n) + r(m,n) \tag{3}$$

According to criterions 1~3, we could generate the exemplar $f\left(x_n|p_n^e\left(I_i^c, d_k\right)\right)$ and its corresponding weight $w_n^e\left(I_i^c, d_k\right) = |e\left(x_m\right) = x_n|/J_i^c$, where $|e\left(x_m\right) =$

$x_n|$ is the number of patches which share the same exemplar x_n, via replacing m, n, m', n', x_m, x_n with the m-th, n-th, m'-th, n'-th patches and $f\left(x_m|p_m\left(I_i^c, d_k\right)\right)$, $f\left(x_n|p_n\left(I_i^c, d_k\right)\right)$, respectively. Therefore, we can use weight-exemplar feature pairs to depict an image $I_i^c = \bigcup_{l=1}^{E_i^c}\{w_l^e(I_i^c, d_k), f\left(x_l|p_l^e(I_i^c, d_k)\right)\}$ as "bag-of-visual-words" of an image, where E_i^c is the total number of exemplars in image I_i^c. Figure 2(c)∼(h) shows an example of finding exemplars under different types of feature descriptors, in which we link patches to the same exemplar shared by them with the same colors through drawing colorful lines.

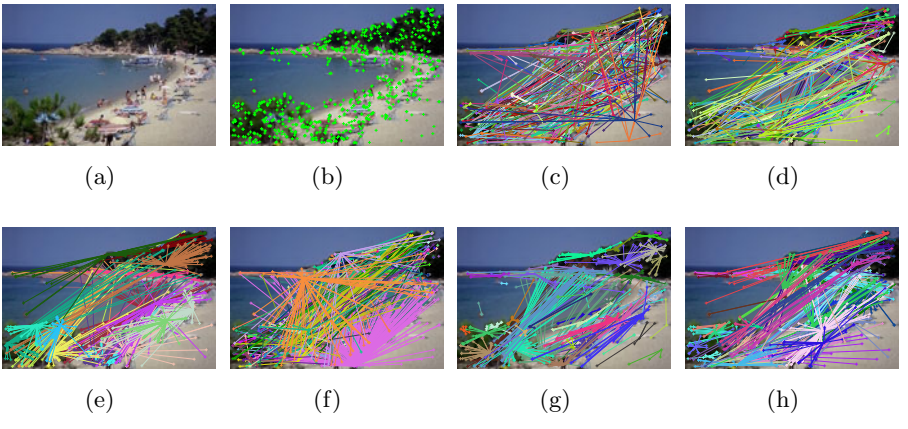

Fig. 2. An example of the results of salient regions detection and finding exemplars under different feature descriptors. (a) original image from the 'beach' class in 1000-image database, (b) result of detecting salient region using Harris-Laplace saliency region detector, (c)∼(h) result of finding exemplars under SIFT, hue-SIFT, color moments, color moment invariants, RGB histogram and rg histogram descriptor respectively.

4 Image-to-Image Distance

Since the Earth Mover's Distance(EMD) [9] has been proved effectiveness in image classification [1], we use this metric to measure the image-to-image distance. EMD is defined as the minimal cost that must be paid to transform one histogram into the other, where there is a "ground distance" between the basic features that are aggregated into the histogram.

Given two image $I_P^c = P$, $I_Q^c = Q$, and viewed them as two histograms: $P = \{(w_{p1}^e(I_P^c, d_k), f(x_{p1}|p_{p1}^e(I_P^c, d_k))), \ldots, (w_{pm}^e(I_P^c, d_k), f(x_{pm}|p_{pm}^e(I_P^c, d_k)))\}$, $Q = \{(w_{q1}^e(I_Q^c, d_k), f(x_{q1}|p_{q1}^e(I_Q^c, d_k))), \ldots, (w_{qm}^e(I_Q^c, d_k), f(x_{qm}|p_{qm}^e(I_Q^c, d_k)))\}$. In brief, let $w_{p1} = w_{p1}^e(I_P^c, d_k)$, $p_{p1} = f(x_{p1}|p_{p1}^e(I_P^c, d_k))$, $w_{pm} = w_{pm}^e(I_P^c, d_k)$, $p_{pm} = f(x_{pm}|p_{p1}^e(I_P^c, d_k))$, $w_{q1} = w_{q1}^e(I_P^c, d_k)$, $q_{q1} = f(x_{q1}|p_{q1}^e(I_q^c, d_k))$ $w_{qn} = w_{qn}^e(I_P^c, d_k)$, $q_{qn} = f(x_{qn}|p_{qn}^e(I_P^c, d_k))$, *i.e.*, $P = \{(p_{p1}, w_{p1}), \ldots, (p_{pm}, w_{pm})\}$ be the first signature with m exemplars, where p_{pi} is the cluster representative, *i.e.*, exemplar and w_{pi} is its corresponding weight; $Q = \{(q_{q1}, w_{q1}), \ldots, (q_{qn}, w_{qn})\}$

the second signature with n exemplars, where q_{qj} is the cluster representative, *i.e.*, exemplar and w_{qj} is its corresponding weight; and let $D = [d_{ij}]$ be Euclidean distance matrix, where d_{ij} is Euclidean distance between p_{pi} and q_{qj}.

Find a flow $F = [f_{ij}]$, with f_{ij} the flow between p_{pi} and q_{qj}, that minimizes the overall cost:

$$WORK(P, Q, F) = \sum_{i=1}^{m} \sum_{j=1}^{n} d_{ij} f_{ij} \tag{4}$$

subjected to the following constraints: $f_{ij} \leq w_{pi} \quad 1 \leq i \leq m, 1 \leq j \leq n$; $\sum_{j=1}^{n} f_{ij} \leq w_{pi} \quad 1 \leq i \leq m$; $\sum_{j=1}^{n} f_{ij} \leq w_{qj} \quad 1 \leq j \leq n$; and $\sum_{i=1}^{m} \sum_{j=1}^{n} f_{ij} = \min(\sum_{i=1}^{m} w_{pi}, \sum_{j=1}^{n} w_{qj})$. Once $WORK(P, Q, F)$ is figured out, and we have found the optimal flow $\boldsymbol{F}$, the earth mover's distance between two image I_P^c and I_Q^c is defined as the resulting work normalized by the total flow:

$$EMD(I_P^c, I_Q^c) = EMD(P, Q) = \frac{\sum_{i=1}^{m} \sum_{j=1}^{n} d_{ij} f_{ij}}{\sum_{i=1}^{m} \sum_{j=1}^{n} f_{ij}} \tag{5}$$

5 Image Classification Formulation

In this section we derive MDMDD. Suppose that there has been a set of labeled images from all classes in a database. Given a new query (unlabeled/unknown) image I_q, we want to find its class: $\hat{c} = \arg\max_c p(c|I_q)$.

For the sake of deriving easily, let $I_i^c(d_k)$ be an image which is the *i-th* image in the *c-th* class and its patches be depicted by the *k-th* descriptor, $i = 1, 2, \ldots, |c|$, $c = 1, 2, \ldots, C$, $k = 1, 2, \ldots, K$ and $I_q(d_k)$ be a query image depicted by the *k-th* type of descriptor, where C is the total number of classes.

Traditionally, NN-based classifier is used to classify image I_q by the class of its nearest image in the database. Although this is the most popular approach among the NN-based image classifiers, it provides inferior performance. We propose a novel image classification algorithm, *i.e.*, MDMNN, which depends on the nearest neighbor images, the classes the nearest neighbor image belong to, and the types of descriptors to images.

Let $dist(I_q(d_k), c) = \min_i EMD(I_q(d_k), I_i^c(d_k))$ denotes the distance between query image $I_q(d_k)$ and *c-th* class when using the *k-th* type of descriptor. Before classifying query image, we normalize this distance to be:

$$N[dist(I_q(d_k), c)] = \frac{dist(I_q(d_k), c)}{\max_c dist(I_q(d_k), c) + \min_c dist(I_q(d_k), c)} \tag{6}$$

We can classify the unlabeled image by the following formulation:

$$\hat{c} = \arg\max_c p(c|I_q) = \arg\max_c \left\{ 1 - \prod_{k=1}^{K} N[dist(I_q(d_k), c)] \right\}$$

$$= \arg\max_c \left\{ 1 - \prod_{k=1}^{K} \frac{dist(I_q(d_k), c)}{\max_c dist(I_q(d_k), c) + \min_c dist(I_q(d_k), c)} \right\} \tag{7}$$

Compared to other NN-based image classification [2] [14], MDMNN combines different kinds of descriptors depicting salient patches with Nearest Neighbors coming from all classes rather than using the K nearest neighbors under only one style of feature descriptor; therefore, MDMNN can boost the object recognition.

6 Experiment and Results

We evaluate our MDMNN on 1000-image[1] and Caltech 101-object[2] databases.

6.1 Exp. 1: 1000-Image Database

The 1000-image challenging database, which was used in [1], consists of ten distinctive categories (Africa people and villages, Beach, Buildings, Buses, Dinosaurs, Elephants, Flowers, Food, Horses, Mountains and glaciers), and each category of which consists of 100 images.

We randomly choose 2, 5, 10, 20 and 30 images per category, use six feature descriptors to represent the patches in each image, and classify all the images in this database. We present our experimental result in two ways: drawing graphs for each class in 1000-image database under different kinds of patches' feature descriptors over the number of 2, 5, 10, 20 and 30 images per category. Meanwhile, for demonstrating the effectiveness of MDMNN on classifying images, we also present the experimental result in the form of mean recognition rate.

Figure 3 shows our experiment on 1000-image database. Figure 3(a) illustrates that when using RGB descriptor, it is the most effective feature descriptor to classify whether an unlabeled image is belong to class 'Africa people and village'; however, Figure 3(j) shows that it is the worst feature descriptor to identify whether unlabeled image is coming from class 'Mountain'. The recognition rate of using Hue-SIFT, SIFT , *et al.*, feature descriptor for image classification is also similar to that of RGB feature descriptor, which demonstrates that different kinds of feature descriptors perform different recognition rate over different classes. Figure 3 also tells that although the combination of different kinds of feature descriptors ('ALL') can not always perform better than any other feature descriptor, it almost outperforms most of the feature descriptors over all of the classes in 1000-image database. More importantly, As shown in Figure 4, for mean recognition over different number of labeled images per class, the combination of all features ('ALL') outperforms any other kinds of feature descriptors apparently, which proofs that MDMNN is an effective algorithm.

6.2 Exp. 2: Caltech-101 Database

The Caltech-101 database [8] consists of images from 101 object categories (approximately 30∼800 images per category). The significant variation in intraclass pose, color and lighting makes this database challenging.

[1] http://wang.ist.psu.edu/docs/related/
[2] http://www.vision.caltech.edu/Image_Datasets/Caltech101

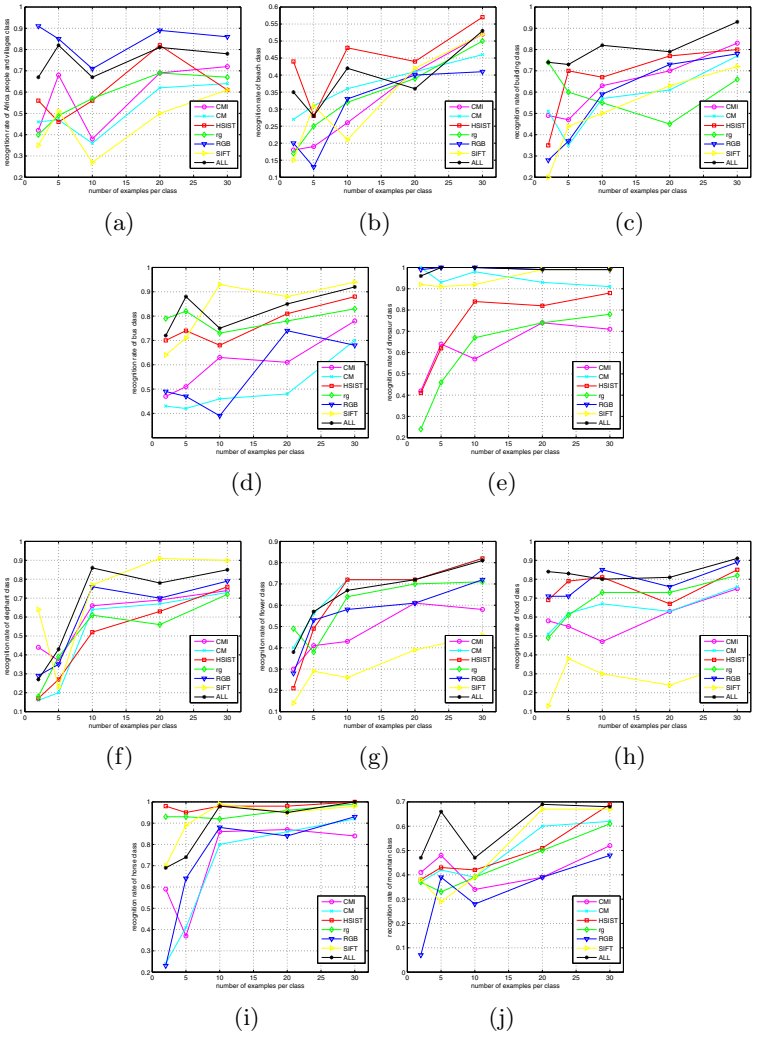

Fig. 3. Image classification result. CMI, CM, HSIFT, rg, RGB, SIFT and All are the patches descriptors respectively, *i.e.*, color moment invariants, color moments, Hue-SIFT rg histogram, RGB histogram, SIFT and combination of all descriptors using in this paper. (a)∼(j) recognition rates (%) of classes in 1000-image database using different kinds of descriptors over number of image per category (2, 5, 10, 20, 30).

To stay as close to the paradigm of the previous work on this dataset, we followed the methodology of [5], and performed experiments using 5, 10, 20, and 30 images per category, using the remaining images in the dataset for testing. We follow the standard approach for evaluation.

Figure 5 compares our results with those of state-of-the-art algorithms published in the last few years. At five and ten images per category, we perform better than [12], [5], [6], [14], [6] and [10] but worse than [2]. At twenty images per category, we achieve a recognition rate of 63.19%, little below that of [6] and almost the same as [14], and at thirty, we achieve 65.80%, smaller than most of the existed algorithms. It makes sense that although our performance would not perform well at large number of images per category, it achieves quite high recognition rate at five and ten images per category, which demonstrates that under certain circumstance, *e.g.*, the case of having difficulty to collect large number of images per category, MDMNN are of great value. More importantly, Figure 5 also shows that although MDMNN is a non-parametric NN-based image classifier, its performance ranks some learning-based image classifiers.

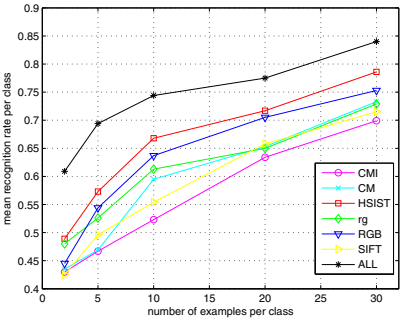

Fig. 4. Mean recognition rate (%) over number of images 2, 5, 10, 20, 30 per category in 1000-image database

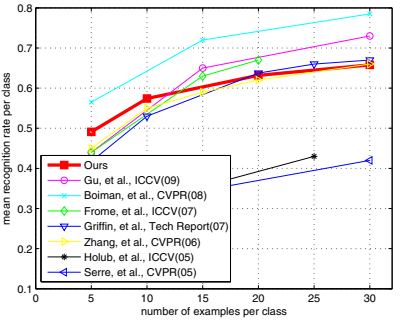

Fig. 5. Mean recognition rate (%) over number of images per category in Caltech 101

7 Conclusion

In this paper, we have proposed a novel non-parametric NN-based image classification algorithm by employing multi-descriptor and multi-nearest neighbor. We have further shown that MDMNN can boost the recognition rate effectively, though it is not a learning based image classifier, and it performs quite well, especially over small number of images per category.

There are some open problems for further studies. For instance, it is still an unsolved problem that what kinds of feature descriptors should be combined in NN-based image classification and how to combine them effectively.

References

1. Chen, Y., Wang, J.Z., Krovetz, R.: Clue: Cluster-based retrieval of images by unsupervised learning. IEEE Transactions on Pattern Analysis and Machine Intelligence (2005)
2. Boiman, O., Shechtman, E., Irani, M.: In defense of nearest-neighbor based image classification. In: IEEE International Conference on Computer Vision and Pattern Recognition (2008)
3. David, A., Sergei, V.: k-means++: the advantages of careful seeding. In: Proceedings of the eighteenth annual ACM-SIAM symposium on Discrete algorithms, pp. 1027–1035 (2007)
4. Frey, B.J., Dueck, D.: Clustering by passing messages between data points. Science 315, 972–976 (2007)
5. Frome, A., Singer, Y., Sha, F., Malik, J.: Learning globally consistent local distance functions for shape-based image retrieval and classification. In: IEEE International Conference on Computer Vision (2007)
6. Griffin, G., Holub, A., Perona, P.: Caltech-256 object category dataset. Technical report California Institute of Technology (2007)
7. Mikolajczyk, K., Schmid, C.: A performance evaluation of local descriptors. IEEE Transactions on Pattern Analysis and Machine Intelligence 27, 31–47 (2005)
8. Fei-Fei, F.L., Perona, P.: Learning generative visual models from few training exmples: an incremental bayesian approach testing on 101 object categories. In: IEEE Workshop on Generative-Model Based Vision (2004)
9. Rubner, Y., Tomasi, C., Guibas, L.J.: A metric for distributions with applications to image databases. In: IEEE International Conference on Computer Vision (1998)
10. Serre, T., Wolf, L., Poggio, T.: object recognition with features inspired by visual cortex. In: IEEE International Conference on Computer Vision and Pattern Recognition (2005)
11. van de Sande, K.E.A., Gevers, T., Snoek, C.G.M.: Evaluation of color descriptors for object and scene recognition. IEEE Transactions on Pattern Analysis and Machine Intelligence (2010)
12. Vedaldi, A., Gulshan, V., Varma, M., Zisserman, A.: Multiple kernels for object detection. In: IEEE International Conference on Computer Vision and Pattern Recognition (2009)
13. Yang, J., Jiang, Y.G., Hauptmann, A.G., Ngo, C.: Evaluating bag-of-visual-words representations in scene classification. In: 9th ACM SIGMM International Conference on Multimedia Information Retrieval (2007)
14. Zhang, H., Berg, A.C., Maire, M., Malik, J.: Svm-knn: Discriminative nearest neighbor classification for visual category recognition. In: IEEE International Conference on Computer Vision and Pattern Recognition (2006)
15. Zhang, J., Marszalek, M.: Local features and kernels for classification of texture and object categories: A comprehensive study. International Journal of Computer Vision (2006)

Orthogonal Locally Discriminant Projection for Palmprint Recognition

Shanwen Zhang and Wei Jia

Institute of Intelligent Machines, Chinese Academy of Sciences, Hefei 230031, P.R. China
wjdw716@163.com, jiawei78@mail.ustc.edu.cn

Abstract. Supervised dimensional reduction methods play an important role in factual applications, which are likely to be more suitable for palmprint recognition. In this paper, a supervised dimensional reduction algorithm called orthogonal locally discriminant projection (OLDP) is proposed, which can effectively extract the low-dimensional discriminative data representation with the generalization ability. In OLDP, an effective weight measurement between two data points is designed combining the sample class information and local information. The experiments on palmprint recognition demonstrate that OLDP is effective and feasible.

Keywords: Manifold learning, Palmprint recognition, Orthogonal locally discriminant projection.

1 Introduction

In information and networked society, automatic personal identification is an impending and crucial problem that needs to be solved properly. As an efficient and safe solution, biometrics technologies have recently been receiving wide attention from researchers. Among them, palmprint based identification has several special advantages such as stable line features, rich texture features, low-resolution imaging, low-cost capturing devices, easy self positioning, and user-friendly interface etc. For these reasons, nowadays the research related to this issue is becoming more active, and there have been many approaches proposed for palmprint recognition including verification and identification [1-7].

In increasingly many cases of interest in palmprint recognition, one is confronted with the situation where the dimensionality of palmprint data is very large. However, there might be reason to suspect that the 'intrinsic dimensionality' of the data is much lower. This leads one to consider methods of dimensionality reduction that allow one to represent the data in a lower dimensional space.

Over the last decade, a great number of dimensionality reduction techniques exist in the literature, among them, a large number of manifold learning techniques for dimensionality reduction have been proposed, such as Locality preserving projections (LPP) [8] and Unsupervised Discriminant Projection (UDP) [9]. Compared to the traditional linear techniques, these manifold learning based techniques have ability to

D.-S. Huang et al. (Eds.): ICIC 2010, LNCS 6215, pp. 524–530, 2010.

deal with complex nonlinear data, which can be available for palmprint recognition. LPP is linear and more crucially defined everywhere in ambient space rather than just on the training data points. Due to introducing the linearization and locality preserving character, the LPP algorithm shows its merits on lowering the computational cost and enhancing the relative robustness to noise and outliers. So it is frequently applied to many areas. Hu et al. [10] employed two dimensionality LPP (2D-LPP) for palmprint recognition. UDP was one of the variations of discriminant LPP, achieved satisfying palmprint recognition results [9]. Yan et al.[11] proposed the discriminant projection embedding (DPE) for face and palmprint recognition. DPE utilizes within-class local manifold variations to characterize the distribution of transformation difference and between-class nearest neighbor variations to characterize the distribution of intrinsic difference. In this paper, we propose an orthogonal locally discriminant projection (OLDP) for palmprint recognition.

The rest paper is organized as follows. Section 2 simply introduces the LPP algorithm. Section 3 describes the OLDP method. Section 4 gives the experimental results. Finally, discussions and conclusions are presented in Section 5.

2 Locality Preserving Projections (LPP)

Given n high-dimensional data points $X=[X_1, X_2, ..., X_n] \in R^{m \times n}$, it is desired to find n corresponding low-dimensional data points $Y=[Y_1, Y_2, ..., Y_n] \in R^{d \times n}$, $Y_i = A^T X_i$, $d \ll m$. The algorithmic procedure of LPP includes three steps, is formally introduced below:

Setp 1: Constructing adjacency graph

An adjacency graph $G=(V, E)$ is constructed using k-nearest neighbor criterion, where G denotes the graph, V is the node set and E is the edge set.

Setp 2: Choosing the weights

If nodes i and j are connected, the affinity matrix W could be defined with the element as follows

$$W_{ij} = \exp(-\frac{\left\| X_i - X_j \right\|^2}{\beta}) \tag{1}$$

Setp 3: Eigenmaps

Compute the eigenvectors and eigenvalues for the generalized eigenvector problem:

$$XLX^T A = \lambda XDX^T A \tag{2}$$

where D is diagonal matrix whose entries are column (or row, since W is symmetric) sums of W, $D_{ii} = \sum_j W_{ji}$. $L=D-W$ is the Laplacian matrix. The ith column of matrix X is x_i.

Matrix D provides a natural measure on the vertices of the graph. The bigger the value D_{ii} (corresponding to the ith node) is, the more 'important' is that node. Laplacian matrix is symmetric, positive semi-definite matrix which can be thought of as an operator on functions defined on vertices of G.

Let $A_0, A_1, ..., A_{k-1}$ be the solutions of Eq.(2), ordered according to their eigenvalues, $\lambda_0 < \lambda_1 < ... < \lambda_{k-1}$. Thus, the embedding is as follows:

$$\begin{aligned} X_i &\to Y_i = A^T X_i \\ A &= (A_0, A_1, ..., A_{k-1}) \end{aligned} \tag{3}$$

where Y_i is a d-dimensional vector, and A is a $d \times n$ matrix, i.e. a linear transformation projecting matrix.

In the LPP algorithm, it is likely that a nearest neighbor search in the low dimensional space will yield similar results to that in the high dimensional space. This makes for an indexing scheme that would allow quick retrieval. LPP is an optimal linear approximation to the eigenfunctions of the Laplace Beltrami operator on the manifold. It is linear and can deal with new data easily, so it is fast and suitable for practical application.

3 Orthogonal Locally Discriminant Projection (OLDP)

In this section, the orthogonal locally discriminant projection is proposed by combining the both the neighbor information and class information, and a locality discriminant criterion is adopted to find the projections that best preserve the within-class local structures while decrease the between-class overlap. OLDP is introduced as follows.

Recall that given a data set we construct a weighted graph G=(V, E) with edges connecting nearby points to each other. Consider the problem of mapping the weighted graph G to a line so that connected points stay as close together as possible. Suppose $X = [X_1, X_2, ..., X_n] \in R^{D \times n}$ is n high-dimensional data points, c_i is the class label of X_i, $N(X_i)$ is the k nearest neighbors of X_i, A is a transformation matrix, $Y_i = A^T X_i$ is the mapping of X_j. Define the intra-class and inter-class weights respectively as follows,

$$W_{ij}^{I} = \begin{cases} \dfrac{\left\| X_i - X_j \right\|^2}{\left\| X_i \right\| \cdot \left\| X_j \right\|}, \text{ if } X_i \in N(X_j) \text{ or } X_j \in N(X_i) \\ \qquad\qquad \text{and } c_i = c_j \\ 0, \qquad \text{otherwise} \end{cases} \tag{4}$$

$$W_{ij}^{B} = \begin{cases} \dfrac{\left\| X_i - X_j \right\|^2}{\left\| X_i \right\| \cdot \left\| X_j \right\|}, \text{ if } X_i \in N(X_j) \text{ or } X_j \in N(X_i) \\ \qquad\qquad \text{and } c_i \neq c_j \\ 0, \qquad \text{otherwise} \end{cases} \tag{5}$$

For the purpose of classification, we try to find a projection A which will draw the within-class samples mapped closer together while simultaneously making the

between-class samples mapped even more distant from each other. From this point of view, a reasonable criterion for choosing a "good" projection is to optimize two following objective functions

$$\min \sum_i \sum_j W_{ij}^I \left\| Y_i - Y_j \right\|^2 \tag{6}$$

$$\max \sum_i \sum_j W_{ij}^B \left\| Y_i - Y_j \right\|^2 \tag{7}$$

with some appropriate constraints.

Following some simple algebraic steps, Eq.(6) is reduced as

$$\begin{aligned} &\frac{1}{2}\sum_{i=1}^{n}\sum_{j=1}^{n} W_{ij}^I \left(Y_i - Y_j\right)^2 \\ &= \frac{1}{2}\sum_{i=1}^{n}\sum_{j=1}^{n} W_{ij}^I \left(A^T X_i - A^T X_j\right)^2 \\ &= \sum_{i=1}^{n}\sum_{i=1}^{n} A X_i^T W_{ii}^I X_i A^T - \sum_{i=1}^{n}\sum_{j=1}^{n} A X_i^T W_{ij}^I X_j A^T \\ &= A^T X D^I X^T A - A^T X W^I X^T A \\ &= A^T X (D^I - W^I) X^T A \\ &= A^T X L^I X^T A \end{aligned} \tag{8}$$

where $L^I = D^I - W^I$, D^I is a diagonal matrix with $D_{ii}^I = \sum_j W_{ji}^I$, W^I is the intra-class weight matrix with W_{ij}^I; D_{ii}^I measures the local density around X_i.

Similarly, Eq.(7) can be reduced to

$$\begin{aligned} &\frac{1}{2}\sum_{i=1}^{n}\sum_{j=1}^{n} W_{ij}^B \left(Y_i - Y_j\right)^2 \\ &= A^T X (D^B - W^B) X^T A \\ &= A^T X L^B X^T A \end{aligned} \tag{9}$$

where $L^B = D^B - W^B$, D^B is a diagonal matrix with $D_{ii}^B = \sum_j W_{ji}^B$, W^B is the inter-class weight matrix with W_{ij}^B.

We combine the two objective functions (6) and (7) by a suitable parameter, and impose the orthogonal condition, then the locality discriminant criterion is given by:

$$\max_{A^T A = I} \frac{A^T X L^B X^T A}{A^T X L^I X^T A} \tag{10}$$

Let $\{A_1, A_2, ..., A_d\}$ be the orthogonal basis vectors, define $A^{(i-1)} = [A_1, A_2, ..., A_{i-1}]$. The orthogonal basis vectors $\{A_1, A_2, ..., A_d\}$ can be computed by step-by-step procedure [12].

After calculating the projections $\{A_1, A_2, ..., A_{i-1}\}$, the i-th projection A_i is calculated by solving the following optimization problem

$$A_i = \arg\max_{A_{i-1}^T A_{i-1}=0} \frac{A_{i-1}^T XL^B X^T A_{i-1}}{A_{i-1}^T XL^I X^T A_{i-1}} \tag{11}$$

Once A has been learnt, the projection of any new test point X_{new} is projected by

$$Y_{\text{new}} = A^T X_{\text{new}} \tag{12}$$

where $A \in R^{n \times d}$, $X_{\text{new}} \in R^D$, $Y_{\text{new}} \in R^d$, $d \ll D$.

From above analysis, the algorithmic procedure of OLDP is expressed as follows:

(1) Constructing the adjacency graph.
(2) Choosing the weights.

The steps (1) and (2) are fulfilled as in LPP.

(3) Initialize A as an arbitrary column-orthogonal matrix.
(4) Compute the trace ratio value $\delta = \frac{tr\left(A^T XL^B X^T A\right)}{tr\left(A^T XL^I X^T A\right)}$.
(5) Form the trace difference problem as $A' = \max_{A^T A=I} tr(A^T (XL^B X^T - \delta XL^I X^T) A)$.
(6) Establish A' by the d eigenvectors of $XL^B X^T - \delta XL^I X^T$ corresponding to the d largest eigenvalues.
(7) Update A by A'.
(8) Iteratively perform steps (4)-(7) until convergence.
(9) Project the new data points to feature space by Eq.(12).

4 Experimental Results

The main objection of palmprint recognition and classification algorithm is to seek a projection characterized by within-class compactness and between-class separability. Owing to the analysis mentioned above, it is obvious that the proposed algorithm can be applied to palmprint recognition.

Usually, a square region is generally identified as the region of interest (ROI) before dimensional reduction and feature extraction. Thus the relevant features can be extracted and matched only in this square region. The benefit of this processing is that it can define a coordinate system to align different palmprint images. Otherwise, the matching result would be unreliable without this processing. In this paper, by using the similar preprocessing approach described in literature [13,14], the central part of each original palmprint image of size 128×128 in the palm is automatically orientated and cropped to be the ROI. Fig. 1 shows an original image and its extracted ROI. Moreover, according to the wavelet theory, we retain the low-frequency sub-band of the approximation coefficients as most of the energy content is concentrated in the low-frequency sub-band, and then we reduce the each image from 128×128 to 32×32. Six palmprint images of an individual are shown in Fig.2.

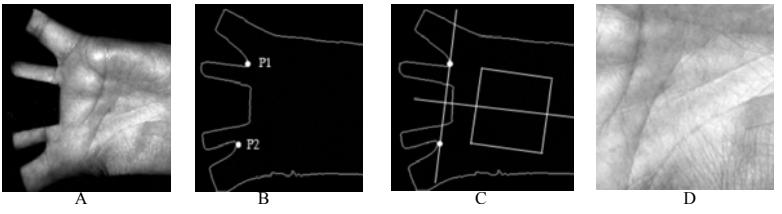

Fig. 1. The process of palmprint preprocessing. (A) Original palmprint; (B) contour line, where p1 and p2 are detecting points; (C) constructing new coordinate axis; (D) extracted ROI.

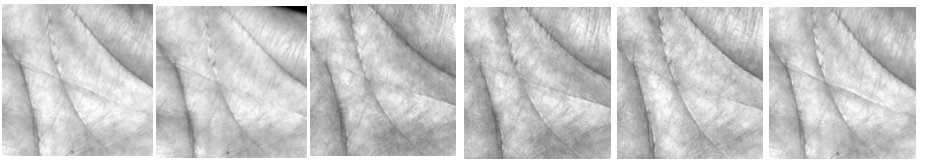

Fig. 2. Six cropped palmprints of one palm on the PolyU palmprint database

For each palm, we randomly select l palmprints from each class as training set, and the rest (6-l) are considered as test set. The recognition process has three steps. First, the palmprint subspace is calculated from the training set. To further reduce computational cost, following an idea proposed in [15], we performed a PCA preprocessing step on the images reducing them to their 100 largest principal components, effectively keeping over 99% of their information.

Then, the palmprint image is projected onto low-dimensionality subspace. Finally, the palmprint image is identified by the 1-nearest-neighbor classifier. For Baseline, we simply perform nearest-neighbor classification in the original 1024-dimensional space. For UDP, LDA, DPE and OLDP, the high-dimensional palmprint dataset are projected into the low-dimensional PCA subspace to avoid the small sample size problem by retaining a 90% portion of energy. For each given l, we perform 20 times experiments to choose randomly the training set. The final result is the average classification rate over 20 splits. Table 1 shows the performance of the Baseline, UDP, LDA, DPE and OLDP with different l.

OLDP is a suitable technique for palmprint recognition. From Table 1, we note that OLDP outperforms LDA, UDP and DPE.

Table 1. Recognition results of Baseline, LDA, UDP, DPE and OLDP

Method	l=2	l=3	l=4	l=5
Baseline	78.34	80.28	80.39	81.52
LDA	81.62	82.94	84.37	90.65
UDP	83.64	84.43	88.22	91.04
DPE	94.31	95.14	95.26	96.36
OLDP	94.08	95.86	96.17	97.49

5 Conclusions

This paper proposed a new discriminant projection algorithm for palmprint recognition, named OLDP. OLDP is a linear supervised dimensional reduction method, which tries to maximize the inter-class objective function, while minimize the intra-class objective function. Experimental results show that OLDP is effective for palmprint recognition. Our future work is to extend OLDP to nonlinear form by kernel trick and multi-dimensionality OLDP by tensor subspace analysis.

Acknowledgments. This work was supported by the grants of the National Science Foundation of China, Nos. 60975005, 60905023, 60873012, 60805021, and 60705007.

References

1. Zhang, D., Kong, A., You, J., Wong, M.: Online palmprint identification. IEEE Trans. Pattern. Anal. Mach. Intell. 25(9), 1041–1050 (2003)
2. Zhang, L., Zhang, D.: Characterization of palmprints by wavelet signatures via directional context modeling. IEEE Transaction on Systems, Man and Cybernetics, Part B 34(3), 1335–1347 (2004)
3. Li, W., You, J.: Texture-based palmprint retrieval using a layered search scheme for personal identification. IEEE Transactions on Multimedia 7(5), 891–898 (2005)
4. Kong, A., Zhang, D., Kamel, M.: Palmprint identification using feature-level fusion. Pattern Recognition 39, 478–487 (2006)
5. Chen, G.Y., Xie, W.F.: Pattern recognition with SVM and dual-tree complex wavelets. Image and Vision Computing 25(6), 960–966 (2007)
6. Liu, L., Zhang, D., You, J.: Detecting wide lines using isotropic nonlinear filtering. IEEE Transaction on Image Procession 16(6), 1584–1595 (2007)
7. Huang, D.S., Jia, W., Zhang, D.: Palmprint verification based on principal lines. Pattern Recognition 41(4), 1215–1428 (2008)
8. Yu, W.W., Teng, X.L., Liu, C.Q.: Face Recognition Using Discriminant Locality Preserving Projections. Image and Vision Computing 24, 239–248 (2006)
9. Yang, J., Zhang, D., Yang, J.Y., Niu, B.: Globally Maximizing, Localy Minimizing: Unsupervised Discriminant Projection with Applications to Face and Palm Biometrics. IEEE Transactions on Pattern Analysis and Machine Intelligence 29(4), 650–664 (2007)
10. Hu, D., Feng, G., Zhou, Z.: Two-dimensional locality preserving projecting (2DLPP) with its application to palmprint recognition. Pattern Recognition 40(3), 339–342 (2007)
11. Yu, Y., Zhang, J.: Discriminant projection embedding for face and palmprint recognition. Neurocomputing 71, 3534–3543 (2008)
12. Cai, D., He, X., Han, J., Zhang, H.J.: Orthogonal Laplacianfaces for Face Recognition. IEEE Trans. on Image Processing 15(11), 3608–3614 (2006)
13. Zhang, D., Kong, A., You, J., Wong, M.: Online palmprint identification. IEEE Transactions on Pattern Analysis and Machine Intelligence 25(9), 1041–1050 (2003)
14. Zhang, L., Zhang, D.: Characterization of palmprints by wavelet signatures via directional context modeling. IEEE Trans. Syst. Man Cybern. B 34(3), 1335–1347 (2004)
15. He, X., Yan, S., Hu, Y., Niyogi, P., Zhang, H.J.: Face recognition using laplacianfaces. IEEE Trans. Pattern Anal. Machine Intelli. 27(3), 328–340 (2005)

OPC UA Based Information Modeling for Distributed Industrial Systems

Vu Van Tan and Myeong-Jae Yi

School of Computer Engineering and Information Technology
University of Ulsan, San-29, Moogu-2 dong, Namgu, Ulsan 680-749, South Korea
{vvtan,ymj}@mail.ulsan.ac.kr

Abstract. Data representation in devices of industrial systems is simple data. However, the structural data organization is used in upper layers of such systems. This information can be modeled by vendors, which of course would lead to different ways of how to model similar information thus makes the life hard for clients, e.g., OPC clients. There are efforts to define a base model to expose device information and device types. A vendor will use this base model and extend it with vendor-specific information about its devices. This paper introduces an object-oriented data model based on the OPC Unified Architecture (UA) specifications and Unified Modeling Language (UML) used for communication in distributed industrial systems. This model is applied for device and information models to provide data for enterprise systems.

Keywords: ERP, MES, OPC Unified Architecture, Industrial system, Information model, Unified modeling language.

1 Introduction

Industrial informatics systems have become more and more distributed from the topological and from the system logic points of view due to the development of microelectronic technology and web service-enabled devices in the last years [3,1,7]. Modern control systems can be divided into layers for control, visualization, and production support systems. These layers are considered in the most of classifications like (i) field layer composing of instrumentation, (ii) control layer with automation devices, (iii) real-time HMI (Human Machine Interface) layer with visualization devices, and (iv) real-time MES (Manufacturing Execution System) layer with data processing devices [2]. Therefore, the ERP (Enterprise Resource Planning) layer is considered as a separate layer that is also used in industrial and informatics systems.

Data exchange has been changed to state-of-the-art, platform independent, secure, and reliable technologies and the capabilities to model information are improved. Clients can achieve the information that they are dealing with the same kind of device at different places or locations. Exposing information in much more semantics will allow clients to process highly sophisticated tasks in industrial and informatics systems.

D.-S. Huang et al. (Eds.): ICIC 2010, LNCS 6215, pp. 531–539, 2010.

Traditionally, information models for industrial systems have been formulated based on domain-specific languages and tools satisfying the requirements of standards such as IEC 750, IEC 61346, and ISO 10303 [4,2]. The solution of IEC 61346 is applied to power plants and other industrial systems [4]. It describes principles for modeling the structure of information about the systems and of the systems themselves. Different viewpoints of a system are modeled such as function-oriented viewpoint, location-oriented viewpoint, and product-oriented viewpoint. ISO 10303 [6] is a specification to address information modeling of industrial systems with different goals. This is a large set of standards for exchange of product data including domain-specific languages and notations. By using open IT standards like UML (Unified Modeling Language) and XML (Extensible Markup Language), another approach is to be able to connect the company industrial IT platform not only to plant-specific systems, but also to general IT systems like ERP systems or office applications. The principle of this approach is based on IEC 61346 to model information about industrial systems.

Due to the new OPC Unified Architecture (UA) specifications from the OPC Foundation [9], there are efforts to define a base model exposing device information and device types for OPC UA based industrial applications [5,3,1,8]. An information modeling approach should be proposed to allow that clients can access device information provided by different, vendor-specific OPC UA servers in the same manner. In addition, this approach should provide data to MES and ERP systems. The OPC UA standard is based on XML, web services, and SOA (Service-Oriented Architecture) to share information in more complex data structure formats. Information modeling is required to expose the measured values of the device as well as configure the device by using device model [4,5]. UML and object-oriented techniques have been applied for software analysis and design. They are widely used not only in pure software companies, but also in the software department of automation companies.

The study of this paper introduces an object-oriented information modeling approach based on the OPC UA specifications and object oriented techniques for communication in distributed industrial systems. The ability of this model is to apply not only for device models, but also for other scenarios to provide data to MES and ERP systems. The principles of OPC UA based information modeling approach are: (i) using object-oriented approach with hierarchies and inheritance to hand all instances of the same type in the same way and to ignore more specialized information, (ii) the type information is provided by server and could be accessed with the same mechanisms, (iii) allowing the same information to be exposed in different ways effectively, and (iv) extensibility regarding the type hierarchies for vendor-specific information.

2 OPC UA and Its Architecture in Industrial Systems

The requirement is to provide better integration of alarms and events in the address space of a Data Access server, especially for the process industry and building automation. Three different types of data such as current data, historical

data, and alarms and events with different semantics have been required. The OPC UA technology enables all three types of data to be accessed by a single OPC server. It unifies the current data access (DA), alarms and events (AE), historical data access (HDA) models and additional process calls into a single integrated address space and makes data management simpler, richer, and more centralized in additional information. An OPC UA server provides access to three kinds of objects and they are available to OPC UA clients as follows:

1. **Type Definition.** Type information is provided not only on data type level, but also on object level as well. Standard types can be defined and inheritance vendor-specific types can be derived from those standard types. They can be used for objects, variables, data, and reference definitions.
2. **Object Definition.** Objects reflect real system structure defined by given type objects with their variables, properties, and methods.
3. **View Mechanism.** A view is used to restrict the number of visible nodes and references in a large address space of the OPC UA server. By using the view mechanism servers can organize large data structures to represent information in the given context.

The OPC UA architecture is designed in a generic manner and therefore can be applied in a diverse range of applications running at various locations on the network of an organization. An ERP system can use an OPC UA client as an interface for consuming services in the corporate network. Four different architectural patterns for OPC UA systems are proposed such as client-server, chained server, server-to-server communication, and aggregating server [8].

3 OPC UA Based Information Modeling Approach

Many field devices from different vendors are being connected to industrial systems through fieldbus communication [5]. A device has some configuration parameters and some measurement values that may differ depending on the configuration. It provides that information in an OPC server, for example OPC UA server. The clients can provide an appropriate interface to expose the measured values of the device as well as configuration of the device. The device data model should include events and historical data. The client can use a generic user interface or a specific-user interface to show a graphical representation of the devices and the main parameters. Based on the OPC UA specifications, the information modeling concepts are related to Nodes, References between nodes, Objects, Variables, and Methods.

3.1 Nodes and References

The address space of an OPC UA based application is composed of nodes and references between nodes. There are two kinds of nodes, one used for representing instances and another one used for representing types. In the concept of the OPC UA standard, seven attributes such as NodeId, NodeClass, BrowseName,

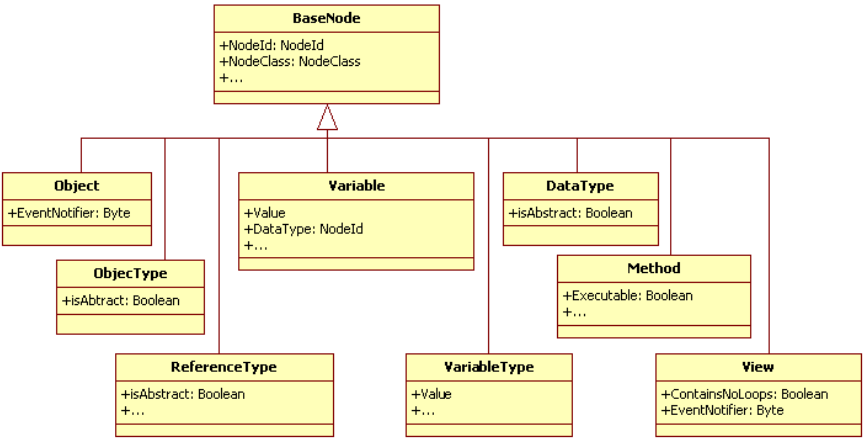

Fig. 1. The UML class diagram for concept of information modeling approach

DisplayName, Description, WriteMask, and UserWriteMask are used to describe nodes (see the BaseNode class in Fig. 1). NodeId uniquely identifies a node in the server. It is used for exchanging in the services to reference nodes. The server returns when browsing or querying the address space and clients use the NodeId to address nodes in the service calls. In normal cases, a node can have several alternative NodeIds that can be used to address the node.

The BrowseName is used for browsing purposes and should not be used for displaying the name of a node. The DisplayName containing the name of a node is used for displaying the name of a node in a user interface. The Description is an optional attribute that contains a localized textual description of the node. The WriteMask and UserWriteMask are also optional attributes that specify which attributes of the node can be modified by an OPC UA client or by the user currently connected to the server [9].

A reference describes the relation between two nodes in the address space. Thus it is uniquely identified by the source node of the reference, the target node, the semantic of the reference, and the direction of the reference. In practice, a server exposes a reference only in one direction and the reference may point to a node in another OPC UA server or nonexisting node.

Reference Types. References are used to expose different semantics on how the nodes are connected. Therefore, a reference type defines the semantic of a reference and every reference is typed and has a defined semantic. References are managed in a Reference Type hierarchy that can be represented in UML class diagram as shown in Fig. 2 [9]. Hierarchical references should be used when a hierarchy is modeled and non-hierarchical references are used for other intention like exposing relationships between different hierarchies.

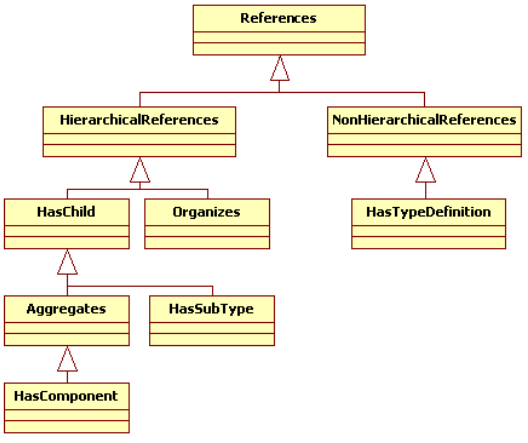

Fig. 2. The UML class diagram of Reference type hierarchy

3.2 Concept of Objects, Variables, and Methods

Object, variable, and method in the introduction of the OPC UA standard are important concepts that come from object-oriented programming. Objects have variables and methods and can also have events. A variable is used to represent a value in which the data type of the value depends on the variable. OPC UA clients can read the value, subscribe to changes of the value, and write the data to OPC servers. A method is represented as a node in the address space of the OPC UA server, called by a client, and returns a result. Each method specifies the input arguments and the output arguments. Objects are used to structure the address space to describe the node with attributes like DisplayName and Description (see Fig. 1 [9]). Methods and variables are always called in the context of the object. For example, the object Motor contains a status variable to identify if the motor is running or not. In addition, the Methods like Start and Stop can be invoked by the client to start or stop the motor.

Two kinds of variables are defined in the OPC UA specifications: Data Variables and Properties. Data variables are used to represent the data of an object, for example, the temperature of a temperature sensor or the flow of a flow transmitter. They can have sub-variables containing parts of the data and properties. Properties are often used to represent the characteristics of a node, for example, the engineering unit of a measured temperature.

(1) **Object Types.** Type information is provided not only on data type level, but also on object level as well. Object types can be simple or complex. Complex object types are used to define a structure of nodes. A server in order to expose complex object types and instance of those types gives clients the possibility of the knowledge of the type information. A client can have a specific mechanism of a user interface based on the object type and displays

it for each instance of the type. For example, the object type of the Sensor is complex.

(2) **Variable Types.** Variable types can be either simple or complex. The complex type exposes a structure of nodes, whereas the simple variable type defines only the semantic of a variable or restricts the usage of the data type of the value attribute on the instances. Variable types can only expose additional variables or either describe the variable like providing the engineering unit, etc., or expose parts of the structure of the values. In general, all the common attributes used for the node class of Variable Types are Value, DataType, ValueRank, ArrayDimensions, and IsAbstract [9]. The Value attribute and the definition of the data type for the Value attribute are contained. However, the Value attribute is optional since it has no real use for Variable Types. All attributes except for the Value attribute of Variables and Variable Types have a fixed data type. The DataType attribute is used to define the type used as scalar or array. Four kinds of Data Types are used in the OPC UA applications such as Built-in Data Types, Simple Data Types, Enumeration Data Types, and Structured Data Types [8].

3.3 Events

Events are received from notifications when subscribing to an Event Notifier. A server needs to expose its Event Types hierarchy in the address space, so that clients can retrieve this information. In fact, the node class of Object Types is used for Event Types: (i) no additional information is needed to expose Event Types; (ii) clients can use their mechanisms to handle Event Types as well as to handle Object Types; (iii) some events can be represented as objects (see Fig. 1).

3.4 Historical Access

Dealing with the history of the data in industrial systems, three facets need to be considered such as historical data, historical events, and historical address space of the server.

(1) **Historical Data and Historical Events.** Two attributes like AccessLevel and UserAccessLevel indicate the history is accessible and changeable. These attributes indicate some history is available if only if currently history is collected. Thus the attribute Historizing is used for indicating whether the history is currently collected or not. For events, the history can be gained from Event Notifiers. The attribute EventNotifier indicates whether the history of events can be accessed and manipulated.

(2) **Historical Address Space.** Nodes and references in the address space of an OPC UA server can be added or deleted over time by the clients. Therefore, allowing to track the changes and to access different versions of the address space by referencing different points of time is an optional feature that should be supported by servers.

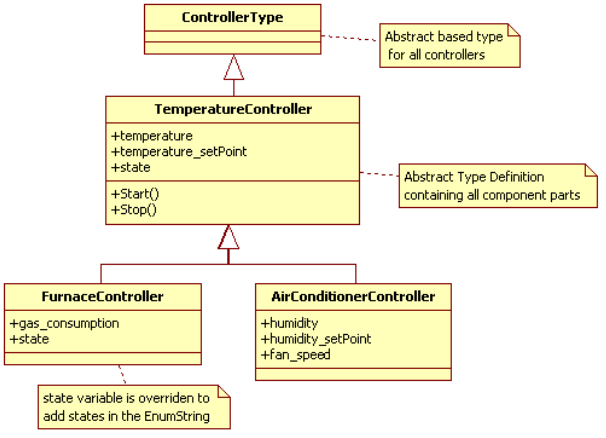

Fig. 3. The UML class diagram of type hierarchy for different controllers

3.5 Views

A view is used to restrict the number of visible nodes and references in a large address space of the server side. With using views a server can organize its address space and provide it to specific-tasks or user cases. In general, two ways can be used for looking at views in OPC UA based applications: (i) A view is represented as a node in the address space. This node gives an entry point into the content of the view. All nodes that are part of a view must be accessible starting from the view node; (ii) The NodeId of the view node can be used as filter parameter when browsing the address space.

4 Example and Discussion

An example is for modeling an air condition machine and a furnace controller that are used in a room [8]. A typical air conditioner application has a control module that the controller application is running. The controller provides two set-points to define the requested temperature and humidity. In addition, the air conditioner is turned on or off depending on the purpose of use. It offers the actual temperature and humidity as well as the power consumption, the fan speed, and the cooler state as measured values.

The controller of the furnace provides the temperature, the power consumption as well as the gas consumption by measuring the gas flow. It provides the state of the burner and allows setting the temperature and turning it on or off. It uses a temperature sensor to measure the temperature, a watt-meter to measure the power consumption, and a flow transmitter to measure the gas consumption. Based on the information modeling approach with the OPC UA specifications, a type hierarchy to expose information and to make it possible for client applications to be more general by using some base Type Definitions

and be programmed based on those supertypes is used. As Fig. 3 shows, the abstract base type ControllerType for all controllers referenced by control modules, TemperatureController, AirConditionerController, and FurnaceController are illustrated in UML class diagram. The AirConditionerController and The FurnaceController inherit from the TemperatureController with overriding the state. The FurnaceController adds the gas consumption and the AirConditionerController adds the humidity and the humidity set point. All the concepts mentioned above can be represented in the C# language as follows:

```
class ControllerType
{
    private void    Initialize();
    private double  m_measurement;
    private double  m_setPoint;
    private double  m_controlOut;
    ...
}
class TemperatureController : ControllerType
{
    // attributes
    public double temperature;
    public double temperature_setPoint;
    public string state;
    public double power_consumption;
    // methods
    public int Start();
    public int Stop();
}
class AirConditionerController : TemperatureController
{   // additional attributes
    public double humidity;
    public double humidity_setPoint;
    public double fan_speed;
}
class FurnaceController : TemperatureController
{   // additional attributes
    public double gas_consumption;
    public override EnumStrings state;
}
```

Typically, a server should support several Information Models where some of them might be based on other information models. Other Information Models can be derived for domain specific types and thus a server specific Information Model is used by the specific data provided by the server. The base Information Model is extended by a topology and a Device Information Model (DIM). The DIM is inherited from the vendor-specific DIM that contains vendor-specific types of devices.

5 Concluding Remarks

An object oriented information modeling approach based on the OPC UA specifications and object oriented techniques was introduced for communication in industrial systems. The proposed approach can be applied not only for device models, but also for other scenarios as well as providing data and related information from devices on the plant floor to MES and ERP systems. By using UML and object oriented technologies for information modeling, this approach in turn allows designers and developers to perform dependency analysis, design, and reuse. Exposing information in much more semantics allows clients to process highly sophisticated tasks in industrial and informatics systems. The presented approach permits clients can access device information and device data provided by different, vendor-specific OPC UA server in the same manner.

Acknowledgements. This work was supported in part by the Korean Ministry of Knowledge Economy and Ulsan Metropolitan City through the Network-based Automation Research Center (NARC) at the University of Ulsan and by the National Research Foundation of Korea (NRF) grant funded by the Korean Government (MEST) (NRF-2009-0076248).

References

1. Bohn, H., Bobek, A., Golatowski, F.: SIRENA – Service Infrastructure for Real-time Embedded Networked Devices: A Service Oriented Framework for Different Domains. In: Proc. of the Int. Conf. on Systems and Int. Conf. on Mobile Comm. and Learning Tech., p. 43. IEEE CS Press, Los Alamitos (2006)
2. Cupek, R., Fojcik, M., Sande, O.: Object Oriented Vertical Communication in Distributed Industrial Systems. In: Kwiecien, A., Gaj, P., Stera, P. (eds.) CN 2009. CCIS, vol. 39, pp. 72–78. Springer, Heidelberg (2009)
3. de Souza, L.M.S., Spiess, P., Guinard, D., Köhler, M., Karnouskos, S., Savio, D.: SOCRADES: A Web Service Based Shop Floor Integration Infrastructure. In: Floerkemeier, C., Langheinrich, M., Fleisch, E., Mattern, F., Sarma, S.E. (eds.) IOT 2008. LNCS, vol. 4952, pp. 50–67. Springer, Heidelberg (2008)
4. Garía, R.G., Gelle, E.: Applying and Adapting the IEC 61346 Standard to Industrial Automation Applications. IEEE Trans. on Industrial Informatics 2(3), 185–191 (2006)
5. Grossmann, D., Bender, K., Danzer, B.: OPC UA based Field Device Integration. In: Proc. of the SICE Annual Conference, pp. 933–938 (2008)
6. ISO 10303 - Industrial Automation Systems and Integration, http://www.iso.org/iso/iso_catalogue/catalogue_tc/catalogue_detail.htm?csnumber=38308
7. Jammes, F., Smit, H.: Service-Oriented Paradigms in Industrial Automation. IEEE Trans. on Industrial Informatics 1(1), 62–70 (2005)
8. Mahnke, W., Leitner, S.-H., Damm, M.: OPC Unified Architecture. Springer, Heidelberg (2009)
9. The OPC Foundation: The OPC Unified Architecture Specifications: Parts 1-12. Version 1.xx (2009), http://www.opcfoundation.org/Downloads.aspx

Voting-Averaged Combination Method for Regressor Ensemble

Kun An[1] and Jiang Meng[2]

[1] School of Information and Communication Engineering, North University of China, Taiyuan 030051, Shanxi, China
[2] School of Mechanical Engineering and Automatization, North University of China, Taiyuan 030051, Shanxi, China
{ankun,meojon}@live.nuc.edu.cn

Abstract. A voting-averaged (VOA) method is presented to combine an ensemble for the regression tasks. VOA can select ensemble components dynamically using the hidden selectivity mechanism of voting, and hence VOA can be regarded as an improvement and extension of both voting and average methods. The experiment results of ten regression tasks show VOA and a representative selective average (SEA) method of GASEN (genetic algorithm-based selective ensemble), are of similar performances to each other, and both of better performance than simple average (SIA) in Bagging ensemble. SEA produces the ensemble subset in the using genetic optimization with validation datasets after the individuals are trained well; however, VOA combines a selective ensemble directly according to the cluster of the component outputs, not to determine ensemble subsets beforehand.

1 Introduction

The importance of ensemble learning has been recognized by many scholars and researchers in recent years, with the development of the statistical learning, manifold learning and multi-instance learning. T. G. Dietterich, the international academic authority of machine learning, believed that the ensemble learning is the first of all four directions in the machine learning field [1]. Therefore, the study on the theories and techniques of the ensemble learning, can not only perfect its structural system, but also facilitate the cooperating development of the machine-learning field.

The first research upsurge was the presentation of two popular strategies for multi-learners training: Bagging and Boosting. The most straightforward way of manipulating the training set is named a *Bagging* (*b*ootstrap *agg*regat*ing*) technique presented by Breiman in 1996 [2]. The other methods to manipulate the training sets are *Boosting* and the developed version of AdaBoost (*ada*ptive *boost*ing), illustrated by Freund and Schapire from 1995 to 1996 [3-4]. From then on, a series of AdaBoost, including AdaBoost.M1 [5] and AdaBoost.MH [6] are contributed for classification tasks, and AdaBoost.R2 [7] and AdaBoost.RT [8] for regression tasks, etc.

D.-S. Huang et al. (Eds.): ICIC 2010, LNCS 6215, pp. 540–546, 2010.

The next upsurge was the development of the ensemble pruning. Margineantu and Dietterich [9] pointed out a drawback that ensemble methods require a large amount of memory to store all of the learners when deploying them in a real application, and thus proposed the idea of pruning AdaBoost ensemble. Before long, Zhou et al. proved the statement of "many could be better than all" [10] and presented the selective ensemble theory [11] and an implementation method of *GASEN* (*g*enetic *a*lgorithm-based *s*elective *en*semble) [12], a famous and popular method to prune an ensemble. Many researchers have proposed various selective or pruning methods [13-16] based on particle swarm optimization [13], immune clonal principle [14], reinforcement learning [15] or semi-definite programming [16], and so on.

According to the current research status, there are two ways to combine an ensemble, voting and average, corresponding to the classification and regression tasks, respectively. Moreover, the clustering tasks can also use voting to combine a clusterer ensemble [17]. In a word, an ensemble needs to take advantage of different combination methods to solve different problems. In order to obtain a unified combination for ensemble, this paper proposes a hybrid strategy of voting-averaged (VOA) combination to solve regression and classification tasks simultaneously. The VOA combination, inheriting the merits of both voting and average, can improve the ensemble performance when constructing ensembles by selecting some of trained learners dynamically.

2 Voting-Averaged Combination

2.1 Hidden Selectivity Mechanism of Voting

Voting is a choosing means between numbers of options based on the input of many voters, which is a common combination method in classifier or clusterer ensembles. Voting covers only parts of the trained learners instead of all of them in the average combination. According to the number of voted results, voting can be divided into plurality and majority voting. For two-class classification tasks, they are equivalent to each other; while for multi-class tasks, many theories and experiments show the majority voting is superior to the plurality one. Therefore, the classifier ensemble usually adopts the majority voting as the combination method.

In fact, a selectivity mechanism is implied in both the majority and the plurality voting. For example, a two-class problem $Q = \{-1, +1\}$ is given with the trained classifiers C_i ($i = 1, 2, \ldots, 2n+1$), where the outputs of m classifiers are +1, and the others are -1. If $m > n$, the voted output of the ensemble is +1 based on the majority voting, and -1 otherwise. In any way, the ensemble output can be regarded as the selection of $\max(m, 2n+1-m)$ classifiers with the same outputs (max is denoted as a maximum function). In contrast, the average combination, either the weighted average or the simple (unweighted) average method, need to consider all of the classifiers to combine the ensemble output. According to this standpoint, there should be a hidden selectivity mechanism in the voting combination. Moreover, the selective ensemble theory that many trained learners could be of better performance than all of them to combine ensembles [10-11], verifies that the selectivity mechanism can be a good way to improve the performance of ensembles in a sense.

2.2 Voting-Averaged Scheme

For regression problems, regressor ensembles usually adopt simple average or weighted average to combine the outputs. In order to improve the ensemble's generalization performance, GASEN [12] is proposed to combine the ensemble output with selective learners instead of all of them. Considering GASEN belongs to the post-training combination and may lose the rapidity of ensemble learning, the voting-averaged combination method is proposed in this paper, which should be used in both classification and regression tasks in a unified format.

Given a single-value regression problem without loss of generality, $f = \{(\boldsymbol{x}_1; y_1), (\boldsymbol{x}_2; y_2), \ldots (\boldsymbol{x}_t; y_t)\}$, there exists n learners or regressors R_i ($i = 1, \ldots, n$) using t training samples. According to the weighted average, the ensemble output $\hat{y}$ is,

$$\hat{y}_j = \sum_{i=1}^{n} w_i z_{ij} = \sum_{i=1}^{n} w_i R_i(\boldsymbol{x}_j) \quad (j = 1, 2, ..., t) \tag{1}$$

where w_i is the weight of the i-th regressor R_i, and z_{ij} is the i-th regressor output corresponding to the j-th training sample $\boldsymbol{x}_j$, $z_{ij} = R_i(\boldsymbol{x}_j)$.

Different from the all-combined ensemble, the voting-averaged ensemble combine the output according to the following steps.

(1) Classifying: The regressor output $z_j = (z_{1j}, z_{2j}, \ldots, z_{nj})^{\mathrm{T}}$ can be divide into m classes C_{jk} ($k = 1, \ldots, m$) according to some strategy, such as $(C_{j1}, C_{j2}, \cdots C_{jm}) = Classifying(\boldsymbol{z}_j)$.

(2) Voting: Based on the majority voting, the k^*-th class is the winner class, such as $C_{jk^*} = Voting(C_{j1}, C_{j2}, \cdots C_{jm})$.

(3) Averaging: The weighted or simple average value of the k^*-th class is taken as the ensemble output corresponding to the j-th sample, such as $\hat{y}_j = Averaging(C_{jk^*})$.

Note that *Classifying*(·) means some classifying strategy, e.g. one clustering method as an unsupervised classifying method, *Voting*(·) indicates some voting strategy, e.g. a majority voting method, and *Averaging*(·) denotes some averaging strategy, e.g. a simple average method. In fact, the designing steps above can construct only a voting-averaged scheme, which is a paradigm and any classifying, voting and averaging algorithm can be applied in.

Moreover, the voting class C_{jk^*} is aimed to the j-th training sample. In other words, C_{jk^*} is a dynamic subset for the original classifiers, varying with different training samples, in contrast to GASEN, a static subset obtained by the genetic algorithm.

2.3 Voting-Averaged Algorithm

Clustering is a feasible way to examine similarities and dissimilarities of observations or objects. Data often falls naturally into groups or clusters of observations, where the characteristics of objects in the same cluster are similar and the characteristics of objects in different. Hierarchical clustering is a way to investigate grouping in the data, simultaneously over a variety of scales of distance, by creating a cluster tree. The tree is not a single set of clusters as in k-Means (a method of cluster analysis

which aims to partition n observations into k clusters in which each observation belongs to the cluster with the nearest mean), but rather a multi-level hierarchy, where clusters at one level are joined as clusters at the next higher level.

Here we take the hierarchical clustering as the reificatory clustering method of the voting-averaged scheme, because it allows users to decide what scale or level of clustering is most appropriate in this application. The corresponding procedure is shown in Fig. 1.

Input: N learners' outputs f_i ($i = 1, \ldots, N$).
Procedure:
1. d = pdist(f), to calculate the pairwise distance of $f = (f_1, f_2, \ldots, f_N)$.
2. t = linkage(d), to create a hierarchical cluster tree according to d.
3. G = cluster(t), to construct the clusters from t, the hierarchical cluster tree.
Output: The clustered classes G.

Fig. 1. Hierarchical clustering

Based on the classification of hierarchical clustering, the majority voting and the simple average methods, we can design a voting-averaged ensemble combination based on the hierarchical clustering (Fig. 2).

Input: N learners' outputs f_i ($i = 1, \ldots, N$).
Procedure:
1. G = Hierarchical-Clustering($f_1, f_2, \ldots, f_N$), to determine the clustering classes G
2. G^* = Majority-Voting (G), to select the voted class G^* from the classes G
3. $\hat{y}$ = Simple-Averaging (G^*), to calculate the regression output from G^*
Output: The ensemble output $\hat{y}$.

Fig. 2. Voting-averaged combination based on hierarchical clustering

3 Experiment and Discussion

3.1 Datasets

In order to compare with the other well-known ensemble combination methods, the datasets listed below were used to test the performance of some well-known methods in machine learning, e.g., Bagging [2] and GASEN [10].

The constraints on the variables are shown in Table 1, where "$U[x, y]$" means a uniform distribution over the interval determined by x and y. Furthermore, we can generate the training, test and validation sets according to the corresponding datasets. The generating functions are neglected in this paper, detailed in [10]. Furthermore, we normalize the datasets to [-1, 1] or [0, 1] to ensure the enough accuracy of single neural network, and add a Gaussian artificial noisy item with the relative noise ratio equal to 0.05 to simulate the real-world data.

Table 1. Datasets for regression tasks

Dataset	Variable	Size	Dataset	Variable	Size
2-D Mexihat	$x \sim U$ [-2π, 2π]	5000	Gabor	$x_i \sim U$ [0, 1]	3000
3-D Mexihat	$x \sim U$ [-4π, 4π]	3000	Multi	$x_i \sim U$ [0, 1]	4000
Friedman #1	$x_i \sim U$ [0, 1]	5000	Plane	$x_i \sim U$ [0, 1]	1000
Friedman #2	$x_1 \sim U$ [0, 100] $x_2 \sim U$ [40π, 560π]	5000	Polynomial	$x_i \sim U$ [0, 1]	3000
Friedman #3	$x_3 \sim U$ [0, 1] $x_4 \sim U$ [1, 11]	3000	Sinc	x ~ U [0, 2π]	3000

3.2 Experiment Results

The performance in the regression tasks are measured as mean squared error (MSE) on the test datasets. We normalize the results of simple average (SIA) in Bagging, selective average (SEA) in GASEN and voting average (VOA) method according to that of the average error of single neural networks. The reported relative results in Table 2 are the average of ten folds on the test datasets with the noise ratio equal to the training datasets. In order to show the hidden selectivity of voting, we compare the combined-learner numbers of three ensembling methods above, listed in Table 3.

Table 2. Relative mean square error of comparison approaches

Dataset	SIA	SEA	VOA	Dataset	SIA	SEA	VOA
2-D Mexihat	0.2537	0.0665	0.0669	Multi	0.5968	0.5465	0.6382
3-D Mexihat	0.8627	0.8139	0.8630	Plane	0.8274	0.8506	0.8394
Friedman #1	0.2890	0.1373	0.3113	Polynomial	0.9750	0.9913	0.9763
Friedman #2	0.1342	0.0373	0.0395	Sinc	0.8302	0.8227	0.8273
Friedman #3	0.5734	0.4442	0.5607	<*Average*>	0.4204	0.2725	0.3815
Gabor	0.4095	0.1356	0.4477				

Table 3. Combined-learner numbers of comparison approaches

Dataset	SIA	SEA	VOA	Dataset	SIA	SEA	VOA
2-D Mexihat	20	2.90	14.79	Multi	20	4.80	12.98
3-D Mexihat	20	3.90	13.75	Plane	20	3.10	12.74
Friedman #1	20	3.10	14.40	Polynomial	20	2.70	12.75
Friedman #2	20	4.10	16.10	Sinc	20	2.50	12.94
Friedman #3	20	4.20	12.90	<*Average*>	20	3.52	13.61
Gabor	20	3.90	12.71				

3.3 Discussions

The results in Tables 2 and 3 show that both the MSE performance and the combined -learner number of the voting-averaged method lie in between those of simple average and selective average. VOA is superior to SIA and inferior to SEA in each and average experimental regression task. These results also indicate that the voting average

method can be regarded as a tradeoff of the simple average and selective average methods.

This fact validates the hidden selectivity in voting makes the voting average more effective than simple average in Bagging, and is of more efficiency than selective average in GASEN with a dynamic selectivity mechanism online instead of a static process of post training in the selective average method.

4 Conclusions

A hybrid combination strategy of the voting average method is proposed in this paper. Voting-averaged combination not only keeps the rapidity and diversity that an averagely-combined ensemble holds, but also improves the accuracy performance by selecting and combining an ensemble dynamically based on the hidden selectivity mechanism of the voting.

Experiment results show that, as for the ensemble, voting average can achieve better performance than simple average in Bagging ensemble, but slightly worse than selective average in GASEN ensemble.

References

1. Dietterich, T.G.: Machine Learning Research: Four Current Directions. AI Magazine 18(4), 97–136 (1997)
2. Breiman, L., Bagging, P.: Machine Learning 24(2), 123–140 (1996)
3. Freund, Y.: Boosting a Weak Algorithm by Majority. Information and Computation 121(2), 256–285 (1995)
4. Schapire, R.: Experiment with a New Boosting Algorithm. In: Proc. of 13th International Conference on Machine Learning, Bari, Italy, pp. 148–156 (1996)
5. Freund, Y., Schapire, R.E.: A Decision-theoretic Generaliation of Online Learning and an Application to Boosting. Journal of Computer and System Sciences 55(1), 119–139 (1997)
6. Schapire, P.E., Singer, Y.: Improved Boosting Algorithms Using Confidence-related Predictions. In: Proceedings of 11th Annual Conf. on Computational Learning Theory, pp. 80–91 (1998)
7. Drucker, H.: Improving Regressor Using Boosting. In: Proc. of 14th International Conference on Machine Learning, pp. 107–115. Morgan Kaufmann, San Francisco (1997)
8. Solomatine, D.P., Shrestha, D.L., AdaBoost, R.T.: A Boosting Algorithm for Regression Problems. In: Proceedings of 2004 IEEE International Joint Conference on Neural Networks, pp. 1163–1168 (2004)
9. Margineantu, D.D., Dietterich, T.G.: Pruning Adaptive Boosting. In: Proceedings of 14th International Conference on Machine Learning, San Francisco, CA, pp. 211–218 (1997)
10. Zhou, Z.H., Wu, J.X., Tang, W.: Ensembling Neural Networks: Many Could Be Better Than All. Artificial Intelligence 137, 239–263 (2002)
11. Zhou, Z.H.: Selective Ensemble. In: Jue, W., et al. (eds.) Machine Learning And Application, pp. 170–171. Tsinghua University Press, Beijing (2005)
12. Zhou, Z.H., Wu, J.X., Jiang, Y., et al.: Genetic Algorithm Based Selective Neural Network Ensemble. In: Proceedings of the 17th International Joint Conference on Artificial Intelligence, Seattle, WA, pp. 797–802 (2001)

13. Shi, Y., Huang, C.M.: An Improved Particle Swarm Optimization Algorithm Based on Ensemble Technique. Journal of China Ordnance 2(4), 310–314 (2006)
14. Zhang, X.R., Wang, S., Tan, S., et al.: Selective SVMs Ensemble Driven by Immune Clonal Algorithm. In: Rothlauf, F., Branke, J., Cagnoni, S., Corne, D.W., Drechsler, R., Jin, Y., Machado, P., Marchiori, E., Romero, J., Smith, G.D., Squillero, G. (eds.) EvoWorkshops 2005. LNCS, vol. 3449, pp. 325–333. Springer, Heidelberg (2005)
15. Partalas, I., Tsoumakas, G., Katakis, I., et al.: Ensemble Pruning via Reinforcement Learning. In: Antoniou, G., Potamias, G., Spyropoulos, C., Plexousakis, D. (eds.) SETN 2006. LNCS (LNAI), vol. 3955, pp. 301–310. Springer, Heidelberg (2006)
16. Zhang, Y., Burer, S., Street, W.N.: Ensemble Pruning via Semi-Definite Programming. Journal of Machine Learning Research 7, 1315–1338 (2006)
17. Zhou, Z.H., Tang, W.: Clusterer Ensemble. Knowledge-Based Systems 19(1), 77–83 (2006)

Face Recognition Using the Feature Fusion Technique Based on LNMF and NNSC Algorithms

Li Shang[1,2], Changxiong Zhou[1,2], Yunian Gu[1], and Yu Zhang[1]

[1] JiangSu Province Support Software Engineering R&D Center for Modern Information Technology Application in Enterprise, Suzhou, China
[2] Department of Electronic Information Engineering, Suzhou Vocational University, Suzhou 215104, Jiangsu, China
{sl0930,zhouchangxiong,gyn,zhy}@jssvc.edu.cn

Abstract. A new face recognition method, realized by the feature fusion technique based on Local Non-negative Sparse Coding (NNSC) and Local Non-negative Matrix Factorization (LNMF) algorithms, is proposed in this paper. NNSC and LNMF are both part-based representations of the multi-dimensional data, used widely and efficiently in image feature extraction and pattern recognition. Here, considered the high recognition rate, the weighting coefficient fusion method between features obtained by algorithms of NNSC and LNMF is discussed in the face recognition task. Using the distance classifier and the Radial Basis Probabilistic Neural Network (RBPNN) classifier, the recognition task is easily implemented on the ORL face database. Moreover, compared with any other algorithm of NNSC and LNMF, experimental results show that the feature fusion method is indeed efficient and applied in the face recognition.

Keywords: Face recognition, LNMF, NNSC, Classifier.

1 Introduction

Over the last ten years, face recognition has become a specialized applications area within the larger field of computer vision. And many methods of face recognition have been exploited, such as methods of eigenfaces [1-2], wavelet –based [3], gabor wavelet [4], Principal Component Analysis (PCA) [5], Independent Component Analysis (ICA) [5-7], Non-negative Matrix Factorization (NMF) [8-9], Local NMF (LNMF) [10], local Non-negative Sparse Coding (NNSC) [10] and so on. Wavelet-based methods depend on the mathematical reasoning, and they are difficult to deal with multi-dimensional data. It is well known that eigenfaces have employed forms of PCA, and PCA is optimal for finding a reduced representation that minimizes the reconstruction error, but it cannot de-correlates the high order moments of input in addition to the second order moments. However, in face recognition, much of the important information is contained in the high-order statistics of the images. So, the high-order statistical methods of NMF, LNMF, ICA and NNSC are used widely in the face recognition task at present [10]. Moreover, ICA and NNSC methods are in fact sparse coding techniques, which are qualitatively very similar to the receptive fields

D.-S. Huang et al. (Eds.): ICIC 2010, LNCS 6215, pp. 547–554, 2010.

of simple cells in the primary visual cortex (V1) in brain, and are successfully applied to the learning of facial features for face recognition. Although any method mentioned above is efficient in implementing face recognition, the illumination changes, out of plane rotations and occlusions are still remain as challenging problems. The recognition rate is still not ideal in application.

In this paper, in order to improve the recognition rate, we attempt to utilize the fusion features, obtained by the weight coefficient fusion between features learned by LNMF and NNSC algorithms, as the new face images' features. Further, using the Distance classifier and RBPNN classifier, the face recognition is implemented on the ORL face database. Under the same experimental condition, compared with the LNMF method and the NNSC method, simulation results show that our feature fusion method based on LNMF and NNSC is the best in performing the face recognition task.

2 Local Non-negative Matrix Factorization (LNMF)

2.1 NMF Algorithm

Non-negative Matrix Factorization (NMF) can be applied to the statistical analysis of multivariate data [10]. Given an $n \times L$ non-negative matrix $\mathbf{V} = [\mathrm{v}_1, \mathrm{v}_2, \cdots, \mathrm{v}_k, \cdots, \mathrm{v}_N]^T$ (each row vector v_k has L samples), the goal of NMF is to find the non-negative matrix $\mathbf{W}$ and $\mathbf{H}$ such that:

$$\mathbf{V} \approx \mathbf{WH} \ . \tag{1}$$

where $\mathbf{W}$ is the feature basis matrix with the size of $n \times m$ (placed in the column), $\mathbf{H}$ is the weight coefficient matrix with the size of $m \times L$ (where $m \le n$). Thus, we minimize the error of reconstruction. This can do so by minimizing the cost function:

$$D = \left\| \mathbf{V} - \mathbf{WH} \right\|_F \ . \tag{2}$$

where $\left\| \cdot \right\|_F$ is the Frobenius norm, and constrains to or by using an alternative measure:

$$D = \sum_{i,j} \left(\mathrm{v}_{ij} \log\left(\frac{\mathrm{v}_{ij}}{\mathrm{w}_{ij}\mathrm{h}_{ij}}\right) - \mathrm{v}_{ij} + \mathrm{w}_{ij}\mathrm{h}_{ij} \right). \tag{3}$$

where $\mathbf{W}, \mathbf{H} \ge 0$, $\sum_i \mathrm{w}_{ij} = 1 \ \ \forall j$. D reduces to Kullback-Leibler divergence when $\sum_{i,j} \mathrm{v}_{ij} = \sum_{i,j} \mathrm{w}_{ij}\mathrm{h}_{ij} = 1$. Otherwise, it is noted that both of these measures equal zero if $\mathbf{V} = \mathbf{WH}$.

2.2 LNMF Algorithm

The Local Non-negative Matrix Factorization (LNMF) algorithm is aimed at learning local features by imposing three additional constraints on the NMF basis [10, 12] in

order to enforce the local property of the main parts of the feature matrix $\mathbf{W}$. The three constraint conditions also emphasize strongly the locality of basic feature components in the decomposition process of original images used in test. Letting $\mathbf{U}=[u_{ij}]=\mathbf{W}^T\mathbf{W}$, $\mathbf{Q}=[q_{ij}]=\mathbf{H}^T\mathbf{H}$, both being the size of $m\times m$. The incorporated of the three constraints leads the following constrained divergence as the objective function for LNMF [12]:

$$D=\sum_{i,j}\left(v_{ij}\log(\frac{v_{ij}}{w_{ij}h_{ij}})-v_{ij}+w_{ij}h_{ij}\right)+\alpha\sum_{i,j}u_{ij}-\beta\sum_{i}q_{ij}. \tag{4}$$

where $\alpha,\beta>0$ are constant parameters. The LNMF factorization is defined as a solution to the constrained minimization of the following formula (5). A local solution to the above constrained minimization can be found by using the following three step update rules:

$$\begin{cases} h_{kl}=\sqrt{h_{kl}\sum_i v_{il}\dfrac{w_{ik}}{\sum_k w_{ik}h_{kl}}} \\ w_{kl}=\dfrac{w_{kl}\sum_j v_{kj}\dfrac{h_{lj}}{\sum_k w_{kl}h_{lj}}}{\sum_j h_{lj}}. \\ w_{kl}=\dfrac{w_{kl}}{\sum_k w_{kl}} \end{cases} \tag{5}$$

3 Local Non-negative Sparse Coding

Non-negative Spare Coding (NNSC) was early proposed by P. O. Hoyer in 2002 [9]. Let a dataset of L training images be given as an $n\times L$ matrix $\mathbf{V}$ with each column denoting an image or a patch sampled from an image. This matrix is approximately factorized into non-negative basis matrix $\mathbf{W}$ with $n\times m$ and non-negative sparse coefficient matrix $\mathbf{H}$ with $m\times L$. Eac facial image can then be represented as a linear combination of the basis images using the approximate factorization (1). As stated earlier, each column of matrix $\mathbf{W}$ contains a basis vector, while each column of H contains the weights needed to approximate the corresponding columns in $\mathbf{V}$ using the bases from $\mathbf{W}$. The rank m of factorization usually is chosen as $m<nL/(n+L)$.

The NNSC algorithm's cost function contains two terms: the small reconstruction error and the sparse penalty function [9,10-11], and it is written as the following form:

$$J(\mathbf{W},\mathbf{H})=\frac{1}{2}\sum_{i=1}^{N}\sum_{j=1}^{L}\left(\mathbf{V}_{ij}-\sum_{i=1}^{N}\mathbf{W}_{ik}\mathbf{H}_{kj}\right)^2+\lambda\sum_{k=1}^{M}\sum_{j=1}^{L}f(\mathbf{H}_{kj})+\alpha\sum_{i}^{N}(w_{ik}^T w_{ik})-\beta\sum_{k}^{M}(h_{kj}h_{kj}^T). \tag{6}$$

subject to the constraints: $\mathbf{V} \geq 0$, $\forall_i$: $\mathrm{w}_k \geq 0$, $\mathrm{h}_k \geq 0$, $\lambda > 0$, $\alpha > 0$, and $\|\mathrm{w}_k\| = 1$ ($k = 1,2,\cdots,m$,). Where $[\cdot]_{kj}$ denotes an element of a matrix. $\sigma_k{}^2 = \langle \mathrm{h}_k^2 \rangle$, $\mathbf{V}$ denotes an image, w_k and h_k denotes respectively the *kth* column of $\mathbf{W}$ and the *kth* row of H, λ is the tradeoff between sparseness and accurate reconstruction, and γ has to do with the variance of the prior distribution of w_k. And the self-adaptive sparse constraint function $f(\cdot)$ is chosen as $f(h_{kj}) = |h_{kj}|$. It can be observed that NNSC subject to the same constraints as those of NMF. The objective function listed in (6) is minimized by the following rules[9,12]:

$$\begin{cases} \Delta h_{kj} \leftarrow h_{kj} \sum_{i=1}^{n} \dfrac{[\mathbf{W}^T \mathbf{V}]_{kj}}{[\mathbf{W}^T \mathbf{W} \mathrm{H}]_{kj} + \lambda} \\ \Delta \mathrm{w}_k \leftarrow -\mu (\mathbf{W}\mathrm{H} - \mathbf{V}) \mathbf{H}^T - \gamma \mathrm{w}_k \,. \\ \mathbf{W} = \dfrac{\mathbf{W}}{\|\mathbf{W}\|} \end{cases} \tag{7}$$

4 Experiment Results

4.1 Face Recogniton in the Part-Based Subspace

Let v_i ($i = 1,2,\cdots,n$) denote the *ith* face image, and $\bar{\mathbf{V}}$ denote the mean of all training face images. Each training face image v_i is projected into the linear space as a feature vector $\mathrm{h}_i = (\mathbf{W}^T \mathbf{W})^{-1} \mathbf{W}^T (\mathrm{v}_i - \bar{\mathbf{V}})$, which is used as a prototype feature point. A query face v_q to be classified is represented by its projection into the space as $\mathrm{h}_q = (\mathbf{W}^T \mathbf{W})^{-1} \mathbf{W}^T (\mathrm{v}_q - \bar{\mathbf{V}})$. Then, the Euclidean distance between the query and each prototype $d(\mathrm{h}_q, \mathrm{h}_i)$ is calculated. The query is classified to the class to which the closest prototype belongs [12].

4.2 Face Databases

The Cambridge ORL face database is used in our test. In this face database, there are 400 images of 40 persons, namely 10 images per person. This database includes both males and females, and each original image is the size of 92×112. To reduce the computation complexity, each image size is reduced to 46×56. A person's 10 images used in this paper are shown in Fig.1. These images are taken at different time, with only slightly varying illumination, different facial details (glasses/no-glasses). All the images are taken against a dark homogeneous background. The faces are in up-right position of frontal view, with slight left-right out-of-plane rotation. Each image is linearly stretched to the full range of pixel values of [0 255]. For 10 images of each person, the first 5 images are used as training images, and last 5 images are used in test images. Thus, the training images and test images are a matrix with the size of

200×2576. The training set is then used to learn basis vectors, and the test set is used to evaluate. All compared methods here take the same training and test data under the same experimental conditions.

Fig. 1. Twenty images of two persons in the ORL database. Each image is the size of 46×56.

4.3 Learning Basis Vectors

Assume that16, 25, 36, 49, 64, 81, 100, 144 basis components are considered in test using different algorithm representations. This was done to determine how the results are affected by the number of dimensions of the feature space. Using the training set, the images of basis coefficients h_i obtained by different algorithms by utilizing the appointed dimension are showed in Fig2. Higher pixels are in darker color, and the components in each basis set of LNMF and NNSC have been ordered (from left to right, and top to bottom) according to the maximum feature values. Clearly, LNMF and NNSC methods both can obtain part-based basis images, but the NNSC basis images have clearer sparseness in feature subspace, further, when the dimensionality is increased, they tend to become more localized compared with LNMF basis images.

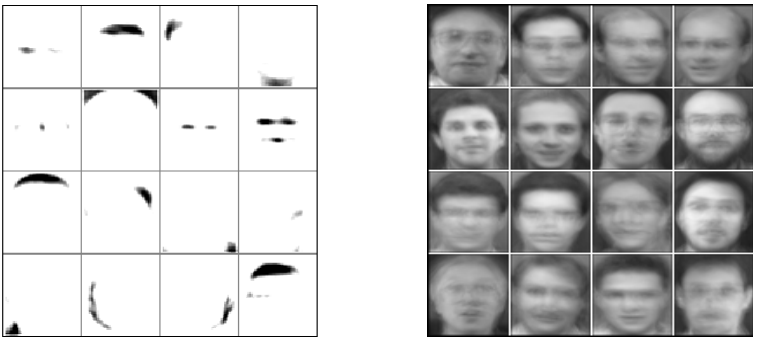

Fig. 2. Bases components (the left panel) and sparse coefficients (the right panel) obtained by the fusion features of LNMF and NNSC with the different dimensions 16 (the top row), 36 (the middle row) and 81 (the last row).

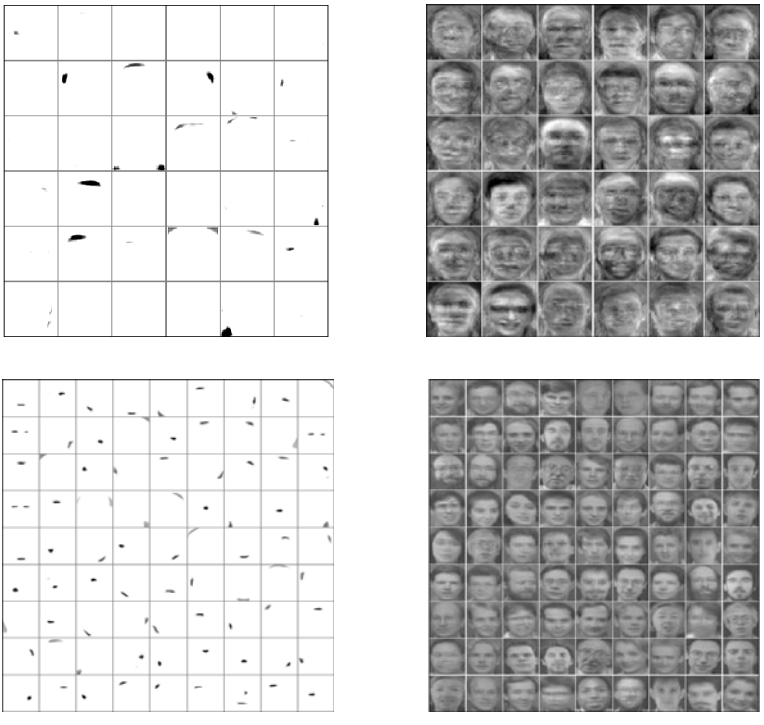

Fig. 2. (*continued*)

4.4 Face Recogniton

In this subsection, for the test set, utilizing the distance classifier and the Radial Basis Probabilistic Neural Network (RBPNN) classifier, the face recognition process can be successfully implemented according to the fusion basis components obtained by LNMF and NNSC algorithms. The recognition accuracy is used as the performance measure. Test was done with different basis components with the level of 25, 64 and 81. The recognition rates obtained by different algorithms responding to different basis components were listed in Table 1. It is easy to see that the larger the dimension, the larger the recognition is in despite of the type of classifiers used. Considering different basis components, for the ORL face database, the recognition rate obtained by NNSC algorithm is better than LNMF, and this is coincident with the reference [12]. And the feature fusion method based on LNMF and NNSC obtained the best recognition rate. However, it must be noted that when the dimension excess 64, the recognition rate increases slowly. In other words, the recognition rate of different algorithm as near as makes no different. Otherwise, when the number of the basis dimensions is very small, the recognition rates of the feature fusion method are still very high. This further proved our method is indeed effective in application.

Table 1. Recognition rate obtained by different algorithms and different classifers

Contents	LNMF		NNSC		LNMF+NNSC	
	RBPNN (%)	Distance (%)	RBPNN (%)	Distance (%)	RBPNN (%)	Distance (%)
16	82.13	79.32	84.85	81.57	86.42	83.28
25	87.43	85.62	89.25	86.92	91.34	88.76
36	91.46	87.96.	94.98	89.47	95.83	90.34
49	93.78	89.56	95.86	91.67	96.56	92.75
64	94.27	91.83	96.69	92.87	97.45	93.92
81	95.16	93.35	97.32	93.56	97.78	94.16
100	95.76	94.06	98.39	94.68	98.05	94.93

5 Conclusions

This paper proposes a novel face image recognition method using the feature fusion technique based on average weighting coefficients. Face image features of ROL database are respectively extracted by the local non-negative matrix factorization (LNMF) and the local non-negative sparse coding. All features behave locality and sparseness. Using the distance classifier and the radial basis probabilistic neural network (RBPNN) classifier, the recognition task was implemented. Considering different basis dimensions of 16, 25, 36,…, 100 , simulation experimental results show that the recognition rates obtained by NNSC algorithm are better than those obtained by LNMF, but they are smaller than those obtained by the feature fusion method proposed here. Importantly, the feature fusion method can obtain higher recognition accuracies with a relatively smaller number of basis dimensions.

Acknowledgement

This work was supported by the Opening Project of Jiangsu Province Support Software Engineering R&D Center for Modern Information Technology Application in Enterprise (No. SX200906), the grants of Natural Science Foundation of Jiangsu Province of China (BK2009131), the grants of National Science Foundation of China (Nos. 60970058 and 60805021), as well as supported by “Qing Lan Project” of Jiangsu Province and the Startup Foundation Research for Young Teachers of Suzhou Vocational University (SZDQ09L05).

References

1. Turk, M.A., Pentland, A.P.: Eigenface for Recognition. Journal of Cognitive Neuroscience 3, 71–86 (1991)
2. Belhumeur, S.D., Hespanha, J., Kriegman, D.: Eigenfaces vs. Fisherfaces: Recognition Using Class Specific Near Projection. IEEE Transaction on Pattern Analysis and Machine Intelligence 19, 711–720 (1997)

3. Garcia, C., Zikos, G., Tziritas, G.: A Wavelet-based Framework for Face Recognition. In: Workshop on Advances in Facial Image Analysis and Recognition, 5th European Conference on Computer Vision, pp. 84–92 (1998)
4. Shen, L.L., Li, B.: A Review on Gabor Wavelets for Face Recognition. Pattern Analysis &Applications 9, 273–292 (2006)
5. Draper, B.A., Kyungim, B., Bartlett, M.S., Ross, B.J.: Recognizing Faces with PCA and ICA. Computer Vision and Image Understanding 9, 115–137 (2003)
6. Bartlett, M.S., Movellan, J.R., Sejnowski, T.J.: Face Recognition by Independent Component Analysis. IEEE Transaction on Neural Networks 13, 1450–1464 (2002)
7. Bartlett, S.M., Lades, H.M., Sejnowski, T.J.: Independent Component Representations for Face Recognition. In: Proceedings of the SPIE Symposium on Electronic Imaging: Science and Technology, Conference on Human Vision and Electronic Imaging III, San Jose, California, pp. 528–539 (1998)
8. David, G., Jordi, V.: Non-negative Matrix Factorization for Face Recognition. In: Escrig, M.T., Toledo, F.J., Golobardes, E. (eds.) CCIA 2002. LNCS (LNAI), vol. 2504, pp. 336–344. Springer, Heidelberg (2002)
9. Hoyer, P.O.: Non-negative Matrix Factorization with Sparseness Constraints. Journal of Machine Learning Research 5, 1427–1469 (2004)
10. Shastri, B.J., Levine, M.D.: Face Recognition Using Localized Features Based on Non-negative Sparse Coding. Machnie Vision and Applications 18, 107–122 (2007)
11. Smaragdis, P., Brown, J.C.: Non-negative Matrix Factorization for Polyphonic Music Transcription. In: 2003 IEEE Workshop on Applications of Signal Processing to Audio and Acoustic, New Paltz, NY, pp. 177–180 (2003)
12. Li, S.Z., Hou, X.W., Zhang, H.J., Cheng, Q.S.: Learning Spatially Localized, Parts-based Representation. IEEE Comput. Vis. Pattern Recognition 1, 207–212 (2001)

A PDOC Method for Topology Optimization Design

Longbiao Zhao[1], Zhimin Chen[2], Haobo Qiu[1], and Liang Gao[1,*]

[1] The State Key Laboratory of Digital Manufacturing Equipment and Technology
Huazhong University of Science and Technology, Wuhan, P.R. China
[2] China Ship Development and Design Center,Wuhan, P.R. China
gaoliang@mail.hust.edu.cn

Abstract. Based on optimality criterion method, proportional and differential optimality criterion（PDOC） method is proposed and applied in topology optimization design. Since the phenomenon of low efficiency and overshoot caused by the uncertain deviation, this method introduces the proportional and differential control to improve the iteration operator, and constructs more reasonable iteration formula to accelerate the convergence. A new algorithm is utilized to calculate the density distribution of new material, so the trend of deviation can be predicted and corrected in advance. Finally, experiment results indicate that PDOC method is feasible and efficient.

Keywords: topology optimization, optimality criteria method, iteration operator, proportional and differential control.

1 Introduction

Topology optimization is to find the optimal topology in design domain. The main idea for solving this problem is to transform it into finding the optimal material distribution. It is a very effective way which could help designers choose the initial topology structure. It has a guiding significance in the conceptual design phase.

Compared with other model solving methods, Optimality Criteria method(OC) [1] is the criteria satisfying a variety of constraints (stress, displacement, frequency, etc.). The original OC includes constant mutual energy design,stress ratio method and fully stressed design [2]. In recent years, many scholars have conducted a lot of research on OC methods. Meske R, et al. has studied the robustness and rapid convergence of OC,and applied OC to the optimization of natural frequency[3]. Logo J, et al. used it in random topology optimization design problem[4]. Chiandussi G, et al. added the genetic path into OC [5].

According to inherent criteria to calculate the density of new material, each iteration is based on the material density and sensitivity in the former in OC. Because of its low search efficiency, it is very difficult to converge in the process of solution. Aiming at these problems, this paper proposes a PDOC method based on traditional OC,

* Corresponding author.

D.-S. Huang et al. (Eds.): ICIC 2010, LNCS 6215, pp. 555–563, 2010.

SIMP[6]density interpolation model and PD control theory. The objective function minimizes the structure's compliance. This method has improved the iteration operator, simultaneously, offered an update scheme of iterative on design variables. On one hand, search efficiency is improved. On the other hand, the speed of optimization is accelerated. Moreover, this method is easier to converge. Furthermore,this paper provides the topology optimization implementation process and experiments the algorithm by Matlab. Finally, the PDOC method is validated by two classic numerical examples.

2 The PDOC Method for Topology Optimization

2.1 PDOC Method

Iterative formula of traditional OC is simple .It is easy for numerical implementation, but its convergence is not ideal. In order to accelerate convergence, we try to construct iterative formula through multi-level iteration in the actual numerical experiments, such as:

$$x^{(k+1)} = \varphi_k(x^{(k)},\ldots,x^{(k-l+1)}), \quad k = 0,1,\ldots, \tag{1}$$

when calculating $x^{(k+1)}$, we take l iterations previous into account. If φ_k is unrelated to k ,the iterative formula can be expressed as follows:

$$x^{(k+1)} = \varphi(x^{(k)},\ldots,x^{(k-l+1)}), \quad k = l, l+1,\ldots, \tag{2}$$

In the process of numerical calculating, multi-level iterative can save more information than single-level iterative method .It increases the storage capacity, and becomes more complex. Therefore, l should not be too large generally. In normal case, when calculating $x^{(k+1)}$, we just take the previous two iterations into considertation. The iterative formula is as follows:

$$x^{(k+1)} = \varphi(x^{(k)}, x^{(k-1)}), \quad k = 2,3,\ldots. \tag{3}$$

In practical optimization problems, the structure of the nonlinear equations is so complex that it is difficult to construct two-level stationary iterative through exact mathematical deduction. This is similar to the cases in system control. In a control system, we can consider $x^{(k+1)}$ as the output variables of $\varphi(x^{(k)}, x^{(k-1)})$. while

$x^{(k)},\ldots,x^{(k-l+1)}$ as input variables. We regard the control system $\varphi(x^{(k)},x^{(k-1)})$ as a black box, nobody knows their internal control mechanism .In control engineering, parameters of the system controller should be determined relying on experience when controlled object is unclear enough, or lack of accurate mathematical model . At this time , the PD control method mentioned above is the more suitable way. PD controller uses the variable figured out by proportional and differential link to control according to the system deviation. The deviation of input signal can be expressed as follows:

$$e^{(k)} = x^{(k)} - x^{(k-1)} \tag{4}$$

Combined with the fixed-point iteration method and differential control theory, two-level stationary iterative formula can be constructed as follows:

$$x_j^{(k+1)} = (D_j^{(k)})^{\zeta} x_j^{(k)} + \alpha(x^{(k)} - x^{(k-1)}) \tag{5}$$

$D_j^{(k)}$ and ζ are consistent with the one in the fixed-point iteration method. α is the impact factor of differential item, we call it differential parameter for short. This two-level stationary iteration method, combining the fixed-point iteration method with differential control theory, is called PDOC.

The iteration operator was improved as follows:

$$x_j^{(k+1)} = \begin{cases} (1)\min\left\{(1+m)x_j^{(k)},1\right\} \\ if\ \min\left\{(1+m)x_j^{(k)},1\right\} \le \alpha\cdot\left(x_j^{(k)}-x_j^{(k-1)}\right)+(D_j^{(k)})^{\zeta}\cdot x_j^{(k)} \\ (2)\alpha\cdot\left(x_j^{(k)}-x_j^{(k-1)}\right)+(D_j^{(k)})^{\zeta}\cdot x_j^{(k)} \\ if\ \max\left\{(1-m)x_j^{k},x_{\min}\right\} < \alpha\cdot\left(x_j^{(k)}-x_j^{(k-1)}\right) \\ \quad +(D_j^{(k)})^{\zeta}\cdot x_j^{(k)} < \min\left\{(1+m)x_j^{(k)},1\right\} \\ (3)\max\left\{(1-m)x_j^{(k)},x_{\min}\right\} \\ if\ \alpha\cdot\left(x_j^{(k)}-x_j^{(k-1)}\right)+(D_j^{(k)})^{\zeta}\cdot x_j^{(k)} \le \max\left\{(1-m)x_j^{(k)},x_{\min}\right\} \end{cases} \tag{6}$$

m represents movement limit ($0<m<1$), k represents iteration steps, ζ is the damping factor ($0<\zeta<1$), $x_{\min}$ is the lower limit value of material density

($x_{\min} = 0.0001$), Λ represents the lagrange multiplier. In each iteration, we ensure that the lagrange multiplier which satisfied volume constraint satisfaction is variable. In the step of k ,we can calculate Λ through bisection method:

Step 1: Define $\Lambda_{\min}^{(0)} = 0$, $\Lambda_{\max}^{(0)} = 100000$; Calculate the current volume ratio $V^{(k)}$; Make $V^{(k)}\Lambda_{\min}^{(0)} < V^*$, $V^{(k)}\Lambda_{\max}^{(0)} > V^*$.

Step 2: Calculate $\Lambda^{(i)} = (\Lambda_{\min}^{(i)} + \Lambda_{\max}^{(i)})/2$.

Step 3: Update the lagrange multiplier: if $V^{(k)} < V^*$, then $\Lambda_{\max}^{(i+1)} = \Lambda^{(i)}$; if $V^{(k)} > V^*$, then $\Lambda_{\min}^{(i+1)} = \Lambda^{(i)}$, $i = i+1$.

Step 4: Repeat **Step2** and **Step3**, until it meets the condition $\left|V^{(k)} - V^*\right| \le \delta$ ($\delta = 0.0001$).

2.2 The Algorithm Implementation

In Fig.1, the flowchart of PDOC method is described for solving topology optimization problem, and we can realize the algorithm by MATLAB. The whole process of solution can be divided into 6 major steps and shown as follows:

Step 1: Pre-treatment of the finite element model: mesh, define constraints and loads.

Step 2: Initialize the design variables: define the density of the initial cell, set the value as 0.5.

Step 3: Analyse and solve the finite element model: calculate the sensitivity of each unit, then analyse and filter.

Step 4: Calculate the material density and the compliance of the structure by PDOC method .

Step 5: Determine whether the results meet the optimal design objectives. If it does not achieve the optimal design goal, then jump to **Step3**; If achieved, then go to **step6**. Generally, there are two kinds of situations to terminate the design goals. Firstly, total material density reaches the minimum constraint limit, and secondly, the change of the structure's compliance reaches the intended boundary.

Step 6: Output the result and end up the procedure.

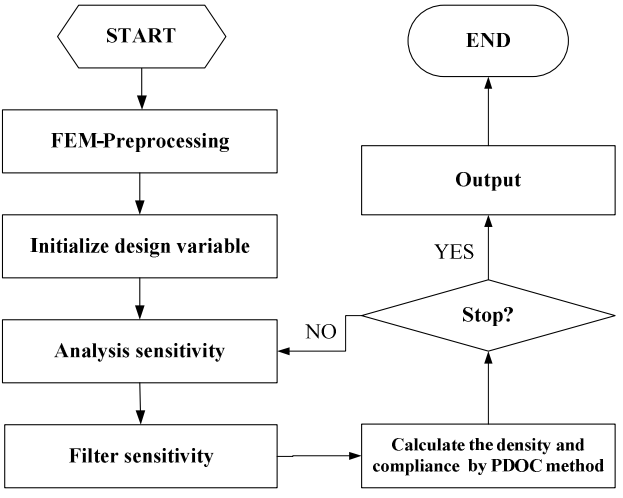

Fig. 1. The flowchart of PDOC

3 Numerical Examples

The proposed PDOC method is applied to minimum compliance structural topology optimization design problems to demonstrate the performance. The minimum compliance optimal topology design problem can be expressed as:

$$\begin{aligned} &\textit{Find}: && x = \{x_1, x_2, ..., x_n\}^T \in R^n \\ &\textit{Minimize}: && C = F^T U = U^T K U \\ & && = \sum_{j=1}^{n} u_j^T k_j u_j = \sum_{j=1}^{n} (x_j)^p u_j^T k_0 u_j \\ &\textit{Subject to}: && V = \sum_{j=1}^{n} x_j v_0 = f \cdot V_0 \le V^* \\ & && F = KU \\ & && x_j \in [0,1],\ j = 1, 2, ..., n \end{aligned} \tag{7}$$

Where C denotes the structural overall compliance. F is the element load vector, and U is the element displacement matrix, K is the structural global stiffness matrix. v_0 represents the initial volume of each element in the design domain, and V_0 is the initial

volume. V is the structural volume after optimization. f declares the optimal volume ratio. u_j is the element displacement column vector.

3.1 Cantilever Beam

In the stiffness optimal problem of cantilever beam, the schematic diagram of design domain is depicted in Fig.2.The length(A) is 60mm and the height(B) is 20mm. Elastic Modulus (E) is 207 GPa and Poisson's ratio υ=0.3. The volume fraction is 50% of the design domain. The structure is subjected to one mid-point concentrated load of 10KN on the right hand. There are freedom constraints in X direction, as well as the Y direction on the left vertical boundary.

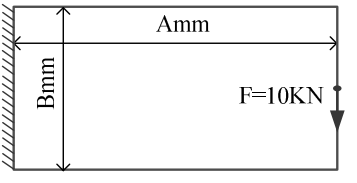

Fig. 2. Design domain of the cantilever beam

First, the influence of the solving effectiveness by differential parameter in the PDOC method is analyzed by experiment. The CPU of the computer for testing is 2.0Ghz, and the internal memory is 2GB. Algorithms are realized by use of Matlab.

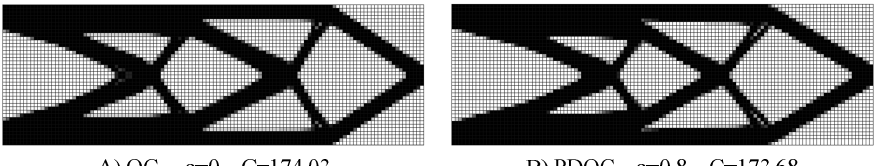

A) OC，a=0，C=174.03　　B) PDOC，a=0.8，C=173.68

Fig. 3. Optimization results of the cantilever beam

Change mesh generation to 120×40, the total number of the elements is 4800. Analysis the solving effectiveness through test, compared PDOC with OC method, which is shown in Fig.3, and the corresponding compliance evolution curve can be seen in Fig.4. From the results, the solving process is relatively stable when the PDOC method is adopted. It is close to the optimal value 173.68 which just need only ten steps of iteration, and the cost of each step is 13.673s. However, it will take 20 steps by use of the OC method, and the cost will be 13.452s by each step. Considering the optimal process, the PDOC method converges easier and faster than the OC method, it can

accelerate the convergence. Meanwhile, we can get a more stiffness structure by PDOC method, compared with the OC method .It can be shown that PDOC has a more efficient search capabilities.

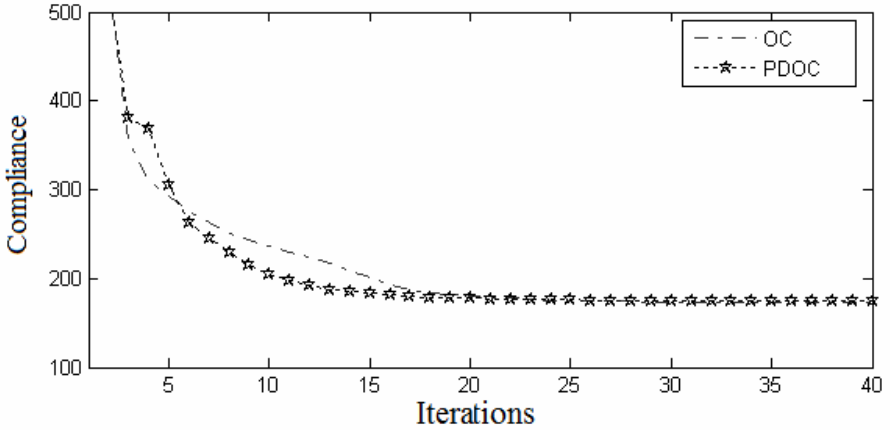

Fig. 4. Comparison of compliance evolution curve

3.2 Flexible Displacement Inverter

Flexible composition is a kind of mechanical structure, which is designed to input load and then generate movement at the output end. Flexible composition belongs to multi-objective design problem, and the two objective functions to be optimized are MSE(Mutual Strain Energy)and SE(Strain Energy)[7].

Now we study topology optimization of displacement inverter to verify the performance of PDOC, and study the objective of topology optimization is to maximize MSE and minimize SE separately. The volume ratio of design is 30%, and its design size is 80um×80um, as shown in Fig.8. We can select the upper part of design domain to analyze because of its symmetry, and there are 80 × 40 meshes distributing uniformly in this part. Elastic modulus is 1MPa, and Poisson ratio is 0.3, input driving force $f_{in} = 0.5mN$. A spring with stiffness $K_{in} = 1$is fixed at the input end, so input energy can be represented by input driving force and the stiffness of spring. Simultaneously, a spring with stiffness $K_{out} = 1$is fixed at the output end to simulate the force from workpiece to composition.

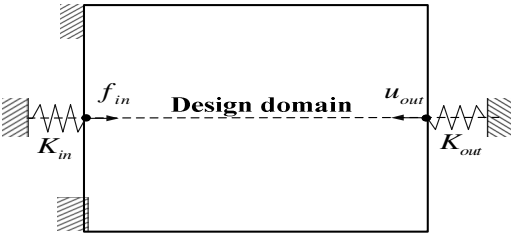

Fig. 5. Design domain of displacement inverter

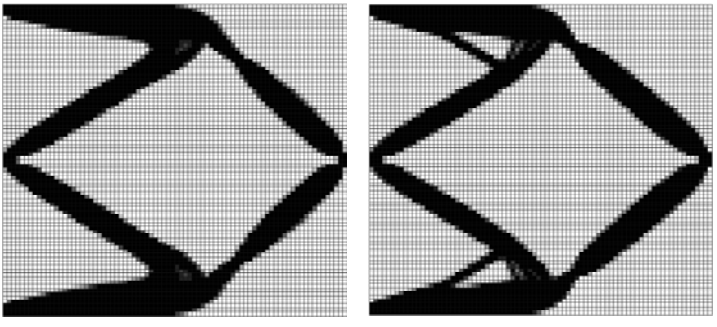

Fig. 6. The inverter solution of beam displacement

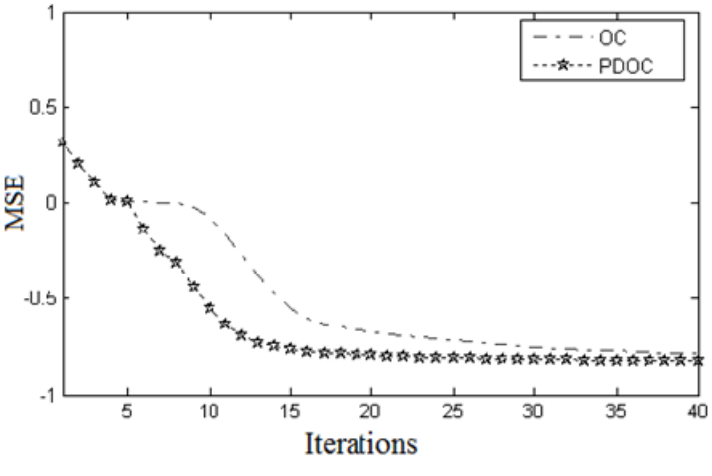

Fig. 7. MSE evolution of the displacement curves of the inverter figure

The results are illustrated in Fig.9 and MSE evolution curve is shown in Fig.10.And it is apparent that process of solution is stable when using PDOC method. And after 15

iterations, it can be close to the optimal value MSE=0.82145 with 9.876 seconds consumed per iteration. while using OC method (a=0), it required probably 40 iterations to gain the optimal value MSE=0.78946, and 9.435 seconds are cost per iteration. Comparing with the process of optimization, PDOC method is better than OC method because of faster convergence. From the optimization results, PDOC method can obtain structures with more rigidity than OC method. Therefore, PDOC method can be applied effectively in practice to solve multi-objective topology optimization problem.

4 Conclusions

In this paper, a new topology optimization method is proposed, and it improves iteration operator by introducing the idea of PD control theory. With some examples tested, this method can construct a more reasonable iteration formula to accelerate the convergence and computing speed, and it has more efficient search capability than OC method. Meanwhile, this method can find a more stiffness structure, and the effectiveness of PDOC method for solving multi-objective topology optimization problem is verified.

Acknowledgment

This research work is supported by the Natural Science Foundation of China under grant No. 50705032, the New Century Excellent Talents in University under Grant no.NCET-08-0232, and the Hi-Tech Research and Development Program of China under grant No. 2007AA04Z120 (863 Program).

References

1. Zhou, M., Ozvany, G.I.N.: The COC algorithm, Part II: Topological geometrical and generalized shape optimization. Computer Methods in Applied Mechanics and Engineering 89, 197–224 (1991)
2. Levy, R., Lavan, O.: Fully stressed design of passive controllers in framed structures for seismic loadings. Structural and Multidisciplinary Optimization 32, 485–498 (2006)
3. Meske, R., Lauber, B., Schnack, E.: A new optimality criteria method for shape optimization of natural frequency problems. Structural and multidisciplinary optimization 31, 135–140 (2006)
4. Logo, J.: New type of optimality criteria method in case of probabilistic loading conditions. Structural and multidisciplinary optimization 35, 147–162 (2007)
5. Chiandussi, G., Codegone, M., Ferrero, S.: Topology optimization with optimality criteria and transmissible loads. Computers and Mathematics with Applications 57, 772–788 (2009)
6. Rietz, A.: Sufficiency of a finite exponent in SIMP (power law) method. Structural and Multidiscipline Optimization 21, 159–163 (2001)
7. Frecker, M., Ananthasuresh, G.K., Nishiwaki, S., Kikuchi, N., Kota, S.: Topological synthesis of compliant mechanisms using multi-criteria optimization. Mech. Des. Trans. ASME 119, 238–245 (1997)

A Decision Support System Based on GIS for Grain Logistics Vehicle Routing Problem

Zhanbiao Bao[1], Jianjun Wu[2], Tong Zhen[2], and Hongyi Ge[2]

[1] Modern Education Technology Center, Henan university of Economics and law
Zhengzhou 450002, China
[2] College of Information Science and Engineering, Henan University of Technology,
Zhengzhou 450001, China
baozhanbiao@126.com

Abstract. Grain logistics Vehicle Routing Problem (VRP) is the one of important problems in the research fields of grain logistics, which represents a problem of finding the optimal route used by a group of vehicles when serving a group of required grain depots. In this paper, we present a Decision Support System (DSS), which help decision-makers to carry out duties. To be most effective, a DSS should be integrated with a geographic information system (GIS), which provides analysis for the problems that helps users of the DSS to visualize the situation. In the system, the data of the required depots, the depot center, and the topologies of the roads are stored and managed by GIS, and a particle swarm optimization method (PSO) is employed to provide the routings of the vehicles. The prototype system has illustrated the effectiveness and feasibility of the DSS using real-world data and showed potentials for grain logistics VRP.

Keywords: Decision Support System, GIS, Grain Logistics.

1 Introduction

Grain safety is the basic safeguard as to human being's survival and development, and grain logistics is very important in achieving the goal of grain safety, at the same time, grain logistics is also the important component of the logistics system for agricultural products. Grain logistics and transportation account for a large portion of the economies of our country. Nowadays, it is lack of technologies to construct our grain logistics system; there are no grain circulation management database and the decision method for grain logistics route planning analysis. Governments and grain logistics companies focus their attention on developing DSS that could aid grain logistics managers to lower costs and achieve greater flexibility. Therefore, research and development grain logistics decision support system based on GIS is an urgent matter.

In grain logistics system, a lot of attention has been given to the problem of determining efficient vehicle routes within a given district. However, more significant cost savings can be achieved if the borders of the districts are optimally determined. Although VRP is widely studied, the studies are limited to the objectives. In particular, it

D.-S. Huang et al. (Eds.): ICIC 2010, LNCS 6215, pp. 564–570, 2010.

is assumed that all limiting conditions are given and the objectives are concrete, such as the total cost or total length.

Geographic information system (GIS) [1] is a technological field that incorporates geographical features with tabular data in order to map, analyze, and assess real-world problems. The key word to this technology is Geography, which means that the data is spatial, in other words, data that is in some way referenced to locations on the earth. Coupled with this data is usually tabular data known as attribute data. Attribute data can be generally defined as additional information about each of the spatial features. An example of this would be grain depot. The actual location of the grain depot is the spatial data. Additional data such as the grain depot name, capacity of grain depot, grain variety would make up the attribute data. It is the partnership of these two data types that enables GIS to be such an effective problem solving tool through spatial analysis or the analysis of vehicle routes.

2 The Model

Determining the optimal route used by a group of vehicles when serving a group of depots represents a Vehicle Routing Problem (VRP) [2]. The vehicles start from the center depot and to reach the required depot they operate on the traffic routes. The solution of the problem is represented by a set of routes. Each route has a starting and the end point at the depot. The objective is to keep the overall transport expenditure at a minimum and all constraints satisfied.

In practice, the basic vehicle routing problem is extended with constraints, for instance, the extended classes of VRP are Capacitated VRP (CVRP), Distance Constrained VRP (DVRP), Distance Constrained Capacitated VRP (DCVRP), VRP with Time Windows (VRPTW), Pickup and Delivery VRP (VRPPD), and Simultaneous Pickup and Delivery VRP (VRPSPD).Fig. 1shows the classification of VRP.The main goal in all VRP problems is to obtain the minimal total cost.

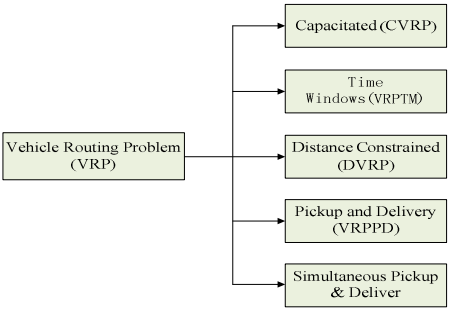

Fig. 1. Classification of VRP, the basic VRP is divided into CVRP, DVRP, VRPTM, etc.

Grain logistics VRP [3] can be briefly described as a set of N required depot with known demands di, that have to be served from a central grain depot with a fleet of t delivery trucks of known capacity Q. Normally, the objective is to minimize the total distance traveled by the truck fleet, but it is also common to minimize route costs.

Given the previous problem statement, the model used for solving the grain logistics VRP is explained below.

Parameters:

Q is capacity of the vehicle;

N is number of required depots;

q_i is the demand of required depot i;

D_k is the maximum travel distance;

t_{ij} represents the travel time between required depot i and j;

C_{ij} is the distance between required depot i and j;

Variables:

$$x_{ijk} = \begin{cases} 1, & \text{vehicle from i to j} \\ 0, & \text{others} \end{cases}$$

$$y_{ik} = \begin{cases} 1, & \text{required depot serviced vehicle k} \\ 0, & \text{others} \end{cases}$$

Where $ij \in (0,1,2,...,N)$ being 0 the central depot.

Objective function:

$$\min Z = \sum_I \sum_J \sum_K c_{ij} x_{ijk} . \tag{1}$$

$$s.t. \sum_i q_i y_{ik} \le q_k . \tag{2}$$

$$\sum_k y_{ik} = 1 . \tag{3}$$

$$\sum_i x_{ijk} = y_{jk} . \tag{4}$$

$$\sum_j x_{ijk} = y_{ik} . \tag{5}$$

$$x_{ijk} = 0 or 1, \quad i, j=0, 1, \cdots, n; \forall k. \tag{6}$$

$$y_{ik} = 0 or 1, \quad i, j=0, 1, \cdots, n; \forall k. \tag{7}$$

We can see that the objective function (1) is minimizing the total distance traveled. Where Constraints (2) ensure that the demand of every required depot is at most a vehicle of capacity Q; Constraints (3) ensure that each required depot is served exactly once; Constraints (4) and (5) ensure that every required depot is visited by a truck and that every truck leaves each depot; Constraints (6), (7) ensure that the variable only

takes the integer 0 or 1; In a word, the ultimate optimization goal is to minimize the total travel distance and the sum of travel time.

3 PSO Algorithm for Grain Logistics VRP

3.1 Particle Swarm Optimization Algorithm

Particle swarm optimization (PSO) algorithm, originally proposed by Dr. Eberhart and Dr. Kennedy in 1995[4], has come to be widely used in computer science. PSO shares many similarities with evolutionary computation techniques such as Genetic Algorithms (GA). The mathematical expression of Particle Swarm Optimization (PSO) algorithm as follows [5]:

Each particle is regarded as a point in a D-dimensional. The position of a particle corresponds to a candidate solution of the considered optimization problem. At any time, Pi has a position, which is represented as X_{it}= （x_{il}, x_{i2}…x_{iD}) and a velocity V_{it}= （v_{i1}, v_{i2}…v_{iD}) associated to it, these particles fly through hyperspace and have two essential reasoning capabilities: their memory of their own best position and knowledge of the global or their neighborhood's best. The particle position and velocity update equations in the simplest form are given by:

$$V_{id}(t+1) = w*V_{id}(t) + c_1 * rand()[P_{id} - X_{id}(t)] + c_2 * rand()[g_{id} - X_{id}(t)] \cdot \quad (8)$$

$$X_{id}(t+1) = X_{id}(t) + V_{id}(t+1) \quad 1 \le i \le n \quad 1 \le d \le D \quad (9)$$

Where w is the inertia weight; V_{id} is the velocity of particle i, X_{id} is the particle position, p_{id} is the current position of particle; c_1, c_2 are the two positive constants, called acceleration parameters; rand () is the random functions in the range[0,1]; The position of particles are restricted in interval[- $X_{\max d}$, $X_{\max d}$],while the velocity of particles are restricted in interval [- $V_{\max d}$, $V_{\max d}$] in the d-dimensional (1≤d≤D). The initial position and velocity are randomly generated, then used to iterate by formula (8), (9), until to meet the end of conditional expression of iteration.

3.2 Algorithm Implementation

Set constants $iter_{\max}$, w_{int}, w_{end}. The initialization process of swarm as follows:

Step1. Parameter setting: acceleration factor c_1, c_2, inertia weight w, the size of the population is m;

Step2. Initialize the swarm

(i)each particle position vector X take real integer in the range[1, L+K-1(required depot number+ vehicle number-1)], each particle velocity vector V take real number in the range [-(L+K-2), (L+K-2)] randomly;

(ii) Use adjustment function Adjust () to adjust all particles;

(iii) Calculate the initial evaluation values of each particle;

Step3. Repeat the following steps, until the end condition appears or the stopping criterion is satisfied

(i) each particle , update the position and the velocity vector according to the formula(8)and (9); if the value X, V exceed the boundary range, set the boundary value;

(ii) Use adjustment function adjust () to adjust all particles;

(iii) Evaluate the fitness values of all particles for new searching point with evaluation function;

(iv) Every particle finds its local best, if evaluated value of each particle is better than best history $pBest$ then set to $pBest$;

(v) Search for the best evaluated value of subgroup and swarm, if better, update the $pBest_l$ in the subgroup and $pBest_g$ among the swarm.

Step4. Output the best optimal solution, if more than one, set one solution randomly.

4 Decision Support System

Decision support systems (DSS) are broadly defined computer-based information systems that support decision-making activities. Once the PSO algorithm and the model proved to work, then we should put it all together under the software application, so the logistics manager at the logistics company could use it. We develop a DSS for solving the grain logistics VRP.

4.1 Architecture of the DSS

The solution process with the DSS can be explained as follows: the solution is based on the required depot data and a professional GIS based system [6]. The grain logistics VRP is modeled and the optimal solutions are searched by PSO. Logistics manager use the GIS based DSS to choose the optimal partitions and make decisions. Fig. 2 shows the architecture of the DSS.

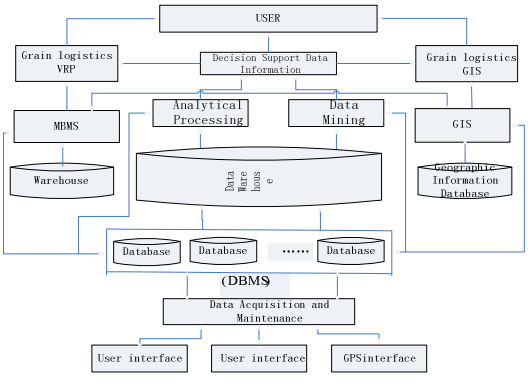

Fig. 2. The architecture of the DSS, the model base is the core part. Developed from traditional grain logistics MIS, grain logistics DSS is an information system to help people make decisions by the core part of model base.

4.2 Analyses of Examples

For VRP problem, computational experiment was carried out on the following instance in the literature [8]: 7 required depots are serviced by 3 vehicles, each with the capacity is 10t, the central depot is 0, and The objective of optimization is to minimize objective functions subject to certain constraints, that is, the reasonable vehicle route is arranged in order to reduce the total cost and distance. The coordinate and the demand of each depot are given in Table 1.

Table 1. The coordinate and the demands

Depot number	Position coordinates	Demands（ton）
0	（18, 54）	—
1	（22, 60）	8.9
2	（58, 69）	1.4
3	（71, 71）	2.8
4	（83, 46）	3.3
5	（91, 39）	2.1
6	（24, 42）	4.1
7	（18, 40）	5.7

The proposed PSO algorithm was used for solving the above problem, set parameters as: swarm size m = 40, c_1 = c_2 =1.49445, w =0.729, $iter_{\max}$ =200. After running the program, we get the results of VRP problem: the minimum distance $\min Z$ =217.813, the corresponding optimal route is: 0→7→6→0, 0→1→0, 0→2→3→4→5→0. The results show the effect of the proposed algorithm.

5 Conclusion

In the present paper, we aimed at solving grain logistics VRP by providing a DSS tool for effective decision making. DSS was designed for grain logistics management, which help user emphasize maximization of grain quality, minimization of vehicle route and cost of the whole system. Simulation results show that the pso algorithm is efficient for grain logistics VRP. The DSS is an effective tool to manage grain logistics, applying GIS to the grain logistics DSS, which can realize visualization management, improve the efficiency of logistics and distribution.

Acknowledgments. This work is partially supported by The 11th Five Years Key Programs for Science and Technology Development of China (No.2008BADA8B03, No. 2006BAD08B01), Henan Program for New Century Excellent Talents in University (No. 2006HANCET-15).

References

1. Kawano, H., Ishii, Y., Komoto, I., Hasegawa, T.: GIS visualization and analysis of traffic flows: Congestion patterns in hanshin expressway data warehouse. In: Proc.of International Conference on Systems Science, Poland, pp. 121–128 (2007)
2. Angelelli, A., Speranza, M.G.: The application of a vehicle routing model to a waste-collection problem: Two Case Studies. Journal of the Operational Research Society 53, 944–952 (2002)
3. Zhen, T., Ge, H.Y., Jiang, Y.Y.: Research on particle swarm optimization for grain logistics vehicle routing problem. In: Proceedings-IITA International Conference on Services Science, Management and Engineering, SSME 2009, pp. 274–277 (2009)
4. Eberhart, R.C., Shi, Y.: Particle swarm optimization: Developments, applications and resources. In: Proc. Congress on Evolutionary Computation, pp. 81–86. IEEE Press, Piscataway (2001)
5. Schutte, J.F., Fregly, B.J.: A parallel particle swarm optimizer. In: Proc. 5th World Congress of Structural and Multidisciplinary Optimization, pp. 19–23. Venice, Italy (2003)
6. Tominaga, T., Sadahiro, Y.: Evaluation of school family system using GIS. Geographical Review of Japan, Series A 76, 743–758 (2003)
7. Lück, I., Schäfer, C., Krumm, H.: Model-based tool-assistance for packet-filter design. In: Sloman, M., Lobo, J., Lupu, E.C. (eds.) POLICY 2001. LNCS, vol. 1995, pp. 120–136. Springer, Heidelberg (2001)
8. Fu, Z., Eglese, R., Li: A new tabu search heuristic for the open vehicle routing problem. Journal of the Operational Research Society 57, 267–274 (2005)
9. Tarantilis, C., Ioannou, G., Kiranoudis, C.: A threshold accepting approach to the open vehicle routing problem. RAIRO Operations Research 38, 345–360 (2004)

On Database Normalization Using User Interface Normal Form

Mohd Zainuri Saringat[1], Rosziati Ibrahim[1], Noraini Ibrahim[1], and Tutut Herawan[2]

[1] Faculty of Information Technology and Multimedia
Universiti Tun Hussein Onn Malaysia,
Parit Raja, Batu Pahat, 86400, Johor, Malaysia
{zainuri,rosziati,noraini}@uthm.edu.my
[2] Department of Mathematics Eduction
Universitas Ahmad Dahlan, Yogyakarta 55166, Indonesia
tutut81@uad.ac.id

Abstract. Database is important to ensure the data can be store, update and retrieve back. The famous data modelling using the Entity Relationship Model already introduced more than thirty years. However, designing a good database is still a big issue especially in designing optimum database because it is very hard to do consistency checking between system design and database design to fulfil user needs. In this paper, we propose an alternative method for designing optimum database system based on object oriented methodology. The schema table is extracted from class diagram and then the schema will be compared with the user interface to normalize the structure. Data sanitization is introduced to remove the unused attributes to provide final schema table.

Keywords: Database, Class Diagram, Object Oriented, Schema Table.

1 Introduction

In modern society, millions of peoples in all over the world are use internet for many purposes. All the relevant information must be store and manage with a good manner to ensure the data can be shared and retrieved back. In producing a system, there are four fundamental software activities such as specification, development, validation and evolution [1]. In software development, software design is to show the logic of the system and database design is to describe the flow of data [2]. There are two famous modelling approaches where is the first approaches is also knows as functional, procedural and imperative [3]. This technique used Data Flow Diagrams (DFD) for designing the system. Meanwhile, the database design is shown by using the Entity Relationship Diagram (ERD). The second approach is object-oriented technique which is using Unified Modelling Language (UML) that consists of thirteen notations [4-5]. Normally, class diagram is used to design the database because these diagram representing the semantic data [1]. Using object oriented methodology, there are two famous ways on how people establish the database. The first technique is the class diagram is transferred to the appropriate tables by considering the class behaviours [6]. However, this technique is not mature and lead to data redundancy. Many researchers

D.-S. Huang et al. (Eds.): ICIC 2010, LNCS 6215, pp. 571–578, 2010.

have given the suggestion to consider the normalization principle in this approach [6-9]. Other famous approach is hybrid technique, which is using UML in system design and ERD with applying normalization concept in constructing the database. Unfortunately, there is lack of integrity checking from system design to database design. Furthermore, the technique will produce many relational tables and cause time consuming in accessing and updating process.

Therefore in this paper, we propose a technique to design the schema table by using class diagram. The schema will be compare with the user interface for normalization and data sanitization to produce an optimum schema. The proposed technique provides the tables at least in Third Normal Form and follows with the recommendation by Connolly and Begg [10]. Using this technique, we can make sure the continuous process from system design until creating database is applied. Furthermore the normalization technique using interface will not drop the accessing time. The rest of the paper is organized as follows; Section 2 presents the related work. Section 3 discusses the framework of this research. We give an example in section 4. Finally, our research conclusion is described in section 5.

2 Related Work

Data is very important because it can be process to generate information for users to make decision and future plan. Major problem in make decision when the data is not accurate [12]. There are two ways how software engineer establish the database which are relational database and object oriented database.

The relational data model concept was introduced by Codd in 1970 [12]. A relational database is collection of tables. To avoid redundancy in the tables, many well know researchers such as Codd, Boyce and Fargin have given the idea to overcome the issues in [2], [4] and [6]. However, the drawback of this normalize form is the higher normal form are applied; the less vulnerable to update anomalies but the number of tables will be increasing. It will drown the accessing time and make the process updating and accessing more complex as well as the programming it self.

Object Oriented Database is a database that store the information based in the form of object. It has been defined around 1990s. The ideas of object oriented are to cover three main activities in software development which are software design, database design and programming capabilities. This technique can improve the accuracy because consistency checking from design to programming can be done. However, it has lack of considering anomaly and lead to be storing redundancy data. It have leads many opportunity in research. A research done by Hadj *et al*. [7] on their paper revealed types of constraints for well-formed conceptual model to produce database from UML class diagram. Alsaadi [8] in his paper wrote that class diagram can be used to produce a schema for system database. He discussed how to check the data structure or data integrities relating to database system using sequence diagram. He *et al*. [9] did a research for designing and building a multimedia database. They proposed an idea to convert the class to schema class declarations using Object Definition Language. Meanwhile, Boufares and Bennaceur wrote on their paper about consistency problems in cardinality constraints [13]. They have discuss on the problems occurred and the suggestion method to solve its.

In related work, we found that many researchers work on data integrity or quality in UML diagram especially in designing system [7-9], [11], [13]. A few of them discussed the idea of extracting schema table from class diagram using OCL [7], [9]. However in our research, we propose an alternative way to produce optimum database with considering semantic data in class diagram, user interface and data sanitization to remove unused attributes. It believed to have improvement in reducing redundancy data and remain the faster accessing time using object oriented technique.

3 The Framework of User Interface Normal Form (UINF)

In this research, we will focus on the class diagram to create schema table. Then, the attributes at the schema table will be comparing with the fields in the user interface. The user interface normalization technique (UNIF) is a process to reorganise the table according the number of accessing the attributes. After UINF process is done, data sanitization process will be applied to remove the attributes which is not retrieve in user interface. The architecture of this research has been illustrated in figure 1, where it shows the process to produce optima schema table.

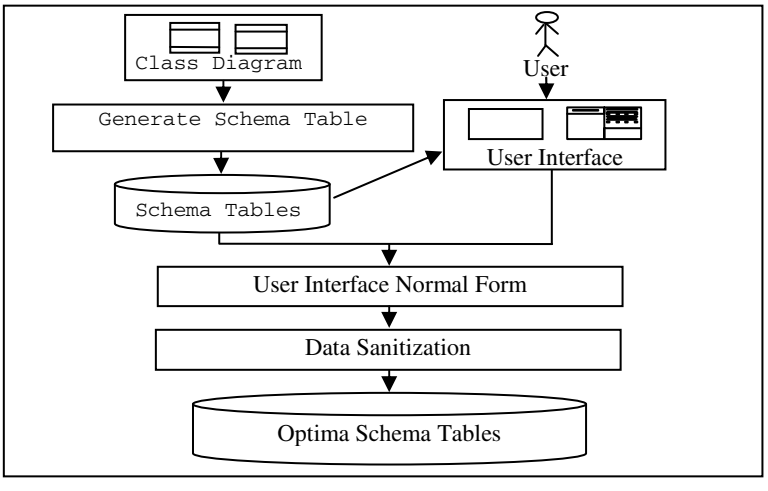

Fig. 1. User Interface Normal Form

3.1 Generate Schema Table Based on Class Behaviours

Transferring process from class diagram to schema table is based on relationships and the behaviours of the classes in class diagram. However in one class diagram, not all criteria will apply concurrently depending on the user requirements and the system needs.

3.2 User Interface

An interface is defined as a point of interaction between two systems. It is referring the place to allow the user to store and retrieve data from the database. This user can

choose from the available attributes from the schema tables. If the user realizes that the attributes in schema tables in not complete or request for adding attributes. The process activities must be come back to the requirements phase. The number of the interface is depending on the user needs. Each interface will be evaluated in User Interface Normal Form (UINF) technique to regroup the tables' structure.

3.3 User Interface Normal Form (UINF)

In the next step, the schema table and user interface are used to perform normalization process. This process will compare the attributes in schema table with the fields in user interface. The tables will be regrouping base on the number of accessing with following the below rules.

3.3.1 Rules of UINF

This section summarizes the rules for modelling the database.

Definition 1. *A schema table, S consists of tables T, where each table consists of at least 2 or more attributes, i.e.,*

$$S = \{T_i\},\ 1 \le i \le n,\ \forall T, \text{card}|T| \ge 2.$$

Definition 2. *User interface, U consists of finite interfaces* $U = \{U_1, U_2, U_3, \ldots, U_m\}$, *where each interfaces contains fields, f i.e., an information that users want to accesses from tables.*

Definition 3. *User Interface Normal Form (UINF) consists of*

a. Schema table, $S = \{T_1, T_2, T_3, \ldots, T_n\}$

b. User interface, $U = \{U_1, U_2, U_3, \ldots, U_m\}$

The Rules of UINF are described as follow.

a. Get the number of intersection between attributes in the tables with fields in interfaces.
   i. The fields in the user interface, *U* will be calculated to get the number of intersection with the attributes in the schema table, *S*, i.e.,
   $$T_j \bigcap U_i, \text{ where } 1 \le j \le m,\ 1 \le i \le n. \quad (1)$$
   ii. From (1), choose the maximum number of such intersection,
   $$M = \max\{T_j \bigcap U_i\}, \text{ where } 1 \le j \le m,\ 1 \le i \le n. \quad (2)$$
   iii. The maximum number in (2) will be divided by two, this is due to lessen the complexity of accessing.
   $$M/2 \quad (3)$$
   iv. Compose the table into two, where the first table contains all attributes which is greater from (3) and the remainder will be contained in table 2.
   $$S_{\text{final}} = \{T_i\}, 1 \le i \le 2,\ \text{card}|T_1| \ge \tfrac{M}{2}, \text{card}|T_2| < \tfrac{M}{2}.$$

b. Get the intersection among the user interfaces.
   i. In case of $U_n \bigcap U_m = U_n$, the table that referring to U_n and U_m will be ignored.
   ii. In case of $U_n \bigcap U_m \neq U_n$ or U_m, two table will be created. The first table contains all fields in $U_n \bigcap U_m$, where the second table contain all fields in $(U_n \bigcup U_m) - (U_n \bigcap U_m)$.

3.4 Data Sanitization

Comparing the attributes in the schema table with the fields in the interface will give the result as zero and non-zero. Zero value means that the users are not interesting with the attributes in schema tables for this moment. Here, data sanitization is the process to remove the zero value. The data sanitization is given as follow.

Definition 4. *Let* $T_i \in S$ *and* $U_i \in U$ *. The attributes in T will be deleted if*

$$T_j \bigcap U_i = \phi .$$

The deletion will be refers as data sanitization.

4 Example

In this paper, we present an example of an application for student registration subject.

```
The system requirements are the student from Faculty IT must be
register subjects that offer by the university and faculty. Each
subject will be taught by one lecturer. The subjects result will
be appear based on registration.
```

Step 1. Base on the requirements we have classify the information into five types of classes which are subject, subjectOffer, Staff, SubjectRegister and Student. Then, we draw the class diagram to represent the user requirements as in Figure 2.

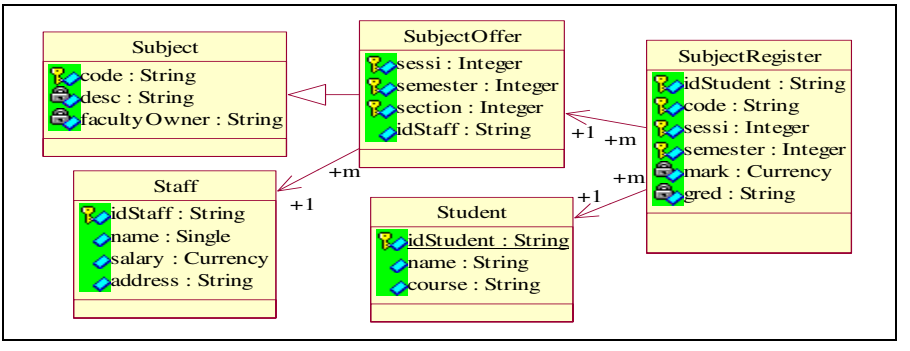

Fig. 2. Class Diagram for Student Registration Subject

Step 2. After drawing class diagram, the schema table will be produce base on class diagram is shown as in Figure 3.

```
Create table Subject                    Create table SubjectRegister
(code char(7), desc char(50),           (idStudent char(7), code char(7),
 facultyOwner char(5),                   sessi int, semester int,
 Primary Key (code);                     section int, mark int,
Create table SubjectOffer                gred char(2),
(code varchar(7), sessi char(6),         Primary Key (idStudent, code,
 semester int, section int,              sessi, semester);
 idStaff char(5),                       Create table Student
 Primary Key (idStudent,code);          (idStudent varchar(7),
Create table Staff                       name varchar(50),
(idStaff char(7), name char(50),         course varchar(3),
 salary float(5,2), address              Primary Key (idStudent);
 char(50), Primary Key (idStaff);
```

Fig. 3. Schema Table

Step 3. The sample user interfaces are shown in Figure 4, Figure 5, Figure 6 and Figure 7.

Registration Subjects

No Student: AQ98203 Name: Ahmad Ali Session/semester 2009/10-1

No.	Subject	Credit
1	Computer Programming	3
2	English Communications	1
3	Asian Culture	3
4	Discrete Math	3
5	Introduction to IT	3

Fig. 4. Interface of Registration Subjects

Result Students

No Student: AQ98203 Name: Ahmad Ali Session/semester 2009/10-1

No.	Subject	Marks
1	Computer Programming	67
2	English Communications	51
3	Asian Culture	73
4	Discrete Math	83
5	Introduction to IT	53

Fig. 5. Interface of Result Students

Staff

No Staff: 00218
Name : Sulaiman Yusof
Salary : RM 4,300.00

Address : NO. 6 Jln Dedap Parit Raja 86400 Batu Pahat

Fig. 6. Interface of Staff

Subject Marks

Subject Code: 1013 (Computer Programming) Lecturer: PM Dr. Gaus Session/semester: 2009/10-1

No.	Student	Marks	Gred
1	AQ98203	67	B-
2	AQ98213	51	C
3	CQ98201	73	B
4	AQ98204	83	C-
5	AQ98213	53	C
6	CQ98202	86	C+

Fig. 7. Interface of Result Marks

Step 5. The schema table and user interface are used to perform UINF normalization process. This process will compare the attributes in schema table with the fields in user interface such as in Table 1.

Table. 1. Intersection between Interface and Schema Table

Table	Attributes	Interface				Total	Keys
		Register Subjects	Result Students	Staff	Subject Marks		
Subject	code	1	1	0	1	3	PK
	desc	1	1	0	1	3	0
	facultyOffer	0	0	0	0	0	0
Subject Offer	code	1	1	0	1	3	PK
	sessi	1	1	0	1	3	PK
	semester	1	1	0	1	3	PK
	section	1	1	0	1	3	PK
	idStaff	0	0	0	1	1	FK
Staff	idStaff	0	0	1	1	2	PK
	name	0	0	1	1	2	0
	salary	0	0	1	0	1	0
	address	0	0	1	0	1	0
Subject Register	idStudent	1	1	0	1	3	PK
	code	1	1	0	1	3	PK
	sessi	1	1	0	1	3	PK
	semester	1	1	0	1	3	PK
	mark	0	1	0	1	2	0
	gred	0	1	0	1	2	0
Student	idStudent	1	1	0	1	3	PK
	name	1	1	0	1	3	0
	course	0	0	0	0	0	0

Using this alternative technique, we suggest to decompose the Staff table to two table which are at the first table will consists of attributes of idStaff and name, and another one consists of idStaff, salary and address.

Step 6. Based on Table 1, the attributes facultyOffer in table subject and attribute course in table student are removed as the process of data sanitization. The suggestion optimum schema table is shown in figure 8.

```
Create table Subject
   (code char(7), desc char(50),
 facultyOwner char(5),
 Primary Key (code);
Create table SubjectOffer
 (code char(7), sessi char(6),
 semester int, section int,
 idStaff char(5),
 Primary Key (idStudent,code);
Create table StaffName
 (idStaff char(7), name char(50),
 Primary Key (idStaff);
Create table StaffSalary
 (idStaff char(7), salary
  float(5,2), address char(50),
  Primary Key (idStaff);
Create table SubjectRegister
 (idStudent char(7), code char(7),
 sessi int, semester int,
 section int, mark int, gred
 char(2),
 Primary Key (idStudent, code,
 sessi, semester);
Create table Student
 (idStudent char(7), name
 char(50),
 course char(3),
 Primary Key (idStudent);
```

Fig. 8. Suggestion Optima Schema Table

5 Conclusion

Object oriented is the well known methodology that using UML to show the user requirements. With this motivation, we have proposed the alternative technique to transferring class diagram to schema table base on behaviour in class diagram. The UNIF is the suggestion idea to creating the tables is based on the user views to achieve minimum accessing time and data sanitization is complement technique to optimum database usage. This alternative technique provide the idea of data consistency checking from system design to database design and the idea to removing the garbage data from the storage for better performing in our database.

References

1. Sommerville, I.: Software Engineering, 8th edn. Pearson, Singapore (2007)
2. Elmasri, R., Navathe, S.: Fundamentals of Database Systems, 4th edn. Pearson, Singapore (2004)
3. Maciaszek, L.A.: Requirements Analysis and System Design, 3rd edn. Pearson, Singapore (2004)
4. Chonoles, M.J., Schardt, J.A.: UML 2 for Dummies. Wiley, Indianapolis (2003)
5. Dobing, B., Parsons, J.: Dimensions of UML Diagram Use: A survey of Practitioners. Journal of Database Management 19, 1–18 (2008)
6. Fitsilis, P., Gerogiannis, V., Kameas, A., Pavlides, G.: Producing Relational Database Schemata from an Object Oriented. In: Proceedings of the 20th EUROMICRO Conference On System Architecture and Integration EUROMICRO 1994, pp. 251–257 (1994)
7. Hadj, A.B., Boufares, F., Abdellatif, A.: Checking Constraints Consistency in UML class diagrams. In: Information and Communication Technologies (ICTTA 2006), vol. 2, pp. 3599–3604 (2006)
8. Alsaadi, A.: Checking Data Integrity Via The UML Class Diagram. In: International Conference on Software Engineering Advances (ICSEA 2006), pp. 37–46. IEEE Computer Society, Los Alamitos (2006)
9. He, Y.L., Ying, Z.L., Zhang, Y.W.: The Design and Implementation of a Multimedia Database with Object Oriented Analysis and Design Method. In: 6th International Conference 9 (ICSP 2002), pp. 1035–1038 (2002)
10. Connolly, T., Begg, C.: Database Systems, 4th edn. Pearson, England (2005)
11. Zhu, B., Shanker, G., Cai, Y.: Integrating Data Quality into Decision-Making Process: An Information Visualization Approach. In: Smith, M.J., Salvendy, G. (eds.) HCII 2007. LNCS, Vol. 4557, pp. 366–369. Springer, Heidelberg (2007)
12. Codd, E.F.: Further Normalization of the Database Relational Model. In: Data base System, pp. 33–64. Prentice Hall, Englewood Cliffs (1972)
13. Boufares, F., Bennaceur, H.: Consistency Problem in ER-schemas for Database Systems. Information Sciences, 263–274 (2003)

Improved Particle Swarm Optimizers with Application on Constrained Portfolio Selection

Li Li[1], Bing Xue[1], Lijing Tan[2], and Ben Niu[1,3,*]

[1] College of Management, Shenzhen University, Shenzhen 518060, China
[2] Measurement Specialties Inc Shenzhen 518107, China
[3] Hefei Institute of Intelligent Machines, Chinese Academy of Sciences, Hefei 230031, China
drniuben@gmail.com

Abstract. Inertia weight is one of the most important adjustable parameters of particle swarm optimization (PSO). The proper selection of inertia weight can prove a right balance between global search and local search. In this paper, a novel PSOs with non-linear inertia weight based on the arc tangent function is provided. The performance of the proposed PSO models are compared with standard PSO with linearly-decrease inertia weight using four benchmark functions. The experimental results demonstrate that our proposed PSO models are better than standard PSO in terms of convergence rate and solution precision. The proposed novel PSOs are also used to solve an improved portfolio optimization model with complex constraints and the primary results demonstrate their effectiveness.

Keywords: Particle swarm optimization, inertia weight, arc tangent function, portfolio optimization.

1 Introduction

Particle swarm optimization (PSO) [1, 2] is a population-based global optimization method proposed by Kennedy and Eberhart, which is motivated by the group organism behavior such as bee swarm and bird flock. Compared with other evolutionary computation techniques such as genetic algorithms (GA), PSO is easy in implementation and there are few parameters to adjust, and it has faster convergence rate [3-6]. PSO has been successfully applied in science and engineering [7, 8].

As a new algorithm, PSO still has many disadvantages. For instance, it shows significant performance in initial iterations, however, the particles are more and more familiar and the swarm loses its diversity along with the developing of the computation. So there may be premature convergence and it is hard to escape the local optimum. There are few parameters to adjust in the PSO, and the inertia weight is the most important one [9, 10], and lots of investigations have been undertaken to provide the improved ways of the inertia weight to enhance the performance of PSO, including the linearly-decrease inertia weight (LIW) [11], the nonlinearly-decrease

* Corresponding author.

D.-S. Huang et al. (Eds.): ICIC 2010, LNCS 6215, pp. 579–586, 2010.

inertia weight (NIW) [12], the random inertia weight (RIW) [13], etc. In this paper, a new non-linear strategy on the inertia weight is proposed. To illustrate the effectiveness and performance of the strategy for optimization problems, a set of four benchmark functions and an improved portfolio optimization model are used.

2 Standard Particle Swarm Optimization

In PSO, each potential solution is called a bird or particle with no weight and no volume. The *i*th particle flies in the n dimension search space to find the optimization. There is a vector $x_i = (x_{i1}, x_{i2} \ldots\ldots, x_{in})$ presenting the position of the *i*th particle, where $x_{id} \in [l_d, u_d]$, $d \in [1, n]$, l_d, u_d are the lower and upper bounds of the *d*th dimension. The velocity for the *i*th particle is represented as $v_i = (v_{i1}, v_{i2}, \ldots\ldots, v_{in})$, which controls the distance and the direction Moreover, the best previous position of the *i*th particle is individual best called *Pbest*. The best one of all the *Pbest* is colonial best called *Gbest* denoting the best previous position of the swarm. The algorithm searches for the optimization by updating generations according to the following formulas:

$$V_{id}(t+1) = wV_{id}(t) + c_1 \cdot rand() \cdot (p_{id} - x_{id}(t)) + c_2 \cdot rand() \cdot (p_{gd} - x_{id}(t)), \tag{1}$$

$$x_i(t+1) = x_i(t) + V_i(t+1), \tag{2}$$

where t means that algorithm is going on the *t*th generation. c_1 and c_2 are set to constant value, which are normally taken as 2. $rand()$ is random value, uniformly distributed in [0, 1]. p_{id} presents the *Pbest* while p_{gd} presents the *Gbest.* w is inertia weight.

3 Novel Non-linear Inertia Weight PSO

Based on the researches on w, it has been proved there will be a faster convergence rate with a larger w, but the precision of the result can not be guaranteed. While a smaller one can get more precise result, but the convergence rate is too slow and the algorithm may get into the local optimal. So a proper variation of w can improve the performance of PSO. During the previous past studies, we tried to introduce monotone increasing or decreasing strategy to update w.

In the arc tangent function $y = arc\tan(x)$ is an increasing function. however the speed of increase is slower and slower. When the independent variable $x = \pi/2$, the result $y = 1$. According to these features, we can use the tangent function to build a new strategy of the w. After a large scale of experiments, the final equation is:

$$w(t) = (w_{start} - w_{end}) * \arctan(\pi/2 * (1 - (\frac{t}{t_{\max}})^k)) + w_{end}, \tag{3}$$

where w_{start} is the initial value of the w and w_{end} is the final value, which also is the smallest one. $t_{\max}$ is the maximum number of iterations. According to the Equation (3), w is decreasing along with t. The difference is that the speed of decrease is slower in prior period and faster in later period. w is also not too small in later period, so it guarantee the convergence rate in prior period and the exploration in later period.

There is a control variable k, which can control the smoothness of the curve that reflects the relationship between the w and t. The experiments show that: when $k = 0.2$, the function between w and t is convex function. When $k = 1$, it is almost a linear one leaning to convex. When $k = 2$, it is a concave function.

Table 1. Results of the Griewank with different k

t	Mean	Std	t	Mean	Std	t	Mean	Std
0.1	0.0280	0.0280	0.8	0.0287	0.0232	1.5	0.0384	0.0373
0.2	0.0273	0.0256	0.9	0.0304	0.0343	1.6	0.0538	0.0707
0.3	0.0331	0.0251	1.0	0.0262	0.0206	1.7	0.0745	0.0850
0.4	0.0245	0.0202	1.1	0.0453	0.0629	1.8	0.0617	0.0769
0.5	0.0270	0.0232	1.2	0.0352	0.0284	1.9	0.0748	0.1130
0.6	0.0247	0.0243	1.3	0.0292	0.0379	2.0	0.1779	0.2043
0.7	0.0245	0.0251	1.4	0.0354	0.0388			

The experiments about the multimode function Griewank were done to choose the best k confined in [0.1~2.0]. The experimental results (i.e., the mean and the standard deviations of the function values found in 20 runs) are listed in Table 1.

In Table 1, when k is during [0.4~0.7], the mean and the standard deviations of the function values are both stable. So k should be chose during [0.4~0.7]. In the following experiments in this paper ATW is used to represent the improved PSO based on this strategy and k is set as 0.4.

4 Experimental Study

4.1 Test Functions and Parameters Setting

To illustrate performance of our proposed method, four nonlinear benchmark functions that are commonly used in evolutionary computation literature [14-16] were performed, and also compared with that of improved PSO based on a linearly-decrease inertia weight (LIW). The four test functions are listed in Table 2.

In every experiment, the w in the two methods (ATW and LIW) are all during [0.9, 0.4], that is $w_{start} = 0.9$, $w_{end} = 0.4$. $c_1 = c_2 = 2.0$, the population size is 40, the allowable error $\sigma = 1e-80$, and $t_{\max} = 1500$. A total of 50 runs for each experimental setting are conducted.

Table 2. Benchmark functions and parameters setting

Function	Dim	Search space	v_{max}
Sphere	20	(-100,100)	100
Rosenbrock	20	(-30,30)	30
Rastrigrin	20	(-10,10)	10
Griewank	20	(-600,600)	600

4.2 The Result and the Analysis

The results of the four functions are listed in Table 3, the mean relative performance generated by three algorithms are shown in Figs 1-4.

The data in Table 3 show that proposed method (ATW) can obtain more precise results (smaller mean of the function) and the stronger robustness (smaller standard deviations) for all of the four functions than LIW. As seen from the figures, ATW is with the faster convergence rate and able to get the best solution.

The results also indicated that the non-liner inertia weight (ATW) performs better than linear one (LIW).

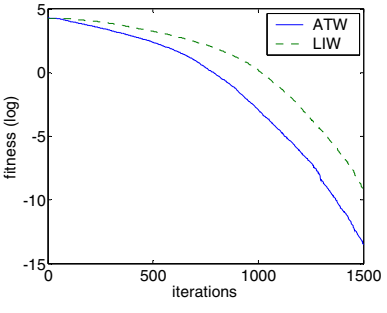

Fig. 1. Sphere function

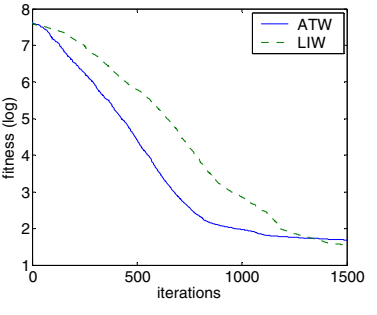

Fig. 2. Rosenbrock function

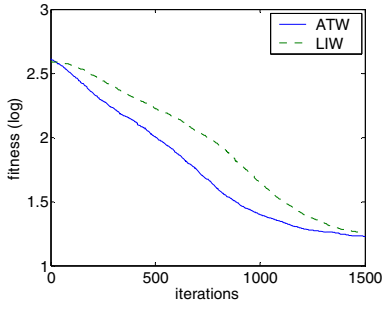

Fig. 3. Rastrigin fuction

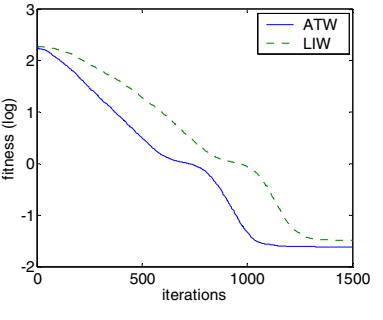

Fig. 4. Griewank function

Table 3. The result for four functions

Function	Algorithm	Max	Min	Std	Mean
Sphere	ATW	5.0653e-013	3.4536e-017	8.0530e-014	3.2708e-014
	LIW	9.7600e-009	4.8377e-012	1.6531e-009	6.8240e-010
Rosenbrock	ATW	248.3628	1.8195	49.6680	48.9274
	LIW	567.3387	4.4772	107.4373	70.1539
Rastrigin	ATW	28.8538	6.9640	5.3089	16.9652
	LIW	33.8585	6.9649	5.8284	18.0666
Griewank	ATW	0.0811	5.7732e-015	0.0205	0.0239
	LIW	0.1052	9.9886e-011	0.0256	0.0328

5 Application on the Portfolio Optimization

5.1 Portfolio Optimization

Modern portfolio analysis started from pioneering research work of Markowitz (1952) [17] who proposed the original mean–variance model. In this paper, based on the original mean-variance model, we present an improved mean–variance model considering the transaction fee produced by selling and buying, and other constraint conditions such as no short sales, the original portfolio owned by the investor. It assumes that an investor allocates his/her wealth among n ($i = 1, \ldots\ldots, n$) assets. Some notations are introduced as follows:

x_i is the proportion of the money used in the ith asset, and $\sum_{i=1}^{n} x_i = 1$. $x_i \geq 0$ means there is no short sales. $x_i^0 \geq 0$ is the original the original portfolio owned by the investor. So when $x_i^0 = 0$, there is no original investment in the ith asset, or it is the new one introdeced in this period. r_i is the yield of the ith asset; $R_i = E(r_i)$ means the expected rate of revenue of the ith asset. $\sigma_{ij} = \mathrm{cov}(r_i, r_j)$ is the covariance of r_i and r_j. k_i^b and k_i^s are the transaction fee when buying and selling the ith asset respectively, which are caculated by proportion. And k_i^s is usuall more than k_i^b. λ is the risk-averse factor, wihch distribute in [0, 1]. Smaller λ represents the investor could bear larger risk.

Based on these defined variables, Our improved portfolio optimization model can be formulated as:

$$\min F(x) = \min\{\lambda \sum_{i=1}^{n}\sum_{i=1}^{n} \sigma_{ij} x_i x_j - (1-\lambda)\sum_{i=1}^{n} R_i x_i - \sum_{i=1}^{n} [\mu \cdot k_i^b \cdot (x_i - x_i^0) + (1-\mu) \cdot k_i^s \cdot (x_i^0 - x_i)]\}$$

$$\begin{cases} \sum_{i=1}^{n} x_i = 1; \\ x_i \geq 0. \end{cases} \quad (4)$$

where $\mu = \begin{cases} 1, \ldots\ldots x_i \geq x_i^0 \\ 0, \ldots\ldots x_i \leq x_i^0 \end{cases}$

5.2 Illustrative Examples

5.2.1 Parameters Representation and Parameters Setting

The position and the velocity of the particle are constructed in the real-number encoding method (see table 4).

Table 4. The encoding of the particle

$x_1, x_2, \ldots\ldots, x_n$	$v_1, v_2, \ldots\ldots, v_n$	F_x
The position of the particle in every dimension	The velocity of the particle in every dimension	The fitness

Five assets are chosed as the sample, which are from different industry and different place. so $n = 5$ .it is assumes that the investor has the same original proportion in every assets, that is $x_i^0 = 0.2$. We set $k_i^b = 0.00065$, $k_i^s = 0.00075$ in the experiment. λ is set as 0.15, 0.65, 0.9 to denote the different kinds investors. In our experimental studies, $w_{start} = 0.9$, $w_{end} = 0.4$. The other parameter $c_1 = c_2 = 2.0$, $k = 0.4$, the swarm size are all 200, and $t_{\max} = 100$. A total of 50 runs for each experimental setting are conducted.

5.2.2 Experimental Results

Numerical results with three different λ obtained by the ATW and LIW are showed in the Table 5. Figs 5-7 present the mean relative performance with different λ generated by the two methods.

The revenue rate and the risk rate, the max value, the min value, the standard deviation and the mean value are summarized in Tables 6. It is obviously that for almost of all the different risk preferences, ATW gets smaller standard deviation and mean value, which demonstrated it outperforms PSO in terms of result robustness and solution quality.

From Figs 5-7, it is clearly found that ATW has quicker convergence rate with LIW in the different situations compared.

Table 5. Numerical results with different λ

	$\lambda = 0.15$		$\lambda = 0.65$		$\lambda = 0.9$	
	ATW	LIW	ATW	LIW	ATW	LIW
Revenue Rate	9.283e-002	8.137e-002	3.058e-002	3.239e-002	1.769e-002	1.200e-002
Risk Rate	1.561e-001	1.062e-001	6.731e-003	7.842e-003	2.409e-003	3.535e-003
Max	-4.840e-002	-4.372e-002	-6.258e-003	-5.578e-003	1.175e-003	3.283e-003
Min	-5.550e-002	-5.324e-002	-6.328e-003	-6.240e-003	3.996e-004	1.182e-003
Mean	-5.307e-002	-4.745e-002	-6.316e-003	-5.9469e-003	6.351e-004	1.967e-003
Std	1.552e-003	2.174e-003	1.869e-005	1.397e-004	2.215e-004	4.735e-004

All the results presented in the tables and figures can proved that the SMPSO could be a more effective way for the investors to solve the portfolio optimizations problems.

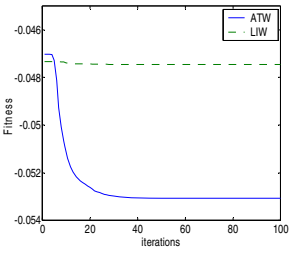

Fig. 5. $\lambda = 0.15$

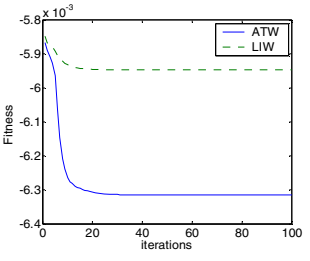

Fig. 6. $\lambda = 0.65$

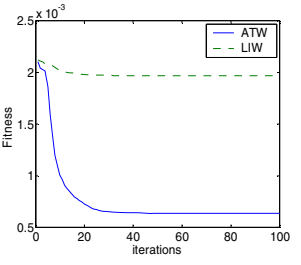

Fig. 7. $\lambda = 0.9$

6 Conclusions

This paper presents a novel PSO algorithm with non-linear inertia weight (ATW) based on the arc tangent function. The performance of ATW is evaluated by the experiments on four representative instances. It provided better quality solutions and more efficacious compared with LIW. They are also used to solve the portfolio optimization, and the result of the study showed that ATW is the more effective approach.

Future work is focused on optimizing the performance of ATW. In addition, extensive study of the applications in more complex practical optimization problems is necessary to fully investigate the properties and evaluate the performance of ATW.

Acknowledgment

This work is supported by Guangdong Natural Science Foundation (Grant no. 9451806001002294), Shenzhen-Hong Kong Innovative Circle project (Grant no. SG200810220137A), 863 Project(No. 008AA04A105), and Project 801-000021 supported by SZU R/D Fund.

References

1. Kennedy, J., Eberhart, R.C.: A New Optimizer Using Particle Swarm Theory. In: 6th International Symposium on Micromachine and Human Science, pp. 39–43 (1995)
2. Kennedy, J., Eberhart, R.C.: Particle Swarm Optimization. In: IEEE International Conference on Neural Networks, vol. IV, pp. 1942–1948 (1995)
3. Clerc, M., Kennedy, J.: The Particle Swarm: Explosion Stability and Convergence in a Multi-Dimensional Complex Space. IEEE Transactions on Evolutionary Computation 6, 58–73 (2002)
4. Eberhart, R.C., Shi, Y.: Comparison between Genetic Algorithms and Particle Swarm Optimization. In: Porto, V.W., Waagen, D. (eds.) EP 1998. LNCS, vol. 1447, pp. 611–616. Springer, Heidelberg (1998)

5. Eberhart, R.C., Shi, Y.: Particle Swarm Optimization: Developments, Applications and Resources. In: Congress on Evolutionary Computation, vol. 1, pp. 68–81 (2001)
6. Shi, Y., Eberhart, R.C.: Empirical Study of Particle Swarm Optimization. In: Congress on Evolutionary Computation, vol. 3, pp. 1945–1949 (1999)
7. Niu, B., Li, L.: A Novel PSO-DE-Based Hybrid Algorithm for Global Optimization. In: Huang, D.-S., Wunsch II, D.C., Levine, D.S., Jo, K.-H. (eds.) ICIC 2008. LNCS (LNAI), vol. 5227, pp. 156–163. Springer, Heidelberg (2008)
8. Niu, B., Xue, B., Li, L.: Symbiotic Multi-swarm PSO for Portfolio Optimization. In: Huang, D.-S., Jo, K.-H., Lee, H.-H., Kang, H.-J., Bevilacqua, V. (eds.) ICIC 2009. LNCS, vol. 5755, pp. 776–784. Springer, Heidelberg (2009)
9. Zhang, L.P., Yu, H.J., Hu, S.X.: Optimal Choice of Parameters for Particle Swarm Optimization. Journal of Zhejiang University Science 6, 528–534 (2004)
10. Shi, Y., Eberhart, R.C.: Parameter Selection in Particle Swarm Optimizations. In: Porto, V.W., et al. (eds.) EP 1998. LNCS, vol. 1447, pp. 591–600. Springer, Heidelberg (1998)
11. Shi, Y., Eberhart, R.C.: A Modified Particle Swarm Optimizer. In: IEEE International Conference on Evolutional Computation, pp. 69–73 (1998)
12. Wang, L., Wang, X.K.: Modified Particle Swarm Optimizer Using Non-Linear Inertia Weight. Computer Engineering and Applications 43, 47–48 (2007)
13. Van den Bergh, F.: An Analysis of Particle Swarm Optimizer, University of Pretoria, South Africa (2002)
14. Niu, B., Zhu, Y.L., He, X.X.: MCPSO: A Multi-Swarm Cooperative Particle Swarm Optimizer. Applied Mathematics and Computation 185, 1050–1062 (2007)
15. Liang, J.J., Suganthan, P.N., Qin, A.K.: Comprehensive Learning Particle Swarm Optimizer for Global Optimization of Multimodal Functions. IEEE Transactions on Evolutionary Computation 10, 281–295 (2006)
16. Parsopoulos, K.E., Vrahatis, M.N.: UPSO-A Unified Particle Swarm Optimization Scheme. Lecture Series on Computational Sciences, pp. 868–873 (2004)
17. Markowitz, H.W.: Foundations of Portfolio Theory. Journal of Finance 46, 469–477 (1991)

An Improved Image Rectification Algorithm Based on Particle Swarm Optimization

Hongwei Gao[1], Ben Niu[2,3,*] , Bin Li[1], and Yang Yu[1]

[1] School of Information Science & Engineering, Shenyang Ligong University Shenyang, 110159 China
[2] Hefei Institute of Intelligent Machines, Chinese Academy of Sciences Hefei 230031, China
[3] College of Management, ShenzhenUniversity Shenzhen, 518060 China
drniuben@gmail.com

Abstract. Image rectification is a method to apply projective transformation to image pair which can ensure the epipolar lines in one horizontal line. There is only horizontal disparity in two images and the matching speed can be improved in this situation. A simple rectification method is described in this paper. It takes the element in the fundamental matrix and epipole as initial value and uses PSO to calculate eight optimal points according with rectification rule by RANSAC robust estimation method. Then, the practical and optimal projective transformation matrixes are confirmed. Epipolar line rectification experiments based on synthetical image and real image show the validity of the algorithm.

Keywords: Image Rectification, Projective Transformation, PSO.

1 Introduction

Epipolar line rectification is an important approach to improve rate and accuracy of stereo match as well as a popular research fields currently. The rectification algorithm proposed by Faugeras[1] is to get rectified images by projecting two images to the common plane once, then the re-projective plane pass the intersection of two planes and parallel to baseline. Faugeras provided a simple image rectification algorithm, but it needs to know two cameras' European projective matrix and it requires two nearly visual angles, otherwise, the size of rectified image will be larger. For this deficiency, a cylindrical projection algorithm is proposed by Meunier and Cox[2] in 1997, the image is not projected in a common plane but is projected in a common cylindrical surface. This method can process a larger visual angle of two images including the situation of polar points being inside the images, however, the calculation is complex. A linear rectifying method was proposed by Hartley[3] in 1999, it relies on the constraint of minimum position of image's point to optimize the projective distortion problems of the image, at the same time, he also put forward the idea of quasi-affine transform in order to prevent the image from splitting after rectifying. A simple rectifying method is given from the above principle in this paper, it does not require high-precision fundamental matrix but just regard the element of fundamental matrix and

* Corresponding author.

D.-S. Huang et al. (Eds.): ICIC 2010, LNCS 6215, pp. 587–594, 2010.

outer polar point as initial value at the same time combines RANSAC robust algorithm and uses PSO algorithm to iterative optimization in order to find the optimal eight points which meet rectifying criterion and gets an optimal projective transformation matrix, after this, processes the image transformation of homogeneous coordinates to obtain the rectified image. Experimental results show that the algorithm presented in this paper is practical.

2 The Theory of Rectification

2.1 The Algorithm of Rectification

H_1 and H_2 are the projective transformation matrix respectively of images I_1 and I_2, m_1, m_2 are the corresponding matching image points, so that the transformed corresponding image points are $\overline{m}_1, \overline{m}_2$,thus we have

$$\overline{m}_1 = H_1 m_1 \ ; \ \overline{m}_2 = H_2 m_2 . \tag{1}$$

Suppose F is fundamental matrix of two images before rectifying, $\overline{F}$ is fundamental matrix of two images after rectifying, according to the nature of the fundamental matrix we can obtain:

$$m_2^T F m_1 = 0; \ \overline{m}_2^T \overline{F} \overline{m}_1 = 0 . \tag{2}$$

After deducing [4,5], the corresponding polar lines of two images all parallel to the X-axis and locate on a common horizontal line. We can obtain the following equation from formula (1), (2), $m_2^T H_2^T \overline{F} H_1 m_1 = 0$. So the relations of fundamental matrix between before and after rectifying can be concluded:

$$F = H_2^T \overline{F} H_1 . \tag{3}$$

From the formula (3), it can be seen that the task of image rectifying is to compute projection transformation matrix H_1, H_2. Document [5] obtained H1 by rotating and translating matrix which make outer polar point translate to infinity, here we present a more simple and direct transformation, so that it is very easy to see the projection transformation matrix

$$H_1 = \begin{bmatrix} a_{11} & a_{12} & a_{13} \\ -e_2 / e_1 & 1 & 0 \\ -1/e_1 & 0 & 1 \end{bmatrix}$$

The polar point can be transformed to infinity, where e_1, e_2 is the coordinates of the outer polar point $e = (e_1, e_2, 1)$ in the first image. Due to the first row of matrix H_1 act as horizontal scale to the image, in order to ensure little distortion for the

rectified image we make $a_{13} = 0$. To deal with shear distortion effectively, determine a_{11}, a_{12} by using the approach of two rectified lines still orthogonality because of the connection line of two mid-points in the original image orthogonality. As Figure1 showed:

$$a = [w/2 \quad 0 \quad 1]; \; b = [w \quad h/2 \quad 1]$$
$$c = [w/2 \quad h \quad 1]; \; d = [0 \quad h/2 \quad 1]$$

Get two straight linear vector t_1, t_2 from connection line between two mid-points:

$$t_1 = [w \quad 0 \quad 0] \quad t_2 = [0 \quad h \quad 0] \; ;$$

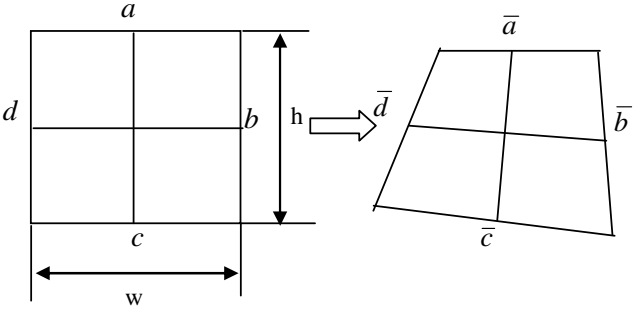

Fig. 1. Projective distortion rectifying

As the straight line of rectified image remains orthogonality, so there should be:

$$(H_1 t_1)^T (H_1 t_2) = 0$$

Put it into formula H_1, we can get easily, $a_{11} a_{12} = \frac{e_1}{e_2}$, Enable $a_{11} = 1; a_{12} = \frac{e_1}{e_2}$ without loss of generality. The latter experiment shows that this is better to handle shear distortion. When we obtained projective transformation matrix H_1, then take it into formula (3) we can get below matrix equation:

$$\mathrm{F} = \begin{bmatrix} -b_{31}\frac{e_2}{e_1} + b_{21}\frac{1}{e_1} & b_{31} & -b_{21} \\ -b_{32}\frac{e_2}{e_1} + b_{22}\frac{1}{e_1} & b_{32} & -b_{22} \\ -b_{33}\frac{e_2}{e_1} + b_{23}\frac{1}{e_1} & b_{33} & -b_{23} \end{bmatrix}. \tag{4}$$

In order to improve the accurately match of the subsequent process we must minimize the horizontal parallax by using the projection matrix which obtained from the first image, as the following equations:

$$\sum_{i=1}^{n}\{(H_1 m_{1i})_x - (H_2 m_{2i})_x\}. \tag{5}$$

Taking formula (4) into formula (2), we can obtain the following equation:

$$(b_{21}-b_{31}e_2)xx' + (b_{22}-b_{32}e_2)xy' + (b_{23}-b_{33}e_2)x + e_1 b_{31} yx' + e_1 b_{32} yy' + e_1 b_{33} y - e_1 b_{21} x' - e_1 b_{22} y' - e_1 b_{23} = 0$$

There are totally eight unknown from the above equation, they are respectively $b_{3i}, b_{2i}\ e_1, e_2, i = 1,2,3$,these equations will become 8-dimesional nonlinear equations when given eight group of the original matching points, so we can use the Gauss - Newton iteration method to solve the initial value of eight unknowns.

The specific steps of robust rectifying algorithm based on RANSAC as follows:

1. Execute random sampling algorithms, i.e. RANSAC technology, progress minimum point set sampling for N times.
2. Select eight group of matching points randomly in two images, seeking the initial value of fundamental matrix and outer polar point by using the Gauss-Newton iteration method, and calculating H_1, H_2 , using PSO algorithm to optimize the horizontal parallax(formula(5)),thus obtained optimized H_1, H_2 ;
3. Make the projection transformation matrix H1 and H2 to act on matching points of each image respectively:
   $\overline{m}_{ij} = H_i m_{ij}, i = 1,2; j = 1,2.....n$, and normalized, then $\overline{m}_{ij} = (\overline{x}_{ij}, \overline{y}_{ij}, 1)$;
4. Assume that $\delta_k = |(\overline{y}_{2j} - \overline{y}_{1j})|$ represents vertical parallax, when given a certain threshold T and $\delta_k < T$,we consider (m_{1j}, m_{2j}) as the correct matching point and statistic the number of correct matching points, then calculate vertical parallax of all matching points and $\delta = \sum_{k=1}^{m} \delta_k$.
5. Find more correct matching points and vertical parallax and projection transformation matrix when δ is minimum value after sampling N times.
6. Resample two images according to the optimal projection transformation matrix.

2.2 Optimization Strategy Based on Particle Swarm Optimization

PSO is derived from the investigation on behavior of bird swarm taking food, as well as GA, it is a kind of optimization tool based on iteration[6]. A set of random solutions are initialized automatically, and then the optimal solution is searched by on

iteration. The particles update its own velocity and position according to equation (6) and (7).

$$v_{id}^{k+1} = v_{id}^{k} + c_1 rand_1^k \left(pbest_{id}^k - x_{id}^k \right) + c_2 rand_2^k \left(gbest_d^k - x_{id}^k \right). \tag{6}$$

$$x_{id}^{k+1} = x_{id}^{k} + v_{id}^{k+1}. \tag{7}$$

The optimized procedure based on PSO is as follows:

1) Initialize the swarm randomly. The initialization of initial searching point position and its speed is finished randomly between the initial value's neighbor domains. The initial number of particle is selected as $d = 20$. (20 matches are selected randomly, and then 8 of the 20 matches are used to calculate the initial value of projective matrix). Calculate $pbest_{id}$ correspondingly, then $gbest_d$ is the best value of $pbest_{id}$.
2) Evaluate every individual in the swarm. Calculate the particle's fitness value according to formula (5), if the value is better than the current $pbest_{id}$, then update the $pbest_{id}$. If the $pbest_{id}$ in all particles is better than current $gbest_d$, then update $gbest_d$.
3) Update the swarm according to formula (6) and (7).
4) If a terminate condition is met, then the searching procedure is terminated, except that return to step 2.

3 Simulation and Experiment Results

Figure2 shows that apply the above algorithm to rectifying for real pairs of images, the fundamental matrix was obtained between them by using robust matching algorithm of previous chapter. Figure2(a) shows the detected 300 pairs corner points, and Figure2(b) shows 42 pairs of remaining matching points through robust matching algorithm. Using line segment represents corresponding points and using length of line segment represents parallax. It can be seen from the figure that both horizontal parallax and vertical parallax consist in image because of unrectified image, this will bring great amount of computation in subsequent dense matching. At first, compute fundamental matrix through 42 pairs of matching points and then compute projective transformation matrix H and H' according to fundamental matrix so that make them act on two original images, we can see from the re-sampling images which are shown in Figure2(c) that the horizontal coordinates of corresponding points are equal and vertical parallax tend to zero. The parallax is nine pixels in the horizontal negative direction and eight pixels in the vertical positive direction. Thus, the search range can be determined by positive and negative parallax in the subsequent dense matching algorithm so that reduce the computation as well as improve matching speed and accuracy.

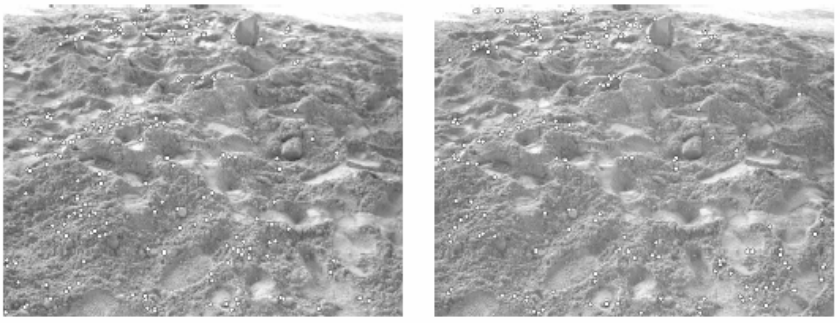

(a) Corner detection results

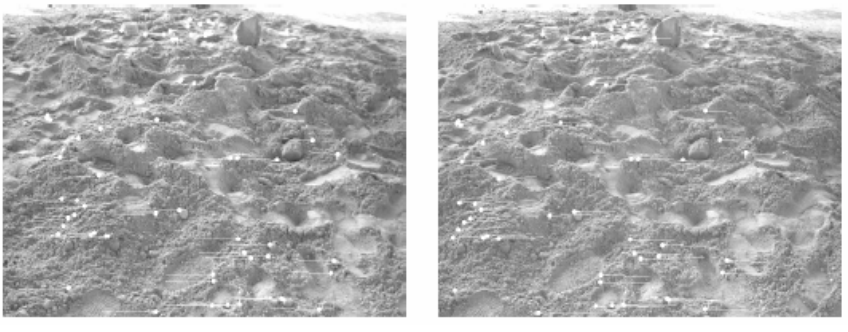

(b) Disparity map of remaining corner points after robust matching

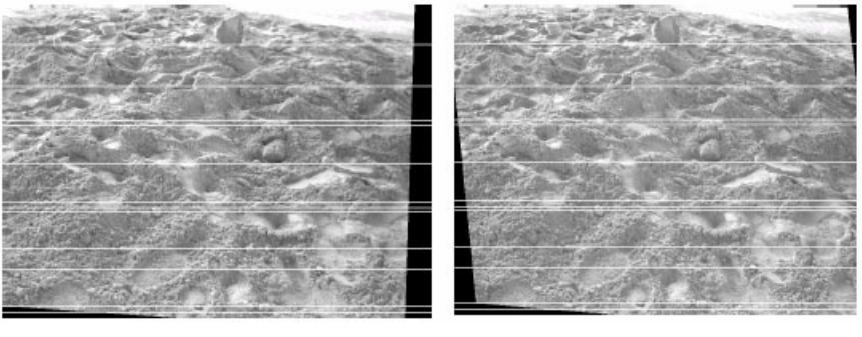

(c) Rectified resampling image

Fig. 2. Rectified results of simulating lunar surface

In order to test the robust of algorithm, we carried out a comparison experiment of algorithm performance between algorithm of this paper and traditional rectifying method based on the fundamental matrix. At first, match 20 to 200 points in every image in turn by using cross-correlation robust matching technology and increase 20 points every time, then take robust iteration method based on RANSAC technology and image rectifying algorithm based on the fundamental matrix, and moreover,

estimate good or bad of image rectifying results according to average vertical parallax of each group i.e.

$$\bar{\delta} = \frac{1}{m}\sum_{k=1}^{m}\delta_k$$

where m is the number of correct matching points. To test the advantage of robust algorithm, we use asterisks and circle respectively to express algorithm of the paper and traditional method based on the fundamental matrix in Figure 3. It can be seen from Figure 3 that the probability of false matching has increased greatly, so that the average vertical parallax also increased gradually which is represented by circle. This is because it is rectified indiscriminate together with false matching which makes the error increase. Using the algorithm of the paper, however, maintains a stable and smaller parallax and it is superior to the traditional method based on the fundamental matrix. It shows that the algorithm is not affected by error matching points, and it has a strong anti-interference only by selecting the best eight points to rectify the image each time.

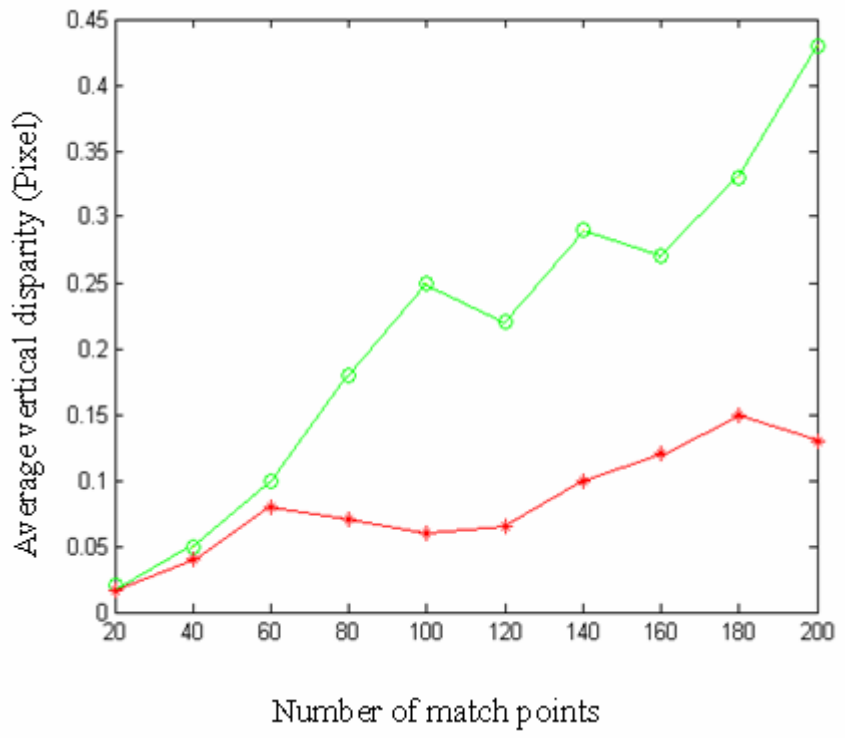

Fig. 3. The relationship between matching points and average vertical disparity

4 Conclusions

This paper presents a robust image rectification method which does not need high-precision fundamental matrix according to basic principles of the image matching, such point-based method has two advantages as follows. On the one hand, the estimation of fundamental matrix is not very accurate because of noise interference. On the other hand, even if set out from a good fundamental matrix, we do not obtain a good rectifying result due to the evaluation criteria both of fundamental matrix and rectifying results. A large number of simulations and real image experiments show that the method has a strong anti-noise and anti-mismatched ability to obtain satisfactory results.

Acknowledgement

This work is supported by China Liaoning Provice Educational Office fund (No.20080611). Shenzhen-Hong Kong Innovative Circle project (Grant no.SG200810220137A) and The Natural Science Foundation of Guangdong Province (Grant no. 9451806001002294), and 863 Project (No. 008AA04A105).

References

1. Faugeras, O.D.: Three-Dimensional Computer Vision: A Geometric View point. The MIT Press, Cambridge (1993)
2. Roy, S., Meunier, J., Cox, I.: Cylindrical rectification to minimize epipolar distortion. In: Proc. IEEE Conference on Computer Vision and Pattern Recognition, pp. 393–399. IEEE Press, Washington (1997)
3. Hartley, R.: Theory and practice of projective rectification. International Journal of Computer Vision 35, 115–127 (1999)
4. Ma, Y.Z., Liu, W.J.: A New Robust Rectification Algorithm of Uncalibrated Stereo Pairs. Computer Engineering 32, 26–28 (2006)
5. Zhang, Z.: Determining the Epipolar Geometry and Its Uncertainty: A Review. International Journal of Computer Vision 27, 161–198 (1998)
6. Niu, B., Xue, B., Li, L.: Symbiotic Multi-swarm PSO for Portfolio Optimization. In: Huang, D.-S., Jo, K.-H., Lee, H.-H., Kang, H.-J., Bevilacqua, V. (eds.) ICIC 2009. LNCS (LNAI), vol. 5755, pp. 776–784. Springer, Heidelberg (2009)

Particle Swarm Optimizer Based on Small-World Topology and Comprehensive Learning

Yanmin Liu[1,2], Dongshen Luo[1], Qingzhen Zhao[1], and Changling Sui[2]

[1] Department of math, and Zunyi Normal College
[2] College of Management and Economics, Shandong Normal University
yanmin7813@sohu.com

Abstract. PSO may easily get trapped in a local optimum, when solving complex multimodal problems. In this paper, an improved PSO based on small world network and comprehensive is proposed. The learning exemplar of each particle includes three parts: the global best particle, its own best particle (pbest) and the pbest of its neighborhood. And a random position around itself is needed to increase a probability to jump to that promising region. These strategies enable the diversity of the swarm to be preserved to discourage premature convergence. In benchmark function test, the SCPSO algorithm achieves better solutions than other PSOs.

Keywords: Particle swarm optimizer, comprehensive learning, small-world.

1 Introduction

Particle swarm optimizer (PSO) is a new entrant to the family of evolutionary algorithms (EAs). It was first proposed by Kenney and Eberhart[1] based on the metaphor of social behavior of birds flocking, fish schooling or the sociological behavior of a group of people. It is easy to implement PSO to solve the optimization problem. But when solving multimodal problems, it may be easily trapped in a local minimum. However, in real-world optimization problem, most of them are multimodal problems. In [2], Clerc indicated that a constriction factor may help to ensure the convergence. Mendes and Kennedy [3] introduced a fully informed PSO to update the particle velocity, in where all the neighbors of the particle are used to update the velocity. In [4], Peram proposed the fitness-distance-ratio-based PSO (FDR-PSO) with near neighbor interactions, when updating each dimension velocity dimension, the FDR-PSO algorithm selects one other particle, which has a higher fitness value and is nearer to the particle being updated. Liang [5] proposed an improved PSO called CLPSO, which uses a novel learning strategy. In [6], the author proposed an improved PSO based on dynamic neighborhood to improve the ability to escape from local optima. The above improved PSOs have achieved a satisfactory result, but at convergence velocity and precision, there are some shortages. Therefore, in order to overcome this defect and improve the PSO performance, some researches investigated neighborhood topology of the swarm. In this paper, on basis of [2], we propose a small world topology and comprehensive learning PSO to improve the PSO performance.

D.-S. Huang et al. (Eds.): ICIC 2010, LNCS 6215, pp. 595–601, 2010.

2 Particle Swarm Optimization (PSO)

Each individual as possible solution can be modeled as a particle that moves in n-dimensional search space. The velocity of each particle is determined by the vector $v_i \subset R^n$, and the velocity and position of the ith particle are updated as follows:

$$\begin{aligned} \overline{v_i}(t+1) &= \overline{v_i}(t) + \varphi_1 \cdot r_1(\overline{p_i}(t) - \overline{x_i}(t)) + \varphi_2 \cdot r_2(\overline{p_g}(t) - \overline{x_i}(t)) \\ \overline{x_i}(t+1) &= \overline{x_i}(t) + \overline{v_i}(t+1) \end{aligned} \tag{1}$$

where, $\overline{x_i}(t)$ represents the position of the ith particle in current iteration t; n is the dimension of the search space. t is the number of current iteration; φ_1 and φ_2 are two positive numbers known as the cognitive and social acceleration coefficients; r_1 and r_2 are two random numbers with the uniform distribution in the range of [0,1]; $\overline{p_i}(t)$ is the best position of the current particle found so far by itself; $\overline{p_g}(t)$ is the best position of all particles found so far by the whole swarm. To make particle fly in the search space, each dimension velocity of a particle is limited to $v_{\max}$, which is constant value defined by the user.

Afterwards, each particle updates its personal best and the global best of the swarm using Eq. (2) and (3). (Assuming a minimization problem):

$$\overline{p_i}(t+1) = \begin{cases} \overline{p_i}(t) & \text{if } f(\overline{p_i}(t)) \le f(\overline{x_i}(t+1)) \\ \overline{x_i}(t+1) & \text{if } f(\overline{p_i}(t)) > f(\overline{x_i}(t+1)) \end{cases} \tag{2}$$

$$\overline{p_g}(t+1) = \arg\min f(\overline{p_i}(t+1)) \tag{3}$$

In PSO domain, there are two main models of the PSO algorithms, called global best (gbest) and local best (lbest), which differ in the way of defining the neighborhood of each particle. In the gbest model, the neighborhood of a particle consists of the particles in the whole swarm, which share information between each other; while in the lbest model, the neighborhood of a particle is defined by several fixed particles. The two models give different optimization performances on different problems. Kennedy and Eberhart [7] pointed out that the gbest model has a faster convergence speed with a higher chance of getting stuck in local optima than lbest. On the contrary, the lbest model is less vulnerable to the attraction of local optima but with a slower convergence speed than the gbest model.

3 Particle Swarm Optimizer Based on Small-World Topology and Comprehensive Learning

In PSO, each individual aims to produce the best solution by learning from other individuals, thereby the different neighborhood topology will effect each particle learning.

In our proposed algorithm, the neighborhood topology is similar to [6], but not the same work. The main difference is the choice of learning exemplar, a kind of comprehensive learning is proposed. The neighborhood of each particle is constructed based on Eq.(1) and the small-world network. Complying with seven criteria, $\overline{p_{ibest}}$ can generate new positions in the process of search by the information derived from different particle historical best positions.

When updating the particle velocity at each iteration, which is shown in Fig.1 (Particle *a, b, c, d* and *e* are connected with particle *i* by probability p. Particle *c* is choose as exemplar based on CC and L.), we firstly produce two small world networks as initial neighborhood topology (denoted as NT), and then choose the learning exemplar of the particle from other particle's pbest as the following criteria:

(1) *If* $CC(1) = CC(2) \& L_1 \neq L_2$, NT_1 wins. If $L_1 < L_2$, particle *i* in NT_1 as exemplar.

(2) *If* $CC(1) = CC(2) \& L_1 = L_2$, NT_1 or NT_2 is chose at will.

(3) *If* $CC(1) \neq CC(2) \& L_1 = L_2$, NT_1 wins. If $CC(1) > CC(2)$, particle *i* in NT_1 as exemplar.

(4) *If* $CC(1) \neq CC(2) \& L_1 < L_2$, NT_1 wins, and particle *i* in NT_1 as the exemplar.

(5) *If* $CC(1) > CC(2) \| L_1 < L_2$, NT_1 wins, then particle *i* in NT_1 as the exemplar.

(6) *If* $CC(1) > CC(2) \| L_1 < L_2$, NT_1 wins, particle *i* in NT_1 is chosen as exemplar.

(7) *If* $CC(1) < CC(2) \| L_1 < L_2$ and the average degree $< K >$ in NT_2 is morn than the $< K >$ in NT_1, NT_2 wins, and we choose particle *i* in NT_2 as the exemplar. Otherwise, population NT_1 wins.

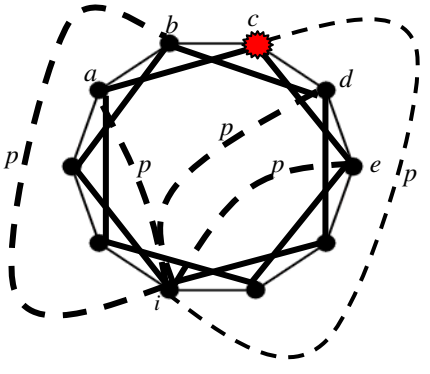

Fig. 1. Neighborhood in small world network

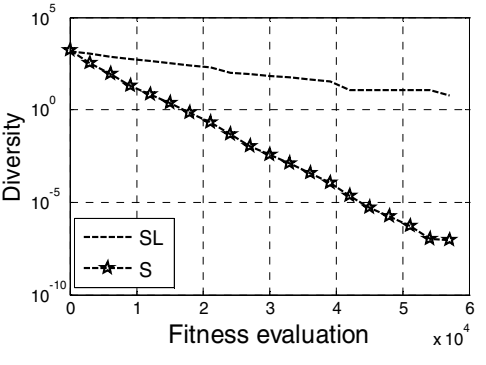

Fig. 2. Swarm diversity

Although there are many improved versions of PSO, how to balance the performance of the gbest and lbest models is still an important issue, especially for multi-modal problems. In the gbest model, all particles' social behavior is strictly constrained by

learning information from the global best particle. Hence, particles are easily attracted by gbest and quickly converge on that region even it is not the global optimum and gbest does not improve. In the lbest model, attraction by the gbest is not too much but the slow convergence speed is unbearable. In the origin PSO, each particle learns from its pbest and the gbest simultaneously, which might cause the above problems. Hence, we can separate the cognition component and the social component to increase diversity based on small-world topology. The information learnt by each particle comes from four sources: the gbest, its own pbest, the pbest of the other neighborhood, and a random position around itself. Once particles converge on a local optimum or there is a more promising region nearby without particles covering it, particles should have a probability to jump to that promising region. Hence, learning from a random position around itself is needed.

So, the velocity updating equation is the following.

$$\begin{aligned} \overline{v_i}(t+1) &= \overline{v_i}(t) + \varphi_1 \cdot r_1(\overrightarrow{p_{ibest}}(t) - \overline{x_i}(t)) + \varphi_2 \cdot r_2(\overrightarrow{p_g}(t) - \overrightarrow{x_i}(t)) + \varphi_3 \cdot r_3(\overrightarrow{p_i}(t) - \overrightarrow{x_i}(t)) \\ \overrightarrow{x_i}(t+1) &= \overrightarrow{v_i}(t+1) + \overrightarrow{x_i}(t) + v_{ave} \cdot N(0,1) \\ ibest &= \{\, i \mid CC_i = \max(CC), L_i = \min(TP_1, TP_2)\}, i \in TP_1 \ \ or \ \ i \in TP_2 \end{aligned} \tag{4}$$

where, TP denotes total population. $CC_i = 3(K-2)/4(K-1)$ is the biggest clustering coefficient for the ith particle in TP; K is the degree of the ith. $ibest$ is the best particle position. v_{avg} is the average velocity of all particles, and $N(0,1)$ is a random number from the normal distribution with mean 0 and variance 1.

PSO with Small-world topology and comprehensive learning makes the swarm more diversity than PSO with Small-world topology. To test diversity, we used Eq.(4) to describe the swarm diversity.

$$D(t) = \frac{\sum_{i=1}^{N} \sqrt{\sum_{d=1}^{n} (x_{id}{}^{t} - \overline{p_d})^2}}{S \cdot L} \tag{5}$$

where S is the swarm, L is the length of longest the diagonal in the search space, N is the dimensionality of the problem, x_{id} is the dth value of the ith particle and $\overline{p_d}$ is the ith value of the average point x. Note that this diversity measure is independent of swarm size, the dimensionality of the problem as well as the search range in each dimension. Small $D(t)$ value means low swarm diversity.

Here, SL denotes the diversity of PSO with Small-world topology and comprehensive learning; S represents PSO with Small-world topology. Fig.2 gives swarm diversity. Algorithm 1 gives the pseudo code of SCPSO.

Algorithm 1
For each particle
Computer *CC* and *L.* (Predefined probability p)
Initialize the particles' position and velocity
Computer fitness value.
If pbestval(i)>pbestval(j) $i \neq j \in popsize$
pbest=pbest(i).
Gbestval=pbestval(i).
End
Endfor
While (stopping criteria)
For each particle
Updating particle velocity and position in terms of Eq.(4).
Choose learning exemplar in terms of *CC* and *L.*
Updating global gbest and global fitness. particle position
End
End While

4 Experiment and Results

To evaluate the performance of the proposed approach, we choose five functions whose formulas are collected in [5]. The experiments were conducted to compare four PSOs on the six test problems with 30 dimensions. The four PSOs are the PSO algorithm with constriction factor (PSO-CF) [2], Fully informed particle swarm (FIPS)[3], FDR-PSO[4], CLPSO [5]. In order to make these different algorithms comparable, all parameters are set as follows: the population size is set at 30 and the maximum fitness evaluations (FEs) is set at 3×10^4. All experiments were run 30 times.

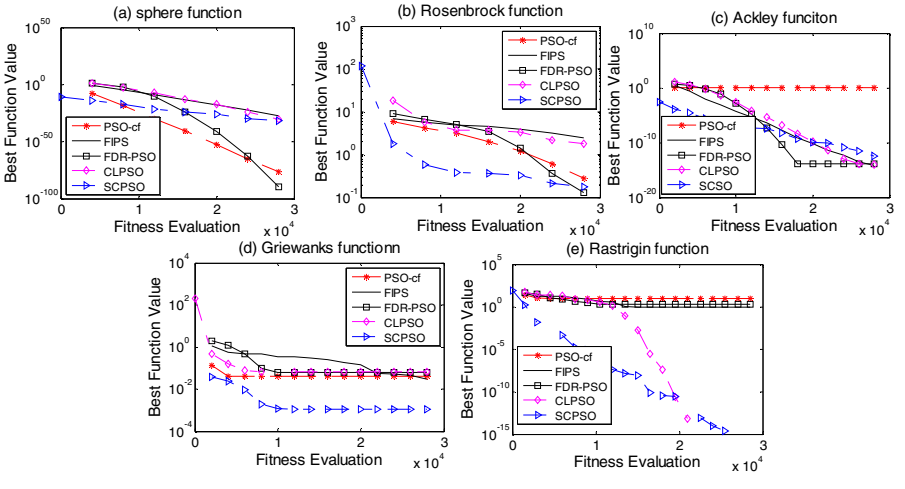

Fig. 3. The convergence characteristics

4.1 Convergence Characteristic Analysis

Fig.3 presents the convergence characteristics in terms of the best fitness value of the median run of each algorithm for each test function. From the results, we observe that in the Sphere function, SCPSO could not converge as fast as other PSO algorithms. Note that on Rosenbrock function, the SCPSO algorithm achieved the almost same best result as FDR-PSO. However, the SCPSO algorithm performs well in all multimodal problems and outperforms all other PSO algorithms, especially on Griewanks and Rastrigin functions.

Additionally, as in SCPSO, small-world topology and comprehensive learning strategies are introduced, it is necessary to explore whether these strategies increase the computations complex. Here, we use (tic, toc) function of software 'matlab' to test the performing time after 3×10^4 FEs. From Table 1, we can conclude the computation complex of SCPSO is the same as other PSOs.

Table 1. The run time when reaching stopping criterion for PSOs (Unit: second)

Algorithm	Sphere	Rosenbrock	Ackley	Griewanks	Rastrigin
PSO-CF	**13**	20	22	29	50
FIPS	12	25	28	45	60
FDR-PSO	14	23	27	39	55
CLPSO	18	27	43	49	76
SCPSO	21	24	41	40	80

4.2 Robustness Analysis

In order to test the robustness of various PSOs, we run the algorithms under different condition of Ackley and Griewanks function. Note that "different condition" denotes function rotation and nonrotation, where the rotation method is the same one as [7]. Table 2 shows the results of the robustness analysis. Note that the "robustness" is used here to express that the algorithm succeeded in a specified threshold. Here, the threshold s of Ackley and Griewank are 0.05 and 0.02, respectively. The "S" column presents the rate at which the function value below the threshold is reached. The "FEs" column means the number of function evaluations needed on average to reach the

Table 2. Robustness Analysis

Algorithm	Ackley		Griewanks		Rotated- Ackley		Rotated- Griewanks	
	FEs	S	FEs	S	FEs	S	FEs	S
PSO-CF	18934	69	9165	39	3146	23	6542	27
FIPS	17835	89	8159	69	12894	88	33678	46
FDR-PSO	18640	100	7902	65	14872	49	19863	42
CLPSO	18931	97	24391	98	2173	93	29316	90
SCPSO	9863	100	11963	100	3419	100	19735	100

threshold. A robust PSO algorithm is the one that manages to reach the threshold consistently. On Ackley and Griewanks function, SCPSO consistently reached the threshold on both the unrotated and the rotated cases. It shows that SCPSO is more robust than other PSOs.

5 Conclusions and Future Work

We have presented an improved PSO based on small world network and comprehensive. These strategies greatly increase swarm diversity and improve the ability to escape from local optima. In benchmark function, SCPSO achieves better solutions than other PSOs.

In the future, we will focus on: (i) experimenting to test our proposed algorithm effectiveness with more multimodal test problems and several composition functions that is more difficult to be optimized; (ii) applying the proposed algorithm to some applications to verify its effectiveness.

Acknowledgments. The first author acknowledges the support from Ministry of Education in Guizhou Province, Zunyi technology division Dean's Office and Department of Scientific Research Of Zunyi Normal College through the project number 0705204, B07015, B07017, [2008]21 and 2007018, respectively.

References

1. Eberhart, R., Kennedy, J.: New optimizer using particle swarm theory. In: Proc. 6th Int. Symp. Micro Machine Human Science, pp. 39–43 (1995)
2. Clerc, M.: The Swarm and the Queen: Toward a Deterministic and Adaptiveparticle Swarm Optimization. In: Proc. ICEC 1999, Washington, DC, pp. 1951–1957 (1999)
3. Mendes, R., Kennedy, J., Neves, J.: The Fully Informed Particle Swarm: Simpler, Maybe Better. IEEE Trans. Evol. Comput. 8, 204–210 (2004)
4. Peram, T., Veeramachaneni, K., Mohan, C.K.: Fitness-distance-ratio based particle swarm optimization. In: Proc. Swarm Intelligence Symp., pp. 174–181 (2003)
5. Liang, J.J., Qin, A.K., Suganthan, P.N., Baskar, S.: Evaluation of Comprehensive Learning Particle Swarm Optimizer. In: Pal, N.R., Kasabov, N., Mudi, R.K., Pal, S., Parui, S.K. (eds.) ICONIP 2004. LNCS, vol. 3316, pp. 230–235. Springer, Heidelberg (2004)
6. Liu, Y., Zhao, Q., Shao, Z., Shang, Z., Sui, C.: Particle swarm optimizer based on dynamic neighborhood topology. In: Huang, D.-S., Jo, K.-H., Lee, H.-H., Kang, H.-J., Bevilacqua, V. (eds.) ICIC 2009. LNCS, vol. 5755, pp. 794–803. Springer, Heidelberg (2009)
7. Mohais, A.S., Mendes, R., Ward, C., Posthoff, C.: Neighborhood re-structuring in Particle Swarm Optimization. In: Zhang, S., Jarvis, R.A. (eds.) AI 2005. LNCS (LNAI), vol. 3809, pp. 776–785. Springer, Heidelberg (2005)

Multi-Objective PSO Based on Evolutionary Programming

Zengzhen Shao[1], Yanmin Liu[2], and Shuxia Dong[3]

[1] School of Information Science and Engineering, Shandong Normal University, Jinan, 250014, China
[2] Department of math, Zunyi Normal College, Zunyi, 563002, China
[3] School of Information and Technology, ShanDong Women's University, Jinan, 250002, China

Abstract. Multi-Objective Particle Swarm Optimizers (MOPSOs) easily converge to a false Pareto front. In this paper, we proposed a hybrid algorithm of MOPSO with evolutionary programming (denoted as EPMOPSO) for solving MOPs. In EPMOPSO, the neighborhood of each particle is dynamically constructed, and the velocity of each particle is adjusted by all particles in its neighborhood including itself, the best performing particle in the swarm and the elite group that is evolved using evolutionary programming. Simulation results show that EPMOPSO is able to find a much better spread of solutions and has faster convergence to true Pareto-optimal front compared with five state-of-the-art MOPSOs.

Keywords: Particle swarm optimizer, Multiobjective optimization, Evolutionary Programming.

1 Introduction

Multiobjective optimization problems (MOPs) represent an important class of real-world problems encountered in various fields. Population-based optimization methods such as evolutionary algorithms (EAs) have become increasingly popular for solving MOPs[1]. These algorithms were developed based on three common goals, namely maximizing the number of elements of the Pareto optimal set found, minimizing the distance of the Pareto front produced by a algorithm with respect to the true Pareto front, and maximizing the distribution of solutions found. Another population-based optimization technique, particle swarm optimization (PSO) [2] has been proved to be an efficient optimization method for single objective optimization, and recently has shown promising results for solving MOPs [3]-[7]. However, the basic PSO algorithm has some serious limitations when dealing with MOPs. In PSO, the velocity of a particle is adjusted by its personal best (pbest) and global best (gbest). At each iteration, if the fitness of the offspring is better than the parent's pbest, the pbest is updated with this offspring, but there is no sharing of information with other particles in the population, except that each particle can access the global best.

D.-S. Huang et al. (Eds.): ICIC 2010, LNCS 6215, pp. 602–610, 2010.

2 Related Work

There have been several proposals to extend PSO to handle MOPs. Li[3] *et al.*proposed a non-dominated sorting Particle Swarm Optimizer (NSPSO), which incorporates the main mechanisms of the NSGA-II [1] into a PSO algorithm. The sigma method allowing the particles to select their global leaders based upon the minimum distance from the sigma values computed for each archive member was introduced by [4]. Coello *et al.*[5] proposed the use of mutation operator to improve the exploration capability. Sierra [6] suggested a new MOPSO (OMOPSO), in which, the population is divided into three subswarms of equal size. Yen *et al.*[7] proposed a multiple-swarm MOPSO algorithm in which the number of swarms is adaptively adjusted throughout the search process.

3 Multi-Objective Particle Swarm Optimizer Based on Elite Learning

3.1 Selection of Pbest

In our algorithm, the updating strategy of pbest is similar to the one used by [5], but not the same. We allow a particle to learn from the exemplars until it ceases improving for a number of generations (which is set as 3 in our algorithm). Then we reassign the exemplars for the particle. The selection principle of the pbest makes use of a basic definition (Pareto Dominance).

3.2 Selection of Gbest

In MOPs, there exist a set of nondominated solutions instead of a single global best solution as in the single objective. However, because all nondominated solutions are good individuals, we could not decide which one is the best. Here, the strategy of selection of gbest is the same as one [6], i.e., randomly choosing a particle from all nondominated solutions in the external archive.

3.3 ε-Dominance Based on External Archive Strategy

According to Pareto optimality, a set of nondominated solutions will be generated at each iteration. As for the store of the nondominated solutions, we use an external archive to store them during the search process. Because convergence and diversity are two main metrics of multi-objective evolutionary algorithm (MOEA), we employ the strategy of ε-dominance to update the external archive. Mostaghim [8] concluded that the ε-dominance method could find solutions much faster than the clustering technique with comparable and even in some cases better convergence and diversity. Therefore, we employ the ε-dominance method to update the external archive in the EPMOPSO algorithm. Usually, there are two levels in the ε-dominance strategy. On the coarse

level, the search space is discretized by a division box, in which each vector uniquely belongs to one box. The box is divided by Equation (1).

$$b_i = \left\lfloor \frac{\log f_i}{\log(1+\varepsilon)} \right\rfloor \tag{1}$$

$$|A| \le \left(\frac{\log f_i}{\log(1+\varepsilon)}\right)^{(m-1)} \tag{2}$$

Note that a generalized dominance relation is used in these boxes. Thus, the algorithm always maintains a set of non-dominated boxes. On the fine level, there is at most one element, which only can be replaced by a dominating one in each box. This method ensures the convergence with the bounded size in terms of Equation (2).

However, as the size of the archive will increase very quickly with the iteration elapsed, the complexity of updating the archive arises with the archive size. In this way, the complexity of the updating process for the complete run is $O(kMN2)$, where M is the total number of iterations, k is the number of objectives and N is the population size. If we don't control the number of the nondominated solutions in the external archive, the complexity of the updating process will be expensive. Here, we apply the nearest neighbor density estimator, which is invoked if the external archived population reaches its maximum size.

3.4 Evolutionary Programming (EP)

Evolutionary Algorithm (EA) and PSO are both population-based algorithms that have known to be successful in solving various complex optimization problems. EAs are robust but require considerable computing cost and slow in converging, while PSOs are relatively fast and simple, but easily converge to local optima. Some researchers proposed a hybrid algorithm of EAs and PSOs[9][10]. Simulation results demonstrate the hybridization algorithm is highly competitive in terms of robustness, accuracy and convergence speed. Additionally, in [11][12], the author summarized MOPSO based on evolutionary programming (EP) and concluded the hybrid algorithm is effective. Consequently, we think that a hybrid algorithm of PSO and evolutionary programming (EP) will be worthy of study issue when solving MOPs.

We proposed a hybrid algorithm of MOPSO and evolutionary programming (EP), in which a particle velocity is adjusted not only by all particles in its neighborhood including itself and the best performing particle in the swarm, but also by the evolving elite group generated by EP.

In EP, initially assume that a population of 2N particles is randomly generated. Each particle is regard as a pair of real valued vectors (x, η), where x is the position of the particle and η is the standard deviation for Gaussian mutations. Each parent particle (x, η) creates a single offspring (x', η') by Equations (3) and (4).

$$x_i^{'} = x_i + \eta_i \cdot r_i \tag{3}$$

$$\eta_i^{'} = \eta_i \cdot \exp(\tau^{'} \cdot r + \tau \cdot r_i) \tag{4}$$

where x_i, η_i, $x_i^{'}$ and $\eta_i^{'}$ represent the i^{th} dimension of the vectors x, η, $x^{'}$ and $\eta^{'}$ respectively; i = 1,...,n, and n denotes the dimension of the position of the particles; r is a normally distributed real random number with mean 0 and standard deviation 1; r_i is the random number corresponding to each value of i; τ and $\tau^{'}$ are set as $(\sqrt{2\sqrt{n}})^{-1}$ and $(\sqrt{2n})^{-1}$, where n is the dimension of the position of the particles.

In our algorithm, the elite group is identified using tournament selection, and then evolved by EP. The visualization of the elite and the ordinary particles on 2-D plane is shown in Figure 1.

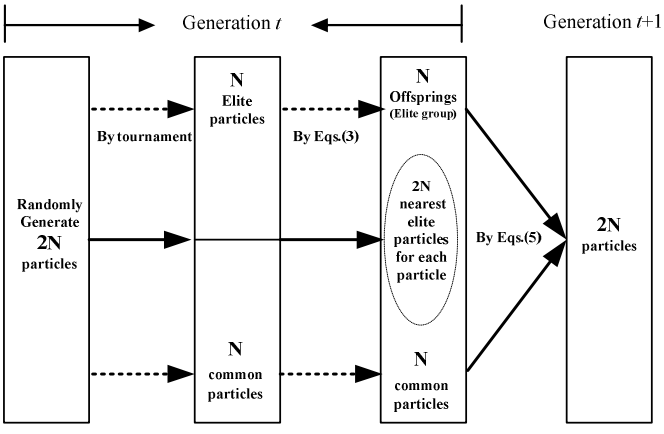

Fig. 1. The process of EP operation

If a particle that learns from all dimensions of the best performing particle will produce 'two steps forward, one step back' phenomenon, which will degrade the efficiency of the algorithm. In our algorithm, a particle's velocity is adjusted not by all dimensions of the best performing particle's pbest in its neighborhood, but by the corresponding dimension of any particle's pbest in its neighborhood, including its own pbest. The updating equations of velocity and position are employed.

$$\begin{aligned} \overline{v_i}(t) &= w \cdot \overline{v_i}(t-1) + \varphi_1 \cdot r_1 (\overline{p_g} - \overline{x_i}(t-1)) + \varphi_2 \cdot r_2 \cdot (\overline{p_{bin_{(i)}}} - \overline{x_i}(t-1)) + \varphi_3 \cdot r_3 \cdot (1-r_2) \cdot (\overline{p_{n\text{-}elite_{(i)}}} - \overline{x_i}(t-1)) \\ \overline{x_i}(t) &= \overline{x_i}(t-1) + \overline{v_i}(t) \end{aligned} \tag{5}$$

$$p_{bin_{(i)}}{}^{d} = \arg\{\max[\frac{sum(Fitness_k(p_j) - Fitness_k(p_i))}{\left|p_{jd} - x_{id}\right|}]\}$$
$$d \in (1,2,\cdots,n), i = 1,2,\cdots,ps \quad j \in neighbor_i \quad k = 1,\cdots,m \tag{6}$$

where w is the inertial weight; ps is the population size; $neighbor_i$ represents the set of all members of the neighborhood of the current particle i, $\overline{v_i}(t) = (v_i^1, v_i^2, \cdots, v_i^n)$ represents the velocity of the ith particle; $\overline{x_i}(t) = (v_i^1, v_i^2, \cdots, v_i^n)$ represents the position of the ith particle at current iteration t; $\overline{p_{n-elite_{(i)}}}$ denotes the nearest elite position of the particle i; $\overline{p_g} = (p_g{}^1, p_g{}^2, \cdots, p_g{}^n)$ is the best position discovered by the whole population; $p_{bin_{(i)}}{}^{d}$ defines the corresponding dimension of the particle i's $\overline{p_{bin_{(i)}}{}^{d}}$; φ_1, φ_2 and φ_3 denote the acceleration coefficients that is randomly varied between 1.5 and 2 to provide different emphasis on the components in Equation (9); r_1, r_2 and r_3 are random vectors with the components uniformly distributed in the range of [0,1]; $\overline{p_j} = (p_j{}^1, p_j{}^2, \cdots, p_j{}^n) \quad j \in neighbor_i$ is any member's pbest of the neighborhood of the particle i; m is the number of the objective function; d defines the particle's dimension; |...| denotes the absolute value; Fitness(p) represents the corresponding fitness value of an array p.In order to guarantee a particle flight in the search space, its velocity on each dimension is limited to $v_{\max}$ which is a constant specified by the user. Algorithm 1 shows the pseudo code of EPMOPSO.

```
Algorithm 1
Begin
    While (fitcount < Max_FES) && (k<iteration)
      For each particle (i=1:ps)//ps=2N
          Generate N elite particles by 2- tournament selection.
          Evolve N elite particles by Evolutionary Programming(Equations (3) and (4)).
          Generate 2N nearest elite particles for each particle.
          Randomly select an exemplar from external archive.
          Updating particle velocity and position in terms of Equations (4) and (5).
          If Pstaynum(i) ≥3
             Pstaynum(i) = 0.
             Update pbest if current position is better than pbest
          End
          Update Nstaynum and Pstaynum
          Evaluate the fitness values of the current particle i.
      End for
      Update the external archive .
      Increase the generation count
    End While
    Output the result.
End Begin
```

4 Experimental Results

4.1 The Comparative Algorithms and Test Functions

We compare EPMOPSO algorithm with other algorithms that are representative of the state of the art. These algorithms are MOPSO [5], OMOPSO [6] and sMOPSO [4]. Table 1 gives the parameter configurations for all MOPSOs. ZDT1 and ZDT2 functions are chosen to compare the relative performance of the proposed EPMOPSO with the other MOPSOs. Their formulas are collected in [6]. ZDT1 and ZDT2 challenge the algorithm's ability to find and produce a good spread of Pareto front.

Table 1. The parameter configurations for all MOPSOs

	Population size	Archive size	Iteration number	Relative parameters
MOPSO	100	100	200	The same parameters
OMOPSO	100	100	200	as the algorithms
sMOPSO	200	100	200	proposed
EPMOPSO	100	100	200	

4.2 Performance Evaluation

Both quantitative and qualitative comparisons are made to validate the EPMOPSO algorithm against other MOPSOs. For qualitative comparison, the plots of final Pareto fronts are presented. As for the quantitative comparison, convergence metric (γ) [5] and spread (Δ) [1] are used. Their formulas are the following.

$$\gamma = \frac{\sqrt{\sum_{i=1}^{N} d_i^{\,2}}}{N} \tag{7}$$

$$\Delta = \frac{\sum_{m=1}^{M} d_m^{\,e} + \sum_{i=1}^{N-1} \left| d_i - \bar{d} \right|}{\sum_{m=1}^{M} d_m^{\,e} + (N-1)\bar{d}} \tag{8}$$

4.3 Results and Discussion

Each algorithm runs 30 times to achieve metric (γ) and (Δ). The mean values and standard deviation of the results are collected in Tables 2-3. The resulting nondominated fronts of six MOPSOs on all test functions are plotted in Figures 2–3.

Table 2. Comparison of performance on ZDT1

	MOPSO		OMOPSO		sMOPSO		EPMOPSO	
	γ	Δ	γ	Δ	γ	Δ	γ	Δ
Best	0.073	0.58	0.061	0.56	0.071	0.56	0.0016	0.18
Worst	0.231	0.94	0.123	0.67	0.163	0.77	0.0043	0.34
Average	0.098	0.66	0.069	0.59	0.089	0.64	**0.0021**	**0.29**
Median	0.097	0.66	0.067	0.58	0.087	0.63	0.0019	0.28
Variance	6.17 e-04	7.23 e-03	4.12 e-05	6.36 e-03	5.61 e-04	3.31 e-04	1.51 e-08	5.63 e-06

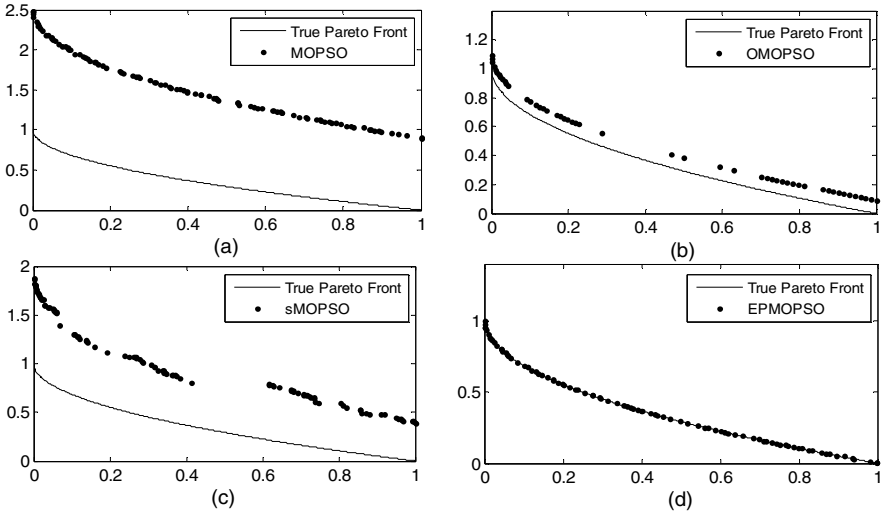

Fig. 2. Pareto fronts on Test Problem ZDT1

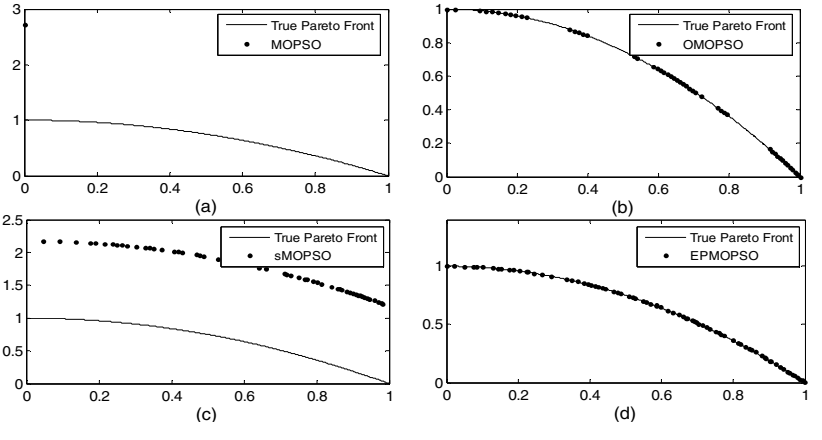

Fig. 3. Pareto fronts on Test Problem ZDT2

Table 3. Comparison of performance on ZDT2

	MOPSO		OMOPSO		sMOPSO		EPMOPSO	
	γ	Δ	γ	Δ	γ	Δ	γ	Δ
Best	0.114	0.58	0.0059	0.56	0.069	0.34	0.0049	0.13
Worst	0.581	0.88	0.0146	0.67	0.121	0.74	0.0112	0.42
Average	0.273	0.87	0.0073	0.59	0.076	0.59	**0.0038**	**0.23**
Median	0.246	0.86	0.0072	0.58	0.075	0.58	0.0036	0.22
Variance	5.77 e-02	4.75 e-02	4.63 e-04	5.63 e-03	5.94 e-04	4.64 e-03	1.08 e-06	`4.21 e-05

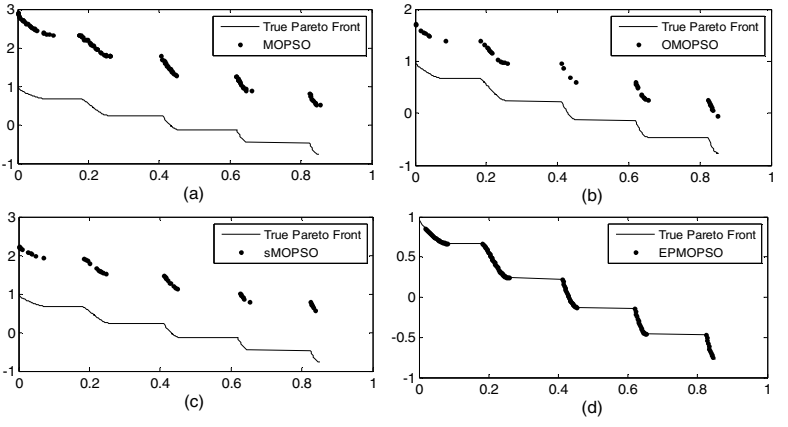

Fig. 4. Pareto fronts on Test Problem ZDT3

From Figures 2-3, we can find that EPMOPSO is able to find the well-distributed and near-optimal Pareto fronts for all test functions. The OMOPSO algorithm can also produce the quality Pareto fronts, but its solution qualities are poor.

Table 4. Comparison of performance on ZDT3

	MOPSO		OMOPSO		sMOPSO		EPMOPSO	
	γ	Δ	γ	Δ	γ	Δ	γ	Δ
Best	0.141	0.46	0.124	0.57	0.137	0.31	0.0021	0.16
Worst	0.274	0.78	0.243	0.68	0.262	0.88	0.0036	0.33
Average	0.189	0.51	0.159	0.59	0.174	0.54	**0.0019**	**0.29**
Median	0.184	0.51	0.153	0.58	0.169	0.51	0.0018	0.28
Variance	3.51 e-03	1.16 e-03	1.45 e-03	2.56 e-03	1.59 e-03	5.12 e-03	3.12 e-07	4.18 e-03

5 Conclusions

This paper presents multi-objective PSO with evolutionary programming for solving MOPs (EPMOPSO for short). The proposed algorithm is tested on various benchmark problems. Both two performance metrics (γ and Δ) indicate that the EPMOPSO algorithm is highly competitive and even outperforms the selected MOPSOs. Thus, the proposed EPMOPSO algorithm can be effectively applied to solve multi-objective optimization problems. In the future, we will focus on (i) testing the proposed algorithm effectiveness with more test problems, (ii) applying the proposed algorithm to solve some combinatorial optimization problems.

References

1. Deb, K., Pratap, A., Agarwal, S., Meyarivan, T.: A Fast and Elitist Multiobjective Genetic Algorithm: NSGA–II. IEEE Transactions on Evolutionary Computation 6, 182–197 (2002)
2. Kennedy, J., Eberhart, R.C.: Particle Swarm Optimization. In: IEEE International Conference on Neural Networks, Piscataway, vol. IV, pp. 1942–1948 (1995)
3. Li, X.: A Non-dominated Sorting Particle Swarm Optimizer for Multi-objective Optimization. In: Cantú-Paz, E., Foster, J.A., Deb, K., Davis, L., Roy, R., O'Reilly, U.-M., Beyer, H.-G., Kendall, G., Wilson, S.W., Harman, M., Wegener, J., Dasgupta, D., Potter, M.A., Schultz, A., Dowsland, K.A., Jonoska, N., Miller, J., Standish, R.K. (eds.) GECCO 2003. LNCS, vol. 2723, pp. 37–48. Springer, Heidelberg (2003)
4. Mostaghim, S., Teich, J.: Strategies for Finding Good Local Guides in Multi-objective Particle Swarm Optimization (MOPSO). In: IEEE Swarm Intelligence Symposium, pp. 26–33 (2003)
5. Coello, C.A.C., Pulido, G.T., Lechuga, M.S.: Handling Multiple Objectives with Particle Swarm Optimization. IEEE Transactions on Evolutionary Computation 8, 256–279 (2004)
6. Sierra, M.R., Coello, C.A.C.: Improving PSO-based Multi-objective Optimization Using Crowding, Mutation and ε-dominance. In: Coello Coello, C.A., Hernández Aguirre, A., Zitzler, E. (eds.) EMO 2005. LNCS, vol. 3410, pp. 505–519. Springer, Heidelberg (2005)
7. Yen, G.G., Leong, W.F.: Dynamic Multiple Swarms in Multiobjective Particle Swarm Optimization. IEEE Transactions on systems, man, and cybernetics-part A: systems and humans 39, 890–911 (2009)
8. Mostaghim, S., Teich, J.: The Role of ε-dominance in Multi Objective Particle Swarm Optimization Methods. In: Mostaghim, S., Teich, J. (eds.) IEEE Congress on Evolutionary Computation, CEC 2003, Canberra, Australia, December 2003, pp. 1764–1771 (2003)
9. Shi, Y., Krohling, R.: Co-evolutionary Particle Swarm Optimization to Solve Min-max Problems. In: IEEE Congress on Evolutionary Computation, vol. 2, pp. 1682–1687 (2002)
10. Juang, C.F.: A Hybrid of Genetic Algorithm and Particle Swarm Optimization for Recurrent Network Design. IEEE Transactions on Systems, Man, and Cybernetics, Part B 34, 997–1006 (2004)
11. Zhou, Z., Dai, G.: An Improved Hybrid Multi-objective Particle Swarm Optimization Algorithm. In: Kang, L., Cai, Z., Yan, X., Liu, Y. (eds.) ISICA 2008. LNCS, vol. 5370, pp. 181–188. Springer, Heidelberg (2008)
12. Yao, X., Liu, Y.: Fast Evolutionary Programming. In: Proc. Of the Fifth Annual Conference on Evolutionary Programming (EP 1996), pp. 451–460. MIT Press, San Diego (1996)

Two-Dimensional Sparse Principal Component Analysis for Palmprint Recognition

Cuntao Xiao[1,2]

[1] Faculty of Information Science and Technology, Sun Yat-Sen University, Guangzhou, 510275, China
[2] Faculty of Applied Mathematics, Guangdong University of Technology, Guangzhou, 510006, China
xiaocuntao@163.com

Abstract. Principal Component Analysis(PCA) is intrinsically a ridge regression problem in statistical view. By imposing l_1 constraint on the regression coefficients, Sparse Principal Component Analysis(SPCA) which is easier to interpret and better for generalization is obtained. But traditional SPCA is difficult to be used on 2-d data for its high dimensionality of covariance matrix because of the matrix-to-vector transformation, especially when the number of dimensionality and training samples are all in large scale. In this paper, Two-dimensional Sparse Principal Component Analysis(2dSPCA) is proposed to overcome the above shortcoming of SPCA. 2dSPCA is directly calculated by elastic net regularization on image covariance matrix without vectorization. Sparsity of projection vectors makes the results more interpretable and generalizable. Experiment on PolyU palmprint databases shows that 2dSPCA achieves comparable or higher performance compared with 2dPCA.

1 Introduction

Palmprint recognition has attracted wide attention of researchers in community of biometrics authentication [1], which is greatly motivated by the needs of military, commercial, and public security applications. Statistical approaches, such as Principal Component Analysis (PCA) [2], Linear Discriminative analysis (LDA) [3] and two dimensional PCA (2dPCA) [4] have proved their effectiveness in feature extraction and dimension reduction. In traditional approaches, 2-d palmprint image matrices must be previously transformed into 1-d image vectors column by column or row by row. But concatenating 2-d matrices into 1-d vectors often leads to a high-dimensional vector space which affects the effectiveness and efficiency of the latter data processing. This problem is commonly referred to as the "curse of dimensionality".

PCA is probably the most popularly unsupervised algorithm of dimension reduction and feature extraction. In statistical literature [6], PCA is equivalent to a ridge regression problem, the projection vectors can be calculated by the regression coefficients, and the projective vectors are usually not sparse since they are the linear combination of all original features. Nonsparsity always results in

D.-S. Huang et al. (Eds.): ICIC 2010, LNCS 6215, pp. 611–618, 2010.

difficulty of interpretation and overfiting of regression model which significantly drops the performance of generalization.

Sparsity has already been used successfully in many fields, like gene expression [7] and face recognition [10]. Zhou, et al. proposed SPCA algorithm which overcomes the shortcoming of PCA [6]. SPCA obtains sparse regression coefficients by imposing l_1 constraint on ridge regression framework corresponding to PCA, which is generally called *elastic net* regularization regression [8].

Although SPCA has proved it's effectiveness in gene expression for it's interpretability, it's difficult to be used directly on 2-d images for the high dimension of covariance matrix, especially when the number of dimension and training samples are all in large scale. Since in the precess of traditional SPCA algorithm, image matrices are first transformed into 1-d vectors column by column or row by row, and then data's covariance matrix with very high dimension can be calculated. As a result, performing SPCA gets time-consuming and even infeasible. Meanwhile, such vectorization ignores the local geometric structure of 2-d images and maybe lose some important information.

In order to overcome the above disadvantages of classical PCA and SPCA simultaneously, a novel feature extraction technique, named Two-dimensional Sparse Principal Component Analysis (2dSPCA) is proposed, which borrows the idea of 2-d Principal Component Analysis (2dPCA) [4]. The novelty of 2dPCA lies in a different data representation model. Under this model, each datum is represented as a matrix without matrix-to-vector transformation, and image covariance matrices was computed instead of conventional covariance matrix to compute eigenvectors. As the size of the image covariance matrix is equal to the width or height of palmprint images, which is quite small compared with the size of covariance of traditional PCA, so 2dPCA is computationally more efficient than classical PCA and better performance in recognition has already been proved in many databases. Similarly, our approach 2dSPCA applies image covariance to perform SPCA. Because it's low dimensionality of image covariance and sparsity of coefficients, 2dSPCA embodies the advantages of both 2dPCA and SPCA, namely computational efficiency and interpretability. Experiment on PolyU palmprint database also has shown that 2dSPCA outperforms 2dPCA in recognition rate.

The rest paper is organized as follows. In Section 2, we briefly review the principles of *elastic net* and SPCA. The details of our 2dSPCA are presented in Section 3. Experimental results are performed and illustrated in Section 4. We conclude this paper in Section 5.

2 Previous Work

2.1 Elastic Net

Elastic net is a regularization and variable selection method [8],which is the generalization of *lasso* [7],but *elastic net* outperforms *lasso* on real world data and encourages a grouping effect where strongly correlated predictors tend to be in or out of the model together.

Suppose that the data set has K samples with P predictors. Let $y = (y_1, ..., y_K)^T$ be the response and $X = (x_1, ..., x_P)$ be the model matrix, where $x_j = (x_{1j}, ..., x_{Kj})^T$, $j = 1, 2, ..., P$, are the predictors.We assume that the response is centered and the predictors are standardized.

For any fixed non-negative λ_1 and λ_2, the naive elastic net criterion is defined as follows

$$L(\lambda_1, \lambda_2, \beta) = ||y - X\beta||_2^2 + \lambda_2||\beta||_2^2 + \lambda_1|\beta|_1, \tag{1}$$

where $||.||_2$ and $|.|_1$ represents l_2 and l_1 norm respectively. The naive elastic net estimator $\hat{\beta}$ is the minimizer of equation (1)

$$\hat{\beta} = arg\min_{\beta}\{L(\lambda_1, \lambda_2, \beta)\}. \tag{2}$$

Let $\theta = \lambda_2/(\lambda_1 + \lambda_2)$,then solving $\hat{\beta}$ is equivalent to the optimization problem

$$\hat{\beta} = arg\min_{\beta} ||y - X\beta||_2^2, (1-\theta)|\beta|_1 + \theta||\beta||_2^2 \leq t. \tag{3}$$

for some $t > 0$. We generally call the function $(1-\theta)|\beta|_1 + \theta||\beta||_2^2$ the *elastic net* penalty, which is a convex combination of the lasso and ridge penalty. If $\theta = 1$, the naive elastic net becomes simple ridge regression, similarly naive net becomes *lasso* problem for $\theta = 0$. In this paper, $0 < \theta < 1$.

If define an artificial data set y^*, X^* by

$$X^*_{(N+P)\times P} = (1+\lambda_2)^{-1/2}\begin{pmatrix} X \\ \sqrt{\lambda_2}I \end{pmatrix}, y^*_{(N+P)} = \begin{pmatrix} y \\ 0 \end{pmatrix},$$

let $\gamma = \lambda_1/\sqrt{1+\lambda_2}$ and $\beta^* = \sqrt{1+\lambda_2}\beta$. Then the naive elastic criterion can be written as

$$L(\gamma, \beta) = L(\gamma, \beta^*) = ||y^* - X^*\beta^*||_2^2 + \gamma|\beta^*|_1, \tag{4}$$

and therein

$$\hat{\beta}^* = arg\min_{\beta^*} L\{(\gamma, \beta^*)\}.$$

Since the naive net estimator appears to incur a double amount of shrinkage which does not help to reduce the variances much and introduces unnecessary extra bias. Then the elastic net estimator $\hat{\beta_{en}}$ are defined by

$$\hat{\beta}_{en} = \sqrt{1+\lambda_2}\hat{\beta}^*.$$

The elastic net regression improves not only the interpretability of prediction variables but also the generalization of the model for prediction. Sparsity makes the predictive variables easy to be explained and help us find the deep information among variables. Especially if there is a group of variables among which the pairwise correlations are very high, elastic net tends to choose all correlative variables as a group into or out of the model. For prediction of unknown data, *elastic net* outperforms lasso and ridge regression. We will show that SPCA obtains sparse prediction variables by *elastic net* regularization.

2.2 Sparse Principal Component Analysis

Zou, et al, firstly introduced sparse principal component analysis (SPCA) [6]. PCA can be formulated as a ridge regression optimization problem, then sparse loadings are obtained by imposing the lasso constraint on the regression coefficients.

Let the data X be a $K \times P$ matrix, where K and P are the number of observations and the number of variables, respectively. Without loss of generality, assume the column means of X are all zeros. Suppose SVD of X as

$$X = UDV^T,$$

where T means transpose. U are the principal components (PCs) of unit length, and the columns of V are the corresponding loadings of the principal components. The following theorem presents a "self-contained" regression-type criterion to derive principal components [6].

Theorem 2.1. *Consider the first L principal components and let α and β be $P \times L$ matrices. X_i denote the $i-th$ row vector of the matrix X. For any $\lambda > 0$, let*

$$(\hat{\alpha}, \hat{\beta}) = arg \min_{\alpha,\beta} \sum_{i=1}^{n} ||X_i - \alpha\beta^T X_i||_2^2 + \lambda \sum_{j=1}^{L} ||\beta_j||_2^2 \tag{5}$$

subjet to $\alpha^T\alpha = I_L$, Then $\hat{\beta}_i \propto V_i$ for $i = 1, 2, \cdots, k$.

Theorem 2.1 effectively transform the PCA problem to a ridge regress problem. To obtain sparse loadings, lasso penalty is added into the criteria (5) and consider the following *elastic net* regularization problem

$$\begin{aligned}(\hat{\alpha}, \hat{\beta}) = arg \min_{\alpha,\beta} &\sum_{i=1}^{n} ||X_i - \alpha\beta^T X_i||_2^2 \\ &+\lambda \sum_{j=1}^{L} ||\beta_j||_2^2 + \sum_{j=1}^{L} \lambda_{1,j}|\beta_j|_1 \end{aligned} \tag{6}$$

subject to $\alpha^T\alpha = I_k$.

Choose appropriate λ_1 and $\lambda_{1,j}$, a sparse solution $\hat{\beta}$ is obtained, hence the sparse vector $\hat{V}_i = \frac{\hat{\beta}}{|\hat{\beta}|}$ with unit length which is an approximation of V_i. is also obtained Then SPCA is transformed to a optimization problem by *elastic net* constraint for fixed α. The problem (6) can be solved by an alternatively minimization algorithm to minimize the SPCA criterion. Detailed numerical algorithm to realize SPCA is seen in [6].

SPCA has been applied in gene expression for it's sparsity which is easier to interpret the results and find the important genes. Also, sparsity can improve the generalization of learned model and avoid over-fitting. So if the sparsity is considered in palmprint recognition, better recognition results should be obtained.

Although SPCA can calculated efficiently when the number of variables is far greater than the number of samples , it is still difficult to be used if they are all in large scale.

2.3 Two-Dimensional Principal Component Analysis

2dPCA is firstly proposed by Yang et al [4]. Compared with 1-d PCA, 2dPCA is based on 2-d image matrices and easier to evaluate the covariance matrix accurately. Instead of transforming image matrices firstly before projection, 2dPCA directly projects original image matrices into low dimensional vector space to keep maximum variance of corresponding image data.

Let $A_k \in R^{m\times n}(k = 1, 2, ..., K)$ represent training image matrices, $\bar{A} = \frac{1}{K}\sum_{k=1}^{K} A_k$ be the average image matrix, $\beta^L \in R^m$ and $\beta^R \in R^n$ are the left and right projection vectors respectively. Then the left and right image covariance matrix can be evaluated by

$$S^L = \frac{1}{K}\sum_{k=1}^{K}(A_k - \bar{A})(A_k - \bar{A})^T, \tag{7}$$

$$S^R = \frac{1}{K}\sum_{k=1}^{K}(A_k - \bar{A})^T(A_k - \bar{A}). \tag{8}$$

Then the problem of searching optimal projection direction is transformed to calculate the eigenvector of maximum eigenvalue of image covariance matrices S^L and S^R. In this paper, 2dPCA represents bidirectional 2dPCA which uses both image matrices. Because the dimension of image covariance matrices are far smaller compared with the 1-d case, it is more efficient and effective than PCA.

3 Two-Dimensional Sparse Principal Component Analysis

In this section, the framework of two-dimensional sparse component analysis(2d**SPCA**) and the algorithm of realization are introduced. Based on the idea of 2dPCA and SPCA, 2dSPCA is naturally proposed which contains the advantages of them. The main technique of 2dSPCA is performing SPCA by using image covariance matrices S^L and S^R instead of X^TX. Since the dimensionality of S^L or S^R is far less than X^TX, then 2dSPCA can be solved efficiently. To the best of our knowledge, this is the first to impose sparsity constrains on image covariance matrices directly.

For fixed α, the optimization problem (5) can be transformed to solve the following naive elastic net problem for $j = 1, 2, \cdots, L$

$$\beta_j = arg\min_{\beta^*}(\beta^*)^T(X^TX + \lambda)\beta^* - 2\alpha_j^T X^T X\beta^* + \lambda_{1,j}|\beta^*|_1. \tag{9}$$

Hence if given α, it amounts to solve L independent elastic net problems to get sparse loadings.

On the other hand, if β is fixed, we should maximize $Tr\alpha^T(X^TX)\beta$ subject to $\alpha^T\alpha = I_k$, whose solution can be obtained by SVD. If $\beta = UDV^T$, then $\hat{\alpha} = UV^T$.

It is particular to note that both PCA and SPCA depend on X only through X^TX. Since X^TX/n is actually the sample covariance matrix of variables. Therefore if the covariance matrix is known, we can use covariance matrix to replace X^TX. For two-dimensional principal component analysis, S^L and S^R are left and right image covariance matrices, which is similar to traditional covariance matrix, but the number of S^L or S^R is very smaller than that of traditional covariance matrix.

Now in community of palmprint recognition, we replace X^TX by image covariance matrix S^L or S^R, we have the following criterion of two-dimensional sparse principal component analysis (**2dSPCA**) in equation (6),

$$\beta_j^L = arg\min_{\beta^*}(\beta^*)^T(S^L + \lambda)\beta^* - 2\alpha_j^T S^L\beta^* + \lambda_{1,j}|\beta^*|_1, \tag{10}$$

and

$$\beta_j^R = arg\min_{\beta^*}(\beta^*)^T(S^R + \lambda)\beta^* - 2\alpha_j^T S^R\beta^* + \lambda_{1,j}|\beta^*|_1. \tag{11}$$

By LARS algorithm [9], sparse projection vectors β^L and β^R can be solved efficiently. Suppose $B^L = (\beta_1^L, \beta_2^L, ..., \beta_p^L)$, where $\beta_i^L (i = 1, 2, ..., p)$ represent the projective vectors corresponding to the largest p eigenvalues of S^L. Similarly we define $B^R = (\beta_1^R, \beta_2^R, ..., \beta_q^R)$ where $\beta_j^R (j = 1, 2, ..., q)$ represent the projective vectors corresponding to the first q eigenvalues of S^R. Next we define

$$Y = (B^L)^T A B^R,$$

here Y is the low dimensional representation of image A which can be used for the consequent classification task.

λ is a very small positive number to overcome potential collinearity of X, the optimal value can be determined by cross validation, but it is generally set to 1×10^{-6} for computation efficiency. Experiments show that the solution tends to become stable when λ is close to this value. $\lambda_{1,j}$ is used to compromise between variance and sparsity, which is automatically selected by LARS algorithm, actually the main parameter we need to determine is the $||\beta||_{l_1}$ which controls the sparsity of β and can be estimated by the l_1-norm of eigenvectors corresponding the traditional PCA.

4 Experimental Results

To evaluate the performance of our technique, the PolyU palmprint Database [5] comprising 100 individual palms captured by CCD-based device was used. Six samples from each individual was collected in two sessions, where three samples were captured in the first session and the other three in the second session. The average interval between the first and the second collection was two months. Some typical samples in this database are shown in Fig.1.

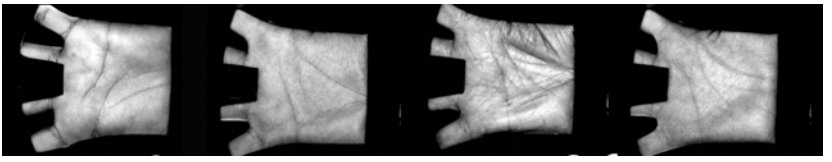

Fig. 1. Samples palmprint from PolyU database

In our experiment, We randomly select three images each subject as training data while the remaining three are deployed as testing data, the size of each cropped image is 128×128 pixels. The nearest neighbor classifier (NN) with Euclidean metric is used for classification. The recognition rate is calculated as ratio of the number of successful recognition and the total number of test samples. Experiments are repeated 10 times, and final recognition rate is the average value of the results. we compare the performance of the 2dSPCA, 2dSPCA+LDA, 2dPCA and 2dPCA+LDA according to different numbers of feature dimension from 5 to 9. Experiments have been performed on an Intel Pentium 4 2.66GHz Windows machine with 2GB memory.

Table 1. Average Recognition Rate on PolyU Palmprint Database(%)

Method	dim=5	dim=6	dim=7	dim=8	dim=9	sparsity
2dPCA	80.00±3.85	82.47±3.10	83.60±2.63	84.27±2.52	84.13±2.83	No
2dSPCA	81.60±4.75	83.31±3.69	83.47±2.72	84.13±2.71	84.33±2.86	Yes
2dPCA+LDA	83.60±4.15	86.13±3.69	87.73±3.48	88.40±2.02	88.87±2.19	No
2dSPCA+LDA	83.60±4.95	87.00±4.09	88.07±3.52	88.60±2.24	88.13±2.63	Yes

(∗)±(∗∗): (∗)represents recognition rate, (∗∗) represents standard deviation.

The comparison results are recorded in Table 1. the average recognition rates of both 2dSPCA and 2dSPCA+LDA increase at low dimension and then get stable at higher dimension, the average recognition rates of 2dSPCA are greater than or very close to 2dPCA, the similar conclusion is also obtained for 2dSPCA+lda and 2dPCA+lda. The best results of 2dSPCA is 84.33% at dimension 9 while the recognition rate is 84.27% at dimension 8. For 2dSPCA+LDA, it is 88.60% at dimension 8, which is almost same as 2dPCA+LDA (88.87% at dimension 9). But the projection vectors obtained by 2dPCA and 2dPCA+LDA are not sparse while 2dSPCA and 2dSPCA+LDA are sparse. It means that 2dSPCA and 2dSPCA+LDA achieve better or comparable performance compared with 2dPCA and 2dPCA+LDA respectively although they make use of less features, and sparsity also means less time and space costs which is benefits for online application. Since 2dPCA works by rows and columns instead of pixel points, so our 2dSPCA algorithm also reserves this advantage which keeps the locally geometric information of images. The transformed features by sparse

projection vectors are constructed by row and column features, which is easily to interpret the structure of new features because of the sparsity of projection vectors.

5 Conclusion

In this paper, in order to overcoming the disadvantages of traditional PCA algorithm in palmprint recognition, we proposed a novel feature extraction technique 2dSPCA which absorbs the advantages of SPCA and 2dPCA. Our method obtains sparse projection by solving a elastic net optimization problem under regression framework which is equivalent to PCA. Sparsity avoids the affect of over-fitting and improves the generalization, also provides a feasible access to interpret the meaning of each component structure. 2dSPCA considers the two-dimensional geometric structure of images and keep more discriminant information than traditional approach. Because of the use of image covariance matrices, the number of dimension is reduced significantly, and the realization for palmprint recognition becomes applicable for online test. Both 2dSPCA and 2dSPCA+LDA achieve satisfied results on PolyU palmprint database.

References

1. Duta, N., Jain, A., Mardia, K.: Matching of Palmprint. Pattern Recognition Letters 23, 477–485 (2002)
2. Lu, G., Zhang, D., Wang, K.: Palmprint Recognition Using Eigenpalms Features. Pattern Recognition Letters 24, 1463–1467 (2003)
3. Wu, X., Zhang, D., Wang, K.: Fisherpalms Based Palmprint Recognition. Pattern Recognition Letters 24, 2829–2838 (2003)
4. Yang, J., Zhang, D., Frangi, A., Yang, J.: Two-dimensional PCA: a New Approach to Appearance-based Face Representation and Recognition. IEEE Transactions on Pattern Analysis and Machine Intelligence 26, 131–137 (2004)
5. Zhang, D.: PolyU palmprint database (2003), http://www4.comp.poly.edu.hk/biometrics
6. Zhou, H., Hastie, T., Tibshirani, R.: Sparse Principle Component Analysis. Journal of Computational and Graphical Statistics 15, 265–286 (2006)
7. Tibshirani, R.: Regression Shrinkage and Selection Via the Lasso. Journal of the Royal Statistical Society (B) 58, 267–288 (1996)
8. Zou, H., Hastie, T.: Regularization and Variable Selection Via the Elastic Net. Journal of the Royal Statistical Society(B) 67, 301–320 (2005)
9. Efron, B., Hastie, T., Johnstone, I., Tibshirani, R.: Least Angle Regression. Annals of Statistics 32, 407–499 (2004)
10. Wright, J., Yang, A., Satry, S., Ma, Y.: Robust Face Recognition Via Sparse Representation. IEEE Transactions on Pattern Analysis and Machine Intelligence 32, 210–227 (2009)

Discovery of Protein's Multifunction and Diversity of Information Transmission

Bo Li[1,3], Jin Liu[2,3], Shuxiong Wang[2], Wensheng Zhang[3], and Shu-Lin Wang[4]

[1] College of Computer Science and Technology,
Wuhan University of Science and Technology, China
[2] State Key Lab of Software Engineering, Computer School, Wuhan University, China
[3] Lab. of Complex Systems and Intelligence Science, Institute of Automation, CAS, China
[4] School of Computer and Communication, Hunan University,
Changsha, Hunan, 410082, China
liberol@mail.ustc.edu.cn

Abstract. To clarify the manifold roles of a protein among different protein complexes and to reveal the diversity of information transmission among these complexes, essential elements, tasks, process and experiment are represented. The proposed method benefits exploring potential physiological function of a protein and clarifying how it contributes to the diversity of information transition.

Keywords: Multifunctional protein, information transmission diversity.

1 Introduction

Proteins often associate in the same space and time to form stable complexes and work together to achieve a physiological function [1]. A single kind of protein can not usually achieve a physiological function without participating in a particular protein complex. A protein performs its biochemical functions by interacting briefly with other proteins [1]. The principle of function homogeneity indicates that proteins in the same complex are more likely to own homothetic function. Protein complexes can be used to investigate physiological function of unfamiliar proteins [2]. A major concern for a multifunctional protein is that the more complexes it participates in the more potential physiological functions it dedicates to. New physiological function of the multifunctional protein may be discovered along this clue. The diversity of information transmission for a protein is represented by its connection between complexes as their intersection. This connection indicates the information transmission between complexes. The more complexes this protein connects the more important it as a messenger. When investigating the diversity of the physiological function and the information transmission for a single protein, it more focused on the protein as a group member rather an individual works because this protein usually contributes to a physiological function in a particular complex.

D.-S. Huang et al. (Eds.): ICIC 2010, LNCS 6215, pp. 619–625, 2010.

2 Basic Idea

Definition 1 (Maximal clique): A clique is a complete subgraph. A maximal clique is defined as a set of vertexes that make up a complete subgraph and is not a subset of any larger complete subgraph [3, 4].

Definition 2 (Similarity): Given a graph set $H=\{H_1, H_2, \ldots, H_t\}$, the similarity of these graphs is defined as follows:

$$\text{similarity}\ (H_1, H_2, \ldots, H_t) = \lambda_1 \frac{|V(H_1 \cap H_2 \cap \ldots \cap H_t)|}{\min\{|V(H_1)|, |V(H_2)|, \ldots, |V(H_t)|\}} + \lambda_2 \frac{|V(H_1 \cap H_2 \cap \ldots \cap H_t)|}{\max\{|V(H_1)|, |V(H_2)|, \ldots, |V(H_t)|\}}$$

where $\lambda_1 + \lambda_2 = 1$, $H_1, H_2, \ldots, H_t$ are compete graphs, $|V(H_i)|$ is the number of nodes in H_i and i= 1, 2, …, n.

There is a value of t_i that corresponds t o H_i satisfies corollary 2. This makes H_i corresponds to a point (t_i, $S(H_1, H_2, \ldots, H_t, t_i)$) on the image of the function $S(H_1, H_2, \ldots, H_t, \lambda)$. And the set of all graphs corresponds to the discrete point set on the image of the function $S(H_1, H_2, \ldots, H_t, \lambda)$, that is $\{H_1, H_2, \ldots, H_t\} \xrightarrow{S(H_1, H_2, \ldots, H_t, \lambda)} Graph\{(t_i, S(H_1, H_2, \ldots, H_t, t_i))\}$.

Definition 3 (Equivalence): Given a graph set $H=\{H_1, H_2, \ldots, H_t\}$, the equivalence relationship of any two graphs $H_i \sim H_j$ is defined as $H_i \sim H_j \Leftrightarrow |1- V(H_i)/V(H_j)| \leq S(H_1, H_2, \ldots, H_t, t_i)$ or $|1- V(H_j)/V(H_i)| \leq S(H_1, H_2, \ldots, H_t, t_j)$, i, j = 1, 2, …*t.* The intersection set $H_1 \cap H_2 \cap \ldots \cap H_t$ reflects the similarity among these graphs. Nodes anot in the intersection indicate the difference among these graphs. The smaller ratio of the difference to the similarity, the more rational these graphs be put into one equivalent category.

Definition 4 (Quotient set): Given a graph set $H=\{H_1, H_2, \ldots, H_t\}$, its quotient set $(H, \sim)$ can be defined as $(H, \sim)=\{[H_k] \mid [H_k] = \{ H_j \mid H_j \sim H_k \}\}$.

The major steps of irregular community discovery can be formalized as follows:

***Task* 1:** (**Maximal clique discovery**) Find out all maximal cliques in a network G, with $C_{max}\{c_1, c_2, \ldots, c_k\}$, for $\forall c_i, c_j \in C_{max}$, $c_i \neq c_j$, $c_i \not\subset c_j$, and $c_j \not\subset c_i$.
***Task* 2:** (**Establish the quotient set of a clique set**) Establish the quotient set for a network G and its the maximal clique set $C_{max}=\{c_1, c_2, \ldots, c_k\}$.
***Task* 3:** (**Sub-graph Scrubbing**) If elements contain only one member graph and no node appears in other graphs, they are removed from the quotient set in Task 2.
***Task* 4:** (**Sub-graph combination and rebuilding quotient set**) If an element in the quotient set in task 2 contains more than two graph members with the same similarity, these graphs are combined into a new one. Then we rebuild the quotient set.
***Task* 5:** (**Analizing potential function and diversity of information transmission**) Take the result of task 4 the quotient set, the potential function of multiproteins and their multifold roles in diversity of information transmission are analyzed with other means.

3 Proposed Method

3.1 Sub-graph Scrubbing

As to task 1, if given a PPI network, the first step is to recognize the maximal cliques from a given PPI network according to the DFS algorithm in graph theory [5]. In a recursive manner, we design a process that explores a vertex v in the PPI network and checks whether the vertex and its adjacent ones s could constitute a clique until all cliques that include v are found out. For task 2, the quotient set is established according to definition 3. It is actually a categorizing process as demonstrated in Fig 1. In this example, the maximal clique set is $\{H_1, H_2, H_3, H_4\}$, where $V(H_1)=\{1,4,5,6,7\}$, $V(H_2)=\{1,4,5,6,7\}$ $V(H_3)=\{1,2,3\}$, $V(H_4)=\{1,5,6,7,9\}$and $V(H_5)=\{10,11,12\}$. According to definition 3, H_1, H_2, H_4 are put into the same equivalent class and H_3 are put into another equivalent class. This is because $|1- V(H_i)/V(H_1)| = 0 < S(H_1, H_2, H_3, H_4, t_1)=4/5$ (i=2,4) and $|1- V(H_j)/V(H_3)|= 2/3 > S(H_1, H_2, H_3, H_4, t_3)=1/3$ (j=1,2,4). And H_5 do not meet any cliques in this case so that $[H_5]$ should be a candidate element of the quotient set. Thus $[H_1, H_2, H_4]$, $[H_3]$ and $[H_5]$ are all candidate elements for the quotient set.

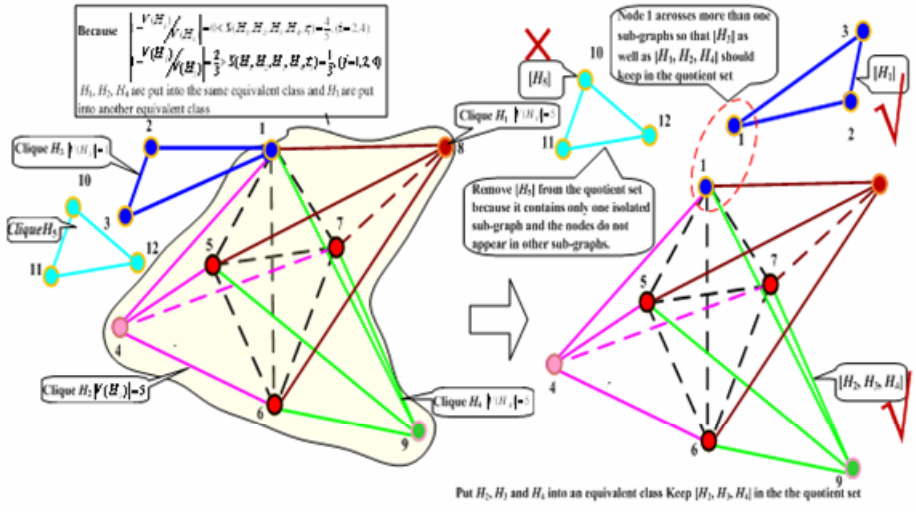

Fig. 1. Establish the quotient set of a clique set and sub-graph Scrubbing

Furthermore, it is noticeable that $[H_5]$ contains only one isolated sub-graph and the nodes of H_5 do not appear in other sub-graphs. $[H_5]$ could be a unwanted noise because it impossible for $[H_5]$ to participate in subsequent probe into manifold roles of multifunctional proteins. Thus, $[H_5]$ is removed from the quotient set. Node 1 acrosses more than one sub-graphs so that $[H_3]$ and $[H_1, H_2, H_4]$ should keep in the quotient set.

3.2 Quotient Graph Combination

Each element of the quotient set is consisted of several sub-graphs, where the intersection of any two sub-graphs is nonempty with the matchable node number. To explore potential function of multifunctional proteins and their multifold roles in information

transmission, we merge sub-graphs of the same quotient set element into a new one. In this way, a one-to-one correspondence relationship is established between the newly combined graph set and the original quotient set. For example, if $[H_1]=\{H_1, H_2\}\in(H, \sim)$, it means that we denotes the combined graph as $[H_1]$. It holds that $|V([H_1])| = |V(H_1)| + |V(H_2)| - |V(H_1\cap H_2)|$. The intersection of sub-graphs works among protein complexes is emphasized by this quotient graph combination, which gives a neat viewpoint on observable objects.

3.3 Protein's Potential Function and Diversity of Information Transmission

An equivalent class containing similar sub-graphs indicates a specific physiological function. If a sub-graph embodies a protein complex in an equivalent class, the potential function of a multifunctional protein is investigated under the circumstances of these complexes' intersection because this multifunctional protein joins several complexes in different equivalent classes. With our iterative approach, the equivalent classes that a common protein stay in can be discovered, which implies the potential new physiological function for this protein. In this process, each element of the quotient set keeps a one-to-one correspondence relationship with a physiological function.

We use the set of generated quotient elements *EF* to represent newly combined sub-graphs that indicate emergent function. It holds that $EF_{inital}= EF_0=(H, \sim)_{initial}$ and $EF_{i+1}= (H, \sim)_{i+1} - ((H, \sim)_{i+1}\cap(H, \sim)_i)$, i=0, 1, …, n-1. If an equivalent class can be transformed into another one by combining its member sub-graphs, these two equivalent classes are regarded to be identical. Then, the cardinality of *EF* is used to indicate the newly appeared function. If the interaction round is *n*, the cardinality of *EF* in the *i*-th round is $|EF_i|$, i=1, 2,…, n. It satisfies that $|EF_0|>|EF_1|>\ldots|EF_{i-1}|>|EF_i|>|EF_{i+1}|\ldots>|EF_n|$. We denote $AF= \sum_{i=0}^{n}|EF_i|$ to indicate the aggregate of physiological function that involves in the iterative process. Likewise, the importance of a given protein *P* in information transmission is that it connects different equivalent classes of a quotient set. We denote the number of these equivalent classes in the *i*-th round interaction as t_i. Thus the number of permutation and combination of these protein groups containing the protein *P* in the *i*-th round interaction is $AD_i= C_{t_i}^2 + C_{t_i}^3 + \ldots\ldots + C_{t_i}^{t_i} = 2^{t_i} - t_i - 1$, which indicates the diversity of information transmission via the protein *P*. And the aggregate of these diversities throughout the iterative process is denoted as $AD = \sum_{i=0}^{n} AD_i$.

4 Experiment

An experimental case of a PPI network segment from IntAct is used to clarify the proposed method [6]. There are 582 proteins in this network. The task 1 identifies 20 maximal cliques and 4 clique groups where cliques connects with each other in a group but do not connect with cliques outside this group. Table 1 illustrates the case of iterative quotient graph combination as stipulated tasks in section 2, where the clique *i* are denote as Gi, *i*=1, 2, …, *n*. This table describes the states of the intersectant sub-graphs, the initial quotient set and 4 round interaction of quotient graph combination.

Table 1. The case of iterative quotient graph combination

Group	intersectant sub-graphs →	initial quotient set →
1	G1,G2,G3,G4,G5	**[G1,G2],[G3,G5],[G4]**
2	G6,G7,G8,G9	**[G6,G7],[G8],[G9]**
3	**G10,G11,G12,G13**	**[G10,G11],[G12],[G13]**
4	G14,G15,G16,G17,G18,G19,G20	**[G14,G15],[G16,G17],[G18],[G19],[G20]**
Group	1st round iteration →	2nd round iteration →
1	[G1-2],**[G3-5,G4]**	[G1-2],[G3-5-4]
2	**[G6-7,G8]**,[G9]	[G6-7-8],[G9]
3	**[G10-11,G12],[G13]**	**[G10-11-12, G13]**
4	[G14-15],**[G16-17,G18]**,[G19],[G20]	[G14-15],**[G16-17-18,G19**],[G20]
Group	3rd round iteration →	4rd round iteration →
1	[G1-2],[G3-5-4]	[G1-2],[G3-5-4]
2	[G6-7-8],[G9]	[G6-7-8],[G9]
3	[G10-11-12-13]	[G10-11-12-13]
4	[G14-15],**[G16-17-18-19,G20]**	[G14-15],[G16-17-18-19-20]

Specially, the iterative quotient graph combination for the group 3 in Table 1 is demonstrated in Fig. 2 to indicate the multifunction of the protein *P* and the diversity of information transmission via *P*, i.e., the number of permutation and combination of these protein groups containing *P* in the *i*-th round interaction. We denote AF and AD for the group 3 as AF-3 and AF-3 respectively. The values of *AF*-3 in the initial group 3 and 3 rounds of the iterative quotient graph combination are 3, 4, 5 and 5. And the values of *DF*-3 in the initial group 3 and 3 rounds of the iterative quotient graph combination are 11, 15, 16 and 16. AF-3 and DF-3 indicate the manifold roles in connecting different protein groups with different potential physiological function. With other methods of phytophysiology & biochemistry, this diversity benefits discovery of proteins' new function and exploration of how a multifunctional protein works in connecting protein complexes and the physiological function they commit to.

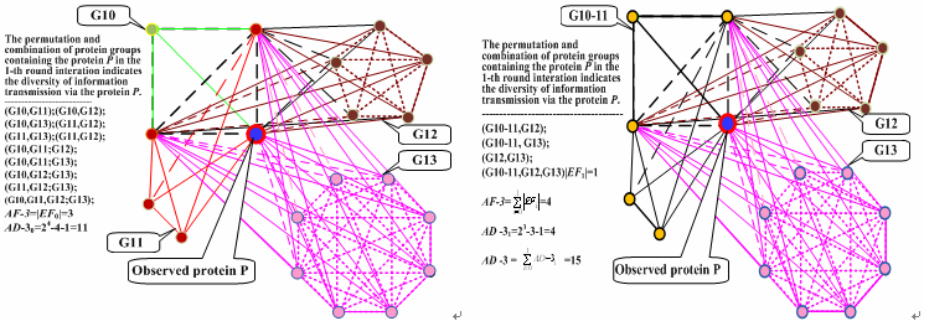

(a) Diversity of information transition via protein P in the initial sub-graph group 3

(b) Diversity of information transition across sub-graph group 3 via protein P after 1st round iteration

Fig. 2. Protein *P* connected diversity of information transition in sub-graph group 3 throughout the iteration of quotient graph combination in Table 1

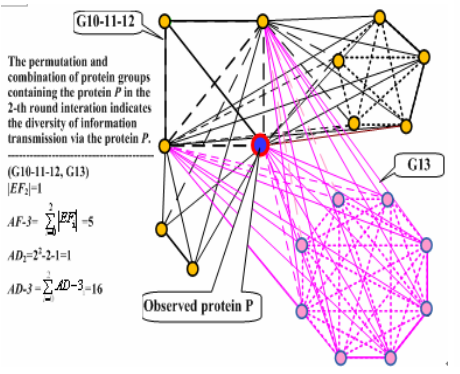

(c) Diversity of information transition across sub-graph group 3 via protein P after 2nd round iteration

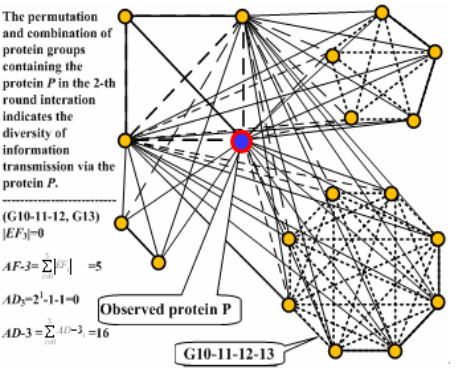

(d) Diversity of information transition across sub-graph group 3 via protein P after 3rd round iteration

Note. The permutation and combination of protein groups containing the protein *P* in the *i*-th round interaction indicates the diversity of information transmission via the protein *P*.

Fig. 2. (*continued*)

A total of 4 sub-graph groups involve the quotient graph combination in Table 1. Fig. 3 records the aggregate process of physiological function *AD* and the permutation and combination of sub-graphs via some multifunctional proteins, which expresses multifunctional proteins' contribution to the diversity of information transmission among protein complexes.

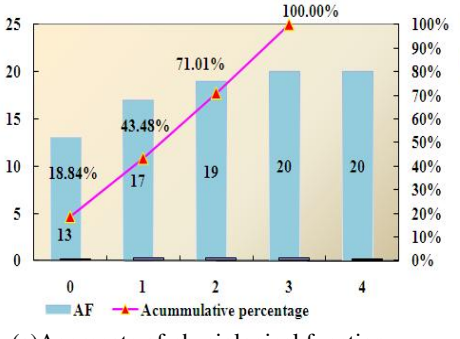

(a)Aggregate of physiological function

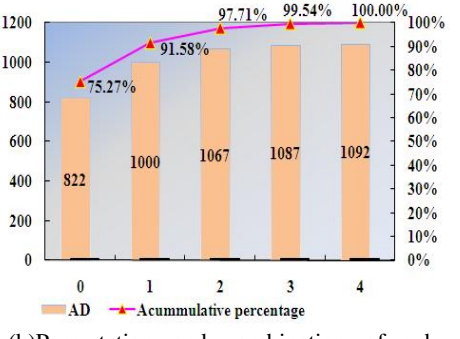

(b)Permutation and combination of sub-graphs via some multifunctional proteins

Fig. 3. Discovery of physiological function and diversities of information transmission throughout the whole iterative quotient graph combination

5 Conclusions

With the novel method, we explore the issue of how to clarify the manifold roles of a protein among different protein complexes and reveal the diversity of information

transmission among these complexes. Metric measurement of AF and AD benefit discovering potential physiological function of a protein and clarifying how it contributes to the diversity of information transition among different protein complexes.

Acknowledgement

This work is funded by the National Natural Science Foundation of China (grant nos., 60703018, 60973153, and 90924026), 973 Program (2007CB310800), 863 Program (2008AA01Z208; 2009AA01Z405), Open Fund Project of State Key Lab. for Novel Software Technology, Nanjing University, the Science and Technology Commission of Wuhan Municipality "Chenguang Jihua" (201050231058), the Doctoral Fund of Ministry of Education of China (20090181110053), and the China Postdoctoral Science Foundation (grant no. 20090450825).

References

1. Protein–protein interaction (2010), http://en.wikipedia.org/wiki/Multiprotein_complex
2. Butland, G., Peregrín-Alvarez, J.M., Li, J., et al.: Interaction network containing conserved and essential protein complexes in Escherichia coli. Nature 433, 531–537 (2005)
3. Cazals, C., Karande, C.: An algorithm for reporting maximal c-cliques. Theoretical Computer Science 349, 484–490 (2005)
4. Koch, E., Wanke, T.L.: An algorithm for finding maximal common subtopologies in a set of protein structures. Journal of Computational Biology 3, 289–306 (1996)
5. Martin, G.: Algorithmic Graph Theory and Perfect Graphs, 2nd edn. Elsevier, Amsterdam (2004)
6. Hermjakob, H., Montecchi-Palazzi, L., Lewington, C.: IntAct - an open source molecular interaction database. Nucleic Acids Research 32, D452–D455 (2004)

Identification and Analysis of Binding Site Residues in Protein Complexes: Energy Based Approach

M. Michael Gromiha[1], S. Selvaraj[2], B. Jayaram[3], and Kazuhiko Fukui[1]

[1] Computational Biology Research Center (CBRC), National Institute of Advanced Industrial Science and Technology (AIST), 2-4-7 Aomi, Koto-ku, Tokyo 135-0064, Japan
{michael-gromiha,k-fukui}@aist.go.jp
[2] Department of Bioinformatics, Bharathidasan University, Tiruchirapalli 620024, Tamilnadu, India
[3] Department of Chemistry and Supercomputing Facility for Bioinformatics and Computational Biology, Indian Institute of Technology Delhi, New Delhi 110016, India

Abstract. Understanding the recognition mechanism of protein complexes is a challenging task in bioinformatics and computational biology. We have developed a novel energy based approach for identifying the binding site residues in protein–protein, protein-RNA and protein-DNA complexes. In protein-protein complexes, the residues and residue-pairs with charged and aromatic side chains are important for binding. These residues influence to form cation–π, electrostatic and aromatic interactions. In protein-RNA complexes, the positively charged, polar and aromatic residues are important for binding. These residues influence to form electrostatic, hydrogen bonding and stacking interactions. The positive charged and polar residues are preferred to bind with DNA in protein-DNA complexes. These results provide an overall view of binding in protein complexes. Our observations have been verified with the experimental binding specificity of protein-protein and protein-nucleic acid complexes and found good agreement with experiments.

Keywords: protein-protein, protein-RNA, complex, interaction energy, binding propensity, binding free energy change.

1 Introduction

The interactions of proteins with other molecules, such as proteins, DNA, RNA, carbohydrate and ligand are important for most of the cellular processes in living organisms. Protein-protein interactions have been approached on two aspects: (i) large scale studies on protein-protein interaction networks and (ii) understanding the principles and predicting the binding sites using protein-protein complex structures. The latter approach has also been applied to protein-DNA and protein-RNA complexes. Unraveling the mechanisms of protein-protein, protein-nucleic acid and protein-ligand are fundamental problems, which would aid in function prediction and drug design.

The availability of protein-protein, protein-RNA and protein-DNA complex structures in Protein Data Bank [1] enables researchers to analyze their binding sites in terms of atomic contacts, amino acid composition, preference of residues, secondary

D.-S. Huang et al. (Eds.): ICIC 2010, LNCS 6215, pp. 626–633, 2010.

structures, solvent accessibility, flexibility, electrostatic interactions, hydrophobic contacts, hydrogen bonding and van der Waals interactions [2-10]. On the other hand, several methods have been proposed for identifying the binding sites in protein-protein, protein-RNA and protein-DNA complexes [11-18]. In most of these studies, binding sites have been defined with a criteria based on the contacts between the partners in protein complexes [11,12,14-17]. The atomic contacts between any atoms or heavy atoms in a pair of proteins or protein-RNA/DNA as well as the distances of 2.5 Å-6.0Å have been used to assign the contacts. These criteria include the repulsive interactions in which two residues or residue-nucleotide pairs are close to each other. In addition, these pairs with different distances have been treated as the same manner.

In this work, we have developed a new approach based on interaction energy for defining the binding sites. We observed that the binding sites are dominated with aromatic and charged residues indicating the importance of electrostatic, aromatic and cation-π interactions in protein-protein complexes. In protein-RNA complexes, the binding sites are dominated with positively charged, aromatic and polar residues indicating the importance of electrostatic, hydrogen bonding and aromatic interactions. The dominance of charged and polar residues are noticed in protein-DNA complexes.

2 Materials and Methods

2.1 Dataset

We have developed non-redundant datasets of 153 protein-protein, 81 protein-RNA and 212 protein-DNA complexes from the information available in the literature [19-21]. In order to avoid the bias in the dataset, have sufficient number of data and obtain reliable of results we have used the conditions, sequence identity and resolution to construct the datasets. All complex structures have been solved with better than 3Å resolution and the sequence identity is less than 25%, 35% and 35%, respectively.

2.2 Computation of Interaction Energy

We have calculated the interaction energy between atoms in protein complexes using AMBER potential [22]. It is given by:

$$E_{inter} = \Sigma\, [(A_{ij}/r_{ij}^{12} - B_{ij}/r_{ij}^{6}) + q_i q_j/\varepsilon r_{ij}] \quad (1)$$

where $A_{ij} = \varepsilon_{ij}^{*}(R_{ij}^{*})^{12}$ and $B_{ij} = 2\ \varepsilon_{ij}^{*}(R_{ij}^{*})^{6}$; $R_{ij}^{*} = (R_i^{*} + R_j^{*})$ and $\varepsilon_{ij}^{*} = (\varepsilon_i^{*}\ \varepsilon_j^{*})^{1/2}$; R^{*} and ε^{*} are, respectively, the van der Waals radius and well depth and these parameters are obtained from Cornell et al. [22]; q_i and q_j are, respectively, the charges for the atoms i and j, and r_{ij} is the distance between them. We have used the distant dependent dielectric constant ($\varepsilon = r_{ij}$) to take account of the dielectric damping effect of the Coulomb interactions, as used in other studies on protein complexes [23].

2.3 Binding Propensity

The binding propensity for the 20 amino acid residues in protein-protein, protein-RNA and protein-DNA complexes has been developed as follows: we have computed

the frequency of occurrence of amino acid residues in binding sites (f_b) and in the protein as a whole (f_t). The binding propensity (P_{bind}) is calculated using the equation:

$$P_{bind}(i) = f_b(i)/f_t(i) \quad (2)$$

where, i represents each of the 20 amino acid residues.

2.4 Binding Segments

The residues identified as binding sites have been analyzed in terms of binding segments. It is based on the number of consecutive binding residues in amino acid sequences. For example, a 4-residue binding segment has a stretch of four consecutive binding residues.

3 Results and Discussion

3.1 Occurrence of Amino Acid Residues at Various Ranges of Interaction Energies

In a protein complex, we have computed the interaction energy (Eqn. 1) of each residue in a protein with all residues in a ligand (protein, RNA or DNA). The total percentage of residues at different intervals of interaction free energies are displayed in Figure 1. In this figure, we present the results obtained with protein-protein, protein-RNA and protein-DNA complexes.

In protein-protein complexes, we observed that 10.8% of the residues have strong interactions with the interaction free energy of <-1 kcal/mol. On the other hand, 6.2% of residues have repulsive energies and 77% of the residues have the interaction energy in the range of -0.3 to 0 kcal/mol, which might be due to the presence of residues that are far away in 3D structures. We have compared the results with those obtained with distance based criteria for defining binding site residues and noticed significant differences between them. Only 28% residues are common to each other and this result indicates the importance of considering the energy between different atoms to define the binding residues. In addition, 4% of the residues have strong repulsive energies and all these residues have been identified as binding residues in distance based criteria, which are not probable binding residues in protein-protein complexes.

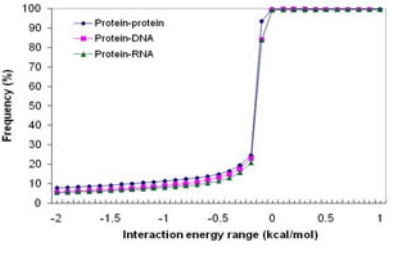

Fig. 1. Occurrence of amino acid residues in different ranges of interaction energies in protein-protein, protein-RNA and protein-DNA complexes

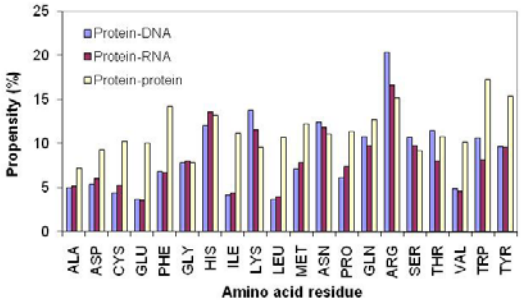

Fig. 2. Binding propensity of amino acid residues in protein-protein, protein-RNA and protein-DNA complexes

In protein-RNA complexes, we observed that 7.6% of the residues have the interaction free energy of < -1 kcal/mol, which is less than that in protein-protein complexes. For the same dataset, the distance based method showed 6.1% of residues as binding sites with the cutoff of 3.5Å.

In protein-DNA complexes, we observed that 8.7% of the residues have strong interactions with nucleotides. Distance based method identified 7.9% of total residues as binding sites.

3.2 Binding Propensity of Residues in Protein Complexes

We have computed the binding propensity in protein complexes and the results for protein-protein, protein-RNA and protein-DNA complexes are presented in Figure 2.

In protein-protein complexes, the aromatic as well as positively charged residues highly contribute to interact between protein partners, indicating the importance of cation-π, aromatic and electrostatic interactions. The comparison between protein-protein and protein-RNA complexes showed that the residues, Asp, Cys, Glu, Phe, Ile, Leu, Met, Val, Trp and Tyr have remarkably high contribution in protein-protein complexes. These residues prefer to form electrostatic, hydrophobic and aromatic interactions in protein-protein complexes. On the other hand, the residues Arg, His, Lys, Asn, Tyr, Gln and Ser highly contribute for the interaction between protein and RNA. Interestingly, these residues belong to positively charged, polar and aromatic groups, which form electrostatic, hydrogen bonds and aromatic interactions with RNA. In protein-DNA complexes, positive charged residues are more dominant than protein-protein and protein-RNA complexes. Further, polar residues prefer to interact with DNA in the form of hydrogen bonds.

3.3 Binding Segments in Protein Complexes

We have analyzed the binding residues in terms of "continuous stretch" in amino acid sequence. The lengths of continuous binding residues are termed as binding segments. The binding segments have been analyzed in protein-protein, protein-RNA and protein-DNA complexes. In protein-protein complexes, about half of the binding

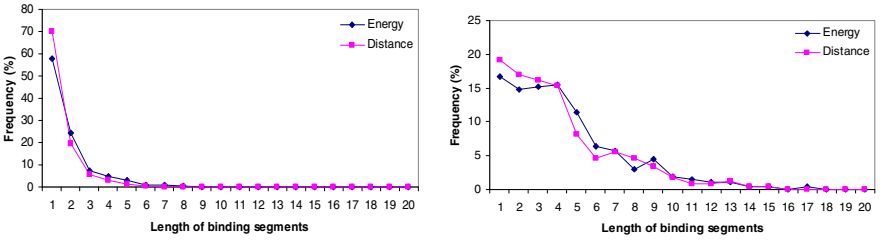

Fig. 3. Frequency of occurrence of (a) amino acid residues (left) and (b) nucleotides (right) at various lengths of binding segments in protein-RNA complexes. The data with distance and energy based criteria are shown.

segments are accommodated with single amino acid residues, which showed that the neighboring residues are non-binding. Similar trend is also observed with distance based criteria used to identify the binding sites. The two and three-residue segments have 25% and 8% of the binding segments, respectively.

In protein-RNA complexes, 58% of the binding segments are accommodated with single amino acid residues (Figure 3a). The two and three-residue segments have 24% and 8% of the binding segments, respectively. The frequency of binding segments based on continuous stretch of nucleotides obtained with energy based and distance based approaches in protein-RNA complexes are shown in Figure 3b. We noticed that the percentage of binding segments accommodated with one, two, three, four and five nucleotides are respectively, 17%, 15%, 15%, 16% and 11%. This result reveals that a stretch of nucleotides in RNAs prefers to interact with amino acid residues in proteins [24]. Protein-DNA complexes have similar behavior to that of protein-RNA complexes.

3.4 Contribution of Different Types of Atoms in Protein Complexes

In order to understand the importance of main chain and side chain atoms for binding we have analyzed the contribution of interaction energy due to different atoms in protein-protein, protein-RNA and protein-DNA complexes. The results are presented in Figure 4.

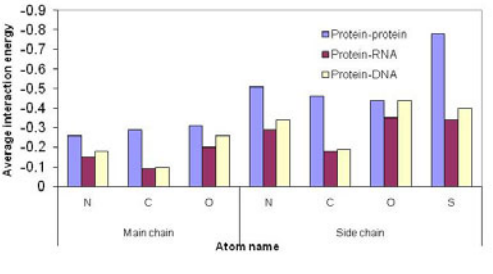

Fig. 4. Contributions of different atoms in protein-DNA, protein-RNA and protein-protein complexes; N: nitrogen, C: carbon, O: oxygen and S: sulfur

We noticed that the contributions of side chain atoms are twice to that of main chain atoms in protein-protein complexes. This result indicates the importance of electrostatic, aromatic and cation-π interactions formed by the side chain atoms of proteins and DNA/RNA in protein-protein and protein-nucleic acid complexes. Further, the main chain atoms of DNA and RNA have appreciable interactions with side chain atoms in protein-RNA and protein-DNA complexes, indicating their role in the formation of electrostatic interactions.

3.5 Comparison with Experiments

We have compared the results obtained in this work with experimental binding free energies of protein-protein and protein-nucleic acid complexes. This has been done with the data on changes in binding free energy upon amino acid substitutions.

The search on protein-protein interactions thermodynamic database [25] showed the presence of 68 unique mutations, which have the difference in binding free energy of >2 kcal/mol. We observed that 32 of them are aromatic and positive charged. On the other hand only seven residues are hydrophobic. This result demonstrates the importance of electrostatic, cation-π and aromatic interactions for the recognition of protein-protein complexes.

The search on protein-nucleic acid interactions thermodynamic database [26] showed the presence of 72 unique interactions, which have the binding free energy of < -1kcal/mol. We observed that the majority of the mutants are due to the replacement of aromatic (19 mutants), charged (19 mutants) and polar (16 mutants) residues. Only few hydrophobic mutants and residues with similar chemical behavior caused the binding free energy change of < -1kcal/mol. This result demonstrates the importance of electrostatic, hydrogen bonds, cation-π and aromatic interactions for the recognition of protein-RNA complexes. Our computational analysis revealed the importance of these interactions, showing good agreement with experiments.

4 Conclusions

We have developed an energy based approach to identify the binding sites and important interactions for the recognition of protein-protein, protein-RNA and protein-DNA complexes. This approach can be commonly used for all macromolecules interacting with proteins. We have delineated the binding site residues using the cutoff interaction energy of -1kcal/mol. Our analysis showed the important residues for binding in protein complexes. Further, the binding residues have been analyzed in terms of binding segments. Most of the binding residues preferred to be in single residue segments. On the other hand, the nucleotides prefer to be in multiple nucleotide segments. The atomic contributions revealed that the side chain atoms are prevalent than main chain atoms in protein-protein complexes and the importance of phosphate atom in the main chain of DNA and RNA. The important interactions have been compared with experimental binding free energy change and we observed good agreements with experiments.

Acknowledgments. This research was supported by Strategic International Cooperative Program, Japan Science and Technology Agency (JST).

References

1. Berman, H., Henrick, K., Nakamura, H., Markley, J.L.: The Worldwide Protein Data Bank (wwPDB): Ensuring a Single. Uniform Archive of PDB Data. Nucleic Acids Res. 35(Database issue), D301–303 (2007)
2. Treger, M., Westhof, E.: Statistical Analysis of Atomic Contacts at RNA-protein Interfaces. J Mol. Recognit. 14, 199–214 (2001)
3. Jones, S., Daley, D.T., Luscombe, N.M., Berman, H.M., Thornton, J.M.: Protein-RNA Interactions: a Structural Analysis. Nucleic Acids Res. 29, 943–954 (2001)
4. Guharoy, M.: Chakrabarti Conservation and Relative Importance of Residues Across Protein-protein Interfaces. P. Proc. Natl. Acad. Sci. U.S.A. 102, 15447–15452 (2005)
5. Gromiha, M.M., Siebers, J.G., Selvaraj, S., Kono, H., Sarai, A.: Intermolecular and Intramolecular Readout Mechanisms in Protein-DNA Recognition. J. Mol. Biol. 337, 285–294 (2004)
6. Morozova, N., Allers, J., Myers, J., Shamoo, Y.: Protein-RNA Interactions: Exploring Binding Patterns with a Three-dimensional Superposition Analysis of High Resolution Structures. Bioinformatics 22, 2746–2752 (2006)
7. Shoemaker, B.A., Panchenko, A.R.: Deciphering Protein-protein Interactions. Part II. Computational methods to predict protein and domain interaction partners PLoS Comput. Biol. 3, 43 (2006)
8. Ellis, J.J., Broom, M., Jones, S.: Protein-RNA Interactions: Structural Analysis and Functional Classes. Proteins 66, 903–911 (2007)
9. Pan, Y., Tsai, C.J., Ma, B., Nussinov, R.: How Do Transcription Factors Select Specific Binding Sites in the Genome? Nat. Struct. Mol. Biol. 16, 1118–1120 (2009)
10. Gromiha, M.M., Yokota, K., Fukui, K.: Energy Based Approach for Understanding the Recognition Mechanism in Protein-protein Complexes. Mol. Biosyst. 5, 1779–1786 (2009)
11. Sikić, M., Tomić, S., Vlahovicek, K.: Prediction of Protein-protein Interaction Sites in Sequences and 3D Structures by Random Forests. PLoS Comput. Biol. 5, e1000278 (2009)
12. Koike, A., Takagi, T.: Prediction of Protein-protein Interaction Sites Using Support Vector Machines. Protein. Eng. Des. Sel. 17, 165–173 (2004)
13. Ofran, Y., Rost, B.: ISIS: Interaction Sites Identified From Sequence. Bioinformatics 23(2), e13-6 (2007)
14. Terribilini, M., Sander, J.D., Lee, J.H., Zaback, P., Jernigan, R.L., Honavar, V., Dobbs, D.: RNABindR: A Server for Analyzing and Predicting RNA-binding Sites in Proteins. Nucleic Acids Res. 35(Web Server issue), W578–W584 (2007)
15. Wang, L., Brown, S.J.: BindN: A web-based Tool for Efficient Prediction of DNA and RNA Binding Sites in Amino Acid Sequences. Nucleic. Acids Res. 34(Web Server issue), W243–W248 (2006)
16. Kumar, M., Gromiha, M.M., Raghava, G.P.: Prediction of RNA Binding Sites in a Protein Using SVM and PSSM Profile. Proteins 71, 189–194 (2008)
17. Ahmad, S., Gromiha, M.M., Sarai, A.: Analysis and Prediction of DNA-binding Proteins and Their Binding Residues Based on Composition, Sequence and Structural Information. Bioinformatics 20, 477–486 (2004)
18. Ofran, Y., Mysore, V., Rost, B.: Prediction of DNA-binding Residues from Sequence. Bioinformatics 53, i347–i353 (2007)

19. Gromiha, M.M., Yokota, K., Fukui, K.: Sequence and Structural Analysis of Binding Site Residues in Protein-protein Complexes. Int. J. Biol. Macromol. 46, 187–192 (2010)
20. Bahadur, R.P., Zacharias, M., Janin, J.: Dissecting Protein-RNA Recognition Sites. Nucleic Acids Res. 36, 2705–2716 (2008)
21. Xu, B., Yang, Y., Liang, H., Zhou, Y.: An All-atom Knowledge-based Energy Function for Protein-DNA Threading, Docking Decoy Discrimination, and Prediction of Transcription-Factor Binding Profiles. Proteins 76, 718–730 (2009)
22. Cornell, W.D., Cieplak, P., Bayly, C.I., Gould, I.R., Merz, K.M., Ferguson, D.M., Spellmeyer, D.C., Fox, T., Caldwell, J.W., Kollman, P.A.: A Second Generation Force Field for the Simulation of Proteins, Nucleic Acids, and Organic Molecules. J. Amer. Chem. Soc. 117, 5179–5197 (1995)
23. Pichierri, F., Aida, M., Gromiha, M.M., Sarai, A.: Free-Energy Maps of Base−Amino Acid Interactions for DNA−Protein Recognition. J. Amer. Chem. Soc. 121, 6152–6157 (1999)
24. Gromiha, M.M., Yokota, K., Fukui, K.: Understanding the Recognition Mechanism in Protein-RNA Complexes Using Energy Based Approach. Curr. Protein Pept. Sci., (in press, 2010)
25. Kumar, M.D., Gromiha, M.M.: PINT: Protein-protein Interactions Thermodynamic Database. Nucleic Acids Res. 34, D195–D198 (2006)
26. Prabakaran, P., An, J., Gromiha, M.M., Selvaraj, S., Uedaira, H., Kono, H., Sarai, A.: Thermodynamic Database for Protein-nucleic Acid Interactions (ProNIT). Bioinformatics 17, 1027–1034 (2001)

Density Based Merging Search of Functional Modules in Protein-Protein Interaction (PPI) Networks

Wei Wang and Jinwen Ma*

Department of Information Science, School of Mathematical Sciences
And LMAM, Peking University, Beijing, 100871, China
jwma@math.pku.edu.cn

Abstract. Discovering functional modules in a protein-protein interaction (PPI) network is very important for understanding the organization and function of the related biological system. The main strategy for this discovery is to translate the PPI network into a mathematical graph which can be analyzed with graph theory. In this paper, we propose a Density Based Merging Search (DBMS) algorithm to discover the complexes of a PPI graph corresponding to the functional modules in the PPI network. The DBMS algorithm starts from a single vertex with the highest density of connecting, then adds it's neighbor vertexes with the sufficiently high density of connecting one by one, and finally obtain one complex when there is no vertex to be added. The same DBMS procedure can be conducted on the rest of the vertexes in the PPI graph till all the complexes are found out. It is demonstrated by the experiments on six PPI datasets that the DBMS algorithm is efficient for discovering the complexes of a PPI network.

Keywords: PPI network; complex; vertex; connecting rate; filter.

1 Introduction

With the development of proteomics technology, a great number of large data sets of protein-protein interactions (PPI) have been accumulated from the proteomic experiments. Actually, a PPI dataset describes a PPI network within a living cell. Recent studies [1] have shown that a large PPI network consists of some complexes which correspond certain functional modules with clear biological meanings. So, it is very important and significant to reveal the structure of a large PI network and find out the existing complexes in it.

As a PPI network can be considered as an interaction graph, a complex can be mathematically represented as a densely connected subgraph in it. In this way, the discovery of the complexes is equivalent to the search of these densely connected subgraphs in the whole PPI interaction graph. To this end, several efficient algorithms have been proposed from different aspects, but they can be generally divided into the splitting and merging search categories.

* Corresponding author.

D.-S. Huang et al. (Eds.): ICIC 2010, LNCS 6215, pp. 634–641, 2010.

In the splitting search, the algorithm starts from the whole PPI interaction graph. It splits the graph into certain subgraphs of densely connecting, and then checks whether these subgraphs fit the conditions of a complex. If some subgraphs satisfy the conditions, we accept them as the complexes. If some subgraphs do not satisfy the conditions, we can further split them into smaller subgraphs of densely connecting, and continue this splitting until all the complexes are finally founded. A typical example of the splitting search is the *GN* algorithm [2] based on *the Hierarchical Clustering*. The *HCS* (Highly Connected Sub-graph) algorithm [3] is another example of this stream, which classifies the vertexes into subgraphs based on *the similarity* between each pair of vertexes. The *RSNC* (Restricted Neighborhood Search Clustering) algorithm [4] is also a such kind of method by implementing a cost based clustering mechanism to identify the complexes.

As for the merging search, the algorithm starts from the most densely connected vertex, extends it into a complex by adding the densely connected vertexes until no such vertex can be founded. Then, the merging search carries on the rest of vertexes and continues the same procedure till all the complexes are found. A representative of the merging search is Newman's Fast Algorithm [5], which conducts the merging process via an evaluation function Q such that a group of vertexes can be merged into a complex as long as Q has the largest increment. Inspired by Newman's work, Clauset further proposed a greedy algorithm [6] which can be applied to very large networks. Recently, Bader and Hogue proposed the MCODE (Molecular Complex Detection) algorithm [8] which utilizes the concept of vertex weighting and can identify the complexes efficiently.

In this paper, in light of the merging search we propose a Density Based Merging Search (DBMS) algorithm for discovering the complexes of a PPI graph with the help of the concept of vertex density of connecting. That is, by defining the connecting density for each vertex, we can find the densest vertex, search its neighbor vertexes with the high enough densities and finally find a complex in the graph. In the same way for the rest of the vertexes and step by step, we can find out all the complexes of the graph. It is demonstrated by the experiments on six PPI datasets that the DBMS algorithm is efficient for discovering the complexes of a PPI network. In comparison with the MCODE algorithm, the DBMS algorithm obtains a better result for discovering the complexes, but it is computationally expensive.

2 The DBMS Algorithm

2.1 The Characteristics of a Complex

A complex in a PPI graph should represent some functional module which involves a number of proteins densely connected together. That is, mathematically, a complex is certainly a densely-connecting subgraph of a graph. However, there has not been a unified definition of a complex yet. In fact, it was defined in different ways related to the complex search methods. For example, Brun [9] and Samanta [10] defined the degree of similarity between two interaction vertexes via their common neighbor vertexes, utilize these similarity degrees for clustering analysis and regard the clusters as the complexes. On the other hand, Watt et al. [11] defined the density of a graph

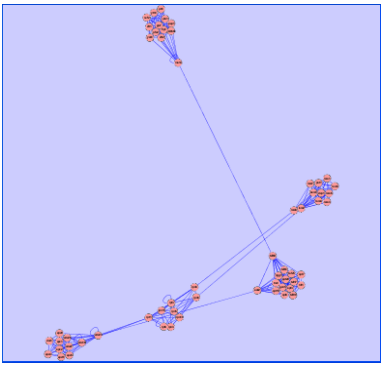

Fig. 1. The PPI graph with five clear complexes

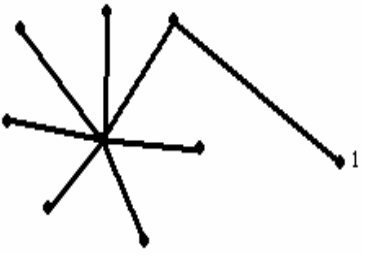

Fig. 2. The sketch of a complex

and consider a dense subgraph as a complex. For graph G with n vertexes, the edges of G will be not more than emax=n(n-1)/2, when G is an undirected graph, the edges of which have no directions. So, d=e/emax can be defined as the density of G, where e is the number of edges in G. We can define that G is dense when d is greater than a certain positive threshold.

In some specific PPI graphs, we can easily find out these dense subgraphs and accept them as the complexes. Figure 1 gives such an example. However, in general, the dense subgraphs are not separated so clearly, especially when there are thousands of vertexes in the graph.

Based on the proteomics experiments and biological experiences, we have the following characteristics of a complex: (1). No vertex belongs to two or more complexes. (2). A vertex belongs to a certain complex if it has a high degree. (3). A vertex with a low degree can be in a complex as a terminal vertex. In fact, as shown Figure 2, the most of the vertexes have one degree, but they can be in the complex. Moreover, if a vertex P belongs to a complex S, the most of the vertexes connecting to P are also in S.

2.2 The Description of the DBMS Algorithm

We begin to define the density of vertex p by

$$\rho_p = \left(\sum_{v \in U_p} d_v + d_p^2 \right) / d_p , \tag{1}$$

where d_v is the degree of the vertex v, U_p is a set of vertexes that are the neighbors of p. Obviously, we can filter the vertexes with a small density since they are generally isolated and do not belong to any complex. Here, a vertex is filtered out before the complex search if its density is less than 3. After then, we try to divide the remaining vertexes into some subgraphs in order to search the complexes. Actually, we further need the concept of correlation between a vertex and a dense subgraph or a complex S

which is assumed to consist of *n* vertexes, i.e., $|S|=n$. Given a vertex P, $d_p = m$, we hope to identify whether $P \in S$. Obviously, P belongs to S if most of P's neighbors are in S. Suppose there are k vertexes of S connecting with P, so $k \le n$ and $k \le d_p$, we define $c = k / n$ as the correlation degree of P to S.

P belongs to S if c is large enough. Assume that $P \in S$ if $c \ge \frac{b}{n}$, so that $P \in S$ if $k \ge b$. Clearly, b should increase with n, but the rate of increase should become relatively small. As we let b be proportional to $\log n$, we then get $b = \min\{\log n, f\}$, where f is a real number related with d_p to balance $\log n$ since it may be too large. In fact, if d_p is smaller than $\log n$ and $b = \log n$, P may not belong to S even if most of the edges connecting to P are in S. In practice, we can set $f = \lambda d_p$, where $\lambda \in (0,1)$.

Given an undirected connected graph G (v, e), S is a subgraph of G, and c is a constant. We consider S as a complex if for any vertex v in S, $k_v / |S| \ge c$, where k_v is the number of the neighbors of v in S, and $|S|$ is the number of vertexes in S. In this way, we propose the Density Based Merging Search (DBMS) algorithm to discover the complexes one by one as follows.

Step 1. Let $S = \varnothing$.

Step 2. Select a vertex P from G such that $\rho_p = \max_{v \in G}\{\rho_v\}$, and let $S = S \cup \{P\}$, N={The neighbors of the vertexes of S in G}, $n = |S|$.

Step 3. Select $Q \in N$ such that $\rho_Q = \max_{v \in N}\{\rho_v\}$, and have

(a). If $c_Q \ge c(n)$, then $S = S \cup \{Q\}$, update N;

(b). If $c_Q < c(n)$, then $N = N / \{Q\}$.

Step 4. If $N \ne \varnothing$, go to 3. Otherwise, if $N = \varnothing$, output S as a complex, and let $G = G - S$, filter out G. If $G = \varnothing$, stop. Else go to 1.

Since |G| is decreased as each complex S is found in a search loop, the DBMS algorithm will certainly converge in a finite iterations. As for the complexity of the DBMS Algorithm, we can consider the worst case to check whether each vertex belongs to S in N. It can be easily found that the time complexity of this step is $O(n^2)$. On the other hand, the time complexity for the filtering in the worst cases is $O(hn^2)$. Therefore, the time complexity of the DBMS Algorithm is $O(hn^3)$. Moreover, we need a memory space with the size of $O(n^2)$ to store the set G, N and S.

3 Experiment Results

3.1 The PPI Datasets

A PPI dataset consists of a group of edges connecting two proteins. In some cases, the PPI datum even represents the strength of the edge, but here, we only consider whether two proteins are connected. So, it is easy to translate the PPI data into a PPI graph where each vertex serves as a protein. Moreover, for each vertex, we can get its neighbor set, i.e., the set of all the neighbors of it.

For the experiments, we use two kinds of PPI datasets. The first kind of dataset is a simulated one as shown by Figure 1, in which there are 59 vertexes and 317 edges. The second kind of datasets are eight real-world PPI datasets downloaded from The Database of Interacting Proteins (DIP: http://dip.doe-mbi.ucla.edu). Specifically, they are Celeg20090126, Dmela20090126, Ecoli20090126, Hpylo20090126, Hsapi20090126, Mmusc20090126, Rnorv20090126, and Scere20090126.

In the experiments, we will compare the DBMS algorithm with the we will take CODE algorithm whose code is downloaded from: http://www.baderlab.org/Software/MCODE/.

3.2 Simulation Results

We begin to implement the DBMS algorithm on the simulated dataset, i.e., the PPI graph given by Figure 1. We set the base of the logarithm is the natural number e, and $\lambda = 0.5$, i.e., $f = 0.4d_p$. The results of the complex discovery by both the DBMS algorithm and the MCODE algorithm on this simulated dataset are given in Table 1.

It can be found from Table 1 that both the DBMS and MCODE algorithms have found five complexes from the PPI graph, but those complexes of the two algorithms are quite different in the way of content as well as the number of vertexes. By checking these results with Figure 1, we have found that the complexes found by the DMBS algorithm are consistent with the five true complexes. However, the complexes found by the MCODE algorithm are not so consistent with those true complexes. Therefore, we can consider the DMBS algorithm is more efficient than the MCODE algorithm on the complex discovery in this experiment.

3.3 Experimental Results on the Real-World PPI Datasets

We further implement the DBMS algorithm on the eight real-world PPI datasets and summarize the experimental results of complex discovery in Table 2, where #vexes denotes the number of vertexes in the PPI graph corresponding to the dataset, #Rvexes denotes the number of remaining vertexes in G at the end of the algorithm, #edges is the number of edges in the PPI graph, #Redges is the number of remaining edges connecting two vertexes in G at the end of the algorithm, #complexes denotes the number of complexes found by the algorithm, and Size-LC denotes the size, i.e., the number of vertexes in the largest complex.

Table 1. The complex discovery results of the DBMS and MCODE algorithms on the simulated PPI dataset, where each column represents a complex found. The blank fill with yellow is the vertexes not be handled by MCODE, and the blank fill with blue is the vertexes which are misclustered by MCODE.

The DBMS algorithm					The MCODE Algorithm				
S_1	S_2	S_3	S_4	S_5	S_1	S_2	S_3	S_4	S_5
taf60	pap1	cdc23	pat1	rpt1	hfi1	cft1	apc11	lsm7	rpn11
ngg1	cft2	cdc16	dcp1	rpn5	taf90	ysh1	apc1	lsm2	rpn5
spt8	yk059	apc1	kem1	rpn10	ngg1	cft2	apc2	lsm6	rpn8
spt3	cft1	apc11	lsm7	rpt3	taf25	pfs2	cdc23	dcp1	rpt1
						yk05			
taf25	pta1	apc5	lsm6	rpn11	spt8	9	cdc16	lsm8	rpn10
spt20	ref2	cdc27	lsm4	rpn6	cdc23	pti1	apc5	rpn6	rpn6
tra1	fip1	apc9	lsm3	rpn3	spt20	pap1	doc1	lsm5	rpt3
						rna1			
gcn5	pfs2	cdc26	lsm2	rpn8	tra1	4	rpt1	lsm4	rpn3
taf17	yth1	apc2	lsm5	rpt6	gcn5	glc7	apc4	lsm3	rpt6
hfi1	ysh1	apc4	lsm1		spt3	yth1	cdc27	kem1	
ada2	pti1	doc1	lsm8		rna14		apc9		
taf90	glc7				spt15		cdc26		
taf61	rna14				taf61				
spt7					taf17				
spt15					ada2				
					spt7				
					taf60				
15	13	11	11	9	17	10	12	10	9

Table 2. The experimental result of complex discovery by the DBMS algorithm on the eight real-world PPI datasets

Dataset	#vexes	#Rvexes	#edges	#Redges	#complexes	Size-LC
Celeg	2643	2098	4043	2278	159	637
Dmela	7494	6403	22872	6651	513	375
Ecoli	1559	1399	7002	5769	21	1282
Hpylo	704	590	1424	601	48	60
Hsapi	1755	1176	2171	1468	141	99
Mmusc	709	372	633	364	62	17
Rnorv	237	115	199	106	22	11
Scere	4965	4309	17612	8102	230	438

Specifically, we give some typical experimental results of complex discovery in Figures 3-6, respectively. The PPI graph of the dataset Rnorv20090126 is given in Figure 3, while 22 complexes found by the DBMS algorithm are shown in Figure 4. It can be observed clearly that all the possible complexes are correctly found.

According to the experimental results on those eight real-world PPI datasets, we find that the DBMS algorithm is applicable for complex discovery. Moreover, the DBMS algorithm generally outperforms the MCODE algorithm on complex

discovery, which can be demonstrated by the experimental results shown in Figures 5 for the datasets Rnorv20090126, respectively. Actually, in Figure 5, we can find that the complexes found by the DBMS algorithm are more reasonable than those found by the MCODE algorithm.

In a summary, the DBMS algorithm can be efficiently implemented to discover the complexes in a PPI graph or dataset. Moreover, it is even better that the MCODE algorithm in certain cases.

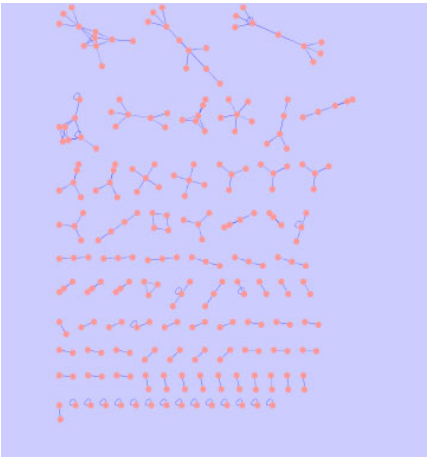

Fig. 3. The PPI graph of forRnorv20090126

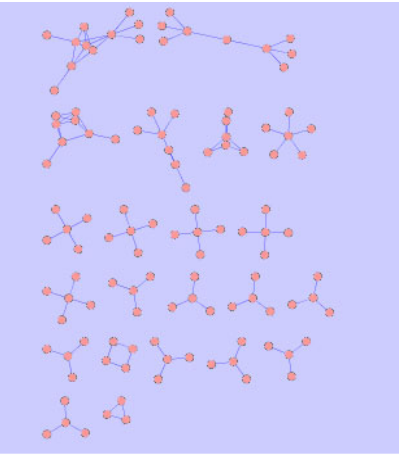

Fig. 4. The complexes found Rnorv20090126

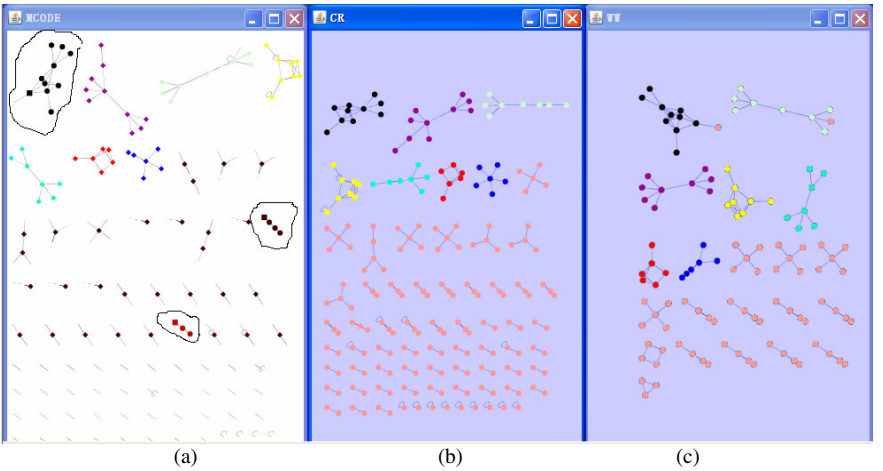

(a) (b) (c)

Fig. 5. The comparison between the DBMS and MCODE algorithms on Rnorv20090126. (a). 3 complexes (circled clusters) found by the MCODE algorithm. (b). The true complexes given in the dataset for check. (c). The complexes found by the DBMS algorithm.

5 Conclusions

We have investigated the discovery of the functional modules or complexes in a protein-protein interaction (PPI) network or graph and have proposed the density based merging search algorithm to discover the complexes for a PPI dataset. The DBMS algorithm is a kind of merging search procedure which combines the highly connected vertexes from any vertex with the highest density step by step to form a complex. It is demonstrated by the experiments on both simulated and real-world PPI datasets that the DBMS algorithm is applicable and efficient for complex discovery and even outperforms the MCODE algorithm.

Acknowledgements

This work was supported by the Natural Science Foundation of China for Project 60771061.

References

1. Hartwell, L.H., et al.: From Molecule to Modular Cell Biology. Nature 402, C47–C52 (1999)
2. Girvan, M., Newman, M.E.J.: Community Structure in Social and Biological Networks. Proc. Natl. Acad. Sci. 99(12), 7821–7826 (2002)
3. Hartuv, E., Shamir, R.: A Clustering Algorithm Based on Graph Connectivity. Information Processing Letters 76(4-6), 175–181 (2000)
4. King, A.D., Przulj, N., Jurisica, I.: Protein Complex Prediction via Cost-based Clustering. Bioinformatics 20(17), 3013–3020 (2004)
5. Newman, M.E.J.: Fast Algorithm for Detecting Community Structure in Networks. Phys. Rev. E 69, 66133 (2004m)
6. Clauset, A., Newman, M.E.J.: Moore c: Finding Community Structure in Very Large Networks. Phys. Rev. E 70(6), 66111 (2004)
7. Palla, G., Dere'nyi, I., Farkas, l., et al.: Uncobering the Overlapping Community Structure of Complex Networks in Nature and Society. Nature 435(7043), 814–818 (2005)
8. Bader, G.D., Hogue, C.: An Automated Method for Finding Molecular Complexes in Large Protein Interaction Networks. BMC Bioinformatics 4, 2 (2003)
9. Brun, C., Chevenet, F., Martin, D., et al.: Functional Classification of Proteins for the Prediction of Cellular Function from a Protein-protein Interaction Network. Genome Biol 5(1), R6 (2003)
10. Samanta, M.P., Liang, S.: Predicting Protein Functions from Redundancies in Large-scale Protein Interaction Networks. Proc Natl. Acad. Sci. USA 100(22), 1257–11258 (2003)
11. Watts, D.J., Strogatz, S.H.: Collective Dynamics of Small-world Networks. Natur. 393, 440–442 (1998)

Topology Prediction of α-Helical and β-Barrel Transmembrane Proteins Using RBF Networks

Shu-An Chen[1], Yu-Yen Ou[1], and M. Michael Gromiha[2]

[1] Department of Computer Science and Engineering,
Yuan Ze University, Chung-Li, Taiwan
[2] Computational Biology Research Center (CBRC), National Institute of Advanced Industrial Science and Technology (AIST), AIST Tokyo Waterfront Bio-IT Research Building, 2-42 Aomi, Koto-ku, Tokyo 135-0064, Japan

Abstract. Transmembrane proteins are difficult to crystallize owing to the presence of lipid environment and the number of membrane protein structures deposited in Protein Data Bank is limited. Hence, computational techniques become essential and powerful tools to aid biologists for understanding the structure and function of membrane proteins.

We propose an architecture for discriminating transmembrane α-helical proteins and transmembrane β-barrel proteins from genomic sequences, and then predict their transmembrane segments with Z-coordinate idea and RBF networks regression techniques.

In the discrimination of transmembrane proteins, our approach has correctly predicted the transmembrane proteins with a cross-validated accuracy of more than 98% in a set of 5888 proteins, which contain 424 α-helical proteins, 203 β-barrel proteins, and 5261 globular proteins. Also, our method showed a TM-segment recall of 97.3% in a independent set of 41 α-helical proteins. The improvement of TM-segment recall is more than 9% when comparing with other modern α-helix transmembrane segment predictors.

1 Introduction

Transmembrane (TM) proteins perform a diverse variety of functions, including the transport of ions and molecules across the membrane, bind to small molecules at the extra cellular space, recognize the immune system and energy transducers. Generally, the functions of proteins are well understood from their structures. However, due to the complex architecture of membrane proteins with lipid environment it is difficult to crystallize them. Consequently, the number of membrane proteins deposited in Protein Data Bank (PDB) is only 2% compared with globular proteins. Hence, computational tools are necessary to understand the structure and function of membrane proteins.

The discrimination of membrane proteins and predicting their membrane spanning segments have been achieved with several methods including statistical analysis, amino acid properties, hidden Markov model and machine learning techniques [4,5,6]. These methods showed different levels of accuracy with their

D.-S. Huang et al. (Eds.): ICIC 2010, LNCS 6215, pp. 642–649, 2010.

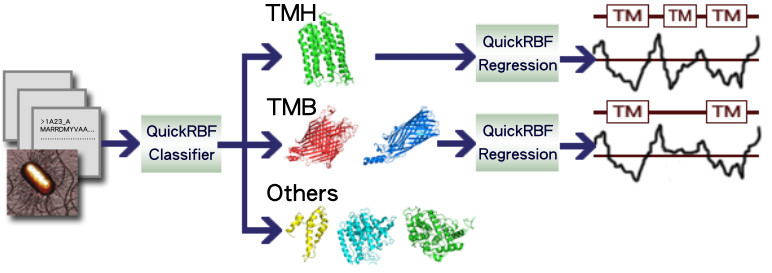

Fig. 1. The architecture of proposed method for discriminating TMH and TMB proteins from genomic sequences

own merits and limitations. Hence, it will be beneficial to develop a method to predict the topology of membrane proteins with high accuracy.

In our earlier works, we have developed different methods based on RBF networks and PSSM profiles to discriminate transmembrane β-barrel (TMB) proteins from other folding types of globular and membrane proteins and predicting their membrane spanning β-strand segments [7,8]. In this work, we have proposed an architecture, Fig. 1, for discriminating transmembrane α-helical (TMH) and TMB proteins from a pool of TMH, TMB and globular proteins. The membrane proteins have been further utilized to predict their membrane spanning α-helical and β-strand segments in TMH and TMB proteins, respectively. Our method showed an accuracy of 98% in discriminating TMH, TMB and globular proteins. Further, the transmembrane α-helical and β-strand segments are predicted with a segment overlap score (SOV) of 0.912 and 0.876, respectively. The residue-wise prediction showed an accuracy of 87.4% and 86.2% in TMH and TMB proteins, respectively. Our method could be effectively used for the structural studies on membrane proteins in terms of discrimination and prediction.

2 Methods

2.1 Design of the Radial Basis Function Networks Classifier and Regression

In this paper, we have employed QuickRBF package [12] for constructing RBF network classifiers. Also, we adopted all default setting of QuickRBF package, and everyone can download the package from the website to verify the results.

Also, we modified QuickRBF package to predict the real value of Z-coordinate. The prediction process is often referred to as the regression process. However, the basic network architecture of RBF classifiers and RBF regression is the same.

2.2 PSSM Profiles

In the structural point of view, several amino acid residues can be mutated without altering the structure of a protein and it is possible that two proteins

have similar structures with different amino acid compositions. Hence, we have adopted the Position Specific Scoring Matrix (PSSM) profiles, which have been widely used in protein secondary structure prediction, subcellular localization and other bioinformatics problems with significant improvement [7,13].

In this paper, we use PSSM profiles and window size 15 to generate 300 dimensions input vector as input features of RBFN classifier. Every element of PSSM profiles is also scaled by $\frac{1}{1+e^{-x}}$, where x means the original value of PSSM profiles.

2.3 Z-Coordinate

Z-coordinate is the distance from the center of the membrane for each residue of transmembrane segment. That is, the Z-coordinate of residue which in the middle of transmembrane segment is 1, and the residue next to the middle residue is 2, and so on.

In [15], authors introduced Z-coordinate idea on the prediction of transmembrane segment of α-helical proteins, and they have shown that the distance to the center of the membrane can be predicted with acceptable accuracy for residues in a-helical membrane proteins. Comparing to the traditional residue base prediction, Z-coordinate idea can provide the information of physical distance from membrane surface to interior, instead of the traditional label of belonging to the transmembrane segment or not.

3 Results and Discussion

3.1 Datasets

In our earlier study [7,5], we have used a set of 208 transmembrane β-barrel (TMB) proteins, 674 globular proteins and 206 transmembrane helix (TMH) proteins. Tusnady et al. [16] developed a data base of transmembrane proteins (PDBTM), which has a set of 161 TMB and 893 TMH protein structures in the latest version 2.2. We have combined the respective sequences from these datasets and constructed a new set of proteins, which have less than 40% sequence identity using the program CD-HIT. Further, the dataset has been refined with BLAST and verified that no two sequences have the identity of more than 40%. The final dataset contains 203 TMB, 424 TMH, and 667 globular proteins, and we name this dataset "Dataset 1". Further, we obtain 5261 globular proteins from ASTRAL database [19] with the sequence identity of less than 25%. By using these 5261 globular proteins, we generate "Dataset 2". Also, we eliminate "Dataset 1" and "Dataset 2" with less than 20% sequence identity to generate "Dataset 3" and "Dataset 4". In Table 1, we list the statistics of four datasets.

Further, PDBTM contains a list of transmembrane α-helical and β-barrel proteins and their membrane spanning segments with crystal structure. We have collected all transmembrane proteins in the latest version of PDBTM and culled them to get the non-redundant set of proteins. The program, BLAST has been used to obtain the non-redundant set of proteins and these proteins have the

Table 1. The statistics of datasets in transmembrane proteins discrimination

	Dataset 1 id <40%	Dataset 2 id <40%	Dataset 3 id <20%	Dataset 4 id <20%
TMH	**424**	**424**	**297**	**297**
TMB	**203**	**203**	**127**	**127**
Globular	**667**	**5261**	**195**	**4889**

Globular proteins of Dataset 2 and Dataset 4 are collected from ASTRAL.

Table 2. The statistics of datasets in TM-segment prediction of membrane proteins

	Validation Dataset	Independent test set	Total
TMH	**152**	**41**	**193**
TMB	**26**	**6**	**32**

sequence identity of less than 30%. The final dataset has 32 non-redundant β-barrel membrane proteins, and 193 α-helical membrane proteins. We select 41 α-helical proteins and 6 β-barrel proteins as our independent test set, and use other membrane proteins as our validation data. Table 2 lists the statistics of datasets used in the topology prediction of membrane proteins.

3.2 Discrimination of α-Helical and β-Barrel Transmembrane Proteins from Other Proteins

We have examined the predictive power of the present method for discriminating transmembrane proteins from four datasets. The results are presented in Table 3. We observed that our method could discriminate the TMH with the accuracy of 95.0% and the TMB with the accuracy of 97.4% in "Dataset 1". Also, the sensitivity of TMH and TMB are 88.0% and 89.2%, respectively. In addition, the specificity and precision are all higher than 90%.

Then, with "Dataset 2", which has a lot of globular proteins as negative samples. We also have good prediction accuracy, but the precision of TMB is from 94.3% to 79.1%. Since the proportion of transmembrane proteins and

Table 3. Results of transmembrane proteins discrimination

		Sensitivity	Specificity	Precision	Accuracy	MCC
Dataset 1	**TMH**	**88.0%**	**98.4%**	**96.4%**	**95.0%**	**0.89**
	TMB	**89.2%**	**99.0%**	**94.3%**	**97.4%**	**0.90**
Dataset 2	**TMH**	**88.4%**	**98.8%**	**85.4%**	**98.1%**	**0.86**
	TMB	**89.7%**	**99.2%**	**79.1%**	**98.8%**	**0.84**
Dataset 3	**TMH**	**87.9%**	**93.8%**	**92.9%**	**91.0%**	**0.82**
	TMB	**90.6%**	**95.7%**	**84.6%**	**94.7%**	**0.84**
Dataset 4	**TMH**	**84.5%**	**99.1%**	**84.2%**	**98.2%**	**0.83**
	TMB	**80.3%**	**98.2%**	**52.6%**	**97.8%**	**0.64**

globular proteins in "Dataset 2" is similar to real case scenario of bacteria genomic sequences, we can understand the prediction power may good enough for practical use.

In addition, we have examined the influence of datasets for discriminating transmembrane proteins using a subset of sequences obtained with less than 20% sequence identity and the results are presented in last two rows of Table 3. We noticed that the different measures (sensitivity, specificity, accuracy and MCC) showed a similar trend to that obtained with previous dataset with 40% identity. However, the precision of TMB in "Dataset 4" is only 52.6% because we may lost too much information of TMB with less than 20% identity.

3.3 Transmembrane Segment Prediction in α-Helical and β-Barrel Proteins

The results for predicting the transmembrane segment of transmembrane proteins are presented in Table 4. First of all, we can discuss the experimental result of segment prediction in β-barrel proteins. We have involved the idea of Z-coordinate [15] and RBF network regression techniques to predict transmembrane segments, and the prediction performance is at the same level of [8]. In Table 5, our proposed method has showed 96.0% TM-segment recall and 95.8% TM-segment precision of 26 proteins validation set. However, by using proposed method in this work, we can not only provide the prediction performance, but also provide a simple output model to help biologist to understand the architecture of whole protein.

Table 4. Results of TM-segment prediction in TMHs and TMBs with segment level

	TMH		TMB	
	Validation Data	**Independent Data**	**Validation Data**	**Independent Data**
Observed TM-Segments	**555**	**149**	**379**	**90**
Predicted TM-Segments	**556**	**153**	**380**	**92**
TM-Segment TP	**533**	**145**	**364**	**85**
TM-Segment FP	**23**	**8**	**16**	**7**
TM-Segment FN	**22**	**4**	**15**	**5**
TM-Segment Precision	**95.9%**	**94.8%**	**95.8%**	**92.4%**
TM-Segment Recall	**96.0%**	**97.3%**	**96.0%**	**94.4%**
SOV1	**0.915**	**0.911**	**0.908**	**0.913**
SOV2	**0.911**	**0.843**	**0.859**	**0.755**
SOV	**0.912**	**0.861**	**0.876**	**0.793**

SOV1: SOV1 means SOV of TM-Segment. SOV2: SOV2 means SOV of non-TM-Segment. SOV: SOV means SOV of all segments of sequence.

Table 5. Results of TM-segment prediction in TMHs and TMBs with residue level

	TMH		TMB	
	Validation Data	**Independent Data**	**Validation Data**	**Independent Data**
Sensitivity	**79.6%**	**79.3%**	**81.1%**	**87.1%**
Specificity	**91.5%**	**94.0%**	**89.2%**	**88.8%**
Accuracy	**87.4%**	**89.7%**	**86.2%**	**88.3%**
MCC	**0.72**	**0.75**	**0.70**	**0.73**

Table 6. Comparison of α-helical segments prediction with SVMtop in segment level

Validation Data	Proposed Method	SVMtop
Observed TM-Segments	555	555
Predicted TM-Segments	556	527
TM-Segment TP	533	505
TM-Segment FP	23	22
TM-Segment FN	22	50
TM-Segment Precision	95.9%	95.8%
TM-Segment Recall	96.0%	91.0%
SOV1	0.915	0.853
SOV2	0.911	0.838
SOV	0.912	0.843
Independent Data	**Proposed Method**	**SVMtop**
Observed TM-Segments	149	149
Predicted TM-Segments	153	138
TM-Segment TP	145	131
TM-Segment FP	8	7
TM-Segment FN	4	18
TM-Segment Precision	94.8%	94.9%
TM-Segment Recall	97.3%	87.9%
SOV1	0.911	0.846
SOV2	0.843	0.831
SOV	0.861	0.835

Table 7. Comparison of α-helical segments prediction with SVMtop in residue level

Validation Data	Proposed Method	SVMtop
Sensitivity	79.6%	82.8%
Specificity	91.5%	84.0%
Accuracy	87.4%	83.6%
MCC	0.72	0.65
Independent Data	**Proposed Method**	**SVMtop**
Sensitivity	79.3%	81.7%
Specificity	94.0%	88.3%
Accuracy	89.7%	86.4%
MCC	0.75	0.68

In the experiment of α-helical transmembrane segment prediction, our method can predict correctly 533 segments from 555 segments in 152 proteins validation set, so the TM-segment recall is 96%. With 41 proteins independent data, our method correctly identified 145 transmembrane segments among the 149 experimentally observed α-helix segments. The precision and recall for segment prediction are 94.8% and 97.3%, respectively.

We also list the results of residue level of transmembrane segment prediction in Table 6. With independent data, the prediction accuracy of TMH segments and TMB segments are 89.7% and 88.3%.

We have compared the performance of α-helical transmembrane segment prediction with SVMtop [24] in Table 7. With the validation set, our method has the same level of TM-segment precision with SVMtop, but the improvement of TM-segment recall is about 5%, from 91.0% to 96.0%. The improvement of TM-segment recall is even more with the independent data, from 87.9% to 97.3%, more than 9%. In Table 8, we also compared the performance in residue level of proposed method and SVMtop. The results are consistent between validation

data and independent data. Our proposed method has shown more than 3% improvement of accuracy.

4 Conclusions

We have developed a novel approach for identifying the transmembrane proteins and predicting their transmembrane segments. Our method could be effectively used for understanding the topology of transmembrane proteins in terms of transmembrane proteins identification and predicting their transmembrane segments.

References

1. Hirokawa, T., Boon-Chieng, S., Mitaku, S.: SOSUI: classification and secondary structure prediction system for membrane proteins. Bioinformatics 14, 378–379 (1998)
2. Tusnady, G., Simon, I.: The HMMTOP transmembrane topology prediction server (2001)
3. Gromiha, M.M., Suwa, M.: A simple statistical method for discriminating outer membrane proteins with better accuracy. Bioinformatics 21, 961–968 (2005)
4. Bagos, P., Liakopoulos, T., Spyropoulos, I., Hamodrakas, S.: A hidden markov model method, capable of predicting and discriminating beta-barrel outer membrane proteins. BMC Bioinformatics 5, 29 (2004)
5. Gromiha, M.M., Suwa, M.: Discrimination of Outer Membrane Proteins Using Machine Learning Algorithms. PROTEINS: Structure, Function, and Bioinformatics 63, 1031–1037 (2006)
6. Gromiha, M., Suwa, M.: Influence of amino acid properties for discriminating outer membrane proteins at better accuracy. BBA-Proteins and Proteomics 1764, 1493–1497 (2006)
7. Ou, Y.Y., Gromiha, M., Chen, S.A., Suwa, M.: TMBETADISC-RBF: Discrimination of β-barrel membrane proteins using RBF networks and PSSM profiles. Computational Biology and Chemistry 32, 227–231 (2008)
8. Ou, Y.Y., Chen, S.A., Gromiha, M.M.: Prediction of membrane spanning segments and topology in beta-barrel membrane proteins at better accuracy. Journal of computational chemistry (2009)
9. Yang, Z., Thomson, R.: Bio-basis function neural network for prediction of protease cleavage sites in proteins. IEEE Transactions on Neural Networks 16, 263–274 (2005)
10. Zhang, G., Huang, D.: Prediction of inter-residue contacts map based on genetic algorithm optimized radial basis function neural network and binary input encoding scheme. Journal of Computer-Aided Molecular Design 18, 797–810 (2004)
11. Su, C.T., Chen, C.Y., Ou, Y.Y.: Protein disorder prediction by condensed PSSM considering propensity for order or disorder. BMC Bioinformatics 7, 319 (2006)
12. Ou, Y.Y.: QuickRBF: a library for radial basis function networks, Software available at `http://csie.org/~yien/quickrbf/`
13. Jones, D.T.: Protein secondary structure prediction based on position-specific scoring matrices. J. Mol. Biol. 292, 195–202 (1999)

14. Xie, D., Li, A., Wang, M., Fan, Z., Feng, H.: LOCSVMPSI: a web server for subcellular localization of eukaryotic proteins using SVM and profile of PSI-BLAST. Nucleic Acids Research 33, W105–W110 (2005)
15. Granseth, E., Viklund, H., Elofsson, A.: ZPRED: Predicting the distance to the membrane center for residues in alpha-helical membrane proteins. Bioinformatics 22, e191–e196 (2006)
16. Tusnády, G., Dosztányi, Z., Simon, I.: PDB_TM: selection and membrane localization of transmembrane proteins in the protein data bank. Nucleic Acids Research 33, D275–D278 (2005)
17. Li, W., Jaroszewski, L., Godzik, A.: Clustering of highly homologous sequences to reduce the size of large protein databases. Bioinformatics 17, 282–283 (2001)
18. Altschul, S., Madden, T., Schaffer, A., Zhang, J., Zhang, Z., Miller, W., Lipman, D.: Gapped BLAST and PSI-BLAST: a new generation of protein database search programs. Nucleic Acids Research 25, 3389–3402 (1997)
19. Chandonia, J., Hon, G., Walker, N., Conte, L., Koehl, P., Levitt, M., Brenner, S., Journals, O.: The ASTRAL Compendium in 2004. Nucl. Acids Res. 32, D189–D192 (2004)
20. Zemla, A., Venclovas, C., Fidelis, K., Rost, B.: A modified definition of Sov, a segment-based measure for protein secondary structure prediction assessment. Proteins 34, 220–223 (1999)
21. Bigelow, H., Rost, B.: PROFtmb: a web server for predicting bacterial transmembrane beta barrel proteins. Nucleic Acids Research 34, W186 (2006)
22. Bagos, P., Liakopoulos, T., Spyropoulos, I., Hamodrakas, S.: PRED-TMBB: a web server for predicting the topology of β-barrel outer membrane proteins. Nucleic acids research 32, 400 (2004)
23. Randall, A., Cheng, J., Sweredoski, M., Baldi, P.: TMBpro: secondary structure, β-contact and tertiary structure prediction of transmembrane β-barrel proteins. Bioinformatics 24, 513 (2008)
24. Lo, A., Chiu, H., Sung, T., Lyu, P., Hsu, W.: Enhanced membrane protein topology prediction using a hierarchical classification method and a new scoring function. Journal of Proteome Research 7, 487–496 (2008)

Palmprint Recognition Based on Neighborhood Rough Set

Shanwen Zhang[1] and Jiandu Liu[2]

[1] Department of Engineering and Technology, Xijing University, Xi'an 710123, China
[2] Missile Institute, Air-Force Engineering University, Sanyuan, 713800, P.R. China
zhangshanwen1965@163.com

Abstract. Feature extraction is viewed as an important preprocessing step for pattern recognition, machine learning and data mining. Neighborhood rough set (NRS) based feature extracting algorithm is able to delete most of the redundant and irrelevant features, which avoid the step of data discretization and hence decreased the information lost in preprocess. In this paper, we firstly introduce the basic definitions and operations of NRS, and propose a palmprint recognition method based on NRS. The neighborhood model is used to reduce the attributes and extract the recognition features. Experimental results on PolyU palmprint database demonstrate that the proposed method is effective and feasible for palmprint recognition.

Keywords: Rough set, Neighborhood rough set, Palmprint recognition, Attribute reduction.

1 Introduction

The key step of the palmprint recognition task is how to effectively reduce the dimensionality of the palmprint images and extract recognition features. Recently, many feature extracting methods have been successfully applied to palmprint recognition [1-12]. Because the palmprint images are more sensitive to the orientations and illumination conditions, and there are a lot of noisy points and outliers in palmprint image dataset, so the recognition rates by the original palmprint recognition algorithms are not high.

Rough set theory, proposed by Pawlak (1982) [13,14], can be seen as a mathematical approach for vague problems, which has been receiving wide attentions from researchers in both theory and applications, and have been applied mainly in data mining tasks like recognition, recognition, clustering and feature selection. An important concept is attribute reduction in rough sets theory. Attribute reduction is to keep the minimal attribute subset of information system, while keeping the same recognition capability of original attribute set. Given a dataset with discretized attribute values, it is possible to find a subset of the original attributes using rough sets that are the most informative and all redundancy attributes can be removed from the original dataset with minimal information loss. However, it is difficult to directly and effectively deal with real-value attributes such as palmprint image dataset. Although feature reduction in classical rough set theory is an effective reduction method, the attributes must be

D.-S. Huang et al. (Eds.): ICIC 2010, LNCS 6215, pp. 650–656, 2010.

discretized before reduction. But discretization of real-number attributes may cause information loss because the degrees of membership of numerical values to discretized values are not considered. While neighborhood rough sets (NRS) based feature extracting algorithm is able to delete most of the redundant and irrelevant features, which avoid the step of data discretization and hence decreased the information lost in preprocess [15,16]. The NRS model is also a natural generalization of Pawlak's rough set model, while NRS can be used to deal with the mixed numerical and categorical data within a uniform framework. In this paper, we introduce a NRS model and apply it to palmprint recognition.

The rest of the paper is organized as follows. Section 2 briefly introduces the basic notions and operations of NRS. Section 3 proposes a palmprint recognition method based on NRS. Experimental results are given in Section 4. Finally, conclusions are drawn in Section 5.

2 Neighborhood Rough Set

Given an information system $T = \langle U , A \rangle$, where U is a nonempty called sample space and finite set of samples $\{x_1, x_2, \ldots, x_n\}$, called a universe, A is a set of attributes $\{a_1, a_2, \ldots, a_m\}$ to characterize the samples. Especially, T is also called a decision table if $A = C \cup D$, where C is the set of condition attributes and D is the decision attribute.

Given arbitrary $\boldsymbol{x_i \in U}$ and $\boldsymbol{B \subset C}$, the neighborhood $\boldsymbol{\delta_B(x_i)}$ of $\boldsymbol{x_i}$ in feature space $\boldsymbol{B}$ is denoted as $\delta_B(x_i) = \{x_j | x_j \in U,\ \Delta_B(x_i, x_j) \le \delta\}$, where Δ is a metric function in subspace B. For $\forall \boldsymbol{x_1, x_2, x_3 \in U}$, Δ usually satisfy three metric functions:

(1) $\boldsymbol{\Delta(x_1, x_2) \ge 0,\ \Delta(x_1, x_2) = 0}$, if and only if $\boldsymbol{x_1 = x_2}$;
(2) $\boldsymbol{\Delta(x_1, x_2) = \Delta(x_2, x_1)}$;
(3) $\boldsymbol{\Delta(x_1, x_3) \le \Delta(x_1, x_2) + \Delta(x_2, x_3)}$.

where (1) if $p = 1$, it is called Manhattan distance Δ_1; (2) if $p = 2$,it is called Euclidean distance Δ_2; (3) if $p = \infty$, it is called Chebychev distance. Here, we use the Manhattan distance.

Given a neighborhood decision table $\boldsymbol{TN = \langle U, C \cup D, N \rangle}$, $X_1, X_2, ..., X_c$ are the sample subsets with decisions 1 to c, $\delta_B(x_i)$ is the neighborhood information granules including x_i, and is generated by gene subset $B \subset G^*$, then the lower and upper approximations of the decision D with respect to gene subset B are respectively defined as

$$Lower_B(D) = \bigcup_{i=1}^{c} Lower_B(X_i),\ Upper_B(D) = \bigcup_{i=1}^{c} Upper_B(X_i) \tag{1}$$

where $Lower_B(X) = \{x_i \mid \delta_B(x_i) \subseteq X, x_i \in S\}$ is the lower approximations of the sample subset X with respect to gene subset B, and is also called positive region denoted by $Pos_B(D)$ which is the sample set that can be classified into one of the classes without uncertainty with the gene subset B. $Upper_B(X) = \{x_i \mid \delta_B(x_i) \cap X \neq \phi, x_i \in S\}$ denotes the upper approximations, obviously $Upper_B(X) = S$. The decision boundary region of D to B is defined as $Bn_B(D) = Upper_B(D) - Lower_B(D)$.

Given a neighborhood decision table $\boldsymbol{TN} = \langle \boldsymbol{U}, \boldsymbol{C} \cup \boldsymbol{D}, \boldsymbol{N} \rangle$, distance function $\boldsymbol{\Delta}$ and neighborhood size $\boldsymbol{\delta}$, the dependency degree of D to B is defined as

$$\boldsymbol{\gamma_B(D)} = \left|\boldsymbol{Pos_B(D)}\right| / \left|\boldsymbol{U}\right| \tag{2}$$

where $|\mathrm{g}|$ is the cardinality of a set. $\boldsymbol{\gamma_B(D)}$ reflects the ability of B to approximate D.

Since $\boldsymbol{Pos_B(D)} \subseteq \boldsymbol{U}$, then $0 \leq \boldsymbol{\gamma_B(D)} \leq 1$. If $\gamma_B(D) = 1$, we say that D depends totally on B and the decision system is consistent in terms of $\boldsymbol{\Delta}$ and $\boldsymbol{\delta}$, otherwise D depends on B in the degree of $\boldsymbol{\gamma}$. If $\gamma_B(D) < 1$, we say that D depends partially. Here we define $\gamma_{\varnothing}(D) = 0$. Given a neighborhood decision system $\boldsymbol{TN} = \langle \boldsymbol{U}, \boldsymbol{C} \cup \boldsymbol{D}, \boldsymbol{N} \rangle$, $\boldsymbol{B} \subseteq \boldsymbol{C}$, $\forall a \in B$ one can define the attribute significance of a in B as $\boldsymbol{Sig(a, B, D)} = \boldsymbol{\gamma_B(D)} - \boldsymbol{\gamma_{B-a}(D)}$.

The above definition can be used to backward feature selection, where redundant features are eliminated from the original set of features one by one. Similarly, a measure applicable to forward selection can be written as

$$\boldsymbol{Sig(a, B, D)} = \boldsymbol{\gamma_{B \cup a}(D)} - \boldsymbol{\gamma_B(D)}, \forall a \in A - B \tag{3}$$

Hu et al. [100] designed a novel feature selection method called forward attribute reduction based on neighborhood model (FARNeM) to select a minimal reduction.

The NRS based on dependence function is chosen as the objective function for evaluating the goodness of the selected recognition feature subset mainly because it is computationally fast, and which is an important consideration given the very time-consuming nature of the search process, and it is no use the feedback information of test data in the training process. There is a parameter δ, which controls the size of neighborhoods, to be specified in the algorithm. To select appropriate δ, we should try different values of parameter δ from 0 to 1 with step 0.01 to gain the attribute subsets with high recognition accuracy.

3 Palmprint Recognition Based on Neighborhood Rough Set

One of the most important aspects of any pattern recognition technique is extracting inherent features in a dataset. Consequently any feature recognition technique would

only be as good as the features extracted from the pattern being analyzed. The difficulty in the process of feature extraction is compounded by the high dimensionality of the feature space. For a two dimensionality continuous function $f(x, y)$ the moments and central moments of order $(p+q)$ are defined as

$$m_{pq} = \int_{-\infty}^{+\infty} \int_{-\infty}^{+\infty} x^p y^q f(x, y) dxdy \tag{4}$$

$$m_{pq} = \int_{-\infty}^{+\infty} \int_{-\infty}^{+\infty} (x - \bar{x})^p (y - \bar{y})^q f(x, y) dxdy \tag{5}$$

where $p, q = 0, 1, 2, \ldots., \bar{x} = m_{10} / m_{00}, \bar{y} = m_{01} / m_{00}$.

If $f(x, y)$ is a digitial image, then (2) becomes

$$\mu_{pq} = \sum_x \sum_y (x - \bar{x})^p (y - \bar{y})^q f(x, y) \tag{6}$$

And the normalized central moments, denoted η_{pq}, are defined as

$$\eta_{pq} = \mu_{pq} / \mu_{00}^{\gamma} \tag{7}$$

where $\gamma = (p + q) / 2 + 1, P + q = 2, 3, \ldots.$

The palmprint recognition system contains two stages: the off-line stage and the on-line stage. In the off-line stage, palmprint images of the different individuals to be verified are first processed by a feature extraction and attribute reduction module then the reduced features are stored as templates in a database for later use, where the recognition features are extracted by μ_{pq} and the decision table is formed by μ_{pq}, then the attributes are reduced by FARNeM [16]. In the on-line stage, a palmprint image of an individual to be verified first processed by a feature extraction and attribute reduction module; the reduced features are then fed to a matching module with one's identity ID by 1-nearest-neighbor (1-NN) classifier, which matches them against one's own templates in the database.

4 Experimental Analysis

The PolyU palmprint database contains 600 grayscale images of 100 different palms with six samples for each palm [4]. Six samples from each of these palms were collected in two sessions, where the first three were captured in the first session and the other three in the second session. The average interval between the first and the second sessions is two months. In experiments, the central part of each original image was automatically cropped. The cropped images was resized to 128×128 pixels and preprocessed by histogram equalization. Fig. 1 shows some images of two palms.

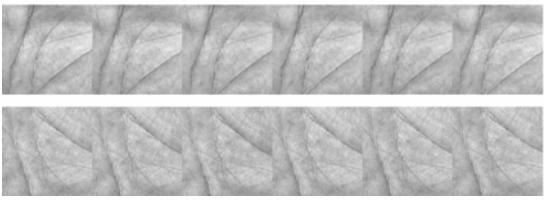

Fig. 1. 12 palmprint images of two palms

The effectiveness of classical rough set method in categorical attribute reduction has been discussed in some literatures [15,16]. Here, we mainly show that the neighborhood model [16] is applicable to the data with numerical attributes or heterogeneous attributes in this paper. In order to test FARNeM, we applied it to palmprint recognition, and show the recognition performances of the algorithm based on 10-fold cross validation, which is a widely used technique to test and evaluate recognition performance. We randomly divide the samples into 10 subsets, and use nine of them as training set and the rest one as the test set. After 10 rounds, we compute the average value and variation as the final performance. In feature extraction, the parameters p and q is set to 10, respectively. Now, we test the effectiveness of the algorithms to recognize the palmprints in the PolyU palmprint database. The maxim average recognition rate is 96.45%.

Threshold δ plays an important role in neighborhood rough sets. It can be considered as a parameter to control the granularity of data analysis. The significances of attributes vary with the granularity levels. Accordingly, the neighborhood based algorithm selects different feature subsets. δ takes the value from 0.1 to 1 with step 0.02 to get different feature subsets. The part results are shown in Table 1. To validate the effectiveness of the proposed method, we compare with other palmprint recognition methods. Table 2 shows the performance comparison with other related work. The comparison results show that our method is effective and feasible.

Table 1. The palmprint recognition results

δ	0.1	0.2	0.3	0.4	0.5	0.6	0.7	0.8	0.9	1
Recognition rate	85.23	85.54	85.25	86.34	89.57	90.16	96.20	96.51	94.38	82.13

Table 2. The palmprint recognition results

Method	DCT [3]	Hierarchical decomposition [4]	Principal Lines [7]	FARNeM
Recognition rate	91.23	94.54	96.25	96.38

5 Conclusion and Future Work

Reducing redundant or irrelevant features can improve recognition performance in most of cases and decrease cost of recognition. The classical rough set model is widely applied to feature selection and attribute reduction tasks. However, the attribute values needed to be discretized. The neighborhood rough set model can be used to deal with attribute reduction without discretization. In this paper, we applied the FARNeM algorithm to palmprint recognition. The experiment results showed that the FARNeM algorithm is effective for palmprint recognition. The future work will be focused on constructing neighborhood classifiers with the proposed model to lay a foundation for neighborhood based learning systems, such as *k*-nearest neighbor methods and neighborhood counting methods.

Acknowledgement

The authors would like to thank the anonymous reviewers for their constructive comments. This work is partly supported by National Natural Science Foundation of China under Grant 60703013 & 60975005.

References

1. Han, C.C., Cheng, H.L., Lin, C.L., Fan, K.C.: Personal authentication using palmprint features. Pattern Recognition 36, 371–381 (2003)
2. Connie, T., Jin, A.T.B., Ong, M.G.K., Ling, D.N.C.: An automated palmprint recognition system. Image Vision Comput. 23, 501–515 (2005)
3. Jing, X.Y., Zhang, D.: A face and palmprint recognition approach based on discriminant DCT feature extraction. IEEE Trans. Syst. Man Cybern. B 34, 2405–2415 (2004)
4. Lin, C.L., Chuang, T.C., Fan, K.C.: Palmprint verification using hierarchical decomposition. Pattern Recognition 38, 2639–2652 (2005)
5. Zhang, L., Zhang, D.: Characterization of palmprints by wavelet signatures via directional context modeling. IEEE Trans. Syst. Man Cybern. B 34, 1335–1347 (2004)
6. Wu, X.Q., Zhang, D., Wang, K.Q.: Palm line extraction and matching for personal authentication. IEEE Trans. Syst. Man Cybern. A 36, 978–987 (2006)
7. Huang, D.S., Jia, W., Zhang, D.: Palmprint Verification Based on Principal Lines. Pattern Recognition 41, 1316–1328 (2008)
8. Jia, W., Huang, D.S., Zhang, D.: Palmprint verification based on robust line orientation code. Pattern Recognition 41, 1521–1530 (2008)
9. Jia, W., Huang, D.S.: Palmprint verification based on robust line orientation code. In: International Joint Conference on Neural Networks, vol. 12-17, pp. 2510–2514 (2007)
10. Zhang, D., Kong, A., You, J., Wong, M.: Online palmprint identification. IEEE Trans. Pattern Anal. Mach. Intell. 25, 1041–1050 (2003)
11. Kong, A., Zhang, D., Kamel, M.: Palmprint identification using feature-level fusion. Pattern Recognition 39, 478–487 (2006)
12. Lu, G.M., Zhang, D., Wang, K.Q.: Palmprint recognition using eigenpalms features. Pattern Recognition Lett. 24, 1463–1467 (2003)

13. Pawlak, Z.: Rough set theory and its applications. Journal of telecommunications and information technology 3, 7–10 (2002)
14. Pawlak, Z., Skowron, A.: Rough Sets: Some Extensions. Information Sciences 177, 28–40 (2007)
15. Hu, Q., Yu, D., Xie, Z.: Numerical attribute reduction based on neighborhood granulation and rough approximation. Journal of Software 19, 640–649 (2008)
16. Hu, Q., Yu, D., Liu, J., Wu, C.: Neighborhood rough set based heterogeneous feature subset selection. Information Sciences 178, 3577–3594 (2008)

Increasing Reliability of Protein Interactome by Combining Heterogeneous Data Sources with Weighted Network Topological Metrics

Zhu-Hong You[1,2], Liping Li[3], Hongjie Yu[1,2,4], Sanfeng Chen[5], and Shu-Lin Wang[1,6]

[1] Intelligent Computing Laboratory, Hefei Institute of Intelligent Machines, Chinese Academy of Sciences, Hefei, Anhui, 230031, China
[2] Department of Automation, University of Science and Technology of China, Hefei, Anhui, 230027, China
[3] The Institute of Soil and Water Conservation of Gansu, Lanzhou, Gansu, 730020, China
[4] School of Science, Anhui Science and Technology University, Fengyang, Anhui, 233100, China
[5] Shenzhen Institute of Information Technology, Shenzhen, Guangdong, 518029, China
[6] School of Computer and Communication, Hunan University, Changsha, Hunan, 410082, China
zhuhongyou@gmail.com

Abstract. Over the last decade, the development of high-throughput techniques has resulted in a rapid accumulation of protein-protein interaction (PPI) data. However, the high-throughput experimental interaction data is prone to exhibit high level of false-positive and false-negative rates. It is therefore highly desirable to develop an approach to deal with these issues from the computational perspective. Meanwhile, as a variety of genomic and proteomic datasets become available, they provide an opportunity to study the interactions between proteins indirectly. In this paper, we introduce a novel approach that employs the Logistic Regression to integrate heterogeneous types of high-throughput biological data into a weighted biological network. Then, a weighted topological metrics of the network is devised to indicate the interacting possibility of two proteins. We evaluate our method on the Gavin's yeast interaction dataset. The experimental results show that by incorporating heterogeneous data types with weighted network topological metrics, our method improved functional homogeneity and localization coherence compared with existing approaches.

Keywords: Protein-protein Interaction, Multiple Data Sources, Weighted Network Topology, False Positive, FSWeight, CD-DIST.

1 Introduction

The development of novel high-throughput techniques, such as mass spectrometry, yeast two-hybrid assays and affinity purification techniques, has been applied to characterize PPI in genome scale and has generated a rapid accumulation of PPI data in the form of networks of interacting proteins [1]. Protein interactions play the crucial

D.-S. Huang et al. (Eds.): ICIC 2010, LNCS 6215, pp. 657–663, 2010.

roles, such as transferring signals, controlling the function of enzymes, in understanding the functional and organizational principles of cellular machinery. The PPI network is useful in obtaining a systems-level understanding of cellular behavior and in context-based functional annotation of genes. Analysis on interactome is expected to obtain biological insights and enable us to collect comprehensive knowledge for the control mechanism and organization of a living cell.

However, the high-throughput methods are prone to a high rate of false-positives, i.e. protein interactions which are identified by the experiment do not take place in the cell. It has been shown that the false positive rate of high-throughput yeast two-hybrid assays is about 50% [1]. Therefore, the PPI data needs to be validated with sophisticated techniques, and computational analysis techniques for assessing and ranking reliability of protein interactions are highly desirable. A large number of such approaches have been introduced for eliminating unreliable interactions and increasing the reliability of protein interactome. *Li et al* [2] combined multiple heterogeneous biological evidences, including gene expression, genome context, functional annotation, interaction domain, and network topology structure, to assign reliability scores to the human protein-protein interactions identified by high throughput experiments. *Saito et al.* developed two indices called IG1 and IG2 which use the local topology of a pair of proteins to rank their interaction probability [3]. *Chen et al.* introduced a novel measure called IRAP for assessing the reliability of protein interaction based on the underlying topology of the PPI network [4]. Similarly, an index called FS-Weight was firstly introduced by *Chua et al*. to predict protein functions [5]. It can be used to assess the reliability of protein interactions base on the number of common partners of a pair of proteins. Another simple measure is the Czekanowski-Dice distance (CD-DIST) [6]. Both of these two indices are initially proposed to predict protein functions, and lately have been shown that they usually outperforme IG and IRAP on large-scale protein interaction networks for assessing the reliability of protein interactions [1].

Although these approaches have yielded satisfactory results, they generally either employ multiple biological data source or topological information of PPI network. In this paper, we attempt to combine heterogeneous data sources with weighted network topological metrics for repurification of the highly erroneous experimentally derived protein interactomes.

2 Materials and Methodology

In this section, we first describe datasets used in this paper. Then we represent how to integrate a variety of genomic and proteomic datasets to derive confidence scores for binary PPI network, and describe how to devise a novel topological metric based on weighted network.

2.1 Datasets

We use Gavin's yeast protein interaction dataset in our experiments [7]. After removing duplicate interactions and self interactions, the dataset contains 8663 interactions involving 1708 proteins. In addition to the PPI data, there are many other types of genomic and proteomic data sources which can reflect the interactions between

proteins indirectly. For example, it has been demonstrated that most of interacting protein pairs are co-expressed. Protein interactions involve physical associations between protein domains, therefore, it will be more reliable if an interaction has a pair of interaction domains [8]. From genome sequences, we can also infer functional linkages for pairs of proteins. It has also been shown that other data source such as essentiality, homology derived PPI, transcription factor binding data provide partial information about the protein interactions [8]. In this study, we integrate above six types of biological evidences to assign reliability weights to yeast PPI identified by high-throughput experiments.

For a Logistic Regression model, the golden standard positive (GSP) and golden standard negative (GSN) training datasets are required to train the LR model and compute the model parameters. We use the hand-curated protein complexes in the MIPS reference database as our GSP training set [9]. Unlike GSP dataset, it is impossible to find a confirmed GSN training dataset on a large scale. Here, we use a random set of protein pairs which located in different cellular localization. Finally, we collect 12279 GSP and 19641036 GSN protein pairs to train LR model, which is used to compute the reliability score of PPI network.

2.2 Integrating the Confidence Scores from Heterogeneous Data Sources by Logistic Regression

The Logistic Regression (LR) model has recently been adopted for estimating the probability of occurrence of an event by fitting data to a logistic curve [8]. In this study, a LR model is used to integrate the confidence scores of six types data sources to calculate the linkage weights of PPI networks. A LR model involves some independent variables which are used to predict a dependent variable (outcome). As stated, the model tries to compute the probability of protein interacting based on heterogeneous data sources. The selected independent variables are gene expression, essentiality, genome sequences, homology derived PPI, transcription factor binding data and protein domain interaction data. These variables are assumed to have a role in predicting the protein interactions.

In our case, the dependent variable is a probability variable representing the presence or absence of protein interaction. The relationship between the occurrence and its dependency on several variables can be written as:

$$p = 1/(1+e^{-z}) \text{ or } p = e^{z}/(1+e^{z}) \tag{1}$$

where p is the probability of an event occurring. In our study, p is the estimated probability of protein interaction. The probability varies from 0 to 1 on an S-shaped curve and z is the linear combination. The linear combination z can be written as:

$$z = b_0 + b_1 x_1 + b_2 x_2 + ... + b_n x_n \tag{2}$$

where x_i $(i = 0, 1, 2, ..., n)$ denotes the score of data source i, b_0 is the intercept of the model and the b_i $(i = 0, 1, 2, ..., n)$ is the slope coefficient of the logistic regression model. The parameters b_0 and b_i are determined using a maximum-likelihood

method. The linear model characterizes a logistic regression with the probability of protein interaction on the independent variables of other heterogeneous data sources.

2.3 Weighted Topological Metric

A protein interaction network can be represented as a non-directed graph $G = (V, E)$, where V denotes a set of vertices and E denotes a set of edges (x, y). For each subset Y of V, let $\Gamma(Y)$ be the set of vertices outside of Y which are connected to Y:

$$\Gamma(Y) = \{x \in V \setminus Y \mid \exists\, y \in Y, (x, y) \in E\} \tag{3}$$

and $\overline{\Gamma}(Y) = Y \cup \Gamma(Y)$. Let $E(Y)$ be the set of internal edges in $Y \in V$:

$$E(Y) = \{(x, y) \in E \,|\, x \in Y \text{ and } y \in Y\} \tag{4}$$

It has been shown that a pair of genuine interacting proteins are generally expected to have common cellular roles and proteins that have common interaction partners have a high chance of sharing a common function, which means protein pairs having many common interaction partners are more likely to be functionally linked; thus they are more likely to be true positive interacting pairs [10]. *Christine B. et al* used an index called Czekanowski-Dice distance (CD-Dist) for the purpose of protein function prediction from protein interaction networks [6]. The CD-Dist index of two proteins x and y can be written as:

$$CD - Dist(x, y) = \frac{\left|\Delta(\overline{\Gamma}(x), \overline{\Gamma}(y))\right|}{\left|\overline{\Gamma}(x)\right| + \left|\overline{\Gamma}(y)\right|} \tag{5}$$

where Δ denotes the symmetric difference between two sets of proteins. The pairs of interacting proteins that are highly ranked by CD-Dist index are more like to be true positives. Conversely, the pairs of proteins that are lowly ranked are likely to be false positives. For example, previous work has shown that using CD-Dist, which assesses the strength of functional association, to eliminate unreliable interactions improves the performance of clustering algorithms. The most interesting feature of the CD-Dist is that it is able to rank the reliability of an protein interaction using only the topology of the interactions between that pair of proteins and their neighbors within a short radius in a PPI network [4].

Although CD-Dist index is originally proposed for protein function prediction, it is also suitable as an index for assessing the reliability of PPI [5]. However, one major limitation of using original CD-Dist to assess the reliability of PPI is that it is devised based on the unweighted networks and the weights of the interactions are not considered. Exploring the information that weights hold allows us to further our understanding of networks. As we saw earlier, the edges of PPI network are assigned reliability scores which can be interpreted as a probability of protein interaction. The successful applications of integrating heterogeneous data have proved that weighted biological network is superior to binary PPI network [8]. Therefore, a new dissimilarity measure which allows to analyze weighted PPI network is highly desirable.

Following *JB Angelelli*'s work [11], a weighted CD-Dist index, denoted $D_W(x, y)$, can be computed by considering the interaction weight of a weighted biological network. We consider two weighted network $\Gamma_w^+(x, y)$ and $\Gamma_w^-(x, y)$. The index D_w^+ corresponds to the graph $\Gamma_w^+(x, y)$, where the weight between x and y is $\omega(x, y)$, and the index D_w^- corresponds to the graph $\Gamma_w^-(x, y)$, where there is no edge between x and y. Thus, the weighted CD-Dist index can be written as

$$\begin{aligned} D_W(x, y) &= \omega(x, y) \times D_w^+(x, y) + (1 - \omega(x, y)) \times D_w^-(x, y) \\ &= \omega(x, y) \times \frac{\sum_{s \in V} \left| \omega(x, s) - \omega(y, s) \right|}{4 + \sum_{s \in V} \left| \omega(x, s) + \omega(y, s) \right| - 2 \times \omega(x, y)} + \\ &\quad (1 - \omega(x, y)) \times \frac{2 + \sum_{s \in V} \left| \omega(x, s) - \omega(y, s) \right|}{2 + \sum_{s \in V} \left| \omega(x, s) + \omega(y, s) \right| - 2 \times \omega(x, y)} \end{aligned} \tag{6}$$

where $\omega(x, y)$ is the weight between x and y in the biological network. V denotes all the proteins in the network. We can see that the smaller the $D_W(x, y)$ is, the more likely the two proteins, x and y, interact with each other. The reliability of the protein pairs can be assessed on the basis of D_W value.

3 Experimental Results

In this section, we compare the performance of our approach with IG [3], CD-Dist [6] and FS-Weight [10] which are considered as three typical topology-based methods for assessing the reliability of protein interactions.

By the "guilt-by-association" principle, interacting proteins usually share common functional role or localize in the same cellular components. Therefore, we use the degree of functional homogeneity and localization coherence of protein pairs to evaluate our method. In the study, the Gene Ontology (GO) based annotations were used to calculate functional homogeneity and localization coherence. The three organizing principles of GO terms are biological processes, molecular functions and cellular components. Here we use the first two taxonomies of the GO terms for functional homogeneity calculation, and the last taxonomies of the GO terms for localization coherence calculation.

We study the impact of eliminating unreliable interactions which defined by D_W value. We eliminate interactions whose D_W values are larger than a given threshold and compute the rate of interacting protein pairs with common function roles and cellular localization. The similar procedures are applied to the other three methods. Fig. 1 shows the functional homogeneity and localization coherence of the interactions in yeast dataset ranked using aforementioned four methods. We show that the

proportion of interacting proteins with a common functional role increases in D_W index filtered interaction data. The similar effect is observed for common cellular localization. As can be seen, all of the four methods can achieve a significant improvement. We noticed that our method performs better than IG, CD-Dist and FS-Weight. The performance of CD-Dist method is comparable to that obtained by FS-Weight approach. For example, in terms of function homogeneity, it can be seen from Fig.1 (a) that over 99% of the top 10% of protein interactions ranked by the proposed method have a common cellular role and about 95% of them have a common subcellular localization. In contrast, about 95% and 91.5% of the top 10% of interacting pairs ranked by FS-Weight and CD-Dist share a common function and subcellular localization respectively. As shown in Fig.1 (a) and (b), IG method performs worst among these four approaches. About 87% and 78.5% of the top 10% of interacting pairs ranked by IG share a common function and subcellular localization respectively.

From the experiment we can see that the protein interactions ranked top by our method have higher localization coherence and functional homogeneity than existing methods.

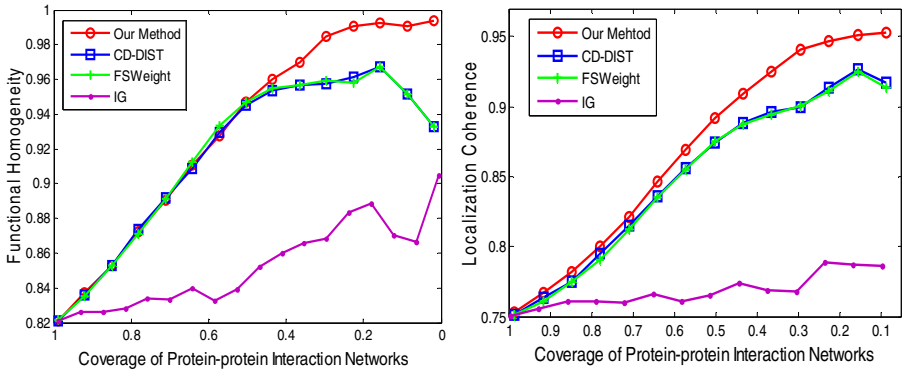

(a) (b)

Fig. 1. Performance of the four approaches, the proposed method, IG, CD-Dist, and FS-Weight, in assessing reliability of interactions. (a) Functional homogeneity. (b) Localization coherence. The horizontal axis denotes the coverage of the PPI network. The vertical axis denotes the proportion of interacting protein pairs which share a common (a) functional roles or (b) cellular localization.

4 Conclusion

In this paper, we have proposed a computational approach to assess the reliability of protein interactomes. Our method incorporates additional genomic and proteomic data with weighted topology information to calculate the reliability scores of protein pairs. Then the annotations in Gene Ontology are employed to evaluate the purified protein interactions. The experimental results show that our method outperforms existing methods and can reduce false positive of protein interaction efficiently.

Acknowledgments

This work was supported by the National Science Foundation of China (grant nos. 30900321, 60973153, and 30700161), the China Postdoctoral Science Foundation (grant no. 20090450825), and the Knowledge Innovation Program of the Chinese Academy of Science (grant no. 0823A16121).

References

1. Chua, H.N., Wong, L.: Increasing the Reliability of Protein Interactomes. Drug Discovery Today 13(15-16), 652–658 (2008)
2. Li, D., Liu, W.L., Liu, Z.Y., Wang, J., Liu, Q.J., Zhu, Y.P., He, F.C.: PRINCESS, a Protein Interaction Confidence Evaluation System with Multiple Data Sources. Molecular & Cellular Proteomics 7(6), 1043–1052 (2008)
3. Saito, R., Suzuki, H., Hayashizaki, Y.: Interaction Generality, a Measurement to Assess the Reliability of a Protein-protein Interaction. Nucleic Acids Research 30(5), 1163–1168 (2002)
4. Chen, J., Hsu, W., Lee, M.L., Ng, S.K.: Increasing Confidence of Protein Interactomes using Network Topological Metrics. Bioinformatics 22(16), 1998–2004 (2006)
5. Chua, H.N., Sung, W.K., Wong, L.: Exploiting Indirect Neighbours and Topological Weight to Predict Protein Function from Protein-Protein Interactions. Bioinformatics 22(13), 1163–1623 (2006)
6. Brun, C., Chevenet, F., Martin, D., Wojcik, J., Guenoche, A., Jacq, B.: Functional Classification of Proteins for the Prediction of Cellular Function from a Protein-Protein Interaction Network. Genome Biology 5(1) (2004)
7. Gavin, A.C., Aloy, P., Grandi, P., Krause, R., Boesche, M.: Proteome Survey Reveals Modularity of the Yeast Cell Machinery. Nature 440(7084), 631–636 (2006)
8. Qi, Y.J., Klein-Seetharaman, J., Bar-Joseph, Z.: A Mixture of Feature Experts Approach for Protein-protein Interaction Prediction. BMC Bioinformatics 8 (2007)
9. Mewes, H.W., Amid, C., Arnold, R., Frishman, D., Guldener, U., Mannhaupt, G., Munsterkotter, M., Pagel, P., Strack, N., Stumpflen, V.: MIPS: Analysis and Annotation of Proteins from Whole Genomes. Nucleic Acids Research 32, 41–44 (2004)
10. Chua, H.N., Sung, W.K., Wong, L.S.: Exploiting Indirect Neighbours and Topological Weight to Predict Protein Function from Protein-protein Interactions. Bioinformatics 24(3), 452 (2008)
11. Angelelli, J.B., Baudot, A., Brun, C., Guenoche, A.: Two Local Dissimilarity Measures for Weighted Graphs with Application to Protein Interaction Networks. Advances in Data Analysis and Classification 2, 3–16 (2008)

Predicting Protein Stability Change upon Double Mutation from Partial Sequence Information Using Data Mining Approach

Lien-Fu Lai[1], Chao-Chin Wu[1], and Liang-Tsung Huang[2,*]

[1] Department of Computer Science and Information Engineering,
National Changhua University of Education, Changhua 500, Taiwan
[2] Department of Information Communication, Mingdao University, Changhua 523, Taiwan
larry@mdu.edu.tw

Abstract. The prediction of stability change for protein mutants is one of the important issues in protein design. Recently, the prediction upon double mutation has attracted more and more attention. In this work, we have employed a data mining approach to discriminating stability change for protein double mutants. We incorporated a reliable rule induction algorithm along with accuracy of 82.2% to construct rule-based knowledge patterns. Further, a fuzzy query method was utilized to value important and similar rule patterns for an input with partial sequence information. The results showed that the approach has two major advantages: (i) A rule-based knowledge representation offers intuitive interpretation on raw data, which is helpful to understand the content; and (ii) A fuzzy query method incorporates the concept of uncertainty, which can make predictions from partial information. Based on the proposed approach, we have also developed a web service for predicting protein stability change upon double mutation from partial sequence information and it is available at http://bioinformatics.myweb.hinet.net/tandem.htm.

Keywords: Protein stability, double mutation, sequence information, data mining, fuzzy query.

1 Introduction

The prediction of stability change for protein mutants is one of the important tasks in protein engineering. It is necessary for understanding the mechanisms responsible for protein stability as well as for designing temperature sensitive protein mutants [1]. For the past several years, many different methods have been developed to address this issue for predicting stability change upon single mutation [2-5].

Moreover, earlier studies revealed that the methods developed for predicting protein stability change upon point mutation are not suitable for predicting the stability of all double mutants [6, 7]. Therefore, the prediction upon double or multiple mutations has attracted more and more attention [8, 9]. However, it is necessary to provide complete information as input when employing these prediction methods.

* Corresponding author.

D.-S. Huang et al. (Eds.): ICIC 2010, LNCS 6215, pp. 664–671, 2010.

Whereas the input information may be incomplete and unavailable in practice, it will be constructive to develop an effective approach to make reliable predictions from partial input information.

2 Materials and Methods

To illustrate the proposed approach, Figure 1 draws a flow chart for the approach of predicting protein stability change upon double mutation. Firstly, experimental observations for protein stability change are collected and a non-redundant dataset is constructed. Next, important rule patterns are derived from the dataset by a reliable rule induction algorithm. These procedures could bring some main advantages: (i) The data amount of derived patterns is usually less than that of original observations, which can improve computational efficiency; (ii) A rule-based knowledge representation (KR) can offer intuitive interpretation on raw data, which is helpful to understand the content; and (iii) The concept of uncertainty can be incorporated, which can develop an integrated application such as fuzzy query in this study [10].

For an input with partial sequence information, a fuzzy query method is utilized to evaluate the importance and the similarity of each rule pattern to the input. The patterns with higher reference level may be used to predict protein stability change.

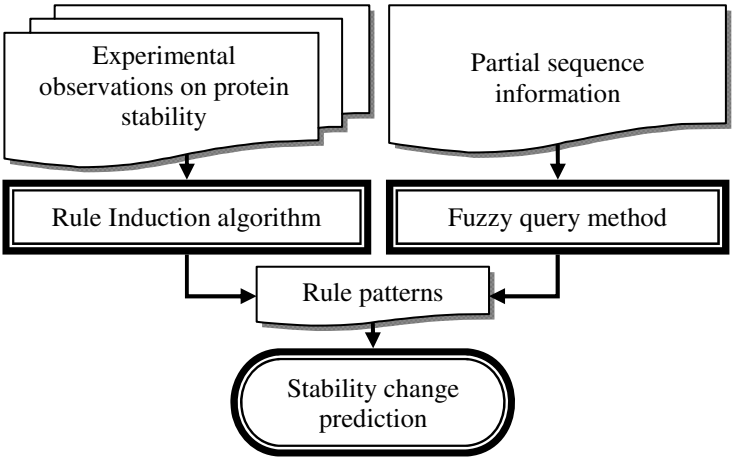

Fig. 1. Flow chart of our proposed approach for predicting protein stability change upon double mutation

2.1 Dataset Construction

In this study, we have collected a set of double mutants from ProTherm database [11, 12] in which the free energy changes of mutants were obtained with thermal denaturation. The final non-redundant dataset consists of 180 mutants acquired from 27 different proteins. The $\Delta\Delta G$ ranges between -8.9kcal/mol and 6.2kcal/mol and the number of stabilizing and destabilizing mutants is 93 and 87, respectively. The datasets

used in the present study are available at http://bioinformatics.myweb.hinet.net/wetstab.htm.

2.2 Rule Induction Algorithm

To represent a double mutant, we have utilized two sets of attributes as input variables. Each refers to a mutation site, including wild-type residue, mutant residue and three neighboring residues of the mutation site along both directions (i.e. 8 attributes for each mutation site). Further, the decision table majority algorithm [13] was implemented to build a set of rules, called decision table majority. The induction algorithm and the derived rules have exhibited reliable performance for predicting protein stability change upon double mutation [8].

2.3 Fuzzy Query Method

For finding important and similar rules to the input, we have utilized fuzzy query method, which consists of three key concepts: (i) fuzzy fit, (ii) fuzzy numbers and (iii) fuzzy weighted average (FWA). Fuzzy fit computes the degree of fit between the input partial information and the antecedent of the rule. Fuzzy numbers [14, 15] can represent linguistic terms. Fuzzy weighted average [16-18] can subsequently calculate the confidence level of a rule to the input. Finally, we calculate the reference level of rules from the degree of fit and the confidence level.

Fuzzy Fit. The input information can be categorized into the known and the unknown parts. For quantifying the degree of fit between the known part and a rule, the elements of the known part are compared to the condition elements of the antecedent of the rule. For example, let us assume that we have N rules (e.g. Ri, i=1…N) with only two condition elements of the antecedent (e.g. Ei1, Ei2, i=1…N):

R_1: IF E_1^1 AND E_1^2 THEN C_1,…, R_i: IF E_i^1 AND E_i^2 THEN C_i,…
R_N: IF E_N^1 AND E_N^2 THEN C_N,

where C_i is the consequent of rule R_i. If the elements of the known part are given as set E, then the score of the degree of fit (DF) for rule R_i, is calculated by: $DF_i = \Phi/2$, where Φ is the number of the intersection between sets E and $\{E_i^1, E_i^2\}$. In this study, the set E with complete input information has 16 elements (8 for each mutation site, including wild-type residue, mutant residue and three neighboring residues of the mutation site along both directions).

Fuzzy Numbers. The importance of a rule may be calculated from its correctness and coverage. As the relative importance between the two factors is uncertainty, we introduce fuzzy numbers and fuzzy weighted average to calculate the confidence level of the rule. Each factor is assigned in terms of “unimportant”, “rather unimportant”, “moderately important”, “rather important”, and “very important”. The five linguistic terms can be represented as fuzzy numbers.

A fuzzy number $\tilde{A}$ can be defined by a triplet (a, b, c) and the membership function $\mu_{\tilde{A}}(x)$ is defined as:

$$\mu_{\tilde{A}}(x)=0,\quad x<a;\quad \frac{x-a}{b-a},\quad a\le x\le b;\quad \frac{c-x}{c-b},\quad b\le x\le c;\quad 0,\quad x>c. \tag{1}$$

Fuzzy Weighted Average (FWA). FWA is a weighted average involving type-1 fuzzy sets. Therefore, fuzzy weighted average y is defined as

$$y=\frac{\sum_{j=1}^{n} w_j x_j}{\sum_{j=1}^{n} w_j}=f(x_1,...,x_n,w_1,...,w_n), \tag{2}$$

where w_j (represented by fuzzy sets or fuzzy numbers) is the weight for the factor value x_j; n is the number of the factors. Since w_j are no longer crisp numbers, $\sum_{j=1}^{n} w_j=1$ is not imposed as a requirement. In this study, the confidence level of a rule is calculated by FWA on two factors, the correctness and coverage of the rule. Both factors are quantified by calculating the confidence and support, respectively (defined in section 2.4).

For example, assigning that confidence is very important and the support is moderately important, for a rule with confidence of 0.78 and support of 0.54, confidence level (CL) for the rule is calculated as follows:

$$\mathrm{CL}=\frac{0.78\otimes(0.75,1,1)\oplus 0.54\otimes(0.25,0.5,0.75)}{(0.75,1,1)\oplus(0.25,0.5,0.75)}=\frac{(0.72,1.05,1.185)}{(1,1.5,1.75)}\approx\frac{0.997}{1.433}=0.6957$$

Applying mathematical operations to fuzzy numbers [19, 20], we have two fuzzy numbers (0.72, 1.05, 1.185) and (1, 1.5, 1.75). The centre of gravity is adopted to defuzzify a fuzzy number [21], which is achieved by mathematical integral. For the example shown in Figure 2, the centre of gravity of (0.72, 1.05, 1.185) is 0.997, which could be obtained by executing *moment-defuzzify* function in FuzzyCLIPS.

Then, the reference level of the rule is calculated by:

$$\mathrm{RL}_i=\mathrm{DF}_i\times\mathrm{CL}_i, \tag{3}$$

namely, the multiplication of DF_i (the degree of fit between the input and rule R_i) and CL_i (the confidence level of rule R_i).

In this study, we implemented the fuzzy query by FuzzyCLIPS [22], which is a knowledge-base programming language and can handle imprecision and uncertainty in an effective way.

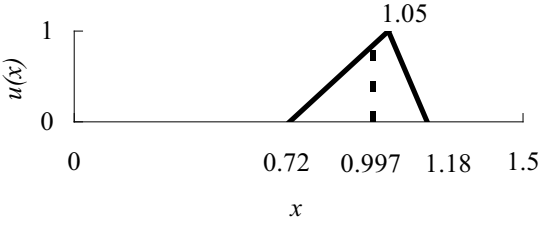

Fig. 2. The defuzzifying of a triangular fuzzy number through the centre of gravity

2.4 Performance Measure Scores

In this study, various measure scores were used to evaluate the performance of discriminating the stabilizing and destabilizing mutants. For the reliability of rule induction, accuracy (AC) indicates the correct prediction of mutants by using the following expression: $AC=(TP+TN)/(TP+TN+FP+FN)\times 100\%$, where TP, TN, FP and FN refer to the number of true positives, true negatives, false positives and false negatives, respectively. In addition, sensitivity (SE) indicates the correct prediction of stabilizing mutants and specificity (SP) about the destabilizing ones by the expression $SE=TP/(TP+FN)\times 100\%$ and $SP=TN/(TN+FP)\times 100\%$, respectively.

In addition, support (SU) shows the coverage of the rule on a dataset and confidence (CO) shows the correctness of the rule. Given a rule: IF A THEN B, where A is the antecedent and B is the consequent, support is calculated by $SU = N_A / N \times 100\%$, where N_A is the number of instances with antecedent A of the rule. Similarly, confidence (CO) is calculated by $CO= N_{A\cup B} / N_A, \times 100\%$ where $N_{A\cup B}$ is the number of instances with both antecedent A and consequent B.

3 Results

3.1 Reliability of Rule Induction Algorithm

An IF-THEN rule assumes the form: IF A THEN B, where A is called the antecedent or premise and B is the consequent or conclusion. N^i_j / C^i_j denotes the *i*-th residue along N- / C-terminus at mutation site *j*; W_j is the wild residue at mutation site *j*; and M_j is the mutant residue at mutation site *j* (*i*=1~2 and *j*=1~3 here).
Based on 10-fold cross-validation, the rules derived by the induction algorithm discriminate the stabilizing and destabilizing mutants with AC, SE, and SP of 82.2%, 76.3% and 88.5%, respectively. For 5-fold, AC, SE and SP are 78.3, 66.7 and 90.8, respectively. In addition, we employed a back-propagation neural network with three layers, showing lower accuracy of 68.3%. The results showed that the induction algorithm could mine reliable rules from the protein mutant dataset.

Further, we have employed the induction algorithm on S180 dataset and then mined total 60 rules. Table 1 lists 4 reliable rules (2 for increasing and 2 for decreasing) along with performance measures.

3.2 Correctness and Coverage of Mined Rules

We have further analyzed the mined rules. Figure 4 exhibits the distribution of rules based on accuracy. It shows that a large proportion of rules have high confidence and there are 83% of rules with confidence above 70%. Interestingly, 46 rules out of 60 ones achieve the confidence of 100%.

In addition, we have observed the coverage of rules for the dataset. The support of the rule lies between 0.56% and 13.3% and the cumulative support of total rules reach 85%. For example, the first rule in Table 1 shows support and confidence of 4.44% and 100%, respectively.

Table 1. Antecedent and consequent of some derived rules along with various measures

Antecedent	Consequent	Support (%)	Confidence (%)
W_2 is Ile, $N^1{}_2$ is Gly, and $C^3{}_2$ is Asp	Decreasing	4.44	100
W_2 is Cys, $N^1{}_2$ is Asp, and $C^3{}_2$ is Thr	Decreasing	3.33	100
W_2 is Glu, $N^1{}_2$ is Lys, and $C^3{}_2$ is none	Increasing	1.67	100
W_2 is Glu, $N^1{}_2$ is Gln, and $C^3{}_2$ is Ser	Increasing	1.11	100

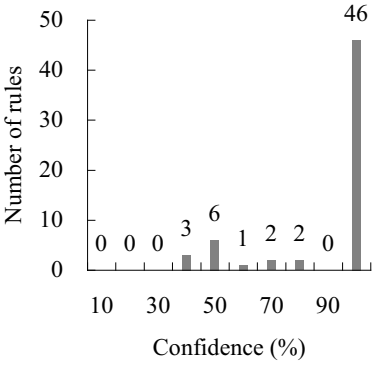

Fig. 4. Distribution of rules based on confidence

3.3 Discrimination from Partial Sequence Information

As an example, we provided the data for the mutants N116D and R119M in 2LZM but removing the information about four residues (i.e. $N^2{}_2$, $N^3{}_2$, $C^1{}_2$ and $C^2{}_2$). For the degree of important factors, confidence and support are assigned to "very important" and "moderately important", respectively.

The results displayed the fit rule(s) for the input along with reference level, which values the rule(s) for prediction reference. In this case, a rule shows the antecedent: W_2 is R, $N^1{}_2$ is L, and $C^3{}_2$ is Q, and the consequent of increasing, which means that the input is similar to the rule of increasing stability. Namely, the input may agree with the experimental observation of 0.15kcal/mol.

Moreover, we removed the information about another three residues (N11, N21, N31) and the results showed it is still a stabilizing mutant.

3.4 Prediction on Web

We have provided a web service for discriminating stability change upon double mutation from partial sequence information using the proposed method (named TANDEM, predicting stability change upon double mutation). The web service is freely available at http://bioinformatics.myweb.hinet.net/tandem.htm.

The input page for the service is illustrated in Figure 5a. It takes the information on wild-type, mutant and three neighboring residues for two mutation sites as input. The output page is shown in Figure 5b.

Fig. 5a. Snapshot of input page with related options

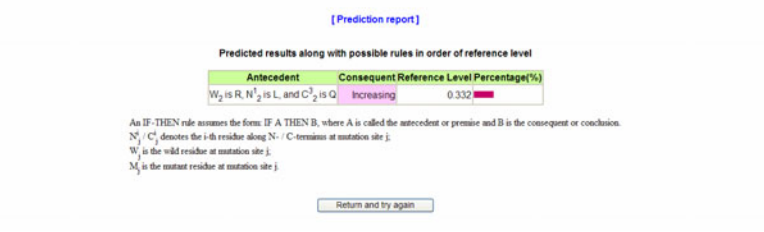

Fig. 5b. Snapshot of output page with predicted results

4 Conclusions

In conclusion, we have proposed a data mining approach to discriminating stability change for protein double mutants by using partial sequence information, which integrated an induction algorithm with a fuzzy query method. The results showed that the approach offers two main advantages: (i) A rule-based knowledge representation offers intuitive interpretation on raw data, which is helpful to understand the content; and (ii) A fuzzy query method incorporates the concept of uncertainty, which can make predictions from partial information. Further, we have also developed a web service for discriminating protein stability change upon double mutation from partial sequence information.

Acknowledgments. The authors would like to thank Dr. M. Michael Gromiha for critical guidance and valuable comments.

References

1. Gromiha, M.M.: Prediction of protein stability upon point mutations. Biochem. Soc. Trans. 35, 1569–1573 (2007)
2. Saraboji, K., Gromiha, M.M., Ponnuswamy, M.N.: Average assignment method for predicting the stability of protein mutants. Biopolymers 82, 80–92 (2006)
3. Huang, L.T., Gromiha, M.M., Ho, S.Y.: iPTREE-STAB: interpretable decision tree based method for predicting protein stability changes upon mutations. Bioinformatics 23, 1292–1293 (2007)

4. Grosfils, A., Dehouck, Y., Gilis, D., Rooman, M., Bogaerts, P.: Neural networks to predict protein stability changes upon mutation. In: Proceedings of the 17th International Federation of Automatic Control World Congress. International Federation of Automatic Control, Seoul, Korea, pp. 12619-12624 (2008)
5. Masso, M., Vaisman, I.I.: Accurate prediction of stability changes in protein mutants by combining machine learning with structure based computational mutagenesis. Bioinformatics 24, 2002–2009 (2008)
6. Wells, J.A.: Additivity of mutational effects in proteins. Biochemistry 29, 8509–8517 (1990)
7. Istomin, A.Y., Gromiha, M.M., Vorov, O.K., Jacobs, D.J., Livesay, D.R.: New insight into long-range nonadditivity within protein double-mutant cycles. Proteins 70, 915–924 (2008)
8. Huang, L.T., Gromiha, M.M.: Reliable prediction of protein thermostability change upon double mutation from amino acid sequence. Bioinformatics 25, 2181–2187 (2009)
9. Montanucci, L., Fariselli, P., Martelli, P.L., Casadio, R.: Predicting protein thermostability changes from sequence upon multiple mutations. Bioinformatics 24, i190–i195 (2008)
10. Giarratano, J.C., Riley, G.: Expert systems: principles and programming, Thomson Course Technology, Boston (2005)
11. Gromiha, M.M., An, J., Kono, H., Oobatake, M., Uedaira, H., Sarai, A.: ProTherm: Thermodynamic Database for Proteins and Mutants. Nucleic Acids Research 27, 286–288 (1999)
12. Kumar, M.D., Bava, K.A., Gromiha, M.M., Prabakaran, P., Kitajima, K., Uedaira, H., Sarai, A.: ProTherm and ProNIT: thermodynamic databases for proteins and protein-nucleic acid interactions. Nucleic Acids Research 34, D204–D206 (2006)
13. Kohavi, R.: The Power of Decision Tables. In: Proceedings of the 8th European Conference on Machine Learning, pp. 174–189. Springer, Heidelberg (1995)
14. Kaufmann, A., Gupta, M.M.: Introduction to fuzzy arithmetic: theory and applications. Van Nostrand Reinhold Co., New York (1985)
15. Ngai, E.W.T., Wat, F.K.T.: Fuzzy decision support system for risk analysis in e-commerce development, vol. 40. Elsevier Science, Amsterdam (2005)
16. Kao, C., Liu, S.-T.: Competitiveness of manufacturing firms: an application of fuzzy weighted average. IEEE Transactions on Systems, Man and Cybernetics, Part A 29, 661–667 (1999)
17. Guu, S.-M.: Fuzzy weighted averages revisited. Fuzzy Sets Syst. 126, 411–414 (2002)
18. Chang, P.T., Hung, K.C., Lin, K.P., Chang, C.H.: A comparison of discrete algorithms for fuzzy weighted average. IEEE Transactions on Fuzzy Systems 14, 663–675 (2006)
19. Lai, Y.-J., Hwang, C.L.: Fuzzy mathematical programming: methods and applications. Springer, Berlin (1992)
20. Zimmermann, H.J.: Fuzzy set theory–and its applications. Kluwer Academic Publishers, Boston (1991)
21. Tseng, T.Y., Cerry, M.K.: A new algorithm for fuzzy multicriteria decision making. Int. J. Approx. Reasoning 6, 45–66 (1992)
22. http://www.iit.nrc.ca/IR_public/fuzzy/fuzzyClips/fuzzyCLIPSIndex.html:

Inference of Gene Expression Regulation via microRNA Transfection

Y-h. Taguchi[1] and Jun Yasuda[2]

[1] Department of Physics, Chuo University, Tokyo 112-8551, Japan
tag@granular.com
http://www.granular.com/tag/
[2] COE Fellow, Graduate School of Medicine, Tohoku University,
Sendai 980-8575, Japan
jun.yasuda@jfcr.or.jp

Abstract. How each microRNA regulates gene expression is unknown problem. Especially, which gene is targeted by each microRNA is mainly depicted via computational method, typically without biological/ experimental validations. In this paper, we propose a computational method to detect gene expression regulation via miRNAs by the use of expression profile data and miRNA target prediction. This method is tested to miRNA transfection experiments to tumor cells and succeeded in inference of transfected miRNA.

Keywords: microRNA, target genes, tumor, computational inference.

1 Introduction

MicroRNAs (miRNAs) are post-transcriptional regulators of gene expression. It binds to target messenger RNAs (mRNAs) through complementary sequences in the three prime untranslated regions (3 UTRs) of the mRNA, and consequently suppresses the expression of the mRNAs. miRNAs are short RNA molecules, on average only 22 nucleotides long, and abundant in many human cell types. The human genome may encode over 1,000 miRNAs, and the coverage by all possible miRNAs may be about 60 % of mammalian genes.

On the other hand, how a miRNA regulates its target genes and which genes are regulated by a miRNA is unclear. Especially, the later is mainly depicted via computational prediction[1], without any biological/experimental validations. There are some direct ways to investigate the bindings of mRNAs to the miRNA-protein complexes, e.g., HITS-CLIP[2] but capability of these methods for identification of miRNA-mRNA relationship is limited since it is unlikely that all the potential target mRNAs for a miRNA simultaneously express in a cell.

Another experimental way to detect miRNA target genes is to analyze the difference of gene expression profiles with or without the transfection of the miRNA to a cell line. However, it is unrealistic to test all the miRNAs with this method because it is time and money consuming.

D.-S. Huang et al. (Eds.): ICIC 2010, LNCS 6215, pp. 672–679, 2010.

In this paper, we describe a computational method to detect miRNAs which regulate the transcriptomes in a cell in response to extracellular stimuli by analyzing the difference of gene expression profiles and computational miRNA target predictions. The validation of our methods were obtained through the analyses of the gene expression profiles with or without the transfection of single miRNAs and our algorithm can quite frequently predict the transfected miRNA.

2 Materials and Methods

2.1 Gene Expression Data for Transfection Experiment

We have downloaded transfection experiment[3] data set, CBX79, which is deposited at CIBEX data base[4] at Center for Information Biology and DNA Data Bank of Japan (DDBJ), National Institute of Genetics (Mishima, Japan). It includes two biological replicates of negative, mir-107, 185, and let-7a trasfection experiments, one day and three days after the transfection. Expression of 45015 genes (probes) are listed. Since our method is robust for the random noise of gene expression variance and the overall distribution of gene expression between technical replicates should be within the acceptable range, we did not apply any normalization procedure.

2.2 Inference of miRNA Which Regulates Target Genes Significantly

The way to detect miRNA whose target genes are significantly differently expressed between negative control and treated one is as follows. First, we have downloaded a list of conserved seed match in 3' UTRs of genes to each miRNA[1][5]. This includes 162 miRNA families. The reason why we do not use major target gene list, e.g., targetScan[6], PITA[7], pictar[8], miranda[9], and others, but use seed match is because Alexiou *et al*[10] recently reported that simple seed match often outperforms more complicated estimations of target genes. Then we have picked up genes which has at least one seed match for any miRNAs in those 3' UTRs. Then, 13270 genes remain.

Hereafter, we denote a set of these genes as G. Next, for each miRNA, m, we have listed genes which has at least one seed match in 3' UTRs. We denote this set of genes as G_m, where m denotes one of miRNA families. Also we define a set of genes, $G'_m \equiv G \setminus G_m$, which is a set of genes included into G, but not into G_m. After denoting expression of gene g under transfection of miRNA m_0, m_0 is one of mir-107, 185, let-7a, and Negative Control (NC), as $x_g^{m_0}$, we compute gene expression difference between post-miRNA transfection and NC,

$$\Delta x_g^{m_0} \equiv \log x_g^{m_0} - \log x_g^{NC}.$$

Then we apply two way t-test beween $\{\Delta x_g^{m_0} \mid g \in G_m\}$ and $\{\Delta x_g^{m_0} \mid g \in G'_m\}$. P-value, P_m, is computed for each miRNA, m. After applying FDR correction

[1] http://hollywood.mit.edu/targetrank/hsa_conserved_miR_family_ranked_targets.txt

(BH method[11]) to 162 P-values, we have selected ms whose FDR corrected P-value is less than 0.05 as miRNA which regulates target genes significantly. For t-test, we have used t.test module in base package in R[12].

2.3 Coincidence between Biological Replicates

We have also checked if two biological replicates satisfy reproducibility in three ways. Firstly, we employed Pearson correlation coefficients between log transformed P_ms and secondly, Spearman correlation coefficients between them. P-values for these are computed as well as 95 percentile significant interval for the form. Thirdly, we analyzed coincidence between significant miRNAs, ms between two biological replicates. If the first(second) replicates have $m_1(m_2)$ significant miRNAs and m_{12} miRNAs are selected for both replicates, P-value computed by binomial distribution $P(m_1,\mathrm{N},m_2/N)$ or $P(m_2,\mathrm{N},m_1/N)$, where $P(x,N,p)$ is the probability that x among N is selected when the probability of selection is p. N is the number of genes in G.

We have used cor.test module in base package of R for P-values of correlation coefficients and pbinom module for binomial distribution.

2.4 Significant Overlap between Target Genes

To compute P-values of accidental agreement between target genes, $P^O_{m,m'}$ of miRNAs m and m', we have employed binomial distribution $P(n_{mm'},n_m,n_{m'}/N)$, where $n_{mm'}$ is the number of co-target genes, $n_m(n_{m'})$ is the number of target genes of m(m').

3 Results

Independent of conditions, i.e., date and transfected miRNA, our method almost always gets non-empty set of significant miRNAs, ms (see Table 1). Thus, in principle, our method can detect miRNA regulation of gene expression. Table 2 shows which miRNA significantly regulates target genes (full list is available as a supplementary material[13]). Most remarkably, P_m has the strong tendency to become smallest when $m = m_0$, especially for one day after transfection. Thus, our method has not only ability to detect miRNA regulation of genes, but also that to infer transfected miRNA correctly, as appearing the transfected one in the highest rank (first or second) for most of the present analyses (Table 1).

In Figs. 1, we have shown comparison of gene expression between $x_g^{m_0}$ and x_g^{NC}. It is generally clear that $x_g^{m_0} < x_g^{NC}$ only for $g \in G_{m_0}$, but not for $g \in G'_{m_0}$. Only exception is mir-185 transfection, replicate 2 where we have failed transfected miRNA correctly (see Table 2). Clearly, for this case, $x_g^{m_0} < x_g^{NC}$ stands for both $g \in G_{m_0}$ and $g \in G'_{m_0}$ (lower row in Fig. 1(b)).

Table 3 shows the results of several statistical tests for the coincidence between biological replicates. For five out of six cases, at least one of tests give the significant P-values < 0.05. Thus, biological replicates are good enough for inference of miRNA transfection.

Table 1. Numbers of significant miRNAs. The ranks of transfected micriRNAs are shown in square brackets.

	Transfected miRNA					
	mir-107		mir-185		let-7a	
time	replicate 1	replicate 2	replicate 1	replicate 2	replicate 1	replicate 2
day 1	25[1st]	36[2nd]	12[1st]	12[—]	2[1st]	2[1st]
day 3	60[17th]	98[—]	0[1st]	24[—]	1[1st]	33[8th]

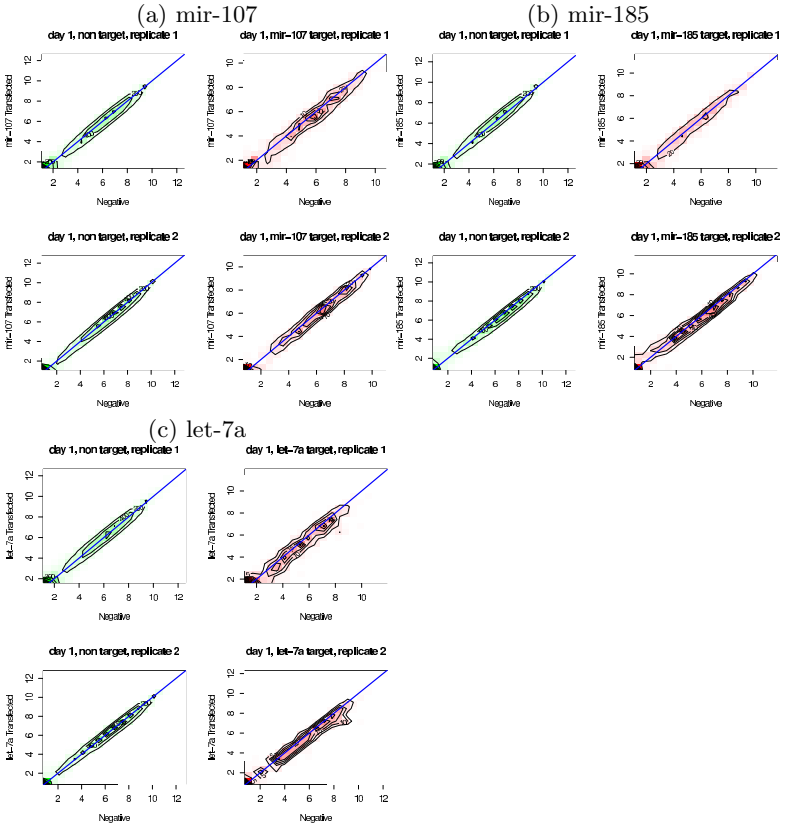

Fig. 1. Comparison between gene expression at one day after transfection (vertical axes) and negative control (horizontal axes). (a) mir-107, (b) mir-185, (c) let-7a . Right column (red) in each block indicates target genes ($g \in G_{m_0}$) and left column (green) in each block is others ($g \in G'_{m_0}$). The upper(lower) row in each block is replicate 1(2). Blue lines are diagonal, i.e., there are no difference between transfeted one and negative control.

Table 2. Top most significant miRNAs, one day or three days after trasnfection. Bold characters are those transfected.

mir-107 transfection, day 1			
replicate 1		replicate 2	
miRNA	P_m	miRNA	P_m
miR-103/107	2.64×10^{-8}	miR-29	1.34×10^{-10}
miR-30-5p	6.43×10^{-7}	**miR-103/107**	9.92×10^{-9}
miR-17-5p/20/93.mr/106/519.d	3.42×10^{-5}	miR-30-5p	2.71×10^{-8}
miR-452	3.73×10^{-5}	miR-17-5p/20/93.mr/106/519.d	3.45×10^{-7}
miR-25/32/92/363/367	2.49×10^{-4}	miR-129-5p	5.66×10^{-7}
mir-107 transfection, day 3			
replicate 1		replicate 2	
miRNA	P_m	miRNA	P_m
miR-17-5p/20/93.mr/106/519.d	1.31×10^{-11}	miR-17-5p/20/93.mr/106/519.d	4.39×10^{-15}
miR-29	8.42×10^{-9}	miR-186	3.27×10^{-13}
miR-25/32/92/363/367	1.07×10^{-7}	miR-203.1	6.56×10^{-13}
miR-181	1.44×10^{-7}	miR-374	2.46×10^{-12}
miR-448	2.30×10^{-7}	miR-369-3p	3.60×10^{-12}
mir-185 transfection, day 1			
replicate 1		replicate 2	
miRNA	P_m	miRNA	P_m
miR-185	8.64×10^{-12}	miR-496	1.87×10^{-7}
miR-326	3.15×10^{-6}	miR-495	1.96×10^{-5}
miR-15/16/195/424/497	1.60×10^{-4}	miR-320	1.98×10^{-5}
miR-410	2.01×10^{-4}	miR-181	2.52×10^{-5}
miR-491	3.98×10^{-4}	miR-381	3.93×10^{-5}
mir-185 transfection, day 3			
replicate 1		replicate 2	
miRNA	P_m	miRNA	P_m
—	—	miR-17-5p/20/93.mr/106/519.d	4.39×10^{-15}
—	—	miR-186	3.27×10^{-13}
—	—	miR-203.1	6.56×10^{-13}
—	—	miR-374	2.46×10^{-12}
—	—	miR-369-3p	3.60×10^{-12}
let-7a transfection, day 1			
replicate 1		replicate 2	
miRNA	P_m	miRNA	P_m
let-7/98	4.37×10^{-14}	**let-7/98**	9.55×10^{-16}
miR-196	3.94×10^{-4}	miR-196	2.81×10^{-4}
let-7a transfection, day 3			
replicate 1		replicate 2	
miRNA	P_m	miRNA	P_m
let-7/98	5.32×10^{-8}	miR-374	1.97×10^{-8}
—	—	miR-130/301	2.67×10^{-6}
—	—	miR-9	2.18×10^{-5}
—	—	miR-223	4.09×10^{-5}
—	—	miR-369-3p	4.96×10^{-5}

Table 3. Comparison of two biological replicates. Bold numbers indicate signifcant P-values (< 0.05). Bold asterisks (*****) indicate $P < 2.2 \times 10^{-16}$.

Transfection	mir-107		mir-185		let-7a	
Time	day 1	day 3	day 1	day 3	day 1	day 3
Pearson	0.67	0.67	0.03	0.16	0.86	0.28
	95 % confidence interval					
lower	0.57	0.58	-0.12	0.00	0.81	0.13
upper	0.74	0.75	0.18	0.30	0.89	0.42
P-value	*	*	0.7	**0.046**	*	**0.00029**
Spearman	0.52	0.70	0.05	0.09	0.28	0.13
P-value	*	*	0.53	0.27	**0.0003**	0.1
	# of significant miRNAs					
common	17	56	1	0	2	1
replicate 1	25	60	12	0	2	1
replicate 2	36	98	12	24	2	33
P-value	$\mathbf{1.6 \times 10^{-7}}$	$\mathbf{8.3 \times 10^{-10}}$	2.2×10^{-1}	—	**0**	**0**

4 Discussion

Although P_{m_0} is mostly the smallest, P_m with $m \neq m_0$ also can take the value as small as P_{m_0} (see Table 2). The reason why it occurs is not because their seed sequence is similar to those of trasnfected miRNA. Actually, seed sequence of miRNA whose P_m is as small as P_{m_0} is very different from that of transfected miRNA.

Thus, the reason why miRNAs not transfected often have P_ms as small as P_{m_0} may be because of the secondary effect. First of all, while transfected miRNA regulates target genes, these genes are targeted by other miRNAs, too. If these genes have significant overlaps with other miRNA's target genes, P_ms of those miRNAs often take significantly small P-value. It is impossible to exclude this possibility, since we do not consider miRNA expression at all. In some sense, it is remarkable that P_{m_0} often has the smallest P-value. Next, genes regulated by tnasfected miRNA induce expression of other genes which are not direct targets of transfected gene. If some of not transfected miRNAs' target genes have siginificant overlap with those secondary induced genes, those miRNA has inevitably significant small P-value. Actually, P_{m_0} for three days after transfection usually does not have small enough P-value. It possibly means that secondary induced genes are apparently more *regulated* than genes directly targeted by transfected miRNA. Thus, it results in the lack of detection of gene regulation by transfected miRNA.

The datasets of day 1for miR-185 transfection is only one case which failed showing significant coincidence between biological replicates. This fact is very interesting because this is also the only the case in which one of biological replicates (replicate 1) cannot infer transfected miRNA correctly within samples at day 1. This possibly means that this replicate may have failed to produce suitable gene expression profile in some sense. For other five cases (one day and three days after mir-107 transfection, three days after mir-185 transfection, one day and three days after let-7a transfection), at least one statistical test can provide

us significant P-value. Therefore, it is unlikely that the detection of regulation of target genes by not transfected miRNA is due to the analytical errors. It is important to clarify the biological reason of this unexpected result.

It is also interesting that miRNA target genes are generally more expressed than the other genes in the present datasets.(in Figs. 1, there are peaks around $\log x_g \simeq 7$, which is far from origin. This tendency cannot be seen in genes not targeted by any miRNA (not shown here). This fact may also be important to understand how each miRNA regulate genes in cancer formation/suppression.

One may wonder that accidental overlap of target genes results in significant regulation of target genes of non-transfected miRNAs. In order to check this point, we have computed P-values of significant overlap of target genes by $P(n_{mm_0}, n_m, n_{m_0}/N)$. As a result, even after correction considering multiple comparison, 156, 157 and 156 miRNAs among in total 162 miRNAs have significant overlap ($P < 0.05$) with transfected miRNA of mir-107, mir-185 and let-7a respectively. This means, almost all of non-transfected miRNAs have significant large number of common target genes with those transfected miRNA.

One may think that this is the evidence that our analysis is erroneous, but it is not the case. Actually, if we compute correlation coefficient between P_m and P^O_{m,m_0}, for most of cases, there are no significant correlations (see Table 4). This means, significant regulation of target genes of non-transfected miRNA cannot be explained by the accidental target gene overlap with those of transfected miRNA, m_0.

Only two exception among total 12 cases (i.e., two biological replicates $\times$ two time points (day 1 or day 3) $\times$ three transfection) is for day 3. Since day 3 is late date when the effects of transfected miRNA become weaker, apparent significant regulation of target genes of non-transfected miRNAs is caused not by accidental overlaps of target genes, but by secondary effect. In other words, these genes are regulated indirectly through direct regulation of target genes by transfection.

Table 4. Significance of correlation between P_m and P^O_{m,m_0}. Bold numbers are significant ($P < 0.05$)

Transfection	mir-107				mir-185				let-7a			
Date	day 1		day 3		day 1		day 3		day 1		day 3	
Replicates	1	2	1	2	1	2	1	2	1	2	1	2
correlation	0.031	0.050	0.15	0.22	0.052	-0.077	-0.045	0.23	0.080	-0.042	-0.019	0.11
P-value	0.70	0.53	0.058	**0.0059**	0.51	0.33	0.57	**0.0035**	0.31	0.6	0.82	0.15

5 Conclusion

In this paper, we have shown that gene expression profile combined with miRNA target genes predicted computationally can often correctly infer transfeted miRNA. This suggests that we may be able to infer miRNA regulation of genes solely from gene expressions without considering any other information than computationally predicted target genes.

References

1. Brennecke, J., Stark, A., Russell, R.B., Cohen, S.M.: Principles of microRNA-target recognition. PLoS Biol. 3, e85 (2005)
2. Chi, S.W., Zang, J.B., Mele, A., Darnell, R.B.: Argonaute HITS-CLIP decodes microRNA-mRNA interaction maps. Nature 460, 479–486 (2009)
3. Takahashi, Y., Forrest, A.A.R., Maeno, E., Hashimoto, T., Daub, C.O., Yasuda, J.: MiR-107 and MiR-185 Can induce cell cycle arrest in human non small cell lung cancer cell lines? PLoS One 4, e6677 (2009)
4. Ikeo, K., Ishii, J., Tamura, T., Gojobori, T., Tateno, Y.: CIBEX: center for information biology gene expression database. C. R. Biol. 326, 1079–1082 (2003)
5. Nielsen, C.B., Shomron, N., Sandberg, R., Hornstein, E., Kitzman, J., Burge, C.B.: Determinants of targeting by endogenous and exogenous microRNAs and siRNAs. RNA 13, 1894–1910 (2007)
6. Friedman, R.C., Farh, K.K., Burge, C.B., Bartel, D.P.: Most mammalian mRNAs are conserved targets of microRNAs. Genome Res. 19, 92–105 (2009)
7. Kertesz, M., Iovino, N., Unnerstall, U., Gaul, U., Segal, E.: The role of site accessibility in microRNA target recognition. Nat. Genet. 39, 1278–1284 (2007)
8. Krek, A., Grün, D., Poy, M.N., Wolf, R., Rosenberg, L., Epstein, E.J., MacMenamin, P., da Piedade, I., Gunsalus, K.C., Stoffel, M., Rajewsky, N.: Combinatorial microRNA target predictions. Nat. Genet. 37, 495–500 (2005)
9. John, B., Enright, A.J., Aravin, A., Tuschl, T., Sander, C., Marks, D.S.: Human MicroRNA targets. PLoS Biol. 2, e363 (2004)
10. Alexiou, P., Maragkakis, M., Papadopoulos, G.L., Reczko, M., Hatzigeorgiou, A.G.: Lost in translation: an assessment and perspective for computational microRNA target identification. Bioinformatics 25, 3049–3055 (2009)
11. Benjamini, Y., Hochberg, Y.: Controlling the false discovery rate: a practical and powerful approach to multiple testing. J. R. Stat. Soc. B 57, 289–300 (1995)
12. R Development Core Team, R: A language and environment for statistical computing. R Foundation for Statistical Computing, Vienna, Austria (2009) ISBN 3-900051-07-0 http://www.R-project.org
13. http://www.granular.com/ICIC2010/SPM.txt

A Residual Level Potential of Mean Force Based Approach to Predict Protein-Protein Interaction Affinity

Xue-Ling Li[1,*], Mei-Ling Hou[1,2], and Shu-Lin Wang[1,3]

[1] Hefei Institute of Intelligent Machines, Chinese Academy of Sciences, Hefei, Anhui 230031, China
xuelingli08@gmail.com
[2] Department of Biology, University of Science and Technology of China, Hefei 230026, China
[3] School of Computer and Communication, Hunan University, Changsha, Hunan, China

Abstract. We develop a knowledge-based statistical energy function on residual level for quantitatively predicting the affinity of protein-protein complexes by using 20 residue types and a distance-free reference state. The correlation coefficients between experimentally measured protein-protein binding affinities (PPIA) and the predicted affinities by our approach are 0.74 for 82 protein-protein (peptide) complexes. Compared to the published results of two other volume corrected knowledge-based scoring functions on atomic level, the proposed approach not only is the simplest but also yields the comparable correlation between theoretical and experimental binding affinities of the test sets with the reported best methods.

Keywords: Protein-protein interaction, affinity, mean force of potential, residue level, protein complex, quaternary structure.

1 Introduction

Most proteins play their functions through interacting with their partners in biological processes. Revealing the structure and energetic characteristics of protein-protein interactions genome-wide is critical in designing effective drugs targeting the interactions. With the increasing number of sequenced genomes, explicit information about the identity of individual proteins are contained, but not the structure and energy of the protein interactions [1]. Thus, the precise and reliable methods for calculating free energy of protein complexes are critical for predicting both the structure and affinity of protein-protein interactions.

The increasing structures of both the single protein and their complexes make this ambitious goal possible. However, obtaining accurate energy estimation is still challenging. Thus computational methods are very important. Existing approaches for predicting protein-protein interaction affinity (PPIA) can be classified into four categories,

* Corresponding author.

D.-S. Huang et al. (Eds.): ICIC 2010, LNCS 6215, pp. 680–686, 2010.

i.e., physical-based force fields, empirical scoring functions and knowledge-based statistical potentials and hybrid scoring functions [2].

Physical-based force fields estimate affinities by summing the strength of intermolecular van der Waals and electrostatic interactions and sometimes polarization energy between all atoms of the two molecules in the complex [3]. Desolvation energies of the ligand and of the protein are sometimes taken into account using implicit solvation methods. Empirical scoring functions count the number of various types of interactions between the two binding protein partners [4] as different terms of the scoring function. The count is based on the number of ligand and receptor atoms in contact with each other or by calculating the change in solvent accessible surface area (ΔSASA) in the complex compared to the uncomplexed ligand and protein. The coefficients of the scoring function are usually fit using multiple linear regression methods. Knowledge-based potentials are based on statistical observations of intermolecular close contacts of interface residues or atoms in large 3D databases (such as the Protein Data Bank) which are used to derive "potentials of mean force". The method is founded on the assumption that close intermolecular interactions between certain types of atoms or functional groups that occur more frequently than one would expect by a random distribution are likely to be energetically favorable and therefore contribute favorably to binding affinity [5]. Finally hybrid scoring functions have also been developed in which the components from two or more of the above scoring functions are combined into one function [6, 7].

Existing energy functions are successful in protein interaction affinity prediction [2-4, 8]. However, their computational cost is still too high for genome-wide PPIA prediction. It is necessary to parameterize the energy function in empirical energy functions. Thus, the structure dissimilarity of training set will greatly affect the accuracy of PPIA prediction and these functions mainly applied in protein-small molecules interaction affinity prediction or a specific protein binding system [9].

Residue level potential of mean force and its derivations are proved to be successful in describing protein-protein interactions [1], ab initio folding [10] and genome-wide measurement for computational predictions of SH2-peptide interactions [11]. We develop a simple approach to predict PPIA based on a distance-independent residue level potential of mean force (DIRPMF) and compare the DIRPMF with its alternatives on atom level with or without volume correlation. We find that DIRPMF are comparable and effective. The technique is sufficiently general that it can be used to predict PPIA in high throughput study and even genome-wide analysis.

2 Materials and Methods

The training and test sets are obtained from [8]. Specifically, the training dataset consists of 178 interfaces of 127 PDB entries of protein-protein and protein-peptide complexes with resolutions better than 2.5 Å and reduced structure similarity. 83 of the 86 protein-protein complexes except 3cpa, 4cpa and 3ssi from [8] are used as our test sets to evaluate the prediction ability of our approach to the affinity prediction of protein-protein complexes.

2.1 Interfacial Statistical Potentials of Mean Force

The DIRPMF or atom pair potential (DIAPMF), P(i,j), are developed from the above training set as described in [1] using the following formula:

$$P(i,j) = -\log\left(\frac{N_{obs}(i,j)}{N_{\exp}(i,j)}\right) \quad (1)$$

where $N_{obs}(i,j)$ is the observed number of interacting residue or atom pairs of *i, j* between two interfacial chains of the protein complex ($i = 1,2,3...20$, $j = 1,2,3,..20$, for residual level PMF; $i = 1,2,3...47$, $j = 1,2,3,..47$ for atomic level PMF; $N_{exp}(i,j)$ is the expected number of interacting pairs of *i, j* between two chains if there are no preferential interactions among them, which is a reference state. The expected number is calculated from:

$$N_{\exp}(i,j) = X_i \times X_j \times N_{total} \quad (2)$$

where X_i is the mole fraction of residue or atom type *i* and is calculated as N_i / N, N_{total} is the total number of interacting pairs.

Four comparison, heavy atom-based distance-dependent and distance-independent (as above) statistical potentials are also built to describe interfacial pair interactions. Based on the atom physicochemical property, connectivity and environment, 47 atom types for all the 167 types of heavy atoms of the 20 amino acids were defined as described in [8]. To obtain more details of interactions, it would be better to define as many types as possible. On the other hand, to obtain statistically sufficient data, not many atom types are preferred.

The distance *r* ranges from 0 to 16 Å at 0.5 Å intervals. The interfacial atom pair potential is:

$$P(i,j,r) = -\log\left(\frac{N_{obs}(i,j,r)}{N_{\exp}(i,j,r)}\right) \quad (i = 1,2,3...47, j = 1,2,3,..47) \quad (3)$$

where $N_{obs}(i,j,r)$ is the observed number of interacting atom pairs *i, j* between two chains at a distance bin of 0.5 Å, $N_{\exp}(i,j,r) = X_i \times X_j \times N_{total}(r)$ is the expected number of interacting atom pairs of *i, j* between two chains if there are no preferential interactions among them; X_i is the mole fraction of atom type *i* and is calculated as N_i / N, where N_i and N are the total number of atom type I and all atoms, respectively, while $N_{total}(r)$ is the total number of interacting atom pairs.

2.2 Scoring and Fitting Experimental Binding Affinity

The scoring functions to a protein-protein complex affinity are defined as the summation over all residue or atom pair interactions of the protein-protein complex for distance-independent and -dependent at all distant bins, respectively:

$$score = \sum_{i=1}^{20}\sum_{j=1}^{20} P(i,j) \quad (4)$$

$$score = \sum_{r}^{r\_cut} \sum_{i=1}^{20} \sum_{j=1}^{20} P(i, j) \tag{5}$$

To relate the score above to the experimentally measured binding affinity, we fit it to the measured binding affinity in a linear manner:

$$\Delta G_{bind} = \alpha \times score + b \tag{6}$$

3 Results and Discussion

3.1 Comparison between Atomic and Residual Levels PMFs

The optimal correlation coefficients (R) between the experimental affinities and the predicted ones are 0.69, 0.54 and 0.53 for the distance-independent residual level PMF (DIRPMF) and distance-dependent and –independent atomic level PMF (DDAPMF and DIAPMF) without volume correction, respectively. The corresponding optimal standard derivations (SD) are 2.46, 2.85, and 2.89 as shown in Fig.1-3. With optimal distance cutoffs of 13 Å and 15.5 Å, the R are 0.54 and 0.53, and the SD are 2.85 and 2.89, respectively for DDAPMF and DIAPMF based approaches, while the optimal cutoffs range from 4.5 Å to 8 Å with the corresponding R ranging from 6.80 to 6.90 and SD varying from 2.46 to 2.49 for the DIRPMF. It can be seen that the DIRPMF based approach is apparently superior to both DDAPMF and DIAPMF based approaches, although numerous reports on the superiority of atomic level PMF to the residual level one. Comparing our DIRPMF based approach with the distance-dependent atomic level PMF (DIAPMF), we find that distance bins only very marginally improve the accuracy of DDAPMF, the corresponding optimal R is 0.55 which is slightly higher the distance-independent one, i.e. 0.53. One explanation for the above results may be that even 47 atom types are used instead of the total 169 atom types for 20 natural amino acids that are commonly found in proteins, still not enough statistical significant number of atom for an defined atom type can be obtained within the little distance bins in the distance-dependent even as a whole bin in the distance-dependent and -independent atomic level PMF methods.

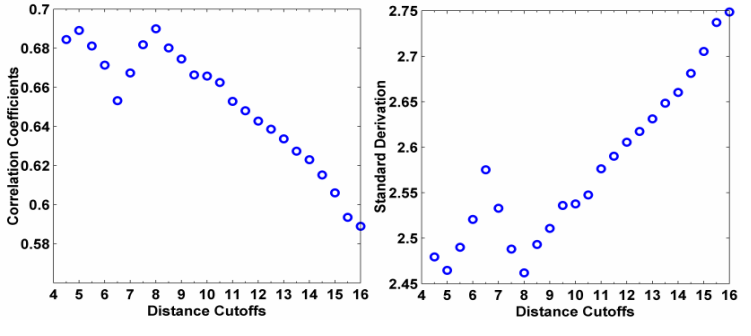

Fig. 1. The linear correlation coefficients (left) and standard deviations (SD) (right)between predicted affinities and the experimental ones based on distance-independent the residual level PMF (DIRPMF) versus the cutoff threshold distance (Å) for contact residues

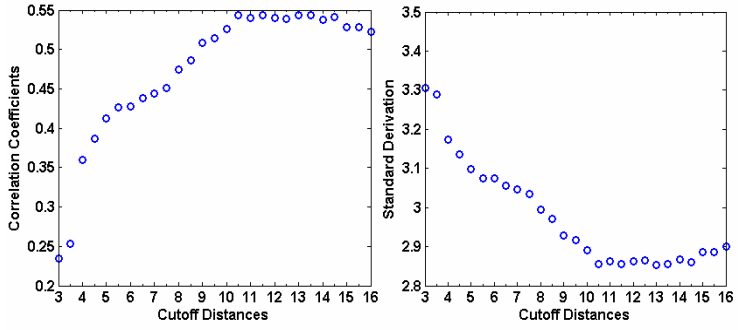

Fig. 2. The linear correlation coefficients (left) and standard deviations (SD) (right) between the predicted affinities based on distance-dependent atomic level PMF (DDAPMF) and the experimental ones versus the cutoff threshold distance (Å) for contact atoms.

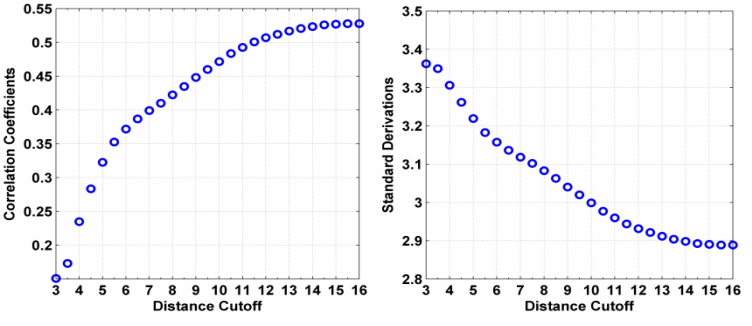

Fig. 3. The linear correlation coefficients (left) and standard deviations (SD) (right)between the predicted affinities based on distance-independent atomic level PMF (DIAPMF) and the experimental ones versus the cutoff threshold distance (Å) for contact atoms

3.2 PPIA Prediction by the Proposed Approach

It can be seen from Fig.4 and Fig.5 that without the outlier 1cho, the optimal linear correlation coefficients between the predicted affinity and the experimental one is improved from 0.69 at 8 Å to 0.74 and 5 Å, respectively for our proposed DIRPMF based approach for PPIA prediction.

We further compared our methods with the volume corrected ones. The correlation obtained here is comparable to the reported best volume corrected ones as shown in Table 3, when one outlier is deleted with the same number of test complexes. Although two of the remaining 82 test complexes used here are different from that in [2] and [8], the total number and the complexity of the text complexes are the same. From the comparison result as shown in Table 3, we can see that the proposed method is comparable to the best ones. Moreover, because of its simplicity, one advantage of the residual level PMF based approach is that it can be used genome-wide and high throughput PPIA prediction if only the contact residues of protein complexes are known or predicted even if the atom coordinate details are not known or not be exact.

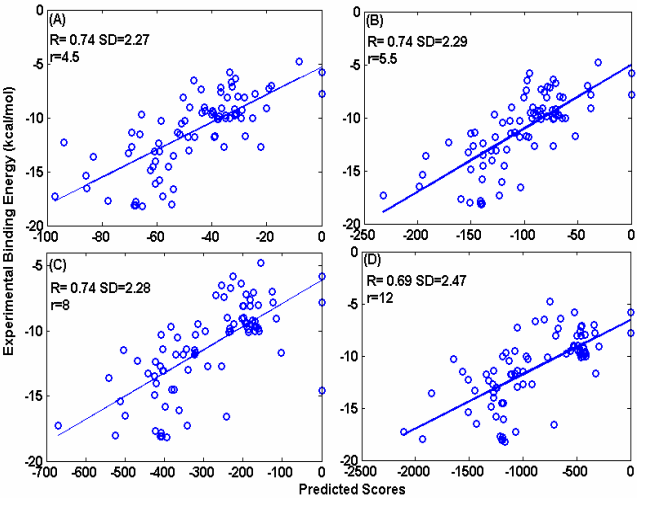

Fig. 4. The predicted binding affinity by the residual level PMF with respected to experimental ones on test set. The linear correlation coefficient (R) and standard deviation (SD) are calculated, where r is the cutoff threshold distance (Å) for contact residues.

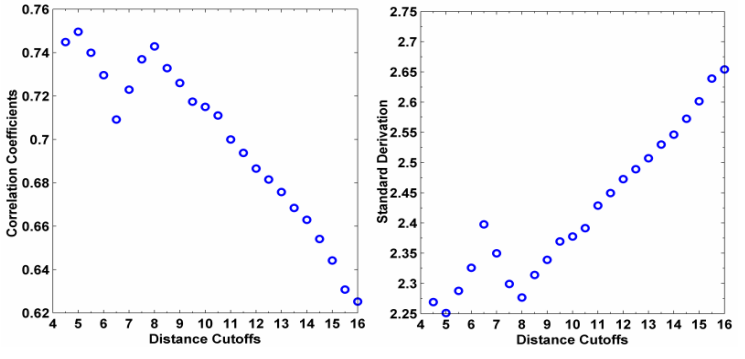

Fig. 5. The linear correlation coefficients (left) and standard deviations (SD) (right) between predicted affinities and the experimental ones based on the residual level PMF versus the cutoff threshold distance (Å) for contact residues when one outlier, 1cho, is not considered

Table 1. Linear correlation between experimental binding affinity and predicted affinity on the independent test set

No. of Complexes [a]	R			SD		
	Ours	Method1[b]	Method2[c]	Ours	Method1[b]	Method2[c]
82	0.74	0.73	0.73	2.25	NA[d]	0.73

[a] Two of the 82 complexes are different between ours and method1 and method2, while the latter two are the same. [b] The results from Ref. 2;
[c] The results from Ref. 8;
[d] NA, no available standard deviation (SD) was reported in the literature.

In conclusion, the proposed method is simple and effective, which may be used for high throughput or genome-wide PPIA prediction.

Acknowledgments. This work was supported by the Knowledge Innovation Program of the Chinese Academy of Sciences (Grant no. 0823A16121), 863 Project of National High Technology of China (2006AA02Z309), the National Science Foundation of China (Grant nos. 30900321, 30700161), the China Postdoctoral Science Foundation (Grant no. 20090450825).

References

1. Lu, H., Lu, L., Skolnick, J.: Development of unified statistical potentials describing protein-protein interactions. Biophysical Journal 84, 1895–1901 (2003)
2. Zhang, C., Liu, S., Zhu, Q.Q., Zhou, Y.Q.: A knowledge-based energy function for protein-ligand, protein-protein, and protein-DNA complexes. Journal of Medicinal Chemistry 48, 2325–2335 (2005)
3. Kollman, P.A., Massova, I., Reyes, C., Kuhn, B., Huo, S., Chong, L., Lee, M., Lee, T., Duan, Y., Wang, W., Donini, O., Cieplak, P., Srinivasan, J., Case, D.A., Cheatham, T.E.: 3rd: Calculating structures and free energies of complex molecules: combining molecular mechanics and continuum models. Acc. Chem. Res. 33, 889–897 (2000)
4. Bohm, H.J.: Prediction of binding constants of protein ligands: a fast method for the prioritization of hits obtained from de novo design or 3D database search programs. J. Comput. Aided Mol. Des. 12, 309–323 (1998)
5. Muegge, I.: PMF scoring revisited. J. Med. Chem. 49, 5895–5902 (2006)
6. Englebienne, P., Moitessier, N.: Docking Ligands into Flexible and Solvated Macromolecules. 4. Are Popular Scoring Functions Accurate for this Class of Proteins? Journal of Chemical Information and Modeling 49, 1568–1580 (2009)
7. Oda, A., Tsuchida, K., Takakura, T., Yamaotsu, N., Hirono, S.: Comparison of consensus scoring strategies for evaluating computational models of protein-ligand complexes. Journal of Chemical Information and Modeling 46, 380–391 (2006)
8. Su, Y., Zhou, A., Xia, X.F., Li, W., Sun, Z.R.: Quantitative prediction of protein-protein binding affinity with a potential of mean force considering volume correction. Protein Science 18, 2550–2558 (2009)
9. Sotriffer, C.A., Sanschagrin, P., Matter, H., Klebe, G.: SFCscore: Scoring functions for affinity prediction of protein-ligand complexes. Proteins-Structure Function and Bioinformatics 73, 395–419 (2008)
10. Skolnick, J., Kolinski, A., Ortiz, A.: Derivation of protein-specific pair potentials based on weak sequence fragment similarity. Proteins-Structure Function and Genetics 38, 3–16 (2000)
11. Wunderlich, Z., Mirny, L.A.: Using genome-wide measurements for computational prediction of SH2-peptide interactions. Nucleic Acids Research 37, 4629–4641 (2009)

Author Index